Aminophosphine Sulfides: Stereoselective Synthesis, Hydrogen-Bond-Based Aggregation and Application as Synthetic Building Blocks

Dissertation

zur Erlangung des

DOKTORGRADES DER NATURWISSENSCHAFTEN

(DR. RER. NAT.)

der Fakultät Chemie und Pharmazie

der Universität Regensburg

vorgelegt von

Tanja Huber

aus Ingolstadt

im Jahr 2024

Eidesstattliche Erklärung

Ich erkläre hiermit an Eides statt, dass ich die vorliegende Arbeit selbstständig verfasst und keine anderen als die angegebenen Quellen und Hilfsmittel benutzt habe. Die aus fremden Quellen direkt oder indirekt übernommenen Gedanken sind als solche gekennzeichnet. Die Arbeit wurde bisher in gleicher oder ähnlicher Form keiner anderen Prüfungsbehörde vorgelegt und auch nicht veröffentlicht.

_____ _____

Ort, Datum Unterschrift

Die vorliegende Arbeit entstand in der Zeit von November 2019 bis März 2024 am Institut für Anorganische Chemie der naturwissenschaftlichen Fakultät IV für Chemie und Pharmazie der Universität Regensburg unter Anleitung von PD Dr. Jonathan O. Bauer.

Promotionsgesuch	April 2024
Promotion	Mai 2024

Prüfungsausschuss:

Vorsitz:	Apl. Prof. Dr. Rainer Müller
Erster Gutachter:	PD Dr. Jonathan O. Bauer
Zweiter Gutachter:	Prof. Dr. Manfred Scheer
Dritter Prüfer:	Prof. Dr. Frank-Michael Matysik

Publikationsliste:

Paper:

Access to Enantiomerically Pure *P*-Stereogenic Primary Aminophosphine Sulfides under Reductive Conditions

T. Huber, N. A. Espinosa-Jalapa, J. O. Bauer

Chem. Eur. J. **2022**, *28*, e202202608.

Review:

A Powerful P–N Connection: Preparative Approaches, Reactivity, and Applications of *P*-Stereogenic Aminophosphines

T. Huber, J. O. Bauer

Chem. Eur. J. **2024**, *30*, e202303760.

Meinen Eltern
Verena und Barthl

„You may say I'm a dreamer.
But I'm not the only one."

John Lennon – Imagine

Preface

Some of the chapters presented herein have already been published during the preparation of this dissertation. The relevant citations and the license numbers are given at the beginning of the corresponding chapters (Chapters one and three).

Each chapter, except for Chapters two and seven, begins by listing the authors and indicating how they have contributed to the chapter. All chapters have their unique compound numbering system. The depicted molecular structures may differ slightly in style. A general introduction (Chapter one) along with the objectives of this thesis (Chapter two) are given at the beginning. For the sake of consistency, all the research chapters (Chapters three to six) are divided into the following sections:

- Abstract, except for Chapter six
- Introduction, except for Chapter six
- Results and Discussion
- Conclusion, except for Chapter six
- References
- Syntheses and Characterizations
- X-ray Crystallographic Details
- Quantum Chemical Calculations, except for Chapter five and Chapter six
- Supplementary References

In addition, a comprehensive conclusion (Chapter seven) of this work is presented at the end of this thesis.

Abbreviations

Å	Ångström (10^{-10} m)
Ac	Acetyl
Ar	Aryl
ATR	Attenuated total reflection
BCF	tris(pentafluorophenyl)borane
°C	Degree Celsius
Ch	Chalcogen (Element of group XVI)
Cy	Cyclohexyl
δ	Chemical shift in ppm
DCM	Dichloromethane
DFT	Density functional theory
de	Diastereomeric excess
d.r.	Diastereomeric ratio
ee	Enantiomeric excess
EI	Electron impact ionization
e.r.	Enantiomeric ratio
ESI	Electrospray ionization
equiv.	Equivalent
Et	Ethyl
g	Gram(s)
GC	Gas chromatography
h	Hour(s)
hexane	*n*-hexane
HR	High resolution
Hz	Hertz (s^{-1})
Int	Intermediate
*i*Pr	*iso*-propyl
IR	Infrared
J	Coupling constant
K	Kelvin
L	Liter
M	Molar ($mol \cdot L^{-1}$)
Me	Methyl
Mes	Mesityl (2,4,6-trimethylphenyl)
min	Minute(s)
mol	Mole(s)
MS	Mass spectrometry
m/z	Mass-to-charge ratio
Naph	Naphthyl
*n*Bu	*n*-butyl
NMR	Nuclear magnetic resonance
pentane	*n*-pentane
Ph	Phenyl
ppm	Parts per million
*p*TsOH	*Para*-toluenesulfonic acid
rac	Racemic
r.t./RT	Room temperature
s/sec	Second(s)
R_X/S_X	*R*/*S*-configuration at element X (if there is no X, axial chirality or the element is C)
t	Time
T	Temperature
*t*Bu	*tert*-butyl
TfOH	Triflic acid
THF	Tetrahydrofuran
Tol	4-Methylphenyl
TS	Transition state
XRD	X-ray diffraction

Table of Contents

1. Introduction: A Powerful P−N Connection: Preparative Approaches, Reactivity, and Applications of *P*-Stereogenic Aminophosphines

Preface

A synthetic version of the following chapter has already been published.

Authors

Tanja Huber, Jonathan O. Bauer, *Chem. Eur. J.* **2024**, *30*, e202303760.

Author contribution

This introductory review article was researched and written by T. Huber and revised by PD Dr. J. O. Bauer.

Acknowledgements

This work was jointly supported by the Elite Network of Bavaria (ENB), the Bavarian State Ministry of Science and the Arts (StMWK), and the University of Regensburg (Project N-LW-NW-2016-366).

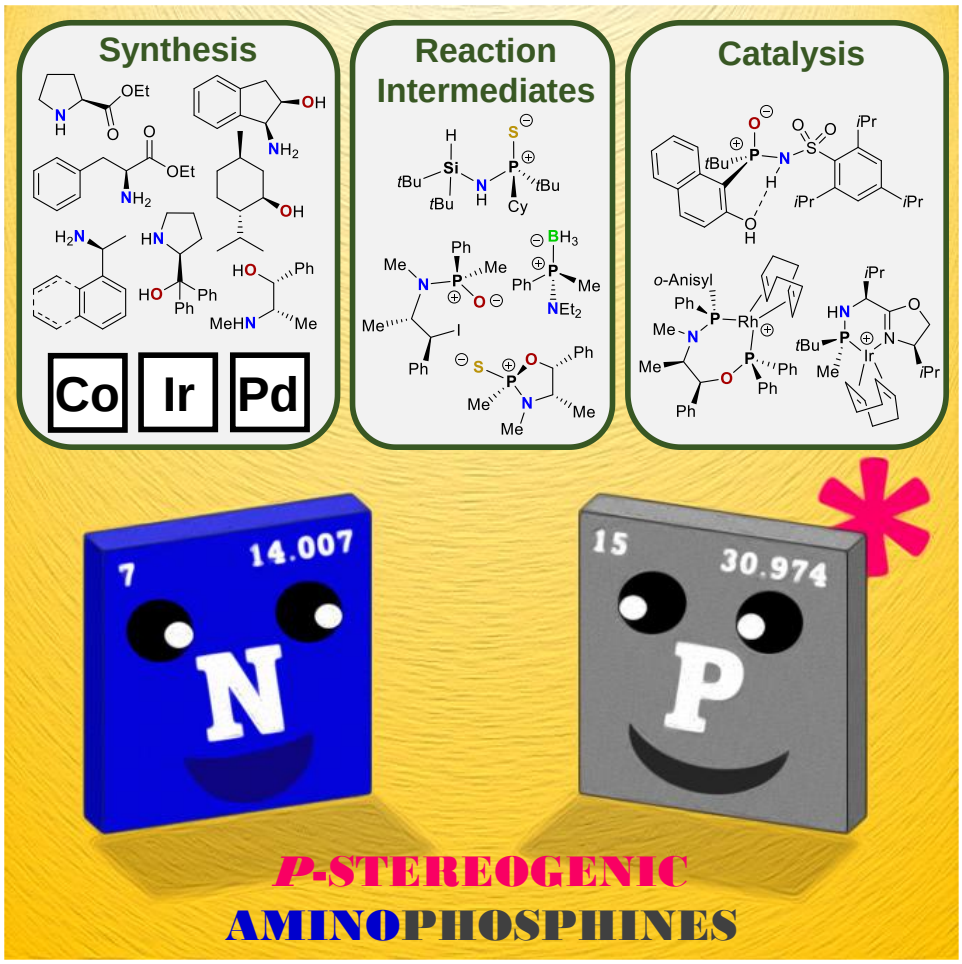

1.1. Abstract

For more than five decades, *P*-stereogenic aminophosphine chalcogenides and boranes have attracted scientific attention and are still in the focus of ongoing research. In the last years, novel transition metal-based synthesis methods have been discovered, in addition to the long-known use of chiral auxiliaries. Enantiomerically pure compounds with N–P^+–X^- (X = O, S, BH_3) motifs served as valuable reactive building blocks to provide new classes of organophosphorus derivatives, thereby preserving the stereochemical information at the phosphorus atom. Over the years, intriguing applications in organocatalysis and transition metal catalysis have been reported for some representatives. Asymmetric reductions of C═C, C═N, and C═O double bonds were feasible with selected *P*-stereogenic aminophosphine oxides in the presence of hydrogen transfer reagents. *P*-stereogenic aminophosphine boranes could be easily deprotected and used as ligands for various transition metals to enable catalytic asymmetric hydrogenations of olefins and imines. This review traces the emergence of a synthetically and catalytically powerful functional compound class with phosphorus-centered chirality in its main lines, starting from classical approaches to modern synthesis methods to current applications.

1.2. Introduction

Organophosphorus compounds, be they phosphines[1] or phosphine chalcogenides[2], have emerged as key derivatives for a variety of reactions in modern synthetic chemistry. Their suitability as intermediates[3] and organocatalysts[1b–e,2b,2c,4] renders them essential and indispensable in today's research. Likewise, they have broad applications as ligands in transition metal catalysis[1a,2a,5] and are used for hydrogenation reactions.[6] In general, P(III) organophosphorus compounds are investigated more frequently. However, a great advantage of P(V) compounds is their stability against air and moisture. Investigations of the latter compounds are therefore rising.[2c,7]

For the further development of catalysis, it is of great interest to introduce specific functional entities into the molecules, which enable them to interact with key intermediates during catalytic processes. This is feasible with heteroatomic moieties like amino groups that are capable of further functionalization[8] or that have exceptional qualities for use as synthesis intermediates and precursors.[9] The N–P^+–Ch^- (Ch = chalcogenide) motif proved to be a beneficial feature for novel ligands,[10] in catalysis,[11] and in medicinal chemistry.[12] In addition, amino- and thiophosphates have recently been proposed as plausible molecules in early Earth scenarios.[13] Especially in the context of ligand design, oxidation of P(III) compounds with selenium has many advantages, as the ^{77}Se NMR spectroscopic parameters such as the $^1J_{P–Se}$ coupling constant provide important information about the electronic nature of the new phosphines.[7c,f,g]

The possibility that both tri- and tetra-substituted phosphorus compounds can exhibit phosphorus-centered chirality is another important feature of these molecules, which is worth taking advantage of. Synthesis methods often involve the use of chiral auxiliaries, leading to diastereomeric mixtures

that need to be separated.[14] A great advantage of P(III) and P(V) compounds with chloro substituents is their ability to be resolved by dynamic kinetic resolution using chiral alcohols and amines, thus leading to the enrichment of one favored stereoisomer.[15] Furthermore, the stereoselectivity of the resolution is strongly dependent on the reaction conditions, such as temperature, solvent, base, and the ratio of starting materials.[16] Highly diastereomerically pure compounds could be obtained by separation techniques like fractional crystallization or chromatography. The desired enantiomers can then be obtained by cleavage of the chiral auxiliary.[14] The first examples were already reported in the late 1960s[17] and various preparation methods for *P*-stereogenic molecules have then been developed in the following decades.[18] While many synthetic routes to all-*C*-substituted *P*-stereogenic compounds are known,[19] heteroatom-substituted analogues have so far received comparatively little attention. Applications can be found as intermediates,[20] in organocatalysis,[21] for enantioselective hydrogenations,[20e,22] and for the design of new ligands.[15a,23]

In this review, we provide a comprehensive overview on the powerful connection between phosphorus and nitrogen under stereochemical aspects. We focus on *P*-stereogenic aminophosphine chalcogenides and boranes and provide a systematic overview of classical and modern synthetic methods and highlight perspectives for applications of these stereochemically valuable functional molecular building blocks in synthesis and asymmetric catalysis. Reports about deprotected aminophosphines for use as ligands in transition metal catalysis are included as well. Aminophosphinic compounds are also discussed in this review, as they have provided impressive utility to the world of asymmetric organocatalysis.

1.3. Auxiliary-Based Approaches Towards *P*-Stereogenic Aminophosphine Chalcogenides and Boranes

The use of monodentate chiral auxiliaries is still a widely used method to introduce a stereogenic phosphorus center. For this purpose, readily available *C*-stereogenic auxiliaries are used. Due to the possibility of diastereomeric separation methods, this approach is often more reliable in terms of stereoselectivity than novel techniques such as the challenging organocatalyzed synthesis of single enantiomers. For example, in 2016, the preparation of *P*-stereogenic oxazaphospholidines catalyzed by tertiary amines only gave moderate enantioselectivities, possibly due to unwanted side reactions.[24] *P*-stereogenic compounds with P–N bonds are often prepared as chalcogenides or boranes and are either used directly as they are or are deprotected prior to use depending on the intended synthetic purpose. Some examples for commonly used chiral auxiliaries are shown in Figure 1.1.

In the late 1970s, the group of Koizumi provided a general route applying L-proline ethyl ester [(*S*C)-**1**] as chiral auxiliary (Scheme 1.1).[25] After coupling the amino acid derivative with phenyldichlorophosphate (**2**), a diastereomeric mixture of **3** was obtained, which could be functionalized stepwise with alcohols. Anhydrous pyridine was used both as solvent and HCl scavenger. In a subsequent reaction, the remaining P–Cl bond was substituted by ethanol or

n-butanol. At this point, the diastereomers (S_C,S_P)-**4** and (S_C,R_P)-**4** were separated by column chromatography before subjecting the individual diastereomers to further functionalization. For cleaving the P–N bond, heating at reflux under strongly acidic conditions in the respective alcohol (methanol, ethanol or *n*-propanol) was required. With this method, the optically active dialkylphenylphosphates (S_P)-**5** and (R_P)-**5** were generated with enantiomeric ratios of 97:3, according to the Eu(hfc)$_3$ shift method.[26] In a follow-up publication the substrate scope was broadened to amino and alkyl groups instead of exclusively alkyloxy moieties, and also to sulfide-functionalized starting compounds.[27]

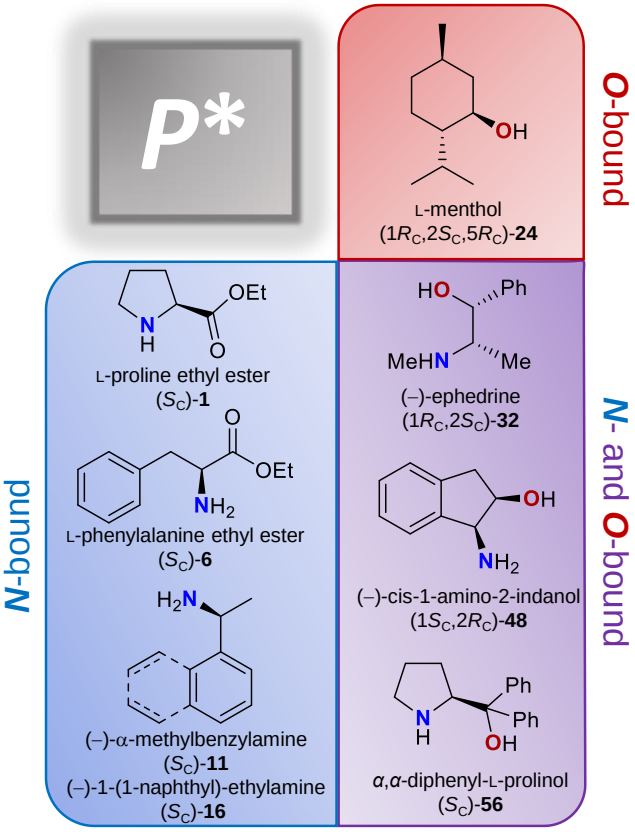

Figure 1.1. Commonly used *O*- and *N*-bound chiral auxiliaries.

A second amino acid derivative-based approach was described by Koizumi et al. using L-phenylalanine ethyl ester [(S_C)-**6**] for synthesizing the alkylphenylphosphoramidates (S_P)-**10** and (R_P)-**10** (Scheme 1.2).[28] Again, phenyldichlorophosphate (**2**) was the starting material of choice and was initially coupled with the amino acid derivative (S_C)-**6** in tetrahydrofuran using triethylamine as HCl scavenger. To introduce the second alkyloxy moiety, the intermediate was then reacted with either methanol or ethanol. Since separation of the resulting 1:1 diastereomeric mixture of **7** has failed at this point, the reaction sequence was continued by *N*-chlorination with *t*BuOCl. The *N*-chlorinated products (S_C,S_P)-**8** and (S_C,R_P)-**8** could then be separated by flash chromatography and further used in their crude state.

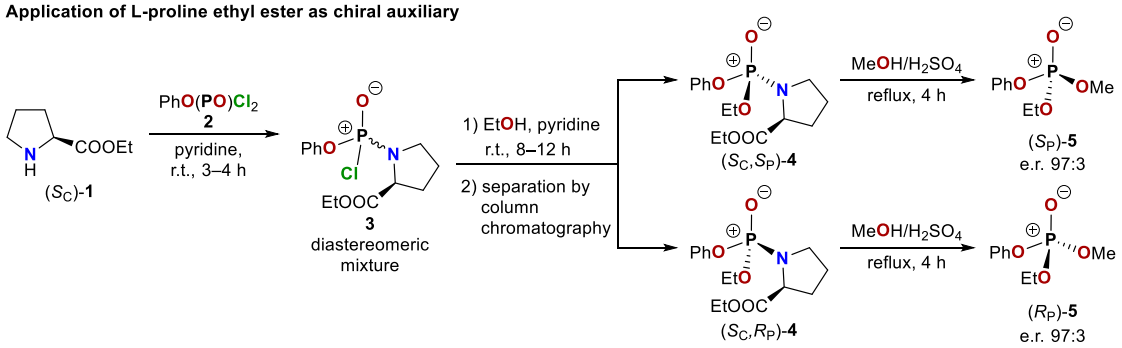

Scheme 1.1. Syntheses of (S_P)-**5** and (R_P)-**5** using L-proline ethyl ester [(S_C)-**1**] as chiral auxiliary and subsequent twofold alcoholysis.[25a]

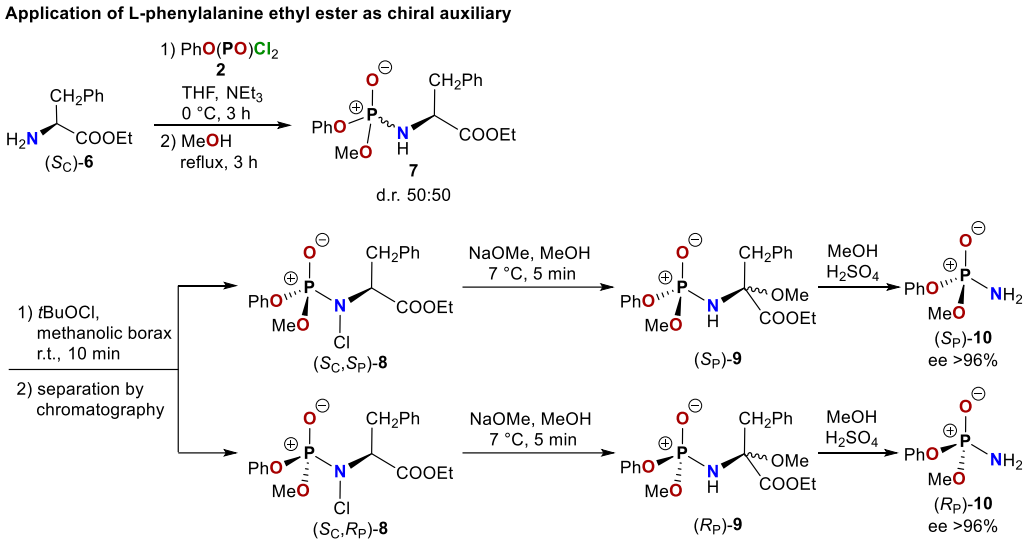

Scheme 1.2. Syntheses of (S_P)-**10** and (R_P)-**10** after using L-phenylalanine ethyl ester [(S_C)-**6**] as chiral auxiliary (THF = tetrahydrofuran).[28]

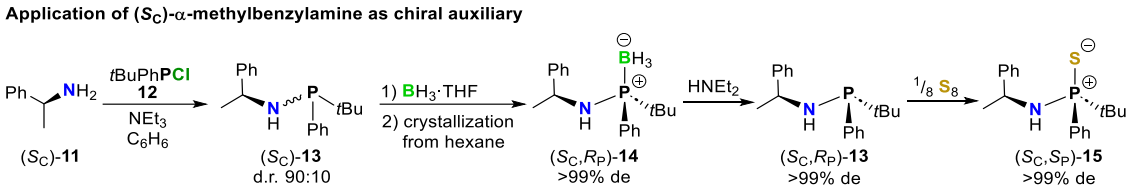

Scheme 1.3. Synthetic pathway towards (S_C,R_P)-**14** and (S_C,S_P)-**15** reported by Kolodiazhnyi.[16,30]

Before the chiral auxiliary could be cleaved to afford the desired phosphoramidate, the pure diastereomers had to be transformed into a species that allowed C–N bond cleavage. For this purpose, the individual diastereomers (S_C,S_P)-**8** and (S_C,R_P)-**8** were subjected to alkaline methanolation by sodium methoxide in dry methanol at 7 °C. The resulting amino acetals (S_P)-**9** and (R_P)-**9** were each formed as epimer mixtures. However, this epimerism was irrelevant, since the concerning part was meant to be cleaved from the actual product in the next step by sulfuric acid in methanol.[28] After purification by silica chromatography, the enantiomeric excesses of products (S_P)-**10** and (R_P)-**10** were determined to be over 96% by the Eu(hfc)$_3$ shift method.[26] Furthermore, the stereochemistry of acid-catalyzed alcoholysis was studied[28] and compared with previous results.[29]

Synthesis and investigation of *P*-chiral N–P$^+$–S$^-$ compounds have been rather neglected compared to the corresponding oxides. In the course of investigations by Kolodiazhnyi and co-workers in 2003,[16,30] diastereomeric *P*-chiral phosphine sulfides with (S_C)-α-methylbenzylamine [(S_C)-**11**] as the chiral auxiliary were reported, but not further considered for follow-up reactions.[16,30] Compound (S_C)-**11** was also used for providing *P*-chiral 4-nitrophenyl alkyl methylphosphonothioates.[31] In Kolodiazhnyi's multiple step preparation (Scheme 1.3), an unsymmetric dialkyl- or alkylaryl-chlorophosphine (**12**) was reacted with the chiral auxiliary (S_C)-**11** to afford (S_C)-**13** (d.r. 90:10), which was subsequently treated with BH$_3$·THF in order to obtain the diastereomerically pure, borane-protected product (S_C,R_P)-**14** after recrystallization from hexane. After removing the borane,

the aminophosphine intermediate (S_C,R_P)-**13** was usable for several further transformations, such as oxidation with hydrogen peroxide or elemental sulfur leading to compound (S_C,S_P)-**15**.[16,30]

In 2010, Riera, Verdaguer, and co-workers presented a way to cleave the C–N bond of the chiral auxiliary in such BH_3-protected *tert*-butylphenylphosphine sulfides (Table 1.1, entries 1 and 2).[32] In a solution of lithium in liquid ammonia, it was possible to attain the desired cleavage. However, due to the strongly reductive conditions, the phenyl substituent at the phosphorus atom underwent a Birch-type reduction when using (S_C)-α-methylbenzylamine [(S_C)-**11**] as chiral auxiliary, leading to compound (S_P)-**19** (Table 1.1, entry 1). This unwanted reduction could be prevented by using (S_C)-1-(1-naphthyl)-ethylamine [(S_C)-**16**] as chiral auxiliary. Thus, the desired product (R_P)-**20** could be obtained (Table 1.1, entry 2).[32] Inspired by those findings, Bauer and co-workers published a thorough investigation on sulfurized analogues in 2022.[33] In the case of aminophosphine sulfides, mixtures with intact and reduced phenyl substituents at the phosphorus atom were observed, no matter if (S_C)-α-methylbenzylamine [(S_C)-**11**] or (S_C)-1-(1-naphthyl)ethylamine [(S_C)-**16**] was used as chiral auxiliary. Furthermore, the molecules were not spared from P–Ph and P–S bond cleavage, which made the phenyl substituent impractical for this kind of reaction. The key to the applicability of the Li/NH_3 mixture was simply to replace the phenyl substituent by an aliphatic cyclohexyl substituent (Table 1.1, entry 3). The resulting cleavage product (R_P)-**21** was the first reported enantiomerically pure *P*-stereogenic primary aminophosphine sulfide. It represents a class of functionalizable precursors, which could be demonstrated by coupling it with a chlorosilane (**22**), affording compound (R_P)-**23** (Scheme 1.4). With that in mind, novel *P*-chiral ligands and organocatalysts might be achievable. Additionally, a new spectroscopic method for determining the enantiomeric purity of aminophosphine sulfides using the lithium salt of (*R*)-BINOL-dithiophosphoric acid as chiral shift reagent was presented and demonstrated that no racemization has occurred during the reductive elimination.[33]

Table 1.1. Reductive C–N bond cleavage of (S_C,R_P)-**14**[32], (S_C,R_P)-**17**,[32] and (S_C,R_P)-**18**[33] under Birch-type reaction conditions.

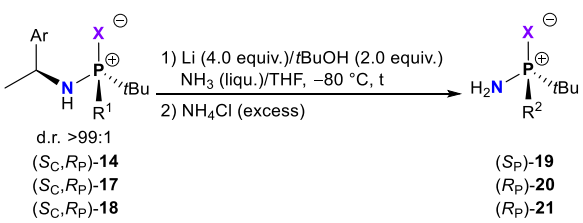

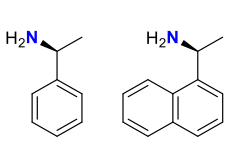

entry	t [min]	Ar	X	R^1	R^2	chiral auxiliary	starting material	product	purity of product	
1	5–10	Ph	BH_3	Ph	1-(cyclo-hexa-2.5-dien)	(S_C)-**11**	(S_C,R_P)-**14**	(S_P)-**19**	not determined	Riera and Verdaguer, **2010**
2	5–10	1-Naph	BH_3	Ph	Ph	(S_C)-**16**	(S_C,R_P)-**17**	(R_P)-**20**	99% ee	Riera and Verdaguer, **2010**
3	2	Ph	S	Cy	Cy	(S_C)-**11**	(S_C,R_P)-**18**	(R_P)-**21**	99% ee	Bauer, **2022**

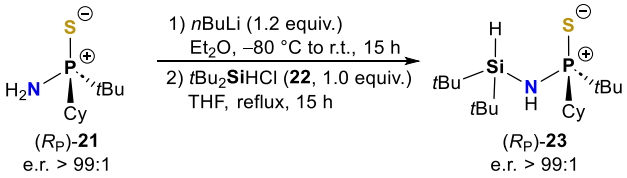

Scheme 1.4. Synthesis of compound (R_P)-**23** by coupling enantiomerically pure (R_P)-**21** with an achiral chlorosilane (**22**).[33]

A long-known[17c,18i,34] *O*-bound auxiliary-based method was applied in 2018 by Stankevič et al.,[35] when diastereomerically pure aminophosphine boranes were synthesized with L-menthol [(1R_C,2S_C,5R_C)-**24**] as chiral auxiliary and used as reactive intermediates to obtain methylphenylphosphinous acid methyl ester borane [(S_P)-**31**] (Scheme 1.5). After coupling of dichlorophenylphosphine (**25**) with L-menthol [(1R_C,2S_C,5R_C)-**24**] in the presence of triethylamine, compound (1R_C,2S_C,5R_C)-**26** was obtained and the remaining chloro substituent was exchanged using diethylamine (**27**), affording compound (1R_C,2S_C,5R_C)-**28**. Protection with borane enabled separation by fractional crystallization of the diastereomeric 1:1 mixture of (1R_C,2S_C,5R_C)-**29** from cyclohexane/Et_2O at –78 °C. One of the diastereomerically pure intermediates [(1R_C,2S_C,5R_C,R_P)-**29**] was then subjected to different electrophilic reagents, such as methyl iodide, after creating Birch-type reaction conditions that caused a P–O bond cleavage. Interestingly, the phenyl moiety was not affected by the strong reductive conditions as it was described by Riera and Verdaguer,[32] and by Bauer et al.[33] It is known, that the outcome of Birch-type reductions of arylphosphoric acid amides is highly dependent on their substituents.[36] The enantiomerically pure product (R_P)-**30** could finally be transformed into a methyl ester (S_P)-**31** by stereospecific exchange of the diethylamino moiety through acidic methanolysis. The absolute configurations of all products were derived from literature precedents.[35]

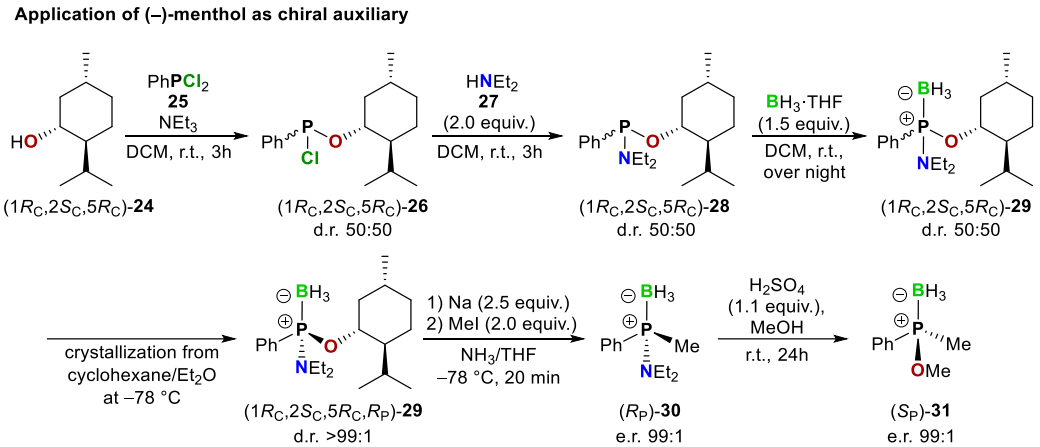

Scheme 1.5. Synthesis towards diastereomerically pure (–)-menthol-substituted aminophosphine borane [(1R_C,2S_C,5R_C,R_P)-**29**], which can be substituted by a methyl and a methoxy entity while maintaining the stereochemical integrity at the phosphorus center (DCM = dichloromethane).[35]

Besides monodentate *N*- and *O*-bound chiral auxiliaries, also bidentate auxiliaries are part of the synthesis repertoire for providing *P*-stereogenic compounds. A prominent example is (–)-ephedrine [(1R_C,2S_C)-**32**], which was introduced by Inch[37] (Scheme 1.6) in the 1970s and further studied by Jugé (Scheme 1.7) around the turn of the millenium.[20a,20b,22b,38] This auxiliary is capable of

chelating a phosphorus center by forming a P–O and P–N bond in the same reaction step. Inch et al. used phosphoryl trichloride (**33**) in benzene and triethylamine as HCl scavenger to obtain a stereochemically pure, five-membered N–P(O)–O heterocycle [(2R_P,4S_C,5R_C)-**34**] after crystallization (Scheme 1.6, top). The remaining P–Cl bond could be subsequently functionalized when subjected to an alcohol in the presence of triethylamine, and compound (2S_P,4S_C,5R_C)-**35** was obtained. The substitution proceeded with retention of configuration.[37a,37c] Chelation of monoalkyl-substituted phosphine sulfide **36** was likewise possible forming the N–P(S)–O heterocycle (2R_P,4S_C,5R_C)-**37**, which could be opened by P–N bond cleavage through acidic alcoholysis with inversion of configuration while forming compound (1R_C,2S_C,S_P)-**38** (Scheme 1.6, bottom). After alkaline treatment with sodium hydroxide, the non-isolated intermediate (R_P)-**39** was reacted with methyl iodide to get to (R_P)-**40**.[37b] The absolute configurations of all products were derived from literature precedents and all syntheses were described to be stereospecific.[37]

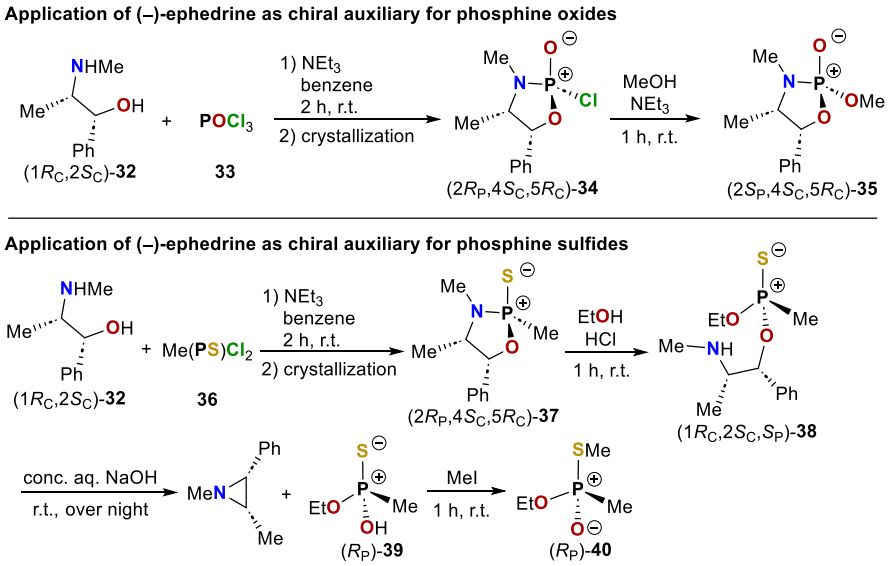

Scheme 1.6. Top: (–)-Ephedrine-based approach to chelate phosphoryl trichloride **33** and functionalization of the remaining P–Cl bond.[37a,37c] Bottom: Synthesis of (R_P)-**40** after ring opening of (2R_P,4S_C,5R_C)-**37**.[37b]

Jugé and co-workers were using P(III) compounds for the reaction with (–)-ephedrine [(1R_C,2S_C)-**32**]. Instead of chloride, their starting materials (such as **41**) had diethylamine as leaving group, which worked well at high temperatures without using any base (Scheme 1.7). The N–P(III)–O ring of (2R_P,4S_C,5R_C)-**42** was opened in a Michaelis-Arbusow rearrangement with retention of configuration at phosphorus through the reaction with alkyl halides such as methyl iodide. Aminophosphine oxide (1R_C,2S_C,R_P)-**43** was thereby formed with high diastereomeric excess featuring a stereogenic P(V) center. Subsequent acidic methanolysis led to cleavage of the P–N bond and afforded compound (R_P)-**44**. The alcoholysis took place with inversion of configuration (Scheme 1.7, top).[38a] After the reaction of (–)-ephedrine [(1R_C,2S_C)-**32**] with bis(diethylamino)-phenylphosphine (**41**), the phosphorus atom of the heterocycle could be protected by borane, obtaining compound (2R_P,4S_C,5R_C)-**45**. Reaction with methyllithium led to cleavage of the P–O bond with retention of configuration at phosphorus [(2R_P,4S_C,5R_C)-**46**]. Acidic methanolysis led to P–N bond cleavage, which allowed (–)-ephedrine [(1R_C,2S_C)-**32**] to be recovered. The

methanolized phosphine borane (S_P)-**31** was obtained with inverted configuration and could be further reacted with aryl lithium compounds, again with inversion of configuration [(R_P)-**47**] (Scheme 1.7, bottom).[20a,20b] Absolute configurations were determined by X-ray crystallography or assumed as previously reported.[20a,20b,38b]

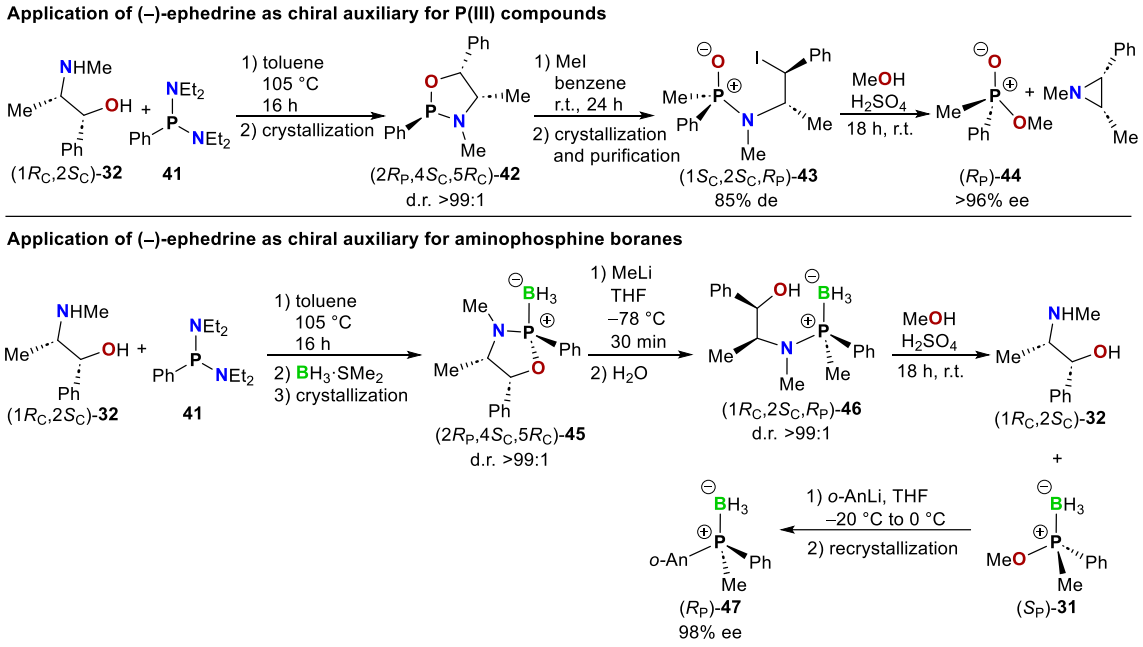

Scheme 1.7. Top: (–)-Ephedrine-based approach to (R_P)-**44** after Michaelis-Arbusow rearrangement and acidic methanolysis.[38a] Bottom: (–)-Ephedrine-based approach to obtain borane-protected phosphine (R_P)-**47** after four steps (*o*An = *ortho*-anisol).[20a,20b,38b]

In 2011, Riera, Verdaguer, and co-workers published a method based on the (–)-ephedrine strategy, but with a variation of the backbone of the chiral auxiliary (Scheme 1.8, top).[20d] Using (–)-*cis*-1-amino-2-indanol [(1S_C,2R_C)-**48**], a highly diastereomerically enriched product (d.r. 18:1) was obtained after reaction with *tert*-butylchlorodiethylaminophosphine (**49**) and borane dimethylsulfide complex. The pure major diastereomer (2R_P,4S_C,5R_C)-**50** could be obtained after recrystallization from hexane and the absolute configuration was determined by the anomalous dispersion method. The chiral auxiliary was removed in two steps. First, ring-opening with organometallic reagents led to cleavage of the P–O bond and gave (1R_C,2S_C,S_P)-**51a** (R = alkyl) or (1R_C,2S_C,R_P)-**51b** (R = aryl), while leaving the P–N bond intact. To the surprise of the authors, this happened in general with inversion of configuration for both alkyl and aryl substituents, no matter if Grignard or other organometallic reagents were used (Scheme 1.8, top).[20d] Previously investigated P–O bond cleavages in monocyclic 1,3,2-oxazaphospholes were reported to proceed with retention of configuration.[20b,38a,39] Excellent diastereomeric ratios were achieved using methylmagnesium bromide. Various other organometallic reagents also gave good ratios, not worse than 90:10, and the corresponding products could be purified by recrystallization from hexane or by column chromatography. In order to finally set the aminophosphine boranes (S_P)-**52a** (R = alkyl) free, the chiral auxiliary was cleaved using lithium in liquid ammonia, whereby the enantiomeric purity was completely maintained (>99% ee). However, as also mentioned in other publications,[32,33] phenyl ring-containing substrates were reduced according to Birch reduction. The authors found a remedy

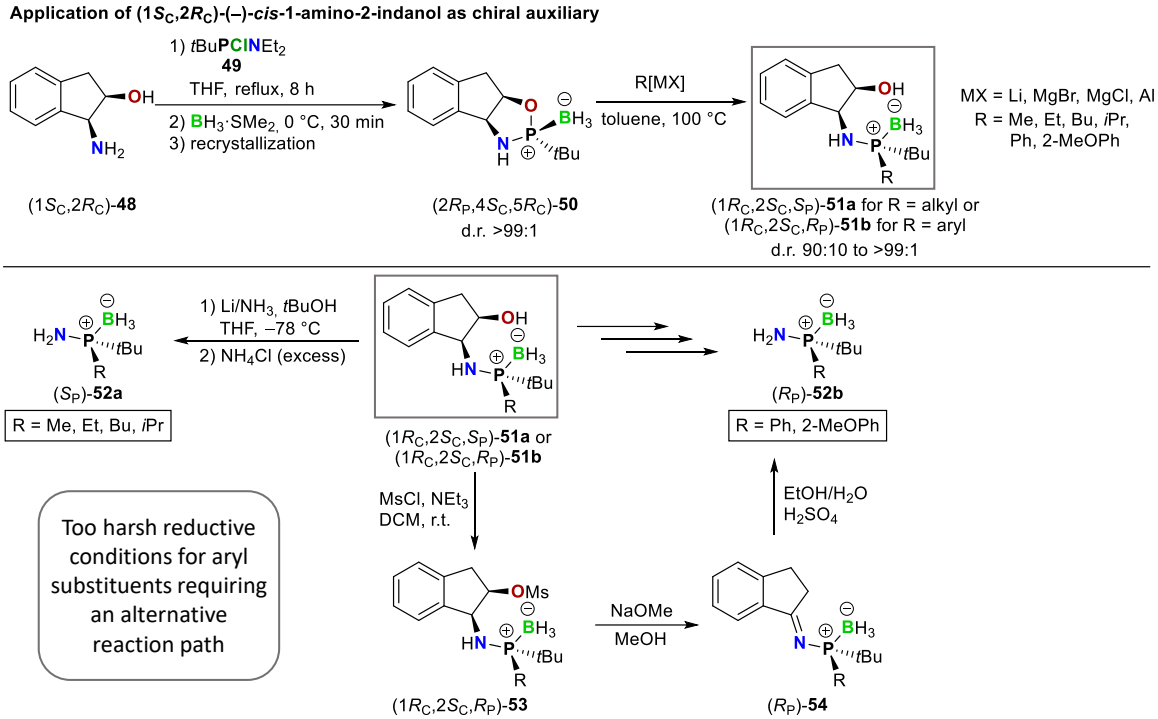

Scheme 1.8. Top: Synthesis of enantiomerically enriched and pure aminophosphine boranes (1R_C,2S_C,S_P)-**51a** (R = alkyl) and (1R_C,2S_C,R_P)-**51b** (R = aryl) using (–)-*cis*-1-amino-2-indanol [(1S_C,2R_C)-**48**] as chiral auxiliary.[20d] Bottom: Differences in cleavage reactions for the substrates (1R_C,2S_C,S_P)-**51a** and (1R_C,2S_C,R_P)-**51b** (Ms = SO_2CH_3).[20d]

for this circumstance by forming an imino-phosphine after mesylation of the hydroxy group [(1R_C,2S_C,R_P)-**53** (R = aryl)] and subsequent alkaline mediated elimination towards (R_P)-**54** (R = aryl). Acidic hydrolysis afforded the corresponding aminophosphine boranes (R_P)-**52b** (R = aryl) with >99% ee (Scheme 1.8, bottom).[20d]

In a follow-up publication two years later,[40] the results of a thorough investigation regarding the stereodivergent P–O ring opening were reported and an explanation of the differing stereochemical pathways of the findings of Riera and Verdaguer[20d] compared to those of Inch[39] and Jugé[20b] was given (Scheme 1.9, top). Three possible reasons were suggested: different substitution at phosphorus (*t*Bu vs. Ph), different substitution at nitrogen (H vs. Me) and different backbones [(–)-*cis*-1-amino-2-indanol vs. (–)-ephedrine].[40]

To find the main factor, Riera and Verdaguer additionally investigated *N*-methylated (–)-*cis*-1-

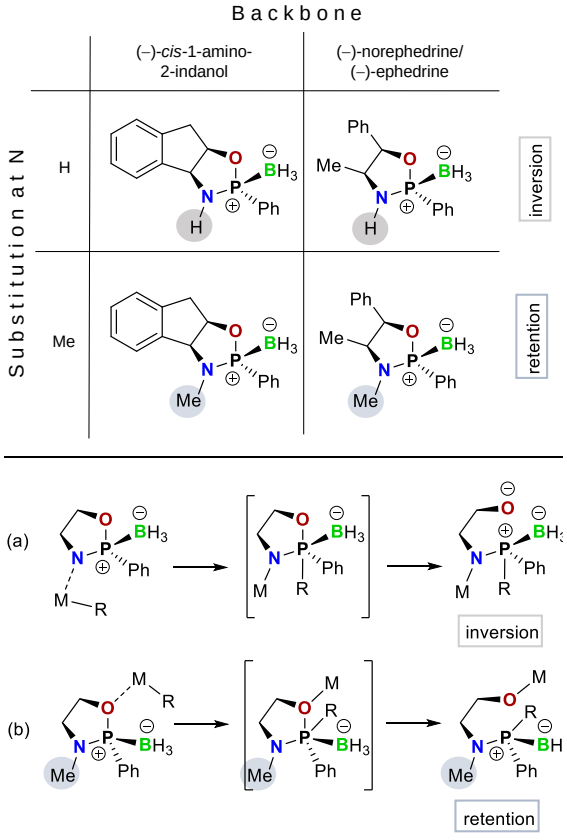

Scheme 1.9. Top: Overview of the different substitution patterns mentioned by Inch[39], Jugé[20b], Riera, and Verdaguer.[20d,40] Bottom: Proposed mechanistic pathways of the reactions with NH or NMe entities.[40]

amino-2-indanol and (−)-norephedrine as chiral backbones. For the reaction of the *N*,*O*-chelated phosphine boranes with organolithium compounds, the presence of an NH moiety provided inversion, while an NMe moiety provided retention at the stereogenic phosphorus atom (Scheme 1.9, top). In case of NH, the cation of the organometallic reagent can deprotonate the nitrogen atom and the attack of R^- takes place from the backside leading to an inversion of configuration (Scheme 1.9, bottom, mechanism a). If the nitrogen atom is blocked by a methyl group, the cation temporarily sticks to oxygen causing R^- to attack from the frontside, which results in retention of configuration (Scheme 1.9, bottom, mechanism b). Proof of this hypothesis was supported by computational investigations of the mechanism. Consequently, the different reactivities of the *N*-methylated and non-*N*-methylated chiral auxiliaries can be exploited to obtain final products with both (R_P)- and (S_P)-configuration.[40]

Another approach with an *N*,*O*-bidentate chiral auxiliary included the application of α,α-diphenyl-L-prolinol [(S_C)-**56**].[41] Using dichlorophenylphosphine oxide **57** in the presence of triethylamine as HCl scavenger and DMAP as organocatalyst, the bicyclic 1,3,2-oxazaphospholidine-2-oxide intermediate (1R_P,3aS_C)-**58** was formed in an excellent diastereomeric ratio of >95:5 (Scheme 1.10). Reaction with MeMgBr resulted in the cleavage of the P–O bond and afforded (S_C,R_P)-**59**. The chiral auxiliary could be removed completely through acidic methanolysis of the P–N bond at −78 °C to form the corresponding methyl ester (R_P)-**44**. The absolute configurations were determined by single-crystal X-ray structure analysis of a follow-up product and the transformations were concluded to be inversion processes.[41b]

Application of α,α-diphenyl-L-prolinol as chiral auxiliary

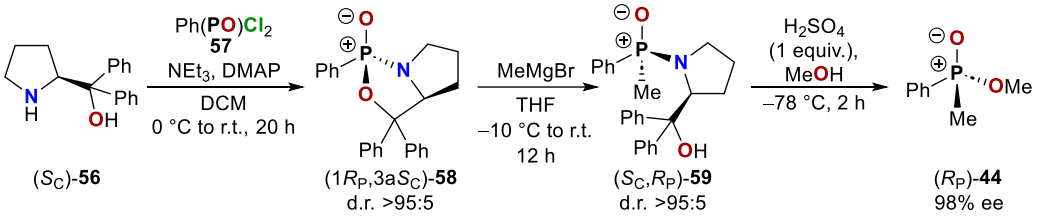

Scheme 1.10. Synthesis of diastereomerically pure α,α-diphenyl-L-prolinol-substituted aminophosphine oxide (1R_P,3aS_C)-**58** and subsequent stereospecific methanolysis (DMAP = 4-(dimethylamino)pyridine).[41b]

1.4. Transition Metal-Catalyzed Approaches Towards *P*-Stereogenic Aminophosphine Chalcogenides and Boranes

Along with the development of novel synthetic methods, the preparation of *P*-stereogenic compounds with P–N functions by means of transition metal catalysis has been increasingly reported. Procedures for non-*P*-chiral or racemic compounds are also known from the literature.[42] Promising results in terms of conversion, stereoselectivity, and catalyst efficiency give reason for further innovative developments in the future.

1.4.1. Synthesis by Copper Catalysis

In 2022, Yin and co-workers presented a general procedure for copper(I)-catalyzed syntheses of *P*-stereogenic aminophosphine chalcogenides and boranes (Table 1.2).[43] The classes of coupling partners were *O*-benzoyl hydroxylamines and diarylphosphines. Several chiral ligands were tested to obtain asymmetric products with the best possible enantiomeric enrichment. The first choice fell on (R_C,R_P)-Ph-FOXAP [(R_C,R_P)-**62**], a diphenylphosphino- and 4-phenyloxazoline-substituted ferrocene derivative (Table 1.2). $Cu(CH_3CN)_4PF_6$ was used as catalyst in the presence of Barton's base. The P–N coupled intermediate was then quenched with hydrogen peroxide. In this context, dibenzylaminoesters (**60**) with electron-deficient aryl groups such as 3,5-$(CF_3)_2$-C_6H_3 were found to increase both yield and stereoselectivity. The same is true for diarylphosphine substrates (**61**) with sterically hindered aryl substituents. The best result for substrates with PO entities [product (S_P)-**63**-O] in terms of enantiomeric excess (90%) was obtained with mesityl-substituted phosphines (**61**-Mes) (Table 1.2, entry 1), as determined by HPLC on a chiral stationary phase. The absolute configuration was determined by single-crystal X-ray structure analysis for one of the synthesized derivatives and deduced for all other obtained products. After finding the best conditions, different reagents (sulfur, selenium, and borane-tetrahydrofuran-complex) were used instead of hydrogen peroxide for quenching the unprotected aminophosphine and afforded products (S_P)-**63**-S, (S_P)-**63**-Se, and (R_P)-**63**-BH_3 with enantiomeric excesses of 90%, 89%, and 92%, respectively (Table 1.2, entries 2–4).

Table 1.2. Comparison of copper(I)-catalyzed syntheses to obtain enantiomerically enriched *N*,*N*-dibenzyl-*P*,*P*-diaryl-aminophosphine borane and chalcogenides yielding similar enantiomeric excesses.[43]

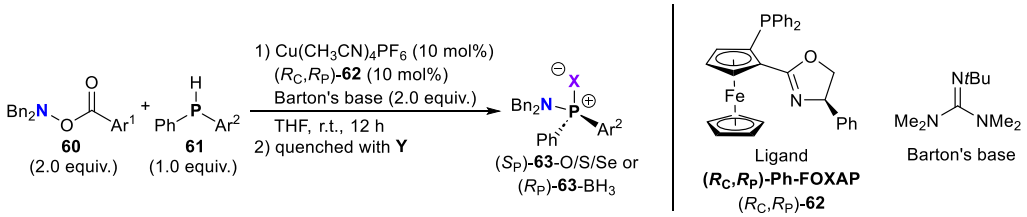

entry	Ar^1	Ar^2	Y	X	product	ee (%)
1	3,5-$(CF_3)_2$-C_6H_3	Mes	H_2O_2	O	(S_P)-**63**-O	90
2	3,5-$(CF_3)_2$-C_6H_3	2,6-Me_2-C_6H_3	S_8	S	(S_P)-**63**-S	90
3	3,5-$(CF_3)_2$-C_6H_3	2,6-Me_2-C_6H_3	Se	Se	(S_P)-**63**-Se	89
4	3,5-$(CF_3)_2$-C_6H_3	2,6-Me_2-C_6H_3	BH_3·THF	BH_3	(R_P)-**63**-BH_3	92

A copper-catalyzed synthesis of diastereomerically enriched *P*-stereogenic compounds containing a P–N bond was reported in 2015 through P–O bond coupling for the purpose of generating the nucleoside-based prodrugs (S_C,S_P)-**66** and (S_C,S_P)-**69** (Scheme 1.11). While purine-based substrates **65** gave the best results with copper(II) triflate (d.r. 1:8.3), the best choice for pyrimidine-

based substrates **68** was copper(I) acetate (d.r. 1:6.3), whereby the absolute configurations were derived from comparable molecules previously reported in a patent. The respective catalytic reactions gave 35–40% conversion with *N*,*N*-diisopropylethylamine (DIPEA) as the base and tetrahydrofuran (THF) or dimethoxyethane (DME) as the solvent.[44] Strategies for several non-metal-catalyzed syntheses of nucleoside-based, *P*-stereogenic drugs, such as remdesivir [(S_C,S_P)-**74**] (Scheme 1.12) that was used during the COVID-19 pandemic,[45] were recently summarized in a review article.[46]

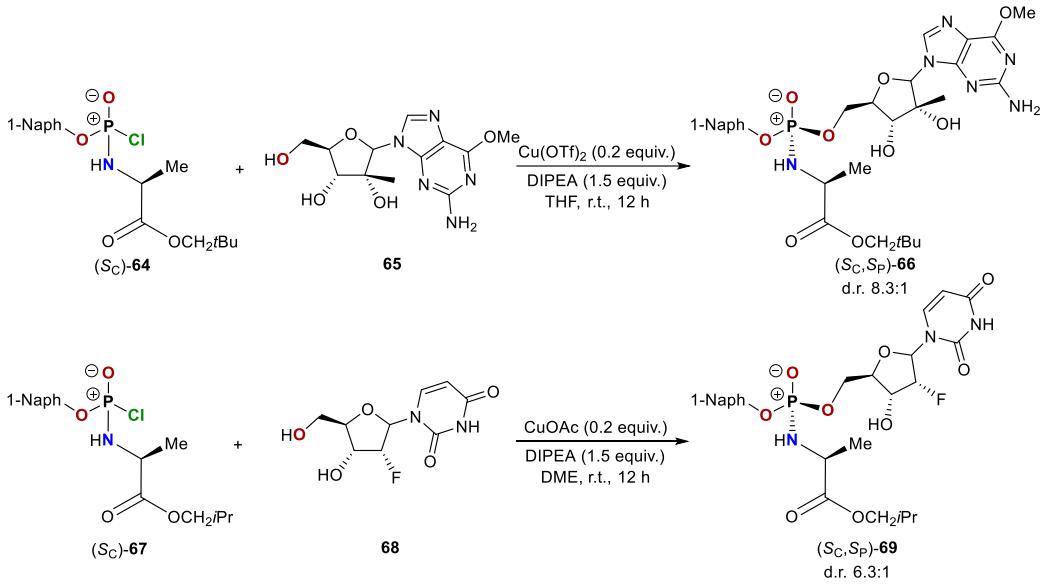

Scheme 1.11. Cu(II)- and Cu(I)-catalyzed syntheses of nucleoside-based prodrugs (S_C,S_P)-**66** and (S_C,S_P)-**69** through P–O bond coupling (DIPEA = *N*,*N*-diisopropylethylamine, DME = dimethoxyethane; stereodescriptors of compounds **65** and **68** have been omitted for clarity).[44]

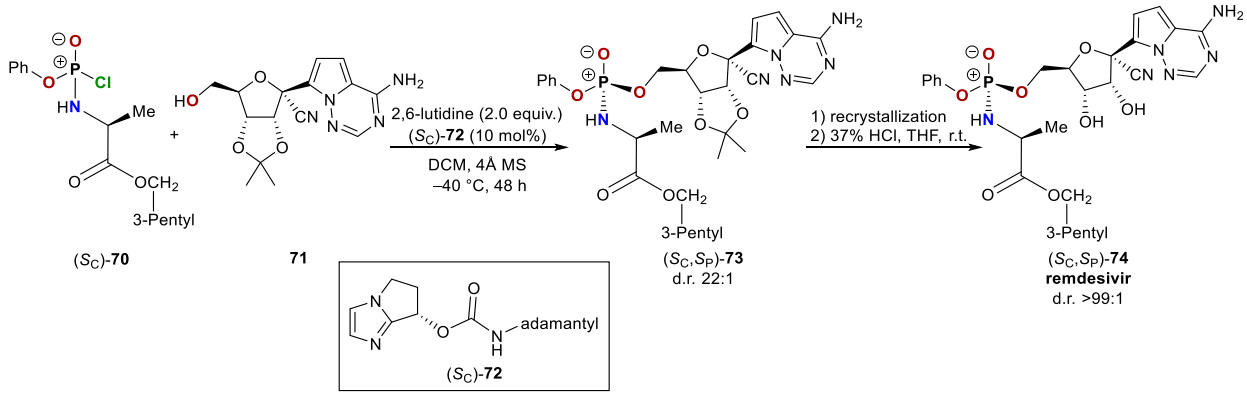

Scheme 1.12. Organocatalyzed synthesis of anti-COVID-19-drug remdesivir [(S_C,S_P)-**74**] through P–O bond coupling (2,6-lutidine = 2,6-dimethylpyridine; stereodescriptors of compound **71** have been omitted for clarity).[45]

Simple copper(I) and copper(II) salts have also been used for dehydrocoupling of P(O)–H bonds with primary amines. Both achiral and enantiomerically pure *P*-stereogenic H-phosphinates were applied and the coupling products showed overall good yields with 2 mol% copper(II) bromide as the catalyst in ethyl acetate. The optically pure starting materials incidentally maintained their stereochemical integrity in the product, albeit with inversion of configuration after the cross-coupling.[47]

1.4.2. Synthesis by Iridium Catalysis

Using $[Ir(cod)Cl]_2$ as the catalyst, an (*R*)-BINOL-based chiral ligand [(R_{ax},R_C)-**77**], and KHMDS as the base, access to *P*-chiral *N*-vinylphosphonamides such as (R_P)-**79** was opened (Scheme 1.13, top). The products were generated in excellent enantiomeric ratios up to 99:1 by asymmetric allylic substitution-isomerization, in which a non-chiral diaminophosphine oxide (**75**) reacted with an allylic compound such as diethyl cinnamylphosphonate (**76**). In the initial kinetically controlled reaction step, both a *C*- and a *P*-stereogenic center were each introduced by the coupling process, accompanied by a shift of the allylic double bond to the terminal position, affording compound (R_P)-**78**. However, due to thermodynamic control, the double bond is shifted back towards the C–N bond and the final product (R_P)-**79** is obtained. The absolute stereochemistry at phosphorus of the final product was determined by X-ray crystallography and deduced for all other obtained derivatives. One of the novel *N*-vinylphosphonamides was investigated for its applicability as chiral catalyst. Both iodocyclization of a phenol derivative and a reductive aldol reaction were investigated in this context. Although they only showed enantiomeric ratios of not more than 60.5:39.5, they provide a valuable basis for further investigations regarding catalytic applications.[48]

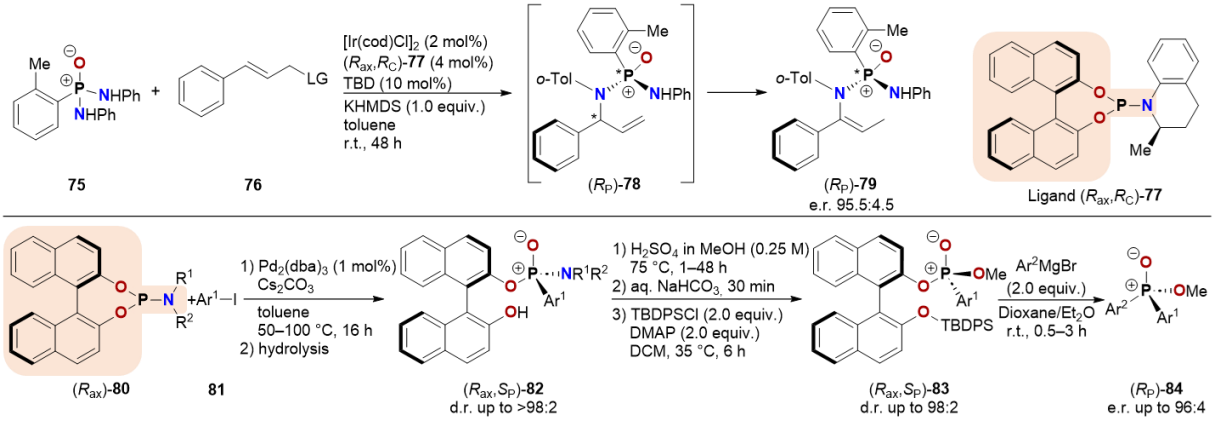

Scheme 1.13. Top: Iridium(I)-catalyzed synthesis of enantiomerically enriched (R_P)-**79** using the (*R*)-BINOL-based ligand (R_{ax},R_C)-**77** (LG = leaving group = OP(O)(OEt)$_2$, cod = 1,5-cyclooctadiene, TBD = 1,5,7-triazabicyclo[4.4.0]dec-5-ene, KHMDS = potassium hexamethyldisilazane).[48] Bottom: Palladium(0)-catalyzed synthesis of enantiomerically enriched, (*R*)-BINOL-substituted aminophosphine oxide (R_{ax},S_P)-**82** using derivatives of (R_{ax},R_C)-**77** as starting compounds and subsequent reaction with acidic methanol and Grignard reagents (dba = dibenzylideneacetone, TBDPS = *tert*-butyldiphenylsilyl, DMAP = 4-dimethylaminopyridine).[49]

1.4.3. Synthesis by Palladium Catalysis

The scaffold of the (*R*)-BINOL-based chiral ligand used for the Ir(I)-catalyzed asymmetric allylic substitution-isomerization (see Scheme 1.13, top)[48] was also used as substrate in recent studies towards enantiomerically pure aminophosphine oxides like (R_{ax},S_P)-**82** (Scheme 1.13, bottom).[49] Using $Pd_2(dba)_3$ as catalyst and Cs_2CO_3 as base, the (*R*)-BINOL-based precursor (R_{ax})-**80** was converted with aryl iodides (**81**) in toluene at 50–100 °C for 16 h and subsequently hydrolyzed to obtain aminophosphine oxides [(R_{ax},S_P)-**82**] with diastereomeric ratios up to >98:2 and good yields (Scheme 1.13, bottom). Formally, this is an auxiliary-based approach using a palladium catalyst

(see also chapter 1.3). The absolute configuration was determined by single-crystal X-ray structure analysis for one of the synthesized derivatives and deduced for all other obtained compounds. The products can be further substituted by alkoxides and Grignard reagents (Scheme 1.13, bottom), each with inversion of configuration, which was again confirmed by single-crystal X-ray diffraction analysis for one representative product. Furthermore, equipping the free hydroxy group of the (*R*)-BINOL fragment with a silane protection group after methanolysis [product (R_{ax},S_P)-**83**] led to better enantiomeric ratios (up to 96:4) for product (R_P)-**84** in the Grignard reaction. Mechanistic studies revealed an oxidative addition of both precursors to the Pd(0) center and a reductive elimination upon C–P bond formation.[49] The same (*R*)-BINOL-based P(III) scaffolds also react with alkenyl halides when catalyzed by Ni(0) catalysts. Diastereomeric ratios of up to >20:1 could be obtained with 10 mol% Ni(cod)(dq) [bis(1,5-cyclooctadiene)(duroquinone) nickel(0)] in 1,2-dichloroethane at 80 °C after 12–24 h.[50]

Palladium(II)-catalyzed approach towards *P*-chiral, enantiomerically enriched phosphinic hydrazones (R_P)-**88**-S and (R_P)-**88**-O was provided in 2020 by Pullarkat, Leung, and co-workers (Scheme 1.14, top). The P–N–N compounds constitute a class of considerable intermediates for the synthesis of diarylphosphinates such as (S_P)-**89**, which can be obtained after acidic methanolysis of the phosphinic hydrazones with inversion of configuration. The modification of the Pd(II) catalysts as well as the substrates, α-diazoesters, and secondary racemic phosphines offered enantiomeric excesses up to 55% for sulfur-protected and up to 81% for oxygen-protected phosphinic hydrazones. The best results could be obtained with **85** and **86** as starting materials and (R_C)-**87** as Pd(II) catalyst. The use of diazabicycloundecene (DBU) as the base in a mixture of chloroform and acetone at −80 °C turned out to be helpful for the stereochemical outcome. The proposed mechanism (Scheme 1.14, bottom) starts with the coordination of two secondary diarylphosphines to the Pd(II) center (**Int1**) followed by coordination of the α-carbon atom of the α-diazoester (**Int2**). Deprotonation of the phosphine (**Int3**) leads to a nucleophilic attack at the azo group forming a rigid, five-membered Pd(II) intermediate (**Int4**). Eventually, the ring is reopened (**Int5**), before the non-oxidized product is eliminated and the catalyst reoccupied.[51]

Quite an intriguing way to obtain enantiomerically enriched aminophosphine oxides [(S_P)-**93**] using Pd(II) catalysis was reported in 2015 (Scheme 1.15, top). Starting from racemic, diarylsubstituted aminophosphine oxide (**90**), a desymmetrizing *ortho*-C–H-arylation was carried out by the reaction with boronic ester **91** in the presence of *N*-Boc-protected amino acid (R_C)-**92** as chiral ligand (Scheme 1.15, top). The best results were obtained by using 10 mol% $Pd(OAc)_2$ in combination with Ag_2CO_3 as oxidant and benzoquinone as additive in dimethylformamide. Enantiomeric excesses up to 98% were achieved as determined by chiral HPLC analysis and the absolute configuration at phosphorus was assigned by single-crystal X-ray diffraction analysis.[52] In a follow-up work, the obtained products were reported to undergo *ortho*-C–N bond coupling through radical oxidation, thus yielding cyclic phosphine amides. Moreover, it could be shown in this work that the oxides could be transferred into sulfides using Lawesson's reagent.[53] In a very recently published article, the selective attachment of alkynyl bromide **95** on the *ortho*-position of a phenyl ring in **94** with the lactam L-pyroglutamic acid [(S_C)-**96**] as chiral ligand was reported (Scheme 1.15, middle).

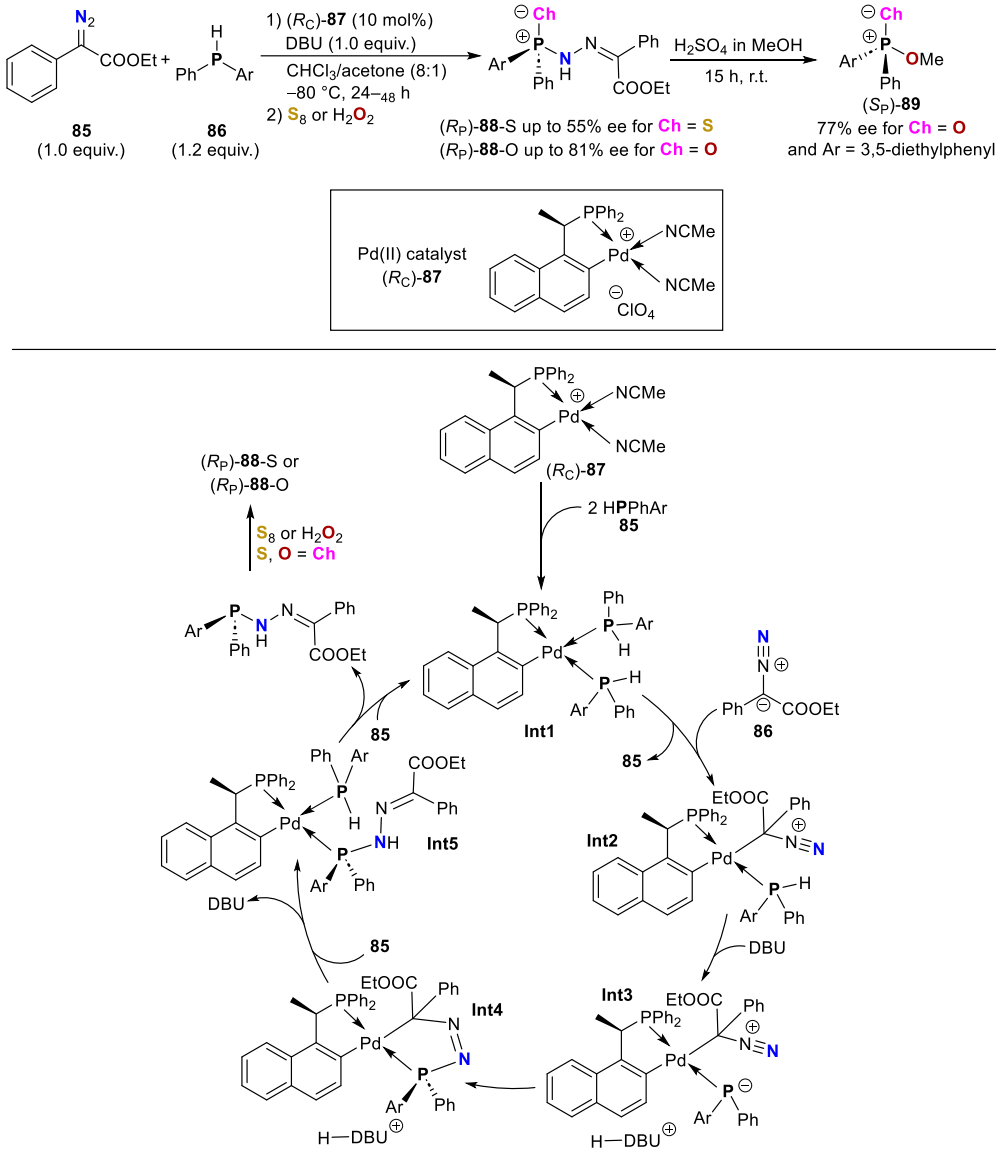

Scheme 1.14. Top: Palladium(II)-catalyzed synthesis of enantiomerically enriched phosphinic hydrazones (R_P)-**88**-S and (R_P)-**88**-O and conversion into diarylphosphinates (S_P)-**89** by acidic methanolysis (DBU = diazabicycloundecene).[51] Bottom: Proposed mechanism for the reaction of α-diazoester **85** with secondary racemic phosphine **86**.[51]

The absolute configuration at phosphorus of product (R_P)-**97** was determined by X-ray crystallography.[54] Related with the aforementioned work,[52–54] further catalytic approaches to enantiomerically pure *P*-stereogenic compounds were investigated and recently reviewed.[55]

A non-metal-based, substrate-controlled desymmetrizing aryl coupling method (Scheme 1.15, bottom) furnished similar stereoselectivity compared to the previously described Pd(II) catalyzed syntheses.[56] Starting from a *C*-stereogenic, (S_C)-α-methylbenzylamine-substituted amino-phosphine oxide [(S_C)-**98**], the electrophilic *ortho*-substitution of one of the phenyl groups was achieved by stereoselective deprotonation of one of the diastereotopic phenyl rings with *t*BuLi followed by the reaction with an electrophile (Scheme 1.15, bottom). Diastereomeric ratios of up to 98:2 were obtained.[56] The absolute configuration at phosphorus of products (S_C,S_P)-**99** could be revealed by X-ray structure determination of a representative derivative.[56c] The newly introduced functional unit at the *ortho*-position could then be replaced by alkyl or aryl moieties[56b] or by the 4-

amino-TEMPO (4-amino-2,2,6,6-tetramethylpiperidinyloxyl) radical.[56d] Analogous asymmetric *ortho*-substitutions were reported for aminophosphazenes, which contain a P^+–N^-–COOMe instead of a P^+–O^- unit. They could be converted to the corresponding aminophosphine oxides or sulfides when subjected to phenyliso(thio)cyanate (Ph–NCO or Ph–NCS).[56a,56b]

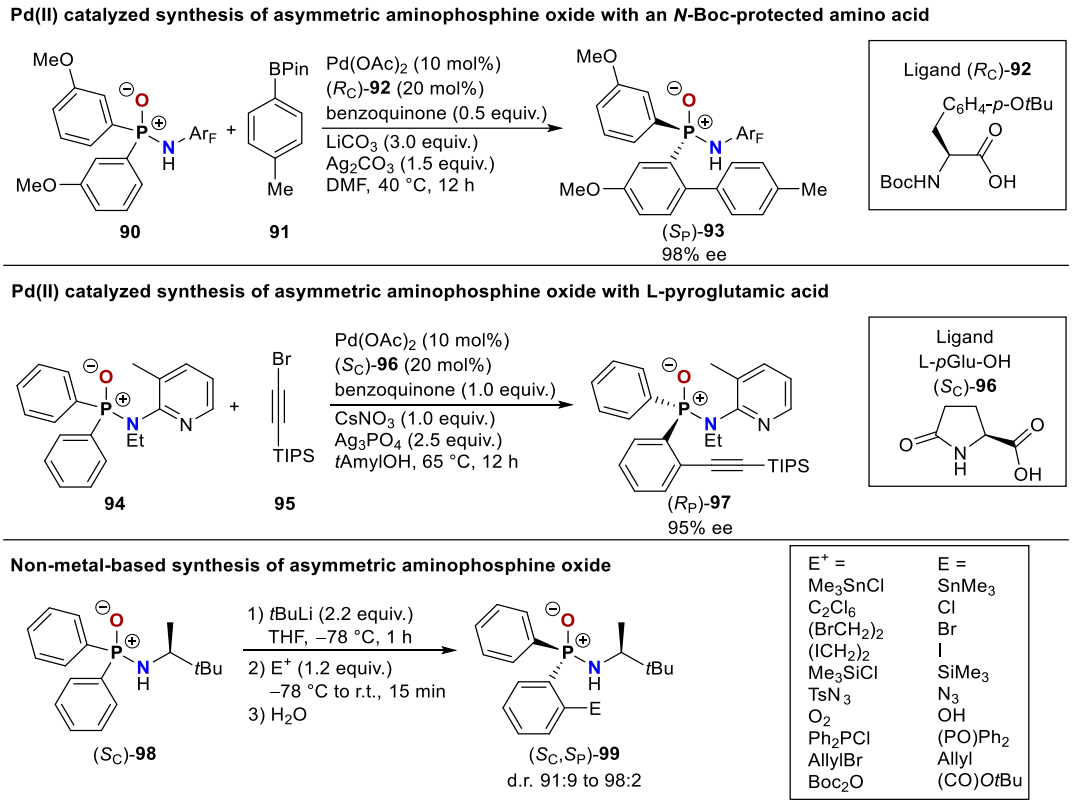

Scheme 1.15. Top: Palladium(II)-catalyzed synthesis of (S_P)-**93** starting from a *P*,*P*-diarylaminophosphine oxide (**90**) by selective *ortho*-arylation of one of the *P*-aryl substituents (Ar_F = 2,3,5,6-tetrafluorobenzonitrile, Bpin = pinacolborane, DMF = dimethylformamide).[52] Middle: Another palladium(II)-catalyzed approach with different chiral ligand (TIPS = triisopropylsilane, *t*AmylOH = 2-methyl-2-butanol).[54] Bottom: Non-metal-based approach.[56]

1.5. Applications of *P*-Stereogenic Aminophosphine Chalcogenides and Boranes

1.5.1. Applications of Aminophosphine Oxides as a Novel Class of Organocatalysts

Many researchers have used the work of Inch[26,37,39] and Jugé[20a,20b,22b,38a] on enantiomerically pure N–P^+–O^- compounds as a starting point for their investigation of functionalized phosphorus-stereogenic compounds.

In 2015, Han et al. found an efficient way to synthesize primary aminophosphine oxides [(S_P)-**103**] with a wide range of substitution patterns (Scheme 1.16, top).[57] They made use of 1,3,2-

benzoxazaphosphinine-2-oxide [(R_C)-**100**] as chiral intermediate for providing the phosphorus-stereogenic products (S_P)-**103** with enantiomeric purities of up to 99% after treatment with an organometallic reagent and lithium amide. Only two years later, they reported the design of efficient asymmetric Lewis base organocatalysts [(S_P)-**105**] by functionalizing the amino group with an *ortho*-phosphine oxide-substituted benzyl moiety. Excellent asymmetric induction of the *P*-stereogenic compound was proven for the reduction of chalcone derivatives **104**, forming products (R_C)-**106** with enantiomeric ratios up to 97.5:2.5 (Scheme 1.16, bottom).[57b] In 2019, the *P*-stereogenic aminophosphine oxides (S_P)-**103** served as precursors for Brønsted acid organocatalysts such as (R_P)-**108**. Catalytically active species of this type have been shown to be effective for certain enantioselective transformations. Through the coupling of the nitrogen atom of the *P*-stereogenic aminophosphine oxides with electron withdrawing groups such as SO_2Ar or $P(O)R_2$, the acidity of the resulting NH function could be increased, which was crucial for the reliability of this type of Brønsted acid catalysts. The substituents at the stereogenic phosphorus center can also affect the NH acidity. Reactivity as well as stereoselectivity of the catalyzed reaction can thereby be modified. The new set of *P*-stereogenic aminophosphine oxides catalyzed hydrogenations using quinoline derivatives such as **107** as substrates and Hantzsch ester as reducing agent (Scheme 1.17, left).[58] Analogous reactions were performed in the past with atropoisomeric (*R*)-BINOL-phosphoric acid derivatives.[59] Full conversion could be achieved with some achiral test catalysts after 24 h. The *P*-stereogenic catalysts also gave full conversion after 24–48 h and yielded enantiomerically enriched products with enantiomeric ratios ranging from 53:47 to 84:16, strongly depending on the substituents of the catalyst, but also on the substituents of the quinoline-based substrate. Highest selectivity was observed with the sterically demanding catalyst (R_P)-**108** and with 2-aryl substituted quinoline derivative **107**, which gave (S_C)-**109** as product.[58]

In the same year, Tsantrizos and co-workers reported similar molecular patterns for Brønsted acid organocatalysis, however, with some innovations (Scheme 1.17, right).[60] (R_P)-**111**, also known as OttoPhosa I, is the prototype of a *P*-stereogenic aminophosphine derivative with an electron withdrawing arylsulfonate moiety attached to the nitrogen atom and a phenolic moiety attached to the phosphorus atom. The hydroxy group of the phenolic moiety is capable of hydrogen bond formation to the NH group. This increases the acidity of the NH moiety on the one hand and stabilizes the transition state structure on the other hand, leading to an increased reaction rate and better enantioselectivities. Using a 2-methyl-substituted quinoline, enantiomeric excesses of 80–89% could be reached with OttoPhosa I [(R_P)-**111**], depending on reaction time and solvent. The best result was achieved for the conversation of **110** into product (S_C)-**112** using cyclohexane as solvent at 22 °C.[60] In a follow-up publication the scope of catalysts and substrates was expanded and it was shown that such catalysts are limited in application at temperatures higher than room temperature, as they tend to racemize upon heating.[61] Nevertheless, this class of organocatalysts provided short reaction times and good enantioselectivities, which could possibly be further enhanced upon crystallization.

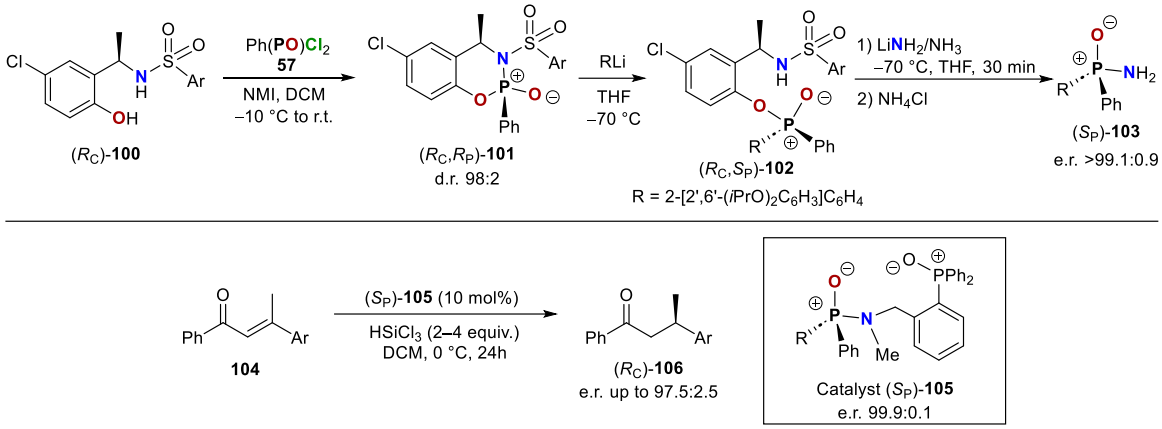

Scheme 1.16. Top: Highly enantioselective method for the synthesis of various *P*-stereogenic aminophosphine oxides [(S_P)-**103**] (NMI = *N*-methylimidazole).[57] Bottom: Asymmetric reduction of chalcone **104** catalyzed by the functionalized aminophosphine oxide (S_P)-**105**.[57b]

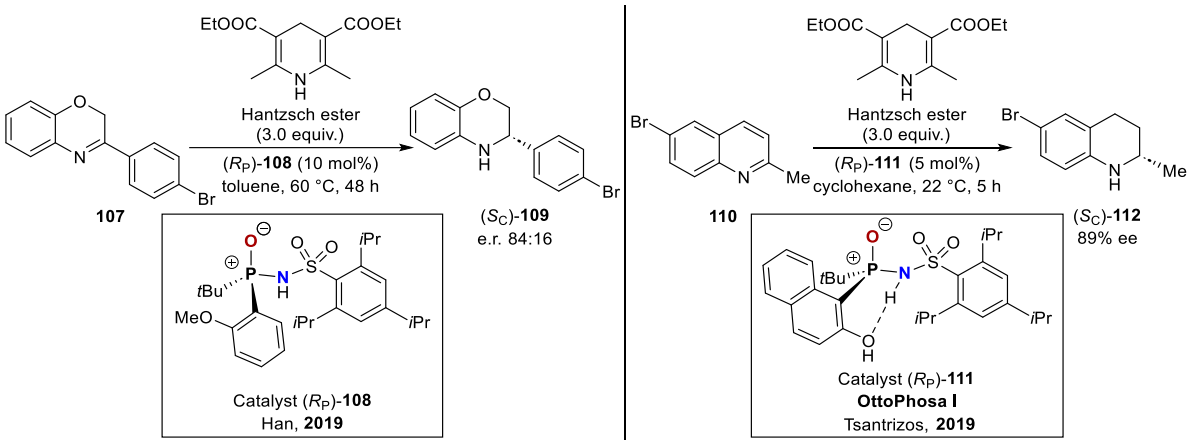

Scheme 1.17. Left: Hydrogen transfer reaction of quinoline derivative **107** using aminophosphine oxide catalyst (R_P)-**108** without intramolecular hydrogen bond stabilization.[58] Right: Hydrogen transfer reaction of quinoline derivative **110** with hydrogen bond-stabilized OttoPhosa I [(R_P)-**111**].[60]

The previously described products of the palladium(II)-catalyzed synthesis of *ortho*-substituted, enantiomerically enriched *P*,*P*-diarylaminophosphine oxides [(S_P)-**93**, Scheme 1.15, top][52] were used as novel organocatalysts in the reductive desymmetrization of cyclic 2,2-disubstituted 1,3-diketones (Scheme 1.18). Five- and six-membered substrates of type **113** could be converted into products of type (S_C,S_C)-**115** with high to excellent enantio- and diastereoselectivities, although the reductions of six-membered derivatives turned out to be challenging in the past. After extensive investigations, the most suitable reaction conditions were found with dichloromethane as solvent, catecholborane as reducing agent, and di-*iso*-propylphenylamine as additive. The reaction was quenched with methanol and subjected to aqueous work-up.[62] The wide substrate scope, easy upscaling, and high selectivity made these findings also applicable in the synthesis of natural products.[63]

The proposed mechanism for the reduction (Scheme 1.19) starts with a coordination of Lewis-acidic catecholborane by the P^+–O^- unit of the catalyst (**Int5**). Following, the addition of di-*iso*-propyl-phenylamine causes the release of one molecule dihydrogen. The resulting intermediate can either be described as a P^+–O–B^- zwitterionic structure (**Int6a**) or as a coordination complex (**Int6b**)

forming an additional O···B interaction with the 1,3-diketone **113**. Due to the different substituents at the 2-position, there is a favored (**Int7a**) and a disfavored (**Int7b**) case. In the favored case, the less bulky substituent (R^S) is pointing towards the activated catalyst. A second catecholborane molecule is then coordinated by the P^+–O^- unit (**Int8**) and capable of reacting with **113** affording the corresponding hydroborane (**Int9**), which finally turns into the alcohol (S_C,S_C)-**115** after aqueous work-up.[62]

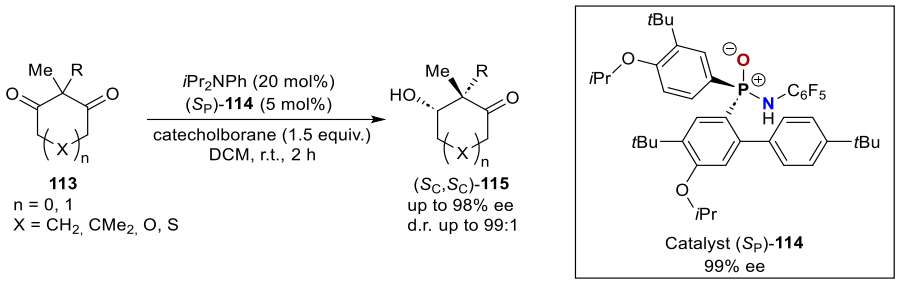

Scheme 1.18. Enantioselective reduction of **113** catalyzed by (S_P)-**114**.[62]

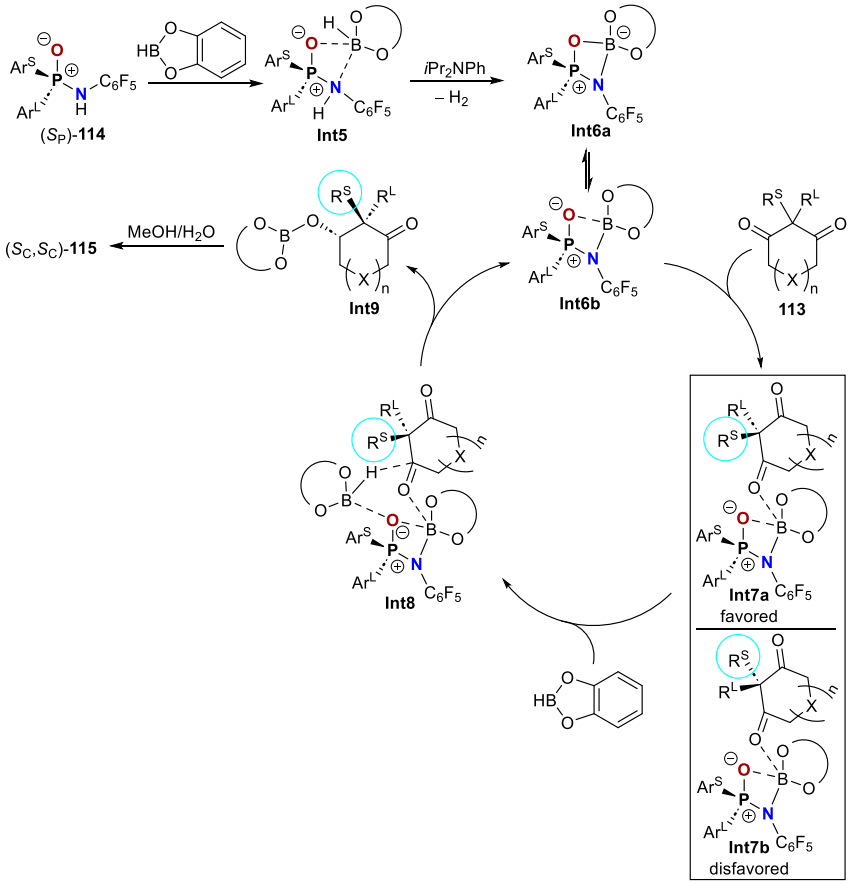

Scheme 1.19. Proposed reaction mechanism of the enantioselective reduction of **113** catalyzed by (S_P)-**114** [R^S/Ar^S = small (aryl-)rest; R^L/Ar^L = large (aryl-)rest].[62]

1.5.2. Transition Metal-Catalyzed Transformations Using *P*-Stereogenic Aminophosphine Ligands

The P(V)–N compounds (S_P)-**105**, (R_P)-**108**, (R_P)-**111**, and (S_P)-**114** containing a stereogenic phosphorus(V) center were shown to have useful properties for many synthetic applications. However, they do not represent the heteroatom-substituted phosphorus species most commonly used in catalysis. As mentioned in several publications,[16,22b,23d,32,64] BH_3 is suitable for protecting phosphorus(III) compounds without changing the oxidation state and a lot of effort has been made in the last twenty years to equip such compounds with *P*-centered chirality.

For their use as ligands in transition metal catalysis, they are deprotected again before coordinating the metal center. Since a comprehensive overview on this topic was published some time ago,[20e] we will only focus on the most groundbreaking achievements in this chapter.

1.5.2.1. Asymmetric Catalysis with Rhodium(I) Complexes

Jugé and co-workers reported that an ephedrine-based pathway led to chiral diphosphines such as (1S_C,2R_C,R_P)-**118**, which represent suitable ligands for rhodium(I) complexes used for homogeneous catalytic hydrogenations of compounds **116** to obtain products (S_C)-**117** (Scheme 1.20, a). Interestingly, the *P*-stereogenic center within the chiral molecule having multiple chirality centers was much more pivotal than the ephedrine backbone for the enantioselectivity of the catalyzed reactions. Up to 99% ee was achieved, strongly depending on the bulkiness of the aminophosphine substituents that determine the conformation of the rhodium chelate complex.[22b,38d]

Work on less traditional analogues of ephedrine-based *P*-stereogenic ligands was carried out by Kamer and de Vries[23f] using solid-phase synthesis (Scheme 1.20, b). The resin-bound molecules (1R_C,2S_C,R_P)-**119** were equally tested in rhodium(I)-catalyzed asymmetric hydrogenations showing an enantiomeric excess up to 89%.

Major contributions to the development of enantiomerically pure P–BH_3-based compounds and their applications were made by Riera, Verdaguer, and co-workers (Scheme 1.20, c). First synthesis approaches in 2010 included the easily available chiral auxiliaries (−)-α-methylbenzylamine [(S_C)-**11**] and (−)-1-(1-naphthyl)- ethylamine [(S_C)-**16**].[32] This in turn was important preparatory work for the studies on aminophosphine sulfides.[33] The primary and secondary aminophosphine boranes could be functionalized at the nitrogen atom without loss of the stereochemical information at the asymmetrically substituted phosphorus-center. Carbon- as well as phosphorus-based substituents were connected to the nitrogen atom. The latter functionalization provided aminodiphosphine (PNP) ligands such as (S_P)-**120** (also known as MaxPHOS ligand) after deprotection, which were used for rhodium(I)-catalyzed highly enantioselective hydrogenations of olefins.[32]

Another example of rhodium(I)-PNP-catalyzed olefin hydrogenations with excellent enantiomeric ratios of up to 99% ee was reported by Kamer and de Vries using ligand (R_C,R_C,S_P,R_P)-**121** with a Betti base backbone (Scheme 1.20, d).[65]

Furthermore, phosphorus-stereogenic PNP ligands based on an axially chiral BINOL backbone such as (R_{ax},S_P)-**122** were also described by Kamer (Scheme 1.20, e) and gave up to 96% ee in asymmetric hydrogenations of olefins **116**. The ligand preparation (Scheme 1.21) started with a well-known method by coupling (R_C)-**11** and phosphine **12** to give an oily product [(R_C,S_P)-**123**] with a diastereomeric ratio of 83:17. In order to achieve optical purity, the authors did not use the common route via oxidation or borane-protection of the phosphorus atom, but formed a lithium amide complex with TMEDA, which could be fractionally crystallized to obtain (R_C,S_P)-**124**. The coupling with the BINOL fragment was achieved using either (S_{ax})- or (R_{ax})-BINOL-phosphorochloridite (**125**) to obtain the PNP ligand (R_{ax},S_P)-**122**.[66]

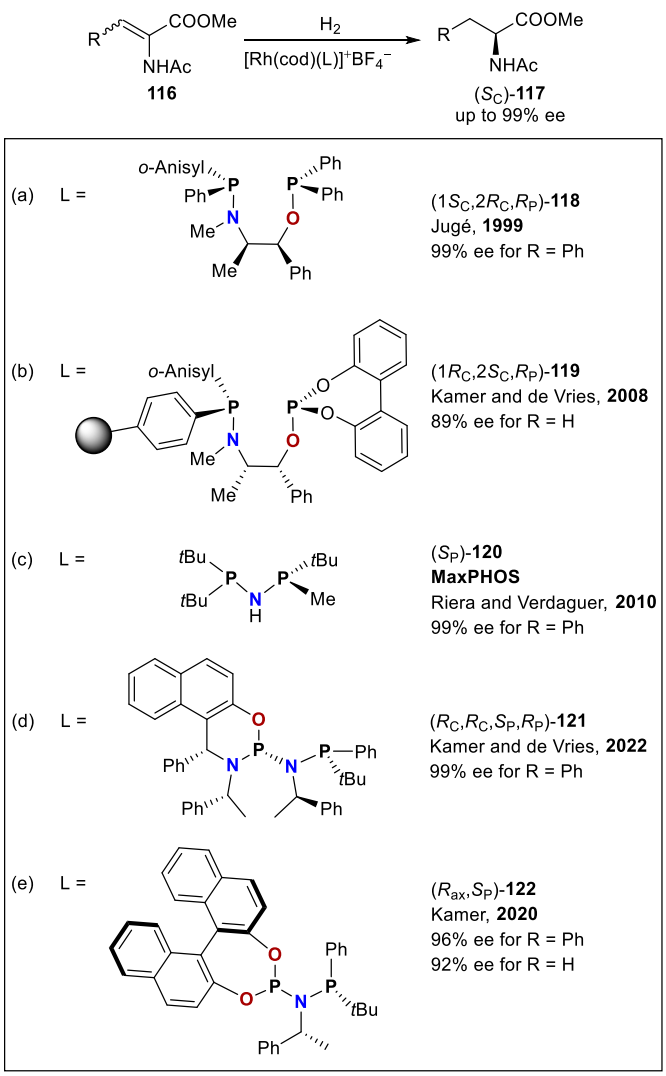

Scheme 1.20. Asymmetric hydrogenation of olefins **116** with different rhodium(I) diphosphine chelate complexes reported by Jugé (a)[22b,38d], Kamer, and de Vries (b[23f] and d[65]), Riera and Verdaguer (c),[32] and Kamer (e)[66] (cod = 1,5-cyclooctadiene).

Two years later, the groups of Riera and Verdaguer reported a new class of rhodium(I) catalysts with phosphinosulfonamide (PNSO) ligands for intramolecular cycloadditions of terminal enediynes **132** (Scheme 1.22).[67] The ligand preparation started from enantiomerically pure (S_P)-**126** with sodium hydride and sulfonyl chlorides **127** or *N*-phenyl-bis(trifluoromethanesulfonimide) in THF to obtain (S_P)-**128** as intermediate product in good to excellent yields. Since the goal was to generate ligands for rhodium(I), the borane entity had to be cleaved in order to release the required coordination site on the stereogenic phosphorus atom. This

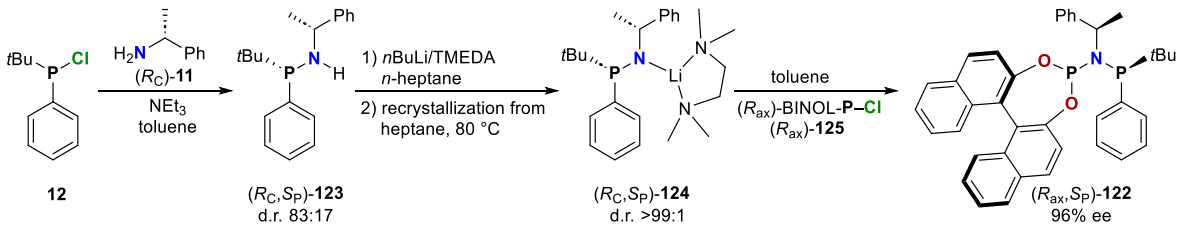

Scheme 1.21. Synthesis of (R_{ax})-BINOL-substituted PNP ligand (R_{ax},S_P)-**122** (TMEDA = *N*,*N*,*N*′,*N*′-tetramethylethane-1,2-diamine).[66]

was achieved under basic (DABCO) or acidic (HBF_4) conditions and heating (Scheme 1.22, top). Surprisingly, the deprotected products were stable under air due to a simple reason: the ability for NH/PH tautomerism led to the PH form (S_P)-**129a** in most of the cases because of the relative basicity of the phosphorus atom. This basic character is increased by electron-rich substituents on the phosphorus atom and by electron-withdrawing substituents at the nitrogen atom. A tautomeric equilibrium in general can be effectively shifted towards the P(III) state by coordinating the phosphorus lone electron pair to a metal center. It is assumed that such molecules do not lose their chiral information during this tautomeric equilibrium, as is indeed the case with the tautomerism of PH/OH compounds. Both, air-stable neutral [(R_P)-**130**] and cationic [(R_P)-**131**] rhodium(I) complexes could be synthesized. In addition to thorough structural investigations of the cationic complex,[67] the complexes were tested for the challenging[68] [2+2+2] intramolecular cycloaddition of enediynes **132**. While the neutral complexes (R_P)-**130** did not lead to any cyclization, the cationic complexes (R_P)-**131** showed remarkable conversions and enantiomeric excesses of up to 94% for products (R_C,R_C)-**133**, depending on the reaction conditions as well as the exact composition of the *O*- or *N*-tethered substrate (Scheme 1.22, bottom).[67]

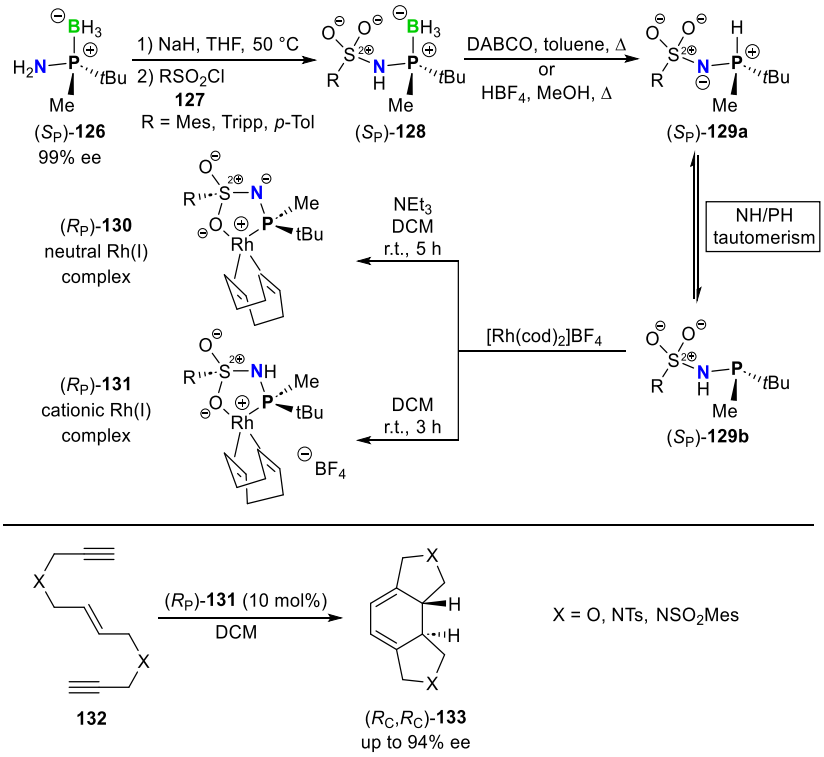

Scheme 1.22. Top: Synthesis of PNSO ligands (S_P)-**129** showing NH/PH tautomerism, and preparation of rhodium(I)-PNSO-complexes.[67] Bottom: Rhodium(I)-catalyzed [2+2+2] intramolecular cycloaddition of enediynes **132** (DABCO = 1,4-diazabicyclo[2.2.2]octane).[67]

1.5.2.2. Asymmetric Catalysis with Iridium(I) Complexes

In 2015, the reactivity of phosphine boranes with adjacent imine functionalities towards organometallic reagents (Scheme 1.23, a and b) was published by Riera and Verdaguer.[64] Borane-protected *N*-phosphonyl imines such as (S_P)-**134** were prepared in a microwave at 80 °C from

enantiomerically pure (S_P)-**126** and various aldehydes. The condensation was promoted by titanium(IV) ethoxide under neat conditions.

The borane moiety proved to be an efficient directing group for the 1,2-addition of organometallic reagents to the imine double bond, leading to unequal mixtures of diastereomers (Scheme 1.23, a and b).[64] Such a directing behavior was previously only known for P(V) compounds[69] (Scheme 1.23, c) and sulfinyles[70]. Depending on the solvent, diastereomerically enriched 1,2-addition products (S_C,S_P)-**135** or (R_C,S_P)-**135** with a diastereomeric ratio of up to 98:2 could be obtained for the phosphine boranes.[64]

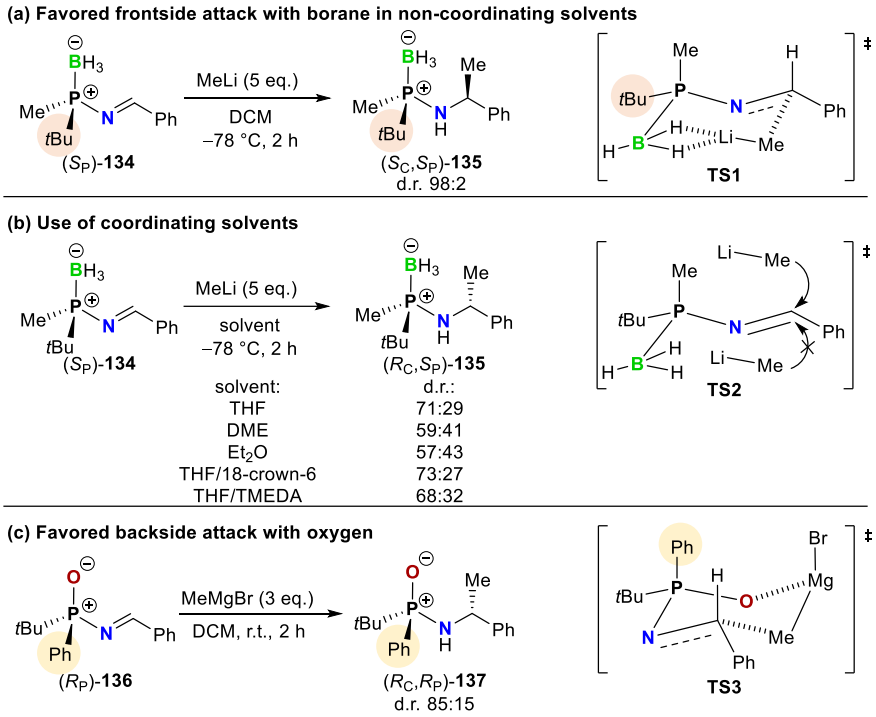

Scheme 1.23. Directing behavior of borane in non-coordinating solvents (a),[64] borane in coordinating solvents (b),[64] and oxygen in non-coordinating solvents (c)[69] in stereoselective 1,2-addition reactions of organometallic reagents with *N*-phosphanylimines (S_P)-**134** and (R_P)-**136** (DME = dimethoxyethane, 18-crown-6 = 1,4,7,10,13,16-hexaoxacyclooctadecane, TMEDA = *N*,*N*,*N*′,*N*′-tetramethylethane-1,2-diamine).

A crucial factor was the coordination ability of the solvents. Coordinating solvents in general provided less stereoselectivity (d.r. values between 41:59 and 27:73), whereas non-coordinating solvents such as dichloromethane gave excellent ratios. Moreover, the selectivity was reversed for the different types of solvent, which means that non-coordinating solvents preferably yielded (S_C,S_P)-**135** (Scheme 1.23, a) and coordinating solvents (R_C,S_P)-**135** (Scheme 1.23, b). The authors provided insight into the stereochemical behavior based on the structure of the transition state. With non-coordinating solvents, a distorted cyclic chair conformation is favorable (**TS1**, Scheme 1.23, a), in which lithium is η^2-coordinated by the BH_3 directing group. This well-defined transition state structure ensures the high stereoselectivity of the 1,2-addition. Since coordinating solvents usually enclose lithium cations, the chair-shaped transition state cannot be built (**TS2**, Scheme 1.23, b). Not even the use of cation scavengers such as TMEDA or 18-crown-6 could prevent the lithium cations from being trapped by the coordinating solvent, resulting in poorer and

reversed stereoselectivity.[64] P^+–O^- compounds build a similar chair-shaped transition state structure compared to P–BH_3 analogues (**TS3**, Scheme 1.23, c). However, reaction of the enantiomerically pure *P*-stereogenic *N*-phosphinoylimine (R_P)-**136** and MeMgBr in dichloromethane yielded a diastereomeric ratio of only 85:15 in (R_C,R_P)-**137**,[69] emphasizing that the borane moiety is a more effective directing group than the P^+–O^- group.[64]

Since the main goal was to establish a new type of ligands for catalytic applications, (R_C,R_P)-**138**, which features a thiophene moiety and a diastereomeric ratio of <99:1, was deprotected using DABCO and coordinated to iridium(I) to obtain (R_C,S_P)-**139** (Scheme 1.24). When treating the resulting neutral complex with NaBArF, the thiophene moiety coordinated as well, yielding the cationic, *P*,*S*-bonded bidentate Ir(I) complex (R_C,S_P)-**140**. The molecular structure of the complex salt in the crystalline state was used to determine the absolute configuration of the ligand.[64] So far, no catalytic activity was reported for exactly this type of complexes.

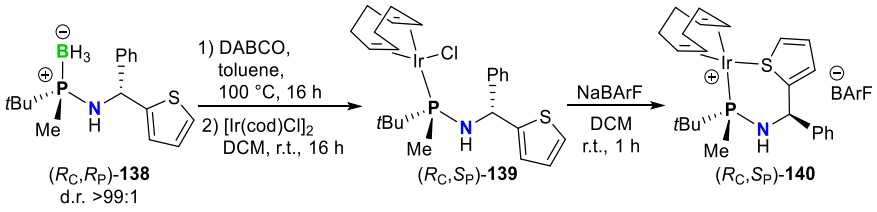

Scheme 1.24. Synthesis of a neutral, *P*-monodentate [(R_C,S_P)-**139**] and a cationic, *P*,*S*-bidentate [(R_C,S_P)-**140**] iridium(I) complex (cod = 1,5-cyclooctadiene, BArF = tetrakis[3,5-bis(trifluoromethyl)phenyl]borate).[64]

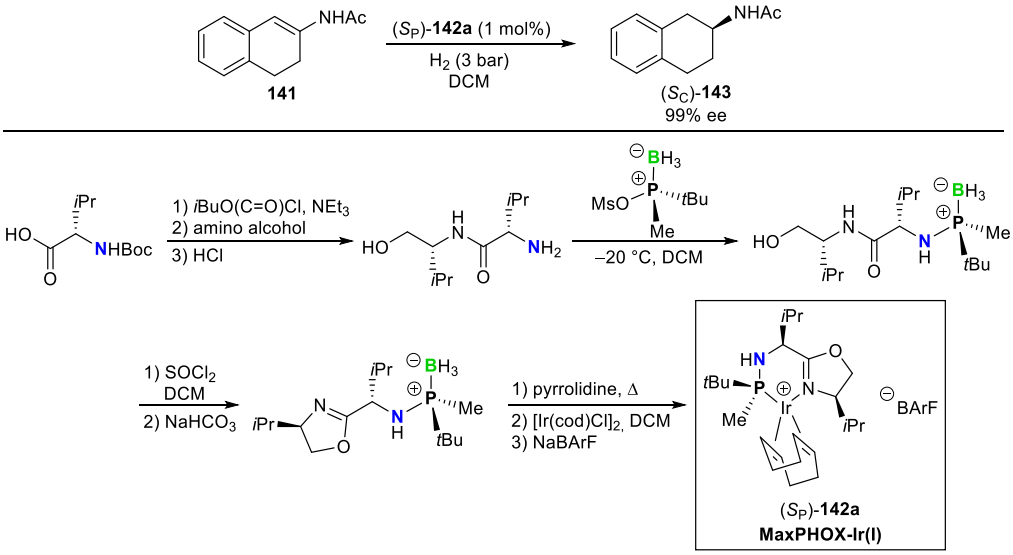

Scheme 1.25. Top: Highly enantioselective iridium(I)-catalyzed asymmetric hydrogenation of the cyclic enamide **141**.[71b] Bottom: Synthesis of (S_P)-**142a**, a representative of the MaxPHOX-Ir(I) family.[71b]

However, also in 2015, the same group[71] presented the MaxPHOX-Ir(I) family with characteristic *P,N*-bidentate phosphine-oxazoline ligands coordinating to iridium(I). (S_P)-**142a** is a representative of this type of catalysts and is capable of highly enantioselective hydrogenation of cyclic enamides (Scheme 1.25, top). This way, the reduction of **141** could be achieved with 99% ee in product (S_C)-**143**, after only 9% ee were achieved with a Rh(I) catalyst some years earlier.[32] The ligands and their corresponding complexes were synthesized in a wide variety of different stereoisomers with various substituents starting from three simple building blocks, each containing a *C*- or *P*-stereogenic center. The synthesis is shown for one example [(S_P)-**142a**] in Scheme 1.25 (bottom).[71b]

Research towards the MaxPHOX-Ir(I)-complex was expanded in the following years. Just recently numerous non-chelating di-, tri-, and tetrasubstituted olefins were reported to undergo catalytic hydrogenations with up to >99% ee. The trisubstituted alkenes were not only exclusively equipped with aryl and alkyl groups (**144**), but also contained poorly coordinating units such as enones (non-cyclic **146** and cyclic **152**), vinyl boronates (**148**), enol phosphinates (**150**), lactams (**152**), and lactones (**152**) (Scheme 1.26, a–e). For the tetrasubstituted species **154** it is noteworthy that even with four different substituents almost enantiomerically pure products with

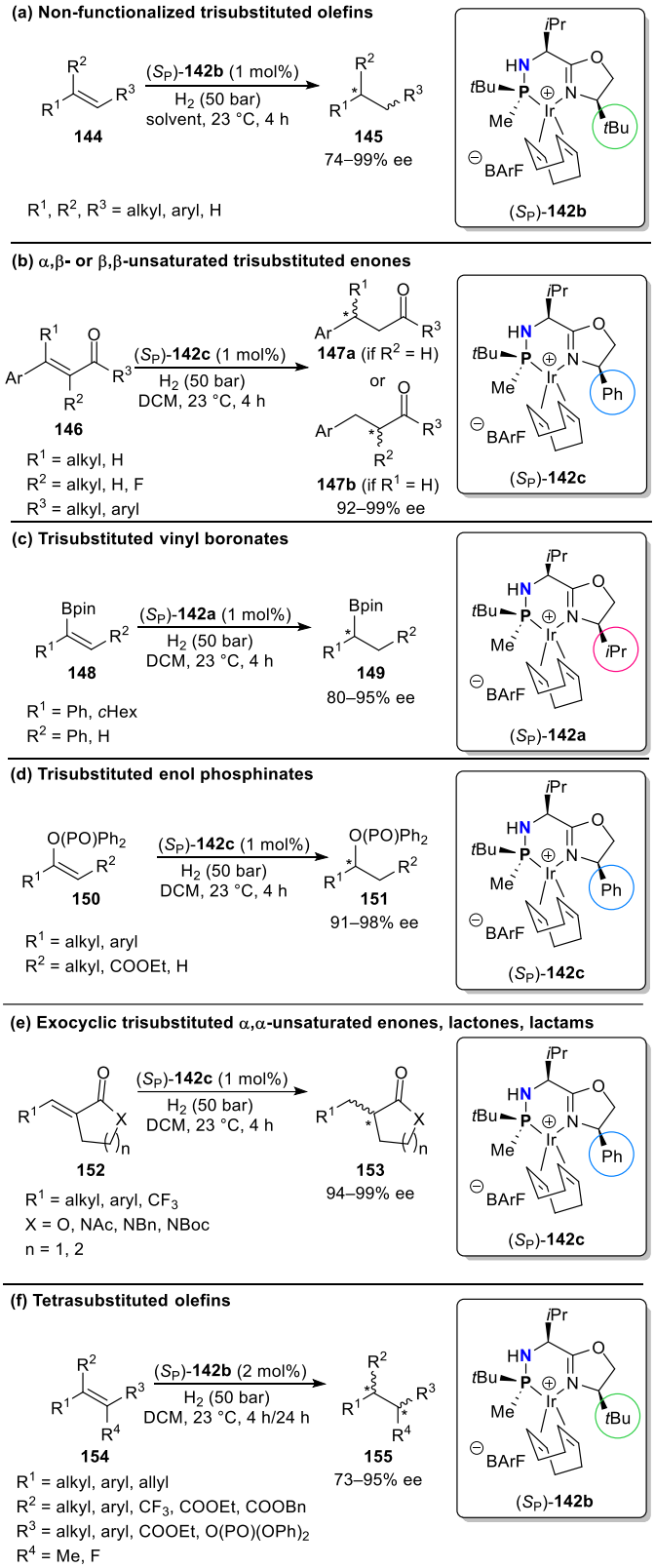

Scheme 1.26. Overview of different MaxPHOX-Ir(I)-complexes being able to catalyze various hydrogenation reactions.[72]

95% ee could be generated (Scheme 1.26, f).[72] The authors thus complemented a library of olefinic substrates, which had originally begun some years earlier with a similar catalyst.[73] In general, the success of asymmetric olefin hydrogenation with excellent enantioselectivity highly depends on the substitution pattern. In Scheme 1.26, the various studied species and the corresponding catalysts for their hydrogenation are shown.[72] DFT calculations supported the proposal of two possible transition states during the catalytic cycle, both of which originate from an Ir(III)/Ir(V) tetrahydride intermediate. The initial hydrogen transfer from the metal center to the coordinated olefin is expected to ultimately determine the enantioselectivity, which in turn can be estimated from the relative energies of the two possible transition states. The respective pathways are either a migration-insertion mechanism (most favorable) or a σ-bond metathesis (energetically feasible according to the calculations, but not favored).[72]

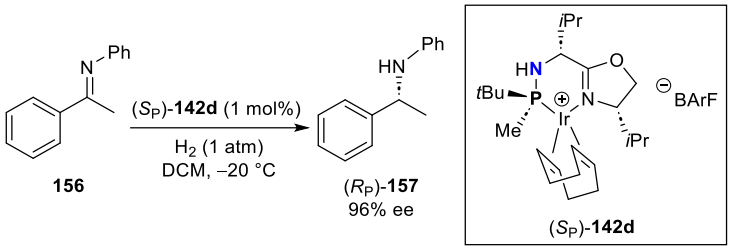

Scheme 1.27. MaxPHOX-Ir(I)-catalyzed asymmetric hydrogenation of *N*-aryl imine **156** (BArF = tetrakis[3,5-bis(trifluoro-methyl)phenyl]borate).[74]

In 2018, MaxPHOX-Ir(I)-mediated hydrogenation of a variety of *N*-aryl imines was achieved. Compound (R_P)-**157** could be obtained with 96% ee from **156** with (S_P)-**142d** as catalyst (Scheme 1.27). This was feasible at atmospheric hydrogen pressure at –20 °C. The stereochemical outcome and the catalyst activity of these reactions were strongly dependent on the substitution pattern at the phosphorus atom and also on the counterion used. Avoiding *P*-centered chirality in the catalyst or replacing the classic BArF anion with borontetrafluoride reduced both the reaction rate and stereoselectivity.[74]

A very striking feature of the MaxPHOX-Ir(I) catalysts was published in 2020 with their ability to enantioselectively isomerize primary allylic alcohols to aldehydes.[75]

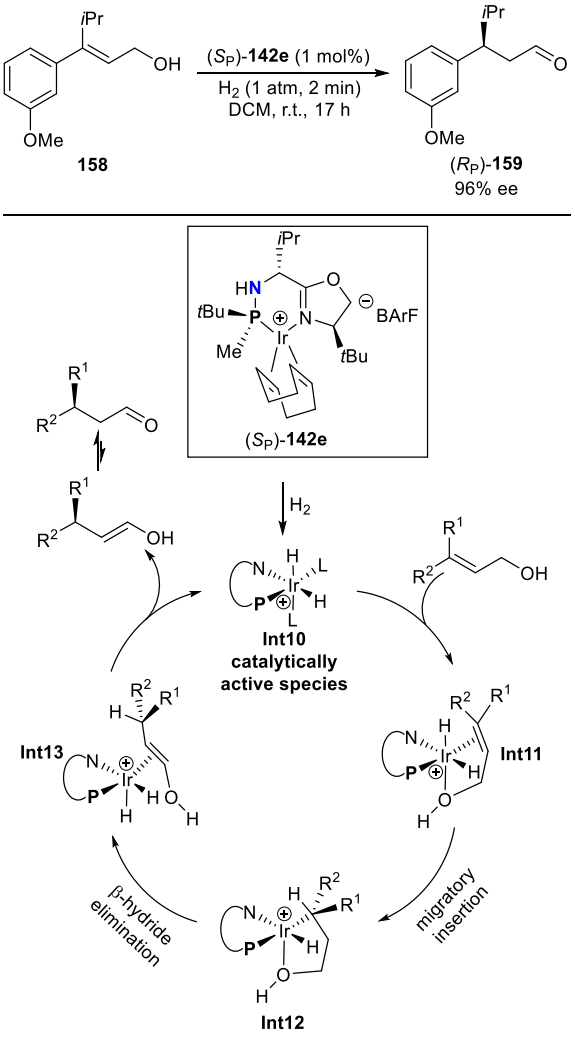

Scheme 1.28. Top: MaxPHOX-Ir(I)-catalyzed isomerization of allylic alcohol **158** to its corresponding aldehyde (R_P)-**159**.[76] Bottom: Proposed catalytic cycle of the upper reaction.[76]

After studying the different derivatives of MaxPHOX-Ir(I) and various olefinic substrates, the best performing catalyst was (S_P)-**142e** and led to 96% ee for the isomerization of **158** to (R_P)-**159** (Scheme 1.28, top). Therefore, the dichloromethane solution containing the starting material was flooded with hydrogen for two minutes and stirred at room temperature under nitrogen atmosphere for 17 hours. The catalytic cycle (Scheme 1.28, bottom) is initiated by activation of (S_P)-**142e** through hydrogenation (**Int10**) and subsequent coordination of the Ir(I) center by the allylic substrate (**Int11**). A migratory insertion of the axial hydrogen atom to the substrate (**Int12**) followed by β-hydride elimination (**Int13**) led to the enol product, which now contains a stereogenic carbon atom and a C═C double bond, the latter being shifted by one position compared to the starting material. Since the enol is now capable of keto-enol tautomerism, it can be converted to the more stable aldehyde. Both the transition state and intermediate structures of the catalytic cycle were confirmed by DFT calculations.[76]

1.6. Summary and Outlook

Phosphorus-stereogenic aminophosphines were shown to provide a unique property profile for two important areas of catalysis, namely organocatalysis and transition metal catalysis. So far, only aminophosphine oxides have been used for organocatalytic reactions. However, the newly created access to other *P*-stereogenic aminophosphine chalcogenides opens up further areas of application in organocatalysis and may stimulate the design of new ligands for transition metal-catalyzed reactions. The ability to achieve outstanding stereoselectivities in a large number of asymmetric transition metal-catalyzed reactions is remarkable and encourages further investigation into complexes with aminophosphine-based ligands.

Synthesis methods for providing *P*-stereogenic, enantiomerically pure aminophosphine chalcogenides and boranes are extensive, ranging from the long-known and still appreciated use of chiral auxiliaries to modern techniques using transition metals such as copper, iridium, and palladium. Stereochemically pure aminophosphine chalcogenides exhibit an interesting bifunctional pattern capable of forming hydrogen bonds, which should be further investigated in terms of defined supramolecular structures with chiral information. This contribution may help researchers in the fields of ligand design, asymmetric catalysis, and chiral supramolecular chemistry to get new ideas and to focus on new building blocks whose potential is far from being exhausted.

Cautionary Note

Some of the presented products and intermediates might potentially be toxic due to their structural similarity to parathion, which inhibits acetylcholinesterase.[77]

1.7. References

[1] For reviews, see: a) D. H. Valentine Jr., J. H. Hillhouse, *Synthesis* **2003**, *16*, 2437–2460; b) J. L. Methot, W. R. Roush, *Adv. Synth. Catal.* **2004**, *346*, 1035–1050; c) Z. Wang, X. Xu, O. Kwon, *Chem. Soc. Rev.* **2014**, *43*, 2927–2940; d) H. Guo, Y. C. Fan, Z. Sun, Y. Wu, O. Kwon, *Chem. Rev.* **2018**, *118*, 10049–10293; e) P. Karanam, G. M. Reddy, S. R. Koppolu, W. Lin, *Tetrahedron Lett.* **2018**, *59*, 59–76.

[2] For reviews, see: a) A. Gallen, A. Riera, X. Verdaguer, A. Grabulosa, *Catal. Sci. Technol.* **2019**, *9*, 5504–5561; b) S. Kotani, M. Nakajima, *Tetrahedron Lett.* **2020**, *61*, 151421; c) M. Hayashi, *Chem. Lett.* **2021**, *50*, 1–6.

[3] M. C. Hilton, X. Zhang, B. T. Boyle, J. V. Alegre-Requena, R. S. Paton, A. McNally, *Science* **2018**, *362*, 799–804.

[4] a) M. Myers, E. F. Connor, T. Glauser, A. Möck, G. Nyce, J. L. Hedrick, *J. Polym. Sci. A Polym. Chem.* **2002**, *40*, 844–851; b) H. Ni, W.-L. Chan, Y. Lu, *Chem. Rev.* **2018**, *118*, 9344–9411; c) C. Xie, A. J. Smaligo, X.-R. Song, O. Kwon, *ACS Cent. Sci.* **2021**, *7*, 536–558.

[5] a) T. M. Shaikh, C.-M. Weng, F.-E. Hong, *Coord. Chem. Rev.* **2012**, *256*, 771–803; b) Y. H. Lee, B. Morandi, *Coord. Chem. Rev.* **2019**, *386*, 96–118.

[6] a) N. L. Dunn, M. Ha, A. T. Radosevich, *J. Am. Chem. Soc.* **2012**, *134*, 11330–11333; b) J. Lam, K. M. Szkop, E. Mosaferi, D. W. Stephan, *Chem. Soc. Rev.* **2019**, *48*, 3592–3612.

[7] a) C. Marquardt, O. Hegen, T. Kahoun, M. Scheer, *Chem. Eur. J.* **2017**, *23*, 4397–4404; b) M. J. Poller, T. Huber, J. Frickel, N. Burford, K. Karaghiosoff, *Phosphorus Sulfur Silicon Relat. Elem.* **2019**, *194*, 513–514; c) A. Denhof, M. Olaru, E. Lork, S. Mebs, L. Chęcińska, J. Beckmann, *Eur. J. Inorg. Chem.* **2020**, 4093–4110; d) N. Fontana, N. A. Espinosa-Jalapa, M. Seidl, J. O. Bauer, *Chem. Eur. J.* **2021**, *27*, 2649–2653; e) N. Fontana, N. A. Espinosa-Jalapa, M. Seidl, J. O. Bauer, *Chem. Commun.* **2022**, *58*, 2144–2147; f) A. Falk, J. O. Bauer, *Inorg. Chem.* **2022**, *61*, 15576–15588; g) N. Fontana, J. O. Bauer, *ChemistrySelect* **2023**, *8*, e202301373.

[8] a) M. Fiorini, G. M. Giongo, *J. Mol. Catal.* **1979**, *5*, 303–310; b) B. Schmid, S. Frieß, A. Herrera, A. Linden, F. W. Heinemann, H. Locke, S. Harder, R. Dorta, *Dalton Trans.* **2016**, *45*, 12028–12040; c) C. Fliedel, A. Ghisolfi, P. Braunstein, *Chem. Rev.* **2016**, *116*, 9237–9304.

[9] a) H. R. Allcock, *Phosphorus-Nitrogen Compounds: cyclic, linear, and high polymeric systems*, Academic Press, New York, NY, USA, **1972**; b) S. Yoshida, K. Igawa, K. Tomooka, *J. Am. Chem. Soc.* **2012**, *134*, 19358–19361; c) M. A. Shameem, A. Orthaber, *Chem. Eur. J.* **2016**, *22*, 10718–10735; d) M. B. Smith, *Molecules* **2022**, *27*, 6293; e) D. Ray, S. Majee, R. N. Yadav, B. K. Banik, *Molecules* **2023**, *28*, 3524.

[10] a) Michael Witt, Herbert W. Roesky, *Chem. Rev.* **1994**, *94*, 1163–1181; b) P. Bhattacharyya, J. Woollins, *Polyhedron* **1995**, *14*, 3367–3388; c) C. A. Kumar, T. K. Panda, *Phosphorus Sulfur Silicon Relat. Elem.* **2017**, *192*, 1084–1101.

[11] W. Zhao, P. K. Yan, A. T. Radosevich, *J. Am. Chem. Soc.* **2015**, *137*, 616–619.

[12] J. B. Rodriguez, C. Gallo-Rodriguez, *ChemMedChem* **2019**, *14*, 190–216.

[13] a) M. Karki, C. Gibard, S. Bhowmik, R. Krishnamurthy, *Life* **2017**, *7*, 32; b) D. J. Ritson, J. Xu, J. D. Sutherland, *Synlett* **2017**, *28*, 64–67; c) C. Gibard, S. Bhowmik, M. Karki, E.-K. Kim, R. Krishnamurthy, *Nat. Chem.* **2018**, *10*, 212–217; d) C. Gibard, I. B. Gorrell, E. I. Jiménez, T. P. Kee, M. A. Pasek, R. Krishnamurthy, *Angew. Chem. Int. Ed.* **2019**, *58*, 8151–8155; *Angew. Chem.*, **2019**, *131*, 8235–8239; e) D. J. Ritson, S. J. Mojzsis, J. D. Sutherland, *Nat. Geosci.* **2020**, *13*, 344–348.

[14] Y. Gnas, F. Glorius, *Synthesis* **2006**, *12*, 1899–1930.

[15] a) K. M. Pietrusiewicz, M. Zablocka, *Chem. Rev.* **1994**, *94*, 1375–1411; b) J.-F. Cavalier, F. Fotiadu, R. Verger, G. Buono, *Synlett* **1998**, 73–75; c) I. Fernández, N. Khiar, A. Roca, A. Benabra, A. Alcudia, J. Espartero, F. Alcudia, *Tetrahedron Lett.* **1999**, *40*, 2029–2032.

[16] O. I. Kolodiazhnyi, E. V. Gryshkun, N. V. Andrushko, M. Freytag, P. G. Jones, R. Schmutzler, *Tetrahedron: Asymmetry* **2003**, *14*, 181–183.

[17] a) O. Korpiun, K. Mislow, *J. Am. Chem. Soc.* **1967**, *89*, 4784–4786; b) O. Korpiun, R. A. Lewis, J. Chickos, K. Mislow, *J. Am. Chem. Soc.* **1968**, *90*, 4842–4846; c) T. L. Emmick, R. L. Letsinger, *J. Am. Chem. Soc.* **1968**, *90*, 3459–3465.

[18] For reviews, see: a) K. M. Pietrusiewicz, M. Zabłocka, *Chem. Rev.* **1994**, *94*, 1375–1411; b) D. Glueck, *Synlett* **2007**, *17*, 2627–2634; c) A. Grabulosa, J. Granell, G. Muller, *Coord. Chem. Rev.* **2007**, *251*, 25–90; d) D. S. Glueck, *Chem. Eur. J.* **2008**, *14*, 7108–7117; e) J. S. Harvey, V. Gouverneur, *Chem. Commun.* **2010**, *46*, 7477–7485; f) O. I. Kolodiazhnyi, *Tetrahedron: Asymmetry* **2012**, *23*, 1–46; g) O. I. Kolodiazhnyi, *Top. Curr. Chem.* **2015**, *360*, 161–236; h) M. Dutartre, J. Bayardon, S. Jugé, *Chem. Soc. Rev.* **2016**, *45*, 5771–5794; i) S. Lemouzy, L. Giordano, D. Hérault, G. Buono, *Eur. J. Org. Chem.* **2020**, *2020*, 3351–3366; j) H. Li, L. Yin, *Chinese J. Org. Chem.* **2022**, *42*, 3183–3200; k) D. S. Glueck, *Synthesis* **2022**, *54*, 271–280.

[19] For examples, see: a) A. N. Serreqi, R. J. Kazlauskas, *J. Org. Chem.* **1994**, *59*, 7609–7615; b) A. R. Muci, K. R. Campos, D. A. Evans, *J. Am. Chem. Soc.* **1995**, *117*, 9075–9076; c) K. Shioji, Y. Ueno, Y. Kurauchi, K. Okuma, *Tetrahedron Lett.* **2001**, *42*, 6569–6571; d) M. J. McGrath, P. O'Brien, *J. Am. Chem. Soc.* **2005**, *127*, 16378–16379; e) D. Wiktelius, M. J. Johansson, K. Luthman, N. Kann, *Org. Lett.* **2005**, *7*, 4991–4994; f) C. Genet, S. J. Canipa, P. O'Brien, S. Taylor, *J. Am. Chem. Soc.* **2006**, *128*, 9336–9337; g) N. F. Blank, K. C. McBroom, D. S. Glueck, W. S. Kassel, A. L. Rheingold, *Organometallics* **2006**, *25*, 1742–1748; h) J. J. Gammon, S. J. Canipa, P. O'Brien, B. Kelly, S. Taylor, *Chem. Commun.* **2008**, 3750–3752; i) J. J. Gammon, P. O'Brien, B. Kelly, *Org. Lett.* **2009**, *11*, 5022–5025; j) S. J. Canipa, P. O'Brien, S. Taylor, *Tetrahedron: Asymmetry* **2009**, *20*, 2407–2412; k) J. S. Harvey, S. J. Malcolmson, K. S. Dunne, S. J. Meek, A. L. Thompson, R. R. Schrock, A. H. Hoveyda, V. Gouverneur, *Angew. Chem. Int. Ed.* **2009**, *48*, 762–766; *Angew. Chem.*, **2009**, *121*, 776–780; l) J. J. Gammon, V. H. Gessner, G. R. Barker, J. Granander, A. C. Whitwood, C. Strohmann, P. O'Brien, B. Kelly, *J. Am. Chem. Soc.* **2010**, *132*, 13922–13927; m) J. Granander, F. Secci, S. J. Canipa, P. O'Brien, B. Kelly, *J. Org. Chem.* **2011**, *76*, 4794–4799.

[20] a) S. Jugé, M. Stephan, J. A. Laffitte, J. P. Genet, *Tetrahedron Lett.* **1990**, *31*, 6357–6360; b) S. Jugé, M. Stephan, R. Merdès, J. P. Genet, S. Halut-Desportes, *J. Chem. Soc., Chem. Commun.* **1993**, 531–533; c) M. Stankevic, K. M. Pietrusiewicz, *J. Org. Chem.* **2007**, *72*, 816–822; d) T. León, A. Riera, X. Verdaguer, *J. Am. Chem. Soc.* **2011**, *133*, 5740–5743; e) A. Cabré, A. Riera, X. Verdaguer, *Acc. Chem. Res.* **2020**, *53*, 676–689.

[21] a) J. Holz, M.-N. Gensow, O. Zayas, A. Borner, *Curr. Org. Chem.* **2007**, *11*, 61–106; b) M. Benaglia, S. Rossi, *Org. Biomol. Chem.* **2010**, *8*, 3824–3830; c) S. Takizawa, E. Rémond, F. A. Arteaga, Y. Yoshida, V. Sridharan, J. Bayardon, S. Jugé, H. Sasai, *Chem. Commun.* **2013**, *49*, 8392–8394; d) C. E. Henry, Q. Xu, Y. C. Fan, T. J. Martin, L. Belding, T. Dudding, O. Kwon, *J. Am. Chem. Soc.* **2014**, *136*, 11890–11893; e) H. Y. Su, M. S. Taylor, *J. Org. Chem.* **2017**, *82*, 3173–3182; f) A. J. Smaligo, S. Vardhineedi, O. Kwon, *ACS Catal.* **2018**, *8*, 5188–5192; g) H. Qiu, Q. Dai, J. He, W. Li, J. Zhang, *Chem. Sci.* **2020**, *11*, 9983–9988.

[22] a) T. Imamoto, H. Tsuruta, Y. Wada, H. Masuda, K. Yamaguchi, *Tetrahedron Lett.* **1995**, *36*, 8271–8274; b) D. Moulin, C. Darcel, S. Jugé, *Tetrahedron: Asymmetry* **1999**, *10*, 4729–4743; c) A. Ohashi, S. Kikuchi, M. Yasutake, T. Imamoto, *Eur. J. Org. Chem.* **2002**, *2002*, 2535–2546; d) W. Tang, X. Zhang, *Chem. Rev.* **2003**, *103*, 3029–3069; e) G. Erre, S. Enthaler, K. Junge, S. Gladiali, M. Beller, *Coord. Chem. Rev.* **2008**, *252*, 471–491; f) A. Vidal-Ferran, A. Grabulosa, X. Verdaguer, A. Riera, *in Catalytic Asymmetric Synthesis*, 4th ed. (Eds: T. Akiyama, I. Ojima), Wiley, Hoboken, NJ, USA, **2022**, Ch. 15; g) P. Rojo, A. Riera, X. Verdaguer, *Coord. Chem. Rev.* **2023**, *489*, 215192.

[23] a) T. Imamoto, T. Oshiki, T. Onozawa, T. Kusumoto, K. Sato, *J. Am. Chem. Soc.* **1990**, *112*, 5244–5252; b) E. J. Corey, Z. Chen, G. J. Tanoury, *J. Am. Chem. Soc.* **1993**, *115*, 11000–11001; c) T. Miura, H. Yamada, S. Kikuchi, T. Imamoto, *J. Org. Chem.* **2000**, *65*, 1877–1880; d) C. Bauduin, D. Moulin, E. B. Kaloun, C. Darcel, S. Jugé, *J. Org. Chem.* **2003**, *68*, 4293–4301; e) J.-V. Naubron, L. Giordano, F. Fotiadu, T. Bürgi, N. Vanthuyne, C. Roussel, G. Buono, *J. Org. Chem.* **2006**, *71*, 5586–5593; f) R. den Heeten, B. H. G. Swennenhuis, P. W. N. M. van Leeuwen, J. G. de Vries, P. C. J. Kamer, *Angew. Chem. Int. Ed.* **2008**, *47*, 6602–6605; *Angew. Chem.*, **2008**, *120*, 6704–6707; g) D. Moraleda, D. Gatineau, D. Martin, L. Giordano, G. Buono, *Chem. Commun.* **2008**, 3031–3033; h) J. Bayardon, S. Jugé, *in Phosphorus(III) Ligands in Homogeneous Catalysis: Design and Synthesis*, 1st ed. (Eds: P. C. J. Kamer, P. W. N. M. van Leeuwen), Wiley, Hoboken, NJ, USA, **2012**, Ch. 12; i) T. Imamoto, *Proc. Jpn. Acad., Ser. B* **2021**, *97*, 520–542.

[24] L. Wang, Z. Du, Q. Wu, R. Jin, Z. Bian, C. Kang, H. Guo, X. Ma, L. Gao, *Eur. J. Org. Chem.* **2016**, *2016*, 2024–2028.
[25] a) T. Koizumi, Y. Kobayashi, H. Amitani, E. Yoshii, *J. Org. Chem.* **1977**, *42*, 3459–3460; b) T. Koizumi, H. Amitani, E. Yoshii, *Synthesis* **1979**, 110–112.
[26] C. R. Hall, T. D. Inch, G. J. Lewis, R. A. Chittenden, *J. Chem. Soc., Chem. Commun.* **1975**, 720–721.
[27] T. Koizumi, H. Takagi, E. Yoshii, *Chem. Lett.* **1980**, *9*, 1403–1406.
[28] Y. Kobayashi, T. Koizumi, E. Yoshii, *Chem. Pharm. Bull.* **1979**, *27*, 1641–1650.
[29] a) T. Koizumi, Y. Kobayashi, E. Yoshii, *J. Chem. Soc., Chem. Commun.* **1974**, 678–679; b) T. Koizumi, Y. Kobayashi, E. Yoshii, *Chem. Pharm. Bull.* **1976**, *24*, 834–835.
[30] E. V. Gryshkun, N. V. Andrushko, O. I. Kolodiazhnyi, *Phosphorus Sulfur Silicon Relat. Elem.* **2004**, *179*, 1027–1046.
[31] P. M. Reddy, I. M. Kovach, *Tetrahedron Lett.* **2002**, *43*, 4063–4066.
[32] M. Revés, C. Ferrer, T. León, S. Doran, P. Etayo, A. Vidal-Ferran, A. Riera, X. Verdaguer, *Angew. Chem. Int. Ed.* **2010**, *49*, 9452–9455; *Angew. Chem.*, **2010**, *122*, 9642–9645.
[33] T. Huber, N. A. Espinosa-Jalapa, J. O. Bauer, *Chem. Eur. J.* **2022**, *28*, e202202608.
[34] a) W. B. Farnham, R. A. Lewis, R. K. Murray Jr., K. Mislow, *J. Am. Chem. Soc.* **1970**, *92*, 5809–5810; b) J. K. Whitesell, *Chem. Rev.* **1992**, *92*, 953–964.
[35] A. Włodarczyk, A. E. Kozioł, M. Stankevič, *Eur. J. Org. Chem.* **2018**, 1589–1600.
[36] M. Stankevič, A. Włodarczyk, D. Nieckarz, *Eur. J. Org. Chem.* **2013**, 4351–4371.
[37] a) D. B. Cooper, J. M. Harrison, T. D. Inch, *Tetrahedron Lett.* **1974**, *15*, 2697–2700; b) D. B. Cooper, C. R. Hall, T. D. Inch, *J. Chem. Soc., Chem. Commun.* **1975**, 721–723; c) D. B. Cooper, C. R. Hall, J. M. Harrison, T. D. Inch, *J. Chem. Soc., Perkin Trans. 1* **1977**, 1969–1980.
[38] a) S. Jugé, J. P. Genet, *Tetrahedron Lett.* **1989**, *30*, 2783–2786; b) S. Jugé, M. Stephan, J. P. Genet, S. Halut-Desportes, S. Jeannin, *Acta Cryst.* **1990**, *C46*, 1869–1872; c) D. Moulin, S. Bago, C. Bauduin, C. Darcel, S. Jugé, *Tetrahedron: Asymmetry* **2000**, *11*, 3939–3956; d) C. Darcel, D. Moulin, J.-C. Henry, M. Lagrelette, P. Richard, P. D. Harvey, S. Jugé, *Eur. J. Org. Chem.* **2007**, 2078–2090.
[39] C. Hall, T. D. Inch, I. W. Lawston, *Tetrahedron Lett.* **1979**, *20*, 2729–2732.
[40] H. Zijlstra, T. León, A. de Cózar, C. Fonseca Guerra, D. Byrom, A. Riera, X. Verdaguer, F. M. Bickelhaupt, *J. Am. Chem. Soc.* **2013**, *135*, 4483–4491.
[41] a) L. Wang, S. Cao, Z. Du, Q. Wu, Z. Bian, C. Kang, L. Gao, J. Zhang, *RSC Adv.* **2016**, *6*, 89665–89670; b) R. Xu, Z. Gao, Y. Yu, Y. Tang, D. Tian, T. Chen, Y. Chen, G. Xu, E. Shi, W. Tang, *Chem. Commun.* **2021**, *57*, 3335–3338.
[42] a) Y. Wu, K. Chen, X. Ge, P. Ma, Z. Xu, H. Lu, G. Li, *Org. Lett.* **2020**, *22*, 6143–6149; b) C. Tan, X. Liu, H. Jia, X. Zhao, J. Chen, Z. Wang, J. Tan, *Chem. Eur. J.* **2020**, *26*, 881–887; c) Y.-Y. Zhu, Y. Niu, Y.-N. Niu, S.-D. Yang, *Org. Biomol. Chem.* **2021**, *19*, 10296–10313; d) Z. Bai, F. Song, H. Wang, W. Cheng, S. Zhu, Y. Huang, G. He, G. Chen, *CCS Chem.* **2022**, *4*, 2258–2266; e) Z. Zhang, Q. Yan, R. Gao, H. Wang, *Phosphorus Sulfur Silicon Relat. Elem.* **2023**, *198*, 789–799.
[43] Y.-B. Li, H. Tian, S. Zhang, J.-Z. Xiao, L. Yin, *Angew. Chem. Int. Ed.* **2022**, *61*, e202117760; *Angew. Chem.*, **2022**, *134*, e202117760.
[44] F. Pertusati, C. McGuigan, *Chem. Commun.* **2015**, *51*, 8070–8073.
[45] M. Wang, L. Zhang, X. Huo, Z. Zhang, Q. Yuan, P. Li, J. Chen, Y. Zou, Z. Wu, W. Zhang, *Angew. Chem. Int. Ed.* **2020**, *59*, 20814–20819; *Angew. Chem.* **2020**, *132*, 21000–21005.
[46] J. Liu, H. Chen, M. Wang, W. He, J.-L. Yan, *Front. Chem.* **2023**, *11*, 1132025.
[47] Y. Zhou, J. Yang, T. Chen, S.-F. Yin, D. Han, L.-B. Han, *Bull. Chem. Soc. Jpn.* **2014**, *87*, 400–402.
[48] X.-L. Zhang, X. Qi, Y.-X. Wu, P. Liu, Y. He, *Cell Rep. Phys. Sci.* **2021**, *2*, 100594.
[49] A. Mondal, N. O. Thiel, R. Dorel, B. L. Feringa, *Nat. Catal.* **2022**, *5*, 10–19.
[50] X.-B. Chen, D. Padín, C. N. Stindt, B. L. Feringa, *Angew. Chem. Int. Ed.* **2023**, *62*, e202307450; *Angew. Chem.* **2023**, *135*, e202307450.
[51] L. B. Balázs, Y. Huang, J. B. Khalikuzzaman, Y. Li, S. A. Pullarkat, P.-H. Leung, *J. Org. Chem.* **2020**, *85*, 14763–14771.

[52] Z.-J. Du, J. Guan, G.-J. Wu, P. Xu, L.-X. Gao, F.-S. Han, *J. Am. Chem. Soc.* **2015**, *137*, 632–635.
[53] Y.-H. Chen, X.-L. Qin, F.-S. Han, *Chem. Commun.* **2017**, *53*, 5826–5829.
[54] T. Zhou, L.-J. Fan, Z.-J. Chen, M.-X. Jiang, P.-F. Qian, X. Hu, K. Zhang, B.-F. Shi, *Org. Lett.* **2023**, *25*, 5724–5729.
[55] P.-F. Qian, J.-Y. Li, T. Zhou, B.-F. Shi, *Synthesis* **2022**, *54*, 4784–4794.
[56] a) M. Casimiro, L. Roces, S. García-Granda, M. J. Iglesias, F. López-Ortiz, *Org. Lett.* **2013**, *15*, 2378–2381; b) M. Casimiro, G. P. Guedes, M. J. Iglesias, F. López-Ortiz, *Tetrahedron: Asymmetry* **2015**, *26*, 53–66; c) M. A. del Águila-Sánchez, Y. Navarro, J. García López, G. P. Guedes, F. López-Ortiz, *Dalton Trans.* **2016**, *45*, 2008–2022; d) Y. Navarro, G. P. Guedes, M. A. del Águila-Sánchez, M. J. Iglesias, F. Lloret, F. López-Ortiz, *Dalton Trans.* **2021**, *50*, 2585–2595.
[57] a) Z. S. Han, N. Goyal, M. A. Herbage, J. D. Sieber, B. Qu, Y. Xu, Z. Li, J. T. Reeves, J.-N. Desrosiers, S. Ma, N. Grinberg, H. Lee, H. P. R. Mangunuru, Y. Zhang, D. Krishnamurthy, B. Z. Lu, J. J. Song, G. Wang, C. H. Senanayake, *J. Am. Chem. Soc.* **2013**, *135*, 2474–2477; b) Z. S. Han, L. Zhang, Y. Xu, J. D. Sieber, M. A. Marsini, Z. Li, J. T. Reeves, K. R. Fandrick, N. D. Patel, J.-N. Desrosiers, B. Qu, A. Chen, D. M. Rudzinski, L. P. Samankumara, S. Ma, N. Grinberg, F. Roschangar, N. K. Yee, G. Wang, J. J. Song, C. H. Senanayake, *Angew. Chem. Int. Ed.* **2015**, *54*, 5474–5477; *Angew. Chem.*, **2015**, *127*, 5564–5567.
[58] Z. S. Han, H. Wu, B. Qu, Y. Wang, L. Wu, L. Zhang, Y. Xu, L. Wu, Y. Zhang, H. Lee, F. Roschangar, J. J. Song, C. H. Senanayake, *Tetrahedron Lett.* **2019**, *60*, 1834–1837.
[59] M. Rueping, A. P. Antonchick, T. Theissmann, *Angew. Chem. Int. Ed.* **2006**, *45*, 3683–3686, *Angew. Chem.*, **2006**, *118*, 3765–3768.
[60] M. Yuan, I. I. Mbaezue, Z. Zhou, F. Topic, Y. S. Tsantrizos, *Org. Biomol. Chem.* **2019**, *17*, 8690–8694.
[61] I. I. Mbaezue, F. Topic, Y. S. Tsantrizos, *Synlett* **2023**, *34*, 1709–1714.
[62] X.-L. Qin, A. Li, F.-S. Han, *J. Am. Chem. Soc.* **2021**, *143*, 2994–3002.
[63] G.-J. Wu, D.-X. Tan, F.-S. Han, *Acc. Chem. Res.* **2021**, *54*, 4354–4370.
[64] A. Flores-Gaspar, S. Orgué, A. Grabulosa, A. Riera, X. Verdaguer, *Chem. Commun.* **2015**, *51*, 1941–1944.
[65] S. Chakrabortty, K. Konieczny, B. H. Müller, A. Spannenberg, P. C. J. Kamer, J. G. de Vries, *Catal. Sci. Technol.* **2022**, *12*, 1392–1399.
[66] J.-O. Moritz, S. Chakrabortty, B. H. Müller, A. Spannenberg, P. C. J. Kamer, *J. Org. Chem.* **2020**, *85*, 14537–14544.
[67] T. León, M. Parera, A. Roglans, A. Riera, X. Verdaguer, *Angew. Chem. Int. Ed.* **2012**, *51*, 6951–6955; *Angew. Chem.*, **2012**, *124*, 7057–7061.
[68] T. Shibata, K. Tsuchikama, *Org. Biomol. Chem.* **2008**, *6*, 1317–1323.
[69] a) I. Notar Francesco, A. Wagner, F. Colobert, *Chem. Commun.* **2010**, *46*, 2139–2141; b) I. Notar Francesco, C. Egloff, A. Wagner, F. Colobert, *Eur. J. Org. Chem.* **2011**, 4037–4045.
[70] a) G. Liu, D. A. Cogan, J. A. Ellman, *J. Am. Chem. Soc.* **1997**, *119*, 9913–9914; b) D. A. Cogan, G. Liu, J. A. Ellman, *Tetrahedron* **1999**, *55*, 8883–8904; c) M. T. Robak, M. A. Herbage, J. A. Ellman, *Chem. Rev.* **2010**, *110*, 3600–3740.
[71] a) S. Orgué, A. Flores-Gaspar, M. Biosca, O. Pàmies, M. Diéguez, A. Riera, X. Verdaguer, *Chem. Commun.* **2015**, *51*, 17548–17551; b) E. Salomó, S. Orgué, A. Riera, X. Verdaguer, *Angew. Chem. Int. Ed.* **2016**, *55*, 7988–7992; *Angew. Chem.*, **2016**, *128*, 8120–8124.
[72] M. Biosca, P. de La Cruz-Sánchez, J. Faiges, J. Margalef, E. Salomó, A. Riera, X. Verdaguer, J. Ferré, F. Maseras, M. Besora, O. Pàmies, M. Diéguez, *ACS Catal.* **2023**, *13*, 3020–3035.
[73] M. Biosca, M. Magre, O. Pàmies, M. Diéguez, *ACS Catal.* **2018**, *8*, 10316–10320.
[74] E. Salomó, P. Rojo, P. Hernández-Lladó, A. Riera, X. Verdaguer, *J. Org. Chem.* **2018**, *83*, 4618–4627.
[75] X.-X. Zhang, Y. Zhang, L. Liao, Y. Gao, H. E. M. Su, J.-S. Yu, *ChemCatChem* **2022**, *14*, e202200126.
[76] A. Cabré, M. Garçon, A. Gallen, L. Grisoni, A. Grabulosa, X. Verdaguer, A. Riera, *ChemCatChem* **2020**, *12*, 4112–4120.
[77] F. Eyer, V. Meischner, D. Kiderlen, H. Thiermann, F. Worek, M. Haberkorn, N. Felgenhauer, T. Zilker, P. Eyer, *Toxicol. Rev.* **2003**, *22*, 143–163.

2. Research Objectives

As mentioned in the introduction, phosphine chalcogenides represent an appreciated and valuable class of functional compounds, that can be further enhanced by the introduction of more heteroatomic elements such as nitrogen. The experimental preparation of such aminophosphine chalcogenides may be straightforward for achiral representatives but is even more challenging for *P*-stereogenic examples.

In Chapter three, we sought for a clean method to prepare *P*-stereogenic primary aminophosphine sulfides with high enantiomeric purity. The long-established use of *N*-bound chiral auxiliaries should allow to provide diastereomerically pure precursors and a subsequent reductive C–N bond cleavage reaction is intended to release the desired primary amino moiety. However, problems with the cleavage of the chiral auxiliary, which had not been thoroughly studied in the previous literature, required investigation and improvement towards the desired products. Furthermore, a method of stereoselective discrimination of the aminophosphine sulfides had to be found due to the lack of mechanical means.

Whether chiral or not, the bifunctional pattern of aminophosphine chalcogenides is suitable for the formation of intermolecular interactions such as hydrogen bonding, which is of great interest for organocatalytic processes and supramolecular topics. The importance to comprehend hydrogen-bond-based structural motifs and self-assembled agglomerates, led us to investigate protonated aminophosphine oxides, sulfides and selenides in terms of their aggregation properties into supramolecular synthons in Chapter four.

The functionalizability of achiral and *P*-stereogenic aminophosphine sulfides was meant to be examined by coupling the amino moiety with a hydrosilyl compound and subsequent ring formation by intramolecular stabilization of the silylium center with the P^{+}–S^{-} moiety. In addition, Chapter five deals with the introduction of *Si*-centered chirality into the heterocyclic products in the presence of a *P*-stereogenic center.

The research objectives can briefly be described as follows:

- Preparation of enantiomerically pure *P*-stereogenic primary aminophosphine sulfides
- Investigation and differences of reductive C–N bond cleavage of the chiral auxiliary in aminophosphine sulfides with a phenyl or only alkyl substituents
- Determination of the enantiomeric purity of *P*-stereogenic primary aminophosphine sulfides using chiral shift reagents in NMR spectroscopy
- Studies on the aggregation properties of protonated aminophosphine chalcogenides in solid state and in solution depending on the use of weakly or strongly coordinating anions
- Application of aminophosphine sulfides as coupling partners for silyl chlorides or triflates
- Ring closing reactions of *N*-hydrosilyl-substituted phosphine sulfides by intramolecular Lewis-base stabilization of a Lewis-acidic silylium center
- Experiments towards the stereoselective preparation of four-membered heterocycles with *P*- and *Si*-centered chirality

3. Access to Enantiomerically Pure *P*-Stereogenic Primary Aminophosphine Sulfides under Reductive Conditions

Preface

A synthetic version of the following chapter has already been published.

Authors

Tanja Huber, Noel-Angel Espinosa-Jalapa, Jonathan O. Bauer

Chem. Eur. J. **2022**, *28*, e202202608.

Author contribution

All syntheses and characterisations reported in this work were performed by T. Huber, except for the synthesis of the chiral shift reagents (*R*)-BINOL-PSSM (M = Li, Na, K) and monolithiated (*R*)-BINOL, which were synthesized by Dr. N. A. Espinosa-Jalapa. Quantum chemical calculations were performed by PD Dr. J. O. Bauer. The manuscript and the supporting information were drafted by T. Huber and revised by both Dr. N. A. Espinosa-Jalapa and PD Dr. J. O. Bauer.

Acknowledgements

This work was jointly supported by the Elite Network of Bavaria (ENB), the Bavarian State Ministry of Science and the Arts (StMWK), and the University of Regensburg (Project N-LW-NW-2016-366). The authors also thank Prof. Dr. Manfred Scheer for generous support, Dr. Michael Seidl for helpful discussions regarding X-ray crystallography, and the Scheer group for kindly providing the reagents benzyl sodium and benzyl potassium.

3.1. Abstract

Stereochemically pure phosphines with phosphorus–heteroatom bonds and *P*-centered chirality are a promising class of functional building blocks for the design of chiral ligands and organocatalysts. A route to enantiomerically pure primary aminophosphine sulfides was opened through stereospecific reductive C–N bond cleavage of phosphorus(V) precursors by lithium in liquid ammonia. The chemoselectivity of the reaction as a function of reaction time, substrate pattern, and chiral auxiliary was investigated. In the presence of exclusively aliphatic groups bound to the phosphorus atom, all competing reductive side reactions are totally prevented. The absolute configurations of all *P*-stereogenic compounds were determined by single-crystal X-ray diffraction analysis. Their use as synthetic building blocks was demonstrated. The lithium salt of (*R*)-BINOL-dithiophosphoric acid proved to be a useful stereochemical probe to determine the enantiomeric purity. Insights into the coordination mode of the lithium-based chiral complex formed in solution was provided by NMR spectroscopy and DFT calculations.

3.2. Introduction

Phosphorus-stereogenic phosphines play a central role in asymmetric transition-metal catalysis[1] and have also been used as organocatalysts.[2] Since the seminal work on phosphine ligands with phosphorus-centered chirality by Knowles and co-workers in the late 1960s and 1970s,[3] numerous synthetic methods for the preparation of *P*-stereogenic compounds have been reported.[4] Many synthetic routes to fully carbon-substituted phosphines with stereogenic phosphorus(III) and (V) centers start from tetravalent phosphine–borane adducts[5] or phosphine sulfides and make use of a desymmetrization through kinetically controlled asymmetric deprotonation.[6] Strategies based on a thermodynamic dynamic resolution via lithiated phosphine boranes and sulfides were also reported.[7] Over the past few decades, further elegant routes toward *P*-chiral compounds have been developed. Prominent examples among them are the dynamic kinetic asymmetric oxidation of trivalent phosphines[8] and the (–)-menthol-mediated dynamic kinetic resolution of *P*-stereogenic phosphine oxides.[9] Enantioselective transition-metal-catalyzed procedures have increasingly gained in importance over the past years.[10–12] These processes are essentially based on catalytic asymmetric C–P cross-couplings reactions of secondary phosphines[10] and secondary phosphine oxides,[11] or rely on desymmetrization reactions.[12] Asymmetric organocatalytic variants of desymmetrization and coupling reactions also demonstrate the enormous research output in this field.[13]

Access strategies to *P*-stereogenic P(III) and P(V) phosphines containing additional phosphorus-heteroatom bonds are very desirable due to their great potential for the design of new types of chiral ligand systems[1] and organocatalysts.[2] However, enantiomerically pure *P*-chiral compounds in which the stereogenic phosphorus atom is directly linked to other reactive functionalities are rare and their synthesis strategies strongly limited in terms of functional group compatibility and substrate scope. Chiral auxiliary-based methods,[14] which often involve the separation of mixtures

of diastereomers, are still an integral part in synthesizing structurally versatile *P*-stereogenic compounds, as these methods have the advantage of providing stereochemically pure phosphine precursors for targeted subsequent transformations.[15] In particular, *P*-stereogenic phosphinic acid and aminophosphine derivatives have proven to be highly efficient intermediates,[16] which have contributed significantly to the emergence of new areas of application in recent times.[17] Riera, Verdaguer, and co-workers opened direct access to enantiomerically pure *P*-chiral borane-protected primary aminophosphines (**A**, Figure 3.1, a) by reductive C–N bond cleavage of diasteromerically pure (*S*)-(–)-1-arylethylamino-functionalized phosphine borane precursors.[17d] Their method relies on the important previous work of Kolodiazhnyi et al., who already reported the diastereoselective synthesis of the used precursors.[18]

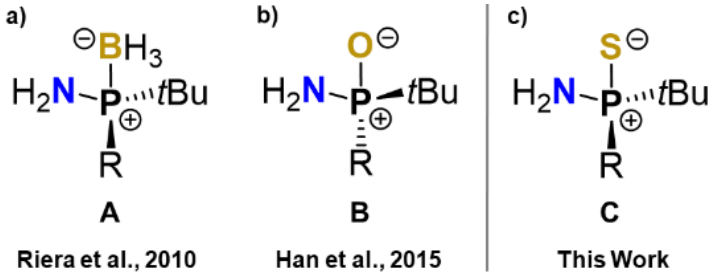

Figure 3.1. Previously reported enantiomerically pure *P*-stereogenic primary aminophosphines. a) Borane-protected aminophosphines (**A**).[17d] b) Aminophosphine oxides (**B**).[17i] c) Aminophosphine sulfides (**C**) reported herein.

The N–P^{+}–O^{-} bonding motif received much attention in asymmetric Brønsted acid[19] and Lewis base organocatalysis[20] and became a central structural feature in the catalyst design. Han et al. reported a chiral auxiliary-based multistep synthesis of enantiomerically pure primary aminophosphine oxides (**B**) via benzoxazaphosphinine-2-oxide templates (Figure 3.1, b).[17i] This is a modification of the widely used[17c,e,g] stereoselective strategy originally developed by Jugé[21] in the way of introducing an inverted reactivity of the P–N and P–O bonds of the cyclic chiral intermediate.[15e,17i] Compounds **B** turned out to be valuable precursors for the design of new organocatalysts.[17i] However their use in catalyst development is strongly limited probably due to the lack of convenient asymmetric synthesis methods.[22] In the context of our work on heterocyclic ring systems,[23] we became interested in stereochemically pure *P*-stereogenic phosphine sulfide moieties. Notably, we found no report in the literature of enantiomerically pure primary aminophosphine sulfides (**C**) exhibiting an H_2N–P^{+}–S^{-} structural motif (Figure 3.1, c).

3.3. Results and Discussion

Herein, we report our studies on the reductive C–N bond cleavage of stereochemically pure *P*-stereogenic phosphorus(V) precursors by lithium dissolved in liquid ammonia to provide enantiomerically pure primary aminophosphine sulfides. We thoroughly investigated the competition between C–N bond cleavage, Birch-type reduction, P–Ph cleavage, and desulfurization in aromatic and aliphatic phosphine sulfides depending on the reaction time and the chiral auxiliary used. The use of the enantiomerically pure primary aminophosphine sulfides as synthetic building

blocks was shown in an example. We also introduced a practical method to determine the enantiomeric purity of primary aminophosphine sulfides using the lithium salt of (*R*)-BINOL-dithiophosphoric acid [(*R*)-BINOL-PSSLi]. NMR spectroscopy accompanied by computational investigations of the chiral complex formed in solution provided important insights into the interplay of hydrogen-bonding and coordinative metal-ligand interactions. To the best of our knowledge, this is the first report on the synthesis of enantiomerically pure *P*-stereogenic primary aminophosphine sulfides.

3.3.1. Synthesis of Diastereomerically Pure (S_P,*S*)-4 and (S_P,*S*)-5

In order to provide suitable stereochemically pure *P*-stereogenic precursors, we resorted to a chiral auxiliary-based method developed by Kolodiazhnyi and co-workers.[18] We first reacted racemic *tert*-butylchlorophenylphosphine (**1**) with (*S*)-(–)-1-phenylethylamine [(*S*)-**2**] and (*S*)-(–)-1-(1-naphthyl)ethylamine [(*S*)-**3**] (Scheme 3.1). It is known that the coupling of both racemic phosphorus(III) and phosphorus(V) chlorides with chiral amines and alcohols leads to unequal mixtures of both diastereomers[17d,18,22b,24], which strongly depends on the reaction conditions.[18,24b] The phosphorus(III) intermediates were not isolated and reacted directly with elemental sulfur in a second step to compounds **4** and **5**, respectively. The diastereomeric ratios of the auxiliary-substituted phosphine sulfides were determined by means of ^{31}P and ^{1}H NMR spectroscopy. The phenyl-substituted compounds (S_P,*S*)-**4** and (S_P,*S*)-**5** were obtained in a diastereomeric ratio of 6:1 and 12:1, respectively. After fractional crystallization, the main diastereomer was obtained in stereochemically pure form for both derivatives **4** and **5**, and with overall yields of 27% [(S_P,*S*)-**4**] and 51% [(S_P,*S*)-**5**].

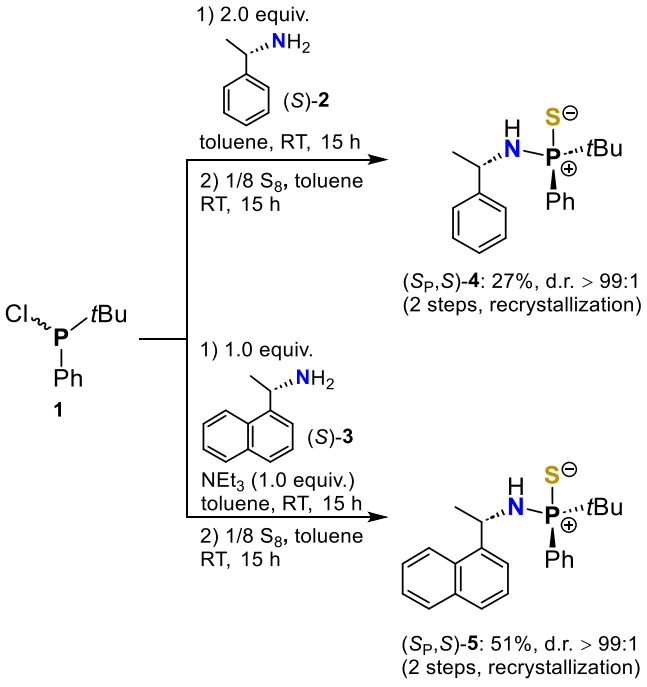

Scheme 3.1. Synthesis of the stereochemically pure phosphorus(V) precursors (S_P,*S*)-**4** and (S_P,*S*)-**5**.

The absolute configuration at the stereogenic phosphorus center was determined to be S_P for both compounds by single-crystal X-ray structural analysis. Diastereomer (S_P,*S*)-**4** crystallized in the orthorhombic crystal system, space group $P2_12_12_1$, and diastereomer (S_P,*S*)-**5** in the monoclinic crystal system, space group $P2_1$ (Figure 3.2).

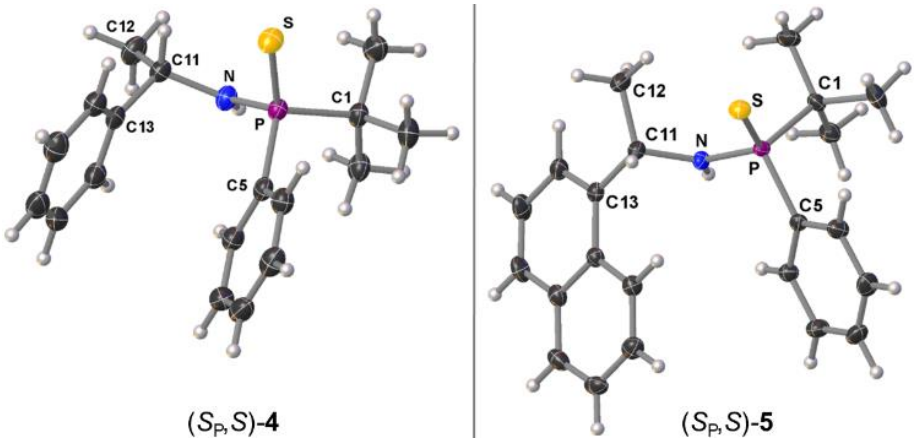

Figure 3.2. Molecular structures of compounds (S_P,*S*)-**4** and (S_P,*S*)-**5** in the crystal (displacement ellipsoids set at the 50 % probability level).

3.3.2. Reductive C–N Bond Cleavage of (S_P,*S*)-4 and (S_P,*S*)-5

In a next step, we investigated whether a selective reductive C–N bond cleavage can be applied to the stereochemically pure phenylethyl- and naphthylethyl-substituted phosphorus(V) starting compounds (S_P,*S*)-**4** and (S_P,*S*)-**5**. At first glance, this seems to be challenging under these strongly reducing conditions as these types of compounds might also be sensitive to reduction of the phosphorus(V) center in addition to the possibility of a Birch-type reduction of the phosphorus-bound phenyl ring or even full cleavage of the P–Ph moiety. For this purpose, we first reacted compound (S_P,*S*)-**4** in a solution of lithium in liquid ammonia in the presence of *tert*-butanol for either one, two, or three minutes before quenching the reaction with ammonium chloride (Table 3.1). We could unequivocally identify and fully characterize two main products, (R_P)-**6** and (R_P,*S*)-**7**, both now having a cyclohexadienyl ring bound to the phosphorus atom. Their ratios, determined by ^{31}P NMR spectroscopy, depended sensitively on the reaction time. Apparently, the Birch-type reduction[25] of the phenyl ring attached to the phosphorus atom occurs before the reductive C–N bond cleavage, a finding consistent with the observation on (*S*)-(–)-1-phenylethylamino-substituted phosphine boranes.[17d] Hence, starting from the phenylethyl-substituted phosphine sulfide (S_P,*S*)-**4**, the product of selective C–N bond cleavage with a still intact P–Ph group [(S_P)-**8**] was never observed. Since the phosphorus atom is unaffected in the reactions toward (R_P)-**6** and (R_P,*S*)-**7**, we expected the formation of both compounds to occur with retention of configuration at the stereogenic phosphorus atom. We were indeed able to isolate single-crystals of (R_P,*S*)-**7** and (R_P)-**6** to confirm the proposed absolute configuration at the phosphorus atom by single-crystal X-ray diffraction analysis (Figure 3.3, top). Both compounds crystallized in the orthorhombic crystal system, space group $P2_12_12_1$.

Table 3.1. Time-dependent product ratios formed under the reductive conditions for the cleavage of the chiral auxiliary.

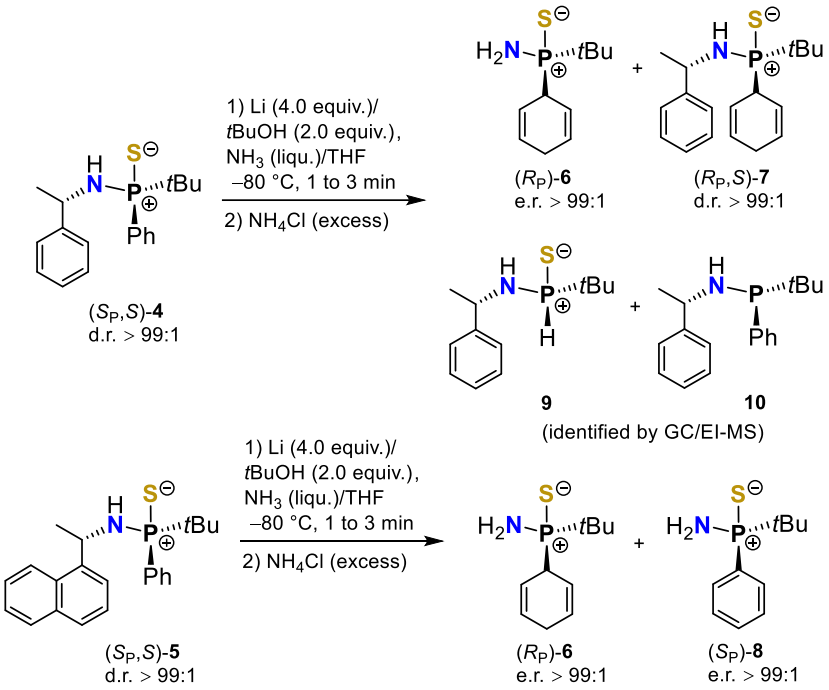

Starting material	(S_P,S)-**4**		
Reaction time [min]	1	2	3
Ratio (R_P)-**6**/(R_P,S)-**7**/**9**/**10**	13:49:21:17	37:22:26:15	41:15:27:17
Starting material	(S_P,S)-**5**		
Reaction time [min]	1	2	3
Ratio (R_P)-**6**/(S_P)-**8**	34:66	38:62	53:47

The Birch-type reduction of phosphorus-bound phenyl rings by metals dissolved in liquid ammonia has previously been studied on phosphine boranes, which was often accompanied by P–Ph cleavage as the most important side reaction.[26] In fact, during the reaction of compound (S_P,S)-**4** with lithium/*tert*-butanol in liquid ammonia, two additional products, **9** and **10**, were obtained in a ratio of approximately 1.5:1, which remained almost constant over all reaction times between 1 to 3 min (Table 3.1). Species **9** and **10** together accounted for about 41% of the total products formed (for details, see Chapter 3.6.2.4). GC/EI-MS analysis indicated that compound **9** was the product of a P–Ph bond cleavage, and **10** the desulfurized phosphorus(III) species. The P–S bond cleavage of phosphine sulfides by alkali metals in liquid ammonia is known.[27] The transfer of an electron from the π* orbital of a phenyl substituent to the σ* orbital of the P–S bond was thought to be an important step in the mechanism.[28] In both compounds **9** and **10**, the chiral auxiliary is still attached to the phosphorus atom. Apparently, the formation of these products competes with the Birch-type reduction of the phosphorus-bound phenyl ring right at the beginning of the reaction. Remarkably, as the reaction proceeds, the product composition depends only on the rate of the subsequent reductive C–N bond cleavage of (R_P,S)-**7**, leading to (R_P)-**6**.

The envisioned product (S_P)-**8** as a result of selective C–N bond cleavage was only formed when using the (*S*)-(–)-1-(1-naphthyl)ethylamino-substituted phosphine (S_P,*S*)-**5** (Table 3.1). One reason may be the different reduction potentials of the phenyl and naphthyl groups of (S_P,*S*)-**4** and (S_P,*S*)-**5**, respectively, in terms of the initial formation of the radical anions.[29] Another explanation might be the higher stability of the 1-(1-naphthyl)ethide anion over the 1-phenylethide anion, which are both formed as a result of the reductive C–N bond cleavage.[29] However, different from what was described for P(III) phosphine boranes,[17d] the phenyl ring of P(V) phosphine sulfides was not necessarily spared from the Birch-type reduction just by using the naphthylethyl fragment within the intramolecular auxiliary. The longer the substrate was exposed to the reductive conditions, the more the product ratio (R_P)-**6**/(S_P)-**8** was shifted toward the Birch-type-reduced product (R_P)-**6** (34:66 after 1 min, 53:47 after 3 min) (Table 3.1). Smaller amounts of unspecified by-products were obtained from the reaction of compound (S_P,*S*)-**5** with lithium/*tert*-butanol in liquid ammonia, which, however, show ^{31}P NMR signals in a chemical shift range similar to that of compounds **9** and **10**.

Also for compound (S_P)-**8** the absolute configuration at the stereogenic phosphorus atom could be unambiguously assigned and confirmed by single-crystal X-ray structural analysis (monoclinic crystal system, space group $P2_1$) (Figure 3.3, bottom). The racemic form of the compound [(*rac*)-**8**] was synthesized separately for determining the stereochemical purity of (S_P)-**8** (see below). The molecular structure of (*rac*)-**8** was also determined by single-crystal X-ray crystallography (monoclinic crystal system, space group $P2_1/n$) (Figure 3.3, bottom).

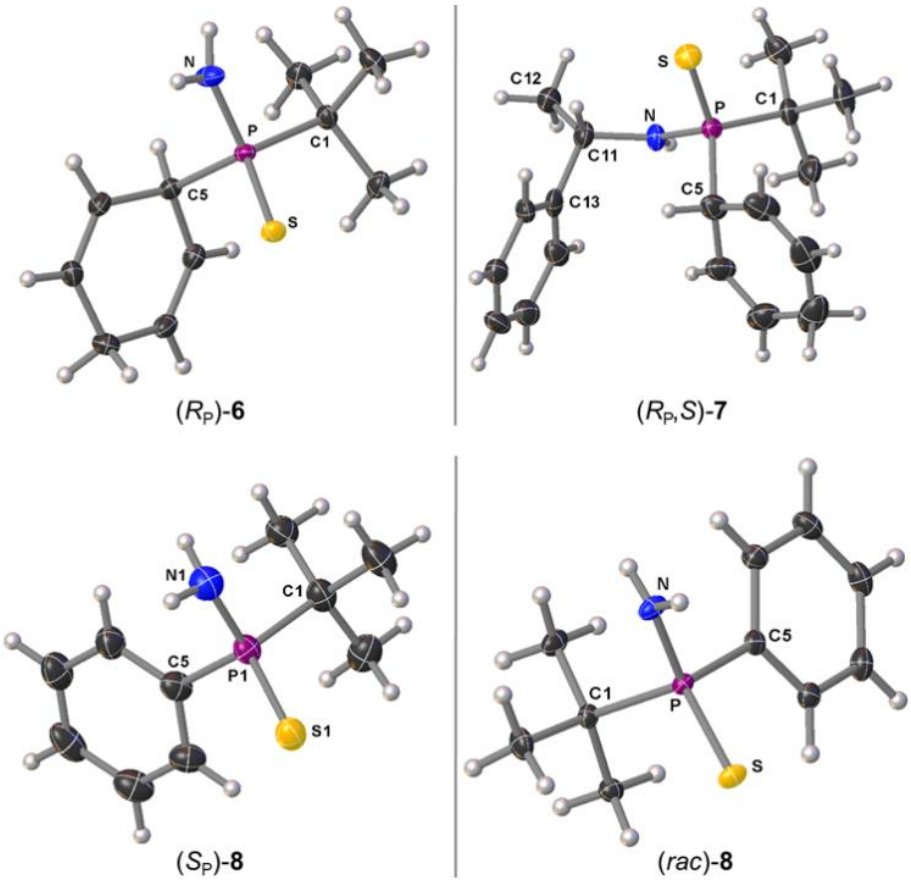

Figure 3.3. Molecular structures of compounds (R_P)-**6** and (R_P,*S*)-**7** (top), and (S_P)-**8** and (*rac*)-**8** (bottom) in the crystal (displacement ellipsoids set at the 50 % probability level).

3.3.3. Synthesis and Reductive C–N Bond Cleavage of (R_P,*S*)-12

Although the use of the (1-naphthyl)ethylamino-patterned starting material (S_P,*S*)-**5** does in fact result in much faster C–N bond cleavage and hence reasonable amounts of the desired primary aminophenylphosphine (S_P)-**8**, the chemoselectivity of the reaction using phosphine sulfides with a phosphorus-bound phenyl group appears to be difficult to control and extremely short reaction times are required to suppress the undesired Birch-type reduction of the phenyl ring. Moreover, phosphorus(V) compounds appear to be generally more susceptible to Birch-type reduction or P–Ph cleavage by alkali metals dissolved in liquid ammonia than phosphorus(III) compounds.

We therefore set out to investigate how phosphorus(V) sulfides with only aliphatic groups bound to the phosphorus atom react under these strongly reductive conditions. For this purpose, we synthesized the cyclohexyl derivative (R_P,*S*)-**12** in two steps starting from *tert*-butylchlorocyclohexylphosphine (**11**) and (*S*)-(–)-1-phenylethylamine [(*S*)-**2**] by using the same proven methodology as outlined above (Scheme 3.2). Compound (R_P,*S*)-**12** was initially obtained in a diastereomeric ratio of 3:1. Recrystallization provided the diastereomerically pure precursor in 32% overall yield. Surprisingly, by replacing the phenyl group with a cyclohexyl group, the subsequent reaction of compound (R_P,*S*)-**12** with lithium in liquid ammonia proceeded with excellent chemoselectivity and led exclusively to the stereospecific C–N bond cleavage to give the desired product (R_P)-**13** in enantiomerically pure form and in a high yield of 94%. The complete absence of a P–S bond cleavage in the case of fully aliphatic substitution patterns impressively shows that a phosphorus-bound aryl group is indeed required for initiating a desulfurization process.

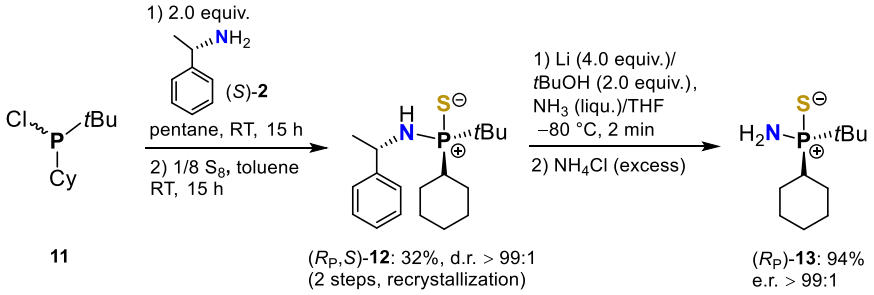

Scheme 3.2. Stereospecific, reductive C–N bond cleavage of (R_P,*S*)-**12** to enantiomerically pure *P*-chiral primary aminophosphine sulfide (R_P)-**13**.

The stereoisomers (R_P,*S*)-**12** and (R_P)-**13** could be obtained in single-crystalline form and subjected to single-crystal X-ray structure analysis for confirming the absolute configuration at the stereogenic phosphorus atom. Compound (R_P,*S*)-**12** crystallized in the orthorhombic crystal system, space group $P2_12_12_1$, and the cleavage product (R_P)-**13** in the trigonal crystal system, space group $P3_2$ (Figure 3.4).

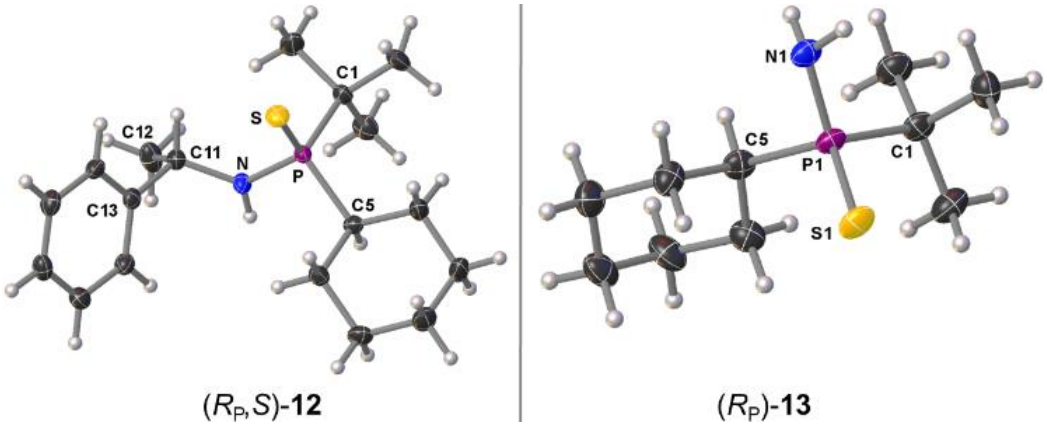

Figure 3.4. Molecular structures of compounds (R_P,*S*)-**12** and (R_P)-**13** in the crystal (displacement ellipsoids set at the 50 % probability level).

3.3.4. Determination of the Stereochemical Purity of (S_P)-8 and (R_P)-13, and Structural Proposal of the Chiral Shift Reagent Complex

In order to determine the enantiomeric purity of compounds (S_P)-**8** and (R_P)-**13**, we first attempted a method that has previously been used for the NMR spectroscopic determination of the enantiomeric purity of silyl pyridines.[30] This method is based on the use of (*R*)-BINOL-dithiophosphoric acid [(*R*)-BINOL-PSSH][31] as Brønsted acidic chiral shift reagent. After preparation of the respective racemic compounds (*rac*)-**8** and (*rac*)-**13**, we tested the ability of (*R*)-BINOL-PSSH as stereochemical probe for our new *P*-stereogenic primary aminophosphine sulfides. However, diastereotopic discrimination could not be achieved for the racemic mixtures either in the ^{1}H or the ^{31}P NMR spectra, which is probably due to the low basicity of the $H_2N–P^+–S^-$ unit. We therefore adapted the procedure for our aminophosphine sulfides by using the lithiated (*R*)-BINOL-dithiophosphoric acid [(*R*)-BINOL-PSSLi] (Scheme 3.3). Apparently, the lithium ion has an important structure-stabilizing effect and consequently leads to significant ^{1}H and ^{31}P NMR spectroscopic discrimination between the two diastereomers formed when the racemic compounds are used. The formation of a structure like **D** in dichloromethane solution was supported by quantum chemical calculations on the M062X/6-31+G(d) level of theory[32] using the polarizable continuum model (PCM)[33] (solvent: dichloromethane). The calculated structure **D**-Cy (R = cyclohexyl) of [(*R*)-BINOL-PSSLi·(R_P)-**13**] exhibits the lowest energy among all optimized, plausible structures in dichloromethane (for details, see Chapter 3.8). It shows that the interplay of both coordinative and hydrogen-bonding interactions may play an important role in the formation of a rigid structure required for efficient diastereotopic discrimination (Scheme 3.3). A tetrahedral coordination of the lithium center and all coordination modes with an involved $H_2N\cdots Li$ interaction turned out to be energetically less favorable than structure **D**-Cy.

In **D**-Cy, the lithium center is coordinated in a trigonal-pyramidal fashion by three sulfide donor atoms. The NH_2 function appears to be involved in the structure formation via a weak N–H···S hydrogen bond. The ^{1}H NMR spectrum of compound (R_P)-**13** in the presence of (*R*)-BINOL-PSSLi in dichloromethane shows a slightly downfield-shifted NH_2 signal at 2.35 ppm compared to the

broad signal of the pure compound (R_P)-**13** (δ = 2.12 ppm). For compound (*rac*)-**8**, which actually shows a broad NH_2 signal at δ = 2.60 ppm in dichloromethane, the presence of (*R*)-BINOL-PSSLi even leads to a splitting of the NH_2 group into two sharp slightly downfield-shifted signals at 2.69 and 2.74 ppm, probably corresponding to the two diagnostic diastereomers. These findings support an involvement of the primary amino group in the complex formation, presumably through weak hydrogen-bonding interaction with a sulfide acceptor of the dithiophosphoric acid unit according to the proposed model **D**.[34] For comparison, the NH signal of the lithium amide (*rac*)-**13**-Li in dichloromethane is considerably highfield-shifted to 0.24 ppm. Therefore, complete deprotonation of the amino function along with an HN···Li interaction in the reaction of the aminophosphine sulfide with (*R*)-BINOL-PSSLi can be excluded. This is also in accordance with acidity considerations (higher Brønsted acidity of the P–SH compared to the NH_2 function). In this context, it seems logical that the same result is also obtained if the reaction is carried out vice versa, i.e. the respective lithium amide and (*R*)-BINOL-PSSH are reacted.

We also examined the sodium and potassium salts of (*R*)-BINOL-dithiophosphoric acid as well as monolithiated (*R*)-BINOL for their ability to discriminate between the two enantiomers of *P*-stereogenic aminophosphine sulfides. However, this resulted in either no splitting at all [in the case of (*R*)-BINOL-Li] or only insufficient splitting [when using (*R*)-BINOL-PSSNa and (*R*)-BINOL-PSSK]. The ^{7}Li NMR spectrum of the complex formed from (*rac*)-**13** and (*R*)-BINOL-PSSLi in dichloromethane shows a signal at δ = 0.4 ppm. In order to strengthen our structural hypothesis in solution, we performed DFT calculations on the ^{7}Li NMR chemical shift for the computed complexes on the M062X/6-311+G(2d,p)//M062X/6-31+G(d) level of theory[32] using the gauge-independent atomic orbital (GIAO)[35] method (for details, see Chapter 3.8). The calculated ^{7}Li NMR chemical shift of δ = 0.3 ppm for **D**-Cy fits perfectly with the experimentally measured shift. Based on all spectroscopic and computational data, we can indeed consider complex **D** as a plausible structural proposal in dichloromethane solution (Scheme 3.3).

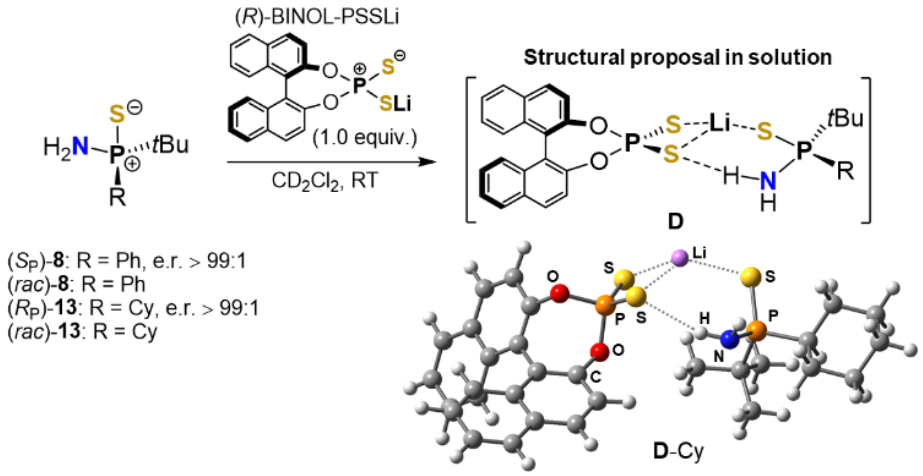

Scheme 3.3. Determination of the enantiomeric purity of primary aminophosphine sulfides by NMR spectroscopy using lithiated (*R*)-BINOL-PSSH as chiral probe (top). Calculated model (**D**-Cy) of the structural proposal **D** (bottom) [M062X/6-31+G(d); PCM solvent: dichloromethane].[32,33]

Finally, the ^{1}H and ^{31}P NMR spectra of the enantiomerically pure samples in the presence of (*R*)-BINOL-PSSLi nicely proved the stereospecificity of the reductive C–N bond cleavage and hence the enantiomeric ratios of e.r. > 99:1 of the primary aminophosphine sulfides (S_P)-**8** and (R_P)-**13** (for details, see Chapter 3.6.2.12). This method, based on the lithium salt of (*R*)-BINOL-PSSH, can be a valuable spectroscopic tool for determining the enantiomeric purity of weakly basic chiral compounds or chiral substances that are sensitive to Brønsted acids.

3.3.5. Functionalization of (R_P)-13

The *P*-stereogenic primary aminophosphine sulfides represent a valuable class of functional precursors that can be added to the molecular repertoire for the synthesis of new phosphine-based asymmetric catalyst systems. In order to demonstrate the applicability for further functionalization, we performed an N–Si coupling through lithiation of the enantiomerically pure compound (R_P)-**13** followed by reaction with di-*tert*-butylchlorosilane (Scheme 3.4). The Si–H bond of the resulting *N*-hydrosilyl-substituted phosphine sulfide (R_P)-**14** has great synthetic potential for carrying out further transformations.[23,36] Stereochemically pure compound (R_P)-**14** was isolated in single-crystalline form from a diethyl ether solution (24% yield) and characterized by single-crystal X-ray crystallography (orthorhombic crystal system, space group $P2_12_12_1$) (Figure 3.5).

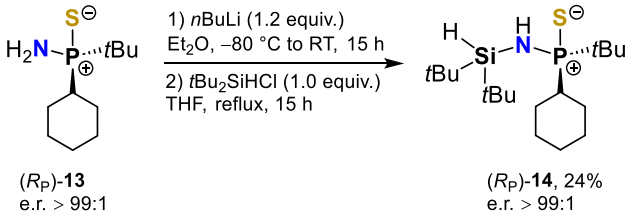

Scheme 3.4. Functionalization of the primary amino group of enantiomerically pure (R_P)-**13** through lithiation and reaction with a chlorohydrosilane. The yield refers to crystalline material obtained directly from the mother liquor.

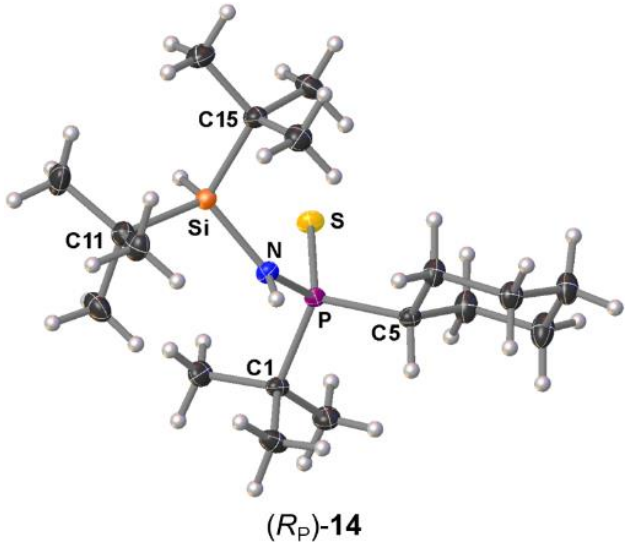

Figure 3.5. Molecular structure of compound (R_P)-**14** in the crystal (displacement ellipsoids set at the 50 % probability level).

3.4. Conclusion

In conclusion, easy synthetic access to enantiomerically pure *P*-stereogenic primary aminophosphine sulfides was opened. By a sequence of P–N coupling of racemic chlorophosphines with a chiral amine, separation of the diastereomers, and subsequent reductive C–N bond cleavage in solutions of lithium in liquid ammonia, enantiomerically pure primary aminophosphine sulfides [(R_P)-**6**, (S_P)-**8**, and (R_P)-**13**] were obtained for the first time. The competition between reductive C–N bond cleavage, Birch-type reduction, P–Ph cleavage, and desulfurization when using phenyl-substituted phosphine sulfides depending on the reaction time and the chiral auxiliary used was investigated in detail. Undesirable reductive side reactions during the cleavage of the chiral auxiliary can be completely avoided by exclusively using aliphatic substitution patterns as shown for a cyclohexyl-substituted derivative. The absolute configuration of all *P*-stereogenic compounds was determined by single-crystal X-ray crystallography and the enantiomeric purity of the primary aminophosphine sulfides determined by NMR spectroscopy using the lithium salt of (*R*)-BINOL-dithiophosphoric acid [(*R*)-BINOL-PSSLi] as an efficient chiral shift reagent. This method could be particularly useful for weakly basic or Brønsted acid-sensitive chiral substances. NMR spectroscopic and computational studies on a plausible [(*R*)-BINOL-PSSLi·(R_P)-**13**] complex in solution provided important insights into structure-forming coordination principles. The *P*-stereogenic primary aminophosphine sulfides can provide a basis for the design of new chiral ligands and organocatalysts. First steps in this direction were shown by the successful functionalization of the primary amino function by a hydrosilyl moiety.

3.5. References

[1] For reviews, see: a) T. Hayashi, *Acc. Chem. Res.* **2000**, *33*, 354–362; b) W. Tang, X. Zhang, *Chem. Rev.* **2003**, *103*, 3029–3069; c) K. V. L. Crépy, T. Imamoto, *Adv. Synth. Catal.* **2003**, *345*, 79–101; d) K. V. L. Crépy, T. Imamoto, *Top. Curr. Chem.* **2003**, *229*, 1–40; e) S. Lühr, J. Holz, A. Börner, *ChemCatChem* **2011**, *3*, 1708–1730; f) P. W. N. M. van Leeuwen, P. C. J. Kamer, C. Claver, O. Pàmies, M. Diéguez, *Chem. Rev.* **2011**, *111*, 2077–2118.

[2] a) J. L. Methot, W. R. Roush, *Adv. Synth. Catal.* **2004**, *346*, 1035–1050; b) A. Marinetti, A. Voituriez, *Synlett* **2010**, 174–194; c) Y. Xiao, Z. Sun, H. Guo, O. Kwon, *Beilstein J. Org. Chem.* **2014**, *10*, 2089–2121; d) A. J. Smaligo, S. Vardhineedi, O. Kwon, *ACS Catal.* **2018**, *8*, 5188–5192; e) H. Y. Su, M. S. Taylor, *J. Org. Chem.* **2017**, *82*, 3173–3182; f) H. Qiu, Q. Dai, J. He, W. Li, J. Zhang, *Chem. Sci.* **2020**, *11*, 9983–9988; g) C. E. Henry, Q. Xu, Y. C. Fan, T. J. Martin, L. Belding, T. Dudding, O. Kwon, *J. Am. Chem. Soc.* **2014**, *136*, 11890–11893.

[3] a) W. S. Knowles, M. J. Sabacky, *Chem. Commun.* **1968**, 1445–1446; b) W. S. Knowles, M. J. Sabacky, B. D. Vineyard, D. J. Weinkauff, *J. Am. Chem. Soc.* **1975**, *97*, 2567–2568; c) B. D. Vineyard, W. S. Knowles, M. J. Sabacky, G. L. Bachman, D. J. Weinkauff, *J. Am. Chem. Soc.* **1977**, *99*, 5946–5952; d) W. S. Knowles, *Angew. Chem. Int. Ed.* **2002**, *41*, 1998–2007; *Angew. Chem.* **2002**, *114*, 2096–2107.

[4] For reviews, see: a) K. M. Pietrusiewicz, M. Zabłocka, *Chem. Rev.* **1994**, *94*, 1375–1411; b) A. Grabulosa, J. Granell, G. Muller, *Coord. Chem. Rev.* **2007**, *251*, 25–90; c) D. S. Glueck, *Synlett* **2007**, 2627–2634; d) J. S. Harvey, V. Gouverneur, *Chem. Commun.* **2010**, *46*, 7477–7485; e) O. I. Kolodiazhnyi, *Tetrahedron: Asymmetry* **2012**, *23*, 1–46; f) O. I. Kolodiazhnyi, *Top. Curr. Chem.* **2014**, *360*, 161–236; g) M. Dutartre, J. Bayardon, S. Jugé, *Chem. Soc. Rev.* **2016**, *45*, 5771–5794; h) D. S. Glueck, *Synthesis* **2022**, *54*, 271–280.

[5] M. Ohff, J. Holz, M. Quirmbach, A. Börner, *Synthesis* **1998**, 1391–1415.

[6] a) A. R. Muci, K. R. Campos, D. A. Evans, *J. Am. Chem. Soc.* **1995**, *117*, 9075–9076; b) T. Imamoto, J. Watanabe, Y. Wada, H. Masuda, H. Yamada, H. Tsuruta, S. Matsukawa, K. Yamaguchi, *J. Am. Chem. Soc.* **1998**, *120*, 1635–1636; c) W. Tang, X. Zhang, *Angew. Chem. Int. Ed.* **2002**, *41*, 1612–1614; *Angew. Chem.* **2002**, *114*, 1682–1684; d) W. Tang, W. Wang, X. Zhang, *Angew. Chem. Int. Ed.* **2003**, *42*, 943–946; *Angew. Chem.* **2003**, *115*, 973–976; e) T. Imamoto, K. Sugita, K. Yoshida, *J. Am. Chem. Soc.* **2005**, *127*, 11934–11935; f) J. J. Gammon, S. J. Canipa, P. O'Brien, B. Kelly, S. Taylor, *Chem. Commun.* **2008**, 3750–3752; g) J. J. Gammon, P. O'Brien, B. Kelly, *Org. Lett.* **2009**, *11*, 5022–5025; h) J. Granander, F. Secci, S. J. Canipa, P. O'Brien, B. Kelly, *J. Org. Chem.* **2011**, *76*, 4794–4799.

[7] a) B. Wolfe, T. Livinghouse, *J. Am. Chem. Soc.* **1998**, *120*, 5116–5117; b) J. J. Gammon, V. H. Gessner, G. R. Barker, J. Granander, A. C. Whitwood, C. Strohmann, P. O'Brien, B. Kelly, *J. Am. Chem. Soc.* **2010**, *132*, 13922–13927.

[8] E. Bergin, C. T. O'Connor, S. B. Robinson, E. M. McGarrigle, C. P. O'Mahony, D. G. Gilheany, *J. Am. Chem. Soc.* **2007**, *129*, 9566–9567.

[9] K. Nikitin, K. V. Rajendran, H. Müller–Bunz, D. G. Gilheany, *Angew. Chem. Int. Ed.* **2014**, *53*, 1906–1909; *Angew. Chem.* **2014**, *126*, 1937–1940.

[10] a) J. R. Moncaraz, N. F. Laritcheva, D. S. Glueck, *J. Am. Chem. Soc.* **2002**, *124*, 13356–13357; b) C. Scriban, D. S. Glueck, *J. Am. Chem. Soc.* **2006**, *128*, 2788–2789; c) V. C. Chan, M. Chiu, R. G. Bergman, F. D. Toste, *J. Am. Chem. Soc.* **2009**, *131*, 6021–6032; d) S. Zhang, J.-Z. Xiao, Y.-B. Li, C.-Y. Shi, L. Yin, *J. Am. Chem. Soc.* **2021**, *143*, 9912–9921.

[11] a) Q. Dai, W. Li, Z. Li, J. Zhang, *J. Am. Chem. Soc.* **2019**, *141*, 20556–20564; b) Z.-H. Wu, A.-Q. Cheng, M. Yuan, Y.-X. Zhao, H.-L. Yang, L.-H. Wie, H.-Y. Wang, T. Wang, Z. Zhang, W.-L. Duan, *Angew. Chem. Int. Ed.* **2021**, *60*, 27241–27246; *Angew. Chem.* **2021**, *133*, 27447–27452; c) Q. Dai, L. Liu, J. Zhang, *Angew. Chem. Int. Ed.* **2021**, *60*, 27247–27252; *Angew. Chem.* **2021**, *133*, 27453–27458; d) Y. Li, X. Jin, P. Liu, H. Zhang, X. Yu, Y. Liu, B. Liu, W. Yang, *Angew. Chem. Int. Ed.* **2022**, *61*, e202117093; *Angew. Chem.* **2022**, *134*, e202117093; e) W.-Q. Cai, Q. Wie, Q.-W. Zhang, *Org. Lett.* **2022**, *24*, 1258–1262.

[12] a) J. S. Harvey, S. J. Malcolmson, K. S. Dunne, S. J. Meek, A. L. Thompson, R. R. Schrock, A. H. Hoveyda, V. Gouverneur, *Angew. Chem. Int. Ed.* **2009**, *48*, 762–766; *Angew. Chem.* **2009**, *121*, 776–780; b) Z.-J. Du, J. Guan, G.-J. Wu, P. Xu, L.-X. Gao, F.-S. Han, *J. Am. Chem.*

Soc. **2015**, *137*, 632–635; c) Z.-Q. Lin, W.-Z. Wang, S.-B. Yan, W.-L. Duan, *Angew. Chem. Int. Ed.* **2015**, *54*, 6265–6269; *Angew. Chem.* **2015**, *127*, 6363–6367; d) Y. Sun, N. Cramer, *Angew. Chem. Int. Ed.* **2017**, *56*, 364–367; *Angew. Chem.* **2017**, *129*, 370–373; e) C. Wang, K. Huang, J. Ye, W.-L. Duan, *J. Am. Chem. Soc.* **2021**, *143*, 5685–5690.

[13] a) Y. Toda, M. Pink, J. N. Johnston, *J. Am. Chem. Soc.* **2014**, *136*, 14734–14737; b) Z. Huang, X. Huang, B. Li, C. Mou, S. Yang, B.-A. Song, Y. R. Chi, *J. Am. Chem. Soc.* **2016**, *138*, 7524–7527; c) G.-H. Yang, Y. Li, X. Li, J.-P. Cheng, *Chem. Sci.* **2019**, *10*, 4322–4327; d) Q.-H. Huang, Q.-Y. Zhou, C. Yang, L. Chen, J.-P. Cheng, X. Li, *Chem. Sci.* **2021**, *12*, 4582–4587.

[14] Y. Gnas, F. Glorius, *Synthesis* **2006**, 1899–1930.

[15] a) E. J. Corey, Z. Chen, G. J. Tanoury, *J. Am. Chem. Soc.* **1993**, *115*, 11000–11001; b) C. Bauduin, D. Moulin, E. B. Kaloun, C. Darcel, S. Jugé, *J. Org. Chem.* **2003**, *68*, 4293–4301; c) T. Kimura, T. Murai, *Chem. Commun.* **2005**, 4077–4079; d) D. Gatineau, L. Giordano, G. Buono, *J. Am. Chem. Soc.* **2011**, *133*, 10728–10731; e) Z. S. Han, N. Goyal, M. A. Herbage, J. D. Sieber, B. Qu, Y. Xu, Z. Li, J. T. Reeves, J.-N. Desrosiers, S. Ma, N. Grinberg, H. Lee, H. P. R. Mangunuru, Y. Zhang, D. Krishnamurthy, B. Z. Lu, J. J. Song, G. Wang, C. H. Senanayake, *J. Am. Chem. Soc.* **2013**, *135*, 2474–2477; f) O. Berger, J.-L. Montchamp, *Angew. Chem. Int. Ed.* **2013**, *52*, 11377–11380; *Angew. Chem.* **2013**, *125*, 11587–11590; g) A. Włodarczyk, A. E. Kozioł, M. Stankevič, *Eur. J. Org. Chem.* **2018**, 1589–1600; h) K. Kuwabara, Y. Maekawa, T. Murai, *Tetrahedron* **2020**, *76*, 131152–131169; i) K. Kuwabara, Y. Maekawa, M. Minoura, T. Maruyama, T. Murai, *J. Org. Chem.* **2020**, *85*, 14446–14455; j) K. R. Winters, J.-L. Montchamp, *J. Org. Chem.* **2020**, *85*, 14545–14558.

[16] a) M. Stankevič, K. M. Pietrusiewicz, *J. Org. Chem.* **2007**, *72*, 816–822; b) A. Cabré, A. Riera, X. Verdaguer, *Acc. Chem. Res.* **2020**, *53*, 676–689.

[17] a) J.-V. Naubron, L. Giordano, F. Fotiadu, T. Bürgi, N. Vanthuyne, C. Roussel, G. Buono, *J. Org. Chem.* **2006**, *71*, 5586–5593; b) D. Moraleda, D. Gatineau, D. Martin, L. Giordano, G. Buono, *Chem. Commun.* **2008**, 3031–3033; c) R. den Heeten, B. H. Swennenhuis, P. W. N. M. van Leeuwen, J. G. de Vries, P. C. J. Kamer, *Angew. Chem. Int. Ed.* **2008**, *47*, 6602–6605; *Angew. Chem.* **2008**, *120*, 6704–6707; d) M. Revés, C. Ferrer, T. León, S. Doran, P. Etayo, A. Vidal-Ferran, A. Riera, X. Verdaguer, *Angew. Chem. Int. Ed.* **2010**, *49*, 9452–9455; *Angew. Chem.* **2010**, *122*, 9642–9645; e) T. León, A. Riera, X. Verdaguer, *J. Am. Chem. Soc.* **2011**, *133*, 5740–5743; f) T. León, M. Parera, A. Roglans, A. Riera, X. Verdaguer, *Angew. Chem. Int. Ed.* **2012**, *51*, 6951–6955; *Angew. Chem.* **2012**, *124*, 7057–7061; g) H. Zijlstra, T. León, A. de Cózar, C. F. Guerra, D. Byrom, A. Riera, X. Verdaguer, F. M. Bickelhaupt, *J. Am. Chem. Soc.* **2013**, *135*, 4483–4491; h) A. Flores-Gaspar, S. Orgué, A. Grabulosa, A. Riera, X. Verdaguer, *Chem. Commun.* **2015**, *51*, 1941–1944; i) Z. S. Han, L. Zhang, Y. Xu, J. D. Sieber, M. A. Marsini, Z. Li, J. T. Reeves, K. R. Fandrick, N. D. Patel, J.-N. Desrosiers, B. Qu, A. Chen, D. M. Rudzinski, L. P. Samankumara, S. Ma, N. Grinberg, F. Roschangar, N. K. Yee, G. Wang, J. J. Song, C. H. Senanayake, *Angew. Chem. Int. Ed.* **2015**, *54*, 5474–5477; *Angew. Chem.* **2015**, *127*, 5564–5567; j) A. Prades, S. Núñez-Pertiñez, A. Riera, X. Verdaguer, *Chem. Commun.* **2017**, *53*, 4605–4608; k) E. Salomó, A. Prades, A. Riera, X. Verdaguer, *J. Org. Chem.* **2017**, *82*, 7065–7069; l) A. Gallen, S. Orgué, G. Muller, E. C. Escudero–Adán, A. Riera, X. Verdaguer, A. Grabulosa, *Dalton Trans.* **2018**, *47*, 5366–5379; m) S. Lemouzy, R. Membrat, E. Olivieri, M. Jean, M. Albalat, D. Nuel, L. Giordano, D. Hérault, G. Buono, *J. Org. Chem.* **2019**, *84*, 4551–4557.

[18] O. I. Kolodiazhnyi, E. V. Gryshkun, N. V. Andrushko, M. Freytag, P. G. Jones, R. Schmutzler, *Tetrahedron: Asymmetry* **2003**, *14*, 181–183.

[19] a) M. Rueping, B. J. Nachtsheim, S. A. Moreth, M. Bolte, *Angew. Chem. Int. Ed.* **2008**, *47*, 593–596; *Angew. Chem.* **2008**, *120*, 603–606; b) S. Vellalath, I. Čorić, B. List, *Angew. Chem. Int. Ed.* **2010**, *49*, 9749–9752; c) I. Čorić, B. List, *Nature* **2012**, *483*, 315–319; d) J. H. Kim, I. Čorić, S. Vellalath, B. List, *Angew. Chem. Int. Ed.* **2013**, *52*, 4474–4477; *Angew. Chem.* **2013**, *125*, 4570–4573; e) D. Parmar, E. Sugiono, S. Raja, M. Rueping, *Chem. Rev.* **2014**, *114*, 9047–9153.

[20] a) S. E. Denmark, S. K. Ghosh, *Angew. Chem. Int. Ed.* **2001**, *40*, 4759–4762; *Angew. Chem.* **2001**, *113*, 4895–4898; b) S. E. Denmark, J. Fu, *Chem. Rev.* **2003**, *103*, 2763–2793; c) M. Bonsignore, M. Benaglia, F. Cozzi, A. Genoni, S. Rossi, L. Raimondi, *Tetrahedron* **2012**, *68*, 8251–8255.

[21] a) S. Jugé, J. P. Genet, *Tetrahedron Lett.* **1989**, *30*, 2783–2786; b) D. Moulin, S. Darcel, S. Jugé, *Tetrahedron: Asymmetry* **1999**, *10*, 4729–4743; c) D. Moulin, S. Bago, C. Bauduin, C. Darcel, S. Jugé, *Tetrahedron: Asymmetry* **2000**, *11*, 3939–3956.
[22] a) M. J. P. Harger, *J. Chem. Soc. Perkin Trans. 1* **1977**, 2057–2063. B) T. A. Hamor, W. B. Jennings, C. L. Lovely, K. A. Reeves, *J. Chem. Soc. Perkin Trans. 2* **1992**, 843–849; c) M. Benamer, S. Turcaud, J. Royer, *Tetrahedron Lett.* **2010**, *51*, 645–648.
[23] a) N. Fontana, N. A. Espinosa-Jalapa, M. Seidl, J. O. Bauer, *Chem. Eur. J.* **2021**, *27*, 2649–2653; b) N. Fontana, N. A. Espinosa-Jalapa, M. Seidl, J. O. Bauer, *Chem. Commun.* **2022**, *58*, 2144–2147; c) A. Falk, J. O. Bauer, *Inorg. Chem.* **2022**, *61*, 15576–15588.
[24] a) J.-F. Cavalier, F. Fotiadu, R. Verger, G. Buono, *Synlett* **1998**, 73–75; b) I. Fernández, N. Khiar, A. Roca, A. Benabra, A. Alcudia, J. L. Espartero, F. Alcudia, *Tetrahedron Lett.* **1999**, *40*, 2029–2032.
[25] a) A. J. Birch, *J. Chem. Soc.* **1944**, 430–436; b) A. J. Birch, D. Nasipuri, *Tetrahedron* **1959**, *6*, 148–153; c) A. J. Birch, *Pure Appl. Chem.* **1996**, *68*, 553–556.
[26] M. Stankevič, M. Pietrusiewicz, *Tetrahedron Lett.* **2009**, *50*, 7093–7095.
[27] Z. Yu, J. G. Verkade, *Phosphorus, Sulfur Silicon Relat. Elem.* **1998**, *133*, 79–82.
[28] M. Stankiewicz, J. Nycz, J. Rachon, *Heteroat. Chem.* **2002**, *13*, 330–339.
[29] a) J. M. Pearson, D. J. Williams, M. Levy, *J. Am. Chem. Soc.* **1971**, *93*, 5478–5482; b) K. Meerholz, J. Heinze, *J. Am. Chem. Soc.* **1989**, *111*, 2325–2326.
[30] A. Fernandes, C. Laye, S. Pramanik, D. Palmeira, Ö. Ö. Pekel, S. Massip, M. Schmidtmann, T. Müller, F. Robert, Y Landais, *J. Am. Chem. Soc.* **2020**, *142*, 564–572.
[31] B.-Q. Gong, W.-Y. Chen, B.-F. Hu, *Phosphorus, Sulfur Silicon Relat. Elem.* **1991**, *57*, 87–94.
[32] M. J. Frisch, G. W. Trucks, H. B. Schlegel, G. E. Scuseria, M. A. Robb, J. R. Cheeseman, G. Scalmani, V. Barone, B. Mennucci, G. A. Petersson, H. Nakatsuji, M. Caricato, X. Li, H. P. Hratchian, A. F. Izmaylov, J. Bloino, G. Zheng, J. L. Sonnenberg, M. Hada, M. Ehara, K. Toyota, R. Fukuda, J. Hasegawa, M. Ishida, T. Nakajima, Y. Honda, O. Kitao, H. Nakai, T. Vreven, J. A. Montgomery Jr., J. E. Peralta, F. Ogliaro, M. Bearpark, J. J. Heyd, E. Brothers, K. N. Kudin, V. N. Staroverov, T. Keith, R. Kobayashi, J. Normand, K. Raghavachari, A. Rendell, J. C. Burant, S. S. Iyengar, J. Tomasi, M. Cossi, N. Rega, J. M. Millam, M. Klene, J. E. Knox, J. B. Cross, V. Bakken, C. Adamo, J. Jaramillo, R. Gomperts, R. E. Stratmann, O. Yazyev, A. J. Austin, R. Cammi, C. Pomelli, J. W. Ochterski, R. L. Martin, K. Morokuma, V. G. Zakrzewski, G. A. Voth, P. Salvador, J. J. Dannenberg, S. Dapprich, A. D. Daniels, O. Farkas, J. B. Foresman, J. V. Ortiz, J. Cioslowski, D. J. Fox, *Gaussian 09*. Revision E.01; Gaussian, Inc.: Wallingford, CT, USA, **2013**.
[33] J. Tomasi, B. Mennucci, R. Cammi, *Chem. Rev.* **2005**, *105*, 2999–3093.
[34] Considering structure **G**-Cy, which is 7 kJ mol^{-1} higher in energy than **D**-Cy (see Chapter 3.8), an $H_2N\cdots Li$ interaction cannot be completely ruled out.
[35] K. Wolinski, J. F. Hinton, P. Pulay, *J. Am. Chem. Soc.* **1990**, *112*, 8251–8260.
[36] a) M. Oestreich, J. Hermeke, J. Mohr, *Chem. Soc. Rev.* **2015**, *44*, 2202–2220; b) M. C. Lipke, A. L. Liberman-Martin, T. D. Tilley, *Angew. Chem. Int. Ed.* **2017**, *56*, 2260–2294; *Angew. Chem.* **2017**, *129*, 2298–2335.

3.6. Syntheses and Characterizations

3.6.1. General Remarks

All experiments were performed in an inert atmosphere of purified nitrogen by using standard Schlenk techniques or an MBraun Unilab 1200/780 glovebox. Glassware was heated at 140 °C prior to use. Dichloromethane (DCM), diethyl ether, hexane, pentane, tetrahydrofuran (THF), and toluene were dried and degassed with an MBraun SP800 solvent purification system. Ammonia (anhydrous, Staub & Co.), ammonium chloride (≥99.8%, Merck KGaA), *tert*-butanol (anhydrous, ≥99.5%, Merck KGaA), *n*-butyllithium (2.5 M or 1.6 M solution in hexane, Merck KGaA), *tert*-butyllithium (1.6 M solution in pentane, Merck KGaA), dichlorocyclohexylphosphine (95%, Merck KGaA), dichlorophenylphosphine (97%, Merck KGaA), di-*tert*-butylchlorosilane (97%, Merck KGaA), (*S*)-(–)-1-phenylethylamine [(*S*)-**2**] (98%, Merck KGaA), (*S*)-(–)-1-(1-naphthyl)ethylamine [(*S*)-**3**] (≥ 99%, Merck KGaA), lithium (granules, 99%, Merck KGaA), sulfur (99%, Merck KGaA), triethylamine (≥99%, Merck KGaA), (*R*)-(+)-1,1'-bi-2-naphthol [(*R*)-BINOL] (99%, Merck KGaA), phosphorus(V) sulfide (99%, Merck KGaA), and *m*-xylene (≥99%) were used as received without further purification. (*R*)-BINOL-dithiophosphoric acid [(*R*)-BINOL-PSSH] (99% ee) was synthesized according to a reported literature procedure.[1] *tert*-Butylchlorophenylphosphine (**1**)[2] and *tert*-butylchlorocyclohexylphosphine (**11**)[3] were synthesized according to modified literature procedures; the new protocols are presented herein. Compound (S_P,*S*)-**4** has been reported previously.[4] C_6D_6 (≥99%, Merck KGaA) and CD_2Cl_2 (≥99.8%, Fluorochem) were dried over 3 Å molecular sieves and degassed by a standard freeze-pump-thaw procedure. NMR spectra were either recorded on a Bruker Avance 400 (400.13 MHz) or on a Bruker Avance III HD 400 (400.13 MHz) at 25 °C. Chemical shifts (δ) are reported in parts per million (ppm). ^{1}H and $^{13}C\{^{1}H\}$ NMR spectra are referenced to tetramethylsilane ($SiMe_4$, δ = 0.0 ppm) as external standard, with the deuterium signal of the solvent serving as internal lock and the residual solvent signal as an additional reference. $^{31}P\{^{1}H\}$ NMR spectra are referenced to 85% H_3PO_4, $^{29}Si\{^{1}H\}$ NMR spectra to $SiMe_4$, and $^{7}Li\{^{1}H\}$ NMR spectra to LiCl (1 M in D_2O). Hydrogen and carbon atoms of aromatic rings are denoted as H_{ar} and C_{ar}, respectively, or specified with the subscripts i = ipso, o = ortho, m = meta, and p = para. For the assignment of the multiplicities, the following abbreviations are used: s = singlet, d = doublet, m = multiplet, br = broad signal. Elemental analyses were performed on a Vario MICRO cube apparatus. High-resolution mass spectrometry was carried out on a Jeol AccuTOF GCX and an Agilent Q-TOF 6540 UHD spectrometer.

3.6.2. Synthetic Procedures

3.6.2.1. Synthesis of *tert*-butylchlorophenylphosphine (1)

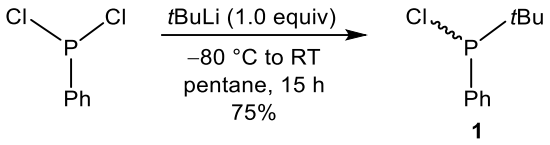

1

tert-Butyllithium (60.0 mL of a 1.6 M solution in pentane, 96.0 mmol, 1.0 equiv.) was slowly added to a solution of dichlorophenylphosphine (17.2 g, 96.0 mmol, 1.0 equiv.) in pentane (150 mL) at –80 °C. The reaction mixture was allowed to slowly warm to room temperature and stirred for 15 h. The precipitated lithium chloride was filtered off *via* cannula filtration. Then, all volatiles of the filtrate were removed *in vacuo*. Compound **1** was obtained as a yellowish liquid (14.4 g, 71.7 mmol, 75%).

^{1}H NMR (400.13 MHz, C_6D_6, 298 K): δ 0.93 [d, $^{3}J_{H–P}$ = 13.5 Hz, 9H, PC(CH_3)$_3$], 7.09–7.05 (m, 3H, H_{ar}), 7.58–7.53 (m, 2H, H_{ar}). **^{31}P{^{1}H} NMR** (162.04 MHz, C_6D_6, 298 K): δ 108.3. **^{13}C{^{1}H} NMR** (100.61 MHz, C_6D_6, 298 K): δ 25.2 [d, $^{2}J_{C–P}$ = 17.8 Hz, PC(CH_3)$_3$], 34.2 [d, $^{1}J_{C–P}$ = 29.9 Hz, PC(CH_3)$_3$], 128.1 (d, $^{3}J_{C–P}$ = 8.5 Hz, C_m), 130.3 (s, C_p), 132.2 (d, $^{2}J_{C–P}$ = 25.4 Hz, C_o), 136.1 (d, $^{1}J_{C–P}$ = 40.8 Hz, C_i).

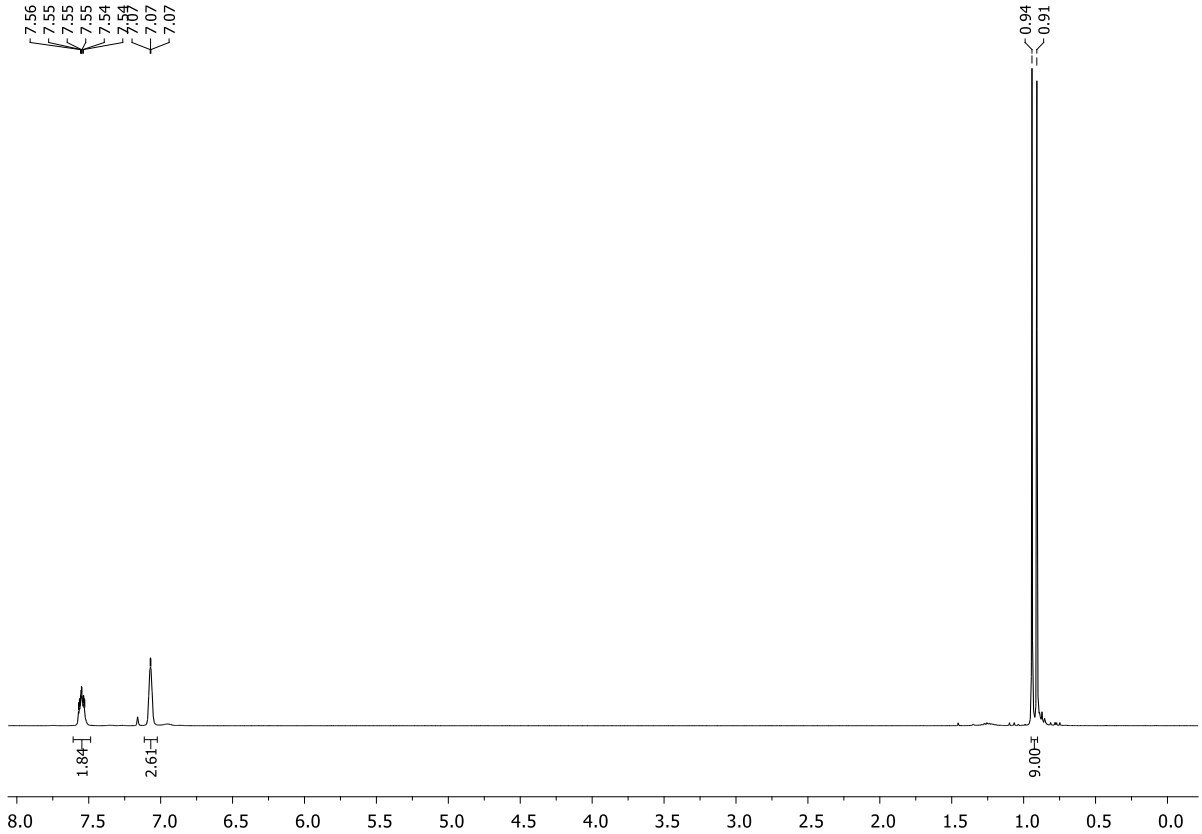

Figure S3.1. ^{1}H NMR spectrum (C_6D_6, 298 K) of compound **1**.

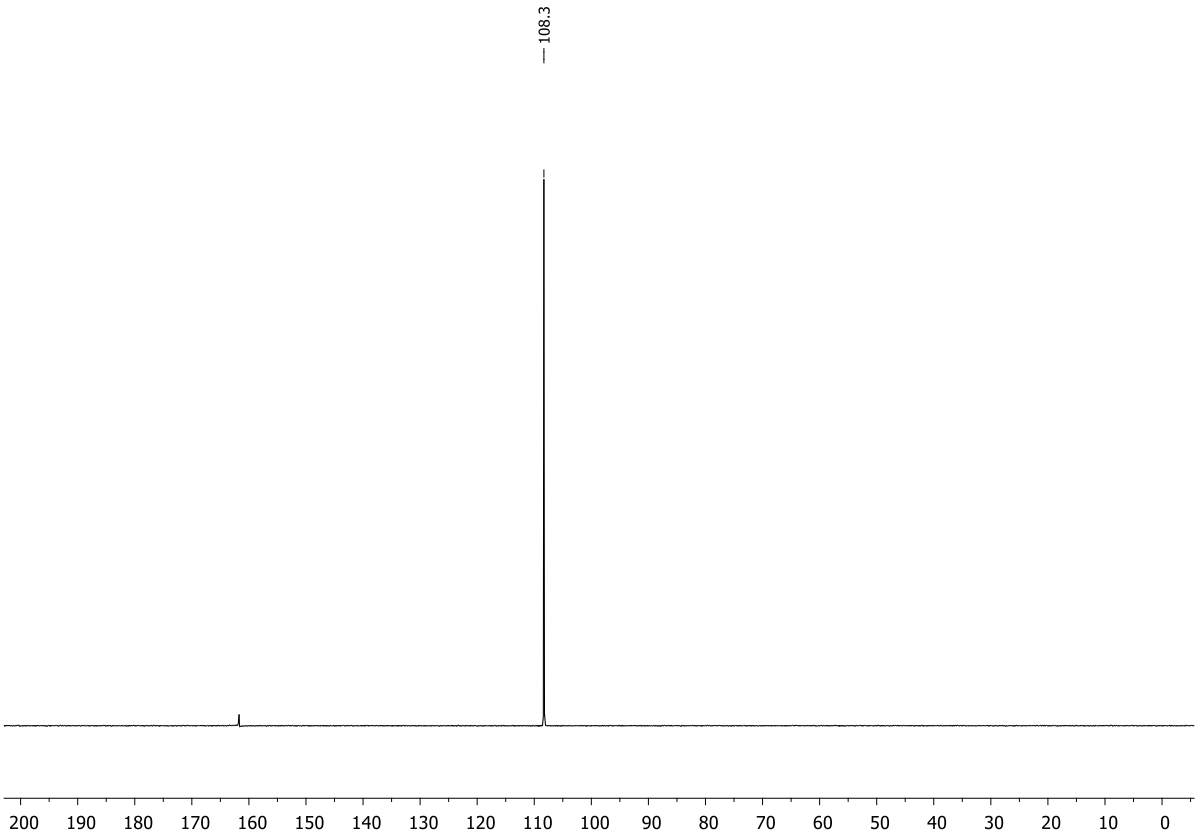

Figure S3.2. $^{31}P\{^{1}H\}$ NMR spectrum (C_6D_6, 298 K) of compound **1**.

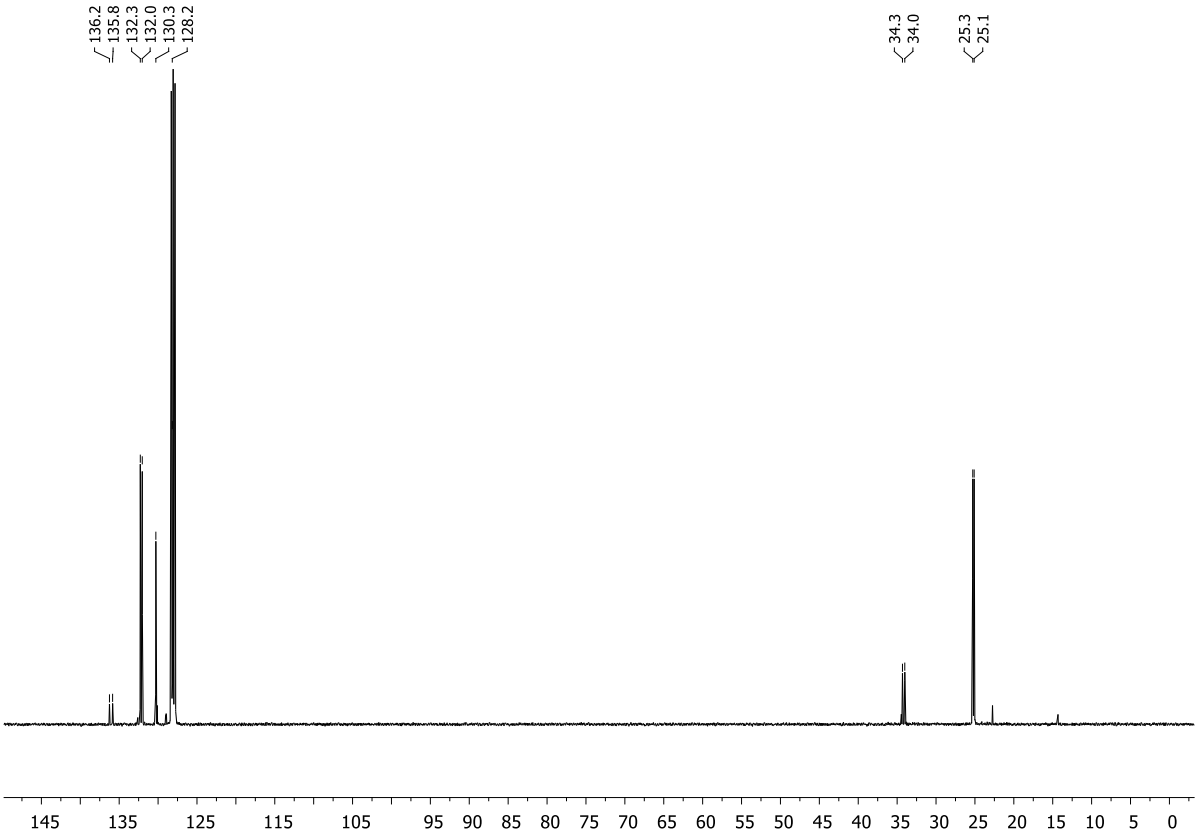

Figure S3.3. $^{13}C\{^{1}H\}$ NMR spectrum (C_6D_6, 298 K) of compound **1**.

3.6.2.2. Synthesis of (S_P,*S*)-4

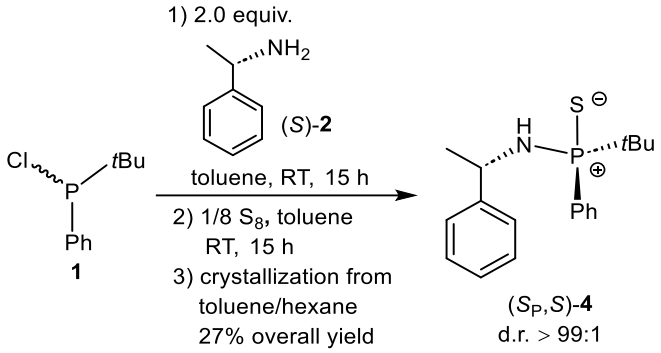

Compound (*S*)-**2** (2.43 mL, 2.28 g, 18.84 mmol, 2.0 equiv.) was added to a solution of compound **1** (1.89 g, 9.42 mmol, 1.0 equiv.) in toluene (50 mL) at room temperature. After stirring for 15 h, the solids were filtered off by transferring the liquid phase *via* cannula filtration directly into another Schlenk tube filled with sulfur (0.30 g, 9.42 mmol, 1.0 equiv.). The reaction mixture was stirred at room temperature for 15 h. Then, all volatiles were removed *in vacuo*. The ^{1}H and ^{31}P{^{1}H} NMR spectra of the crude product showed the formation of the desired product (S_P,*S*)-**4** in a 6:1 diastereomeric ratio. The crude product was recrystallized from toluene/hexane at −25 °C. Compound (S_P,*S*)-**4** (0.82 g, 2.58 mmol, 27% overall yield, d.r. > 99:1) was obtained as colorless crystals suitable for single-crystal X-ray diffraction analysis.

^{1}H NMR (400.13 MHz, C_6D_6, 298 K): δ 1.05 [d, $^{3}J_{H-P}$ = 16.3 Hz, 9H, PC(CH_3)$_3$], 1.52 (d, $^{4}J_{H-P}$ = 6.7 Hz, 3H, CHCH_3), 2.33–2.29 (m, 1H, N*H*), 4.62–4.52 (m, 1H, C*H*CH$_3$), 7.10–6.92 (m, 8H, H_{ar}), 7.88–7.83 (m, 2H, H_{ar}). **^{31}P{^{1}H} NMR** (162.04 MHz, C_6D_6, 298 K): δ 80.7. **^{13}C{^{1}H} NMR** (100.61 MHz, C_6D_6, 298 K): δ 24.9 [d, $^{2}J_{C-P}$ = 1.4 Hz, PC(*C*H$_3$)$_3$], 26.2 (d, $^{3}J_{C-P}$ = 2.8 Hz, CH*C*H$_3$), 35.2 [d, $^{1}J_{C-P}$ = 66.7 Hz, P*C*(CH$_3$)$_3$], 51.5 (d, $^{2}J_{C-P}$ = 1.5 Hz, *C*HCH$_3$), 126.5 (s, C_{ar}), 127.0 (s, C_{ar}), 127.6 (d, $^{2}J_{C-P}$ = 12.0 Hz, C_o), 128.6 (s, C_{ar}), 131.1 (d, $^{4}J_{C-P}$ = 2.9 Hz, C_p), 132.0 (d, $^{1}J_{C-P}$ = 91.4 Hz, PC_i), 134.1 (d, $^{3}J_{C-P}$ = 10.0 Hz, C_m), 146.0 (d, $^{3}J_{C-P}$ = 6.1 Hz, CC_i). **HR(ESI)-MS**: Calcd *m*/*z* for $C_{18}H_{25}NPS$ [(M + H)$^+$]: 318.1440. Found: 318.1441. **CHN Analysis**: Calcd for $C_{18}H_{24}NPS$: C, 68.11; H, 7.62; N, 4.41. Found: C, 68.27; H, 7.51; N, 4.42.

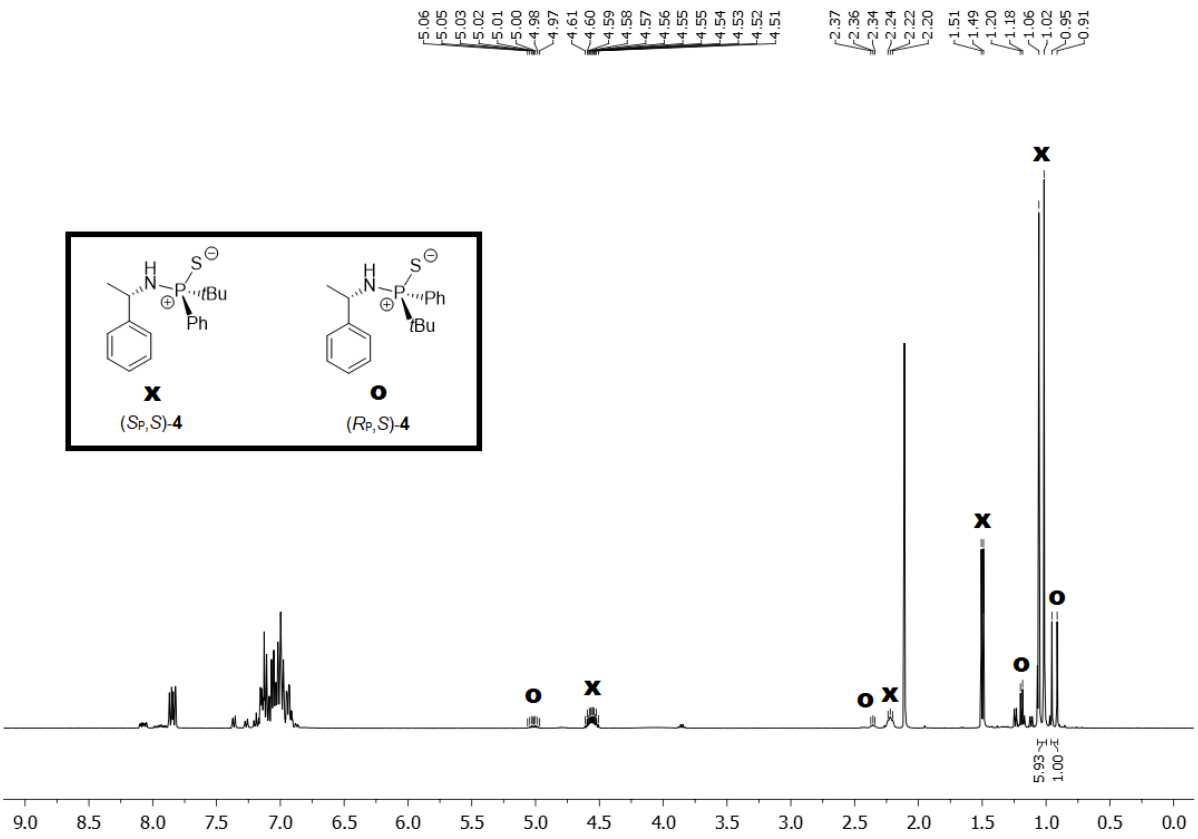

Figure S3.4. ^{1}H NMR spectrum (C_6D_6, 298 K) of the crude reaction mixture for determining the diastereomeric ratio. Compounds (S_P,*S*)-**4** and (R_P,*S*)-**4** were formed in a 6:1 diastereomeric ratio.

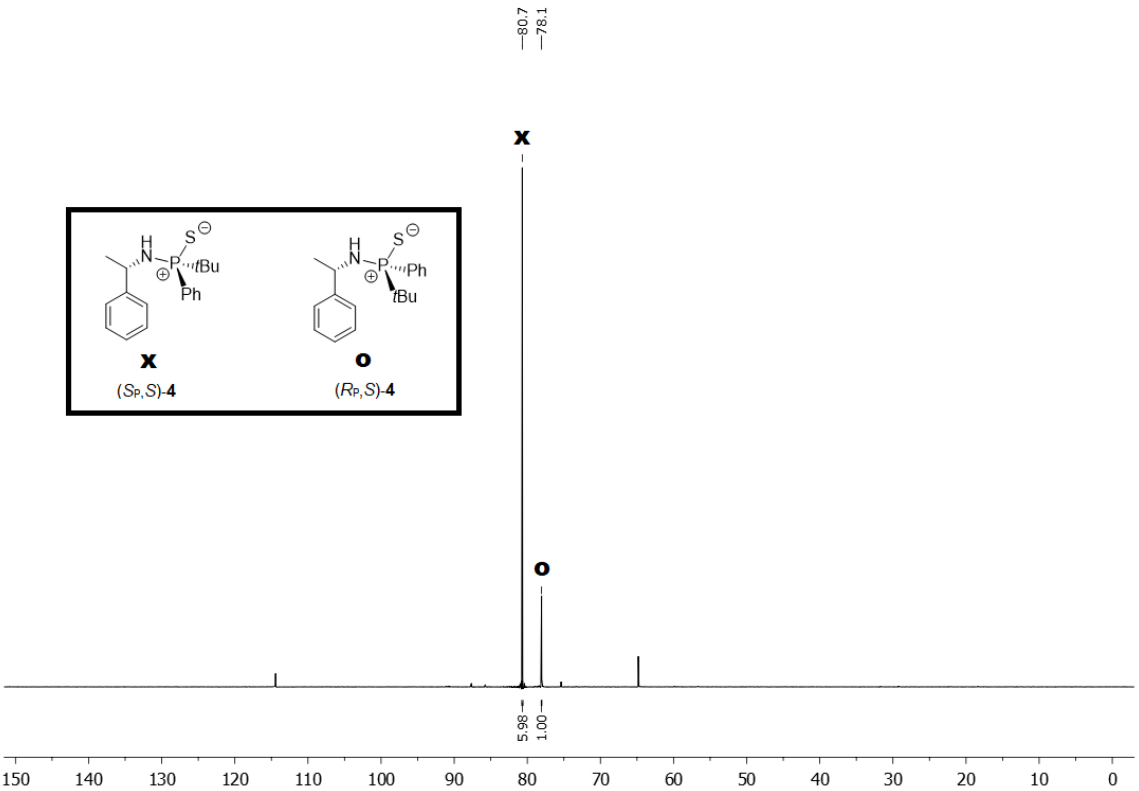

Figure S3.5. $^{31}P\{^{1}H\}$ NMR spectrum (C_6D_6, 298 K) of the crude reaction mixture for determining the diastereomeric ratio. Compounds (S_P,*S*)-**4** and (R_P,*S*)-**4** were formed in a 6:1 diastereomeric ratio.

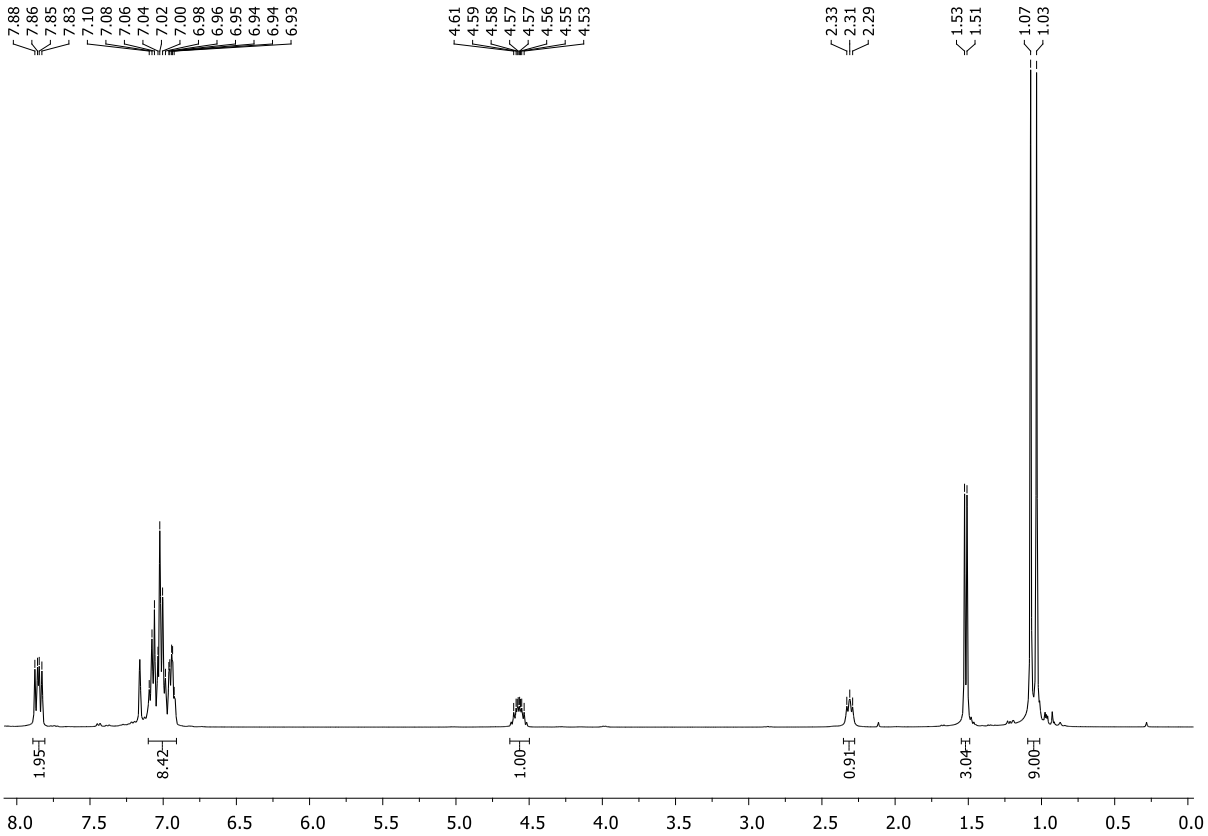

Figure S3.6. ^{1}H NMR spectrum (C_6D_6, 298 K) of compound (S_P,*S*)-**4**.

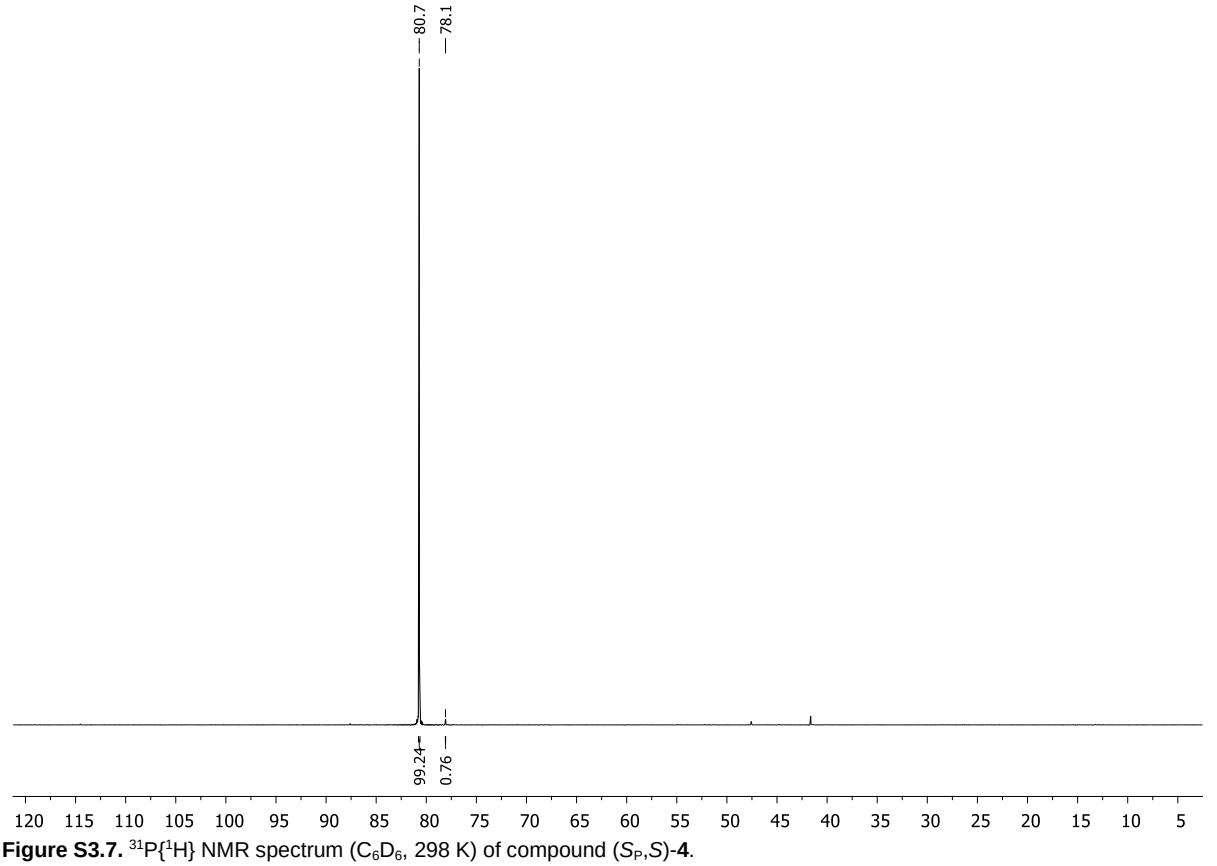

Figure S3.7. $^{31}P\{^{1}H\}$ NMR spectrum (C_6D_6, 298 K) of compound (S_P,*S*)-**4**.

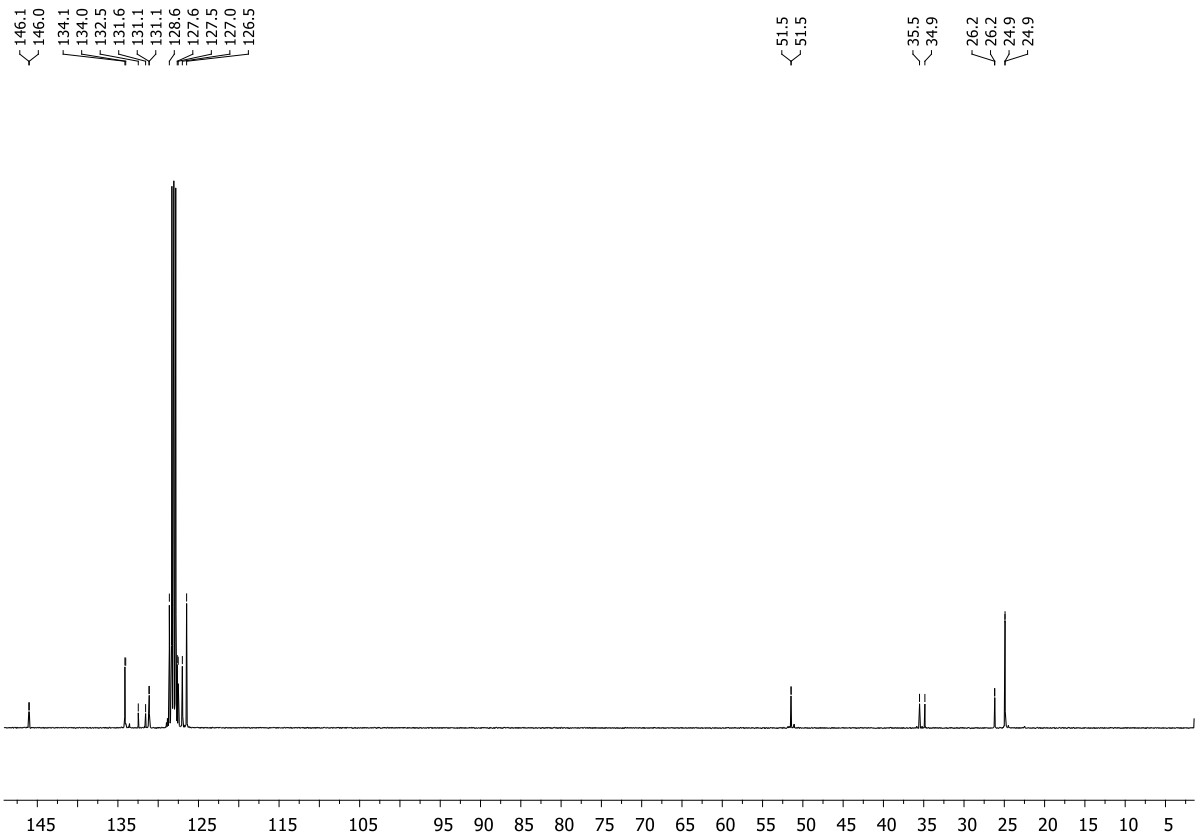

Figure S3.8. $^{13}C\{^{1}H\}$ NMR spectrum (C_6D_6, 298 K) spectrum of compound (S_P,*S*)-**4**.

3.6.2.3. Synthesis of (S_P,S)-5

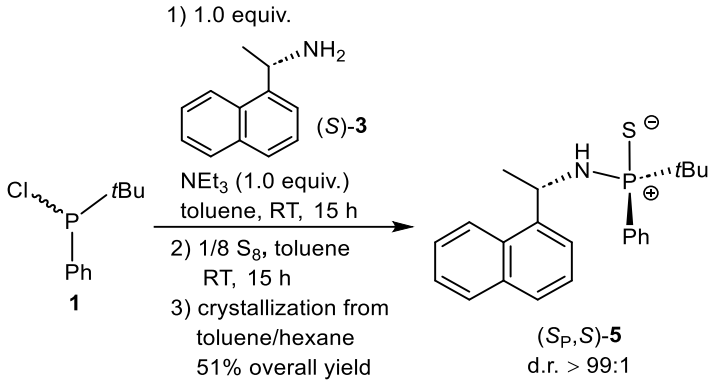

Compound **1** (0.48 g, 2.39 mmol, 1.0 equiv.) was added to a solution of compound (*S*)-**3** (0.38 mL, 0.41 g, 2.39 mmol, 1.0 equiv.) and triethylamine (0.33 mL, 0.24 g, 2.39 mmol, 1.0 equiv.) in toluene (7 mL) at room temperature. After stirring for 15 h, the solids were filtered off by transferring the liquid phase *via* cannula filtration directly into another Schlenk tube filled with sulfur (0.08 g, 2.39 mmol, 1.0 equiv.). The reaction mixture was stirred at room temperature for 15 h. Then, all volatiles were removed *in vacuo*. The ^{1}H and ^{31}P{^{1}H} NMR spectra of the crude product showed the formation of the desired product (S_P,S)-**5** in a 12:1 diastereomeric ratio. The crude product was recrystallized from toluene/hexane at **–**25 °C. Compound (S_P,S)-**5** (0.45 g, 1.22 mmol, 51% overall yield, d.r. > 99:1) was obtained as pale beige crystals suitable for single-crystal X-ray diffraction analysis.

^{1}H NMR (400.13 MHz, C_6D_6, 298 K): δ 1.06 [d, $^{3}J_{H-P}$ = 16.3 Hz, 9H, PC(CH_3)$_3$], 1.67 (d, $^{4}J_{H-P}$ = 6.7 Hz, 3H, CHCH_3), 2.32 (m, 1H, N*H*), 5.37–5.48 (m, 1H, C*H*CH$_3$), 6.76–6.72 (m, 2H, H_{ar}), 6.85–6.81 (m, 1H, H_{ar}), 7.02–6.97 (m, 1H, H_{ar}), 7.14–7.12 (d, $^{3}J_{H-H}$ = 7.7 Hz, 1H, H_{ar}), 7.35–7.32 (m, 1H, H_{ar}), 7.45–7.44 (d, $^{3}J_{H-H}$ = 7.1 Hz, 1H, H_{ar}), 7.59 (dd, $^{3}J_{H-H}$ = 8.0, $^{4}J_{H-H}$ = 4.9 Hz, 2H, H_{ar}), 7.69 (d, $^{3}J_{H-H}$ = 8.6 Hz, 1H, H_{ar}), 7.82–7.77 (m, 2H, H_{ar}). **^{31}P{^{1}H} NMR** (162.04 MHz, C_6D_6, 298 K): δ 81.2. **^{13}C{^{1}H} NMR** (100.61 MHz, C_6D_6, 298 K): δ 24.9 [d, $^{2}J_{C-P}$ = 1.4 Hz, PC(*C*H$_3$)$_3$], 26.5 (d, $^{3}J_{C-P}$ = 1.8 Hz, CH*C*H$_3$), 35.3 [d, $^{1}J_{C-P}$ = 66.6 Hz, P*C*(CH$_3$)$_3$], 47.9 (s, *C*HCH$_3$), 122.8 (s, C_{ar}), 123.8 (s, C_{ar}), 125.6 (s, C_{ar}), 125.8 (s, C_{ar}), 126.3 (s, C_{ar}), 127.5 (d, $^{2}J_{C-P}$ = 12.0 Hz, C_o), 127.9 (s, C_{ar}), 128.9 (s, C_{ar}), 130.7 (s, C_{ar}), 131.1 (d, $^{4}J_{C-P}$ = 2.9 Hz, C_p), 131.9 (d, $^{1}J_{C-P}$ = 91.7 Hz, PC_i), 133.8 (d, $^{3}J_{C-P}$ = 10.0 Hz, C_m), 134.4 (s, C_{ar}), 142.4 (d, $^{3}J_{C-P}$ = 6.5 Hz, CC_i). **HR(ESI)-MS**: Calcd *m*/*z* for $C_{22}H_{27}NPS$ [(M + H)$^+$]: 368.1596. Found: 368.1598. **CHN Analysis**: Calcd $C_{22}H_{26}NPS$: C, 71.90; H, 7.13; N, 3.81. Found: C, 71.64; H, 7.00; N, 3.74.

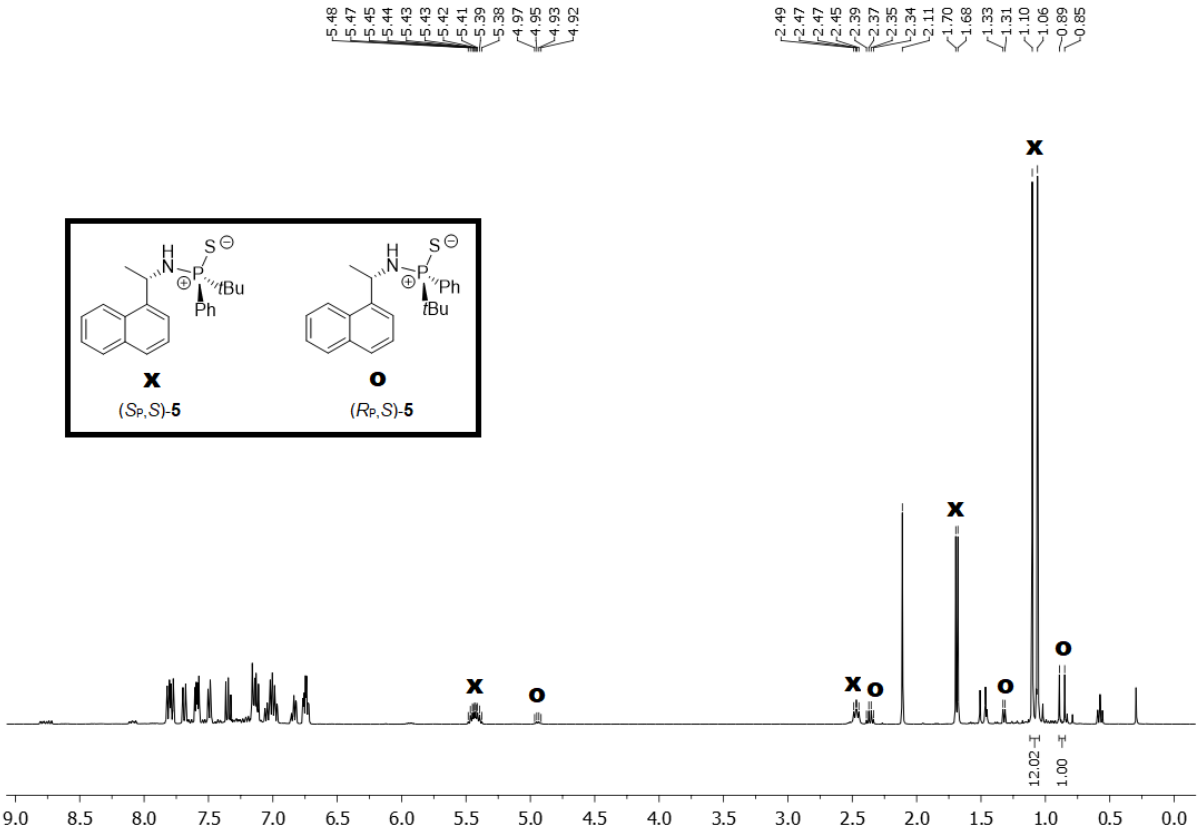

Figure S3.9. ^{1}H NMR spectrum (C_6D_6, 298 K) of the crude reaction mixture for determining the diastereomeric ratio. Compounds (S_P,*S*)-**5** and (R_P,*S*)-**5** were formed in a 12:1 diastereomeric ratio.

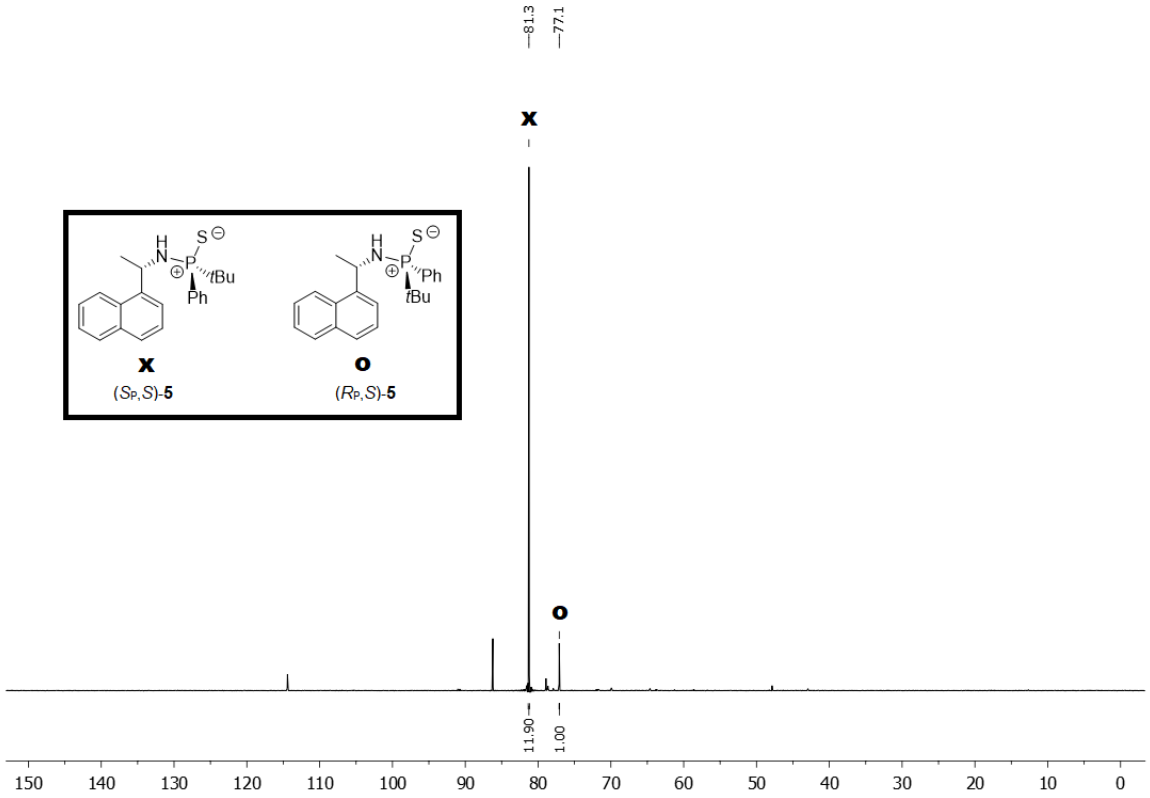

Figure S3.10. $^{31}P\{^{1}H\}$ NMR spectrum (C_6D_6, 298 K) of the crude reaction mixture for determining the diastereomeric ratio. Compounds (S_P,*S*)-**5** and (R_P,*S*)-**5** were formed in a 12:1 diastereomeric ratio.

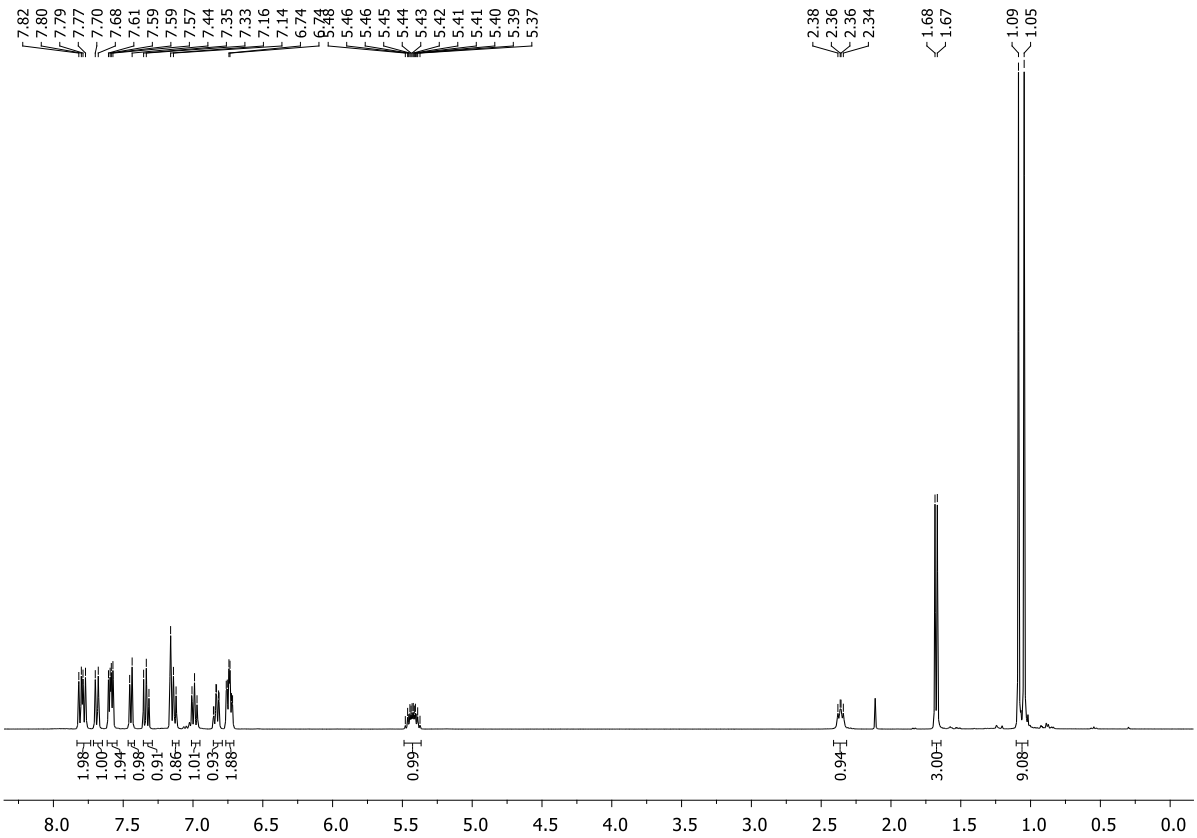

Figure S3.11. ^{1}H NMR spectrum (C_6D_6, 298 K) of compound (S_P,*S*)-**5**.

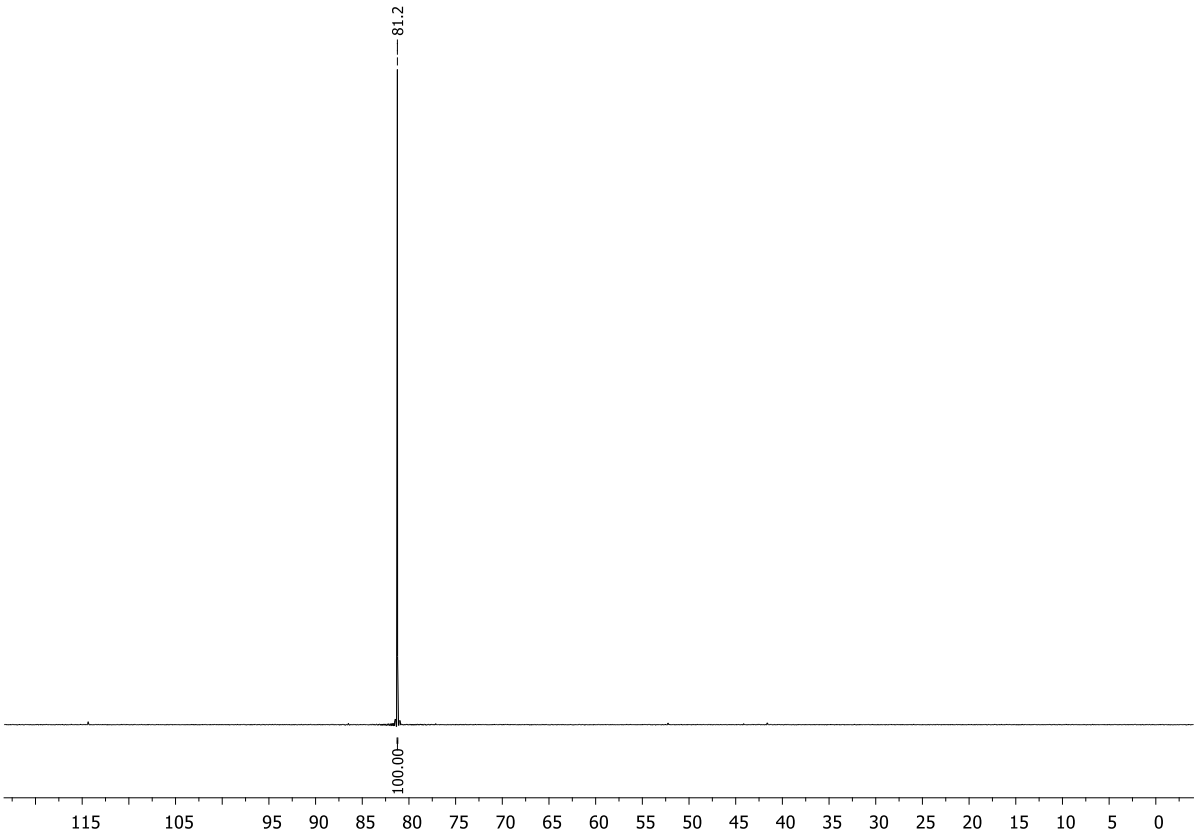

Figure S3.12. $^{31}P\{^{1}H\}$ NMR spectrum (C_6D_6, 298 K) of compound (S_P,*S*)-**5**.

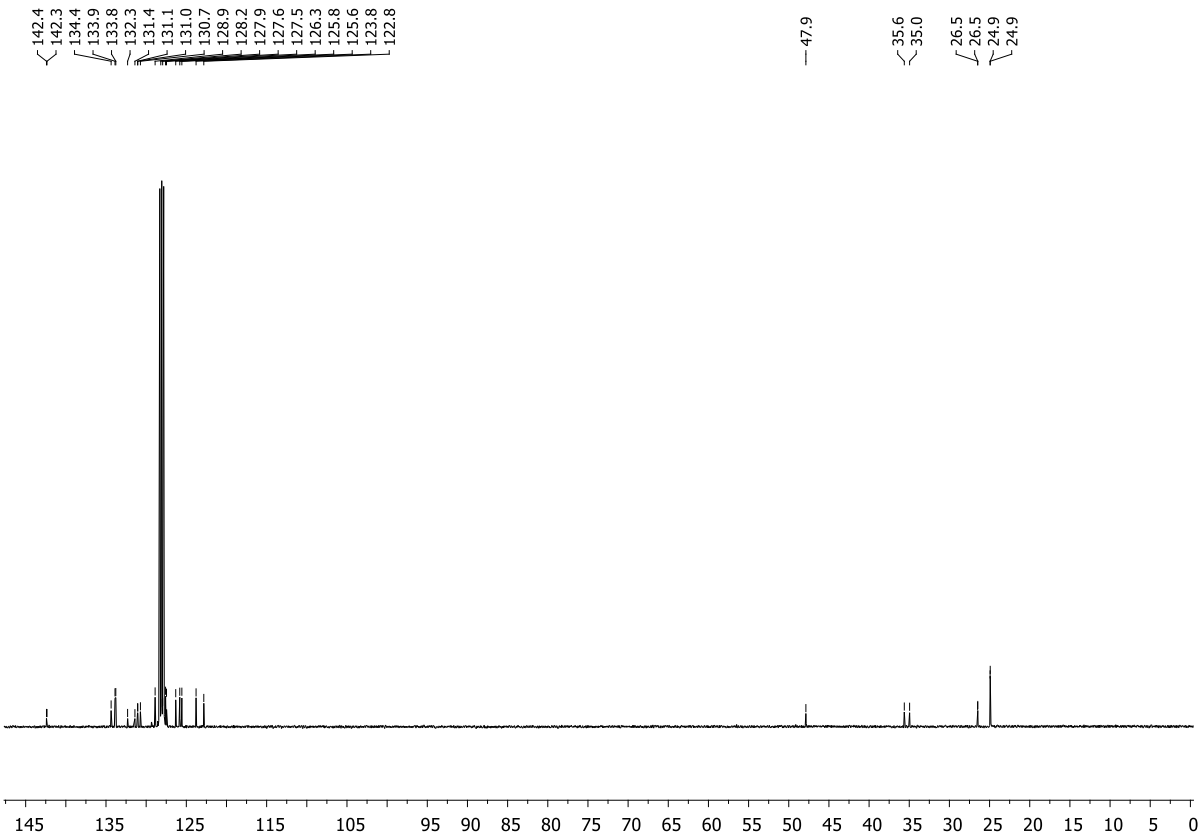

Figure S3.13. $^{13}C\{^{1}H\}$ NMR spectrum (C_6D_6, 298 K) of compound (S_P,*S*)-**5**.

3.6.2.4. General procedure for the reductive C–N bond cleavage of compounds (S_P,S)-4 and (S_P,S)-5

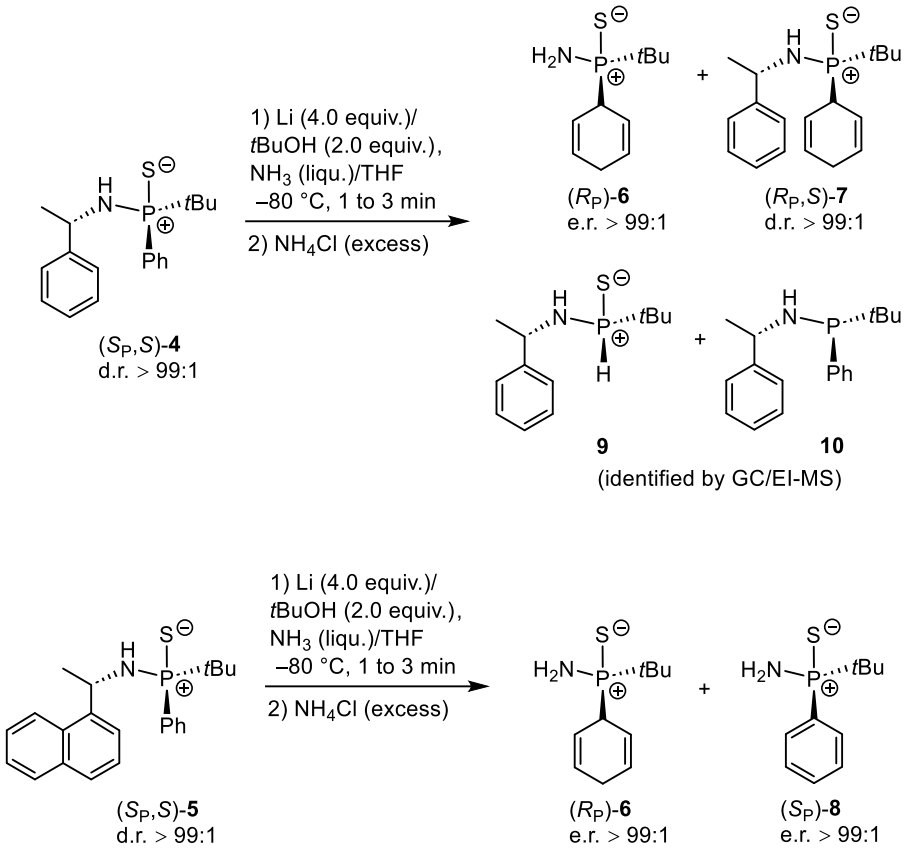

Ammonia (5 mL) was condensed into a flask containing lithium (9.0 mg, 1.28 mmol, 4.0 equiv.) at **–**80 °C. The mixture was stirred for 5 to 10 min while turning into a dark blue solution. Meanwhile, a solution of either (S_P,S)-**4** (0.102 g, 0.32 mmol, 1.0 equiv.) or (S_P,S)-**5** (0.118 g, 0.32 mmol, 1.0 equiv.) and *tert*-butanol (0.06 mL, 0.64 mmol, 2.0 equiv.) in THF (2.5 mL) was prepared and then added to the solution of lithium in liquid ammonia in one portion. After stirring for 1, 2, or 3 min (see Table 3.1 in Chapter 3.3.2), the mixture was quenched with ammonium chloride. Reaction times longer than 3 min up to 10 min led to a significant increase in undesired by-products. After quenching, the cooling bath was removed allowing ammonia to evaporate. The crude mixture was extracted with diethyl ether (1 × 5 mL, 2 × 2.5 mL) and the solids removed *via* cannula filtration. All volatiles were removed *in vacuo* and the ratios of the products [(R_P)-**6**/(R_P,S)-**7**/**9**/**10** or (R_P)-**6**/(S_P)-**8**, depending on the starting compound used] in the crude mixture determined by $^{31}P\{^1H\}$ NMR spectroscopy (see Table 3.1 in Chapter 3.3.2 and Figures S3.23–28). Separation attempts using Kugelrohr distillation were challenging and mostly resulted in mixed fractions of the products. However, very few crystals of pure (R_P)-**6**, (S_P)-**8**, and (R_P,S)-**7**, suitable for single-crystal X-ray diffraction analysis, could be obtained. Crystals of (R_P)-**6** were obtained from the crude reaction mixture of the reduction of (S_P,S)-**4** after 3 min reaction time. The crude product mixture was dissolved in diethyl ether (5 mL) and the solvent was slowly evaporated from a half-sealed vial at room temperature for two days until colorless crystalline needles of (R_P)-**6** were formed. Crystals of

(R_P,*S*)-**7** were obtained from the crude reaction mixture of the reduction of (S_P,*S*)-**4** after 1 min reaction time. The crude product was dissolved in diethyl ether (2 mL) and the solvent was slowly evaporated from a half-sealed vial at room temperature for two days until colorless crystalline blocks of (R_P,*S*)-**7** were formed. Crystals of (S_P)-**8** were obtained from the crude reaction mixture of the reduction of (S_P,*S*)-**5** after 1 min reaction time. After dissolving the crude product in dichloromethane (2 mL), the solution was slowly layered with pentane (4 mL) and stored at −35 °C in a sealed vial for four weeks until colorless crystalline blocks of (S_P)-**8** were formed. The crystalline material of compounds (R_P)-**6**, (R_P,*S*)-**7**, and (S_P)-**8** was sufficient to obtain all analytical data (NMR spectroscopy, elemental analysis, high-resolution mass spectrometry, and X-ray crystallography). The enantiomeric purity of crude compound (S_P)-**8** was determined by ^{1}H and ^{31}P{^{1}H} NMR spectroscopy in the presence of (*R*)-BINOL-PSSLi (99% ee) in CD_2Cl_2 (for details, see Chapter 3.6.2.12). Compounds **9** and **10** were identified by GC/EI-MS analysis. For this purpose, a diethyl ether extract of the crude mixture of the reaction of compound (S_P,*S*)-**4** with lithium/*tert*-butanol in liquid ammonia after 3 min reaction time was subjected to GC/EI-MS analysis.

Compound (R_P)-**6**:

^{1}H NMR (400.13 MHz, C_6D_6, 298 K): δ 1.09 [d, $^{3}J_{H–P}$ = 16.0 Hz, 9H, PC(C*H*$_3$)$_3$], 1.60 (br, 2H, N*H*$_2$), 2.36–2.32 (m, 1H, C*H*), 2.41–2.38 (m, 1H, C*H*), 3.41–3.30 (m, 1H, C*H*), 5.58–5.52 (m, 1H, C*H*), 5.66–5.61 (m, 1H, C*H*), 5.80–5.76 (m, 1H, C*H*), 6.04–5.99 (m, 1H, C*H*). **^{31}P{^{1}H} NMR** (162.04 MHz, C_6D_6, 298 K): δ 81.2. **^{13}C{^{1}H} NMR** (100.61 MHz, C_6D_6, 298 K): δ 55.9 [d, $^{2}J_{C–P}$ = 0.9 Hz, PC(*C*H$_3$)$_3$], 26.7 (d, $^{4}J_{C–P}$ = 6.1 Hz, *C*H$_2$), 37.3 [d, $^{1}J_{C–P}$ = 59.2 Hz, P*C*(CH$_3$)$_3$], 43.7 (d, $^{1}J_{C–P}$ = 53.5 Hz, P*C*H), 123.3 (d, $^{3}J_{C–P}$ = 6.5 Hz, *C*H), 123.6 (d, $^{3}J_{C–P}$ = 7.2 Hz, *C*H), 126.7 (d, $^{2}J_{C–P}$ = 10.0 Hz, *C*H), 127.5 (d, $^{2}J_{C–P}$ = 9.9 Hz, *C*H). **HR(ESI)-MS**: Calcd *m*/*z* for $C_{10}H_{19}NPS$ [(M + H)$^+$]: 216.0970. Found: 216.0973. **CHN Analysis**: Calcd for $C_{10}H_{18}NPS$: C, 55.79; H, 8.43; N, 6.51. Found: C, 56.36; H, 8.28; N, 6.27.

Compound (R_P,*S*)-**7**:

^{1}H NMR (400.13 MHz, C_6D_6, 298 K): δ 1.17 [d, $^{3}J_{H–P}$ = 15.9 Hz, 9H, PC(C*H*$_3$)$_3$], 1.35 (d, $^{4}J_{H–P}$ = 6.8 Hz, 3H, CHC*H*$_3$), 2.04–1.87 (m, 1H, N*H*), 2.27–2.14 (m, 2H, C*H*$_2$), 3.39–3.26 (m, 1H, C*H*), 5.08–4.97 (m, 1H, C*H*), 5.45–5.39 (m, 2H, C*H*), 5.88–5.83 (m, 1H, C*H*), 5.98–5.92 (m, 1H, C*H*), 7.05–7.01 (m, 1H, *H*$_{ar}$), 7.12–7.08 (m, 2H, *H*$_{ar}$), 7.23–7.20 (m, 2H, *H*$_{ar}$). **^{31}P{^{1}H} NMR** (162.04 MHz, C_6D_6, 298 K): δ 82.6. **^{13}C{^{1}H} NMR** (100.61 MHz, C_6D_6, 298 K): δ 25.5 (d, $^{3}J_{C–P}$ = 4.5 Hz, CH*C*H$_3$), 26.2 [s, PC(*C*H$_3$)$_3$], 26.5 (d, $^{4}J_{C–P}$ = 6.0 Hz, *C*H$_2$), 38.0 [d, $^{1}J_{C–P}$ = 59.7 Hz, P*C*(CH$_3$)$_3$], 43.9 (d, $^{1}J_{C–P}$ = 53.7 Hz, P*C*H), 50.6 (d, $^{3}J_{C–P}$ = 1.5 Hz, *C*HCH$_3$), 123.5 (d, $^{3}J_{C–P}$ = 7.3 Hz, *C*H), 123.6 (d, $^{3}J_{C–P}$ = 6.2 Hz, *C*H), 126.3 (d, $^{2}J_{C–P}$ = 10.0 Hz, *C*H), 126.8 (s, *C*$_{ar}$), 127.1 (d, $^{2}J_{C–P}$ = 9.7 Hz, C*H*), 127.2 (s, *C*$_{ar}$), 128.7 (s, *C*$_{ar}$), 146.5 (d, $^{3}J_{C–P}$ = 3.5 Hz, C*C*$_i$). **HR(ESI)-MS**: Calcd *m*/*z* for $C_{18}H_{27}NPS$ [(M + H)$^+$]: 320.1596. Found: 320.1594. **CHN Analysis**: Calcd for $C_{18}H_{26}NPS$: C, 67.68; H, 8.20; N, 4.38. Found: C, 67.62; H, 8.26; N, 4.38.

Compound (S_P)-**8**:

^{1}H NMR (400.13 MHz, C_6D_6, 298 K): δ 0.98 [d, $^3J_{H–P}$ = 16.7 Hz, 9H, PC(CH_3)$_3$], 1.76 (br, 2H, NH_2), 7.07–7.04 (m, 3H, H_{ar}), 7.91–7.86 (m, 2H, H_{ar}). **^{31}P{^{1}H} NMR** (162.04 MHz, C_6D_6, 298 K): δ 75.4. **^{13}C{^{1}H} NMR** (100.61 MHz, C_6D_6, 298 K): δ 24.7 [d, $^2J_{C–P}$ = 2.0 Hz, PC(CH_3)$_3$], 35.6 [d, $^1J_{C–P}$ = 67.5 Hz, PC(CH_3)$_3$], 127.9 (d, $^2J_{C–P}$ = 11.8 Hz, C_o), 131.2 (d, $^4J_{C–P}$ = 2.9 Hz, C_p), 133.2 (d, $^3J_{C–P}$ = 9.8 Hz, C_m), 133.2 (d, $^1J_{C–P}$ = 88.8 Hz, PC_i). **GC/EI-MS**: *m*/*z* (%) = 213 (21) [M$^{+\bullet}$], 157 (53) [(M – C_4H_8)$^{+\bullet}$], 156 (24) [(M – C_4H_9)$^+$], 124 (100) [H_2NPPh$^{+\bullet}$]. **CHN Analysis**: Calcd for $C_{10}H_{16}$NPS: C, 56.32; H, 7.56; N, 6.57. Found: C, 56.40; H, 7.51; N, 6.52.

Compound **9**:

^{31}P{^{1}H} NMR (162.04 MHz, C_6D_6, 298 K): δ 66.1. GC/EI-MS [80 °C (1 min) – 320 °C (15 min) with 25 °C·min^{-1}], (70 eV, t_R = 7.02 min): *m*/*z* (%) for $C_{12}H_{20}$NPS: 241 (2) [M$^{+\bullet}$], 208 (16) [{C_8H_9(NH)P*t*Bu}$^{+\bullet}$], 184 (29) [(M **–** C_4H_9)$^{+\bullet}$], 120 (100) [(C_8H_{10}N)$^{+\bullet}$], 105 (85) [(C_8H_9)$^{+\bullet}$], 77 (22) [(C_6H_5)$^{+\bullet}$], 57 (38) [(C_4H_9)$^{+\bullet}$].

Compound **10**:

^{31}P{^{1}H} NMR (162.04 MHz, C_6D_6, 298 K): δ 47.5. GC/EI-MS [80 °C (1 min) – 320 °C (15 min) with 25 °C·min^{-1}], (70 eV, t_R = 7.47 min): *m*/*z* (%) for $C_{18}H_{24}$NP: 285 (8) [M$^{+\bullet}$], 228 (55) [(M – C_4H_9)$^{+\bullet}$], 124 (88) [(C_6H_7NP)$^{+\bullet}$], 105 (100) [(C_8H_9)$^{+\bullet}$], 77 (13) [(C_6H_5)$^{+\bullet}$].

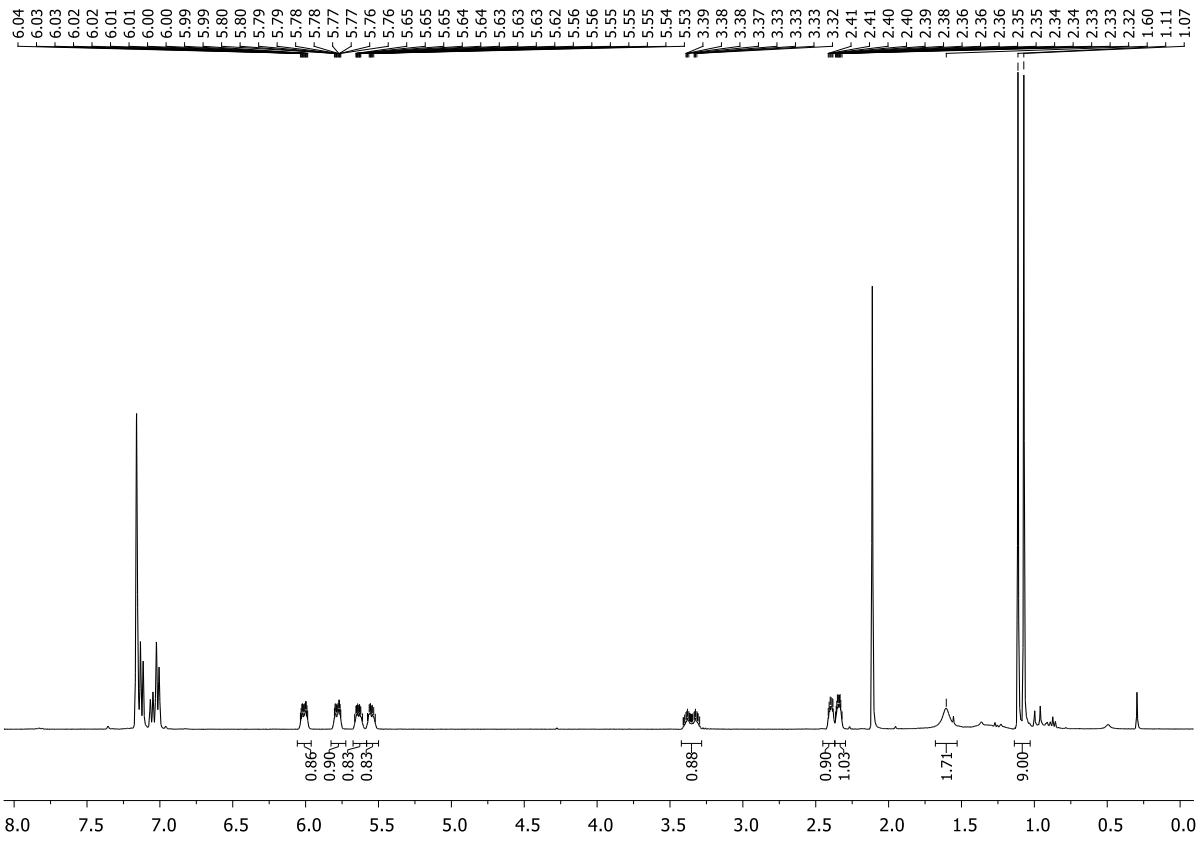

Figure S3.14. ^{1}H NMR spectrum (C_6D_6, 298 K) of compound (R_P)-**6** (with impurity of toluene).

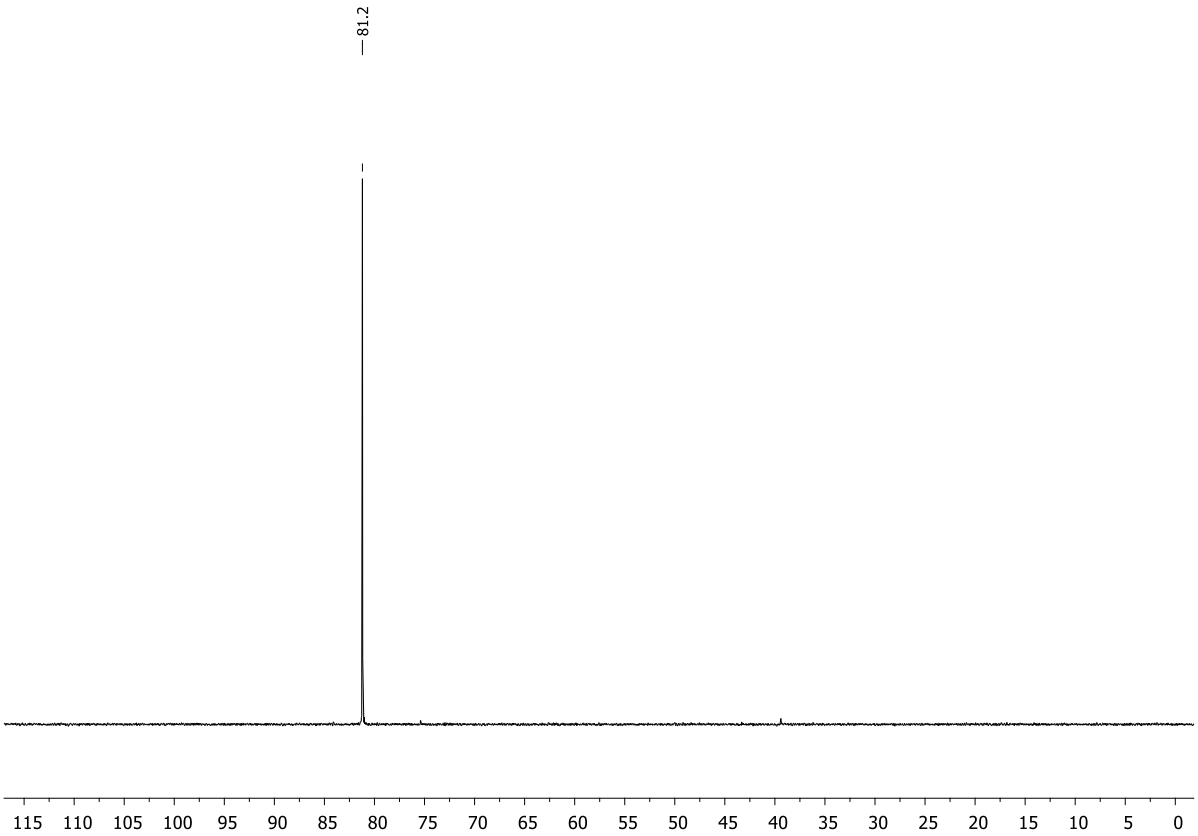

Figure S3.15. $^{31}P\{^{1}H\}$ NMR spectrum (C_6D_6, 298 K) of compound (R_P)-**6**.

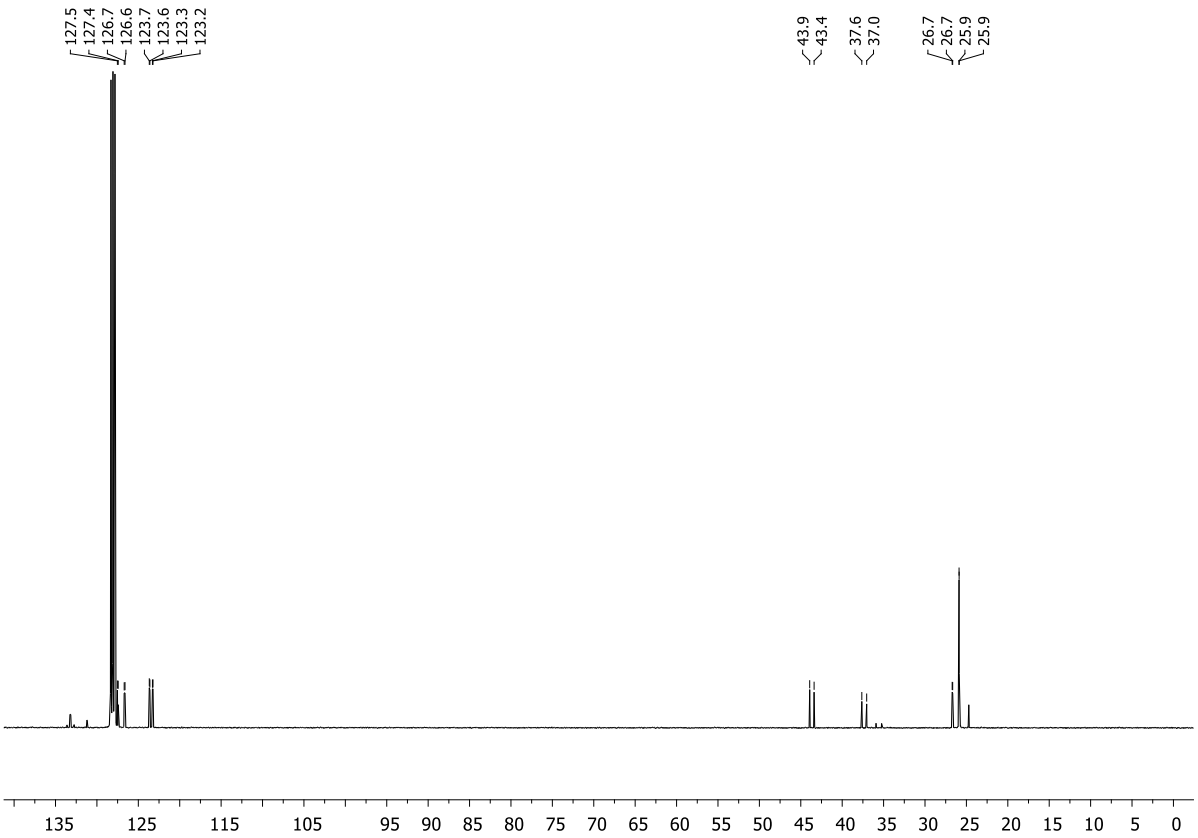

Figure S3.16. $^{13}C\{^{1}H\}$ NMR spectrum (C_6D_6, 298 K) of compound (R_P)-**6**.

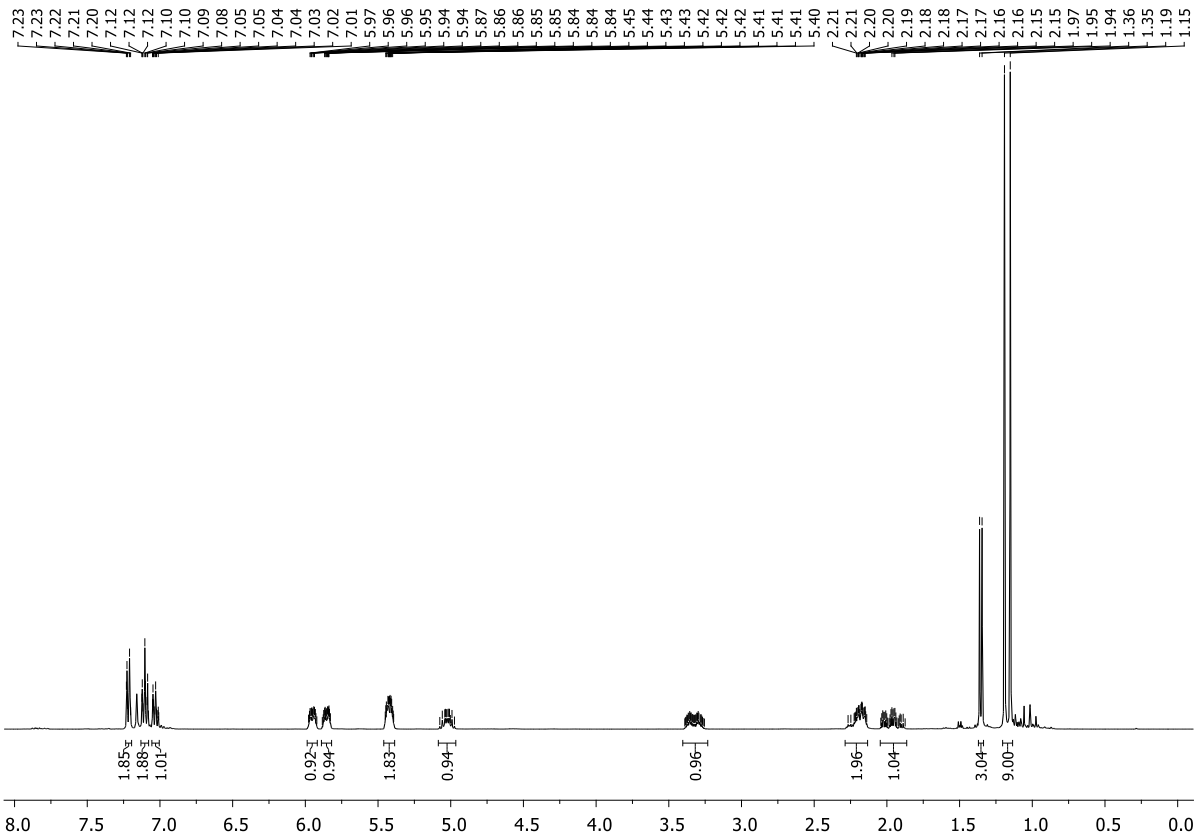

Figure S3.17. ^{1}H NMR spectrum (C_6D_6, 298 K) of compound (R_P,*S*)-**7**.

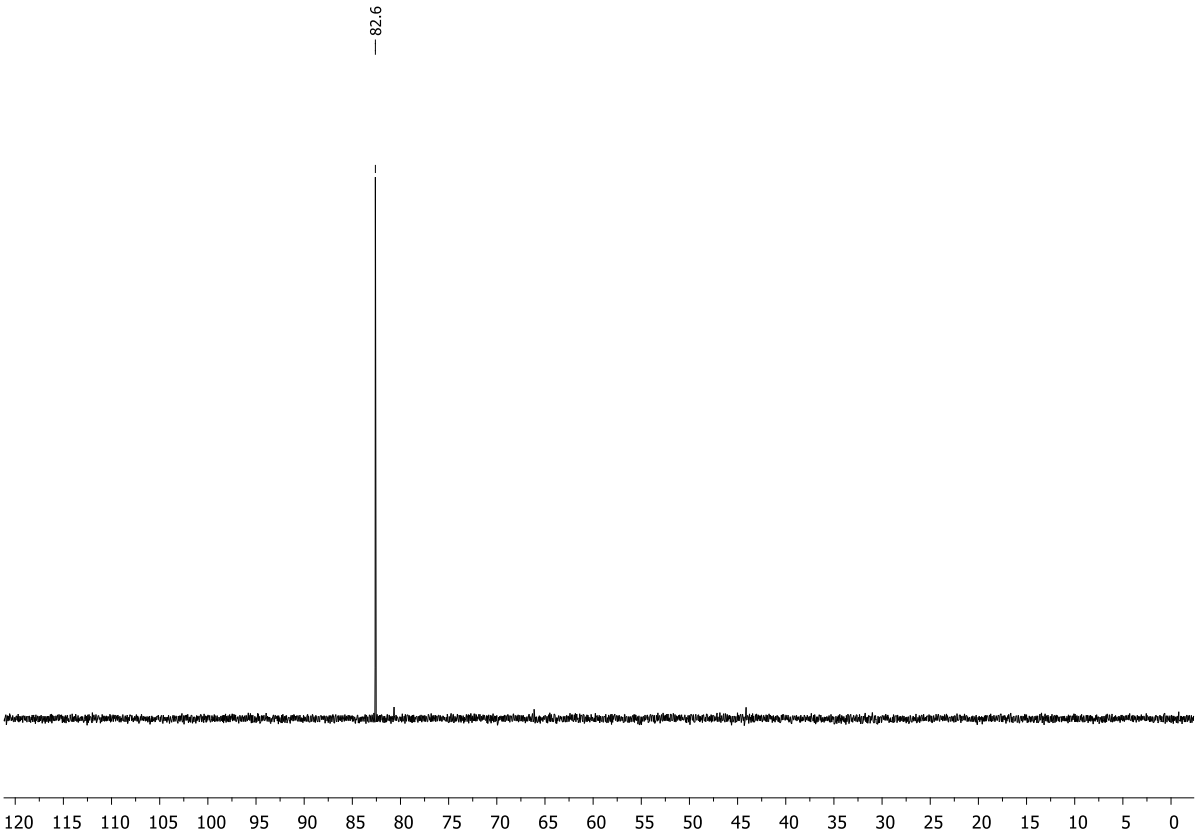

Figure S3.18. $^{31}P\{^{1}H\}$ NMR spectrum (C_6D_6, 298 K) of compound (R_P,*S*)-**7**.

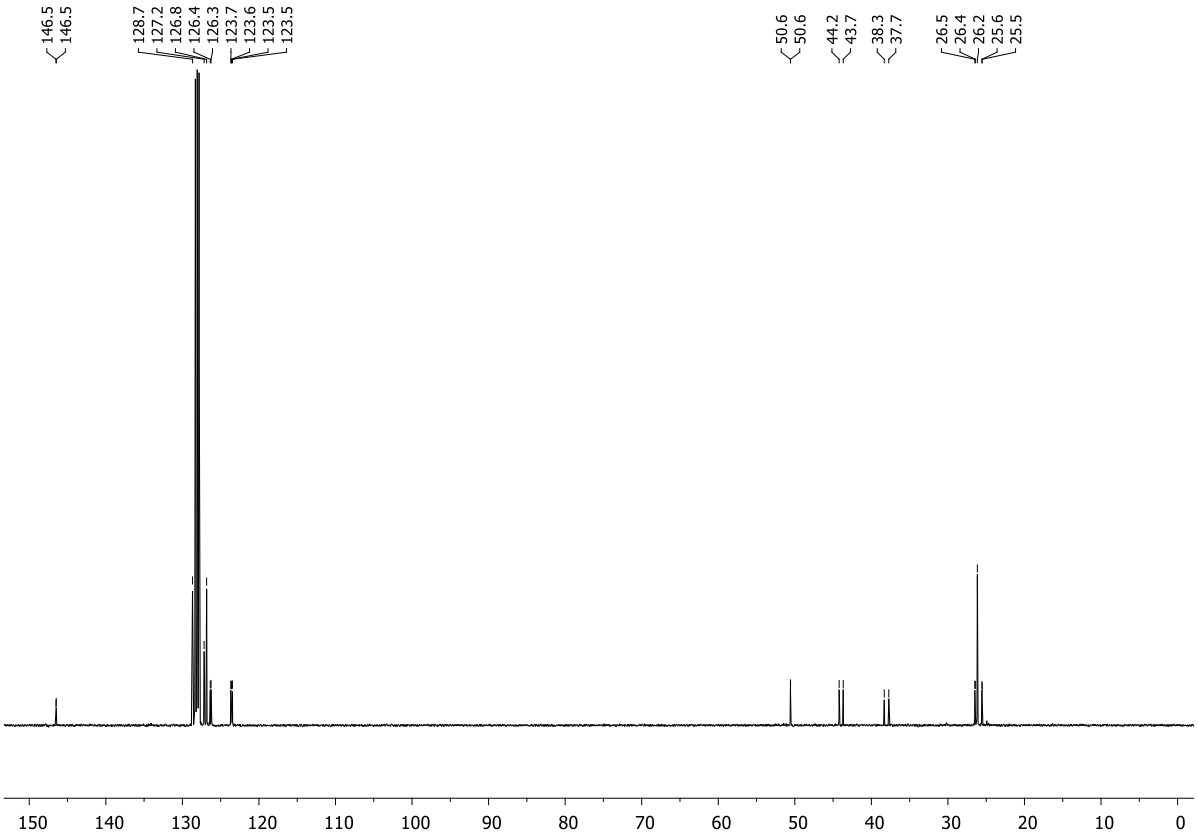

Figure S3.19. $^{13}C\{^{1}H\}$ NMR spectrum (C_6D_6, 298 K) of compound (R_P,S)-**7**.

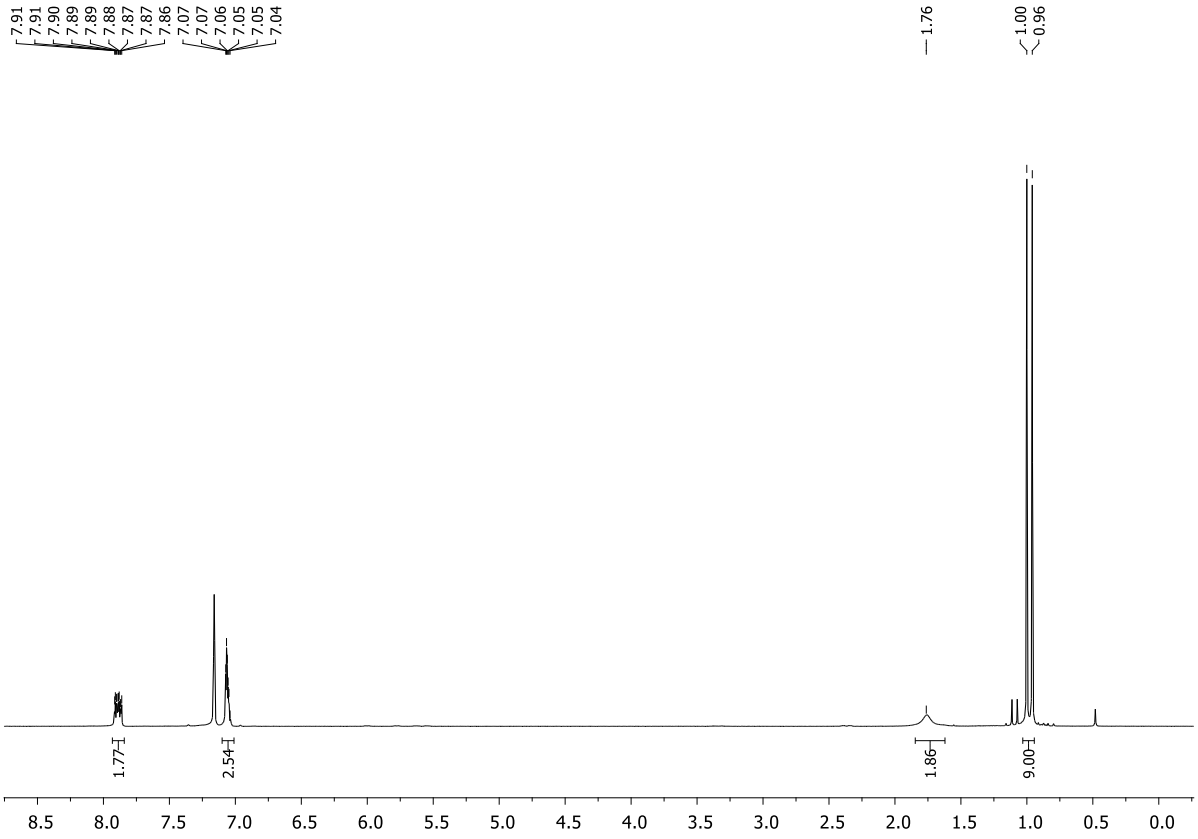

Figure S3.20. ^{1}H NMR spectrum (C_6D_6, 298 K) of compound (S_P)-**8**.

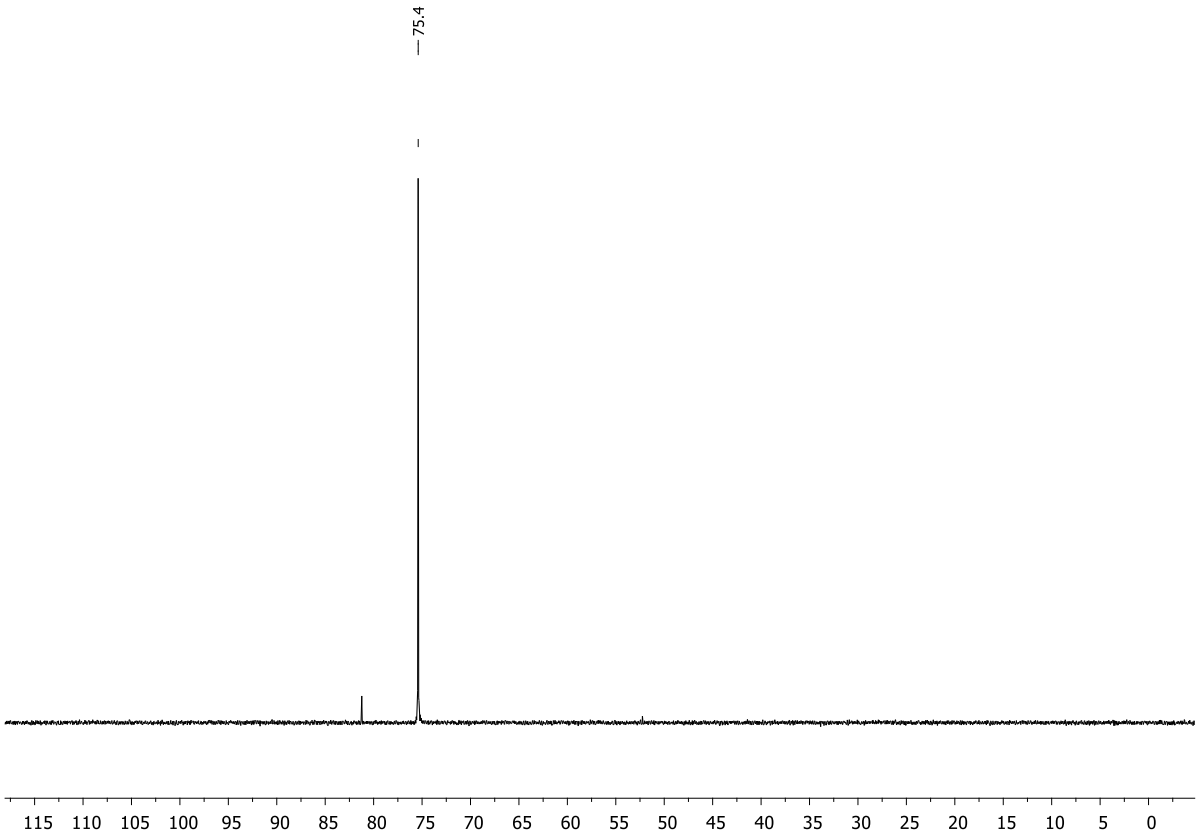

Figure S3.21. $^{31}P\{^{1}H\}$ NMR spectrum (C_6D_6, 298 K) of compound (S_P)-**8**.

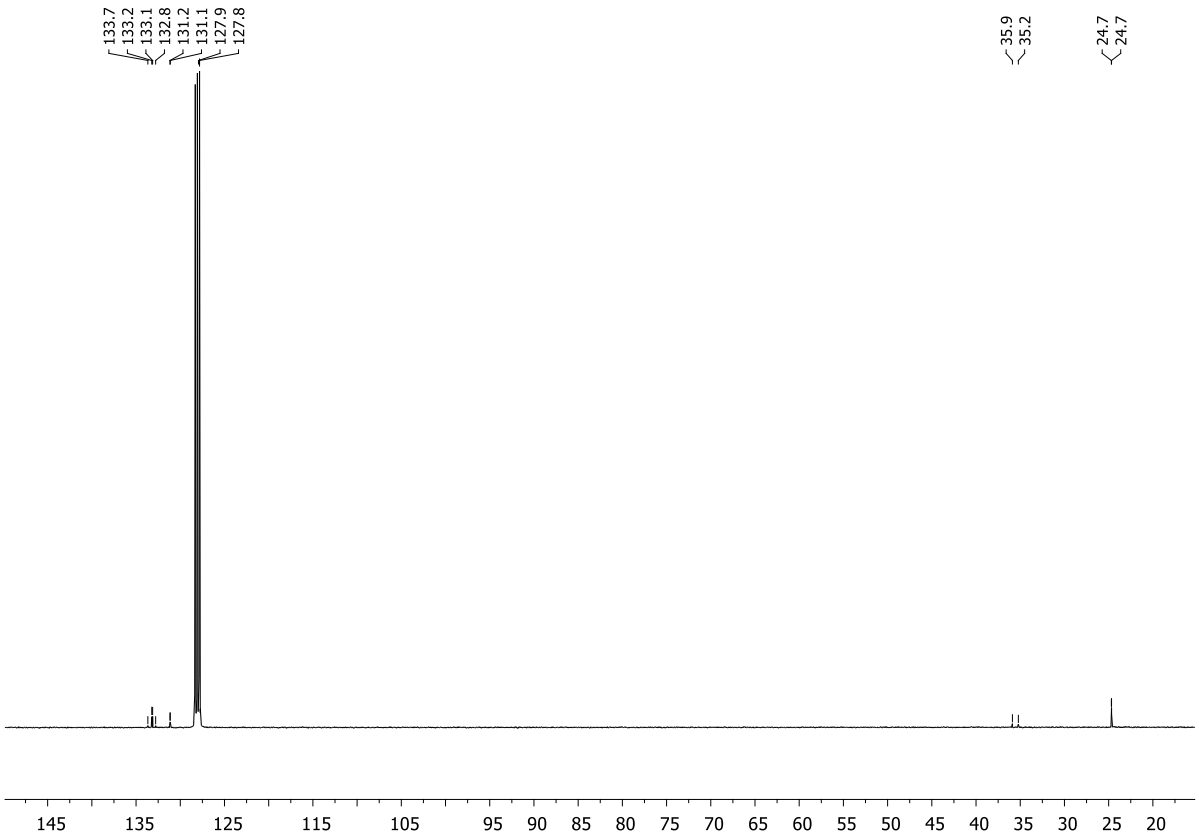

Figure S3.22. $^{13}C\{^{1}H\}$ NMR spectrum (C_6D_6, 298 K) of compound (S_P)-**8**.

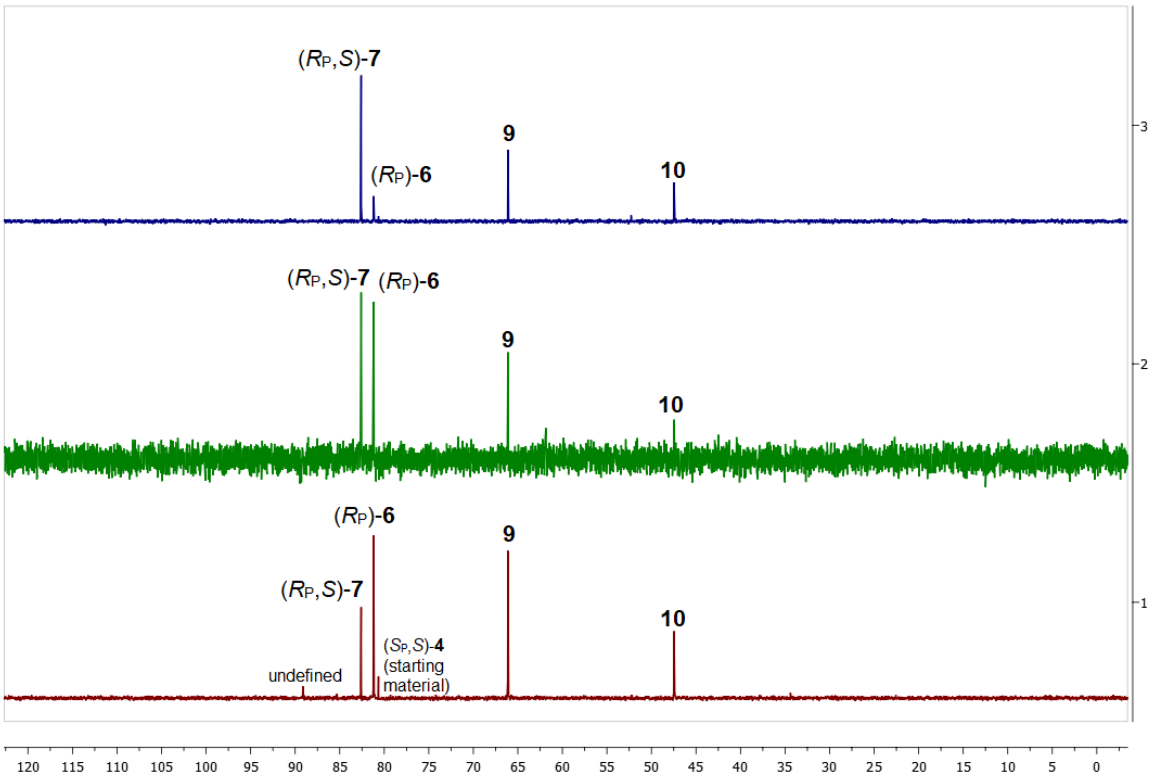

Figure S3.23. $^{31}P\{^{1}H\}$ NMR spectra (C_6D_6, 298 K) of the crude mixture of the reaction of compound (S_P,*S*)-**4** with lithium/*tert*-butanol in liquid ammonia after one (top/blue), two (middle/green), and three (bottom/red) minutes.

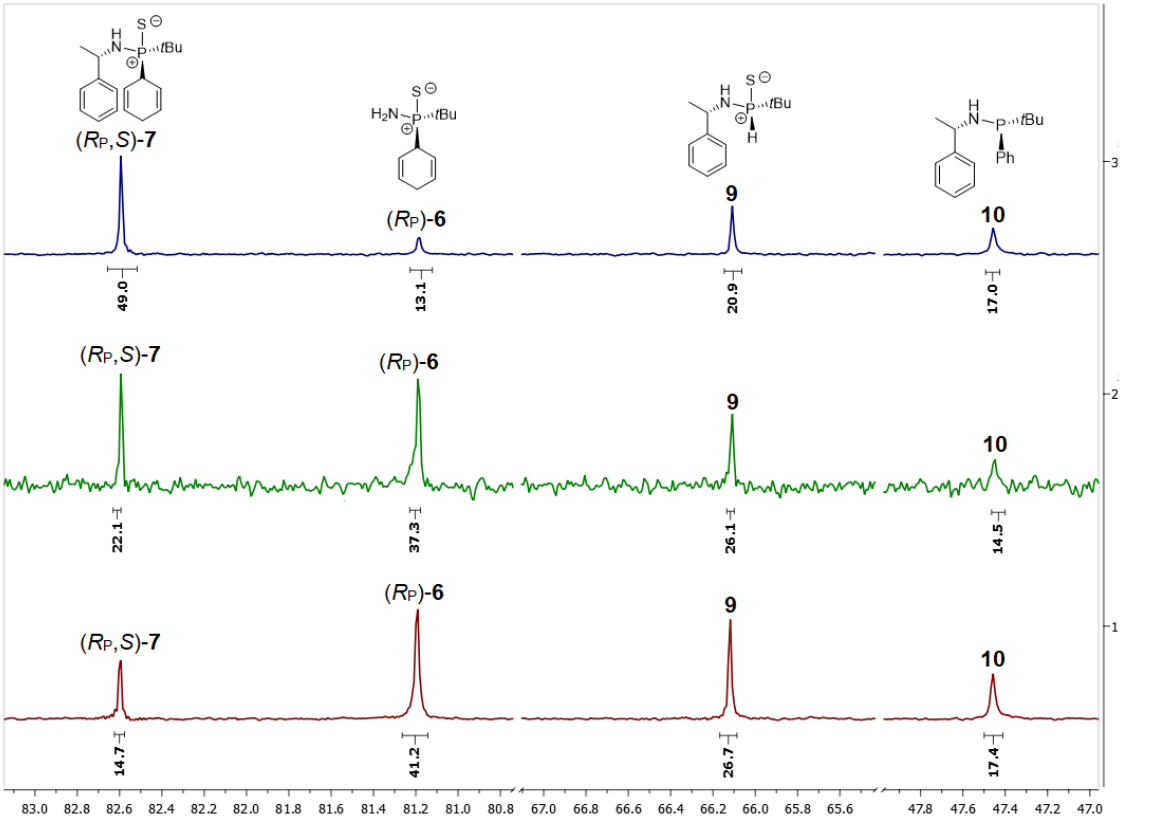

Figure S3.24. $^{31}P\{^{1}H\}$ NMR spectra (C_6D_6, 298 K) of the crude mixture of the reaction of compound (S_P,*S*)-**4** with lithium/*tert*-butanol in liquid ammonia after one (top/blue), two (middle/green), and three (bottom/red) minutes. Integration over all main products formed.

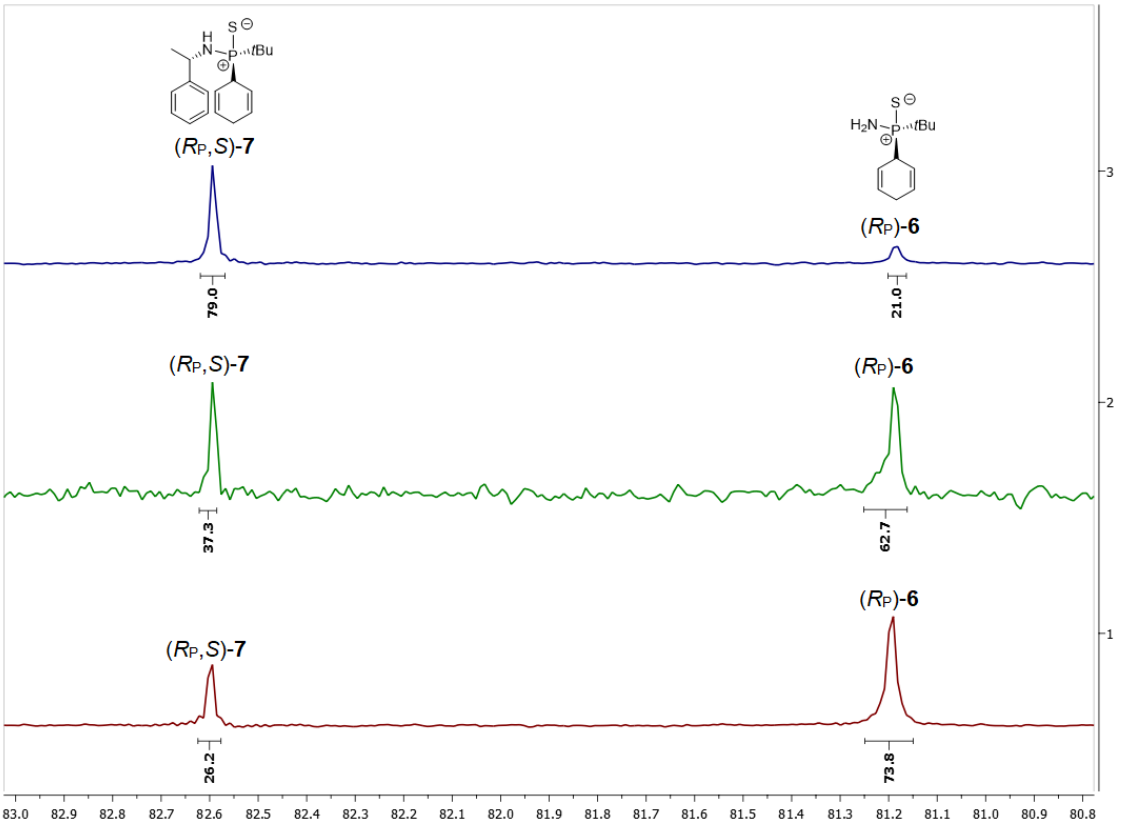

Figure S3.25. $^{31}P\{^{1}H\}$ NMR spectra (C_6D_6, 298 K) of the crude mixture of the reaction of compound (S_P,*S*)-**4** with lithium/*tert*-butanol in liquid ammonia after one (top/blue), two (middle/green), and three (bottom/red) minutes. Integration only over the products (R_P)-**6** and (R_P,*S*)-**7**.

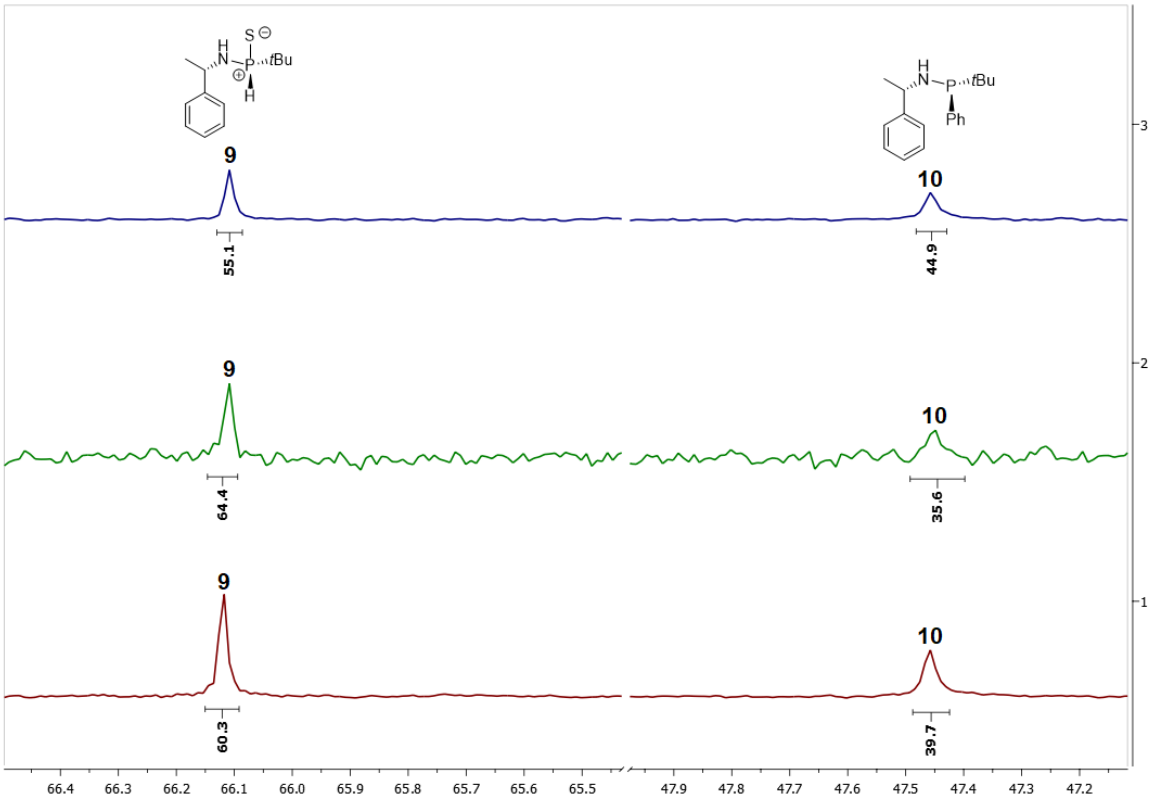

Figure S3.26. $^{31}P\{^{1}H\}$ NMR spectra (C_6D_6, 298 K) of the crude mixture of the reaction of compound (S_P,*S*)-**4** with lithium/*tert*-butanol in liquid ammonia after one (top/blue), two (middle/green), and three (bottom/red) minutes. Integration only over the products **9** and **10**.

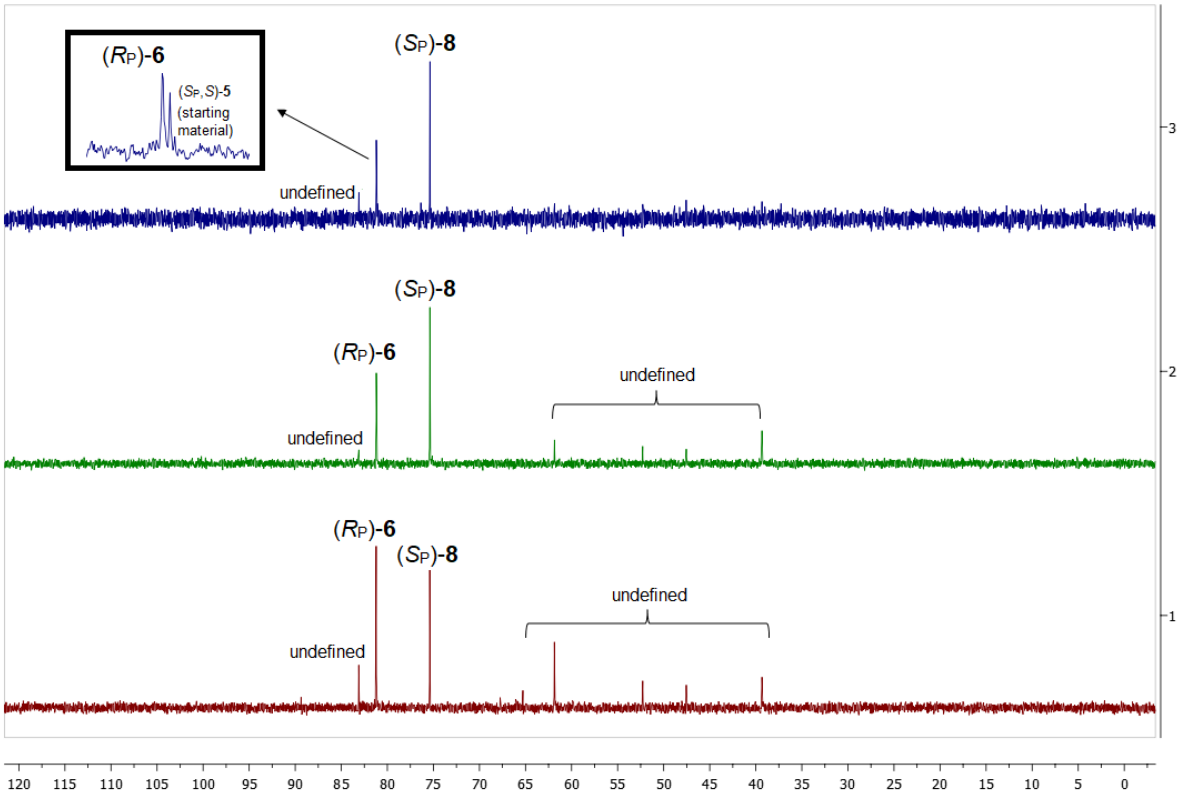

Figure S3.27. $^{31}P\{^{1}H\}$ NMR spectra (C_6D_6, 298 K) of the crude mixture of the reaction of compound (S_P,*S*)-**5** with lithium/*tert*-butanol in liquid ammonia after one (top/blue), two (middle/green), and three (bottom/red) minutes. The unspecified signals in the chemical shift region between 39 ppm and 63 ppm are likely to be attributed to P–Ph cleavage products and desulfurized compounds.

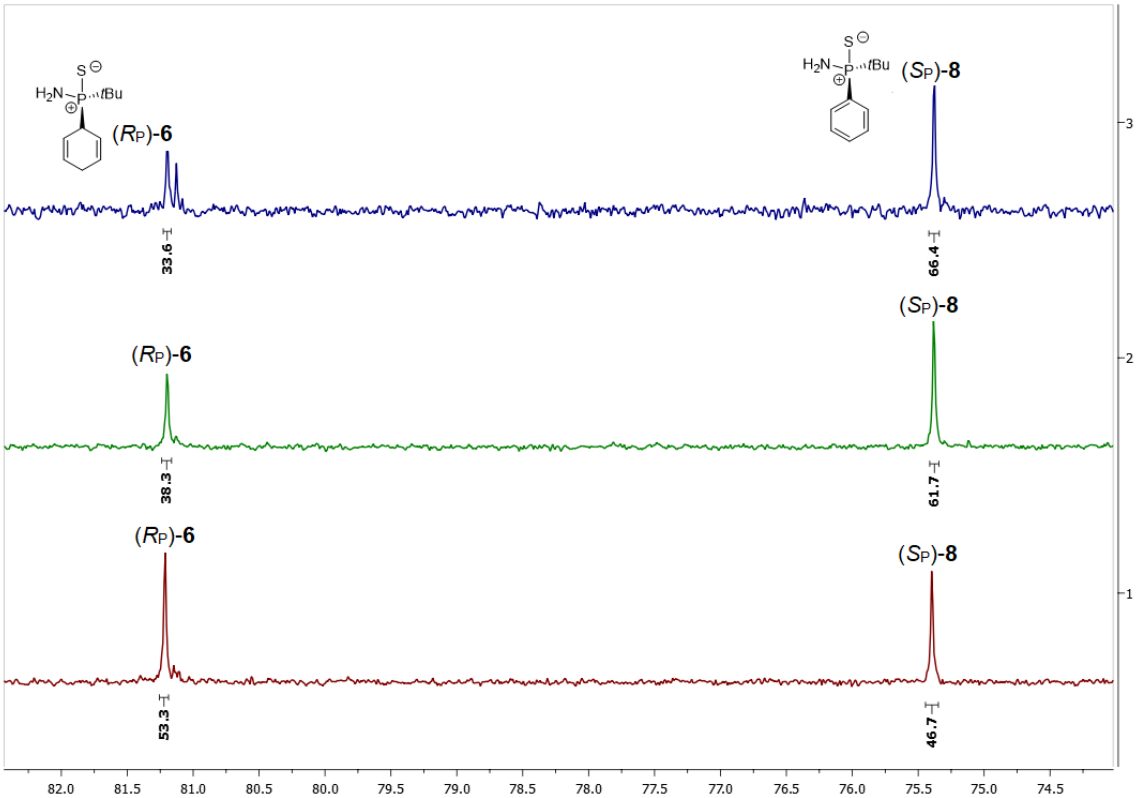

Figure S3.28. $^{31}P\{^{1}H\}$ NMR spectra (C_6D_6, 298 K) of the crude mixture of the reaction of compound (S_P,*S*)-**5** with lithium/*tert*-butanol in liquid ammonia after one (top/blue), two (middle/green), and three (bottom/red) minutes. Integration only over the products (R_P)-**6** and (S_P)-**8**.

3.6.2.5. Synthesis of (*rac*)-8

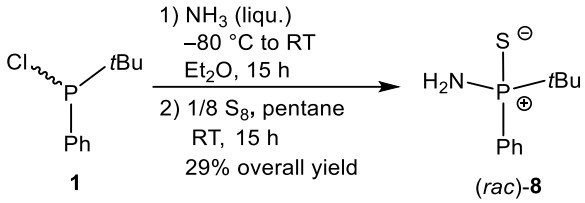

A solution of compound **1** (4.41 g, 22.0 mmol, 1.0 equiv.) in diethyl ether (50 mL) was cooled to –80 °C and ammonia was condensed into the solution. The reaction mixture was allowed to slowly warm to room temperature and stirred for 15 h. The formed precipitate was filtered off *via* cannula filtration and all volatiles of the filtrate were removed *in vacuo*. The crude intermediate was dissolved in pentane (50 mL), added to a flask loaded with sulfur (0.70 g, 22.0 mmol, 1.0 equiv.), and stirred for 15 h yielding a colorless suspension. The liquid phase was removed *via* cannula filtration and the remaining solid extracted with dichloromethane. Then, all volatiles were removed *in vacuo* to yield (*rac*)-**8** as a colorless solid (1.35 g, 6.33 mmol, 29% overall yield). Crystals suitable for single-crystal X-ray diffraction analysis were obtained by recrystallization from dichloromethane/pentane at room temperature.

^{1}H NMR (400.13 MHz, C_6D_6, 298 K): δ 0.98 [d, $^{3}J_{H-P}$ = 16.7 Hz, 9H, PC(CH_3)$_3$], 1.79 (br, 2H, NH_2), 7.08–7.05 (m, 3H, H_{ar}), 7.91–7.86 (m, 2H, H_{ar}). **^{31}P{^{1}H} NMR** (162.04 MHz, C_6D_6, 298 K): δ 75.4. **^{13}C{^{1}H} NMR** (100.61 MHz, C_6D_6, 298 K): δ 24.7 [d, $^{2}J_{C-P}$ = 2.0 Hz, PC(CH$_3$)$_3$], 35.6 [d, $^{1}J_{C-P}$ = 67.3 Hz, PC(CH$_3$)$_3$], 127.9 (d, $^{2}J_{C-P}$ = 11.8 Hz, C_o), 131.2 (d, $^{4}J_{C-P}$ = 2.9 Hz, C_p), 133.0 (d, $^{1}J_{C-P}$ = 89.3 Hz, PC_i), 133.2 (d, $^{3}J_{C-P}$ = 9.8 Hz, C_m). **^{1}H NMR** (400.13 MHz, CD_2Cl_2, 298 K): δ 1.15 [d, $^{3}J_{H-P}$ = 16.9 Hz, 9H, PC(CH_3)$_3$], 2.60 (br, 2H, NH_2), 7.54–7.45 (m, 3H, H_{ar}), 7.93–7.98 (m, 2H, H_{ar}). **^{31}P{^{1}H} NMR** (162.04 MHz, CD_2Cl_2, 298 K): δ 76.4. **^{13}C{^{1}H} NMR** (100.61 MHz, CD_2Cl_2, 298 K): δ 25.0 [d, $^{2}J_{C-P}$ = 2.0 Hz, PC(CH$_3$)$_3$], 36.0 [d, $^{1}J_{C-P}$ = 66.7 Hz, PC(CH$_3$)$_3$], 128.4 (d, $^{2}J_{C-P}$ = 11.9 Hz, C_o), 131.9 (d, $^{4}J_{C-P}$ = 2.9 Hz, C_p), 132.8 (d, $^{1}J_{C-P}$ = 89.6 Hz, PC_i), 133.2 (d, $^{3}J_{C-P}$ = 9.8 Hz, C_m). **HR(ESI)-MS**: Calcd *m*/*z* for $C_{10}H_{17}NPS$ [(M + H)$^+$]: 214.0814. Found: 214.0814. **CHN Analysis**: Calcd for $C_{10}H_{16}NPS \cdot 0.05\ CH_2Cl_2$: C, 55.49; H, 7.46; N, 6.44. Found: C, 55.71; H, 7.07; N, 6.38.

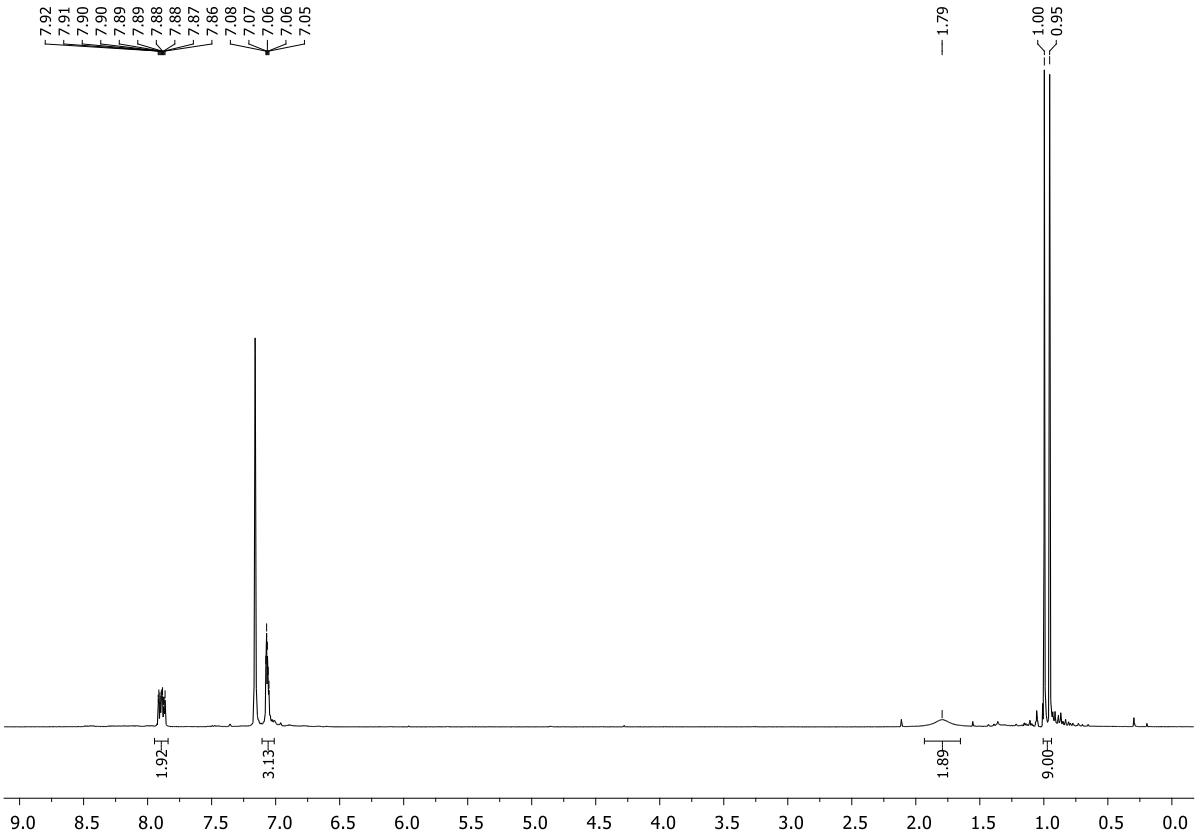

Figure S3.29. ^{1}H NMR spectrum (C_6D_6, 298 K) of compound (*rac*)-**8**.

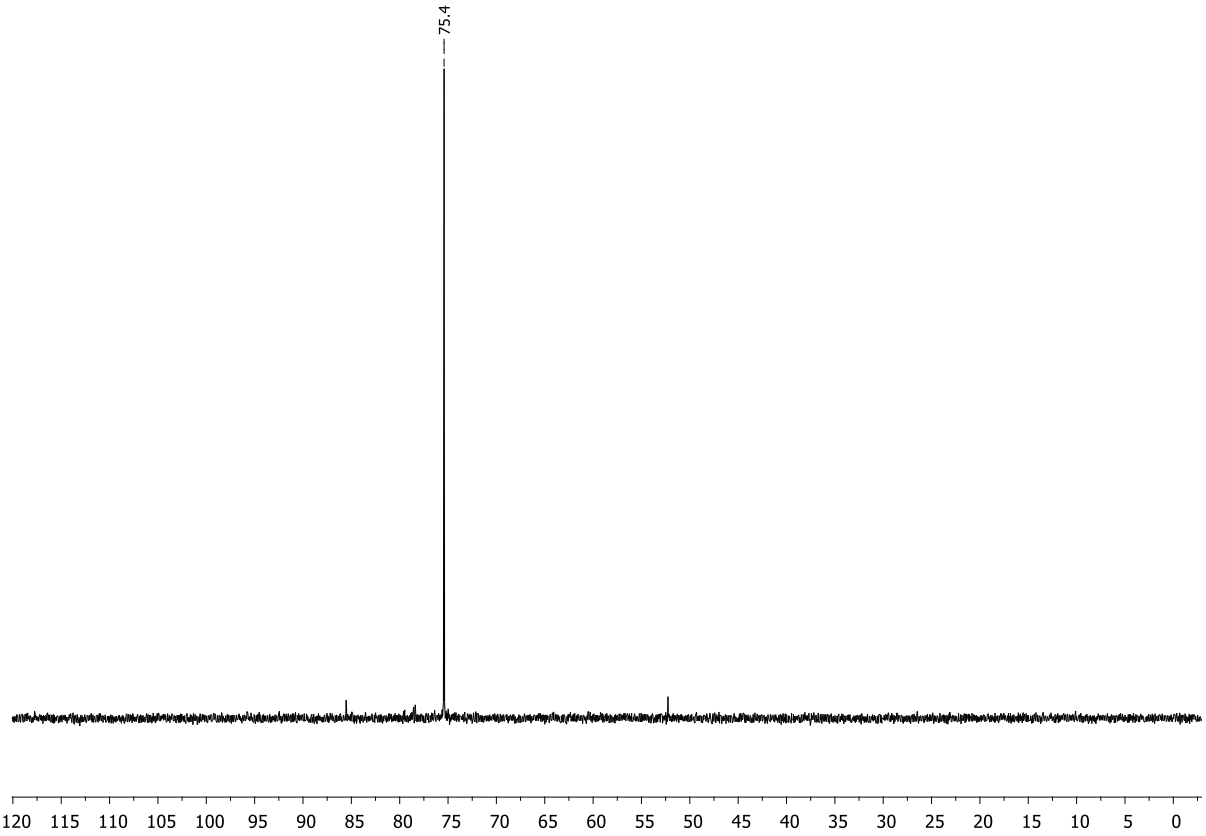

Figure S3.30. $^{31}P\{^{1}H\}$ NMR spectrum (C_6D_6, 298 K) of compound (*rac*)-**8**.

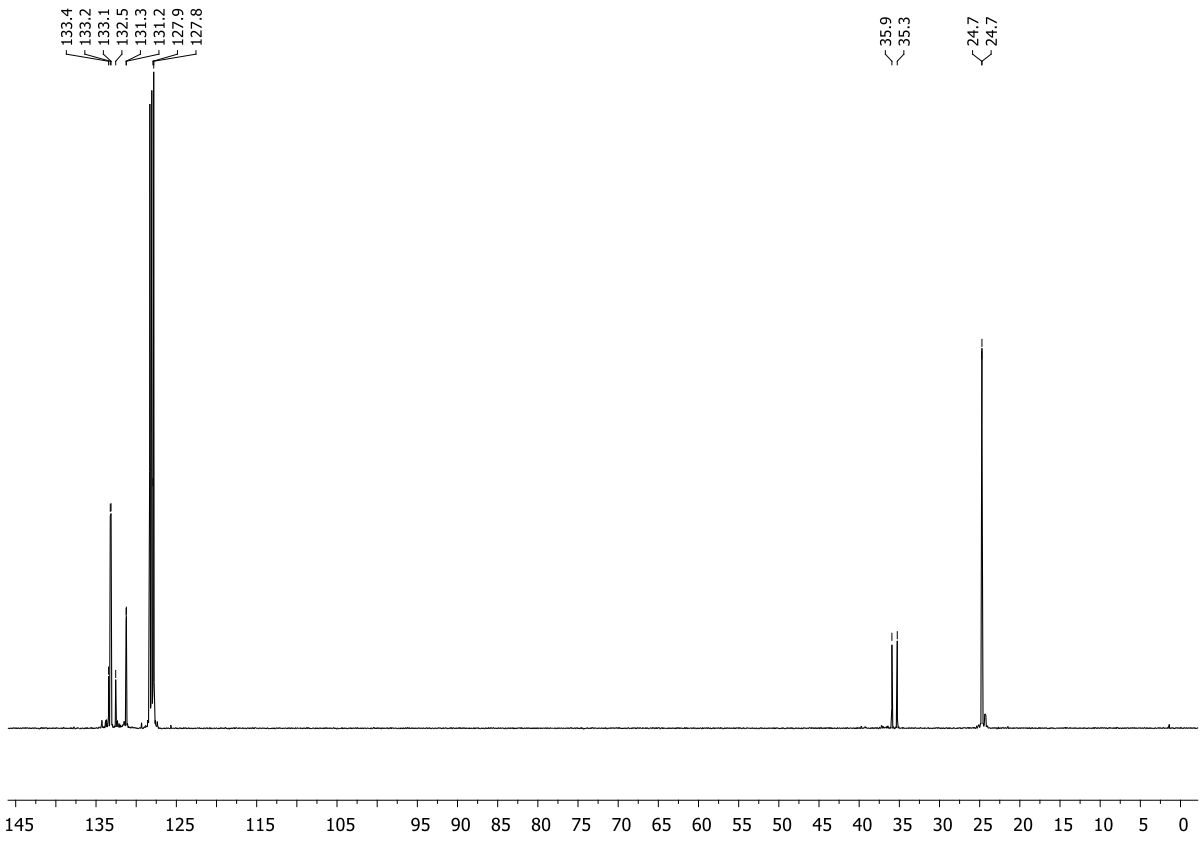

Figure S3.31. $^{13}C\{^{1}H\}$ NMR spectrum (C_6D_6, 298 K) of compound (*rac*)-**8**.

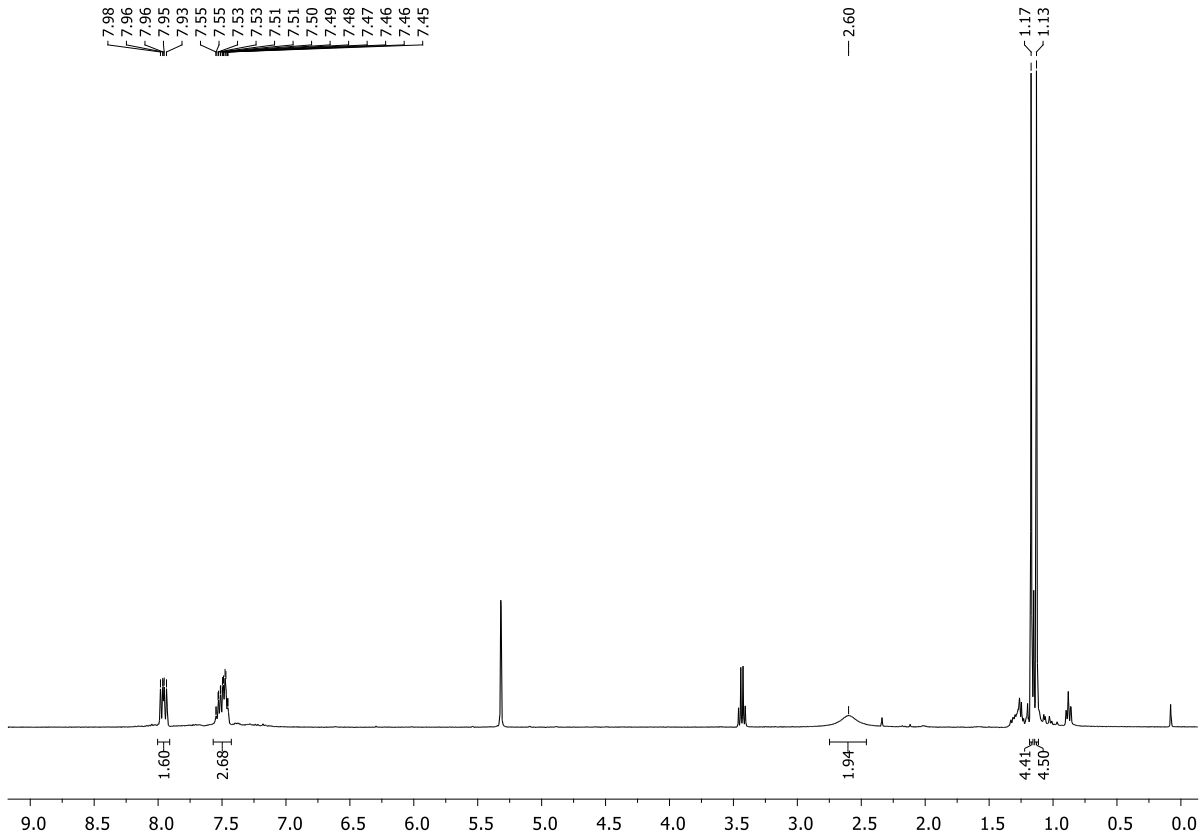

Figure S3.32. ^{1}H NMR spectrum (CD_2Cl_2, 298 K) of compound (*rac*)-**8**.

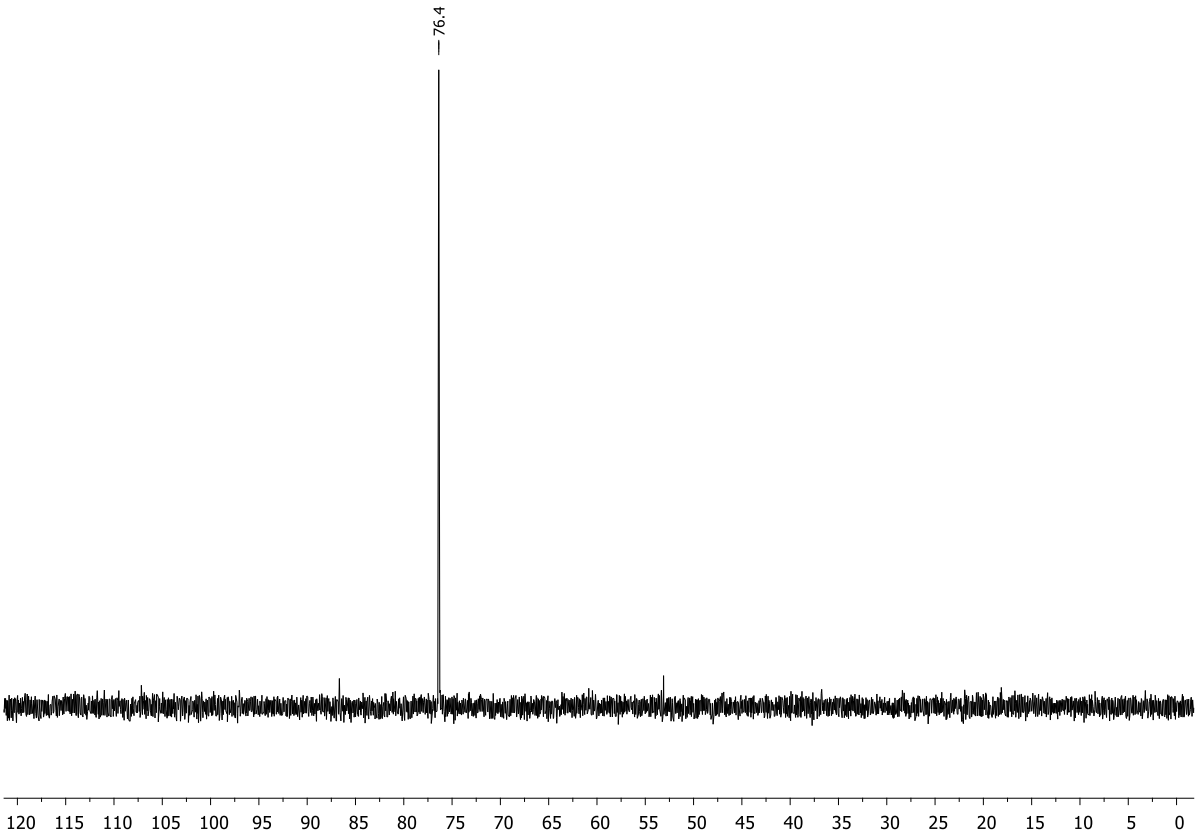

Figure S3.33. $^{31}P\{^{1}H\}$ NMR spectrum (CD_2Cl_2, 298 K) of compound (*rac*)-**8**.

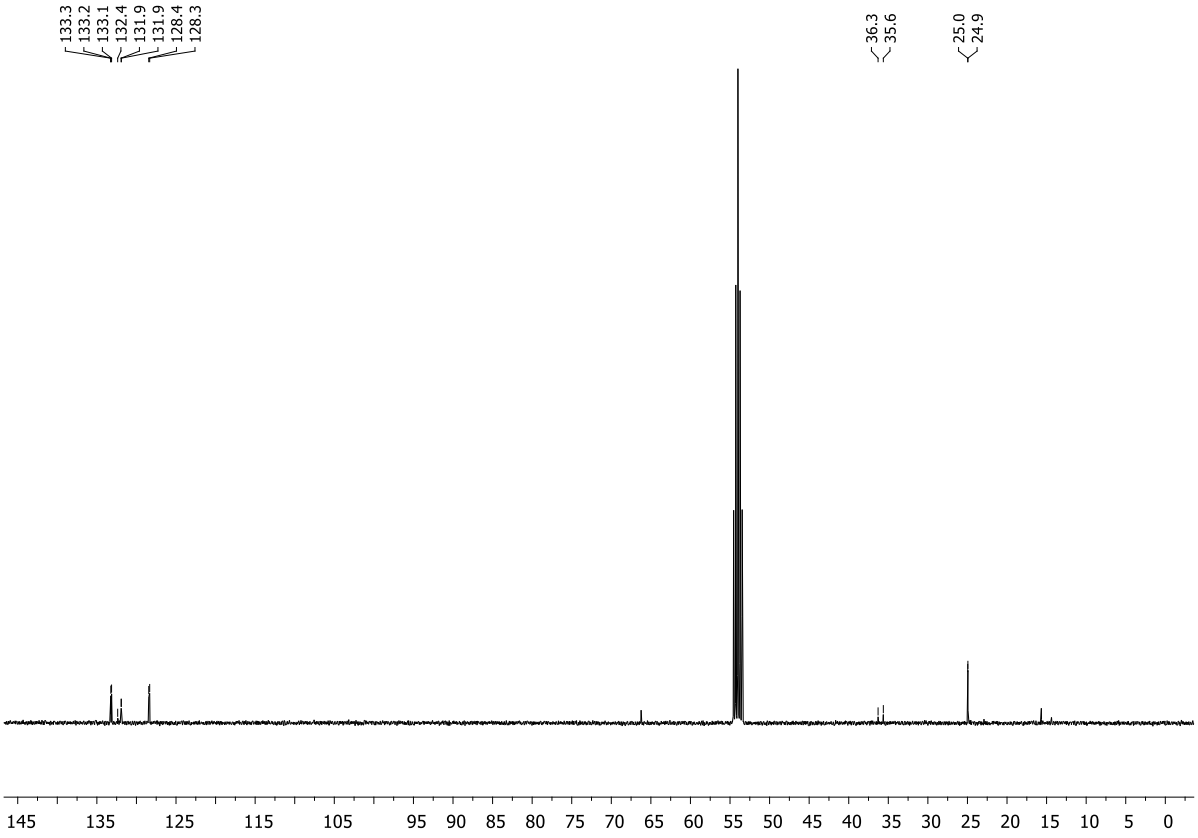

Figure S3.34. $^{13}C\{^{1}H\}$ NMR spectrum (CD_2Cl_2, 298 K) of compound (*rac*)-**8**.

3.6.2.6. Synthesis of *tert*-butylchlorocyclohexylphosphine (11)

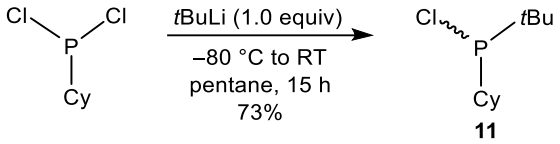

11

tert-Butyllithium (2.97 mL of a 1.6 M solution in pentane, 4.76 mmol, 1.0 equiv.) was slowly added to a solution of dichlorocyclohexylphosphine (0.88 g, 4.76 mmol, 1.0 equiv.) in pentane (10 mL) at –80 °C. The reaction mixture was allowed to slowly warm to room temperature and stirred for 15 h. The precipitated lithium chloride was filtered off *via* cannula filtration. Then, all volatiles of the filtrate were removed *in vacuo*. Compound **11** was obtained as a yellowish liquid (0.72 g, 3.48 mmol, 73%).

^{1}H NMR (400.13 MHz, C_6D_6, 298 K): *δ* 1.05 [d, $^{3}J_{H–P}$ = 12.2 Hz, 9H, PC(C*H*$_3$)$_3$], 1.22–1.10 (m, 4H, C*H*$_2$), 1.38–1.24 (m, 2H, C*H*$_2$), 1.50–1.46 (m, 1H, C*H*$_2$), 1.61–1.54 (m, 1H, C*H*$_2$), 1.68–1.64 (m, 2H, C*H*$_2$), 2.09–2.05 (m, 1H, PC*H*). **^{31}P{^{1}H} NMR** (162.04 MHz, C_6D_6, 298 K): *δ* 137.8. **^{13}C{^{1}H} NMR** (100.61 MHz, C_6D_6, 298 K): *δ* 26.2 [d, $^{2}J_{C–P}$ = 1.1 Hz, PC(*C*H$_3$)$_3$], 26.5 (s, *C*H$_2$), 26.7 (s, *C*H$_2$), 26.9 (s, *C*H$_2$), 33.5 [d, $^{1}J_{C–P}$ = 33.5 Hz, P*C*(CH$_3$)$_3$], 39.2 (d, $^{1}J_{C–P}$ = 37.9 Hz, P*C*H). **GC/EI-MS**: *m*/*z* (%) = 206 (8) [M$^{+\bullet}$], 83 (14) [$C_6H_{11}^{+\bullet}$], 57 (100) [$C_4H_9^{+\bullet}$].

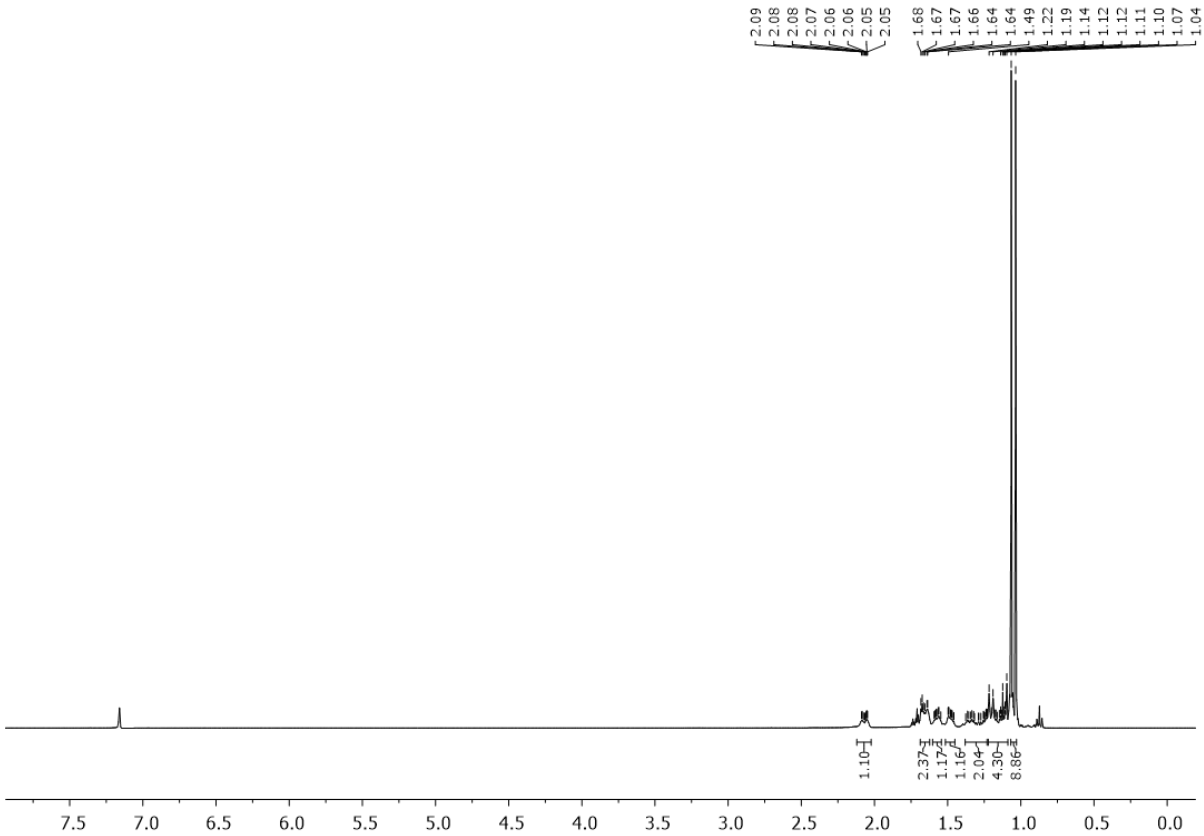

Figure S3.35. ^{1}H NMR spectrum (C_6D_6, 298 K) of compound **11**.

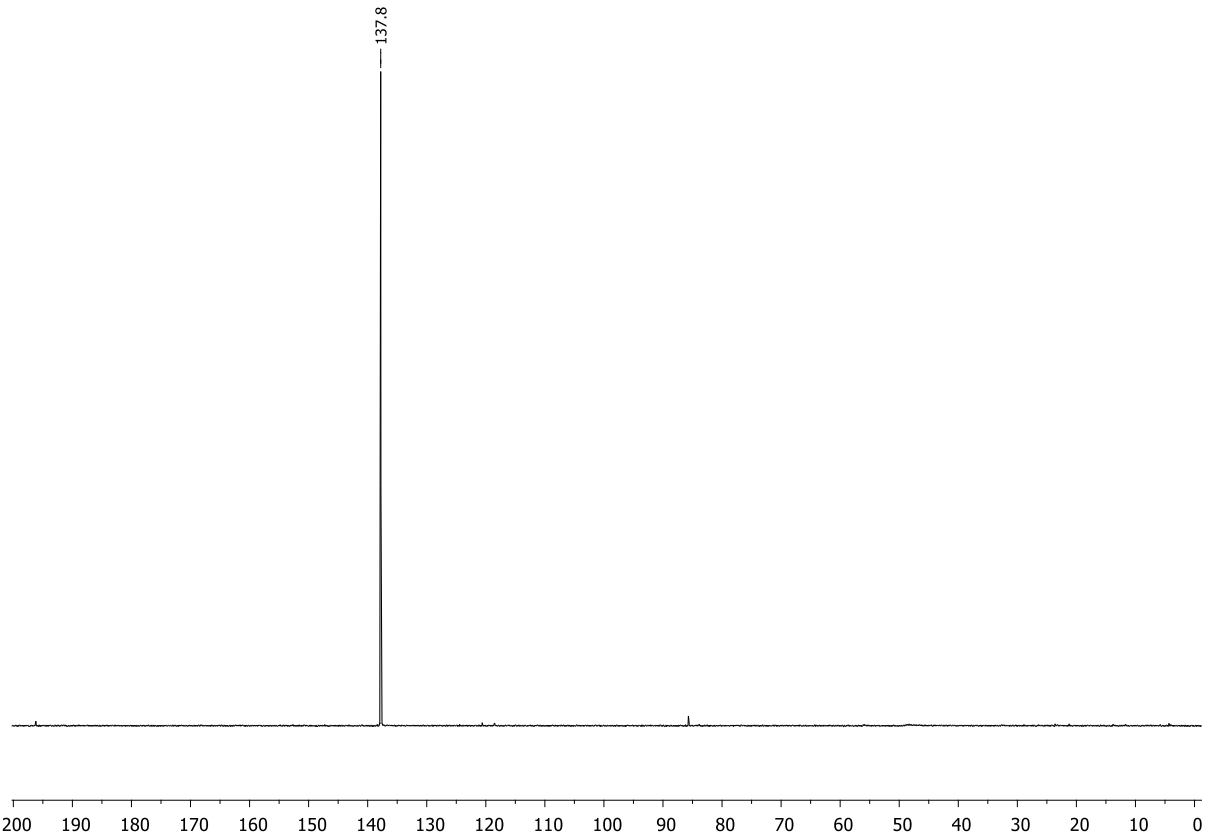

Figure S3.36. $^{31}P\{^{1}H\}$ NMR spectrum (C_6D_6, 298 K) of compound **11**.

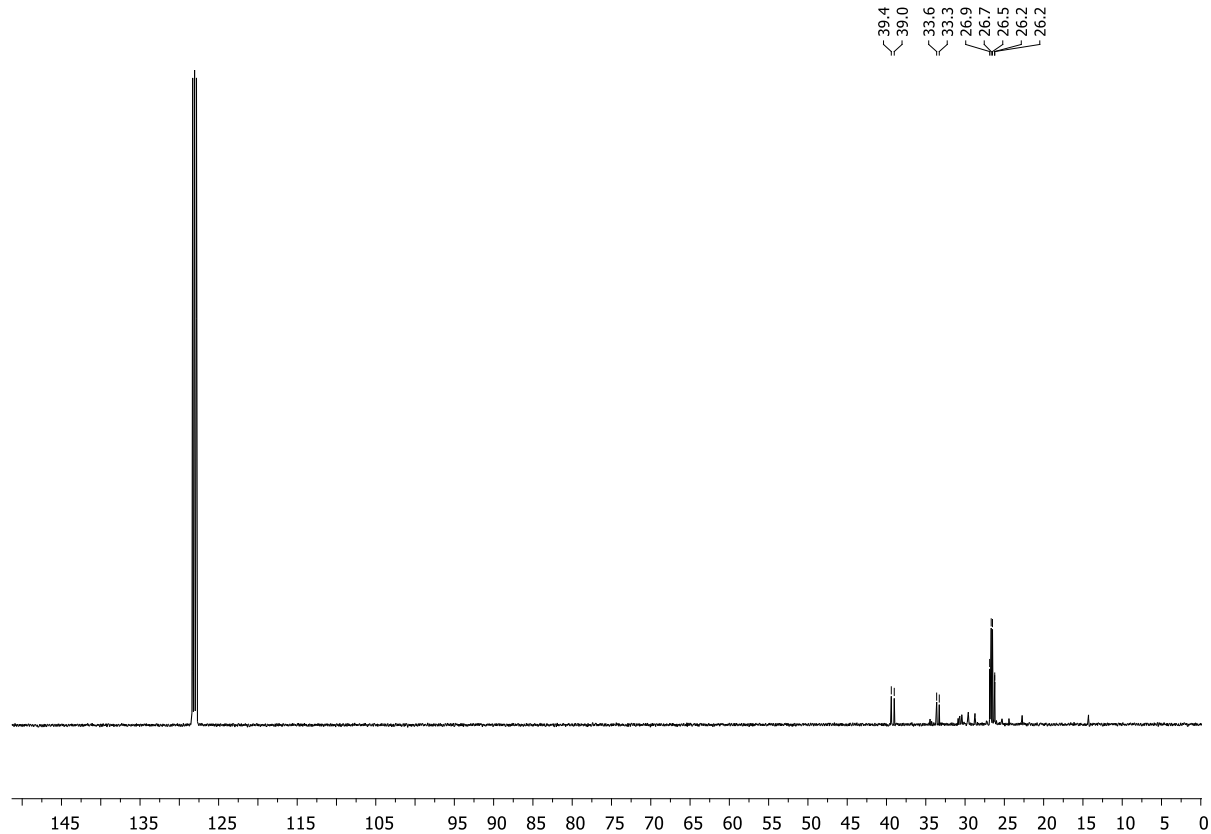

Figure S3.37. $^{13}C\{^{1}H\}$ NMR spectrum (C_6D_6, 298 K) of compound **11**.

3.6.2.7. Synthesis of (R_P,S)-12

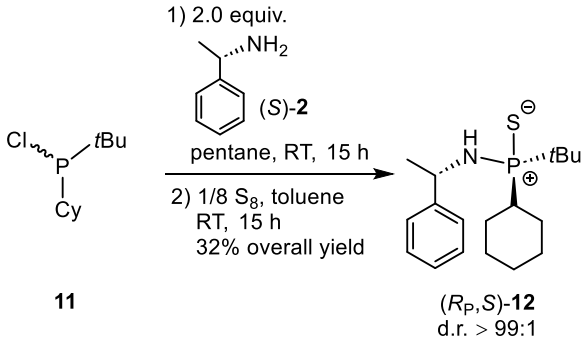

Compound (*S*)-**2** (4.24 mL, 3.99 g, 32.96 mmol, 2.0 equiv.) was added to a solution of compound **11** (3.41 g, 16.48 mmol, 1.0 equiv.) in pentane (40 mL) at room temperature. After stirring for 15 h, the solids were filtered off by transferring the liquid phase *via* cannula filtration directly into another Schlenk tube filled with sulfur (0.53 g, 16.48 mmol, 1.0 equiv.). The reaction mixture was stirred at room temperature for 15 h. Then, all volatiles were removed *in vacuo*. The ^{1}H and ^{31}P{^{1}H} NMR spectra of the crude product showed the formation of the desired product (R_P,S)-**12** in a 3:1 diastereomeric ratio. The crude product was recrystallized from toluene/hexane at **–**25 °C. Compound (R_P,S)-**12** (1.70 g, 5.25 mmol, 32% overall yield, d.r. > 99:1) was obtained as colorless crystals suitable for single-crystal X-ray diffraction analysis.

^{1}H NMR (400.13 MHz, C_6D_6, 298 K): δ 0.87–0.96 (m, 3H, CH_2), 1.11 [d, $^{3}J_{H-P}$ = 15.4 Hz, 9H, PC(CH_3)$_3$], 1.18–1.29 (m, 1H, CH_2), 1.35 (d, $^{4}J_{H-P}$ = 6.8 Hz, 3H, CHCH_3), 1.38–1.44 (m, 2H, CH_2), 1.48–1.65 (m, 5H, CH_2, PCH), 1.94–1.98 (m, 1H, NH), 4.94–5.04 (m, 1H, CHCH$_3$), 7.03–7.07 (m, 1H, H_{ar}), 7.13–7.15 (m, 2H, H_{ar}), 7.21–7.23 (m, 2H, H_{ar}). **^{31}P{^{1}H} NMR** (162.04 MHz, C_6D_6, 298 K): δ 89.1. **^{13}C{^{1}H} NMR** (100.61 MHz, C_6D_6, 298 K): δ 25.8 (d, $^{3}J_{C-P}$ = 4.4 Hz, CH$_2$), 25.9 [d, $^{2}J_{C-P}$ = 1.1 Hz, PC(CH$_3$)$_3$], 26.0 (d, $^{4}J_{C-P}$ = 1.7 Hz, CH$_2$), 26.9 (d, $^{2}J_{C-P}$ = 10.7 Hz, CH$_2$), 27.0 (d, $^{2}J_{C-P}$ = 9.7 Hz, CH$_2$), 27.4 (d, $^{3}J_{C-P}$ = 3.4 Hz, CH$_2$), 28.7 (d, $^{3}J_{C-P}$ = 1.4 Hz, CHCH$_3$), 36.8 [d, $^{1}J_{C-P}$ = 61.3 Hz, PC(CH$_3$)$_3$], 40.6 (d, $^{1}J_{C-P}$ = 57.8 Hz, PCH), 50.8 (d, $^{2}J_{C-P}$ = 1.2 Hz, CHCH$_3$), 126.9 (s, C_{ar}), 127.1 (s, C_{ar}), 128.7 (s, C_{ar}), 146.7 (d, $^{3}J_{C-P}$ = 3.6 Hz, PC_i). **HR(ESI)-MS**: Calcd *m*/*z* for $C_{18}H_{31}NPS$ [(M + H)$^{+}$]: 324.1909. Found: 324.1914. **CHN Analysis**: Calcd for $C_{18}H_{30}NPS$: C, 66.84; H, 9.35; N, 4.33. Found: C, 66.75; H, 9.12; N, 4.22.

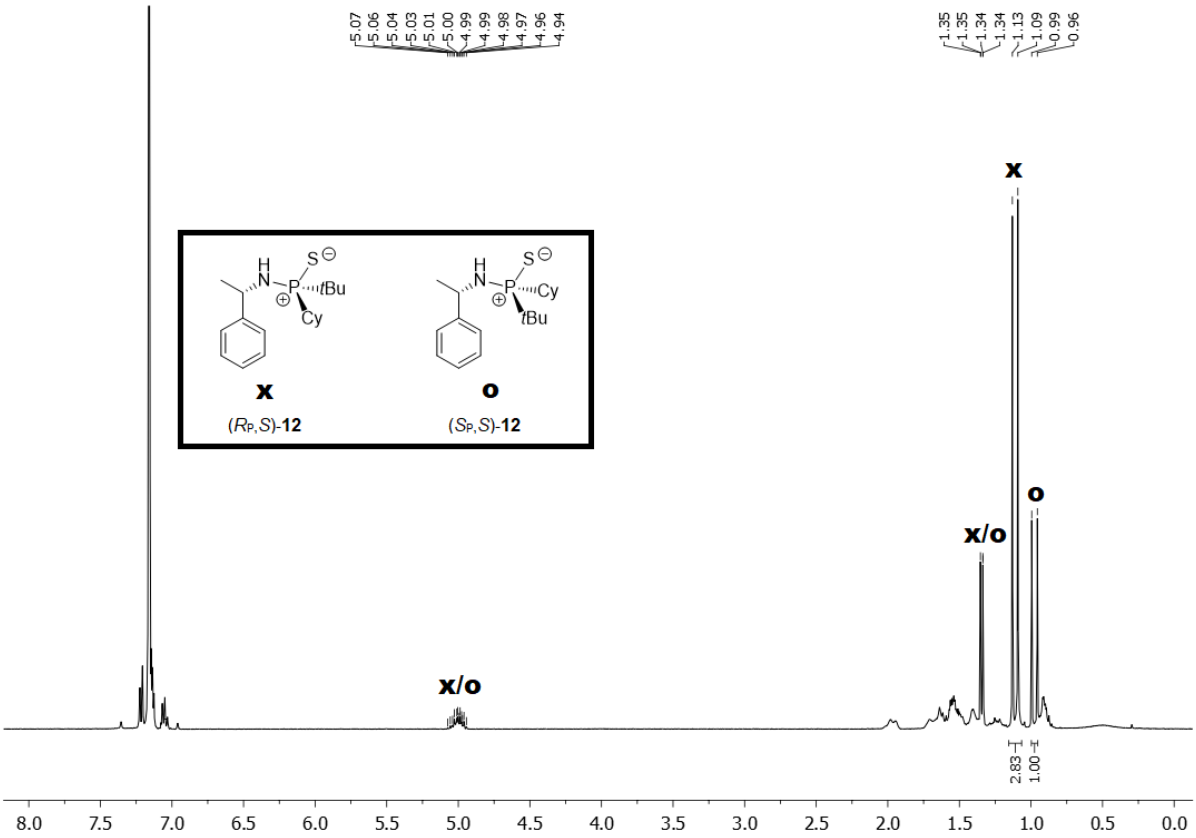

Figure S3.38. ^{1}H NMR spectrum (C_6D_6, 298 K) of the crude reaction mixture for determining the diastereomeric ratio. Compounds (R_P,S)-**12** and (S_P,S)-**12** were formed in a 3:1 diastereomeric ratio.

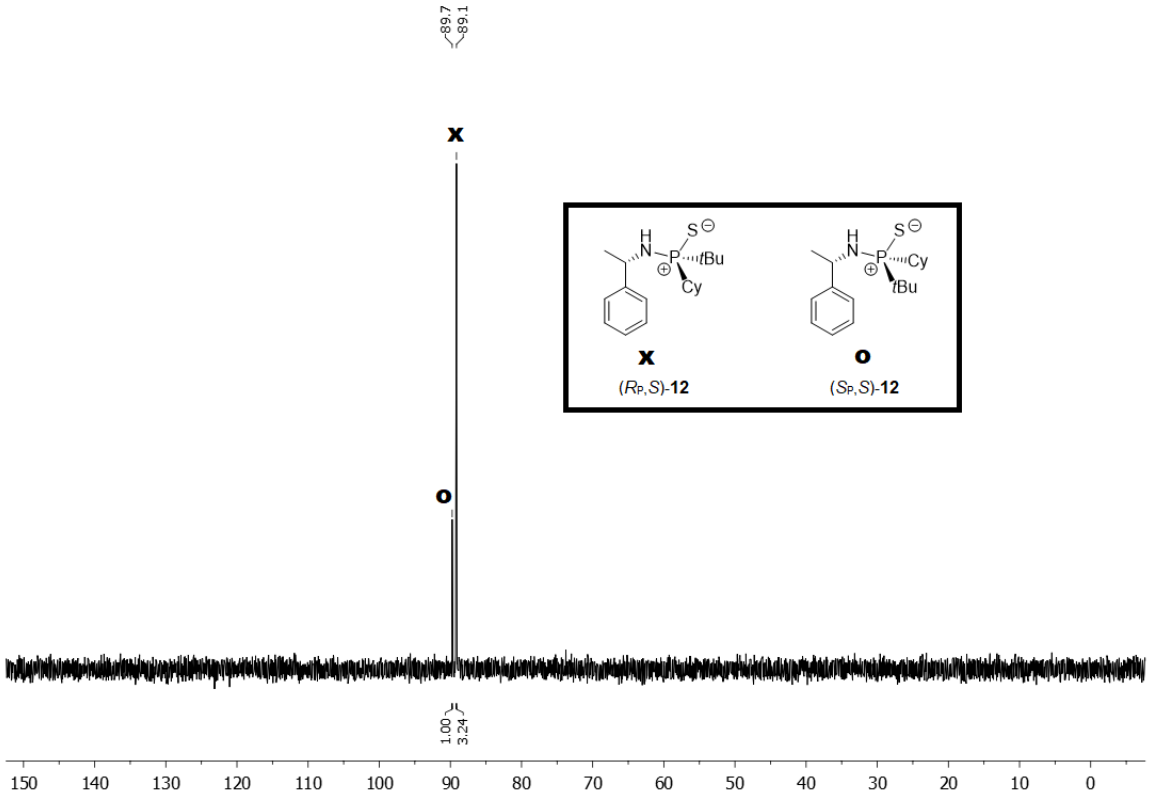

Figure S3.39. ^{31}P{^{1}H} NMR spectrum (C_6D_6, 298 K) of the crude reaction mixture for determining the diastereomeric ratio. Compounds (R_P,S)-**12** and (S_P,S)-**12** were formed in a 3:1 diastereomeric ratio.

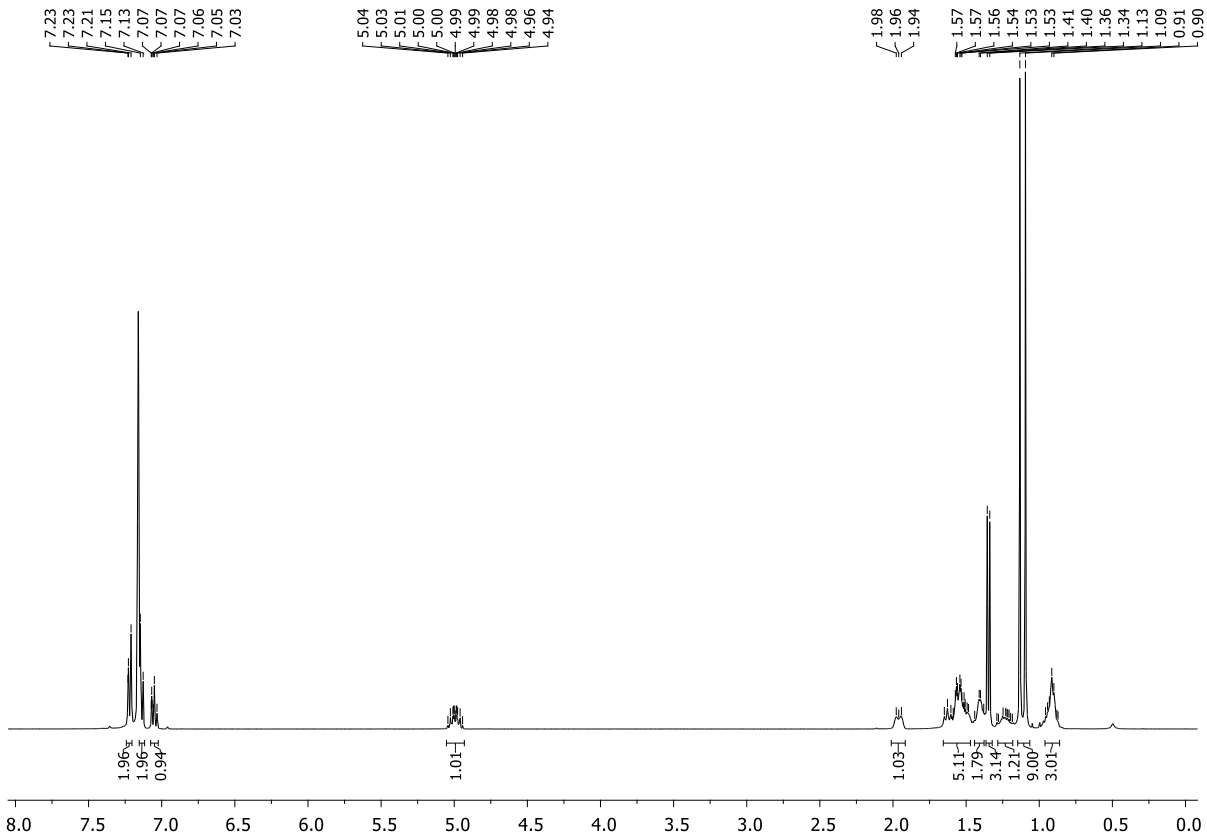

Figure S3.40. ^{1}H NMR spectrum (C_6D_6, 298 K) of compound (R_P,*S*)-**12**.

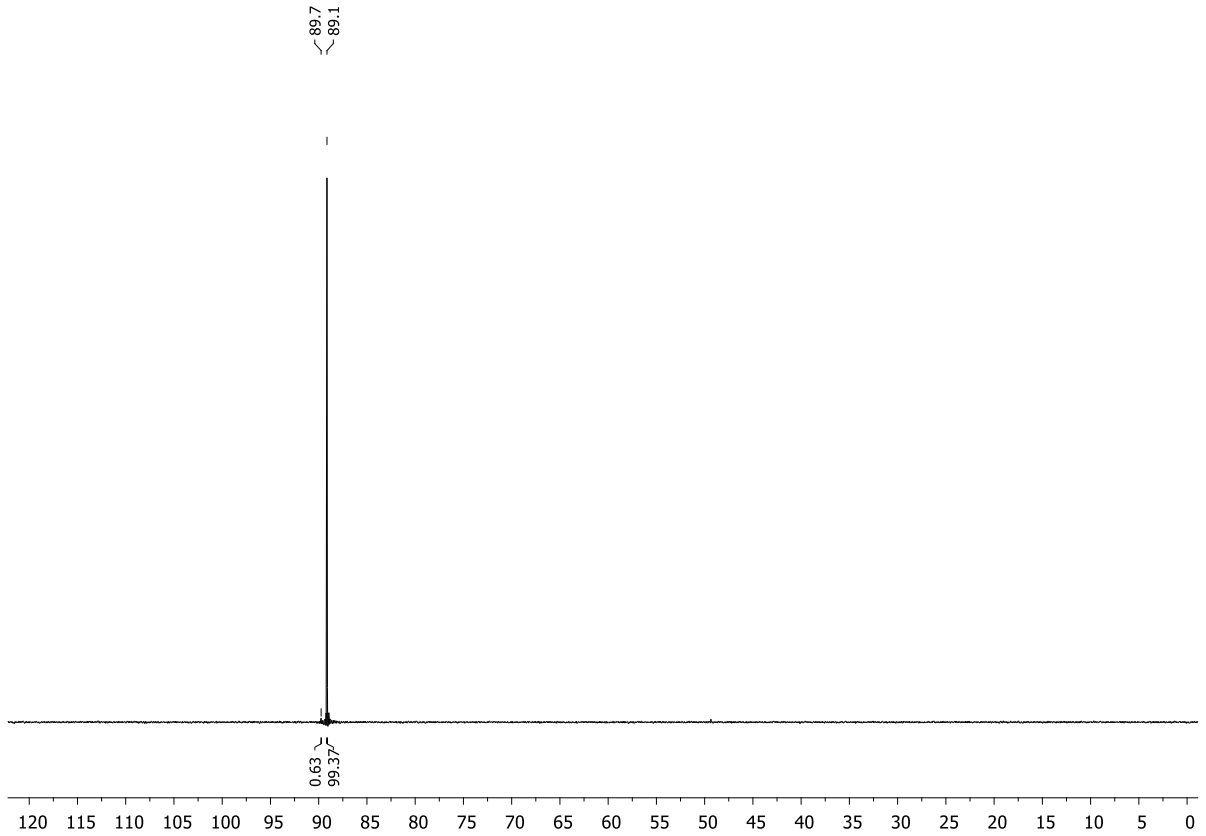

Figure S3.41. ^{31}P{^{1}H} NMR spectrum (C_6D_6, 298 K) of compound (R_P,*S*)-**12**.

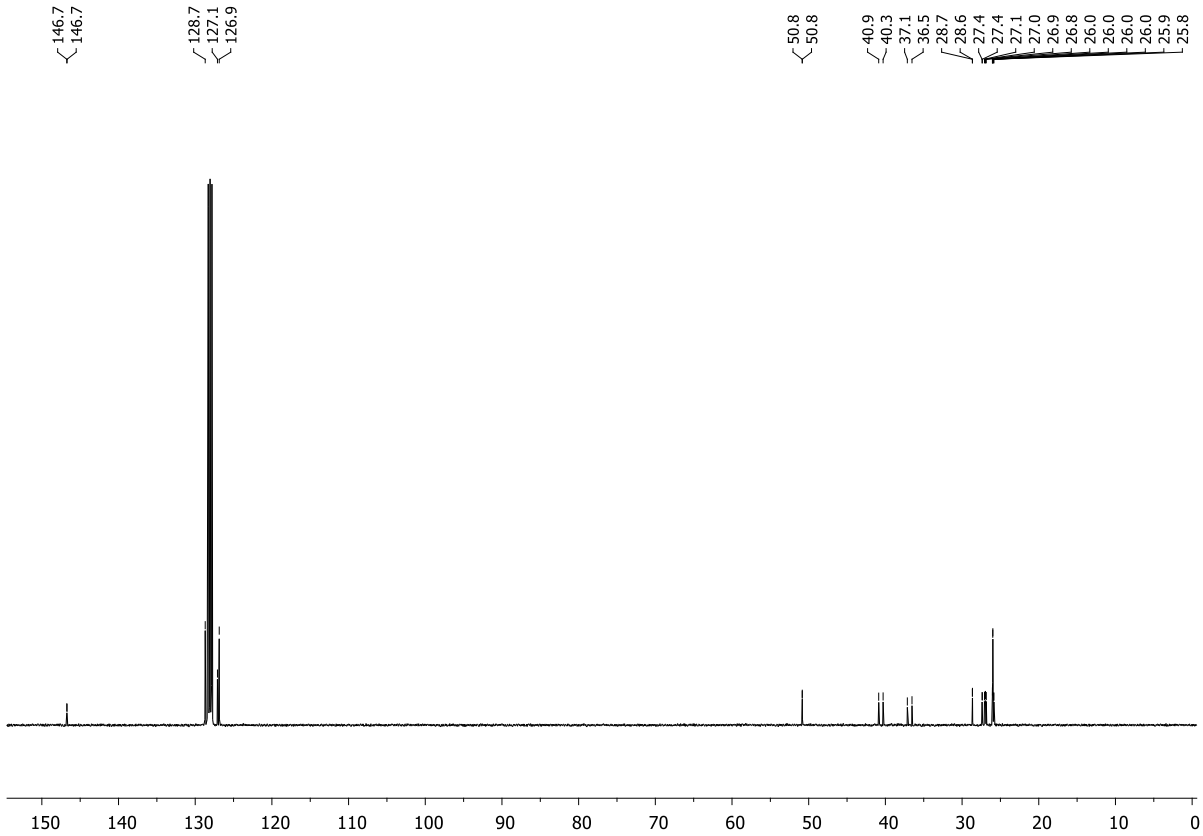

Figure S3.42. $^{13}C\{^{1}H\}$ NMR spectrum (C_6D_6, 298 K) of compound (R_P,*S*)-**12**.

3.6.2.8. Synthesis of (R_P)-13

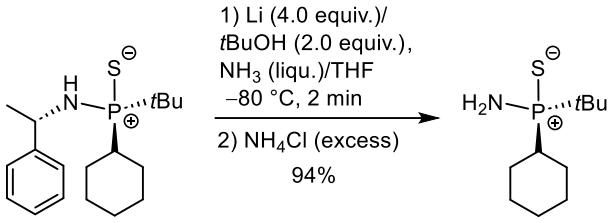

(R_P,S)-**12**
d.r. > 99:1

(R_P)-**13**
e.r. > 99:1

Ammonia (5 mL) was condensed into a flask containing lithium (24 mg, 3.48 mmol, 4.0 equiv.) at –80 °C. The mixture was stirred for 10 min while turning into a dark blue solution. Meanwhile, a solution of compound (R_P,S)-**12** (0.28 g, 0.87 mmol, 1.0 equiv.) and *tert*-butanol (0.17 mL, 1.74 mmol, 2.0 equiv.) in THF (5 mL) was prepared and then added to the solution of lithium in liquid ammonia in one portion. After stirring for 2 min, the mixture was quenched with ammonium chloride and the cooling bath removed allowing ammonia to evaporate. The crude mixture was extracted with diethyl ether (1 × 10 mL, 2 × 5 mL) and the solids were removed *via* cannula filtration. Then, all volatiles were removed *in vacuo* and the gel-like substance purified *via* Kugelrohr distillation (100**–**120 °C oven temperature, $1.0 \cdot 10^{-2}$ mbar). Compound (R_P)-**13** (0.18 g, 0.82 mmol, 94%, e.r. > 99:1) was obtained as a colorless solid. Crystals suitable for single-crystal X-ray diffraction analysis were obtained from diethyl ether by slow evaporation of the solvent. The enantiomeric purity of crude compound (R_P)-**13** was determined by ^{1}H and ^{31}P{^{1}H} NMR spectroscopy in the presence of (*R*)-BINOL-PSSLi (99% ee) in CD_2Cl_2 (for details, see Chapter 3.6.2.12).

^{1}H NMR (400.13 MHz, C_6D_6, 298 K): δ 1.06 [d, $^3J_{H–P}$ = 15.5 Hz, 9H, PC(CH_3)$_3$], 1.09–1.06 (m, 2H, CH_2), 1.48–1.42 (br, 2H, NH_2), 1.52–1.49 (m, 1H, CH_2), 1.66–1.56 (m, 7H, CH_2), 1.91–1.88 (m, 1H, PC*H*). **^{31}P{^{1}H} NMR** (162.04 MHz, C_6D_6, 298 K): δ 85.4. **^{13}C{^{1}H} NMR** (100.61 MHz, C_6D_6, 298 K): δ 25.7 [d, $^2J_{C–P}$ = 1.4 Hz, PC(*C*H$_3$)$_3$], 26.0 (d, $^3J_{C–P}$ = 1.6 Hz, *C*H$_2$), 26.6 (d, $^2J_{C–P}$ = 14.4 Hz, *C*H$_2$), 26.8 (d, $^2J_{C–P}$ = 13.5 Hz, *C*H$_2$), 28.3 (s, *C*H$_2$), 30.2 (s, *C*H$_2$), 36.2 [d, $^1J_{C–P}$ = 61.3 Hz, P*C*(CH$_3$)$_3$], 38.6 (d, $^1J_{C–P}$ = 58.2 Hz, P*C*H). **^{1}H NMR** (400.13 MHz, CD_2Cl_2, 298 K): δ 1.23 [d, $^3J_{H–P}$ = 15.8 Hz, 9H, PC(CH_3)$_3$], 1.38–1.26 (m, 3H, CH_2), 1.57–1.41 (m, 2H, CH_2), 1.71–1.67 (m, 1H, PC*H*), 1.92–1.79 (m, 3H, CH_2), 2.02–1.93 (m, 2H, CH_2), 2.12 (br, 2H, NH_2). **^{31}P{^{1}H} NMR** (162.04 MHz, CD_2Cl_2, 298 K): δ 86.7. **^{13}C{^{1}H} NMR** (100.61 MHz, CD_2Cl_2, 298 K): δ 25.9 [d, $^2J_{C–P}$ = 1.4 Hz, PC(*C*H$_3$)$_3$], 26.3 (d, $^3J_{C–P}$ = 1.6 Hz, *C*H$_2$), 26.8 (d, $^2J_{C–P}$ = 14.5 Hz, *C*H$_2$), 27.1 (d, $^2J_{C–P}$ = 12.8 Hz, *C*H$_2$), 27.2 (d, $^3J_{C–P}$ = 4.0 Hz, *C*H$_2$), 28.7 (s, *C*H$_2$), 36.5 [d, $^1J_{C–P}$ = 60.7 Hz, P*C*(CH$_3$)$_3$], 38.6 (d, $^1J_{C–P}$ = 58.1 Hz, P*C*H). **HR(ESI)-MS**: Calcd *m*/*z* for $C_{10}H_{23}NPS$ [(M + H)$^+$]: 220.1283. Found: 220.1276. **CHN Analysis**: Calcd for $C_{10}H_{22}NPS$: C, 54.76; H, 10.11; N, 6.39. Found: C, 55.21; H, 10.46; N, 6.15.

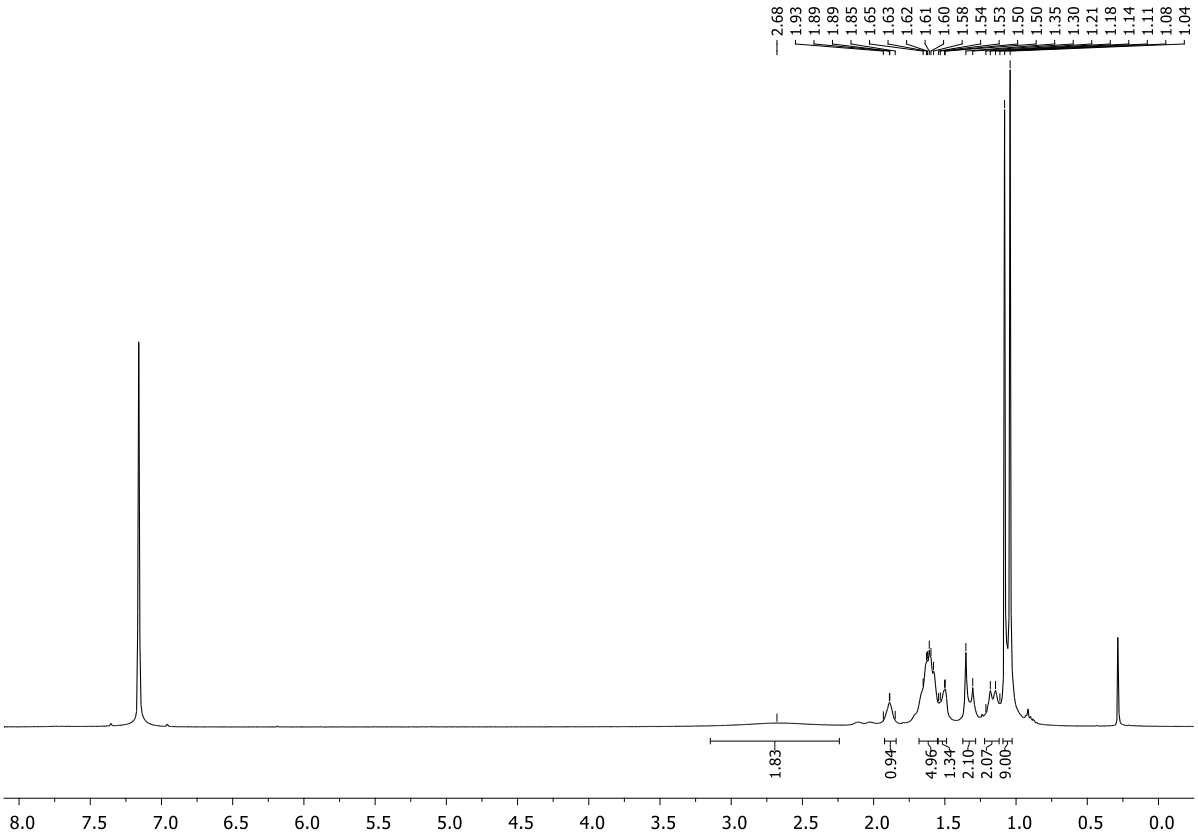

Figure S3.43. ^{1}H NMR spectrum (C_6D_6, 298 K) of the crude reaction mixture confirming that no by-products were formed.

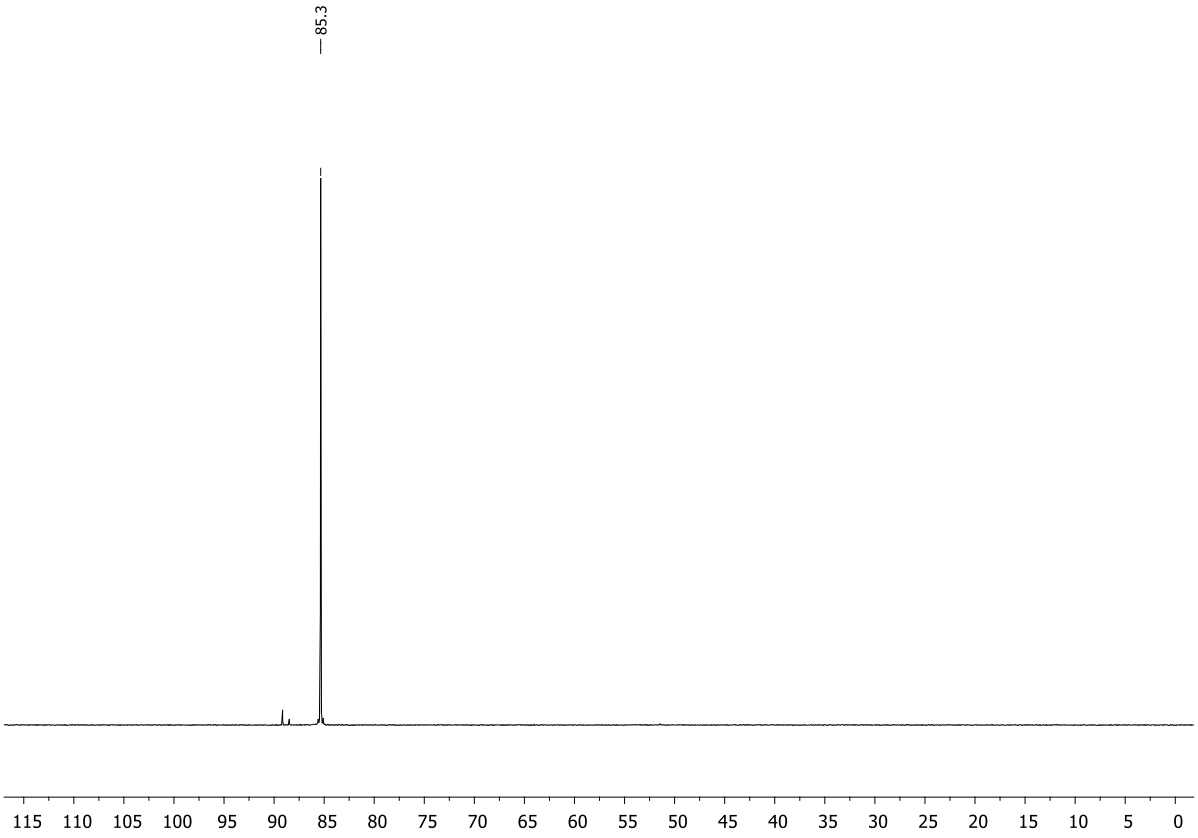

Figure S3.44. $^{31}P\{^{1}H\}$ NMR spectrum (C_6D_6, 298 K) of the crude reaction mixture confirming that no by-products were formed.

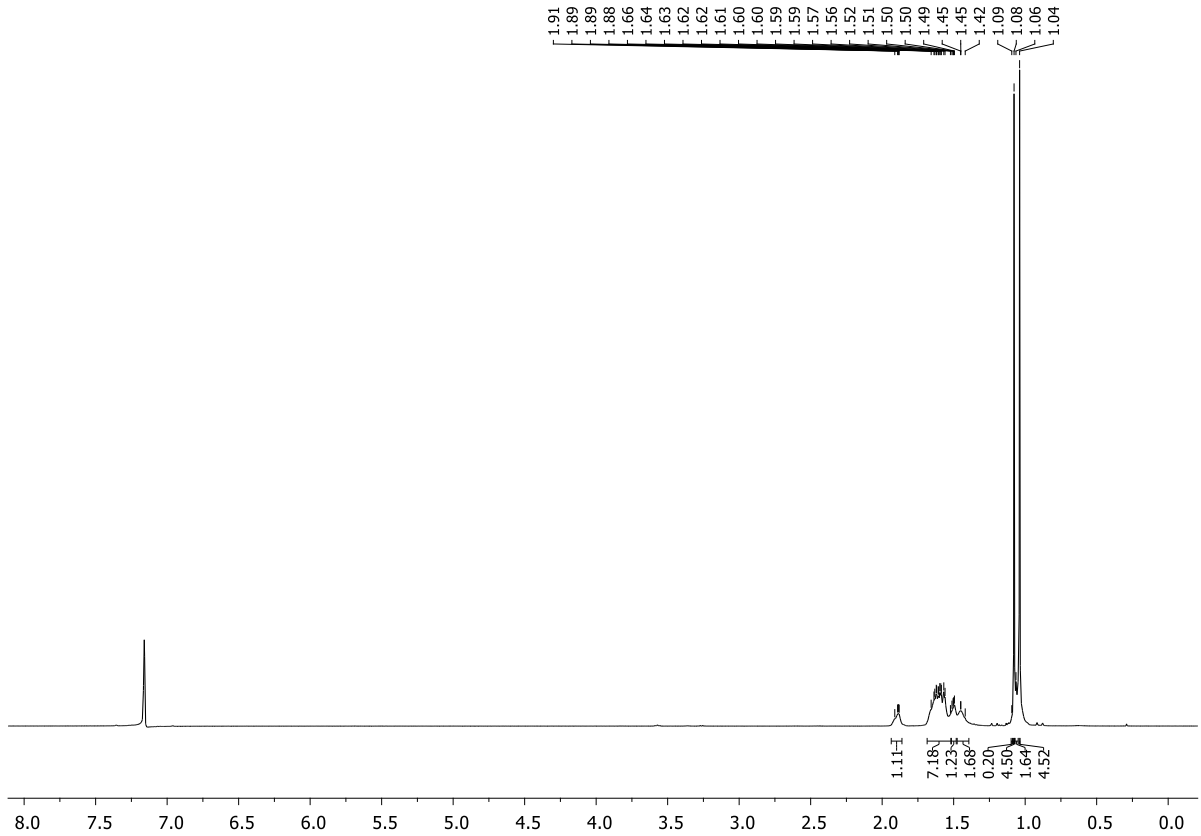

Figure S3.45. ^{1}H NMR spectrum (C_6D_6, 298 K) of compound (R_P)-**13**.

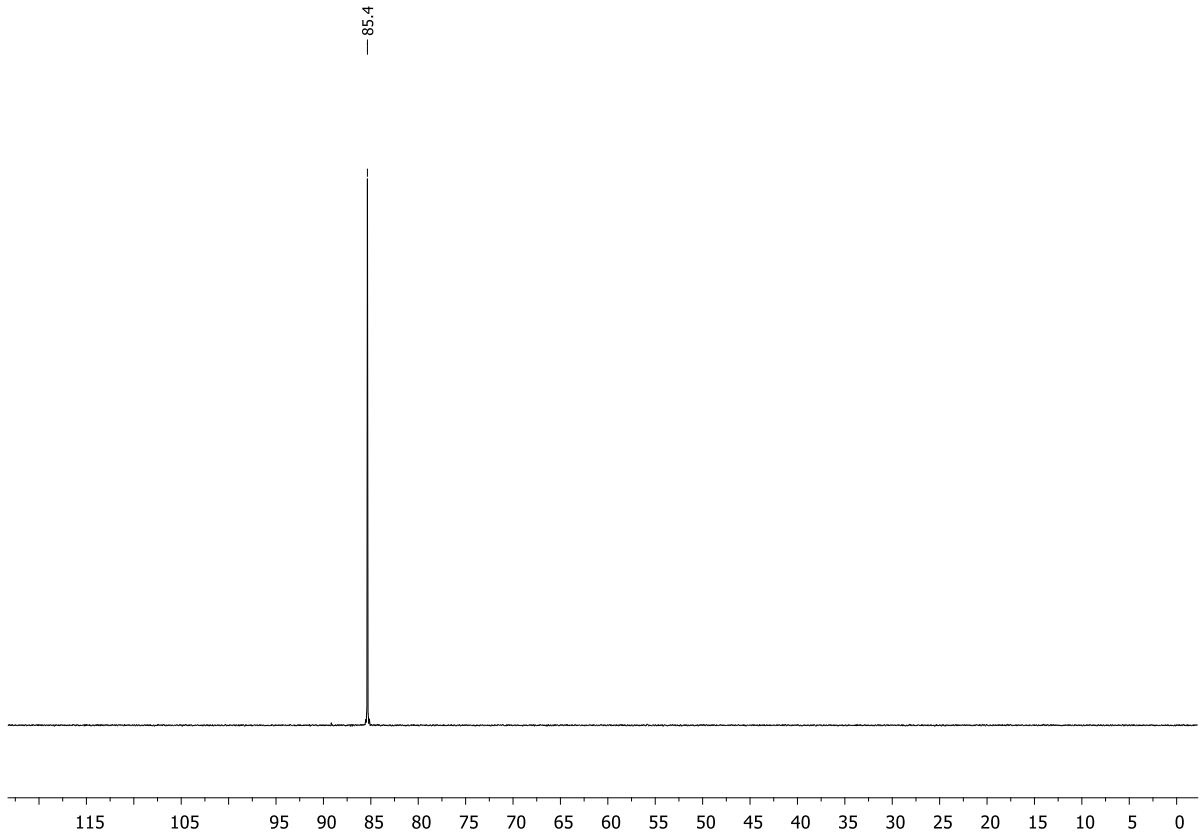

Figure S3.46. $^{31}P\{^{1}H\}$ NMR spectrum (C_6D_6, 298 K) of compound (R_P)-**13**.

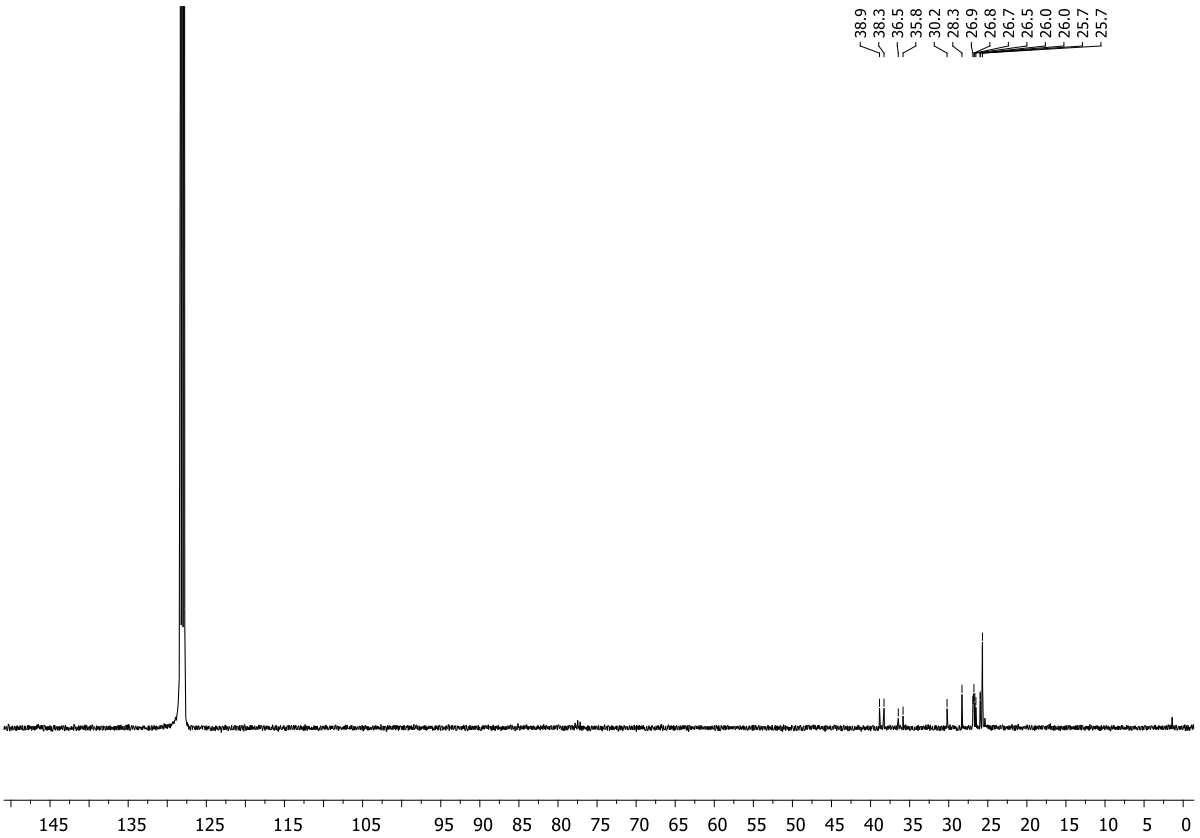

Figure S3.47. $^{13}C\{^{1}H\}$ NMR spectrum (C_6D_6, 298 K) of compound (R_P)-**13**.

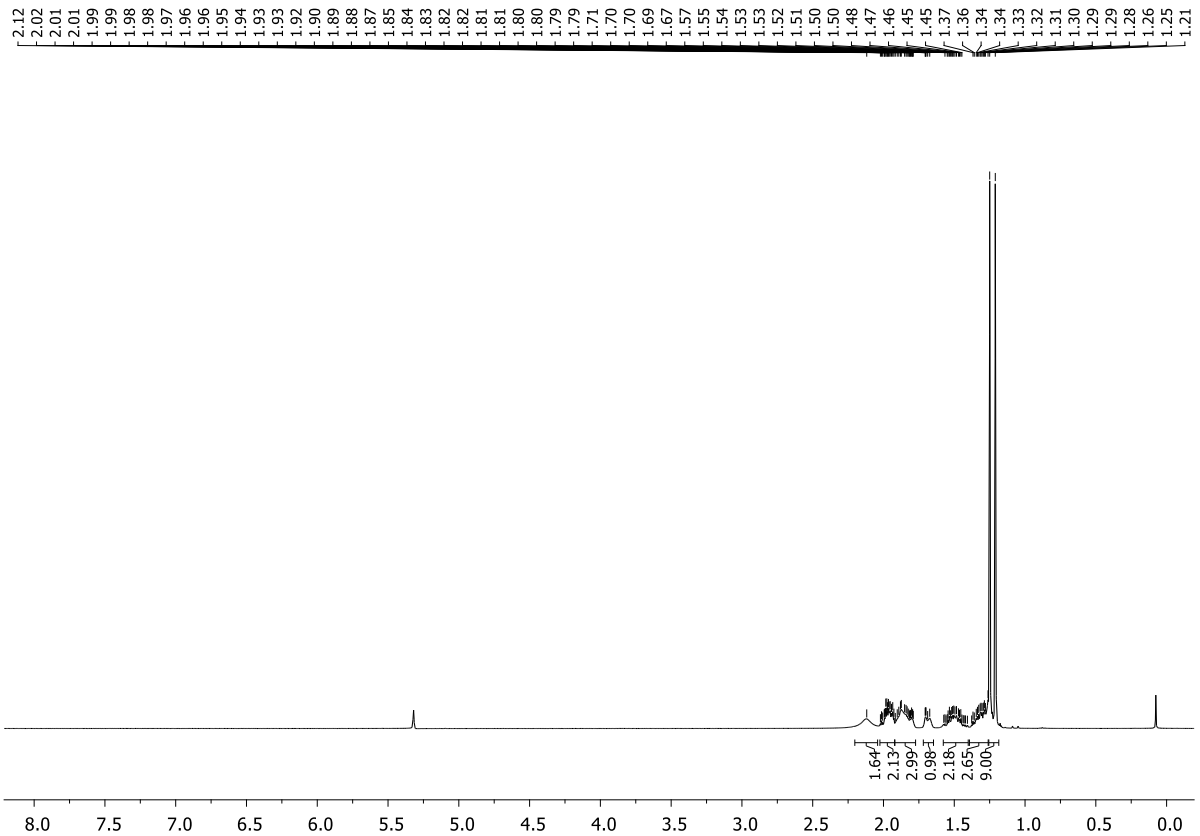

Figure S3.48. ^{1}H NMR spectrum (CD_2Cl_2, 298 K) of compound (R_P)-**13**.

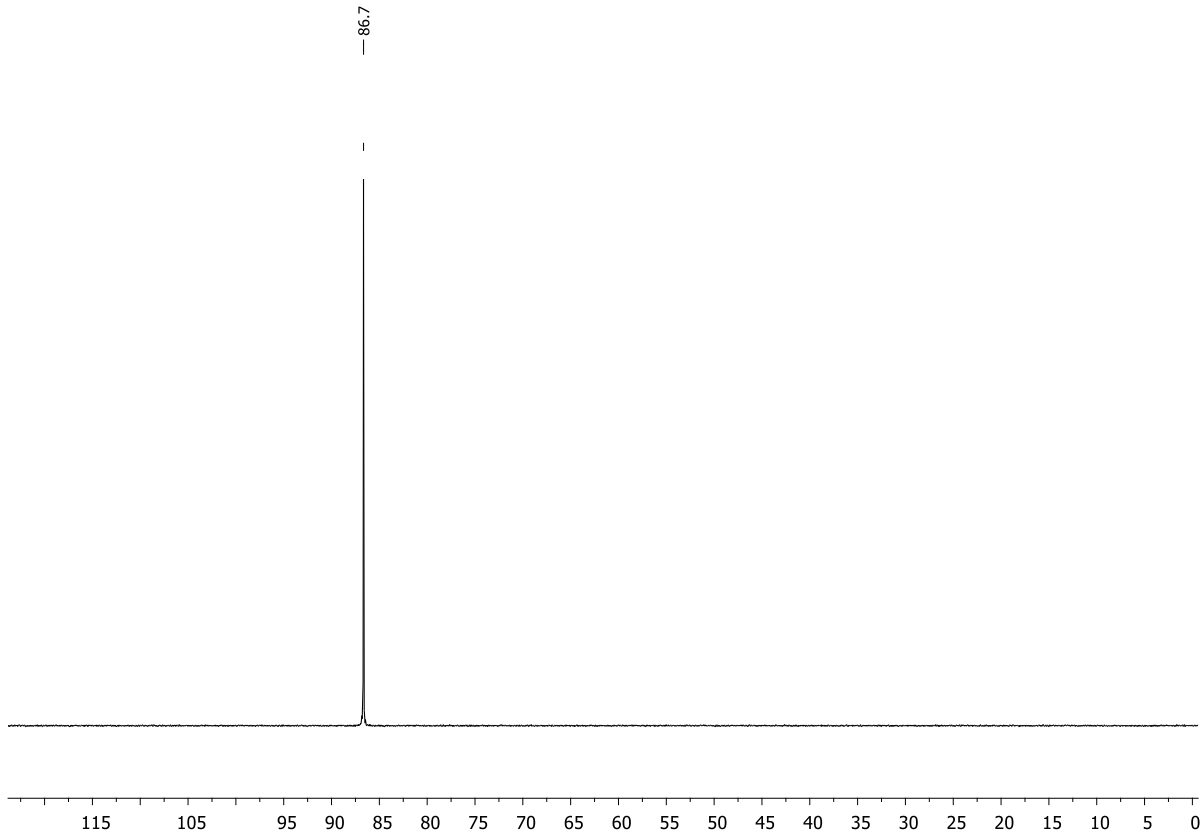

Figure S3.49. $^{31}P\{^{1}H\}$ NMR spectrum (CD_2Cl_2, 298 K) of compound (R_P)-**13**.

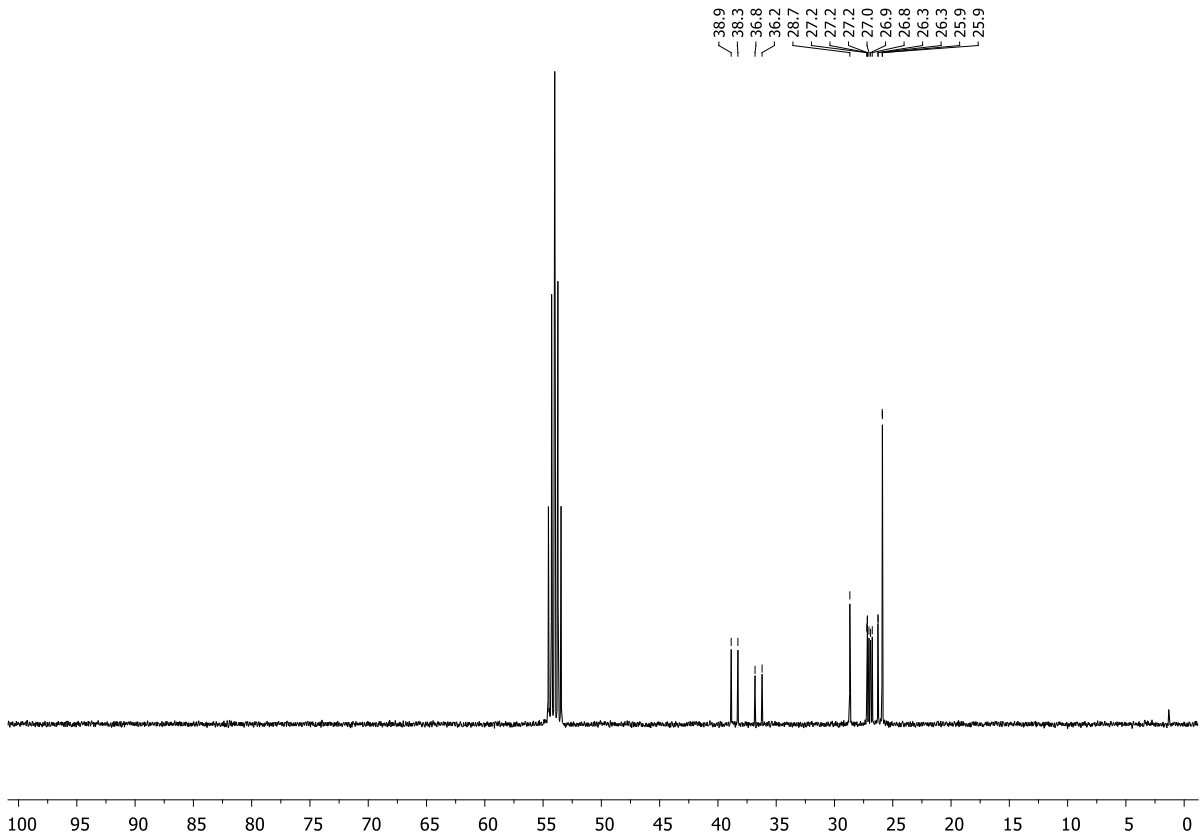

Figure S3.50. $^{13}C\{^{1}H\}$ NMR spectrum (CD_2Cl_2, 298 K) of compound (R_P)-**13**.

3.6.2.9. Synthesis of (*rac*)-13

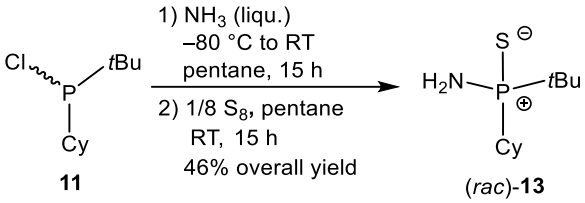

A solution of compound **11** (1.02 g, 4.93 mmol, 1.0 equiv.) in pentane (15 mL) was cooled to –80 °C and ammonia was condensed into the solution. The reaction mixture was allowed to slowly warm to room temperature and stirred for 15 h. The formed precipitate was filtered off *via* cannula filtration and the filtrate directly transferred into a Schlenk tube loaded with sulfur (0.16 g, 4.93 mmol, 1.0 equiv.) at room temperature. The reaction mixture was stirred for 15 h. All volatiles were removed *in vacuo* and the remaining solid extracted with diethyl ether. Then, all volatiles were removed *in vacuo* to yield (*rac*)-**13** as a colorless liquid (0.50 g, 2.28 mmol, 46% overall yield).

^{1}H NMR (400.13 MHz, C_6D_6, 298 K): δ 1.07 [d, $^{3}J_{H-P}$ = 15.6 Hz, 9H, PC(CH_3)$_3$], 1.07–1.03 (m, 2H, CH_2), 1.54–1.47 (br, 2H, NH_2), 1.68–1.60 (m, 6H, CH_2), 1.95–1.75 (m, 3H, PCH/CH_2). **^{31}P{^{1}H} NMR** (162.04 MHz, C_6D_6, 298 K): δ 85.4. **^{13}C{^{1}H} NMR** (100.61 MHz, C_6D_6, 298 K): δ 25.7 [d, $^{2}J_{C-P}$ = 1.4 Hz, PC(CH$_3$)$_3$], 26.0 (d, $^{3}J_{C-P}$ = 1.6 Hz, CH$_2$), 26.6 (d, $^{2}J_{C-P}$ = 14.4 Hz, CH$_2$), 26.8 (d, $^{2}J_{C-P}$ = 13.5 Hz, CH$_2$), 28.3 (s, CH$_2$), 30.2 (s, CH$_2$), 36.2 [d, $^{1}J_{C-P}$ = 61.3 Hz, PC(CH$_3$)$_3$], 38.6 (d, $^{1}J_{C-P}$ = 58.2 Hz, PCH). **HR(ESI)-MS**: Calcd *m*/*z* for [(M + H)$^{+}$]: 220.1283. Found: 220.1276. **CHN Analysis**: Calcd for $C_{10}H_{22}NPS$: C, 54.76; H, 10.11; N, 6.39. Found: C, 55.12; H, 10.59; N, 6.09.

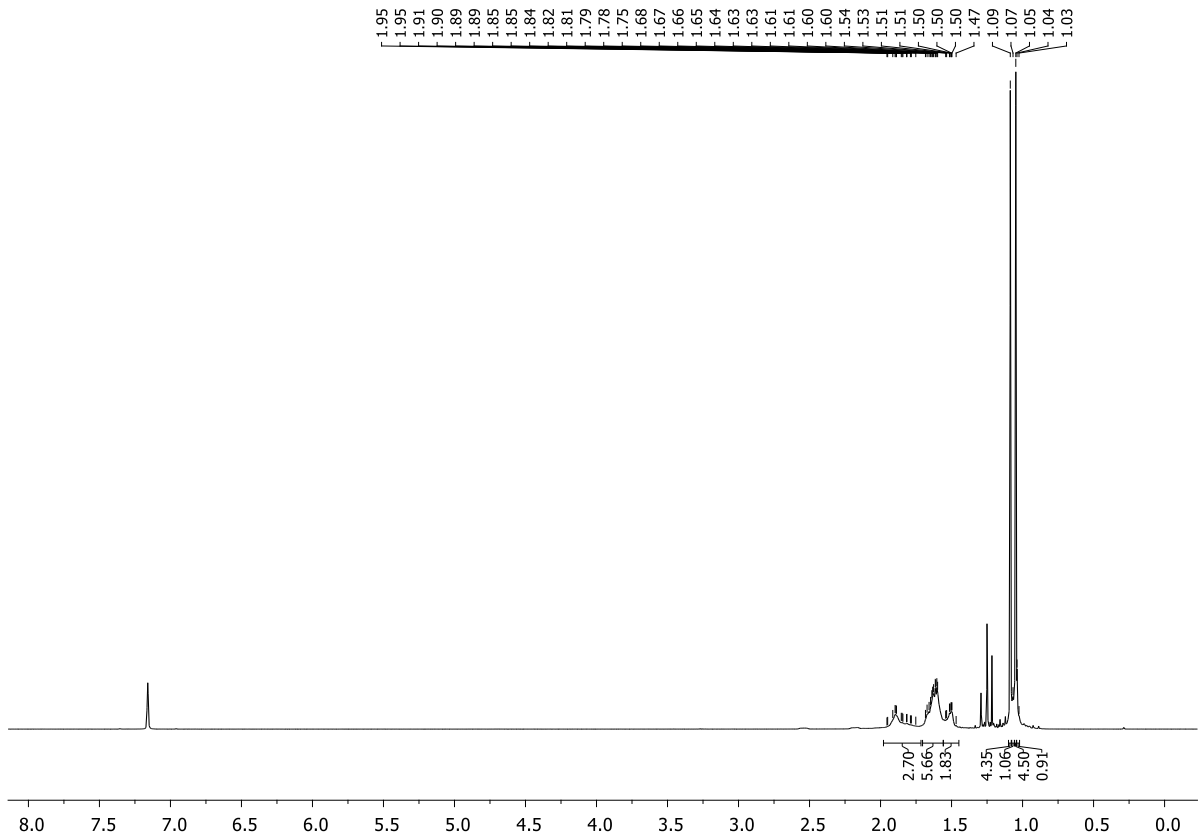

Figure S3.51. ^{1}H NMR spectrum (C_6D_6, 298 K) of compound (*rac*)-**13**.

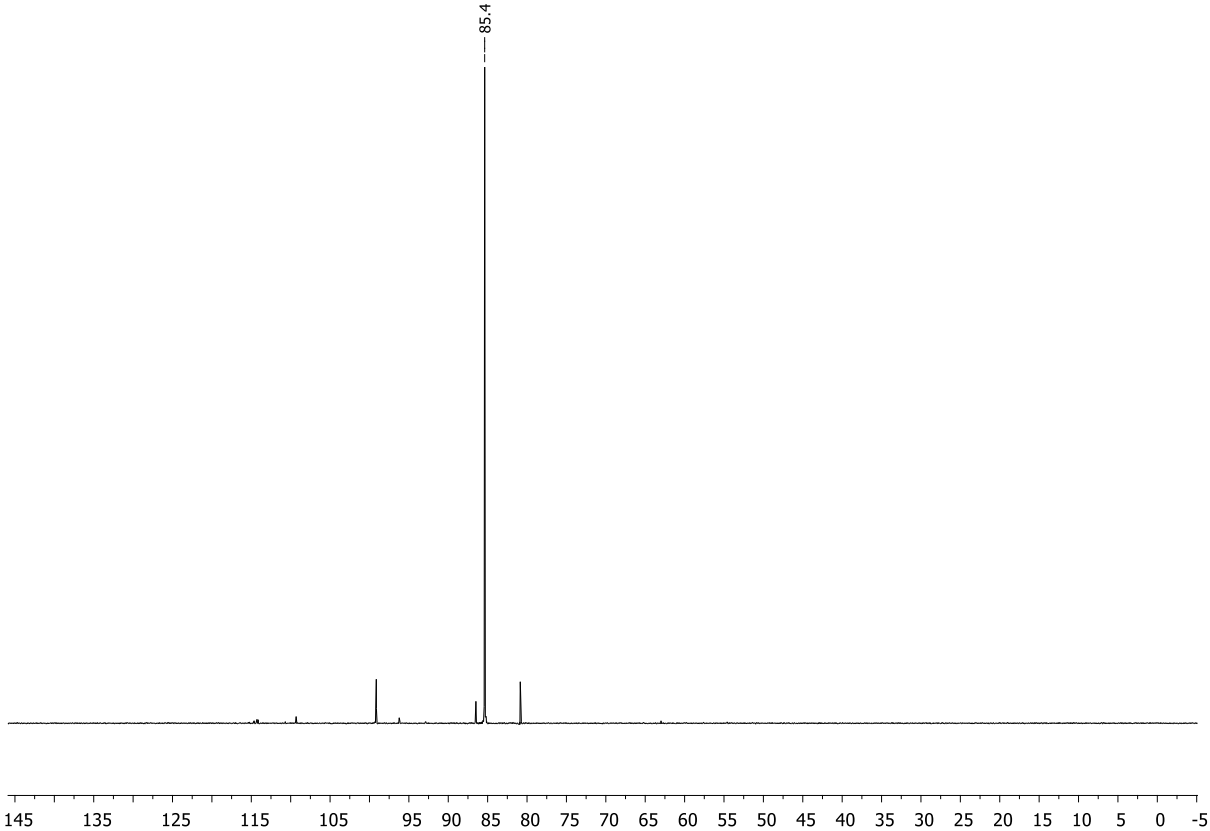

Figure S3.52. $^{31}P\{^{1}H\}$ NMR spectrum (C_6D_6, 298 K) of compound (*rac*)-**13**.

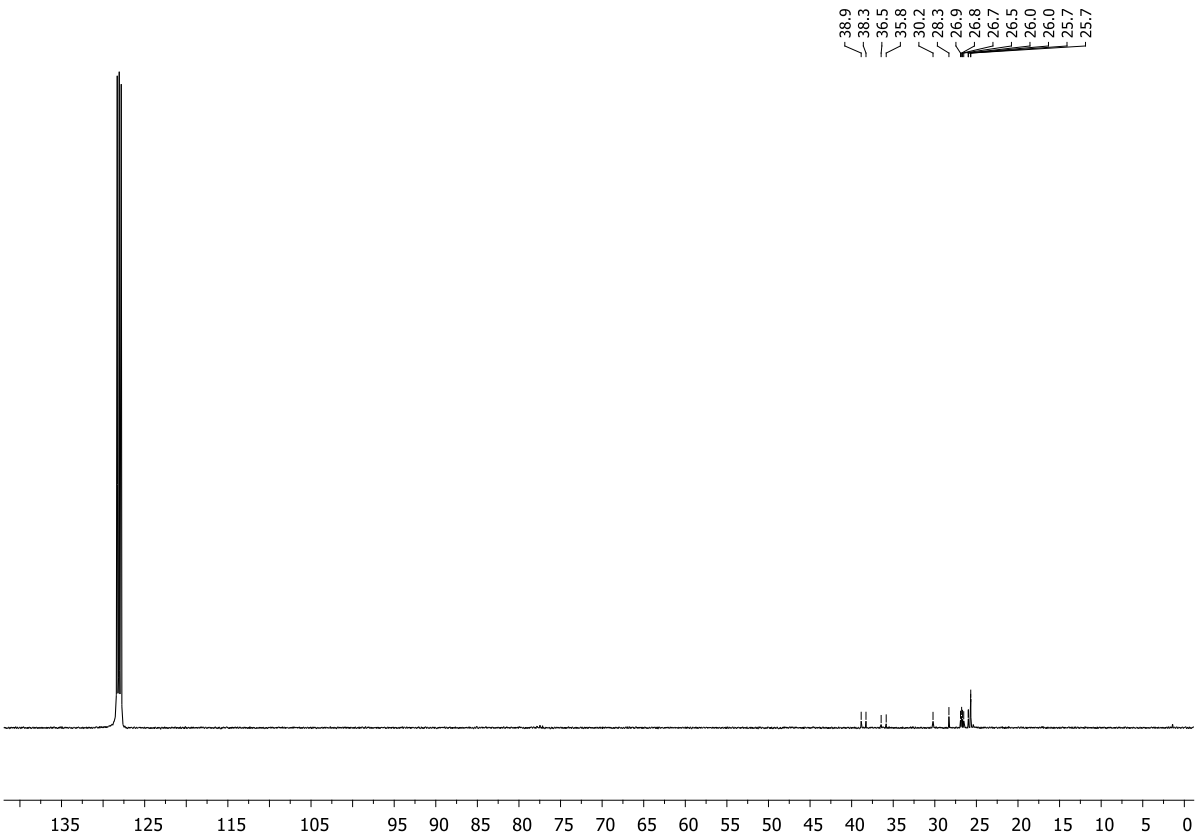

Figure S3.53. $^{13}C\{^{1}H\}$ NMR spectrum (C_6D_6, 298 K) of compound (*rac*)-**13**.

3.6.2.10. Synthesis of (*rac*)-13-Li

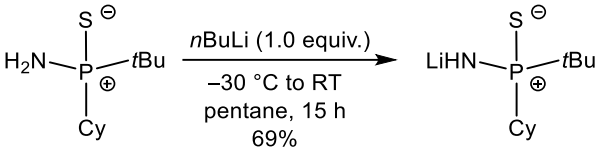

n-Butyllithium (0.44 mL of a 2.5 M solution in hexane, 1.09 mmol, 1.0 equiv.) was added dropwise to a solution of (*rac*)-**13** (0.24 g, 1.09 mmol, 1.0 equiv.) in pentane (20 mL) at –30 °C. The suspension was allowed to slowly warm to room temperature and then stirred for 15 h. The remaining solid was filtered off and dried *in vacuo* to yield (*rac*)-**13**-Li as a colorless solid (0.17 g, 0.75 mmol, 69%).

^{1}H NMR (400.13 MHz, CD_2Cl_2, 298 K): *δ* 0.24 (d, $^{2}J_{H–P}$ = 12.3 Hz, 1H, N*H*), 1.20 [d, $^{3}J_{H–P}$ = 15.1 Hz, 9H, PC(C*H*$_3$)$_3$], 1.46–1.25 (m, 5H, C*H*$_2$), 1.68 (d, $^{2}J_{H–P}$ = 11.3 Hz 1H, PC*H*), 1.88–1.78 (m, 3H, C*H*$_2$), 2.02–1.90 (m, 1H, C*H*$_2$), 2.19–2.05 (m, 1H, C*H*$_2$). **^{31}P{^{1}H} NMR** (162.04 MHz, CD_2Cl_2, 298 K): *δ* 92.6. ^{7}Li{^{1}H} NMR (155.51 MHz, CD_2Cl_2) δ 1.13. **^{13}C{^{1}H} NMR** (100.61 MHz, CD_2Cl_2, 298 K): *δ* 26.0 [s, PC(*C*H$_3$)$_3$], 26.6 (s, *C*H$_2$), 27.6 (s, *C*H$_2$), 29.7 (s, *C*H$_2$) 30.3 (s, *C*H$_2$), 37.4 [d, $^{1}J_{C–P}$ = 52.7 Hz, P*C*(CH$_3$)$_3$], 40.0 (d, $^{1}J_{C–P}$ = 49.2 Hz, P*C*H).

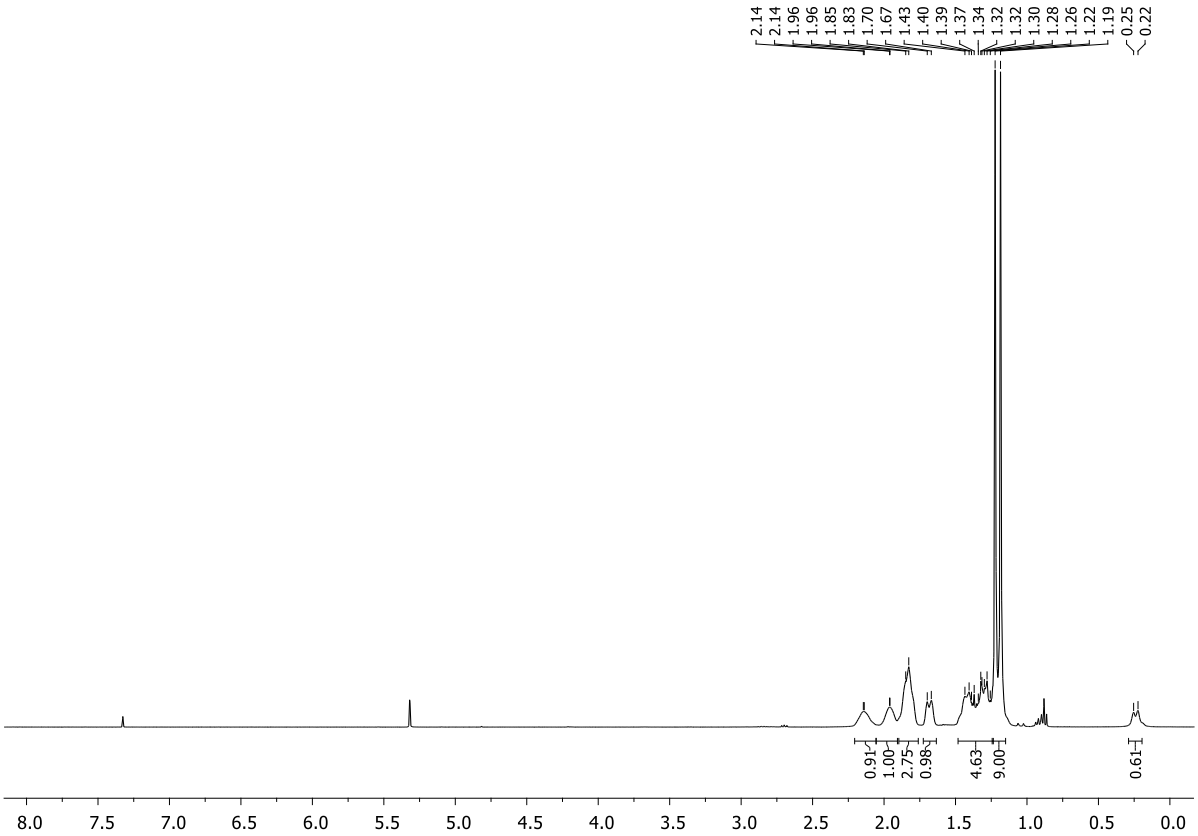

Figure S3.54. ^{1}H NMR spectrum (CD_2Cl_2, 298 K) of compound (*rac*)-**13**-Li.

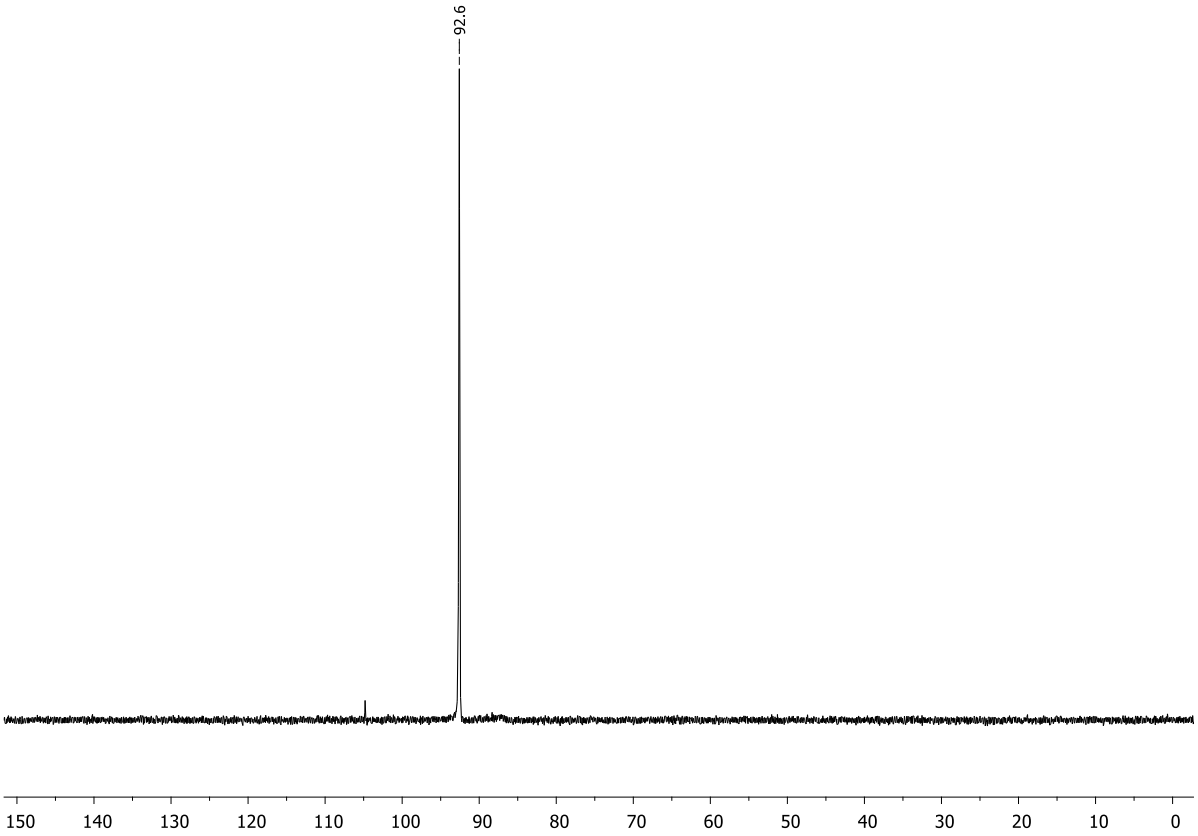

Figure S3.55. $^{31}P\{^{1}H\}$ NMR spectrum (CD_2Cl_2, 298 K) of compound (*rac*)-**13**-Li.

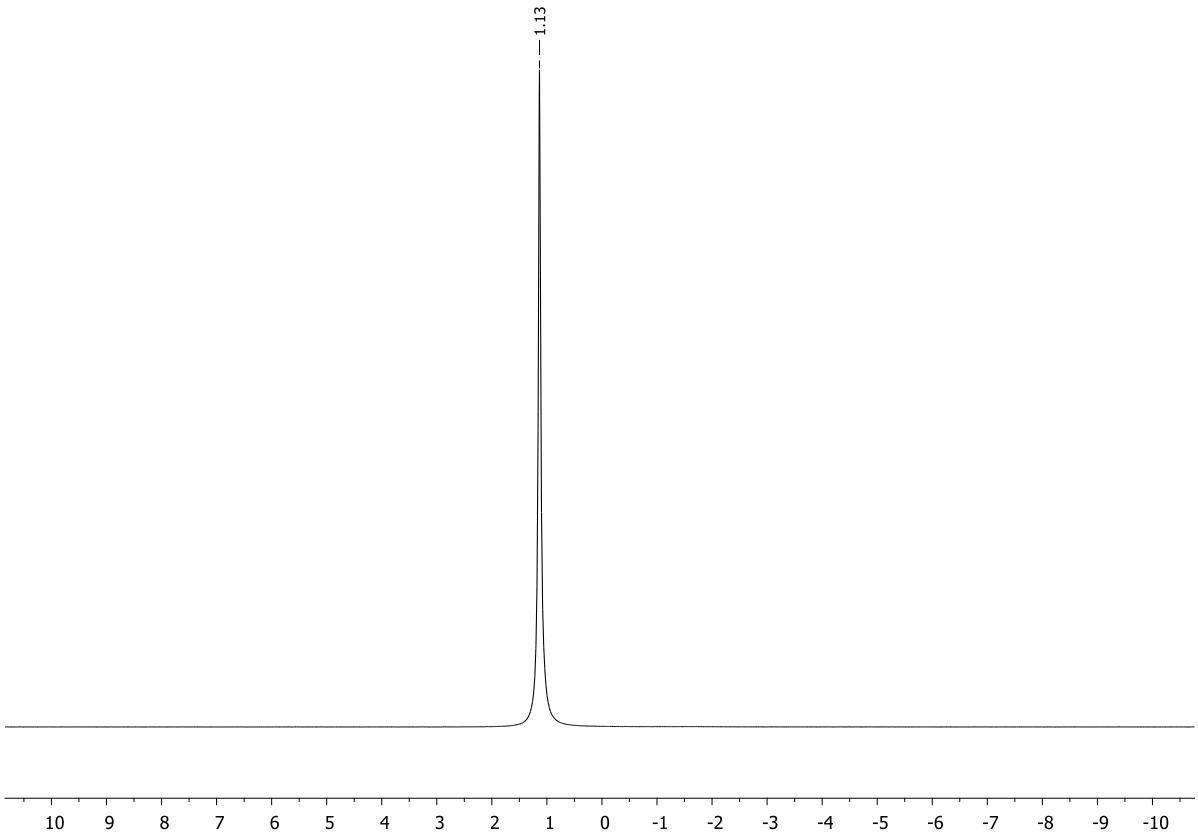

Figure S3.56. $^{7}Li\{^{1}H\}$ NMR spectrum (CD_2Cl_2, 298 K) of compound (*rac*)-**13**-Li.

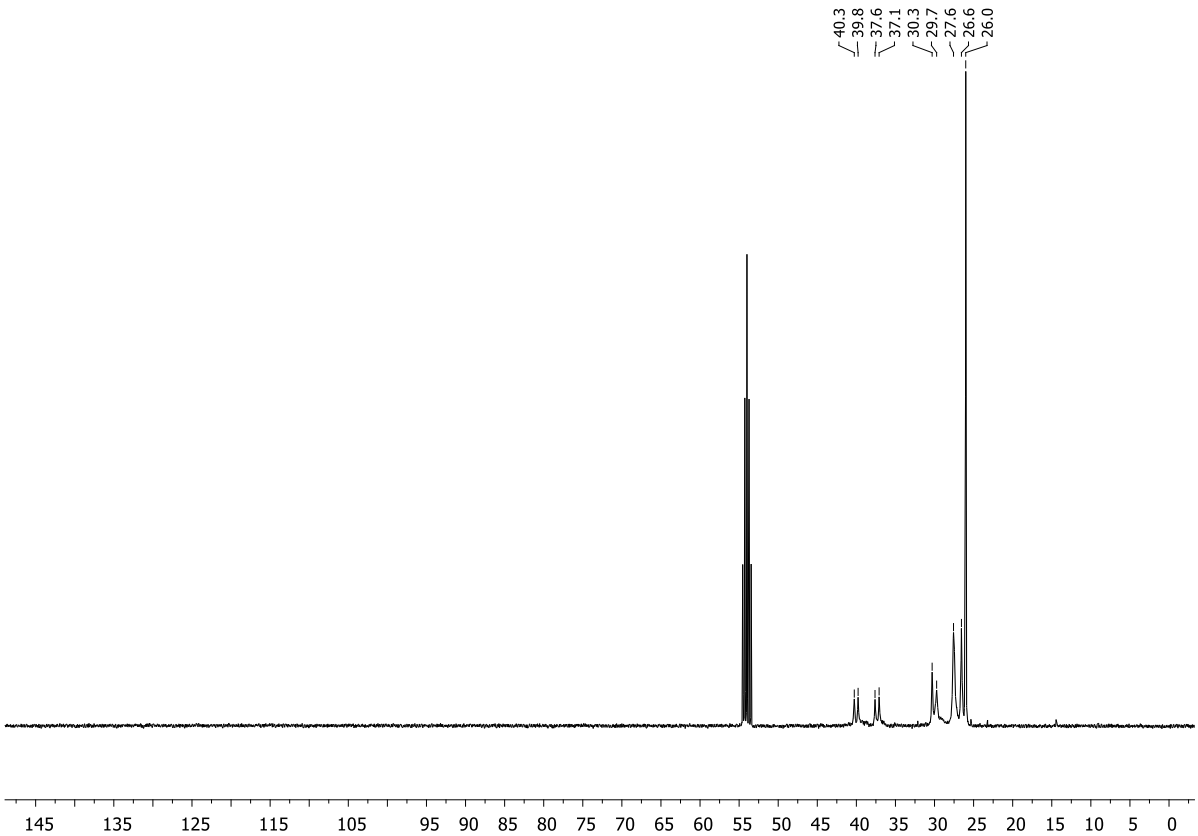

Figure S3.57. $^{13}C\{^{1}H\}$ NMR spectrum (CD_2Cl_2, 298 K) of compound (*rac*)-**13**-Li.

3.6.2.11. Synthesis of (R_P)-14

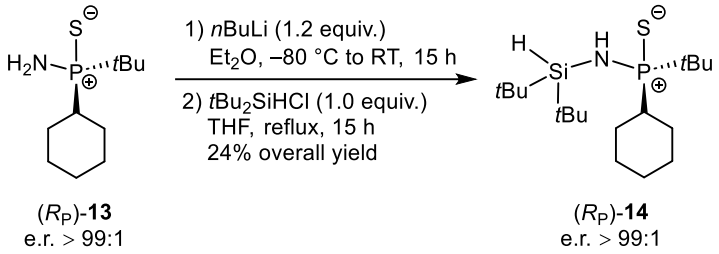

(R_P)-**13**
e.r. > 99:1

(R_P)-**14**
e.r. > 99:1

n-Butyllithium (0.22 mL of a 1.6 M solution in hexane, 0.55 mmol, 1.2 equiv.) was added to a solution of compound (R_P)-**13** (100 mg, 0.46 mmol, 1.0 equiv., e.r. > 99:1) in diethyl ether (2 mL) at –80 °C. The reaction mixture was allowed to slowly warm to room temperature and stirred for 15 h. The resulting colorless solution was again cooled to –80 °C and di-*tert*-butylchlorosilane (82 mg, 0.46 mmol, 1.0 equiv.), dissolved in diethyl ether (3 mL), was added. The reaction mixture was allowed to slowly warm to room temperature and stirred for 15 h. Since no reaction occurred, the solvent was changed to THF (5 mL) and the reaction mixture was heated at reflux for 15 h turning into a yellow solution. Then, all volatiles were removed *in vacuo* and the crude product was extracted with diethyl ether. Colorless crystals of compound (R_P)-**14** (40 mg, 0.11 mmol, 24%) suitable for single-crystal X-ray diffraction analysis were obtained by slow crystallization from the diethyl ether solution at **–**25 °C.

^{1}H NMR (400.13 MHz, C_6D_6, 298 K): δ 1.07–1.03 (m, 3H, CH_2), 1.08 [s, 9H, SiC(CH_3)$_3$], 1.12 [s, 9H, SiC(CH_3)$_3$], 1.17 [d, $^3J_{H–P}$ = 15.5 Hz, 9H, PC(CH_3)$_3$], 1.53–1.40 (m, 4H, CH_2), 1.70–1.64 (m, 2H, CH_2/NH), 1.84–1.74 (m, 1H, CH), 2.12–2.08 (m, 1H, CH_2), 2.28–2.23 (m, 1H, CH_2), 4.65–4.63 (m, 1H, SiH). **^{31}P{^{1}H} NMR** (162.04 MHz, C_6D_6, 298 K): δ 85.1. **^{13}C{^{1}H} NMR** (100.61 MHz, C_6D_6, 298 K): δ 20.0 [d, $^3J_{C–P}$ = 2.4 Hz, SiC(CH$_3$)$_3$], 20.1 [d, $^3J_{C–P}$ = 0.9 Hz, SiC(CH$_3$)$_3$], 26.2 [d, $^2J_{C–P}$ = 1.4 Hz, PC(CH$_3$)$_3$], 27.3 (d, $^3J_{C–P}$ = 2.3 Hz, CH$_2$), 27.4 (d, $^2J_{C–P}$ = 3.3 Hz, CH$_2$), 29.1 (d, $^2J_{C–P}$ = 3.4 Hz, CH$_2$), 29.1 [s, SiC(CH$_3$)$_3$], 29.2 [s, SiC(CH$_3$)$_3$], 29.3 (d, $^3J_{C–P}$ = 2.4 Hz, CH$_2$), 38.2 [d, $^1J_{C–P}$ = 59.7 Hz, PC(CH$_3$)$_3$], 42.9 [d, $^1J_{C–P}$ = 56.9 Hz, PCH]. **^{29}Si{^{1}H} NMR** (79.49 MHz, C_6D_6, 298 K): δ 4.5 (d, $^2J_{C–P}$ = 6.5 Hz). **HR(ESI)-MS**: Calcd *m*/*z* for $C_{18}H_{41}NPSSi$ [(M + H)$^+$]: 362.2461. Found: 362.2464. **CHN Analysis**: Calcd for $C_{18}H_{40}NPSSi$: C, 59.78; H, 11.15; N, 3.87. Found: C, 59.29; H, 11.03; N, 3.42.

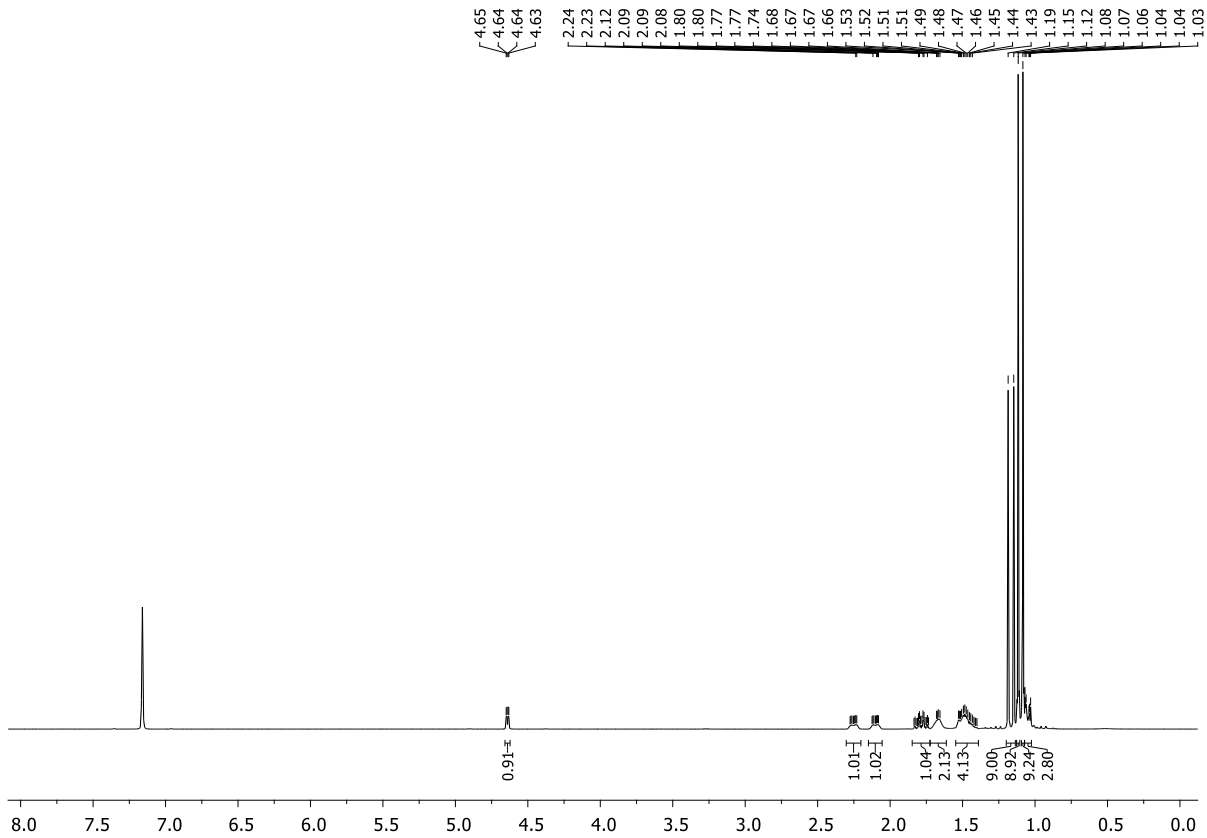

Figure S3.58. ^{1}H NMR spectrum (C_6D_6, 298 K) of compound (R_P)-**14**.

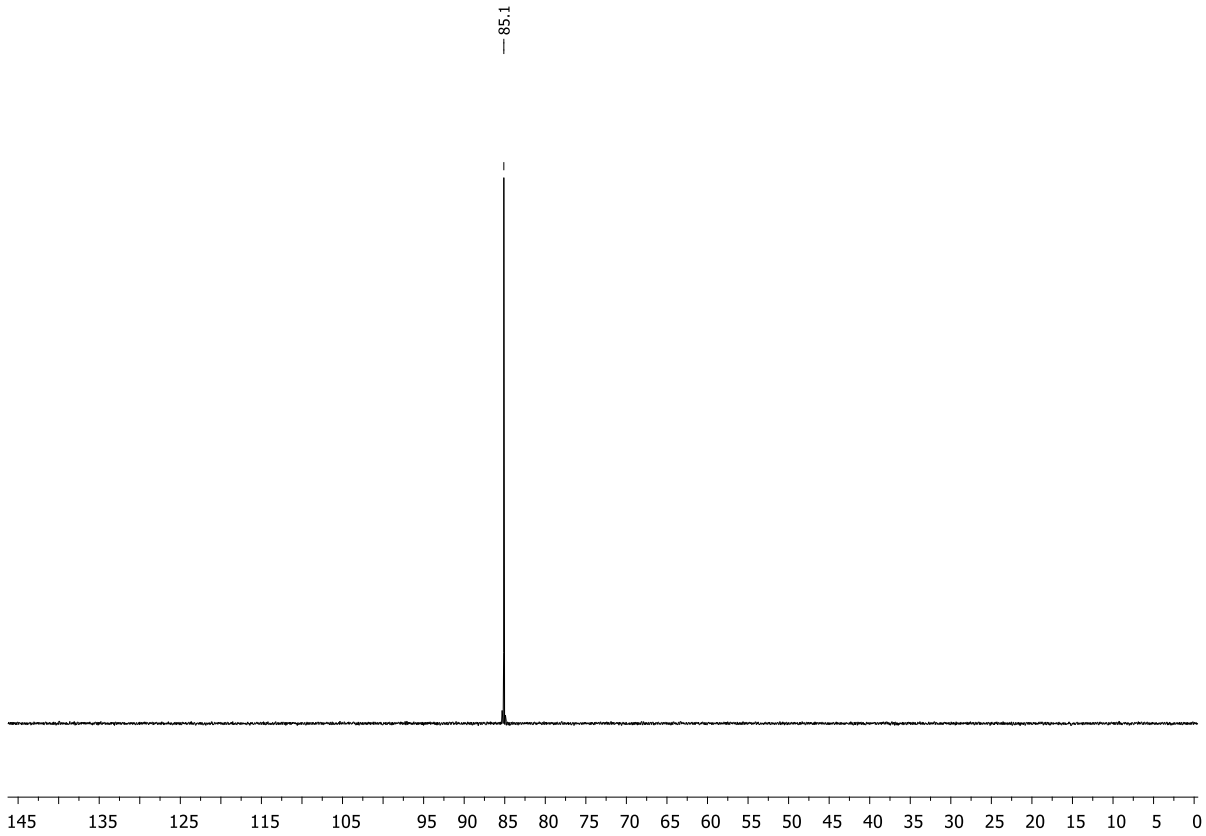

Figure S3.59. $^{31}P\{^{1}H\}$ NMR spectrum (C_6D_6, 298 K) of compound (R_P)-**14**.

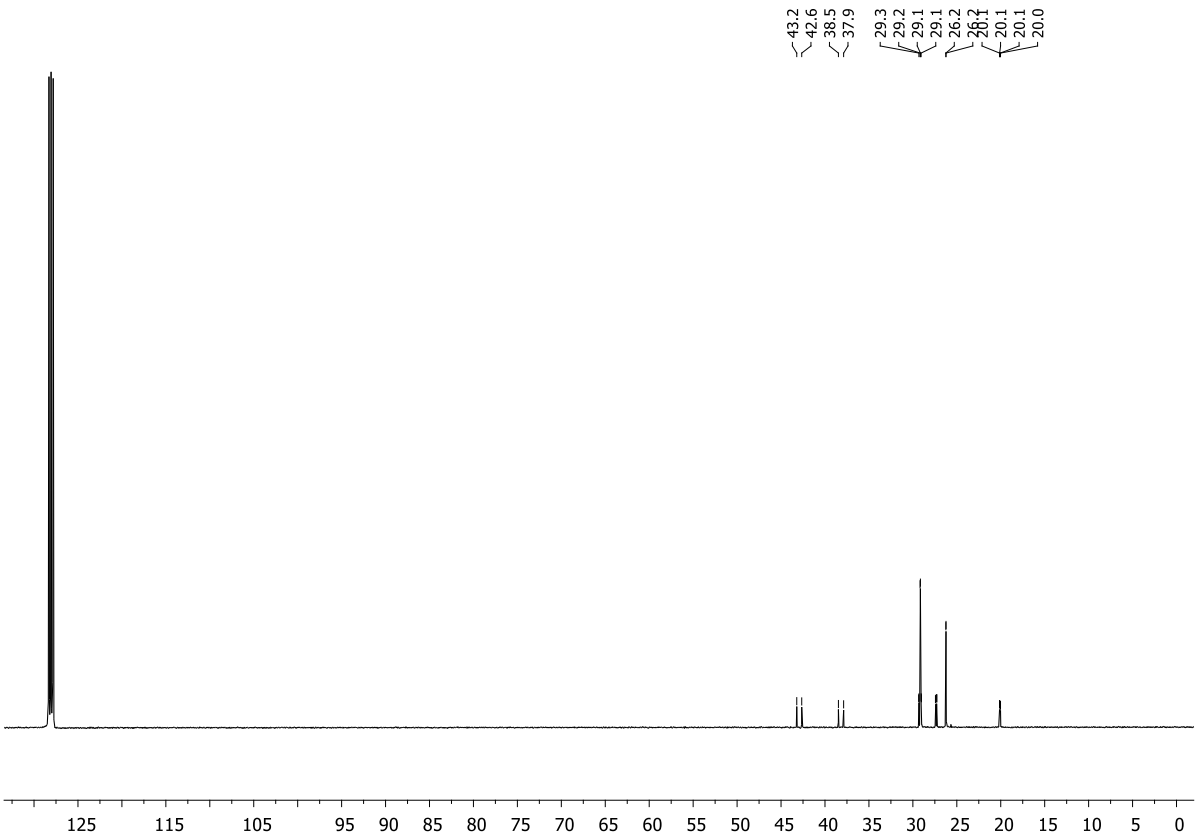

Figure S3.60. $^{13}C\{^{1}H\}$ NMR spectrum (C_6D_6, 298 K) of compound (R_P)-**14**.

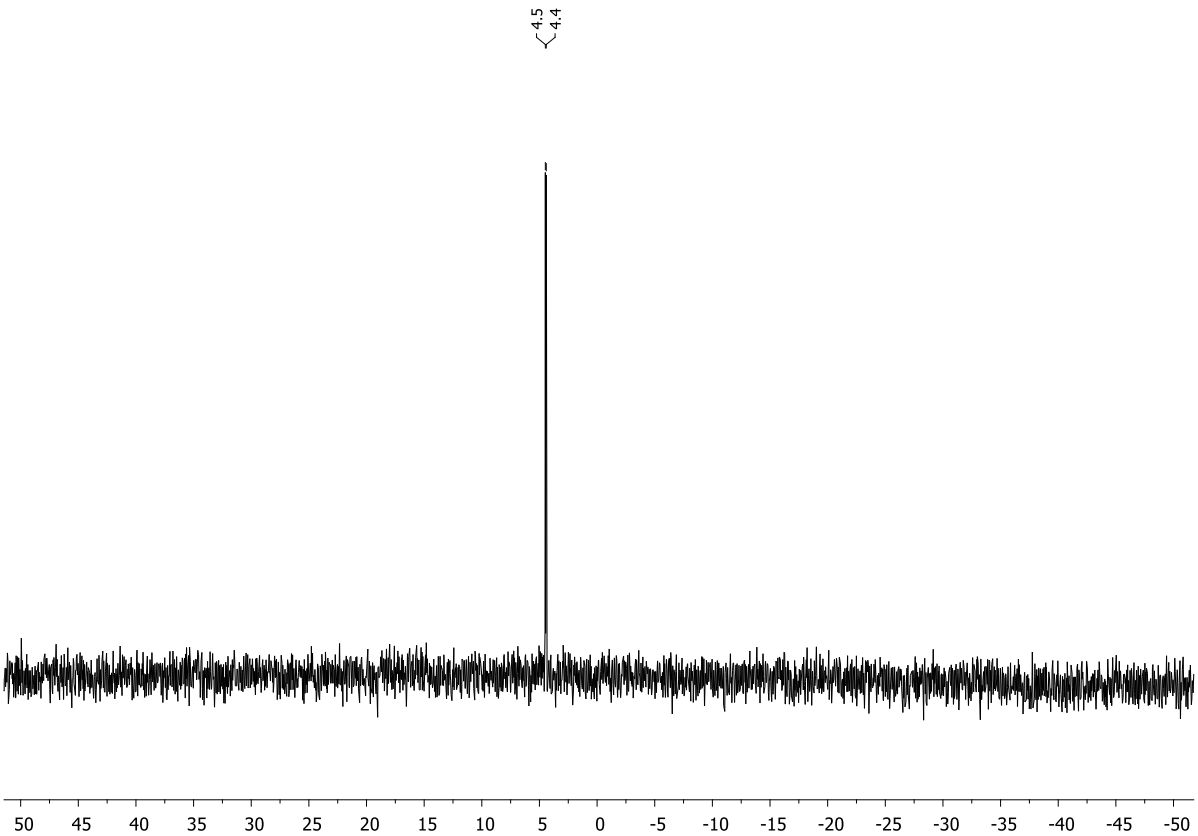

Figure S3.61. $^{29}Si\{^{1}H\}$ NMR spectrum (C_6D_6, 298 K) of compound (R_P)-**14**.

3.6.2.12. Determination of the enantiomeric ratios of compounds (S_P)-8 and (R_P)-13 using (*R*)-BINOL-PSSLi

n-Butyllithium (0.06 mL of a 2.5 M solution in hexane, 0.14 mmol, 1.0 equiv.) was added to a suspension of (*R*)-BINOL-PSSH (53 mg, 0.14 mmol, 1.0 equiv.) in pentane (20 mL) at **–**30 °C. The mixture was allowed to slowly warm to room temperature. The resulting colorless solid was filtered off, washed with pentane and dried *in vacuo*. Then, the freshly prepared sample of (*R*)-BINOL-PSSLi and the respective primary aminophosphine sulfide [(*rac*)-**8**, (S_P)-**8**, (*rac*)-**13**, or (R_P)-**13**] (0.14 mmol, 1.0 equiv.) were dissolved in CD_2Cl_2 (0.5 mL), the mixture transferred to a Young NMR tube and subjected to ^1H and $^{31}P\{^1H\}$ NMR spectroscopy. The enantiomeric ratios were determined by integration of either the ^1H NMR signals of the *tert*-butyl groups or the $^{31}P\{^1H\}$ NMR signals. For details, see Figures S3.64–79.

(*rac*)-**8** in the presence of (*R*)-BINOL-PSSLi:
^1H NMR (400.13 MHz, CD_2Cl_2, 298 K): δ 0.97 [d, 9H, $^3J_{H-P}$ = 17.2 Hz, PC(CH_3)$_3$], 1.00 [d, 9H, $^3J_{H-P}$ = 17.2 Hz, PC(CH_3)$_3$], 2.69 (s, 2H, NH_2), 2.74 (s, 2H, NH_2), 7.23–7.20 (m, 7H, H_{ar}), 7.33–7.31 (m, 7H, H_{ar}), 7.42–7.36 (m, 7H, H_{ar}), 7.48–7.44 (m, 14H, H_{ar}), 7.81–7.72 (m, 5H, H_{ar}), 7.94–7.91 (m, 14H, H_{ar}). $^{31}P\{^1H\}$ NMR (162.04 MHz, CD_2Cl_2, 298 K): δ 77.3 (s, 1P, S*P*N), 77.5 (s, 1P, S*P*N), 126.3 (s, 2P, O_2PS_2).

(S_P)-**8** in the presence of (*R*)-BINOL-PSSLi:
^1H NMR (400.13 MHz, CD_2Cl_2, 298 K): δ 1.07 [d, 9H, $^3J_{H-P}$ = 17.2 Hz, PC(CH_3)$_3$], 2.82 (s, 2H, NH_2), 7.26–7.23 (m, 17H, H_{ar}), 7.36–7.34 (m, 17H, H_{ar}), 7.47–7.44 (m, 17H, H_{ar}), 7.53–7.51 (m, 17H, H_{ar}), 7.97–7.92 (m, 34H, H_{ar}). $^{31}P\{^1H\}$ NMR (162.04 MHz, CD_2Cl_2, 298 K): δ 77.3 (s, 1P, S*P*N), 127.8 (s, O_2PS_2).

(*rac*)-**13** in the presence of (*R*)-BINOL-PSSLi:
^1H NMR (400.13 MHz, CD_2Cl_2, 298 K): δ 1.04 [d, 9H, $^3J_{H-P}$ = 16.3 Hz, PC(CH_3)$_3$], 1.05 [d, 9H, $^3J_{H-P}$ = 16.3 Hz, PC(CH_3)$_3$], 1.25–1.10 (m, 6H, CH_2), 1.43–1.26 (m, 4H, CH_2), 1.61–1.58 (m, 2H, 2 × C*H*), 1.78–1.64 (m, 7H, CH_2), 1.95–1.80 (m, 3H, CH_2), 2.52 (s, 4H, 2 × NH_2), 7.27–7.24 (m, 4H, H_{ar}), 7.40–7.37 (m, 4H, H_{ar}), 7.48–7.45 (m, 4H, H_{ar}), 7.60–7.58 (m, 4H, H_{ar}), 7.97–7.95 (m, 4H, H_{ar}), 8.01–7.99 (m, 4H, H_{ar}). $^{31}P\{^1H\}$ NMR (162.04 MHz, CD_2Cl_2, 298 K): δ 88.5 (s, 1P, S*P*N), 88.6 (s, 1P, S*P*N), 122.5 (s, 2P, O_2PS_2). $^7Li\{^1H\}$ NMR (155.51 MHz, CD_2Cl_2, 298 K): δ 0.4.

(R_P)-**13** in the presence of (*R*)-BINOL-PSSLi:
^1H NMR (400.13 MHz, CD_2Cl_2, 298 K): δ 1.11 [d, 9H, $^3J_{H-P}$ = 16.1 Hz, PC(CH_3)$_3$], 1.45–1.17 (m, 5H, CH_2), 1.63–1.60 (m, 1H, C*H*), 1.79–1.70 (m, 3H, CH_2), 1.93–1.80 (m, 2H, CH_2), 2.35 (s, 2H, NH_2), 7.29–7.23 (m, 2H, H_{ar}), 7.40–7.34 (m, 2H, H_{ar}), 7.49–7.43 (m, 2H, H_{ar}), 7.58–7.51 (m, 2H, H_{ar}), 8.01–7.89 (m, 4H, H_{ar}). $^{31}P\{^1H\}$ NMR (162.04 MHz, CD_2Cl_2, 298 K): δ 87.9 (s, 1P, S*P*N), 126.3 (s, 1P, O_2PS_2).

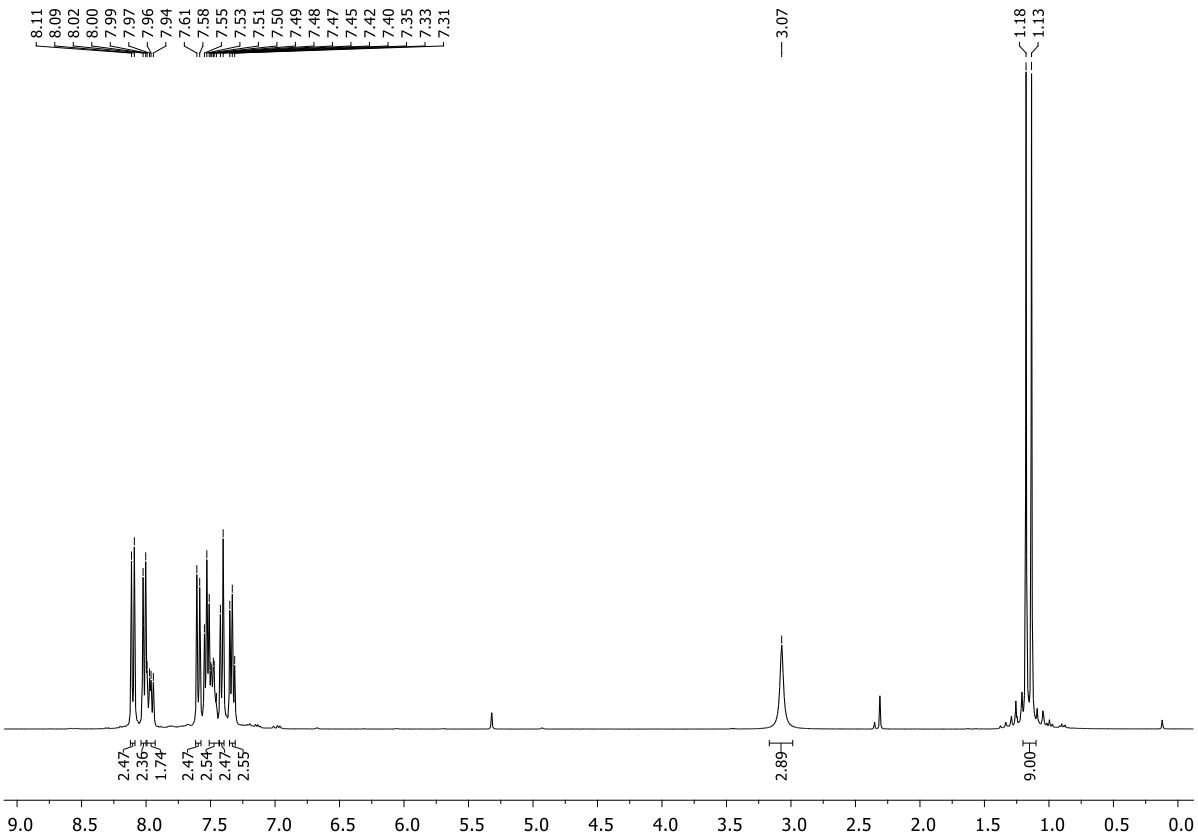

Figure S3.62. ^{1}H NMR spectrum (0.5 mL CD_2Cl_2, 298 K) of (*rac*)-**8** (21 mg, 0.10 mmol, 1.0 equiv.) in the presence of (*R*)-BINOL-PSSH (38 mg, 0.10 mmol, 1.0 equiv.). No diastereotopic discrimination was achieved.

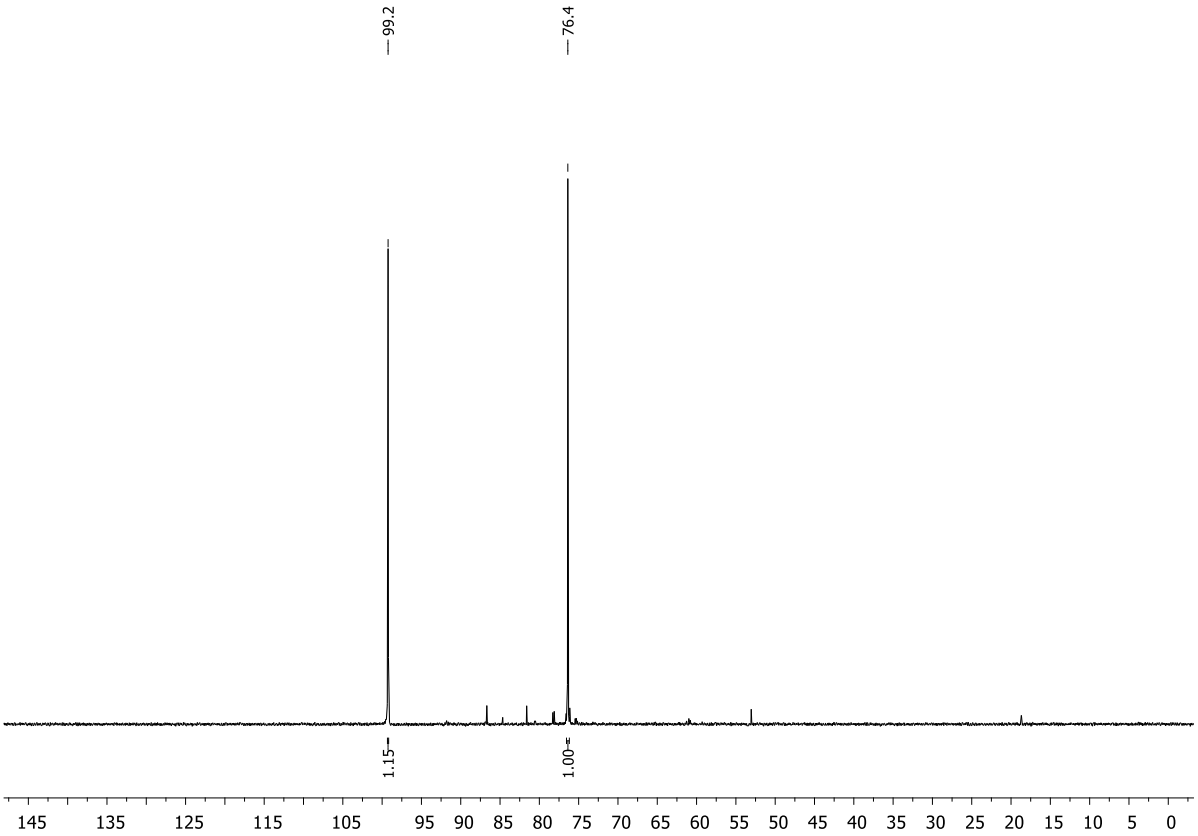

Figure S3.63. $^{31}P\{^{1}H\}$ NMR spectrum (0.5 mL CD_2Cl_2, 298 K) of (*rac*)-**8** (21 mg, 0.10 mmol, 1.0 equiv.) in the presence of (*R*)-BINOL-PSSH (38 mg, 0.10 mmol, 1.0 equiv.). No diastereotopic discrimination was achieved.

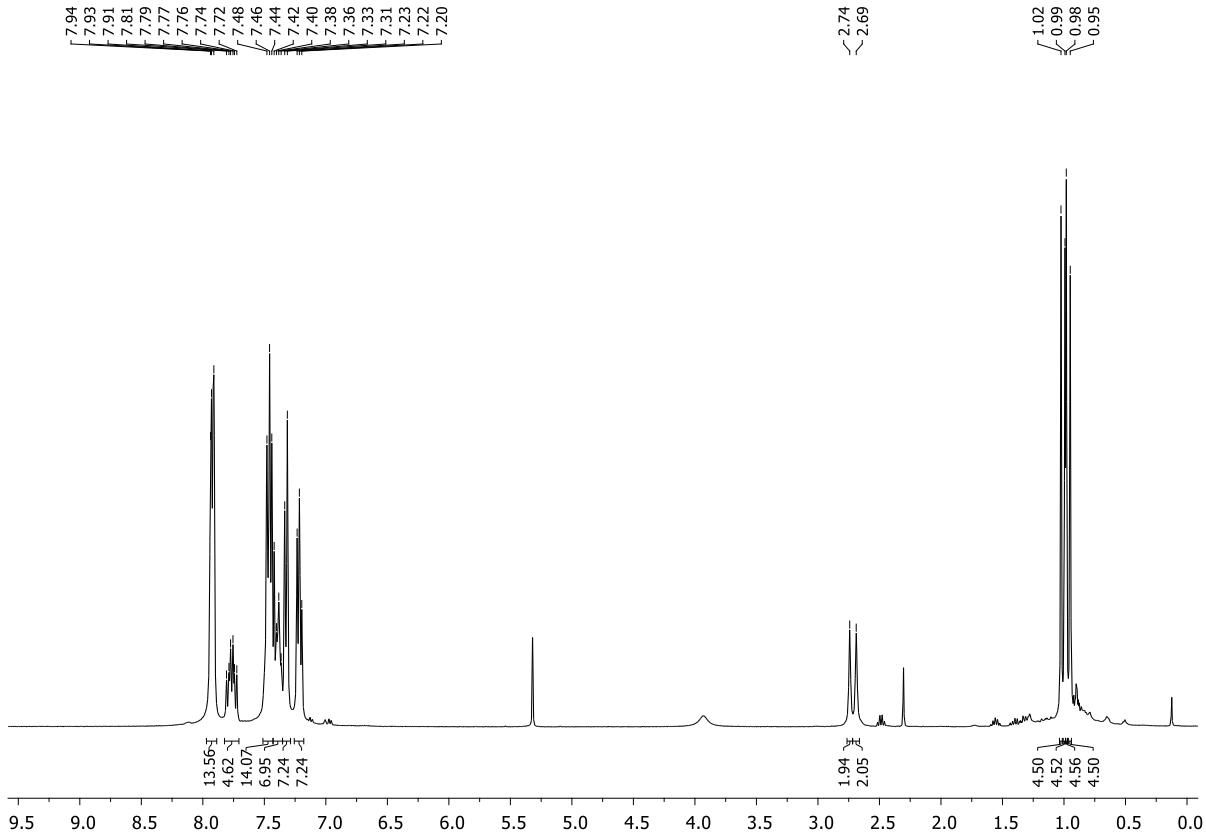

Figure S3.64. ^{1}H NMR spectrum (CD_2Cl_2, 298 K) of (*rac*)-**8** in the presence of (*R*)-BINOL-PSSLi.

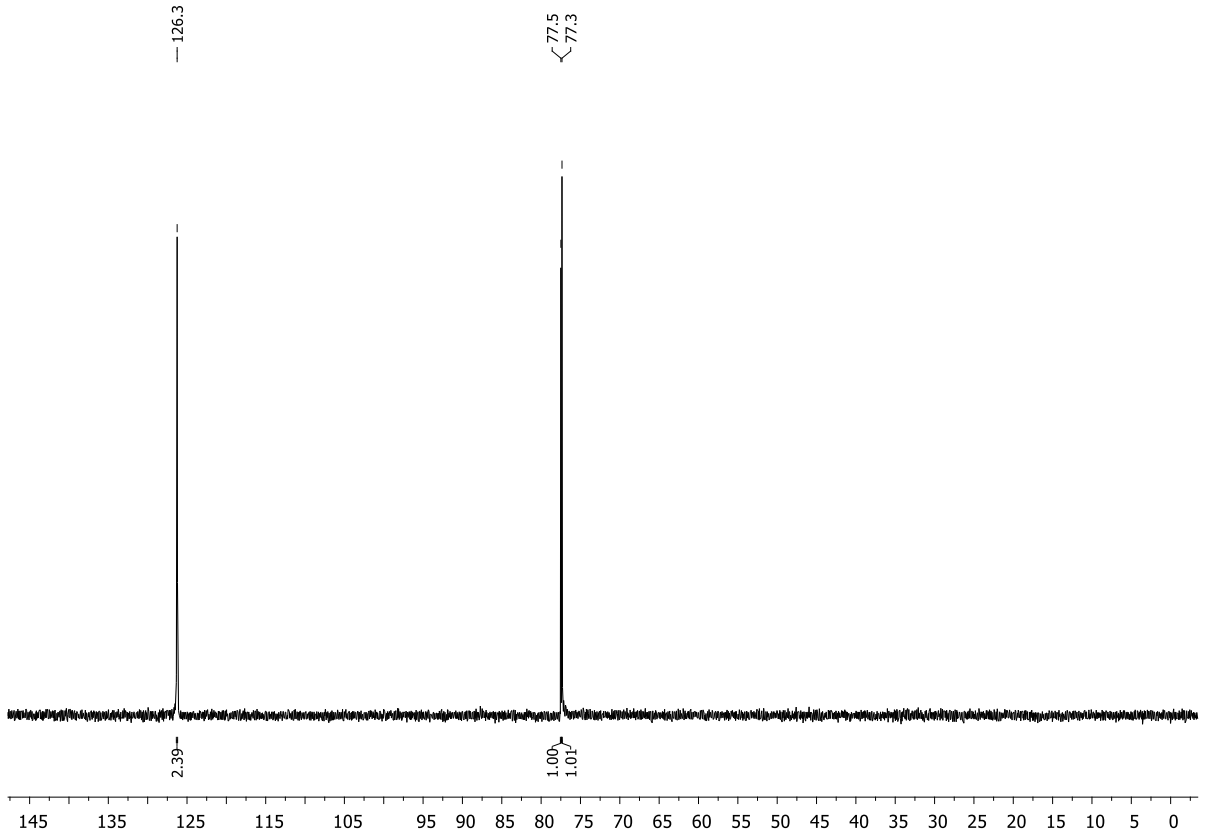

Figure S3.65. $^{31}P\{^{1}H\}$ NMR spectrum (CD_2Cl_2, 298 K) of (*rac*)-**8** in the presence of (*R*)-BINOL-PSSLi.

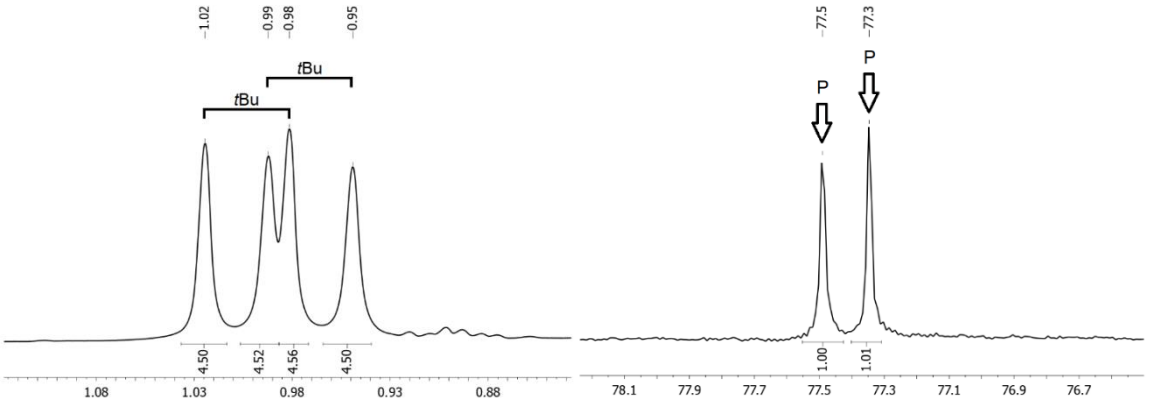

Figure S3.66. Details of the ^{1}H NMR spectrum (left) and ^{31}P{^{1}H} NMR spectrum (right) of (*rac*)-**8** in the presence of (*R*)-BINOL-PSSLi (CD_2Cl_2, 298 K).

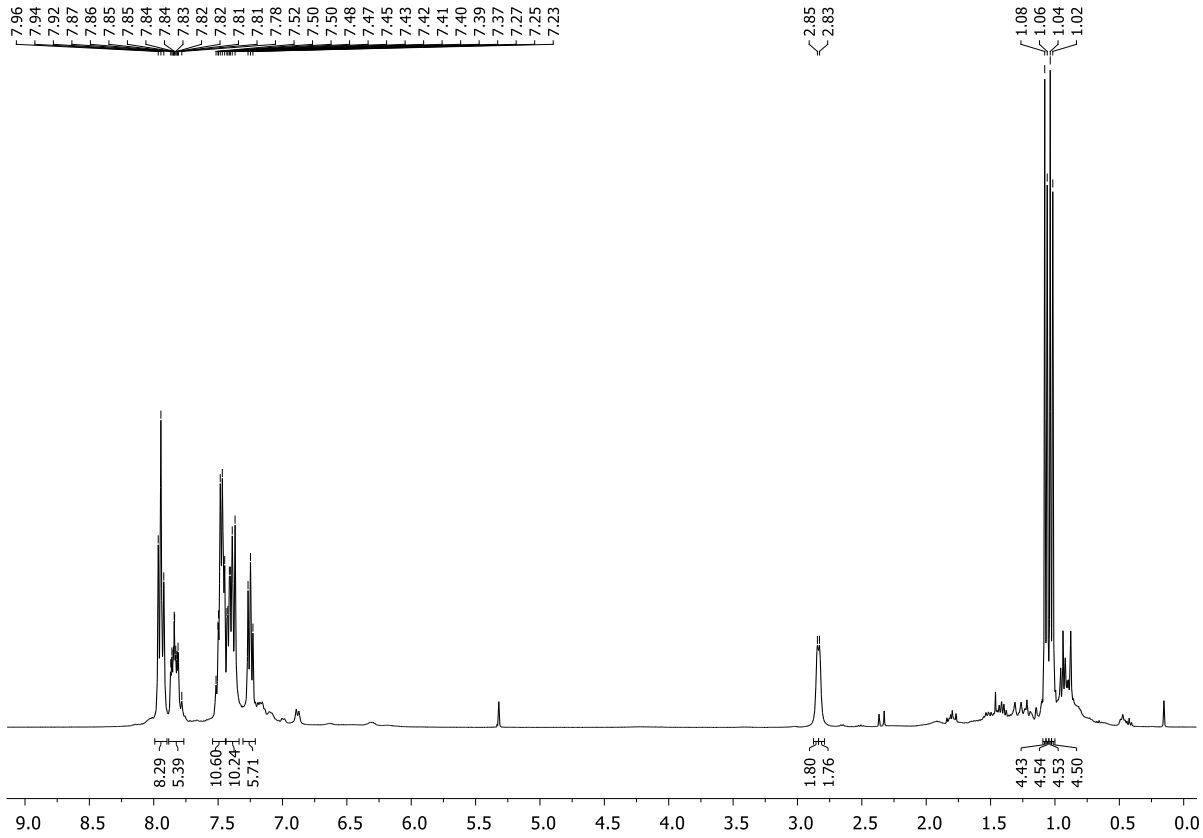

Figure S3.67. ^{1}H NMR spectrum (CD_2Cl_2, 298 K) of lithiated (*rac*)-**8** [(*rac*)-**8**-Li] in the presence of (*R*)-BINOL-PSSH, showing that complex formation also works vice versa.

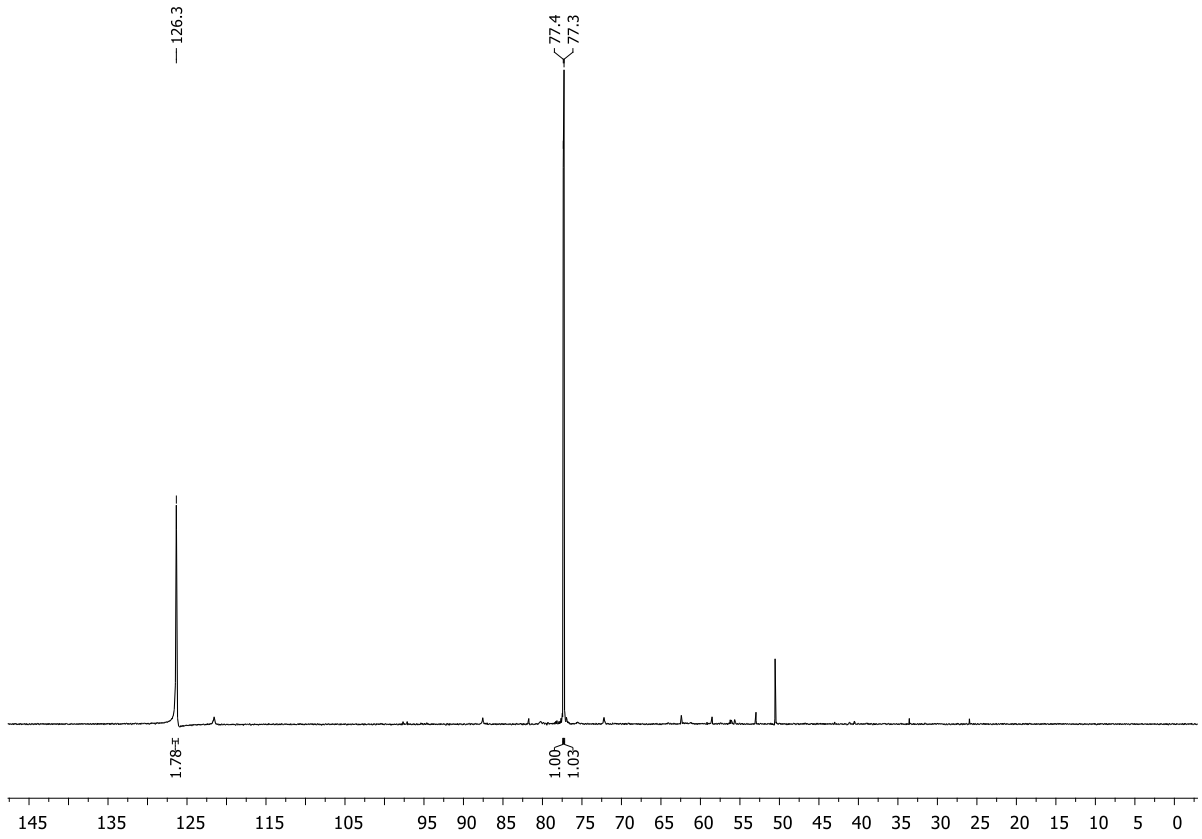

Figure S3.68. $^{31}P\{^{1}H\}$ NMR spectrum (CD_2Cl_2, 298 K) of lithiated (*rac*)-**8** [(*rac*)-**8**-Li] in the presence of (*R*)-BINOL-PSSH, showing that complex formation also works vice versa.

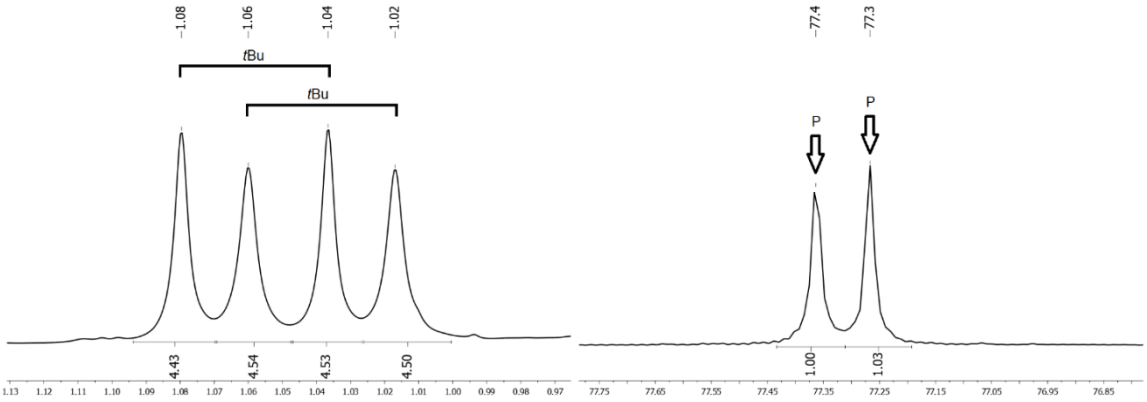

Figure S3.69. Details of the ^{1}H NMR spectrum (left) and $^{31}P\{^{1}H\}$ NMR spectrum (right) of lithiated (*rac*)-**8** [(*rac*)-**8**-Li] in the presence of (*R*)-BINOL-PSSH (CD_2Cl_2, 298 K).

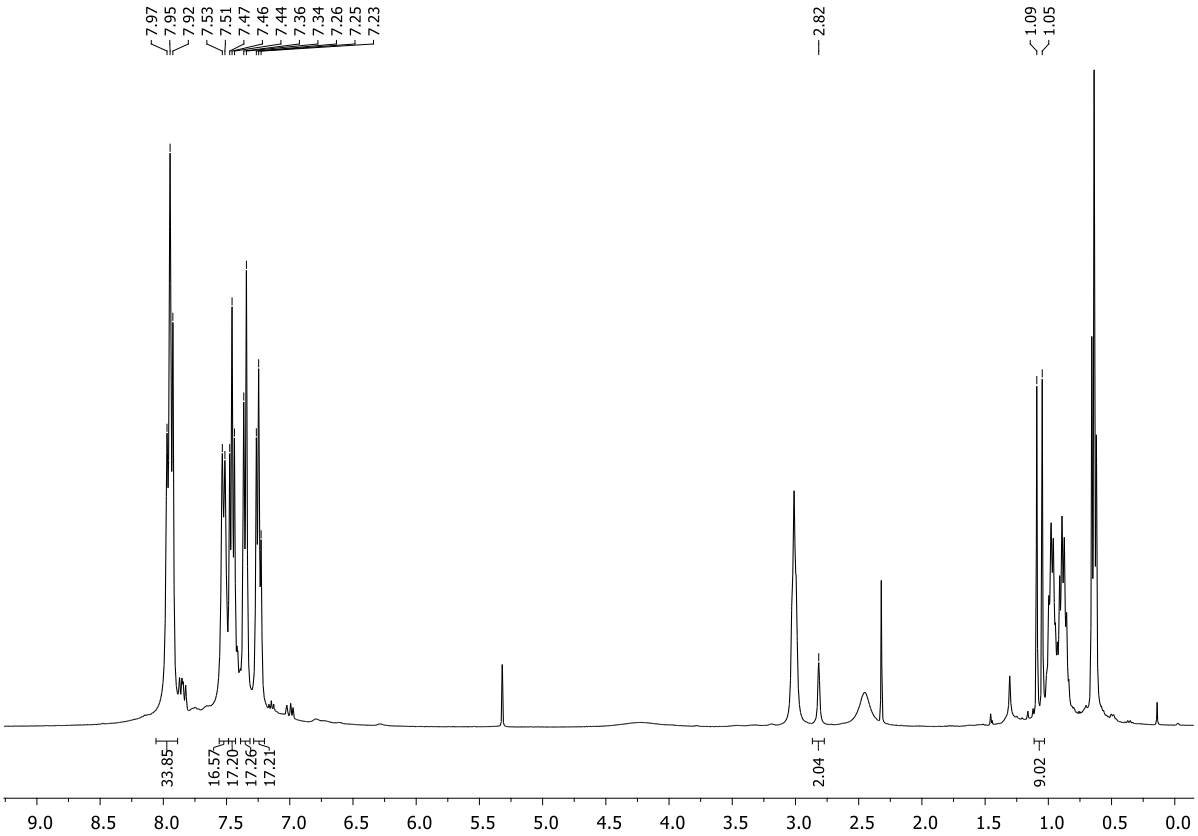

Figure S3.70. ^{1}H NMR spectrum (CD_2Cl_2, 298 K) of crude (S_P)-**8** in the presence of (*R*)-BINOL-PSSLi. Due to the small amount of sample, the shift reagent was used in a slight excess.

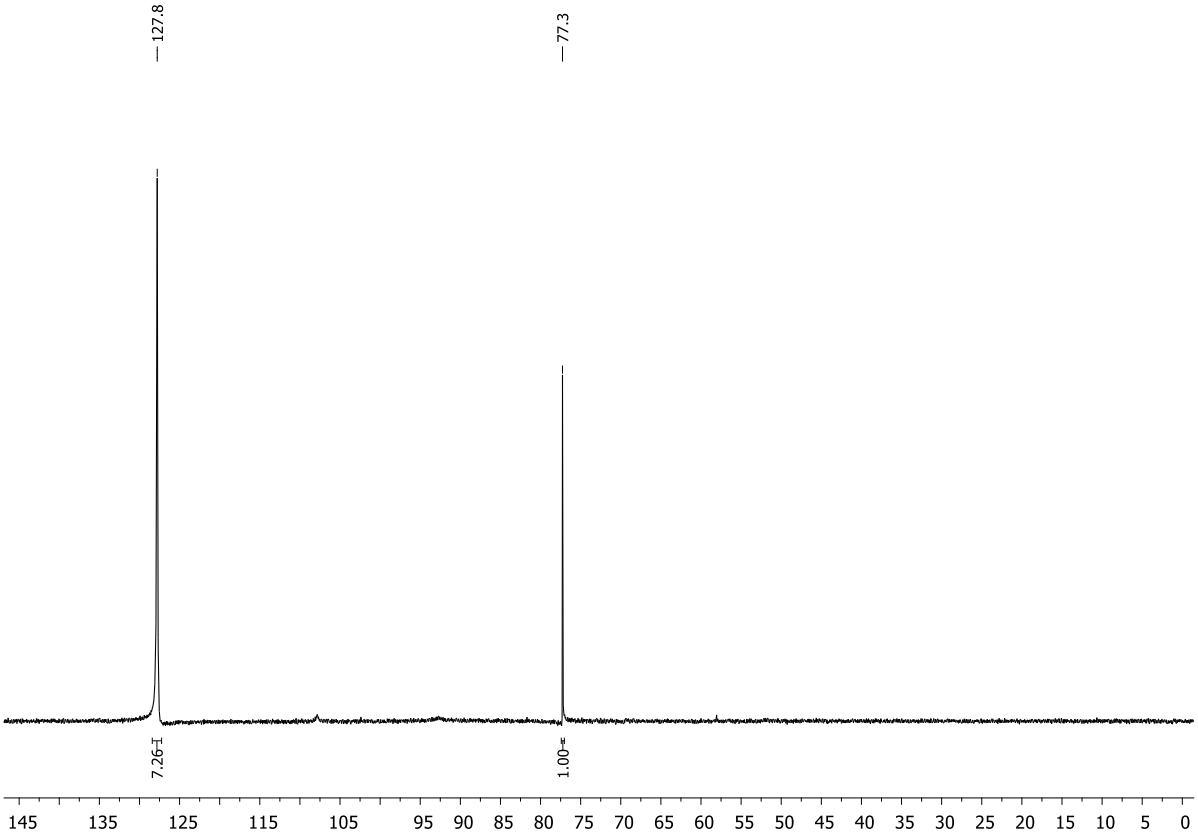

Figure S3.71. ^{31}P{^{1}H} NMR spectrum (CD_2Cl_2, 298 K) of crude (S_P)-**8** in the presence of (*R*)-BINOL-PSSLi. Due to the small amount of sample, the shift reagent was used in a slight excess.

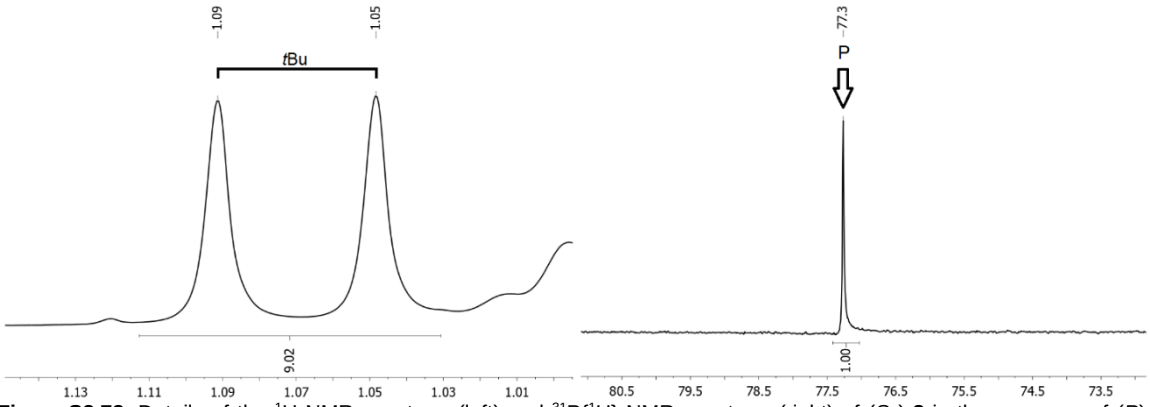

Figure S3.72. Details of the ^{1}H NMR spectrum (left) and ^{31}P{^{1}H} NMR spectrum (right) of (S_P)-**8** in the presence of (*R*)-BINOL-PSSLi (CD_2Cl_2, 298 K).

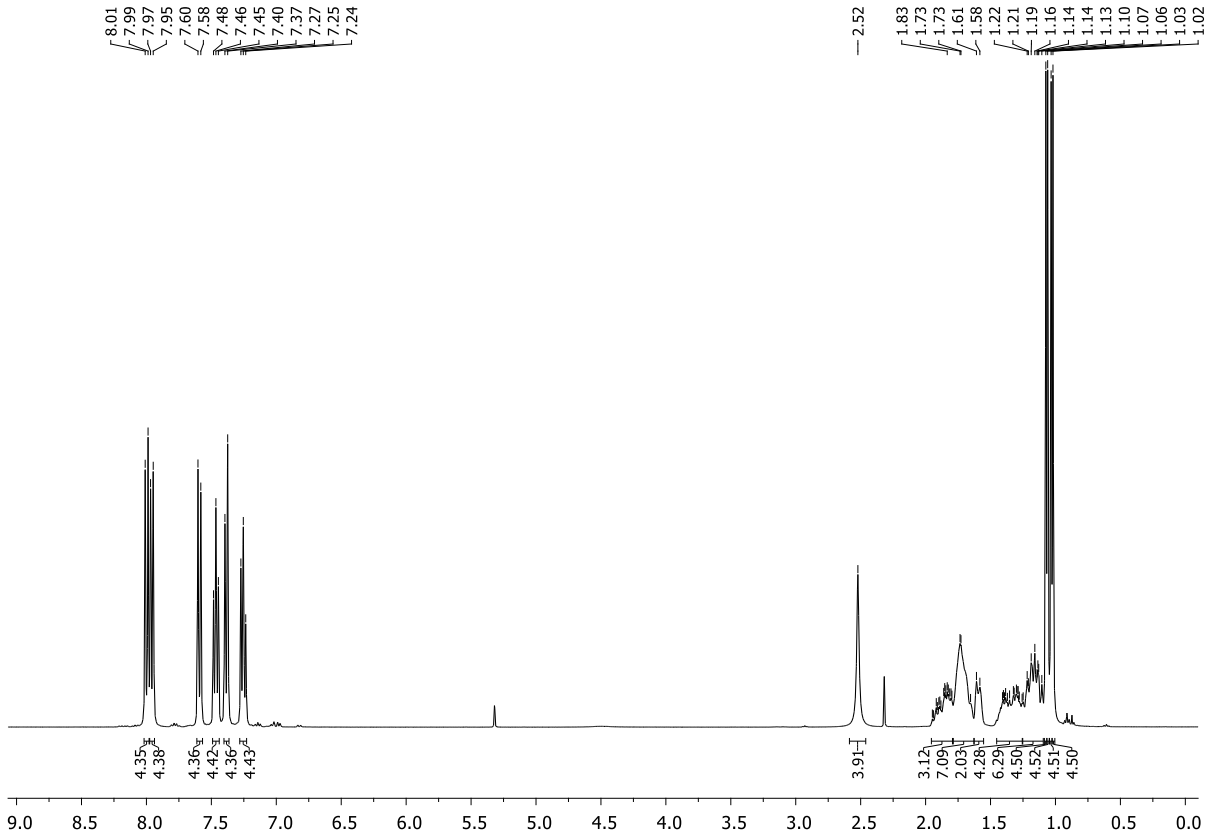

Figure S3.73. ^{1}H NMR spectrum (CD_2Cl_2, 298 K) of (*rac*)-**13** in the presence of (*R*)-BINOL-PSSLi.

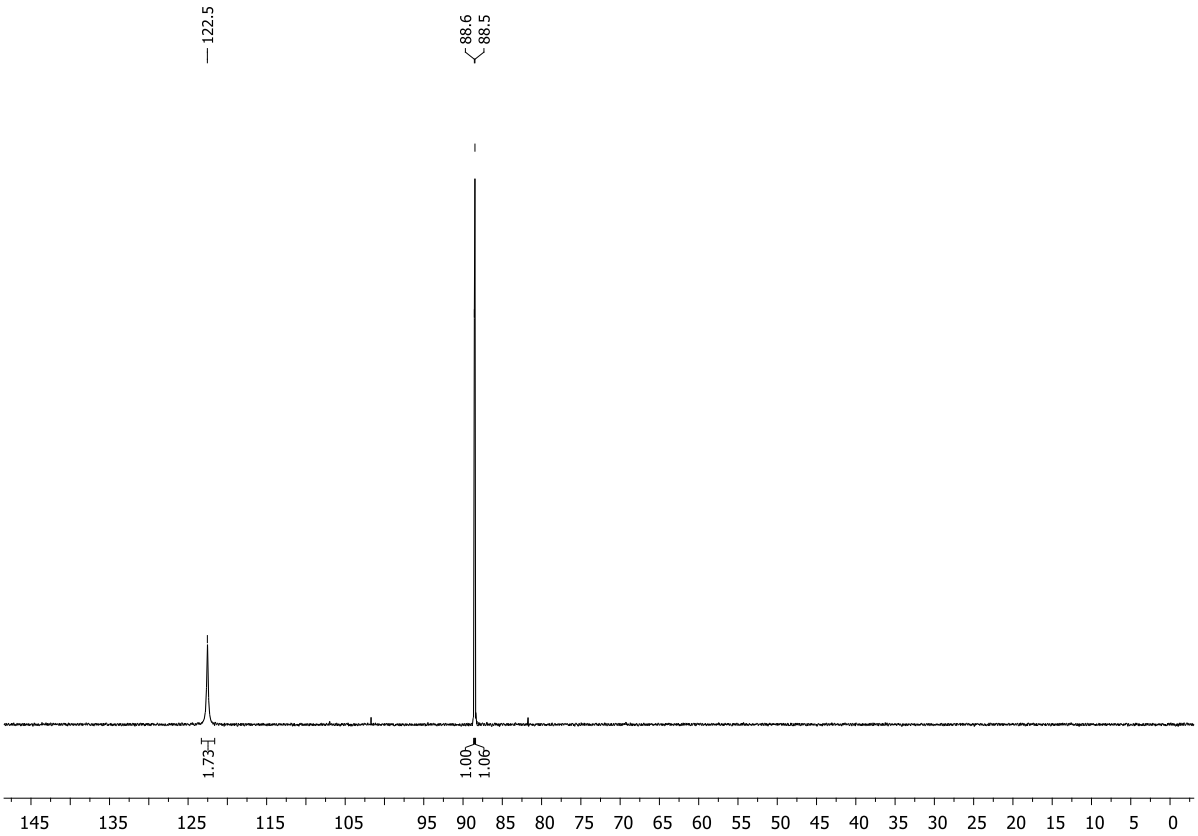

Figure S3.74. $^{31}P\{^{1}H\}$ NMR spectrum (CD_2Cl_2, 298 K) of (*rac*)-**13** in the presence of (*R*)-BINOL-PSSLi.

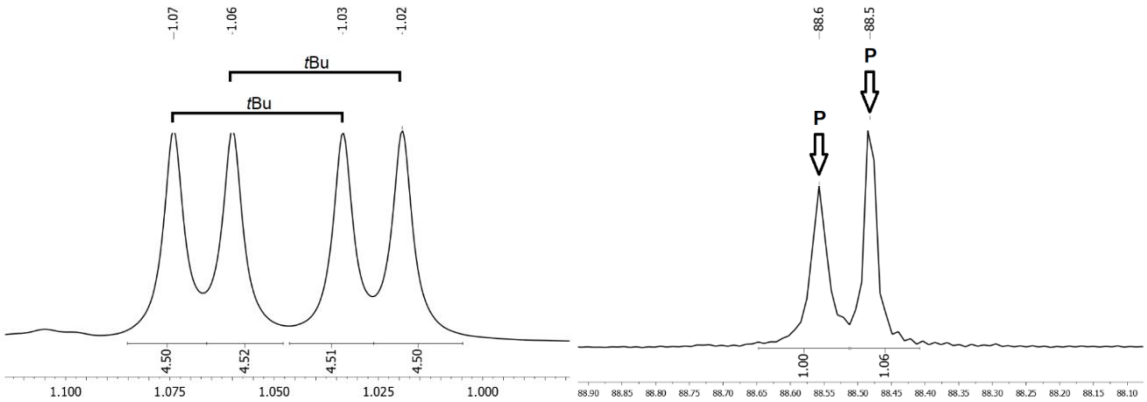

Figure S3.75. Details of the ^{1}H NMR spectrum (left) and $^{31}P\{^{1}H\}$ NMR spectrum (right) of (*rac*)-**13** in the presence of (*R*)-BINOL-PSSLi (CD_2Cl_2, 298 K).

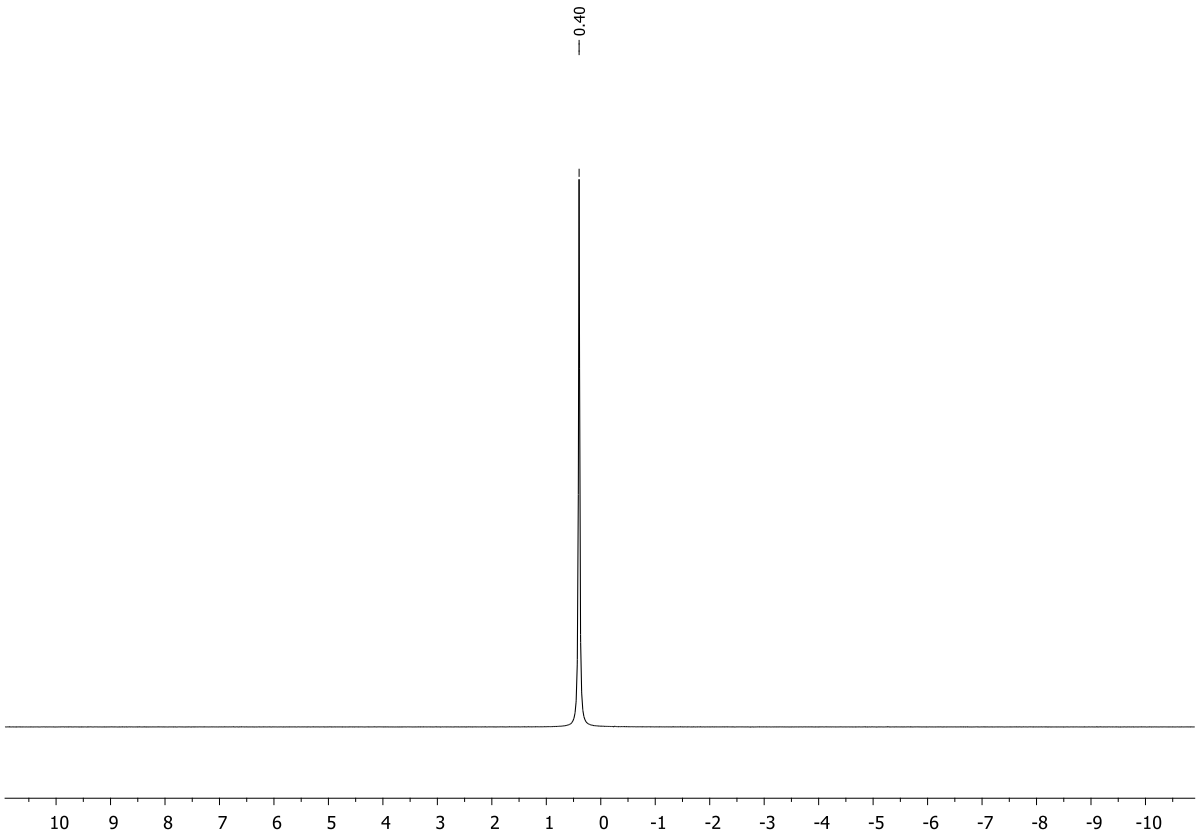

Figure S3.76. $^{7}Li\{^{1}H\}$ NMR spectrum (CD_2Cl_2, 298 K) of (*rac*)-**13** in the presence of (*R*)-BINOL-PSSLi.

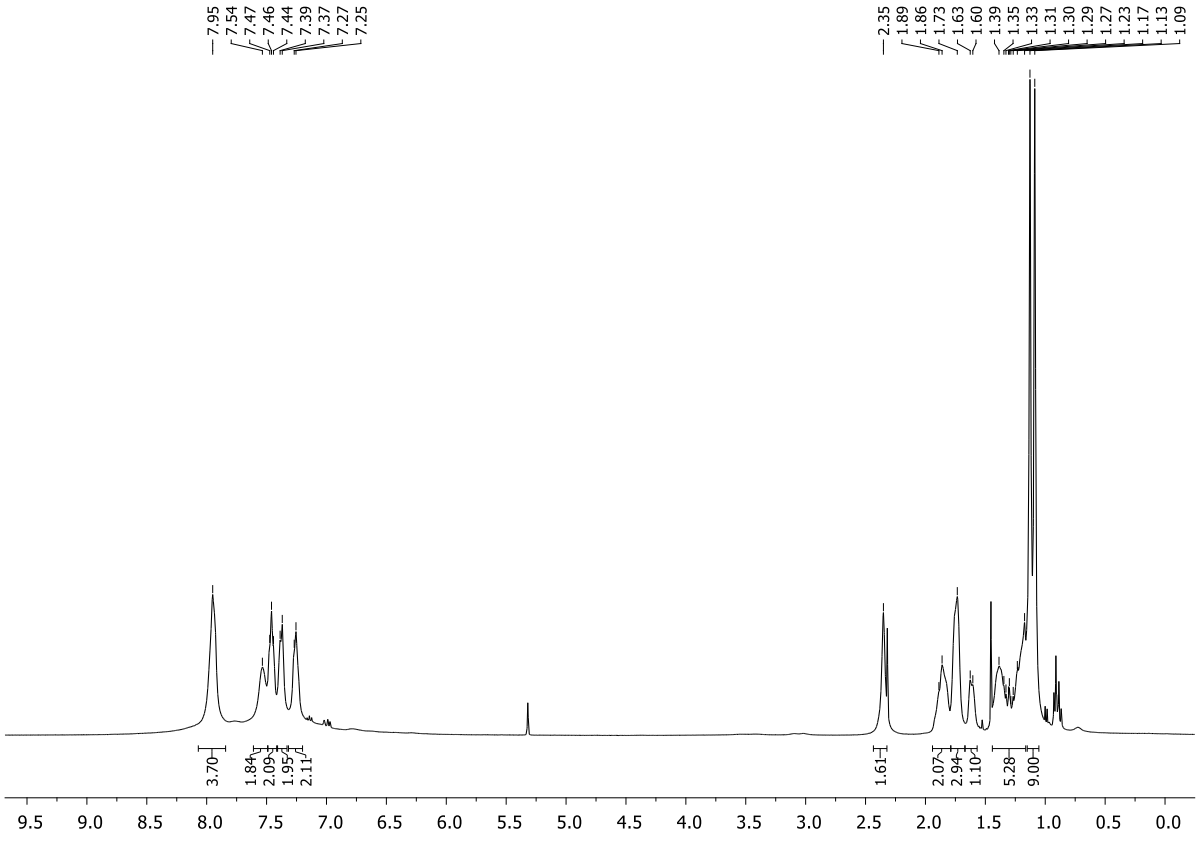

Figure S3.77. ^{1}H NMR spectrum (CD_2Cl_2, 298 K) of crude (R_P)-**13** in the presence of (*R*)-BINOL-PSSLi.

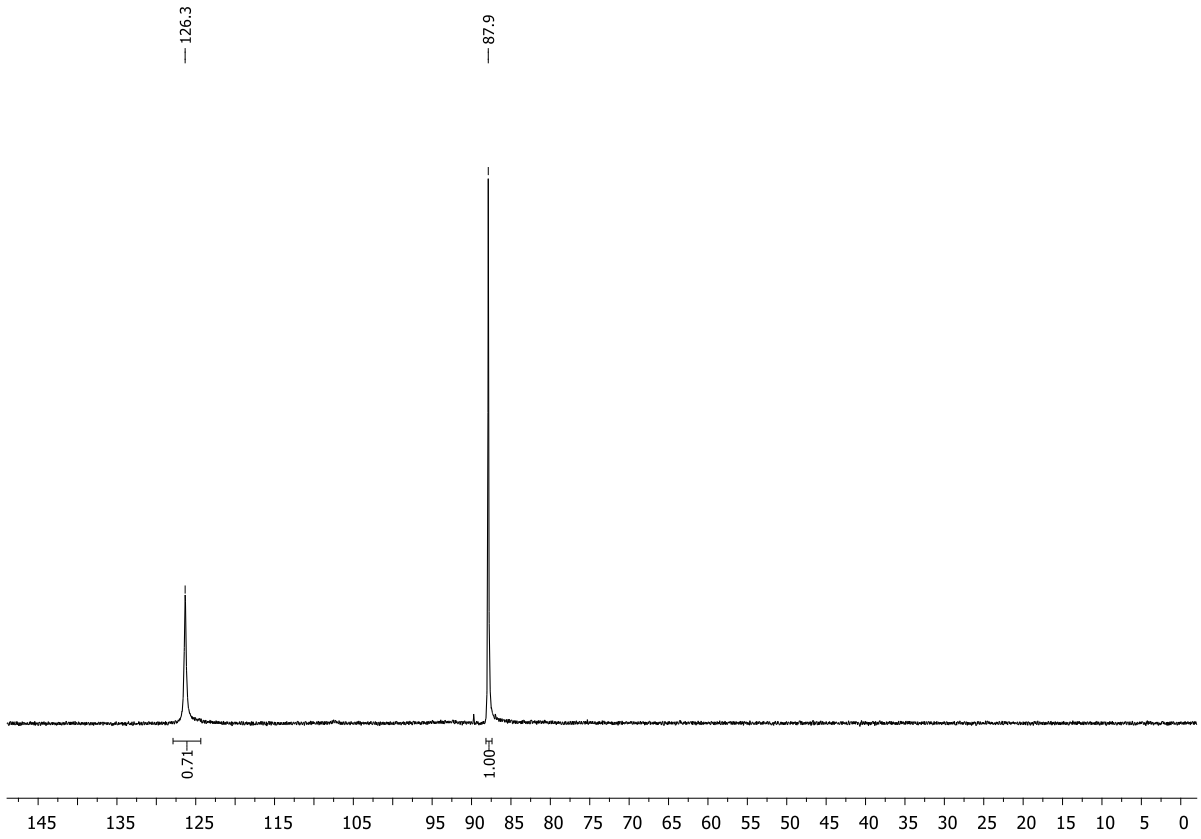

Figure S3.78. $^{31}P\{^{1}H\}$ NMR spectrum (CD_2Cl_2, 298 K) of crude (R_P)-**13** in the presence of (*R*)-BINOL-PSSLi (CD_2Cl_2, 298 K).

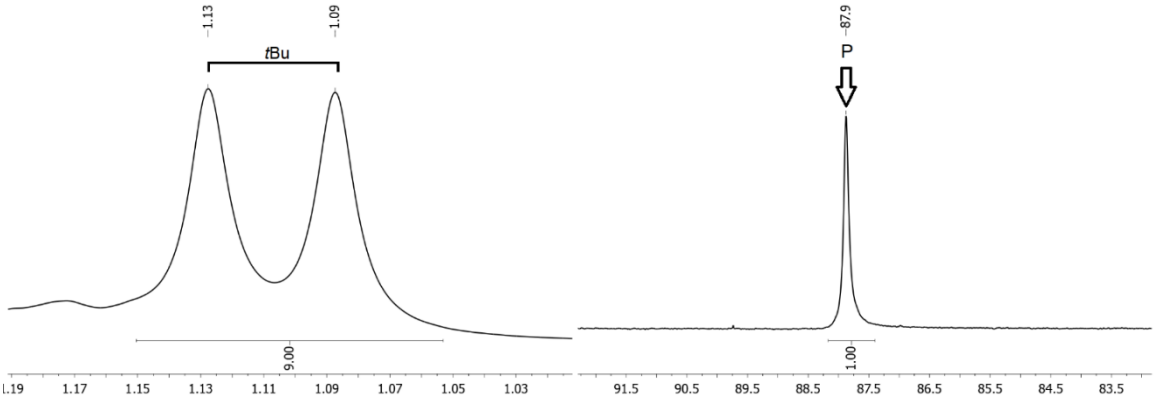

Figure S3.79. Details of the ^{1}H NMR spectrum (left) and $^{31}P\{^{1}H\}$ NMR spectrum (right) of (R_P)-**13** in the presence of (*R*)-BINOL-PSSLi (CD_2Cl_2, 298 K).

3.6.2.13. Preparation of (*R*)-BINOL-PSSNa and (*R*)-BINOL-PSSK

A suspension of benzyl sodium (0.18 g, 1.6 mmol, 1.0 equiv.) or benzyl potassium (0.17 g, 1.3 mmol, 1.0 equiv.) in hexane (20 mL) was added to a suspension of (*R*)-BINOL-PSSH (1.6 or 1.3 mmol, 1.0 equiv.) in hexane (30 mL) at **–**30 °C. The mixture was allowed to slowly warm to room temperature and stirred for 48 h. Then, the resulting colorless solid was filtered off, washed with hexane and dried *in vacuo* to yield (*R*)-BINOL-PSSNa (0.58 g, 1.45 mmol, 91%) and (*R*)-BINOL-PSSK (0.46 g, 1.10 mmol, 85%), respectively. The reagents were used directly.

3.6.2.14. Preparation of monolithiated (*R*)-BINOL

n-Butyllithium (1.0 mL of a 2.5 M solution in hexane, 2.5 mmol, 1.0 equiv.) was added to a suspension of (*R*)-BINOL (0.69 g, 2.5 mmol, 1.0 equiv.) in hexane (60 mL) at **–**30 °C. The mixture was allowed to slowly warm to room temperature and stirred for 48 h. Then, the resulting colorless solid was filtered off, washed with hexane and dried *in vacuo* to yield monolithiated (*R*)-BINOL (0.67 g, 2.3 mmol, 92%). The reagent was used directly.

3.6.2.15. Investigation of (*R*)-BINOL-PSSNa, (*R*)-BINOL-PSSK, and monolithiated (*R*)-BINOL for use as chiral shift reagents

Freshly prepared (*R*)-BINOL-PSSNa, (*R*)-BINOL-PSSK, or monolithiated (*R*)-BINOL (0.14 mmol, 1.0 equiv.) and (*rac*)-**8** (29 mg, 0.14 mmol, 1.0 equiv.) were dissolved in CD_2Cl_2 (0.5 mL), the mixture transferred to a Young NMR tube and subjected to ^{1}H and $^{31}P\{^{1}H\}$ NMR spectroscopy. With (*R*)-BINOL-PSSNa and (*R*)-BINOL-PSSK, no sufficient diastereotopic discrimination was achieved. With monolithiated (*R*)-BINOL, no diastereotopic discrimination was achieved. For details, see Figures S3.80–87.

(*rac*)-**8** in the presence of (*R*)-BINOL-PSSNa:
^{1}H NMR (400.13 MHz, CD_2Cl_2, 298 K): δ 1.03 [d, 18H, $^{3}J_{H-P}$ = 17.1 Hz, PC(CH_3)$_3$], 2.61 (s, 2H, NH_2), 2.67 (s, 2H, NH_2), 7.22–7.18 (m, 7H, H_{ar}), 7.53–7.32 (m, 23H, H_{ar}), 7.76–7.71 (m, 3H, H_{ar}), 7.90–7.82 (m, 12H, H_{ar}). **^{31}P{^{1}H} NMR** (162.04 MHz, CD_2Cl_2, 298 K): δ 76.6 (s, 1P, S*P*N), 76.6 (s, 1P, S*P*N), 130.1 (s, 2P, O_2PS_2).

(*rac*)-**8** in the presence of (*R*)-BINOL-PSSK:
^{1}H NMR (400.13 MHz, CD_2Cl_2, 298 K): δ 1.10 [d, 9H, $^{3}J_{H-P}$ = 17.0 Hz, PC(CH_3)$_3$], 1.10 [d, 9H, $^{3}J_{H-P}$ = 17.0 Hz, PC(CH_3)$_3$], 2.76 (br, 4H, 2 × NH_2), 7.20–7.16 (m, 6H, H_{ar}), 7.55–7.32 (m, 28H, H_{ar}), 7.94–7.85 (m, 16H, H_{ar}). **^{31}P{^{1}H} NMR** (162.04 MHz, CD_2Cl_2, 298 K): δ 76.4 (s, 2P, S*P*N), 130.4 (s, 2P, O_2PS_2).

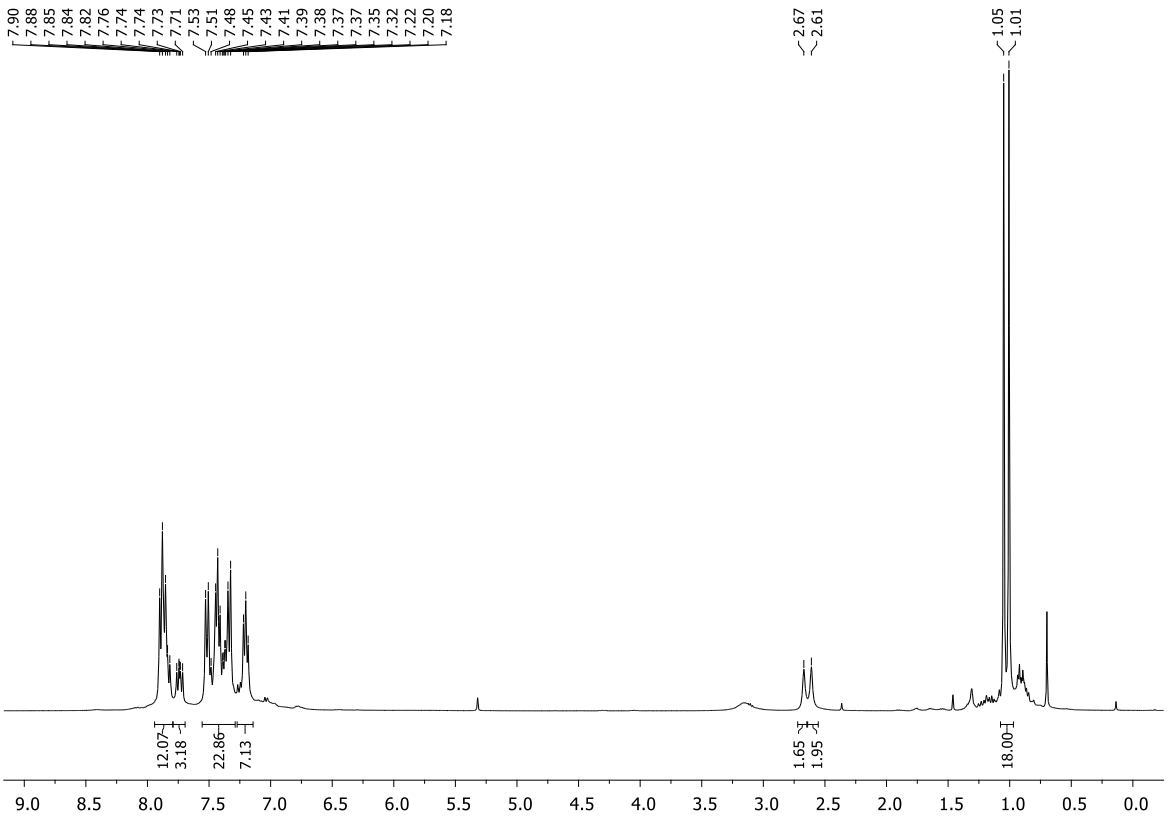

Figure S3.80. ^{1}H NMR spectrum (CD_2Cl_2, 298 K) of (*rac*)-**8** in the presence of (*R*)-BINOL-PSSNa.

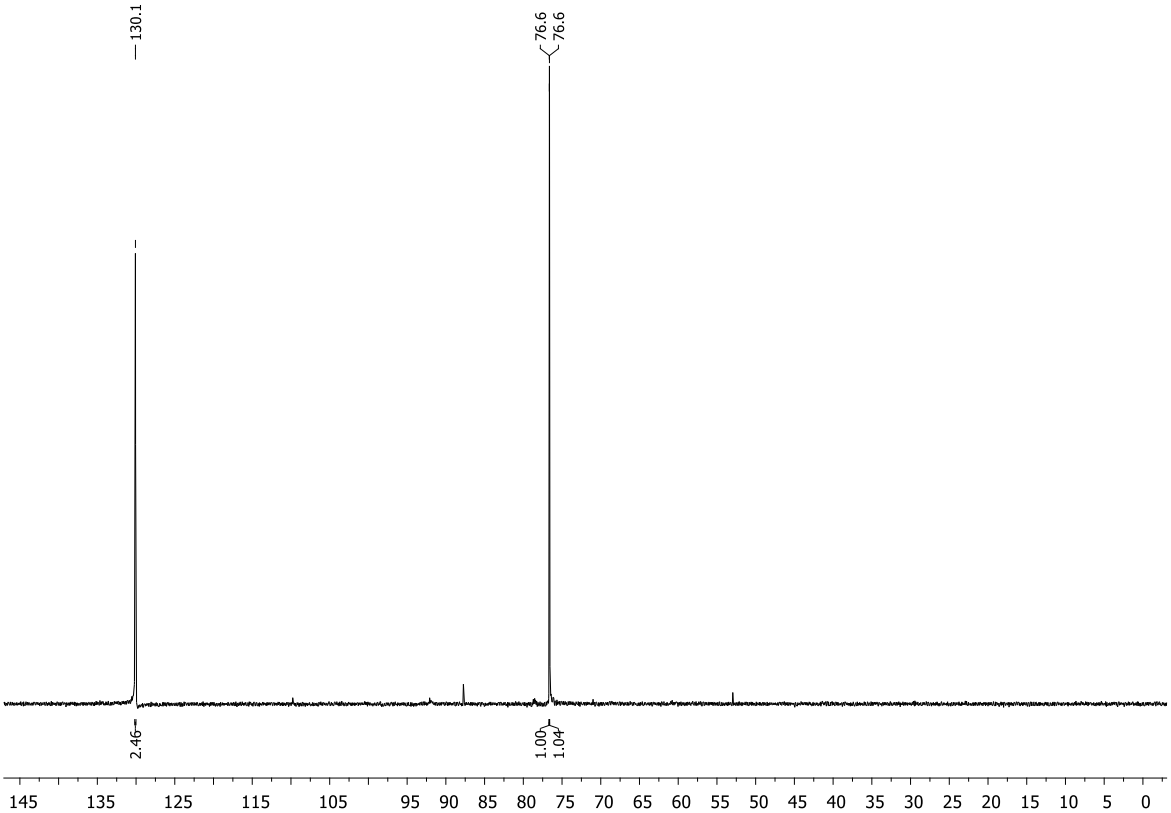

Figure S3.81. $^{31}P\{^{1}H\}$ NMR spectrum (CD_2Cl_2, 298 K) of (*rac*)-**8** in the presence of (*R*)-BINOL-PSSNa.

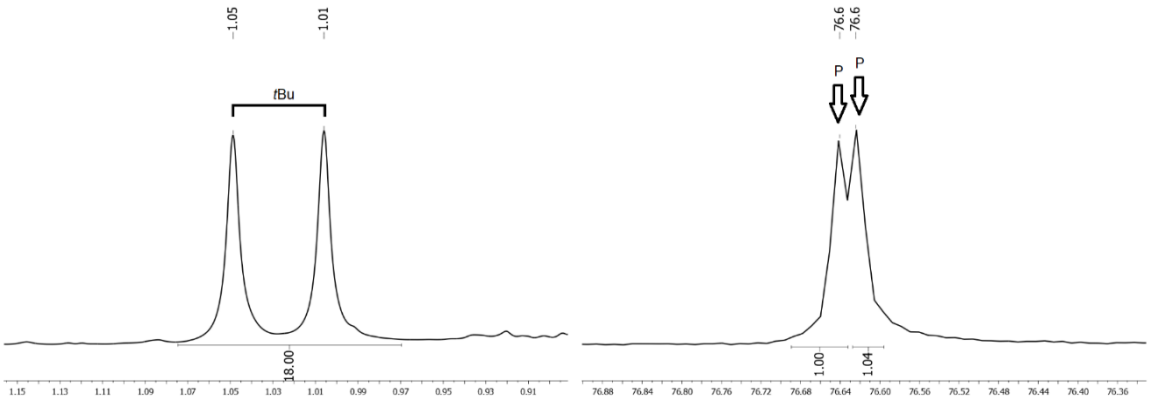

Figure S3.82. Details of the ^{1}H NMR spectrum (left) and $^{31}P\{^{1}H\}$ NMR spectrum (right) of (*rac*)-**8** in the presence of (*R*)-BINOL-PSSNa (CD_2Cl_2, 298 K). No sufficient diastereotopic discrimination was achieved.

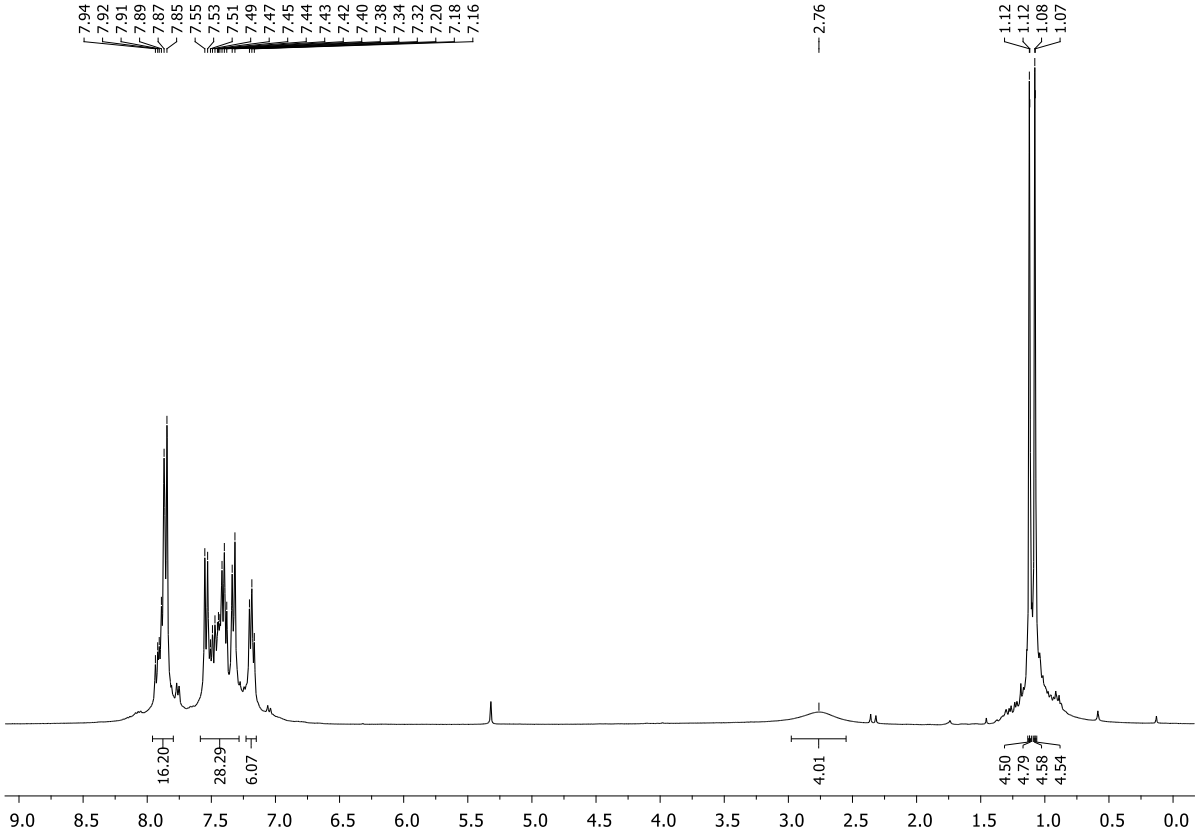

Figure S3.83. ^{1}H NMR spectrum (CD_2Cl_2, 298 K) of (*rac*)-**8** in the presence of (*R*)-BINOL-PSSK.

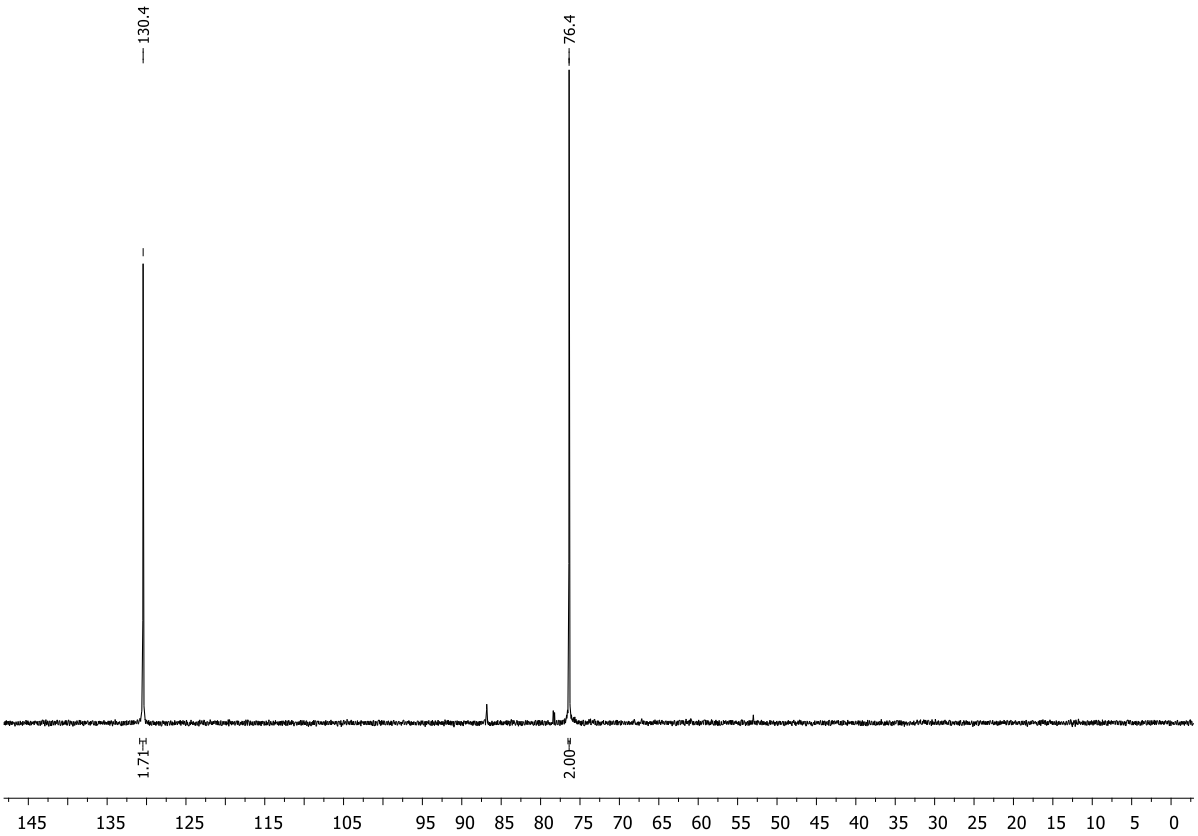

Figure S3.84. $^{31}P\{^{1}H\}$ NMR spectrum (CD_2Cl_2, 298 K) of (*rac*)-**8** in the presence of (*R*)-BINOL-PSSK.

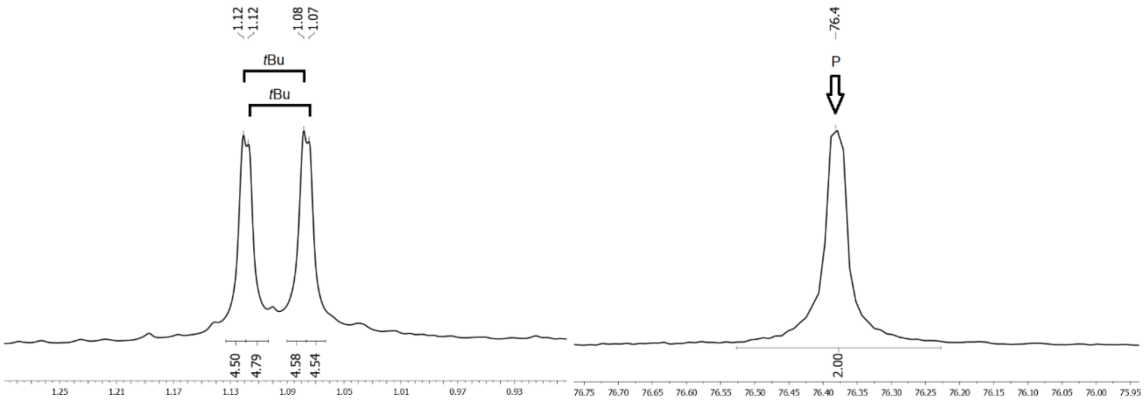

Figure S3.85. Details of the ^{1}H NMR spectrum (left) and $^{31}P\{^{1}H\}$ NMR spectrum (right) of (*rac*)-**8** in the presence of (*R*)-BINOL-PSSK (CD_2Cl_2, 298 K). No sufficient diastereotopic discrimination was achieved.

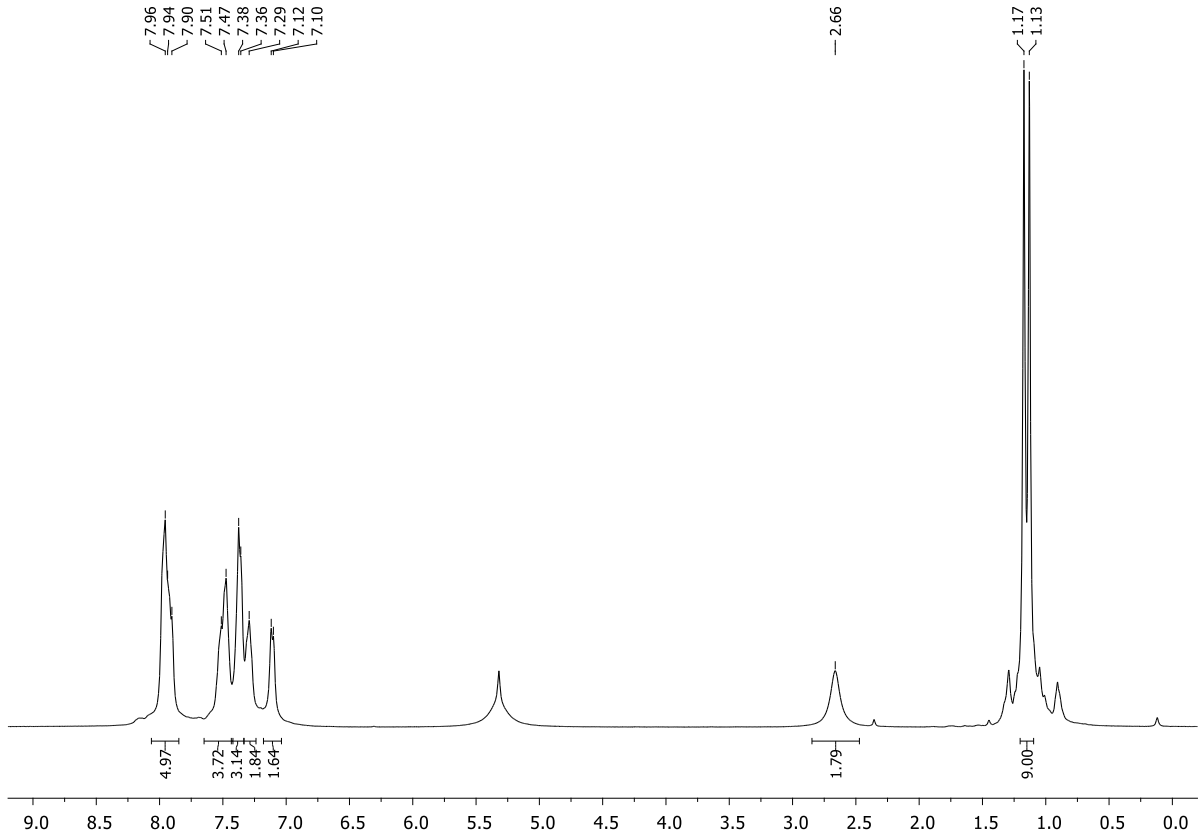

Figure S3.86. ^{1}H NMR spectrum (CD_2Cl_2, 298 K) of (*rac*)-**8** in the presence of monolithiated (*R*)-BINOL. No diastereotopic discrimination was achieved.

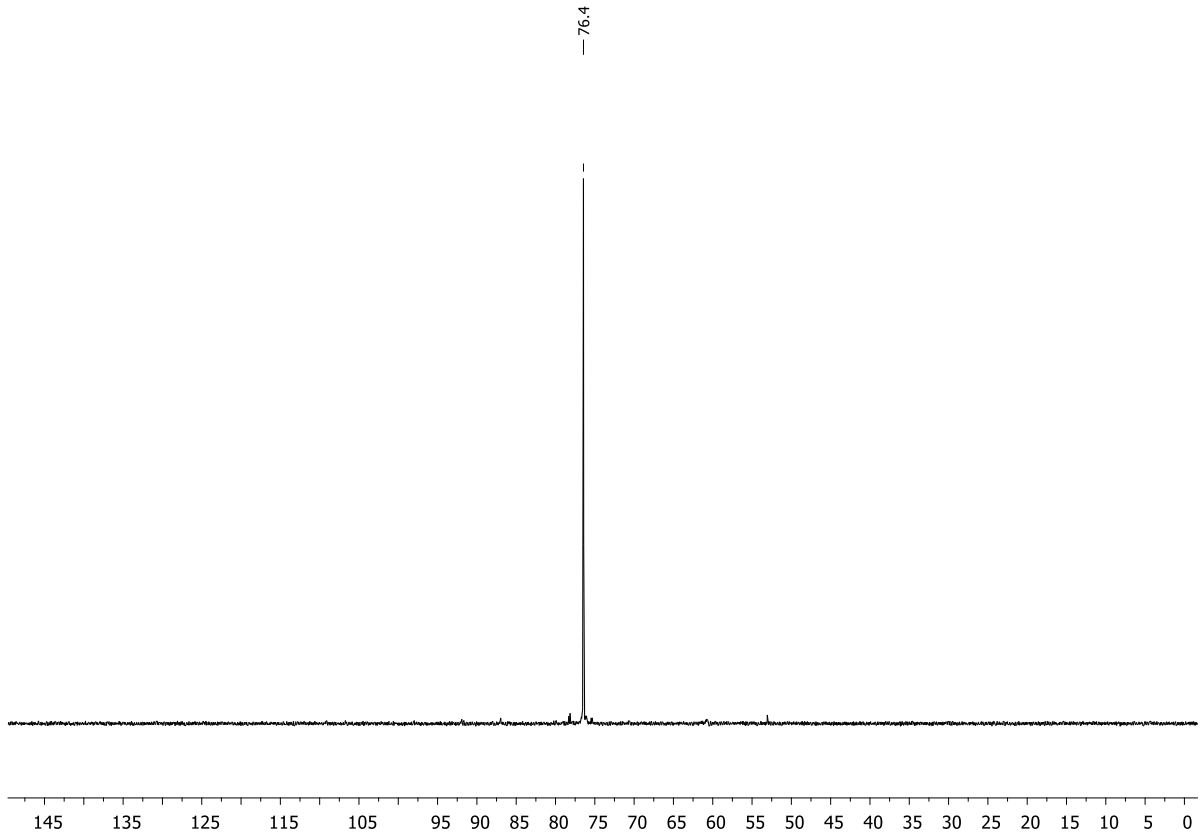

Figure S3.87. $^{31}P\{^{1}H\}$ NMR spectrum (CD_2Cl_2, 298 K) of (*rac*)-**8** in the presence of monolithiated (*R*)-BINOL. No diastereotopic discrimination was achieved.

3.7. X-Ray Crystallographic Details

The crystals were selected and measured either on an Xcalibur Gemini Ultra diffractometer, equipped with a TitanS2 detector [(S_P,*S*)-**4**, (R_P,*S*)-**7**], an XtaLAB Synergy R, DW system, equipped with a HyPix-Arc 150 detector [(S_P,*S*)-**5**, (R_P)-**6**, (*rac*)-**8**, and (R_P)-**14**], or on a SuperNova Dualflex diffractometer, equipped with a TitanS2 detector [(S_P)-**8**, (R_P,*S*)-**12**, and (R_P)-**13**]. The crystals were kept at T = 123(1) K [(S_P,*S*)-**4**, (S_P,*S*)-**5**, (R_P,*S*)-**7**, (S_P)-**8**, (R_P,*S*)-**12**, (R_P)-**13**, and (R_P)-**14**] or 100(1) K [(R_P)-**6** and (*rac*)-**8**] during data collection. Data collection and reduction were performed with CrysAlisPro, Version 1.171.41.83a [(S_P,*S*)-**4**, (S_P,*S*)-**5**, (R_P,*S*)-**7**, (R_P)-**6**, (*rac*)-**8**, (R_P,*S*)-**12** and (R_P)-**14**] or Version 1.171.41.90a [(S_P)-**8**, (R_P)-**13**].[5] For all compounds a numerical absorption correction based on Gaussian integration over a multifaceted crystal model, and an empirical absorption correction using spherical harmonics as implemented in SCALE3 ABSPACK scaling algorithm was applied. Using Olex2,[6] the structures were solved with ShelXT[7] and a least-square refinement on F^2 was carried out with ShelXL[8]. All non-hydrogen atoms were refined anisotropically. Hydrogen atoms at the carbon atoms were located in idealized positions and refined isotropically according to the riding model. Hydrogen atoms at the nitrogen atoms in compounds (S_P,*S*)-**4**, (S_P,*S*)-**5**, (R_P,*S*)-**7**, and (R_P,*S*)-**12** were located in idealized positions and refined isotropically according to the riding model. Hydrogen atoms at the nitrogen atoms in compounds (R_P)-**6**, (S_P)-**8**, (*rac*)-**8**, (R_P)-**13** and (R_P)-**14** were located from the difference Fourier map and refined without restraints. The hydrogen atom at the silicon atom was located from the difference Fourier map and refined without restraints. All figures were created with Olex2.[6]

Compound (S_P,*S*)-**4**: The asymmetric unit contains one molecule.
Compound (S_P,*S*)-**5**: The asymmetric unit contains one molecule.
Compound (R_P)-**6**: The asymmetric unit contains one molecule.
Compound (R_P,*S*)-**7**: The asymmetric unit contains one molecule.
The phenyl moiety (C14, C15, C16, C17, C18) is disordered over two positions and split into two parts with occupancies of 66:34. SIMU and SADI restraints were used to model this disorder.
Compound (S_P)-**8**: The asymmetric unit contains four molecules. DFIX and DANG restraints were used for this structure.
Compound (*rac*)-**8**: The asymmetric unit contains one molecule.
Compound (R_P,*S*)-**12**: The asymmetric unit contains one molecule.
Compound (R_P)-**13**: The asymmetric unit contains three molecules.
One of the cyclohexyl moieties (C25, C26, C27, C28) is disordered over two positions and split into two parts with occupancies of 50:50. SIMU and SADI restraints were used to model this disorder.
Compound (R_P)-**14**: The asymmetric unit contains one molecule.

Table S3.1. Crystallographic data for compounds (S_P,S)-**4**, (S_P,S)-**5**, and (R_P)-**6**.

Compound	(S_P,S)-**4**	(S_P,S)-**5**	(R_P)-**6**
Data Set (internal naming)	**TH179_2**	**TH139**	**TH147_dest_1B**
CCDC Number	2201330	2201331	2201332
Formula	$C_{18}H_{24}NPS$	$C_{22}H_{26}NPS$	$C_{10}H_{18}NPS$
$\rho_{calc.}$ / g·cm^{-3}	1.208	1.264	1.273
μ/mm^{-1}	2.442	2.282	3.538
Formula Weight	317.41	367.47	215.28
Color	clear colorless	clear colorless	clear colorless
Shape	block	block	needle
Size/mm^3	0.48 × 0.20 × 0.20	0.22 × 0.2 × 0.16	0.81 × 0.09 × 0.09
T/K	123.00(10)	123.00(10)	100.00(10)
Crystal System	orthorhombic	monoclinic	orthorhombic
Flack Parameter	−0.011(9)	−0.004(6)	−0.004(10)
Hooft Parameter	−0.011(5)	−0.014(3)	−0.011(8)
Space Group	$P2_12_12_1$	$P2_1$	$P2_12_12_1$
a/Å	6.4057(2)	10.1070(10)	6.23200(10)
b/Å	14.4006(5)	8.01210(10)	10.2303(2)
c/Å	18.9245(7)	11.9370(10)	17.6171(3)
α/°	90	90	90
β/°	90	92.340(10)	90
γ/°	90	90	90
V/Å^3	1745.71(10)	965.832(17)	1123.18(3)
Z	4	2	4
Z'	1	1	1
Wavelength/Å	1.54184	1.54184	1.54184
Radiation Type	Cu K_α	Cu K_α	Cu K_α
$2\theta_{min}$/°	7.714	7.412	9.998
$2\theta_{max}$/°	135.13	150.556	154.208
Measured Refl.	18713	15260	8284
Independent Refl.	3137	3910	2320
R_{int}	0.0406	0.0209	0.0311
Parameters	194	230	129
Restraints	0	1	0
Largest Peak	0.41	0.26	0.33
Deepest Hole	−0.32	−0.23	−0.27
GooF	1.079	1.032	1.053
wR_2 (all data)	0.0857	0.0587	0.0699
wR_2	0.0834	0.0586	0.0696
R_1 (all data)	0.0328	0.0222	0.0258
R_1	0.0312	0.0220	0.0252

Table S3.2. Crystallographic data for compounds (R_P,S)-**7**, (S_P)-**8**, and (*rac*)-**8**.

Compound	(R_P,S)-**7**	(S_P)-**8**	(*rac*)-**8**
Data Set (internal naming)	**TH186_1A**	**TH250_2A**	**KS02**
CCDC Number	2201333	2201334	2201335
Formula	$C_{18}H_{26}NPS$	$C_{10}H_{16}NPS$	$C_{10}H_{16}NPS$
$\rho_{calc.}$ / g·cm^{-3}	1.175	1.242	1.249
μ/mm^{-1}	2.361	3.484	3.502
Formula Weight	319.43	213.27	213.27
Color	clear colorless	clear colorless	clear colorless
Shape	block	block	block
Size/mm^3	0.22 × 0.17 × 0.09	0.19 × 0.13 × 0.11	0.49 × 0.36 × 0.29
T/K	123.00(10)	122.97(16)	100.00(10)
Crystal System	orthorhombic	monoclinic	monoclinic
Flack Parameter	−0.042(18)	0.04(2)	–
Hooft Parameter	−0.045(15)	0.04(2)	–
Space Group	$P2_12_12_1$	$P2_1$	$P2_1/n$
a/Å	6.3088(3)	6.31750(10)	12.77968(9)
b/Å	16.3220(10)	21.0281(2)	6.28987(4)
c/Å	17.5362(12)	17.1702(2)	14.39331(10)
α/°	90	90	90
β/°	90	90.0680(10)	101.3194(7)
γ/°	90	90	90
V/Å^3	1805.74(19)	2280.97(5)	1134.466(14)
Z	4	8	4
Z'	1	4	1
Wavelength/Å	1.54184	1.54184	1.54184
Radiation Type	Cu K_α	Cu K_α	Cu K_α
$2\theta_{min}$/°	10.088	8.41	8.466
$2\theta_{max}$/°	133.634	132.992	150.866
Measured Refl.	10712	8020	13598
Independent Refl.	3208	8020	2308
R_{int}	0.0548	– (twin)	0.0298
Parameters	234	506	129
Restraints	96	10	0
Largest Peak	0.19	0.26	0.47
Deepest Hole	−0.21	−0.30	−0.36
GooF	1.024	1.067	1.103
wR_2 (all data)	0.0803	0.1241	0.0774
wR_2	0.0775	0.1238	0.0773
R_1 (all data)	0.0392	0.0452	0.0288
R_1	0.0343	0.0450	0.0287

Table S3.3. Crystallographic data for compounds (R_P,*S*)-**12**, (R_P)-**13**, and (R_P)-**14**.

Compound	(R_P,*S*)-**12**	(R_P)-**13**	(R_P)-**14**
Data Set (internal naming)	**TH208**	**TH222**	**TH302**
CCDC Number	2201336	2201337	2202270
Formula	$C_{18}H_{30}NPS$	$C_{10}H_{22}NPS$	$C_{18}H_{40}NPSSi$
$\rho_{calc.}$ / g·cm^{-3}	1.152	1.146	1.109
μ/mm^{-1}	2.287	3.125	2.518
Formula Weight	323.46	219.31	361.63
Color	clear colorless	clear colorless	clear colourless
Shape	needle	needle	needle
Size/mm^3	0.52 × 0.09 × 0.08	0.89 × 0.10 × 0.09	0.3 × 0.05 × 0.03
T/K	123.00(10)	123.01(10)	122.99(10)
Crystal System	orthorhombic	trigonal	orthorhombic
Flack Parameter	−0.002(11)	−0.02(3)	0.000(10)
Hooft Parameter	−0.003(8)	−0.02(3)	−0.010(8)
Space Group	$P2_12_12_1$	$P3_2$	$P2_12_12_1$
a/Å	6.03120(10)	23.0281(4)	11.1841(3)
b/Å	16.7373(2)	23.0281(4)	12.1617(3)
c/Å	18.4734(3)	6.23040(10)	15.9245(5)
α/°	90	90	90
β/°	90	90	90
γ/°	90	120	90
V/Å^3	1864.82(5)	2861.29(11)	2166.01(10)
Z	4	9	4
Z'	1	3	1
Wavelength/Å	1.54184	1.54184	1.54184
Radiation Type	Cu K_α	Cu K_α	Cu K_α
$2\theta_{min}$/°	9.576	7.678	9.15
$2\theta_{max}$/°	133.632	133.75	147.602
Measured Refl.	13208	5128	15742
Independent Refl.	3303	5128	4170
R_{int}	0.0491	– (twin)	0.0323
Parameters	194	400	216
Restraints	0	52	0
Largest Peak	0.28	0.31	0.22
Deepest Hole	−0.39	−0.46	−0.17
GooF	1.040	1.075	1.053
wR_2 (all data)	0.0845	0.1192	0.0659
wR_2	0.0839	0.1188	0.0650
R_1 (all data)	0.0325	0.0459	0.0280
R_1	0.0319	0.0453	0.0256

Compound (S_P,S)-4:

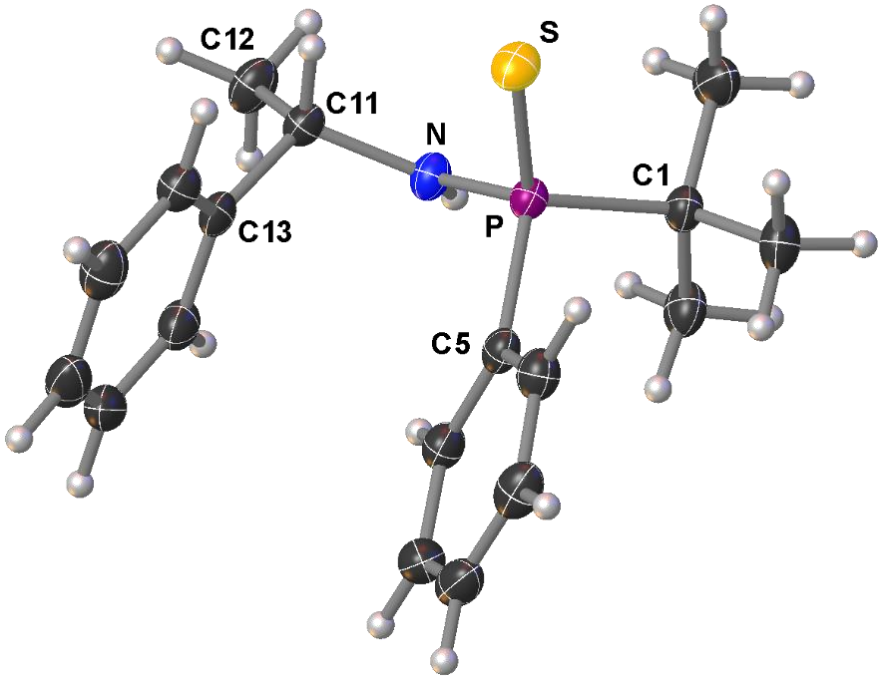

Selected Bond Lengths in Å		Selected Bond Angles in °	
S–P	1.9485(9)	N–P–S	111.32(8)
P–N	1.659(2)	N–P–C1	104.67(11)
P–C1	1.850(2)	N–P–C5	109.64(11)
P–C5	1.822(2)	C5–P–S	111.25(9)
N–C11	1.479(3)	C5–P–C1	105.81(11)
		C1–P–S	113.79(8)

Compound (S_P,S)-5:

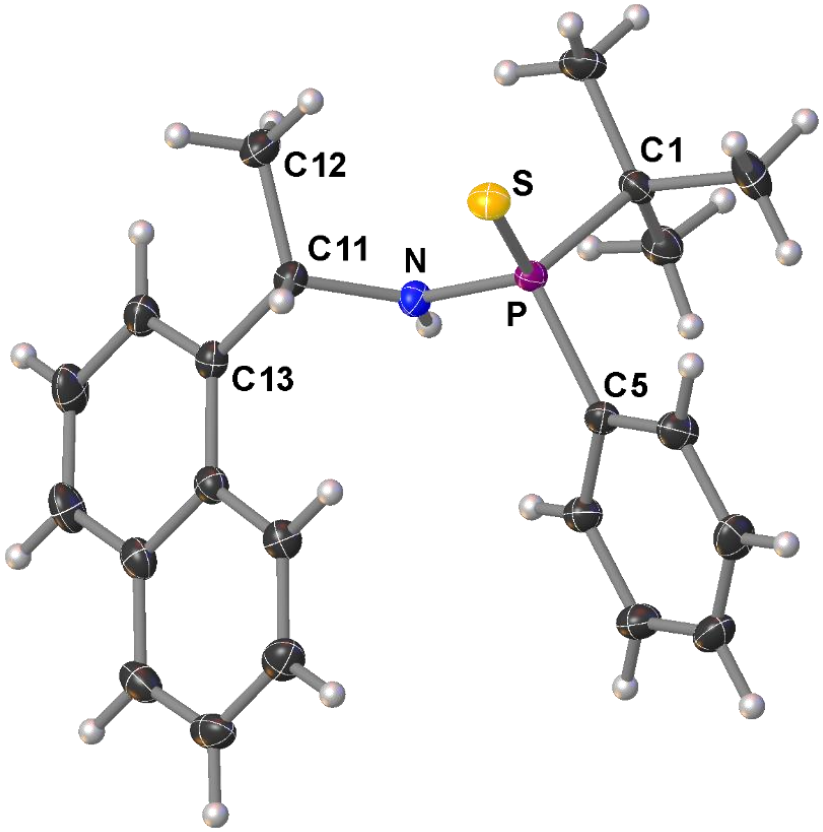

Selected Bond Lengths in Å		Selected Bond Angles in °	
S–P	1.9547(6)	N–P–S	113.01(6)
P–N	1.6702(15)	N–P–C1	106.08(8)
P–C1	1.8546(18)	N–P–C5	107.52(8)
P–C5	1.8213(17)	C5–P–S	111.01(6)
N–C11	1.478(2)	C5–P–C1	106.09(8)
		C1–P–S	112.69(6)

Compound (R_P)-6:

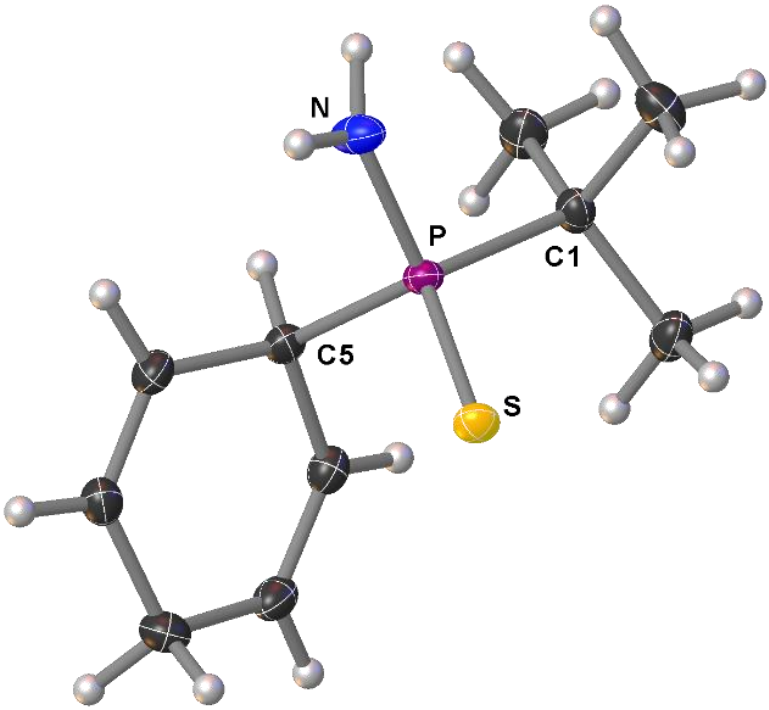

Selected Bond Lengths in Å		Selected Bond Angles in °	
S–P	1.9625(7)	N–P–S	112.65(8)
P–N	1.6417(19)	N–P–C1	104.24(10)
P–C1	1.860(2)	N–P–C5	106.47(10)
P–C5	1.862(2)	C5–P–S	110.91(7)
		C5–P–C1	108.60(9)
		C1–P–S	113.52(7)

Compound (R_P,S)-7:

Part 1 (66%)

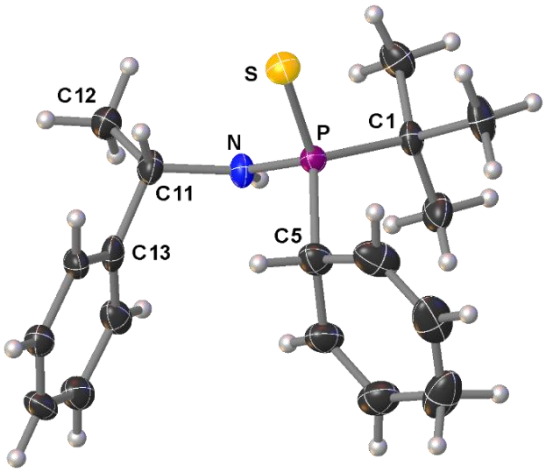

Part 2 (34%)

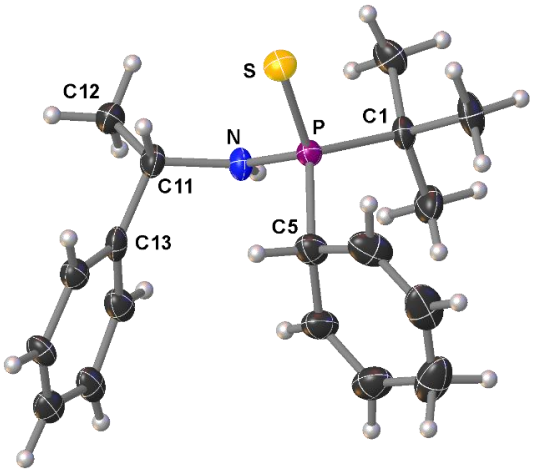

Selected Bond Lengths in Å		Selected Bond Angles in °	
S–P	1.9625(10)	N–P–S	111.33(10)
P–N	1.650(2)	N–P–C1	104.05(13)
P–C1	1.842(3)	N–P–C5	107.30(14)
P–C5	1.866(3)	C5–P–S	107.69(11)
N–C11	1.473(4)	C5–P–C1	113.53(16)
		C1–P–S	112.83(11)

Compound (S_P)-8:

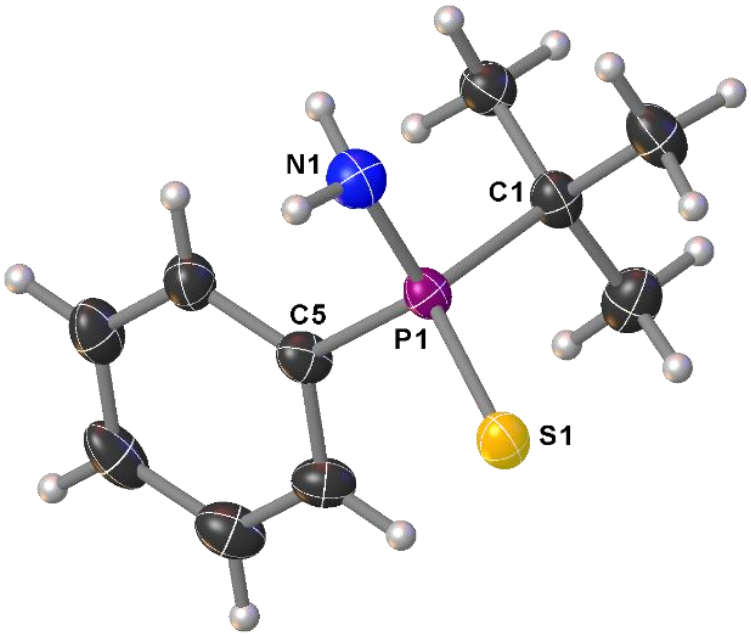

(one of four molecules in the asymmetric unit)

Selected Bond Lengths in Å		Selected Bond Angles in °	
S1–P1	1.953(3)	N1–P1–S1	110.5(3)
P1–N1	1.642(7)	N1–P1–C1	104.6(3)
P1–C1	1.846(7)	N1–P1–C5	110.0(3)
P1–C5	1.821(7)	C5–P1–S1	111.2(2)
		C5–P1–C1	106.8(3)
		C1–P1–S1	113.4(3)

Compound (*rac*)-8:

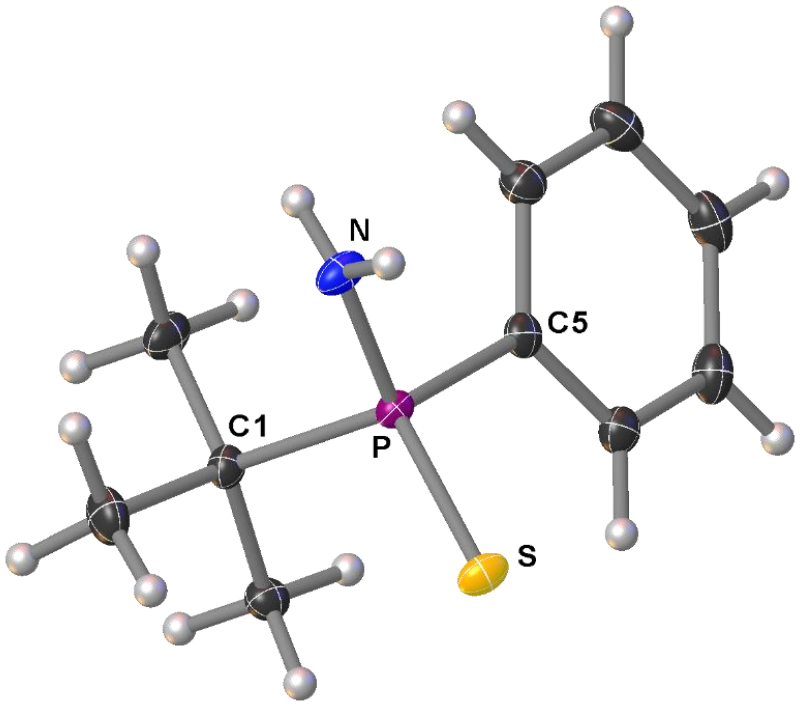

Selected Bond Lengths in Å		Selected Bond Angles in °	
S–P	1.9651(4)	N–P–S	110.96(5)
P–N	1.6446(12)	N–P–C1	105.57(6)
P–C1	1.8446(12)	N–P–C5	109.31(6)
P–C5	1.8188(13)	C5–P–S	112.19(4)
		C5–P–C1	105.96(6)
		C1–P–S	112.50(4)

Compound (R_P,S)-12:

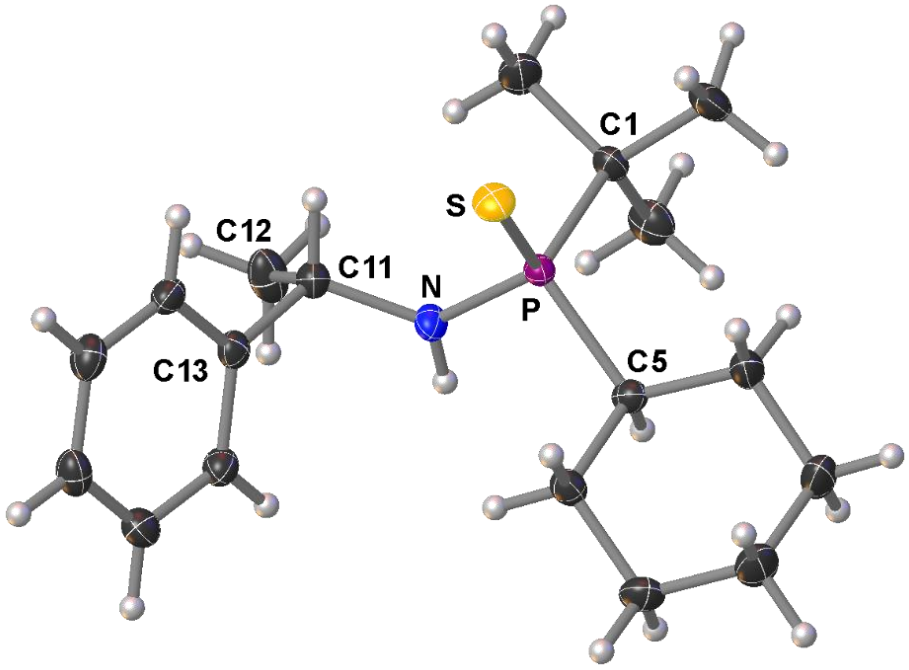

Selected Bond Lengths in Å		Selected Bond Angles in °	
S–P	1.9609(8)	N–P–S	113.29(8)
P–N	1.651(2)	N–P–C1	106.58(11)
P–C1	1.863(2)	N–P–C5	101.56(11)
P–C5	1.830(2)	C5–P–S	113.06(8)
N–C11	1.468(3)	C5–P–C1	110.19(11)
		C1–P–S	111.56(8)

Compound (R_P)-13:

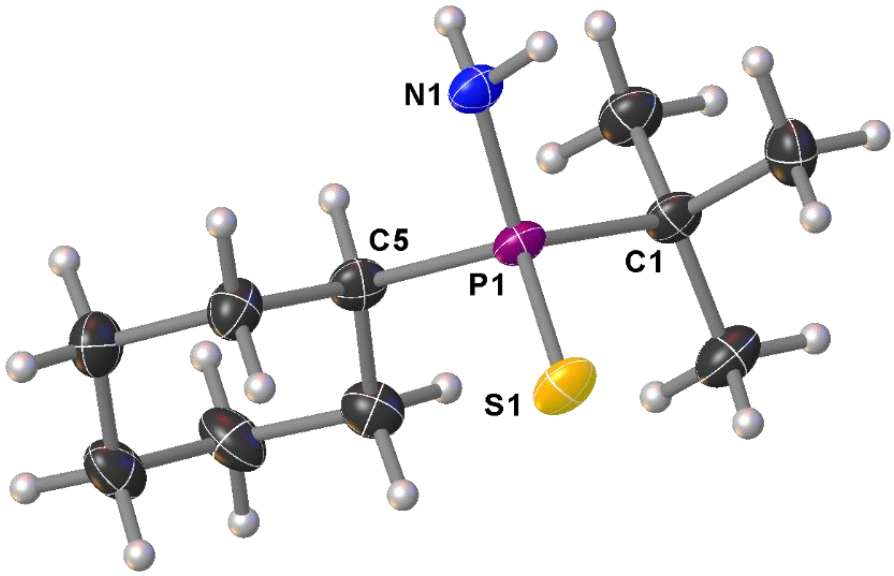

(one of three molecules in the asymmetric unit)

Selected Bond Lengths in Å		Selected Bond Angles in °	
S1–P1	1.967(3)	N1–P1–S1	111.8(2)
P1–N1	1.653(6)	N1–P1–C1	109.2(3)
P1–C1	1.862(7)	N1–P1–C5	101.0(3)
P1–C5	1.835(7)	C5–P1–S1	113.3(3)
		C5–P1–C1	110.9(3)
		C1–P1–S1	110.3(2)

Compound (R_P)-14:

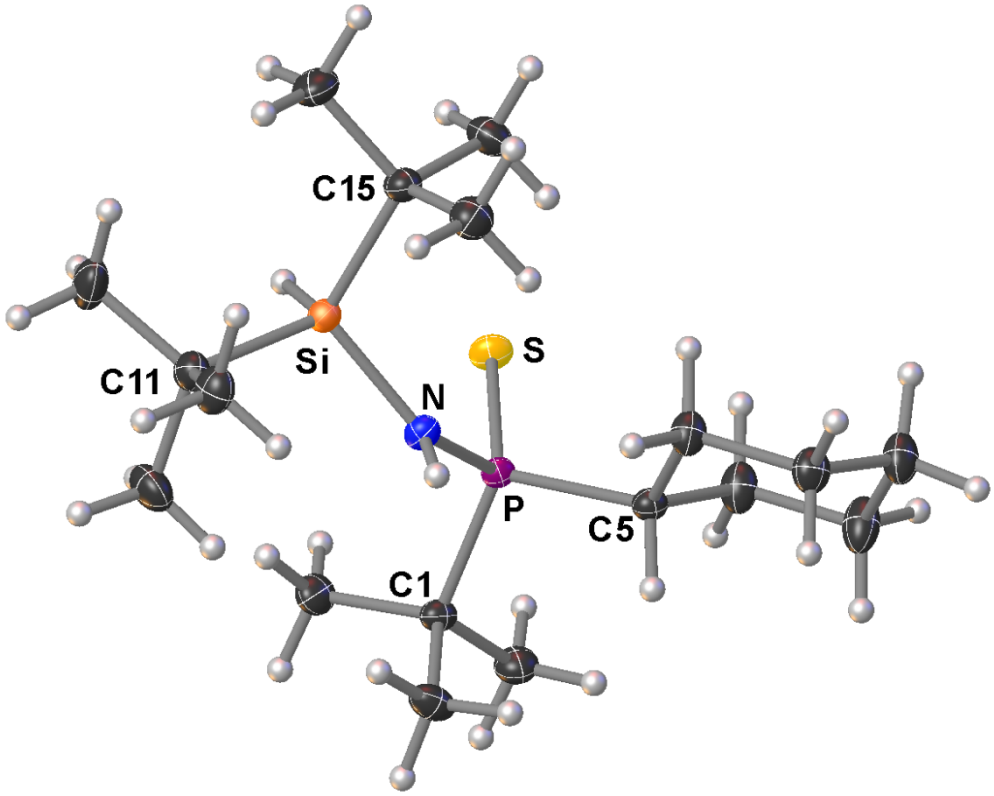

Selected Bond Lengths in Å		Selected Bond Angles in °	
S–P	1.9615(8)	N–P–S	111.27(7)
P–N	1.6679(19)	N–P–C1	107.27(10)
P–C1	1.860(2)	N–P–C5	107.73(10)
P–C5	1.849(2)	C5–P–S	112.72(8)
Si–N	1.761(2)	C5–P–C1	105.08(11)
Si–C11	1.908(3)	C1–P–S	112.38(8)
Si–C15	1.907(2)	N–Si–C11	109.16(10)
		N–Si–C15	110.75(10)
		C15–Si–C11	115.27(11)

3.8. Quantum Chemical Calculations

Optimization and additional harmonic vibrational frequency analyses were performed with the software package Gaussian 09 (Revision E.01) on the M062X/6-31+G(d) level of theory[9] without symmetry restrictions applying the Polarizable Continuum Model (PCM)[10] [solvent: dichloromethane for **D**-Cy, **E**-Cy, **F**-Cy, **G**-Cy, and **H**-Cy, tetrahydrofuran for $(LiCl{\cdot}THF)_2$]. The GJF input files and the figures of the optimized structures were created with the program GaussView version 5.0.9.[11] For the ground state structures, the vibrational frequency analysis showed no imaginary frequency in the harmonical approximation. The relative energies (ΔG) of the computed structures are given based on the sum of electronic and thermal free energies (Gibbs energies) at 298.15 K in kJ mol^{-1}. The Hartree units were converted as follows: 1 Hartree = 2625.4995 kJ mol^{-1}.[12] The total electronic energies (SCF), the sum of electronic and zero-point energies (ZPE), the sum of electronic and thermal free energies (Gibbs energies) at 298.15 K, ^{7}Li GIAO magnetic shieldings together with the derived ^{7}Li NMR chemical shifts, and the Cartesian coordinates of the optimized structures can be found in Tables S3.4–S3.11. The ^{7}Li NMR chemical shift calculations were performed with the software package Gaussian 09 (Revision E.01) on the M062X/6-311+G(2d,p) level of theory[9] applying the Gauge-Independent Atomic orbital (GIAO)[13] method on the M062X/6-31+G(d)-optimized structures. The ^{7}Li NMR chemical shifts of **D**-Cy, **E**-Cy, **F**-Cy, **G**-Cy, and **H**-Cy were calculated relative to that of $(LiCl{\cdot}THF)_2$ (δ = 0.5 ppm, measured in THF)[14]. The existence of the dimeric structure [$(LiCl{\cdot}THF)_2$] of LiCl in THF solution is very well supported by work from Stalke[15] and Reich[16].

Table S3.4. Total electronic energies (SCF), sum of electronic and zero-point energies (ZPE), and sum of electronic and thermal free energies (Gibbs energies) at 298.15 K of the optimized structures.

Optimized structure	Method/Basis	SCF [Hartree]	ZPE [Hartree]	Gibbs energies [Hartree]
D-Cy	M062X/6-31+G(d) (PCM, solvent: dichloromethane)	–3253.25704881	–3252.665282	–3252.736368
E-Cy	M062X/6-31+G(d) (PCM, solvent: dichloromethane)	–3253.25843306	–3252.664853	–3252.732020
F-Cy	M062X/6-31+G(d) (PCM, solvent: dichloromethane)	–3253.25677601	–3252.663693	–3252.732728
G-Cy	M062X/6-31+G(d) (PCM, solvent: dichloromethane)	–3253.25499484	–3252.662789	–3252.733531
H-Cy	M062X/6-31+G(d) (PCM, solvent: dichloromethane)	–3253.25306666	–3252.660900	–3252.731598
$(LiCl{\cdot}THF)_2$	M062X/6-31+G(d) (PCM, solvent: tetrahydrofuran)	–1865.12249575	–1864.635955	–1864.702577

Table S3.5. Calculated ^{7}Li NMR chemical shifts of the optimized structures relative to $(LiCl\cdot THF)_2$ (δ = 0.5 ppm, measured in THF).

Optimized structure	Method/Basis	^{7}Li GIAO magnetic shieldings [ppm]	^{7}Li NMR chemical shift [ppm]
D-Cy	M062X/6-311+G(2d,p) (GIAO)	90.7801	0.3
E-Cy	M062X/6-311+G(2d,p) (GIAO)	90.5556	0.5
F-Cy	M062X/6-311+G(2d,p) (GIAO)	90.8234	0.3
G-Cy	M062X/6-311+G(2d,p) (GIAO)	90.8782	0.2
H-Cy	M062X/6-311+G(2d,p) (GIAO)	90.5105	0.6
$(LiCl\cdot THF)_2$ (Reference)	M062X/6-311+G(2d,p) (GIAO)	90.4436, 90.7595	

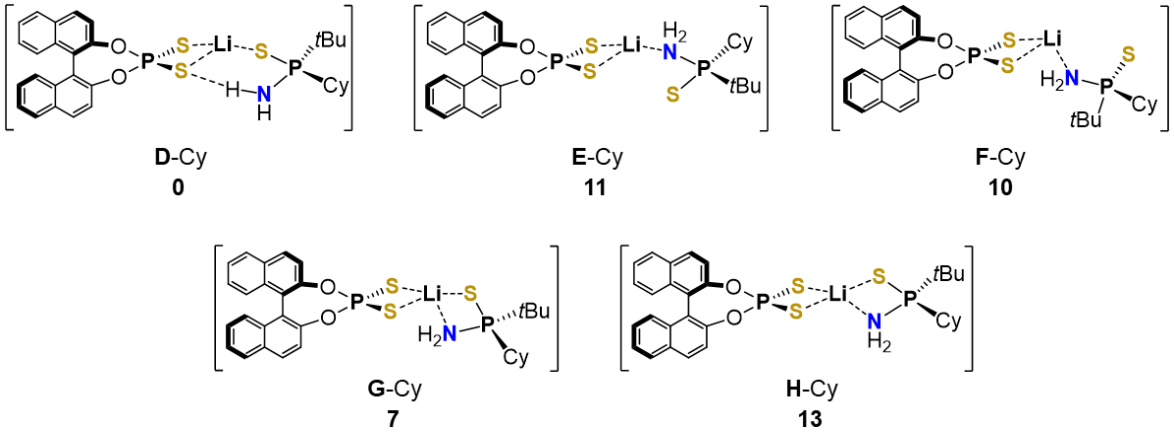

Figure S3.88. Relative energies [kJ mol^{-1}] of different coordination modes of [(*R*)-BINOL-PSSLi·(R_P)-**13**] structures in dichloromethane solution [M062X/6-31+G(d)] (PCM, solvent: dichloromethane). In **E**-Cy, the amino and not the sulfide functionality like in **D**-Cy coordinates to the lithium center; this eliminates the possibility of an additional N–H···S hydrogen bond. Structure **F**-Cy shows an alternative S_2N coordination mode of the lithium center. In **G**-Cy, the lithium cation can be considered tetra-coordinate, with the NH_2 function capping the trigonal S_3Li plane. Structure **H**-Cy features a nearly tetrahedrally coordinated lithium center.

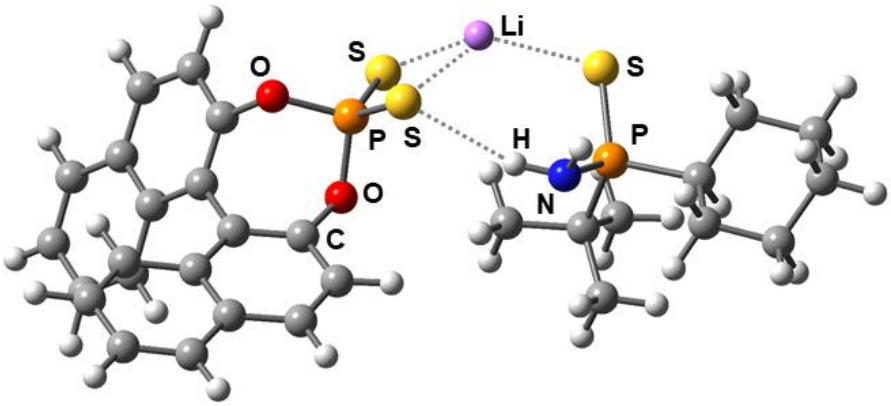

Figure S3.89. Optimized structure **D**-Cy [M062X/6-31+G(d)] (PCM, solvent: dichloromethane).

Table S3.6. Cartesian coordinates of the optimized structure **D**-Cy [M062X/6-31+G(d)] (PCM, solvent: dichloromethane).

Atomic symbol	x	y	z
C	–3.885688	–0.473452	–0.195404
C	–3.216477	0.849501	–0.098786

C	–1.867344	0.900449	0.184801
C	–3.356343	–1.431611	–1.034389
C	–3.950842	–2.697902	–1.226655
C	–5.092689	–3.010809	–0.538013
C	–5.651471	–2.093805	0.393958
C	–5.037031	–0.822053	0.586610
C	–6.800077	–2.436515	1.158278
C	–7.305760	–1.571601	2.096550
C	–6.673200	–0.323327	2.316943
C	–5.570733	0.042091	1.582946
C	–3.903092	2.086315	–0.341086
C	–3.203414	3.316923	–0.172877
C	–1.828295	3.300200	0.186698
C	–1.162309	2.113788	0.341538
C	–5.254332	2.134168	–0.784387
C	–5.881386	3.335826	–1.009501
C	–5.195874	4.558066	–0.801953
C	–3.884826	4.544175	–0.396874
H	–3.487416	–3.391233	–1.921032
H	–5.571642	–3.976141	–0.678788
H	–7.263063	–3.406308	0.992724
H	–8.180036	–1.844814	2.679547
H	–7.060596	0.348886	3.076896
H	–5.090989	0.997761	1.769884
H	–1.306590	4.244992	0.314428
H	–0.106145	2.077121	0.587569
H	–5.789079	1.205601	–0.958167
H	–6.910995	3.349174	–1.354788
H	–5.705695	5.500688	–0.976813
H	–3.339771	5.474012	–0.253088
O	–2.209590	–1.141013	–1.759042
O	–1.163501	–0.280815	0.370010
P	–0.766663	–1.168538	–0.961871
S	0.524928	–0.225865	–2.133009
S	–0.284220	–2.975581	–0.328131
S	4.186244	–2.150953	–0.644434
P	4.315422	–0.299763	0.123184
C	3.478682	–0.175135	1.775869
C	3.969748	–1.312804	2.679052

H	5.055162	–1.285944	2.829281
H	3.495800	–1.207392	3.661570
H	3.702491	–2.290511	2.269064
C	1.966711	–0.306013	1.556152
H	1.704028	–1.246548	1.060023
H	1.460908	–0.287975	2.528843
H	1.567330	0.523348	0.963448
C	3.788634	1.181210	2.424423
H	3.486693	2.014327	1.782889
H	3.225213	1.251068	3.362191
H	4.850544	1.289701	2.670915
N	3.579612	0.923853	–0.781986
H	4.066044	1.121853	–1.655766
H	2.606708	0.700988	–1.011154
C	6.076402	0.241110	0.328483
C	7.063197	–0.554147	–0.539803
C	6.276470	1.753208	0.112276
H	6.300320	0.010507	1.381911
C	8.504344	–0.148752	–0.217327
H	6.851467	–0.359259	–1.601001
H	6.927915	–1.627417	–0.381852
C	7.717239	2.148110	0.452470
H	6.083432	1.996029	–0.941423
H	5.569877	2.340061	0.704693
C	8.721617	1.355621	–0.385391
H	9.192769	–0.710211	–0.858931
H	8.731282	–0.434881	0.819861
H	7.847276	3.224188	0.291385
H	7.899740	1.960092	1.520401
H	9.746695	1.625800	–0.107855
H	8.595912	1.622958	–1.444561
Li	1.886030	–2.418990	–1.624769

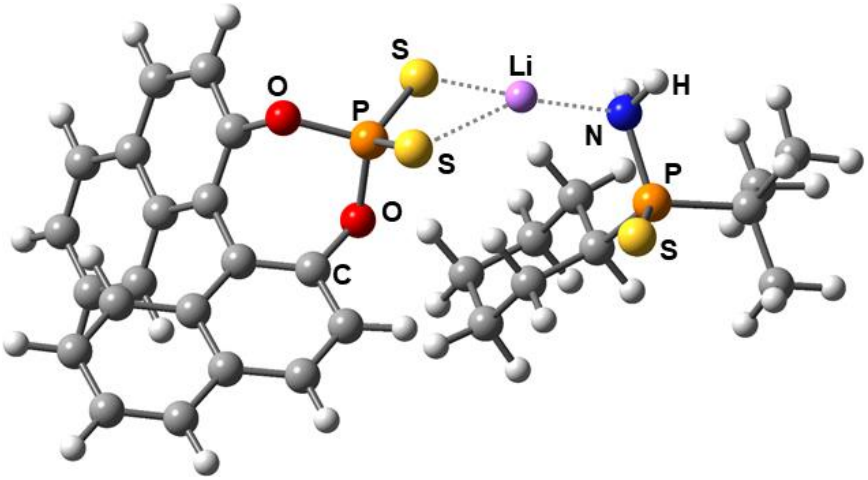

Figure S3.90. Optimized structure **E**-Cy [M062X/6-31+G(d)] (PCM, solvent: dichloromethane).

Table S3.7. Cartesian coordinates of the optimized structure **E**-Cy [M062X/6-31+G(d)] (PCM, solvent: dichloromethane).

Atomic symbol	x	y	z
C	–3.31807900	–0.58439700	–0.42465100
C	–2.87521200	0.78380300	–0.04899500
C	–1.52692100	1.02313600	0.11258200
C	–2.75023700	–1.20159300	–1.52142500
C	–3.14314200	–2.48272500	–1.96764100
C	–4.11544200	–3.16253700	–1.28328800
C	–4.69396600	–2.61062400	–0.10814500
C	–4.27807500	–1.32444100	0.34353400
C	–5.66237100	–3.33439500	0.63973900
C	–6.17771700	–2.82484300	1.80535800
C	–5.73182900	–1.56699400	2.28059700
C	–4.80933200	–0.83715100	1.57081300
C	–3.77952600	1.88717300	0.10689100
C	–3.26871000	3.15281600	0.51932500
C	–1.87099900	3.31606100	0.72514100
C	–1.00721800	2.27706600	0.50317700
C	–5.17025100	1.77968500	–0.17322000
C	–6.00784500	2.85730800	–0.01396600
C	–5.50443700	4.10293100	0.43506700
C	–4.16297300	4.24438800	0.68957000
H	–2.66630700	–2.89389200	–2.85159600
H	–4.44081400	–4.14330600	–1.62002200
H	–5.97949300	–4.30770000	0.27322400
H	–6.91436800	–3.38675600	2.37165800
H	–6.11951400	–1.17841100	3.21774100
H	–4.47060800	0.12049200	1.95335600

H	–1.49474000	4.28721000	1.03574300
H	0.06811800	2.38613300	0.61161700
H	–5.56881200	0.83450800	–0.52858700
H	–7.06519700	2.75537900	–0.24037100
H	–6.17925500	4.94409200	0.56233700
H	–3.75871800	5.19976800	1.01544100
O	–1.78958100	–0.53457800	–2.26570500
O	–0.63001600	–0.01278900	–0.09350200
P	–0.26271700	–0.38805400	–1.65902700
S	0.58651700	1.12583500	–2.60156600
S	0.73081800	–2.09635400	–1.60854600
P	4.80368800	0.27018000	–0.05261900
Li	2.62333900	–0.40876000	–2.31725700
N	4.45590000	–0.86498600	–1.30879400
H	4.51088700	–1.84321500	–1.01811700
H	5.10462300	–0.73604400	–2.08796400
S	4.51767000	2.08826900	–0.77143100
C	6.56022900	–0.00562900	0.50867400
C	6.72492500	–1.38136400	1.16800200
H	7.78311100	–1.51973800	1.41866600
H	6.15326600	–1.46473100	2.09797600
H	6.43945400	–2.20302700	0.50153200
C	7.48303300	0.09151900	–0.71337400
H	8.52301500	0.02940900	–0.37316600
H	7.32137200	–0.73250400	–1.41724000
H	7.35432700	1.04128600	–1.24174000
C	6.92677600	1.09371200	1.51541500
H	6.26703900	1.09248900	2.39013800
H	7.94878300	0.91727100	1.87048200
H	6.88585200	2.08395800	1.05395200
C	3.67464500	–0.24755300	1.31734600
C	2.37579800	0.57423700	1.32257100
C	3.34768300	–1.75349900	1.30120700
H	4.23419800	–0.01558900	2.23705500
C	1.48322500	0.18352700	2.50341000
H	1.83598400	0.39098300	0.38383100
H	2.60813900	1.64338100	1.35245500
C	2.48570800	–2.12544800	2.51186000
H	2.77601100	–1.98240100	0.39250200

H	4.25484100	–2.36606000	1.29178600
C	1.18872800	–1.31623700	2.52028200
H	0.54632300	0.75079300	2.45117300
H	1.98071000	0.47249200	3.44120400
H	2.26838200	–3.19918000	2.48379700
H	3.05152500	–1.93528600	3.43561400
H	0.58457200	–1.57470900	3.39755900
H	0.59931500	–1.57045900	1.62916500

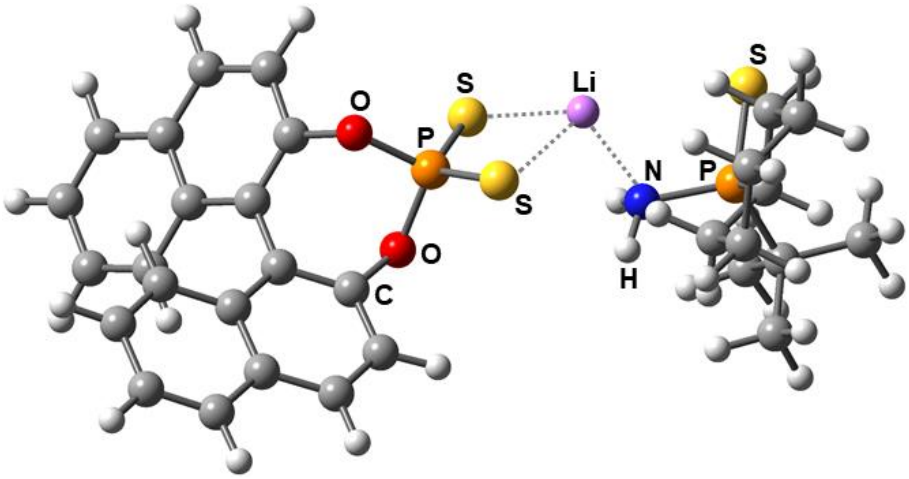

Figure S3.91. Optimized structure **F**-Cy [M062X/6-31+G(d)] (PCM, solvent: dichloromethane).

Table S3.8. Cartesian coordinates of the optimized structure **F**-Cy [M062X/6-31+G(d)] (PCM, solvent: dichloromethane).

Atomic symbol	x	y	z
C	–3.81316000	–0.59348800	–0.32647900
C	–3.46072100	0.71518300	0.28407300
C	–2.19157800	0.89965500	0.79288000
C	–2.99837900	–1.11228400	–1.31165500
C	–3.28138300	–2.31848500	–1.98857700
C	–4.40106000	–3.02892500	–1.64750500
C	–5.24657800	–2.58522300	–0.59448400
C	–4.94495700	–1.37196300	0.09007600
C	–6.37682100	–3.34952800	–0.19592500
C	–7.16247300	–2.94964300	0.85610000
C	–6.84003300	–1.76652600	1.56530000
C	–5.76296500	–0.99864500	1.19300100
C	–4.36652400	1.82828800	0.31369200
C	–3.96761100	3.03671400	0.95642300
C	–2.66601600	3.13727700	1.51913100
C	–1.78231300	2.09580600	1.42191100
C	–5.64299900	1.78910700	–0.31385800

C	–6.48606300	2.87318900	–0.26887200
C	–6.10334300	4.05824600	0.40624500
C	–4.86820400	4.13554400	0.99985300
H	–2.60245400	–2.65023200	–2.76745800
H	–4.64337200	–3.95414100	–2.16363600
H	–6.59983000	–4.26614700	–0.73645200
H	–8.02128500	–3.54261200	1.15574700
H	–7.44659200	–1.46713700	2.41496300
H	–5.52280400	–0.09995700	1.75256300
H	–2.37342600	4.06258500	2.00857900
H	–0.77283800	2.15737000	1.81560300
H	–5.94721100	0.89320400	–0.84583900
H	–7.45295200	2.82308000	–0.76110300
H	–6.78187600	4.90527500	0.43951800
H	–4.55189700	5.04566700	1.50390300
O	–1.86598800	–0.41249100	–1.70028400
O	–1.27446600	–0.13904500	0.73484700
P	–0.54781200	–0.46130200	–0.71136100
S	0.64969800	0.99681200	–1.30500100
S	0.22600000	–2.27396900	–0.55886100
Li	2.30063900	–0.96776500	–1.30007700
S	5.33800700	–2.52077800	–0.46304000
N	3.22157400	–0.69137200	0.58117400
H	2.86825700	0.15939700	1.02256900
H	2.80637500	–1.49725900	1.05250500
P	4.93149700	–0.82955900	0.47883900
C	5.64974700	–0.76451600	2.19393200
C	4.99440000	–1.86571500	3.03750500
H	5.11438200	–2.85174700	2.57836200
H	5.47581700	–1.88695000	4.02198700
H	3.92732600	–1.67597400	3.19817800
C	7.16042000	–1.01655300	2.09694500
H	7.66449600	–0.27742200	1.46416500
H	7.59528300	–0.94662600	3.10065200
H	7.36974800	–2.01220200	1.69656300
C	5.39000800	0.60023400	2.84634000
H	5.77200100	0.56993900	3.87326000
H	5.90590300	1.41546400	2.32859900
H	4.32176100	0.83723000	2.90522000

C	5.42888200	0.72463400	–0.39678200
C	5.68076700	0.49069800	–1.89441100
C	4.42382400	1.87493200	–0.19494600
H	6.38617800	1.01108400	0.06518000
C	6.16280400	1.77686000	–2.57097500
H	4.74902500	0.15055500	–2.36956400
H	6.41202200	–0.31095100	–2.03148700
C	4.92908900	3.15614500	–0.86478900
H	3.46251900	1.59676600	–0.64805400
H	4.23768400	2.06533600	0.86765900
C	5.18316700	2.93087000	–2.35542900
H	6.30983500	1.59184100	–3.64088300
H	7.14405700	2.05146100	–2.15770100
H	4.19450600	3.95521300	–0.71618000
H	5.85969700	3.47905600	–0.37657600
H	5.56633500	3.84689300	–2.81867600
H	4.22989700	2.69567900	–2.85069800

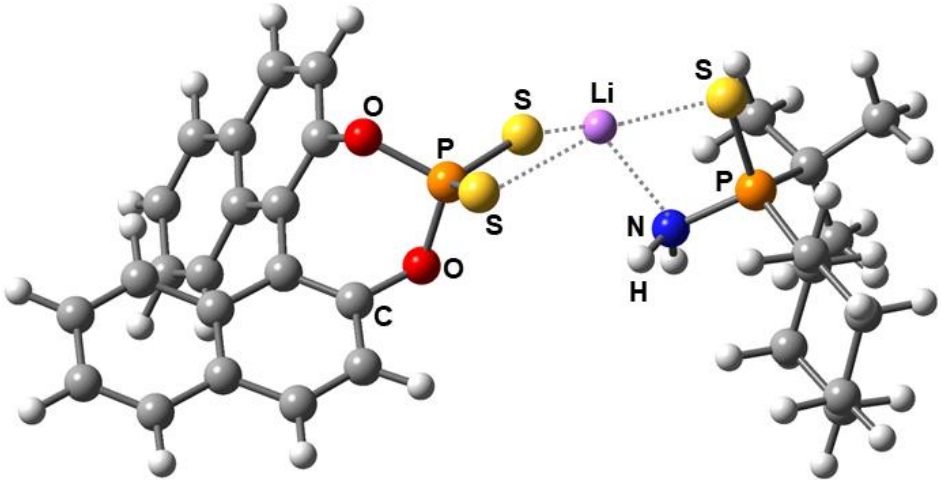

Figure S3.92. Optimized structure **G**-Cy [M062X/6-31+G(d)] (PCM, solvent: dichloromethane).

Table S3.9. Cartesian coordinates of the optimized structure **G**-Cy [M062X/6-31+G(d)] (PCM, solvent: dichloromethane).

Atomic symbol	x	y	z
C	–3.59442700	0.86395500	0.07749300
C	–3.91723800	–0.56750100	–0.15598100
C	–3.12989800	–1.29896800	–1.02026600
C	–2.31479400	1.21144800	0.45784200
C	–1.93373400	2.54101800	0.74264700
C	–2.85909700	3.54321600	0.61938400
C	–4.17732700	3.26081300	0.16853200
C	–4.54790800	1.91646000	–0.12771400

C	–5.12569300	4.30366400	–0.01749300
C	–6.38088300	4.03576000	–0.50352800
C	–6.73754200	2.70599700	–0.83714700
C	–5.84782500	1.67528200	–0.65449400
C	–4.98845300	–1.24345600	0.51796100
C	–5.26868800	–2.60298900	0.19395400
C	–4.46101400	–3.27874400	–0.76109000
C	–3.39425300	–2.64797200	–1.34429200
C	–5.76164400	–0.61813400	1.53534400
C	–6.77667300	–1.29526500	2.16698100
C	–7.07900100	–2.63410100	1.81597800
C	–6.33614500	–3.27145300	0.85362900
H	–0.91304900	2.73397900	1.05713800
H	–2.58932100	4.57171800	0.84448600
H	–4.83079800	5.32208000	0.22375800
H	–7.09747800	4.83880500	–0.64687100
H	–7.72213200	2.50138700	–1.24756500
H	–6.13229700	0.66331300	–0.92526200
H	–4.68719200	–4.31389300	–1.00313500
H	–2.74107700	–3.15046700	–2.05051300
H	–5.53526800	0.40439100	1.82123900
H	–7.34857000	–0.80180500	2.94737000
H	–7.88828100	–3.15492300	2.31875300
H	–6.54428600	–4.30512500	0.58785500
O	–1.35911400	0.21986600	0.61824600
O	–2.04629900	–0.68791700	–1.63367500
P	–0.68514500	–0.45136400	–0.73099900
S	0.14445800	–2.15127900	–0.15672100
S	0.44579400	0.82530200	–1.73215800
Li	2.11552100	–1.09155100	–1.35776700
P	4.77945000	–0.61565700	–0.20558000
S	4.69635400	–0.90789400	–2.17062400
N	3.18983800	–0.20881100	0.27893600
C	5.97650500	0.69098100	0.33918300
C	6.43984400	1.60046800	–0.80785500
C	5.42486900	1.53698400	1.50134400
H	6.85417400	0.13300100	0.70016600
C	7.50262900	2.58304700	–0.30664800
H	5.57713200	2.15612000	–1.20219000

H	6.83330300	0.99920700	–1.63265700
C	6.49714300	2.50880200	2.00449000
H	4.56146500	2.11546600	1.14503600
H	5.07111600	0.90825700	2.32516500
C	6.99455900	3.41177600	0.87452800
H	7.81140200	3.23761000	–1.12917700
H	8.39338700	2.01749000	0.00251100
H	6.08895800	3.10912100	2.82514800
H	7.33978700	1.93434500	2.41523600
H	7.78518900	4.07636400	1.24042700
H	6.16794900	4.05350500	0.53763000
C	5.14672500	–2.15496600	0.76813700
C	4.01038000	–3.16511000	0.55477500
H	3.87088700	–3.39029000	–0.50768900
H	4.27212000	–4.09772100	1.06707300
H	3.05801100	–2.81270700	0.96498500
C	5.28862800	–1.83856200	2.26457500
H	5.47763700	–2.77780300	2.79663500
H	6.13024900	–1.16966200	2.47129100
H	4.38038100	–1.40279800	2.69523000
C	6.46253800	–2.74187600	0.23782700
H	7.30222300	–2.04592400	0.34273500
H	6.70213700	–3.64024100	0.81738200
H	6.37673000	–3.02393100	–0.81533600
H	2.92274900	0.75188600	0.05692700
H	2.95088700	–0.39619500	1.25254900

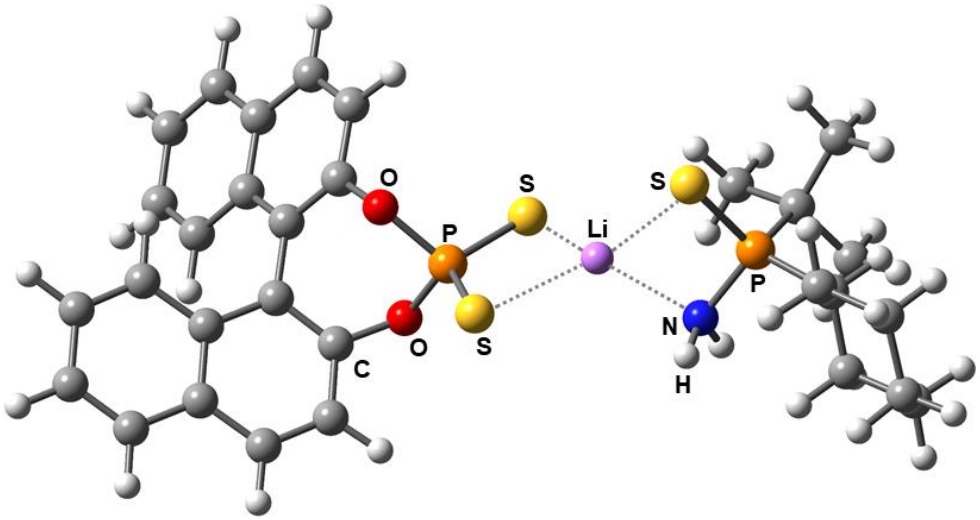

Figure S3.93. Optimized structure **H**-Cy [M062X/6-31+G(d)] (PCM, solvent: dichloromethane).

Table S3.10. Cartesian coordinates of the optimized structure **H**-Cy [M062X/6-31+G(d)] (PCM, solvent: dichloromethane).

Atomic symbol	x	y	z
C	4.07713700	–0.58645100	0.21632900
C	4.04583100	0.83075600	–0.23100300
C	2.94974600	1.28743600	–0.93389500
C	3.00853100	–1.08606100	0.93177100
C	2.96709600	–2.40513700	1.43359300
C	4.01920200	–3.24626800	1.18862400
C	5.12240100	–2.81536400	0.40212500
C	5.14903400	–1.48443800	–0.10862300
C	6.18910400	–3.70317800	0.09448100
C	7.22845500	–3.30468400	–0.70829200
C	7.23722800	–1.99593400	–1.24949200
C	6.22715800	–1.11090200	–0.95908700
C	5.08503000	1.77109300	0.08044100
C	5.00113000	3.09870000	–0.43290400
C	3.87292900	3.48462300	–1.20714400
C	2.85137000	2.60287500	–1.43725900
C	6.18661000	1.44241500	0.91955900
C	7.16436300	2.36716600	1.19637400
C	7.09888800	3.67295400	0.65153800
C	6.03586900	4.02815700	–0.14047800
H	2.09844300	–2.71592000	2.00505700
H	4.01240700	–4.26256000	1.57374900
H	6.15725400	–4.71138700	0.50053300
H	8.03650300	–3.99164600	–0.94134600
H	8.04779200	–1.69138900	–1.90510600
H	6.24241100	–0.11526000	–1.39139300
H	3.82182000	4.49874600	–1.59462500
H	1.96504600	2.87925500	–1.99901900
H	6.24631500	0.44955800	1.35435000
H	7.99346600	2.09637500	1.84351500
H	7.88230000	4.39159400	0.87289400
H	5.96010900	5.03289800	–0.54919300
O	1.93377300	–0.25834500	1.21784600
O	1.90326300	0.41978000	–1.20808700
P	0.85364500	0.05904400	0.01201900
S	–0.19889600	1.62418500	0.60970400
S	–0.15090100	–1.54410800	–0.56412400
Li	–2.06446500	–0.05025900	0.24118000

P	–5.00128500	–0.45631600	0.15567600
S	–4.14851700	–0.53427200	1.94589600
N	–3.89433700	0.38431600	–0.85604600
C	–6.65490100	0.38015400	0.10748400
C	–6.94172400	1.21806600	1.36164900
C	–6.84374300	1.23435400	–1.15917800
H	–7.38182100	–0.44623800	0.08128600
C	–8.36162200	1.79001600	1.30477700
H	–6.21325100	2.03902800	1.42424600
H	–6.81095700	0.61016500	2.26166200
C	–8.27105800	1.78894800	–1.21547900
H	–6.13810500	2.07624500	–1.13475800
H	–6.62672600	0.66294600	–2.06755500
C	–8.59259700	2.60979800	0.03448200
H	–8.54347700	2.40351100	2.19419400
H	–9.08197300	0.95994900	1.33852500
H	–8.38904900	2.39956400	–2.11755200
H	–8.97903400	0.95212600	–1.29951800
H	–9.62752300	2.96753300	–0.00343900
H	–7.94738200	3.49960400	0.05533100
C	–5.19353700	–2.11310500	–0.66352600
C	–3.80634000	–2.72428100	–0.90134600
H	–3.23595200	–2.79966600	0.03031200
H	–3.93454600	–3.73519700	–1.30396100
H	–3.21707200	–2.14959200	–1.62362100
C	–5.94390300	–1.98866100	–1.99795100
H	–6.01263900	–2.98622800	–2.44621900
H	–6.96520800	–1.61617100	–1.86919500
H	–5.42535400	–1.34750600	–2.71931100
C	–5.99065900	–3.01281800	0.29287700
H	–6.98756800	–2.61315600	0.50953300
H	–6.12192600	–3.99194900	–0.18076800
H	–5.46176600	–3.15597800	1.23931600
H	–3.91196300	1.39238000	–0.68984900
H	–4.00765900	0.23227200	–1.85909700

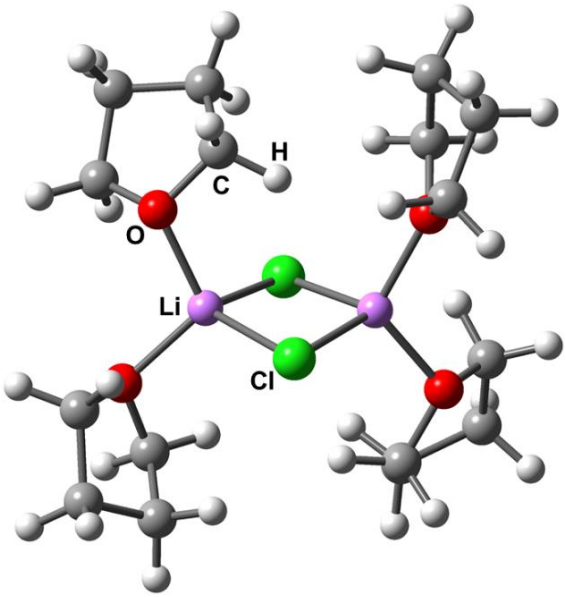

Figure S3.94. Optimized structure $(LiCl{\cdot}THF)_2$ [M062X/6-31+G(d)] (PCM, solvent: tetrahydrofuran).

Table S3.11. Cartesian coordinates of the optimized structure $(LiCl{\cdot}THF)_2$ [M062X/6-31+G(d)] (PCM, solvent: tetrahydrofuran).

Atomic symbol	x	y	z
Li	–1.083475	0.968382	0.034134
Cl	0.011688	–0.239488	–1.599762
Li	0.791049	–1.108620	0.436119
Cl	–0.555050	–0.092420	2.017615
O	–2.967956	1.039520	–0.236243
O	–0.375942	2.739447	–0.032013
O	2.611812	–0.589907	0.628959
O	0.535292	–3.000798	0.286954
C	3.443670	–0.078385	–0.430972
C	4.371672	0.930158	0.237450
C	4.535896	0.325515	1.635070
C	3.129105	–0.190154	1.914065
C	–0.855517	–3.366834	0.183790
C	–1.030293	–3.881735	–1.238257
C	0.324927	–4.550465	–1.489567
C	1.283727	–3.582785	–0.800847
C	–3.667195	1.660129	0.866269
C	–4.740216	0.659991	1.309300
C	–4.194594	–0.673426	0.785288
C	–3.560903	–0.239241	–0.527237
C	–0.759373	3.438394	–1.234555
C	0.494085	4.174968	–1.692031

C	1.597154	3.210915	–1.244604
C	1.061526	2.727453	0.098682
H	2.787922	0.346520	–1.195558
H	4.004936	–0.916128	–0.862262
H	5.315303	1.044896	–0.301113
H	3.889000	1.912532	0.303523
H	4.867866	1.047911	2.384312
H	5.250663	–0.504217	1.608869
H	3.094049	–1.057898	2.577034
H	2.478386	0.594742	2.318242
H	–1.452078	–2.479908	0.418359
H	–1.063242	–4.145368	0.927807
H	–1.876009	–4.567492	–1.332066
H	–1.169883	–3.039167	–1.923860
H	0.556954	–4.674361	–2.549927
H	0.360619	–5.533757	–1.007783
H	2.171968	–4.062630	–0.382315
H	1.588107	–2.773836	–1.476314
H	–4.081360	2.611342	0.520635
H	–2.932954	1.851728	1.655827
H	–4.884486	0.670217	2.391995
H	–5.698596	0.888690	0.831496
H	–4.969893	–1.431294	0.648278
H	–3.423708	–1.062537	1.458967
H	–2.763502	–0.892395	–0.893581
H	–4.313608	–0.111170	–1.315729
H	–1.598217	4.093667	–0.987989
H	–1.081794	2.698837	–1.978173
H	0.493131	4.361600	–2.768433
H	0.588000	5.133899	–1.170728
H	2.577814	3.685584	–1.156488
H	1.667334	2.369522	–1.942789
H	1.367585	1.707452	0.355599
H	1.336445	3.403084	0.917581

3.9. Supplementary References

[1] B.-Q. Gong, W.-Y. Chen, B.-F. Hu, *Phosphorus, Sulfur Silicon Relat. Elem.* **1991**, *57*, 87–94.
[2] S. Schweizer, J.-M. Becht, C. Le Drian, *Org. Lett.* **2007**, *9*, 3777–3780.
[3] H. Zhang, P. Ruiz-Castillo, S. L. Buchwald, *Org. Lett.* **2018**, *20*, 1580–1583.
[4] O. I. Kolodiazhnyi, E. V. Gryshkun, N. V. Andrushko, M. Freytag, P. G. Jones, R. Schmutzler, *Tetrahedron: Asymmetry* **2003**, *14*, 181–183.
[5] Rigaku Oxford Diffraction, CrysAlisPro Software System, **2020**.
[6] O. V. Dolomanov, L. J. Bourhis, R. J. Gildea, J. A. K. Howard, H. Puschmann, *J. Appl. Crystallogr.* **2009**, *42*, 339–341.
[7] G. M. Sheldrick, *Acta Crystallogr*. **2015**, *A71*, 3–8.
[8] G. M. Sheldrick, *Acta Crystallogr.* **2015**, *C71*, 3–8.
[9] M. J. Frisch, G. W. Trucks, H. B. Schlegel, G. E. Scuseria, M. A. Robb, J. R. Cheeseman, G. Scalmani, V. Barone, B. Mennucci, G. A. Petersson, H. Nakatsuji, M. Caricato, X. Li, H. P. Hratchian, A. F. Izmaylov, J. Bloino, G. Zheng, J. L. Sonnenberg, M. Hada, M. Ehara, K. Toyota, R. Fukuda, J. Hasegawa, M. Ishida, T. Nakajima, Y. Honda, O. Kitao, H. Nakai, T. Vreven, J. A. Montgomery Jr., J. E. Peralta, F. Ogliaro, M. Bearpark, J. J. Heyd, E. Brothers, K. N. Kudin, V. N. Staroverov, T. Keith, R. Kobayashi, J. Normand, K. Raghavachari, A. Rendell, J. C. Burant, S. S. Iyengar, J. Tomasi, M. Cossi, N. Rega, J. M. Millam, M. Klene, J. E. Knox, J. B. Cross, V. Bakken, C. Adamo, J. Jaramillo, R. Gomperts, R. E. Stratmann, O. Yazyev, A. J. Austin, R. Cammi, C. Pomelli, J. W. Ochterski, R. L. Martin, K. Morokuma, V. G. Zakrzewski, G. A. Voth, P. Salvador, J. J. Dannenberg, S. Dapprich, A. D. Daniels, O. Farkas, J. B. Foresman, J. V. Ortiz, J. Cioslowski, D. J. Fox, Gaussian 09. Revision E.01; Gaussian, Inc.: Wallingford, CT, USA, **2013**.
[10] J. Tomasi, B. Mennucci, R. Cammi, *Chem. Rev.* **2005**, *105*, 2999–3093.
[11] R. D. Dennington, II; T. A. Keith, J. M. Millam, *GaussView 5.0*; Gaussian, Inc.: Wallingford, CT, USA, **2008**.
[12] J. B. Foresman, A. Frisch, *Exploring Chemistry with Electronic Structure Methods*, 2nd Ed.; Gaussian, Inc.: Pittsburgh, PA, USA, **1996**.
[13] K. Wolinski, J. F. Hinton, P. Pulay, *J. Am. Chem. Soc.* **1990**, *112*, 8251–8260.
[14] N. A. Espinosa-Jalapa, N. Berg, M. Seidl, I. G. Shenderovich, R. M. Gschwind, J. O. Bauer, *Chem. Commun.* **2020**, *56*, 13335–13338.
[15] R. Neufeld, T. L. Teuteberg, R. Herbst-Irmer, R. A. Mata, D. Stalke, *J. Am. Chem. Soc.* **2016**, *138*, 4796–4806.
[16] H. J. Reich, J. P. Borst, R. R. Dykstra, D. P. Green, *J. Am. Chem. Soc.* **1993**, *115*, 8728–8741.

4. Hydrogen Bonding Patterns of Protonated Aminophosphine Chalcogenides in Solid-State and in Solution

Preface

The following chapter and supporting information are based on a manuscript in preparation on a model study about hydrogen bonding modes of protonated, bifunctional aminophosphine oxides, sulfides and selenides in the presence of a strongly or weakly coordinating anion. Special focus is put on the investigation of aminophosphine sulfide aggregates in CD_2Cl_2 solution.

Authors

Tanja Huber, Nicolò Fontana, Alexander Falk, Simon H. F. Schreiner, Wagner Silva, Johannes Gramüller, Ruth M. Gschwind, Gabriel Mayer, Patrick Nürnberger, Dominik Horinek, Michael Seidl, Jonathan O. Bauer.

Author contribution

All syntheses and characterisations reported in this work were performed by T. Huber, except for the initial preparation of compounds **1**, **(1·HCl)$_4$**, **(1–SH)$^+$ WCA$^-$**, which were synthesized for the first time by Dr. N. Fontana, compound **4**, which was synthesized and characterized for the first time by S. H. F. Schreiner and compound **(6–SH)$^+$ WCA$^-$**, which was synthesized and characterized by A. Falk. DOSY NMR spectroscopy was performed by Dr. J. Gramüller and Dr. W. Silva (Gschwind group). IR spectroscopy in solution was performed by G. Mayer (Nürnberger/Horinek group). Single crystal X-ray diffraction and structure refinements for compounds **(4·HCl)$_4$**, **(4–SeH)$^+$ WCA$^-$** and **5·HCl** were performed by T. Huber, for compounds **1**, **(1·HCl)$_4$**, **(1–SH)$^+$ WCA$^-$** and **[(*R*$_P$)-2·HCl]$_4$** by Dr. M. Seidl, for compound **4** by S. H. F. Schreiner and for compound **(6–SH)$^+$ WCA$^-$** by A. Falk. Quantum chemical calculations were performed by PD Dr. J. O. Bauer. The manuscript and the supporting information were drafted by T. Huber and revised by PD Dr. J. O. Bauer.

Acknowledgements

This work was financed by the Deutsche Forschungsgemeinschaft (DFG, German Research Foundation) through the Research Training Group “Ion Pair Effects in Molecular Reactivity” (RTG 2620, Project 426795949). Further support was provided jointly by the Elite Network of Bavaria (ENB), the Bavarian State Ministry of Science and the Arts (StMWK), and the University of Regensburg (N-LW-NW-2016-366).

4.1. Abstract

Cube-like structures held together solely by non-covalent interactions have long attracted the attention. Reaction of di-*tert*-butylaminophosphine sulfide **1**, *P*-stereogenic (*tert*-butyl)cyclohexyl-aminophosphine sulfides (R_P)-**2**/*rac*-**2** and di-*tert*-butylaminophosphine selenide **4** with hydrogen chloride led to well-defined supramolecular structures in the crystalline state consisting of a cubic hydrogen-bonded ammonium chloride core. The assembly behavior of these supermolecules was examined in dichloromethane at different concentrations and temperatures by means of classical analytical methods. Diffusion-ordered (DOSY), ^{1}H, ^{2}H, ^{15}N{^{1}H}, ^{15}N, ^{31}P{^{1}H}, ^{77}Se{^{1}H} NMR and infrared spectroscopy were applied. The measurements showed that, depending on the conditions, a switch from the tetrameric, possibly cube-like P–NH_3···Cl association to the monomeric species occurs. Possibilities to protonate the less basic chalcogenide entity were the use of a weakly coordinating anion or the replacement of the heavier chalcogen homologues by oxygen. Computational studies supported our findings on the protonation behavior of sulfide-substituted cations.

4.2. Introduction

Hydrogen-bond-based aggregation plays a crucial and indispensable role in modern organocatalysis.[1] Non-covalent interactions often have a significant impact on catalytic processes and should not be neglected when considering mechanistic studies.[2] The behavior of the aggregation is often dependent on external factors, such as solvents, temperature and concentration.[3] Perhaps the best examples of hydrogen bonding catalysts can be found in the human body. Enzymes, which catalyze important biochemical reactions, form the basis for biomimetic images of potent organocatalysts.[1c,4] Since hydrogen-bonded functional species often do not necessarily contain metal centers, they represent an environmentally friendly alternative to classic transition-metal catalysts.[1b,5] Well-known analytical methods suitable to detect hydrogen bonding[2c,6] and other non-covalent interactions[6b,6e,7] are NMR spectroscopy[2c,6a,6c,6d,6f,6g] and, in the case of supramolecular aggregation, diffusion NMR spectroscopy.[6b,6c,6e,6f,6g,7]

While the definition of self-assembled aggregates was limited to host-guest chemistry a few decades ago, structural motifs with hydrogen bonding have become a valuable representative of this broad field.[8] Well-defined structural patterns form the basis for the self-organization of the molecules of life[9] and for mineralization processes in our nature.[10] The exploration of novel supramolecular assemblies and the targeted design of metal-containing clusters for use as functional materials with diverse applications is a cutting edge research with a high level of interdisciplinary.[11] Knowledge about non-covalent interactions in clearly defined supramolecular units is a key to understanding the molecular mechanisms of their formation and the origins of complex matter.[12]

For a clearer comprehension, G. R. Desiraju introduced the modern concept of crystal engineering and defined supramolecular synthons as secondary building units, that are connected by

intermolecular interactions such as hydrogen bonds or coordination bonds.[12b,12d,13] The spatial layout of such aggregated synthons is often accompanied by the formation of stacked or ladder-shaped structures.[14] An astonishing pattern in crystal structures is the three-dimensional cube. Firstly found in 1985,[15] more and more cubic aggregates were reported in the early 2000s.[16–21] Protonated primary amines have always played an important role in cubic structure formation, as they can form a three-dimensional network by incorporation of all three hydrogen atoms, provided appropriate hydrogen bonding acceptor atoms are present. Halides,[15,17] sulfonates,[18] silanethiolates,[19] phosphonates,[20] and carboxylates[21] have been found to be suitable counteranions. However, the cubic, supramolecular entities known from the literature are often limited in their expandability and only little is known about the solution structures of fundamental inorganic functional patterns regarding their involvement in different hydrogen-bonding motifs. At the same time, it is known that many compounds exhibit different aggregation behavior in solution than they do in the solid state.[22] By studying defined molecular model systems, which focus on a few basic structural patterns, the complexity of questions on the nature of matter can often be simplified. This can help to gain in-depth information about fundamental formation principles, hydrogen-bonding motifs and structure-interaction relationships.[23]

4.3. Results and Discussion

Herein, we present a simple bifunctional molecular model system that contains both an amino (NH_2) group and a phosphorus chalcogenide [P^+–Ch^- (Ch = O, S, Se)] moiety within the same molecule. Both functional units show an affinity to protons and are in principle capable of forming hydrogen bonds. These aminophosphine chalcogenides thus combine an interesting structural motif, which will be studied in terms of their hydrogen bonding modes and supramolecular arrangements. An achiral, a racemic and an enantiomerically pure phosphorus-stereogenic model system will be studied for aminophosphine sulfides. As they were found to exhibit virtually identical aggregation properties according to NMR measurements, the achiral probe was studied in more detail and compared with the selenide and the oxide analogue. The investigations address the question of how the two competing acceptor atoms (N or Ch) are involved in hydrogen bonding both in the solid state and in solution, and under what conditions one of the two bonding modes is favored.

4.3.1. Protonation of Aminophosphine Chalcogenides in the Presence of a Strongly Coordinating Anion

Di-*tert*-butyl-substituted aminophosphine chalcogenides (compounds **1**, **4** and **5**)[24] were used as achiral starting materials and modified by exchange through a cyclohexyl moiety for the *P*-stereogenic enantiomerically pure [(R_P)-**2**][25] and racemic (*rac*-**2**)[25] samples. All precursors were subjected to a protonation with an excess of hydrogen chloride in diethyl ether at room temperature (Scheme 4.1).

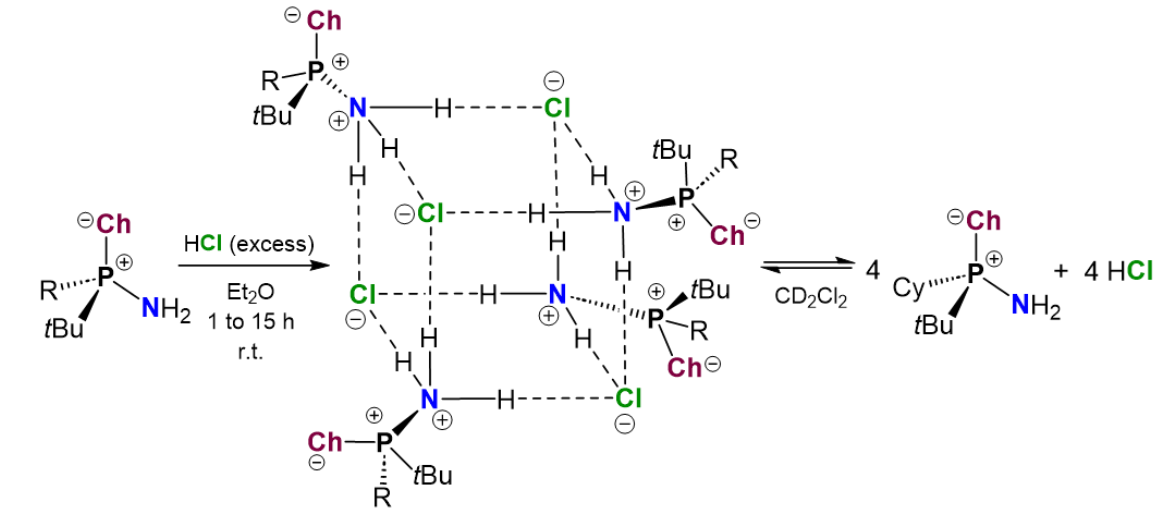

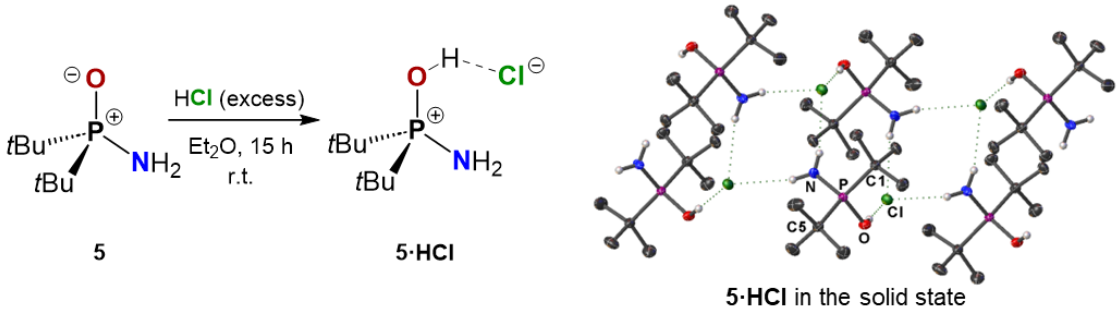

Scheme 4.1. Synthesis of the protonated products **(1·HCl)$_4$**, **[(*R*$_P$)-2·HCl]$_4$**, **(*rac*-2·HCl)$_4$**, **(4·HCl)$_4$** and **5·HCl** and grown crystal structure of **5·HCl** (displacement ellipsoids set at the 50% probability level). The phosphorus atom in ***rac*-2** must be seen without stereoinformation. The structure of **(*rac*-2·HCl)$_4$** is derived from NMR data only, not from XRD data.

The products **(1·HCl)$_4$**, **[(*R*$_P$)-2·HCl]$_4$**, **(*rac*-2·HCl)$_4$**, **(4·HCl)$_4$** and **5·HCl** were obtained as colorless solids in yields between 40% and 89%. Crystals suitable for single crystal X-ray analysis were obtained for compounds **(1·HCl)$_4$**, **[(*R*$_P$)-2·HCl]$_4$**, **(4·HCl)$_4$** and **5·HCl** from Et2O at −35 °C, from Et$_2$O by slow evaporation of the solvent, from DCM by slowly evaporating the solvent or from a DCM solution by layering with *n*-pentane, respectively. The crystal structures of **(1·HCl)$_4$**, **[(*R*$_P$)-2·HCl]$_4$** (Figure 4.1) and **(4·HCl)$_4$** consist of a tetrameric, hydrogen-bonded synthon with a cubic core whose corners are alternately occupied by ammonium and chloride ions. The three hydrogen atoms of each NH_3 unit point along the edges of the cube towards a chloride acceptor. The H···Cl distances range from 2.24 Å to 2.33 Å, which is in correlation with hydrogen bonds of chloride acceptors known from the literature.[12a] It is thus proven, that the precursors **1**, (*R*$_P$)-**2** and **4** are protonated at the amino moiety, while the P^+–Ch^- functional units remain unprotonated in the solid state. In contrast to that, precursor **5**, which has oxygen as a harder Lewis basic moiety,[26] is protonated at the P^+–Ch^- unit. The product **5·HCl** is therefore unable to form a cubic structure in the solid state, but still forms a two-dimensional network constructed by hydrogen bonds between anionic chloride acceptors and both OH and NH_2 groups (Scheme 4.1, bottom right).

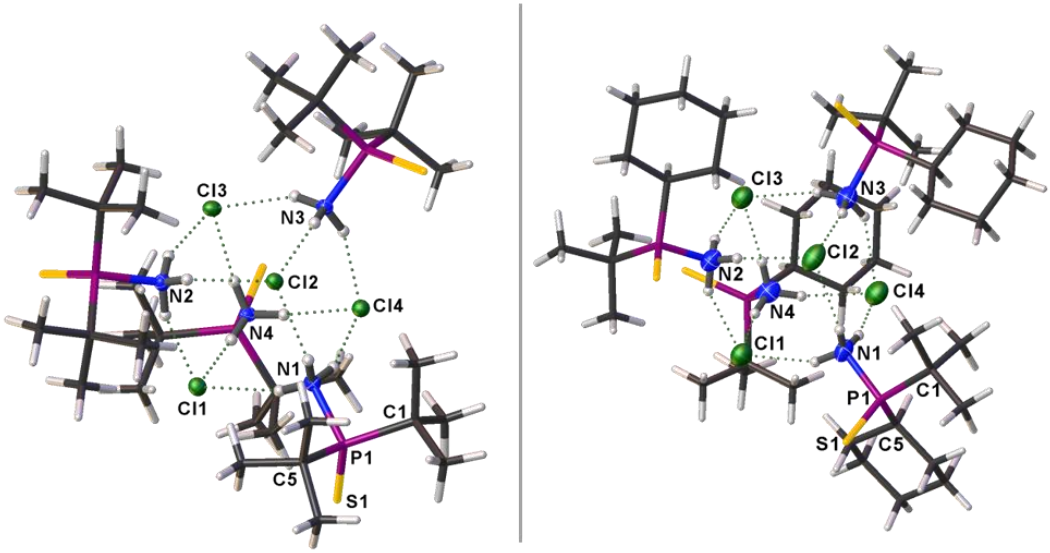

Figure 4.1. Molecular structures of **(1·HCl)$_4$** (left) and **[(*R*$_P$)-2·HCl]$_4$** (right) in the crystalline state (displacement ellipsoids set at the 50% probability level).

4.3.2. ^{1}H DOSY Experiments of (1·HCl)$_4$, [(*R*$_P$)-2·HCl]$_4$ and (4·HCl)$_4$

In order to get insight into the cubic structures in solution, we performed ^{1}H DOSY measurements of the isolated supermolecules **(1·HCl)$_4$**, **[(*R*$_P$)-2·HCl]$_4$** and **(4·HCl)$_4$** in deuterated dichloromethane (DCM) at room temperature with different concentrations. The hydrodynamic volume of sample **(1·HCl)$_4$** has increased continuously from 435 Å^3 (30 mM) via 670 Å^3 (50 mM) to 905 Å^3 (100 mM). For the monomeric reference compound **1** a volume of 248 Å^3 was obtained. Any potential hydrogen bonding interaction between the amino and the sulfur moiety in **1**, that could distort the reference result, was excluded by preparing and measuring compound **3** (di-*tert*-butyl-chlorophosphine sulfide, see experimental section), which had a volume of 228 Å^3. Thus, the hydrodynamic volume of **(1·HCl)$_4$** in 100 mM DCM-d$_2$ solution is approximately four times greater than of the non-protonated compounds **1** and **3**. This indicates a tetrameric arrangement also in DCM solution and corresponds well with a cubic synthon composition as found in the crystal structure (Figure 4.1, left). The same conclusion can be drawn for **[(*R*$_P$)-2·HCl]$_4$**, which has a hydrodynamic volume of 713 Å^3 in 50 mM solution, compared to 280 Å^3 for monomeric (*R*$_P$)-**2**. For **(4·HCl)$_4$** a concentration of 500 mM is required to obtain a hydrodynamic volume of 855 Å^3, which is approximately four times the value of the monomeric reference compound **4** (235 Å^3) and again corresponds to the crystal structure of the cubic synthon.

Surprisingly, reducing the concentration of compounds **(1·HCl)$_4$**, **[(*R*$_P$)-2·HCl]$_4$** and **(4·HCl)$_4$** to 5 mM resulted in the formation of a solution species that is clearly indicative of a monomer according to the measured hydrodynamic volumes of 265 Å^3, 273 Å^3 and 251 Å^3, respectively. It can be assumed that in this entropically favored dissociation process now also the sulfide function becomes involved in hydrogen bonding before hydrogen chloride is released from the monomeric species. Quantum chemical calculations on the M062X/6-311+G(d,p) level of theory using the polarizable continuum model (PCM) (solvent: DCM) showed that the energy of the transition state

between $H_2N\cdots H$ and $S\cdots H$ hydrogen bonding is only 13 kJ·mol^{-1} in the presence of a coordinating anion such as chloride. Without a coordinating anion the energy of the transition state would be 100 kJ·mol^{-1} higher. Furthermore, $S\cdots H$ bonding is even thermodynamically favored over the $H_2N\cdots H$ bonding, but in practice the cubic arrangement seems to lead to an energy gain. As explained in this chapter, this can only be achieved in a sufficiently concentrated solution. As the concentration is reduced, the equilibrium between tetramer and monomer (Scheme 4.1) is shifted towards the latter.

4.3.3. NMR Studies of (1·HCl)$_4$, [(*R*$_P$)-2·HCl]$_4$, (*rac*-2·HCl)$_4$, (4·HCl)$_4$ and 5·HCl

The results of ^{1}H and ^{31}P{^{1}H} NMR measurements in CD_2Cl_2 solution substantiate the DOSY experiments. A comparison of the values for the *tert*-butyl, amino/ammonium and phosphorus signals shows that these are broadened and shifted towards the lower field for the HCl adducts **(1·HCl)$_4$** (100 mM), **[(*R*$_P$)-2·HCl]$_4$** (100 mM), **(*rac*-2·HCl)$_4$** (100 mM) and **(4·HCl)$_4$** (500 mM) in contrast to the precursors **1**, (*R*$_P$)-**2**, *rac*-**2** and **4**. In addition, the integrals of the NH signals correspond well with the presence of an NH_3 moiety and the coupling constants of the *tert*-butyl signals are each increased by about 2 Hz. This indicates deshielding and hence confirms the presence of hydrogen bonding. The samples in low concentrations (5 mM or 10 mM) give ^{1}H and ^{31}P{^{1}H} NMR spectra, which are essentially identical to those of the corresponding starting materials. The low concentration structures can therefore be considered as monomers in the presence of solvated hydrogen chloride [**1 + HCl$_{solv}$**, (*R*$_P$)-**2 + HCl$_{solv}$**, *rac*-**2 + HCl$_{solv}$**, **4 + HCl$_{solv}$**] (Scheme 4.1, top right).

As expected from the crystal structure, the situation is different for compound **5·HCl**. No dependence on the concentration of the NMR samples was found and the formation of a cubic aggregation can be safely excluded. Considering the Lewis basic properties of oxygen in comparison to sulfur and selenium,[26] it is logical that the proton is attached to oxygen. However, an exchange between OH and NH_2 protons in solution is likely and gives an averaged signal in the ^{1}H NMR spectrum.

Compounds **(1·HCl)$_4$** and **(4·HCl)$_4$** were subjected to thorough dilution- and temperature-dependent ^{1}H and ^{31}P{^{1}H} NMR studies in CD_2Cl_2. **(1·HCl)$_4$** was measured in seven different concentrations at 298 K (Figure 4.2, left). In the ^{31}P{^{1}H} NMR spectra at 10 mM and 15 mM only one signal at around δ = 94.5 ppm, that can be assigned to the monomeric species **1 + HCl$_{solv}$**, was observed. Two signals were visible between 20 mM and 30 mM, indicating the coexistence of monomer and tetramer. The downfield shifted signal at around δ = 111.5 ppm, that can be assigned to the tetrameric aggregate, rose with increasing concentration. From 50 mM only the signal of the tetramer remained. The same tendency was observed with decreasing temperature for a 5 mM sample (Figure 4.2, right). Only the monomer was present at room temperature and coexisted with the tetramer at 283 K. At temperatures below 273 K only the tetrameric aggregate remained. ^{1}H NMR spectra confirmed these findings by changing from an NH_2 signal at around δ = 2.0 ppm to a

broad NH_3 signal at around δ = 9.5 ppm with increasing concentration or decreasing temperature (see experimental section).

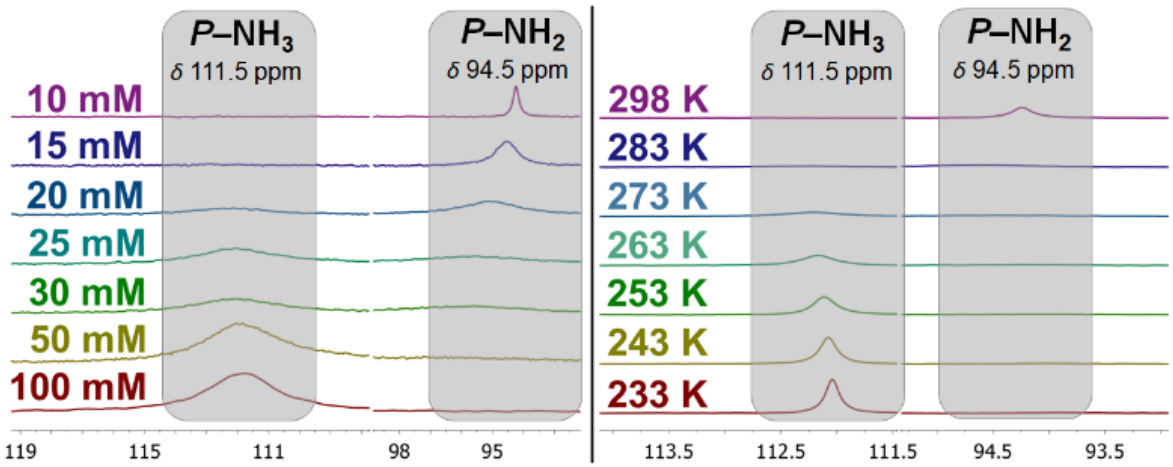

Figure 4.2. Results of variable concentration (left) and variable temperature (right) $^{31}P\{^1H\}$ NMR measurements of **(1·HCl)$_4$**.

(4·HCl)$_4$ was investigated in the same way as **(1·HCl)$_4$**, but with different concentrations (see experimental section). As explained for the DOSY experiments, a concentration five times higher than for the sulfur analogue was required to obtain a hydrodynamic volume corresponding to the tetrameric structure. Indeed, the $^{31}P\{^1H\}$ NMR spectrum of the 500 mM sample showed a single signal at around δ = 114.0 ppm, that can be assigned to the tetramer. Between 20 mM and 200 mM two signals were observed for coexisting monomer and tetramer, while at even lower concentrations only the monomer signal at around δ = 95.0 ppm is present. Variable temperature measurements were performed with a 10 mM sample. In contrast to the measurements with the sulfur analogue, the monomer signal did not disappear and coexisted with the tetramer up to the lowest possible measurement temperature (193 K).

^2H NMR spectra in a 9:1 mixture of CH_2Cl_2 and CD_2Cl_2 were measured after reaction of **1**, **4** and **5** with deuterium chloride instead of hydrogen chloride. It was found that the signals corresponding to NH_2D [100 mM **(1·DCl)$_4$** or 500 mM **(4·DCl)$_4$**], NH*D* [5 mM **(1·DCl)$_4$** or 10 mM **(4·DCl)$_4$**] and O*D* (**5·DCl**) are indeed approximately at the same chemical shift values in the ^2H NMR spectrum as the corresponding ^1H NMR chemical shifts of the non-deuterium labelled samples. This suggests a rapid exchange between the hydrogen and deuterium atoms of the nitrogen and chalcogen atoms. ^{15}N and $^{15}N\{^1H\}$ NMR measurements were recorded after labelling the precursor **1** with 98% ^{15}N enriched ammonia (see experimental section). The spectra should provide further information and confirmation of the previously predicted structures of **(1·HCl)$_4$** in high (100 mM) and low (5 mM) concentrated CD_2Cl_2 solution. The reference spectrum of **1** showed a ^{15}N chemical shift of δ = 29.1 ppm (td). Coupling of the nitrogen atom with the phosphorus atom ($^1J_{N–P}$ = 22 Hz) and with the NH_2 protons ($^1J_{N–H}$ = 76 Hz) was clearly observed. At a concentration of 5 mM, the chemical shift and the N–P coupling constant of the protonated species turned out to be the same as for **1**, which corroborates the presence of **1 + HCl$_{solv}$** in a low concentrated solution of compound **(1·HCl)$_4$**. The N–H coupling constant could not be observed, possibly due to the insufficient concentration.

Lowering the temperature was not an option regarding the results of the variable temperature experiments. A 100 mM concentrated solution of **(1·HCl)$_4$** showed a broad downfield shifted ^{15}N signal at δ = 60.1 ppm, which showed no couplings at all. Measuring the same sample at 193 K resulted in a slightly shifted signal at δ = 62.6 ppm (qd) due to the temperature change. It revealed the coupling constants of the nitrogen atom with the phosphorus atom ($^1J_{N–P}$ = 34 Hz) and with the NH_3^+ protons ($^1J_{N–H}$ = 68 Hz), which are also visible in the corresponding ^{1}H and ^{31}P{^{1}H} NMR spectra at 193 K.

Compound **(4·HCl)$_4$**, as the selenium-containing sample, was subjected to studies of the ^{77}Se NMR-active core. Precursor **4** showed a ^{77}Se chemical shift of δ = –351 ppm with a phosphorus-selenium coupling constant of 727 Hz. Very similar values were obtained for the protonated species at a concentration of 10 mM, again supporting the assumption of the presence of a monomeric species (**4 + HCl$_{solv}$**). A chemical shift of δ = –348 ppm for the 500 mM sample of compound **(4·HCl)$_4$** suggests, that the chalcogen atom is not much affected by the tetrameric aggregation. However, the coupling constant between the phosphorus and the selenium atom is increased by almost 100 Hz ($^1J_{P–Se}$ = 815 Hz) upon protonation of the nitrogen atom.

4.3.4. IR Spectroscopy Studies of (1·HCl)$_4$

Based on the results of the crystal structure and the NMR experiments of compound **(1·HCl)$_4$**, we expected to observe IR vibrations for a primary ammonium cation in the solid state and at concentrations in CD_2Cl_2 higher than 15 mM. In the transmission IR spectrum of the solid, the broad signal at 2713 cm^{-1} can be assigned to the NH_3^+ stretching vibration. While the transmission IR spectrum of a 5 mM CD_2Cl_2 solution appeared identical to the reference spectrum of compound **1**, the 50 mM CD_2Cl_2 solution unequivocally showed a broad NH_3^+ signal at 2750 cm^{-1}. The same observation was made for 10 mM and 500 mM CD_2Cl_2 solutions of **(4·HCl)$_4$**.

Screening of different concentrations of compound **(1·HCl)$_4$** revealed that the signal at 2750 cm^{-1} becomes larger with increasing concentration. At the same time, the two NH_2 bands at about 3400 cm^{-1} decrease. This can be clearly seen by stacking the difference absorption spectra [difference between **(1·HCl)$_4$** and **1**]. Figure 4.3 shows the difference absorption spectra normalized to the respective concentrations. Despite the normalization, the order of the concentrations remains the same, suggesting in fact an increasing formation of the tetrameric structure with increasing concentration.

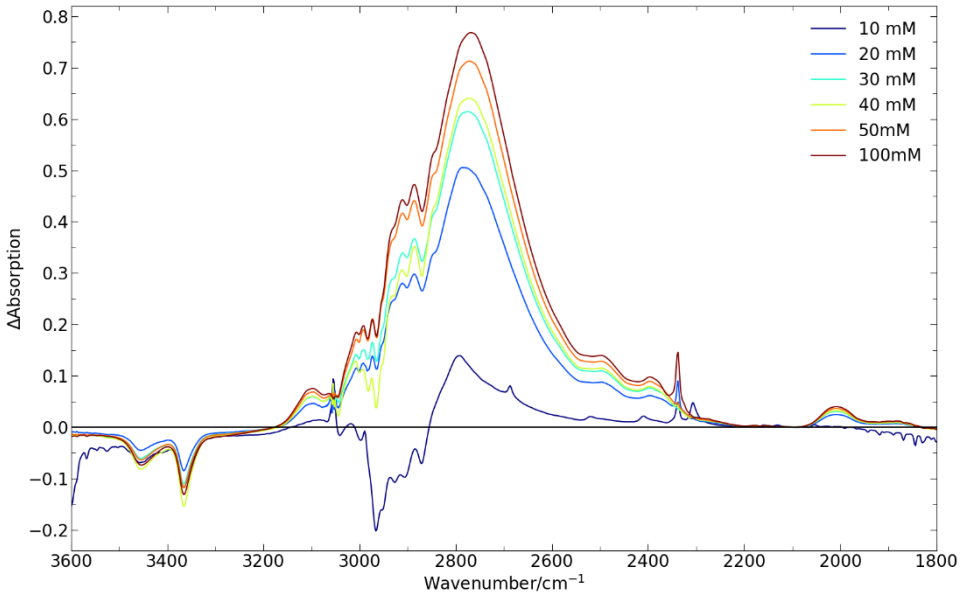

Figure 4.3. Cutout of the difference absorption spectra [**(1·HCl)$_4$** – **1**] of the IR spectroscopy measurements normalized to the concentration in CH_2Cl_2 with concentrations 10 mM to 100 mM showing the broad signal of the NH_3^+ moiety at 2750 cm^{-1} and the NH_2 signals in the range of 3400 cm^{-1}.

4.3.5. Protonation of Aminophosphine Chalcogenides in the Presence of a Weakly Coordinating Anion

The same achiral and chiral precursors as for the protonation reactions with hydrogen chloride [**1**, (R_P)-**2**, *rac*-**2**, **4** and **5**] were subjected to a protonation with Jutzi's acid {[H(OEt$_2$)$_2$][B(C$_6$F$_5$)$_4$]}[27] in DCM (Scheme 4.2). The reactions were performed at room temperature, except for the synthesis of **(4–SeH)$^+$ WCA$^-$**, which was carried out from –30 °C to –10 °C.

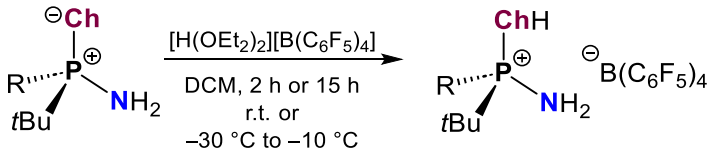

1:	R = *t*Bu, **Ch** = **S**	**(1–SH)$^+$ WCA$^-$**:	R = *t*Bu, **Ch** = **S**; 87%
(R_P)-**2**:	R = Cy, **Ch** = **S**	**[(R_P)-2–SH]$^+$ WCA$^-$**:	R = Cy, **Ch** = **S**; 82%
rac-**2**:	R = Cy, **Ch** = **S**	**(*rac*-2–SH)$^+$ WCA$^-$**:	R = Cy, **Ch** = **S**; 73%
4:	R = *t*Bu, **Ch** = **Se**	**(4–SeH)$^+$ WCA$^-$**:	R = *t*Bu, **Ch** = **Se**; 74%
5:	R = *t*Bu, **Ch** = **O**	**(5–OH)$^+$ WCA$^-$**:	R = *t*Bu, **Ch** = **O**; 85%

Scheme 4.2. Synthesis of the protonated products **(1–SH)$^+$ WCA$^-$**, **[(R_P)-2–SH]$^+$ WCA$^-$**, **(*rac*-2–SH)$^+$ WCA$^-$**, **(4–SeH)$^+$ WCA$^-$** and **(5–OH)$^+$ WCA$^-$**. The phosphorus atom in *rac*-**2** must be seen without stereoinformation.

The products **(1–SH)$^+$ WCA$^-$**, **[(R_P)-2–SH]$^+$ WCA$^-$**, **(*rac*-2–SH)$^+$ WCA$^-$** and **(5–OH)$^+$ WCA$^-$** were obtained as colorless solids, while **(4–SeH)$^+$ WCA$^-$** was a pale rose solid, due to a slight decomposition forming red selenium. The yields are approximately 80% for each of the products. Crystals suitable for single crystal X-ray analysis of compounds **(1–SH)$^+$ WCA$^-$** and **(4–SeH)$^+$ WCA$^-$** could be grown from a toluene or DCM solution, respectively, by layering with *n*-pentane. As

$[B(C_6F_5)_4]^-$ is a non-coordinating anion, no cube formation, as observed for the HCl adducts, is possible. The crystal structures of compounds **(1–SH)$^+$ WCA$^-$** and **(4–SeH)$^+$ WCA$^-$** showed, that the chalcogenide moiety, instead of the amino moiety, is protonated in the solid state (Figure 4.4).

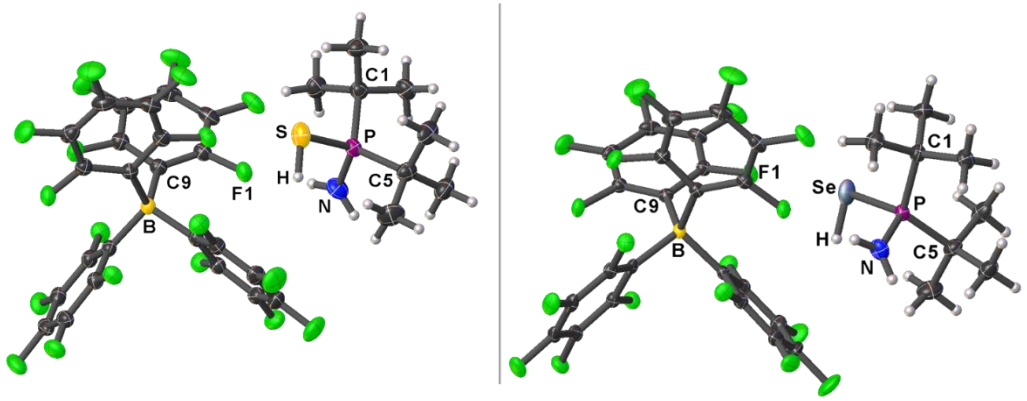

Figure 4.4. Molecular structures of **(1–SH)$^+$ WCA$^-$** (left) and **(4–SeH)$^+$ WCA$^-$** (right) in the crystalline state (displacement ellipsoids set at the 50% probability level).

4.3.6. ^{1}H and ^{11}B DOSY Experiments of (1–SH)$^+$ WCA$^-$

Indeed, the question is what the structure of the protonation products with a weakly coordinating anion looks like in solution. First, it should be noted that no concentration or temperature dependence, as observed for the HCl adducts, was found in CD_2Cl_2. Quantum chemical calculations on the M062X/6-311+G(d,p) level of theory using the polarizable continuum model (PCM) (solvent: DCM) showed that in the absence of a coordinating anion in CD_2Cl_2 solution the intrinsic proton affinity is higher for sulfur than for the amino group. In addition, ^{1}H and ^{11}B DOSY experiments of compound **(1–SH)$^+$ WCA$^-$** in CD_2Cl_2 and DMSO-d_6 revealed a solvent dependence of the hydrodynamic volumes. In DMSO-d_6, as a strongly coordinating solvent, the volume of the cation **(1–SH)$^+$** remained roughly the same (394 Å^3) as for the reference molecule **1** (324 Å^3), which suggests the presence of a monomeric cation. The corresponding monomeric volume of the anion $[B(C_6F_5)_4]^-$ was 583 Å^3 in DMSO-d_6. However, in CD_2Cl_2 the hydrodynamic volumes of both cation (579 Å^3) and anion (1052 Å^3) were approximately twice as high as it was expected for monomers. It is therefore assumed, that in CD_2Cl_2 solution units consisting of two cations and two anions are formed and that a rapid intermolecular exchange of the SH and NH_2 protons between two cations might take place.

4.3.7. NMR Studies of (1–SH)$^+$ WCA$^-$, [(*R*$_P$)-2–SH]$^+$ WCA$^-$, (*rac*-2–SH)$^+$ WCA$^-$, (4–SeH)$^+$ WCA$^-$ and (5–OH)$^+$ WCA$^-$

The fast exchange of SH and NH_2 protons is confirmed by the ^{1}H NMR spectra of compounds **(1–SH)$^+$ WCA$^-$**, **[(*R*$_P$)-2–SH]$^+$ WCA$^-$** and **(*rac*-2–SH)$^+$ WCA$^-$**, which all show an averaged signal at δ ≈ 2.95 ppm for these three protons. The same is true for compound **(4–SeH)$^+$ WCA$^-$** for the SeH and the NH_2 protons (δ = 2.48 ppm), while the OH and NH_2 protons in compound **(5–OH)$^+$ WCA$^-$**

have different shifts at δ = 3.55 ppm (NH_2) and at δ = 6.04 ppm (OH). As with the HCl adducts, the oxygenated compound is again the odd one out, which can be attributed to the higher Lewis basicity and proton affinity of oxygen.[26] A comparable exchange of the OH and the NH_2 protons can therefore be excluded.

For further confirmation of the presence of an SH or SeH moiety in CD_2Cl_2 solution, compound **(6–SH)$^+$ WCA$^-$** (see experimental section), which is intrinsically unable to intramolecularly exchange its SH proton, can be used. For **(6–SH)$^+$ WCA$^-$**, the SH signal is visible at δ = 2.42 ppm in the ^{1}H NMR spectrum, which roughly correlates with the ChH values for **(1–SH)$^+$ WCA$^-$**, **[**(R_P)-**2–SH]$^+$ WCA$^-$** (*rac*-**2–SH)$^+$ WCA$^-$** and **(4–SeH)$^+$ WCA$^-$**.

Furthermore, ^{2}H NMR spectra of the deuterated analogues **(1–SD)$^+$ WCA$^-$** and **(4–SeD)$^+$ WCA$^-$** in a 9:1 mixture of CH_2Cl_2 and CD_2Cl_2 were measured. The chemical shifts of the ^{2}H signals at δ ≈ 2.85 ppm are another indication for the S···H/D···N exchange.

The ^{31}P{^{1}H} NMR values of **(1–SH)$^+$ WCA$^-$**, **[**(R_P)-**2–SH]$^+$ WCA$^-$** (*rac*-**2–SH)$^+$ WCA$^-$** and **(4–SeH)$^+$ WCA$^-$** are slightly shifted towards lower field (Δδ ≈ 3.5–5.7 ppm) compared to the starting materials **1**, (R_P)-**2**, *rac*-**2** and **4**. In contrast to that, the different Ch–H bonding situation[26] of compound (**5–OH)$^+$ WCA$^-$** in solution leads to a much greater downfield shift of Δδ = 25 ppm compared to **5**.

^{15}N and ^{15}N{^{1}H} NMR measurements of compound **(1–SH)$^+$ WCA$^-$** were recorded after labelling the precursor **1** with 98% ^{15}N enriched ammonia (see experimental section). The spectra showed a doublet signal at 21.2 ppm ($^1J_{N–P}$ = 16 Hz), which is slightly highfield shifted compared to compound **1** (δ = 29.1 ppm). This is indicative of higher shielding of the nitrogen atom in compound **(1–SH)$^+$ WCA$^-$** and further supports the idea that the nitrogen atom is not protonated. The coupling between the nitrogen and the hydrogen atom could not be observed, possibly due to the fast SH/NH_2 proton exchange. Even lowering the temperature to 193 K did not make the coupling visible.

Compound **(4–SeH)$^+$ WCA$^-$** was used for ^{77}Se NMR measurement. Compared to precursor **4** (δ = –351 ppm, $^1J_{P–Se}$ = 727 Hz), a strong downfield shift to δ = –43 ppm and a significant decrease in the coupling constant ($^1J_{P–Se}$ = 406 Hz) was observed. The differences in the chemical shift and the phosphorus-selenium coupling constant compared to compound **4**, and also compound **(4·HCl)$_4$**, provide solid evidence for a change in the immediate vicinity of the selenium atom. In addition to protonation, as in the case described, similar differences have been observed for intramolecularly coordinated silylium centers by phosphine selenide functions.[28]

4.3.8. IR Spectroscopy Studies of (1–SH)$^+$ WCA$^-$

IR measurements of compound **(1–SH)$^+$ WCA$^-$** were carried out in solid state and in CH_2Cl_2 solution (Figure 4.5). Both transmission spectra show a characteristic, weak thiol signal at about 2560 cm^{-1}. The signals at about 3370 cm^{-1} and 3450 cm^{-1} can be attributed to amine vibrations. In the difference absorption spectrum [difference between **(1–SH)$^+$ WCA$^-$** and **1**] (Figure 4.6) the weak SH signal is clearly observable as well. The two NH_2 bands are actually present for both compounds **(1–SH)$^+$ WCA$^-$** and **1** (see experimental section), but in **(1–SH)$^+$ WCA$^-$** they are more pronounced,

although the compounds were measured in the same solvent and in the same concentration. The opposite applies to the signals at around 3000 cm^{-1}, which are most likely hydrocarbon vibrations.

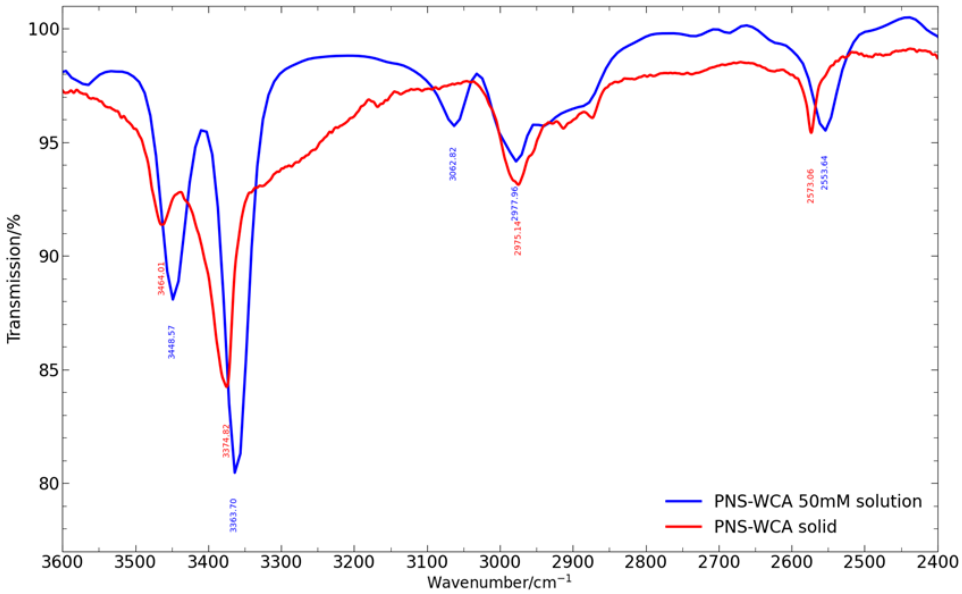

Figure 4.5. Cutout of the transmission spectra of **(1–SH)⁺ WCA⁻** in 50 mM DCM solution (blue line) and in the solid state (red line).

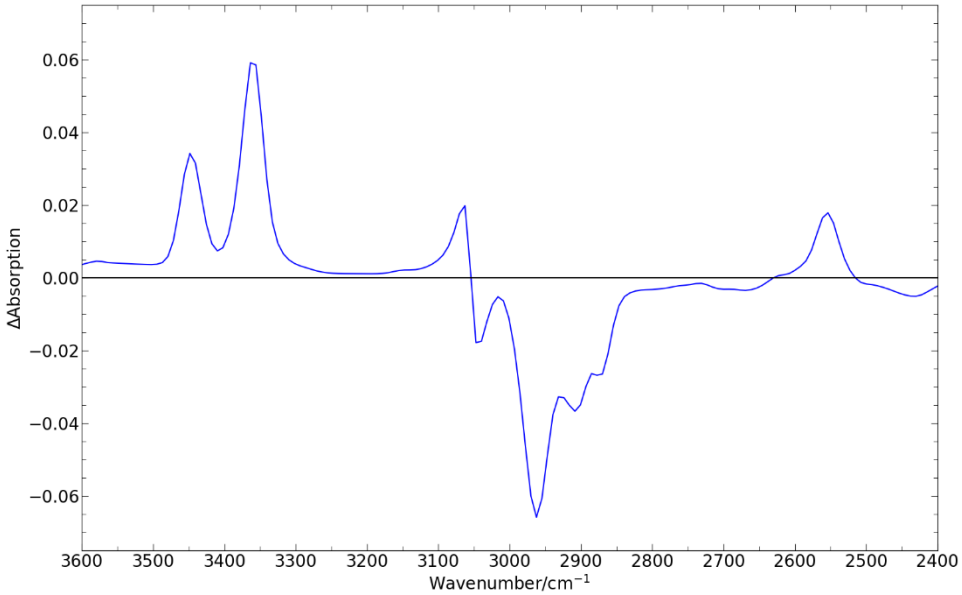

Figure 4.6. Cutout of the difference absorption spectrum [**(1–SH)⁺ WCA⁻** – **1**] in 50 mM DCM solution.

4.4. Conclusion

In conclusion, it has been demonstrated that the formation of hydrogen bonding after the protonation of model systems with NH_2 and P^+–Ch^- (Ch = O, S, Se) moiety is highly dependent on the counteranion, but also on external conditions such as solvent, concentration and temperature. Several bifunctional molecular model systems in combination with two different counterions were examined, one of which is generally able to coordinate (Cl^-), while the other one is a classic representative of weakly coordinating anions {WCA^-/$[B(C_6F_5)_4]^-$}. The bifunctional substrates were all protonated on the chalcogenide entity when using the WCA and no evidence of hydrogen bonding networks could be observed in the solid state and in solution. However, intermolecular exchange of the ChH and NH_2 protons might take place for sulfur- and selenium-substituted congeners in CD_2Cl_2 solution. In contrast to this, two different supramolecular aggregation modes were found for the chloride products. The oxygen analogue, which was protonated on the oxygen moiety, formed a two-dimensional, hydrogen-bonded network by interaction with the chloride anions in the solid state. Due to their lower basicity, it was not possible to protonate the sulfur or selenium entity under the same conditions. Instead, an ammonium cation was generated, which formed a cube-shaped synthon with the chloride anions in the solid state. We assume that the number of hydrogen bonding interactions leads to an energy gain compared to the protonation of the chalcogenide function. The tetrameric structure remained intact in sufficiently high concentrations in CD_2Cl_2 solution but disintegrated in too low concentrations. Furthermore, it was discovered that *P*-stereogenic enantiomerically pure aminophosphine sulfides exhibit comparable aggregation properties to an achiral sulfide. Our findings were supported by single crystal X-ray analysis, NMR spectroscopy, IR spectroscopy and computational studies. The results of this model study could provide insights into important structural patterns that have implications for a variety of topics and further investigations. Of particular importance appear the tailored formation of supramolecular synthons by gradual cluster expansion due to free sulfide or selenide coordination sites and the field of hydrogen-bonding/ion-pairing organocatalysis.

4.5. References

[1] a) L. J. Prins, D. N. Reinhoudt, P. Timmerman, *Angew. Chem. Int. Ed.* **2001**, *40*, 2382–2426; b) P. R. Schreiner, *Chem. Soc. Rev.* **2003**, *32*, 289–296; c) M. S. Taylor, E. N. Jacobsen, *Angew. Chem. Int. Ed.* **2006**, *45*, 1520–1543; *Angew. Chem.* **2006**, *118*, 1550–1573; d) A. G. Doyle, E. N. Jacobsen, *Chem. Rev.* **2007**, *107*, 5713–5743; e) D. Parmar, E. Sugiono, S. Raja, M. Rueping, *Chem. Rev.* **2014**, *114*, 9047–9153.

[2] a) P. H.-Y. Cheong, C. Y. Legault, J. M. Um, N. Çelebi-Ölçüm, K. N. Houk, *Chem. Rev.* **2011**, *111*, 5042–5137; b) U. Gellrich, W. Seiche, M. Keller, B. Breit, *Angew. Chem. Int. Ed.* **2012**, *51*, 11033–11038; *Angew. Chem.* **2012**, *124*, 11195–11200; c) J. Greindl, J. Hioe, N. Sorgenfrei, F. Morana, R. M. Gschwind, *J. Am. Chem. Soc.* **2016**, *138*, 15965–15971; d) D. D. Ford, D. Lehnherr, C. R. Kennedy, E. N. Jacobsen, *J. Am. Chem. Soc.* **2016**, *138*, 7860–7863; e) N. Lokesh, J. Hioe, J. Gramüller, R. M. Gschwind, *J. Am. Chem. Soc.* **2019**, *141*, 16398–16407; f) N. Berg, S. Bergwinkl, P. Nürnberger, D. Horinek, R. M. Gschwind, *J. Am. Chem. Soc.* **2021**, *143*, 724–735; g) I. Harden, F. Neese, G. Bistoni, *Chem. Sci.* **2023**, *14*, 10580–10590.

[3] a) D. Jansen, J. Gramüller, F. Niemeyer, T. Schaller, M. C. Letzel, S. Grimme, H. Zhu, R. M. Gschwind, J. Niemeyer, *Chem. Sci.* **2020**, *11*, 4381–4390; b) M. Franta, J. Gramüller, P. Dullinger, S. Kaltenberger, D. Horinek, R. M. Gschwind, *Angew. Chem. Int. Ed.* **2023**, *62*, e202301183; *Angew. Chem.* **2023**, *135*, e202301183.

[4] A. Berkessel, H. Gröger, *Asymmetric Organocatalysis: From Biomimetic Concepts to Applications in Asymmetric Synthesis*, Wiley-VCH Verlag GmbH & Co. KGaA, Weinheim, **2005**.

[5] L. Chen, B. Zhang, L. Chen, H. Liu, Y. Hu, S. Qiao, *Mater. Adv.* **2022**, *3*, 3680–3708.

[6] a) R. M. Gschwind, M. Armbrüster, I. Z. Zubrzycki, *J. Am. Chem. Soc.* **2004**, *126*, 10228–10229; b) Y. Cohen, L. Avram, L. Frish, *Angew. Chem. Int. Ed.* **2005**, *44*, 520–554; *Angew. Chem.* **2005**, *117*, 524–560; c) M. Fleischmann, D. Drettwan, E. Sugiono, M. Rueping, R. M. Gschwind, *Angew. Chem. Int. Ed.* **2011**, *50*, 6364–6369; *Angew. Chem.* **2011**, *123*, 6488–6493; d) N. Sorgenfrei, J. Hioe, J. Greindl, K. Rothermel, F. Morana, N. Lokesh, R. M. Gschwind, *J. Am. Chem. Soc.* **2016**, *138*, 16345–16354; e) Y. Cohen, S. Slovak, *Org. Chem. Front.* **2019**, *6*, 1705–1718; f) D. Jansen, J. Gramüller, F. Niemeyer, T. Schaller, M. C. Letzel, S. Grimme, H. Zhu, R. M. Gschwind, J. Niemeyer, *Chem. Sci.* **2020**, *11*, 4381–4390; g) J. Gramüller, P. Dullinger, D. Horinek, R. M. Gschwind, *Chem. Sci.* **2022**, *13*, 14366–14372.

[7] Y. Cohen, L. Avram, T. Evan-Salem, S. Slovak, N. Shemesh, L. Frish, *in Analytical Methods in Supramolecular Chemistry*, 2nd ed. (Ed.: C. A. Schalley), Wiley-VCH Verlag GmbH & Co. KGaA, Weinheim, **2012**, Ch. 6.

[8] R. P. Sijbesma, E. W. Meijer, *Curr. Opin. Colloid Interface Sci.* **1999**, *4*, 24–32.

[9] a) L. E. Orgel, *Nature* **1992**, *358*, 203–209; b) J. M. Lehn, *Science* **1993**, *260*, 1762–1763.

[10] a) T. W. Swaddle, J. Salerno, P. A. Tregloan, *Chem. Soc. Rev.* **1994**, *23*, 319–325; b) G. V. Gibbs, R. T. Downs, D. F. Cox, N. L. Ross, C. T. Prewitt, K. M. Rosso, T. Lippmann, A. Kirfel, *Z. Kristallogr.* **2008**, *223*, 1–40; c) G. V. Gibbs, A. F. Wallace, D. F. Cox, R. T. Downs, N. L. Ross, K. M. Rosso, *Am. Mineral.* **2009**, *94*, 1085–1102.

[11] a) J.-M. Lehn, *Supramolecular Chemistry: Concepts and Perspectives*, Wiley-VCH, Weinheim, **2006**; b) I. Beletskaya, V. S. Tyurin, A. Y. Tsivadze, R. Guilard, C. Stern, *Chem. Rev.* **2009**, *109*, 1659–1713; c) D. A. Uhlenheuer, K. Petkau, L. Brunsveld, *Chem. Soc. Rev.* **2010**, *39*, 2817–2826; d) T. Aida, E. W. Meijer, S. I. Stupp, *Science* **2012**, *335*, 813–817; e) M. J. Webber, E. A. Appel, E. W. Meijer, R. Langer, *Nature Mater.* **2016**, *15*, 13–26; f) Y. Tu, F. Peng, A. Adawy, Y. Men, L. K. E. A. Abdelmohsen, D. A. Wilson, *Chem. Rev.* **2016**, *116*, 2023–2078; g) C. Sutton, C. Risko, J.-L. Brédas, *Chem. Mater.* **2016**, *28*, 3–16; h) D. B. Amabilino, D. K. Smith, J. W. Steed, *Chem. Soc. Rev.* **2017**, *46*, 2404–2420; i) M. P. Hendricks, K. Sato, L. C. Palmer, S. I. Stupp, *Acc. Chem. Res.* **2017**, *50*, 2440–2448; j) A. V. Virovets, E. Peresypkina, M. Scheer, *Chem. Rev.* **2021**, *121*, 14485–14554; k) J. E. M. Lewis, *Chem. Commun.* **2022**, *58*, 13873–13886; l) A. J. McConnell, *Chem. Soc. Rev.* **2022**, *51*, 2957–2971; m) J. E. M. Lewis, *Trends Chem.* **2023**, *5*, 717–719; n) P. P. Mehta, V. Dhapte-Pawar (Eds.) *Crystal Engineering: A Versatile Platform for Pulmonary Drug Delivery*, Springer, Singapore, **2023**; o)

S.-Z. Zhao, H.-W. Zhou, C.-Y. Qin, H.-Z. Zhang, Y.-H. Li, M. Yamashita, S. Wang, *Chem. Eur. J.* **2023**, *29*, e202300554; p) R. Banerjee, D. Chakraborty, P. S. Mukherjee, *J. Am. Chem. Soc.* **2023**, *145*, 7692–7711; q) W. Drożdż, A. Ciesielski, A. R. Stefankiewicz, *Angew. Chem. Int. Ed.* **2023**, *62*, e202307552; *Angew. Chem.* **2023**, *135*, e202307552; r) J. Martí-Rujas, *Mater. Adv.* **2023**, *4*, 4333–4343.

[12] a) T. Steiner, *Angew. Chem. Int. Ed.* **2002**, *41*, 48–76; *Angew. Chem.* **2002**, *114*, 50–80; b) G. R. Desiraju, *Angew. Chem. Int. Ed.* **2007**, *46*, 8342–8356; *Angew. Chem.* **2007**, *119*, 8492–8508; c) R. J. Davey, S. L. M. Schroeder, J. H. ter Horst, *Angew. Chem. Int. Ed.* **2013**, *52*, 2166–2179; *Angew. Chem.* **2013**, *125*, 2220-2234; d) G. R. Desiraju, *J. Am. Chem. Soc.* **2013**, *135*, 9952–9967; e) J. S. Du, Y. Bae, J. J. de Yoreo, *Nat. Rev. Mater.* **2024**, accepted (DOI: 10.1038/s41578-023-00637-y).

[13] a) G. R. Desiraju, *Crystal Engineering: The design of Organic Solids*, Elsevier, Amsterdam, **1989**; b) G. R. Desiraju, *Angew. Chem. Int. Ed.* **1995**, *34*, 2311–2327; c) G. R. Desiraju, *J. Mol. Struct.* **2003**, *656*, 5–15; d) G. R. Desiraju, *J. Chem. Sci.* **2010**, *122*, 667–675.

[14] A. D. Bond, *Chem. Eur. J.* **2004**, *10*, 1885–1898.

[15] G. Knupp, A. W. Frahm, A. Kirfel, T. Fröhlich, G. Will, *Acta Crystallogr. C* **1985**, *41*, 468–470.

[16] a) T. Gröb, K. Harms, K. Dehnicke, *Z. Anorg. Allg. Chem.* **2000**, *626*, 1065–1072; b) T. Gröb, S. Chitsaz, K. Harms, K. Dehnicke, *Z. Anorg. Allg. Chem.* **2002**, *628*, 473–479; c) S. Courtenay, P. Wei, D. W. Stephan, *Can. J. Chem.* **2003**, *81*, 1471–1476; d) A. Pladzyk, Ł. Ponikiewski, Y. Lan, A. K. Powell, *Inorg. Chem. Commun.* **2012**, *20*, 66–69.

[17] a) J. Büchler, C. Maichle-Mössmer, K.-A. Kovar, *Z. Naturforsch. B* **2000**, *55*, 1124–1130; b) A. D. Bond, E. L. Doyle, *Chem. Commun.* **2003**, 2324–2325; c) A. D. Bond, *Cryst. Growth Des.* **2005**, *5*, 755–771; d) A. D. Bond, *Coord. Chem. Rev.* **2005**, *249*, 2035–2055; e) A. D. Bond, W. H. Jørgensen, J. M. Pløger, *Chem. Commun.* **2007**, 3273–3275.

[18] N. Tohnai, Y. Mizobe, M. Doi, S. Sukata, T. Hinoue, T. Yuge, I. Hisaki, Y. Matsukawa, M. Miyata, *Angew. Chem. Int. Ed.* **2007**, *46*, 2220–2223; *Angew. Chem.* **2007**, *119*, 2270–2273.

[19] B. Becker, K. Baranowska, J. Chojnacki, W. Wojnowski, *Chem. Commun.* **2004**, 620–621.

[20] T. Yuge, N. Kai, I. Hisaki, M. Miyata, N. Tohnai, *Chem. Lett.* **2007**, *36*, 1390–1391.

[21] a) K. Sada, T. Watanabe, J. Miyamoto, T. Fukuda, N. Tohnai, M. Miyata, T. Kitayama, K. Maehara, K. Ute, *Chem. Lett.* **2004**, *33*, 160–161; b) T. Yuge, N. Tohnai, T. Fukuda, I. Hisaki, M. Miyata, *Chem. Eur. J.* **2007**, *13*, 4163–4168; c) T. Yuge, I. Hisaki, M. Miyata, N. Tohnai, *CrystEngComm* **2008**, *10*, 263–266.

[22] a) V. H. Gessner, C. Däschlein, C. Strohmann, *Chem. Eur. J.* **2009**, *15*, 3320–3334; b) N. A. Espinosa-Jalapa, N. Berg, M. Seidl, I. G. Shenderovich, R. M. Gschwind, J. O. Bauer, *Chem. Commun.* **2020**, *56*, 13335–13338; c) Y. Cohen, S. Slovak, L. Avram, *Chem. Commun.* **2021**, *57*, 8856–8884; d) N. Geue, R. E. P. Winpenny, P. E. Barran, *Chem. Soc. Rev.* **2022**, *51*, 8–27.

[23] G. Ashkenasy, T. M. Hermans, S. Otto, A. F. Taylor, *Chem. Soc. Rev.* **2017**, *46*, 2543–2554.

[24] a) M. J. P. Harger, M. A. Stephen, *J. Chem. Soc., Perkin Trans.* **1980**, *0*, 705–711; b) M. Köster, A. Kreher, C. von Hänisch, *Dalton Trans.* **2018**, *47*, 7875–7878; c) T. C. Jankins, Z. Qin, K. M. Engle, *Tetrahedron* **2019**, *75*, 3272–3281.

[25] T. Huber, N. A. Espinosa-Jalapa, J. O. Bauer, *Chem. Eur. J.* **2022**, *28*, e202202608.

[26] R. G. Pearson, *J. Am. Chem. Soc.* **1963**, *85*, 3533–3539.

[27] P. Jutzi, C. Müller, A. Stammler, H.-G. Stammler, *Organometallics* **2000**, *19*, 1442–1444.

[28] A. Falk, J. O. Bauer, *Inorg. Chem.* **2022**, *61*, 15576–15588.

4.6. Syntheses and Characterizations

4.6.1. General Remarks

All experiments were performed in an inert atmosphere of purified nitrogen by using standard Schlenk techniques or an MBraun Unilab 1200/780 glovebox. Glassware was heated at 140 °C prior to use. Diethyl ether (Et_2O), dichloromethane (DCM), *n*-hexane, *n*-pentane, tetrahydrofuran (THF), and toluene were dried and degassed with an MBraun SP800 solvent purification system.

Di-*tert*-butylchlorophosphine (98%, abcr or 96%, Merck), ammonia (anhydrous, Staub & Co.), *s*ulfur (99%, Merck), ammonia (98% ^{15}N, Eurisotop), hydrogen chloride (2.0 M solution in diethyl ether, Merck) and deuterium chloride (2.0 M solution in diethyl ether, Merck) were used without further purification.

(R_P)-**2** and *rac*-**2** were synthesized following a procedure published by our group.[1] $[H(OEt_2)_2][B(C_6F_5)_4]$ and $[D(OEt_2)_2][B(C_6F_5)_4]$ were synthesized following a reported procedure.[2] $tBu_2(PO)NH_2$ (**5**) was synthesized following a reported procedure.[3a] **6** was prepared following a procedure published by our group.[5]

C_6D_6 (≥ 99.6%, Merck) was used for NMR spectroscopy as purchased. CD_2Cl_2 (> 99.8%, Fluorochem) was degassed and dried over molecular sieve (3 Å) prior to use. NMR spectra were either recorded using a Bruker Avance 400 (400.13 MHz) or a Bruker Avance III HD 400 (400.13 MHz) at 25 °C. Chemical shifts (δ) are reported in parts per million (ppm). ^1H, ^2H and $^{13}C\{^1H\}$ NMR spectra are referenced to tetramethylsilane ($SiMe_4$, δ = 0.0 ppm) as external standard, with the deuterium signal of the solvent serving as internal lock and the residual solvent signal as an additional reference. $^{31}P\{^1H\}$, $^{77}Se\{^1H\}$, $^{11}B\{^1H\}$, $^{19}F\{^1H\}$ and $^{29}Si\{^1H\}$ NMR spectra are referenced to H_3PO_4, $Se(CH_3)_2$, $BF_3{\cdot}OEt_2$, $CFCl_3$ and $SiMe_4$, respectively. For the assignment of the multiplicities, the following abbreviations are used: s = singlet, d = doublet, t = triplet, q = quartet, m = multiplet, br = broad signal.

Elemental analyses were performed on a Vario MICRO cube apparatus.

High-resolution mass spectrometry was carried out on a Jeol AccuTOF GCX and an Agilent Q-TOF 6540 UHD spectrometer.

Infrared spectroscopy for solids was carried out on a Thermo Scientific Nicolet™ iS™ 5 FT-IR-Spectrometer.

Infrared spectroscopy in solution was performed in CH_2Cl_2 on a Bruker Vertex 80 spectrometer with OPUS software. All measurements were performed at 25 °C. IR data was processed, evaluated, and plotted with Python 3 software. For the peak intensities, the following abbreviations are used: vw = very weak, w = weak, m = medium, s = strong, vs = very strong, br = broad.

4.6.2. Synthetic Procedures

4.6.2.1. Synthesis of *t*Bu$_2$(PS)NH$_2$ (1)

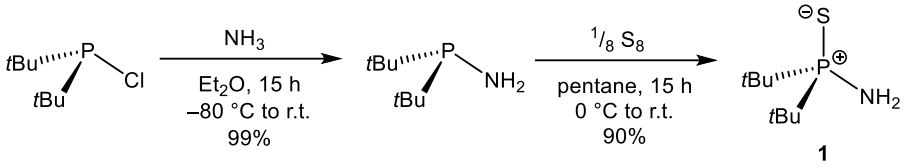

1

1 was synthesized in a modified literature procedure.[3]

Di-*tert*-butylchlorophosphine (15.4 g, 85.2 mmol) in diethyl ether (100 mL) was cooled to −50 °C and ammonia was passed through the solution for 45 min. The reaction mixture was allowed to slowly warm to room temperature and stirred for 15 h. The precipitated NH_4Cl was filtered off *via* cannula filtration and washed with diethyl ether. The solvent was removed *in vacuo* from the filtrate yielding amino-di-*tert*-butylphosphine as a colorless liquid (13.6 g, 84.3 mmol, 99%). The values of ^{1}H and $^{31}P\{^{1}H\}$ NMR are in accordance with the literature.

Amino-di-*tert*-butylphosphine (7.00 g, 43.4 mmol, 1.0 equiv.) was added dropwise to a suspension of sulfur (1.39 g, 43.4 mmol, 1.0 equiv.) in *n*-pentane (90 mL) at 0 °C. The reaction mixture was allowed to slowly warm to room temperature and stirred for 15 h yielding a colorless suspension. The liquid phase was removed by cannula filtration and the remaining solid was extracted with the minimum amount of diethyl ether. After removal of insoluble solids *via* cannula filtration, the solvent was removed *in vacuo* to obtain **1** as a colorless solid (7.58 g, 39.2 mmol, 90%). Crystals suitable for single crystal X-ray diffraction were obtained from *n*-pentane at −25 °C.

For the ^{15}N NMR measurements, the first reaction was proceeded using 98% ^{15}N labelled ammonia as reagent. In order not to waste the enriched ammonia, the gas was condensed into an empty Schlenk tube at −196 °C (gas flow at 3.9 bar for 30 sec). Di-*tert*-butylchlorophosphine (2.85 g, 15.77 mmol) in diethyl ether (10 mL) was precooled to −70 °C and then added to enriched ammonia at −70 °C. The reaction mixture was allowed to slowly warm to room temperature and stirred for 15 h. The precipitated $^{15}NH_4Cl$ was filtered off *via* cannula filtration and washed with diethyl ether. The solvent was removed *in vacuo* from the filtrate yielding ^{15}N labelled amino-di-*tert*-butylphosphine as a colorless liquid (1.71 g, 10.5 mmol, 66%). The values of ^{1}H and $^{31}P\{^{1}H\}$ NMR are in accordance with the literature.

^{15}N labelled amino-di-*tert*-butylphosphine (1.00 g, 6.16 mmol, 1.0 equiv.) was added dropwise to a suspension of sulfur (0.20 g, 6.16 mmol, 1.0 equiv.) in *n*-pentane (15 mL) at 0 °C. The reaction mixture was allowed to slowly warm to room temperature and stirred for 15 h yielding a colorless suspension. The liquid phase was removed by cannula filtration and the remaining solid was extracted with the minimum amount of diethyl ether. After removal of insoluble solids *via* cannula filtration, the solvent was removed *in vacuo* to obtain ^{15}N labelled **1** as a colorless solid (0.67 g, 3.45 mmol, 56%).

^{1}H NMR (400.13 MHz, C_6D_6, 298 K): δ = 1.14 (d, $^{3}J_{H–P}$ = 15.2 Hz, 18H, PC(CH_3)$_3$), 1.54 (br, 2H, NH_2). **^{31}P{^{1}H} NMR** (162.04 MHz, C_6D_6, 298 K): δ = 92.9 (s). **^{13}C{^{1}H} NMR** (100.61 MHz, C_6D_6, 298 K): δ = 27.3 (d, $^{2}J_{C–P}$ = 1.7 Hz, PC(CH$_3$)$_3$), 38.5 (d, $^{1}J_{C–P}$ = 55.7 Hz, PC(CH$_3$)$_3$). **^{1}H NMR** (400.13 MHz, CD_2Cl_2, 298 K): δ = 1.32 (d, $^{3}J_{H–P}$ = 15.4 Hz, 18H, PC(CH_3)$_3$), 2.20 (br, 2H, NH_2). **^{31}P{^{1}H} NMR** (162.04 MHz, CD_2Cl_2, 298 K): δ = 94.1 (s). **^{13}C{^{1}H} NMR** (100.61 MHz, CD_2Cl_2, 298 K): δ = 27.6 (d, $^{2}J_{C–P}$ = 1.6 Hz, PC(CH$_3$)$_3$), 38.9 (d, $^{1}J_{C–P}$ = 55.3 Hz, PC(CH$_3$)$_3$). **^{15}N NMR** (40.54 MHz, CD_2Cl_2, 298 K, ^{15}N labelled): δ = 29.1 (td, $^{1}J_{N–H}$ = 76.0 Hz, $^{1}J_{N–P}$ = 22.2 Hz). **Elemental analysis**: $C_8H_{20}NPS$: calcd.: C 49.71, H 10.43, N 7.25; found: C 49.92, H 10.15, N 7.29. **HR(EI+)-MS**: calcd. *m/z* for $C_8H_{20}NPS$ [$M^{+\cdot}$]: 193.1049, found: 193.1054.

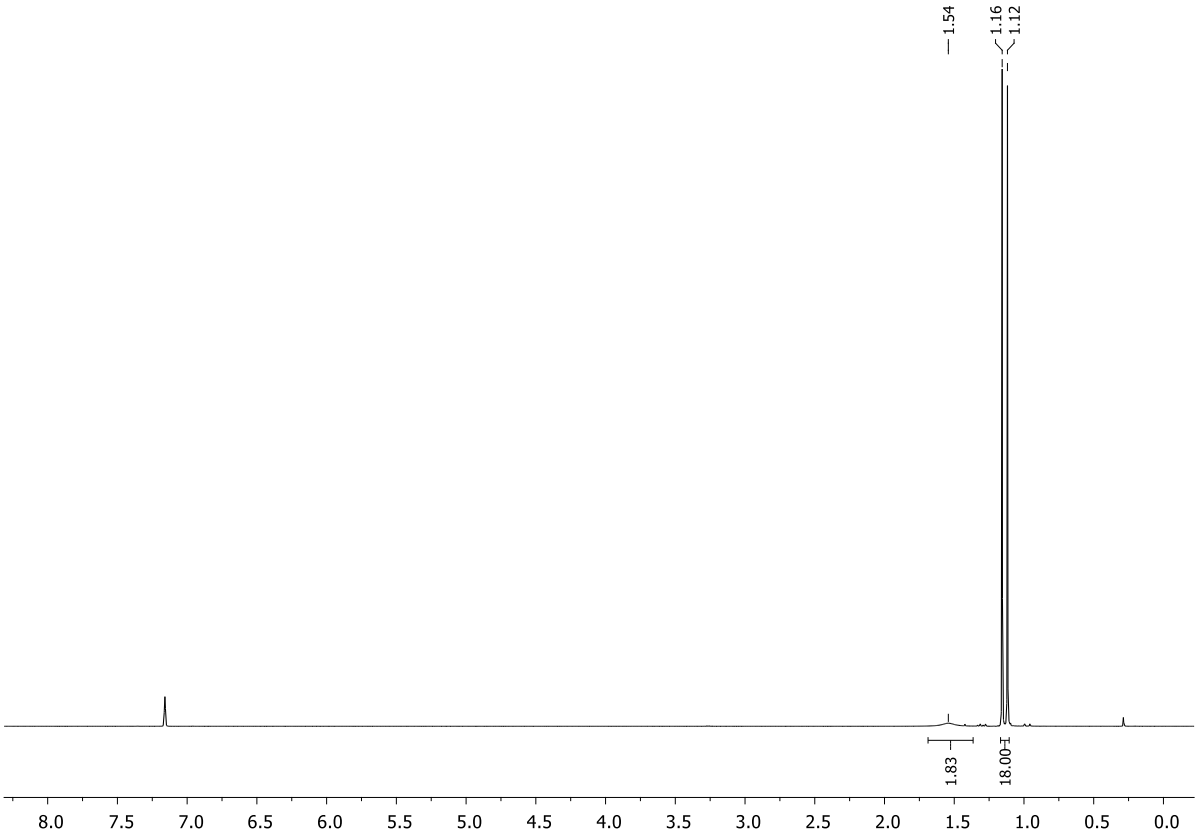

Figure S4.1. ^{1}H NMR spectrum (C_6D_6, 298 K) of **1**.

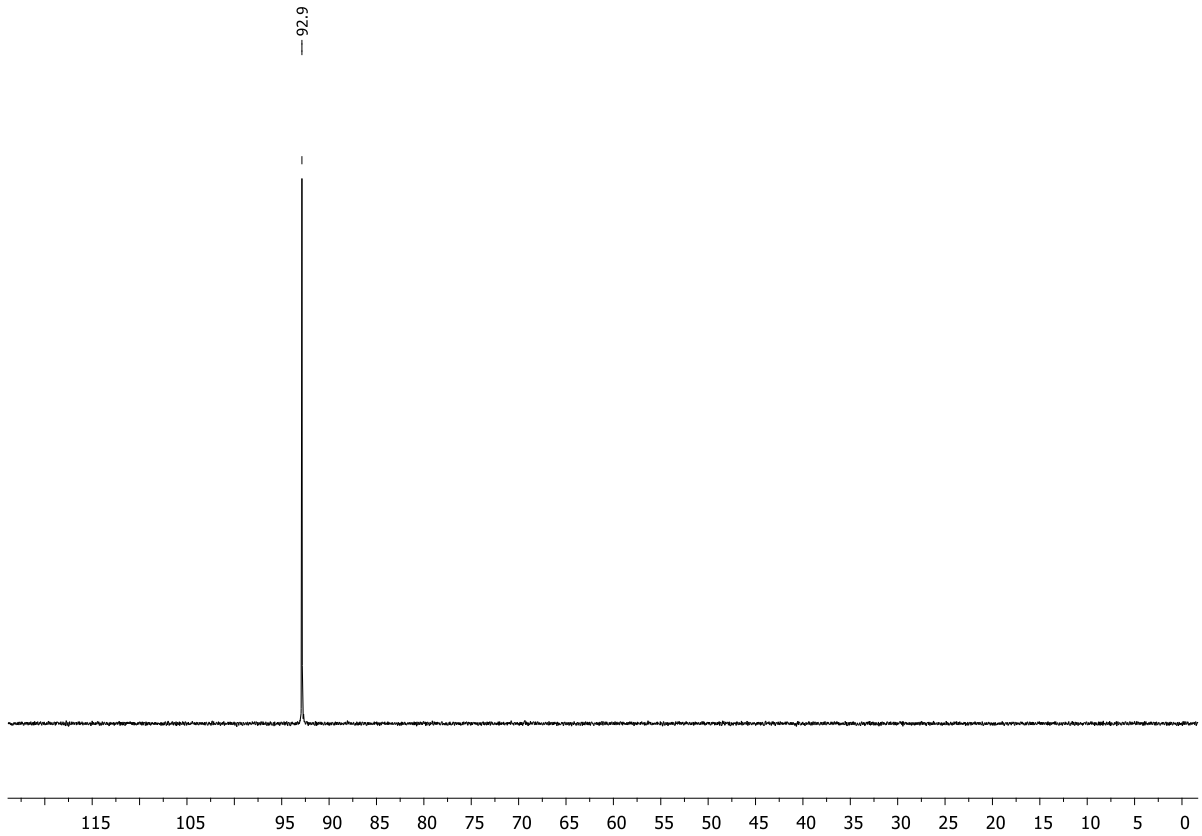

Figure S4.2. $^{31}P\{^{1}H\}$ NMR spectrum (C_6D_6, 298 K) of **1**.

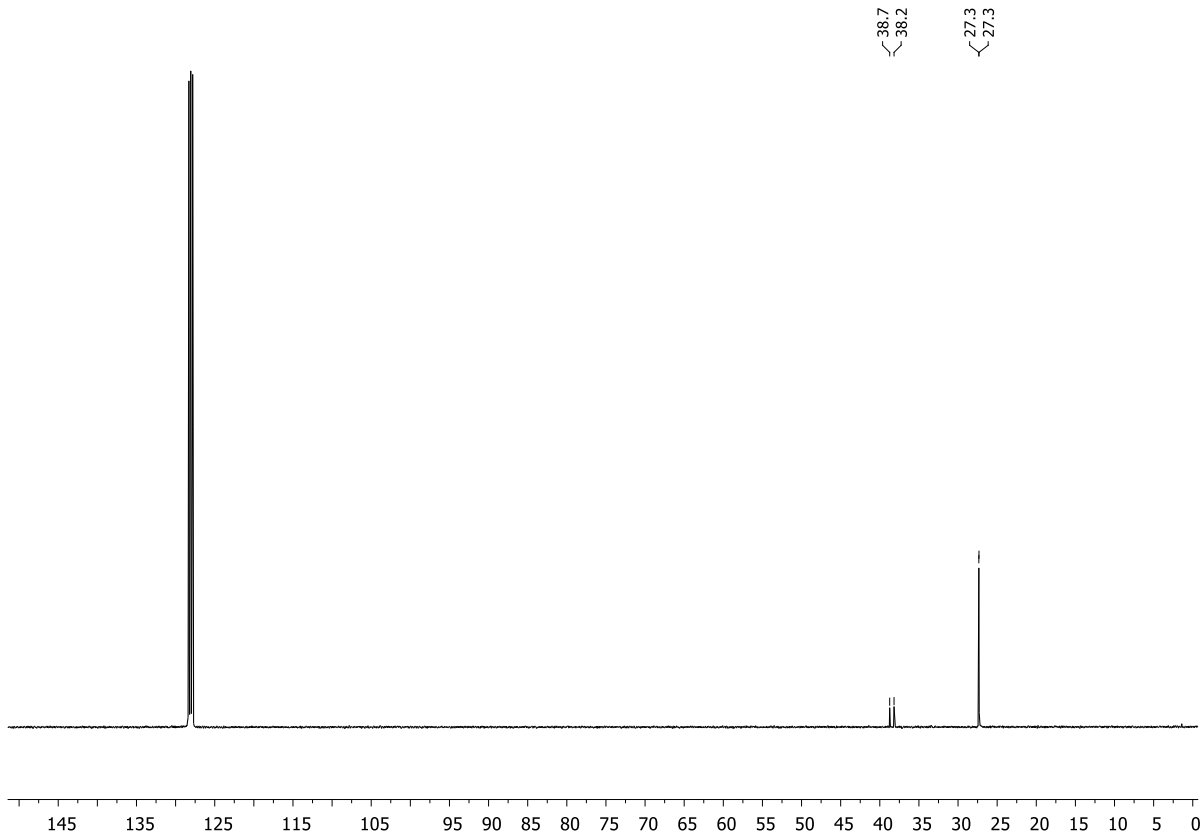

Figure S4.3. $^{13}C\{^{1}H\}$ NMR spectrum (C_6D_6, 298 K) of **1**.

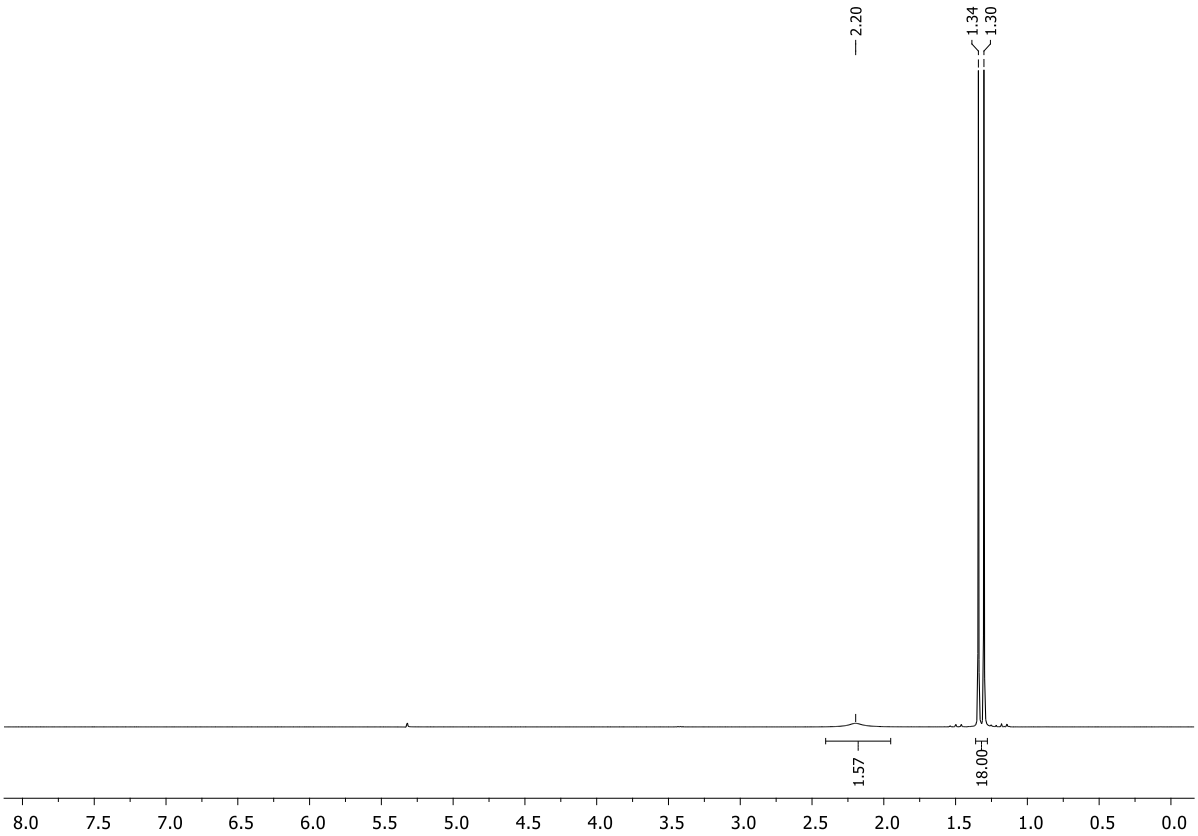

Figure S4.4. ^{1}H NMR spectrum (CD_2Cl_2, 298 K) of **1**.

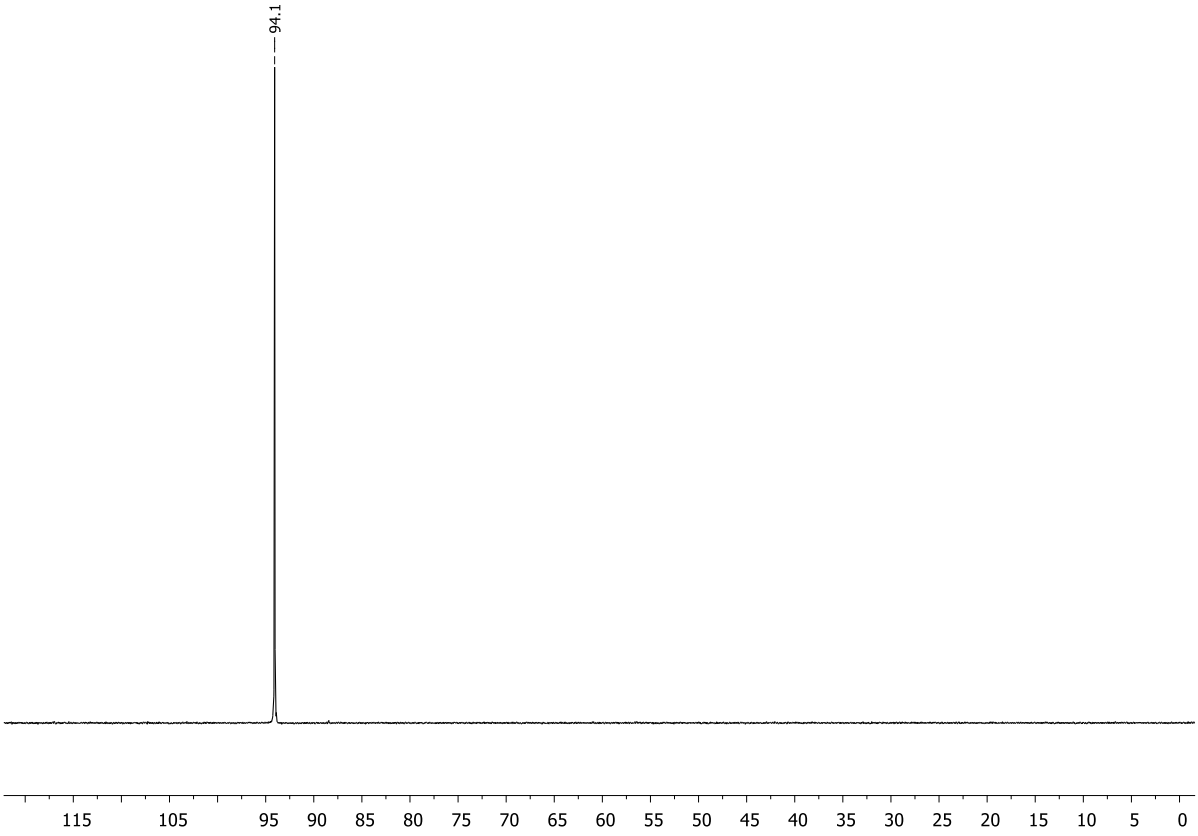

Figure S4.5. $^{31}P\{^{1}H\}$ NMR spectrum (CD_2Cl_2, 298 K) of **1**.

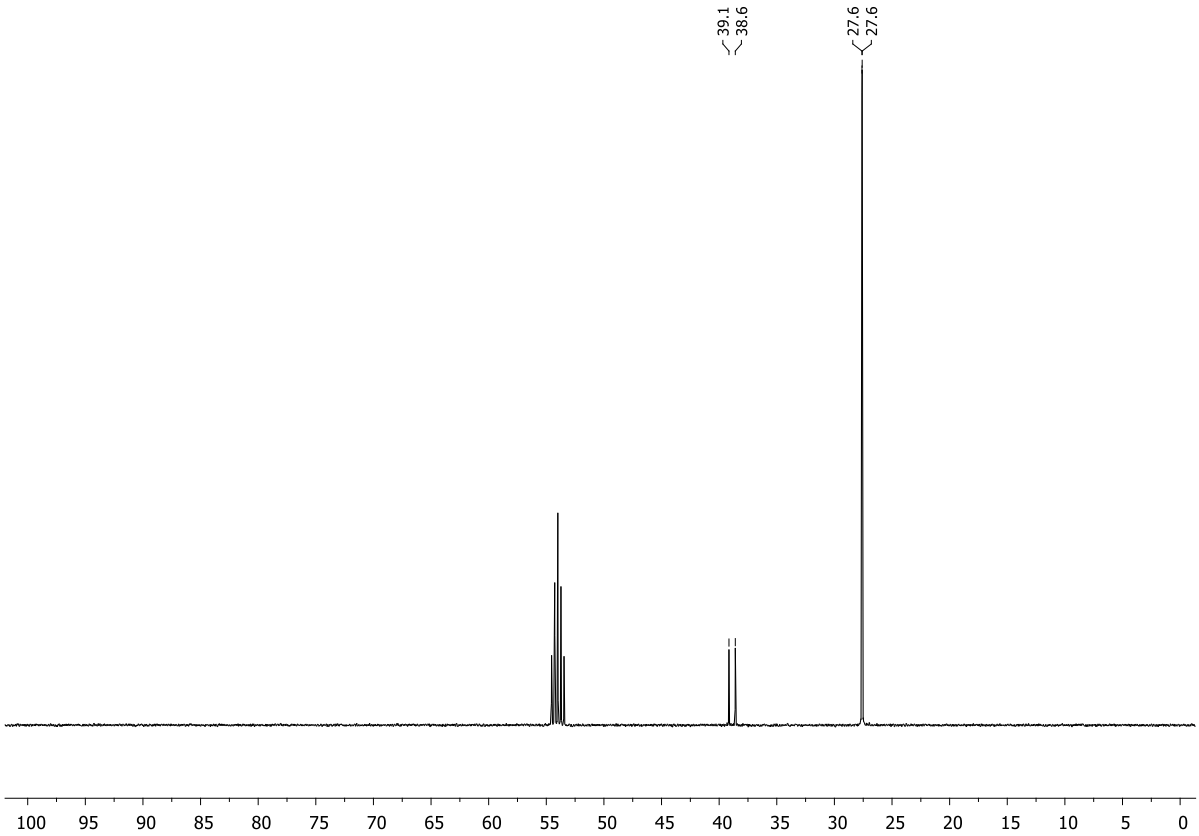

Figure S4.6. $^{13}C\{^{1}H\}$ NMR spectrum (CD_2Cl_2, 298 K) of **1**.

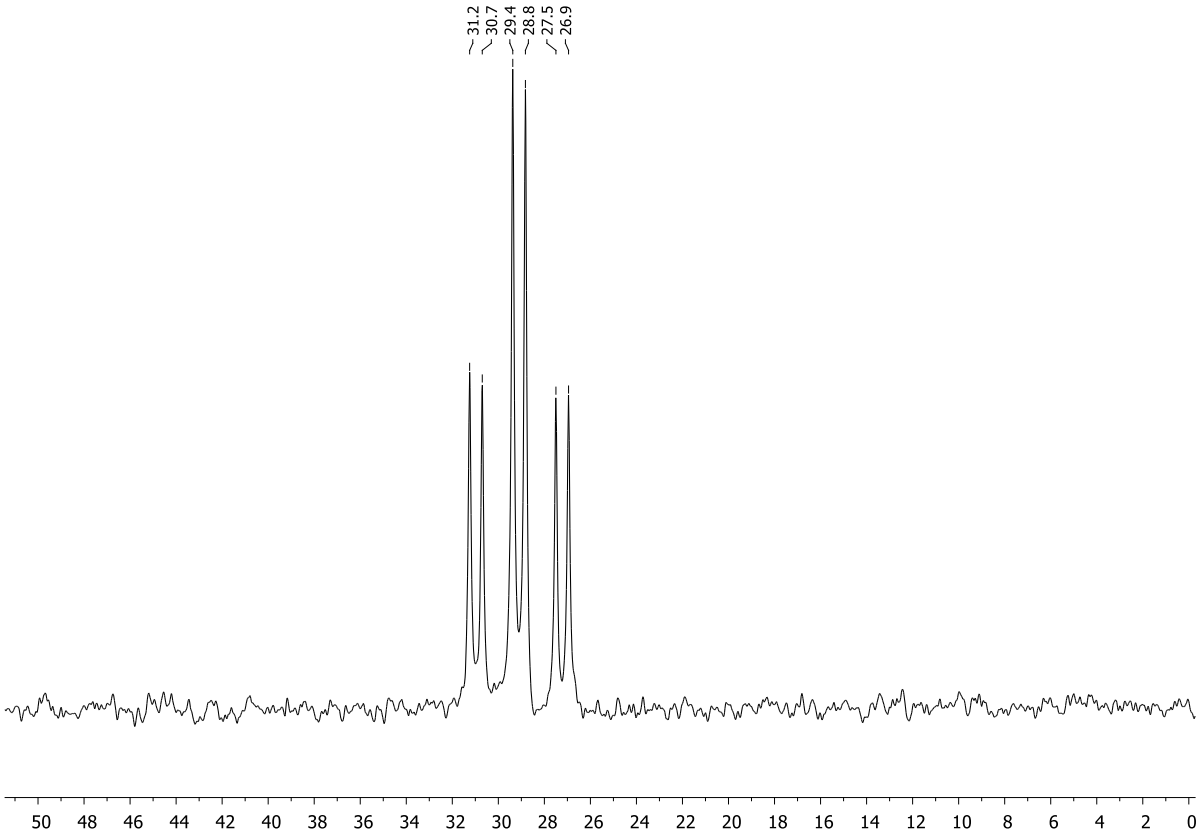

Figure S4.7. ^{15}N NMR spectrum (CD_2Cl_2, 298 K) of ^{15}N labelled **1**.

4.6.2.2. Synthesis of *t*Bu$_2$(PS)NH$_3^+$ Cl$^-$ [(1·HCl)$_4$]

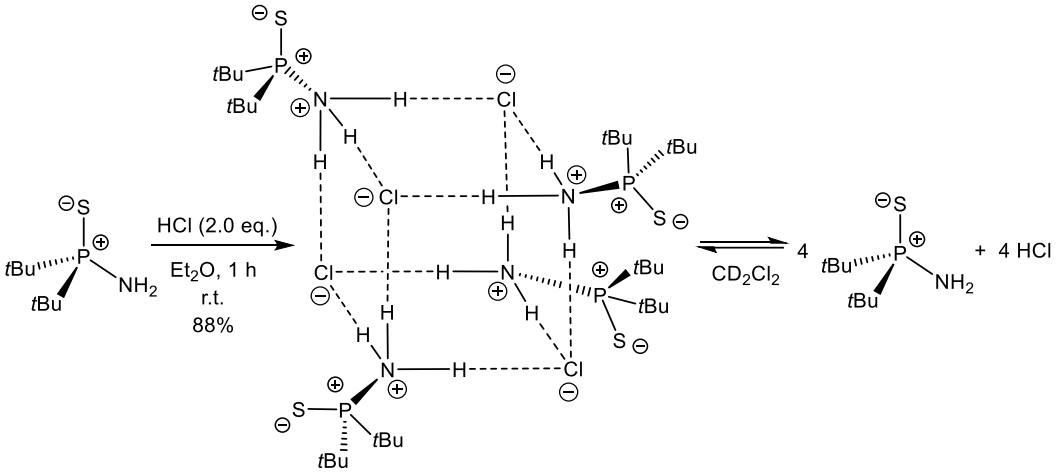

1 (0.60 g, 3.10 mmol, 1.0 equiv.) was dissolved in diethyl ether (20 mL) and HCl (3.10 mL, 6.20 mmol, 2.0 equiv., 2.0 M in diethyl ether) was added dropwise at room temperature resulting in a colorless suspension after a few minutes. After 1 h of stirring, the solvent was removed *in vacuo* and the solid further dried. **(1·HCl)$_4$** was obtained as a colorless solid (0.63 g, 2.74 mmol, 88%). Crystals suitable for single crystal X-ray diffraction were grown from Et$_2$O at –35 °C.

^{1}H NMR (400.13 MHz, 100 mM in CD_2Cl_2, 298 K): δ = 1.50 (d, $^3J_{H–P}$ = 17.4 Hz, 18H, PC(C*H*$_3$)$_3$), 9.32 (br, 3H, N*H*$_3$). **^{1}H NMR** (400.13 MHz, 100 mM in CD_2Cl_2, 193 K, ^{15}N labelled): δ = 1.40 (d, $^3J_{H–P}$ = 17.7 Hz, 18H, PC(C*H*$_3$)$_3$), 9.56 (d, $^1J_{H–N}$ = 68.1 Hz, 3H, N*H*$_3$). **^{31}P{^{1}H} NMR** (162.04 MHz, 100 mM in CD_2Cl_2, 298 K): δ = 111.5 (br). **^{31}P{^{1}H} NMR** (162.04 MHz, 100 mM in CD_2Cl_2, 193 K, ^{15}N labelled): δ = 111.9 (d, $^1J_{P–N}$ = 34.1 Hz). **^{13}C{^{1}H} NMR** (100.61 MHz, 100 mM in CD_2Cl_2, 298 K): δ = 27.5 (d, $^2J_{C–P}$ = 2.0 Hz, PC(*C*H$_3$)$_3$), 40.8 (d, $^1J_{C–P}$ = 43.2 Hz, P*C*(CH$_3$)$_3$). **^{15}N NMR** (40.54 MHz, 100 mM in CD_2Cl_2, 298 K, ^{15}N labelled): δ = 60.1 (br; no N–H or N–P coupling visible). **^{15}N NMR** (40.54 MHz, 100 mM in CD_2Cl_2, 193 K, ^{15}N labelled): δ = 62.6 (qd, $^1J_{N–H}$ = 68.0 Hz, $^1J_{P–N}$ = 34.0 Hz). **^{1}H NMR** (400.13 MHz, 5 mM in CD_2Cl_2, 298 K): δ = 1.33 (d, $^3J_{H–P}$ = 15.4 Hz, 18H, PC(C*H*$_3$)$_3$), 2.14 (br, 2H, N*H*$_2$). **^{31}P{^{1}H} NMR** (162.04 MHz, 5 mM in CD_2Cl_2, 298 K): δ = 94.2 (s). **^{13}C{^{1}H} NMR** (100.61 MHz, 5 mM in CD_2Cl_2, 298 K): δ = 27.6 (d, $^2J_{C–P}$ = 1.3 Hz, PC(*C*H$_3$)$_3$), P*C*(CH$_3$)$_3$ not visible. **^{15}N NMR** (40.54 MHz, 5 mM in CD_2Cl_2, 298 K, ^{15}N labelled): δ = 29.5 (br; no N–H or N–P coupling visible). **^{15}N{^{1}H} NMR** (40.54 MHz, 5 mM in CD_2Cl_2, 298 K, ^{15}N labelled): δ = 29.0 (d, $^1J_{N–P}$ = 22.4 Hz). **Elemental analysis**: $C_8H_{21}ClNPS$: calcd.: C 41.82, H 9.21, N 6.10; found: C 41.90, H 8.81, N 6.06. **IR (solid, ATR)**: 2713 (s, br, NH_3^+), 2002 (vw), 1866 (vw), 1556 (vw), 1466 (m), 1435 (s), 1403 (m), 1375 (m), 1184 (w), 1024 (w).

For ^{2}H NMR measurements, the reaction was proceeded using **1** (0.50 g, 2.59 mmol, 1.0 equiv.) in diethyl ether (2 mL) and DCl (5.2 mL, 5.18 mmol, 2.0 equiv., 1.0 M in diethyl ether). ^{2}H labelled

compound **(1·DCl)$_4$** was obtained as a colorless solid (0.50 g, 2.17 mmol, 84%). The ^{2}H NMR samples were prepared using a mixture of CH_2Cl_2 and CD_2Cl_2 (9:1) as solvent.

^{1}H NMR (400.13 MHz, 100 mM in CD_2Cl_2, 298 K): δ = 1.49 (d, $^3J_{H–P}$ = 17.3 Hz, 18H, PC(C*H*$_3$)$_3$), 9.59 (br, 2H, N*H*$_2$D). **^{2}H NMR** (61.42 MHz, 100 mM in CH_2Cl_2/CD_2Cl_2 (9:1), 298 K): δ = 8.96 (br, 1D, NH$_2$*D*). **^{1}H NMR** (400.13 MHz, 5 mM in CD_2Cl_2, 298 K): δ = 1.33 (d, $^3J_{H–P}$ = 15.4 Hz, 18H, PC(C*H*$_3$)$_3$), 1.90 (br, 1H, N*H*D). **^{2}H NMR** (61.42 MHz, 5 mM in CH_2Cl_2/CD_2Cl_2 (9:1), 298 K): δ = 2.08 (br, 1D, NH*D*).

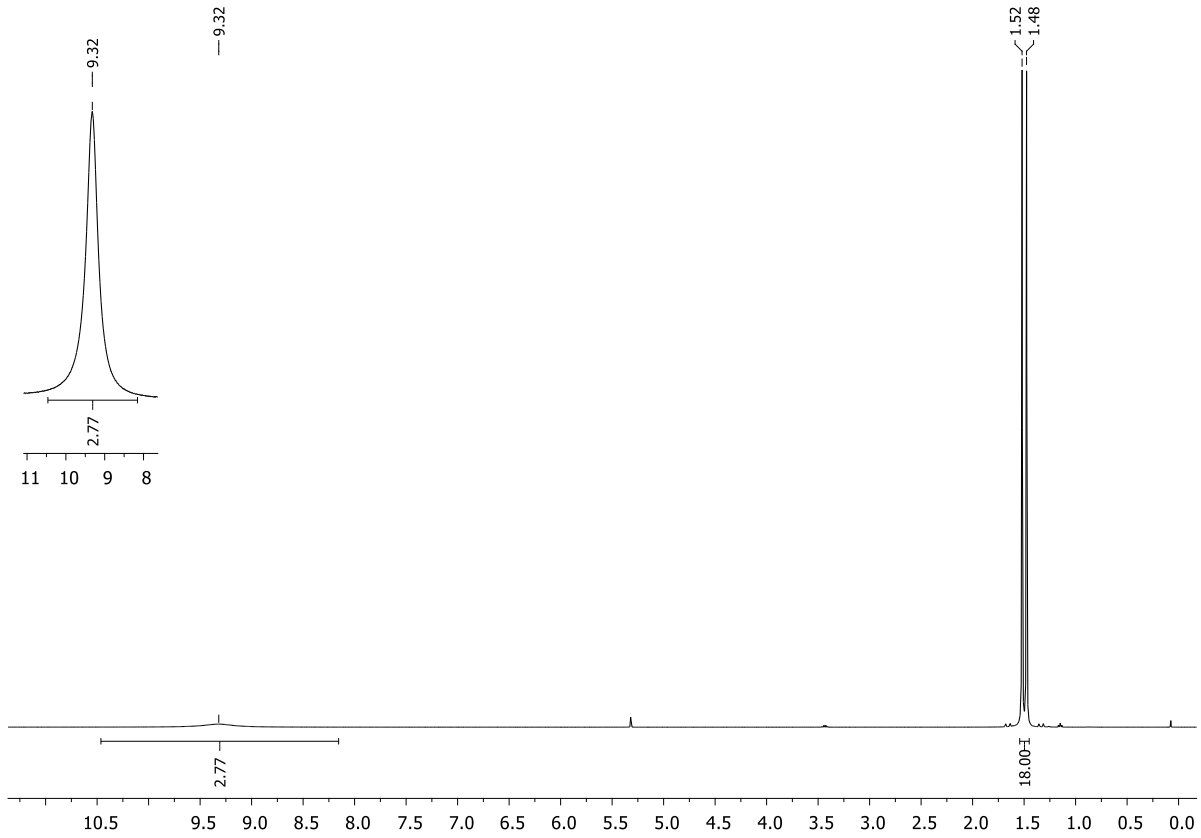

Figure S4.8. ^{1}H NMR spectrum (100 mM in CD_2Cl_2, 298 K) of **(1·HCl)$_4$**.

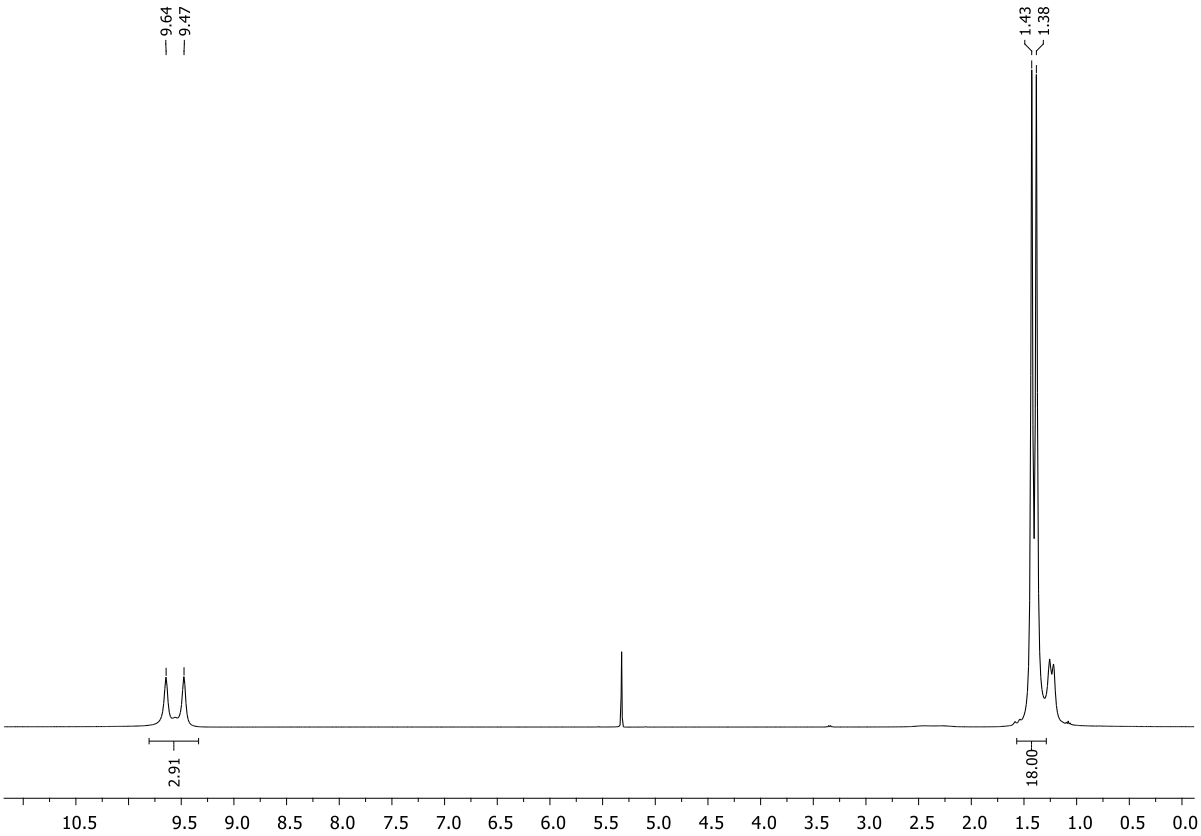

Figure S4.9. ^{1}H NMR spectrum (100 mM in CD_2Cl_2, 193 K) of ^{15}N labelled **(1·HCl)$_4$**.

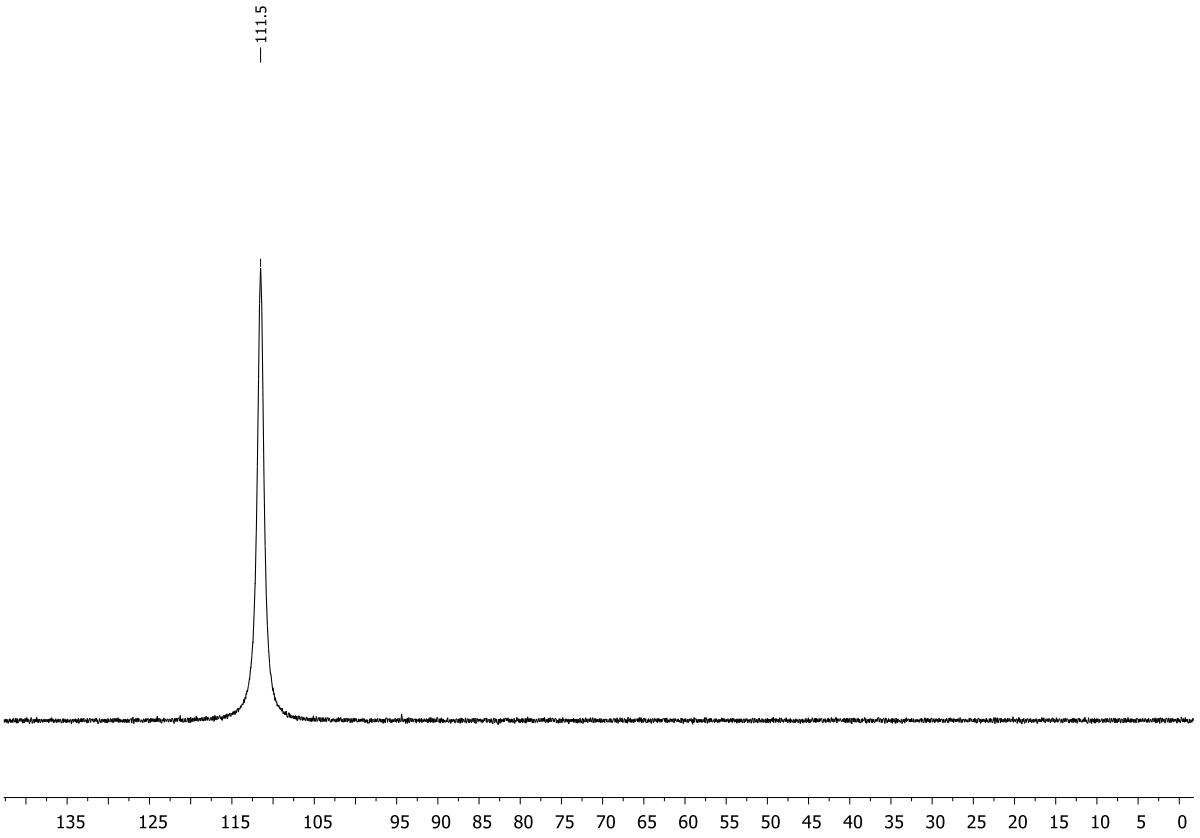

Figure S4.10. $^{31}P\{^{1}H\}$ NMR spectrum (100 mM in CD_2Cl_2, 298 K) of **(1·HCl)$_4$**.

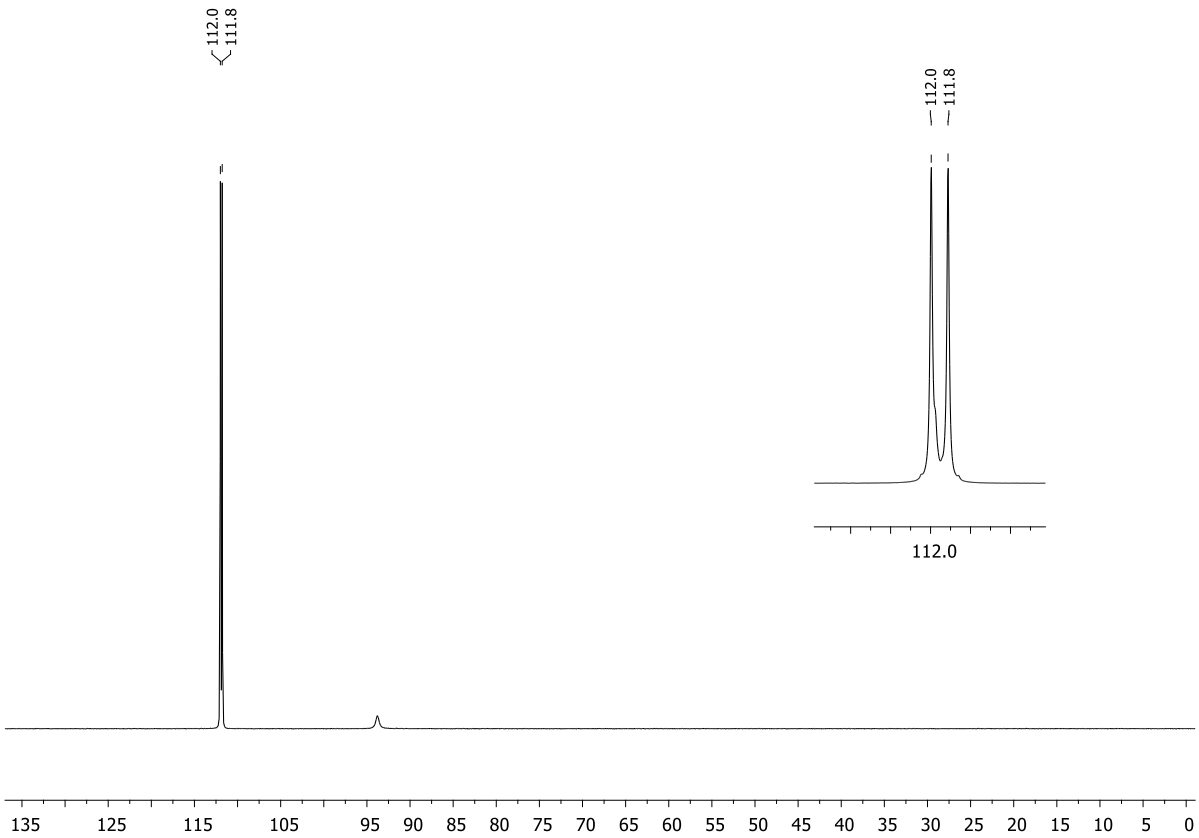

Figure S4.11. $^{31}P\{^{1}H\}$ NMR spectrum (100 mM in CD_2Cl_2, 193 K) of ^{15}N labelled **(1·HCl)$_4$**.

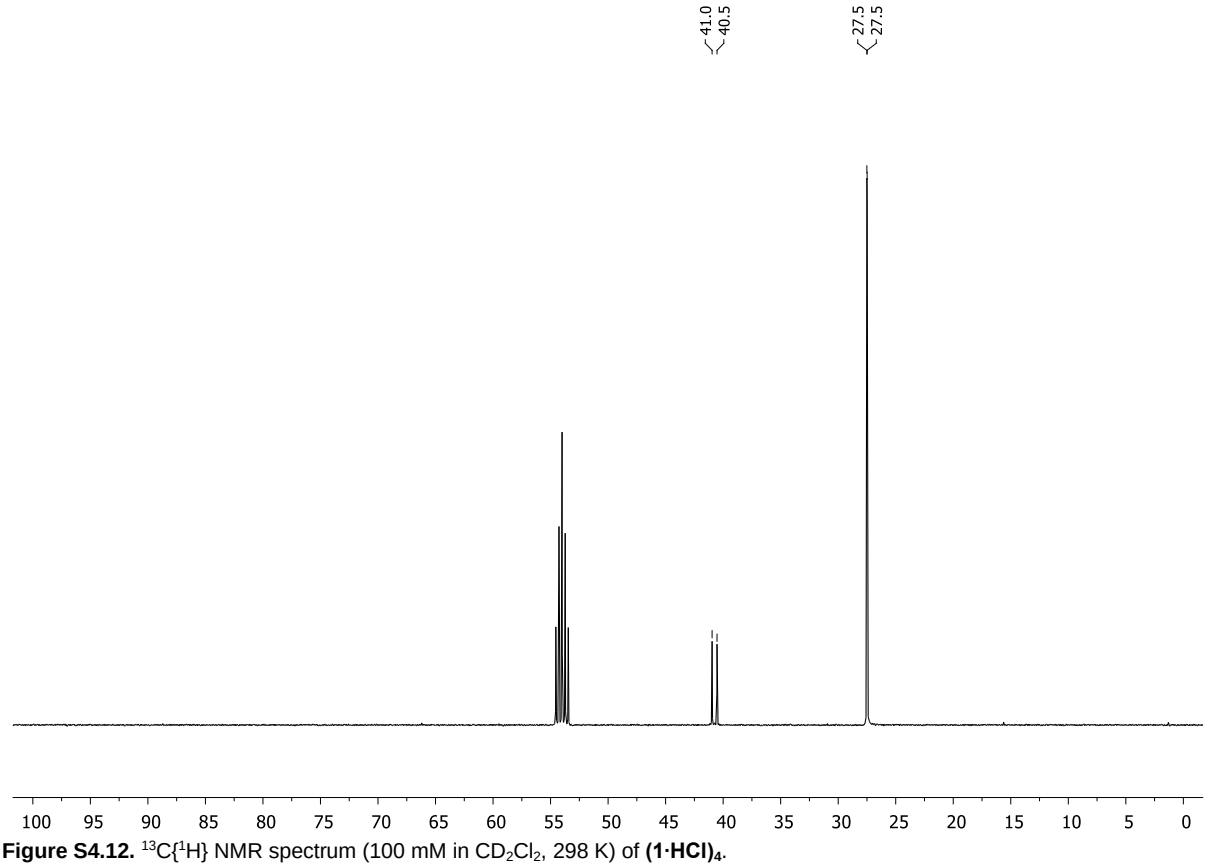

Figure S4.12. $^{13}C\{^{1}H\}$ NMR spectrum (100 mM in CD_2Cl_2, 298 K) of **(1·HCl)$_4$**.

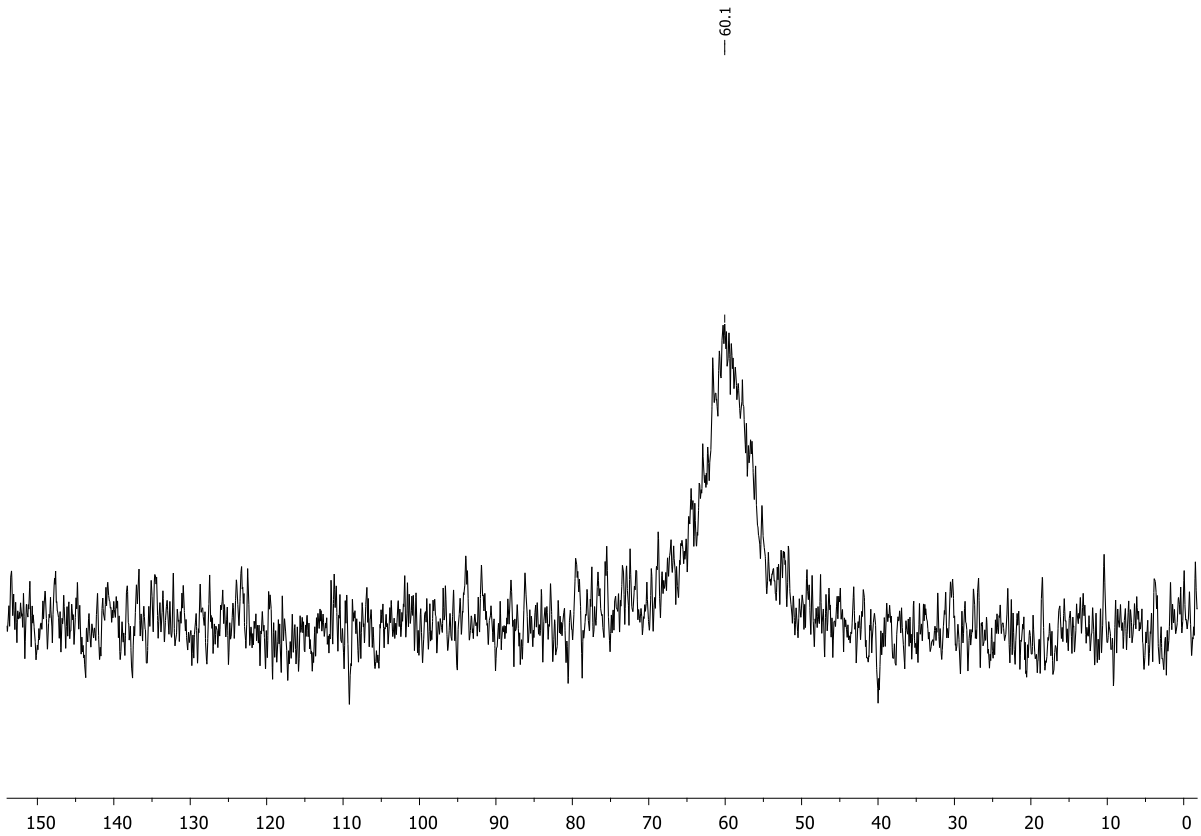

Figure S4.13. ^{15}N NMR spectrum (100 mM in CD_2Cl_2, 298 K) of ^{15}N labelled **(1·HCl)$_4$** (no N–H or N–P coupling visible).

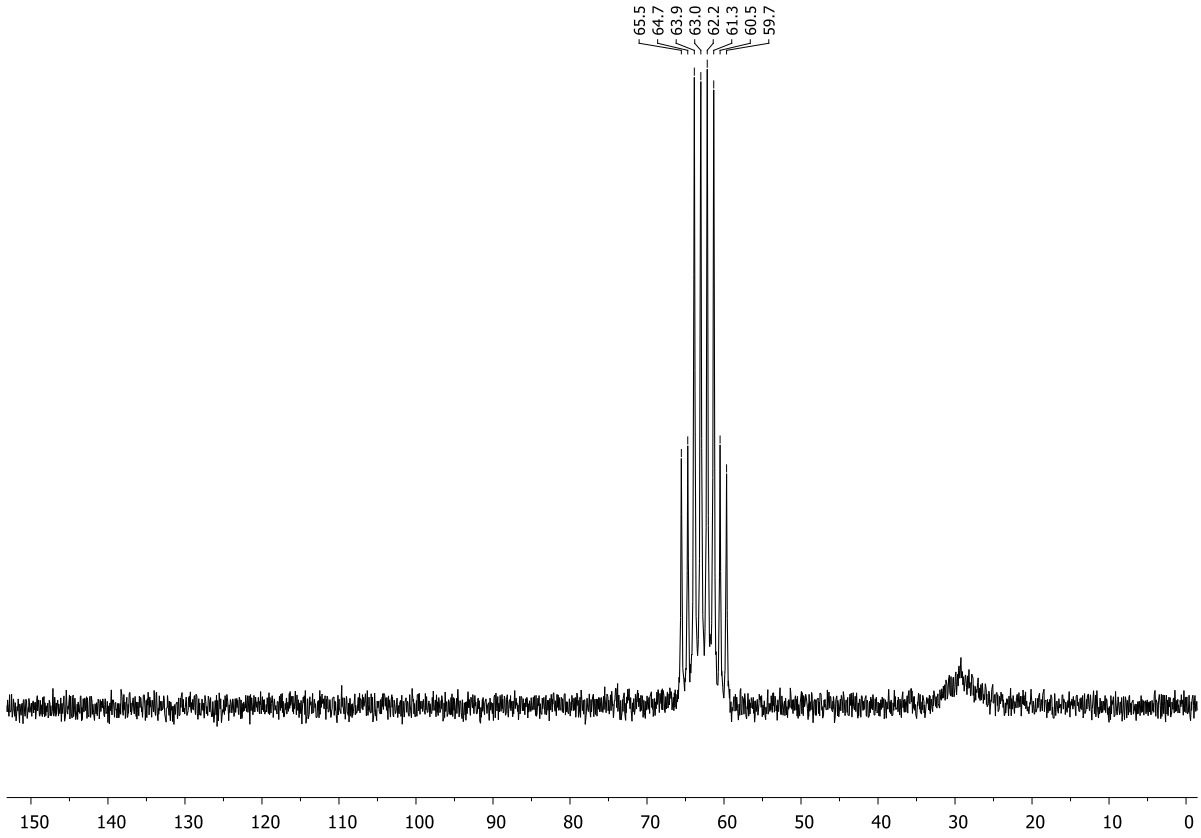

Figure S4.14. ^{15}N NMR spectrum (100 mM in CD_2Cl_2, 193 K) of ^{15}N labelled **(1·HCl)$_4$**.

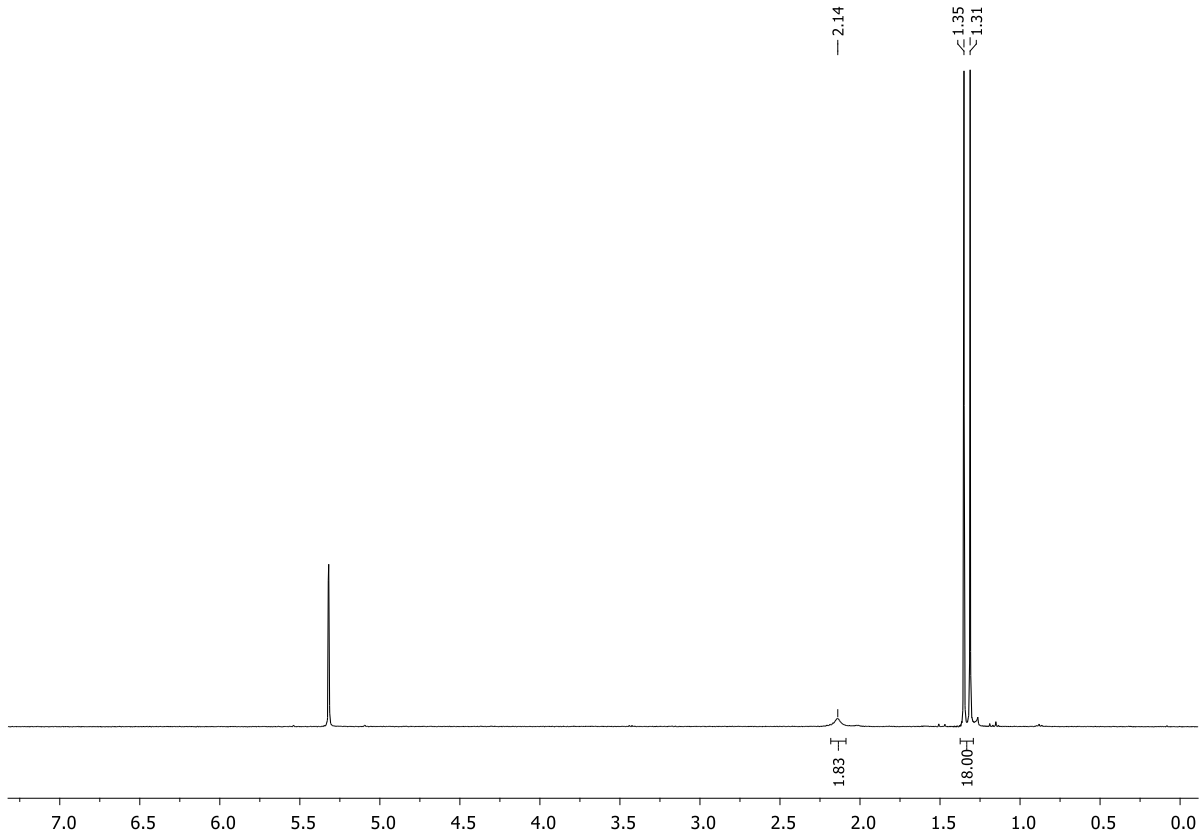

Figure S4.15. ^{1}H NMR spectrum (5 mM in CD_2Cl_2, 298 K) of **1 + HCl$_{solv}$**.

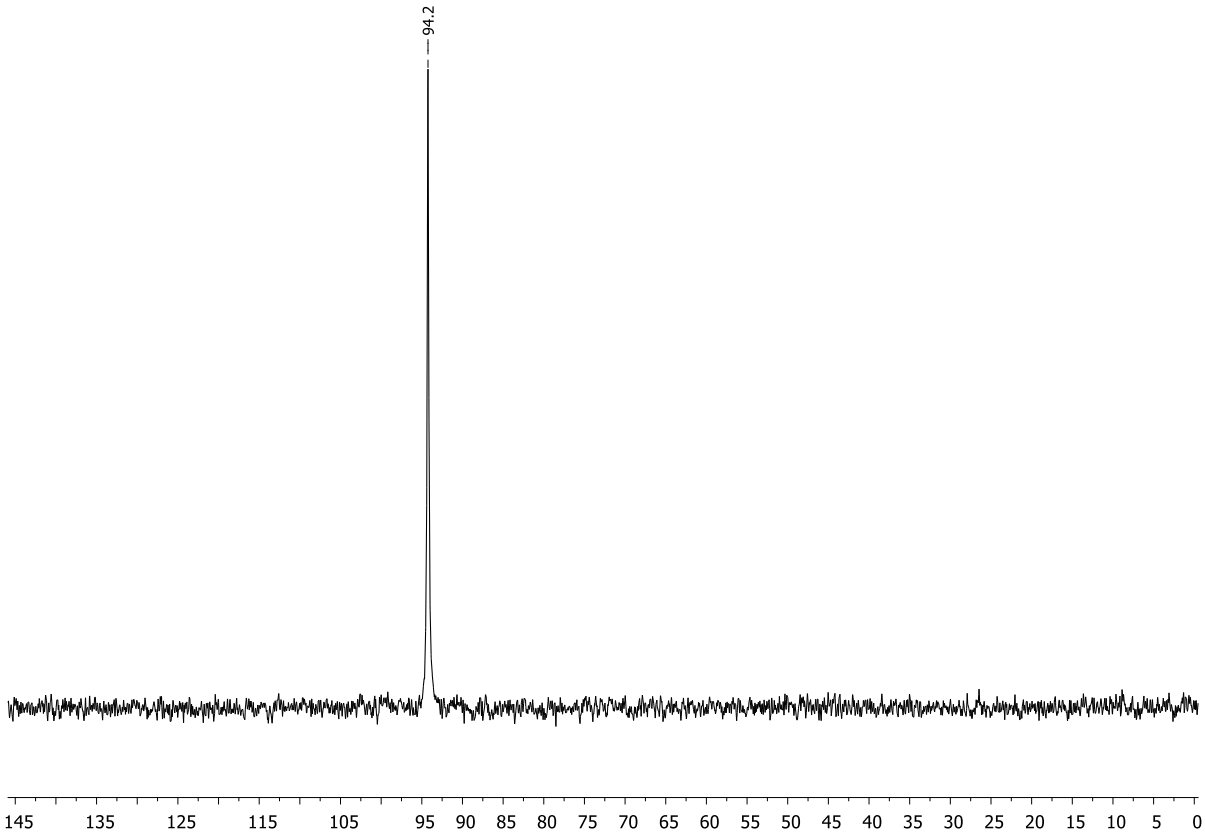

Figure S4.16. $^{31}P\{^{1}H\}$ NMR spectrum (5 mM in CD_2Cl_2, 298 K) of **1 + HCl$_{solv}$**.

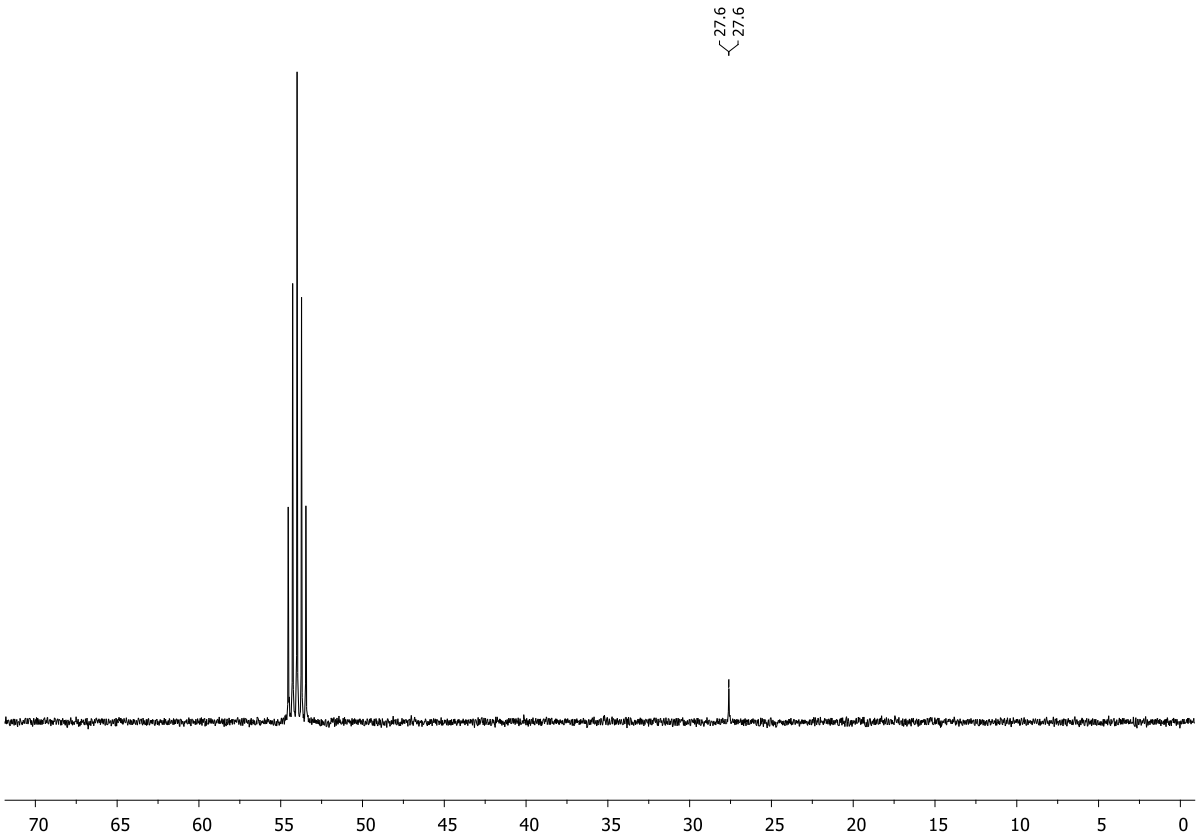

Figure S4.17. $^{13}C\{^{1}H\}$ NMR spectrum (5 mM in CD_2Cl_2, 298 K) of **1 + HCl$_{solv}$**.

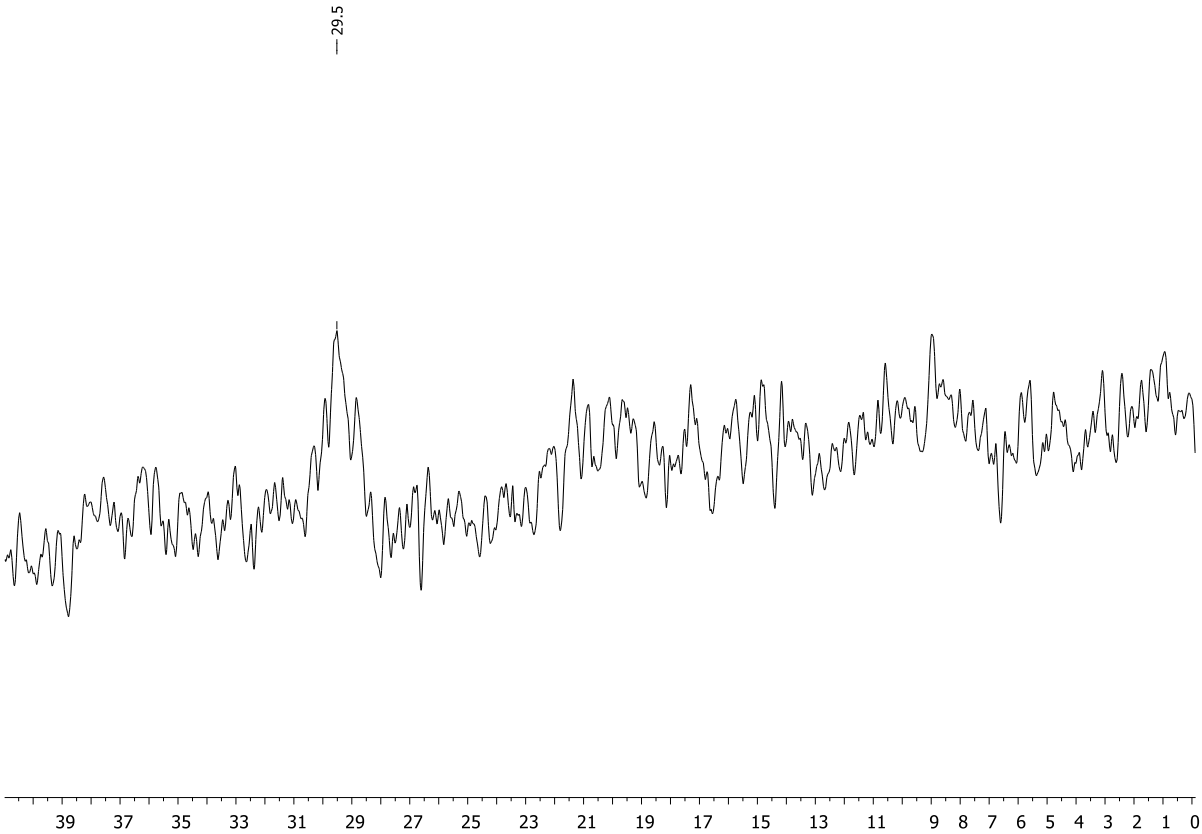

Figure S4.18. ^{15}N NMR spectrum (5 mM in CD_2Cl_2, 298 K) of ^{15}N labelled **1 + HCl$_{solv}$** (no N–H or N–P coupling visible).

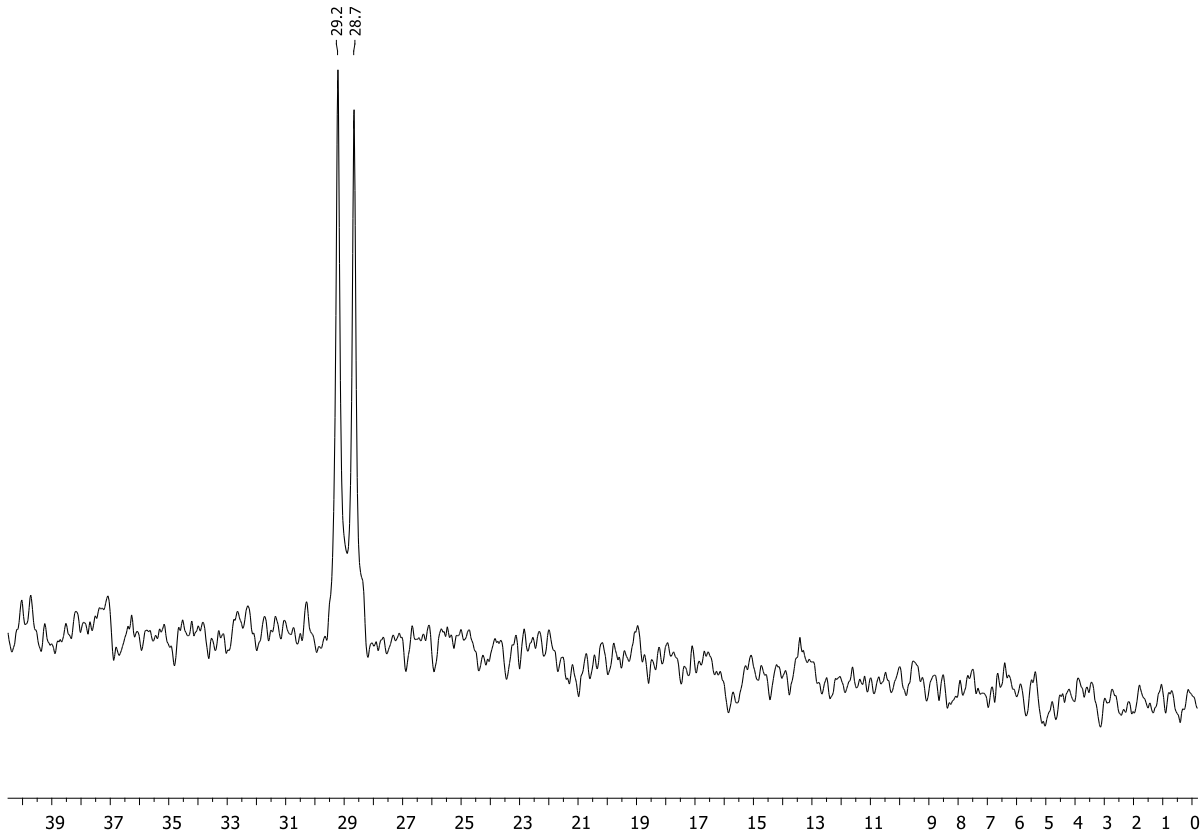

Figure S4.19. $^{15}N\{^{1}H\}$ NMR spectrum (5 mM in CD_2Cl_2, 298 K) of ^{15}N labelled **1 + HCl$_{solv}$**.

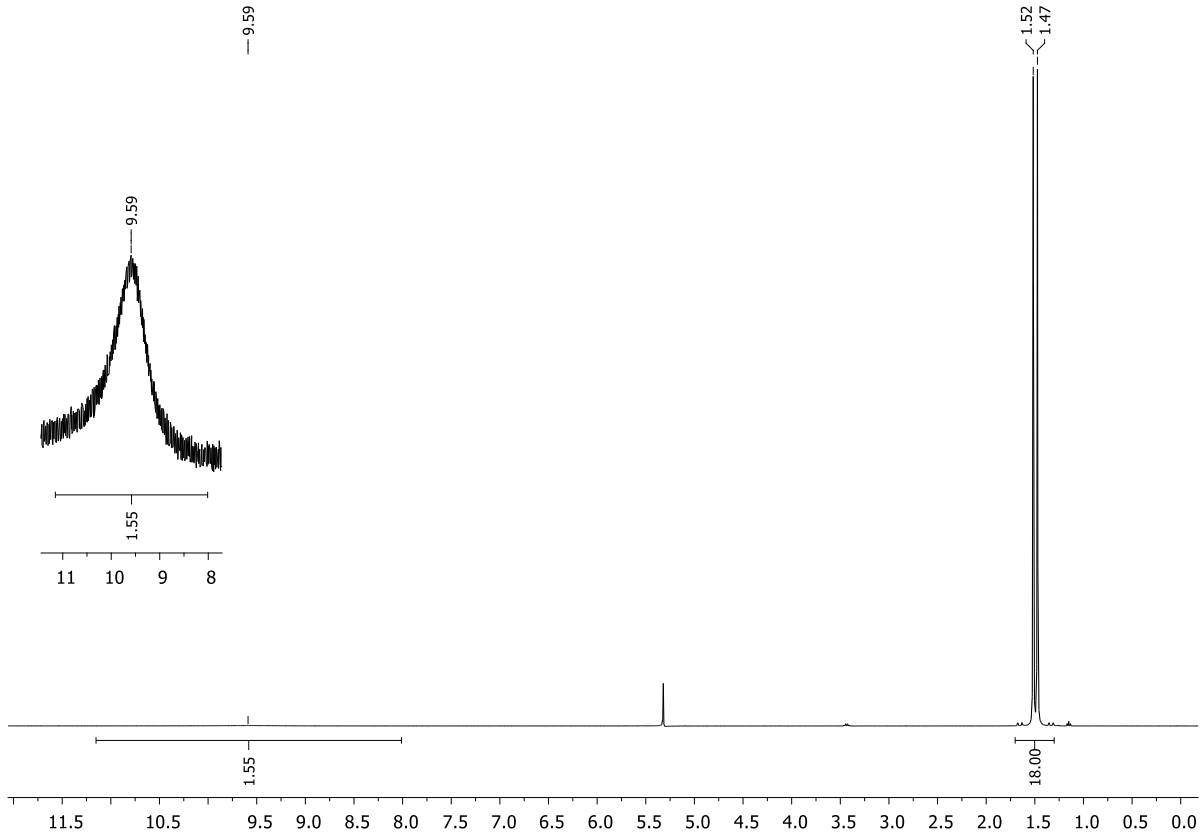

Figure S4.20. ^{1}H NMR spectrum (100 mM in CD_2Cl_2, 298 K) of **(1·DCl)$_4$**.

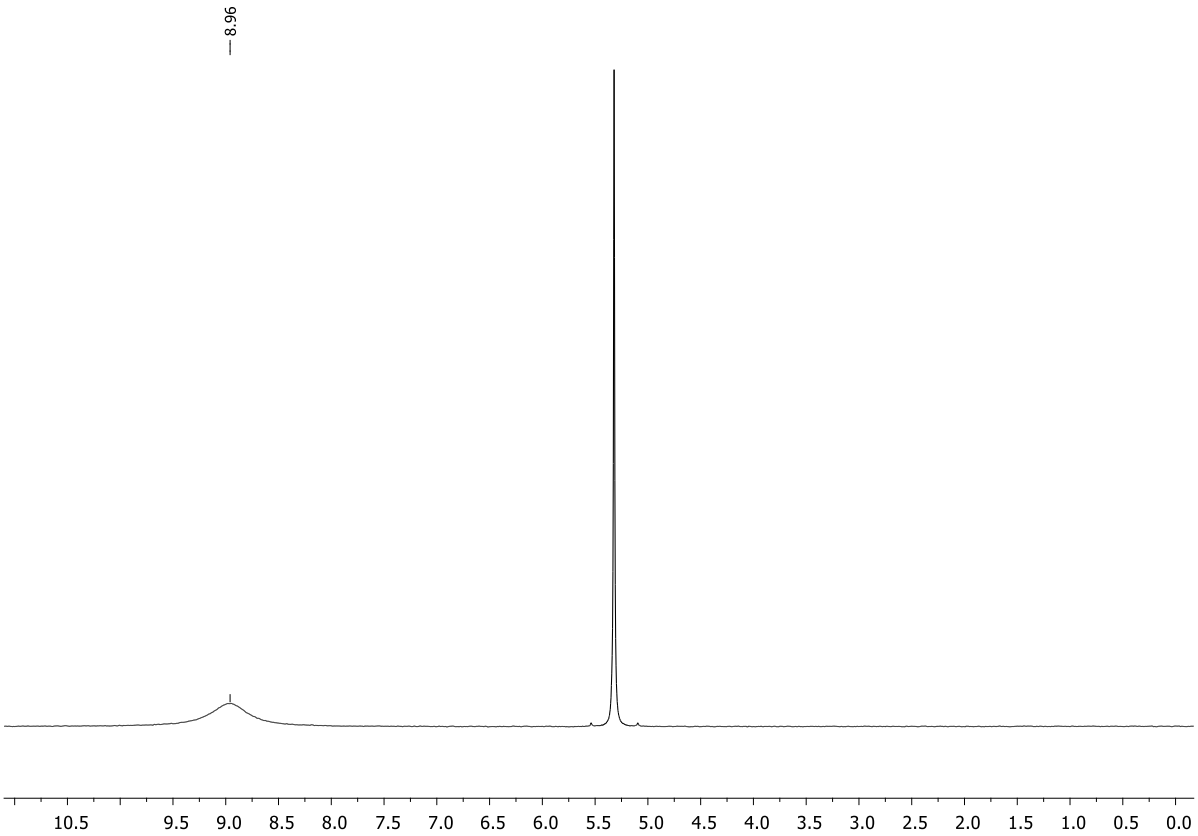

Figure S4.21. ^{2}H NMR spectrum (100 mM in CH_2Cl_2/CD_2Cl_2 (9:1), 298 K) of **(1·DCl)$_4$**.

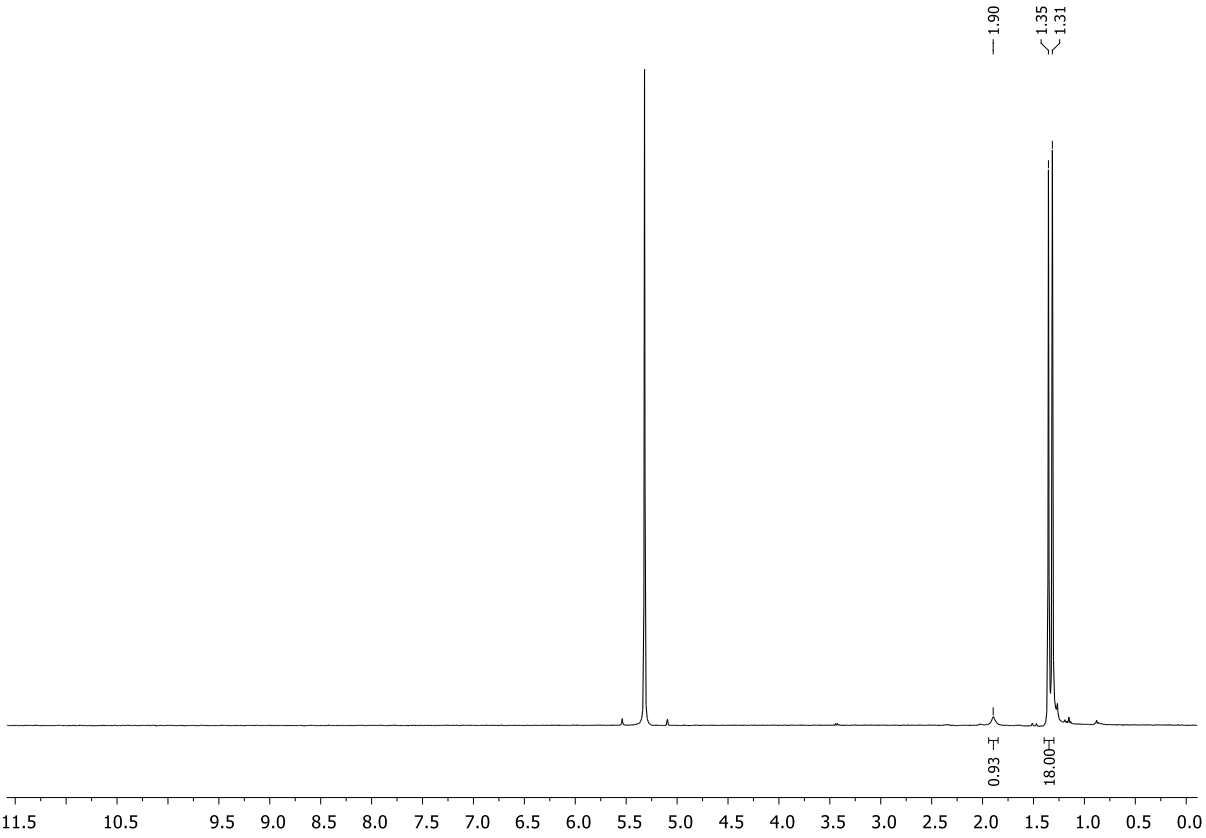

Figure S4.22. ^{1}H NMR spectrum (5 mM in CD_2Cl_2, 298 K) of **1 + DCl$_{solv}$**.

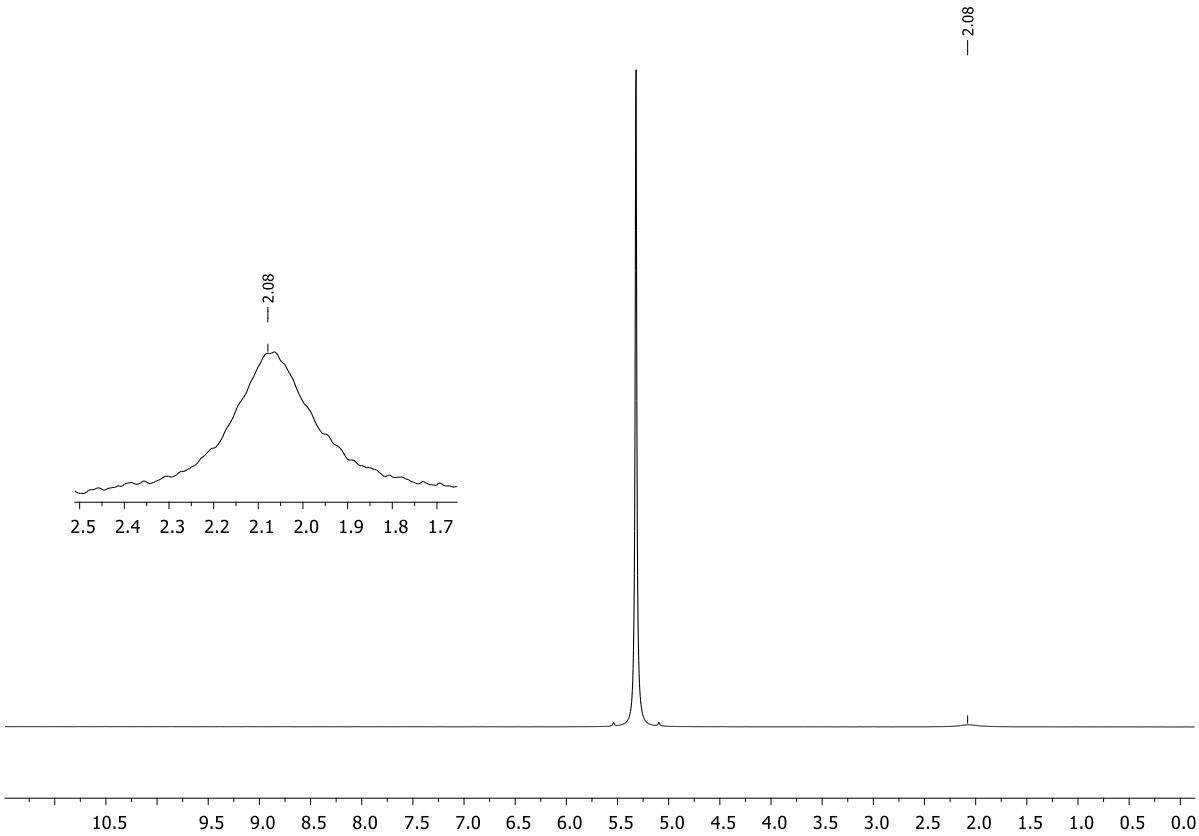

Figure S4.23. ^{2}H NMR spectrum (5 mM in CH_2Cl_2/CD_2Cl_2 (9:1), 298 K) of **1 + DCl$_{solv}$**.

4.6.2.3. Synthesis of *t*Bu$_2$(P$^+$–SH)NH$_2$ B(C$_6$F$_5$)$_4^-$ [(1–SH$^+$) WCA$^-$]

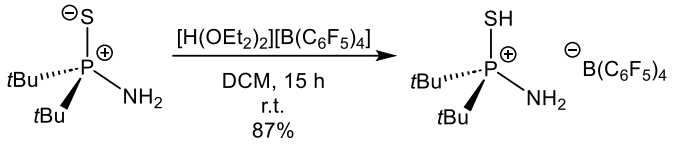

1 **(1–SH)$^+$ WCA$^-$**

1 (117 mg, 0.60 mmol, 1.0 equiv.) and [H(OEt$_2$)$_2$][B(C$_6$F$_5$)$_4$] (500 mg, 0.60 mmol, 1.0 equiv.) were dissolved in dichloromethane (10 mL) and the resulting suspension was stirred for 15 h at room temperature. All volatiles were removed *in vacuo* and the solid further dried. **(1–SH)$^+$ WCA$^-$** was obtained as a colorless solid (450 mg, 0.52 mmol, 87%). Crystals suitable for single crystal X-ray diffraction were grown from toluene after layering with *n*-pentane.

^{1}H NMR (400.13 MHz, CD_2Cl_2, 298 K): δ = 1.48 (d, $^3J_{H–P}$ = 18.4 Hz, 18H, PC(C*H*$_3$)$_3$), 2.96 (br, 3H, N*H*$_2$/S*H*). **^{31}P{^{1}H} NMR** (162.04 MHz, CD_2Cl_2, 298 K): δ = 97.6 (s). **^{13}C{^{1}H} NMR** (100.61 MHz, CD_2Cl_2, 298 K): δ = 26.6 (d, $^2J_{C–P}$ = 0.6 Hz, PC(*C*H$_3$)$_3$), 39.6 (d, $^1J_{C–P}$ = 44.6 Hz, P*C*(CH$_3$)$_3$), *C*$_{Ar\text{-}borate}$ not visible. **^{15}N NMR** (40.54 MHz, CD_2Cl_2, 298 K, ^{15}N labelled): δ = 21.2 (d, $J_{N–P}$ = 15.9 Hz; no N–H coupling visible). **^{15}N NMR** (40.54 MHz, CD_2Cl_2, 193 K, ^{15}N labelled): δ = 22.9 (d, $J_{N–P}$ = 16.5 Hz; no N–H coupling visible). **^{15}N{^{1}H} NMR** (40.54 MHz, CD_2Cl_2, 298 K, ^{15}N labelled): δ = 21.2 (d, $J_{N–P}$ = 15.9 Hz). **^{11}B{^{1}H} NMR** (128.43 MHz, CD_2Cl_2, 298 K): *δ* = −16.9 (s). **^{19}F{^{1}H} NMR** (376.66 MHz, CD_2Cl_2, 298 K): *δ* = −167.2 (m, 8F, *meta*-*F*$_{Ar\text{-}borate}$), −163.3 (m, 4F, *para*-*F*$_{Ar\text{-}borate}$), −132.9 (s, 8F, *ortho*-*F*$_{Ar\text{-}borate}$). **Elemental analysis**: $C_{32}H_{21}BF_{20}NPS$: calcd.: C 44.01, H 2.42, N 1.60; found: C 42.85, H 2.74, N 1.64. **IR (ATR)**: 3464 (vw, NH_2), 3375 (w, NH_2), 2975 (vw), 2573 (vw, SH), 1644 (m), 1547 (w), 1514 (s), 1456 (vs), 1411 (w), 1375 (w), 1274 (m), 1186 (vw), 1084 (s), 1022 (vw), 973 (vs).

For ^{2}H NMR measurements, the reaction was proceeded using **1** (30.0 mg, 0.16 mmol, 1.0 equiv.) and [D(OEt$_2$)$_2$][B(C$_6$F$_5$)$_4$] (129 mg, 0.16 mmol, 1.0 equiv.) in dichloromethane (1 mL). ^{2}H labelled compound **(1–SD)$^+$ WCA$^-$** was obtained as a colorless solid (105 mg, 0.12 mmol, 75%). The ^{2}H NMR sample was prepared using a mixture of CH_2Cl_2 and CD_2Cl_2 (9:1) as solvent.
^{1}H NMR (400.13 MHz, CD_2Cl_2, 298 K): δ = 1.49 (d, $^3J_{H–P}$ = 18.4 Hz, 18H, PC(C*H*$_3$)$_3$), 2.91 (br, 2H, N*H*$_2$ or N*H*D/S*H*). **^{2}H NMR** (61.42 MHz, CH_2Cl_2/CD_2Cl_2 (9:1), 298 K): δ = 2.90 (br, 1D, NH*D* or S*D*).

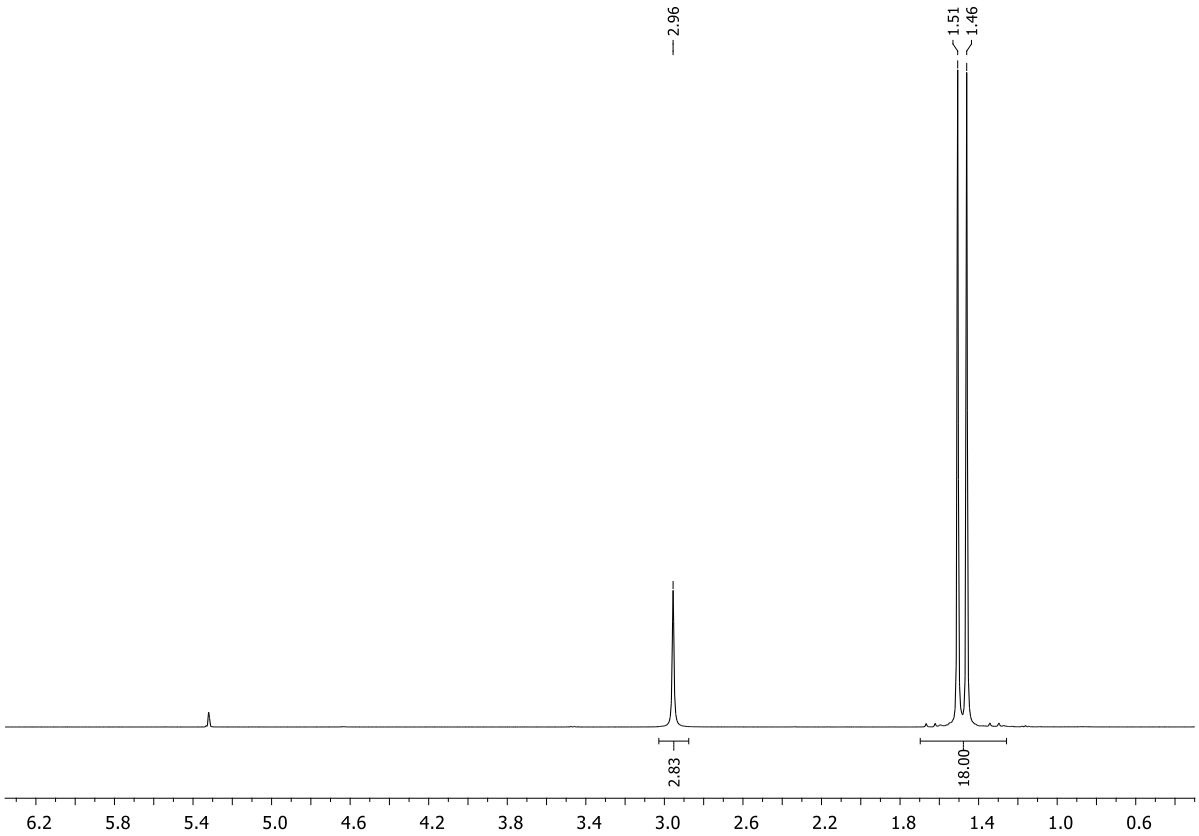

Figure S4.24. ^{1}H NMR spectrum (CD_2Cl_2, 298 K) of **(1–SH)$^+$ WCA$^-$**.

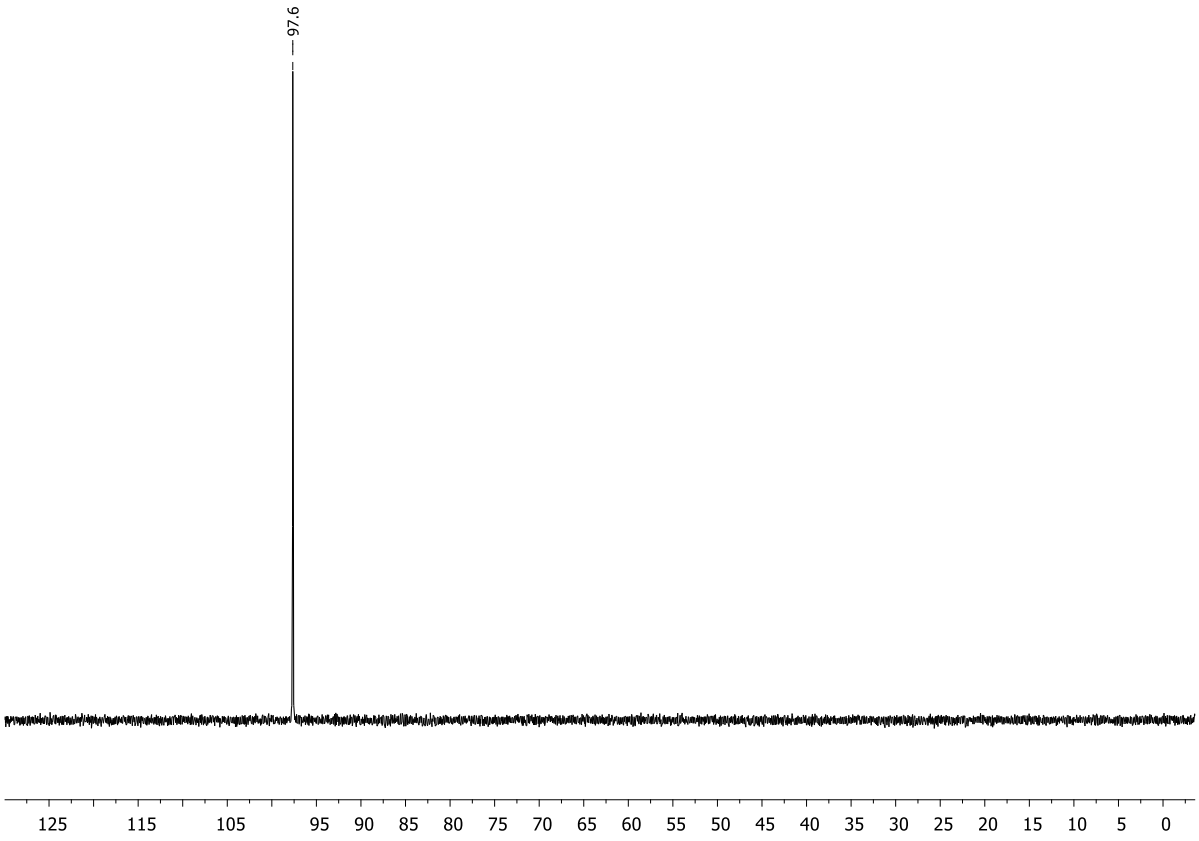

Figure S4.25. $^{31}P\{^{1}H\}$ NMR spectrum (CD_2Cl_2, 298 K) of **(1–SH)$^+$ WCA$^-$**.

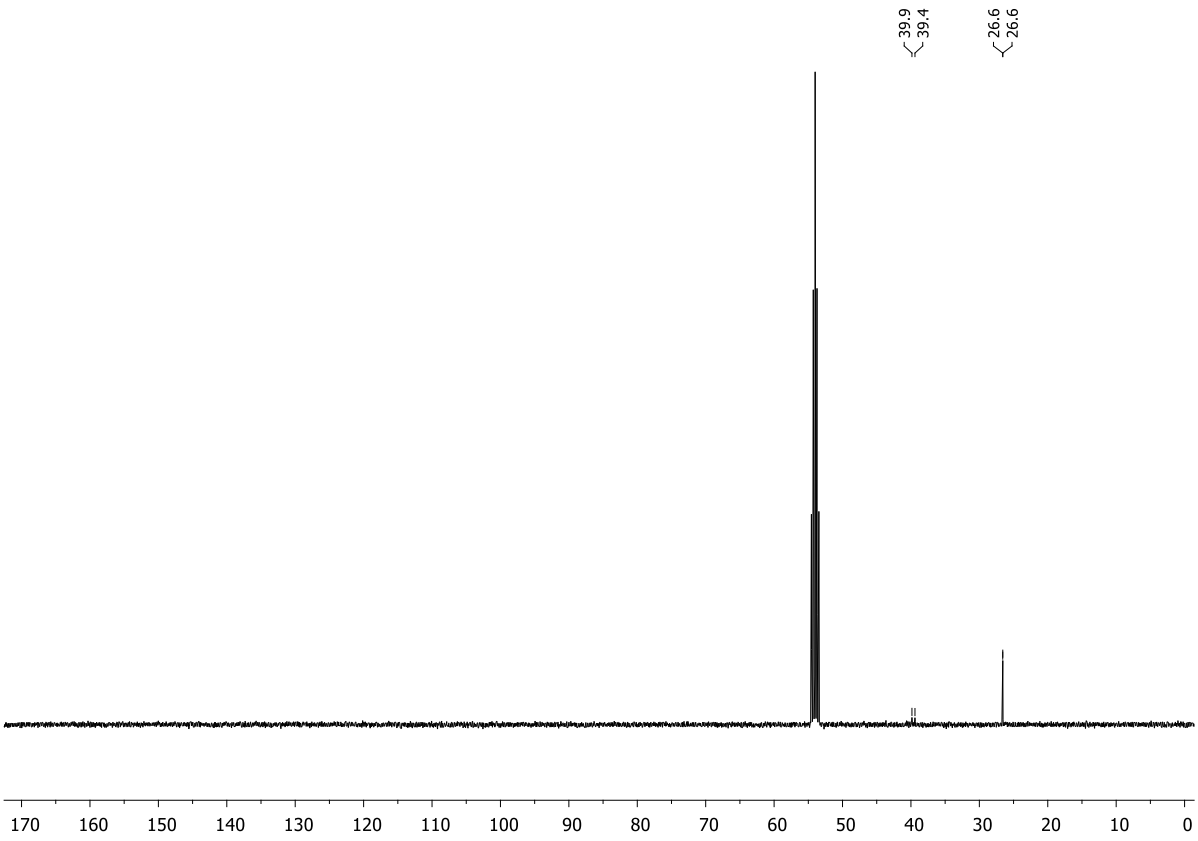

Figure S4.26. $^{13}C\{^{1}H\}$ NMR spectrum (CD_2Cl_2, 298 K) of **(1–SH)$^+$ WCA$^-$**.

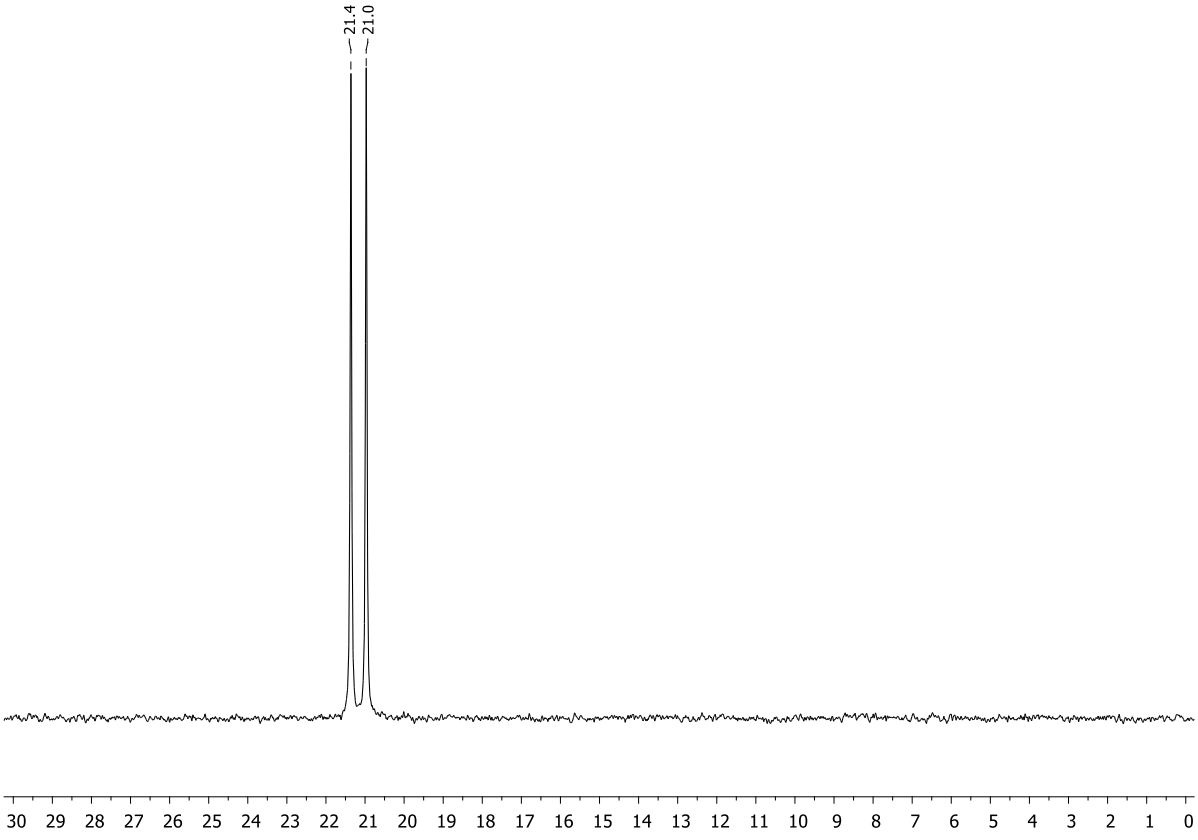

Figure S4.27. ^{15}N NMR spectrum (CD_2Cl_2, 298 K) of ^{15}N labelled **(1–SH)$^+$ WCA$^-$** (no N–H coupling visible).

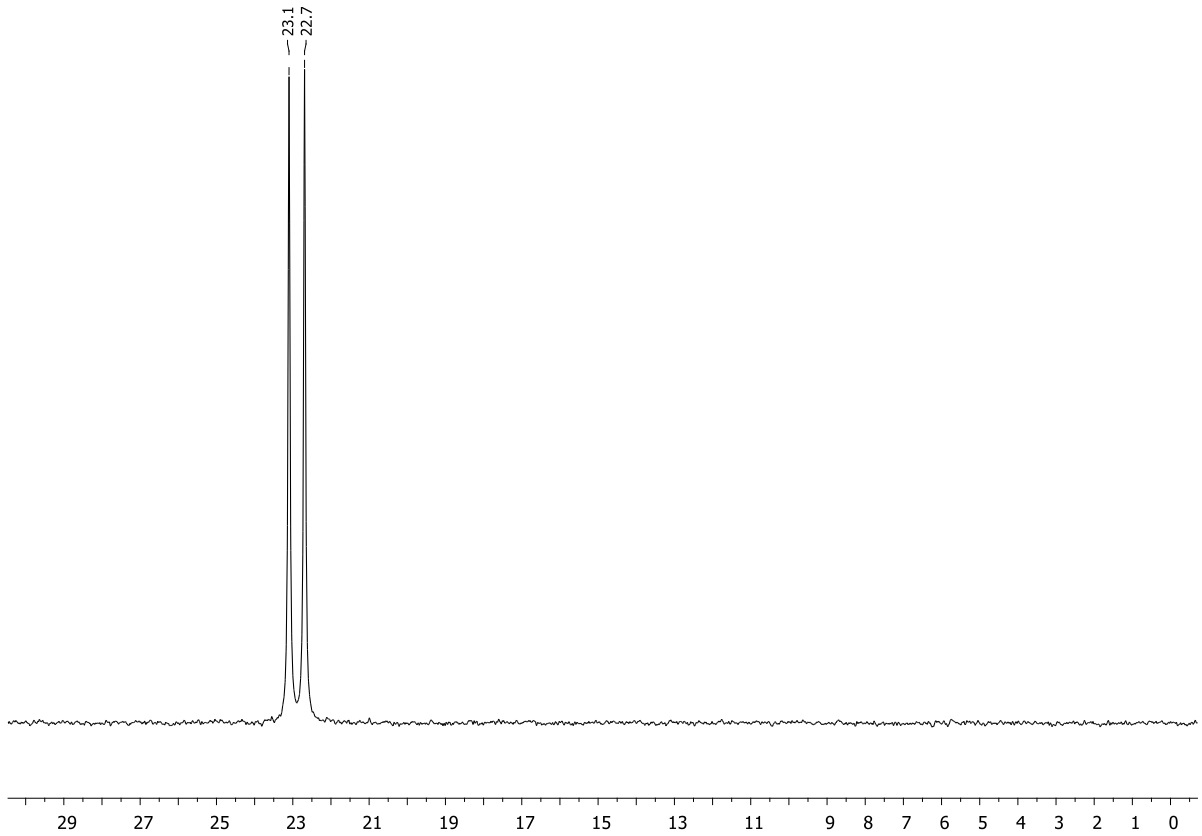

Figure S4.28. ^{15}N NMR spectrum (CD_2Cl_2, 193 K) of ^{15}N labelled **(1–SH)$^+$ WCA$^-$** (no N–H coupling visible).

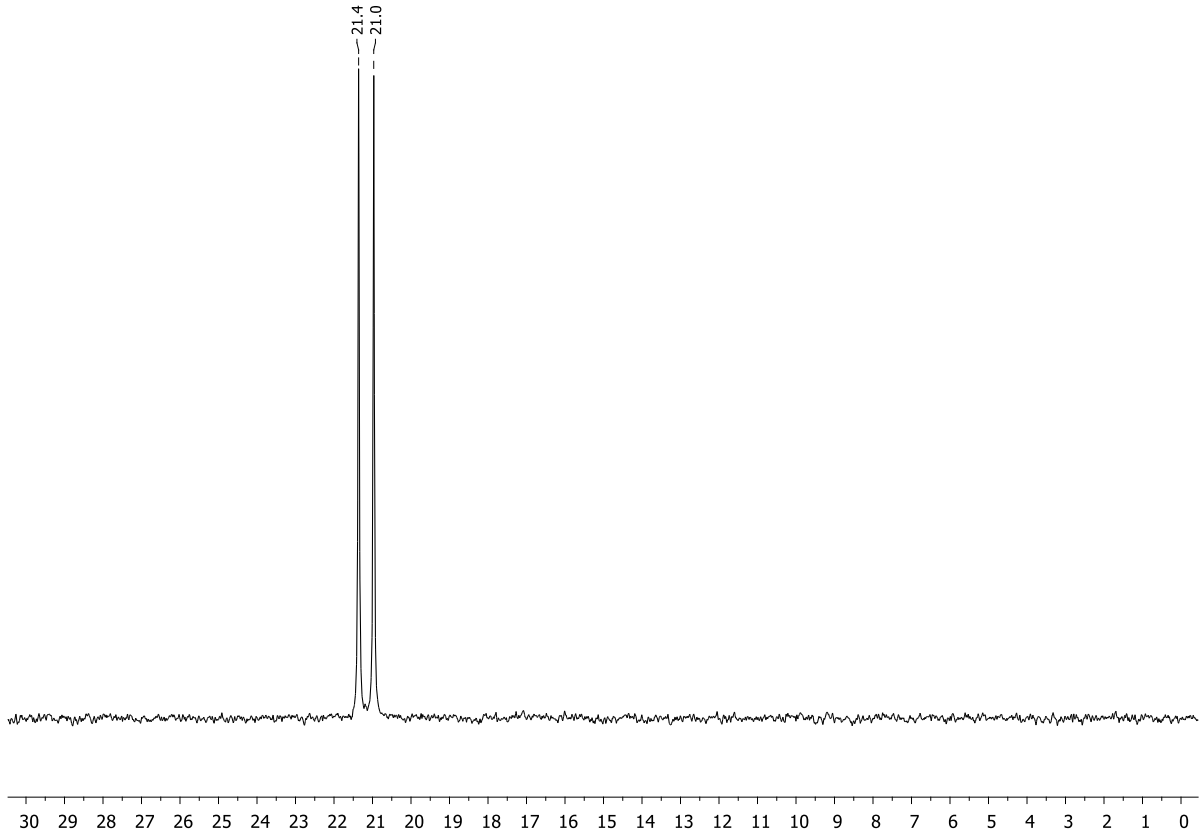

Figure S4.29. $^{15}N\{^1H\}$ NMR spectrum (CD_2Cl_2, 298 K) of ^{15}N labelled **(1–SH)$^+$ WCA$^-$**.

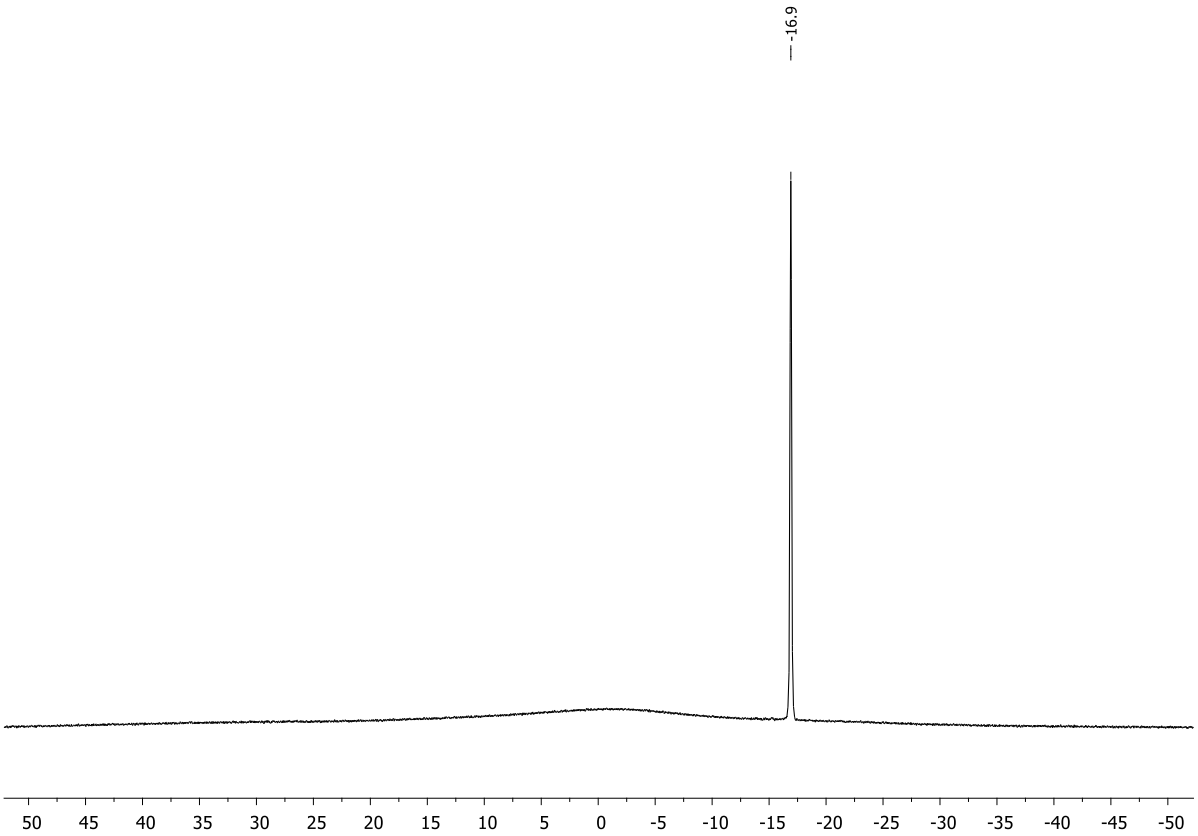

Figure S4.30. $^{11}B\{^{1}H\}$ NMR spectrum (CD_2Cl_2, 298 K) of **(1–SH)$^+$ WCA$^-$**.

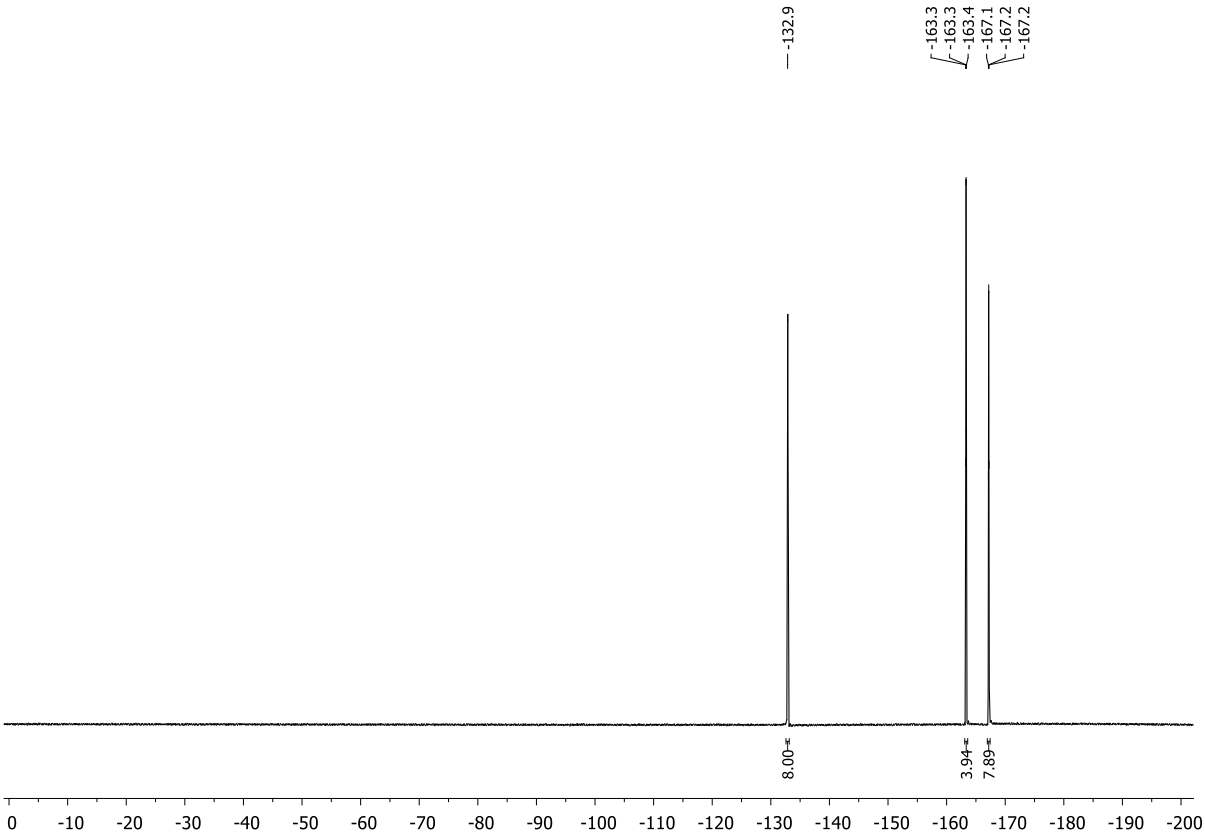

Figure S4.31. $^{19}F\{^{1}H\}$ NMR spectrum (CD_2Cl_2, 298 K) of **(1–SH)$^+$ WCA$^-$**.

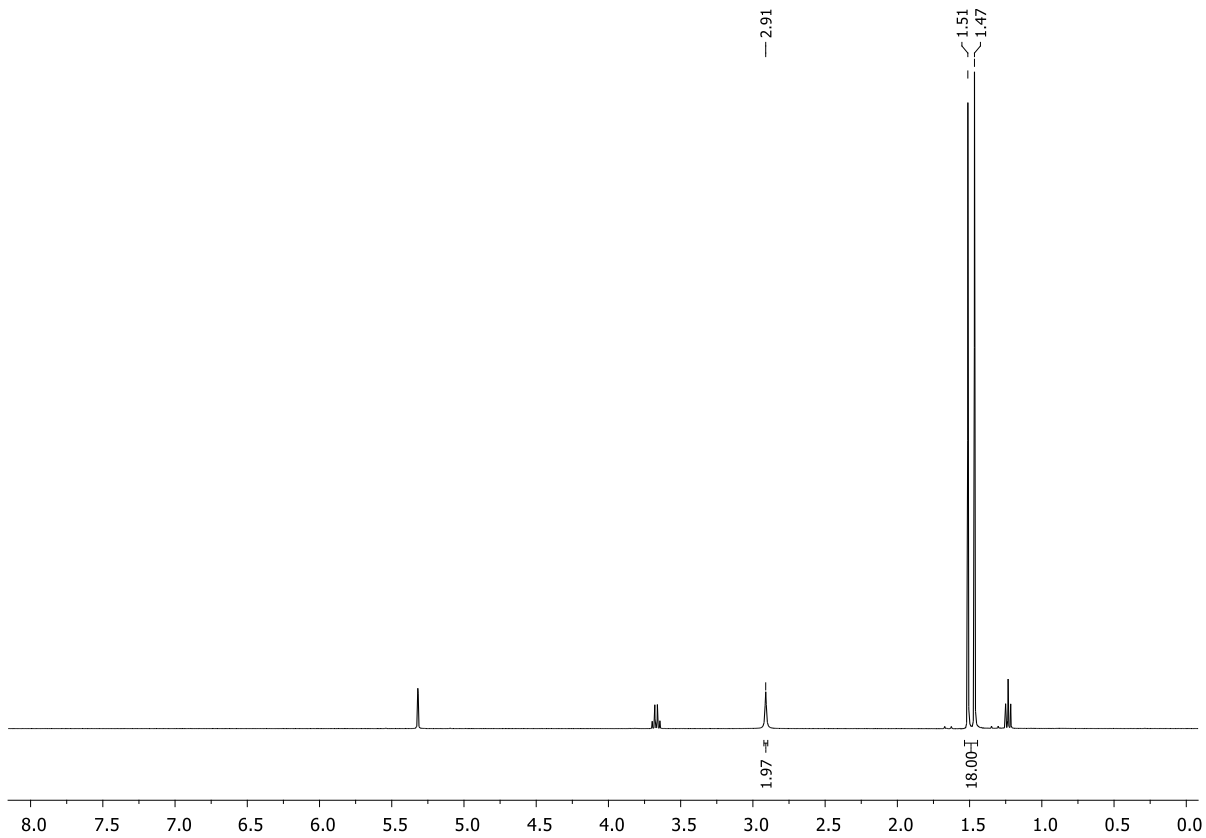

Figure S4.32. ^{1}H NMR spectrum (CD_2Cl_2, 298 K) of **(1–SD)$^+$ WCA$^–$**.

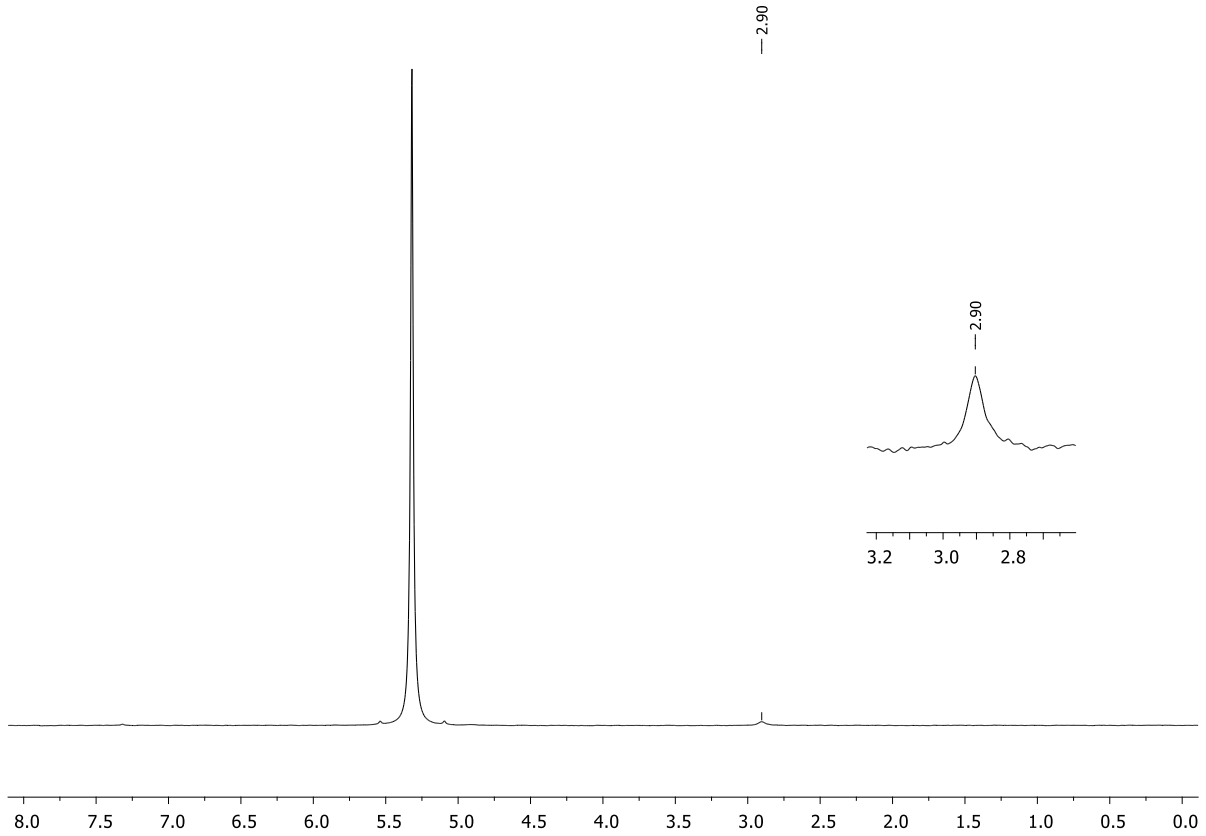

Figure S4.33. ^{2}H NMR spectrum (CH_2Cl_2/CD_2Cl_2 (9:1), 298 K) of **(1–SD)$^+$ WCA$^–$**.

4.6.2.4. Synthesis of (R_P)-*t*BuCy(PS)NH$_3^+$ Cl$^-$ {[(R_P)-2·HCl]$_4$}

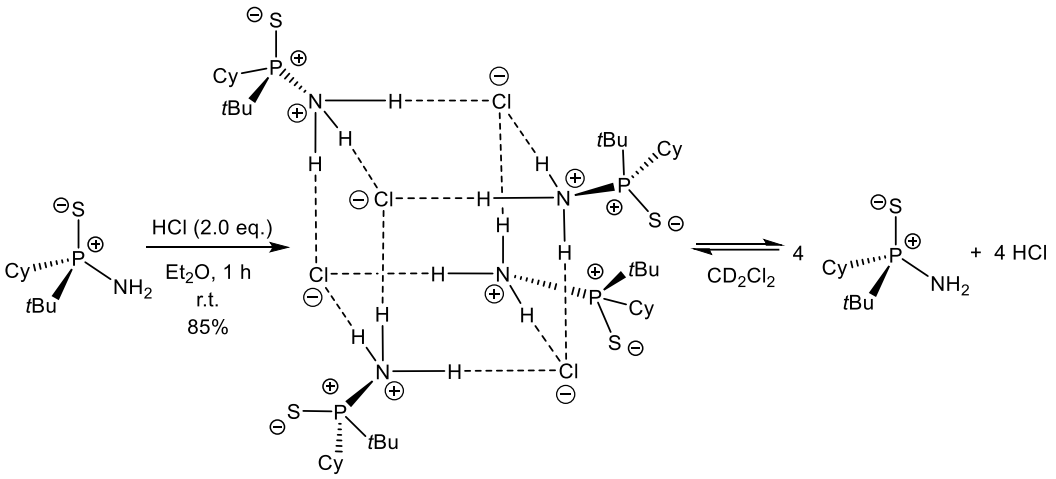

(R_P)-**2** was synthesized following a procedure published by our group.[1]

(R_P)-**2** (100 mg, 0.46 mmol, 1.0 equiv., e.r. > 99:1) was dissolved in diethyl ether (2 mL) and HCl (0.46 mL, 0.92 mmol, 2.0 equiv., 2.0 M in diethyl ether) was added dropwise at room temperature resulting in a colorless suspension after a few minutes. After 1 h of stirring, the solvent was removed *in vacuo* and the remaining solid further dried. **[(R_P)-2·HCl]$_4$** was obtained as a colorless solid (99 mg, 0.39 mmol, 85%). Crystals suitable for single crystal X-ray diffraction were grown from Et_2O by slow evaporation of the solvent.

^{1}H NMR (400.13 MHz, 100 mM in CD_2Cl_2, 298 K): δ = 1.34–1.20 (m, 3H, CH_2), 1.38 (d, $^3J_{H–P}$ = 17.5 Hz, 9H, PC(CH_3)$_3$), 1.72–1.52 (m, 3H, CH_2), 1.86–1.83 (m, 1H, CH_2), 1.98–1.92 (m, 2H, CH_2), 2.14–2.11 (m, 1H, CH_2), 2.38–2.32 (m, 1H, CH_2), 8.37 (br, 3H, NH_3). **^{31}P{^{1}H} NMR** (162.04 MHz, 100 mM in CD_2Cl_2, 298 K): δ = 99.7 (br). **^{13}C{^{1}H} NMR** (100.61 MHz, 100 mM in CD_2Cl_2, 298 K): δ = 25.8 (d, $^3J_{C–P}$ = 1.6 Hz, *C*H$_2$), 26.0 (d, $^2J_{C–P}$ = 1.8 Hz, PC(*C*H$_3$)$_3$), 26.6 (d, $^2J_{C–P}$ = 15.3 Hz, *C*H$_2$), 26.9 (d, $^2J_{C–P}$ = 13.4 Hz, *C*H$_2$), 27.4 (d, $^3J_{C–P}$ = 4.5 Hz, *C*H$_2$), 27.9 (s, *C*H$_2$), 38.2 (d, $^1J_{C–P}$ = 50.2 Hz, P*C*(CH$_3$)$_3$), 39.0 (d, $^1J_{C–P}$ = 49.3 Hz, P*C*H). **^{1}H NMR** (400.13 MHz, 5 mM in CD_2Cl_2, 298 K): δ = 1.22–1.18 (m, 1H, CH_2), 1.26 (d, $^3J_{H–P}$ = 16.0 Hz, 9H, PC(CH_3)$_3$), 1.26–1.25 (m, 1H, CH_2), 1.39–1.29 (m, 2H, CH_2), 1.60–1.44 (m, 2H, CH_2), 1.72–1.68 (m, 1H, CH_2), 1.99–1.80 (m, 4H, CH_2), 2.29 (br, 2H, NH_2). **^{31}P{^{1}H} NMR** (162.04 MHz, 5 mM in CD_2Cl_2, 298 K): δ = 87.0 (s). **^{13}C{^{1}H} NMR** (100.61 MHz, 5 mM in CD_2Cl_2, 298 K): δ = 25.3 (d, $^2J_{C–P}$ = 1.5 Hz, PC(*C*H$_3$)$_3$), P*C*(CH$_3$)$_3$, *C*H and *C*H$_2$ not visible. **Elemental analysis**: $C_{10}H_{23}ClNPS \cdot 0.2\ Et_2O$: calcd.: C 47.94, H 9.31, N 5.18; found: C 48.24, H 8.99, N 5.24.

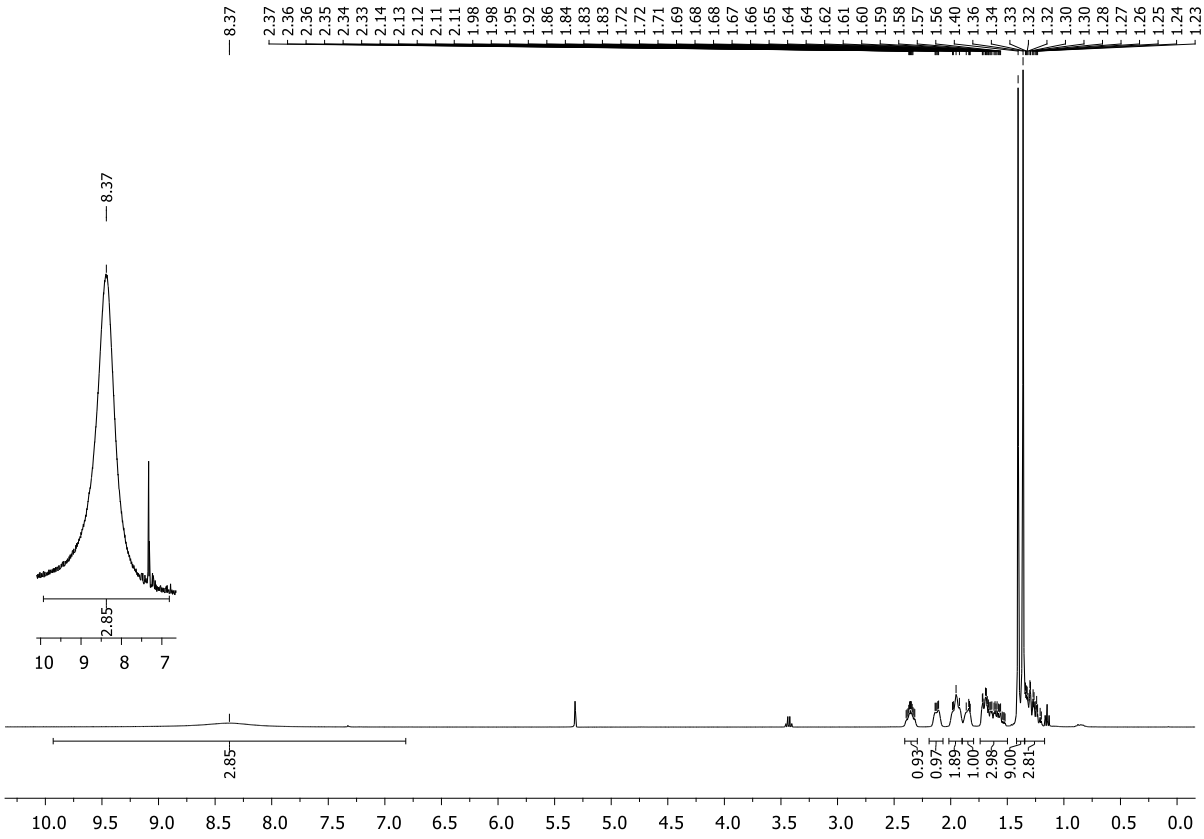

Figure S4.34. ^{1}H NMR spectrum (100 mM in CD_2Cl_2, 298 K) of **[(*R*$_P$)-2·HCl]$_4$**.

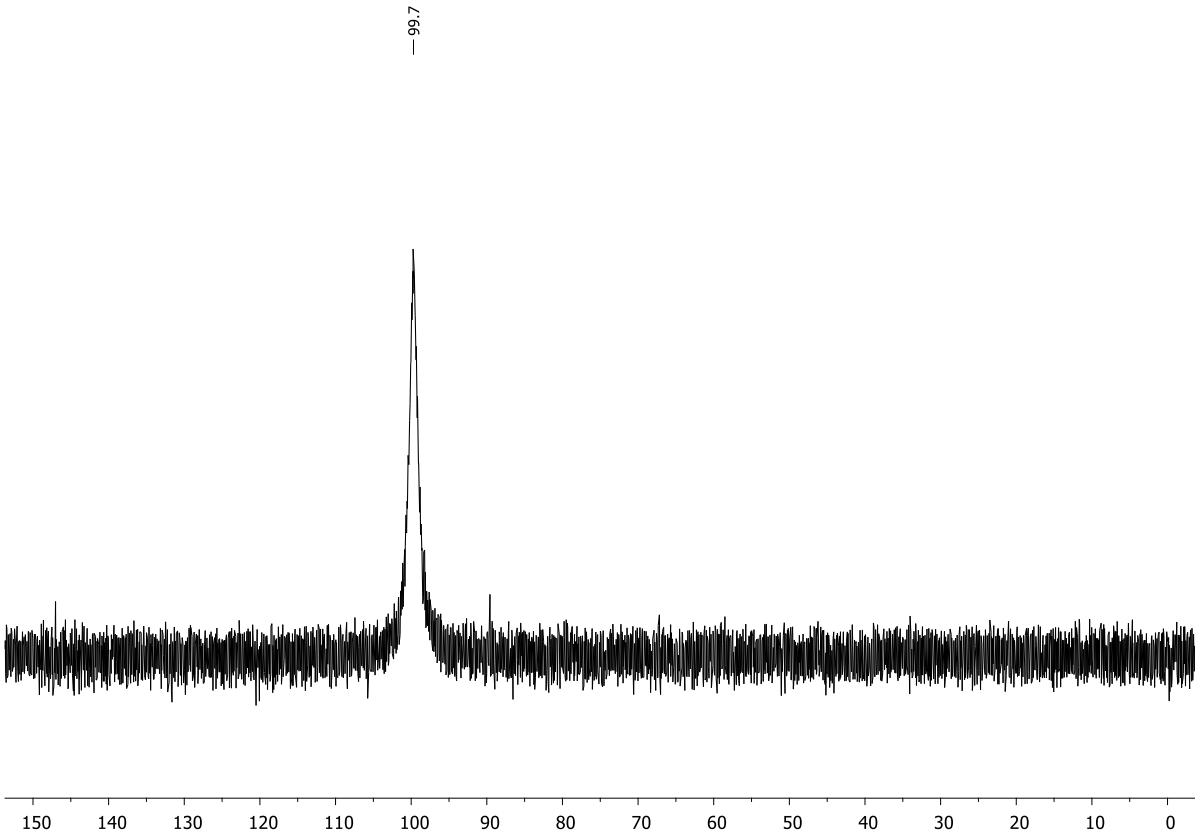

Figure S4.35. $^{31}P\{^{1}H\}$ NMR spectrum (100 mM in CD_2Cl_2, 298 K) of **[(*R*$_P$)-2·HCl]$_4$**.

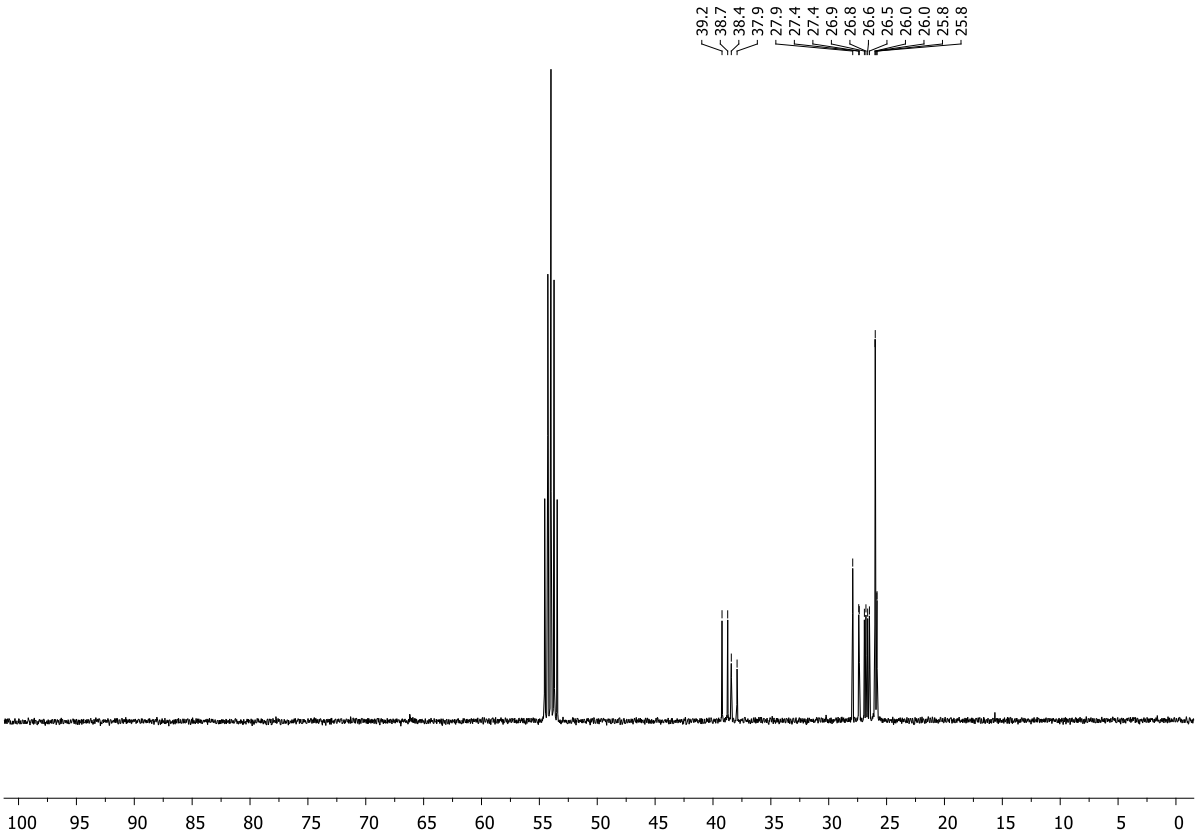

Figure S4.36. $^{13}C\{^{1}H\}$ NMR spectrum (100 mM in CD_2Cl_2, 298 K) of **[(*R*$_P$)-2·HCl]$_4$**.

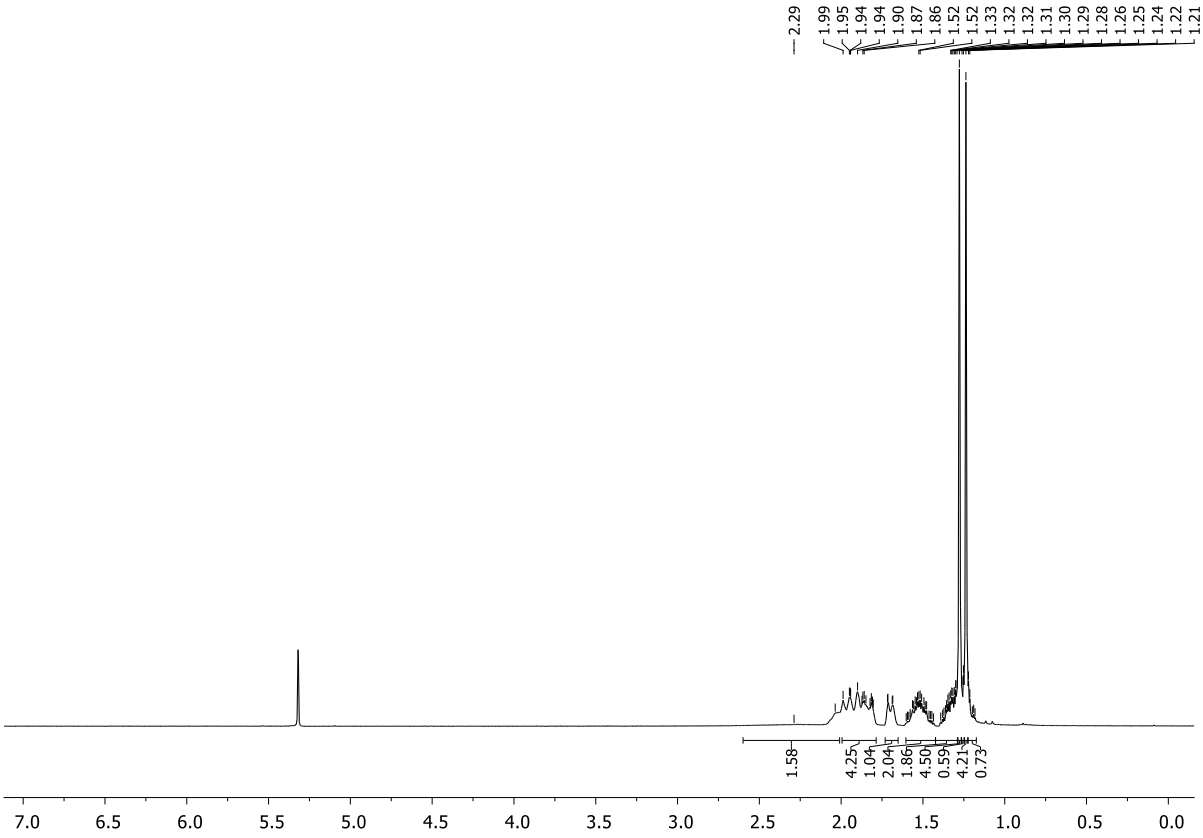

Figure S4.37. ^{1}H NMR spectrum (5 mM in CD_2Cl_2, 298 K) of (*R*$_P$)-**2 + HCl$_{solv}$**.

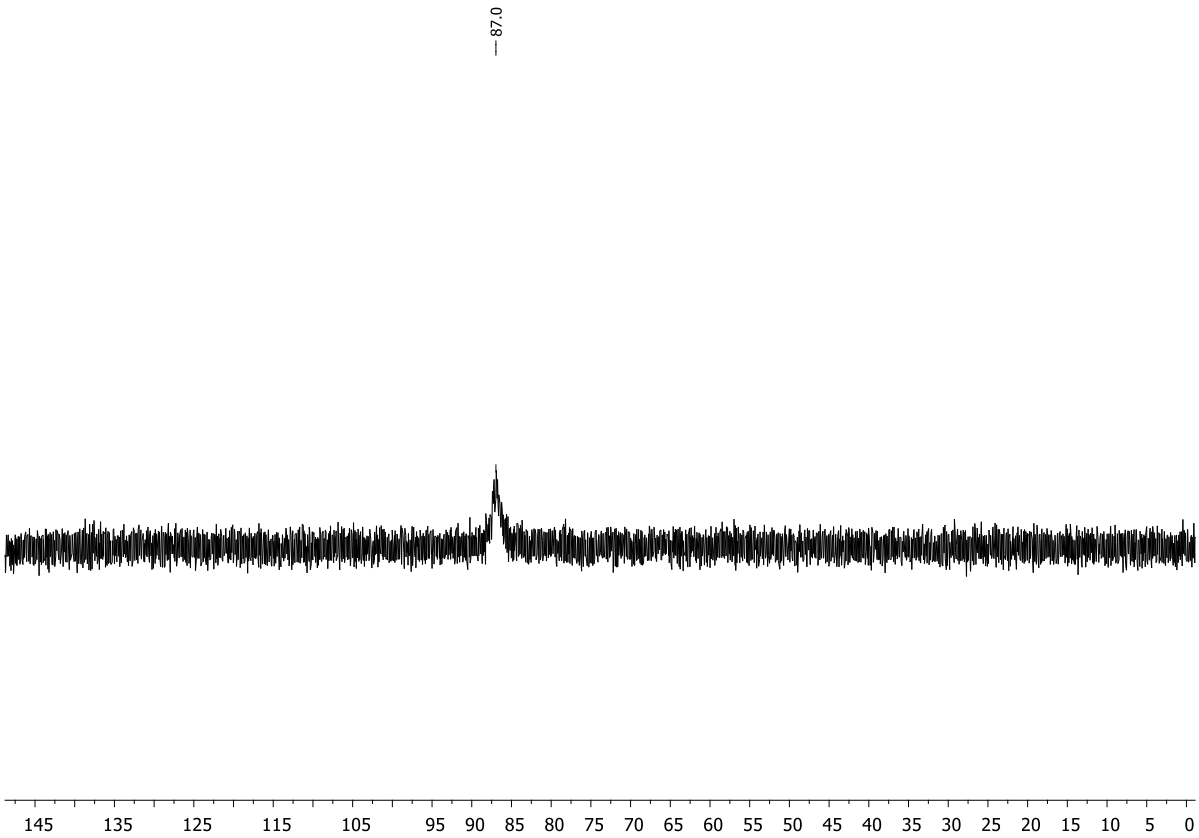

Figure S4.38. $^{31}P\{^{1}H\}$ NMR spectrum (5 mM in CD_2Cl_2, 298 K) of (R_P)-**2 + HCl$_{solv}$**.

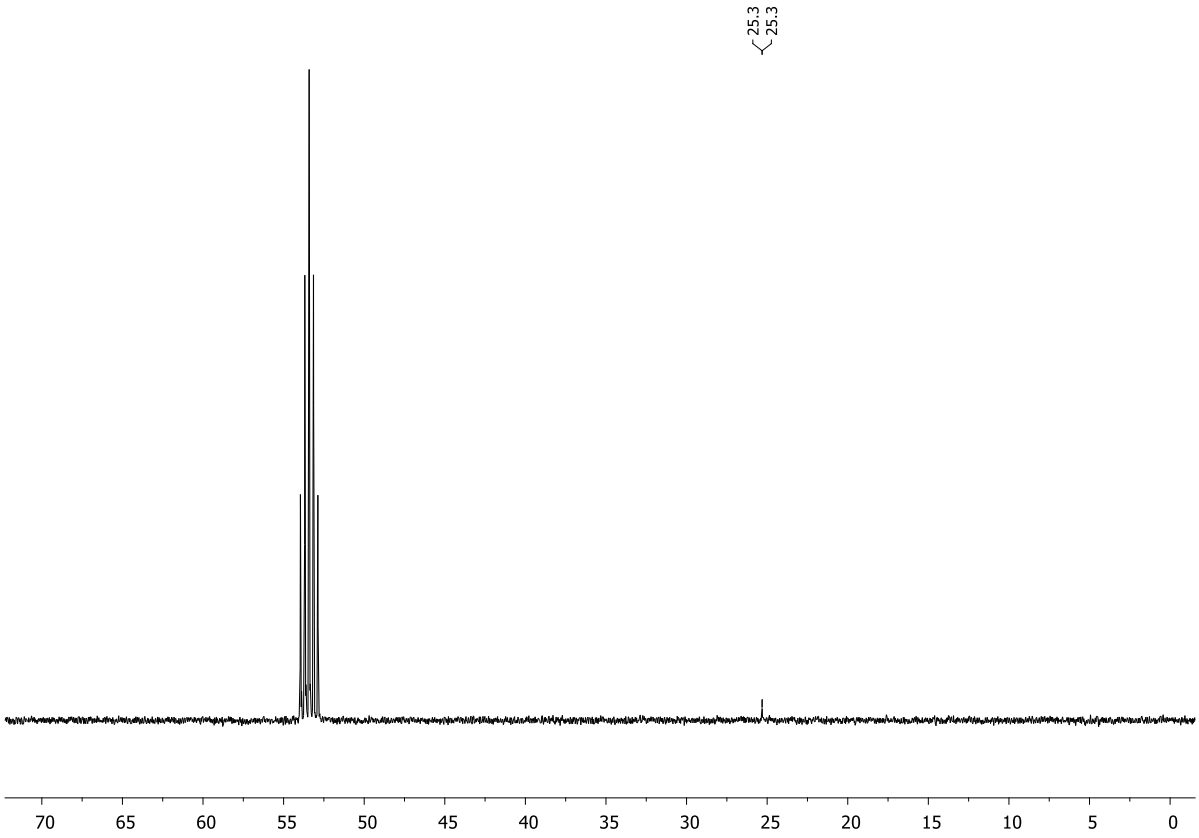

Figure S4.39. $^{13}C\{^{1}H\}$ NMR spectrum (5 mM in CD_2Cl_2, 298 K) of (R_P)-**2 + HCl$_{solv}$**.

4.6.2.5. Synthesis of (R_P)-*t*BuCy(P$^+$–SH)NH$_2$ B(C$_6$F$_5$)$_4^-$ {[(R_P)-2–SH]$^+$ WCA$^-$}

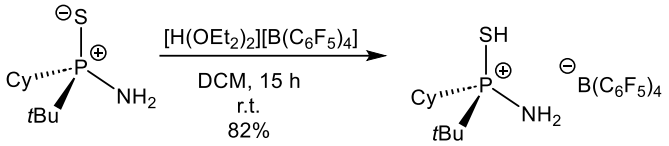

(R_P)-**2** [**[(R_P)-2–SH]$^+$ WCA$^-$**]

(R_P)-**2** was synthesized following a procedure published by our group.[1]

(R_P)-**2** (8.0 mg, 31.3 µmol, 1.0 equiv.) and [H(OEt$_2$)$_2$][B(C$_6$F$_5$)$_4$] (26 mg, 31.3 µmol, 1.0 equiv.) were dissolved in dichloromethane (1 mL) and the resulting suspension was stirred for 15 h at room temperature. All volatiles were removed *in vacuo* and the solid further dried. **[(R_P)-2–SH]$^+$ WCA$^-$** was obtained as a colorless solid (23 mg, 25.6 µmol, 82%).

^{1}H NMR (400.13 MHz, CD_2Cl_2, 298 K): δ = 1.21–1.35 (m, 1H, CH_2), 1.39–1.41 (m, 1H, CH_2), 1.40 (d, $^3J_{H–P}$ = 18.8 Hz, 9H, PC(CH_3)$_3$), 1.45–1.59 (m, 3H, CH_2), 1.78–1.84 (m, 1H, CH_2), 1.94–2.07 (m, 4H, CH_2), 2.37–2.45 (m, 1H, CH_2), 2.94 (s, 3H, NH_2/SH). **^{31}P{^{1}H} NMR** (162.04 MHz, CD_2Cl_2, 298 K): δ = 90.2 (s). **^{13}C{^{1}H} NMR** (100.61 MHz, CD_2Cl_2, 298 K): δ = 25.1 (s, PC(CH$_3$)$_3$), 25.4 (d, $^3J_{C–P}$ = 1.8 Hz, CH$_2$), 26.3 (d, $^2J_{C–P}$ = 15.1 Hz, CH$_2$), 26.4 (d, $^2J_{C–P}$ = 13.6 Hz, CH$_2$), 27.0 (d, $^3J_{C–P}$ = 5.1 Hz, CH$_2$), 28.0 (d, $^4J_{C–P}$ = 2.6 Hz, CH$_2$), 37.3 (d, $^1J_{C–P}$ = 51.3 Hz, PC(CH$_3$)$_3$), 37.7 (d, $^1J_{C–P}$ = 49.4 Hz, PCH), 124.7 (s, *ipso*-$C_{Ar\text{-}borate}$), 136.9 (d, $^1J_{C–F}$ = 246.9 Hz, *meta*-$C_{Ar\text{-}borate}$), 138.8 (d, $^1J_{C–F}$ = 246.7 Hz, *para*-$C_{Ar\text{-}borate}$), 148.8 (d, $^1J_{C–F}$ = 244.2 Hz, *ortho*-$C_{Ar\text{-}borate}$). **^{11}B{^{1}H} NMR** (128.43 MHz, CD_2Cl_2, 298 K): δ = −16.9 (s). **^{19}F{^{1}H} NMR** (376.66 MHz, CD_2Cl_2, 298 K): δ = −167.3 (m, 8F, *meta*-$F_{Ar\text{-}borate}$), −163.5 (m, 4F, *para*-$F_{Ar\text{-}borate}$), −132.9 (s, 8F, *ortho*-$F_{Ar\text{-}borate}$). **Elemental analysis**: $C_{34}H_{23}BF_{20}NPS$: calcd.: C 45.41, H 2.58, N 1.56; found: C 45.10, H 3.07, N 1.68.

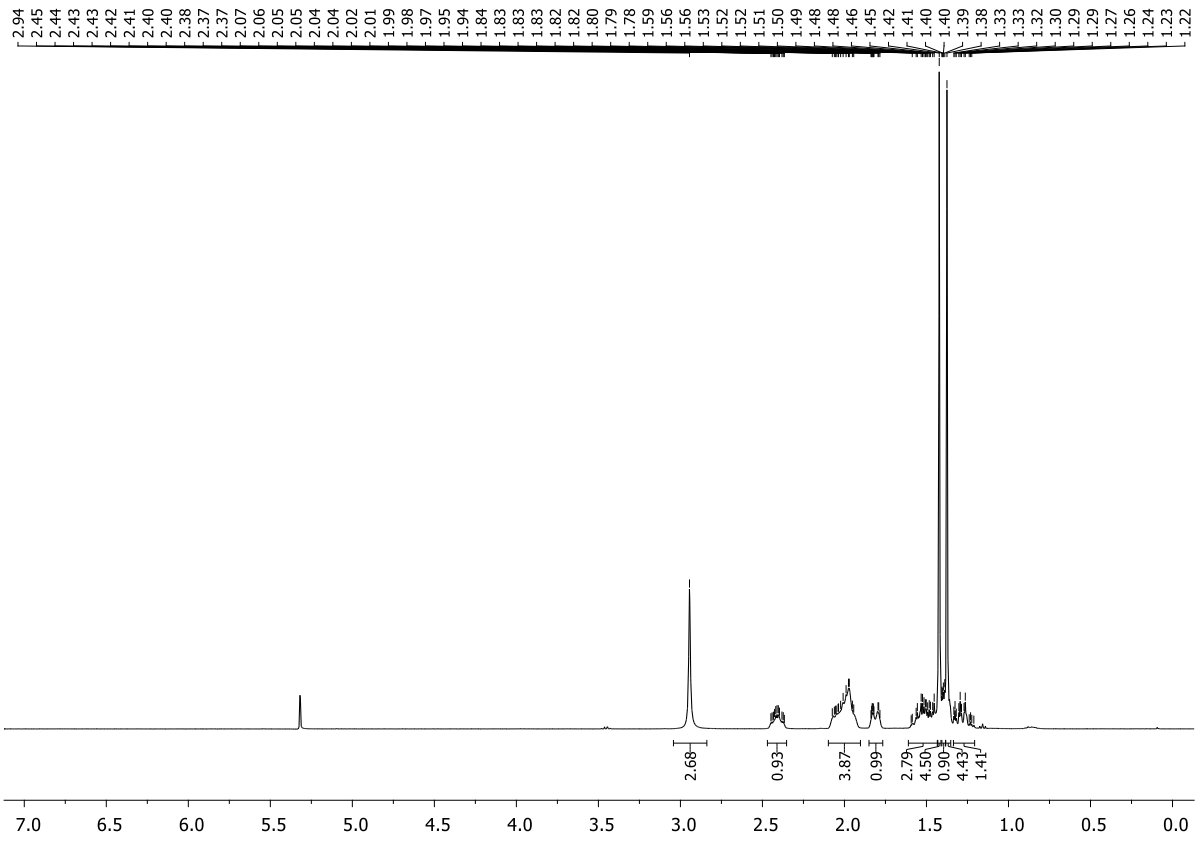

Figure S4.40. ^{1}H NMR spectrum (CD_2Cl_2, 298 K) of **[(R_P)-2–SH]$^+$ WCA$^–$**.

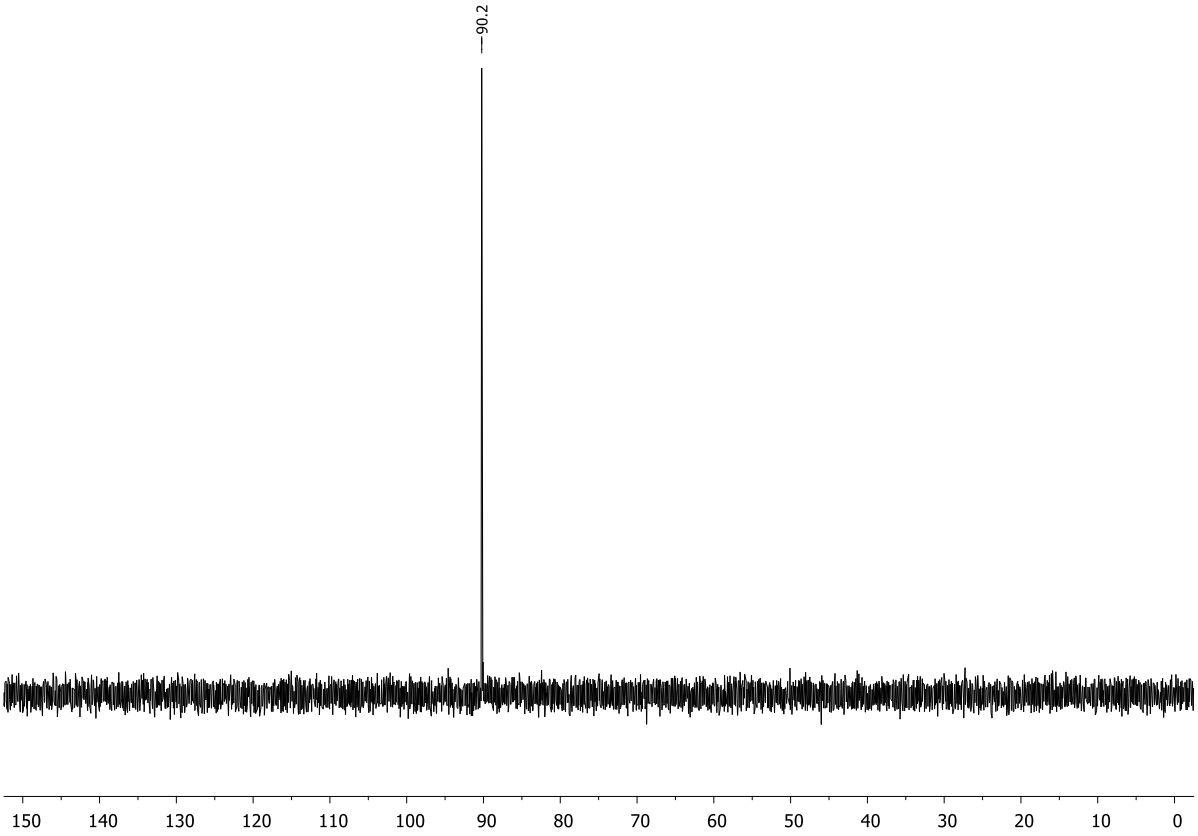

Figure S4.41. ^{31}P{^{1}H} NMR spectrum (CD_2Cl_2, 298 K) of **[(R_P)-2–SH]$^+$ WCA$^–$**.

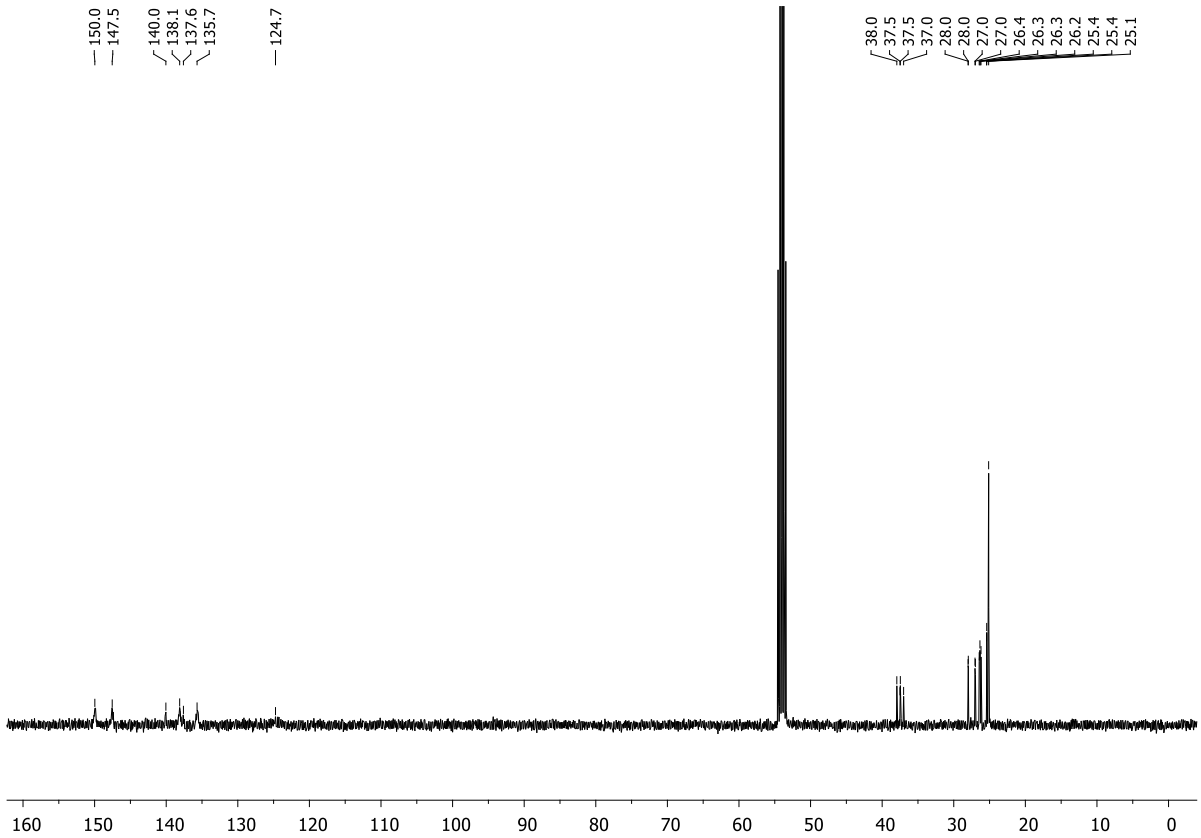

Figure S4.42. $^{13}C\{^{1}H\}$ NMR spectrum (CD_2Cl_2, 298 K) of **[(R_P)-2–SH]$^+$ WCA$^-$**.

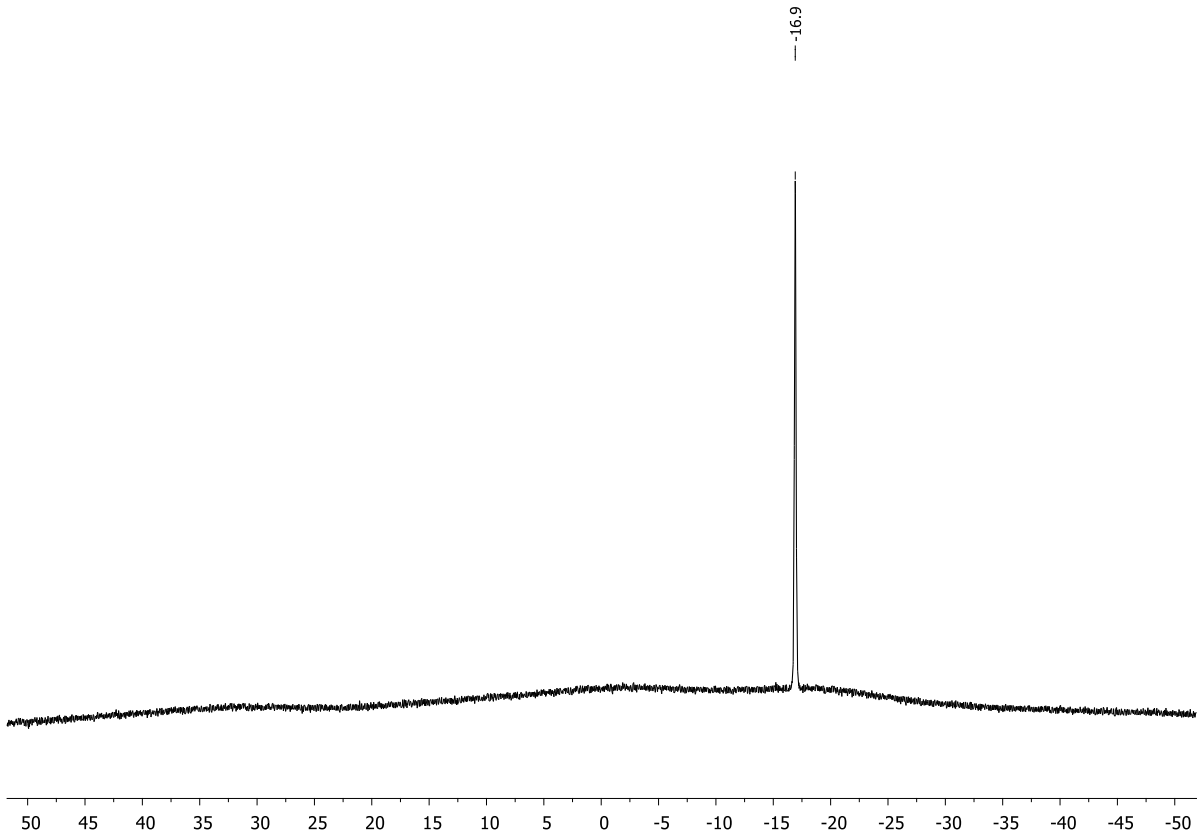

Figure S4.43. $^{11}B\{^{1}H\}$ NMR spectrum (CD_2Cl_2, 298 K) of **[(R_P)-2–SH]$^+$ WCA$^-$**.

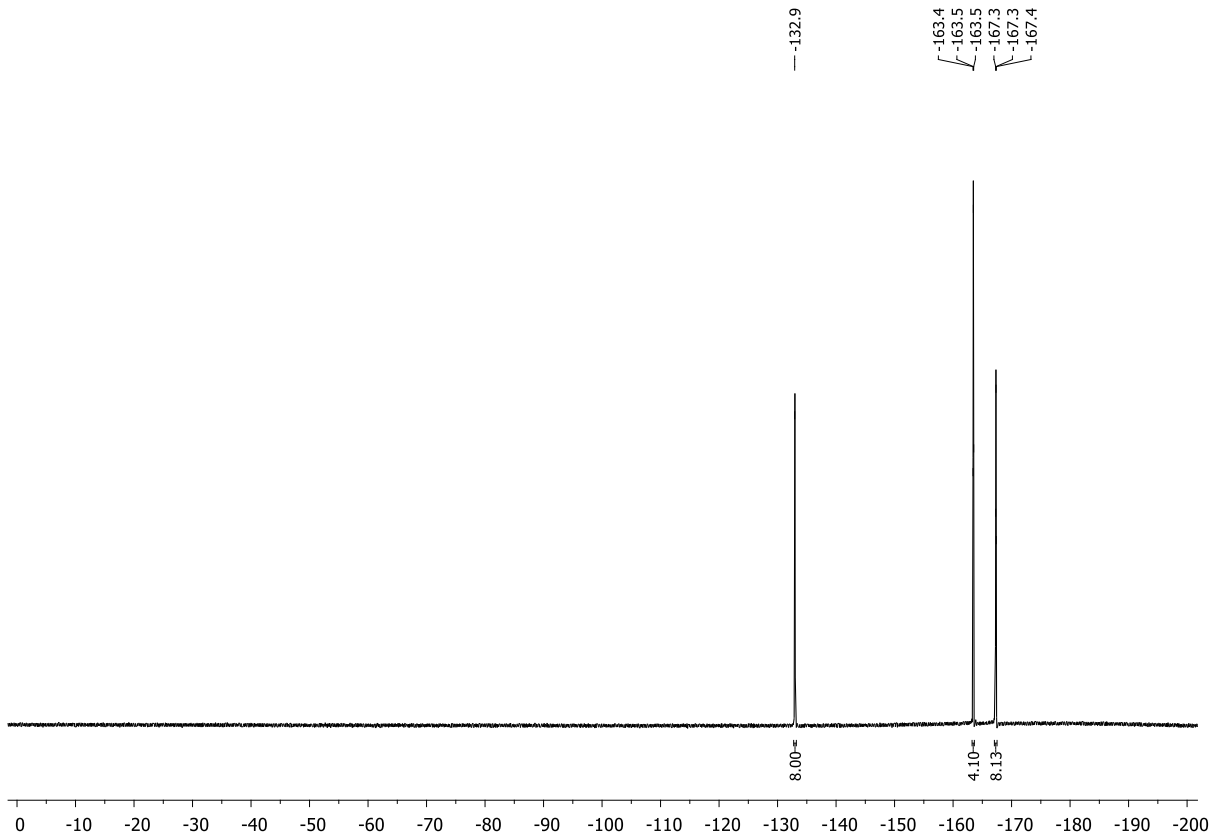

Figure S4.44. $^{19}F\{^{1}H\}$ NMR spectrum (CD_2Cl_2, 298 K) of **[(*R*$_P$)-2–SH]$^+$ WCA$^–$**.

4.6.2.6. Synthesis of *rac*-*t*BuCy(PS)NH$_3^+$ Cl$^-$ [(*rac*-2·HCl)$_4$]

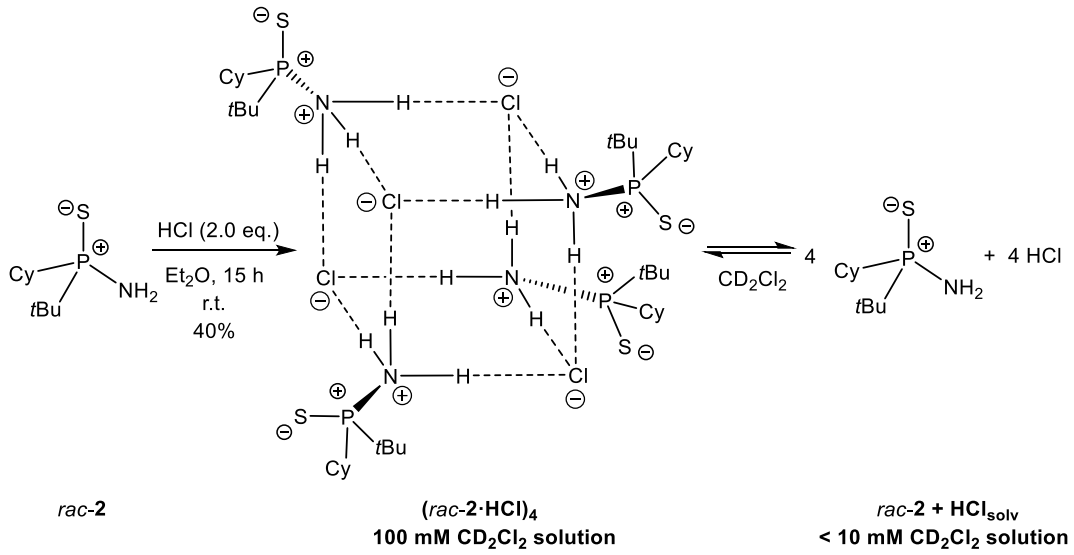

rac-**2** was synthesized following a procedure published by our group.[1]

rac-**2** (1.00 g, 4.56 mmol, 1.0 equiv.) was dissolved in diethyl ether (5 mL) and HCl (4.6 mL, 9.12 mmol, 2.0 equiv., 2.0 M in diethyl ether) was added dropwise at room temperature resulting in a colorless suspension after a few minutes. After 15 h of stirring, the solvent was removed *in vacuo* and the remaining solid further dried. **(*rac*-2·HCl)$_4$** was obtained as a colorless solid (0.47 g, 1.84 mmol, 40%).

^{1}H NMR (400.13 MHz, 100 mM in CD_2Cl_2, 298 K): δ = 1.34–1.20 (m, 3H, C*H*$_2$), 1.38 (d, $^3J_{H–P}$ = 17.4 Hz, 9H, PC(C*H*$_3$)$_3$), 1.66–1.44 (m, 2H, C*H*$_2$), 1.72–1.69 (m, 1H, C*H*$_2$), 1.87–1.84 (m, 1H, C*H*$_2$), 1.99–1.92 (m, 2H, C*H*$_2$), 2.13–2.10 (m, 1H, C*H*$_2$), 2.40–2.29 (m, 1H, C*H*$_2$), 8.64 (br, 3H, N*H*$_3$). **^{31}P{^{1}H} NMR** (162.04 MHz, 100 mM in CD_2Cl_2, 298 K): δ = 100.3 (br). **^{13}C{^{1}H} NMR** (100.61 MHz, 100 mM in CD_2Cl_2, 298 K): δ = 25.9 (d, $^3J_{C–P}$ = 1.3 Hz, *C*H$_2$), 26.2 (d, $^2J_{C–P}$ = 1.3 Hz, PC(*C*H$_3$)$_3$), 26.8 (d, $^2J_{C–P}$ = 14.6 Hz, *C*H$_2$), 27.1 (d, $^2J_{C–P}$ = 12.9 Hz, *C*H$_2$), 27.2 (d, $^3J_{C–P}$ = 4.0 Hz, *C*H$_2$), 28.6 (s, *C*H$_2$), 36.8 (d, $^1J_{C–P}$ = 59.3 Hz, P*C*(CH$_3$)$_3$), 38.6 (d, $^1J_{C–P}$ = 56.5 Hz, P*C*H). **^{1}H NMR** (400.13 MHz, 5 mM in CD_2Cl_2, 298 K): δ = 1.23 (d, $^3J_{H–P}$ = 15.8 Hz, 9H, PC(C*H*$_3$)$_3$), 1.37–1.29 (m, 2H, C*H*$_2$), 1.58–1.41 (m, 3H, C*H*$_2$), 1.71–1.67 (m, 1H, C*H*$_2$), 1.89–1.78 (m, 3H, C*H*$_2$), 1.92 (br, 2H, N*H*$_2$), 2.02–1.92 (m, 2H, C*H*$_2$). **^{31}P{^{1}H} NMR** (162.04 MHz, 5 mM in CD_2Cl_2, 298 K): δ = 86.7 (s). **^{13}C{^{1}H} NMR** (100.61 MHz, 5 mM in CD_2Cl_2, 298 K): δ = 25.3 (d, $^3J_{C–P}$ = 1.4 Hz, *C*H$_2$), 25.7 (d, $^2J_{C–P}$ = 1.9 Hz, PC(*C*H$_3$)$_3$), 26.3 (d, $^2J_{C–P}$ = 14.5 Hz, *C*H$_2$), 26.5 (d, $^2J_{C–P}$ = 12.9 Hz, *C*H$_2$), 26.6 (d, $^3J_{C–P}$ = 3.9 Hz, *C*H$_2$), 28.1 (s, *C*H$_2$), 38.0 (d, $^1J_{C–P}$ = 58.1 Hz, P*C*H), P*C*(CH$_3$)$_3$ not visible.

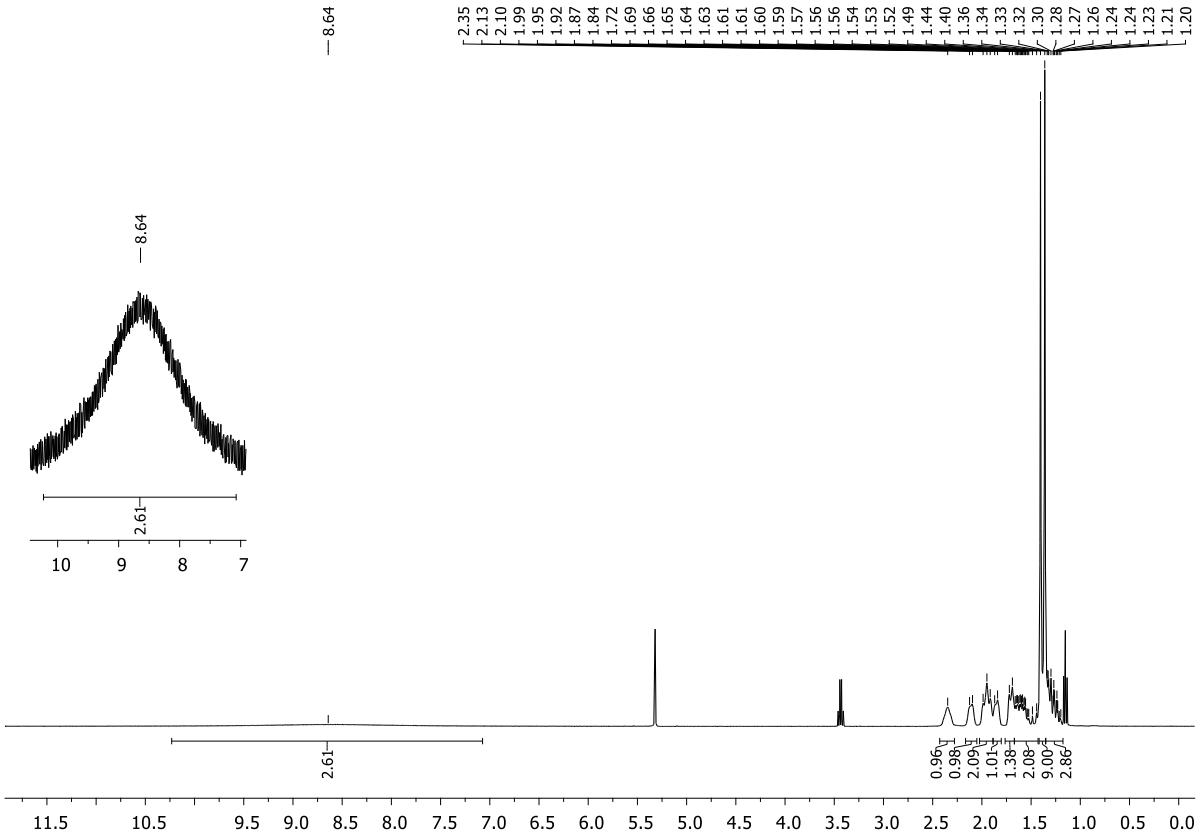

Figure S4.45. ^{1}H NMR spectrum (100 mM in CD_2Cl_2, 298 K) of **(*rac*-2·HCl)$_4$**.

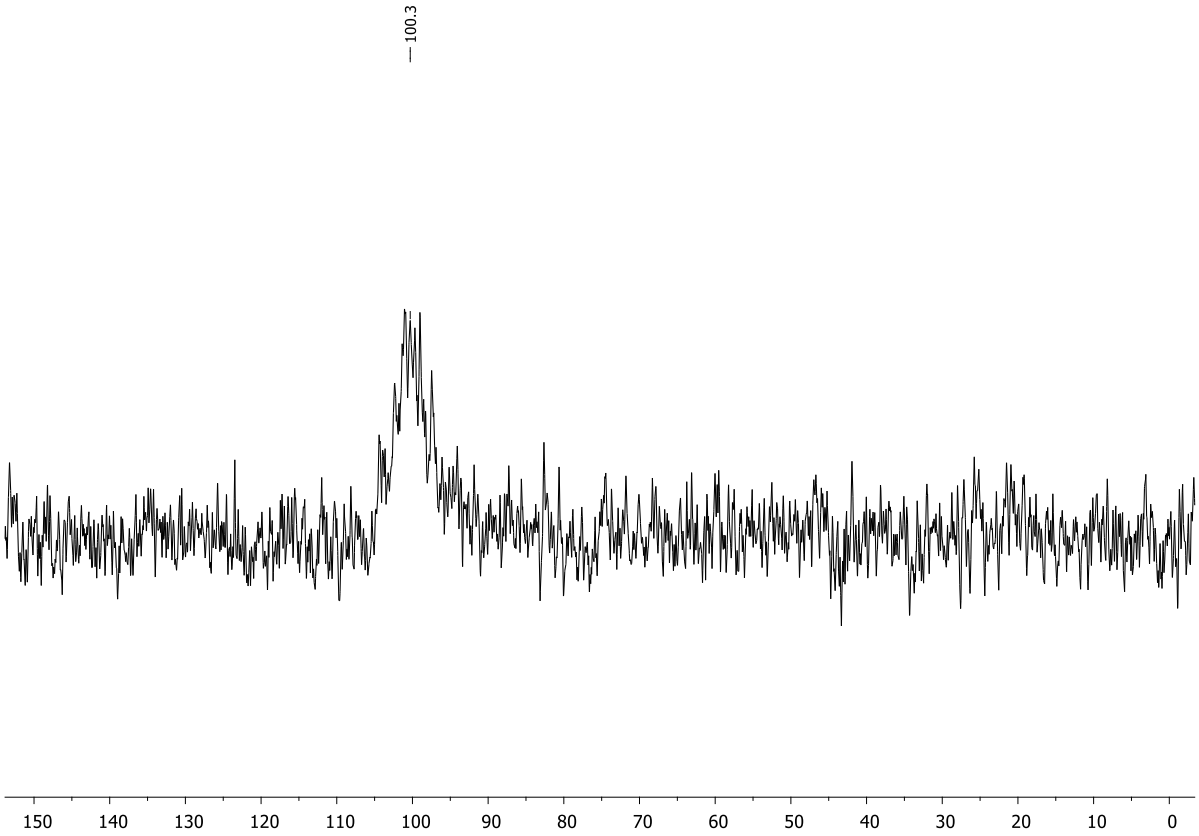

Figure S4.46. $^{31}P\{^{1}H\}$ NMR spectrum (100 mM in CD_2Cl_2, 298 K) of **(*rac*-2·HCl)$_4$**.

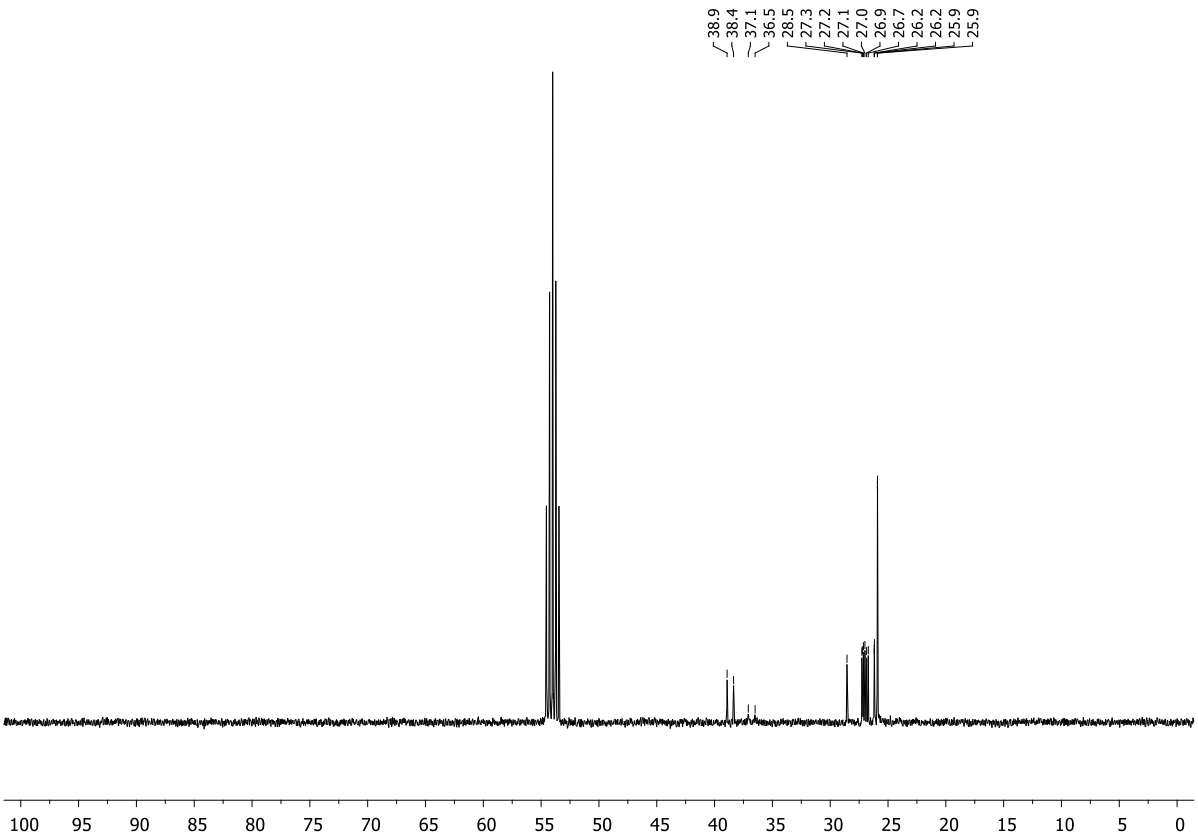

Figure S4.47. $^{13}C\{^{1}H\}$ NMR spectrum (100 mM in CD_2Cl_2, 298 K) of **(*rac*-2·HCl)$_4$**.

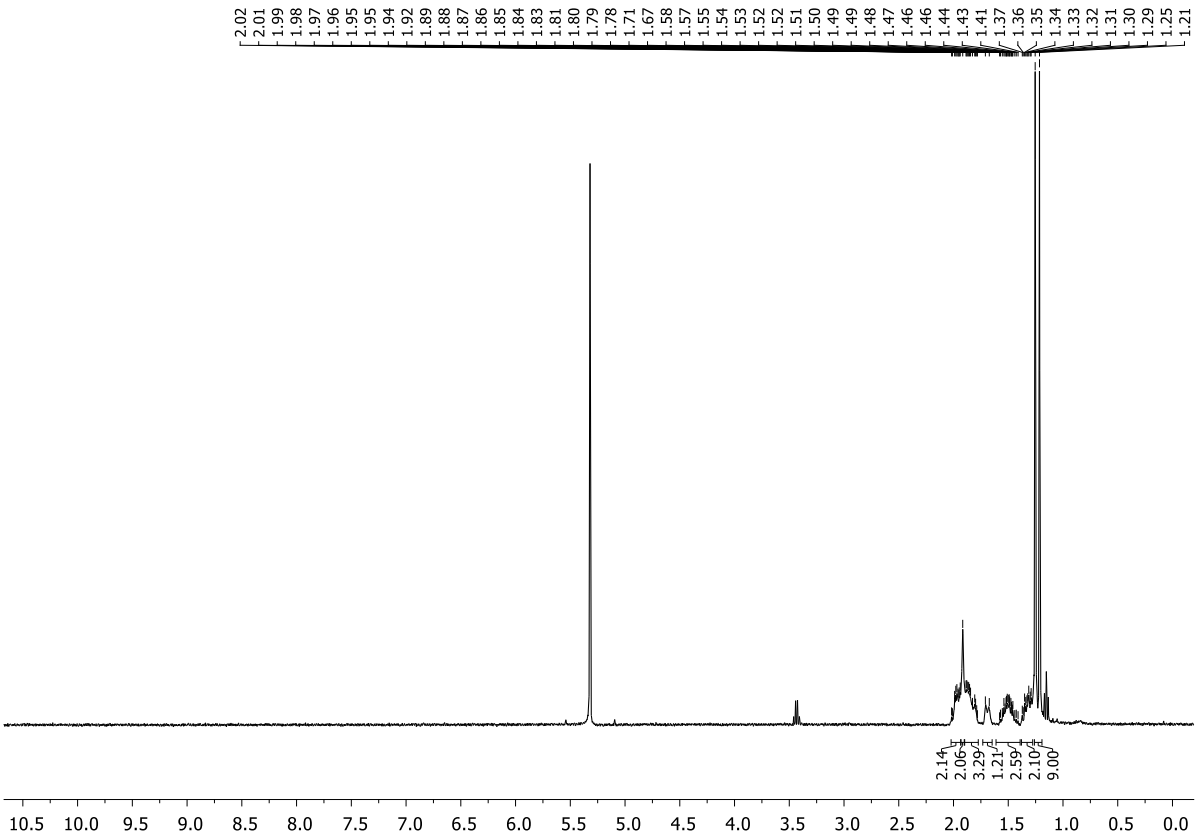

Figure S4.48. ^{1}H NMR spectrum (5 mM in CD_2Cl_2, 298 K) of *rac*-**2 + HCl$_{solv}$**.

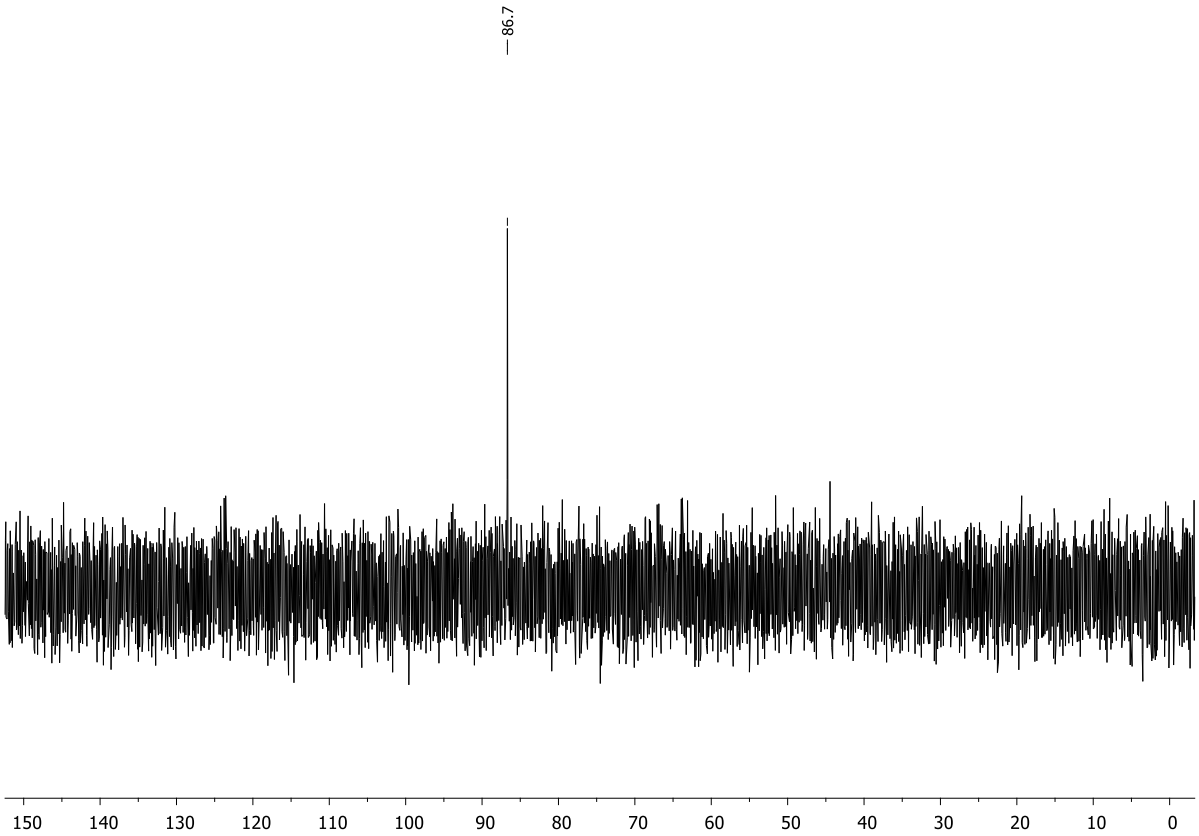

Figure S4.49. $^{31}P\{^{1}H\}$ NMR spectrum (5 mM in CD_2Cl_2, 298 K) of *rac*-**2 + HCl$_{solv}$**.

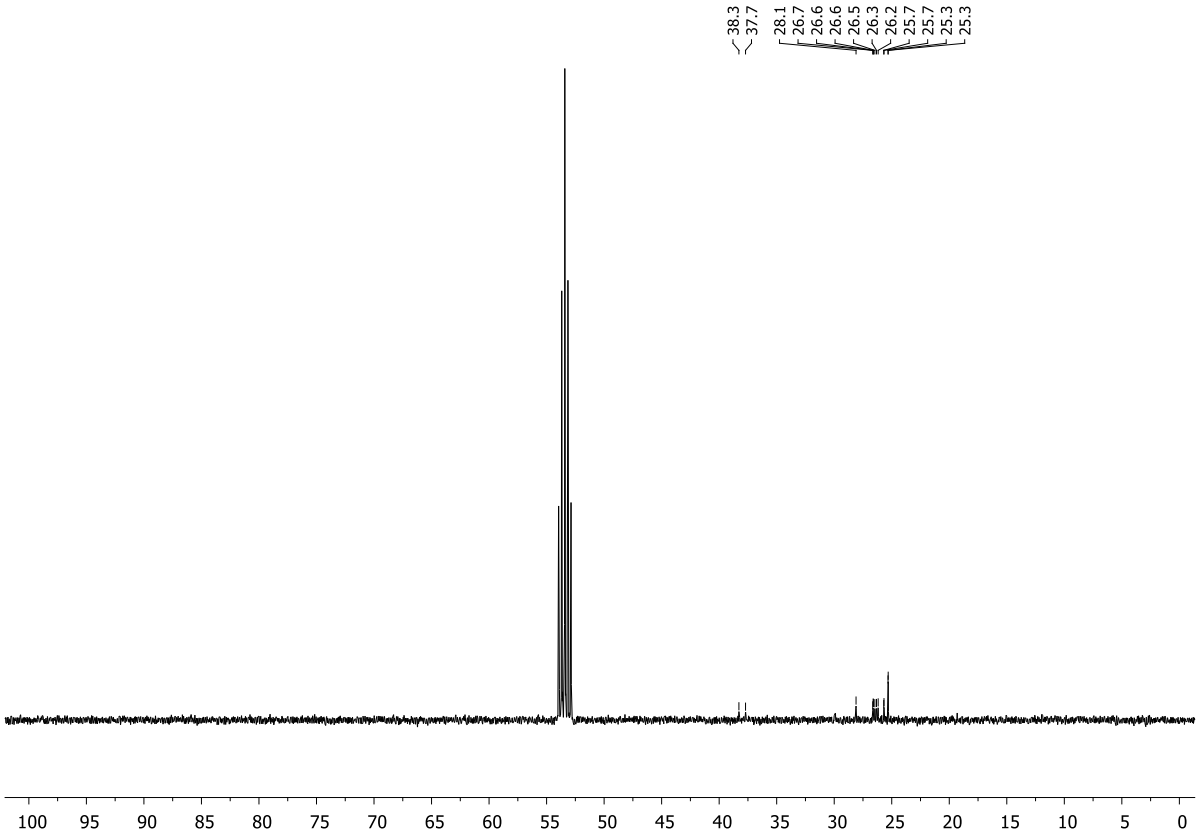

Figure S4.50. $^{13}C\{^{1}H\}$ NMR spectrum (5 mM in CD_2Cl_2, 298 K) of rac-**2 + HCl$_{solv}$**.

4.6.2.7. Synthesis of *rac*-*t*BuCy(P$^+$–SH)NH$_2$ B(C$_6$F$_5$)$_4^-$ [(*rac*-2–SH)$^+$ WCA$^-$]

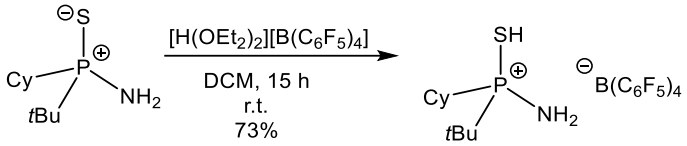

rac-**2** (*rac*-**2–SH)$^+$ WCA$^-$**

rac-**2** was synthesized following a procedure published by our group.[1]

rac-**2** (24 mg, 0.11 mmol, 1.0 equiv.) and [H(OEt$_2$)$_2$][B(C$_6$F$_5$)$_4$] (90 mg, 0.11 mmol, 1.0 equiv.) were dissolved in dichloromethane (1 mL) and the resulting suspension was stirred for 15 h at room temperature. All volatiles were removed *in vacuo* and the solid further dried. **(***rac*-**2–SH)$^+$ WCA$^-$** was obtained as a colorless solid (70 mg, 0.08 mmol, 73%).

^{1}H NMR (400.13 MHz, CD_2Cl_2, 298 K): δ = 1.23–1.38 (m, 2H, C*H*$_2$), 1.41–1.43 (m, 1H, C*H*$_2$), 1.42 (d, $^3J_{H–P}$ = 19.3 Hz, 9H, PC(C*H*$_3$)$_3$), 1.46–1.61 (m, 3H, C*H*$_2$), 1.80–1.84 (m, 1H, C*H*$_2$), 1.91–2.09 (m, 4H, C*H*$_2$), 2.43–2.52 (m, 1H, C*H*$_2$), 2.99 (s, 3H, N*H*$_2$/S*H*). **^{31}P{^{1}H} NMR** (162.04 MHz, CD_2Cl_2, 298 K): δ = 90.4 (s).

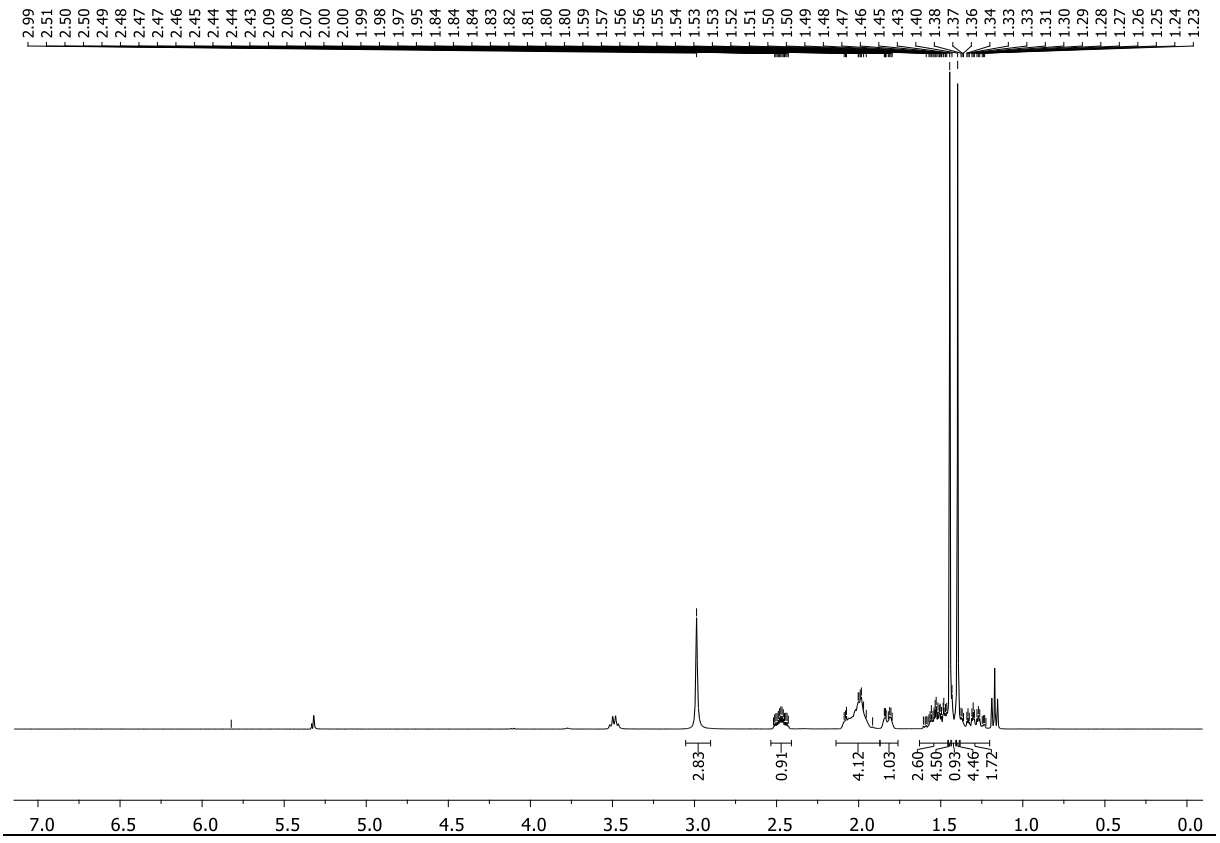

Figure S4.51. ^{1}H NMR spectrum (CD_2Cl_2, 298 K) of **(*rac*-2–SH)$^+$ WCA$^-$**.

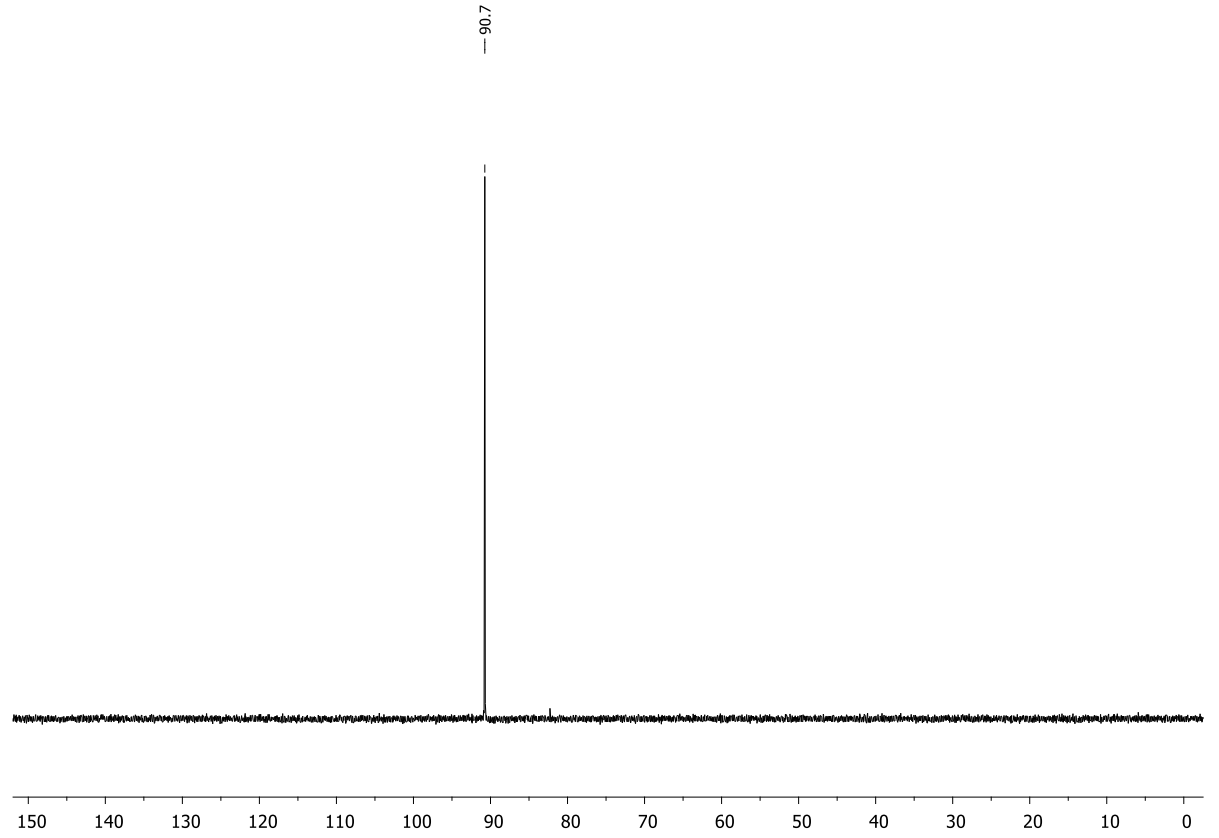

Figure S4.52. $^{31}P\{^{1}H\}$ NMR spectrum (CD_2Cl_2, 298 K) of **(*rac*-2–SH)$^+$ WCA$^-$**.

4.6.2.8. Synthesis of *t*Bu$_2$(PS)Cl (3)

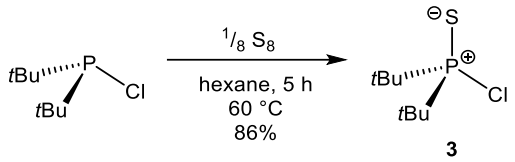

3 was synthesized in a modified literature procedure.[4]
Di-*tert*-butylchlorophosphine (2.00 g, 11.1 mmol, 1.0 equiv.) and sulfur (0.36 g, 11.1 mmol, 1.0 equiv.) were suspended in *n*-hexane (10 mL) and heated to 60 °C for 5 h. The solvent was removed *in vacuo* and the remaining solid was extracted with the minimum amount of *n*-pentane. After removal of insoluble solids *via* cannula filtration, the solvent was removed *in vacuo* to obtain **3** as a colorless solid (2.02 g, 9.50 mmol, 86%).

^{1}H NMR (400.13 MHz, C_6D_6, 298 K): δ = 1.21 (d, $^3J_{H–P}$ = 18.2 Hz, 18H, PC(C*H*$_3$)$_3$). **^{31}P{^{1}H} NMR** (162.04 MHz, C_6D_6, 298 K): δ = 145.3 (s). **^{13}C{^{1}H} NMR** (100.61 MHz, C_6D_6, 298 K): δ = 27.5 (d, $^2J_{C–P}$ = 2.0 Hz, PC(*C*H$_3$)$_3$), 45.2 (d, $^1J_{C–P}$ = 40.8 Hz, P*C*(CH$_3$)$_3$). **^{1}H NMR** (400.13 MHz, CD_2Cl_2, 298 K): δ = 1.46 (d, $^3J_{H–P}$ = 18.4 Hz, 18H, PC(C*H*$_3$)$_3$). **^{31}P{^{1}H} NMR** (162.04 MHz, CD_2Cl_2, 298 K): δ = 146.4 (s). **^{13}C{^{1}H} NMR** (100.61 MHz, CD_2Cl_2, 298 K): δ = 27.9 (d, $^2J_{C–P}$ = 2.0 Hz, PC(*C*H$_3$)$_3$), 45.7 (d, $^1J_{C–P}$ = 39.9 Hz, P*C*(CH$_3$)$_3$). **Elemental analysis**: $C_8H_{18}ClPS$: calcd.: C 45.17, H 8.53; found: C 45.01, H 8.21. **HR(EI+)-MS**: calcd. *m/z* for $C_8H_{18}ClPS$ [M$^{+\cdot}$]: 212.0550, found: 212.0556.

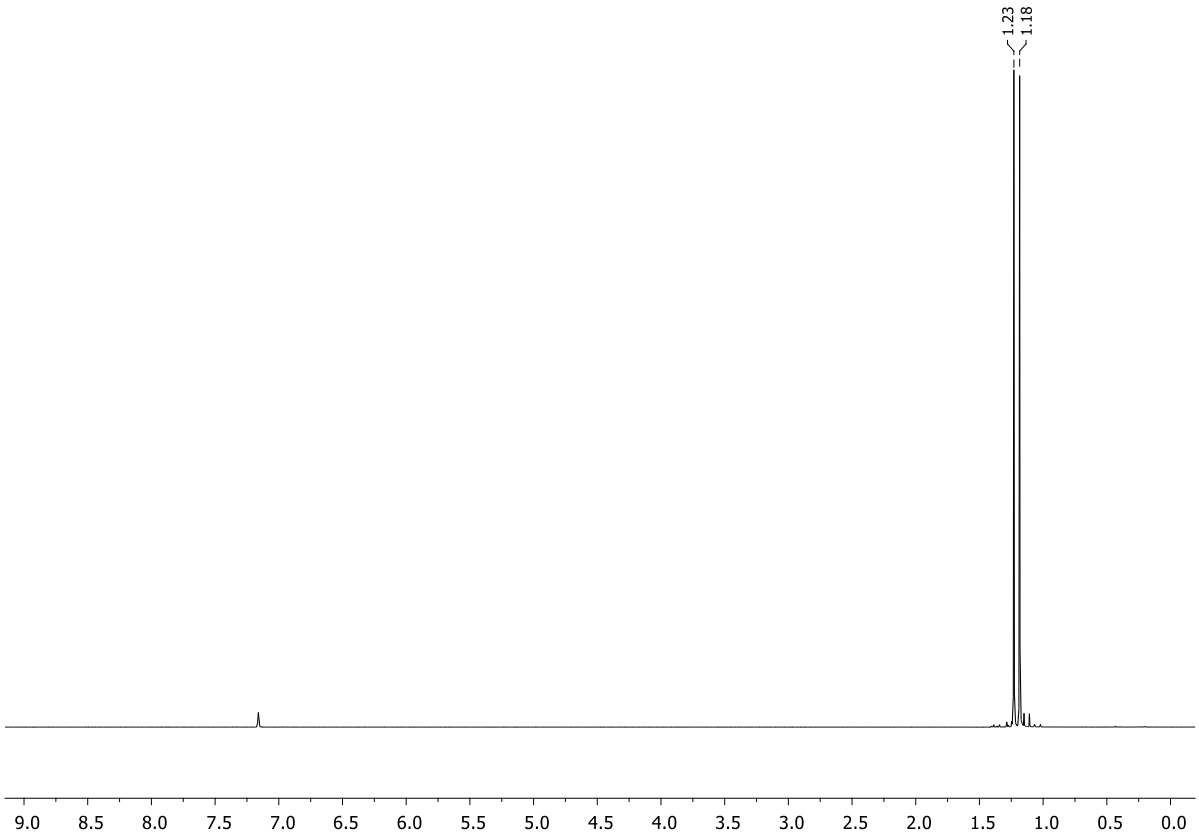

Figure S4.53. ^{1}H NMR spectrum (C_6D_6, 298 K) of **3**.

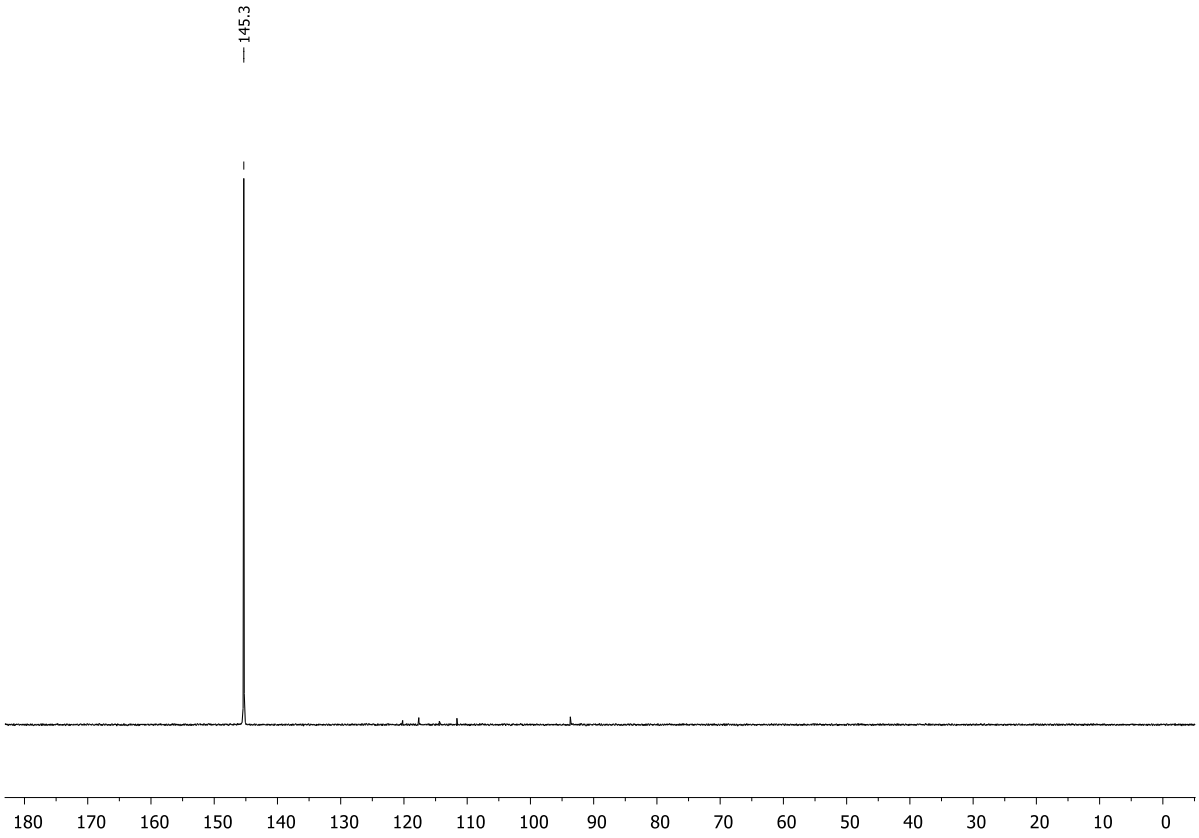

Figure S4.54. $^{31}P\{^{1}H\}$ NMR spectrum (C_6D_6, 298 K) of **3**.

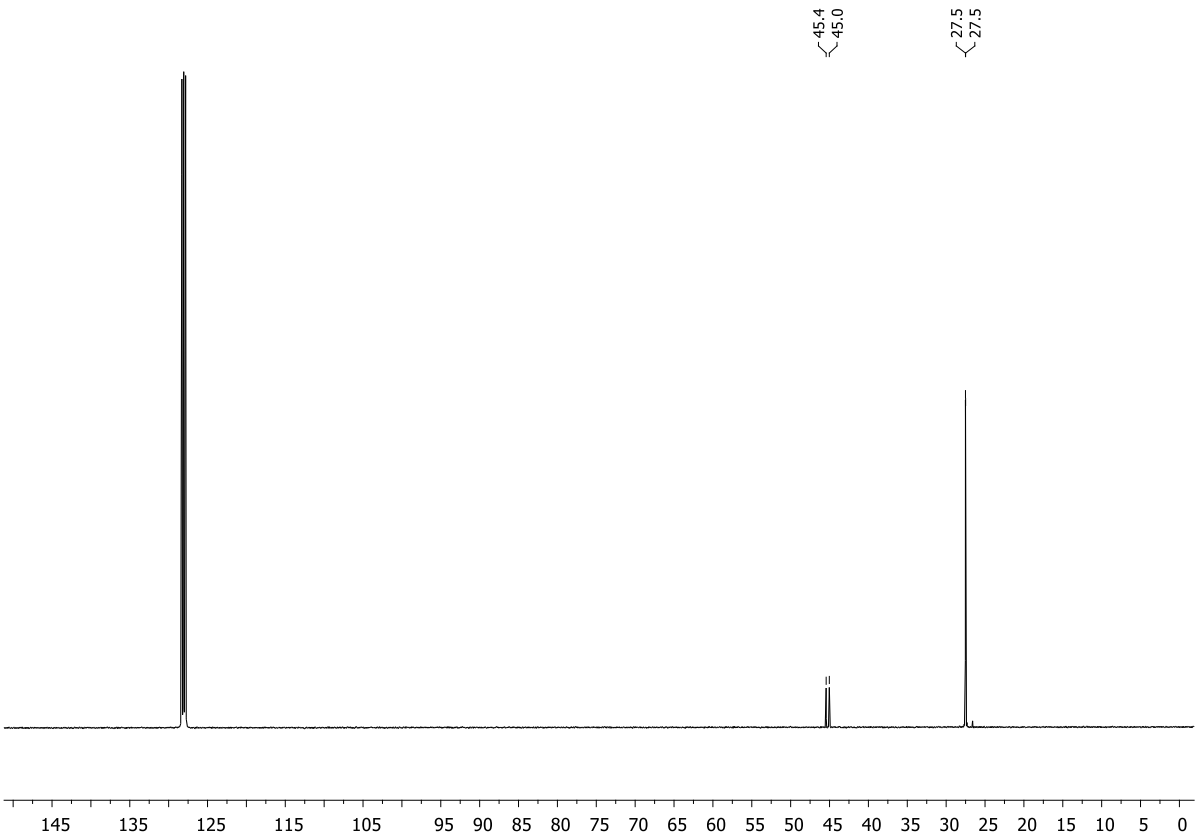

Figure S4.55. $^{13}C\{^{1}H\}$ NMR spectrum (C_6D_6, 298 K) of **3**.

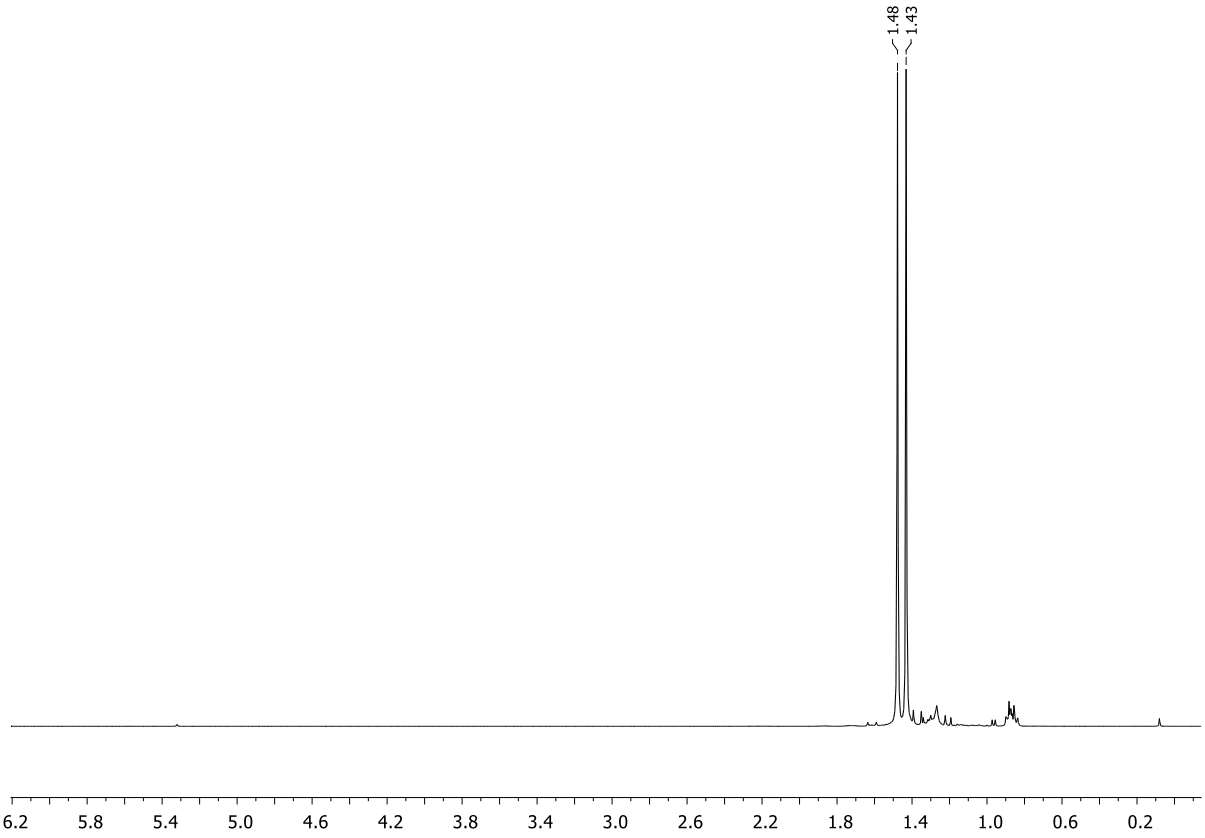

Figure S4.56. ^{1}H NMR spectrum (CD_2Cl_2, 298 K) of **3**.

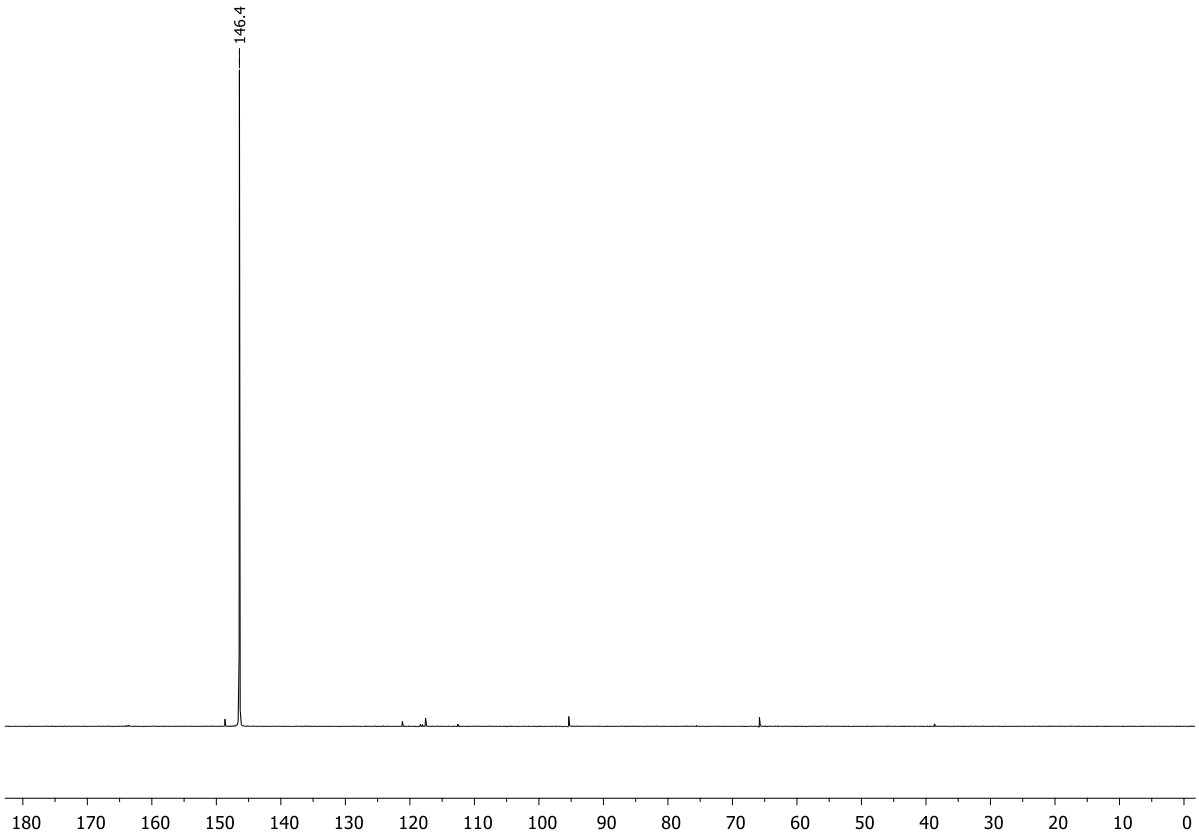

Figure S4.57. $^{31}P\{^{1}H\}$ NMR spectrum (CD_2Cl_2, 298 K) of **3**.

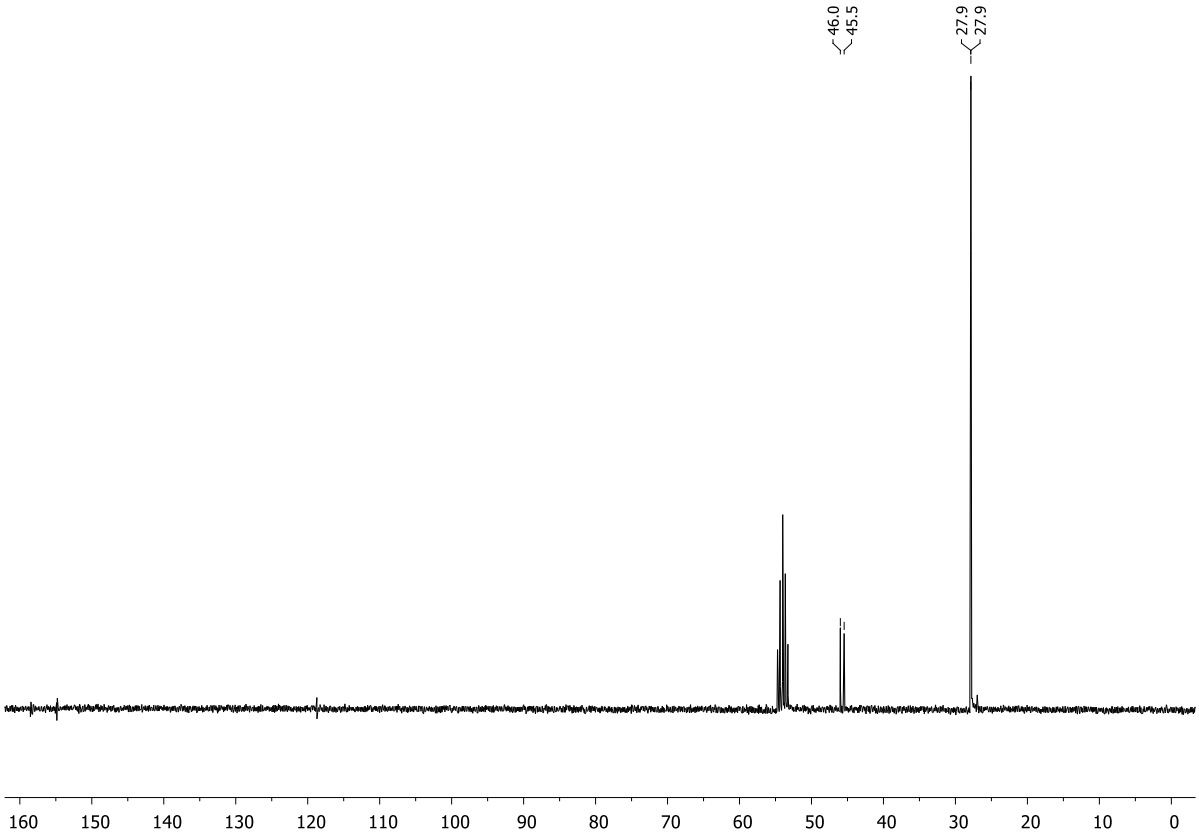

Figure S4.58. $^{13}C\{^{1}H\}$ NMR spectrum (CD_2Cl_2, 298 K) of **3**.

4.6.2.9. Synthesis of *t*Bu$_2$(PSe)NH$_2$ (4)

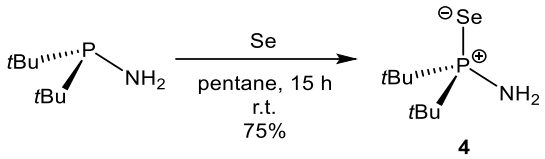

4

Amino-di-*tert*-butylphosphine (3.00 g, 18.6 mmol, 1.0 equiv.) was added dropwise to a suspension of grey selenium (1.47 g, 18.6 mmol, 1.0 equiv.) in *n*-pentane (20 mL). The reaction mixture was stirred for 15 h yielding a light grey suspension. The liquid phase was removed by cannula filtration and the remaining solid was extracted with the minimum amount of diethyl ether. After removal of insoluble solids *via* cannula filtration, the solvent was removed *in vacuo* to obtain **4** as a colorless solid (3.33 g, 13.9 mmol, 75%). Crystals suitable for single crystal X-ray diffraction were obtained at the wall of the reaction Schlenk tube after stirring for 15 h.

^{1}H NMR (400.13 MHz, C_6D_6, 298 K): δ = 1.14 (d, $^3J_{H–P}$ = 15.6 Hz, 18H, PC(C*H*$_3$)$_3$), 1.66 (br, 2H, N*H*$_2$). **^{31}P{^{1}H} NMR** (162.04 MHz, C_6D_6, 298 K): δ = 93.8 (s). **^{13}C{^{1}H} NMR** (100.61 MHz, C_6D_6, 298 K): δ = 27.6 (d, $^2J_{C–P}$ = 2.2 Hz, PC(*C*H$_3$)$_3$), 38.6 (d, $^1J_{C–P}$ = 45.9 Hz, P*C*(CH$_3$)$_3$). **^{77}Se{^{1}H} NMR** (76.31 MHz, C_6D_6, 298 K): δ = −356.2 (d, $^1J_{Se–P}$ = 744.5 Hz). **^{1}H NMR** (400.13 MHz, CD_2Cl_2, 298 K): δ = 1.34 (d, $^3J_{H–P}$ = 15.8 Hz, 18H, PC(C*H*$_3$)$_3$), 2.33 (br, 2H, N*H*$_2$). **^{31}P{^{1}H} NMR** (162.04 MHz, CD_2Cl_2, 298 K): δ = 95.0 (s). **^{13}C{^{1}H} NMR** (100.61 MHz, CD_2Cl_2, 298 K): δ = 27.8 (d, $^2J_{C–P}$ = 2.1 Hz, PC(*C*H$_3$)$_3$), 39.1 (d, $^1J_{C–P}$ = 45.5 Hz, P*C*(CH$_3$)$_3$). **^{77}Se{^{1}H} NMR** (76.31 MHz, CD_2Cl_2, 298 K): δ = −350.8 (d, $^1J_{Se–P}$ = 726.6 Hz). **Elemental analysis**: $C_8H_{20}NPSe \cdot 0.25\ Et_2O$: calcd.: C 41.78, H 8.77, N 5.41; found: C 41.74, H 8.55, N 5.59. **HR(EI+)-MS**: calcd. *m/z* for $C_8H_{20}NPSe$ [M$^{+\cdot}$]: 241.0499, found: 241.0495.

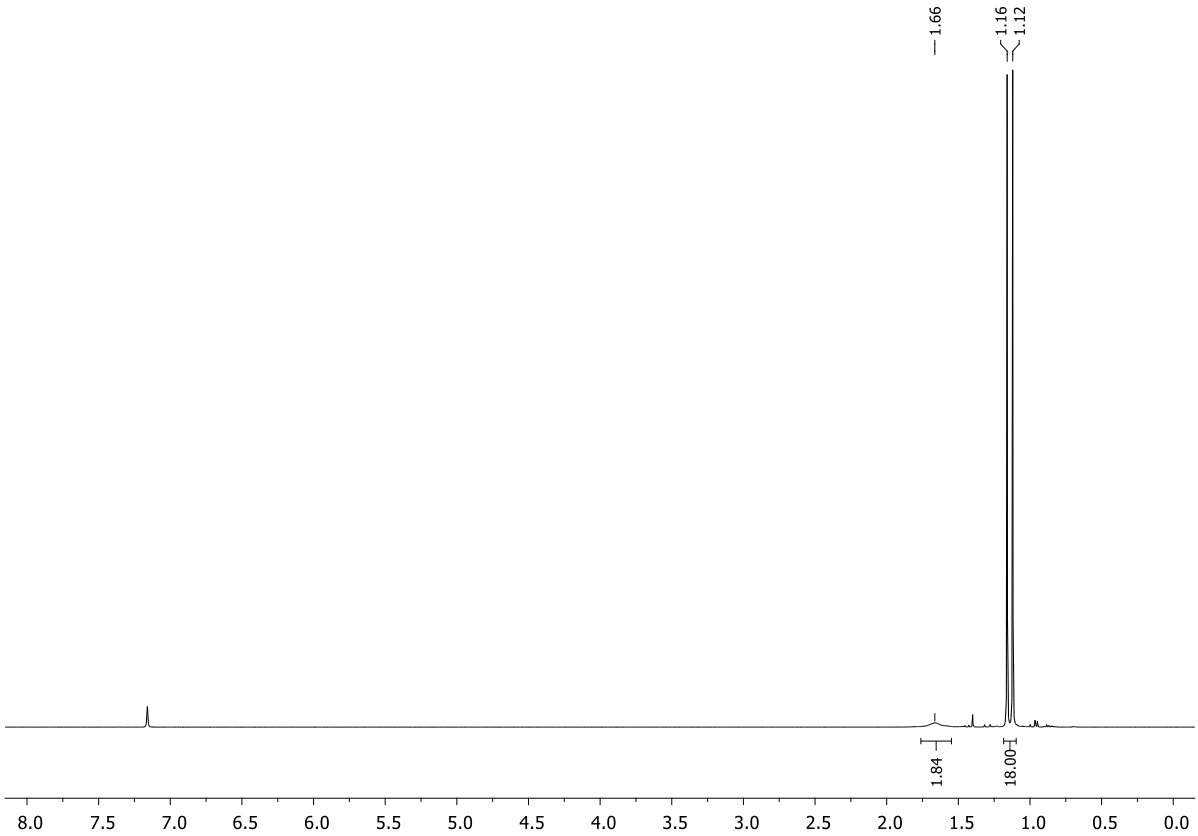

Figure S4.59. ^{1}H NMR spectrum (C_6D_6, 298 K) of **4**.

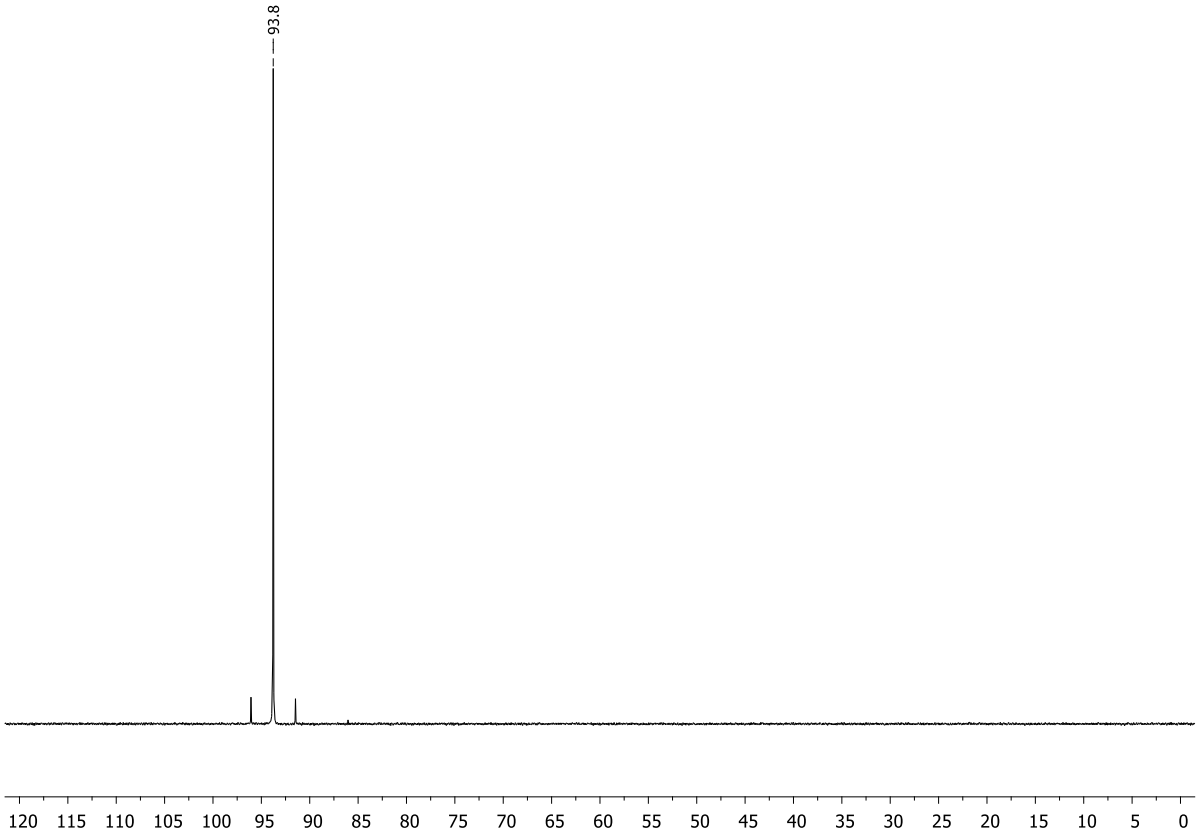

Figure S4.60. $^{31}P\{^{1}H\}$ NMR spectrum (C_6D_6, 298 K) of **4**.

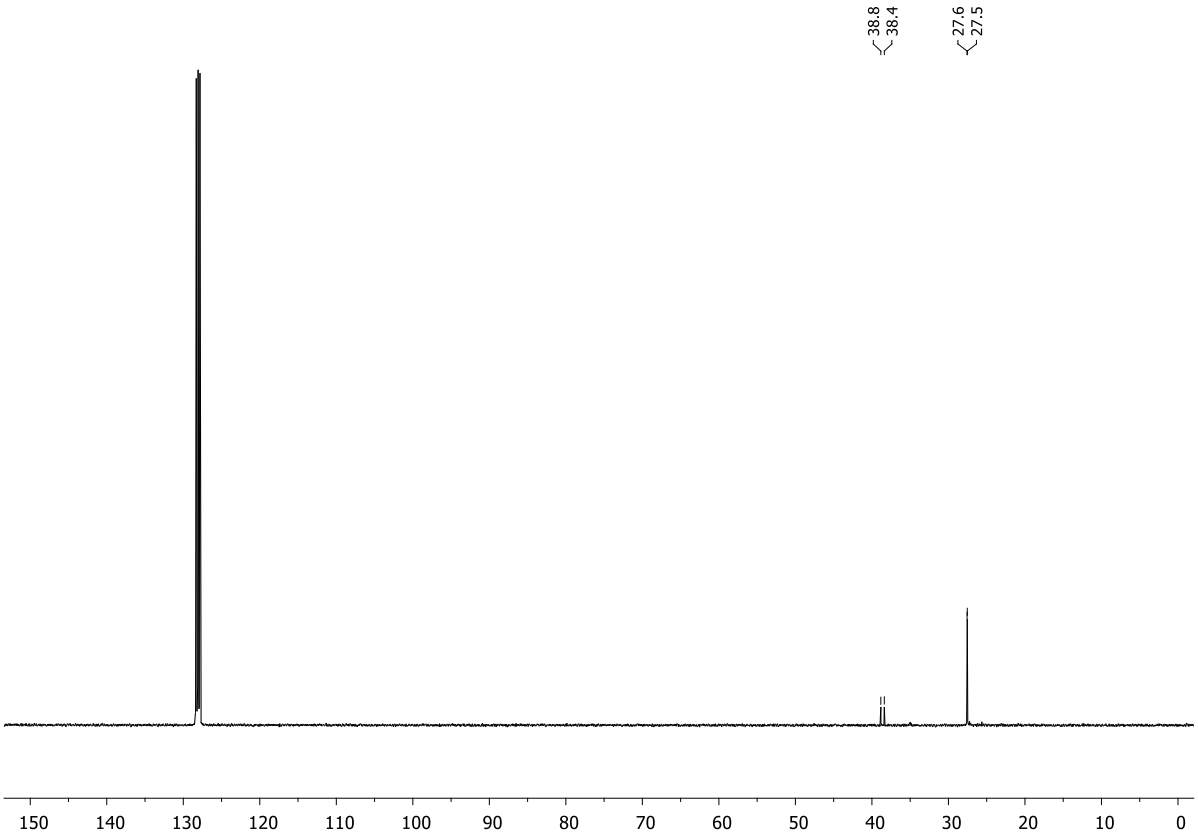

Figure S4.61. $^{13}C\{^{1}H\}$ NMR spectrum (C_6D_6, 298 K) of **4**.

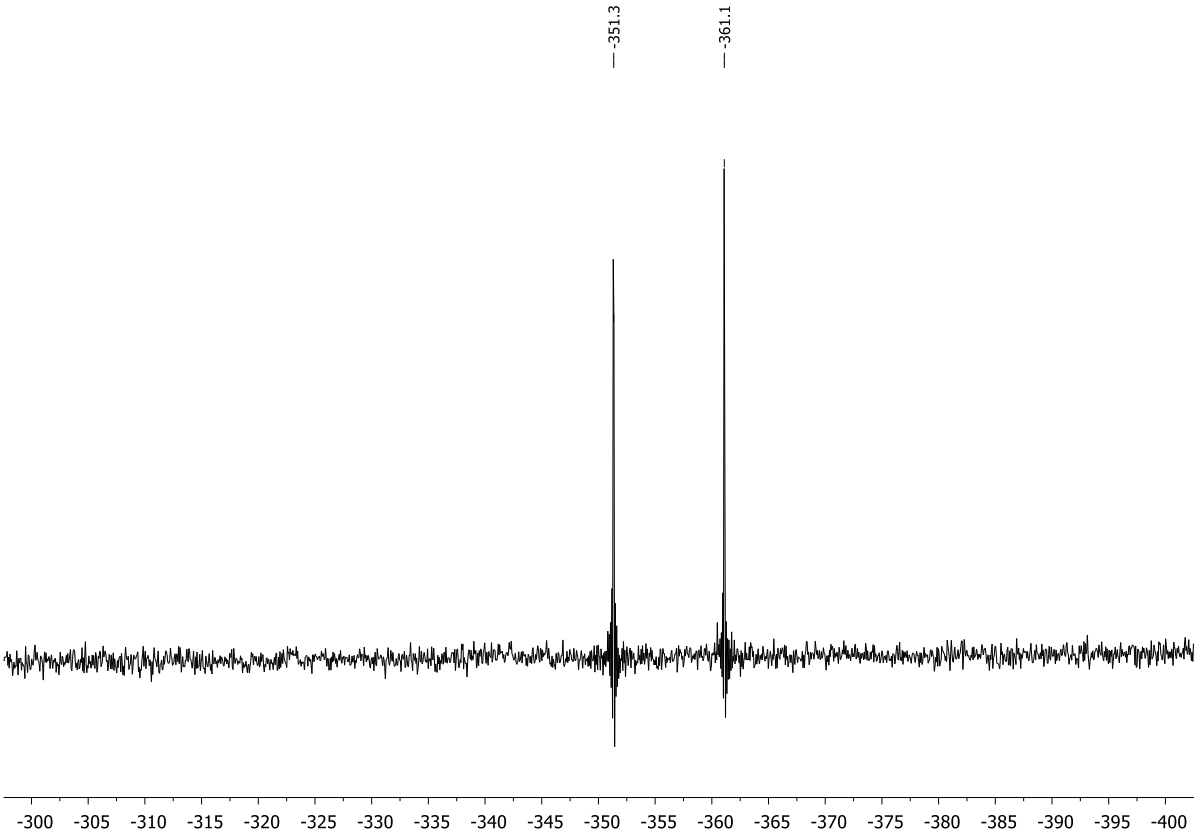

Figure S4.62. $^{77}Se\{^{1}H\}$ NMR spectrum (C_6D_6, 298 K) of **4**.

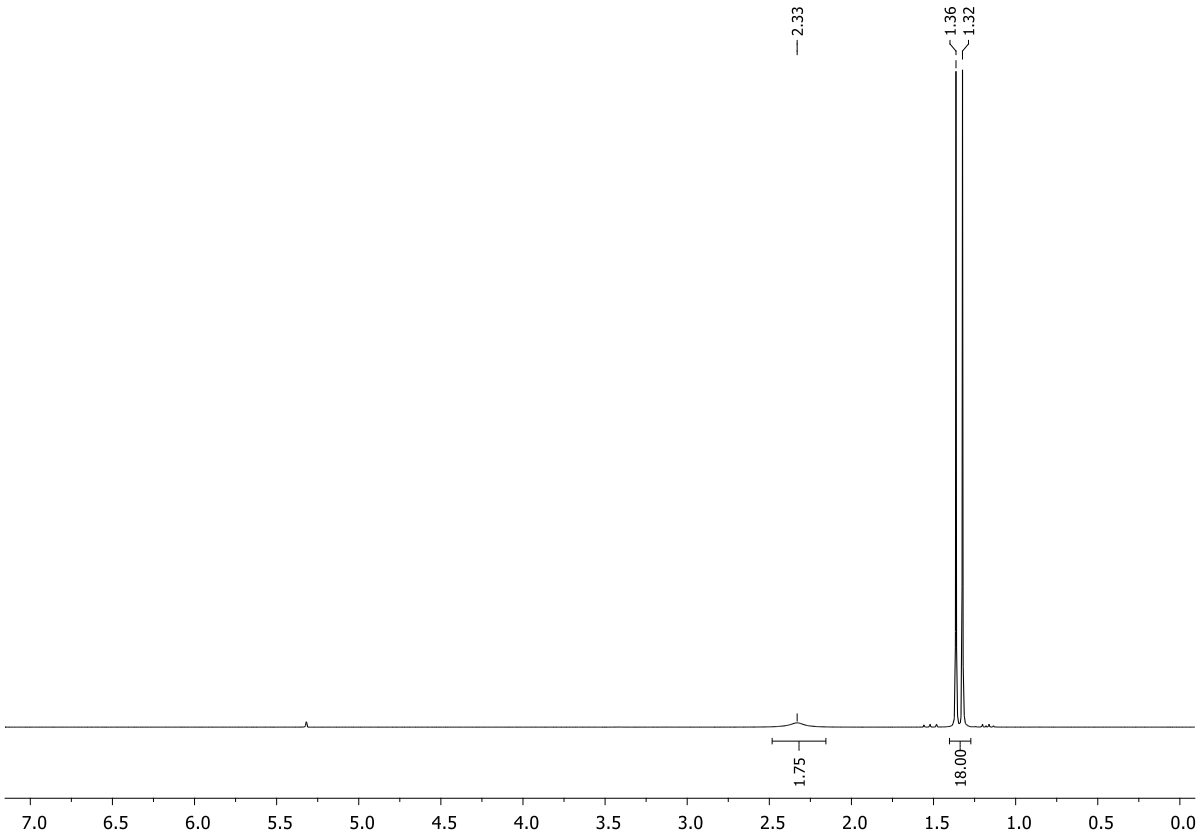

Figure S4.63. ^{1}H NMR spectrum (CD_2Cl_2, 298 K) of **4**.

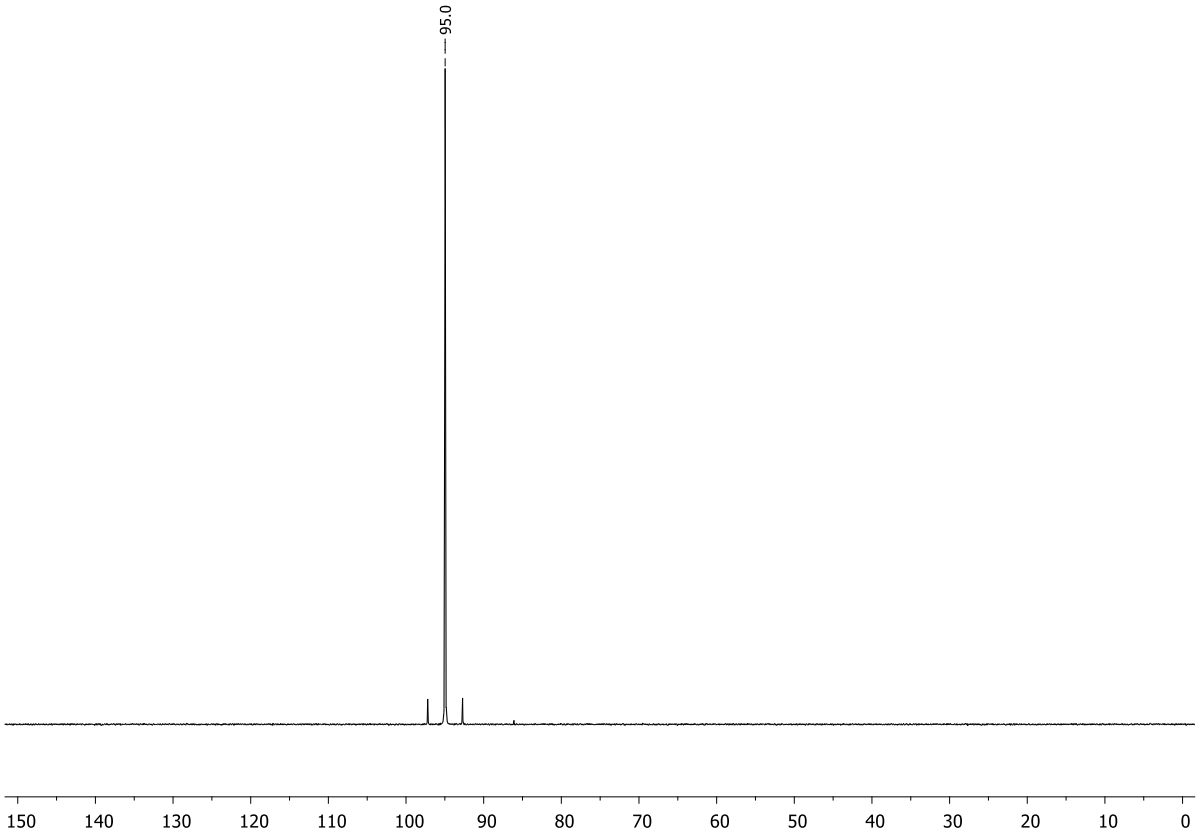

Figure S4.64. $^{31}P\{^{1}H\}$ NMR spectrum (CD_2Cl_2, 298 K) of **4**.

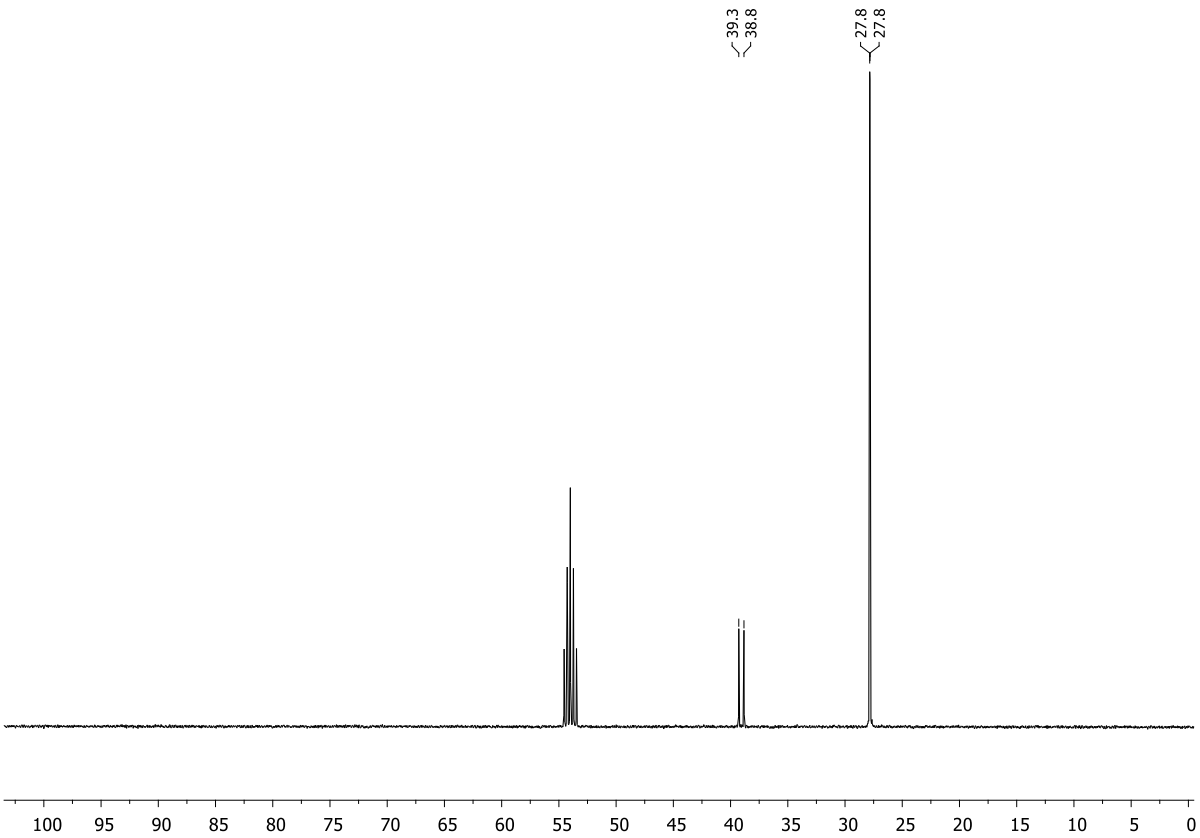

Figure S4.65. $^{13}C\{^{1}H\}$ NMR spectrum (CD_2Cl_2, 298 K) of **4**.

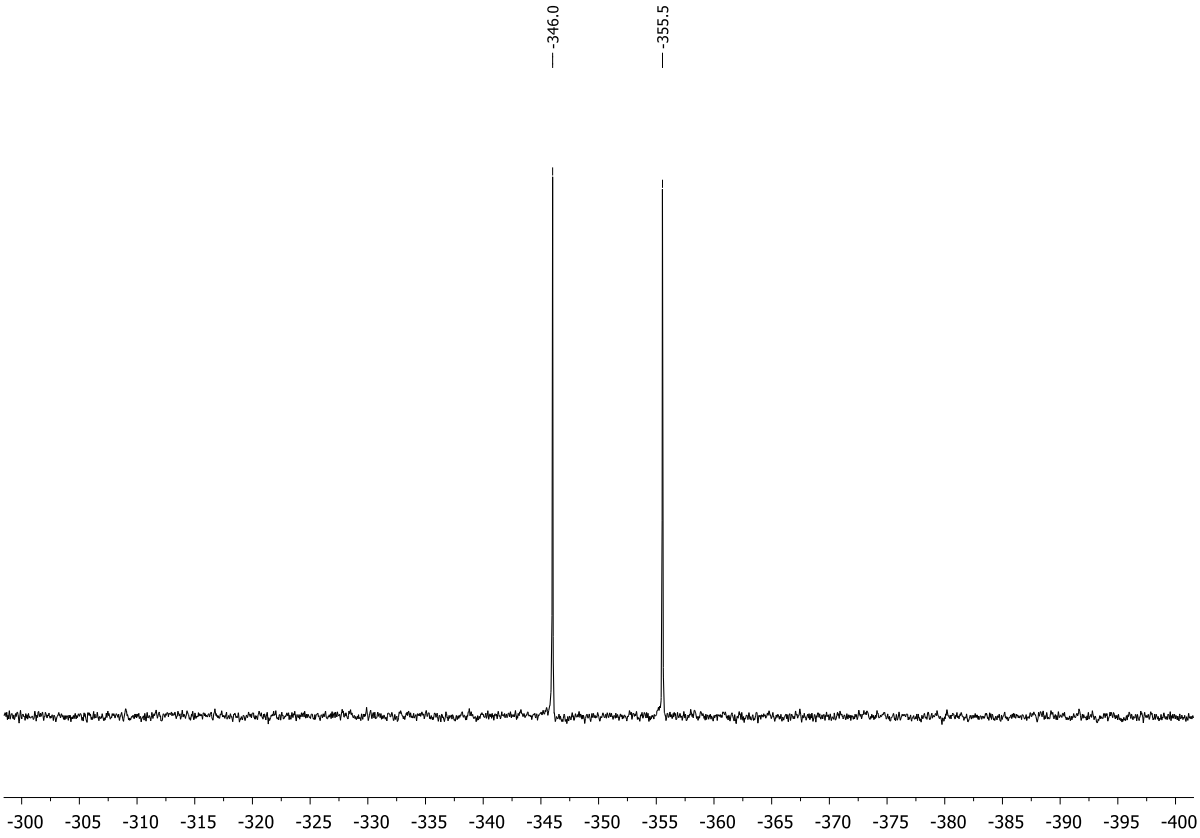

Figure S4.66. $^{77}Se\{^{1}H\}$ NMR spectrum (CD_2Cl_2, 298 K) of **4**.

4.6.2.10. Synthesis of *t*Bu$_2$(PSe)NH$_3^+$ Cl$^-$ [(4·HCl)$_4$]

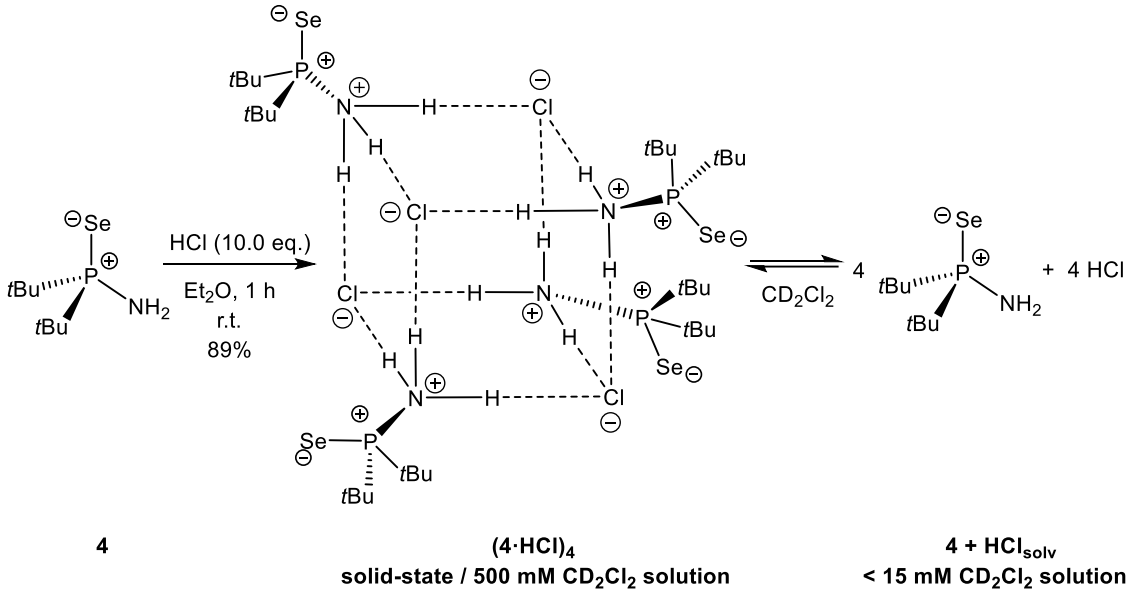

4 (1.00 g, 4.16 mmol, 1.0 equiv.) was dissolved in diethyl ether (4 mL) and HCl (21 mL, 41.6 mmol, 10.0 equiv., 2.0 M in diethyl ether) was added dropwise at room temperature resulting in a colorless suspension after a few minutes. After 1 h of stirring, the solvent was removed *in vacuo* and the solid further dried. **(4·HCl)$_4$** was obtained as a colorless solid (1.03 g, 3.72 mmol, 89%). Crystals suitable for single crystal X-ray diffraction were grown from DCM by slowly evaporating the solvent.

^{1}H NMR (400.13 MHz, 500 mM in CD_2Cl_2, 298 K): δ = 1.50 (d, $^3J_{H–P}$ = 17.7 Hz, 18H, PC(C*H*$_3$)$_3$), 9.52 (br, 3H, N*H*$_3$). **^{31}P{^{1}H} NMR** (162.04 MHz, 500 mM in CD_2Cl_2, 298 K): δ = 114.3. **^{13}C{^{1}H} NMR** (100.61 MHz, 500 mM in CD_2Cl_2, 298 K): δ = 27.9 (d, $^2J_{C–P}$ = 2.4 Hz, PC(*C*H$_3$)$_3$), 40.6 (d, $^1J_{C–P}$ = 33.8 Hz, P*C*(CH$_3$)$_3$). **^{77}Se{^{1}H} NMR** (76.31 MHz, 500 mM in CD_2Cl_2, 298 K): δ = −348.4 (d, $^1J_{Se–P}$ = 814.5 Hz). **^{1}H NMR** (400.13 MHz, 10 mM in CD_2Cl_2, 298 K): δ = 1.36 (d, $^3J_{H–P}$ = 15.9 Hz, 18H, PC(C*H*$_3$)$_3$), 2.12 (br, 2H, N*H*$_2$). **^{31}P{^{1}H} NMR** (162.04 MHz, 10 mM in CD_2Cl_2, 298 K): δ = 95.1. **^{13}C{^{1}H} NMR** (100.61 MHz, 10 mM in CD_2Cl_2, 298 K): δ = 27.3 (d, $^2J_{C–P}$ = 2.0 Hz, PC(*C*H$_3$)$_3$), P*C*(CH$_3$)$_3$ not visible. **^{77}Se{^{1}H} NMR** (76.31 MHz, 10 mM in CD_2Cl_2, 298 K): δ = −350.3 (d, $^1J_{Se–P}$ = 732.5 Hz). **Elemental analysis**: $C_8H_{21}ClNPS \cdot 0.2\ Et_2O$: calcd.: C 36.26, H 7.95, N 4.81; found: C 36.47, H 7.80, N 5.17.

For ^{2}H NMR measurements, the reaction was proceeded using **4** (0.50 g, 2.08 mmol, 1.0 equiv.) in diethyl ether (2 mL) and DCl (15.6 mL, 15.6 mmol, 7.5 equiv., 1.0 M in diethyl ether). ^{2}H labelled compound **(4·DCl)$_4$** was obtained as a colorless solid (0.52 g, 1.87 mmol, 90%). The ^{2}H NMR samples were prepared using a mixture of CH_2Cl_2 and CD_2Cl_2 (9:1) as solvent.
^{1}H NMR (400.13 MHz, 500 mM in CD_2Cl_2, 298 K): δ = 1.51 (d, $^3J_{H–P}$ = 17.7 Hz, 18H, PC(C*H*$_3$)$_3$), 9.71 (br, 2H, N*H*$_2$D). **^{2}H NMR** (61.42 MHz, 500 mM in CH_2Cl_2/CD_2Cl_2 (9:1), 298 K): δ = 9.13 (br, 1D, NH$_2$*D*). **^{1}H NMR** (400.13 MHz, 10 mM in CD_2Cl_2, 298 K): δ = 1.38 (d, $^3J_{H–P}$ = 15.9 Hz, 18H,

PC(C*H*$_3$)$_3$), 2.11 (br, 1H, N*H*D). **^{2}H NMR** (61.42 MHz, 10 mM in CH_2Cl_2/CD_2Cl_2 (9:1), 298 K): δ = 2.27 (br, 1D, NH*D*).

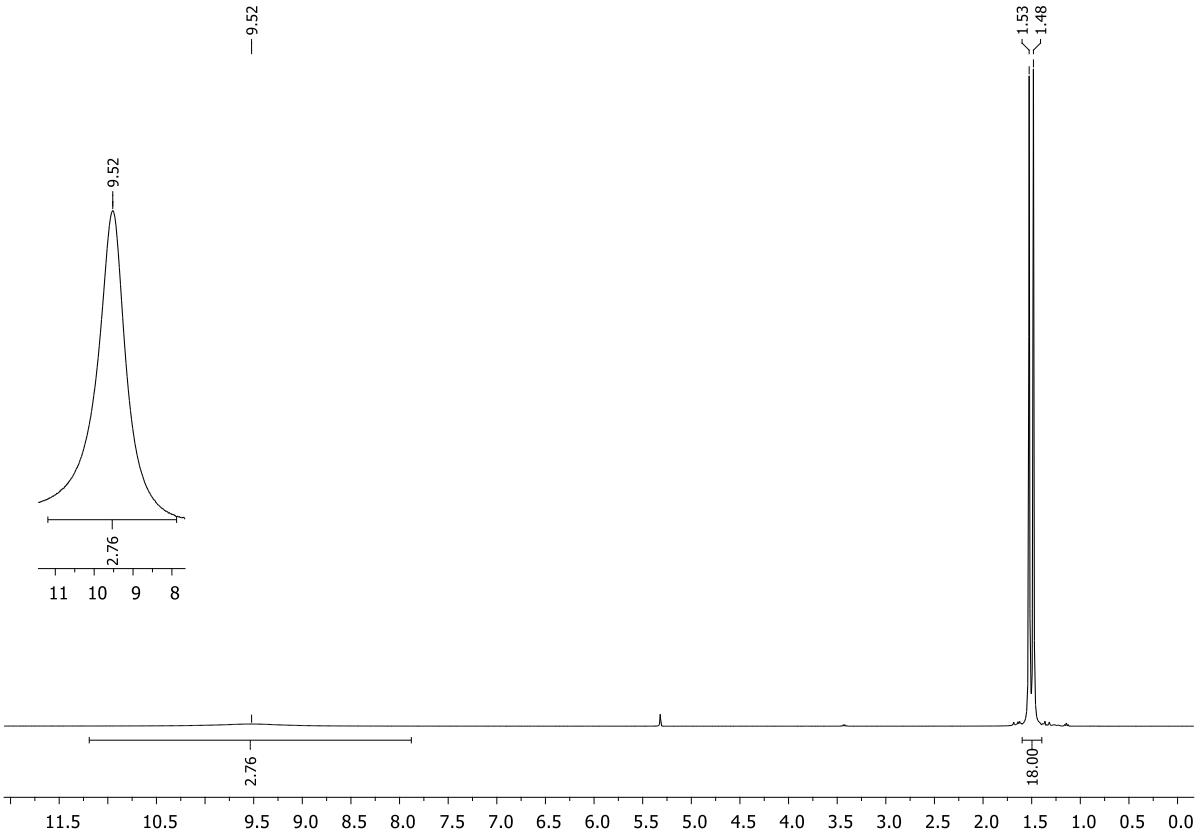

Figure S4.67. ^{1}H NMR spectrum (500 mM in CD_2Cl_2, 298 K) of **(4·HCl)$_4$**.

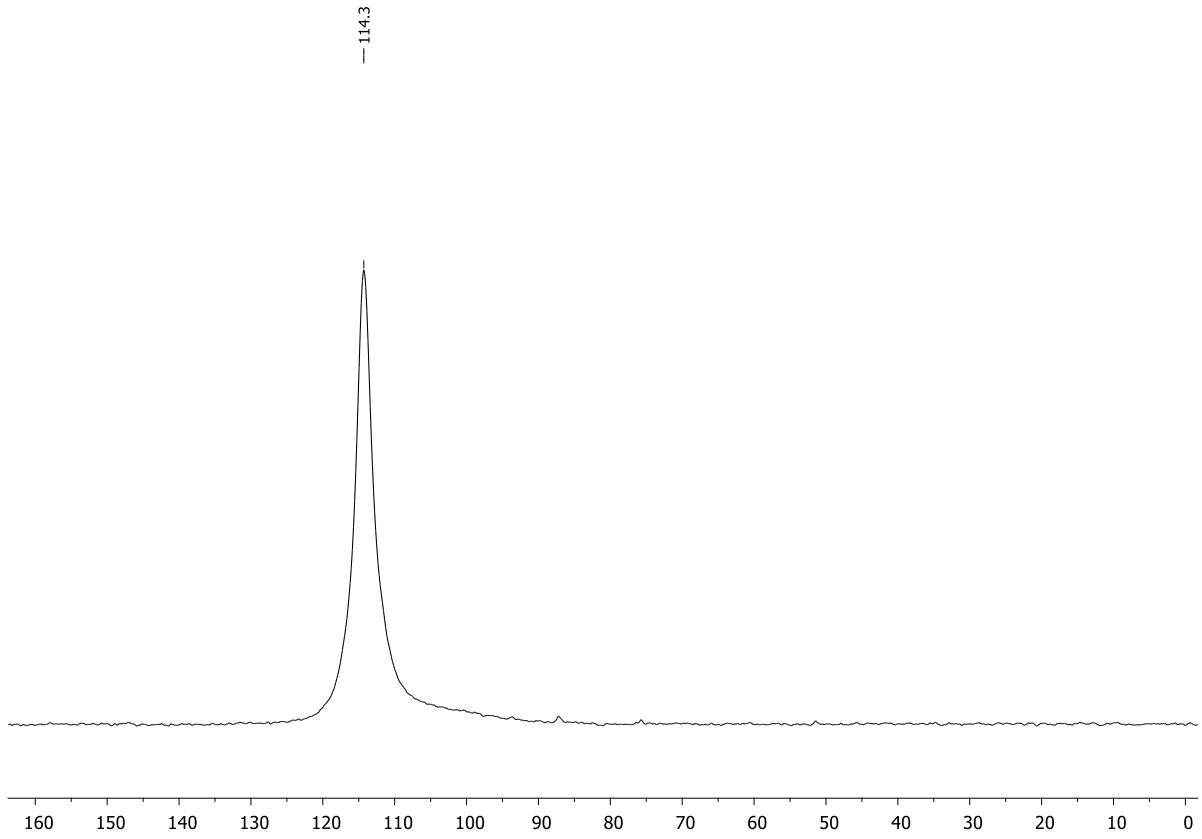

Figure S4.68. $^{31}P\{^{1}H\}$ NMR spectrum (500 mM in CD_2Cl_2, 298 K) of **(4·HCl)$_4$.**

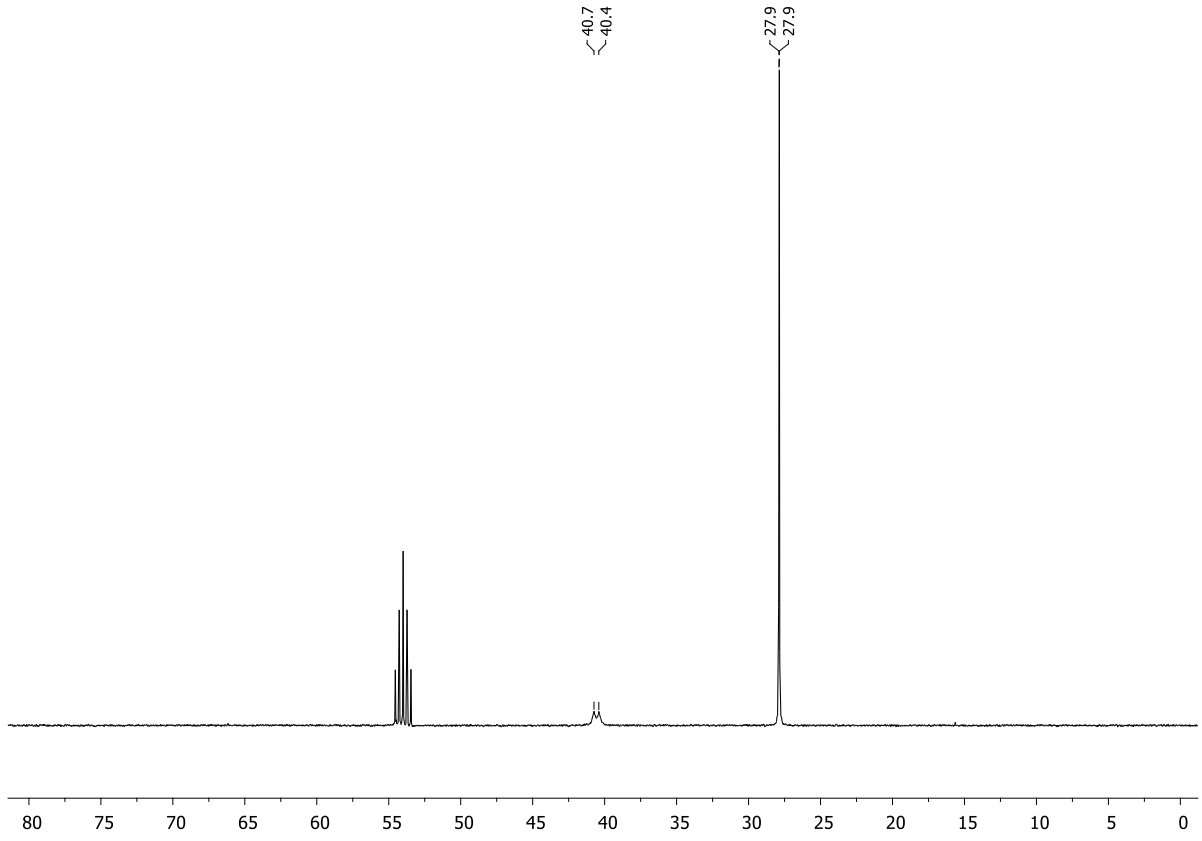

Figure S4.69. $^{13}C\{^{1}H\}$ NMR spectrum (500 mM in CD_2Cl_2, 298 K) of **(4·HCl)$_4$.**

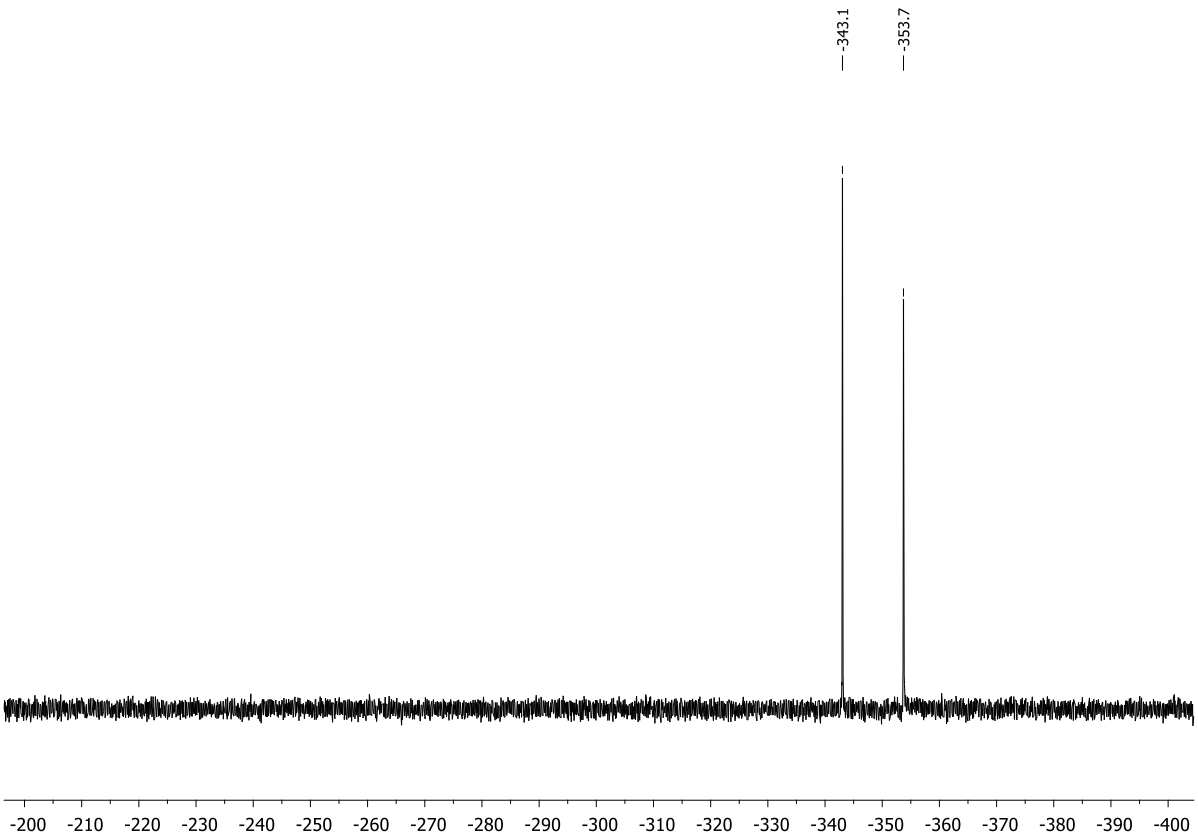

Figure S4.70. $^{77}Se\{^{1}H\}$ NMR spectrum (500 mM in CD_2Cl_2, 298 K) of **(4·HCl)$_4$.**

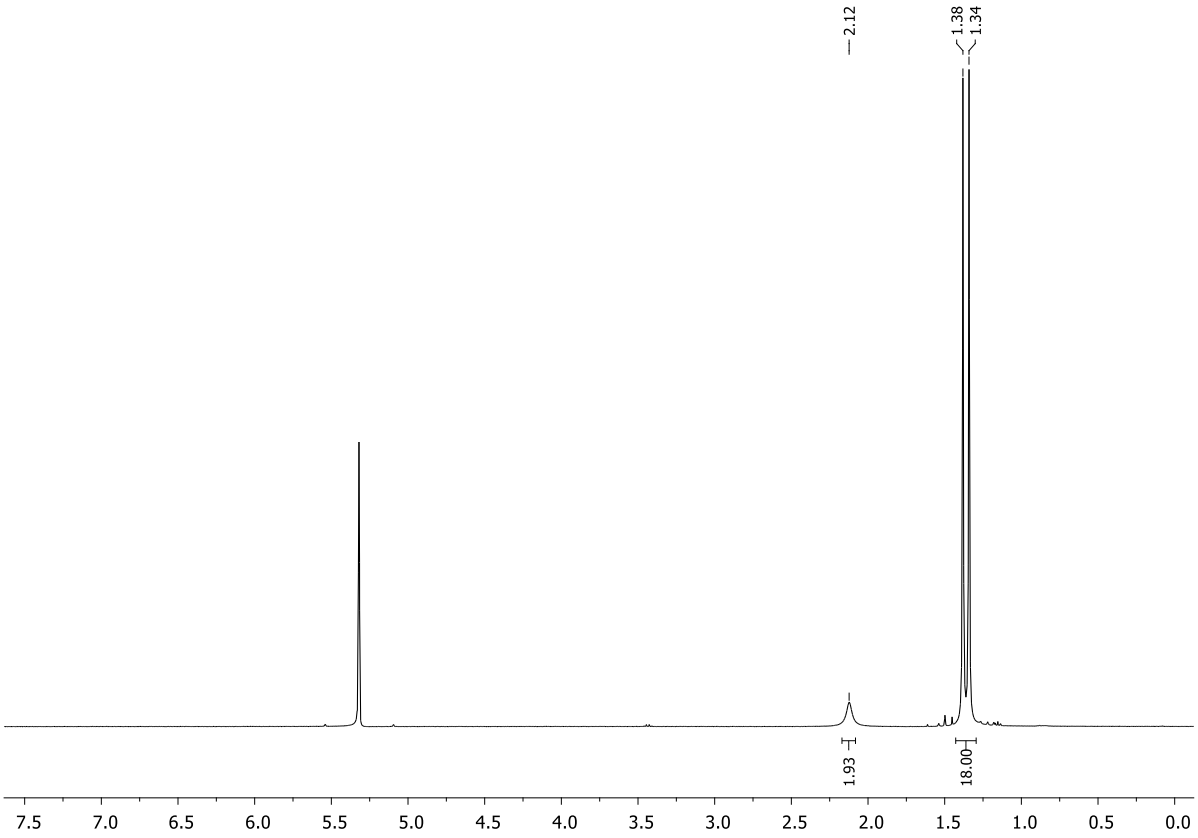

Figure S4.71. ^{1}H NMR spectrum (10 mM in CD_2Cl_2, 298 K) of **4 + HCl$_{solv}$**.

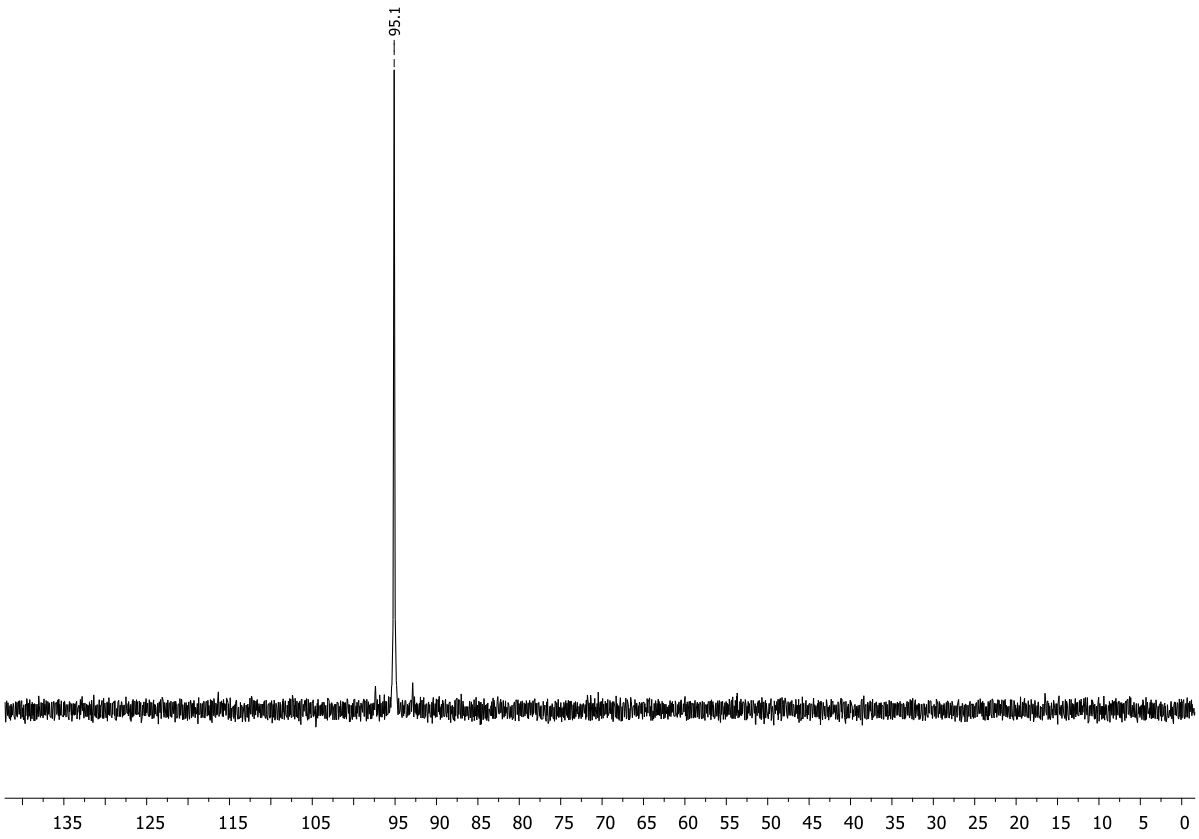

Figure S4.72. $^{31}P\{^{1}H\}$ NMR spectrum (10 mM in CD_2Cl_2, 298 K) of **4 + HCl$_{solv}$**.

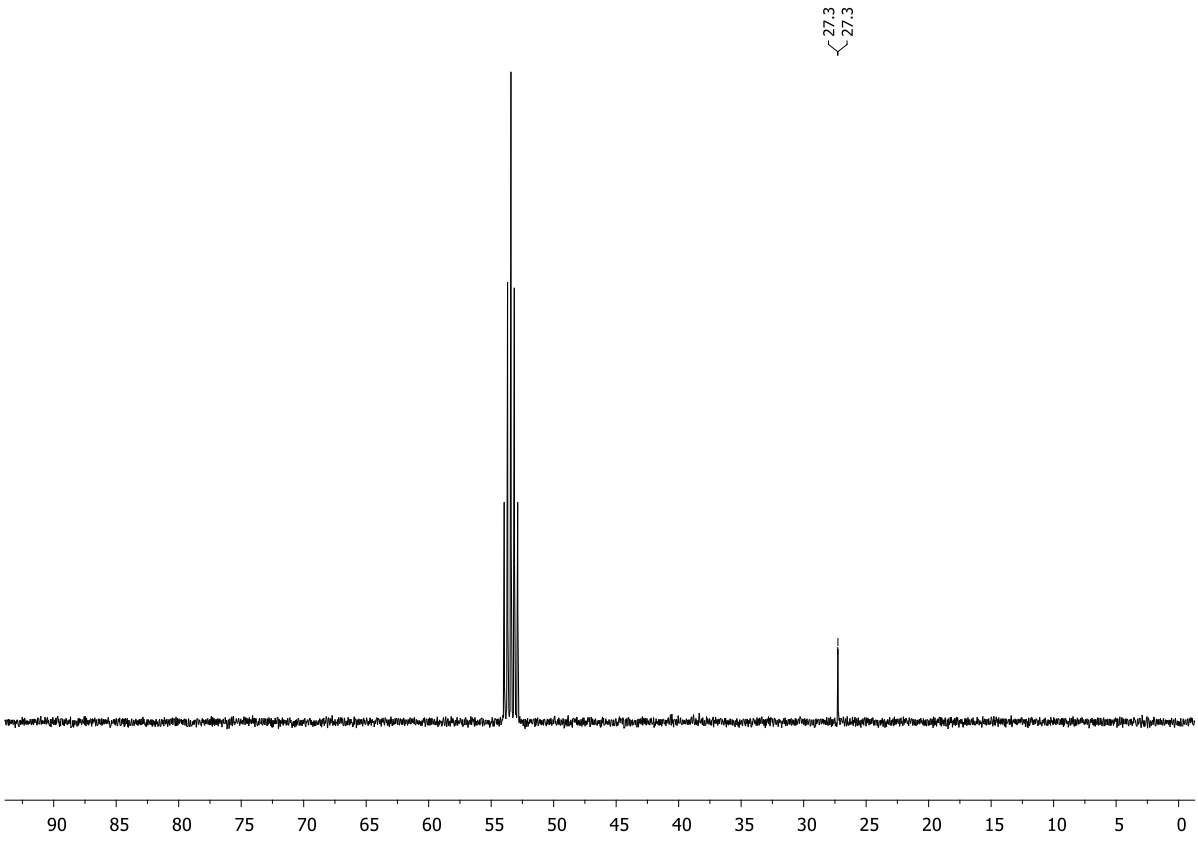

Figure S4.73. $^{13}C\{^{1}H\}$ NMR spectrum (10 mM in CD_2Cl_2, 298 K) of **4 + HCl$_{solv}$**.

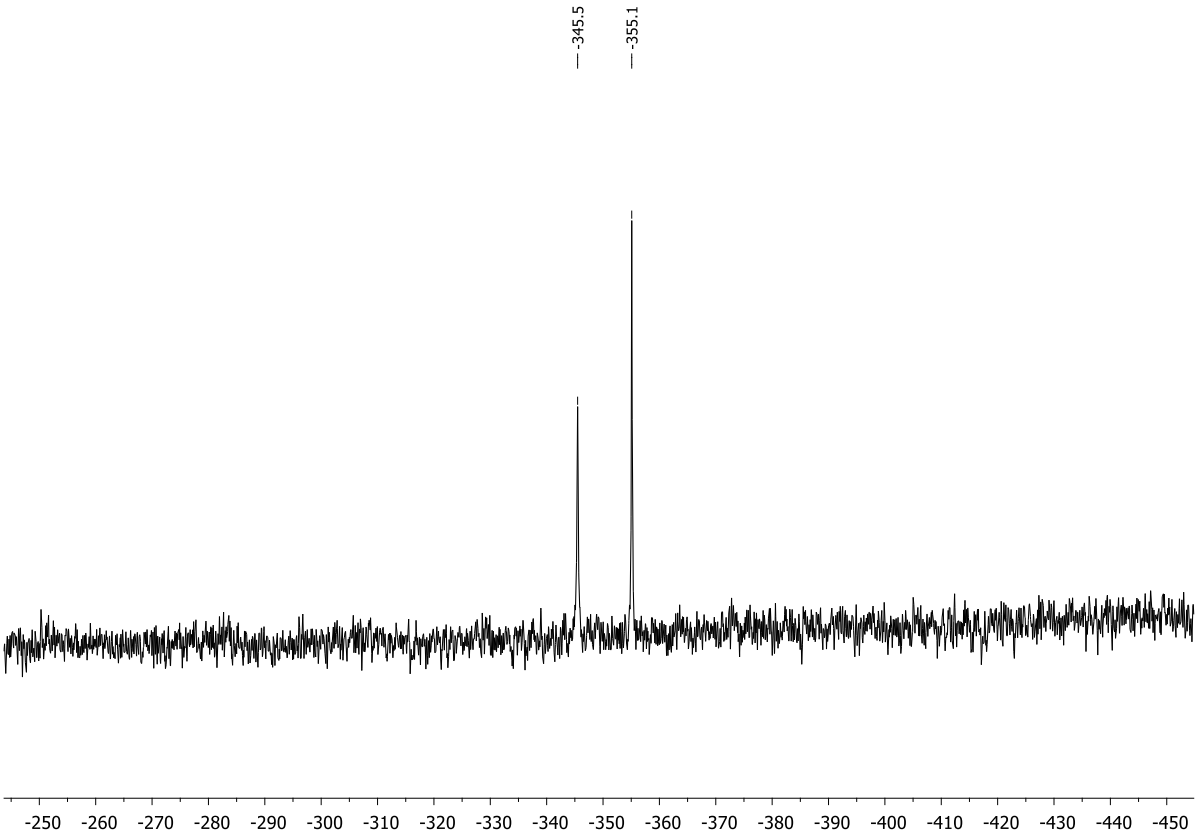

Figure S4.74. $^{77}Se\{^{1}H\}$ NMR spectrum (10 mM in CD_2Cl_2, 298 K) of **4 + HCl$_{solv}$**.

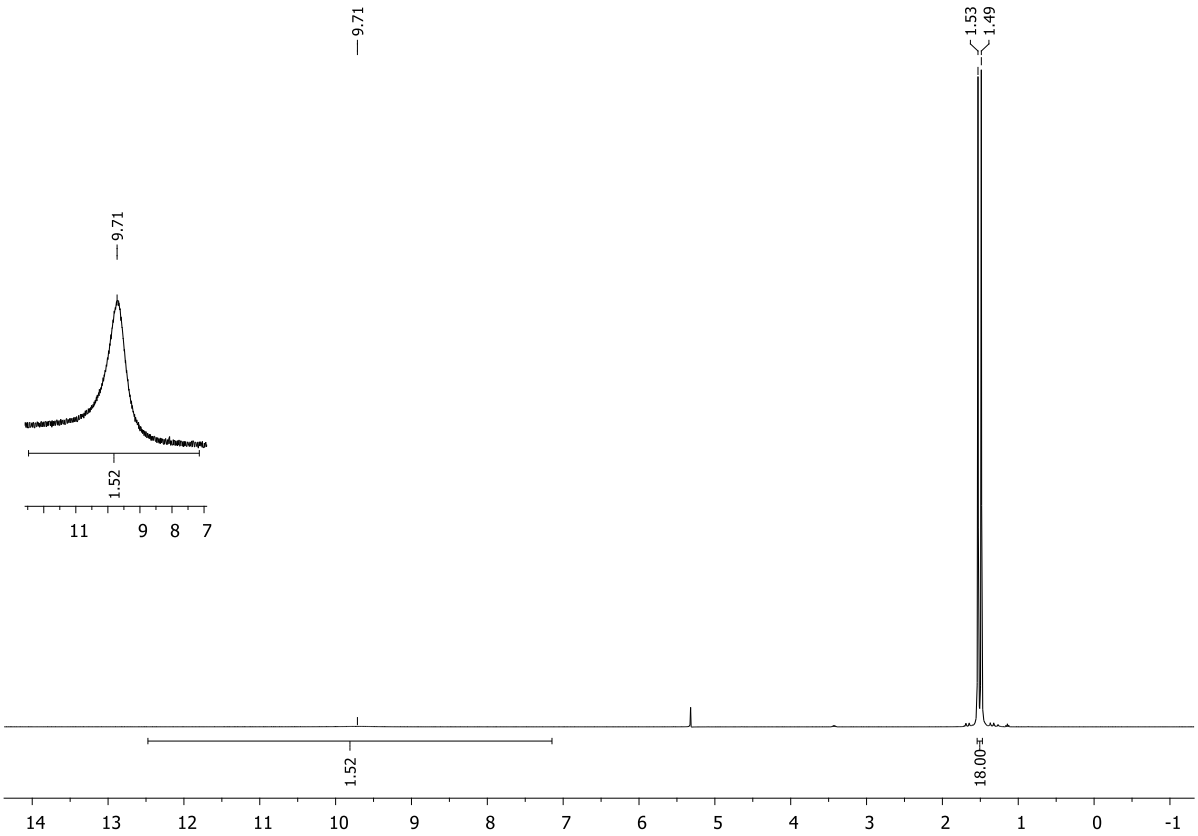

Figure S4.75. ^{1}H NMR spectrum (500 mM in CD_2Cl_2, 298 K) of **(4·DCl)$_4$**.

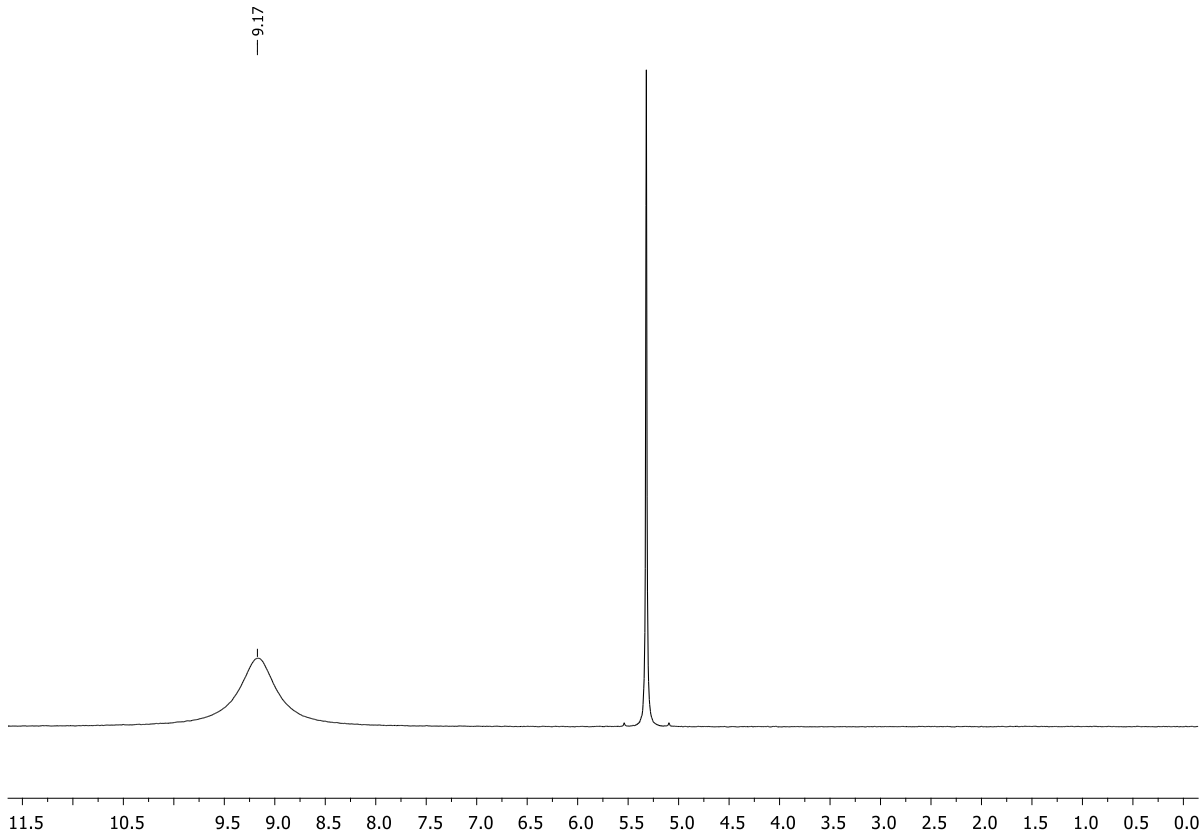

Figure S4.76. ^{2}H NMR spectrum (500 mM in CH_2Cl_2/CD_2Cl_2 (9:1), 298 K) of **(4·DCl)$_4$.**

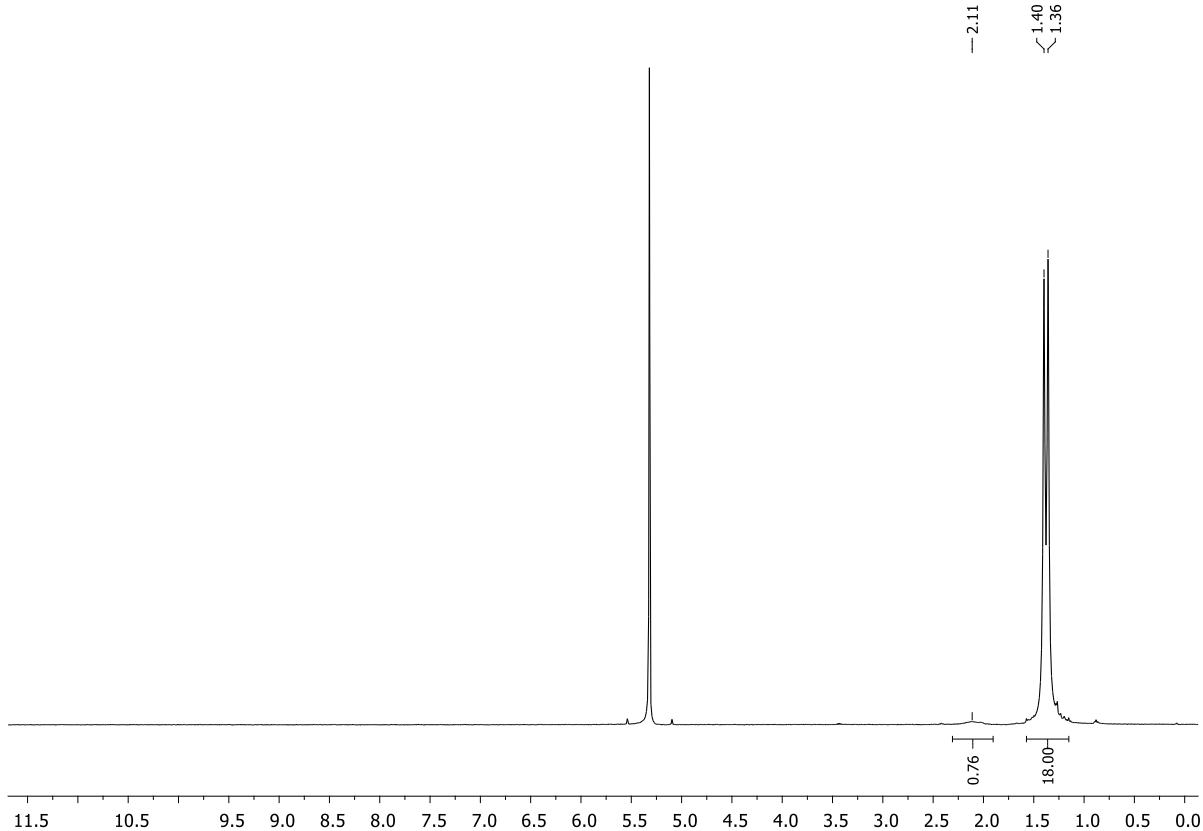

Figure S4.77. ^{1}H NMR spectrum (10 mM in CD_2Cl_2, 298 K) of **4 + DCl$_{solv}$**.

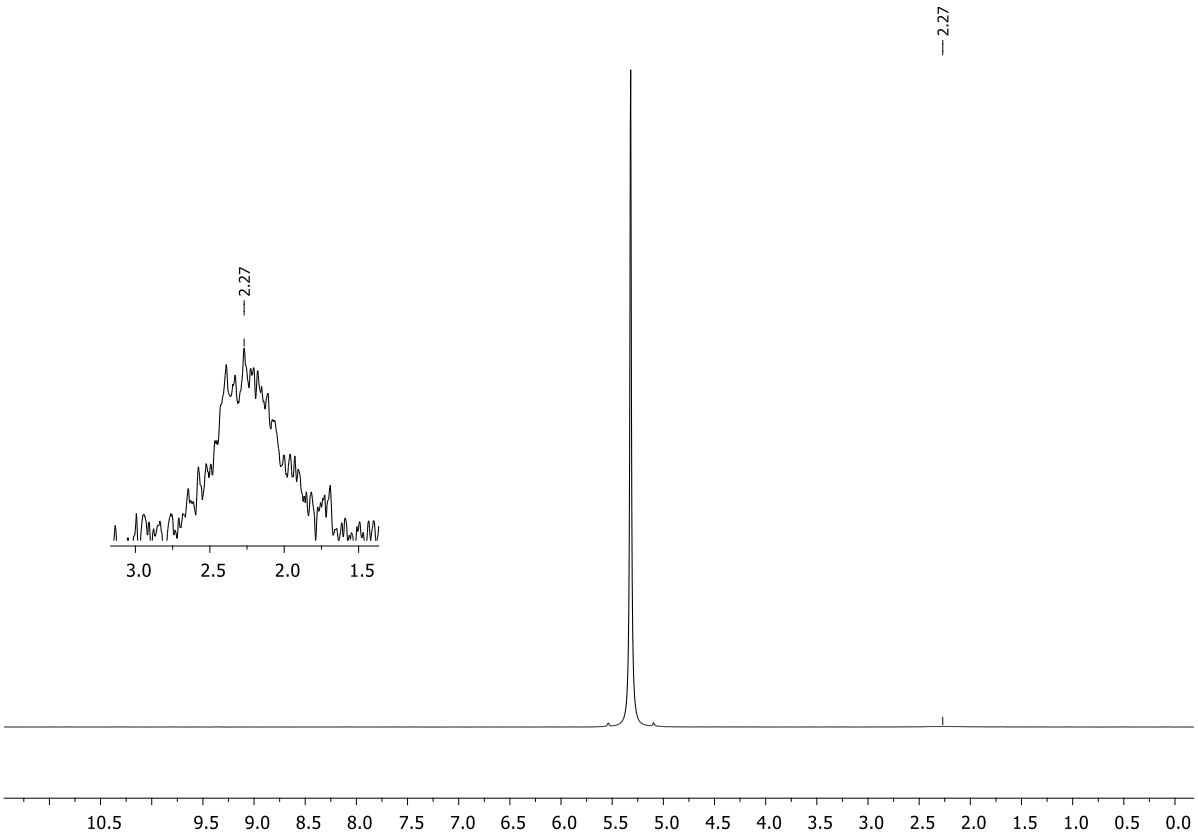

Figure S4.78. ^{2}H NMR spectrum (10 mM in CH_2Cl_2/CD_2Cl_2 (9:1), 298 K) of **4 + DCl$_{solv}$**.

4.6.2.11. Synthesis of tBu$_2$(P$^+$–SeH)NH$_2$ B(C$_6$F$_5$)$_4^-$ [(4–SeH)$^+$ WCA$^-$]

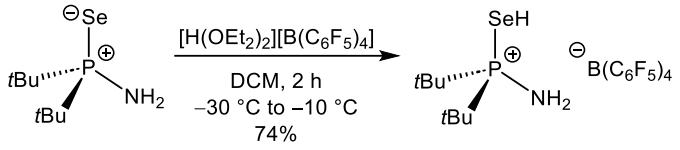

4 **(4–SeH)$^+$ WCA$^-$**

4 (100 mg, 0.42 mmol, 1.0 equiv.) and [H(OEt$_2$)$_2$][B(C$_6$F$_5$)$_4$] (340 mg, 0.42 mmol, 1.0 equiv.) were dissolved in dichloromethane (for each 2 mL) in separate flasks. The solutions were combined at −30 °C and stirred until the temperature of the acetone bath reached −10 °C. After removal of the cooling bath, all volatiles were removed *in vacuo* and the solid further dried. **(4–SeH)$^+$ WCA$^-$** was obtained as a pale rose solid (284 mg, 0.31 mmol, 74%). Crystals suitable for single crystal X-ray diffraction were grown from DCM after slow layering with *n*-pentane.

^{1}H NMR (400.13 MHz, CD_2Cl_2, 298 K): δ = 1.51 (d, $^3J_{H–P}$ = 19.1 Hz, 18H, PC(C*H*$_3$)$_3$), 2.48 (br, 3H, N*H*$_2$/S*H*). **^{31}P{^{1}H} NMR** (162.04 MHz, CD_2Cl_2, 298 K): δ = 100.7 (s). **^{13}C{^{1}H} NMR** (100.61 MHz, CD_2Cl_2, 298 K): δ = 26.8 (d, $^2J_{C–P}$ = 1.2 Hz, PC(*C*H$_3$)$_3$), 40.4 (d, $^1J_{C–P}$ = 36.9 Hz, P*C*(CH$_3$)$_3$), *C*$_{Ar\text{-}borate}$ not visible. **^{11}B{^{1}H} NMR** (128.43 MHz, CD_2Cl_2, 298 K): *δ* = −17.0 (s). **^{19}F{^{1}H} NMR** (376.66 MHz, CD_2Cl_2, 298 K): *δ* = −167.3 (m, 8F, *meta-F*$_{Ar\text{-}borate}$), −163.5 (m, 4F, *para-F*$_{Ar\text{-}borate}$), −133.0 (s, 8F, *ortho-F*$_{Ar\text{-}borate}$). **^{77}Se{^{1}H} NMR** (76.31 MHz, CD_2Cl_2, 298 K): δ = −43.4 (d, $^1J_{Se–P}$ = 406.3 Hz). **Elemental analysis**: $C_{32}H_{21}BF_{20}NPSe$: calcd.: C 41.77, H 2.30, N 1.52; found: C 42.20, H 2.47, N 1.44.

For ^{2}H NMR measurements, the reaction was proceeded using **4** (10.0 mg, 0.42 mmol, 1.0 equiv.) and [D(OEt$_2$)$_2$][B(C$_6$F$_5$)$_4$] (348 mg, 0.42 mmol, 1.0 equiv.) in dichloromethane (2 × 2 mL). ^{2}H labelled compound **(4–SeD)$^+$ WCA$^-$** was obtained as a pale rose solid (307 mg, 0.35 mmol, 83%). The ^{2}H NMR sample was prepared using a mixture of CH_2Cl_2 and CD_2Cl_2 (9:1) as solvent.
^{1}H NMR (400.13 MHz, CD_2Cl_2, 298 K): δ = 1.49 (d, $^3J_{H–P}$ = 18.8 Hz, 18H, PC(C*H*$_3$)$_3$), 2.45 (br, 2H, N*H*$_2$ or N*H*D/Se*H*). **^{2}H NMR** (61.42 MHz, CH_2Cl_2/CD_2Cl_2 (9:1), 298 K): δ = 2.83 (br, 1D, NH*D* or Se*D*).

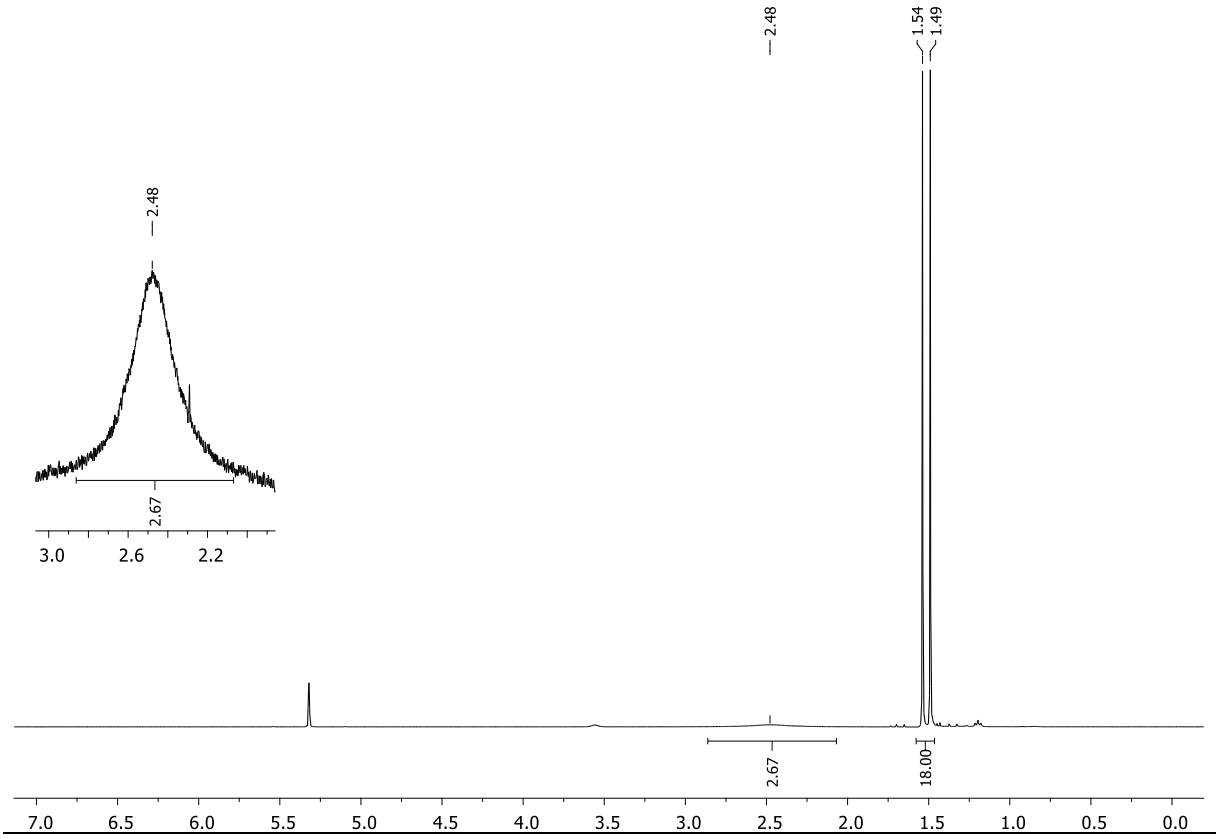

Figure S4.79. ^{1}H NMR spectrum (CD_2Cl_2, 298 K) of **(4–SeH)$^+$ WCA$^-$**.

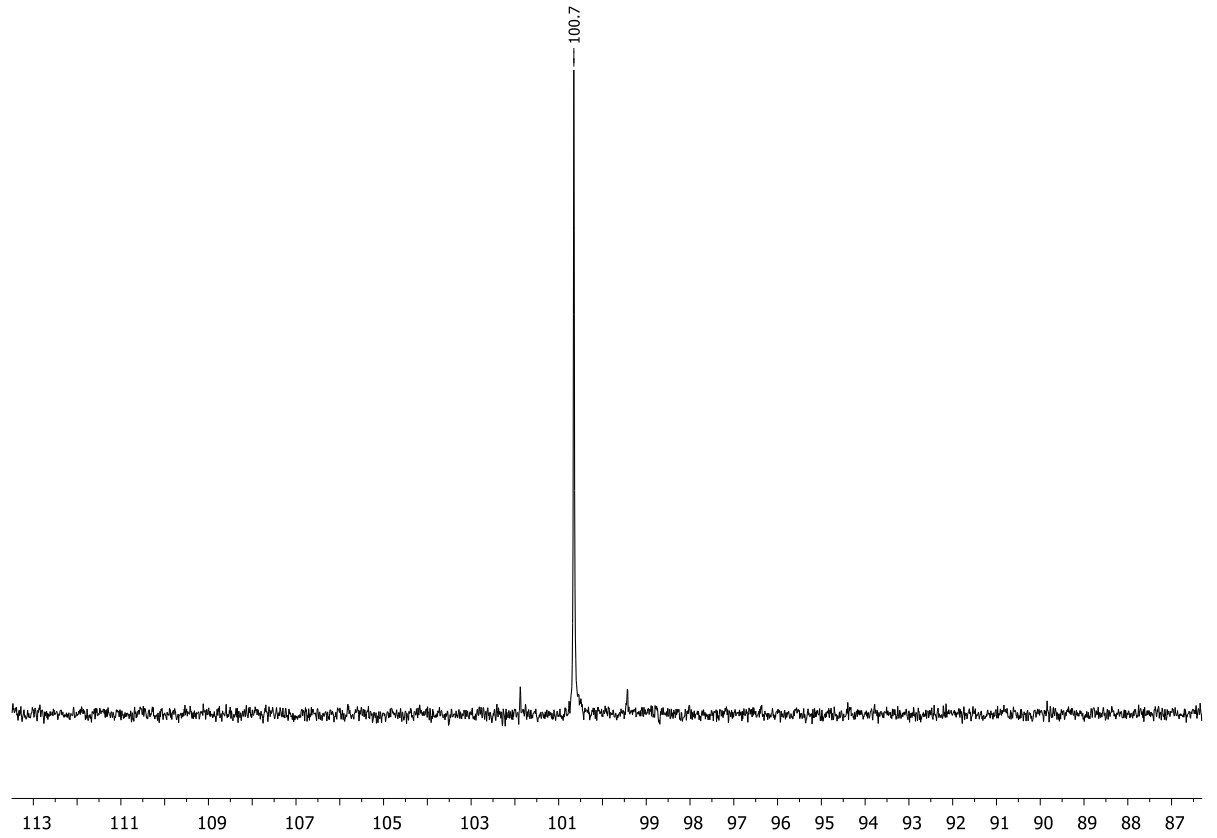

Figure S4.80. ^{31}P{^{1}H} NMR spectrum (CD_2Cl_2, 298 K) of **(4–SeH)$^+$ WCA$^-$**

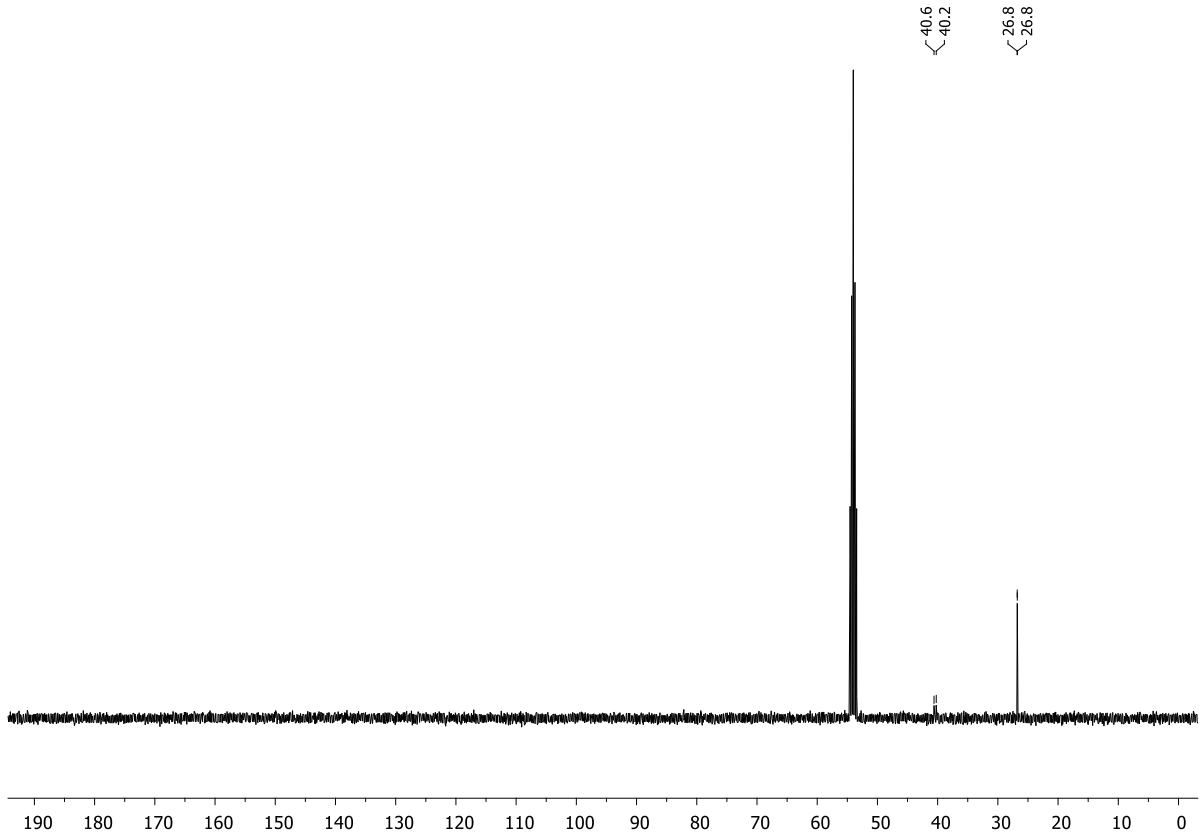

Figure S4.81. $^{13}C\{^{1}H\}$ NMR spectrum (CD_2Cl_2, 298 K) of **(4–SeH)$^+$ WCA$^-$**.

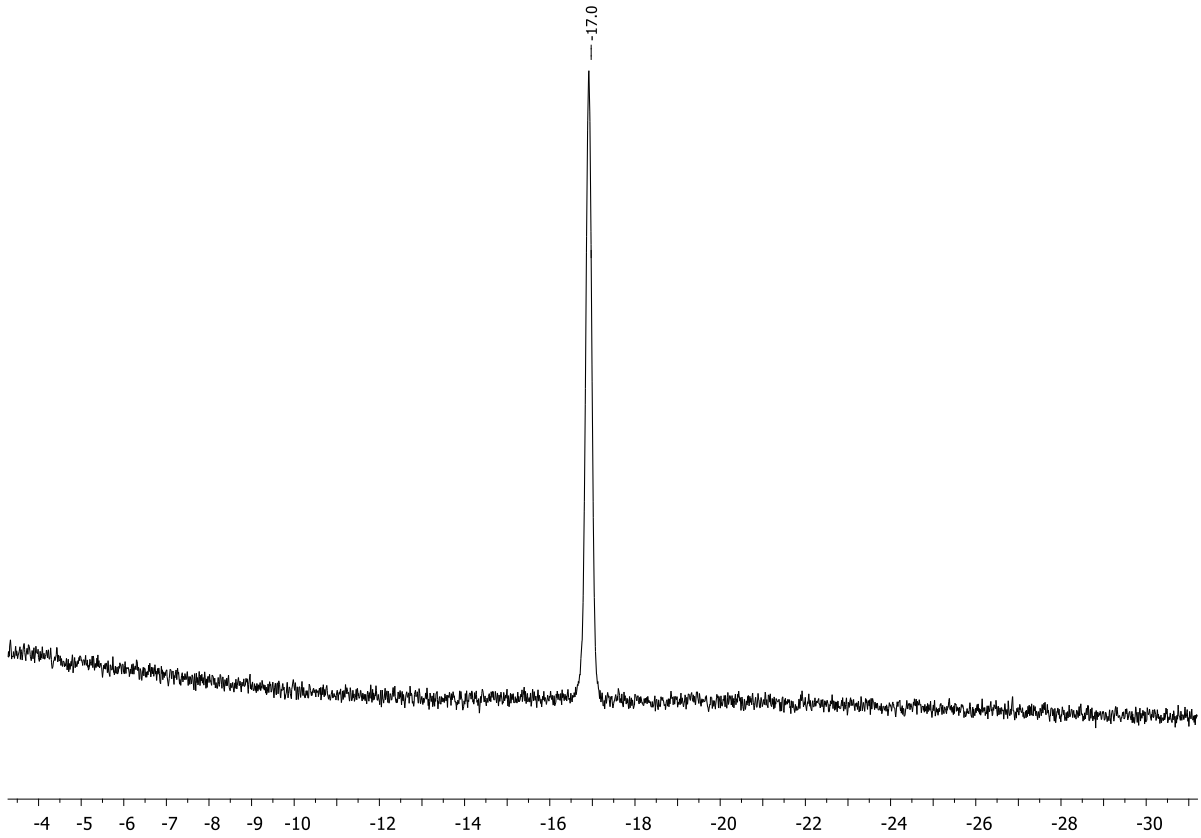

Figure S4.82. $^{11}B\{^{1}H\}$ NMR spectrum (CD_2Cl_2, 298 K) of **(4–SeH)$^+$ WCA$^-$**.

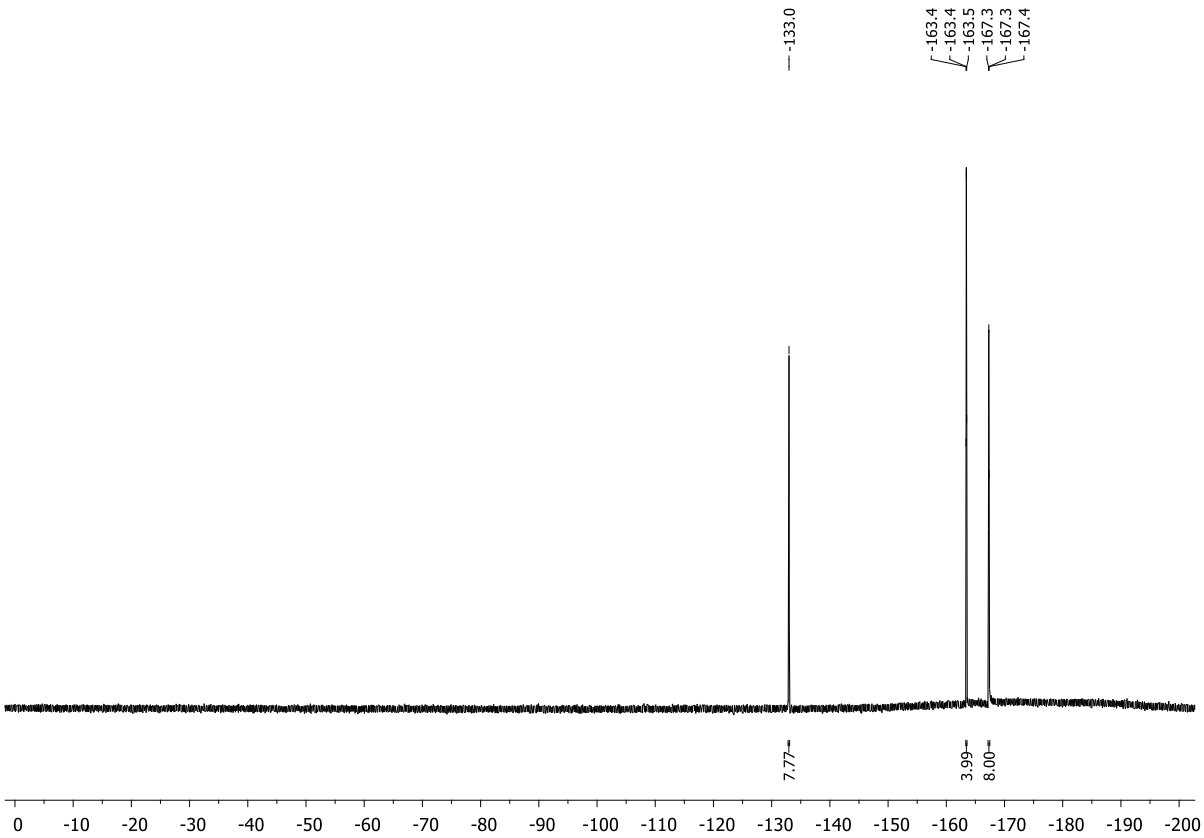

Figure S4.83. $^{19}F\{^{1}H\}$ NMR spectrum (CD_2Cl_2, 298 K) of **(4–SeH)$^+$ WCA$^-$**.

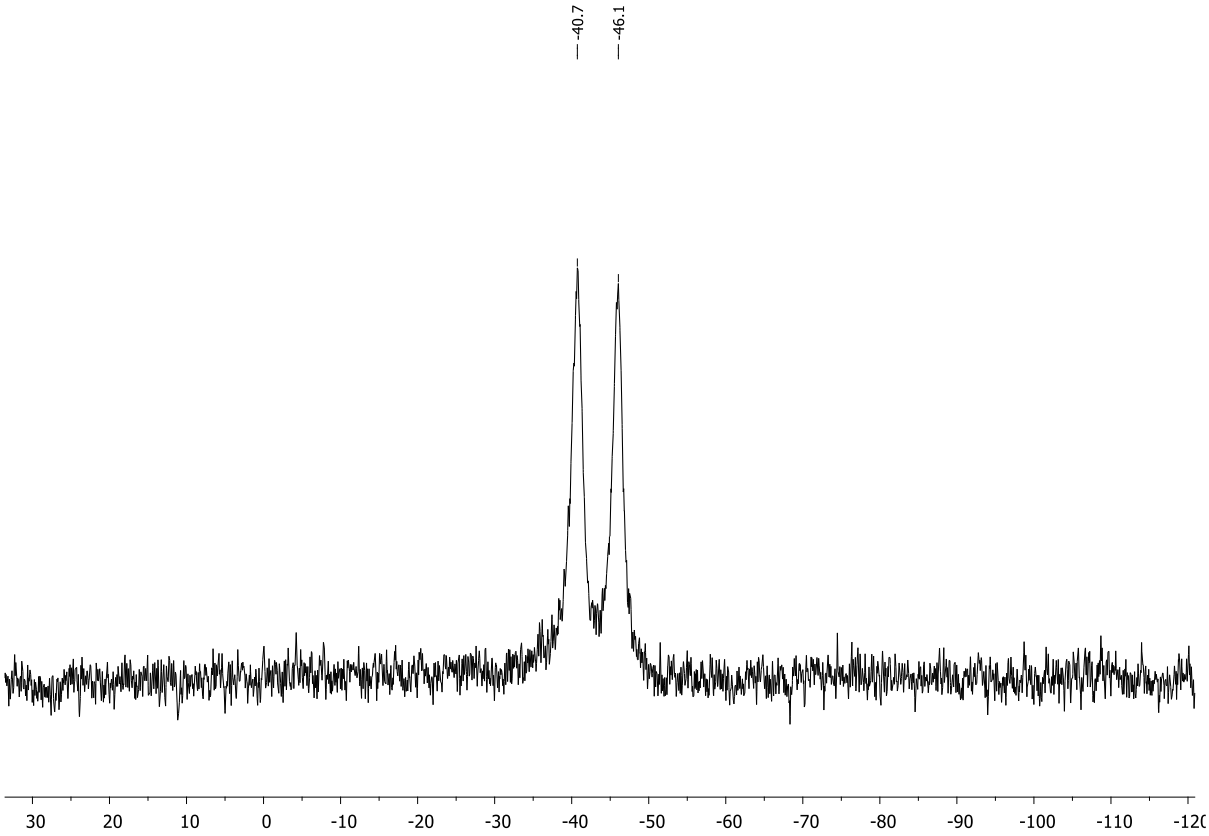

Figure S4.84. $^{77}Se\{^{1}H\}$ NMR spectrum (CD_2Cl_2, 298 K) of **(4–SeH)$^+$ WCA$^-$**.

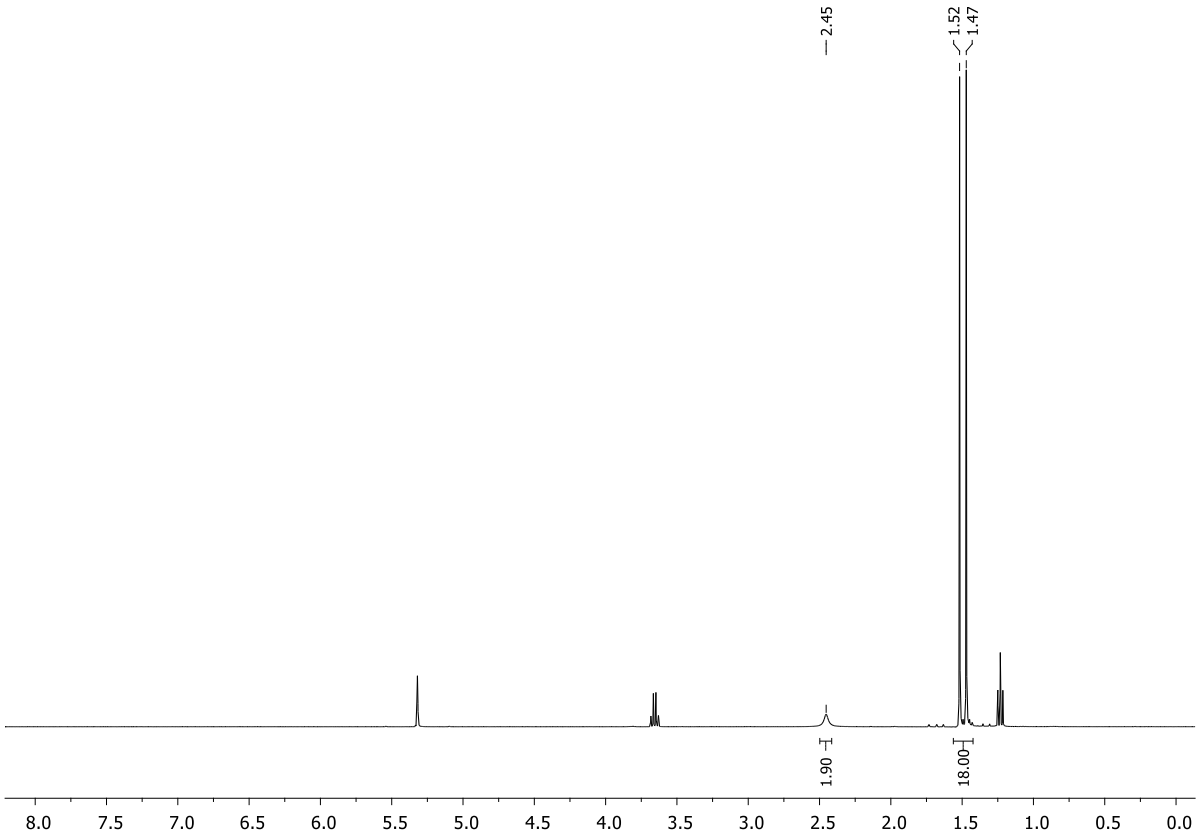

Figure S4.85. ^{1}H NMR spectrum (CD_2Cl_2, 298 K) of **(4–SeH)$^+$ WCA$^-$**.

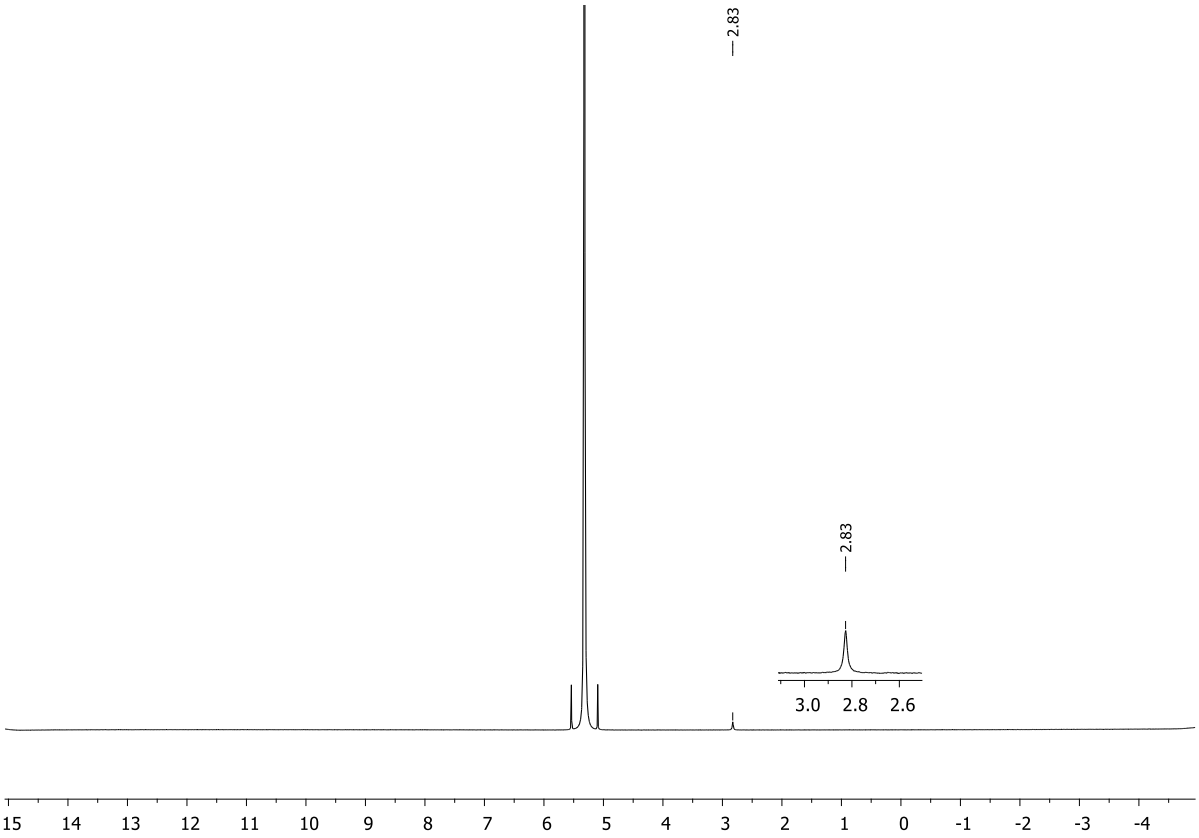

Figure S4.86. ^{2}H NMR spectrum (CH_2Cl_2/CD_2Cl_2 (9:1), 298 K) of **(4–SeH)$^+$ WCA$^-$**.

4.6.2.12. Synthesis of *t*Bu$_2$(P$^+$–OH)NH$_2$ Cl$^-$ (5·HCl)

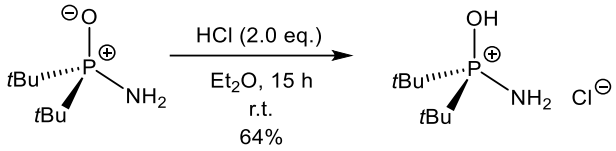

5 **5·HCl**

*t*Bu$_2$(PO)NH$_2$ (**5**) was synthesized following a reported procedure.[3a]

5 (0.30 g, 1.69 mmol, 1.0 equiv.) was dissolved in diethyl ether (10 mL) and HCl (1.7 mL, 3.38 mmol, 2.0 equiv., 2.0 M in diethyl ether) was added dropwise at room temperature resulting in a colorless suspension after a few minutes. After 15 h of stirring, the liquid phase was filtered off, the solid was washed with *n*-hexane and dried *in vacuo*. **5·HCl** was obtained as a colorless solid (0.23 g, 1.08 mmol, 64%). Crystals suitable for single crystal X-ray diffraction were grown from a DCM solution by layering with *n*-pentane.

^{1}H NMR (400.13 MHz, CD_2Cl_2, 298 K): δ = 1.41 (d, $^3J_{H–P}$ = 15.5 Hz, 18H, PC(C*H*$_3$)$_3$), 7.57 (br, 3H, N*H*$_2$/O*H*). **^{31}P{^{1}H} NMR** (162.04 MHz, CD_2Cl_2, 298 K): δ = 71.7 (s). **^{13}C{^{1}H} NMR** (100.61 MHz, CD_2Cl_2, 298 K): δ = 26.5 (s, PC(*C*H$_3$)$_3$), 35.1 (d, $^1J_{C–P}$ = 78.5 Hz, P*C*(CH$_3$)$_3$). **Elemental analysis**: $C_8H_{21}ClNOP$: calcd.: C 44.97, H 9.91, N 6.55; found: C 44.92, H 9.71, N 6.21.

For ^{2}H NMR measurements, the reaction was proceeded using **5** (0.05 g, 0.28 mmol, 1.0 equiv.) in diethyl ether (0.5 mL) and DCl (0.56 mL, 0.56 mmol, 2.0 equiv., 1.0 M in diethyl ether). ^{2}H labelled compound **5·DCl** was obtained as a colorless solid (0.052 g, 0.24 mmol, 86%). The ^{2}H NMR samples were prepared using a mixture of CH_2Cl_2 and CD_2Cl_2 (9:1) as solvent.

^{1}H NMR (400.13 MHz, CD_2Cl_2, 298 K): δ = 1.40 (d, $^3J_{H–P}$ = 15.7 Hz, 18H, PC(C*H*$_3$)$_3$), 8.33 (br, 1H, N*H*$_2$). **^{2}H NMR** (61.42 MHz, CH_2Cl_2/CD_2Cl_2 (9:1), 298 K): δ = 7.25 (br, 1D, O*D*).

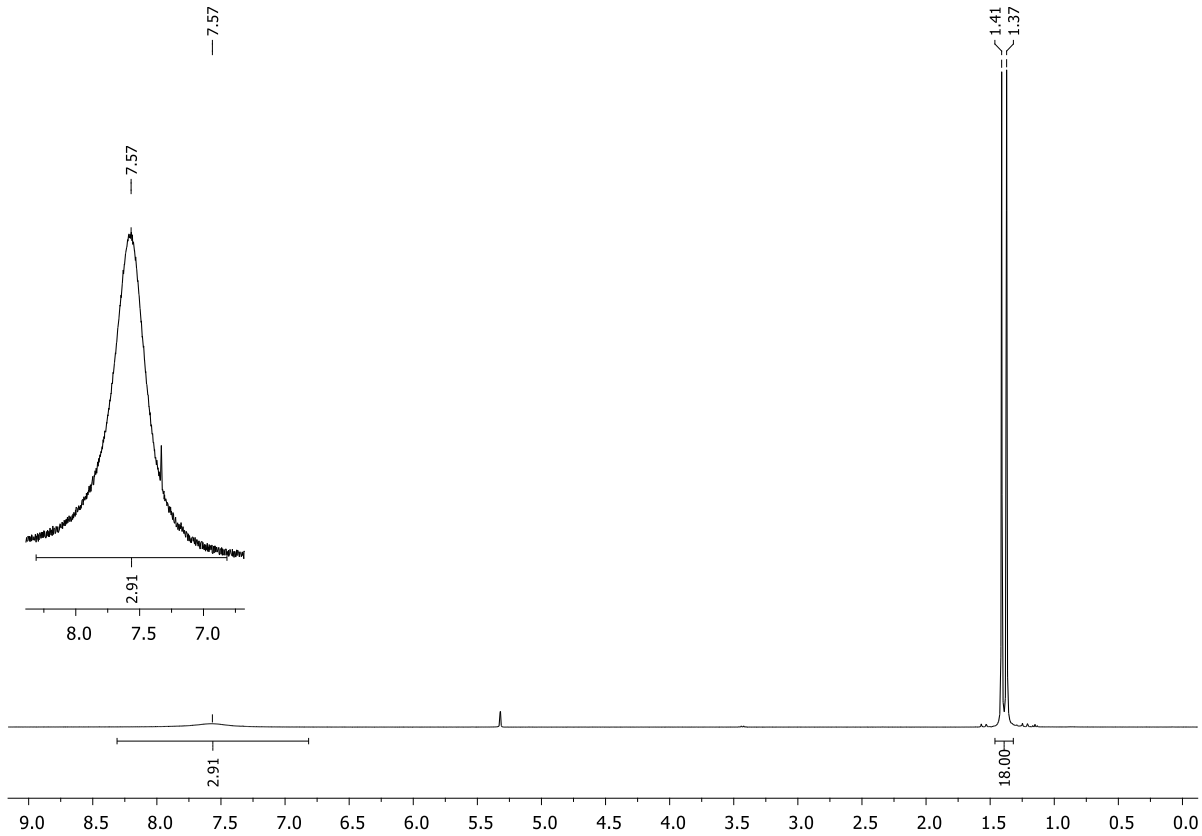

Figure S4.87. ^{1}H NMR spectrum (CD_2Cl_2, 298 K) of **5·HCl**.

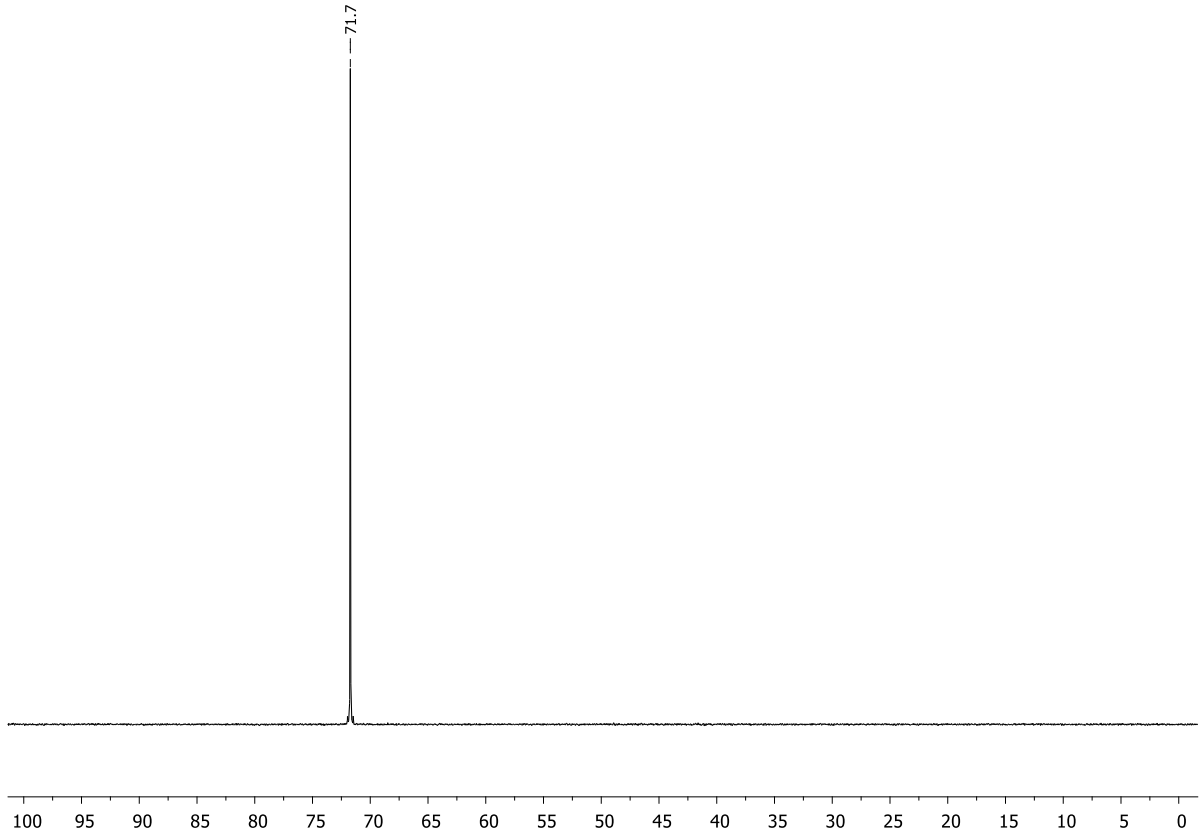

Figure S4.88. $^{31}P\{^{1}H\}$ NMR spectrum (CD_2Cl_2, 298 K) of **5·HCl**.

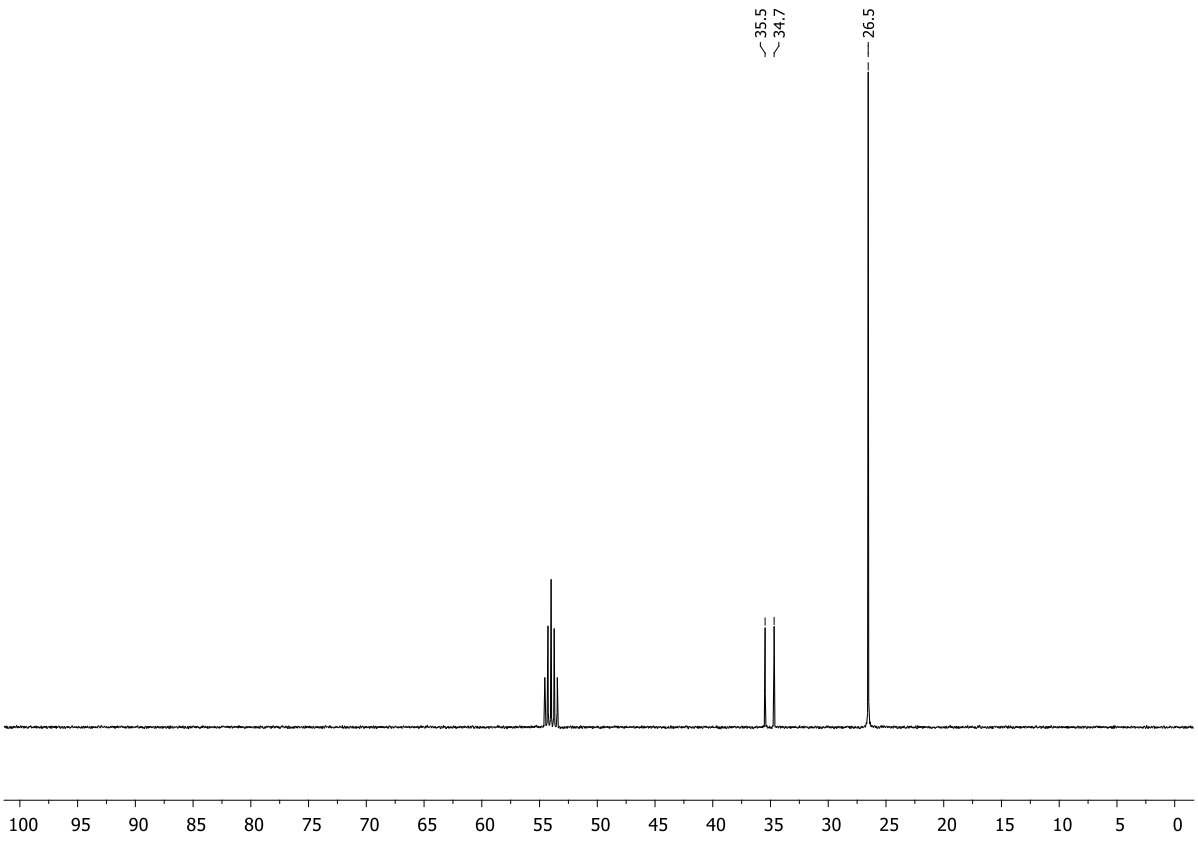

Figure S4.89. $^{13}C\{^{1}H\}$ NMR spectrum (CD_2Cl_2, 298 K) of **5·HCl**

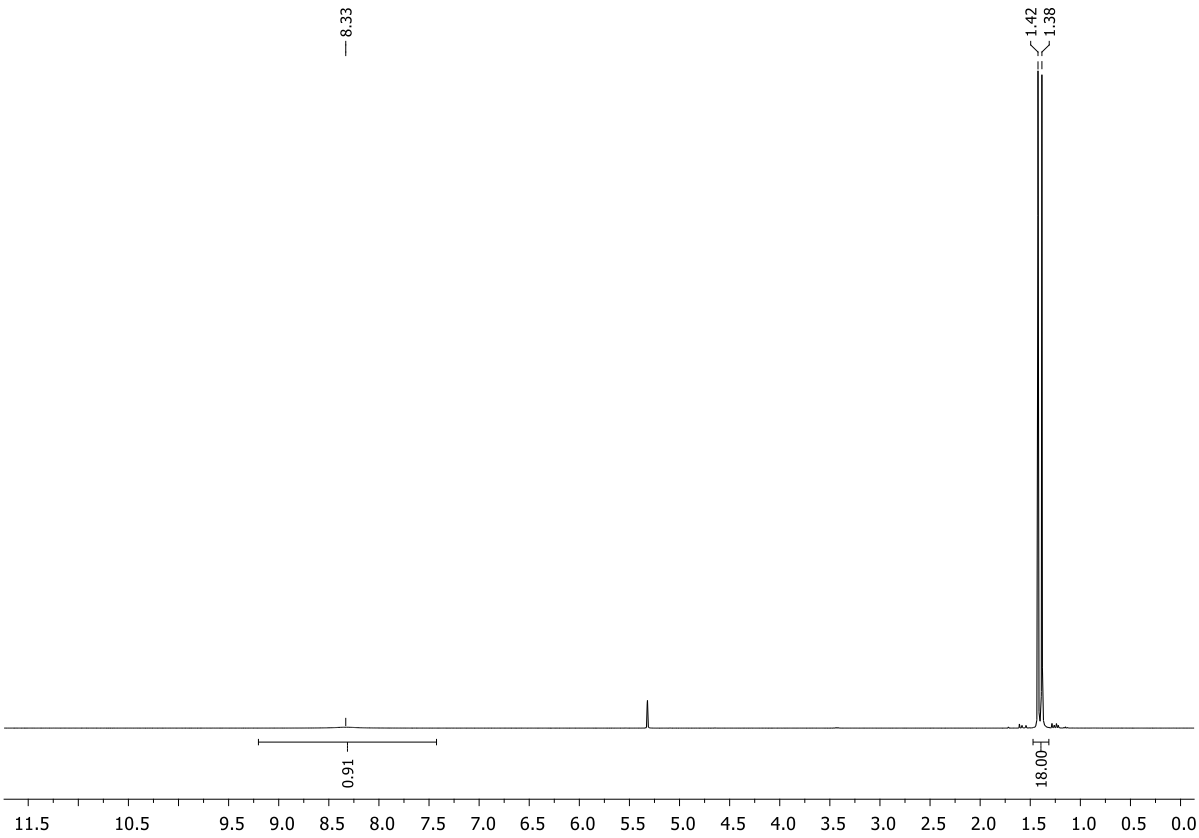

Figure S4.90. ^{1}H NMR spectrum (CD_2Cl_2, 298 K) of **5·DCl**.

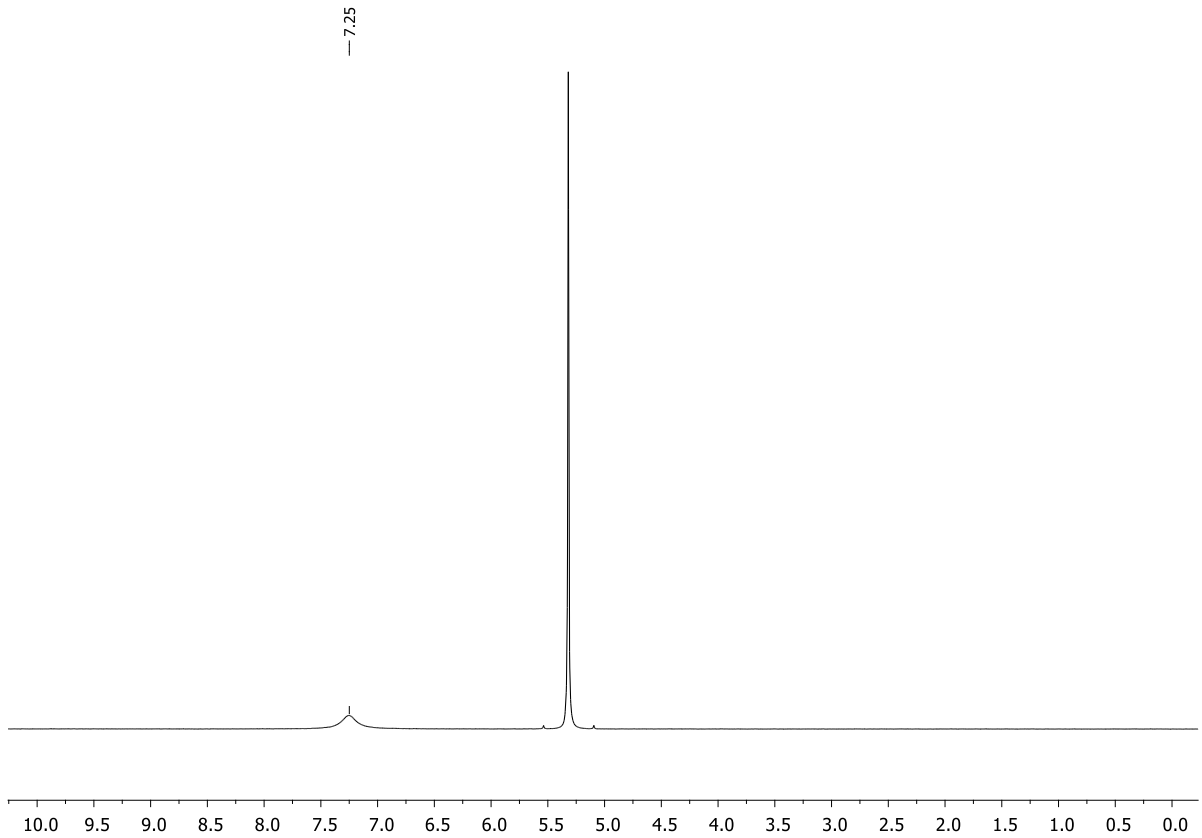

Figure S4.91. ^{2}H NMR spectrum (CH_2Cl_2/CD_2Cl_2 (9:1), 298 K) of **5·DCl**.

4.6.2.13. Synthesis of *t*Bu$_2$(P$^+$–OH)NH$_2$ B(C$_6$F$_5$)$_4^-$ [(5–OH)$^+$ WCA$^-$]

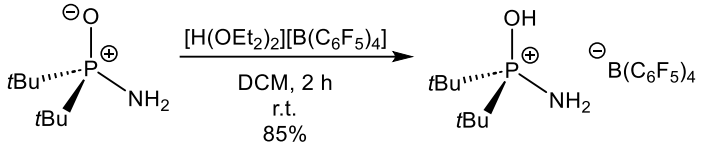

5 **(5–OH)$^+$ WCA$^-$**

*t*Bu$_2$(PO)NH$_2$ (**5**) was synthesized following a reported procedure.[3a]

5 (55.0 mg, 0.47 mmol, 1.0 equiv.) and [H(OEt$_2$)$_2$][B(C$_6$F$_5$)$_4$] (390 mg, 0.47 mmol, 1.0 equiv.) were dissolved in dichloromethane (2 mL) and the resulting solution was stirred for 2 h at room temperature. All volatiles were removed *in vacuo* and the solid further dried. **(5–OH)$^+$ WCA$^-$** was obtained as a colorless solid (343 mg, 0.40 mmol, 85%).

^{1}H NMR (400.13 MHz, CD_2Cl_2, 298 K): δ = 1.44 (d, $^3J_{H–P}$ = 17.0 Hz, 18H, PC(C*H*$_3$)$_3$), 3.55 (br, 2H, N*H*$_2$), 6.04 (br, 1H, O*H*). **^{31}P{^{1}H} NMR** (162.04 MHz, CD_2Cl_2, 298 K): δ = 82.4 (s). **^{13}C{^{1}H} NMR** (100.61 MHz, CD_2Cl_2, 298 K): δ = 25.9 (s, PC(*C*H$_3$)$_3$), 35.2 (d, $^1J_{C–P}$ = 70.9 Hz, P*C*(CH$_3$)$_3$), 136.9 (d, $^1J_{C–F}$ = 247.3 Hz, *C*$_{Ar\text{-}borate}$), 138.8 (d, $^1J_{C–F}$ = 255.6 Hz, *C*$_{Ar\text{-}borate}$), 148.7 (d, $^1J_{C–F}$ = 245.4 Hz, *C*$_{Ar\text{-}borate}$), *ipso*-*C*$_{Ar\text{-}borate}$ not visible. **^{11}B{^{1}H} NMR** (128.43 MHz, CD_2Cl_2, 298 K): *δ* = −16.9 (s). **^{19}F{^{1}H} NMR** (376.66 MHz, CD_2Cl_2, 298 K): *δ* = −167.3 (m, 8F, *meta*-*F*$_{Ar\text{-}borate}$), −163.3 (m, 4F, *para*-*F*$_{Ar\text{-}borate}$), −133.1 (s, 8F, *ortho*-*F*$_{Ar\text{-}borate}$). **Elemental analysis**: $C_{32}H_{21}BF_{20}NPO \cdot 0.4\ Et_2O$: calcd.: C 45.50, H 2.84, N 1.58; found: C 45.54, H 2.75, N 1.54.

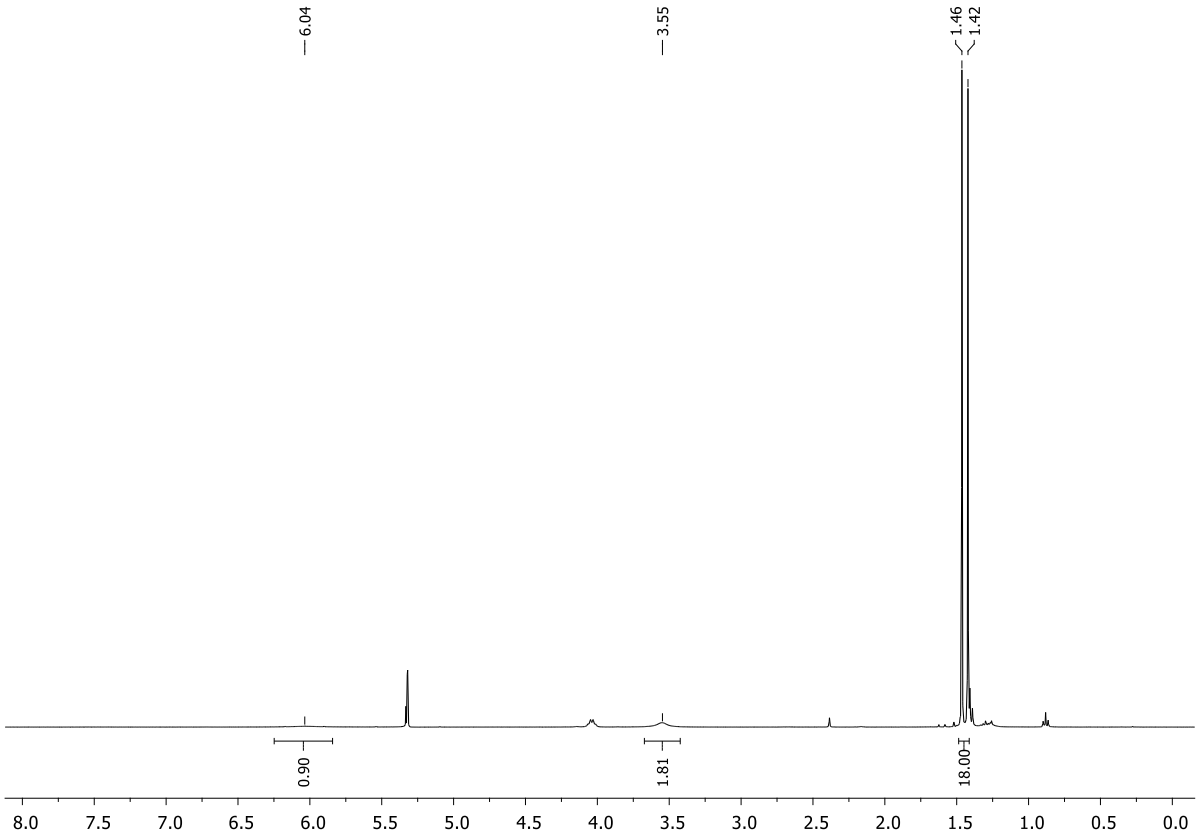

Figure S4.92. ^{1}H NMR spectrum (CD_2Cl_2, 298 K) of **(5–OH)$^+$ WCA$^-$**.

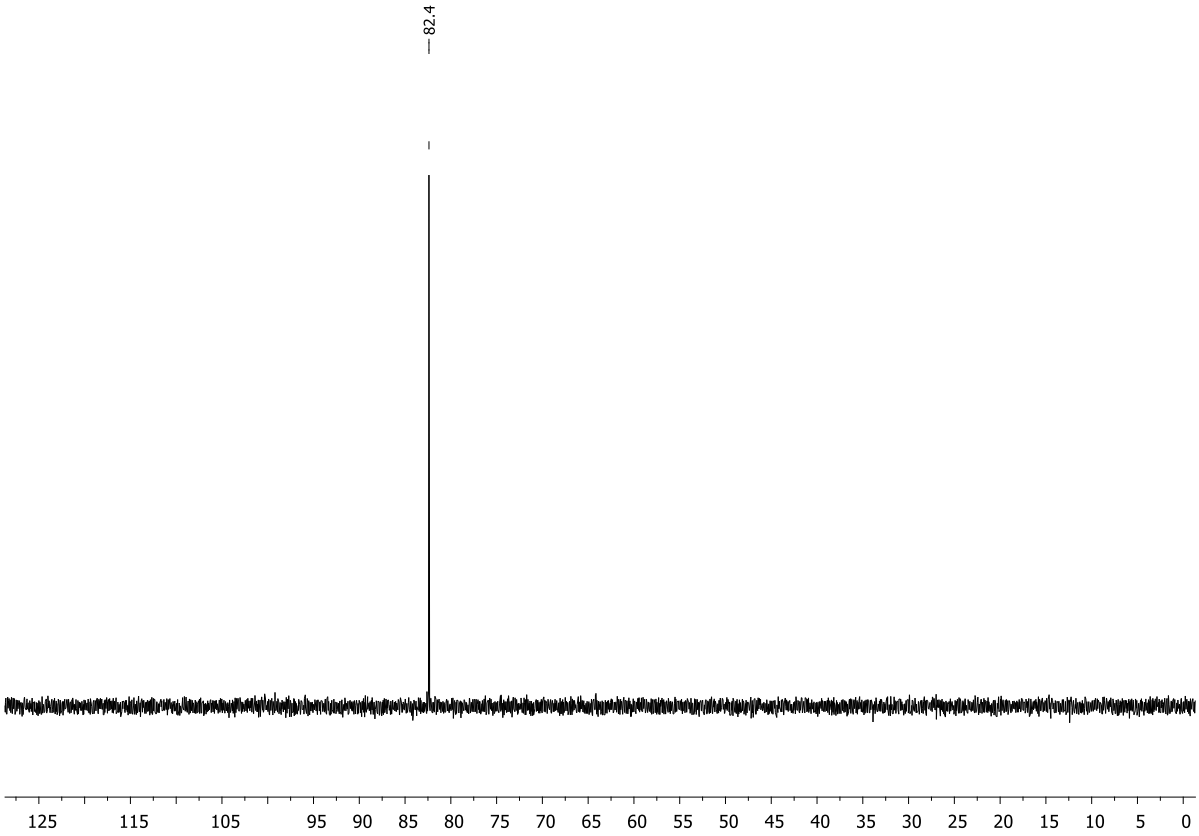

Figure S4.93. $^{31}P\{^{1}H\}$ NMR spectrum (CD_2Cl_2, 193 K) of **(5–OH)$^+$ WCA$^-$**.

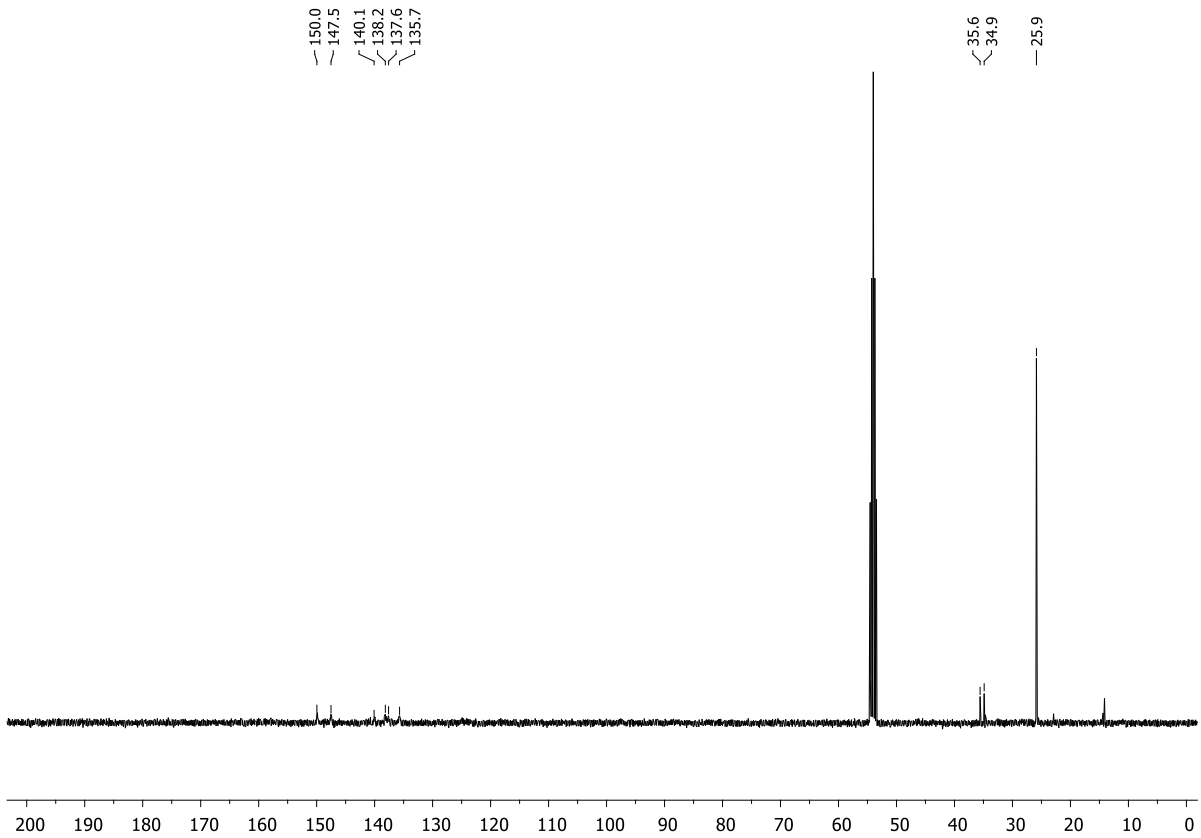

Figure S4.94. $^{13}C\{^{1}H\}$ NMR spectrum (CD_2Cl_2, 298 K) of **(5–OH)$^+$ WCA$^-$**.

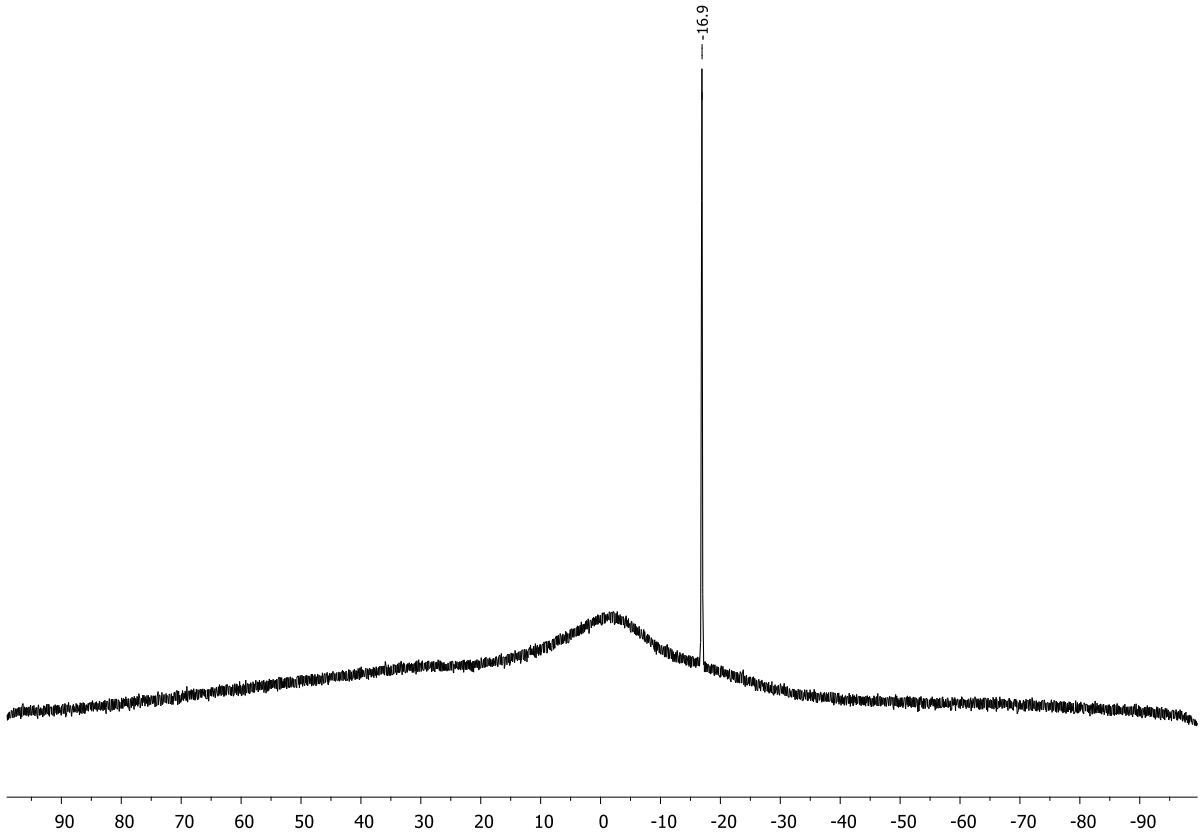

Figure S4.95. $^{11}B\{^{1}H\}$ NMR spectrum (CD_2Cl_2, 298 K) of **(5–OH)$^+$ WCA$^-$**.

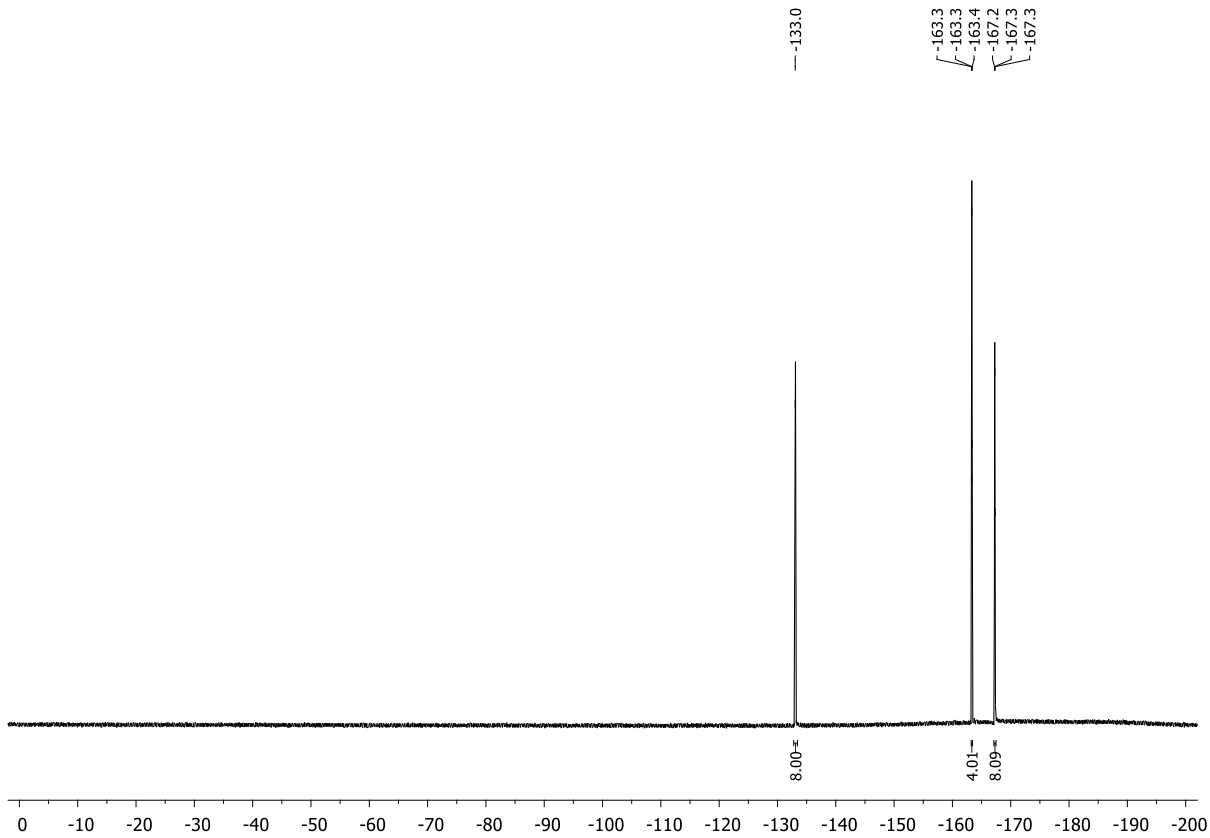

Figure S4.96. $^{19}F\{^{1}H\}$ NMR spectrum (CD_2Cl_2, 298 K) of **(5–OH)$^+$ WCA$^-$**.

4.6.2.14. Synthesis of *t*Bu$_2$(P$^+$–SH)CH$_2$Si(H)*t*Bu$_2$ B(C$_6$F$_5$)$_4^-$ [(6–SH)$^+$ WCA$^-$]

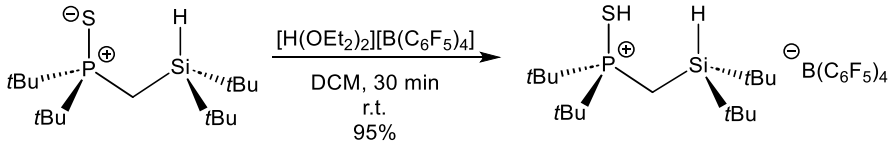

6 **(6–SH)$^+$ WCA$^-$**

6 was prepared following a procedure published by our group.[5]

6 (202 mg, 0.60 mmol, 1.0 equiv.) and [H(OEt$_2$)$_2$][B(C$_6$F$_5$)$_4$] (500 mg, 0.60 mmol, 1.0 equiv.) were dissolved in dichloromethane (4 mL) and the resulting solution was stirred for 30 min at room temperature. All volatiles were removed *in vacuo* and the solid further dried. Then the white powder was washed twice with 2 mL *n*-hexane. Subsequently the dry white powder was dissolved in 1 mL DCM and layered with 3 mL *n*-hexane. **[(6–SH)$^+$ WCA$^-$]** was obtained as fine colorless needles suitable for single crystal X-Ray crystallography (585 mg, 0.58 mmol, 95 %).

^{1}H NMR (400.13 MHz, CD_2Cl_2, 298 K): δ = 1.15 (s, 18H, SiC(C*H*$_3$)$_3$), 1.53 (d, $^3J_{P–H}$ = 17.8 Hz, 18H, PC(C*H*$_3$)$_3$), 1.55 (dd, $^2J_{P–H}$ = 14.4 Hz, $^3J_{H–H}$ = 2.0 Hz, 2H, P–C*H*$_2$–Si), 2.42 (br, 1H, S–*H*), 3.90 (m, 1H, Si–*H*). **^{31}P{^{1}H} NMR** (162.04 MHz, CD_2Cl_2, 298 K): δ = 89.3 (s). **^{13}C{^{1}H} NMR** (100.61 MHz, CD_2Cl_2, 298 K): δ = −1.7 (d, $^1J_{P–C}$ = 27.2 Hz, P–*C*H$_2$–Si), 20.2 (d, $^3J_{P–C}$ = 2.4 Hz, Si*C*(CH$_3$)$_3$), 27.6 (d, $^2J_{P–C}$ = 0.6 Hz, PC(*C*H$_3$)$_3$), 29.5 (s, SiC(*C*H$_3$)$_3$), 40.8 (d, $^1J_{P–C}$ = 29.3 Hz, P*C*(CH$_3$)$_3$), 124.1 (br, *ipso*-*C*$_{Ar\text{-}borate}$), 136.9 (d, $^1J_{C–F}$ = 243.3 Hz, *C*$_{Ar\text{-}borate}$), 138.8 (d, $^1J_{C–F}$ = 245.1 Hz, *C*$_{Ar\text{-}borate}$), 148.8 (d, $^1J_{C–F}$ = 238.6 Hz, *C*$_{Ar\text{-}borate}$). **^{11}B{^{1}H} NMR** (128.43 MHz, CD_2Cl_2, 298 K): δ = −16.9 (s). **^{19}F{^{1}H} NMR** (376.66 MHz, CD_2Cl_2, 298 K): δ = −167.3 (m, 8F, *meta*-*F*$_{Ar\text{-}borate}$), −163.5 (m, 4F, *para*-*F*$_{Ar\text{-}borate}$), −132.9 (m, 8F, *ortho*-*F*$_{Ar\text{-}borate}$). **^{29}Si{^{1}H} NMR** (79.49 MHz, CD_2Cl_2, 298 K): δ = 6.6 (d, $^2J_{P–Si}$ = 11.9 Hz). **Elemental analysis**: $C_{41}H_{40}BF_{20}PSSi$: calcd.: C 48.50, H 3.97; found: C 48.45, H 3.97.

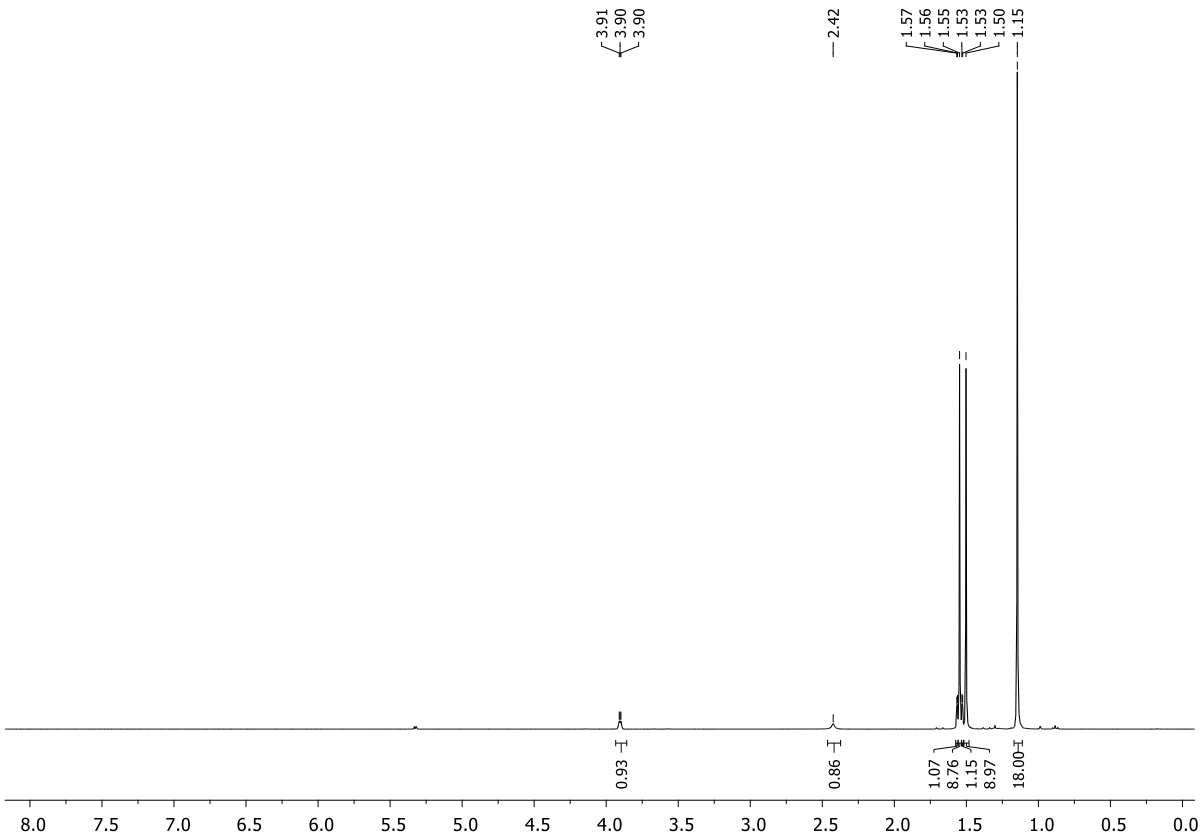

Figure S4.97. ^{1}H NMR spectrum (CD_2Cl_2, 298 K) of **(6–SH)$^{+}$ WCA^{-}**.

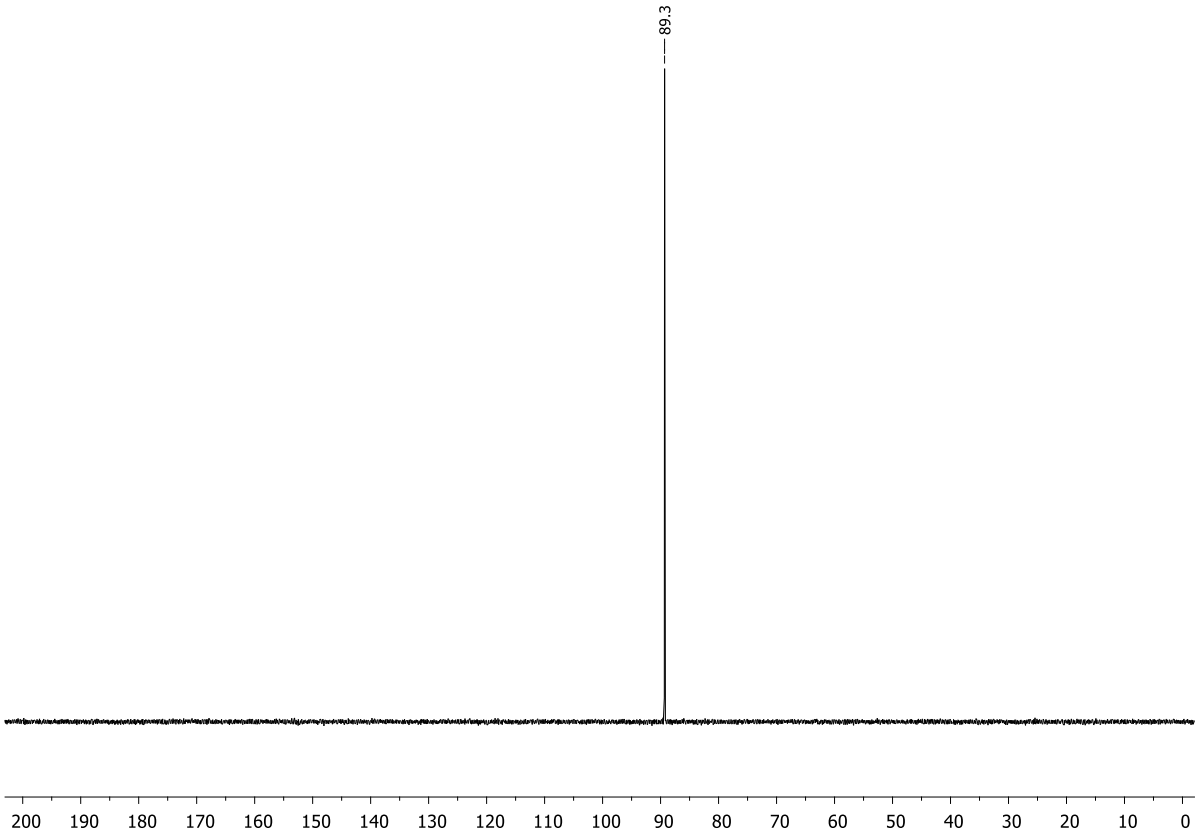

Figure S4.98. $^{31}P\{^{1}H\}$ NMR spectrum (CD_2Cl_2, 298 K) of **(6–SH)$^{+}$ WCA^{-}**.

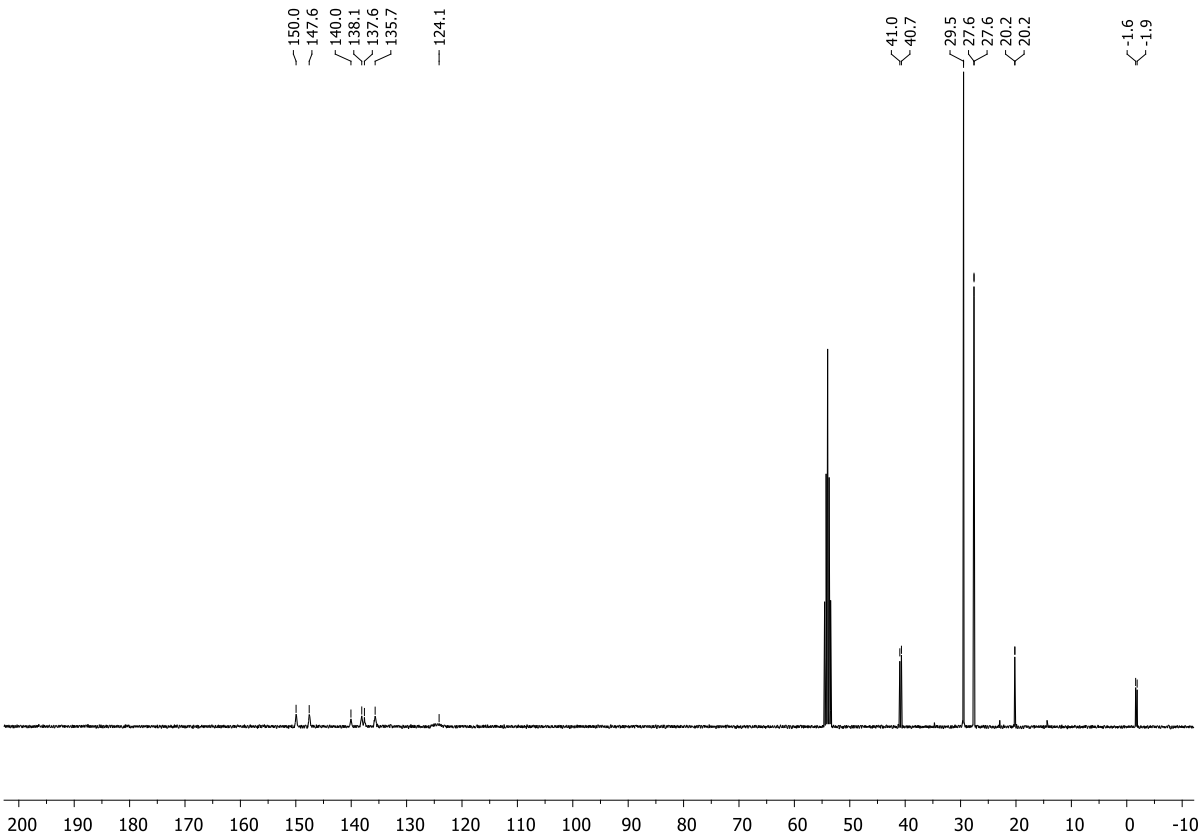

Figure S4.99. $^{13}C\{^{1}H\}$ NMR spectrum (CD_2Cl_2, 298 K) of **(6–SH)$^+$ WCA$^-$**.

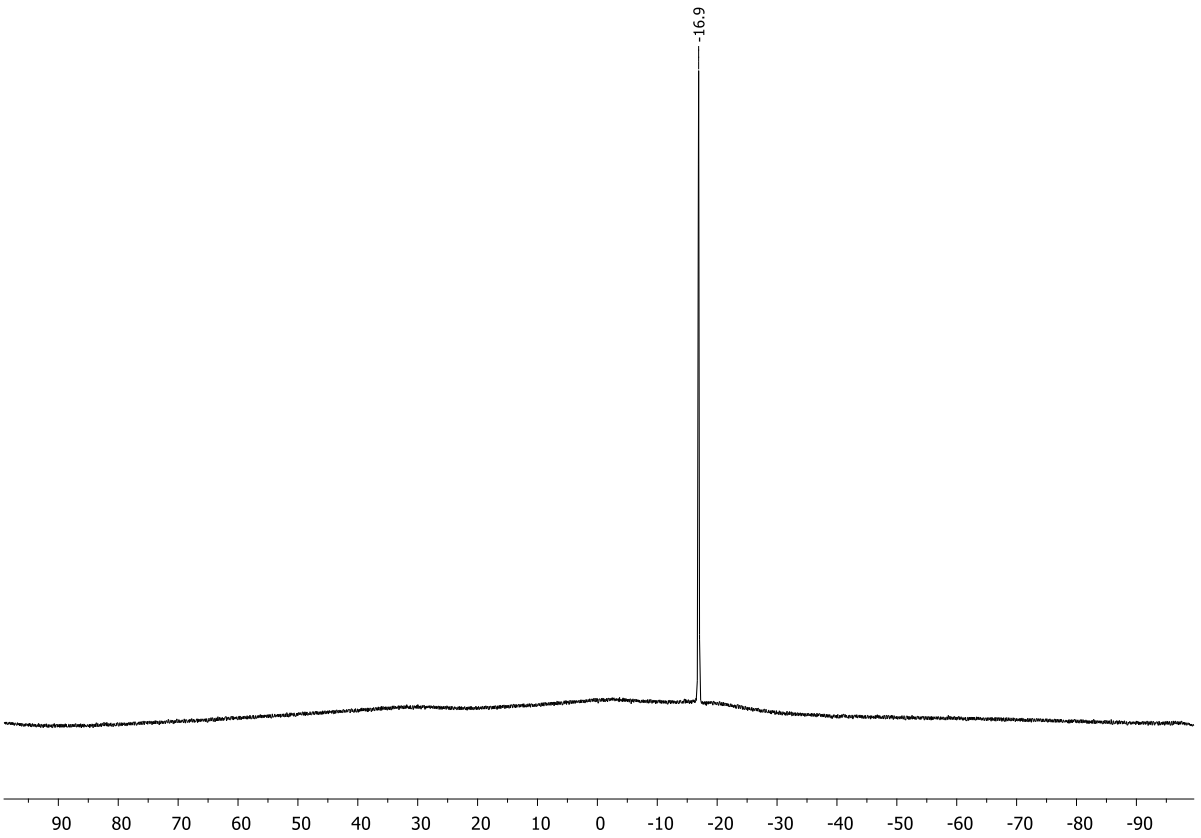

Figure S4.100. $^{11}B\{^{1}H\}$ NMR spectrum (CD_2Cl_2, 298 K) of **(6–SH)$^+$ WCA$^-$**.

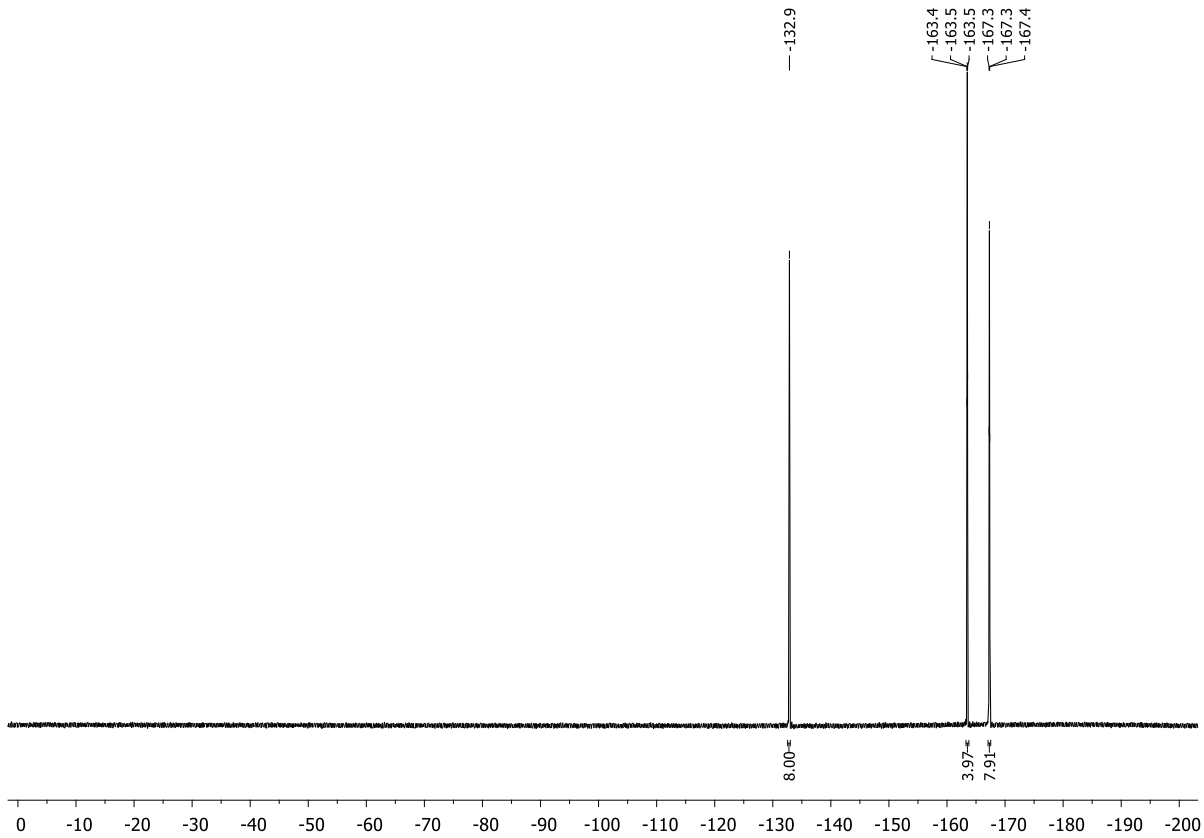

Figure S4.101. $^{19}F\{^{1}H\}$ NMR spectrum (CD_2Cl_2, 298 K) of **(6–SH)$^+$ WCA$^-$**.

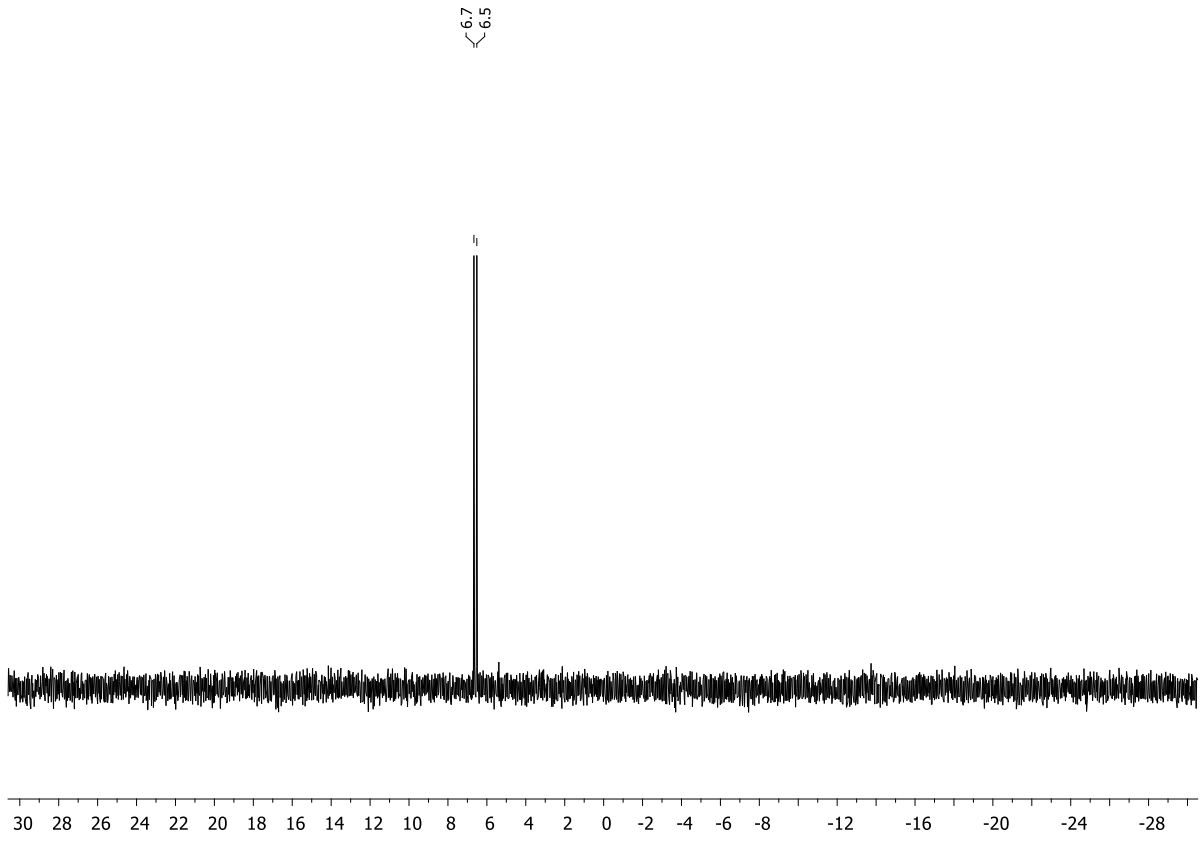

Figure S4.102. $^{29}Si\{^{1}H\}$ NMR spectrum (CD_2Cl_2, 298 K) of **(6–SH)$^+$ WCA$^-$**.

4.6.3. Concentration- and Temperature-Dependent Investigations

4.6.3.1. Diffusion-Ordered NMR Spectroscopy (DOSY)

General information

Diffusion ordered NMR spectroscopy experiments were performed in CD_2Cl_2 on Bruker Avance III HD 600 MHz spectrometer, equipped with a 5 mm CPPBBO BB-1H/19F. All measurements were performed at 298 K and temperature was controlled by BVTE 3900. NMR Data were processed, evaluated and plotted with TopSpin 3.2 software. Further analysis of the measurements was performed with Microsoft Excel (Version 16.0.10359.20023 64 Bit). The results of the measurements are shown in Table S4.1.

Diffusion-ordered spectroscopy (DOSY)

The DOSY measurements were performed with the convection suppressing DSTE (double stimulated echo) pulse sequence developed by Jerschow and Müller in a pseudo 2D mode.[6] Smoothed square (SMSQ10.100) gradient shapes and a linear gradient ramp with 20 increments between 5% and 95% of the maximum gradient strength (5.35 G/mm) were used. The diffusion time delay was set to 45 ms. For the homospoil gradient strengths, values of 100, −13.17, 20 and −17.13% were used. Gradient pulse lengths (p16) were first optimized to obtain a sigmoidal signal decay for increasing gradient strength (0.75 ms for TMS, 0.9–1.2 ms for the investigated molecules). NMR spectra were processed with Bruker TopSpin 3.2 (T1/T2 relaxation package) and diffusion coefficients were derived according to Jerschow and Müller[6]. Tetramethylsilane was added to the samples to reference chemical shifts and the viscosity of each sample.

The molecular radii were derived by the Stokes-Einstein equation[7] using Chens correction[8].

$$D_i = \frac{k_B T}{6\pi\eta r_H} * \left[1 + 0.695 * \left(\frac{r_{solv}}{r_H}\right)^{2.234}\right]$$

D_i is the self-diffusion coefficient derived by the measurement, η is the viscosity of the solvent, r_H is the hydrodynamic radius of the observed molecule and r_{solv} the radius of the solvent. No form factor correction was applied. The viscosity was determined by measuring the diffusion coefficient of the reference tetramethylsilane (TMS) and solving the equation for η with the literature value[9] of the radius of 2.96 Å. The solvent radius of CD_2Cl_2 (2.46 Å) was taken from literature.[10]

Table S4.1. Results of the DOSY measurements (600 MHz).

Compound	Sample	Solvent	Nucleus	Diffusion coefficient in m^2/s	Diffusion coefficient of TMS in m^2/s	Concentration in mmol/L	Temperature in K	Hydrodynamic Radius in Å	Volume in $Å^3$
1	TH120	CD_2Cl_2	^1H	1.84E-09	2.83E-09	50	298	3.90	248
(1·HCl)$_4$	TH231	CD_2Cl_2	^1H	1.70E-09	2.70E-09	5	298	3.98	265
(1·HCl)$_4$	TH231	CD_2Cl_2	^1H	1.35E-09	2.69E-09	30	298	4.70	435
(1·HCl)$_4$	TH231	CD_2Cl_2	^1H	1.12E-09	2.68E-09	50	298	5.43	670
(1·HCl)$_4$	TH231	CD_2Cl_2	^1H	1.01E-09	2.73E-09	100	298	6.00	905
(R_P)-**2**	TH288	CD_2Cl_2	^1H	1.69E-09	2.75E-09	50	298	4.06	280
[(R_P)-2 · HCl]$_4$	TH282	CD_2Cl_2	^1H	1.72E-09	2.77E-09	5	298	4.02	273
[(R_P)-2 · HCl]$_4$	TH282	CD_2Cl_2	^1H	1.12E-09	2.74E-09	50	298	5.54	713
3	TH111	CD_2Cl_2	^1H	1.90E-09	2.80E-09	50	298	3.79	228
4	TH488	CD_2Cl_2	^1H	1.80E-09	2.70E-09	50	298	3.83	235
(4·HCl)$_4$	TH474	CD_2Cl_2	^1H	1.91E-09	2.96E-09	5	298	3.92	251
(4·HCl)$_4$	TH474	CD_2Cl_2	^1H	8.06E-10	2.13E-09	500	298	5.89	855
(1–SH)$^+$ WCA$^-$	TH357 Cation	CD_2Cl_2	^1H	1.50E-09	3.38E-09	100	298	5.17	579
(1–SH)$^+$ WCA$^-$	TH357 Anion	CD_2Cl_2	^{11}B	1.18E-09	3.38E-09	100	298	6.31	1052
1	TH120	DMSO-d_6	^1H	5.14E-10	9.18E-10	100	298	4.26	324
(1–SH)$^+$ WCA$^-$	TH357 Cation	DMSO-d_6	^1H	3.41E-10	6.67E-10	100	298	4.55	394
(1–SH)$^+$ WCA$^-$	TH357 Anion	DMSO-d_6	^{11}B	2.86E-10	6.67E-10	100	298	5.18	583

4.6.3.2. $^{31}P\{^{1}H\}$ and ^{1}H NMR Spectroscopy

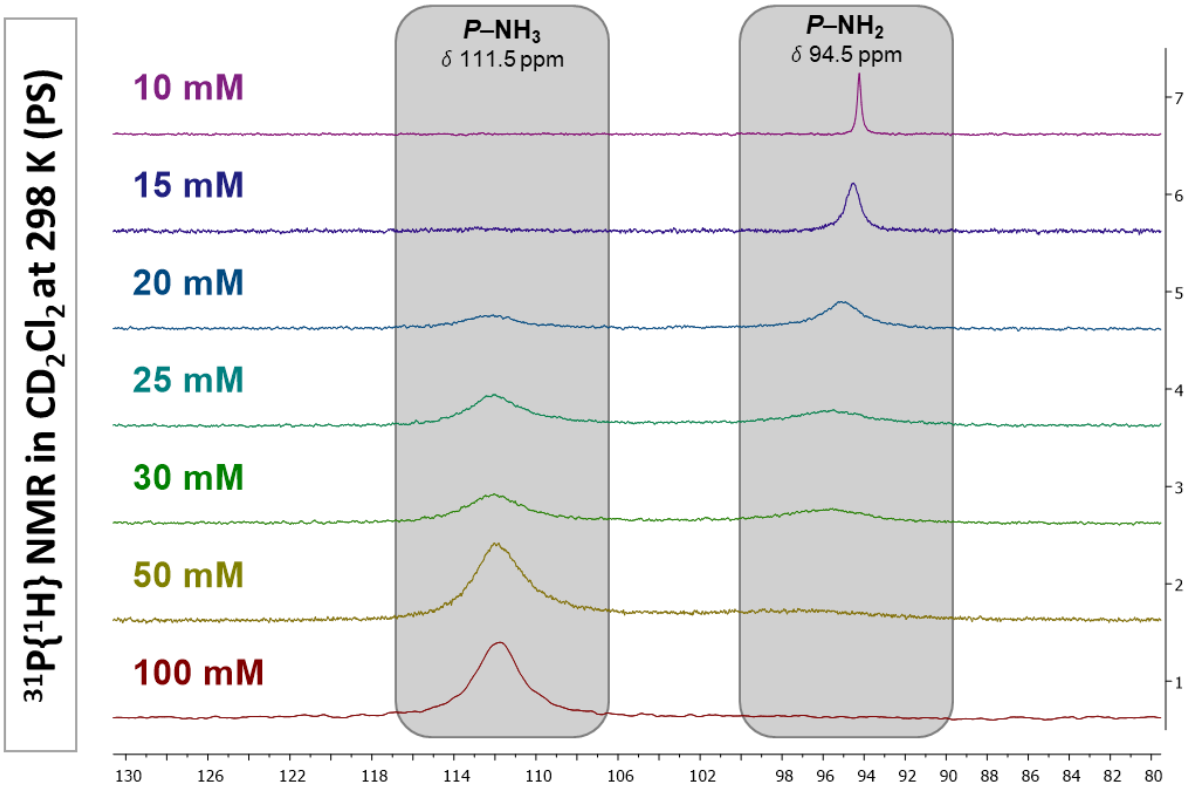

Figure S4.103. $^{31}P\{^{1}H\}$ NMR spectra (CD_2Cl_2, 298 K) of **$(1{\cdot}HCl)_4$/(1+HCl)** in different concentrations.

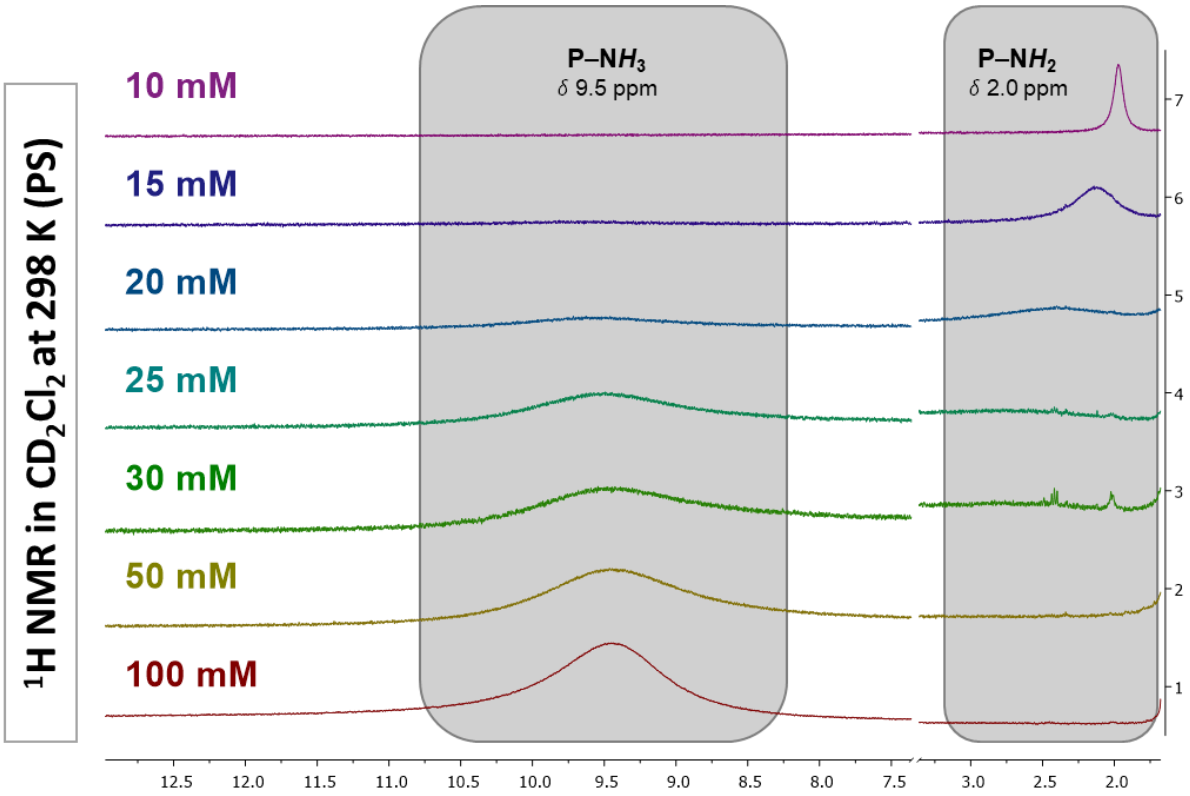

Figure S4.104. Enlarged cutout of ^{1}H NMR spectra (CD_2Cl_2, 298 K) of **$(1{\cdot}HCl)_4$/(1+HCl)** in different concentrations showing the signals for NH_3^+ (left) and NH_2 (right).

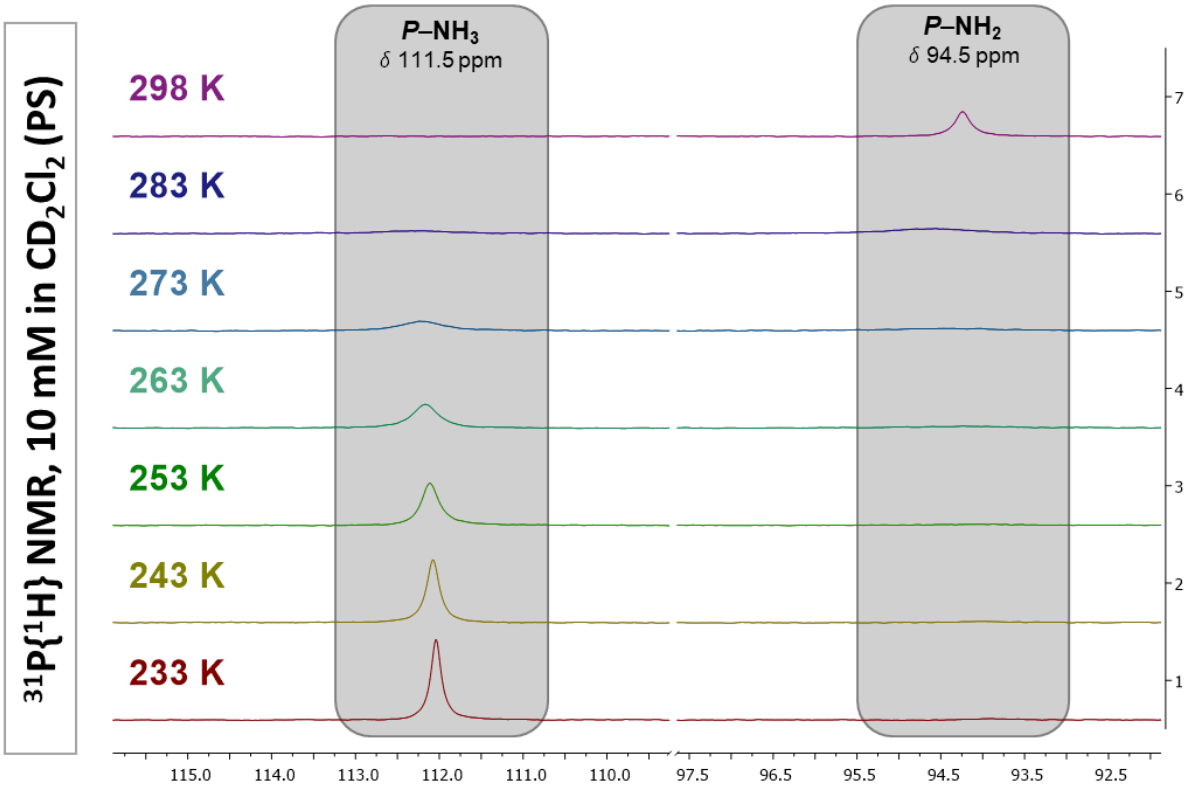

Figure S4.105. $^{31}P\{^{1}H\}$ NMR spectra (10 mM in CD_2Cl_2) of **(1·HCl)$_4$/(1+HCl)** at variable temperatures.

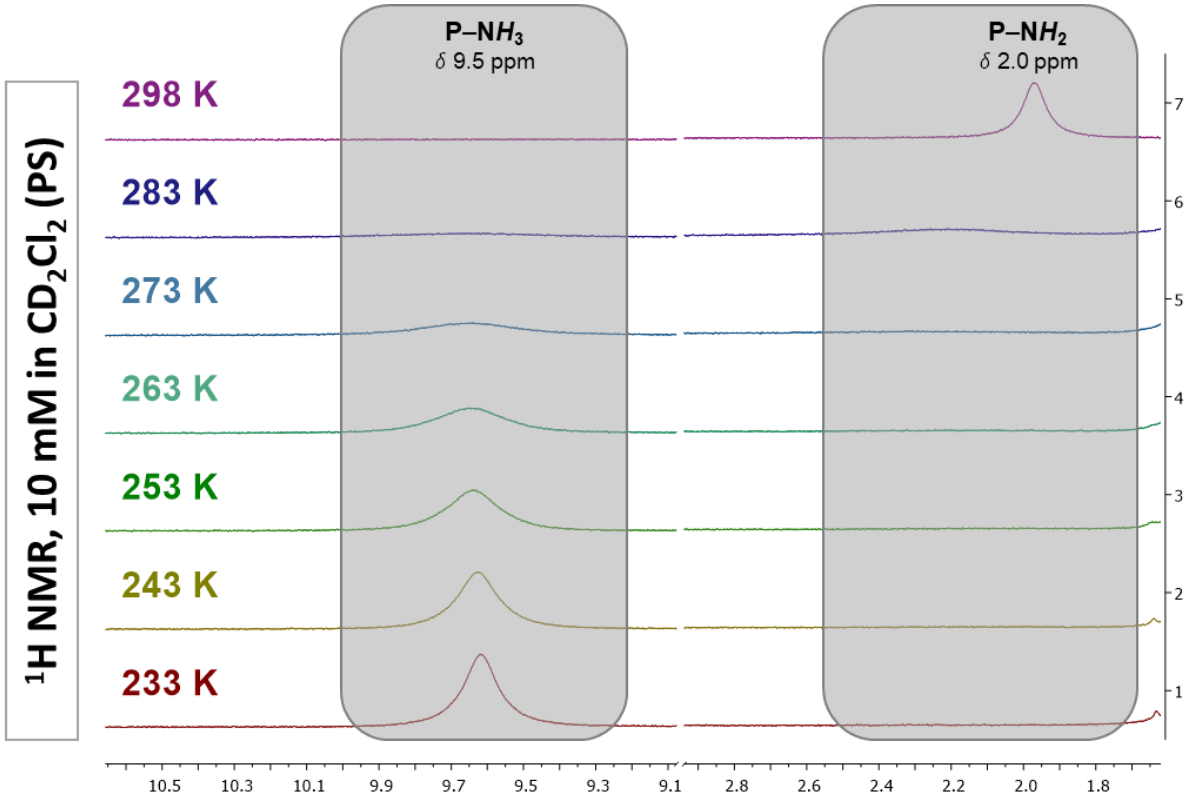

Figure S4.106. Enlarged cutout of ^{1}H NMR spectra (10 mM in CD_2Cl_2) of **(1·HCl)$_4$/(1+HCl)** at variable temperatures showing the signals for NH_3^+ (left) and NH_2 (right).

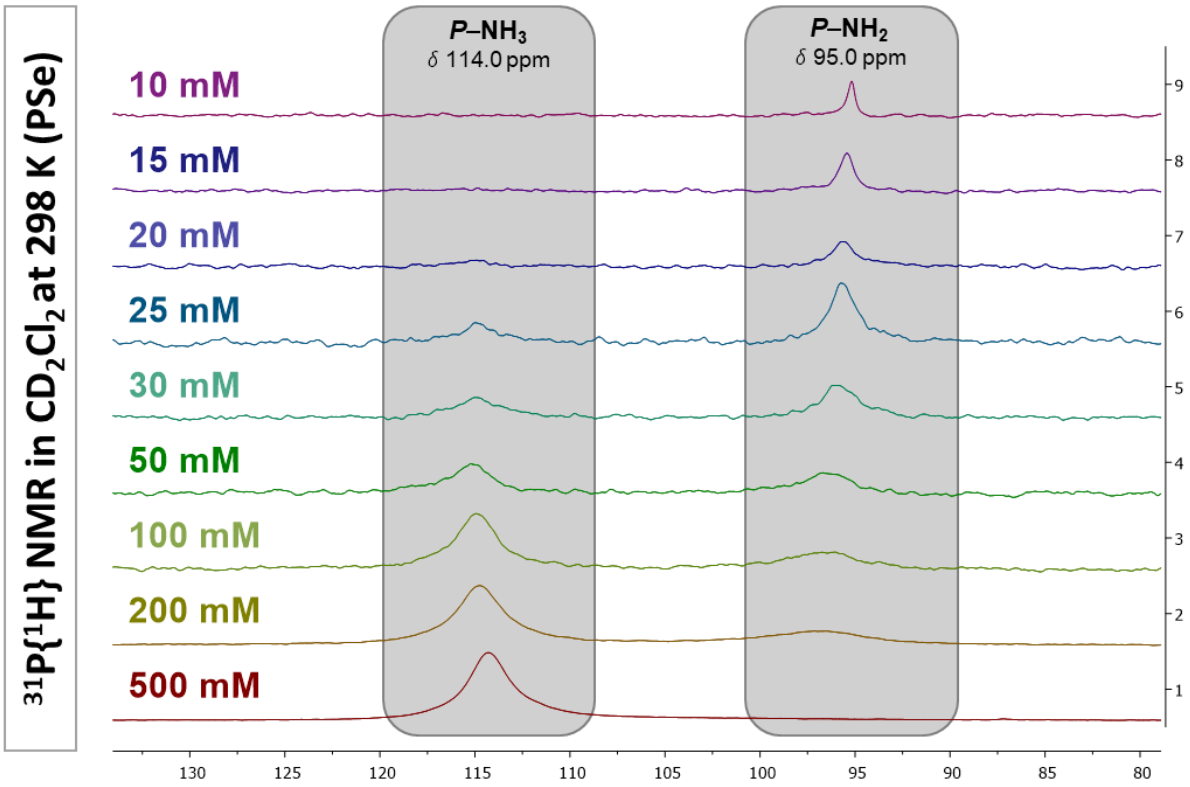

Figure S4.107. $^{31}P\{^{1}H\}$ NMR spectra (CD_2Cl_2, 298 K) of **$(4\cdot HCl)_4$/(4+HCl)** in different concentrations.

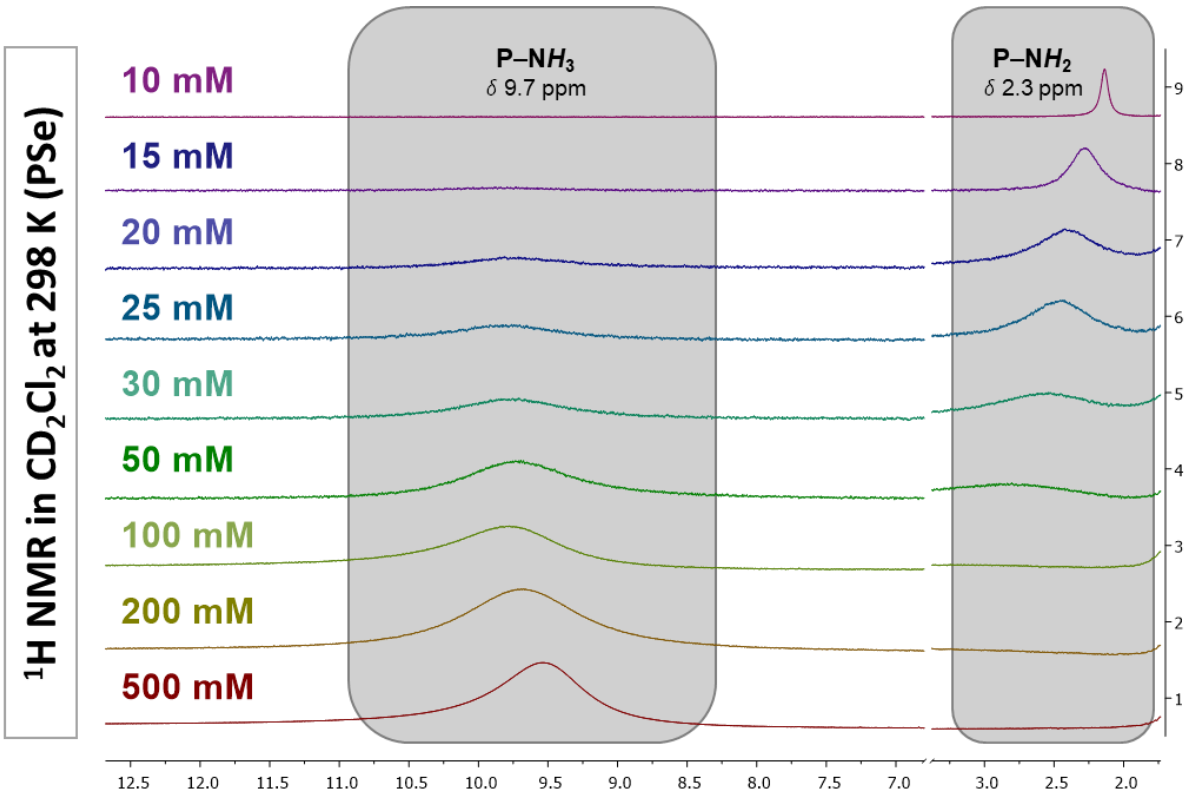

Figure S4.108. Enlarged cutout of ^{1}H NMR spectra (CD_2Cl_2, 298 K) of **$(4\cdot HCl)_4$/(4+HCl)** in different concentrations showing the signals for NH_3^+ (left) and NH_2 (right).

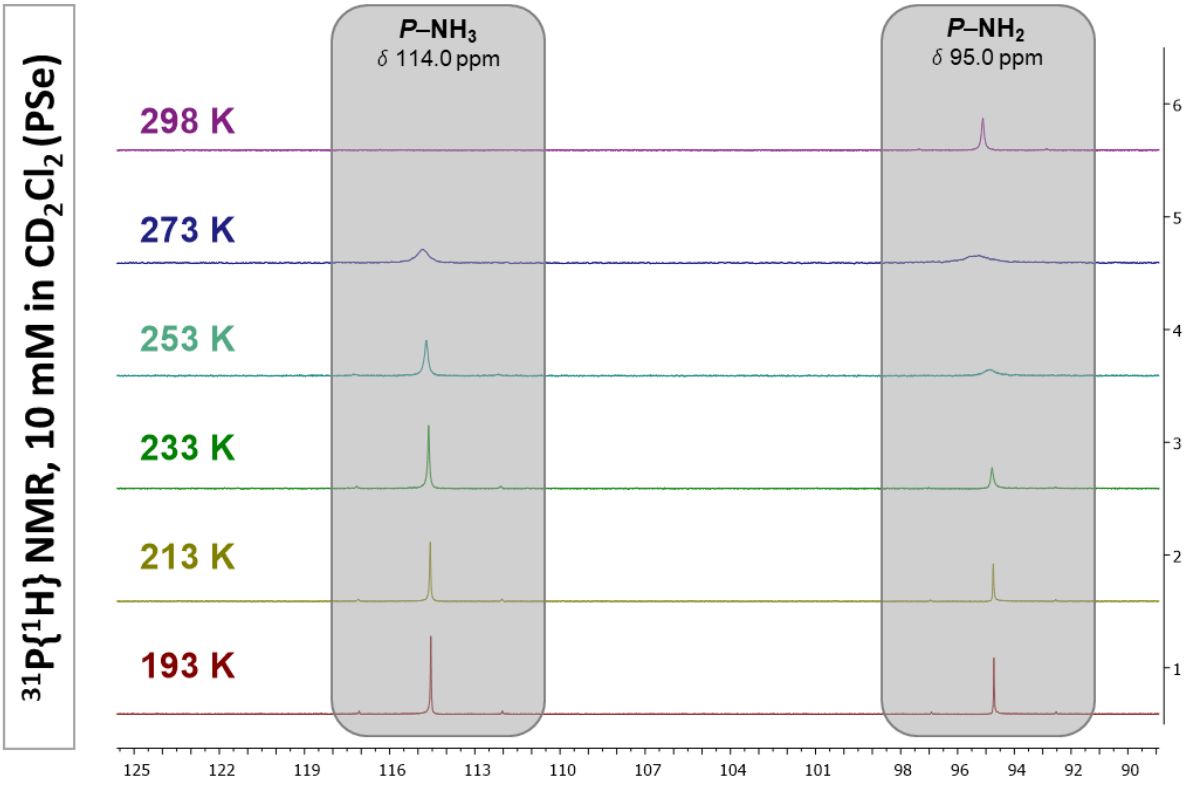

Figure S4.109. $^{31}P\{^{1}H\}$ NMR spectra (10 mM in CD_2Cl_2) of **(4·HCl)$_4$/(4+HCl)** at variable temperatures.

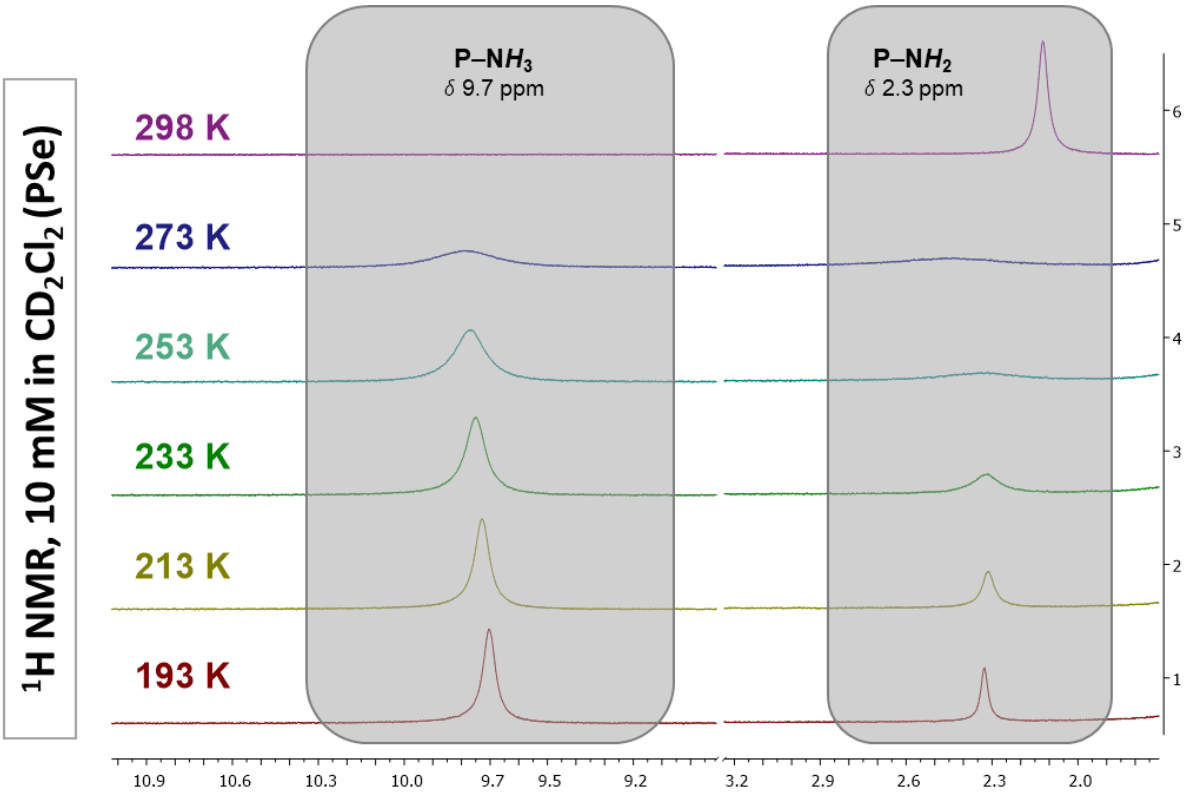

Figure S4.110. Enlarged cutout of ^{1}H NMR spectra (10 mM in CD_2Cl_2) of **(4·HCl)$_4$/(4+HCl)** at variable temperatures showing the signals for NH_3^+ (left) and NH_2 (right).

4.6.3.3. Infrared Spectroscopy (IR)

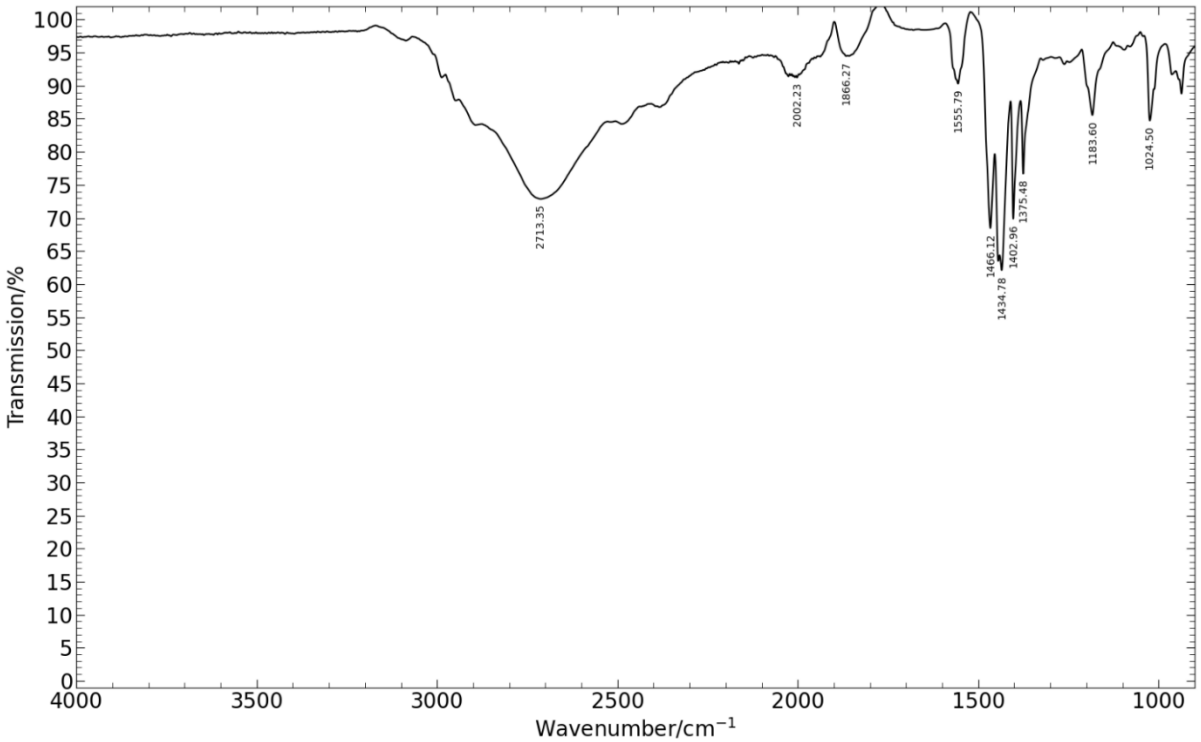

Figure S4.111. IR spectrum (298 K) of **(1·HCl)$_4$** in the solid state.

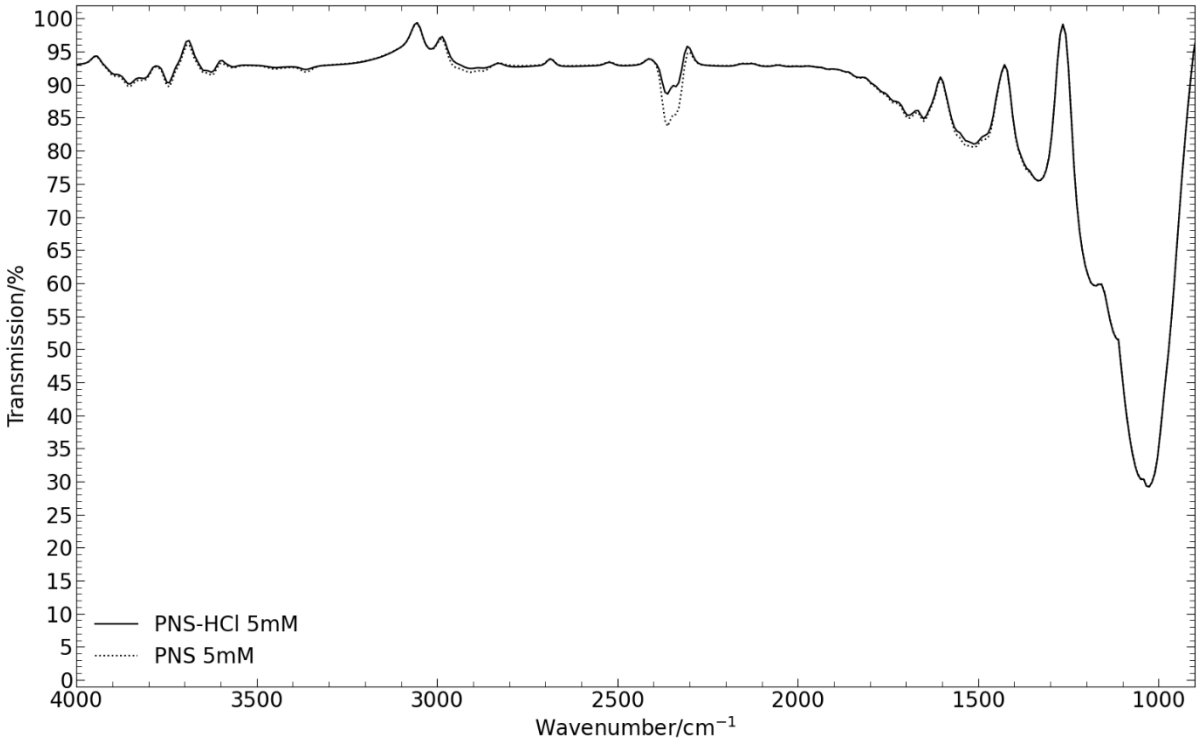

Figure S4.112. IR spectra (298 K) of **1** in 5 mM CH_2Cl_2 solution (dotted line) and **1 + HCl$_{solv}$** in 5 mM CH_2Cl_2 solution (solid line) showing almost no difference.

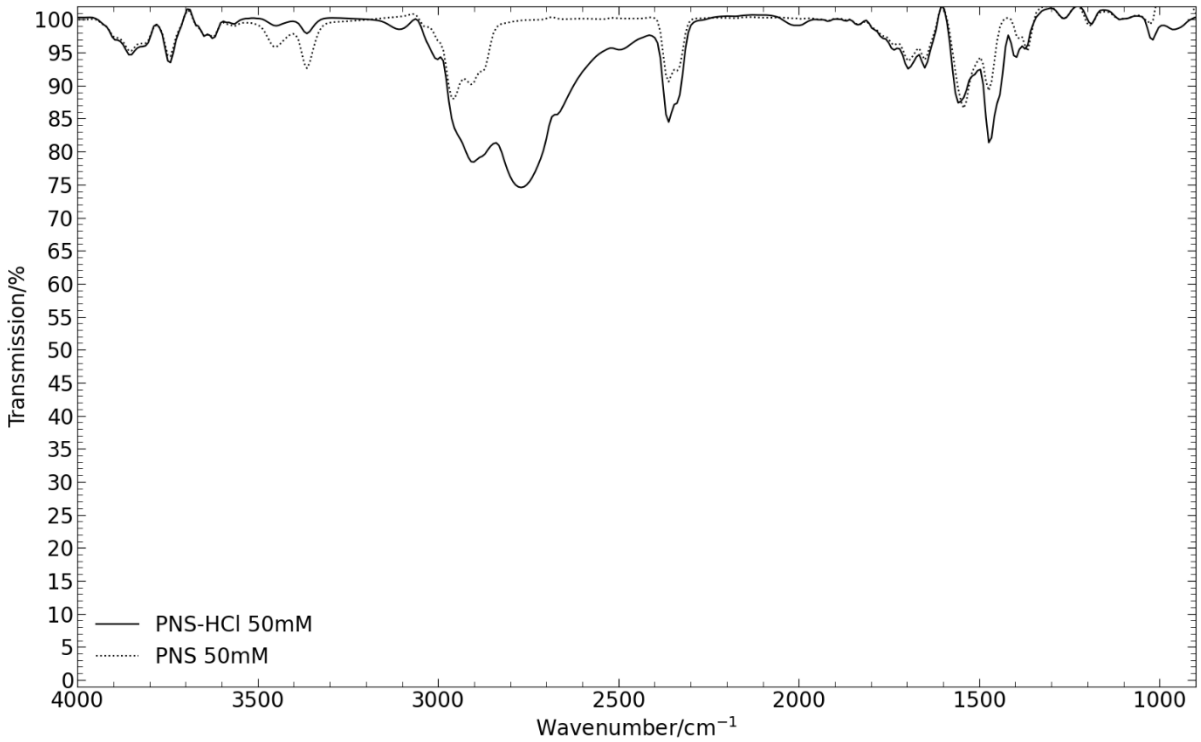

Figure S4.113. IR spectra (298 K) of **1** in 50 mM CH_2Cl_2 solution (dotted line) and **(1·HCl)$_4$** in 50 mM CH_2Cl_2 solution (solid line). The broad signal at about 2750 cm^{-1} shows that the NH_3^+ moiety is present in 50 mM solution of **(1·HCl)$_4$**.

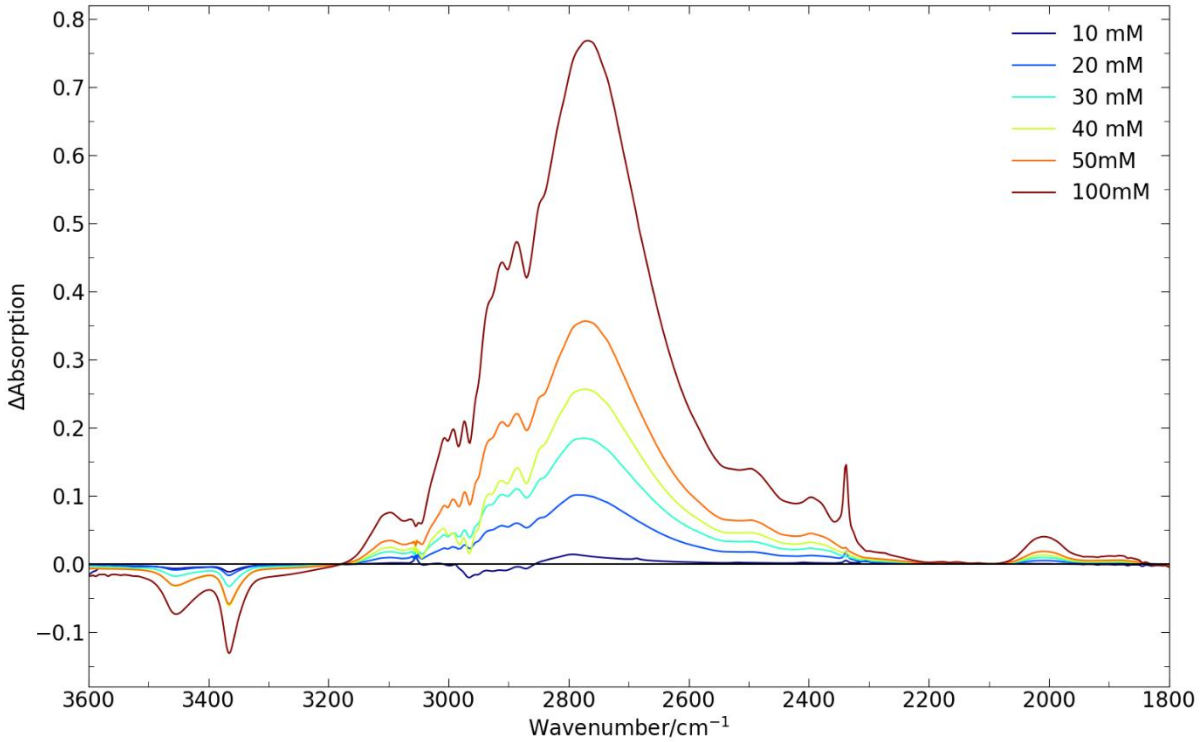

Figure S4.114. Cutout of the difference absorption spectra [**(1·HCl)$_4$** – **1**] of the IR spectroscopy measurements in CH_2Cl_2 with concentrations 10 mM to 100 mM showing the broad signal of the NH_3^+ moiety at 2750 cm^{-1} and the NH_2 signals at 3400 cm^{-1}.

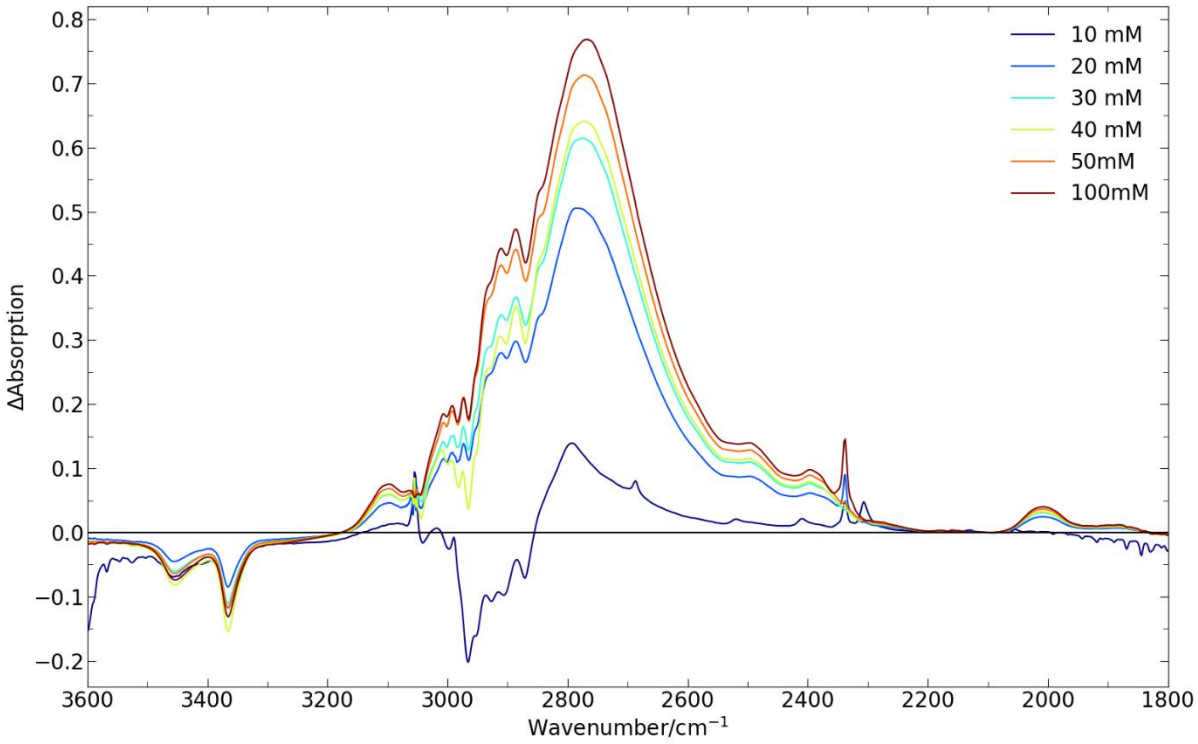

Figure S4.115. Cutout of the difference absorption spectra [**(1·HCl)$_4$** – **1**] of the IR spectroscopy measurements normalized to the concentration in CH_2Cl_2 with concentrations 10 mM to 100 mM showing the broad signal of the NH_3^+ moiety at 2750 cm^{-1} and the NH_2 signals at 3400 cm^{-1}.

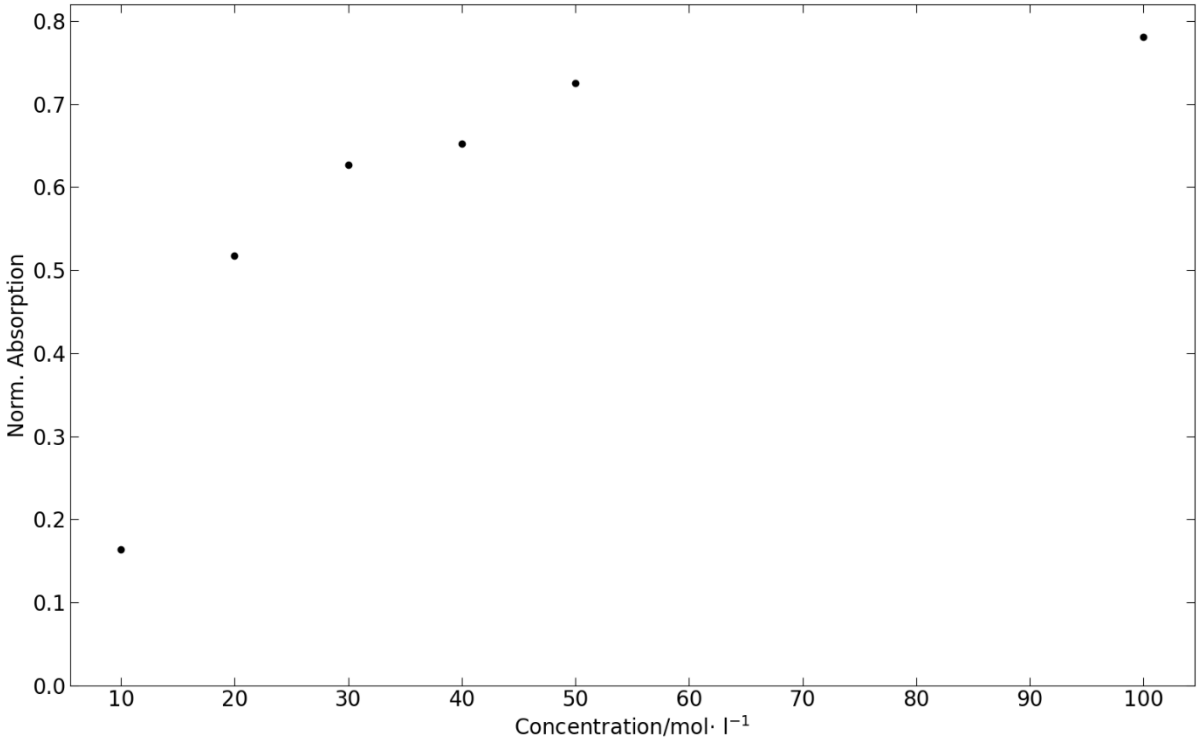

Figure S4.116. Plot of absorption against the concentration of normalized absorption spectra in Figure S4.115. The increase in normalized absorption shows the formation of the cubic structure; otherwise no change would be expected.

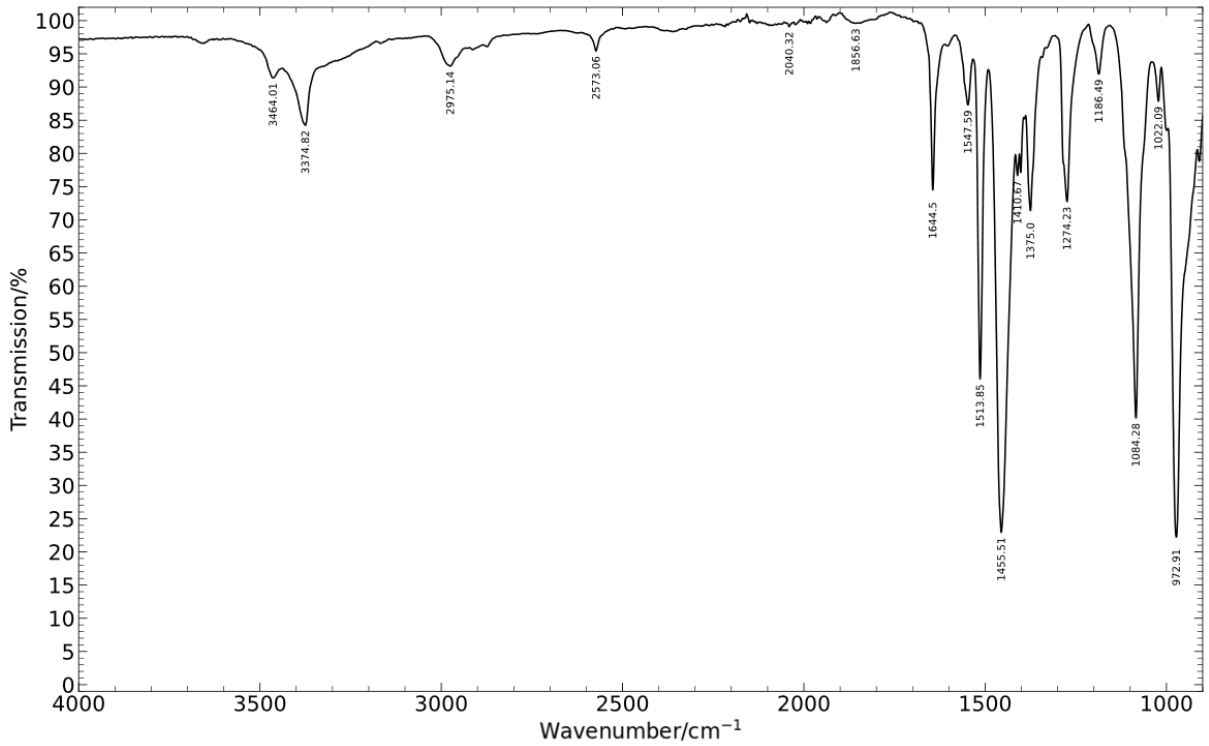

Figure S4.117. IR spectrum (298 K) of **(1–SH)$^+$ WCA$^-$** in the solid state.

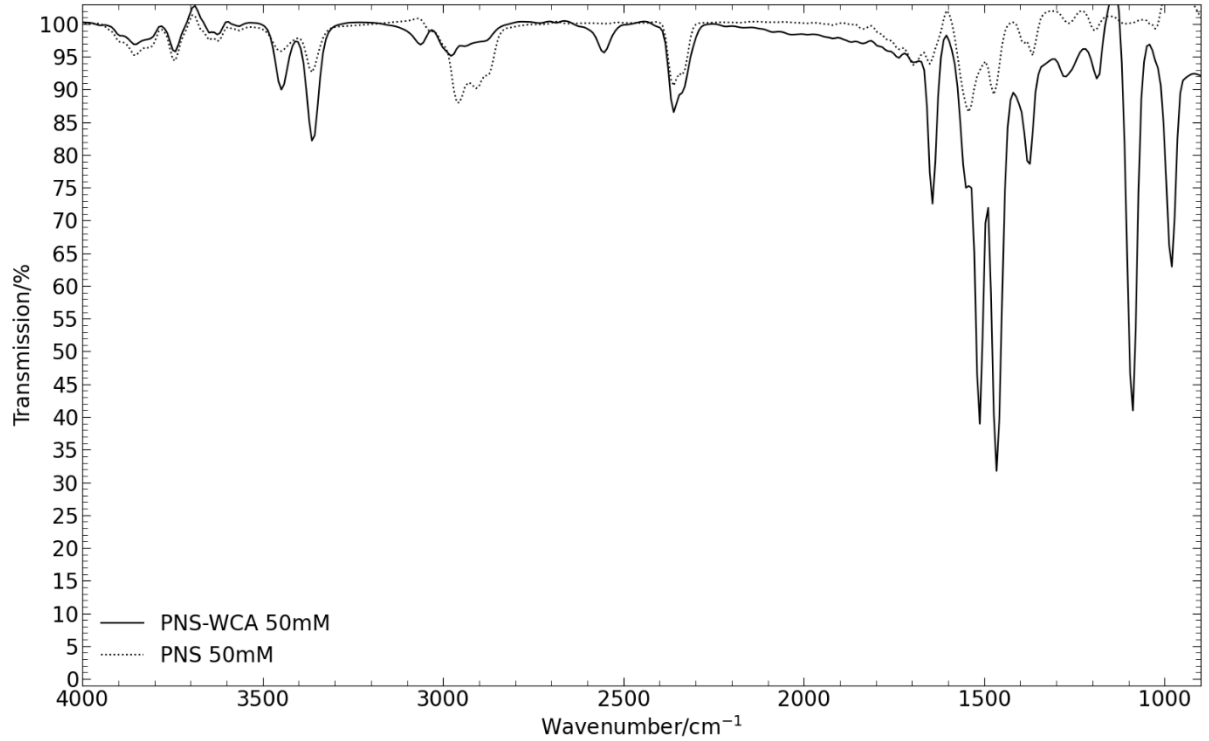

Figure S4.118. IR spectra (298 K) of **1** in 50 mM CH_2Cl_2 solution (dotted line) and **(1–SH)$^+$ WCA$^-$** in 50 mM CH_2Cl_2 solution (solid line). The weak signal at about 2500 cm^{-1} shows that an SH moiety in present in the solution of **(1–SH)$^+$ WCA$^-$**.

4.7. X-Ray Crystallographic Details

The crystals were selected and measured on a SuperNova, single source at offset/far, Atlas {**1**}, on a Xcalibur, AtlasS2, Gemini ultra {**(1·HCl)$_4$**}, on a GV1000, TitanS2 {**(1–SH)$^+$ WCA$^-$**} on a SuperNova, Dualflex, TitanS2 {**[**(*R*$_P$)-**2·HCl]$_4$**, **4**, **(4–SeH)$^+$ WCA$^-$**} or on a XtaLAB Synergy R, DW system, HyPix-Arc 150 {**(4·HCl)$_4$**, **5·HCl**, **(6–SH)$^+$ WCA$^-$**}. The crystals were kept at T = 123(1) K {**1**, **(1–SH)$^+$ WCA$^-$**, **[**(*R*$_P$)-**2 · HCl]$_4$**, **4**, **(4·HCl)$_4$**, **(1–SeH)$^+$ WCA$^-$**, **5·HCl**, **(6–SH)$^+$ WCA$^-$**} or 293(2) K {**(1·HCl)$_4$**} during data collection. Data collection and reduction were performed with **CrysAlisPro** Version 1.171.39.46 {**1**}, Version 1.171.40.18c {**(1–SH)$^+$ WCA$^-$**}, Version 1.171.41.83a {**(1·HCl)$_4$**, **4**}, Version 1.171.41.90a {**[**(*R*$_P$)-**2·HCl]$_4$**}, Version 1.171.41.93a {**(4·HCl)$_4$**, **(1–SeH)$^+$ WCA$^-$**, **5·HCl**} or Version 1.171.43.36a {**(6–SH)$^+$ WCA$^-$**}.[11] For all compounds a numerical absorption correction based on gaussian integration over a multifaceted crystal model and an empirical absorption correction using spherical harmonics as implemented in SCALE3 ABSPACK was applied. Using **Olex2**[12], the structures were solved with **ShelXT**[13] and a least-square refinement on F_2 was carried out with **ShelXL**[14] for all structures. All non-hydrogen atoms were refined anisotropically. Hydrogen atoms at the carbon atoms were located in idealized positions and refined isotropically according to the riding model. Hydrogen atoms at the nitrogen atoms in compounds **(1·HCl)$_4$**, **(1–SH)$^+$ WCA$^-$**, **[**(*R*$_P$)-**2·HCl]$_4$**, **(4·HCl)$_4$**, **(4–SeH)$^+$ WCA$^-$** were located in idealized positions and refined isotropically according to the riding model. Hydrogen atoms at the nitrogen atoms in compounds **1**, **4**, **5·HCl** were located from the difference Fourier map and refined without restraints. Hydrogen atoms at sulfur, selenium and oxygen were located from the difference Fourier map and refined without restraints. Figures were created with Olex2.[12]

Compound **1**: The asymmetric unit contains one molecule. One of the *tert*-butyl moieties (C6, C7, C8) is disordered over two positions and split into two parts with occupancies of 55:45. SIMU and SADI restraints were used to model this disorder.

Compound **(1·HCl)$_4$**: The asymmetric unit contains one cation and one chloride anion.

Compound **(1–SH)$^+$ WCA$^-$** : The asymmetric unit contains one cation and one anion.

Compound **[**(*R*$_P$)-**2·HCl]$_4$**: The asymmetric unit contains one cation, one chloride anion and one molecule of diethyl ether. One of the cyclohexyl moieties (C25, C26, C27, C28, C29, C30) is disordered over two positions and split into two parts with occupancies of 60:40. Another one of the cyclohexyl moieties (C36, C37, C38, C39, C40) is disordered over two positions and split into two parts with occupancies of 83:17. SIMU and SADI restraints were used to model these disorders.

Compound **4**: The asymmetric unit contains one molecule. The squeeze tool was used for solvent masking.

Compound **(4·HCl)$_4$**: The asymmetric unit contains two cations, two chloride anions and half a molecule of DCM.

Compound **(4–SeH)$^+$ WCA$^-$** : The asymmetric unit contains one cation and one anion.

Compound **5·HCl**: The asymmetric unit contains one cation and one chloride anion.

Compound **(6–SH)$^+$ WCA$^-$**: The asymmetric unit contains one cation and one anion.

Table S4.2. Crystallographic data for compounds **1**, **(1·HCl)$_4$** and **(1–SH)$^+$ WCA$^-$**.

Compound	**1**	**(1·HCl)$_4$**	**(1–SH)$^+$ WCA$^-$**
Data Set (internal naming)	**nf-341**	**nf-349_2**	**nf-268**
Formula	$C_8H_{20}NPS$	$C_{32}H_{84}Cl_4N_4P_4S_4$	$C_{32}H_{21}BF_{20}NPS$
$\rho_{calc.}$ / g·cm^{-3}	1.125	1.190	1.733
μ/mm^{-1}	3.421	0.544	1.889
Formula Weight	193.28	918.95	873.34
Color	clear colorless	clear colorless	yellow
Shape	needle	block	block
Size/mm^3	0.221 × 0.059 × 0.04	0.33 × 0.27 × 0.15	0.24 × 0.12 × 0.07
T/K	123.00(10)	293(2)	123.01(13)
Crystal System	tetragonal	triclinic	triclinic
Flack Parameter	0.01(5)	–	–
Hooft Parameter	0.01(5)	–	–
Space Group	*I*–4	*P*–1	*P*–1
a/Å	16.6871(2)	13.2417(3)	10.5988(5)
b/Å	16.6871(2)	13.8445(4)	12.7849(5)
c/Å	8.1933(2)	14.2299(5)	13.9950(6)
α/°	90	81.033(3)	73.714(3)
β/°	90	88.006(2)	72.120(4)
γ/°	90	84.805(2)	71.221(4)
V/Å^3	2281.50(8)	2565.66(13)	1673.66(14)
Z	8	2	2
Z'	1	1	1
Wavelength/Å	1.54184	0.71073	1.39222
Radiation Type	Cu K$_\alpha$	Mo K$_\alpha$	Cu K$_\beta$
2θ$_{min}$/°	7.492	6.628	6.118
2θ$_{max}$/°	152.642	64.134	132.154
Measured Refl.	5805	23418	21688
Independent Refl.	2313	15490	7745
R_{int}	0.0178	0.0219	0.0273
Parameters	143	461	515
Restraints	70	0	0
Largest Peak	0.42	0.46	0.44
Deepest Hole	−0.49	−0.32	−0.41
GooF	1.038	1.088	1.028
wR_2 (all data)	0.1002	0.0908	0.1057
wR_2	0.0995	0.0841	0.1010
R_1 (all data)	0.0425	0.0601	0.0408
R_1	0.0417	0.0430	0.0368

Table S4.3. Crystallographic data for compounds **[(R_P)-2·HCl]$_4$**, **4** and **(4·HCl)$_4$**.

Compound	**[(R_P)-2·HCl]$_4$**	**4**	**(4·HCl)$_4$**
Data Set (internal naming)	**TH263**	**SiS110**	**TH380**
Formula	$C_{80}H_{184}Cl_8N_8P_8S_8 \cdot (C_2H_5)_2O$	$C_8H_{20}NPSe$	$C_8H_{21}ClNPSe \cdot ½\ CH_2Cl_2$
$\rho_{calc.}$ / g·cm^{-3}	1.177	1.306	1.446
μ/mm^{-1}	4.349	4.994	7.588
Formula Weight	2120.30	239.74	319.10
Color	clear colorless	clear colorless	clear colorless
Shape	block	plate	plate
Size/mm^3	0.791 × 0.418 × 0.297	0.32 × 0.10 × 0.06	0.36 × 0.24 × 0.20
T/K	122.97(13)	123.15	123.00(10)
Crystal System	monoclinic	trigonal	orthorhombic
Flack Parameter	0.008(9)	–	0.05(5)
Hooft Parameter	0.008(9)	–	0.05(5)
Space Group	$P2_1$	$R\bar{3}$	$Fdd2$
a/Å	12.50990(10)	32.0113(3)	46.4889(3)
b/Å	21.9387(2)	32.0113(3)	23.3534(2)
c/Å	22.3873(2)	6.18430(10)	10.80290(10)
α/°	90	90	90
β/°	103.2050(10)	90	90
γ/°	90	120	90
V/Å^3	5981.75(9)	5488.17(14)	11728.43(17)
Z	2	18	32
Z'	1	1	2
Wavelength/Å	1.54184	1.54184	1.54184
Radiation Type	Cu K$_\alpha$	Cu K$_\alpha$	Cu K$_\alpha$
2θ$_{min}$/°	7.258	9.57	7.606
2θ$_{max}$/°	134.536	133.73	150.466
Measured Refl.	167804	16785	29677
Independent Refl.	20205	2160	5773
R_{int}	0.0596	0.0333	0.0433
Parameters	1236	181	258
Restraints	400	0	1
Largest Peak	0.94	0.33	1.54
Deepest Hole	−0.44	−0.27	−0.96
GooF	1.031	1.092	1.073
wR_2 (all data)	0.1188	0.0534	0.1744
wR_2	0.1178	0.0519	0.1737
R_1 (all data)	0.0452	0.0196	0.0670
R_1	0.0444	0.0192	0.0663

Table S4.4. Crystallographic data for compounds **(4–SeH)$^+$ WCA$^-$**, **5·HCl** and **(6–SH)$^+$ WCA$^-$**.

Compound	**(4–SeH)$^+$ WCA$^-$**	**5·HCl**	**(6–SH)$^+$ WCA$^-$**
Data Set (internal naming)	**TH473**	**TH402**	**AF119b**
Formula	$C_{32}H_{21}BF_{20}NPSe$	$C_8H_{21}ClNOP$	$C_{41}H_{40}BF_{20}PSSi$
$\rho_{calc.}$ / g·cm^{-3}	1.817	1.209	1.555
μ/mm^{-1}	3.264	3.860	2.357
Formula Weight	920.24	213.68	1014.66
Color	clear colorless	clear colorless	clear colorless
Shape	plate	block	cube
Size/mm^3	0.49 × 0.38 × 0.11	0.59 × 0.39 × 0.19	0.16 × 0.15 × 0.07
T/K	123.01(10)	123.00(10)	123.00(10)
Crystal System	triclinic	monoclinic	monoclinic
Flack Parameter	–	–	–
Hooft Parameter	–	–	–
Space Group	*P*–1	*I* 2/*a*	$P2_1/n$
a/Å	10.5767(2)	12.33050(10)	13.96480(10)
b/Å	12.7396(2)	11.95060(10)	20.74560(10)
c/Å	14.0847(2)	16.90260(10)	15.03350(10)
α/°	73.7310(10)	90	90
β/°	72.177(2)	109.4890(10)	95.6630(10)
γ/°	71.968(2)	90	90
V/Å^3	1681.57(5)	2348.01(3)	4334.07(5)
Z	2	8	4
Z'	1	1	1
Wavelength/Å	1.54184	1.54184	1.54184
Radiation Type	Cu K_α	Cu K_α	Cu K_α
$2\theta_{min}$/°	7.456	9.25	7.286
$2\theta_{max}$/°	133.908	150.246	150.602
Measured Refl.	29498	22570	46340
Independent Refl.	5968	2407	8842
R_{int}	0.0551	0.0540	0.0221
Parameters	515	127	606
Restraints	0	0	0
Largest Peak	0.52	0.48	0.41
Deepest Hole	–0.87	–0.52	–0.47
GooF	1.054	1.097	1.109
wR_2 (all data)	0.1196	0.0967	0.1268
wR_2	0.1191	0.0965	0.1234
R_1 (all data)	0.0433	0.0345	0.0357
R_1	0.0429	0.0344	0.0326

Compound 1:

Part 1 (55%)

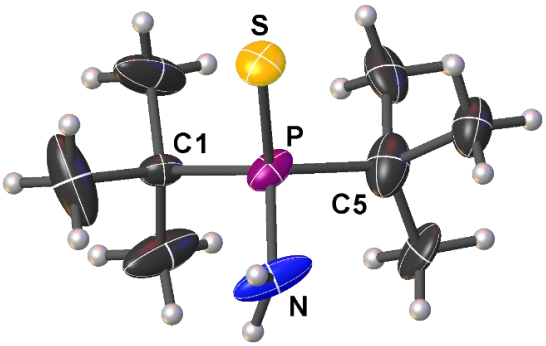

Part 2 (45%)

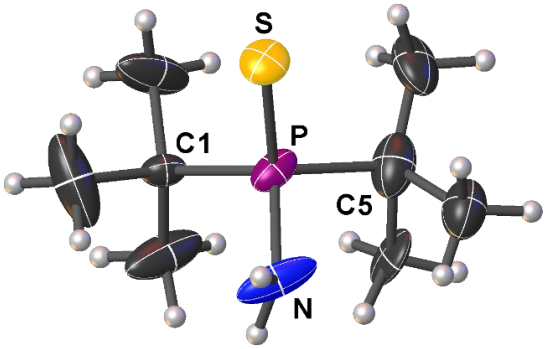

Selected Bond Lengths in Å		Selected Bond Angles in °	
S–P	1.9667(12)	N–P–S	110.64(14)
P–N	1.664(4)	N–P–C1	107.0(2)
P–C1	1.858(4)	N–P–C5	103.8(3)
P–C5	1.850(5)	C5–P–S	110.96(16)
		C5–P–C1	113.72(19)
		C1–P–S	110.46(12)

Compound $(1 \cdot HCl)_4$:

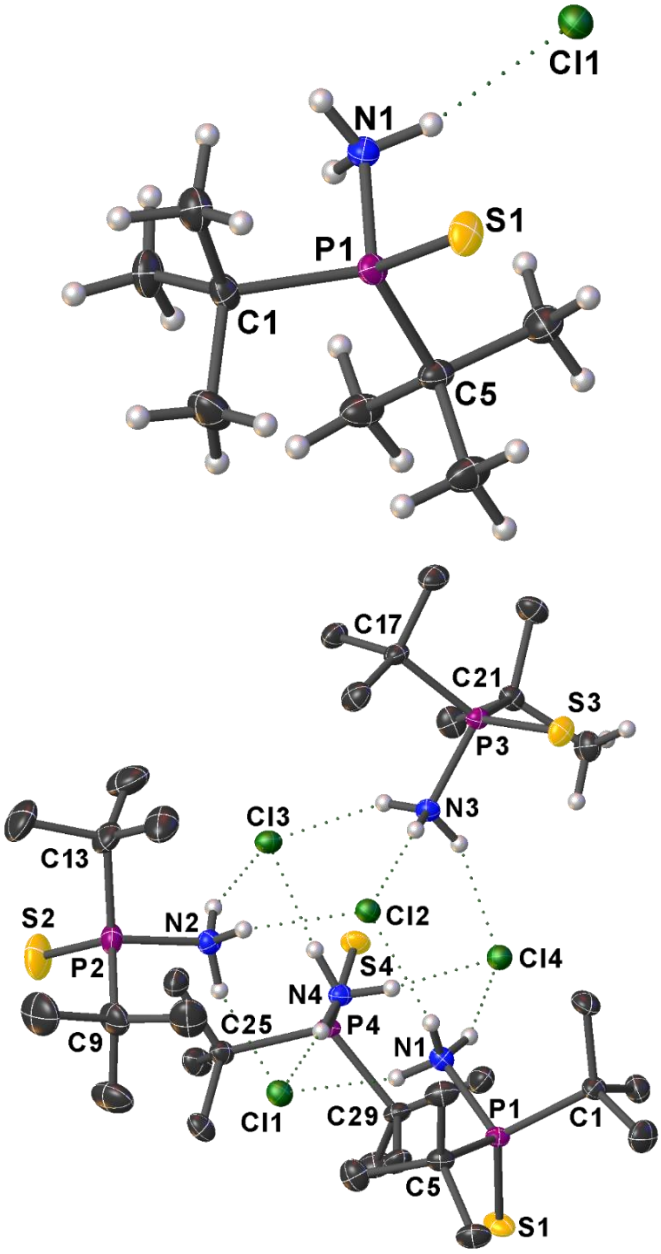

Selected Bond Lengths in Å		Selected Bond Angles in °	
P1–S1	1.9292(6)	N1–P1–S1	108.99(5)
P1–N1	1.7791(13)	N1–P1–C5	102.34(7)
P1–C5	1.8525(16)	N1–P1–C1	101.29(7)
P1–C1	1.8559(16)	C5–P1–S1	111.98(5)
		C5–P1–C1	115.92(8)
		C1–P1–S1	114.69(6)

Compound $(1–SH)^+$ WCA^-:

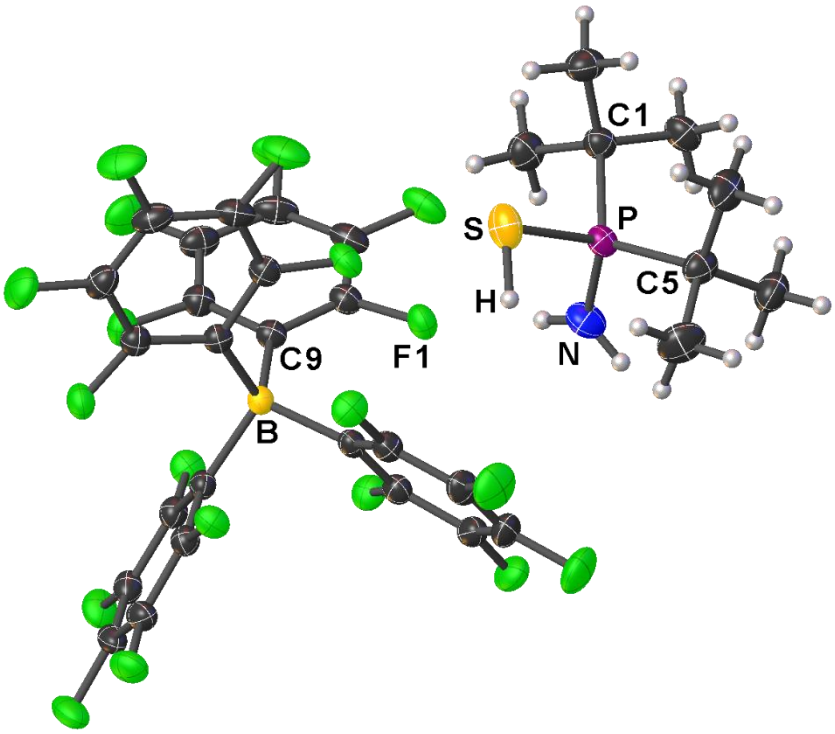

Selected Bond Lengths in Å		Selected Bond Angles in °	
P–S	2.0705(6)	N–P–S	112.43(6)
P–N	1.6345(15)	N–P–C5	105.68(8)
P–C5	1.8382(17)	N–P–C1	107.54(8)
P–C1	1.8392(16)	C5–P–S	108.50(6)
S–H	1.19(3)	C5–P–C1	118.24(8)
		C1–P–S	104.62(5)
		P–S–H	91.6(12)

Compound [(R_P)-2 · HCl]$_4$:

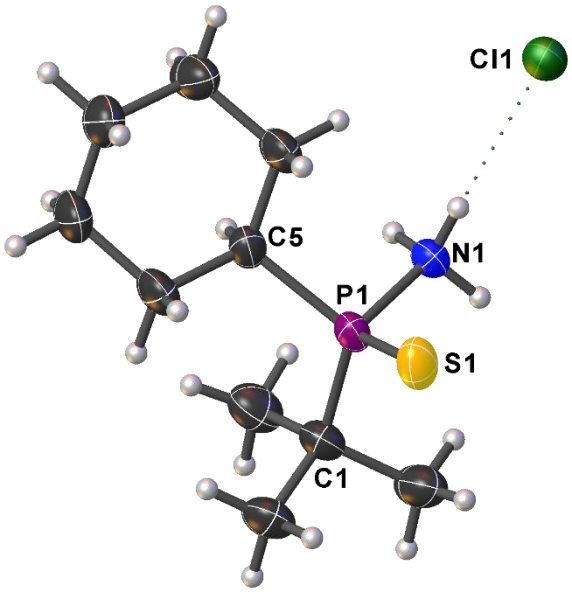

Part 1 [60%(C25A–C30A)/83%(C36A–C40A)] Part 2 [40%(C25B–C30B)/17%(C36B–C40B)]

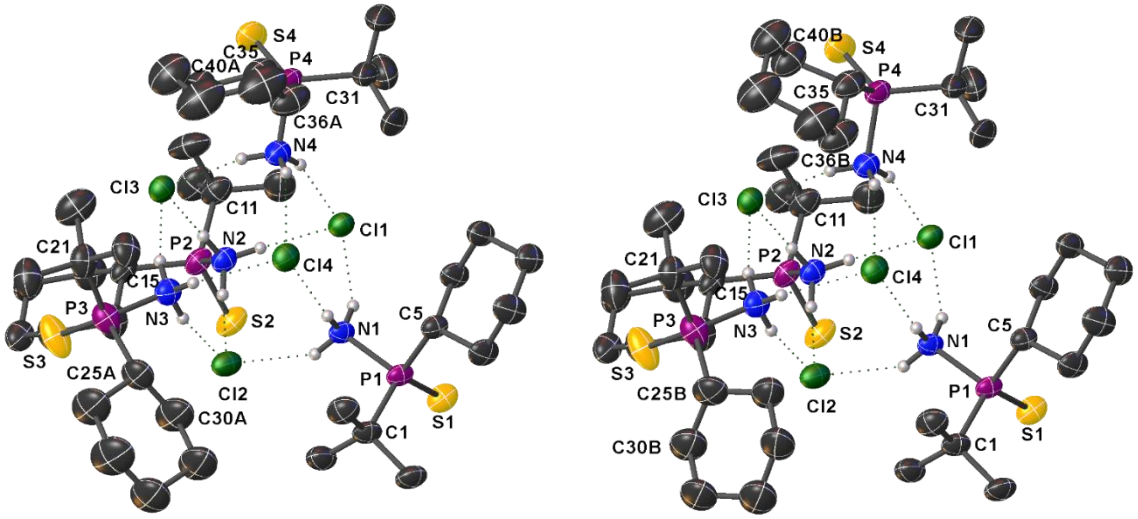

Selected Bond Lengths in Å		Selected Bond Angles in °	
P1–S1	1.9296(18)	N1–P1–S1	111.87(15)
P1–N1	1.792(4)	N1–P1–C5	98.7(2)
P1–C5	1.809(5)	N1–P1–C1	103.0(2)
P1–C1	1.836(5)	C5–P1–S1	115.26(18)
		C5–P1–C1	111.6(2)
		C1–P1–S1	114.61(18)

Compound 4:

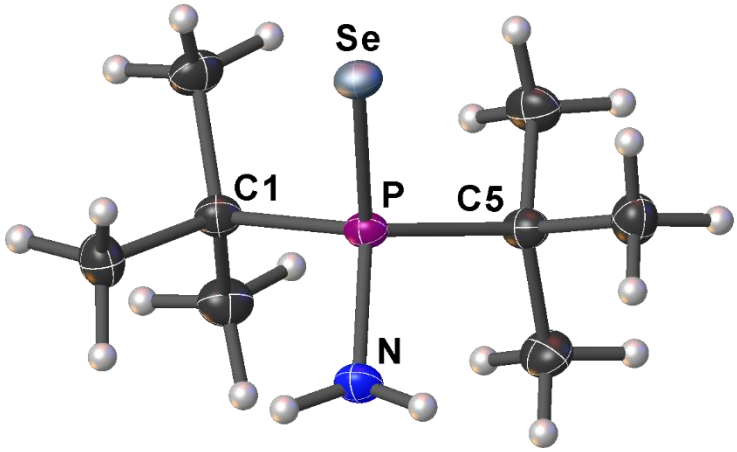

Selected Bond Lengths in Å		Selected Bond Angles in °	
Se–P	2.1425(4)	N–P–Se	116.79(5)
P–N	1.6583(14)	N–P–C1	102.97(8)
P–C1	1.8683(17)	N–P–C5	101.96(7)
P–C5	1.8707(16)	C5–P–Se	111.58(5)
		C5–P–C1	114.98(7)
		C1–P–Se	108.43(5)

Compound $(4 \cdot HCl)_4$:

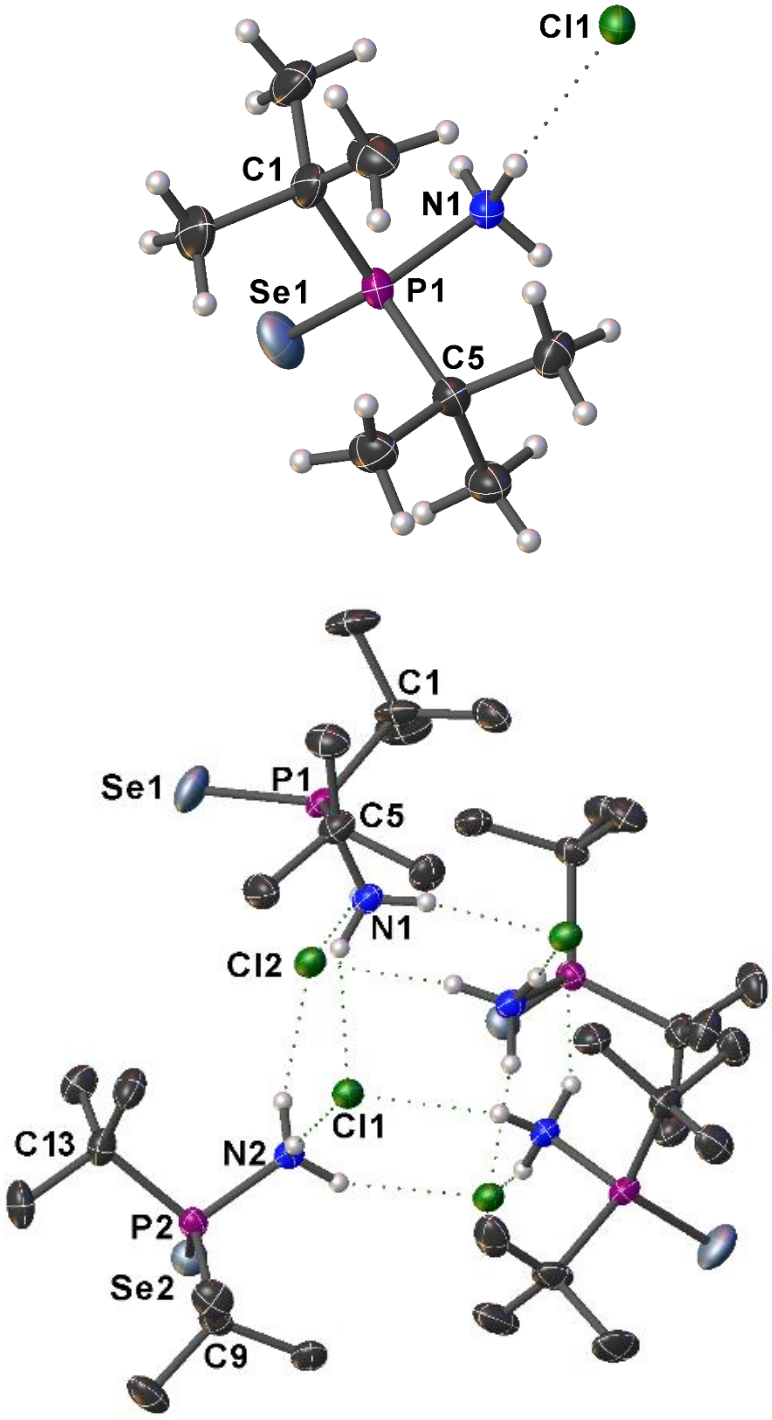

Selected Bond Lengths in Å		Selected Bond Angles in °	
P1–Se1	2.076(2)	N1–P1–Se1	107.7(2)
P1–N1	1.781(7)	N1–P1–C5	102.1(3)
P1–C5	1.846(9)	N1–P1–C1	101.5(3)
P1–C1	1.872(9)	C5–P1–Se1	116.0(3)
		C5–P1–C1	114.1(4)
		C1–P1–Se1	113.4(3)

Compound $(4–SeH)^+$ WCA^-:

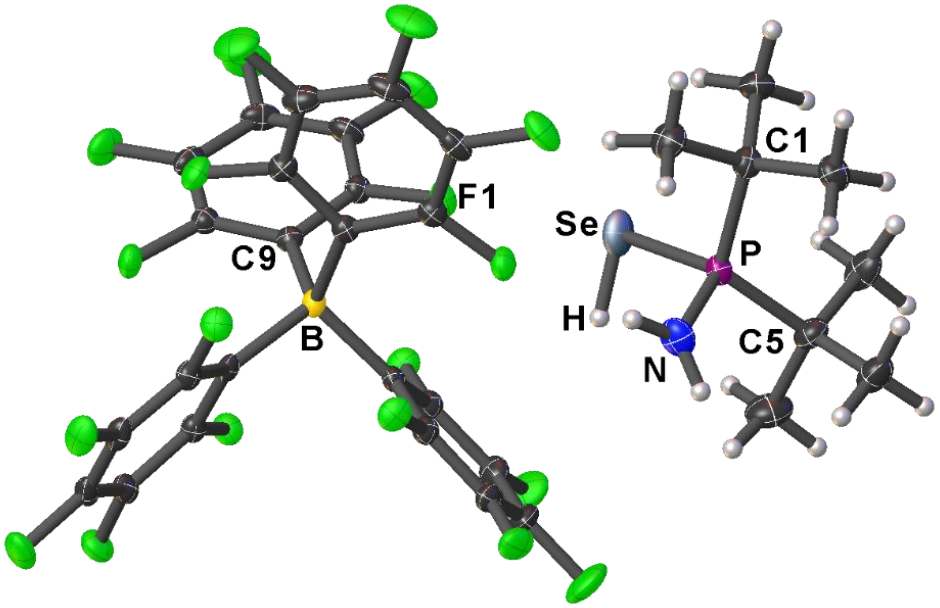

Selected Bond Lengths in Å		Selected Bond Angles in °	
P–Se	2.2221(6)	N–P–Se	112.40(9)
P–N	1.631(2)	N–P–C5	105.56(12)
P–C5	1.843(2)	N–P–C1	107.46(12)
P–C1	1.844(2)	C5–P–Se	108.67(9)
Se–H	1.28(4)	C5–P–C1	118.18(11)
		C1–P–Se	104.74(8)
		P–Se–H	86.3(16)

Compound 5·HCl:

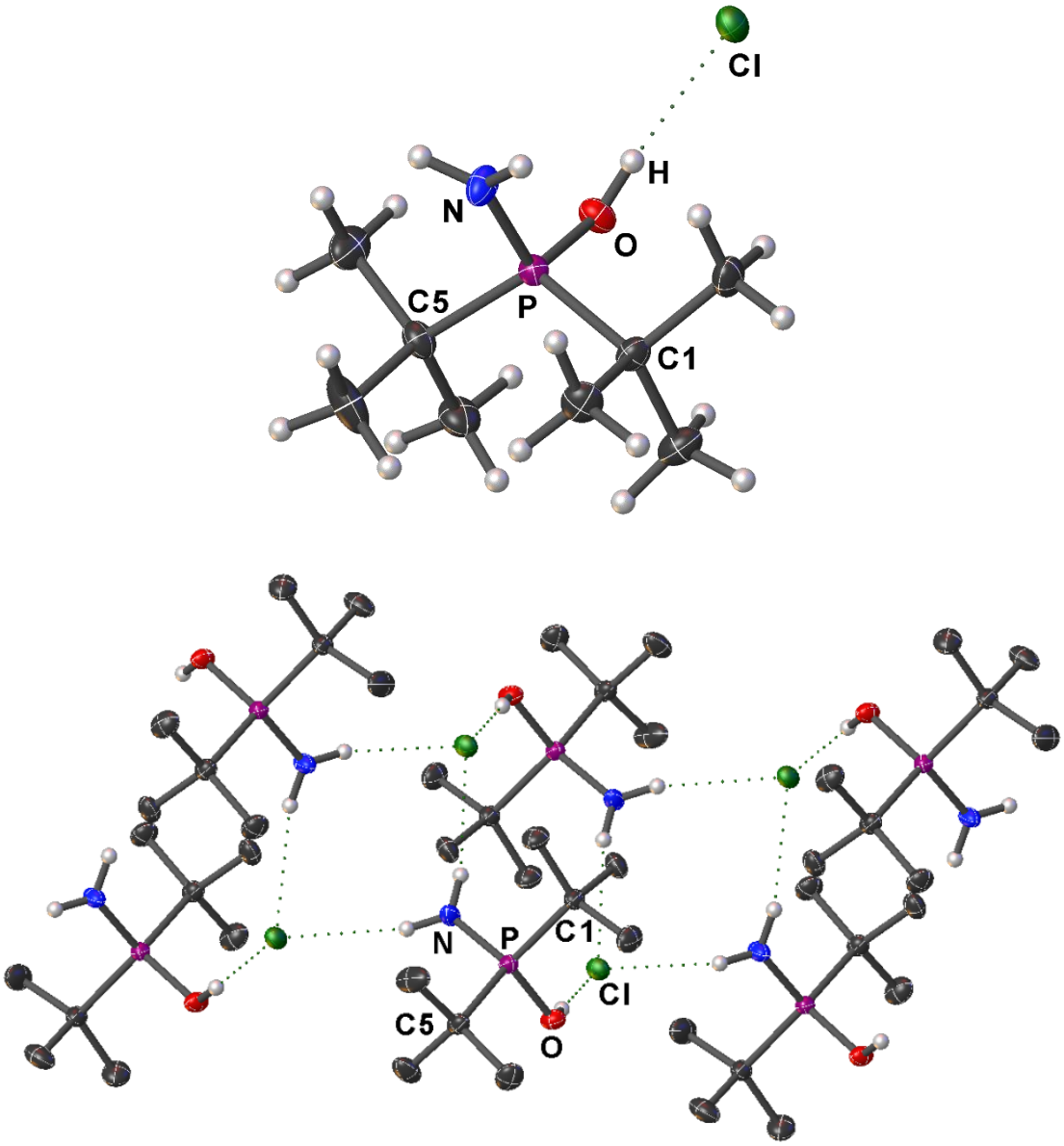

Selected Bond Lengths in Å		Selected Bond Angles in °	
P–O	1.5668(9)	N–P–O	115.27(6)
P–N	1.6112(12)	N–P–C5	107.90(6)
P–C5	1.8324(13)	N–P–C1	105.91(6)
P–C1	1.8335(13)	C5–P–O	102.75(6)
O–H	0.81(3)	C5–P–C1	118.51(7)
		C1–P–O	106.94(6)

Compound $(6–SH)^+$ $WCA^–$:

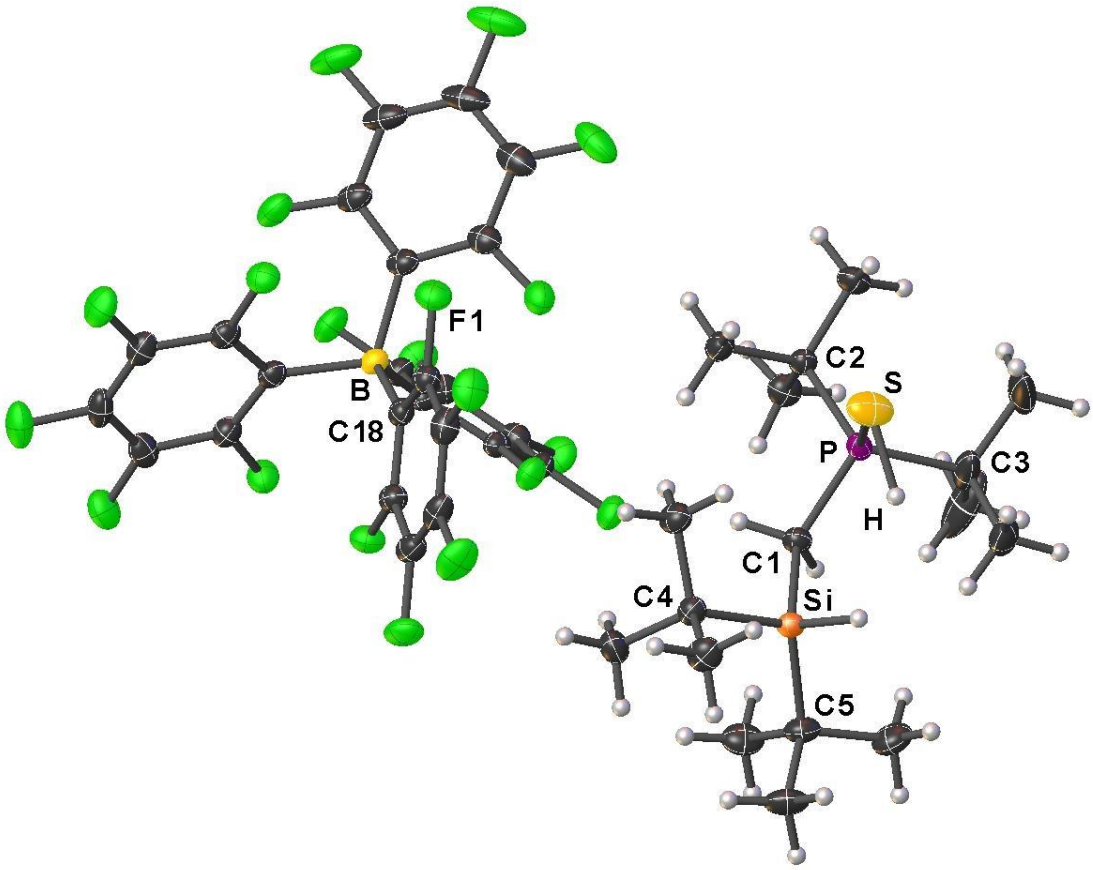

Selected Bond Lengths in Å		Selected Bond Angles in °	
P–S	2.0647(6)	C1–P–S	110.22(5)
P–C1	1.8022(13)	C1–P–C2	107.99(6)
P–C2	1.8576(14)	C1–P–C3	108.70(8)
P–C3	1.8613(17)	C2–P–S	106.80(5)
Si–C1	1.9241(14)	C2–P–C3	115.69(7)
S–H	1.47(5)	C3–P–S	107.38(7)
		P–S–H	82(2)

4.8. Quantum Chemical Calculations

Optimization and additional harmonic vibrational frequency analyses were performed with the software package Gaussian 09 (Revision E.01) on the M062X/6-31+G(d) level of theory[15] without symmetry restrictions applying the Polarizable Continuum Model (PCM)[16] (solvent: dichloromethane). The GJF input files and the figures of the optimized structures were created with the program GaussView version 5.0.9.[17] For the ground state structures, the vibrational frequency analysis showed no imaginary frequency in the harmonical approximation. The relative energies (ΔG) of the computed structures are given based on the sum of electronic and thermal free energies (Gibbs energies) at 298.15 K in kJ mol^{-1}. The Hartree units were converted as follows: 1 Hartree = 2625.4995 kJ mol^{-1}.[18] The sum of electronic and thermal free energies (Gibbs energies) at 298.15 K are summarized in Table S.4.5, and the Cartesian coordinates of the calculated systems can be found in Tables S4.6–S4.11.

Table S4.5. Total electronic energies (SCF), sum of electronic and zero-point energies (ZPE), and sum of electronic and thermal free energies (Gibbs energies) at 298.15 K of the optimized structures.

Optimized structure	Method/Basis	SCF [Hartree]	ZPE [Hartree]	Gibbs energies [Hartree]
1-SH_Cl	M062X/6-31+G(d) (PCM, solvent: dichloromethane)	−1571.97261507	−1571.687688	−1571.731178
1-TS_Cl	M062X/6-31+G(d) (PCM, solvent: dichloromethane)	−1571.96666983	−1571.682339	−1571.726215
1-NH_Cl	M062X/6-31+G(d) (PCM, solvent: dichloromethane)	−1571.97490240	−1571.685693	−1571.728813
1-SH_WCA	M062X/6-31+G(d) (PCM, solvent: dichloromethane)	−1111.57385463	−1111.287671	−1111.327229
1-TS_WCA	M062X/6-31+G(d) (PCM, solvent: dichloromethane)	−1111.52805261	−1111.244421	−1111.283791
1-NH_WCA	M062X/6-31+G(d) (PCM, solvent: tetrahydrofuran)	−1111.57331216	−1111.282740	−1111.322266

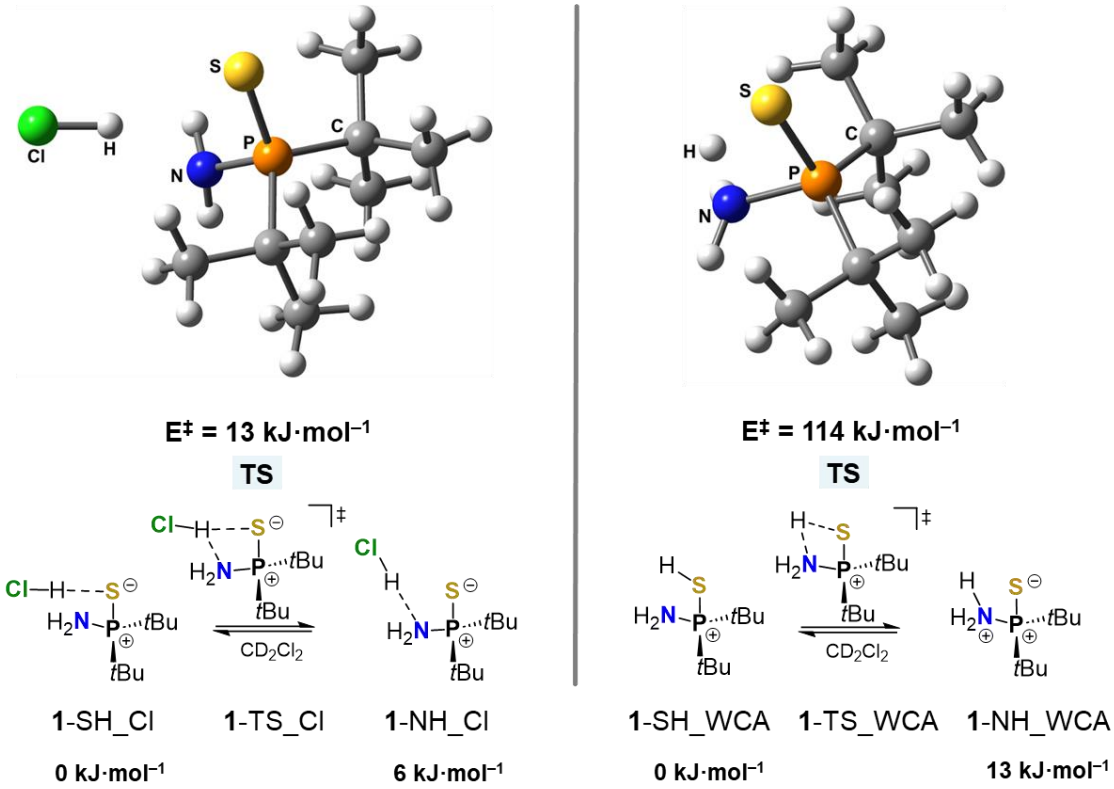

Figure S4.119 Relative energies of different protonation modes and transition states (TS) in the presence of a coordinating anion (left) and in the absence of a coordinating anion (right) in dichloromethane solution [M062X/6-31+G(d)] (PCM, solvent: dichloromethane). The energy differences in the calculations are based on the Gibbs energies.

Table S4.6. Cartesian coordinates of the optimized structure **1**-SH_Cl [M062X/6-31+G(d)] (PCM, solvent: dichloromethane).

Atomic symbol	x	y	z
C	-1.69046200	-2.32793400	-0.71789000
C	-1.89158500	-0.91723800	-0.13501200
C	-2.48807400	-1.04549600	1.27199000
C	-2.84219800	-0.13549500	-1.04861500
C	1.25898300	2.15897200	0.37805100
C	-0.18927600	1.72849000	0.09165000
C	-0.65983900	2.42065300	-1.19623600
C	-1.07524200	2.13954300	1.27359100
H	-0.95073700	-2.89878800	-0.15227700
H	-1.39804200	-2.29377600	-1.76936800
H	0.65326900	-1.33949200	-1.80651900
H	-2.64482700	-2.85735000	-0.65760800
H	1.20062000	0.20883000	-1.84713000
H	2.57278500	-0.81853100	0.40176400
H	-1.86286900	-1.67008300	1.91091200
H	-2.40480200	0.03735600	-2.03401000
H	-3.46929800	-1.51949800	1.18015700
H	-3.75013700	-0.73055000	-1.18217600
H	1.95446900	1.83829100	-0.40238800
H	-0.00636000	2.19978800	-2.04110000
H	1.61396700	1.77100500	1.33307000
H	-2.62771200	-0.07966300	1.75854600
H	-3.13951900	0.81970600	-0.61268000
H	-1.67858600	2.15692900	-1.47283400
H	1.28356100	3.25128500	0.41433100
H	-0.80571600	1.59924800	2.18444600
H	-0.62969200	3.50016100	-1.02362600
H	-2.13455200	1.98080400	1.06450800
H	-0.92988300	3.20711800	1.45872700
N	0.39749900	-0.37301700	-1.62676300
S	0.87066000	-1.00255400	1.39480700
P	-0.20478400	-0.13013300	-0.06757100
Cl	3.70464400	-0.69928200	-0.36035000

Table S4.7. Cartesian coordinates of the optimized structure **1**-TS_Cl [M062X/6-31+G(d)] (PCM, solvent: dichloromethane).

Atomic symbol	x	y	z
C	-1.98802100	-2.32839100	0.05200400
C	-2.00756300	-0.81442300	-0.20901100
C	-2.96330800	-0.14805700	0.78615600
C	-2.48646800	-0.58778700	-1.65078100
C	1.36615700	2.02426900	-0.09786600
C	-0.12246300	1.67554900	0.06998100
C	-0.92834100	2.34820100	-1.04849000
C	-0.58664700	2.20243900	1.43476600
H	-1.76751300	-2.55148900	1.09558100
H	-1.25181300	-2.84250300	-0.57184300
H	0.71046800	-1.58673100	-1.52379300
H	-2.97529100	-2.72897100	-0.19472300
H	0.32712500	-0.13247900	-2.23291800
H	2.69381500	-0.68568100	-0.17550500
H	-2.58601000	-0.21375200	1.80971700
H	-1.88645300	-1.15586900	-2.36446000
H	-3.92421700	-0.66894900	0.74731200
H	-3.51582200	-0.94981900	-1.72685800
H	1.75553500	1.72077200	-1.07053800
H	-0.66555300	1.97586700	-2.04217300
H	1.97112700	1.55971100	0.68374400
H	-3.14724700	0.89939100	0.54099500
H	-2.48484000	0.45963100	-1.94886000
H	-2.00353600	2.23872900	-0.90249700
H	1.47120600	3.10896600	-0.00826000
H	-0.01179000	1.75072800	2.24433800
H	-0.70218500	3.41816300	-1.03362800
H	-1.64599000	2.02613100	1.61824000
H	-0.41994700	3.28294800	1.45470200
N	0.61902400	-0.58691200	-1.37291100
S	0.64360500	-1.02889200	1.58346000
P	-0.25586900	-0.18851200	0.02523600
Cl	3.97447300	-0.69160300	-0.38368600

Table S4.8. Cartesian coordinates of the optimized structure **1**-NH_Cl [M062X/6-31+G(d)] (PCM, solvent: dichloromethane).

Atomic symbol	X	y	z
C	-1.48461700	1.96948100	0.00111000
C	0.02716100	1.69278000	-0.05145200
C	0.70980400	2.45448200	1.09577100
C	0.58833200	2.16271200	-1.39885000
C	1.99402500	-2.27507500	0.17899100
C	1.89256700	-0.83195000	-0.34025200
C	2.01604200	-0.84964700	-1.87177700
C	3.02251600	0.00176600	0.28117000
H	-1.93693600	1.57977500	0.91453100
H	-2.02166200	1.55355900	-0.85372000
H	-1.93033900	-0.76175200	-0.68920400
H	-1.62353100	3.05324600	-0.01736300
H	-0.69552300	-1.83252800	-1.09261400
H	0.29171800	2.16852600	2.06151600
H	0.16698200	1.62518700	-2.25228000
H	0.52504400	3.52039100	0.94152800
H	0.31562400	3.21414300	-1.52110600
H	1.16011500	-2.90223400	-0.14751500
H	1.32016700	-1.55356600	-2.33410200
H	2.03461500	-2.30624000	1.26711000
H	1.78900500	2.30139500	1.11995800
H	1.67581300	2.09905200	-1.44208200
H	1.89053100	0.12836500	-2.33313700
H	2.91403400	-2.70890800	-0.22086100
H	2.90479400	0.09747700	1.36331200
H	3.02263400	-1.19823400	-2.11644900
H	3.09310100	0.99689000	-0.16003500
H	3.96782700	-0.51251700	0.09115000
N	-0.87064100	-0.82941700	-0.98659400
S	-0.28921500	-0.73390300	2.01661500
P	0.26620400	-0.13056000	0.24849200
H	-0.78395200	-0.40600400	-1.91460100
Cl	-3.76153900	-0.85862000	-0.41878600

Table S4.9. Cartesian coordinates of the optimized structure **1**-SH_WCA [M062X/6-31+G(d)] (PCM, solvent: dichloromethane).

Atomic symbol	x	y	z
C	-2.68364600	0.00791800	0.75924600
C	-1.57198800	-0.53639100	-0.15604300
C	-1.89267400	-0.19169500	-1.61769000
C	-1.46168400	-2.05581700	0.03151000
C	2.72364900	0.56804700	0.07669600
C	1.61211700	-0.46373300	-0.18163400
C	1.90893600	-1.74805900	0.61037800
C	1.53918700	-0.75847600	-1.68500900
H	-2.73593200	1.09867200	0.75110900
H	-2.57190800	-0.34675900	1.78507900
H	-0.70768900	0.66683100	2.53210900
H	-3.63488700	-0.37426200	0.38214500
H	0.93284800	0.32821300	2.48728900
H	0.81103300	2.70130700	0.40062100
H	-2.09960500	0.87149800	-1.75461400
H	-1.15443000	-2.31943000	1.04546600
H	-2.79814600	-0.73804200	-1.89160100
H	-2.45354500	-2.48135500	-0.13922700
H	2.74671100	0.92784700	1.10865900
H	2.04733800	-1.55563400	1.67483300
H	2.64518600	1.42193400	-0.59693800
H	-1.10336200	-0.49086500	-2.30699400
H	-0.77949600	-2.51284100	-0.68635900
H	1.13728300	-2.50686800	0.49090600
H	3.67896400	0.07569300	-0.11759600
H	1.25689000	0.12535500	-2.26172900
H	2.84425000	-2.15833400	0.22218500
H	0.85155400	-1.57382000	-1.91236900
H	2.53548800	-1.06507700	-2.01204300
N	0.03871800	0.20285700	2.02676600
S	-0.17675100	2.22245000	-0.37801900
P	0.00433800	0.26639800	0.37568600

Table S4.10. Cartesian coordinates of the optimized structure **1**-TS_WCA [M062X/6-31+G(d)] (PCM, solvent: dichloromethane).

Atomic symbol	x	y	z
C	-2.73678100	0.47326300	-0.06223400
C	-1.60094700	-0.56132900	-0.09700600
C	-1.55875500	-1.22629500	-1.48019900
C	-1.82116900	-1.60836700	1.00462500
C	2.68539400	0.16477500	0.67663400
C	1.58190100	-0.59745900	-0.07451600
C	1.49051500	-2.03153500	0.45885200
C	1.89623100	-0.59289100	-1.58007900
H	-2.66967300	1.17312600	-0.89440500
H	-2.76800000	1.04416700	0.86885100
H	-0.87648400	0.80139000	2.34620000
H	-3.67810200	-0.07496100	-0.14382600
H	0.78502900	0.88263900	2.34632100
H	-0.04998100	2.15549200	0.99594100
H	-1.34260400	-0.50757700	-2.27457800
H	-1.90135800	-1.16292800	1.99843900
H	-2.54732900	-1.64882500	-1.67469900
H	-2.77433100	-2.10055900	0.79619900
H	2.61003200	0.03741900	1.75879400
H	1.20189800	-2.06853800	1.51157000
H	2.70269100	1.22784000	0.42845000
H	-0.83642600	-2.04195600	-1.52387300
H	-1.05135800	-2.37649000	1.02315500
H	0.81038300	-2.65052700	-0.12676900
H	3.64276300	-0.26392000	0.37253700
H	2.01986900	0.42292300	-1.95893100
H	2.48698100	-2.47285200	0.37510400
H	1.13468900	-1.10290400	-2.17056500
H	2.83961100	-1.12542500	-1.72079900
N	-0.05421600	1.01498700	1.78155000
S	0.06530100	2.21771300	-0.63703100
P	-0.00146200	0.34287800	0.15413700

Table S4.11. Cartesian coordinates of the optimized structure **1**-NH_WCA [M062X/6-31+G(d)] (PCM, solvent: dichloromethane).

Atomic symbol	x	y	z
C	-2.69050800	0.16363500	0.64084100
C	-1.57076100	-0.53223100	-0.15278000
C	-1.89023200	-0.42785100	-1.65386300
C	-1.47864700	-2.00292000	0.26986200
C	2.75171200	0.51178500	-0.05724000
C	1.59814400	-0.49738300	-0.15439900
C	1.82687900	-1.62821400	0.85781900
C	1.53828900	-1.05534500	-1.58555800
H	-2.72300400	1.23796800	0.45109700
H	-2.61871700	-0.01803600	1.71560500
H	-0.74646900	1.09794300	2.32341000
H	-3.64140300	-0.26290100	0.31396800
H	0.87603400	0.86115100	2.36093200
H	-2.00713300	0.61167400	-1.96203500
H	-1.21778500	-2.13561900	1.32332600
H	-2.83620800	-0.94644600	-1.82630300
H	-2.46776500	-2.44705300	0.13172600
H	2.80987300	0.99996300	0.91882900
H	2.01151400	-1.25237200	1.86671500
H	2.67396800	1.28313200	-0.82252400
H	-1.13216700	-0.89801800	-2.28044600
H	-0.77900400	-2.57096700	-0.34283100
H	1.01912300	-2.35687100	0.88552200
H	3.68366400	-0.03851900	-0.20693100
H	1.30744000	-0.27593400	-2.31564100
H	2.73202200	-2.16067000	0.55541100
H	0.81670000	-1.86673200	-1.68543700
H	2.52461000	-1.45784600	-1.82798600
N	-0.00312400	0.46348600	2.01457700
S	-0.04296900	2.26719900	-0.45292100
P	0.00379300	0.42197600	0.14035300
H	-0.14205900	-0.44192000	2.47491600

4.9. Supplementary References

[1] T. Huber, N.-A. Espinosa-Jalapa, J. O. Bauer, *Chem. Eur. J.* **2022**, *28*, e202202608.
[2] S. F. Rach, E. Herdtweck, F. E. Kühn, *J. Organomet. Chem.* **2011**, *696*, 1817–1823.
[3] a) M. J. P. Hargar, M. A. Stephen, *J. Chem. Soc.*, *Perkin Trans.*, **1980**, 705–711; b) M. Köster, A. Kreher, C. von Hänisch, *Dalton Trans.* **2018**, *47*, 7875–7878. c) T. C. Jankins, Z.-Y. Qin, K. M. Engle, *Tetrahedron* **2019**, *75*, 3272–3281.
[4] a) A. P. Stewart, S. Trippett, *J. Chem. Soc. C* **1970**, 1263–1266; b) W. Kuchen, G. Hägele, *Chem. Ber.* **1970**, *103*, 2114–2121.
[5] A. Falk, J. O. Bauer, *Inorg. Chem.* **2022**, *61*, 15576–15588.
[6] A. Jerschow, N. Müller, *J. Magn. Reson.* **1997**, *125*, 372–375.
[7] A. Macchioni, G. Ciancaleoni, C. Zuccaccia, D. Zuccaccia, *Chem. Soc. Rev.* **2008**, *37*, 479–489.
[8] H. C. Chen, S. H. Chen, *J. Phys. Chem.* **1984**, *88*, 5118–5121.
[9] D. Ben-Amotz, K. G. Willis, *J. Phys. Chem.* **1993**, *97*, 7736–7742.
[10] D. Zuccaccia, A. Macchioni, *Organometallics* **2005**, *24*, 3476–3486.
[11] CrysAlisPro Software System, Rigaku Oxford Diffraction, **2023**.
[12] O. V. Dolomanov, L. J. Bourhis, R. J. Gildea, J. A. K. Howard, H. Puschmann, *J. Appl. Crystallogr.* **2009**, *42*, 339–341.
[13] G. M. Sheldrick, *Acta Cryst.* **2015**, *A71*, 3–8.
[14] G. M. Sheldrick, *Acta Cryst.* **2015**, *C71*, 3–8.
[15] M. J. Frisch, G. W. Trucks, H. B. Schlegel, G. E. Scuseria, M. A. Robb, J. R. Cheeseman, G. Scalmani, V. Barone, B. Mennucci, G. A. Petersson, H. Nakatsuji, M. Caricato, X. Li, H. P. Hratchian, A. F. Izmaylov, J. Bloino, G. Zheng, J. L. Sonnenberg, M. Hada, M. Ehara, K. Toyota, R. Fukuda, J. Hasegawa, M. Ishida, T. Nakajima, Y. Honda, O. Kitao, H. Nakai, T. Vreven, J. A. Montgomery Jr., J. E. Peralta, F. Ogliaro, M. Bearpark, J. J. Heyd, E. Brothers, K. N. Kudin, V. N. Staroverov, T. Keith, R. Kobayashi, J. Normand, K. Raghavachari, A. Rendell, J. C. Burant, S. S. Iyengar, J. Tomasi, M. Cossi, N. Rega, J. M. Millam, M. Klene, J. E. Knox, J. B. Cross, V. Bakken, C. Adamo, J. Jaramillo, R. Gomperts, R. E. Stratmann, O. Yazyev, A. J. Austin, R. Cammi, C. Pomelli, J. W. Ochterski, R. L. Martin, K. Morokuma, V. G. Zakrzewski, G. A. Voth, P. Salvador, J. J. Dannenberg, S. Dapprich, A. D. Daniels, O. Farkas, J. B. Foresman, J. V. Ortiz, J. Cioslowski, D. J. Fox, *Gaussian 09*. Revision E.01; Gaussian, Inc.: Wallingford, CT, USA, **2013**.
[16] J. Tomasi, B. Mennucci, R. Cammi, *Chem. Rev.* **2005**, *105*, 2999–3093.
[17] R. D. Dennington, II; T. A. Keith, J. M. Millam, *GaussView 5.0*; Gaussian, Inc.: Wallingford, CT, USA, **2008**.
[18] J. B. Foresman, A. Frisch, *Exploring Chemistry with Electronic Structure Methods*, 2nd Ed.; Gaussian, Inc.: Pittsburgh, PA, USA, **1996**.

5. New Cyclic Four-Membered NPSSi-Based Cationic Rings and Their Investigation Towards *P*- and *Si*-Centered Chirality

Preface

The following chapter and supporting information are based on a manuscript in preparation on inorganic ring systems. For four-membered NPSSi cycles with the aim of introducing *P*- and *Si*-centered chirality are investigated in terms of the stereochemistry of the ring-closing reactions.

Authors

Tanja Huber, Nicolò Fontana, Michael Seidl, Florian Meurer, Jonathan O. Bauer.

Author contribution

All syntheses and characterisations reported in this work were performed by T. Huber, except for the initial preparation of compounds *rac*-**6** and *rac*-**19**, which were synthesized for the first time by Dr. N. Fontana. Single crystal X-ray diffraction and structure refinements were performed by T. Huber, except for *rac*-**7**[$HB(C_6F_5)_3$], which was solved and refined by Dr. M. Seidl, and except for *rac*-**8** · NH_4^+ $HB(C_6F_5)_3^-$ and (R_P,S_{Si})-**18**[$HB(C_6F_5)_3$], which were solved and refined by F. Meurer. The manuscript and the supporting information were drafted by T. Huber and revised by PD Dr. J. O. Bauer.

Acknowledgements

This work was jointly supported by the Elite Network of Bavaria (ENB), the Bavarian State Ministry of Science and the Arts (StMWK), and the University of Regensburg (N-LW-NW-2016-366). Intellectual support was given by the Deutsche Forschungsgemeinschaft (DFG) through the Research Training Group “Ion Pair Effects in Molecular Reactivity” (RTG 2620, Project 426795949).

5.1. Abstract

A simple method for the synthesis of *N*-hydrosilyl-substituted aminophosphine sulfides is provided by coupling lithiated achiral or enantiomerically pure aminophosphine sulfides with chlorohydrosilanes. The same procedure can be used starting from chlorohydrodisiloxanes to obtain *N*-hydrodisiloxy-substituted aminophosphine sulfides. Both species serve as precursors for the preparation of four- or six-membered cationic rings, respectively, when subjected to hydride abstraction with the Lewis acid $B(C_6F_5)_3$. The investigation of the stereochemistry of the ring-closing reaction using a substrate with defined *P*- and *Si*-centered chirality provided insights into the equilibrium processes of diastereomeric enrichment.

5.2. Introduction

Chiral, quaternary phosphonium ions have been considered as an important class of catalysts in a variety of asymmetric organic synthesis protocols.[1] In general, carbon-centered chirality often seems to be the most straightforward option to obtain enantiomerically enriched products, but research on phosphorus-stereogenic analogues has been rising in the past decades and has shown to contribute beneficial properties to asymmetric catalysis.[2] When combined with other heteroatom functional groups such as amino groups or chalcogen atoms directly bonded to phosphorus, a powerful functional pattern is created for applications as chiral organocatalysts or ligands.[3]

The introduction of a silicon atom as a potential Lewis-acidic site features another interesting aspect to consider in terms of catalytic activity and bond activation.[4] In recent years, several elegant ways have been found to tame highly reactive silicon centers, including intramolecular stabilization by a Lewis-basic moiety,[5] three-center-two-electron Si–H–Si[6] or Si–H–B[7] bridges, as well as counteranion-mediated stabilization.[8] Compounds with tetrasubstituted stereogenic silicon centers were part of chiral memory studies towards hydride abstraction reactions and subsequent intramolecular stabilization.[5a,5b,5c,5f] In terms of applications, stereochemical studies on the exchange of functional groups at asymmetrically substituted silicon centers provide important information about the maintenance of configurational integrity at stereogenic silicon centers during reactions.[9]

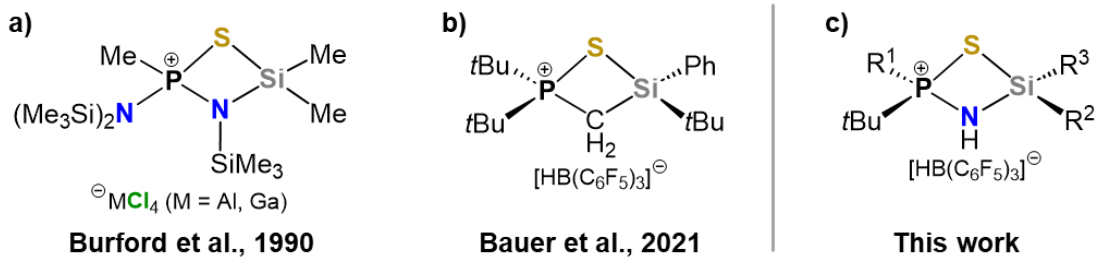

Figure 5.1. Overview of four-membered, cationic heterocyclic ring systems. a) First published cationic NPSSi cycle.[10] b) Enantiomerically pure CPSSi cycle with *Si*-centered chirality.[5f] c) First stereochemically pure NPSSi cycle with both phosphorus and silicon as stereogenic centers, reported herein.

The first examples of four-membered NPSSi cycles were reported by Burford et al. in the 1990s (Figure 5.1, a). Ring closure was achieved by chloride abstraction via P–Cl bond cleavage using the Lewis acids aluminium trichloride ($AlCl_3$) or gallium trichloride ($GaCl_3$).[10,11] The cationic cycle was found to be unstable to heating and was converted to an NPNSi species (Scheme 5.1, top). A new approach using a different starting material resulted in a zwitterionic compound with an NPSSi core that is thermally stable up to at least 80 °C (Scheme 5.1, bottom).[10]

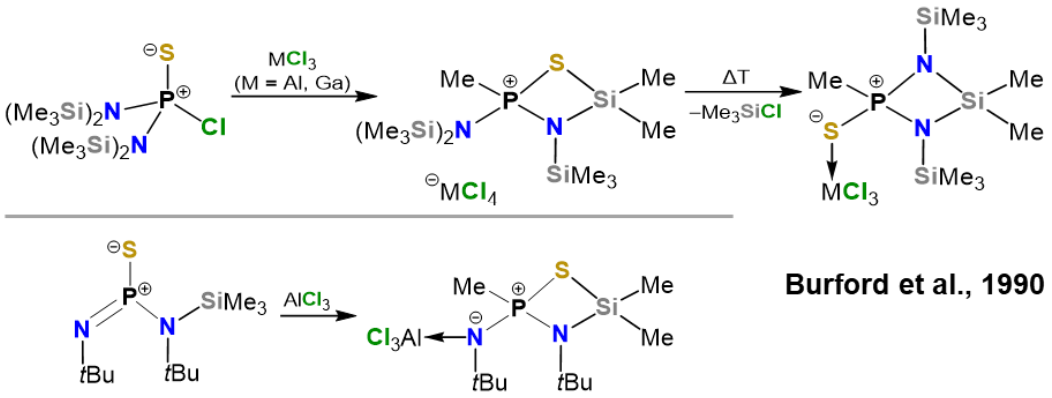

Scheme 5.1. Top: Synthesis of a thermally unstable cationic NPSSi cycle using the Lewis acids $AlCl_3$ and $GaCl_3$, and conversion to an NPNSi cycle.[10] Bottom: Synthesis of a thermally stable NPSSi cycle using $AlCl_3$.[10]

In contrast to this, cyclic CPChSi (Ch = S, Se) cations (Figure 5.1, b) have recently been prepared by hydride abstraction from a silane moiety with Lewis-acidic tris(pentafluorophenyl)borane [$B(C_6F_5)_3$/BCF].[5f,5k,5n] A six-membered cationic CPSSiOSi ring system and its ion pair reactivity have also been reported by our group.[5j] The present work aimed to investigate cationic ring systems based on a NPSSi core. Instead of the CH_2-bridge, an NH moiety was introduced (Figure 5.1, c), which provides an additional Brønsted acidic functionality and therefore enlarges the scope of applications.

5.3. Results and Discussion

Herein, we report the synthesis of *N*-hydrosilyl-substituted aminophosphine sulfides as valuable precursors for heterocyclic systems and present ring formation reactions using tris(pentafluorophenyl)borane (BCF) as hydride abstractor. The scope of precursors does not only include achiral and racemic, but also *P*-chiral as well as *P*-and *Si*-chiral molecules. Particular attention will be paid to the possibility of introducing both *P*- and *Si*-centered chirality into the cyclic system. While achiral or racemic precursors were relatively easy to convert into the ring structure, the enantiomerically and diastereomerically pure products showed high sensitivity when subjected to classical workup such as washing with pentane. Nevertheless, it was possible to perform small scale reactions and to obtain preliminary information by NMR spectroscopy and X-ray structural analysis. Among other things, it was found that the cyclization of diastereomerically pure (R_P,R_{Si})-**17** (d.r. 97:3) does not proceed completely stereospecific. Moreover, an example of the formation of a racemic six-membered ring system starting from an *N*-hydrodisiloxy-substituted aminophosphine

sulfide is presented. All obtained products have been characterized in the best possible way. If no crystal structure could be obtained, ^{1}H, $^{29}Si\{^{1}H\}$ and $^{31}P\{^{1}H\}$ NMR data such as chemical shifts or coupling constants could be used as perfect indicators for the success of the ring formations.

5.3.1. Synthesis of Achiral and Racemic Four-Membered NPSSi Ring Systems and Their Precursors

For the synthesis of achiral or racemic starting materials *P*,*P*-di-*tert*-butylaminophosphine sulfide (**1**)[12] was lithiated using *n*-butyllithium at –80 °C and subsequently subjected to a nucleophilic substitution with the respective hydrosilyl chloride or triflate (Scheme 5.2)

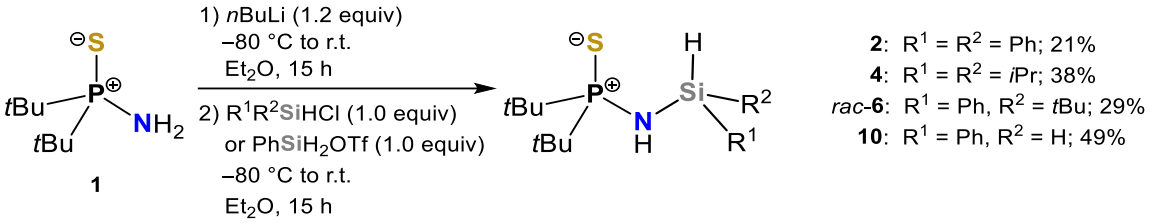

Scheme 5.2. Synthesis of the achiral or racemic precursors **2**, **4**, *rac*-**6** and **10**.

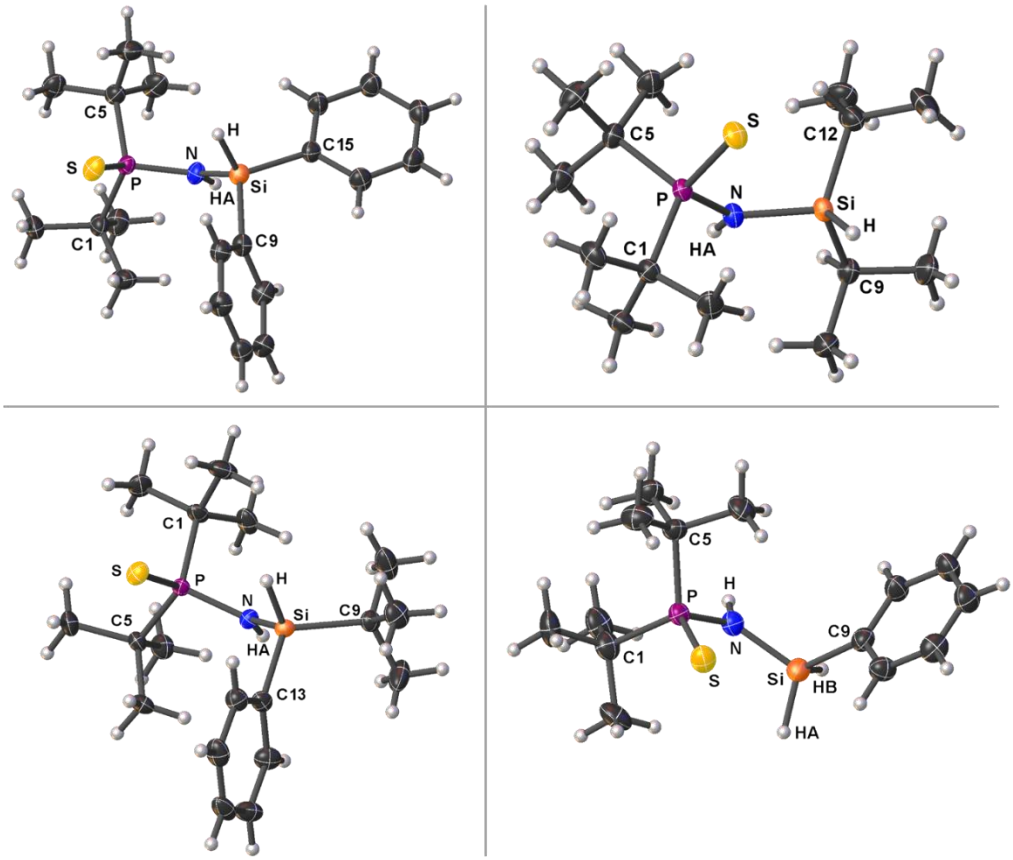

Figure 5.2. Molecular structures of **2** (top left), **4** (top right), *rac*-**6** (bottom left) and **10** (bottom right). in the crystalline state (displacement ellipsoids set at the 50% probability level). Selected bond lengths [Å] and angles [°]: Compound **2**: P–S 1.9631(17), P–N 1.654(4), Si–N 1.751(4), N–P–S 111.11(16), P–N–Si 127.3(3); Compound **4**: P–S 1.9647(5), P–N 1.6551(11), Si–N 1.7550(12), N–P–S 110.16(4), P–N–Si 127.90(7); Compound *rac*-**6**: P–S 1.9646(5), P–N 1.6683(11), Si–N 1.7500(11), N–P–S 111.36(4), P–N–Si 125.83(8); Compound **10**: P–S 1.9669(18), P–N 1.645(4), Si–N 1.744(5), N–P–S 109.20(17); P–N–Si 127.4(3).

The *N*-hydrosilyl-substituted phosphine sulfides were purified by either crystallization (**2**, **4**), Kugelrohr distillation (*rac*-**6**) or washing with pentane (**10**) and obtained in yields between 21% and 49%. All products are stable in air for a long time and do not need to be stored under inert gas. Colorless crystals suitable for single-crystal X-ray analysis (see Figure 5.2) were grown from either diethyl ether (**2**, **4**, *rac*-**6**) or toluene (**10**) solutions.

As being achieved with CH_2-bridged analogues,[5f,5j,5k] hydride abstraction of the synthesized *N*-hydrosilyl-substituted phosphine sulfides could be accomplished using the Lewis acid tris(pentafluorophenyl)borane (BCF). While the hydride remains at the boron atom of BCF to form the anion $[HB(C_6F_5)_3]^-$, the cation undergoes an intermolecular stabilization of the Lewis-acidic silylium moiety by the sulfur atom. Formally, a cyclic aminophosphonium cation is formed and the still Lewis-acidic silylium atom is tamed.

The reactions were conducted at low temperature by slowly combining toluene solutions of both reagents and the mixtures were allowed to warm to ambient temperature overnight while stirring (Scheme 5.3).

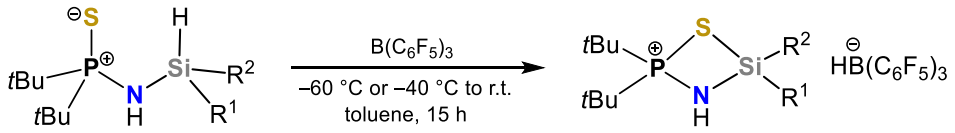

2: $R^1 = R^2$ = Ph
4: $R^1 = R^2$ = *i*Pr
rac-**6**: R^1 = Ph, R^2 = *t*Bu
10: R^1 = Ph, R^2 = H

3[$HB(C_6F_5)_3$]: $R^1 = R^2$ = Ph; 52%
5[$HB(C_6F_5)_3$]: $R^1 = R^2$ = *i*Pr; 62%
rac-**7**[$HB(C_6F_5)_3$]: R^1 = Ph, R^2 = *t*Bu; 62%
rac-**11**[$HB(C_6F_5)_3$]: R^1 = Ph, R^2 = H; n.d.

Scheme 5.3. Synthesis of the achiral or racemic cyclic aminophosphonium compounds **3**[$HB(C_6F_5)_3$], **5**[$HB(C_6F_5)_3$], *rac*-**7**[$HB(C_6F_5)_3$] and *rac*-**11**[$HB(C_6F_5)_3$] (n.d. = yield not defined).

After removal of the solvent and washing with pentane, the product salts were obtained as colorless amorphous solids in yields between 52% and 62% (only the yield of compound *rac*-**11**[$HB(C_6F_5)_3$] was not defined due to irremovable impurities, but expected to be similar). It was possible to crystalize compounds **3**[$HB(C_6F_5)_3$] and **5**[$HB(C_6F_5)_3$] from a toluene solution by layering with pentane and compound *rac*-**7**[$HB(C_6F_5)_3$] from a DCM solution by layering with pentane. Those crystals were suitable for single-crystal X-ray diffraction analysis (see Figure 5.3).

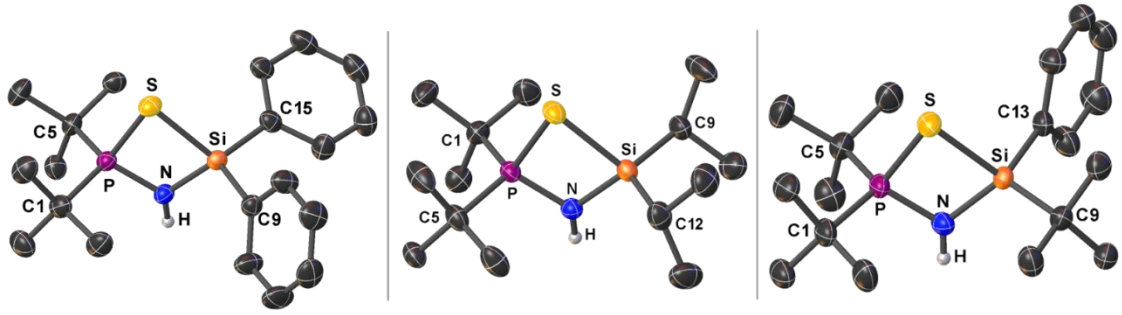

Figure 5.3. Molecular structures of the cyclic cations of compounds **3**[$HB(C_6F_5)_3$] (left), **5**[$HB(C_6F_5)_3$] (middle) and *rac*-**7**[$HB(C_6F_5)_3$] (right) in the crystalline state (displacement ellipsoids set at the 50% probability level). Hydrogen atoms, except for N*H*, are omitted for clarity. Anions are omitted for clarity. Selected bond lengths [Å] and angles [°]: Compound **3**[$HB(C_6F_5)_3$]: P–S 2.0657(6), P–N 1.6458(14), Si–N 1.7490(15), S–Si 2.1967(6); N–P–S 93.69(5), P–S–Si 76.95(2), N–Si–S 86.49(5), P–N–Si 102.81(8); Compound **5**[$HB(C_6F_5)_3$]: P–S 2.0586(6), P–N 1.6434(15), Si–N 1.7530(15), S–Si 2.2074(6), N–P–S 94.24(6), P–S–Si 76.83(2), N–Si–S 86.24(5), P–N–Si 102.69(8); Compound *rac*-**7**[$HB(C_6F_5)_3$]: P–S 2.0692(16), P–N 1.646(4), Si–N 1.752(4), S–Si 2.1937(16), N–P–S 93.57(16), P–S–Si 76.83(6), N–Si–S 86.51(15), P–N–Si 102.5(2).

All three cations have the shape of a distorted square with phosphorus, nitrogen, silicon and sulfur at the edges. The acute P–S–Si angles of about 77° and the wider P–N–Si angles of about 103° indicate that the rings are highly strained systems. While the lengths of the P–N and Si–N bonds hardly changed due to the ring formation compared to the precursor molecules, each P–S bond is lengthened by about 0.1 Å. Modifying the substituents on silicon does not seem to make a big difference at first glance. However, it is noteworthy that compound **5**[$HB(C_6F_5)_3$] with two aliphatic entities on silicon exhibits, by small margin, the longest S–Si distance of all three cations shown in Figure 5.3. This fact is especially reflected when comparing the $^{29}Si\{^1H\}$ NMR shifts in CD_2Cl_2: δ = 35.2 ppm for **5**[$HB(C_6F_5)_3$], δ = 4.4 ppm for **3**[$HB(C_6F_5)_3$] and δ = 20.7 ppm for *rac*-**7**[$HB(C_6F_5)_3$]. It is known that the Lewis-acidic character of a silicon center is increased with a higher downfield shift in $^{29}Si\{^1H\}$ NMR spectra,[13] which means that the silicon atom in compound **5**[$HB(C_6F_5)_3$] is the most Lewis-acidic of the three cycles due to the lack of electron-rich aromatic groups. Electronic effects in four-membered CPSSi heterocyclic molecules were already investigated by the Bauer group.[5k]

Not only the signal of the silicon atom, but also of the phosphorus atom experiences a downfield shift according to $^{31}P\{^1H\}$ NMR spectroscopy in CD_2Cl_2, when comparing the precursors **2**, **4**, *rac*-**6** and **10** (δ = 93.3–95.0 ppm) with the corresponding cyclic aminophosphonium cations **3**, **5**, *rac*-**7** and *rac*-**11** (δ = 111.8–116.1 ppm). In the ^1H NMR spectra, downfield shifts of up to Δδ = 0.3 ppm for the *tert*-butyl groups on the phosphorus atom and about Δδ = 2.0 ppm for the hydrogen atom on the nitrogen atom were observed. The coupling constants ($^3J_{H–P}$) of the *tert*-butyl doublets also changed upon ring formation and increased by about 4 Hz.

Although it was not possible to obtain single-crystals of compound *rac*-**11**[$HB(C_6F_5)_3$] and thus, to unambiguously determine the molecular structure, the ^1H and $^{31}P\{^1H\}$ NMR data strongly indicate, that ring formation by S–Si stabilization took place, since the changes are fairly comparable with the ones observed for compounds **3**[$HB(C_6F_5)_3$], **5**[$HB(C_6F_5)_3$] and *rac*-**7**[$HB(C_6F_5)_3$]. However, compound *rac*-**11**[$HB(C_6F_5)_3$] could only be obtained in 85% pure form. A small signal at δ = 4.60 ppm in the ^1H NMR spectrum in CD_2Cl_2, which becomes larger when the same sample is subjected to another NMR measurement one day later, provides a conceivable explanation for the presence of impurities. Due to the close proximity of protic (N*H*) and hydridic (Si*H*) hydrogen atoms in the strained ring, dihydrogen formation appears to occur and increases with time. The proposed decomposition product still contains an NPSSi cycle, but with an N=Si double bond due to the dihydrogen cleavage (Scheme 5.4). In a previous publication,[5f] it was shown that dihydrogen formation upon Si–H bond cleavage is feasible in the presence of protic hydrogen at higher temperatures.

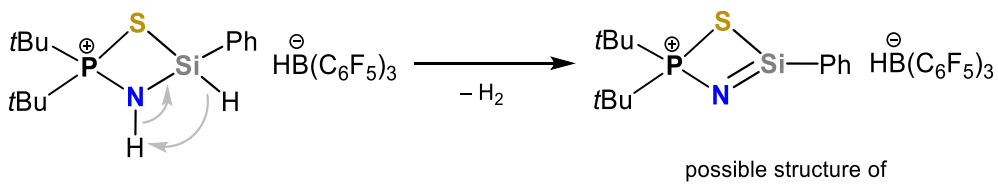

rac-**11**[$HB(C_6F_5)_3$]

possible structure of dehydrogenated *rac*-**11**[$HB(C_6F_5)_3$]

Scheme 5.4. Possible mechanism and proposed result of dihydrogen formation in *rac*-**11**[$HB(C_6F_5)_3$].

An indication that the cationic ring has indeed not completely been opened upon decomposition is the still downfield shifted signal (δ = 106.0 ppm) in the $^{31}P\{^{1}H\}$ NMR spectrum and the higher coupling constant ($\Delta^{3}J_{H-P}$ = 2.2 Hz) of the *tert*-butyl doublet compared to precursor **10**. However, it is assumed that the dehydrogenated cation is a highly reactive intermediate and immediately reacts further. In turn it is possible that the $^{31}P\{^{1}H\}$ NMR signal at 106.0 ppm may not belong to the proposed structure in Scheme 5.4. As there are a number of other small, unidentifiable signals in the $^{31}P\{^{1}H\}$ NMR spectrum at lower values, also partial ring opening cannot be excluded with certainty.

5.3.2. Activation Experiments of compound *rac*-7[HB(C$_6$F$_5$)$_3$]

Activation experiments with gaseous carbon dioxide and hydrogen were carried out based on literature-known models,[14] however, with no significant result for *rac*-**7**[HB(C$_6$F$_5$)$_3$]. A more promising attempt was made with ammonia.[15] The small molecule could certainly open the ring structure of the cation *rac*-**7** after being condensed into the reaction flask at –80 °C and stirring overnight in toluene at room temperature. It was expected that ammonia would attack on the silicon atom to form a terminal aminosilane moiety (Scheme 5.5). Surprisingly, single-crystal X-ray analysis of colorless crystals obtained from a toluene solution, that was layered with pentane, revealed that a terminal Si–OH functionality was present (*rac*-**8**). Even the use of dried ammonia did not prevent the hydrolysis reaction. It is likely that the use of solvents introduced moisture into the reaction solution or product, although the solvents used were generally dry enough to handle the water-sensitive cationic phosphonium cycles such as *rac*-**7**. The terminal Si–N bond is therefore thought to be relatively unstable. Potentially, changing the substituents could help to solve this problem. In addition, NH_4^+ HB(C$_6$F$_5$)$_3^-$ was present in the crystal structure (Scheme 5.5). *Rac*-**8** is a potential precursor for the chain extension with a silane moiety, leading to an *N*-hydrodisiloxy-substituted aminophosphine sulfide.

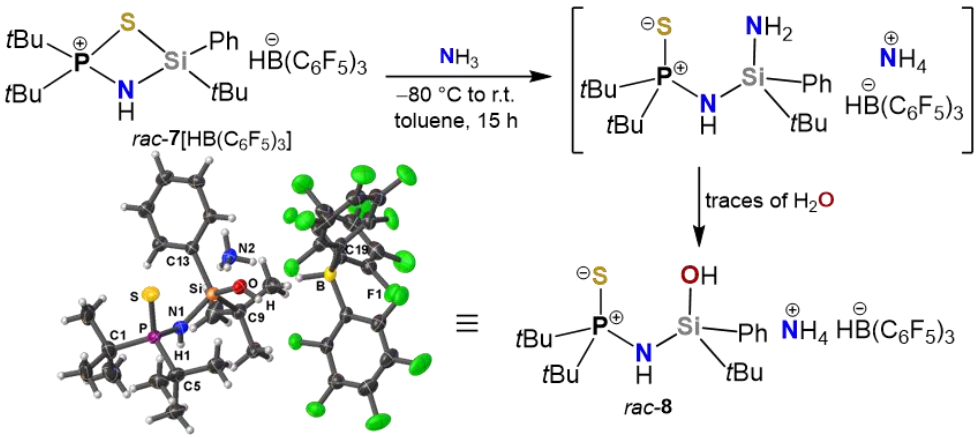

Scheme 5.5. Possible reaction pathway of the ammonia activation of *rac*-**7**[HB(C$_6$F$_5$)$_3$] and subsequent hydrolysis of the labile intermediate.

Besides the activation of small molecules, *rac*-**7**[$HB(C_6F_5)_3$] itself bears potential for further modification such as deprotonation of the NH bridge. This is essentially the second step of a stepwise removal of dihydrogen from compound *rac*-**6**, which has both hydridic (Si*H*) and protic hydrogen (N*H*). In order to avoid ring opening of cation *rac*-**7** during the deprotonation step, non-nucleophilic bases were used for the experiment. Admittedly, the interpretation of such experiments was challenging due to the presence of several products. An attempt with the non-nucleophilic base 1,8-diazabicyclo[5.4.0]undec-7-en (DBU) led to a crystalline product, which is the by-product of the expected deprotonated cyclic main product. The presence of DBU–H^+ $HB(C_6F_5)_3^-$ {**9**[$HB(C_6F_5)_3$]} (Figure 5.5) suggests, that deprotonation of the cationic ring *rac*-**7** was indeed successful, but the zwitterionic, formally dehydrogenated, cycle could not be isolated. Due to the presence of several products in the crude NMR spectra, it is likely that the zwitterionic cycle could have reacted further and decomposed. If the isolation can be achieved in the future, the proposed zwitterionic structure (Scheme 5.6) could serve as a model for a novel type of *N*-binding ligands.

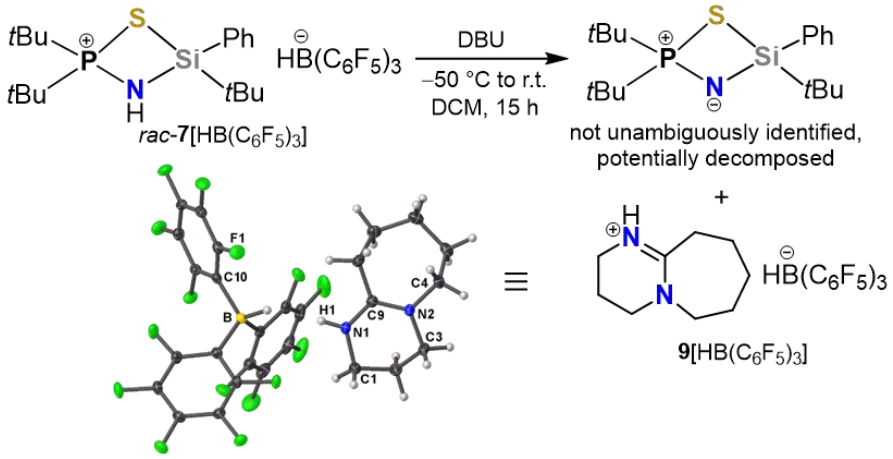

Scheme 5.6. Possible zwitterionic deprotonation product of *rac*-**7**[$HB(C_6F_5)_3$] and crystal structure of the by-product **9**[$HB(C_6F_5)_3$] (DBU = 1,8-diazabicyclo[5.4.0]undec-7-en).

5.3.3. Attempted Synthesis of Chiral Four-Membered NPSSi Ring Systems and Synthesis of Their Precursors

To introduce chirality into the ring structures, phosphorus- and silicon-centered chirality are thinkable. With the goal to investigate *P*-chiral NPSSi cycles, we prepared enantiomerically pure (R_P)-*P*-(*tert*-butyl)-*P*-cyclohexylphosphinothioic amide [(R_P)-**12**], which has already been published,[16] and coupled it with achiral hydrosilyl chloride or triflate after lithiation with *n*-butyllithium. A first test reaction with achiral di-*tert*-butylchlorosilane was already included in the mentioned publication.[16] Two more examples are shown in Scheme 5.7.

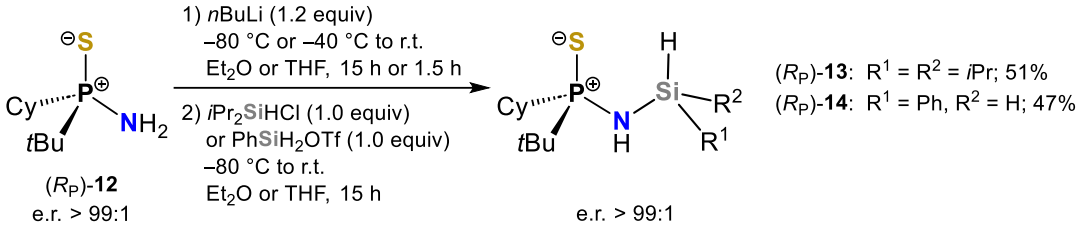

Scheme 5.7. Synthesis of the *P*-chiral precursors (R_P)-**13** and (R_P)-**14**.

The *P*-chiral *N*-hydrosilyl-substituted phosphine sulfides were purified by crystallization and obtained in yields around 50%. The products seemed to be air-stable but were stored under inert gas as a precaution. Colorless crystals suitable for single-crystal X-ray analysis (see Figure 5.4) were grown from either diethyl ether [(R_P)-**13**] or toluene [(R_P)-**14**] solutions.

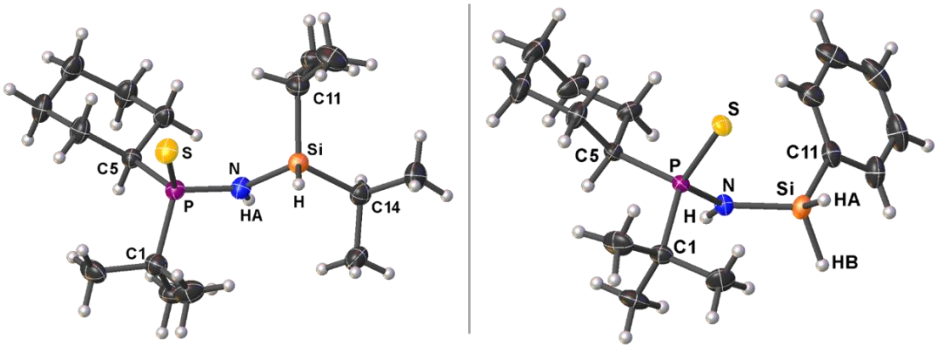

Figure 5.4. Molecular structures of compounds (R_P)-**13** (left) and (R_P)-**14** (right) in the crystalline state (displacement ellipsoids set at the 50% probability level). Selected bond lengths [Å] and angles [°]: Compound (R_P)-**13**: P–S 1.9593(10), P–N 1.649(3), Si–N 1.756(3), N–P–S 109.60(10), P–N–Si 128.02(16); Compound (R_P)-**14**: P–S 1.9656(7), P–N 1.6653(18), Si–N 1.7385(18), N–P–S 111.51(7), P–N–Si 128.39(11).

So far, it was not possible to achieve the ring formation of compound (R_P)-**13** using the same procedure as for the achiral substrates. It is assumed that the chiral cycles are less stable than the achiral ones and break during work-up. In general, it is known that the stability of silicon-nitrogen bonds decreases with a lower steric demand of the substituents at the silicon atom.[17] In the present case, also the steric demand of the substituents at phosphorus, which is lower in the chiral samples due to the exchange of one *tert*-butyl by a cyclohexyl group, could have an influence on the stability of the products. The reaction of (R_P)-**14** with tris(pentafluorophenyl)borane (BCF) was therefore carefully conducted as a small-scale reaction in a Young NMR tube at 0 °C. Deuterated benzene was used as the solvent in order to be able to measure NMR spectra of the crude reaction mixture before the work-up. In the crude $^{31}P\{^1H\}$ NMR spectrum, two signals at δ = 108.2 ppm and δ = 95.6 ppm in a ratio of 62:38 were visible. Due to the downfield shift (Δδ = 20 ppm) the one with the higher integral at δ = 108.2 ppm could easily be assigned to the corresponding desired NPSSi four-membered cycle (R_P)-**15** (Scheme 5.8), which is supported by the increase of the coupling constant of the *tert*-butyl doublet by 3.8 Hz. It is noteworthy, that this is indeed only one signal for the NPSSi cycle. This suggests that only one diastereomer was obtained and that stereochemical induction from the configurationally defined *P*-chiral center to the silicon atom had most likely occurred. However, the absolute configuration at the silicon atom is unknown. After the classic work-up (removing the solvent and washing with pentane) only the second signal at δ = 95.6 ppm (C_6D_6)/ δ = 96.3 ppm (CD_2Cl_2) was left and the coupling constant of the *tert*-butyl doublet was still

increased by 2.4 Hz compared to precursor (R_P)-**14**. The most interesting hint for the identification of this decomposed molecule, however, could be observed in the $^{29}Si\{^1H\}$ NMR spectrum. Surprisingly, it showed a strongly upfield shifted signal of δ = –81.7 ppm, which is in the range for anionic pentacoordinated silicon atoms in a spirocyclic environment.[18] According to the ^1H NMR spectra, the presence of a molecule with the structure of (R_P,R_P)-**16** (Scheme 5.8) is possible. In both, the crude ^1H NMR spectrum in C_6D_6 and the ^1H NMR spectrum in CD_2Cl_2, that was taken after work up, a signal corresponding to dihydrogen is visible at δ = 4.47 ppm or δ = 4.60 ppm, respectively. Dihydrogen formation in cationic NPSSi ring systems was already discussed for compound *rac*-**11**[$HB(C_6F_5)_3$]. This formation is feasible due to the proximity of protic (N*H*) and hydridic (Si*H*) hydrogen in the cyclic cation. Molecules with the same NH–SiHPh motif have been shown to be unstable and prone to further reactions, especially when traces of water are present.[19] Furthermore, it is likely that $[HB(C_6F_5)_3]^-$-induced silane release has occurred upon N–Si bond cleavage and the free aminophosphine sulfide has reacted with an equivalent of cation (R_P)-**15** or its dehydrogenated analogue. Several possibilities for the mechanism are thinkable. Two proposals are presented in Scheme 5.8. The by-products phenylsilane or phenylsilanol could not be observed in the NMR spectra, however, polymerization due to moisture, which gives insoluble products, is likely.

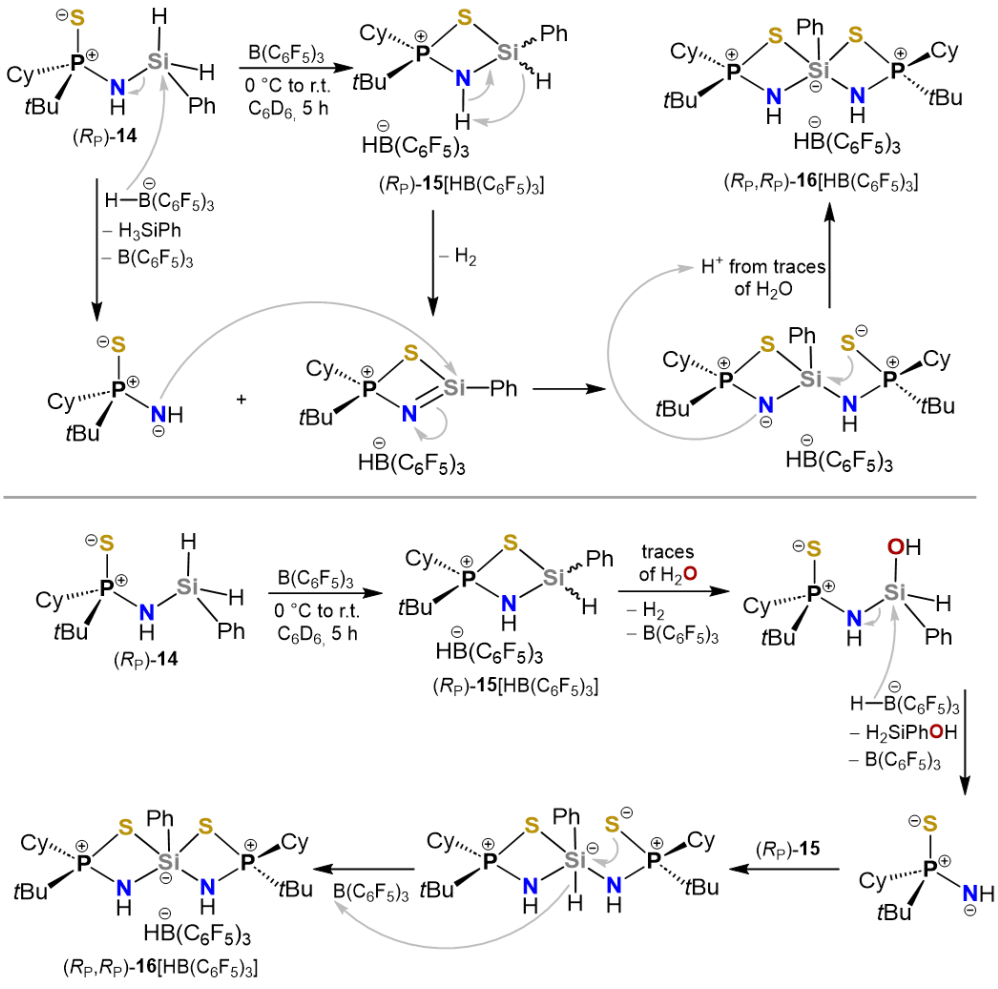

Scheme 5.8. Two possible mechanisms for the formation of the bicyclic compound (R_P,R_P)-**16**[$HB(C_6F_5)_3$].

5.3.4. Synthesis of a *P*- and *Si*-Chiral Four-Membered NPSSi Ring System and Its Precursor

After the successful attachment of an achiral silane moiety to enantiomerically pure (R_P)-*P*-(*tert*-butyl)-*P*-cyclohexylphosphinothioic amide [(R_P)-**12**], a chiral alkylarylchlorosilane was used for the coupling reaction after lithiation of the amino entity (Scheme 5.9). Basically, (R_P)-**12** functioned as a *P*-stereogenic chiral auxiliary and, as expected, two *P*- and *Si*-chiral diastereomers [(R_P,S_{Si})-**17** and (R_P,R_{Si})-**17**] were formed, which had to be separated. The crude reaction mixture showed a diastereomeric ratio of 11:89 according to the signals at δ = 86.8 ppm and δ = 86.1 ppm in the $^{31}P\{^1H\}$ NMR spectrum. After three crystallization steps (for details see experimental section) from a diethyl ether solution, that was layered with pentane, the diastereomerically pure *P*- and *Si*-chiral *N*-hydrosilyl-substituted phosphine sulfides (R_P,S_{Si})-**17** (d.r. >99:1) and (R_P,R_{Si})-**17** (d.r. 97:3) could be separated.

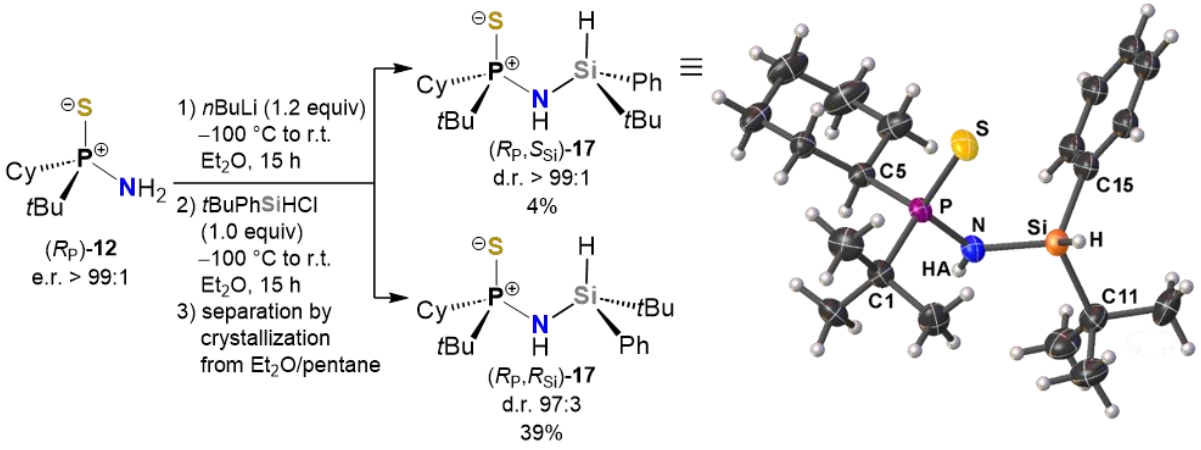

Scheme 5.9. Synthesis of the *P*- and *Si*-chiral precursors (R_P,S_{Si})-**17** and (R_P,R_{Si})-**17**, and molecular structure of compound (R_P,S_{Si})-**17** in the crystalline state (displacement ellipsoids set at the 50% probability level).

After the many crystallization steps, yields of 4% and 39% were achieved in total for the air-stable products. Colorless crystals could be obtained for compound (R_P,S_{Si})-**17** after the second crystallization step and the absolute configuration could be determined by single-crystal X-ray diffraction analysis (see Scheme 5.9). (R_P,R_{Si})-**17** could never be obtained in a crystalline form good enough to be analyzed by single-crystal X-ray diffraction.

With (R_P,R_{Si})-**17**, the stereoselectivity of the ring closure of *P*- and *Si*-chiral *N*-hydrosilyl-substituted phosphine sulfides was investigated for the first time. Previous experiments on *Si*-chiral hydrosilyl phosphine sulfides showed that both ring formation with BCF and re-opening using $NaHBEt_3$ were stereospecific.[5f] For the ring closure experiment, (R_P,R_{Si})-**17** was dissolved in C_6D_6 and slowly added to a solution of tris(pentafluorophenyl)borane (BCF) in C_6D_6 in a Young NMR tube at 0 °C (Scheme 5.10). Five hours later, NMR spectra of the crude mixture were recorded without any purification and showed two signals at δ = 106.4 ppm and δ = 105.8 ppm in a ratio of 22:78 in the $^{31}P\{^1H\}$ NMR spectrum. The downfield shift (Δδ = 20 ppm) and the change in the coupling constants of the *tert*-butyl doublets ($\Delta^3J_{H-P} \approx 4.3$ Hz) compared to the precursor (R_P,R_{Si})-**17** indicate that the two possible diastereomeric cyclic cations (R_P,S_{Si})-**18** and (R_P,R_{Si})-**18** had been formed. Also, the

^{29}Si{^{1}H} NMR signals were shifted downfield (Δδ ≈ 15 ppm). We strongly believe that the poor stereoselectivity, as observed in the ^{31}P{^{1}H} NMR spectrum, is based on thermodynamic reasons. Since neighbor-group-participated hydride abstraction with Lewis acids such as BCF has been shown to be an inversion process,[5c,5f,20] (R_P,R_{Si})-**18**[HB(C_6F_5)$_3$] is the kinetic product, which is gradually converted into the thermodynamically stable (R_P,S_{Si})-**18**[HB(C_6F_5)$_3$]. This hypothesis is additionally supported by the structure of the diastereomers. In the cation (R_P,R_{Si})-**18**, both *tert*-butyl groups (P*t*Bu and Si*t*Bu) are located on the same side of the NPSSi ring and are quite close to each other. Since this is sterically unfavorable, the cation (R_P,S_{Si})-**18**, which carries the *tert*-butyl groups on the opposite sides of the ring, is formed over time. In previous studies, this circumstance was not discovered, since exclusively an achiral phosphine sulfide moiety was used.[5f] In addition, it should be noted that the recorded NMR spectra only represent a momentary snapshot and that an increasing formation of the more stable product with longer reaction time cannot be ruled out.

In order to unequivocally prove the ring formation, a crystallization experiment was set up by layering the crude C_6D_6 solution with pentane. Colorless crystals of (R_P,S_{Si})-**18**[HB(C_6F_5)$_3$] could be obtained after five days at room temperature and were subjected to a single-crystal X-ray diffraction analysis (see Scheme 5.10).

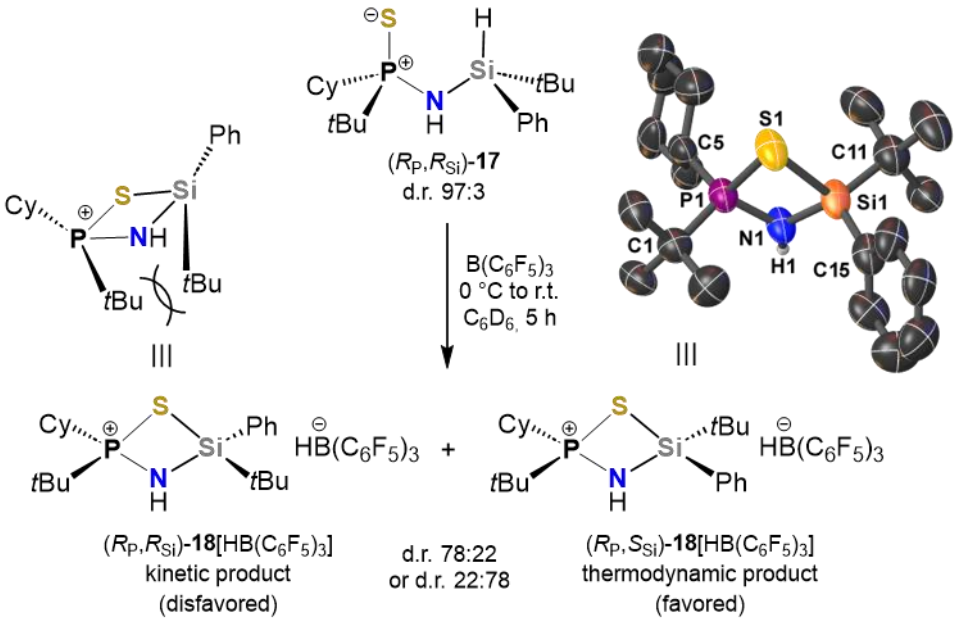

Scheme 5.10. Synthesis of the diastereomeric *P*- and *Si*-chiral cyclic aminophosphonium compounds (R_P,R_{Si})-**18**[HB(C_6F_5)$_3$] and (R_P,S_{Si})-**18**[HB(C_6F_5)$_3$], and molecular structure of cation (R_P,S_{Si})-**18** in the crystalline state (displacement ellipsoids set at the 50% probability level; hydrogen atoms, except for N*H*, are omitted for clarity).

After a second ring closure experiment of (R_P,R_{Si})-**17**, re-opening of the cyclic cation (R_P,R_{Si}/S_{Si})-**18** (d.r.78:22) using NaHBEt$_3$[5f] was attempted. Although it was expected that the starting materials would be recovered, two broad signals at δ = 70.3 ppm and δ = 71.4 ppm were obtained in the ^{31}P{^{1}H} NMR spectra in C_6D_6, which are not consistent with the shift values of the starting materials (R_P,S_{Si})-**17** and (R_P,R_{Si})-**17**. Furthermore, the ratio of these new signals (66:34) suggests that the presumed ring opening reaction was again not stereoselective in the case of diastereomeric signals. Due to the broadness of the signals, also in the ^{1}H NMR spectrum, no statement on the possible

structure of the products can be made. Regarding the highfield-shifted $^{31}P\{^{1}H\}$ NMR values, it is likely that ring opening has occurred, but presumably not in the expected manner between sulfur and silicon. Cleavage between nitrogen and silicon seems likely according to our own experiences during the experimental collection and work with N–Si bridged *N*-hydrosil(ox)yl-substituted phosphine sulfides.

5.3.5. Synthesis of a Racemic Six-Membered NPSSiOSi Ring System and Its Precursor

While hydrosilyl chlorides and triflates could be directly coupled with *P*,*P*-di-*tert*-butylaminophosphine sulfide (**1**) after lithiation to give silane-based precursors, this reaction proved less efficient for chlorodisiloxanes. Instead, a chlorodisiloxane was coupled with the unoxidized *P*,*P*-di-*tert*-butylaminophosphine after lithiation at –80 °C and subsequently oxidized with elemental sulfur to obtain compound *rac*-**19** (Scheme 5.11).

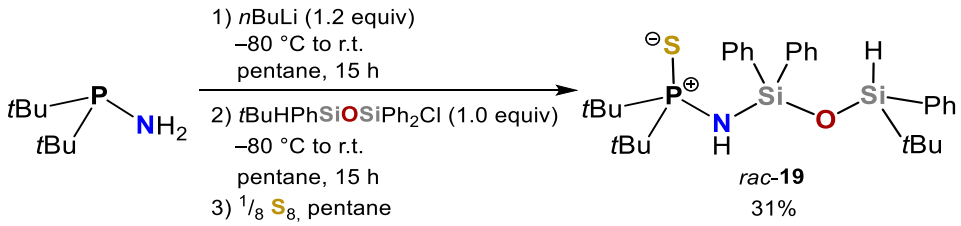

Scheme 5.11. Synthesis of the racemic disiloxane-based precursor *rac*-**19**.

The *N*-hydrodisiloxy-substituted phosphine sulfide *rac*-**19** was obtained in an overall yield of 31% after three reaction steps. Since Kugelrohr distillation was carried out after the second reaction step, no further purification was necessary after oxidation with sulfur. The oxidized product *rac*-**19** was obtained as a colorless viscous oil and stored under inert gas.

Hydride abstraction of *rac*-**19** was performed with tris(pentafluorophenyl)borane (BCF) at –40 °C by slowly combining toluene solutions of both reagents and allowing the mixture to warm to ambient temperature overnight while stirring (Scheme 5.12). The oily crude product of *rac*-**20**[$HB(C_6F_5)_3$] was isolated by precipitation in pentane and eventually obtained as a colorless foamy solid in 49% yield after washing with pentane and drying in vacuo.

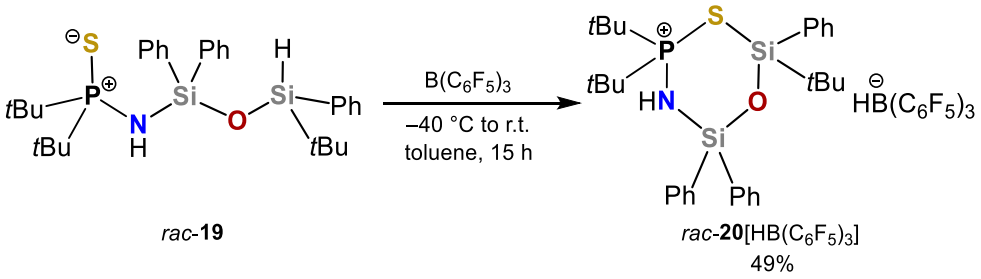

Scheme 5.12. Synthesis of the racemic disiloxane-based cyclic aminophosphonium compound *rac*-**20**[$HB(C_6F_5)_3$].

Although several attempts to obtain single crystals of *rac*-**20**[HB(C_6F_5)$_3$] remained unsuccessful, the structure of the six-membered aminophosphonium cation could be validated by NMR spectroscopy. The missing Si*H* signal and the coupling constants of the *tert*-butyl doublets ($^3J_{H-P}$ = 18.7 Hz in cation *rac*-**20** vs. $^3J_{H-P}$ = 15.5 Hz in precursor *rac*-**19**) in the ^{1}H NMR spectrum strongly suggest the successful hydride abstraction and ring formation by intermolecular stabilization of the Lewis-acidic silylium moiety by the sulfur atom. Also the downfield shift from δ = 91.0 ppm in *rac*-**19** to δ = 100.1 ppm in *rac*-**20**[HB(C_6F_5)$_3$] in the ^{31}P{^{1}H} NMR spectrum confirms this assumption. Compared to the four-membered cycles, the overall downfield shift is indeed lower, which means that the influence of the P–S–Si stabilization is less in six-membered cycles. The same suggestion is underlined by the small downfield shift to δ = –3.3 ppm in the ^{29}Si{^{1}H} NMR spectrum for the tamed silylium atom (*t*BuPh*Si*) in *rac*-**20**[HB(C_6F_5)$_3$] compared to the *t*BuPhH*Si* moiety of the precursor *rac*-**19** (δ = –5.6 ppm). These findings are in line with previous investigations on six-membered CH_2-bridged substrates.[5j] As there too, it should be mentioned at this point that increased shielding of silicon atoms with increasing ring size is a known fact.[21]

Failed crystallization attempts of compound *rac*-**20**[HB(C_6F_5)$_3$] included classical methods such as layering a DCM solution of the aminophosphonium hydroborate with pentane, as well as prior anion exchange experiments. The latter were carried out with Jutzi's acid {[H(OEt_2)$_2$]$^+$[B(C_6F_5)$_4$]$^-$}, Li$^+$[B(C_6F_5)$_4$]$^-$ or (CPh_3)$^+$[B(C_6F_5)$_4$]$^-$. The aim was to replace the anion [HB(C_6F_5)$_3$]$^-$ by the tetraaryl-substituted borate [B(C_6F_5)$_4$]$^-$, which features a better crystallizability. After anion exchange with lithium or trityl tetraaryl-substituted borate, single crystals of *rac*-**20**[B(C_6F_5)$_4$] could still not be obtained. Jutzi's acid, previously used successfully for weakly coordinating anion exchange,[5j] induced cleavage of the N–Si bond in cation *rac*-**20**. The same bond cleavage happened when trying to crystallize *rac*-**20**[HB(C_6F_5)$_3$] in the unintended presence of moisture. Not only the cation turned out to be very sensitive, but also the anion, which dimerized with a hydroxyl moiety in between. The crystal structure of **21**[(μ-OH)($BCF)_2$] (Figure 5.5) was obtained from a DCM solution after layering with pentane.

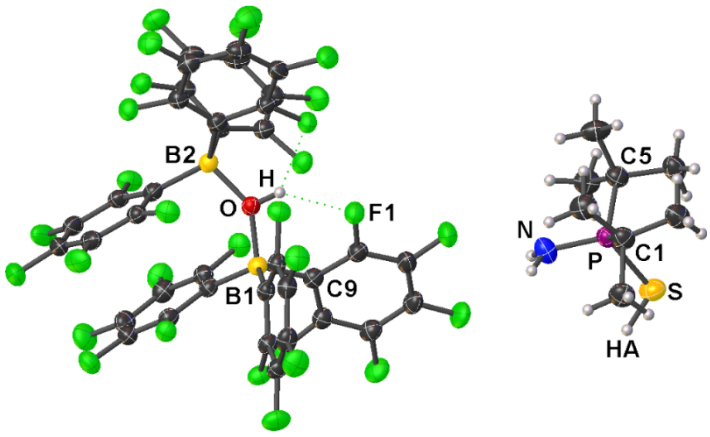

Figure 5.5. Molecular structure of compound **21**[(μ-OH)($BCF)_2$] in the crystalline state (displacement ellipsoids set at the 50% probability level). Selected bond lengths [Å] and angles [°]: P–S 2.0796(9), P–N 1.626(2), S–HA 1.30(3), N–P–S 112.94(10).

5.4. Conclusion

In conclusion, we have synthesized *N*-hydrosilyl-substituted aminophosphine sulfides in four categories: 1) achiral, 2) *Si*-racemic, 3) enantiomerically pure *P*-chiral and 4) diastereomerically pure *P*- and *Si*-chiral. A great challenge was the unprecedented fractional crystallization of the diastereomeric compounds (R_P,S_{Si})-**17** and (R_P,R_{Si})-**17**. *N*-hydrosilyl-substituted phosphine sulfides constitute valuable precursors for the formation of four-membered, cationic, heterocyclic ring systems upon hydride abstraction with BCF. The phosphine sulfide, as a Lewis basic functionality, provides an effective stabilization for the Lewis-acidic silylium-type centers through the formation of strong intramolecular bonds. While the preparation of achiral cyclic cations was a straightforward undertaking, all chiral samples were prone to decomposition. Nevertheless, it was possible to study the stereoselectivity of the ring formation of (R_P,R_{Si})-**17**, which is likely influenced by epimerization processes. Two examples of follow-up reactions of *rac*-**7**[$HB(C_6F_5)_3$] that give rise to further investigation were presented and can be considered as model experiments for the applicability of aminophosphonium ions in organic synthesis. It was also shown that six-membered cyclic cations can be prepared using the same hydride abstraction method. Application of the presented molecules in the design of new ligand systems and transition metal-free catalysis will be further investigated in the future.

5.5. References

[1] a) T. Werner, *Adv. Synth. Catal.* **2009**, *351*, 1469–1481; b) D. Enders, T. V. Nguyen, *Org. Biomol. Chem.* **2012**, *10*, 5327–5331; c) A. Golandaj, A. Ahmad, D. Ramjugernath, *Adv. Synth. Catal.* **2017**, *359*, 3676–3706; d) N. Noroozi-Shad, M. Gholizadeh, H. Sabet-Sarvestani, *J. Mol. Struct.* **2022**, *1257*, 132628; e) S. Fang, Z. Liu, T. Wang, *Angew. Chem. Int. Ed.* **2023**, *62*, e202307258; *Angew. Chem.* **2023**, *135*, e202307258.

[2] T. Huber, J. O. Bauer, *Chem. Eur. J.* **2024**, *30*, e202303760.

[3] a) C. Fliedel, A. Ghisolfi, P. Braunstein, *Chem. Rev.* **2016**, *116*, 9237–9304; b) M. B. Smith, *Molecules* **2022**, *27*, 6293; c) D. Ray, S. Majee, R. N. Yadav, B. K. Banik, *Molecules* **2023**, *28*, 3524.

[4] a) H. F. T. Klare, L. Albers, L. Süsse, S. Keess, T. Müller, M. Oestreich, *Chem. Rev.* **2021**, *121*, 5889–5985; b) A. Y. Timoshkin, *Chem. Eur. J.* **2024**, *30*, e202302457.

[5] a) P. Ducos, V. Liautard, F. Robert, Y. Landais, *Chem. Eur. J.* **2015**, *21*, 11573–11578; b) S. Künzler, S. Rathjen, K. Rüger, M. S. Würdemann, M. Wernke, P. Tholen, C. Girschik, M. Schmidtmann, Y. Landais, T. Müller, *Chem. Eur. J.* **2020**, *26*, 16441–16449; c) A. Fernandes, C. Laye, S. Pramanik, D. Palmeira, Ö. Ö. Pekel, S. Massip, M. Schmidtmann, T. Müller, F. Robert, Y. Landais, *J. Am. Chem. Soc.* **2020**, *142*, 564–572; d) A. Dajnak, E. Maerten, N. Saffon-Merceron, A. Baceiredo, T. Kato, *Organometallics* **2020**, *39*, 3403–3412; e) A. Denhof, M. Olaru, E. Lork, S. Mebs, L. Chęcińska, J. Beckmann, *Eur. J. Inorg. Chem.* **2020**, 4093–4110; f) N. Fontana, N. A. Espinosa-Jalapa, M. Seidl, J. O. Bauer, *Chem. Eur. J.* **2021**, *27*, 2649–2653; g) N. Kumar, C. Laye, F. Robert, Y. Landais, *Eur. J. Org. Chem* **2021**, 3613–3621; h) A. Dajnak, G. Altınbaş Özpınar, R. Lenk, N. Saffon-Merceron, A. Baceiredo, T. Kato, T. Müller, E. Maerten, *Dalton Trans.* **2022**, *51*, 1407–1414; i) R. Nougué, S. Takahashi, A. Dajnak, E. Maerten, A. Baceiredo, N. Saffon-Merceron, V. Branchadell, T. Kato, *Chem. Eur. J.* **2022**, *28*, e202202037; j) N. Fontana, N. A. Espinosa-Jalapa, M. Seidl, J. O. Bauer, *Chem. Commun.* **2022**, *58*, 2144–2147; k) A. Falk, J. O. Bauer, *Inorg. Chem.* **2022**, *61*, 15576–15588; l) A. Dajnak, L. Shi, G. Altınbaş Özpınar, R. Lenk, N. Saffon-Merceron, A. Baceiredo, T. Kato, T.

Müller, E. Maerten, *Dalton Trans.* **2023**, *52*, 3052–3058; m) S. Takahashi, R. Nougué, T. Troadec, A. Baceiredo, N. Saffon-Merceron, V. Branchadell, T. Kato, *Inorg. Chem.* **2023**, *62*, 6488–6498; n) N. Fontana, J. O. Bauer, *ChemistrySelect* **2023**, *8*, e202301373.

[6] a) T. Müller, *Angew. Chem. Int. Ed.* **2001**, *40*, 3033–3036; *Angew. Chem.* **2001**, *113*, 3123–3126; b) A. Y. Khalimon, Z. H. Lin, R. Simionescu, S. F. Vyboishchikov, G. I. Nikonov, *Angew. Chem. Int. Ed.* **2007**, *46*, 4530–4533; *Angew. Chem.* **2007**, *119*, 4614–4617; c) S. J. Connelly, W. Kaminsky, D. M. Heinekey, *Organometallics* **2013**, *32*, 7478–7481; d) L. Albers, J. Baumgartner, C. Marschner, T. Müller, *Chem. Eur. J.* **2016**, *22*, 7970–7977.

[7] H. Gao, R. Müller, E. Irran, H. F. T. Klare, M. Kaupp, M. Oestreich, *Chem. Eur. J.* **2022**, *28*, e202104464.

[8] a) L. Omann, B. Pudasaini, E. Irran, H. F. T. Klare, M.-H. Baik, M. Oestreich, *Chem. Sci.* **2018**, *9*, 5600–5607; b) Q. Wu, A. Roy, G. Wang, E. Irran, H. F. T. Klare, M. Oestreich, *Angew. Chem. Int. Ed.* **2020**, *59*, 10523–10526; *Angew. Chem.* **2020**, *132*, 10609–10613.

[9] M. Kümper, T. Götz, N. A. Espinosa-Jalapa, A. Falk, R. Rothfelder, J. O. Bauer, *Z. Anorg. Allg. Chem.* **2023**, *649*, e202300067.

[10] N. Burford, R. E. H. Spence, J. M. Whalen, R. D. Rogers, J. F. Richardson, *Organometallics* **1990**, *9*, 2854–2856.

[11] a) N. Burford, S. Mason, R. E. H. Spence, J. M. Whalen, J. F. Richardson, R. D. Rogers, *Organometallics* **1992**, *11*, 2241–2250; b) N. Burford, R. E. H. Spence, J. M. Whalen, J. F. Richardson, R. D. Rogers, *Phosphorus, Sulfur Relat. Elem.* **1992**, *64*, 137–144.

[12] a) M. J. P. Harger, M. A. Stephen, *J. Chem. Soc., Perkin Trans.* **1980**, 705–711; b) M. Köster, A. Kreher, C. von Hänisch, *Dalton Trans.* **2018**, *47*, 7875–7878; c) T. C. Jankins, Z. Qin, K. M. Engle, *Tetrahedron* **2019**, *75*, 3272–3281.

[13] a) H. F. T. Klare, M. Oestreich, *Dalton Trans.* **2010**, *39*, 9176–9184; b) J. C. L. Walker, H. F. T. Klare, M. Oestreich, *Nat. Rev. Chem.* **2020**, *4*, 54–62.

[14] a) A. Berkefeld, W. E. Piers, M. Parvez, *J. Am. Chem. Soc.* **2010**, *132*, 10660–10661; b) M. Reißmann, A. Schäfer, S. Jung, T. Müller, *Organometallics* **2013**, *32*, 6736–6744; c) B. Waerder, M. Pieper, L. A. Körte, T. A. Kinder, A. Mix, B. Neumann, H.-G. Stammler, N. W. Mitzel, *Angew. Chem. Int. Ed.* **2015**, *54*, 13416–13419; *Angew. Chem.* **2015**, *127*, 13614–13617; d) S. A. Weicker, D. W. Stephan, *Chem. Eur. J.* **2015**, *21*, 13027–13034.

[15] J. Cui, Y. Li, R. Ganguly, A. Inthirarajah, H. Hirao, R. Kinjo, *J. Am. Chem. Soc.* **2014**, *136*, 16764–16767.

[16] T. Huber, N. A. Espinosa-Jalapa, J. O. Bauer, *Chem. Eur. J.* **2022**, *28*, e202202608.

[17] a) S. S. Dua, C. Eaborn, D. A. R. Harper, S. P. Hopper, K. D. Safa, D. R. M. Walton, *J. Organomet. Chem.* **1979**, *178*, 75–82; b) C. Eaborn, F. M. S. Mahmoud, *J. Organomet. Chem.* **1981**, *220*, 139–143.

[18] a) J. A. Cella, J. D. Cargioli, E. A. Williams, *J. Organomet. Chem.* **1980**, *186*, 13–17; b) R. Tacke, M. Pülm, B. Wagner, *Adv. Organomet. Chem.* **1999**, *44*, 221–273.

[19] T. Götz, *PhD thesis,* **2023**, Universität Regensburg.

[20] S. Rendler, M. Oestreich, *Angew. Chem. Int. Ed.* **2008**, *47*, 5997–6000; *Angew. Chem.* **2008**, *120*, 6086–6089.

[21] D. Seyferth, H. Friedrich, S. W. Krska, *Z. Naturforsch.* **1994**, *49b*, 1818–1826.

5.6. Syntheses and Characterizations

5.6.1. General Remarks

All experiments were performed in an inert atmosphere of purified nitrogen by using standard Schlenk techniques or an MBraun Unilab 1200/780 glovebox. Glassware was heated at 140 °C prior to use. Diethyl ether (Et_2O), dichloromethane (DCM), hexane, pentane, tetrahydrofuran (THF), and toluene were dried and degassed with an MBraun SP800 solvent purification system.

n-Butyllithium (1.6 M or 2.5 M solution in hexane, Merck), chlorodiphenylsilane (90%, abcr), chlorodiisopropylsilane (95%, abcr), diphenylsilane (97%, Merck), triflic acid (98%, Merck), *s*ulfur (99%, Merck), ammonia (anhydrous, Staub & Co.), 1,8-diazabicyclo[5.4.0]undec-7-en (DBU) (for synthesis, Merck) were used without further purification.

P,*P*-Di-*tert*-butylaminophosphine sulfide (**1**) and *P*,*P*-di-*tert*-butylaminophosphine were synthesized following literature procedures.[1] *tert*-Butylchlorophenylsilane and $ClPh_2Si–O–Si$*t*$BuPhH$ were synthesized following a procedure published by our group.[2] Tris(pentafluorophenyl)borane (BCF) was synthesized following a reported procedure.[3] Phenylsilyl triflate was synthesized following a reported procedure.[4] (R_P)-*P*-(*tert*-butyl)-*P*-cyclohexylphosphinothioic amide [(R_P)-**12**, e.r. >99:1] was synthesized following a procedure published by our group.[5]

C_6D_6 (≥ 99.6%, Merck) was used for NMR spectroscopy as purchased. CD_2Cl_2 (> 99.8%, Fluorochem) was degassed and dried over molecular sieve (3 Å) prior to use. NMR spectra were either recorded using a Bruker Avance 400 (400.13 MHz) or a Bruker Avance III HD 400 (400.13 MHz) at 25 °C. Chemical shifts (δ) are reported in parts per million (ppm). ^{1}H and $^{13}C\{^{1}H\}$ NMR spectra are referenced to tetramethylsilane ($SiMe_4$, δ = 0.0 ppm) as external standard, with the deuterium signal of the solvent serving as internal lock and the residual solvent signal as an additional reference. $^{31}P\{^{1}H\}$, $^{29}Si\{^{1}H\}$, $^{11}B\{^{1}H\}$ and $^{19}F\{^{1}H\}$ NMR spectra are referenced to H_3PO_4, $SiMe_4$, $BF_3{\cdot}OEt_2$ and $CFCl_3$, respectively. For the assignment of the multiplicities, the following abbreviations are used: s = singlet, d = doublet, t = triplet, m = multiplet, br = broad signal. Elemental analyses were performed on a Vario MICRO cube apparatus. High-resolution mass spectrometry was carried out on a Jeol AccuTOF GCX and an Agilent Q-TOF 6540 UHD spectrometer.

5.6.2. Four-Membered NPSSi Ring Systems and Their Precursors

5.6.2.1. Synthesis of *t*Bu$_2$(PS)NH(SiHPh$_2$) (2)

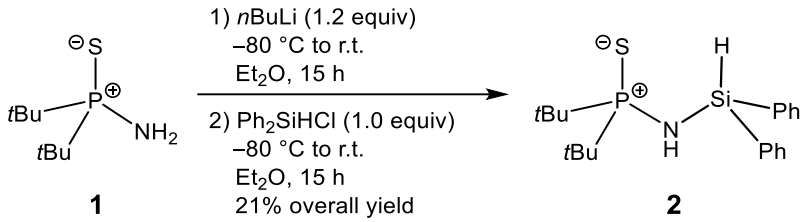

1 **2**

*n*Butyllithium (3.92 mL, 9.80 mmol, 1.2 equiv., 2.5 M in hexane) was added dropwise to a solution of *P*,*P*-di-*tert*-butylaminophosphine sulfide (**1**) (1.58 g, 8.17 mmol, 1.0 equiv.) in diethyl ether (50 mL) at −80 °C. The solution was allowed to slowly warm to room temperature and stirred for 15 h. Following, the colorless solution was cooled to −80 °C again and chlorodiphenylsilane (1.79 g, 8.17 mmol, 1.0 equiv.) was added dropwise. The reaction mixture was allowed to slowly warm to room temperature and stirred for 15 h affording a yellow suspension. The precipitated lithium chloride was filtered off via cannula filtration and washed with diethyl ether. The crude solution was kept at −28 °C for 20 h to yield colorless crystalline needles suitable for single-crystal X-ray analysis, which were filtered off via cannula filtration and washed with pentane. After drying in vacuo, compound **2** was obtained as colorless needle-shaped crystals (0.63 g, 1.68 mmol, 21%).

^{1}H NMR (400.13 MHz, C_6D_6, 298 K): δ = 1.12 (d, $^3J_{H–P}$ = 15.4 Hz, 18H, PC(C*H*$_3$)$_3$), 2.11 (br, 1H, N*H*), 6.15 (m, 1H, Si*H*), 7.18–7.23 (m, 6H, *H*$_{Ph}$), 7.76–7.80 (m, 4H, *H*$_{Ph}$). **^{31}P{^{1}H} NMR** (162.04 MHz, C_6D_6, 298 K): δ = 93.3 (s). **^{13}C{^{1}H} NMR** (100.61 MHz, C_6D_6, 298 K): δ = 27.4 (d, $^2J_{C–P}$ = 1.9 Hz, PC(*C*H$_3$)$_3$), 39.7 (d, $^1J_{C–P}$ = 53.2 Hz, P*C*(CH$_3$)$_3$), 128.3 (s, *C*$_{meta}$), 130.3 (s, *C*$_{para}$), 135.5 (d, $^3J_{C–P}$ = 2.9 Hz, *C*$_{ipso}$), 135.6 (s, *C*$_{ortho}$). **^{29}Si{^{1}H} NMR** (79.49 MHz, C_6D_6, 298 K): δ = −20.9 (d, $^2J_{Si–P}$ = 2.1 Hz).

^{1}H NMR (400.13 MHz, CD_2Cl_2, 298 K): δ = 1.30 (d, $^3J_{H–P}$ = 15.5 Hz, 18H, PC(C*H*$_3$)$_3$), 2.31 (br, 1H, N*H*), 5.69 (m, 1H, Si*H*), 7.37–7.46 (m, 6H, *H*$_{Ph}$), 7.66–7.68 (m, 4H, *H*$_{Ph}$). **^{31}P{^{1}H} NMR** (162.04 MHz, CD_2Cl_2, 298 K): δ = 94.2 (s). **^{13}C{^{1}H} NMR** (100.61 MHz, CD_2Cl_2, 298 K): δ = 27.7 (d, $^2J_{C–P}$ = 1.8 Hz, PC(*C*H$_3$)$_3$), 40.2 (d, $^1J_{C–P}$ = 52.8 Hz, P*C*(CH$_3$)$_3$), 128.5 (s, *C*$_{meta}$), 130.6 (s, *C*$_{para}$), 135.6 (s, *C*$_{ortho}$), 135.6 (s, *C*$_{ipso}$). **^{29}Si{^{1}H} NMR** (79.49 MHz, CD_2Cl_2, 298 K): δ = −21.8 (d, $^2J_{P–Si}$ = 2.3 Hz).

Elemental analysis: $C_{20}H_{30}NPSSi$: calcd.: C 63.96, H 8.05, N 3.73; found: C 63.73, H 7.84, N 3.64.

HR(+ESI)-MS: calcd. *m/z* for $C_{20}H_{31}NPSSi$ [(M+H)$^+$]: 376.1679, found: 376.1685.

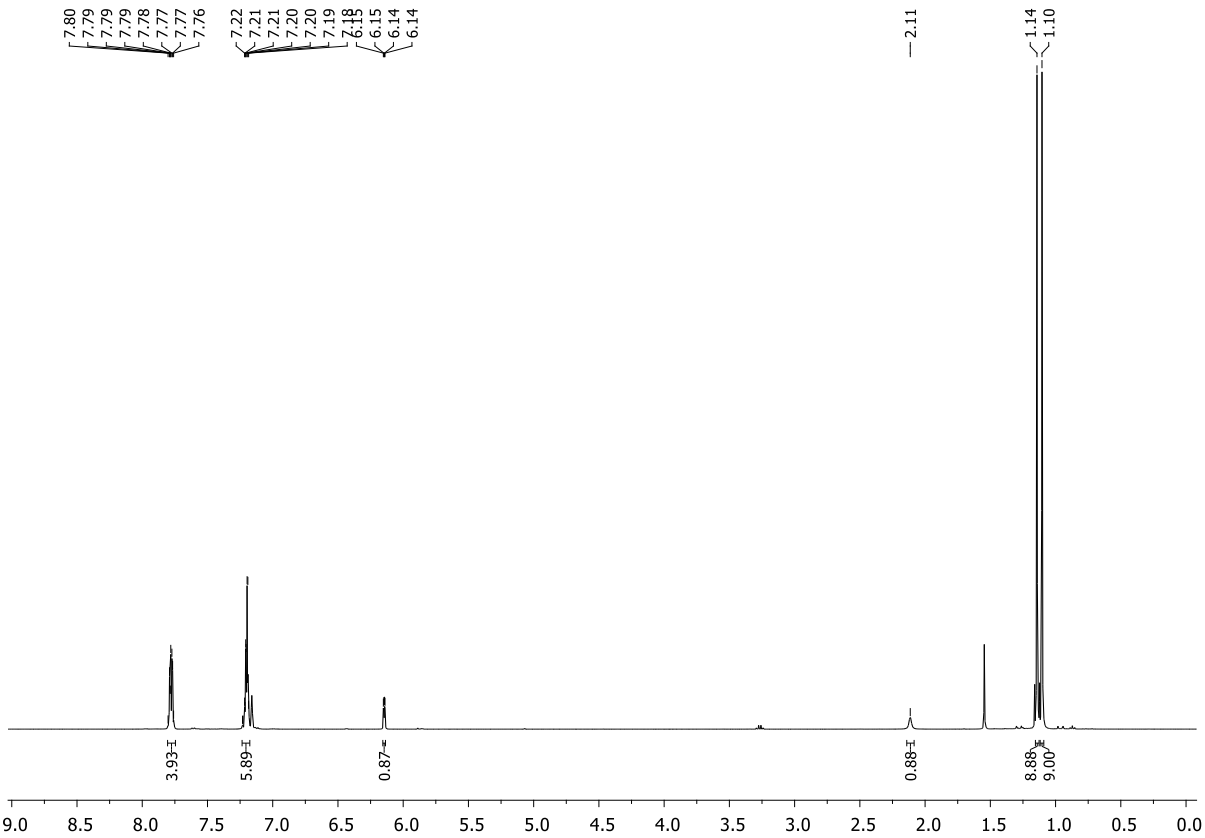

Figure S5.1. ^{1}H NMR spectrum (C_6D_6, 298 K) of **2**.

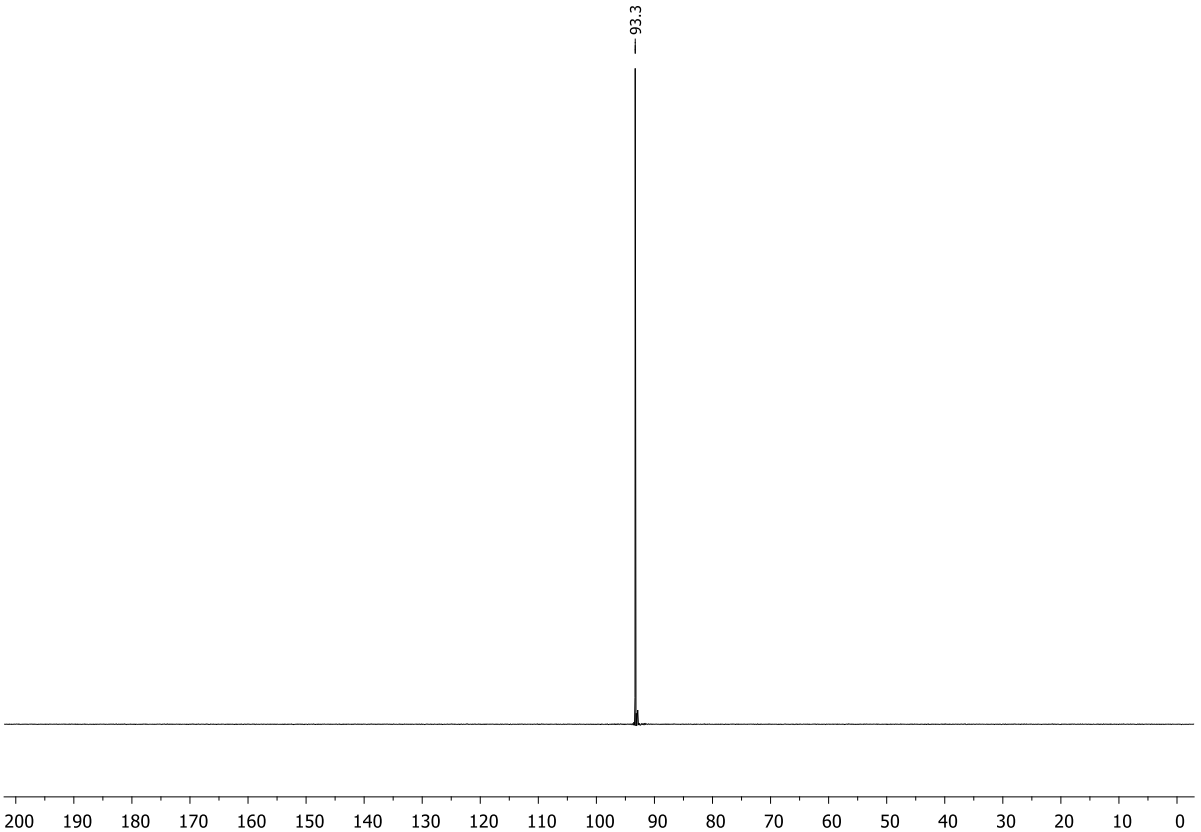

Figure S5.2. $^{31}P\{^{1}H\}$ NMR spectrum (C_6D_6, 298 K) of **2**.

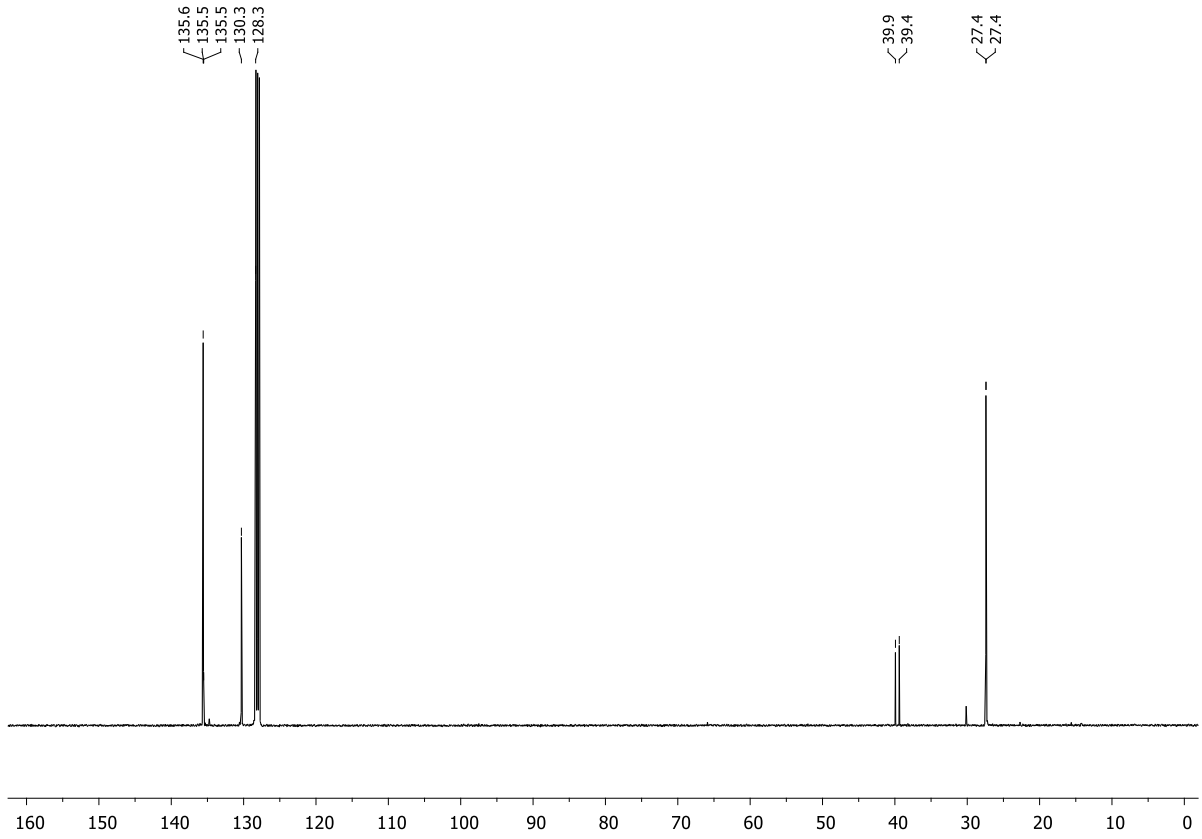

Figure S5.3. $^{13}C\{^{1}H\}$ NMR spectrum (C_6D_6, 298 K) of **2**.

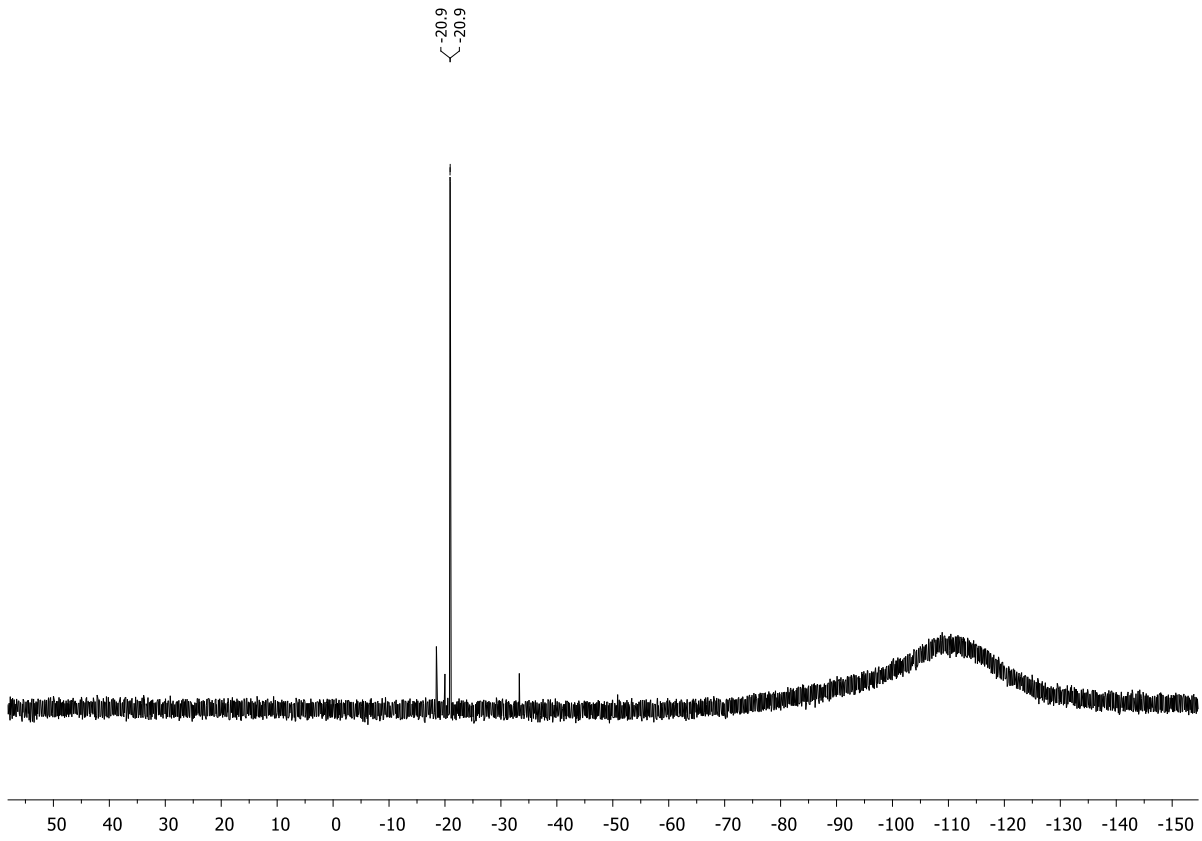

Figure S5.4. $^{29}Si\{^{1}H\}$ NMR spectrum (C_6D_6, 298 K) of **2**.

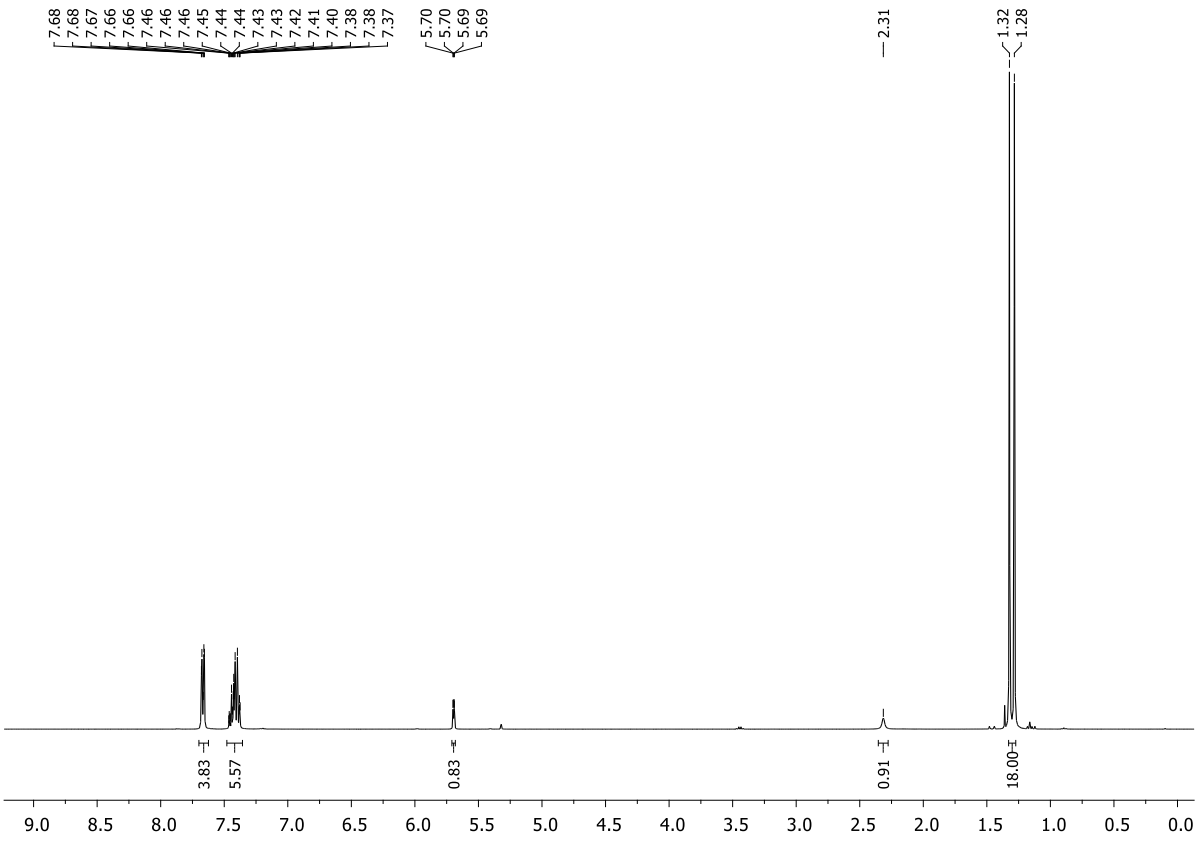

Figure S5.5. ^{1}H NMR spectrum (CD_2Cl_2, 298 K) of **2**.

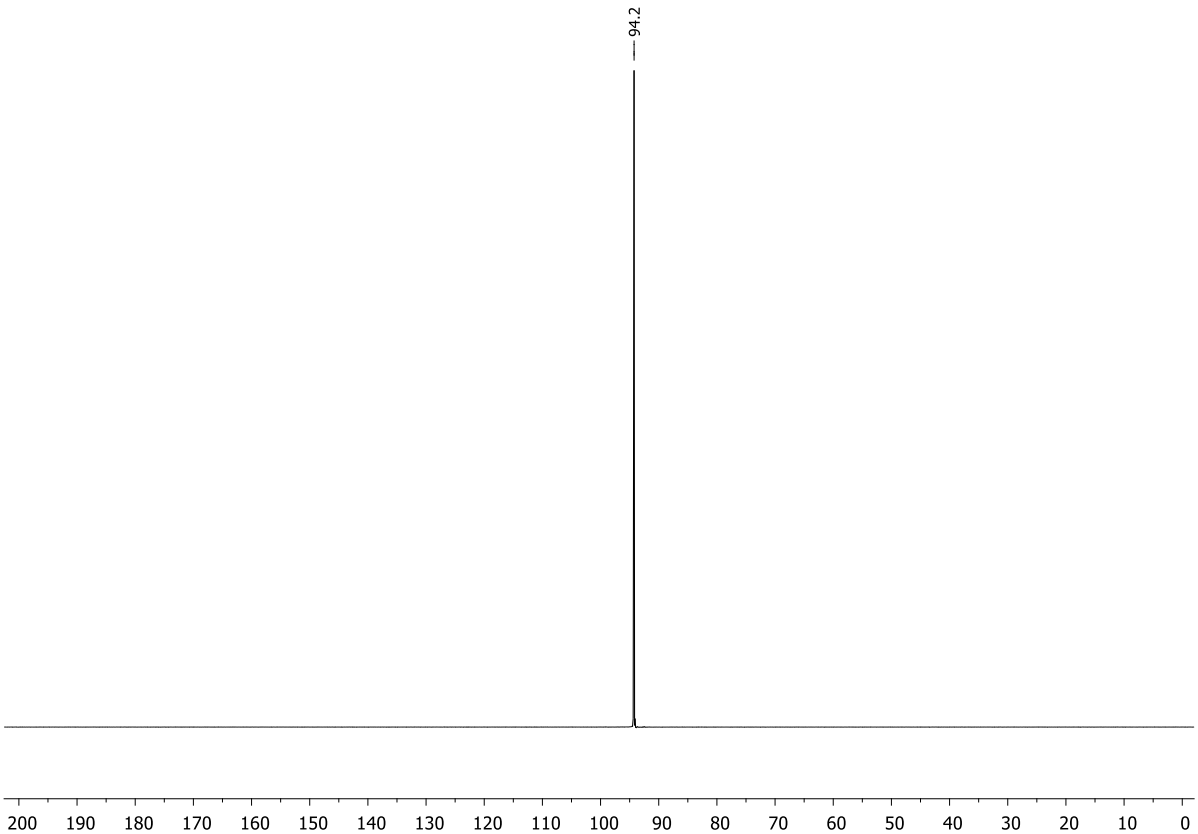

Figure S5.6. $^{31}P\{^{1}H\}$ NMR spectrum (CD_2Cl_2, 298 K) of **2**.

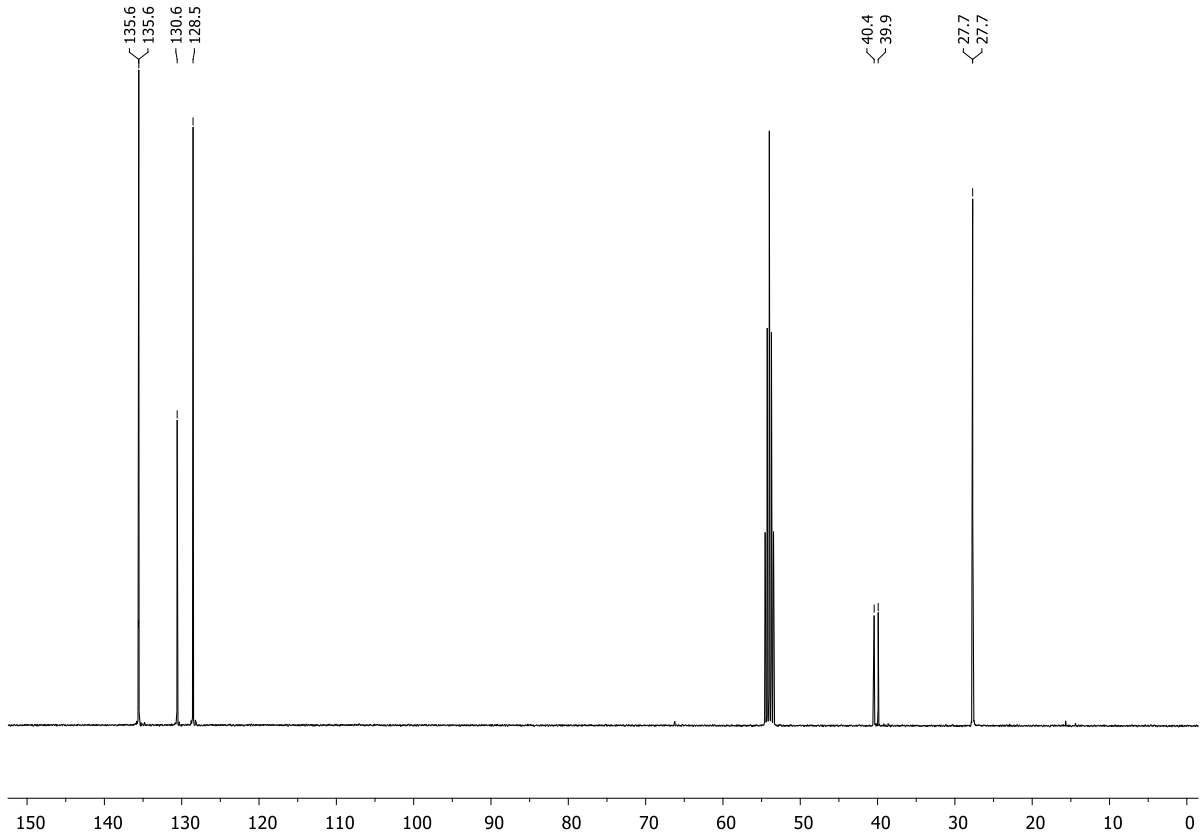

Figure S5.7. $^{13}C\{^{1}H\}$ NMR spectrum (CD_2Cl_2, 298 K) of **2**.

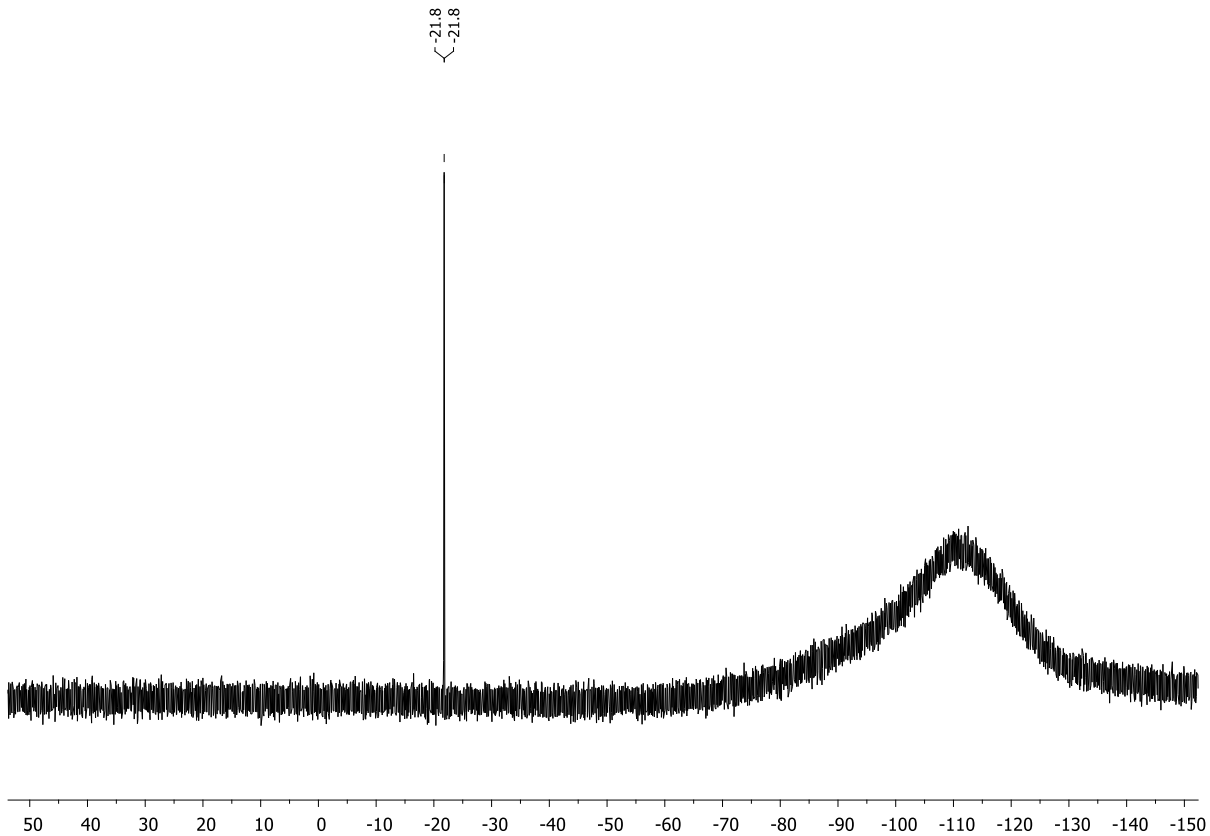

Figure S5.8. $^{29}Si\{^{1}H\}$ NMR spectrum (CD_2Cl_2, 298 K) of **2**.

5.6.2.2. Synthesis of [*t*Bu$_2$(PS)NH(SiPh$_2$)]$^+$ [HB(C$_6$F$_5$)$_3$]$^-$ {3[HB(C$_6$F$_5$)$_3$]}

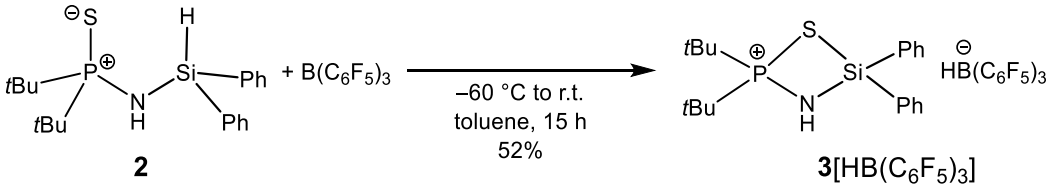

A solution of compound **2** (0.32 g, 0.84 mmol, 1.0 equiv.) in toluene (3 mL) was added to a solution of tris(pentafluorophenyl)borane (0.43 g, 0.84 mmol, 1.0 equiv.) in toluene (2 mL) at –60 °C. The solution was allowed to slowly warm to room temperature and stirred for 15 h. The solvent was then removed in vacuo and the remaining solid was washed with pentane. After drying in vacuo, compound **3**[HB(C$_6$F$_5$)$_3$] was obtained as a colorless solid (0.39 g, 0.44 mmol, 52%). Crystals suitable for single-crystal X-ray analysis were obtained by layering a toluene solution with pentane.

^{1}H NMR (400.13 MHz, CD_2Cl_2, 298 K): δ = 1.49 (d, $^3J_{H–P}$ = 19.2 Hz, 18H, PC(C*H*$_3$)$_3$), 4.36 (d, $^2J_{H–P}$ = 3.1 Hz, 1H, N*H*), 7.45–7.49 (m, 4H, *H*$_{Ph}$), 7.59–7.63 (m, 2H, *H*$_{Ph}$), 7.68–7.70 (m, 4H, *H*$_{Ph}$). **^{31}P{^{1}H} NMR** (162.04 MHz, CD_2Cl_2, 298 K): δ = 113.2 (s). **^{13}C{^{1}H} NMR** (100.61 MHz, CD_2Cl_2, 298 K): δ = 26.7 (d, $^2J_{C–P}$ = 2.5 Hz, PC(*C*H$_3$)$_3$), 42.7 (d, $^1J_{C–P}$ = 29.7 Hz, P*C*(CH$_3$)$_3$), 129.3 (s, *C*$_{Ph}$), 130.0 (s, *C*$_{Ph}$), 133.6 (s, *C*$_{Ph}$), 135.2 (s, *C*$_{Ph}$). **^{11}B{^{1}H} NMR** (128.43 MHz, CD_2Cl_2, 298 K): δ = –25.1 (s). **^{19}F{^{1}H} NMR** (376.66 MHz, CD_2Cl_2, 298 K): δ = –166.9 (m, 6F, *meta-F*$_{Ar\text{-}borate}$), –163.9 (m, 3F, *para-F*$_{Ar\text{-}borate}$), –133.6 (m, 6F, *ortho-F*$_{Ar\text{-}borate}$). **^{29}Si{^{1}H} NMR** (79.49 MHz, CD_2Cl_2, 298 K): δ = 4.4 (d, $^2J_{P–Si}$ = 5.5 Hz).

Elemental analysis: $C_{38}H_{30}BF_{15}NPSSi$: calcd.: C 51.42, H 3.41, N 1.58; found: C 51.52, H 3.32, N 1.64.

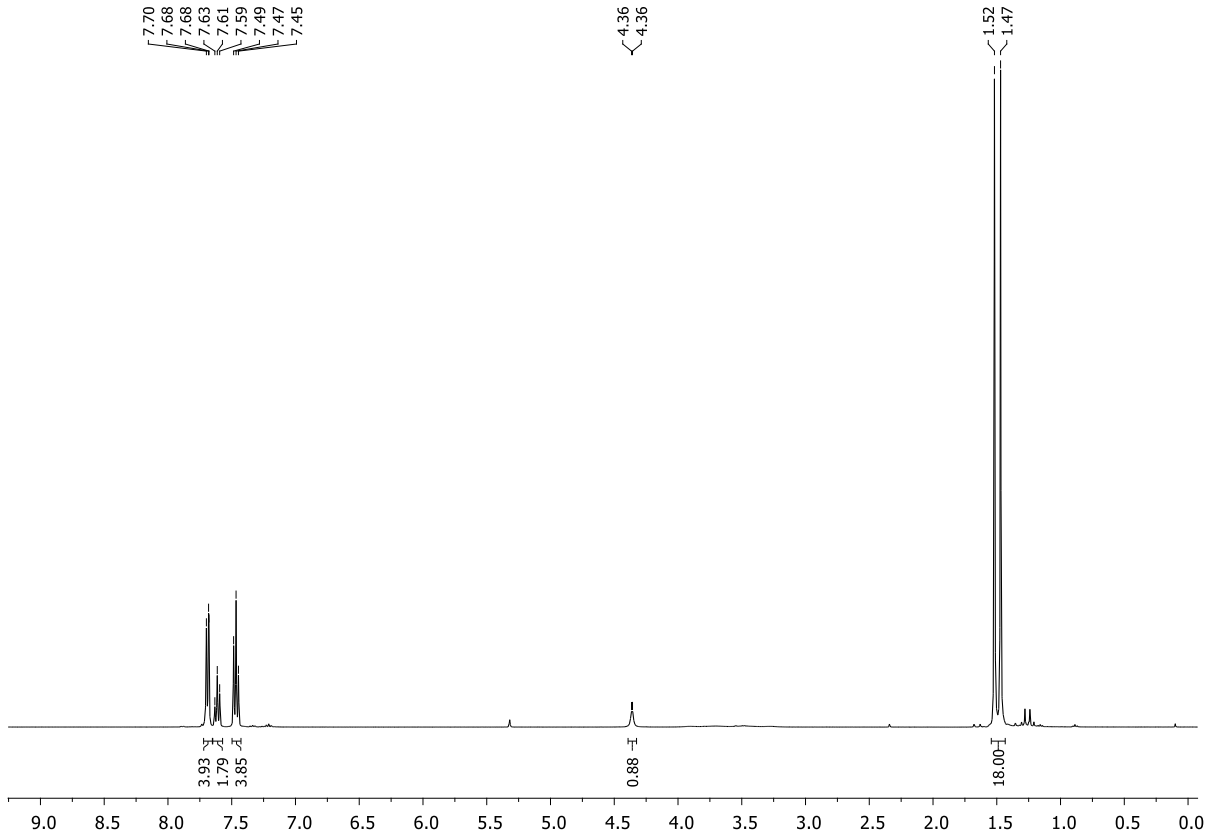

Figure S5.9. ^{1}H NMR spectrum (CD_2Cl_2, 298 K) of **3**[$HB(C_6F_5)_3$].

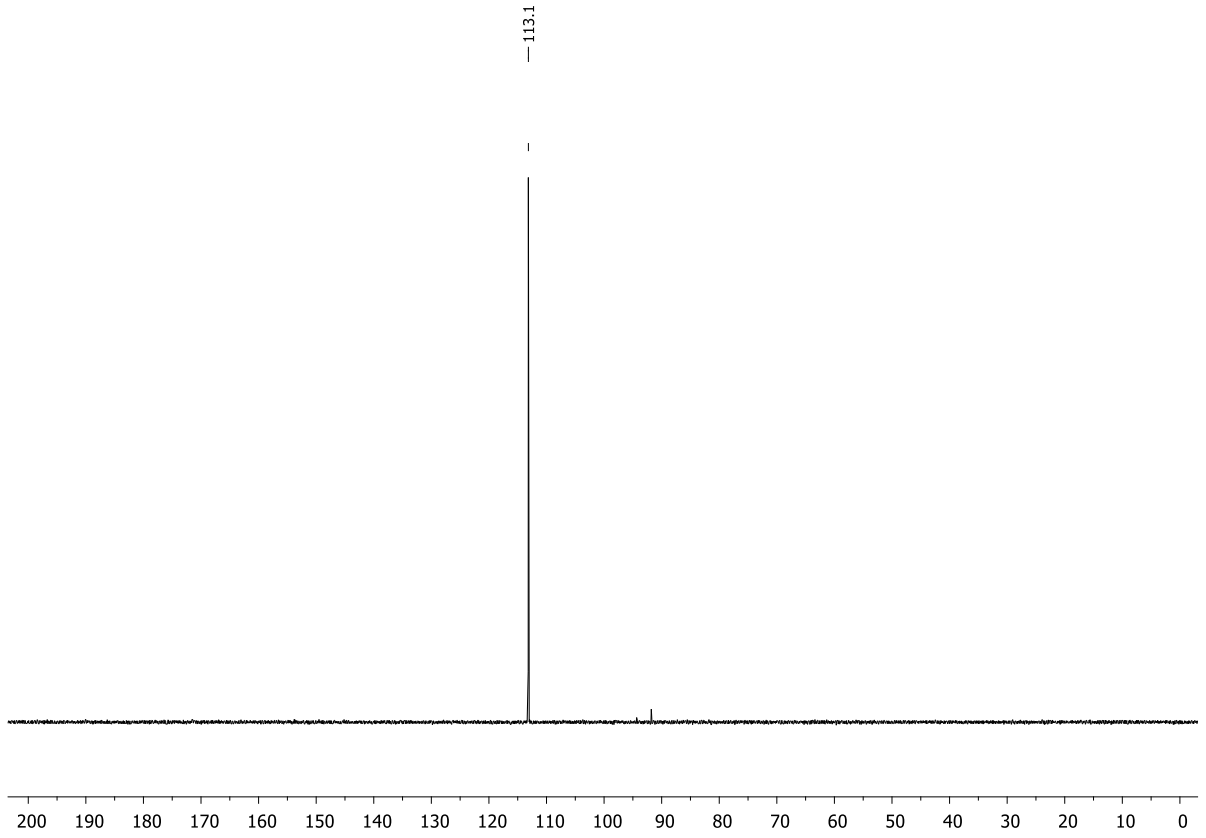

Figure S5.10. $^{31}P\{^{1}H\}$ NMR spectrum (CD_2Cl_2, 298 K) of **3**[$HB(C_6F_5)_3$].

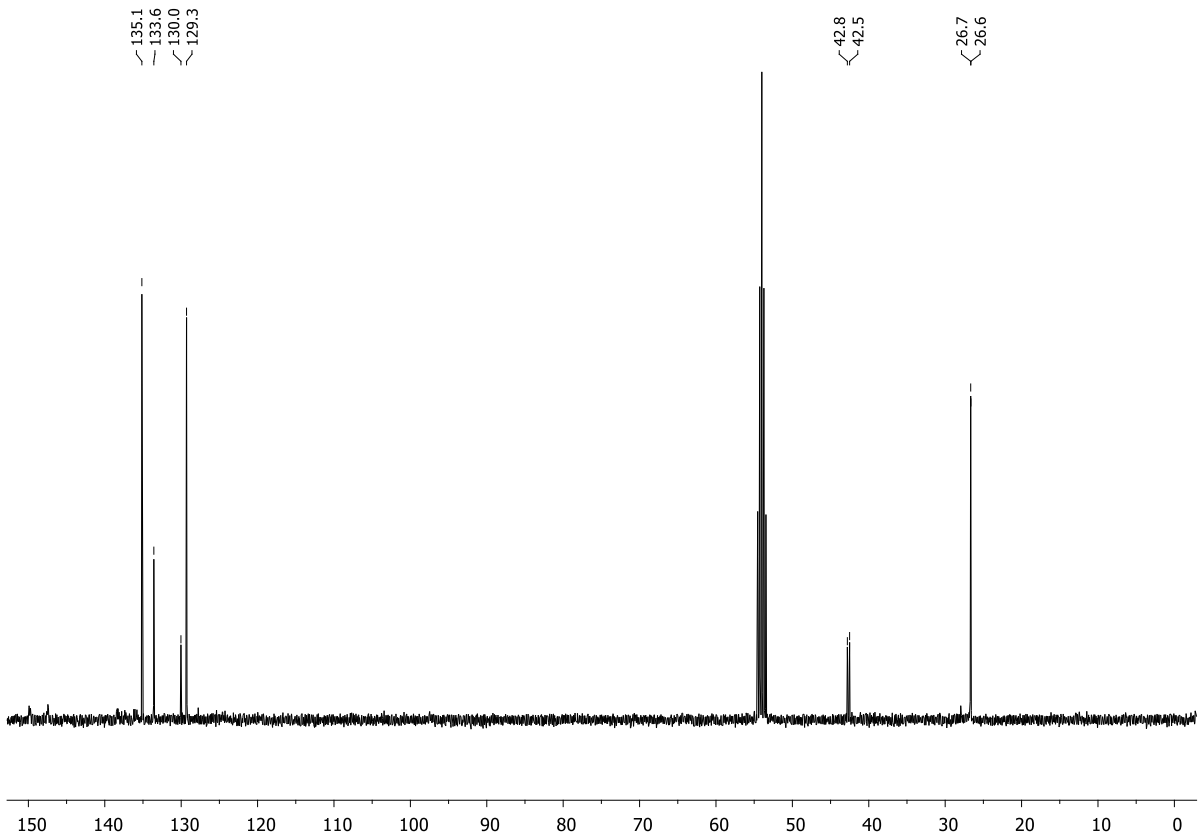

Figure S5.11. $^{13}C\{^{1}H\}$ NMR spectrum (CD_2Cl_2, 298 K) of **3**[$HB(C_6F_5)_3$].

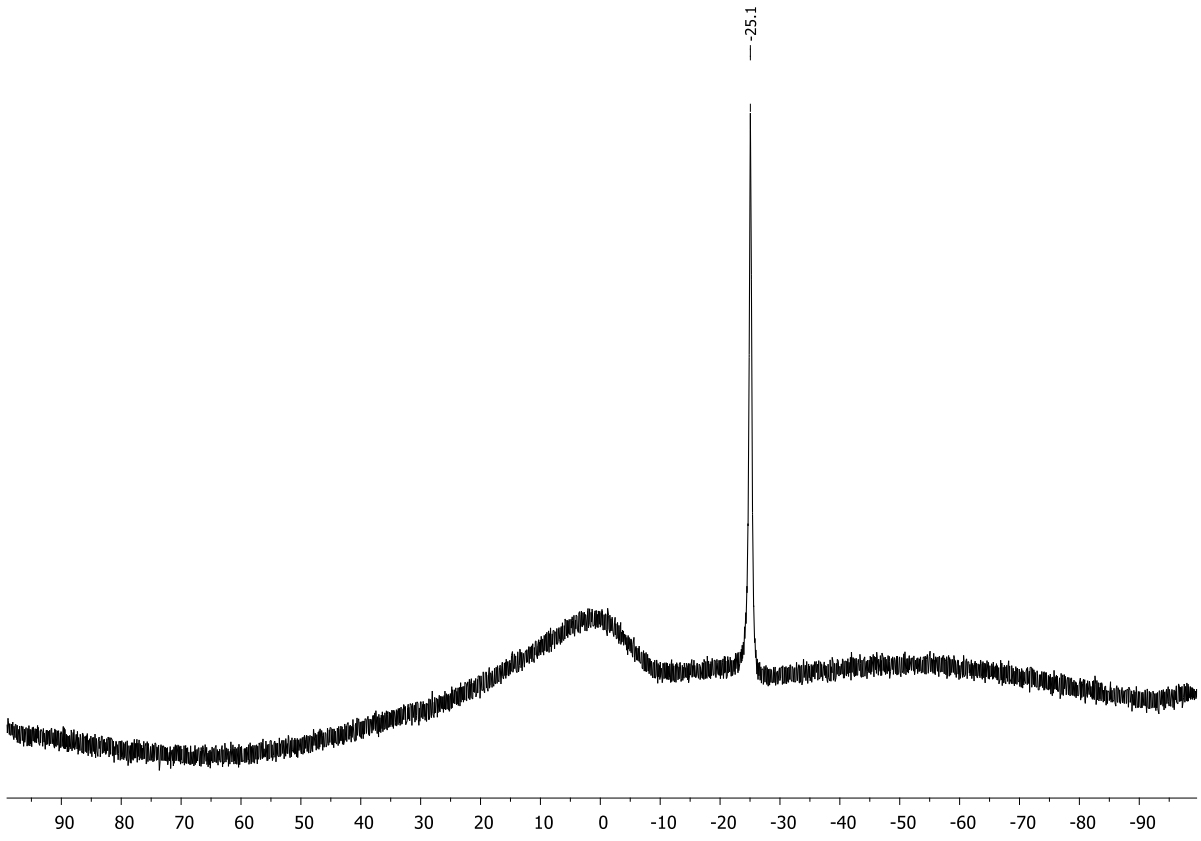

Figure S5.12. $^{11}B\{^{1}H\}$ NMR spectrum (CD_2Cl_2, 298 K) of **3**[$HB(C_6F_5)_3$].

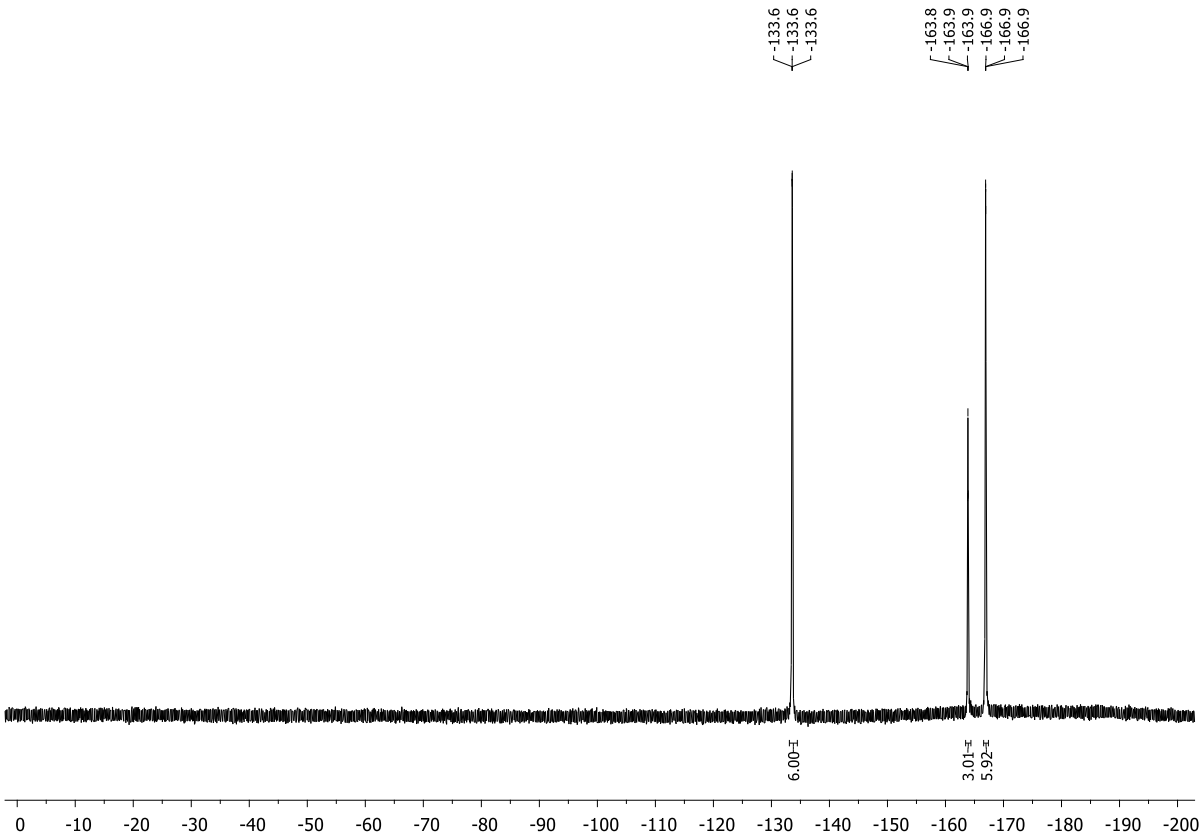

Figure S5.13. $^{19}F\{^{1}H\}$ NMR spectrum (CD_2Cl_2, 298 K) of **3**[$HB(C_6F_5)_3$].

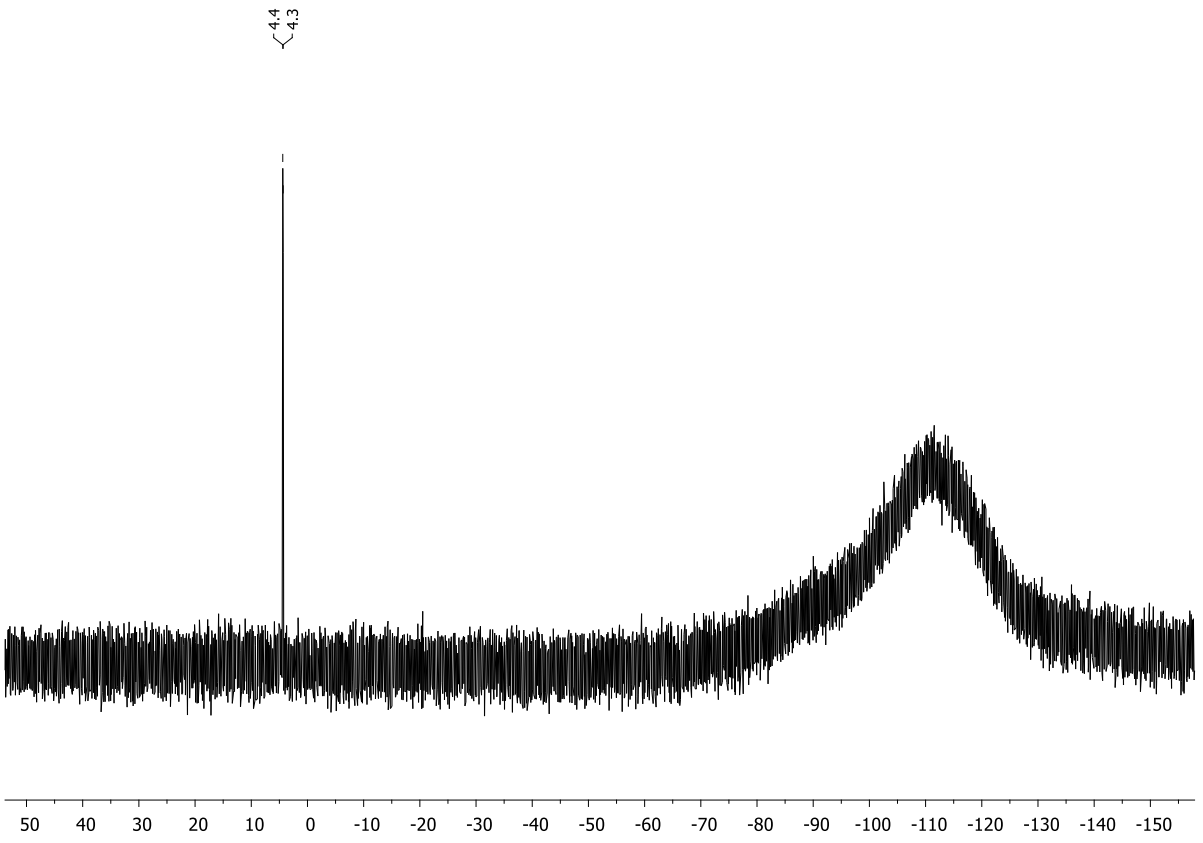

Figure S5.14. $^{29}Si\{^{1}H\}$ NMR spectrum (CD_2Cl_2, 298 K) of **3**[$HB(C_6F_5)_3$].

5.6.2.3. Synthesis of *t*Bu$_2$(PS)NH(SiH*i*Pr$_2$) (4)

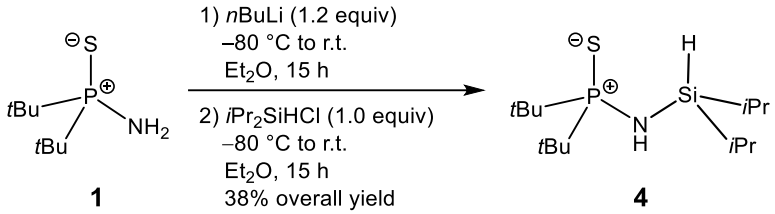

1 **4**

*n*Butyllithium (2.48 mL, 6.20 mmol, 1.2 equiv., 2.5 M in hexane) was added dropwise to a solution of *P*,*P*-di-*tert*-butylaminophosphine sulfide (**1**) (1.00 g, 5.17 mmol, 1.0 equiv.) in diethyl ether (20 mL) at −80 °C. The solution was allowed to slowly warm to room temperature and stirred for 15 h. Following, the colorless solution was cooled to −80 °C again and chlorodiisopropylsilane (0.78 g, 5.17 mmol, 1.0 equiv.) was added dropwise. The reaction mixture was allowed to slowly warm to room temperature and stirred for 15 h affording a colorless suspension. The precipitated lithium chloride was filtered off via cannula filtration and washed with diethyl ether. The crude solution was kept at −28 °C for 20 h to yield colorless crystalline needles suitable for single-crystal X-ray analysis, which were filtered off via cannula filtration and washed with pentane. After drying in vacuo, compound **4** was obtained as colorless needle-shaped crystals (0.60 g, 1.95 mmol, 38%).

^{1}H NMR (400.13 MHz, C_6D_6, 298 K): δ = 1.08–1.04 (m, 12H, SiCH(C*H*$_3$)$_2$), 1.20 (d, $^3J_{H–P}$ = 15.2 Hz, 18H, PC(C*H*$_3$)$_3$), 1.34–1.25 (m, 2H, SiC*H*(CH$_3$)$_2$), 1.48 (br, 1H, N*H*), 4.73 (m, 1H, Si*H*). **^{31}P{^{1}H} NMR** (162.04 MHz, C_6D_6, 298 K): δ = 92.3 (s). **^{13}C{^{1}H} NMR** (100.61 MHz, C_6D_6, 298 K): δ = 13.0 (d, $^3J_{C–P}$ = 2.2 Hz, Si*C*H(CH$_3$)$_2$), 18.4 (d, $^4J_{C–P}$ = 22.2 Hz, SiCH(*C*H$_3$)$_2$), 27.5 (d, $^2J_{C–P}$ = 1.7 Hz, PC(*C*H$_3$)$_3$), 39.9 (d, $^1J_{C–P}$ = 53.8 Hz, P*C*(CH$_3$)$_3$).

^{1}H NMR (400.13 MHz, CD_2Cl_2, 298 K): δ = 1.08–1.06 (m, 12H, SiCH(C*H*$_3$)$_2$), 1.26–1.20 (m, 2H, SiC*H*(CH$_3$)$_2$), 1.30 (d, $^3J_{H–P}$ = 15.3 Hz, 18H, PC(C*H*$_3$)$_3$), 1.69 (br, 1H, N*H*), 4.34 (m, 1H, Si*H*). **^{31}P{^{1}H} NMR** (162.04 MHz, CD_2Cl_2, 298 K): δ = 93.3 (s). **^{13}C{^{1}H} NMR** (100.61 MHz, CD_2Cl_2, 298 K): δ = 13.3 (d, $^3J_{C–P}$ = 2.2 Hz, Si*C*H(CH$_3$)$_2$), 18.5 (d, $^4J_{C–P}$ = 26.4 Hz, SiCH(*C*H$_3$)$_2$), 27.8 (d, $^2J_{C–P}$ = 1.7 Hz, PC(*C*H$_3$)$_3$), 40.3 (d, $^1J_{C–P}$ = 53.6 Hz, P*C*(CH$_3$)$_3$). **^{29}Si{^{1}H} NMR** (79.49 MHz, CD_2Cl_2, 298 K): δ = 3.0 (d, $^2J_{P–Si}$ = 4.5 Hz).

Elemental analysis: $C_{14}H_{34}NPSSi \cdot 0.15\ Et_2O$: calcd.: C 53.81, H 11.23, N 4.30; found: C 53.73, H 11.42, N 4.51.

HR(+ESI)-MS: calcd. *m/z* for $C_{14}H_{35}NPSSi$ [(M+H)$^+$]: 308.1992, found: 308.1998.

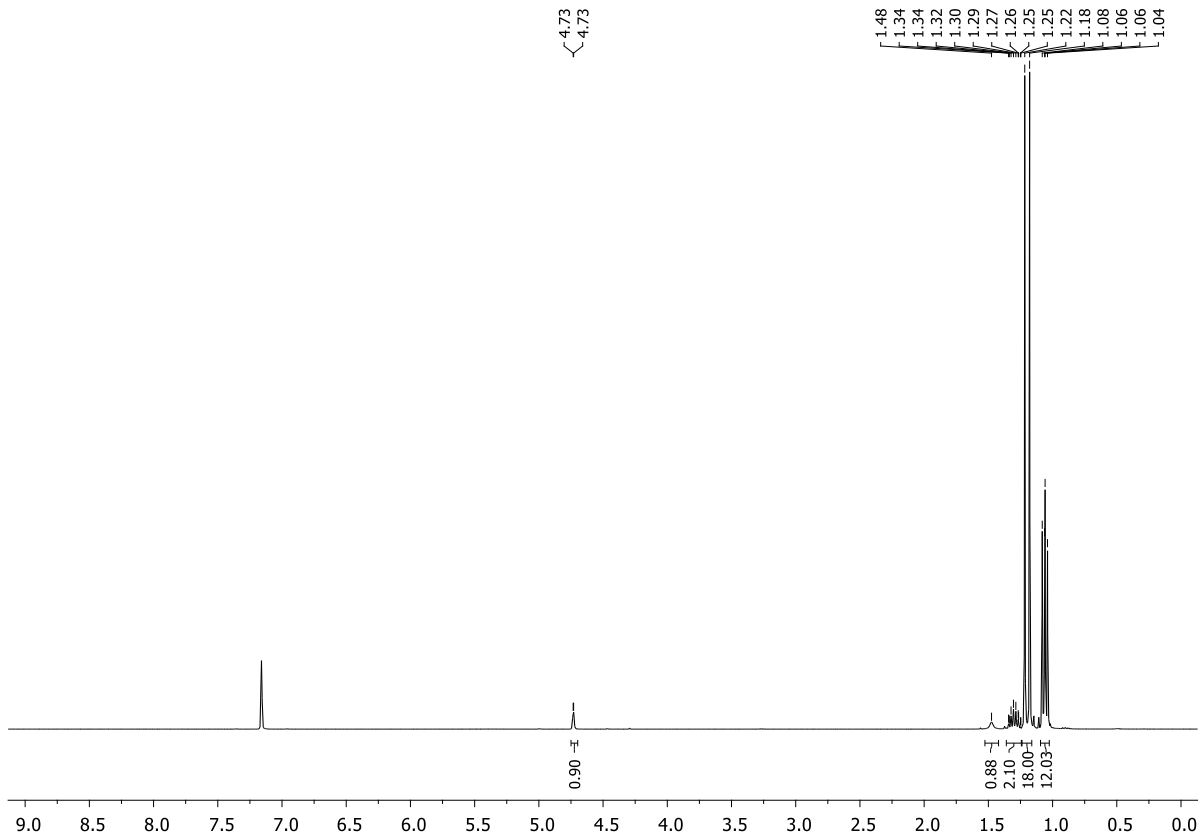

Figure S5.15. ^{1}H NMR spectrum (C_6D_6, 298 K) of **4**.

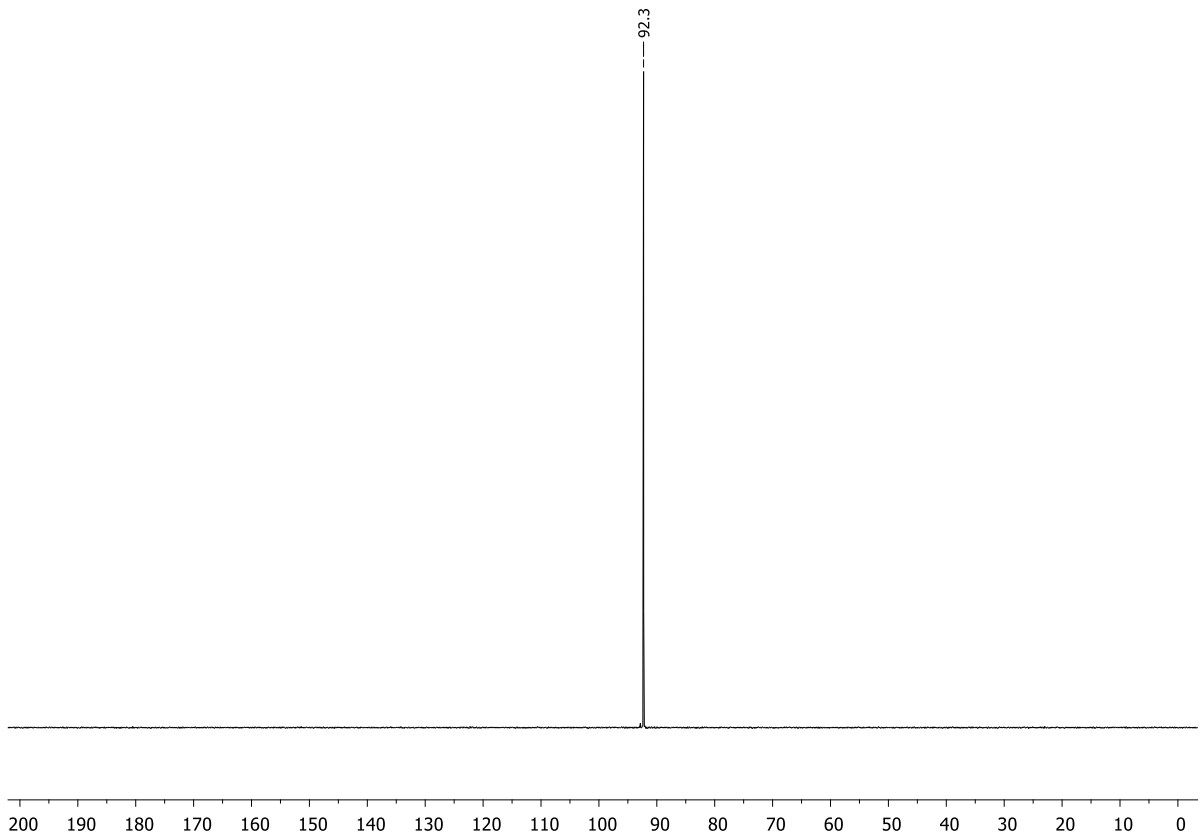

Figure S5.16. $^{31}P\{^{1}H\}$ NMR spectrum (C_6D_6, 298 K) of **4**.

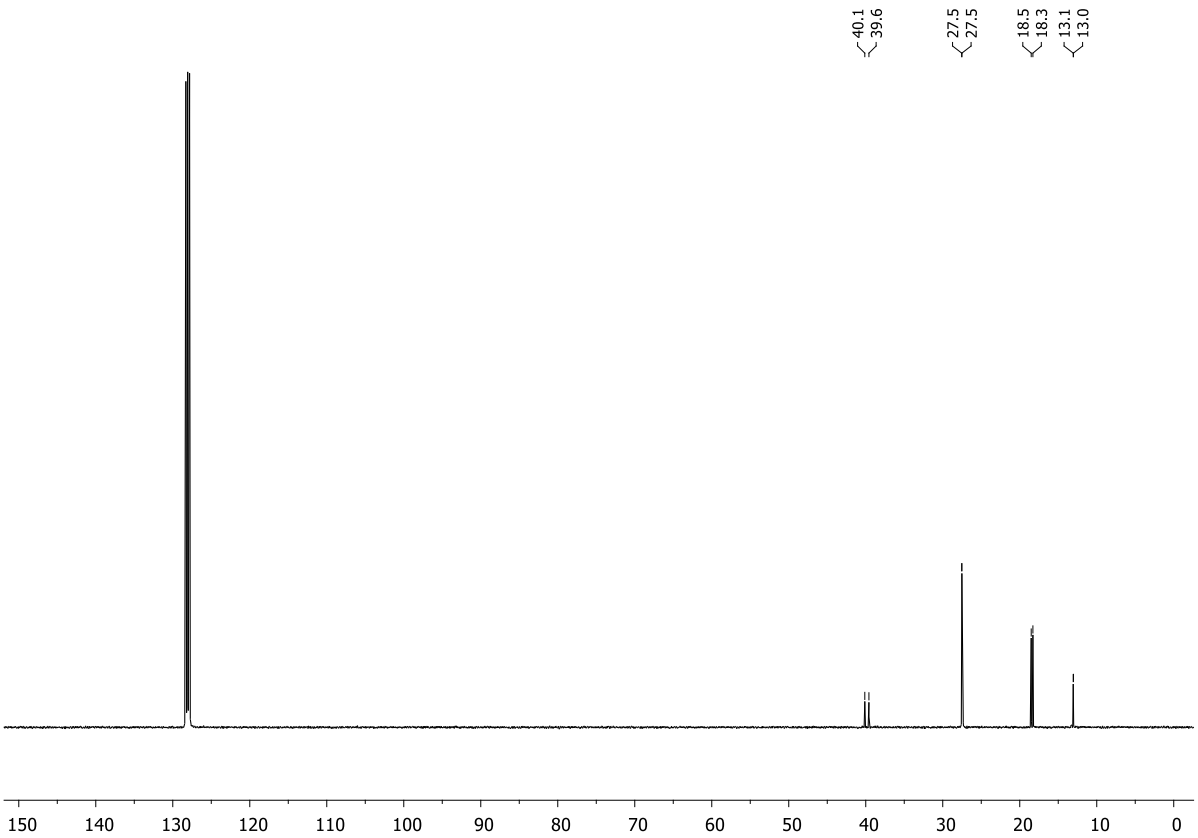

Figure S5.17. $^{13}C\{^{1}H\}$ NMR spectrum (C_6D_6, 298 K) of **4**.

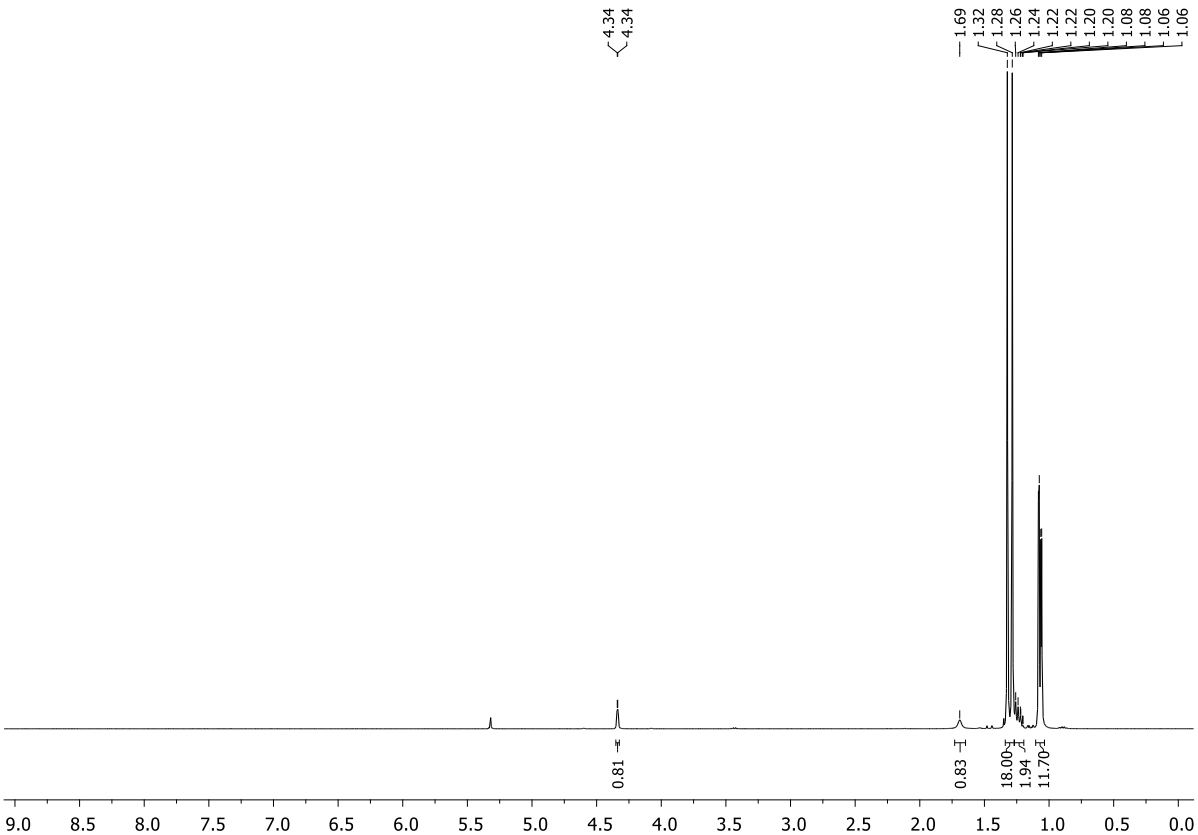

Figure S5.18. ^{1}H NMR spectrum (CD_2Cl_2, 298 K) of **4**.

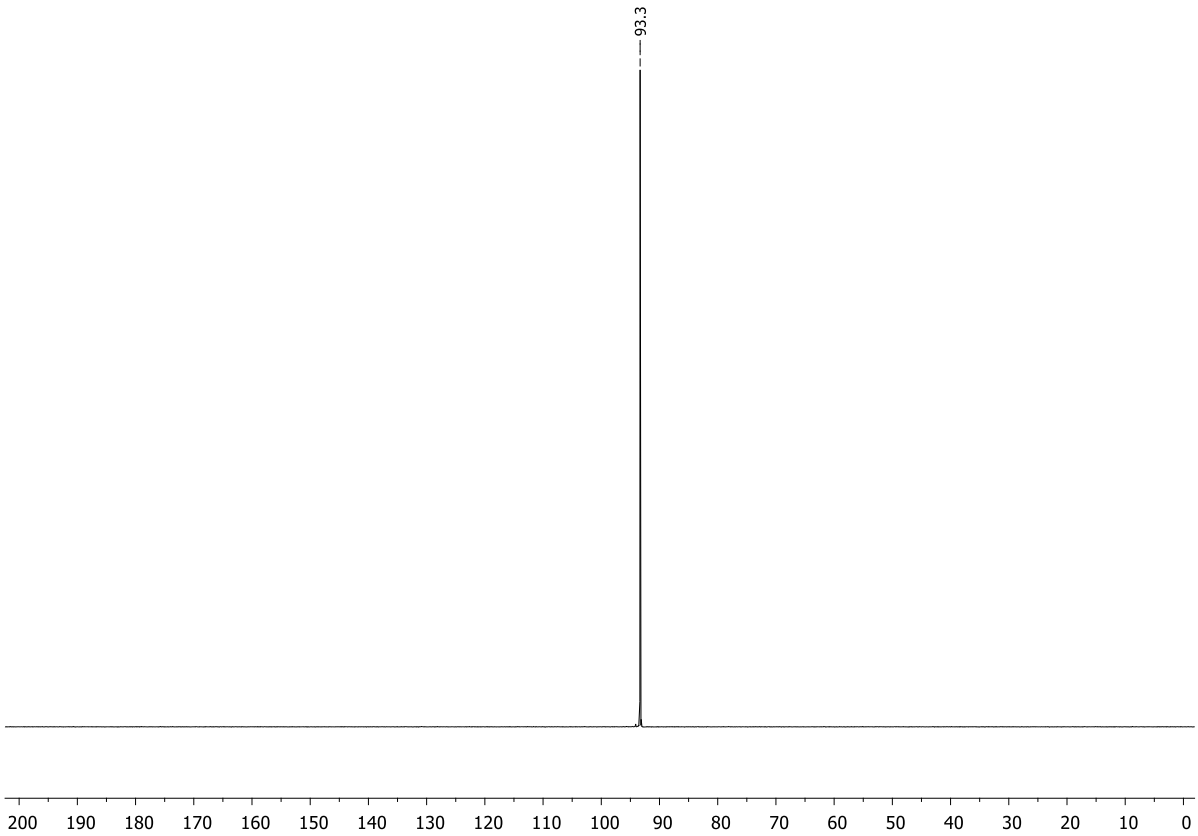

Figure S5.19. $^{31}P\{^{1}H\}$ NMR spectrum (CD_2Cl_2, 298 K) of **4**.

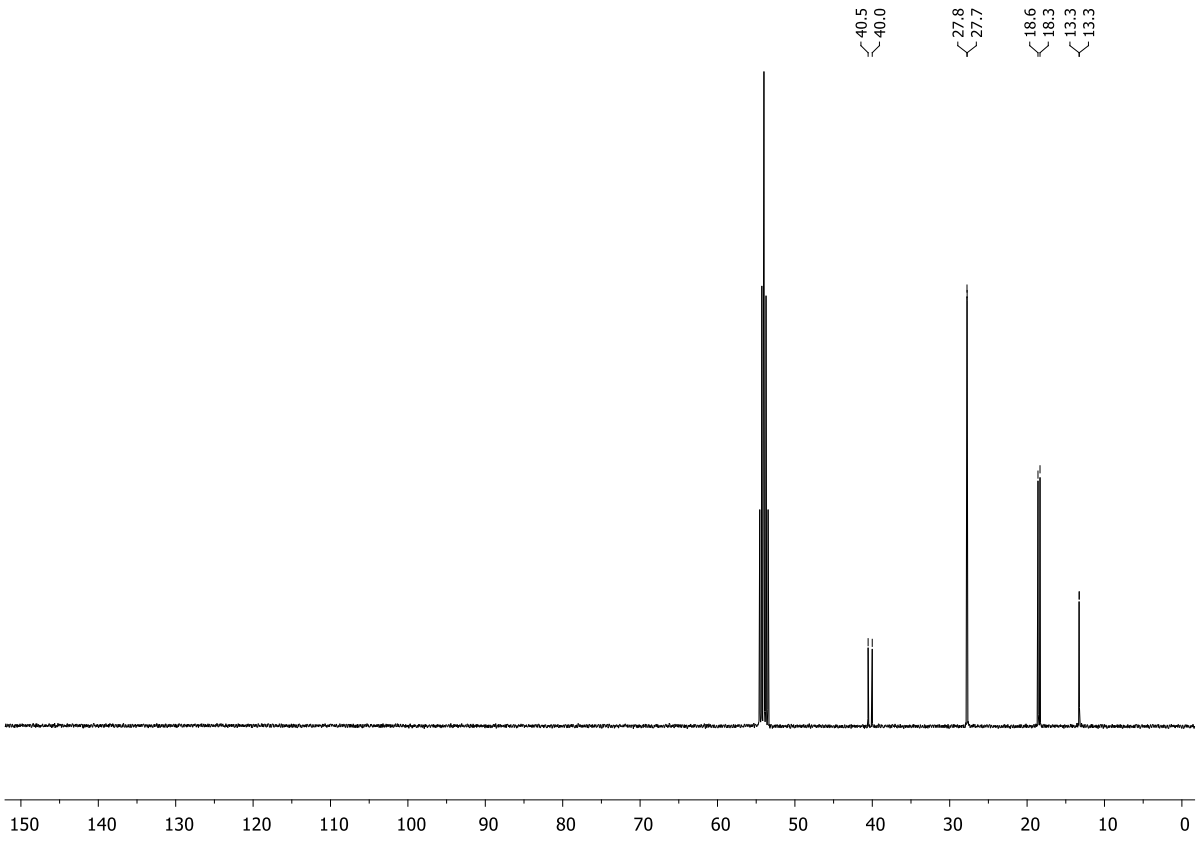

Figure S5.20. $^{13}C\{^{1}H\}$ NMR spectrum (CD_2Cl_2, 298 K) of **4**.

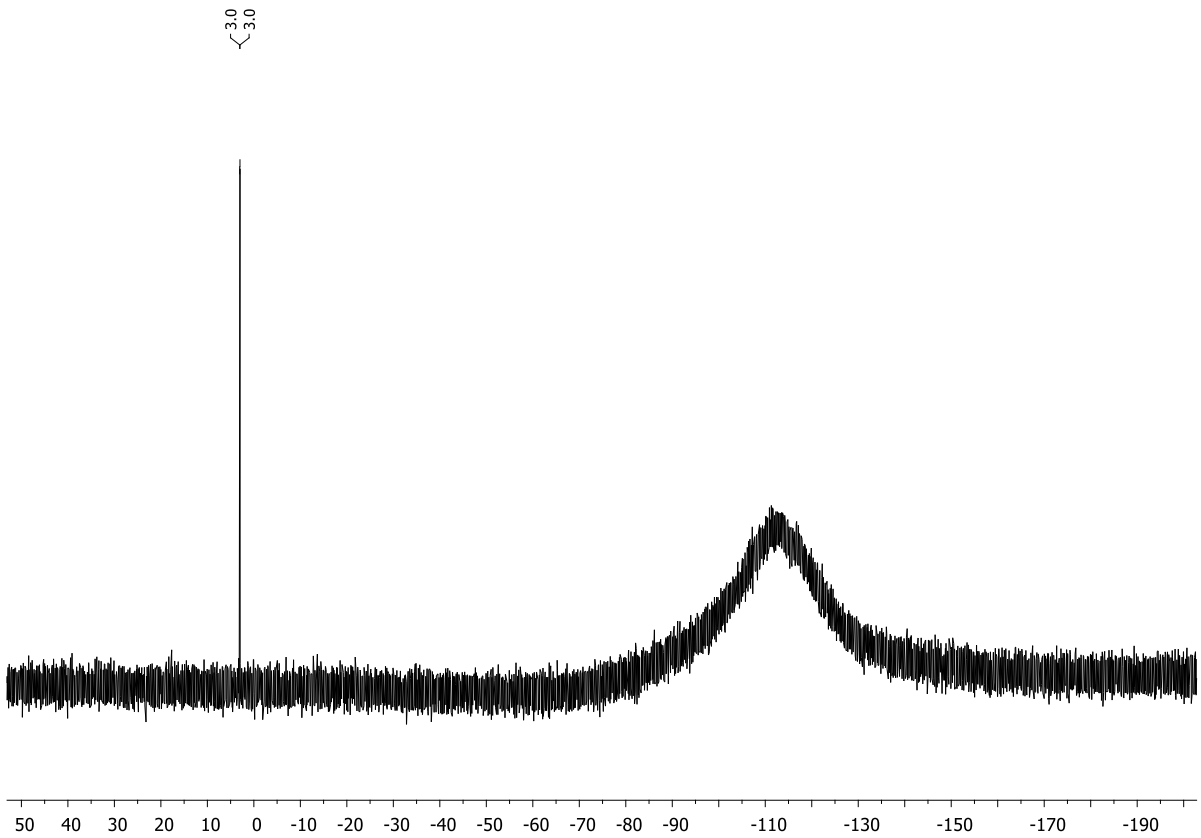

Figure S5.21. $^{29}Si\{^{1}H\}$ NMR spectrum (CD_2Cl_2, 298 K) of **4**.

5.6.2.4. Synthesis of [*t*Bu$_2$(PS)NH(Si*i*Pr$_2$)]$^+$ [HB(C$_6$F$_5$)$_3$]$^-$ {5[HB(C$_6$F$_5$)$_3$]}

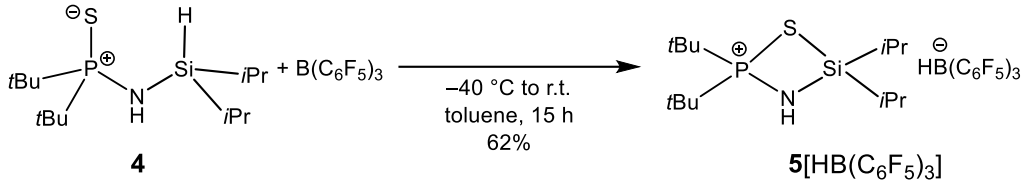

A solution of compound **4** (0.26 g, 0.84 mmol, 1.0 equiv.) in toluene (4 mL) was added to a solution of tris(pentafluorophenyl)borane (0.43 g, 0.84 mmol, 1.0 equiv.) in toluene (6 mL) at –40 °C. The solution was allowed to slowly warm to room temperature and stirred for 15 h. The solvent was then removed in vacuo and the remaining solid was washed with pentane. After drying in vacuo, compound **5**[HB(C$_6$F$_5$)$_3$] was obtained as a colorless solid (0.43 g, 0.52 mmol, 62%). Crystals suitable for single-crystal X-ray analysis were obtained by layering a toluene solution with pentane.

^{1}H NMR (400.13 MHz, CD_2Cl_2, 298 K): δ = 1.23–1.20 (m, 12H, SiCH(C*H*$_3$)$_2$), 1.49 (d, $^3J_{H–P}$ = 18.9 Hz, 18H, PC(C*H*$_3$)$_3$), 1.69–1.58 (m, 2H, SiC*H*(CH$_3$)$_2$), 3.61 (br, 1H, N*H*). **^{31}P{^{1}H} NMR** (162.04 MHz, CD_2Cl_2, 298 K): δ = 111.8 (s). **^{13}C{^{1}H} NMR** (100.61 MHz, CD_2Cl_2, 298 K): δ = 16.6 (s, SiCH(*C*H$_3$)$_2$), 19.1 (s, Si*C*H(CH$_3$)$_2$), 26.6 (d, $^2J_{C–P}$ = 2.5 Hz, PC(*C*H$_3$)$_3$), 42.4 (d, $^1J_{C–P}$ = 30.8 Hz, P*C*(CH$_3$)$_3$). **^{11}B{^{1}H} NMR** (128.43 MHz, CD_2Cl_2, 298 K): δ = –25.3 (s). **^{19}F{^{1}H} NMR** (376.66 MHz, CD_2Cl_2, 298 K): δ = –167.2 (m, 6F, *meta-F*$_{Ar\text{-}borate}$), –164.1 (m, 3F, *para-F*$_{Ar\text{-}borate}$), –133.8 (m, 6F, *ortho-F*$_{Ar\text{-}borate}$). **^{29}Si{^{1}H} NMR** (79.49 MHz, CD_2Cl_2, 298 K): δ = 35.2 (d, $^2J_{P–Si}$ = 2.7 Hz).
Elemental analysis: $C_{32}H_{34}BF_{15}NPSSi$: calcd.: C 46.90, H 4.18, N 1.71; found: C 47.55, H 4.24, N 1.79.

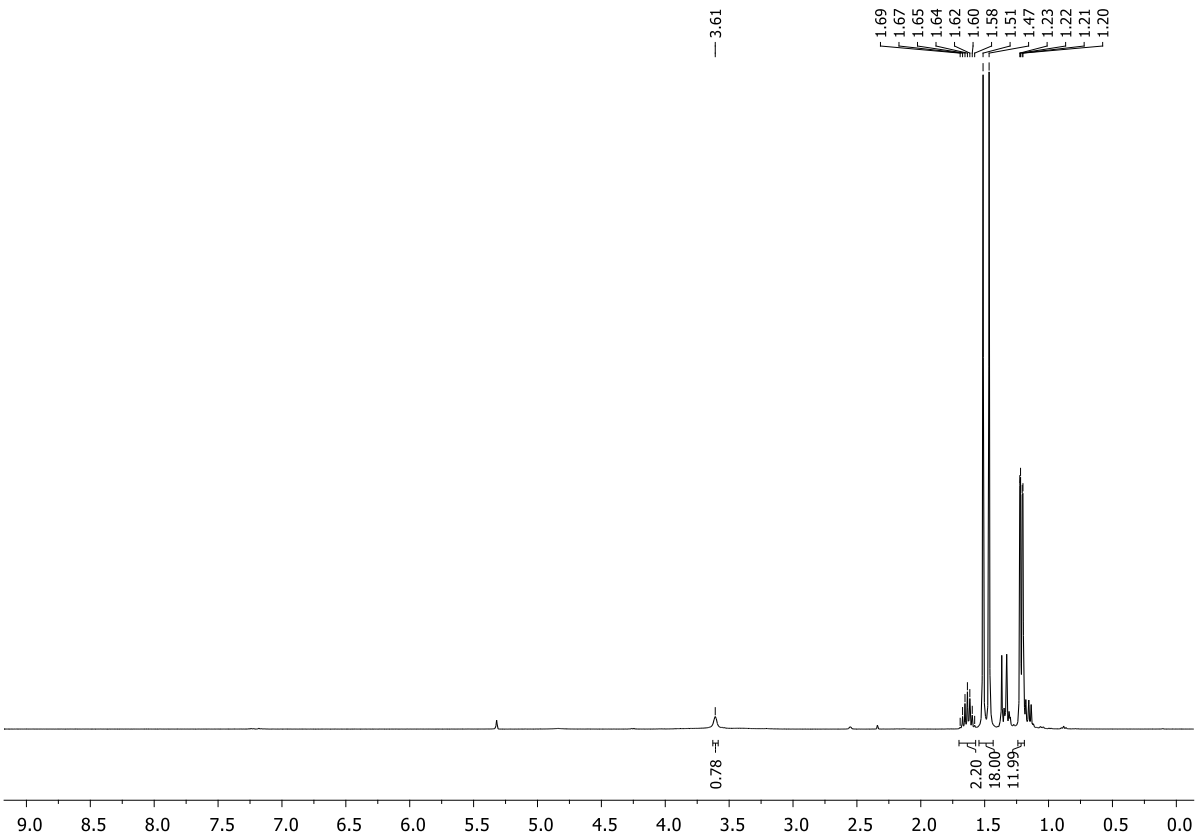

Figure S5.22. ^{1}H NMR spectrum (C_6D_6, 298 K) of **5**[$HB(C_6F_5)_3$].

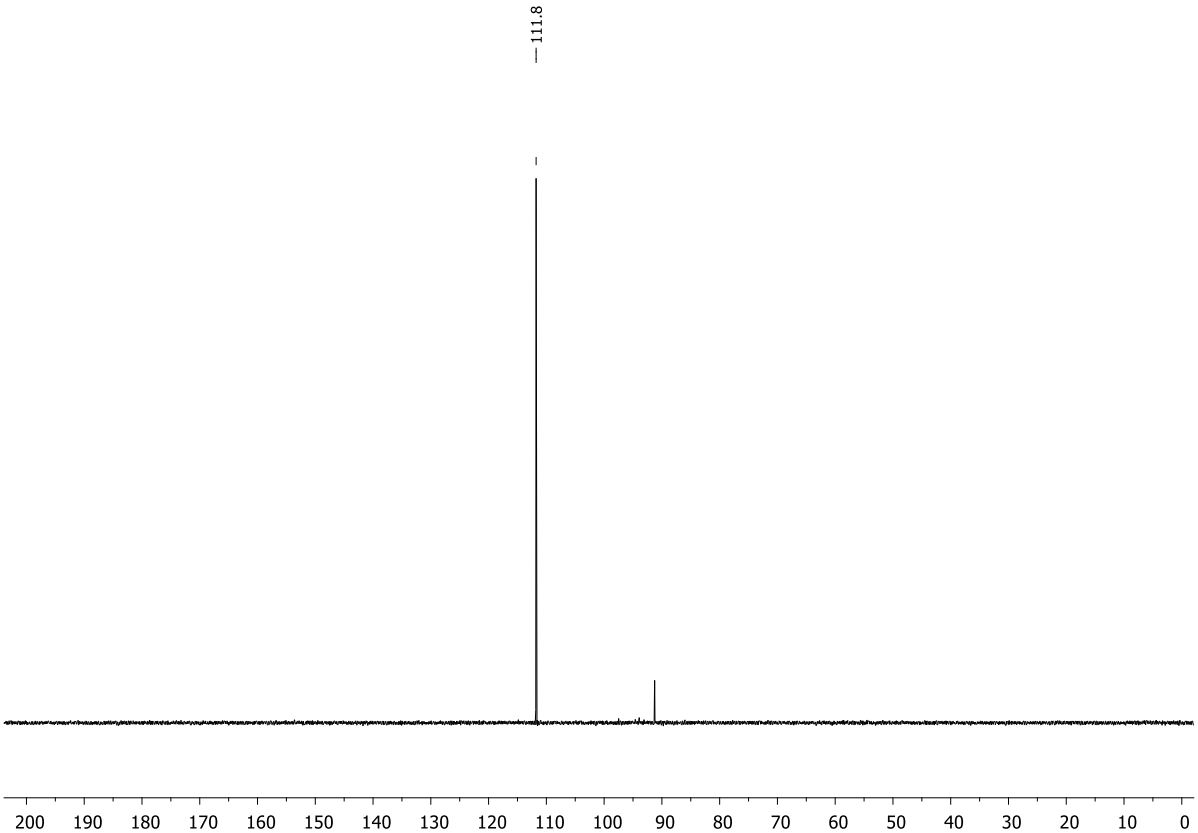

Figure S5.23. $^{31}P\{^{1}H\}$ NMR spectrum (CD_2Cl_2, 298 K) of **5**[$HB(C_6F_5)_3$].

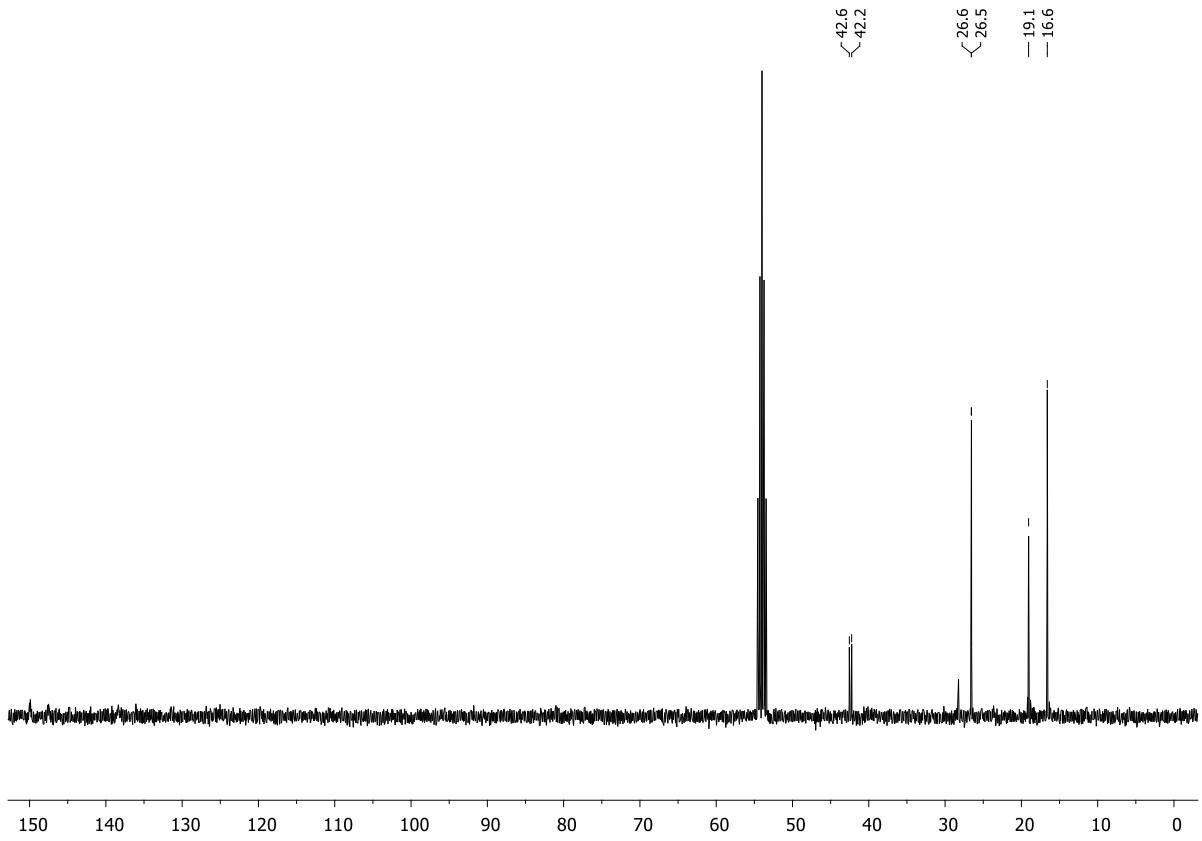

Figure S5.24. $^{13}C\{^{1}H\}$ NMR spectrum (CD_2Cl_2, 298 K) of **5**[$HB(C_6F_5)_3$].

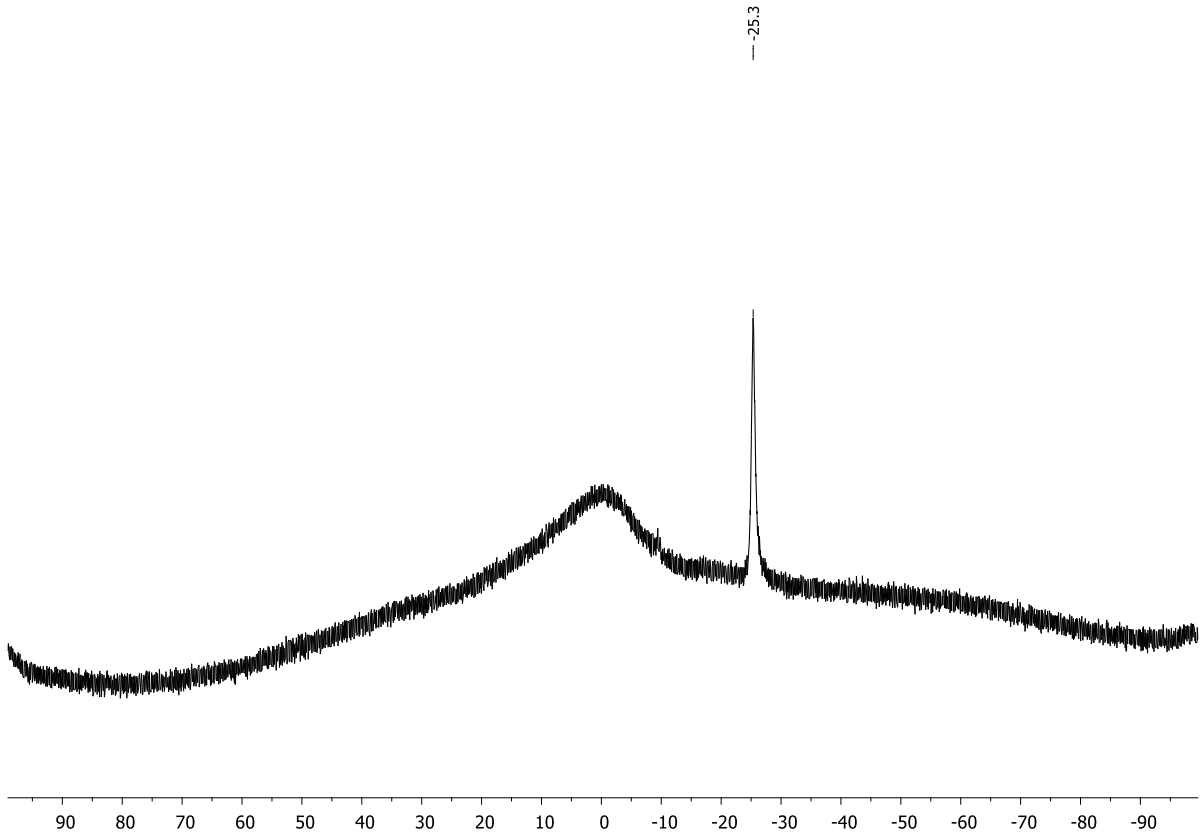

Figure S5.25. $^{11}B\{^{1}H\}$ NMR spectrum (CD_2Cl_2, 298 K) of **5**[$HB(C_6F_5)_3$].

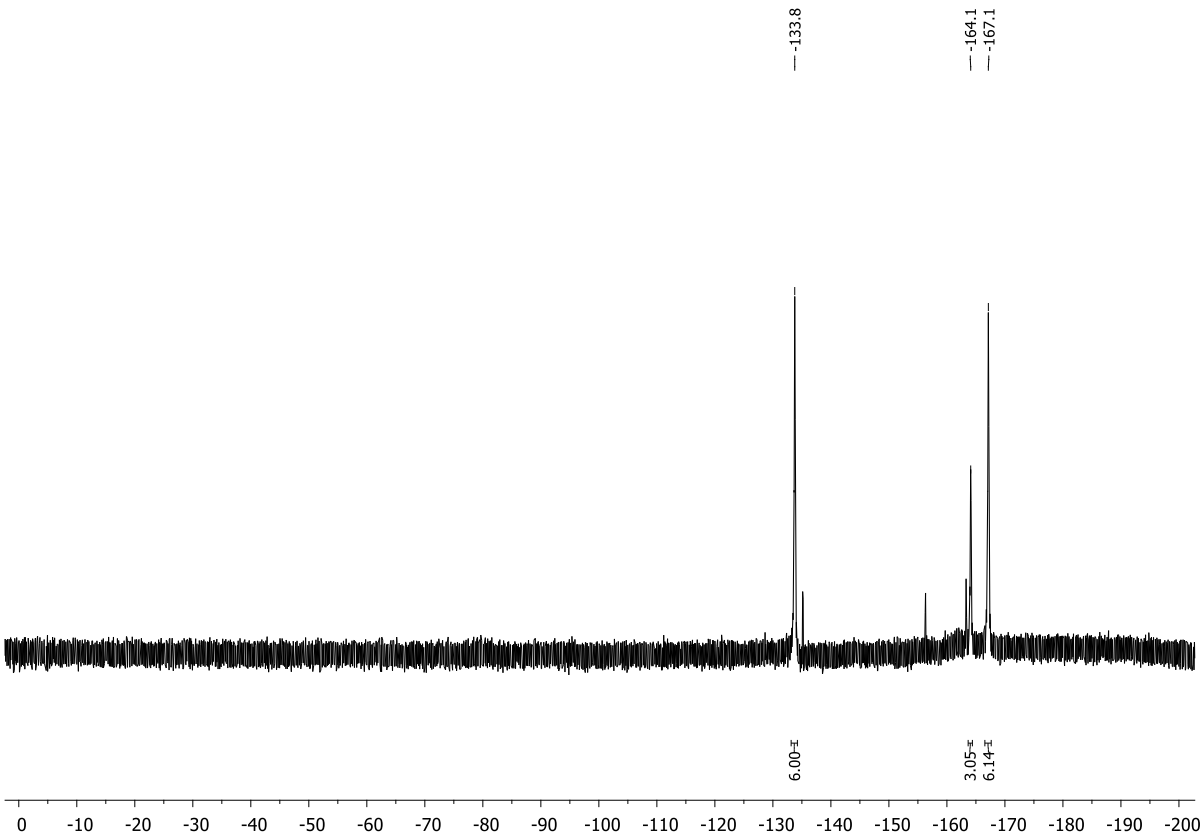

Figure S5.26. $^{19}F\{^{1}H\}$ NMR spectrum (CD_2Cl_2, 298 K) of **5**[$HB(C_6F_5)_3$].

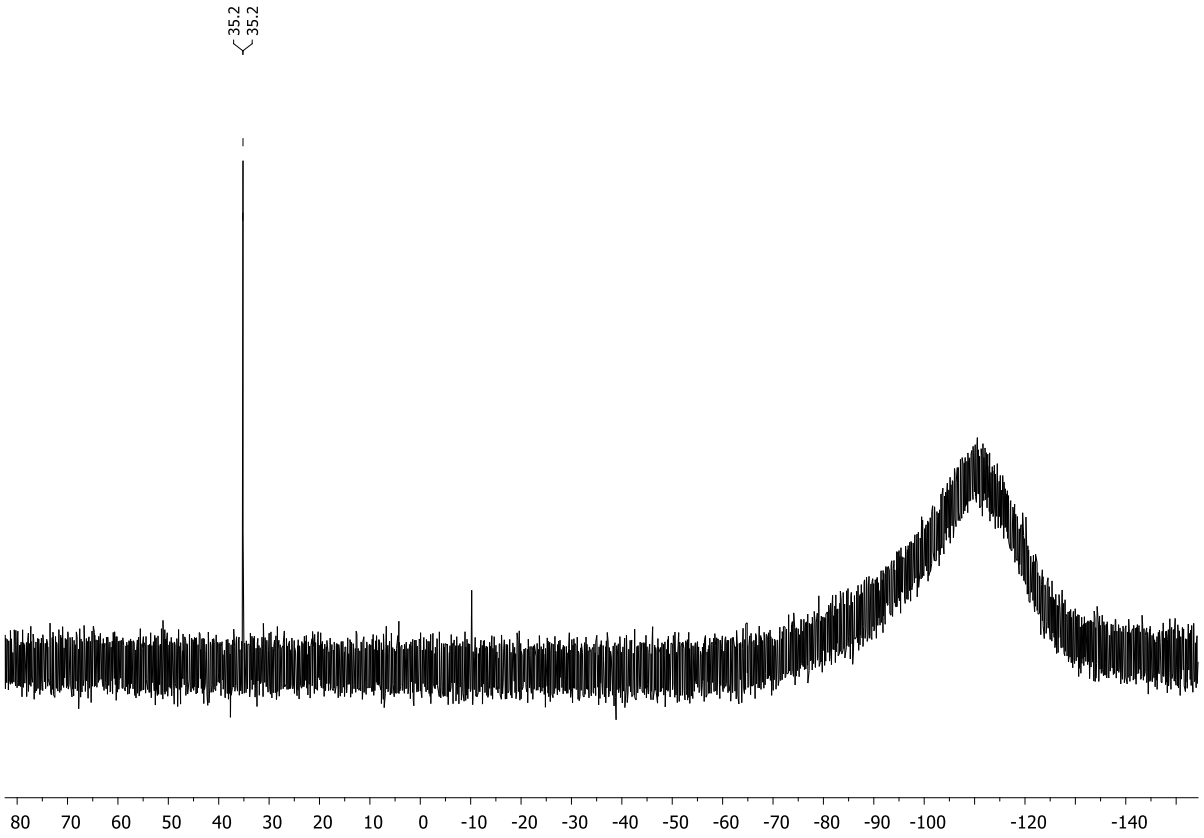

Figure S5.27. $^{29}Si\{^{1}H\}$ NMR spectrum (CD_2Cl_2, 298 K) of **5**[$HB(C_6F_5)_3$].

5.6.2.5. Synthesis of *t*Bu$_2$(PS)NH(SiH*t*BuPh) (*rac*-6)

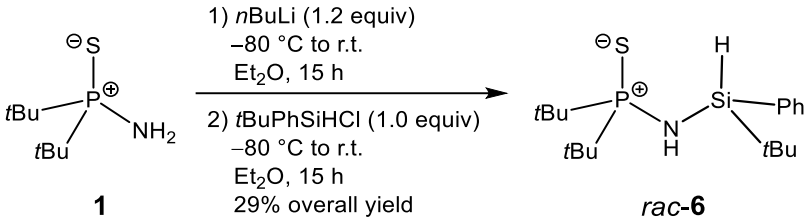

*n*Butyllithium (4.40 mL, 11.0 mmol, 1.2 equiv., 2.5 M in hexane) was added dropwise to a solution of *P*,*P*-di-*tert*-butylaminophosphine sulfide (**1**) (1.77 g, 9.16 mmol, 1.0 equiv.) in diethyl ether (50 mL) at −80 °C. The solution was allowed to slowly warm to room temperature and stirred for 15 h. Following, the colorless solution was cooled to −80 °C again and *tert*-butylchlorophenylsilane (1.82 g, 9.16 mmol, 1.0 equiv.) was added dropwise. The reaction mixture was allowed to slowly warm to room temperature and stirred for 15 h affording a colorless suspension. The precipitated lithium chloride was filtered off via cannula filtration and washed with diethyl ether. Then, all volatiles of the filtrate were removed under vacuum. The crude solid mixture was purified by Kugelrohr distillation (115 °C oven temperature, 1.3×10^{-2} mbar). Compound *rac*-**6** was obtained as a colorless solid (0.95 g, 2.67 mmol, 29%). Crystals suitable for single-crystal X-ray analysis were obtained from a diethyl ether solution by slow evaporation of the solvent.

^{1}H NMR (400.13 MHz, C_6D_6, 298 K): δ = 0.99 (s, 9H, SiC(C*H*$_3$)$_3$), 1.09 (d, $^3J_{H–P}$ = 15.3 Hz, 9H, PC(C*H*$_3$)$_3$), 1.24 (d, $^3J_{H–P}$ = 15.1 Hz, 9H, PC(C*H*$_3$)$_3$), 1.90 (br, 1H, N*H*), 5.29 (m, 1H, Si*H*), 7.18–7.22 (m, 3H, *H*$_{Ph}$), 7.63–7.65 (m, 2H, *H*$_{Ph}$). **^{31}P{^{1}H} NMR** (162.04 MHz, C_6D_6, 298 K): δ = 92.9 (s). **^{13}C{^{1}H} NMR** (100.61 MHz, C_6D_6, 298 K): δ = 18.0 (d, $^3J_{C–P}$ = 4.0 Hz, Si*C*(CH$_3$)$_3$), 27.2 (s, SiC(*C*H$_3$)$_3$), 27.5 (s, PC(*C*H$_3$)$_3$), 27.6 (s, PC(*C*H$_3$)$_3$), 39.5 (d, $^1J_{C–P}$ = 55.0 Hz, P*C*(CH$_3$)$_3$), 40.2 (d, $^1J_{C–P}$ = 54.7 Hz, P*C*(CH$_3$)$_3$), 128.0 (s, *C*$_{Ph}$), 129.9 (s, *C*$_{Ph}$), 135.0 (s, *C*$_{Ph}$), 135.7 (s, *C*$_{Ph}$). **^{29}Si NMR** (79.49 MHz, C_6D_6, 298 K): δ = −6.0 (d, $^1J_{Si–H}$ = 221.4 Hz).

^{1}H NMR (400.13 MHz, CD_2Cl_2, 298 K): δ = 0.99 (s, 9H, SiC(C*H*$_3$)$_3$), 1.21 (d, $^3J_{H–P}$ = 15.5 Hz, 9H, PC(C*H*$_3$)$_3$), 1.36 (d, $^3J_{H–P}$ = 15.4 Hz, 9H, PC(C*H*$_3$)$_3$), 2.06 (br, 1H, N*H*), 4.90 (d, $^3J_{H–P}$ = 2.9 Hz, 1H, Si*H*), 7.34–7.40 (m, 3H, *H*$_{Ph}$), 7.57–7.59 (m, 2H, *H*$_{Ph}$). **^{31}P{^{1}H} NMR** (162.04 MHz, CD_2Cl_2, 298 K): δ = 94.0 (s). **^{13}C{^{1}H} NMR** (100.61 MHz, CD_2Cl_2, 298 K): δ = 18.1 (d, $^3J_{C–P}$ = 4.3 Hz, Si*C*(CH$_3$)$_3$), 27.3 (s, SiC(*C*H$_3$)$_3$), 27.8 (d, $^2J_{C–P}$ = 1.8 Hz, PC(*C*H$_3$)$_3$), 27.8 (d, $^2J_{C–P}$ = 1.9 Hz, PC(*C*H$_3$)$_3$), 39.8 (d, $^1J_{C–P}$ = 53.4 Hz, P*C*(CH$_3$)$_3$), 40.9 (d, $^1J_{C–P}$ = 53.0 Hz, P*C*(CH$_3$)$_3$), 128.1 (s, *C*$_{Ph}$), 130.1 (s, *C*$_{Ph}$), 135.1 (s, *C*$_{Ph}$), 136.0 (s, *C*$_{Ph}$).

Elemental analysis: $C_{18}H_{34}NPSSi$: calcd.: C 60.80, H 9.64, N 3.94; found: C 60.35, H 9.76, N 3.65.

HR(APCI+)-MS: calcd. *m/z* for $C_{18}H_{35}NPSSi$ [(M+H)$^+$]: 356.1996, found: 356.1992.

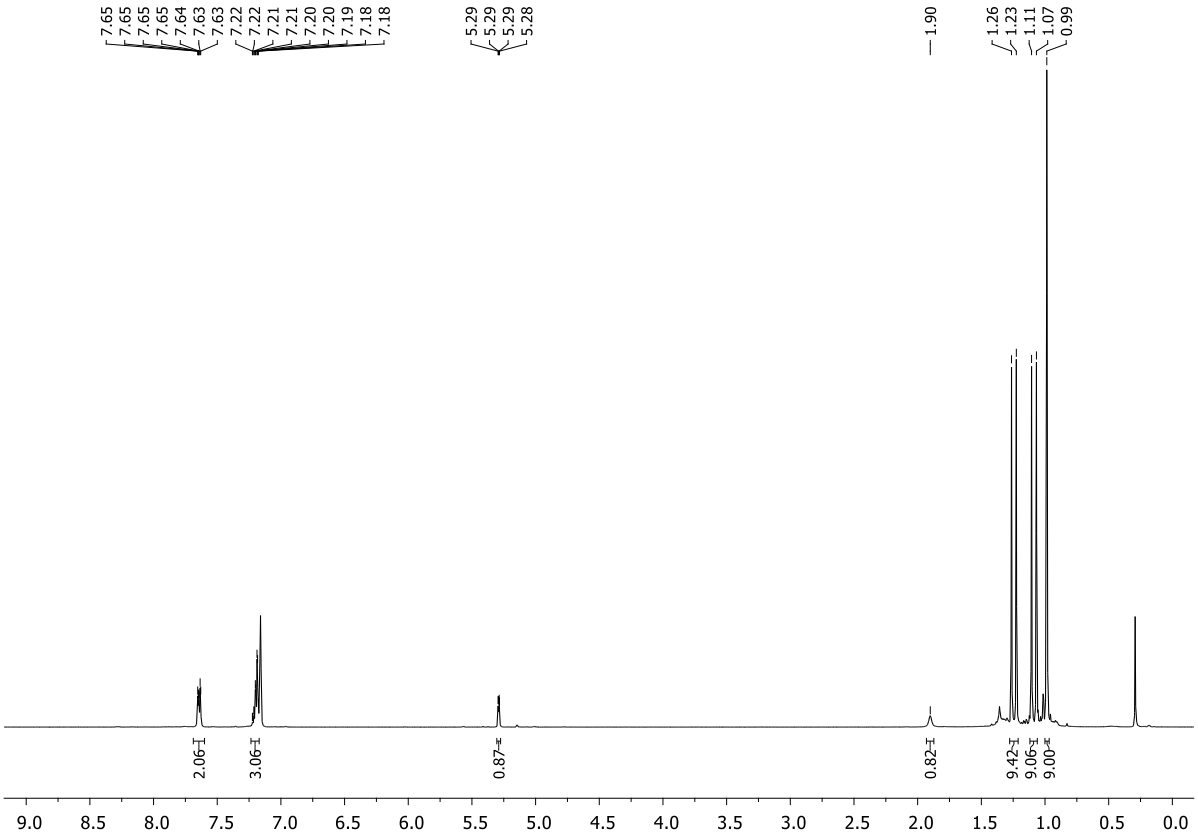

Figure S5.28. ^{1}H NMR spectrum (C_6D_6, 298 K) of *rac*-**6**.

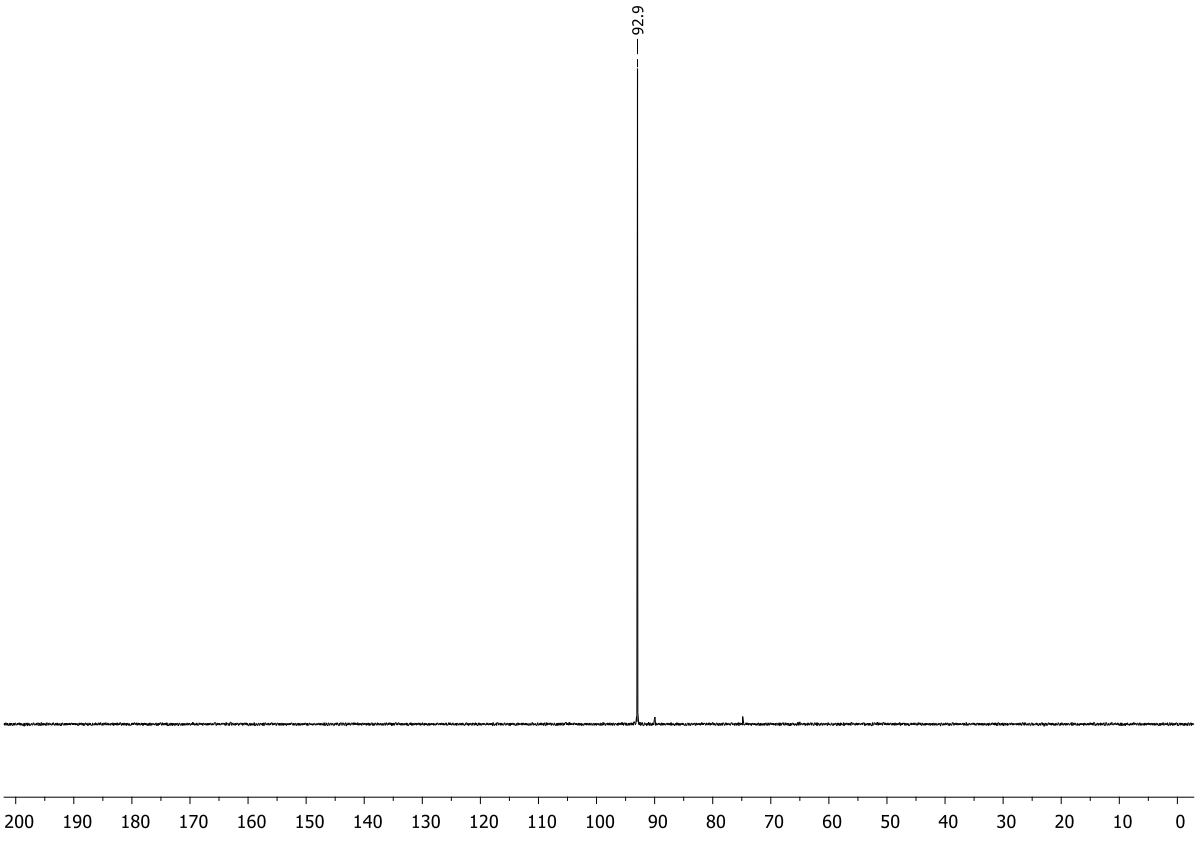

Figure S5.29. $^{31}P\{^{1}H\}$ NMR spectrum (C_6D_6, 298 K) of *rac*-**6**.

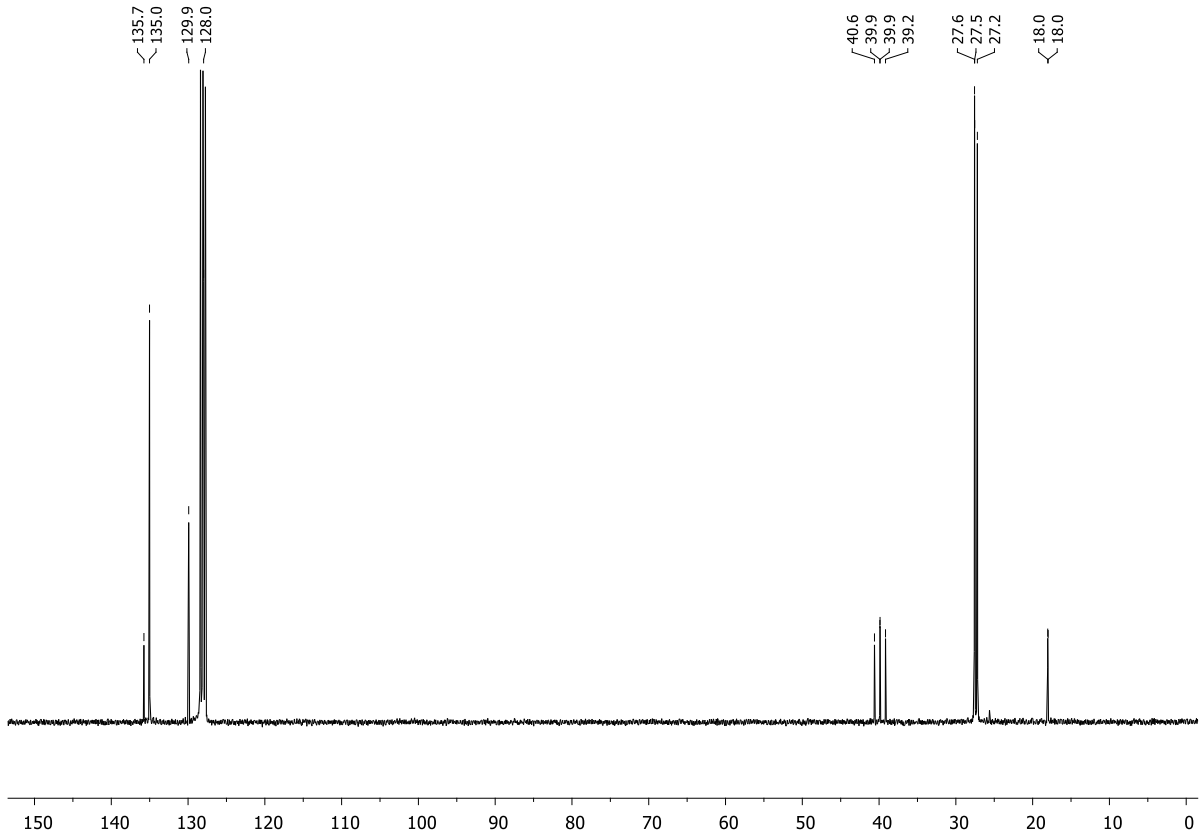

Figure S5.30. $^{13}C\{^{1}H\}$ NMR spectrum (C_6D_6, 298 K) of *rac*-**6**.

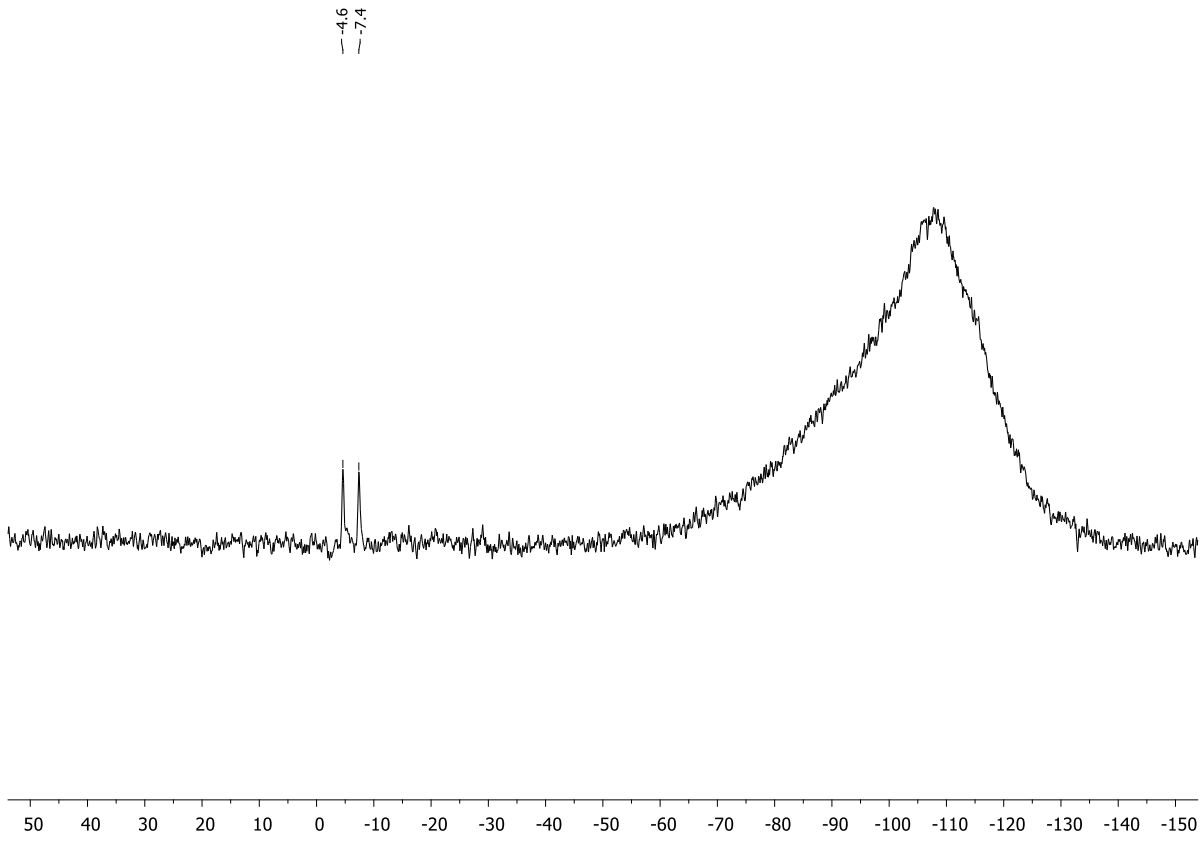

Figure S5.31. ^{29}Si NMR spectrum (C_6D_6, 298 K) of *rac*-**6**.

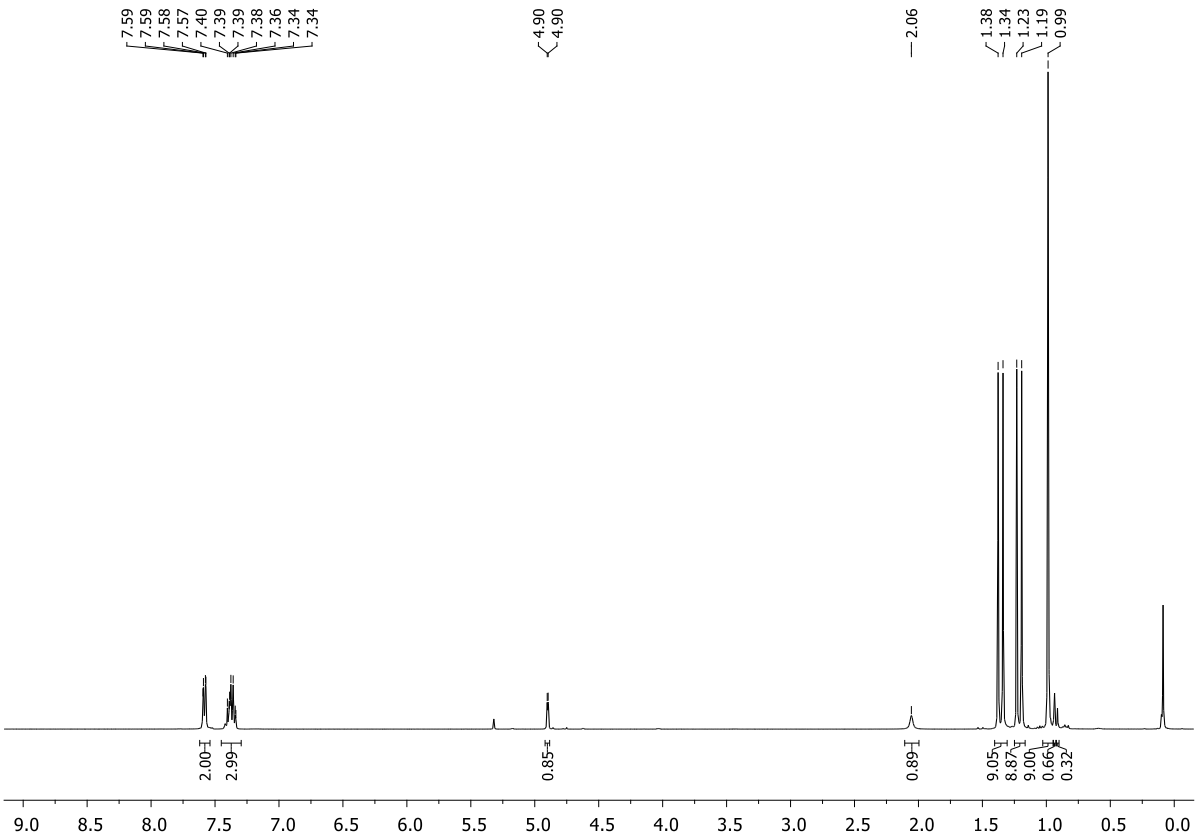

Figure S5.32. ^{1}H NMR spectrum (CD_2Cl_2, 298 K) of *rac*-**6**.

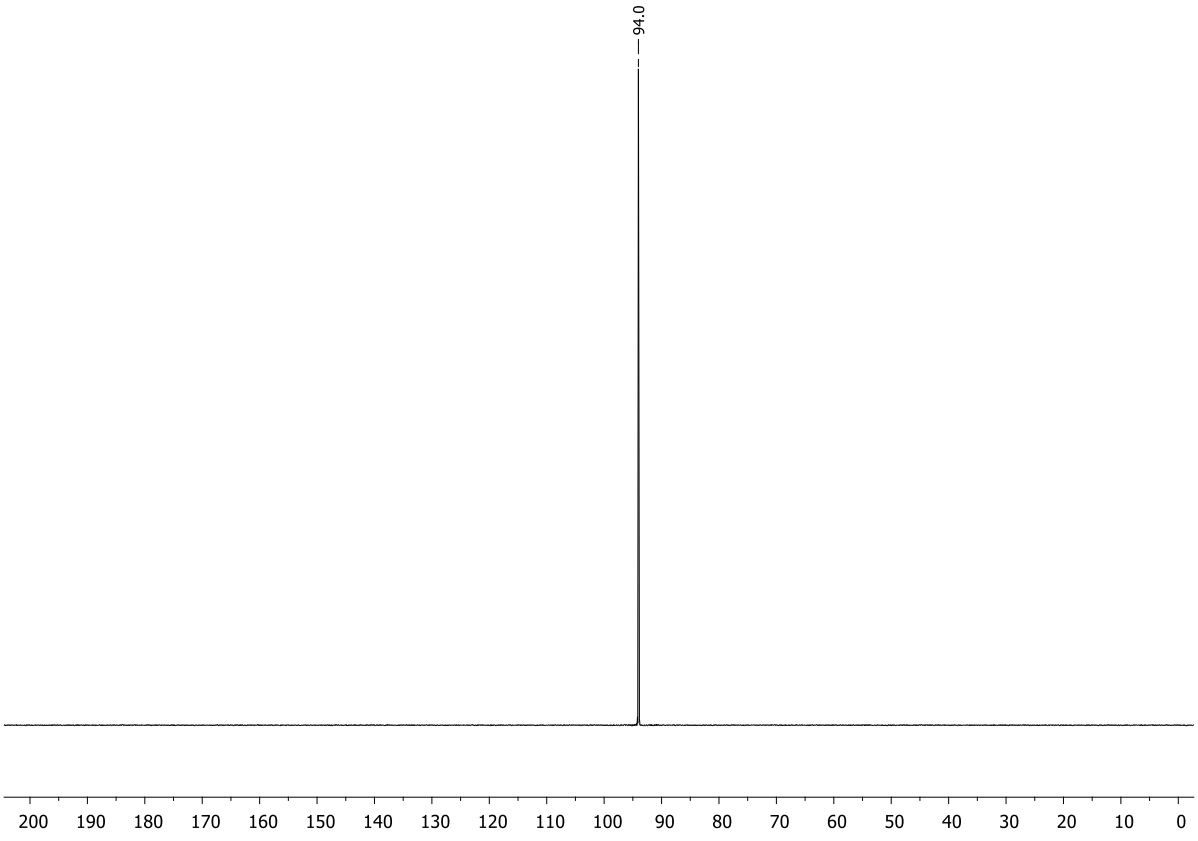

Figure S5.33. $^{31}P\{^{1}H\}$ NMR spectrum (CD_2Cl_2, 298 K) of *rac*-**6**.

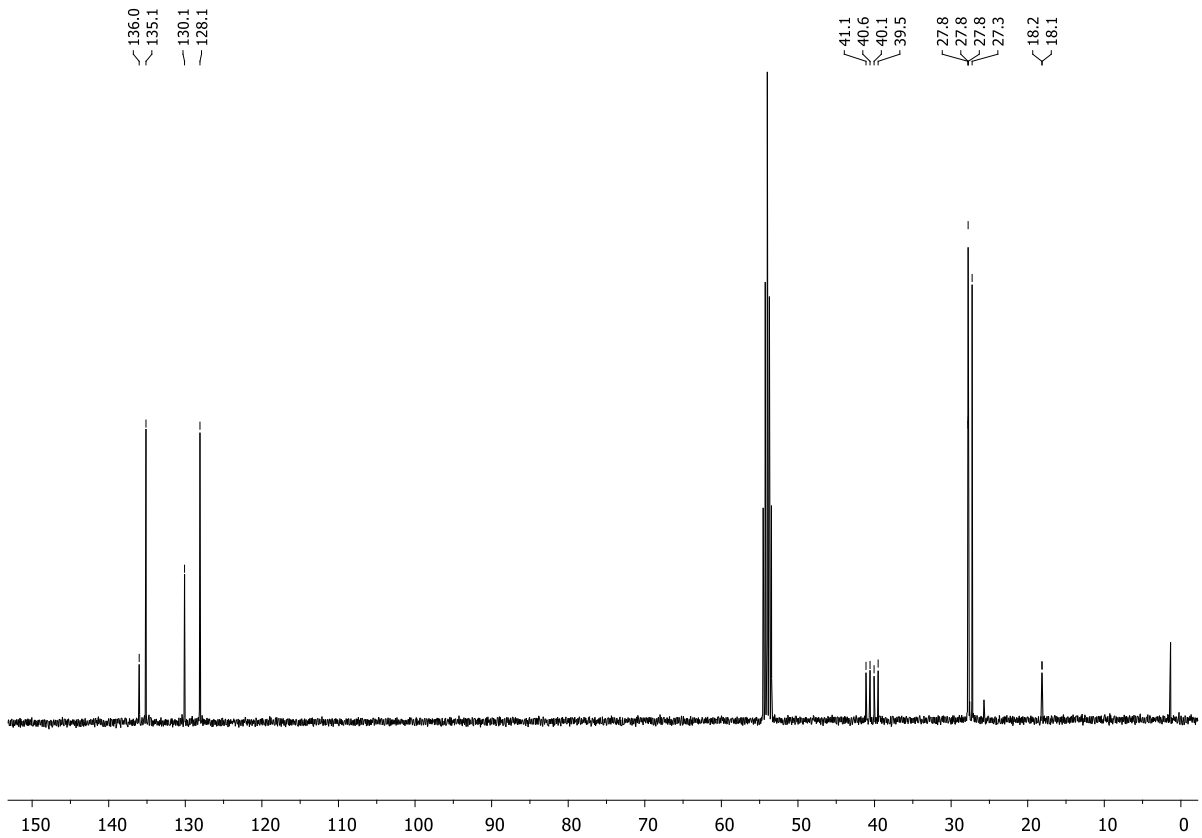

Figure S5.34. $^{13}C\{^{1}H\}$ NMR spectrum (CD_2Cl_2, 298 K) of *rac*-**6**.

5.6.2.6. Synthesis of [*t*Bu$_2$(PS)NH(Si*t*BuPh)]$^+$ [HB(C$_6$F$_5$)$_3$]$^-$ {*rac*-7[HB(C$_6$F$_5$)$_3$]}

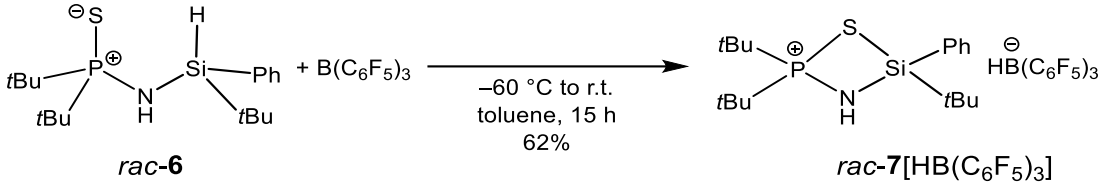

rac-**6** *rac*-**7**[HB(C$_6$F$_5$)$_3$]

A solution of compound *rac*-**6** (0.30 g, 0.84 mmol, 1.0 equiv.) in toluene (3 mL) was added to a solution of tris(pentafluorophenyl)borane (0.43 g, 0.84 mmol, 1.0 equiv.) in toluene (2 mL) at –60 °C. The solution was allowed to slowly warm to room temperature and stirred for 15 h. The solvent was then decanted and the remaining solid was washed with pentane. After drying in vacuo, compound *rac*-**7**[HB(C$_6$F$_5$)$_3$] was obtained as a colorless solid (0.45 g, 0.52 mmol, 62%). Crystals suitable for single-crystal X-ray analysis were obtained by slow layering of a DCM solution with pentane.

^{1}H NMR (400.13 MHz, CD_2Cl_2, 298 K): δ = 1.10 (s, 9H, SiC(C*H*$_3$)$_3$), 1.22 (d, $^3J_{H–P}$ = 19.1 Hz, 9H, PC(C*H*$_3$)$_3$), 1.55 (d, $^3J_{H–P}$ = 19.2 Hz, 9H, PC(C*H*$_3$)$_3$), 3.99 (d, $^2J_{H–P}$ = 1.5 Hz, 1H, N*H*), 7.45–7.49 (m, 2H, *H*$_{Ph}$), 7.54–7.61 (m, 3H, *H*$_{Ph}$). **^{31}P{^{1}H} NMR** (162.04 MHz, CD_2Cl_2, 298 K): δ = 114.3 (s). **^{13}C{^{1}H} NMR** (100.61 MHz, CD_2Cl_2, 298 K): δ = 24.4 (s, Si*C*(CH$_3$)$_3$), 25.6 (s, SiC(*C*H$_3$)$_3$), 26.8 (d, $^2J_{C–P}$ = 2.7 Hz, PC(*C*H$_3$)$_3$), 26.9 (d, $^2J_{C–P}$ = 2.6 Hz, PC(*C*H$_3$)$_3$), 43.0 (d, $^1J_{C–P}$ = 29.5 Hz, P*C*(CH$_3$)$_3$), 43.1 (d, $^1J_{C–P}$ = 29.2 Hz, P*C*(CH$_3$)$_3$), 129.2 (s, *C*$_{Ph}$), 130.7 (s, *C*$_{Ph}$), 132.3 (s, *C*$_{Ph}$), 133.4 (s, *C*$_{Ph}$). **^{11}B{^{1}H} NMR** (128.43 MHz, CD_2Cl_2, 298 K): δ = –25.1 (s). **^{19}F{^{1}H} NMR** (376.66 MHz, CD_2Cl_2, 298 K): δ = –166.9 (m, 6F, *meta*-*F*$_{Ar\text{-}borate}$), –164.0 (m, 3F, *para*-*F*$_{Ar\text{-}borate}$), –133.4 (m, 6F, *ortho*-*F*$_{Ar\text{-}borate}$). **^{29}Si{^{1}H} NMR** (79.49 MHz, CD_2Cl_2, 298 K): δ = 20.7 (d, $^2J_{P–Si}$ = 3.4 Hz).

Elemental analysis: $C_{36}H_{34}BF_{15}NPSSi$: calcd.: C 49.84, H 3.95, N 1.61; found: C 49.91, H 3.98, N 1.58.

HR(+ESI)-MS: calcd. *m/z* for $C_{18}H_{35}NOPSSi^+$ [Cation+H_2O]$^+$, $C_{18}HBF_{15}^-$ [Anion]$^-$: 372.1941, 512.9937, found: 372.1993, 513.0017.

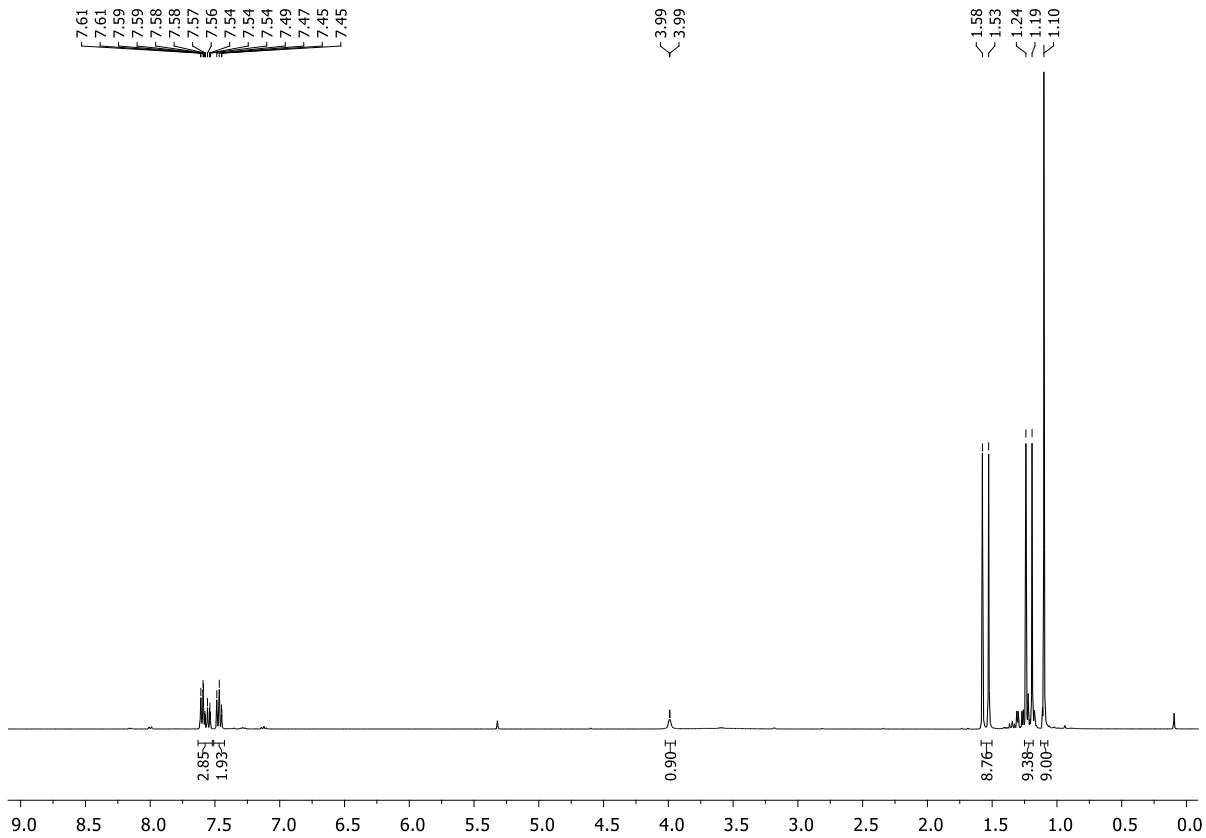

Figure S5.35. ^{1}H NMR spectrum (CD_2Cl_2, 298 K) of *rac*-**7**[$HB(C_6F_5)_3$].

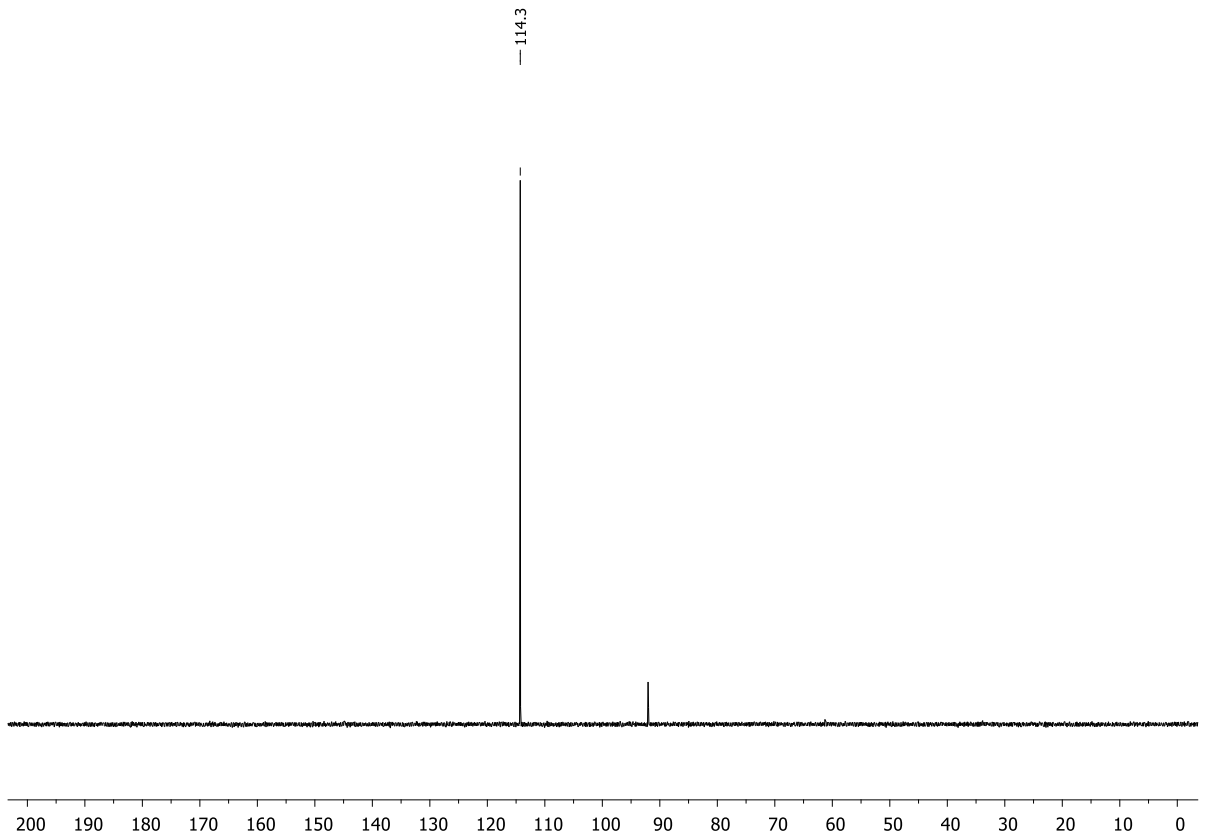

Figure S5.36. $^{31}P\{^{1}H\}$ NMR spectrum (CD_2Cl_2, 298 K) of *rac*-**7**[$HB(C_6F_5)_3$].

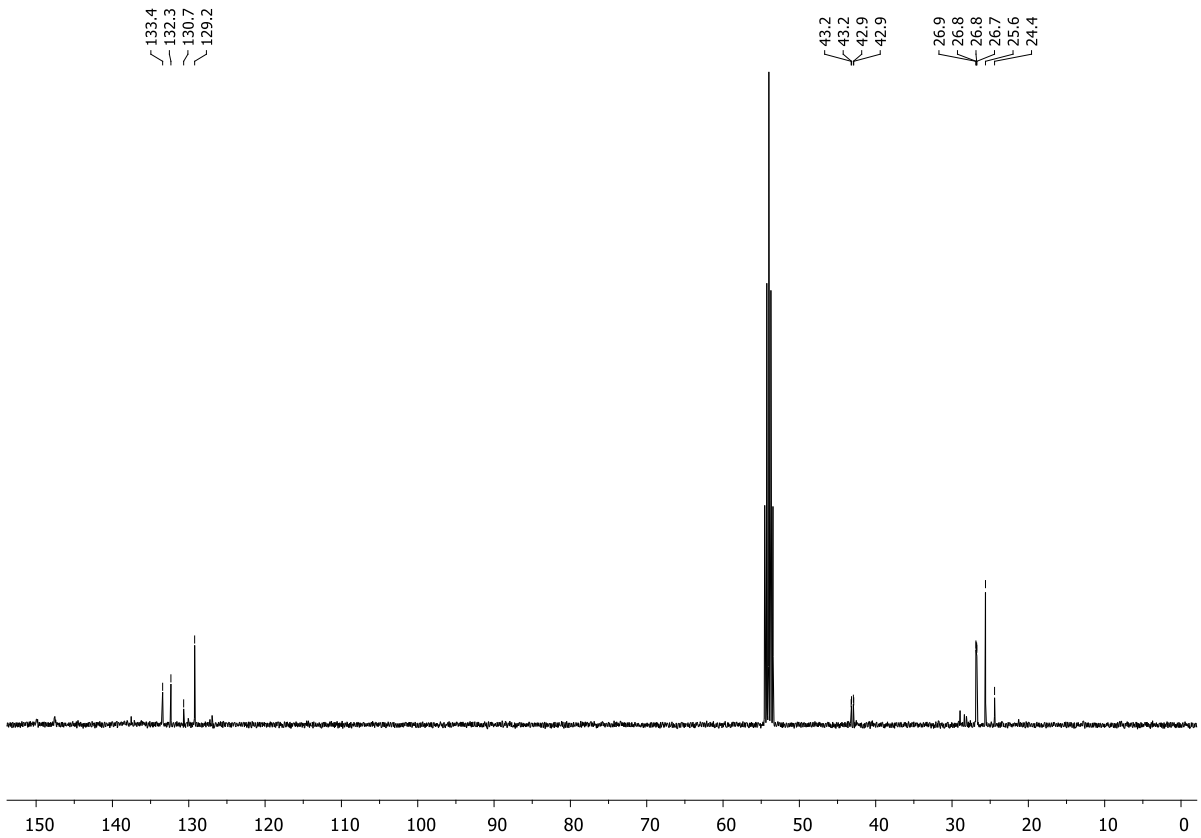

Figure S5.37. $^{13}C\{^{1}H\}$ NMR spectrum (CD_2Cl_2, 298 K) of *rac*-**7**[$HB(C_6F_5)_3$].

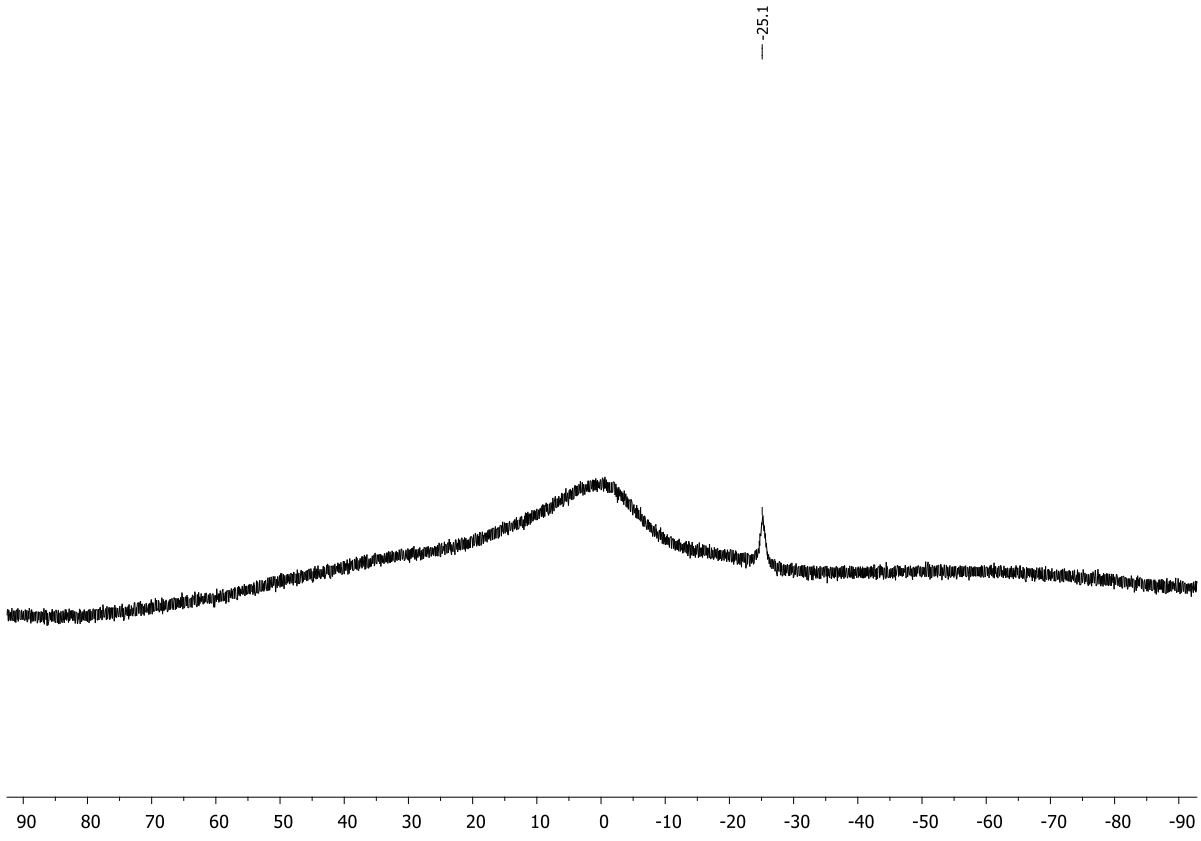

Figure S5.38. $^{11}B\{^{1}H\}$ NMR spectrum (CD_2Cl_2, 298 K) of *rac*-**7**[$HB(C_6F_5)_3$].

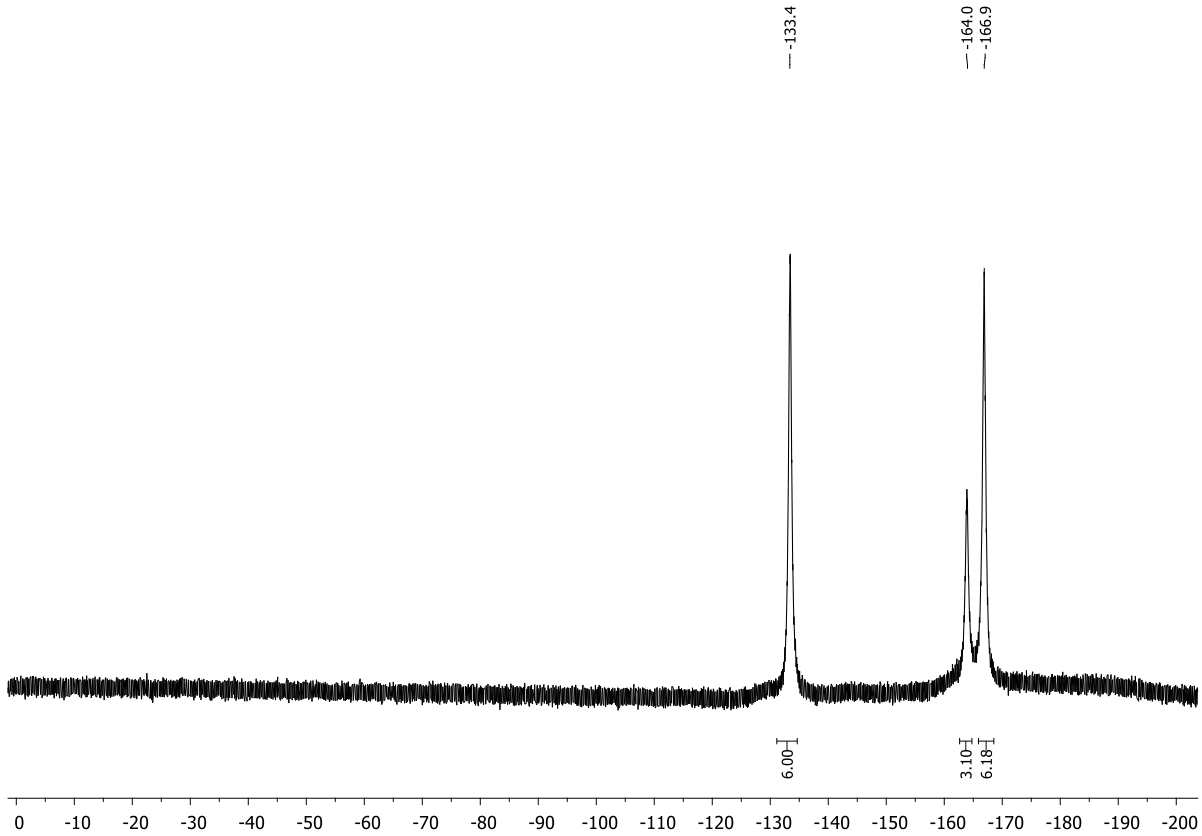

Figure S5.39. $^{19}F\{^{1}H\}$ NMR spectrum (CD_2Cl_2, 298 K) of *rac*-**7**[$HB(C_6F_5)_3$].

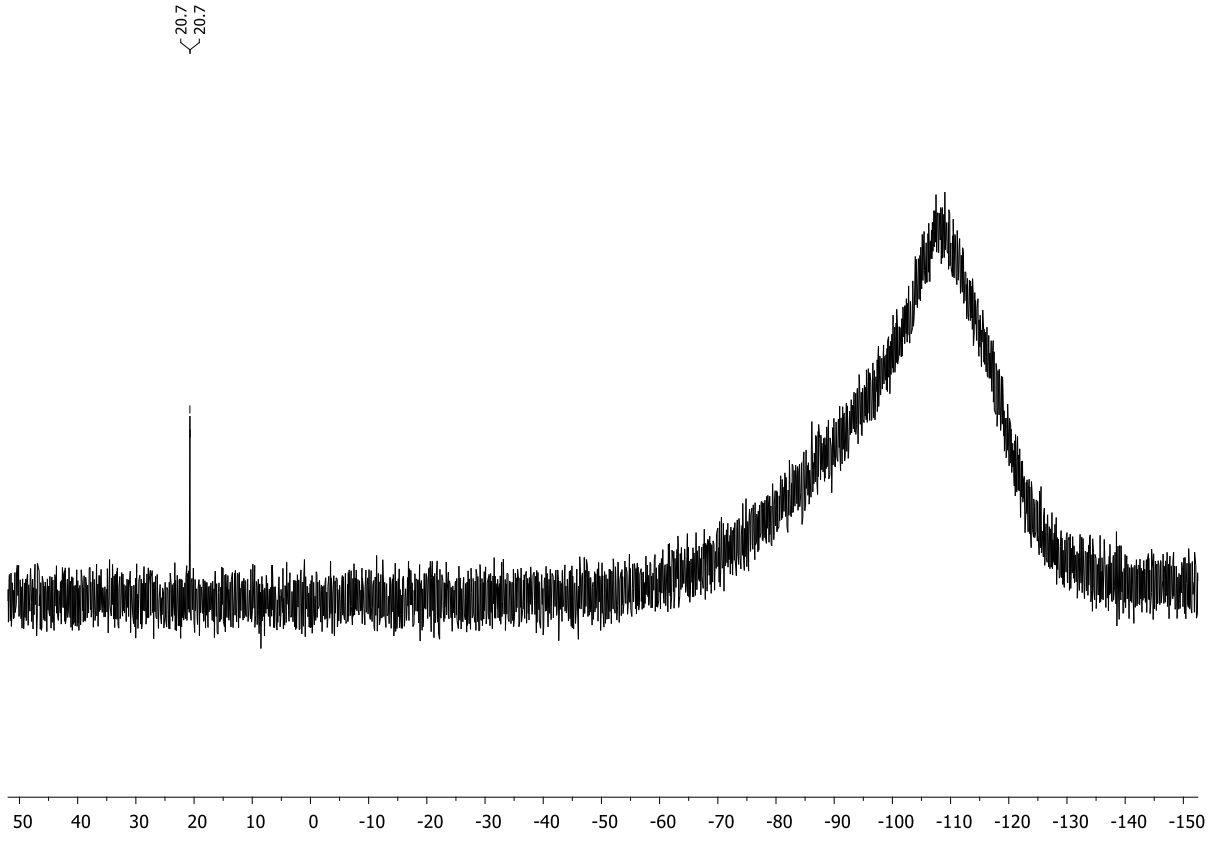

Figure S5.40. $^{29}Si\{^{1}H\}$ NMR spectrum (CD_2Cl_2, 298 K) of *rac*-**7**[$HB(C_6F_5)_3$].

5.6.2.7. Reaction of *rac*-7[HB(C$_6$F$_5$)$_3$] with ammonia

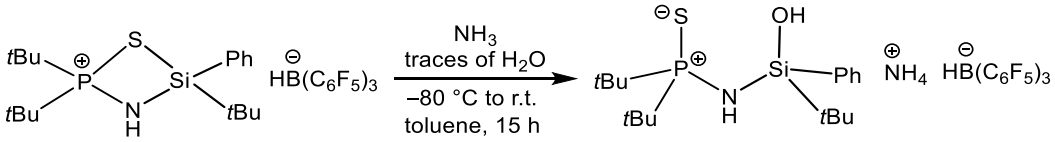

rac-**7**[HB(C$_6$F$_5$)$_3$] *rac*-**8** · NH4$^+$ HB(C$_6$F$_5$)$_3^-$

rac-**7**[HB(C$_6$F$_5$)$_3$] (100 mg, 0.115 mmol) was solved in toluene (7 mL) and cooled to –80 °C. Anhydrous, gaseous ammonia (a few mL) was condensed into the reaction flask. The mixture was allowed to slowly warm to room temperature and stirred for 15 h affording a colorless solution. All volatiles were removed in vacuo. Crystals suitable for single-crystal X-ray analysis were obtained by layering a toluene solution with pentane. X-ray measurement revealed that the expected amino-substituted product [*t*Bu$_2$(PS)NHSiNH$_2$*t*BuPh] had not crystallized. Instead, the hydrolysed product *rac*-**8** had co-crystallized with NH$_4^+$ HB(C$_6$F$_5$)$_3^-$.

^{1}H NMR (400.13 MHz, CD_2Cl_2, 298 K): δ = 0.96 (s, 9H, SiC(C*H*$_3$)$_3$), 1.18 (d, $^3J_{H–P}$ = 15.9 Hz, 9H, PC(C*H*$_3$)$_3$), 1.38 (d, $^3J_{H–P}$ = 15.7 Hz, 9H, PC(C*H*$_3$)$_3$), 2.29 (br, 1H, N*H*), 4.42 (br, 1H, O*H*), 4.82 (br, 4H, NH$_4$), 7.35–7.43 (m, 3H, *H*$_{Ph}$), 7.63–7.66 (m, 2H, *H*$_{Ph}$). **^{31}P{^{1}H} NMR** (162.04 MHz, CD_2Cl_2, 298 K): δ = 94.5 (s). **^{13}C{^{1}H} NMR** (100.61 MHz, CD_2Cl_2, 298 K): δ = 19.3 (d, $^3J_{C–P}$ = 3.3 Hz, Si*C*(CH$_3$)$_3$), 26.4 (s, SiC(*C*H$_3$)$_3$), 27.6 (d, $^2J_{C–P}$ = 1.8 Hz, PC(*C*H$_3$)$_3$), 27.7 (d, $^2J_{C–P}$ = 1.9 Hz, PC(*C*H$_3$)$_3$), 40.2 (d, $^1J_{C–P}$ = 52.6 Hz, P*C*(CH$_3$)$_3$), 40.5 (d, $^1J_{C–P}$ = 52.1 Hz, P*C*(CH$_3$)$_3$), 128.0 (s, *C*$_{Ph}$), 130.1 (s, *C*$_{Ph}$), 135.2 (s, *C*$_{Ph}$), 136.2 (s, *C*$_{Ph}$). **^{11}B{^{1}H} NMR** (128.43 MHz, CD_2Cl_2, 298 K): δ = –24.9 (s). **^{19}F{^{1}H} NMR** (376.66 MHz, CD_2Cl_2, 298 K): δ = –166.3 (m, 6F, *meta*-*F*$_{Ar\text{-}borate}$), –162.7 (m, 3F, *para*-*F*$_{Ar\text{-}borate}$), –134.5 (m, 6F, *ortho*-*F*$_{Ar\text{-}borate}$). **^{29}Si NMR** (79.49 MHz, CD_2Cl_2, 298 K): δ = –12.1 (d, $^2J_{Si–P}$ = 6.2 Hz).

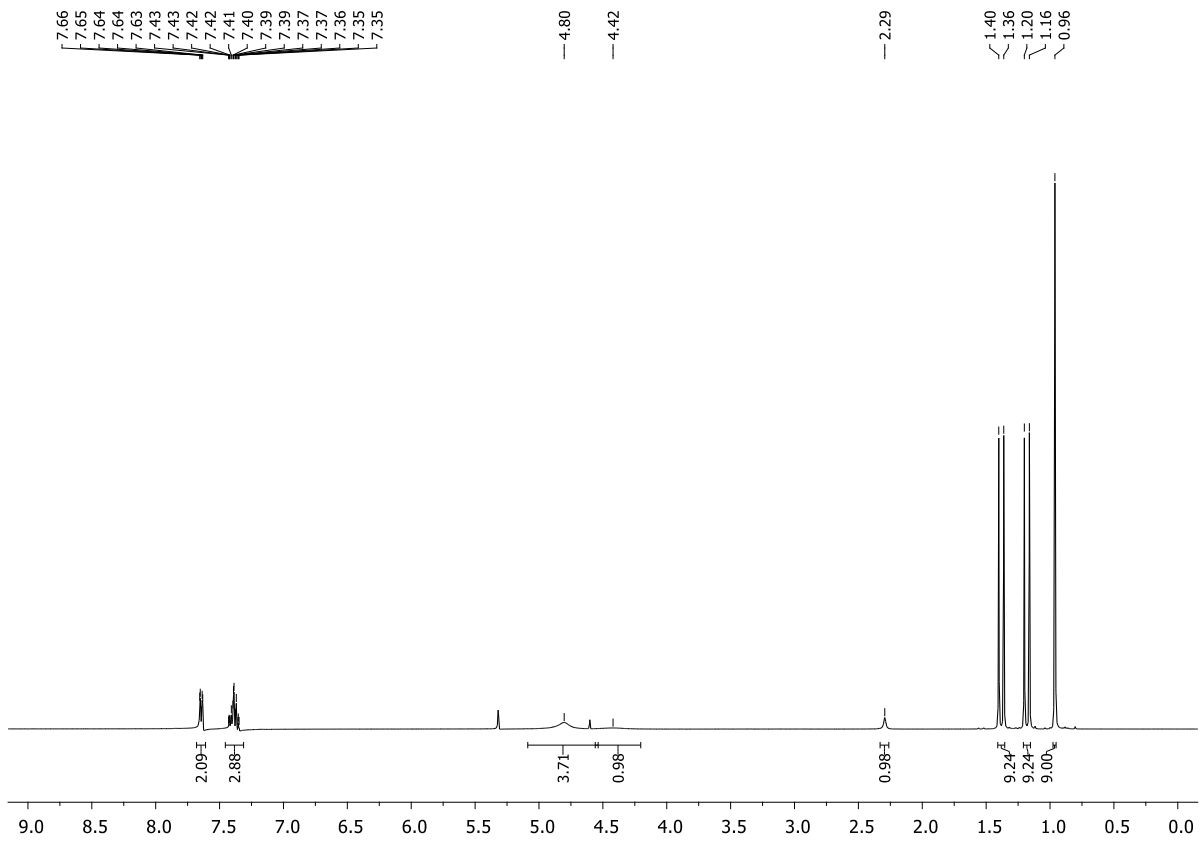

Figure S5.41. ^{1}H NMR spectrum (CD_2Cl_2, 298 K) of *rac*-**8** · NH_4^+ $HB(C_6F_5)_3^-$.

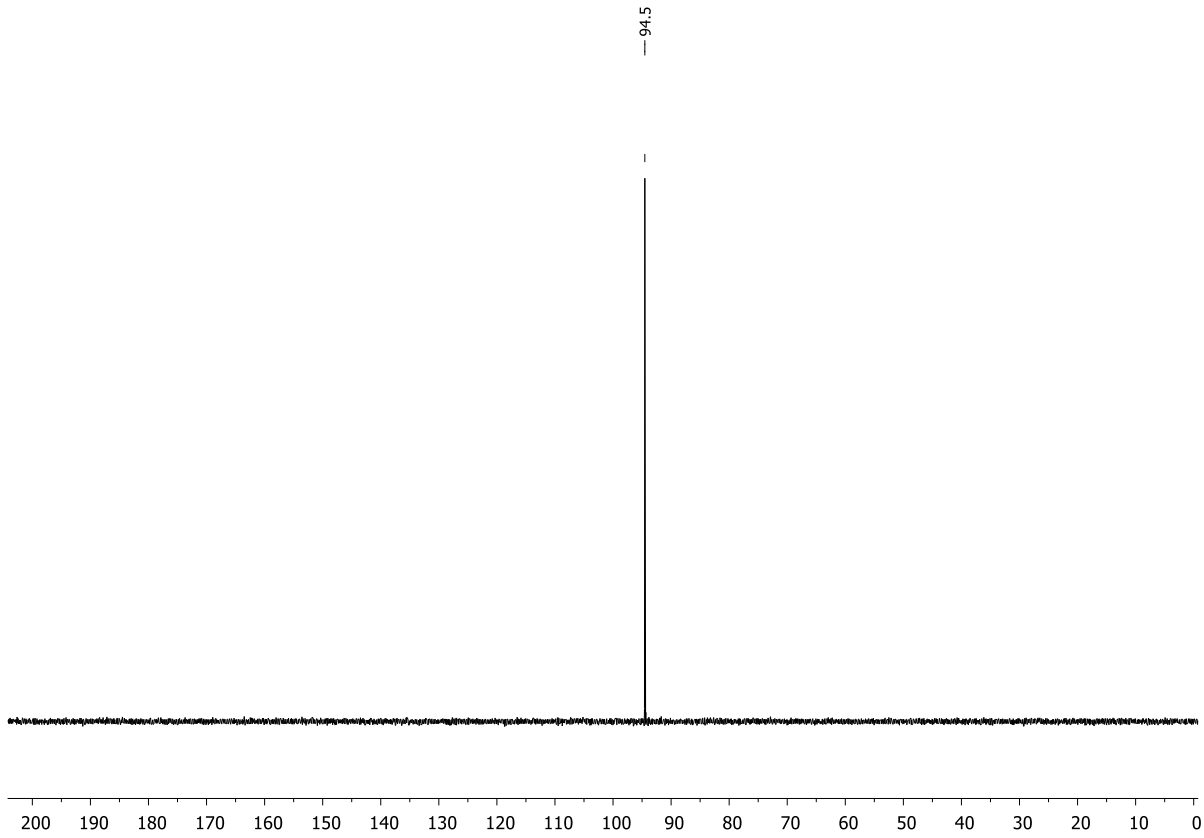

Figure S5.42. $^{31}P\{^{1}H\}$ NMR spectrum (CD_2Cl_2, 298 K) of *rac*-**8** · NH_4^+ $HB(C_6F_5)_3^-$.

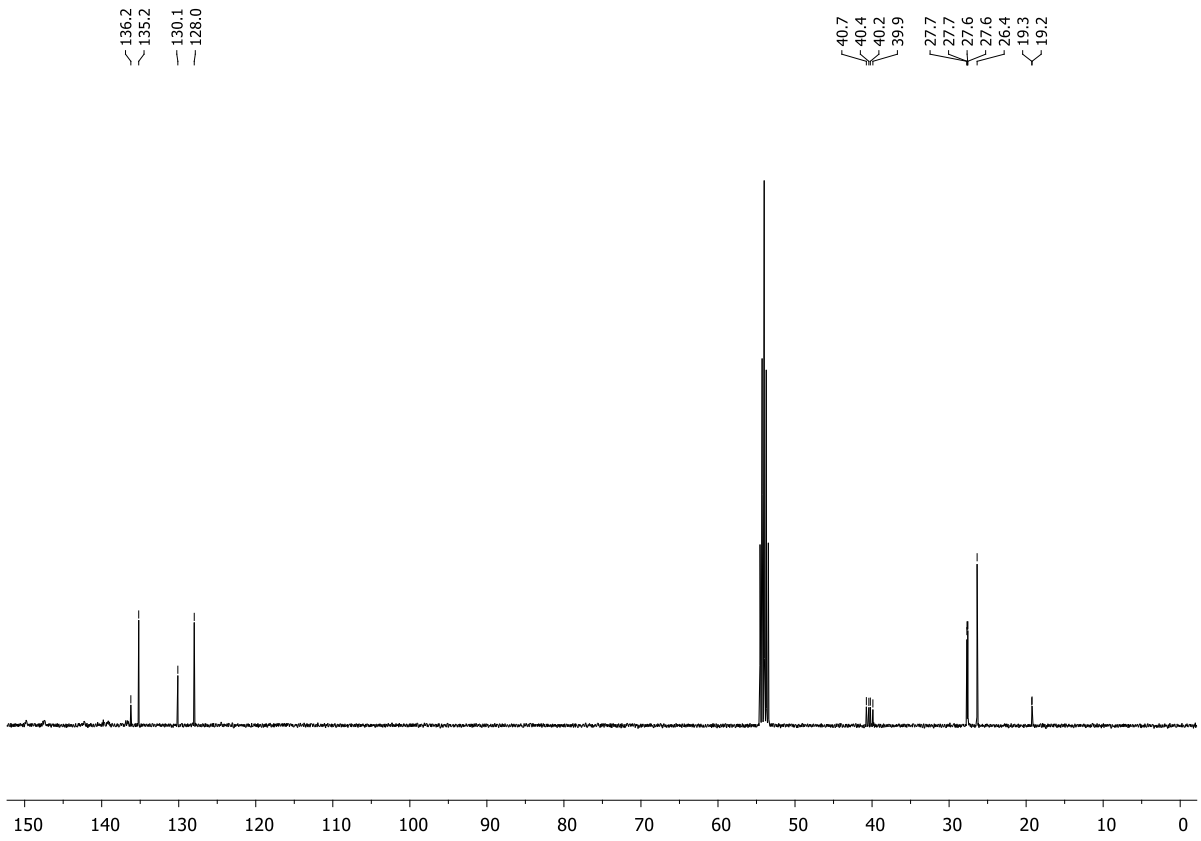

Figure S5.43. $^{13}C\{^{1}H\}$ NMR spectrum (CD_2Cl_2, 298 K) of *rac*-**8** · NH_4^+ $HB(C_6F_5)_3^-$.

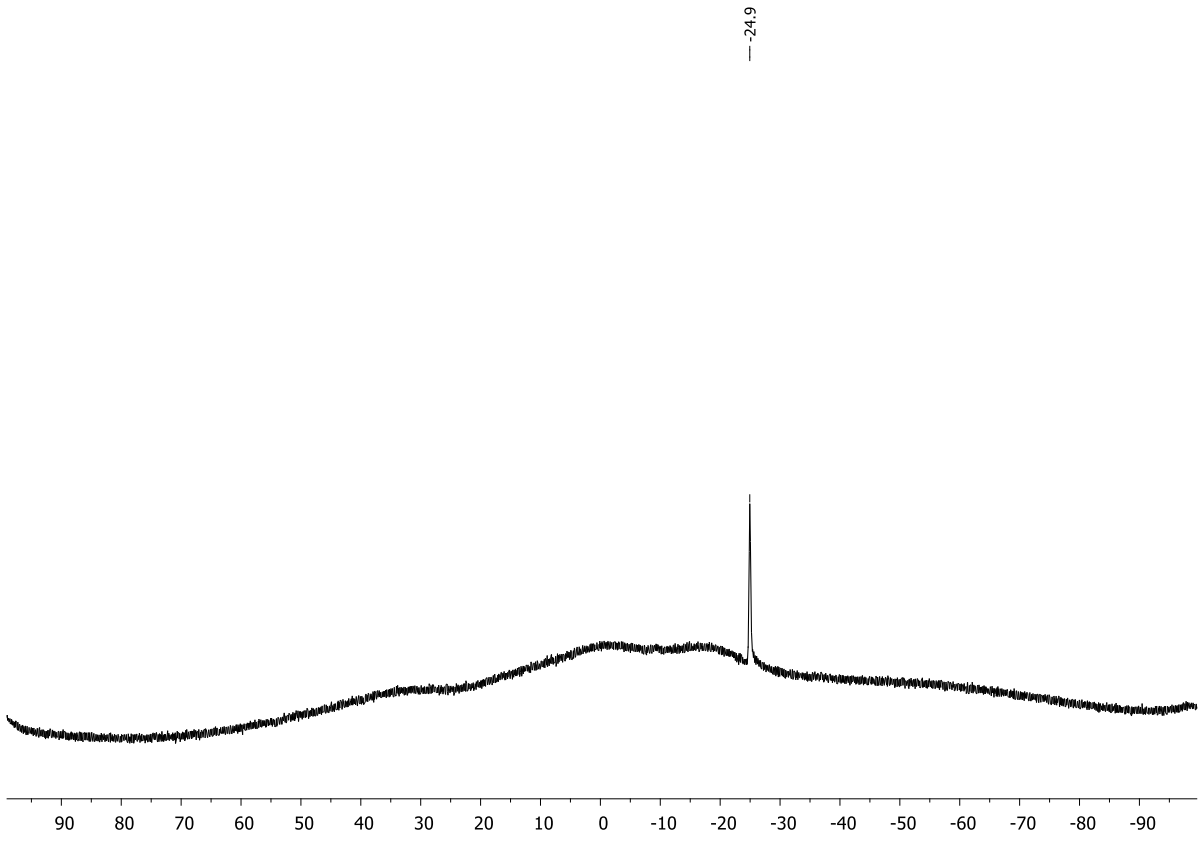

Figure S5.44. $^{11}B\{^{1}H\}$ NMR spectrum (CD_2Cl_2, 298 K) of *rac*-**8** · NH_4^+ $HB(C_6F_5)_3^-$.

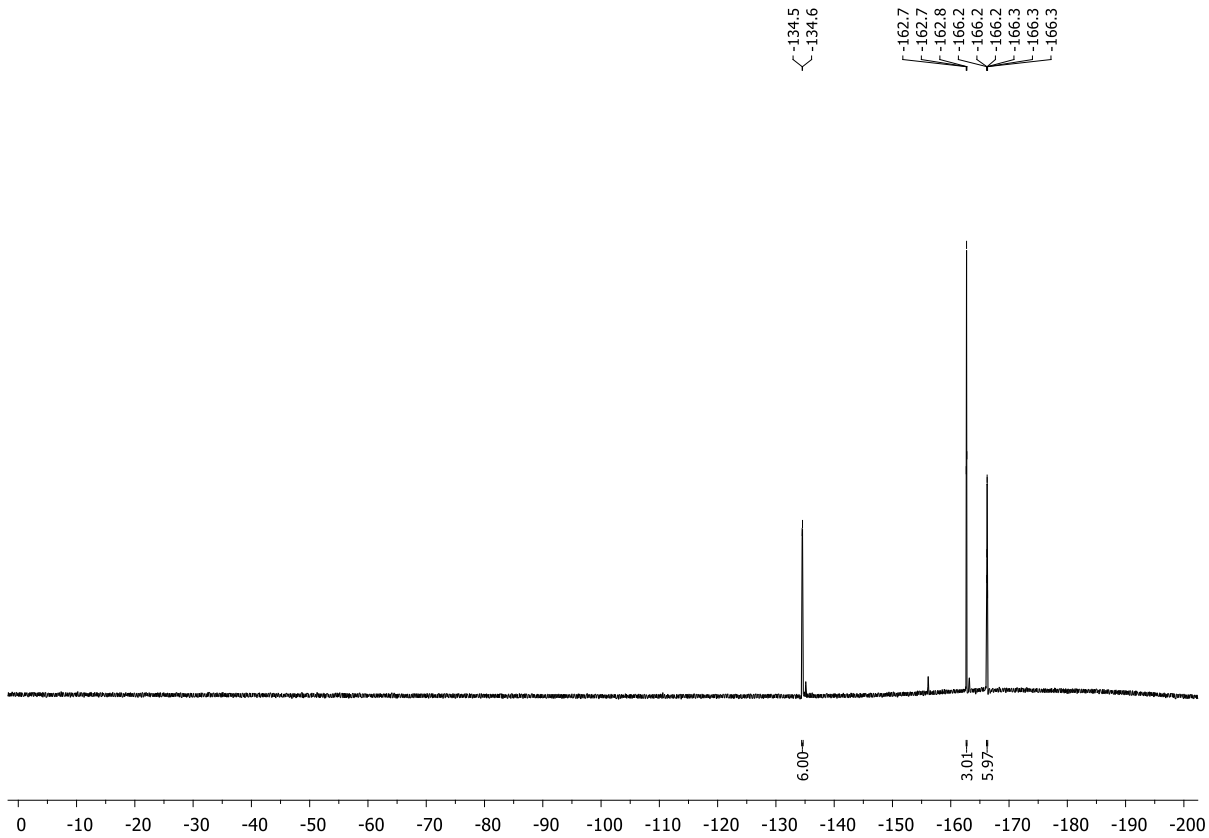

Figure S5.45. $^{19}F\{^{1}H\}$ NMR spectrum (CD_2Cl_2, 298 K) of *rac*-**8** · NH_4^+ $HB(C_6F_5)_3^-$.

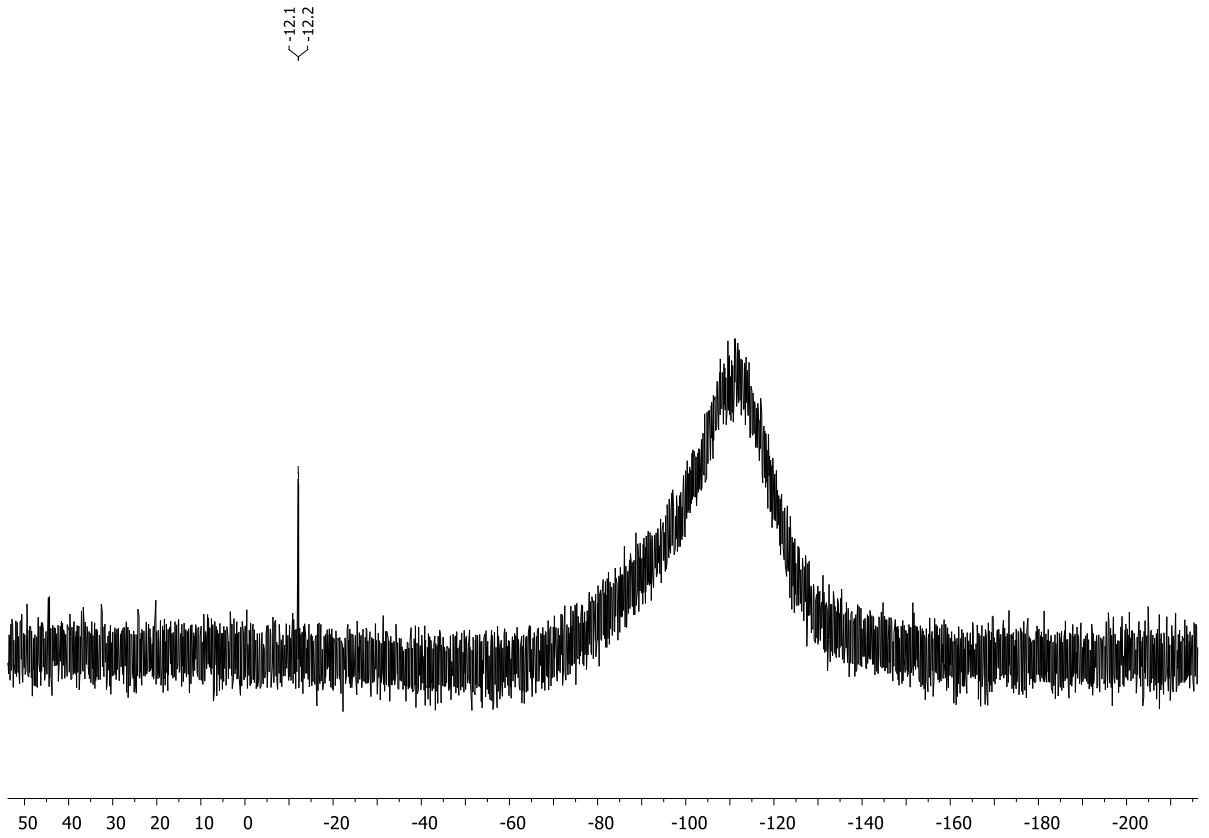

Figure S5.46. $^{29}Si\{^{1}H\}$ NMR spectrum (CD_2Cl_2, 298 K) of *rac*-**8** · NH_4^+ $HB(C_6F_5)_3^-$.

5.6.2.8. Reaction of *rac*-7[HB(C$_6$F$_5$)$_3$] with DBU

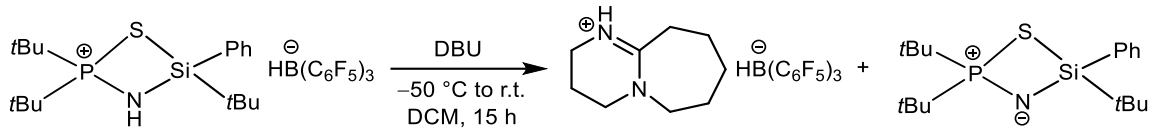

rac-**7**[HB(C$_6$F$_5$)$_3$] **9**[HB(C$_6$F$_5$)$_3$] not unambiguously identified

DBU (9 mg, 0.0576 mmol, 1.0 equiv.) was added to a solution of *rac*-**7**[HB(C$_6$F$_5$)$_3$] (50 mg, 0.0576 mmol, 1.0 equiv.) in DCM (1.5 mL) at –50 °C. The reaction mixture was allowed to slowly warm to room temperature and stirred for 15 h affording a colorless solution. All volatiles were removed in vacuo. Crystals suitable for single-crystal X-ray analysis were obtained by layering a DCM solution with pentane. X-ray measurement revealed that not the desired zwitterionic product had crystallized, but the by-product, which is DBU–H$^+$ HB(C$_6$F$_5$)$_3^-$ {**9**[HB(C$_6$F$_5$)$_3$]}.

5.6.2.9. Synthesis of *t*Bu$_2$(PS)NH(SiH$_2$Ph) (10)

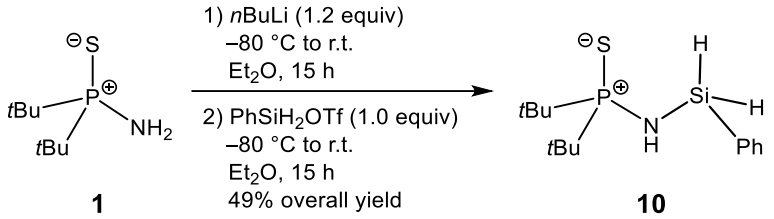

1 **10**

*n*Butyllithium (2.48 mL, 6.20 mmol, 1.2 equiv., 2.5 M in hexane) was added dropwise to a solution of *P*,*P*-di-*tert*-butylaminophosphine sulfide (**1**) (1.00 g, 5.17 mmol, 1.0 equiv.) in diethyl ether (20 mL) at −80 °C. The solution was allowed to slowly warm to room temperature and stirred for 15 h. Following, the colorless solution was cooled to −80 °C again and phenylsilyl triflate (1.32 g, 5.17 mmol, 1.0 equiv.), which was prepared shortly before addition in a separate Schlenk tube according to a literature procedure,[4] was added dropwise. The reaction mixture was allowed to slowly warm to room temperature and stirred for 15 h affording a colorless solution. All volatiles were removed in vacuo, the remaining solid was washed with pentane and the product was extracted with toluene. After removing toluene again and drying in vacuo, compound **10** was obtained as a colorless solid (0.76 g, 2.54 mmol, 49%). Crystals suitable for single-crystal X-ray analysis were obtained by layering a toluene solution with pentane.

^{1}H NMR (400.13 MHz, C_6D_6, 298 K): δ = 1.06 (d, $^3J_{H–P}$ = 15.4 Hz, 18H, PC(C*H*$_3$)$_3$), 1.63 (br, 1H, N*H*), 5.36 (m, 2H, Si*H*), 7.17–7.22 (m, 3H, *H*$_{Ph}$), 7.79–7.84 (m, 2H, *H*$_{Ph}$). **^{31}P{^{1}H} NMR** (162.04 MHz, C_6D_6, 298 K): δ = 94.2 (s). **^{13}C{^{1}H} NMR** (100.61 MHz, C_6D_6, 298 K): δ = 27.2 (d, $^2J_{C–P}$ = 1.8 Hz, PC(*C*H$_3$)$_3$), 39.5 (d, $^1J_{C–P}$ = 52.9 Hz, P*C*(CH$_3$)$_3$), 128.3 (s, *C*$_{meta}$), 130.5 (s, *C*$_{para}$), 134.7 (d, $^3J_{C–P}$ = 2.5 Hz, *C*$_{ipso}$), 135.8 (s, *C*$_{ortho}$).

^{1}H NMR (400.13 MHz, CD_2Cl_2, 298 K): δ = 1.29 (d, $^3J_{H–P}$ = 15.6 Hz, 18H, PC(C*H*$_3$)$_3$), 2.07 (br, 1H, N*H*), 5.03 (m, 2H, Si*H*), 7.37–7.46 (m, 3H, *H*$_{Ph}$), 7.72–7.75 (m, 2H, *H*$_{Ph}$). **^{31}P{^{1}H} NMR** (162.04 MHz, CD_2Cl_2, 298 K): δ = 95.0 (s). **^{13}C{^{1}H} NMR** (100.61 MHz, CD_2Cl_2, 298 K): δ = 27.5 (d, $^2J_{C–P}$ = 1.9 Hz, PC(*C*H$_3$)$_3$), 40.1 (d, $^1J_{C–P}$ = 52.6 Hz, P*C*(CH$_3$)$_3$), 128.5 (s, *C*$_{meta}$), 130.8 (s, *C*$_{para}$), 134.4 (d, $^3J_{C–P}$ = 3.2 Hz, *C*$_{ipso}$), 135.8 (s, *C*$_{ortho}$). **^{29}Si{^{1}H} NMR** (79.49 MHz, CD_2Cl_2, 298 K): δ = −33.3 (d, $^2J_{P–Si}$ = 2.5 Hz).

Elemental analysis: $C_{14}H_{26}NPSSi$: calcd.: C 56.15, H 8.75, N 4.68; found: C 56.18, H 8.54, N 4.62. **HR(+ESI)-MS**: calcd. *m/z* for $C_{14}H_{27}NPSSi$ [(M+H)$^+$]: 299.1293, found: 194.1131 {fragmentation peak equals [(*t*Bu$_2$(PS)NH$_2$+H)$^+$]: calcd. *m/z* for $C_8H_{21}NPS$ [(M+H)$^+$]: 194.1127.}

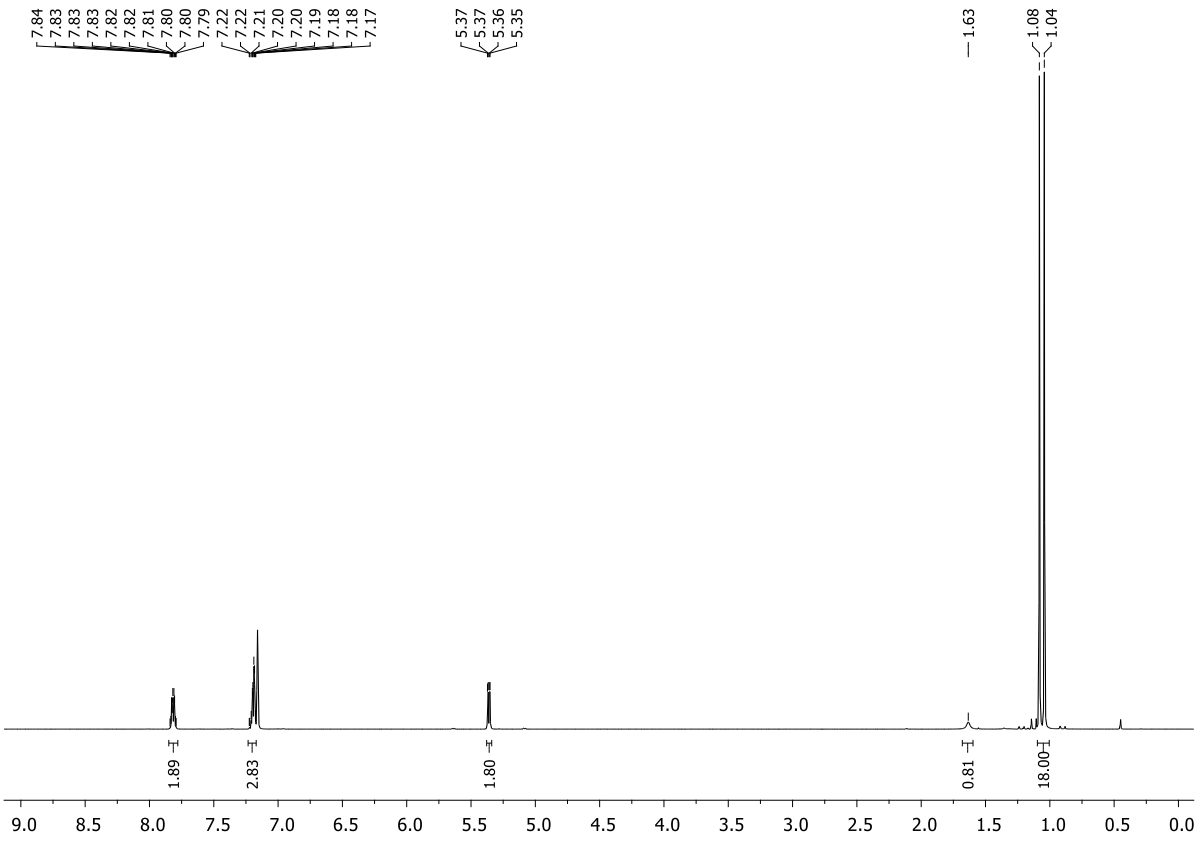

Figure S5.47. ^{1}H NMR spectrum (C_6D_6, 298 K) of **10**.

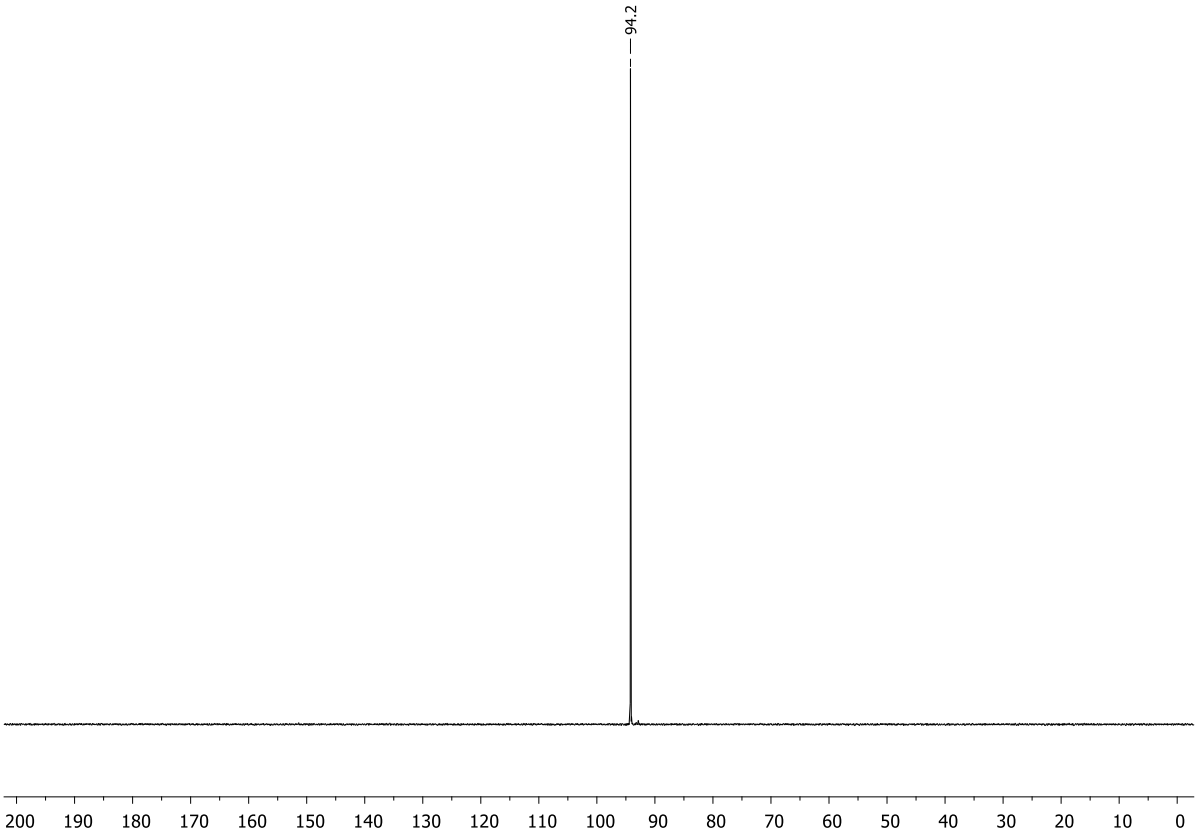

Figure S5.48. $^{31}P\{^{1}H\}$ NMR spectrum (C_6D_6, 298 K) of **10**.

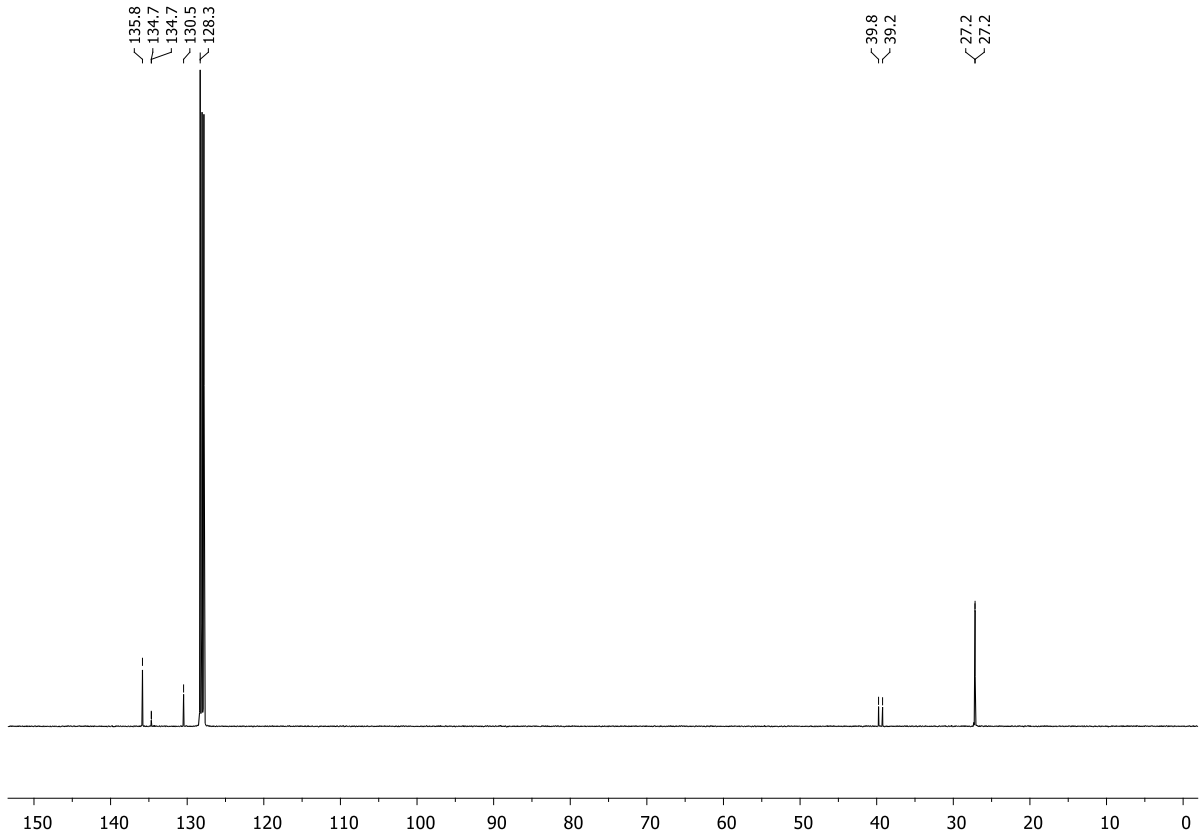

Figure S5.49. $^{13}C\{^{1}H\}$ NMR spectrum (C_6D_6, 298 K) of **10**.

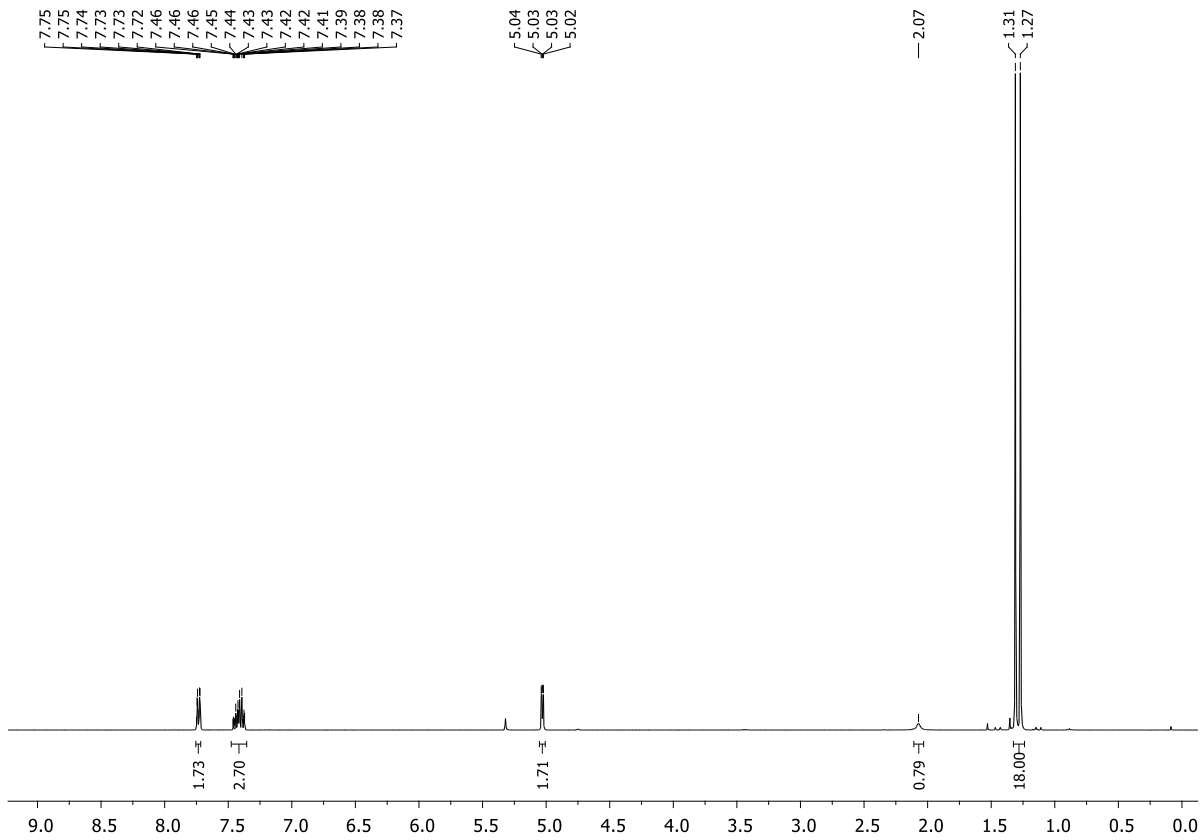

Figure S5.50. ^{1}H NMR spectrum (CD_2Cl_2, 298 K) of **10**.

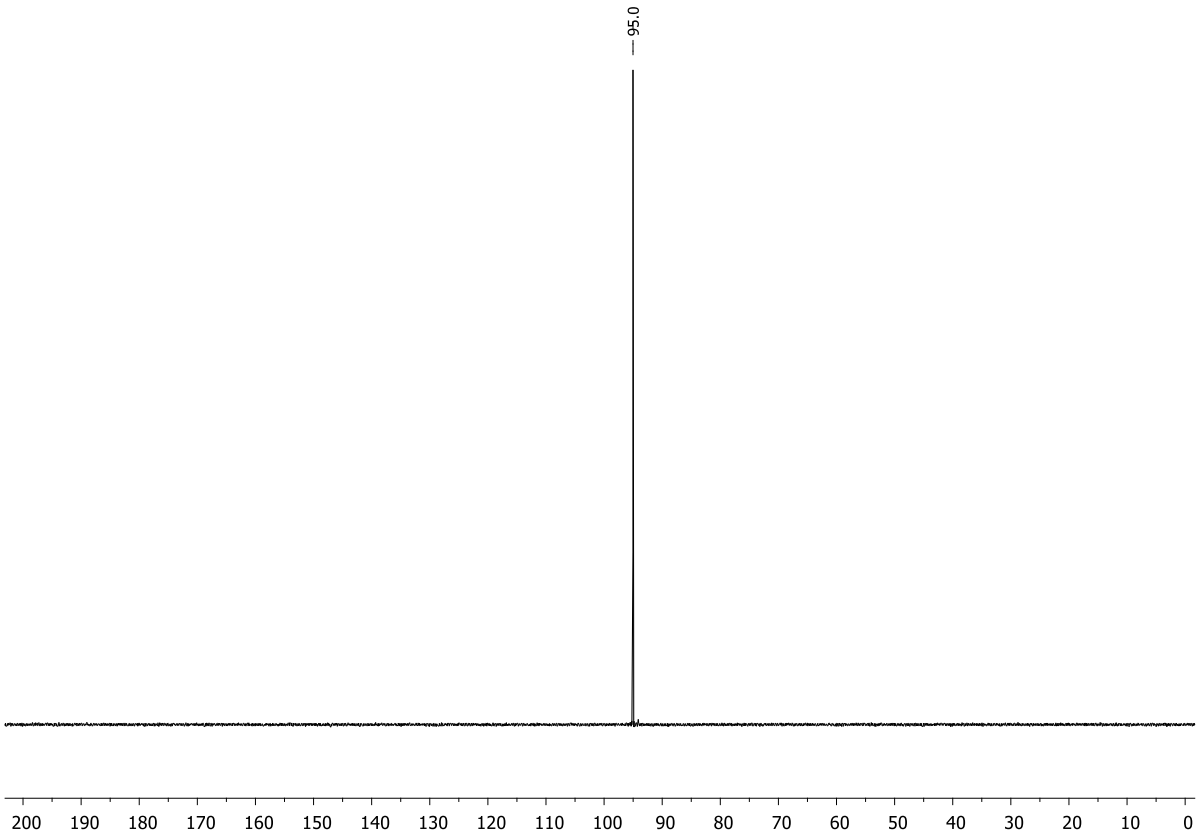

Figure S5.51. $^{31}P\{^{1}H\}$ NMR spectrum (CD_2Cl_2, 298 K) of **10**.

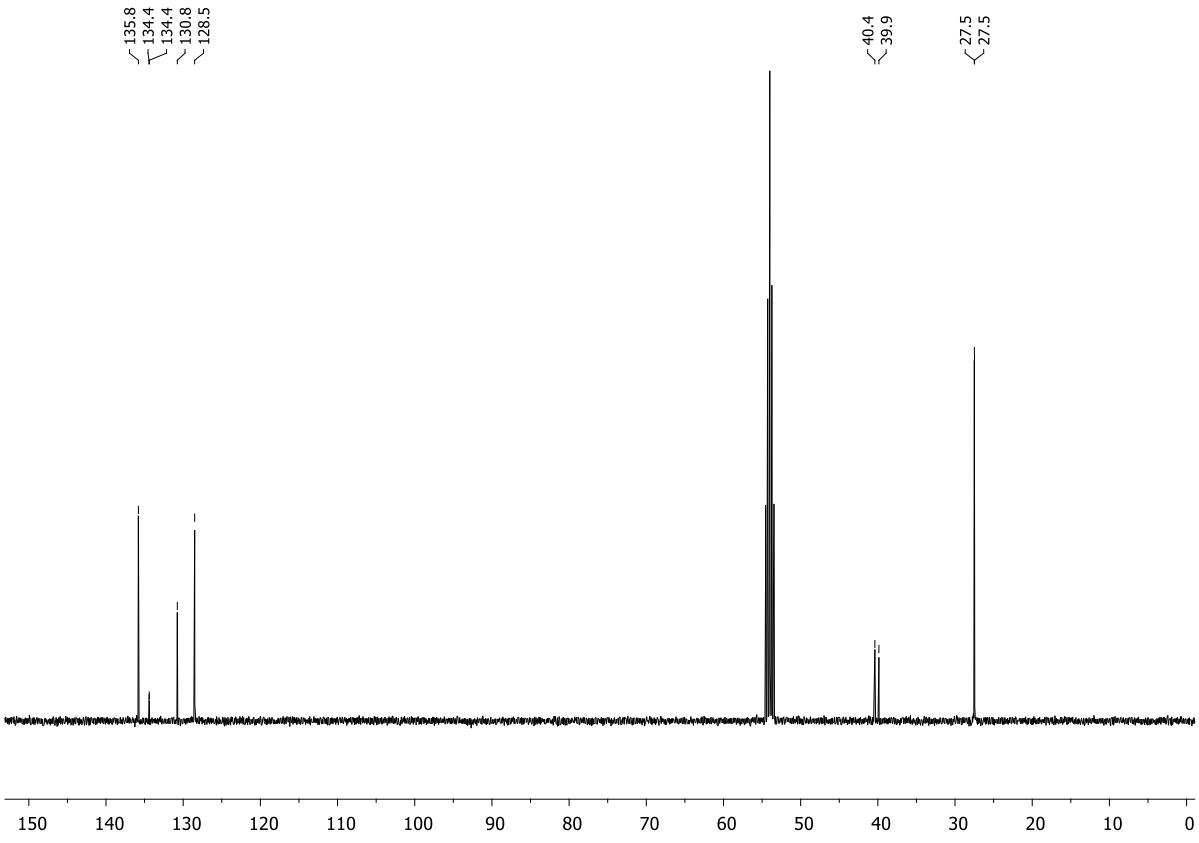

Figure S5.52. $^{13}C\{^{1}H\}$ NMR spectrum (CD_2Cl_2, 298 K) of **10**.

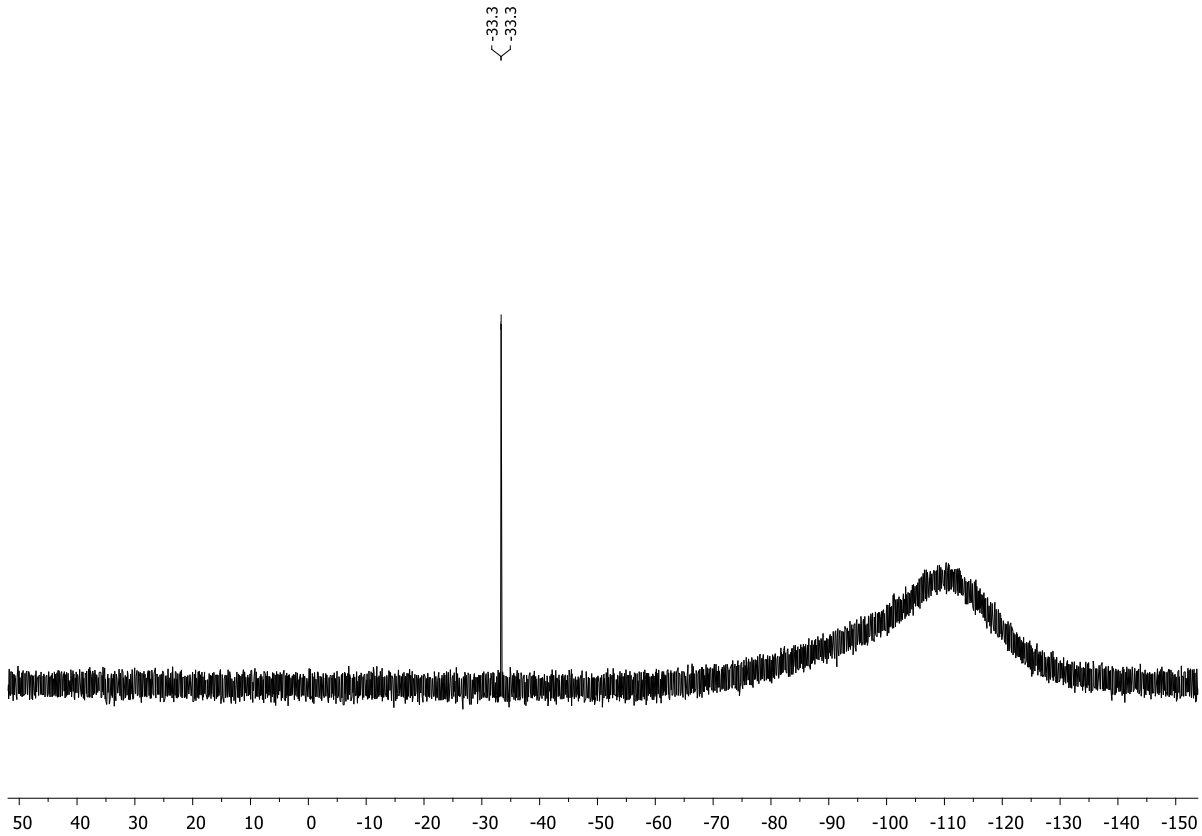

Figure S5.53. $^{29}Si\{^{1}H\}$ NMR spectrum (CD_2Cl_2, 298 K) of **10**.

5.6.2.10. Synthesis of [*t*Bu$_2$(PS)NH(SiHPh)]$^+$ [HB(C$_6$F$_5$)$_3$]$^-$ {*rac*-11[HB(C$_6$F$_5$)$_3$]}

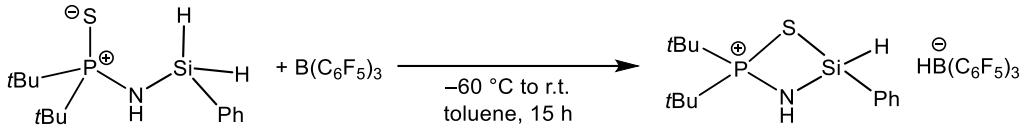

10 *rac*-**11**[HB(C$_6$F$_5$)$_3$]

A solution of compound **10** (0.25 g, 0.84 mmol, 1.0 equiv.) in toluene (4 mL) was added to a solution of tris(pentafluorophenyl)borane (0.43 g, 0.84 mmol, 1.0 equiv.) in toluene (4 mL) at –40 °C. The solution was allowed to slowly warm to room temperature and stirred for 15 h. The solvent was then removed in vacuo and the remaining colorless solid was washed with pentane. Compound *rac*-**11**[HB(C$_6$F$_5$)$_3$] was identified by ^{1}H and ^{31}P{^{1}H} NMR spectroscopy and could only be obtained in 85% pure form with several small impurities. Attempts to obtain single crystals of compound *rac*-**11**[HB(C$_6$F$_5$)$_3$] have failed so far, leading to an oily precipitate.

^{1}H NMR (400.13 MHz, CD_2Cl_2, 298 K): δ = 1.58 (d, $^3J_{H–P}$ = 19.2 Hz, 18H, PC(C*H*$_3$)$_3$), 4.14 (br, 1H, N*H*), 6.00 (br, 1H, Si*H*), 7.48–7.59 (m, 3H, *H*$_{Ph}$), 7.74–7.76 (m, 2H, *H*$_{Ph}$). **^{31}P{^{1}H} NMR** (162.04 MHz, CD_2Cl_2, 298 K): δ = 116.1 (s). **^{13}C{^{1}H} NMR** (100.61 MHz, CD_2Cl_2, 298 K): δ = 26.3 (d, $^2J_{C–P}$ = 2.4 Hz, PC(*C*H$_3$)$_3$), 42.7 (d, $^1J_{C–P}$ = 29.6 Hz, P*C*(CH$_3$)$_3$), 128.7 (s, *C*$_{Ph}$), 129.6 (s, *C*$_{Ph}$), 134.7 (s, *C*$_{Ph}$), 134.9 (s, *C*$_{Ph}$). **^{11}B{^{1}H} NMR** (128.43 MHz, CD_2Cl_2, 298 K): δ = –24.8 (s). **^{19}F{^{1}H} NMR** (376.66 MHz, CD_2Cl_2, 298 K): δ = –166.6 (m, 6F, *meta*-*F*$_{Ar\text{-}borate}$), –163.8 (m, 3F, *para*-*F*$_{Ar\text{-}borate}$), –133.3 (m, 6F, *ortho*-*F*$_{Ar\text{-}borate}$).

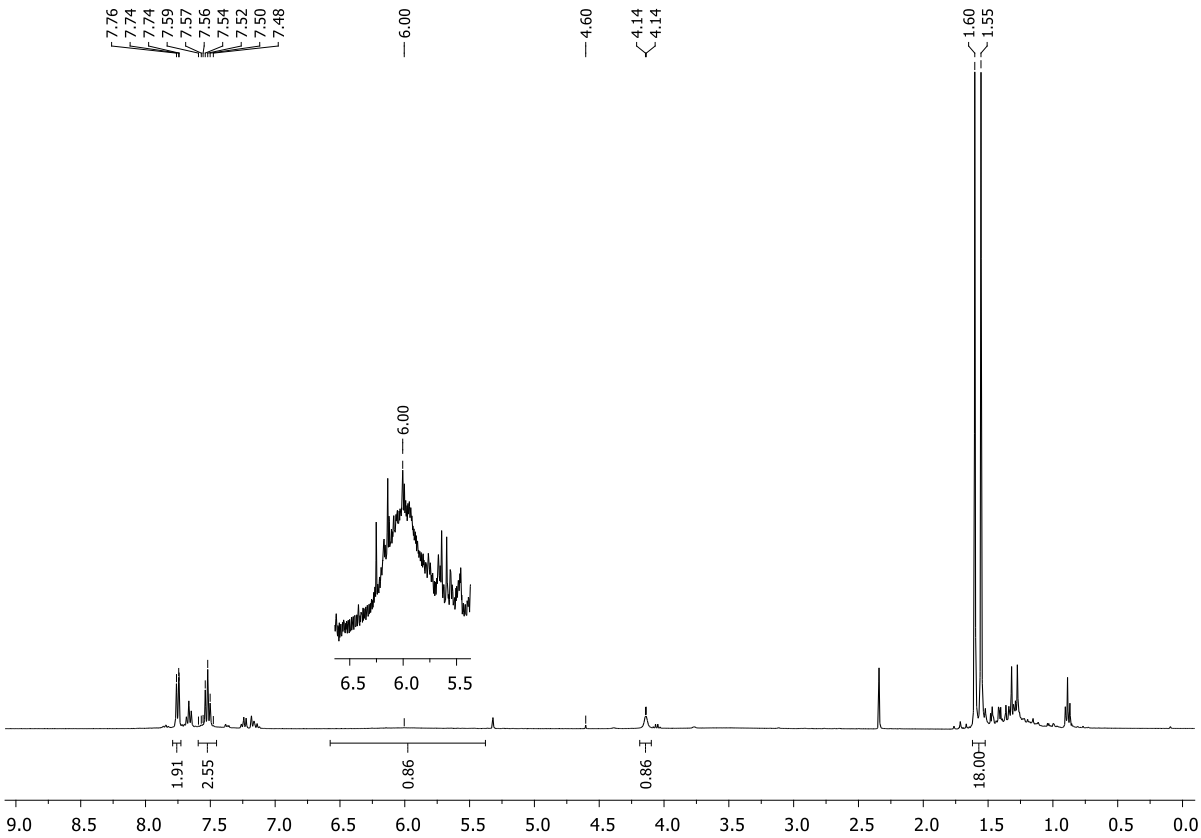

Figure S5.54. ^{1}H NMR spectrum (CD_2Cl_2, 298 K) of *rac*-**11**[$HB(C_6F_5)_3$].

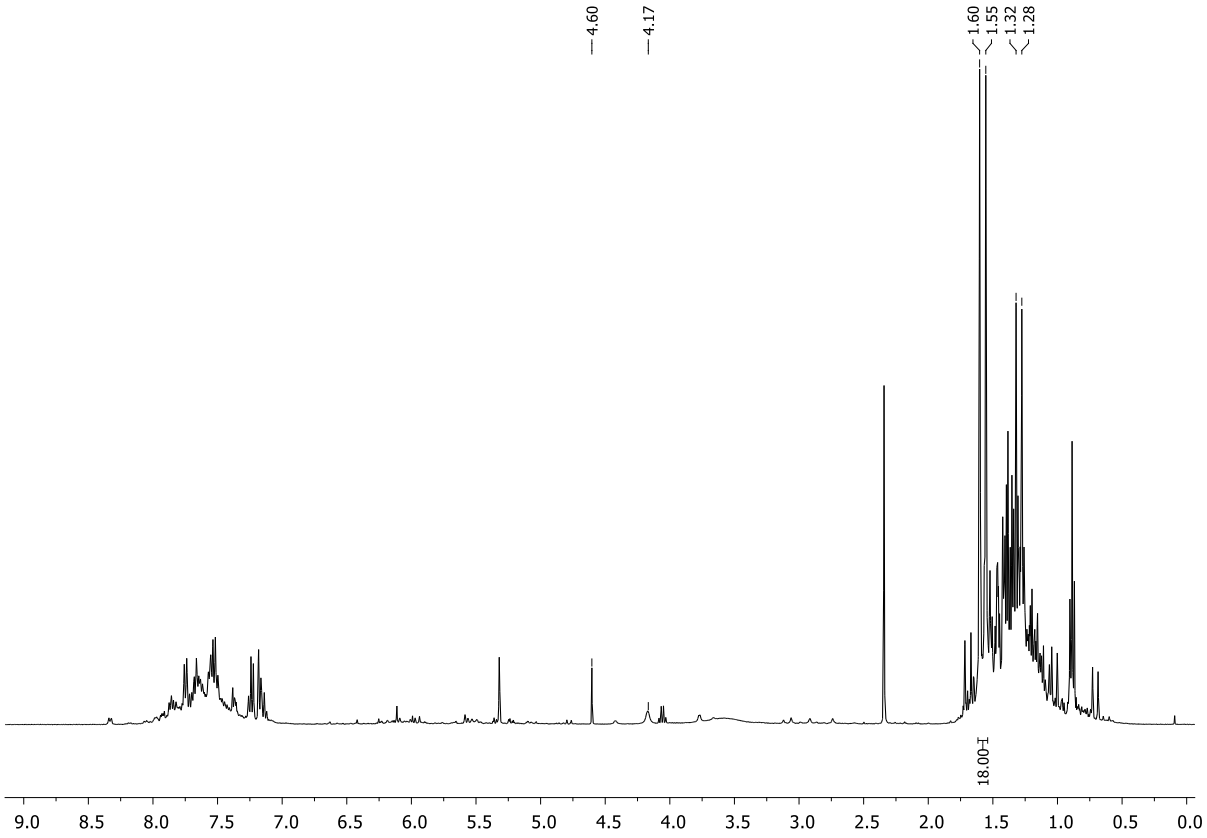

Figure S5.55. ^{1}H NMR spectrum (CD_2Cl_2, 298 K) of *rac*-**11**[$HB(C_6F_5)_3$] after one day at room temperature showing increasing dihydrogen formation at 4.60 ppm and progressive decomposition.

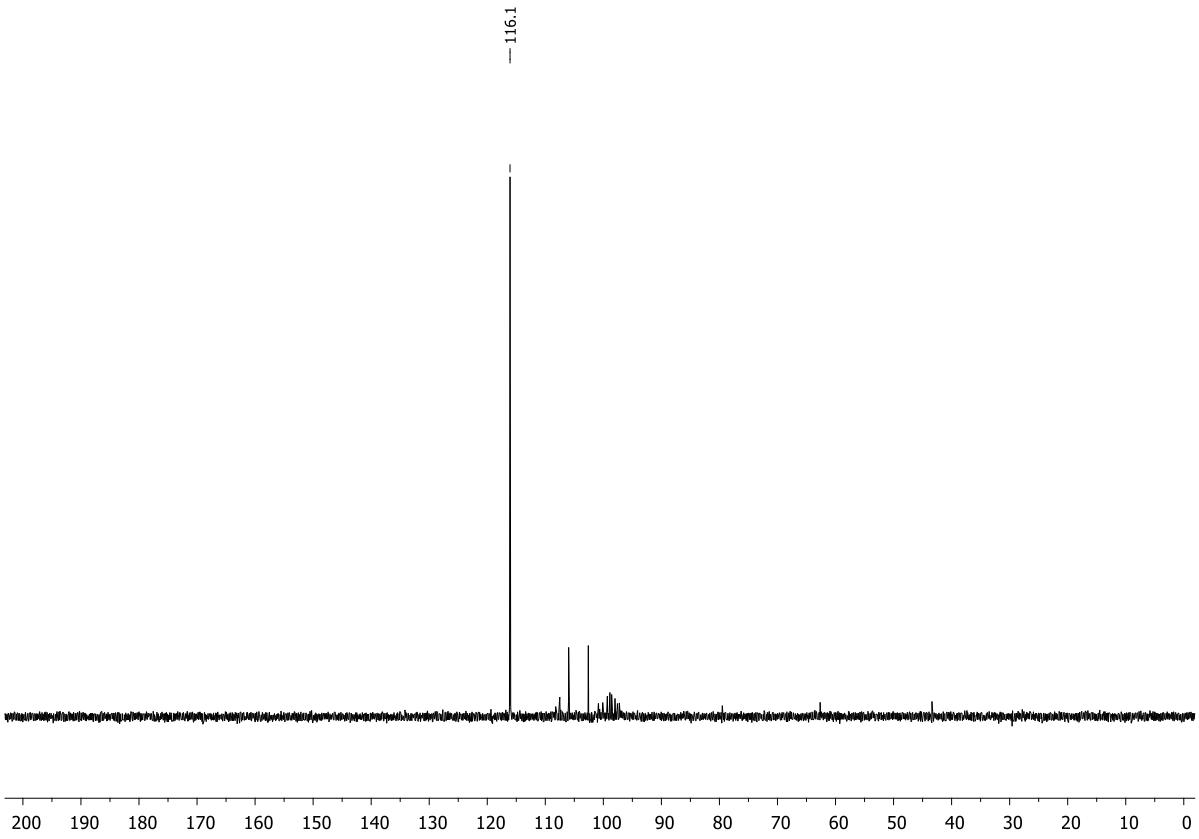

Figure S5.56. $^{31}P\{^{1}H\}$ NMR spectrum (CD_2Cl_2, 298 K) of *rac*-**11**[$HB(C_6F_5)_3$].

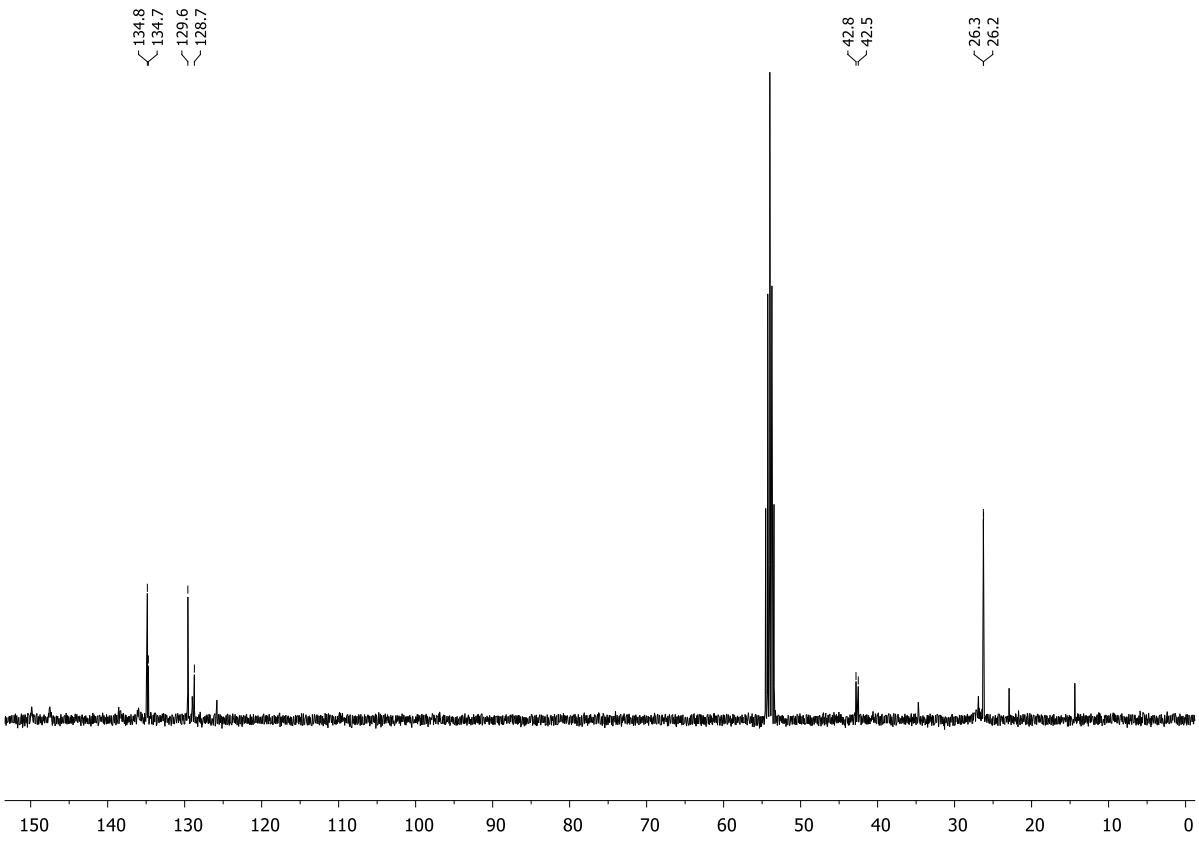

Figure S5.57. $^{13}C\{^{1}H\}$ NMR spectrum (CD_2Cl_2, 298 K) of *rac*-**11**[$HB(C_6F_5)_3$].

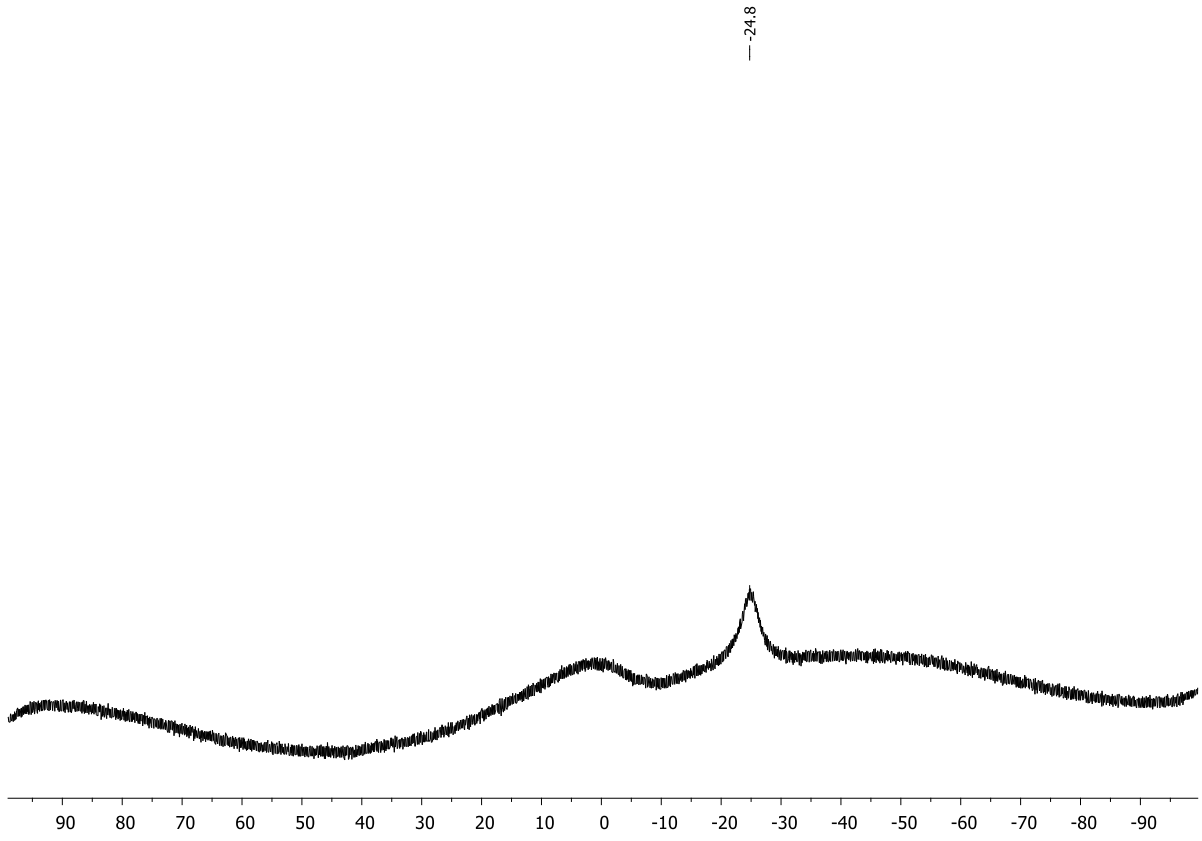

Figure S5.58. $^{11}B\{^{1}H\}$ NMR spectrum (CD_2Cl_2, 298 K) of *rac*-**11**[$HB(C_6F_5)_3$].

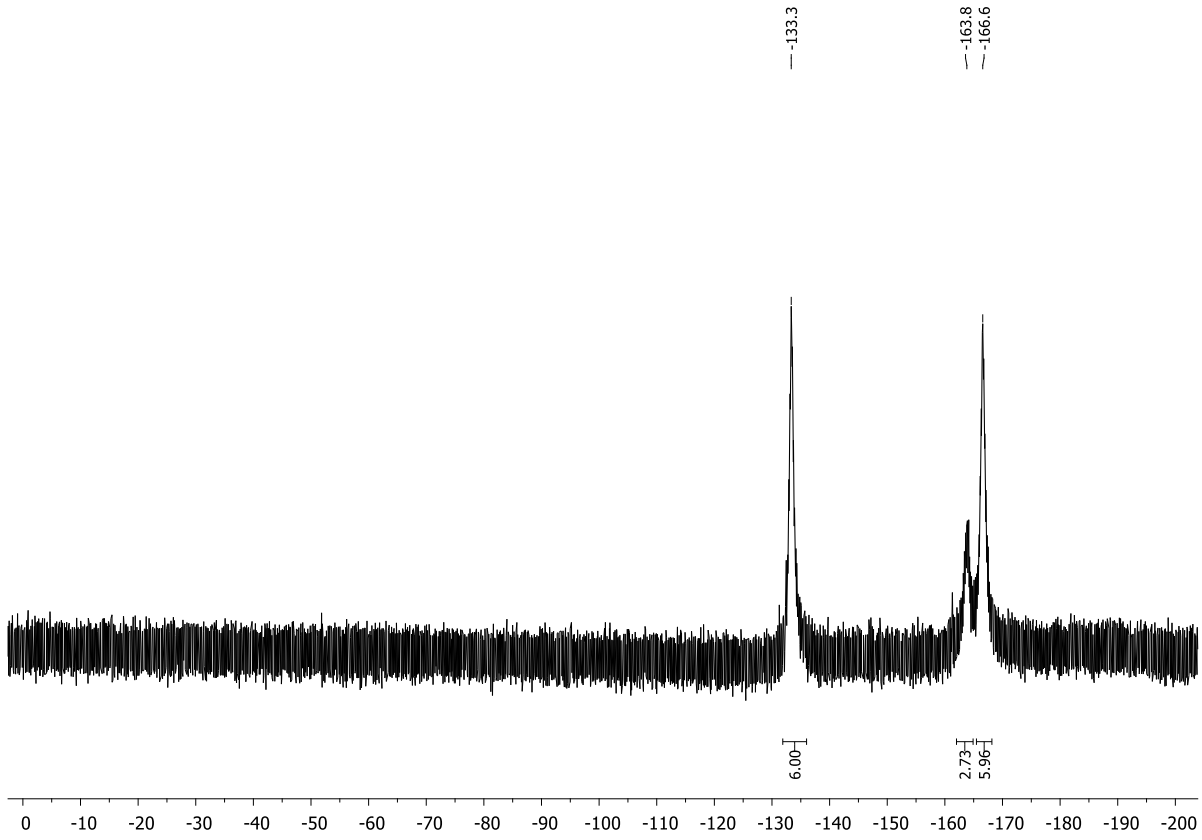

Figure S5.59. $^{19}F\{^{1}H\}$ NMR spectrum (CD_2Cl_2, 298 K) of *rac*-**11**[$HB(C_6F_5)_3$].

5.6.2.11. Synthesis of (R_P)-*t*BuCy(PS)NH(SiH*i*Pr$_2$) [(R_P)-13]

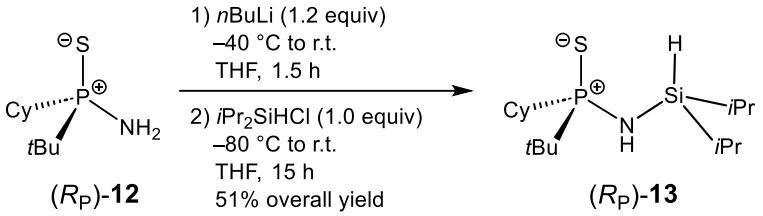

*n*Butyllithium (0.33 mL, 0.82 mmol, 1.2 equiv., 2.5 M in hexane) was added dropwise to a solution of (R_P)-*P*-(*tert*-butyl)-*P*-cyclohexylphosphinothioic amide [(R_P)-**12**] (150 mg, 0.68 mmol, 1.0 equiv.) in THF (6 mL) at −30 °C. The solution was allowed to warm to room temperature and stirred for 1.5 h. Following, the yellow solution was cooled to −80 °C and chlorodiisopropylsilane (102 mg, 0.68 mmol, 1.0 equiv.) was added dropwise. The reaction mixture was allowed to slowly warm to room temperature and stirred for 15 h affording a colorless solution. All volatiles were removed in vacuo and the product was extracted with diethyl ether. The filtered solution was kept at 8 °C for 20 h to yield colorless crystals suitable for single-crystal X-ray analysis, which were filtered off via cannula filtration and washed with pentane. After drying in vacuo, compound (R_P)-**13** was obtained as colorless crystals (117 mg, 0.35 mmol, 51%).

^{1}H NMR (400.13 MHz, C_6D_6, 298 K): δ = 1.02–1.11 (m, 12H, SiCH(CH_3)$_2$), 1.11 (d, $^3J_{H–P}$ = 15.6 Hz, 9H, PC(CH_3)$_3$), 1.15–1.19 (m, 1H, CH_2), 1.20–1.29 (m, 1H, SiCH(CH$_3$)$_2$), 1.31–1.44 (m, 1H, SiCH(CH$_3$)$_2$), 1.53 (br, 1H, NH), 1.55–1.73 (m 4H, CH_2), 1.79–1.86 (m, 1H, CH_2), 2.03–2.11 (m 1H, CH_2), 4.71 (m, 1H, SiH). **^{31}P{^{1}H} NMR** (162.04 MHz, C_6D_6, 298 K): δ = 85.2 (s).

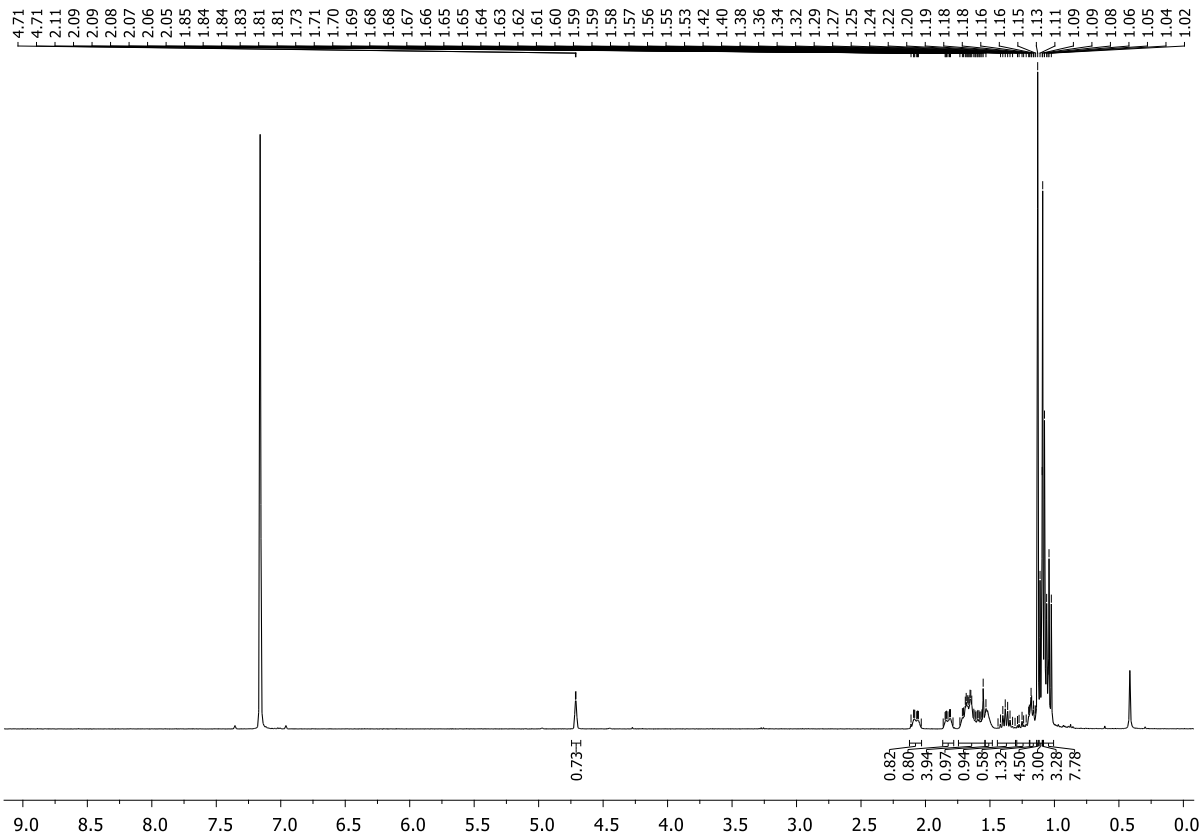

Figure S5.60. ^{1}H NMR spectrum (C_6D_6, 298 K) of (R_P)-**13**.

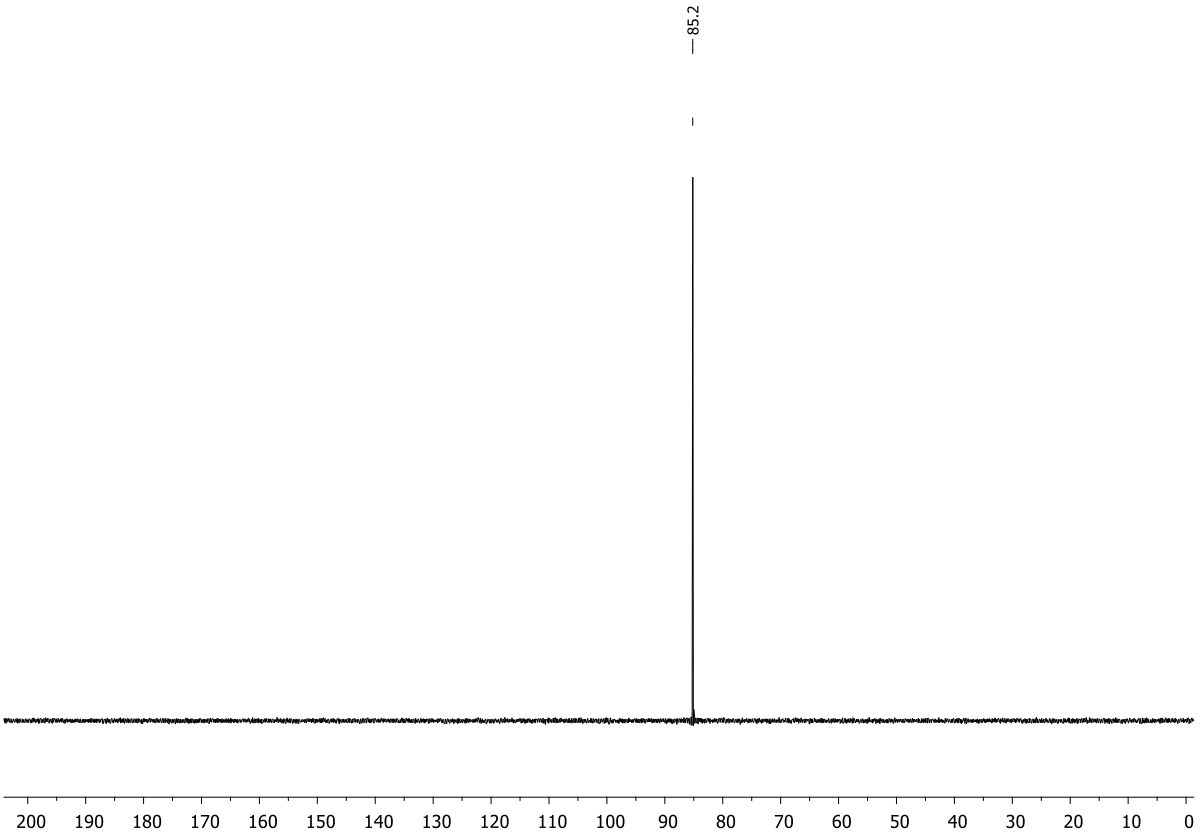

Figure S5.61. $^{31}P\{^{1}H\}$ NMR spectrum (C_6D_6, 298 K) of (R_P)-**13**.

5.6.2.12. Synthesis of (R_P)-*t*BuCy(PS)NH(SiH$_2$Ph) [(R_P)-14]

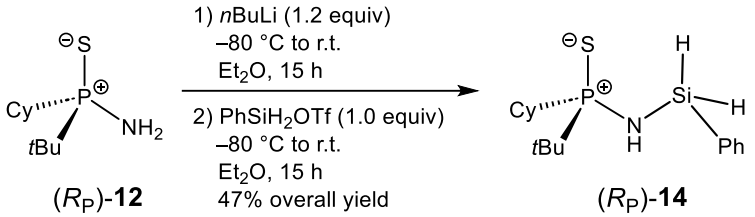

(R_P)-**12** (R_P)-**14**

*n*Butyllithium (0.9 mL, 2.18 mmol, 1.2 equiv., 2.5 M in hexane) was added dropwise to a solution of (R_P)-*P*-(*tert*-butyl)-*P*-cyclohexylphosphinothioic amide [(R_P)-**12**] (400 mg, 1.82 mmol, 1.0 equiv.) in diethyl ether (10 mL) at –80 °C. The solution was allowed to slowly warm to room temperature and stirred for 15 h. Following, the colorless solution was cooled to –80 °C again and phenylsilyl triflate (466 mg, 1.82 mmol, 1.0 equiv.), which was prepared shortly before addition in a separate Schlenk tube according to a literature procedure,[4] was added dropwise. The reaction mixture was allowed to slowly warm to room temperature and stirred for 15 h affording a colorless solution. All volatiles were removed in vacuo, the remaining solid was washed with pentane and the crude product was extracted with toluene. By layering the toluene solution with pentane, colorless crystals suitable for single-crystal X-ray analysis were obtained. Those were filtered off via cannula filtration and washed with pentane. After drying in vacuo, compound (R_P)-**14** was obtained as colorless crystals (0.28 g, 0.86 mmol, 47%).

^{1}H NMR (400.13 MHz, C_6D_6, 298 K): δ = 1.01 (d, $^3J_{H–P}$ = 15.8 Hz, 9H, PC(C*H*$_3$)$_3$), 1.34 (br, 1H, N*H*), 1.43–1.70 (m, 7H, C*H*$_2$), 1.79–1.92 (m, 1H, C*H*), 5.32 (m, 2H, Si*H*), 7.18–7.23 (m, 3H, *H*$_{Ph}$), 7.78–7.82 (m, 2H, *H*$_{Ph}$). **^{31}P{^{1}H} NMR** (162.04 MHz, C_6D_6, 298 K): δ = 87.4 (s). **^{13}C{^{1}H} NMR** (100.61 MHz, CD_2Cl_2, 298 K): δ = 25.7 (d, $^2J_{C–P}$ = 1.7 Hz, PC(*C*H$_3$)$_3$), 25.9 (d, $^3J_{C–P}$ = 1.6 Hz, *C*H$_2$), 26.6 (d, $^2J_{C–P}$ = 10.9 Hz, *C*H$_2$), 26.7 (s, *C*H$_2$), 26.9 (d, $^2J_{C–P}$ = 12.8 Hz, *C*H$_2$), 28.3 (s, *C*H$_2$), 37.2 (d, $^1J_{C–P}$ = 58.5 Hz, P*C*(CH$_3$)$_3$), 39.6 (d, $^1J_{C–P}$ = 55.8 Hz, P*C*H), 128.3 (s, *C*$_{Ph}$), 130.4 (s, *C*$_{Ph}$), 134.6 (d, $^3J_{C–P}$ = 2.5 Hz, *C*$_{ipso}$), 135.8 (s, *C*$_{Ph}$).

^{1}H NMR (400.13 MHz, CD_2Cl_2, 298 K): δ = 1.21 (d, $^3J_{H–P}$ = 16.0 Hz, 9H, PC(C*H*$_3$)$_3$), 1.27 (br, 1H, N*H*), 1.30–1.34 (m, 1H, C*H*$_2$), 1.40–1.54 (m, 2H, C*H*$_2$), 1.67–1.69 (m, 1H, C*H*), 1.75–2.02 (m, 7H, C*H*$_2$), 5.01 (m, 2H, Si*H*), 7.38–7.46 (m, 3H, *H*$_{Ph}$), 7.71–7.73 (m, 2H, *H*$_{Ph}$). **^{31}P{^{1}H} NMR** (162.04 MHz, CD_2Cl_2, 298 K): δ = 88.2 (s). **^{13}C{^{1}H} NMR** (100.61 MHz, CD_2Cl_2, 298 K): δ = 25.8 (d, $^2J_{C–P}$ = 1.6 Hz, PC(*C*H$_3$)$_3$), 26.3 (d, $^3J_{C–P}$ = 1.6 Hz, *C*H$_2$), 26.9 (d, $^2J_{C–P}$ = 14.5 Hz, *C*H$_2$), 27.1 (d, $^2J_{C–P}$ = 12.8 Hz, *C*H$_2$), 27.3 (d, $^3J_{C–P}$ = 3.8 Hz, *C*H$_2$), 28.7 (s, *C*H$_2$), 37.6 (d, $^1J_{C–P}$ = 58.3 Hz, P*C*(CH$_3$)$_3$), 39.9 (d, $^1J_{C–P}$ = 55.5 Hz, P*C*H), 128.5 (s, *C*$_{Ph}$), 130.8 (s, *C*$_{Ph}$), 134.3 (d, $^3J_{C–P}$ = 3.1 Hz, *C*$_{ipso}$), 135.7 (s, *C*$_{Ph}$). **^{29}Si{^{1}H} NMR** (79.49 MHz, CD_2Cl_2, 298 K): δ = –34.3 (d, $^2J_{P–Si}$ = 2.2 Hz).

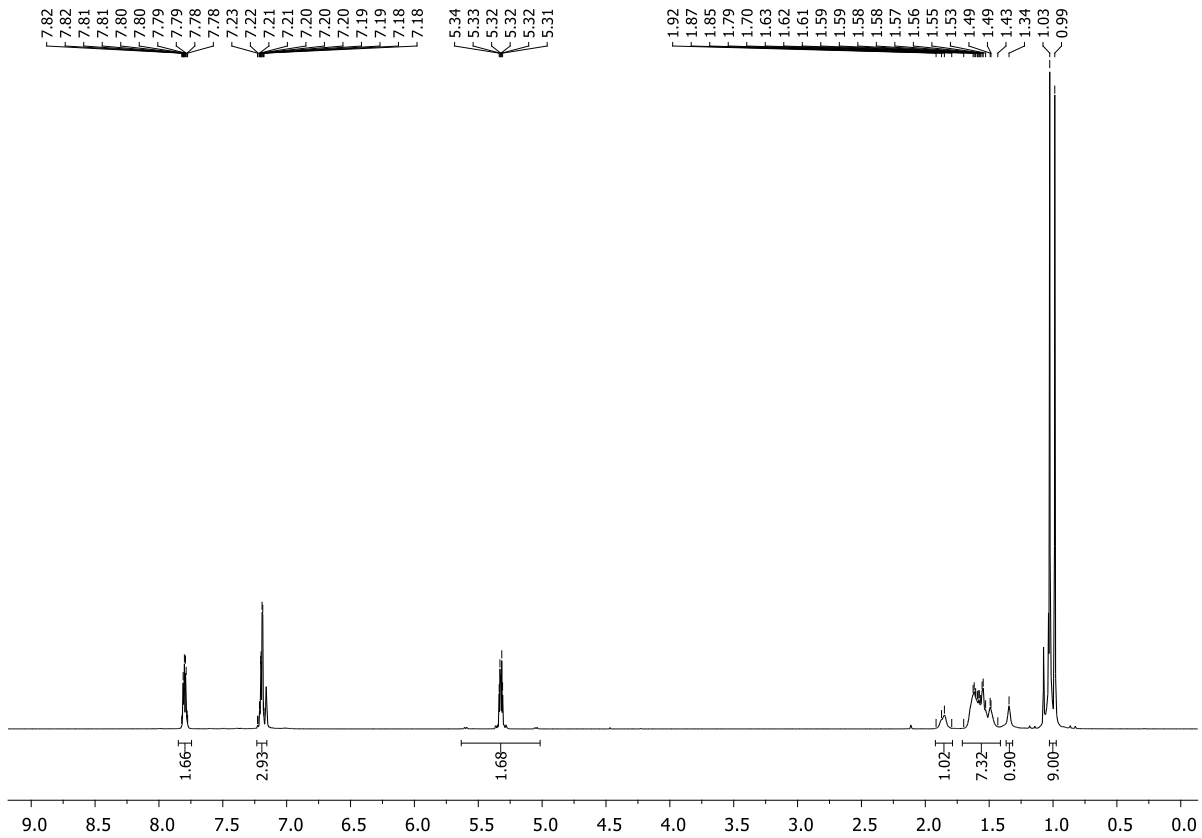

Figure S5.62. ^{1}H NMR spectrum (C_6D_6, 298 K) of (R_P)-**14**.

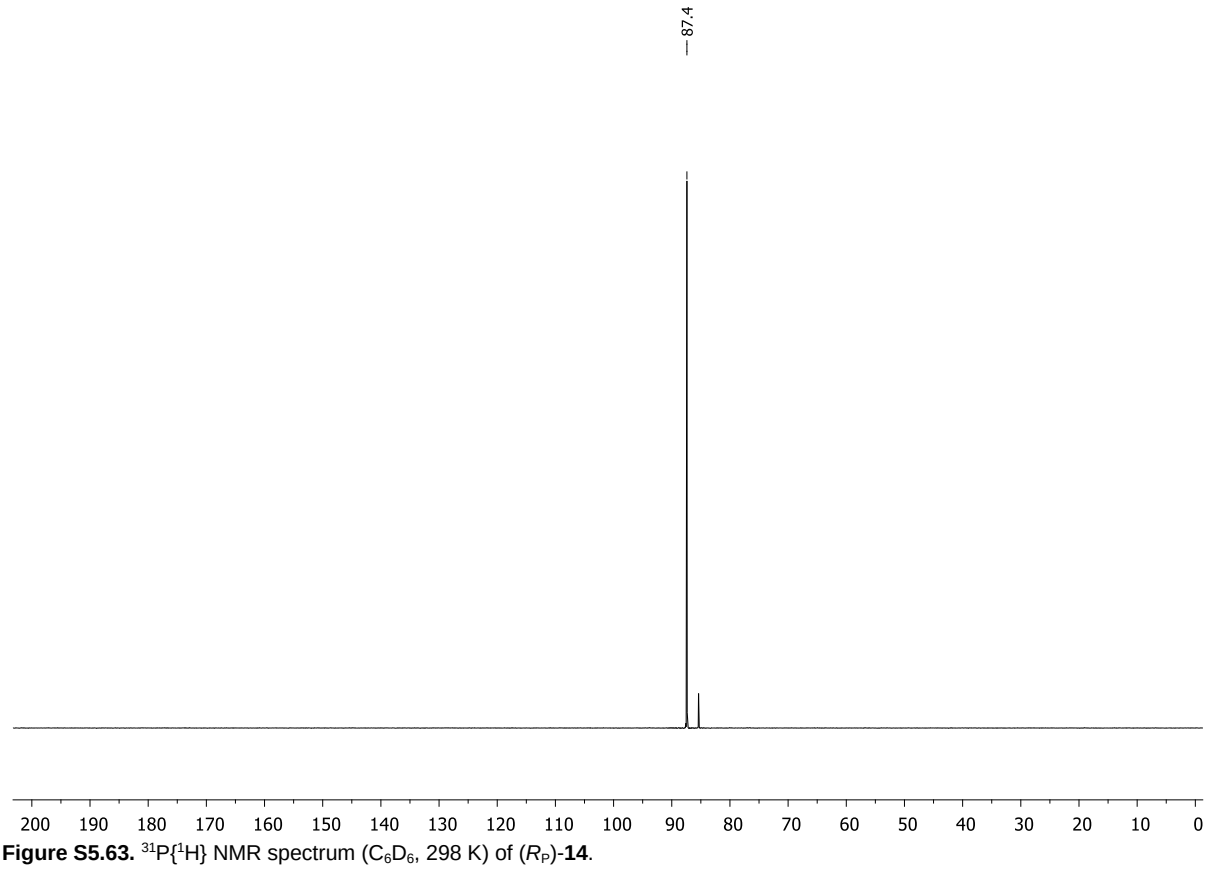

Figure S5.63. ^{31}P{^{1}H} NMR spectrum (C_6D_6, 298 K) of (R_P)-**14**.

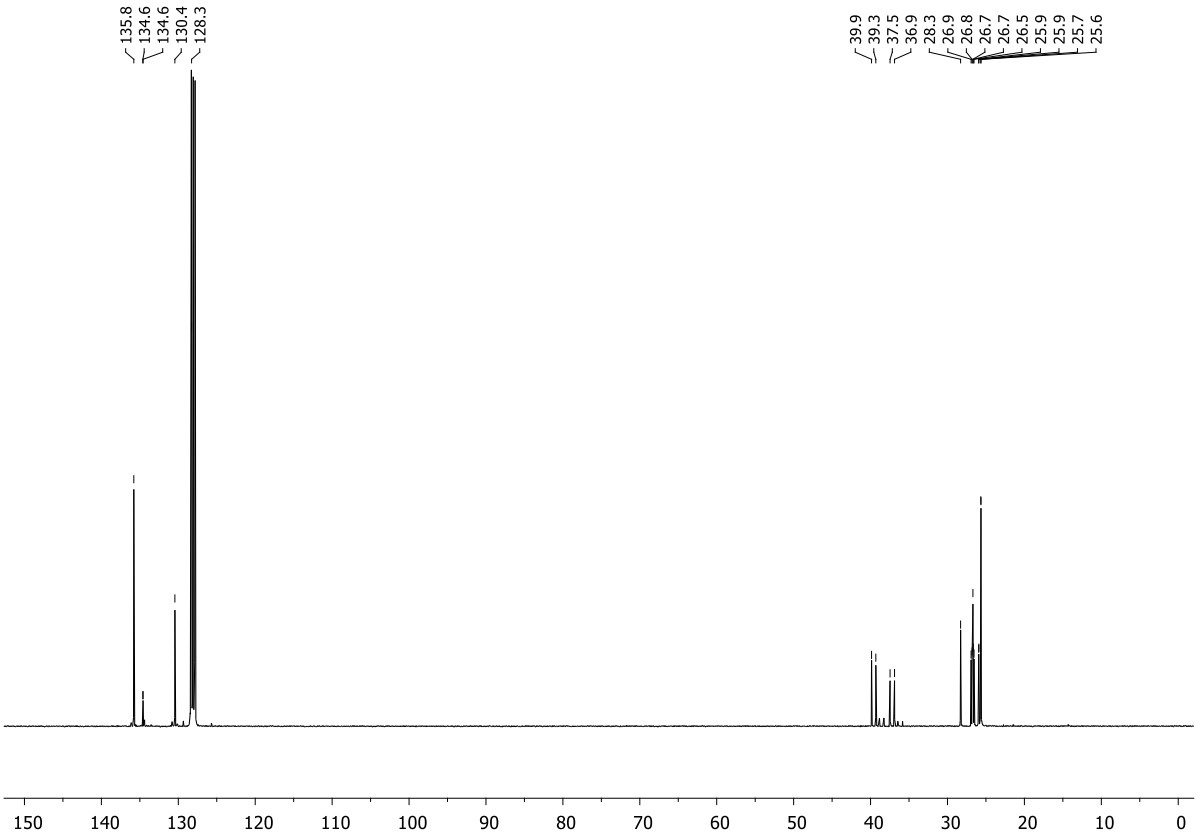

Figure S5.64. $^{13}C\{^{1}H\}$ NMR spectrum (C_6D_6, 298 K) of (R_P)-**14**.

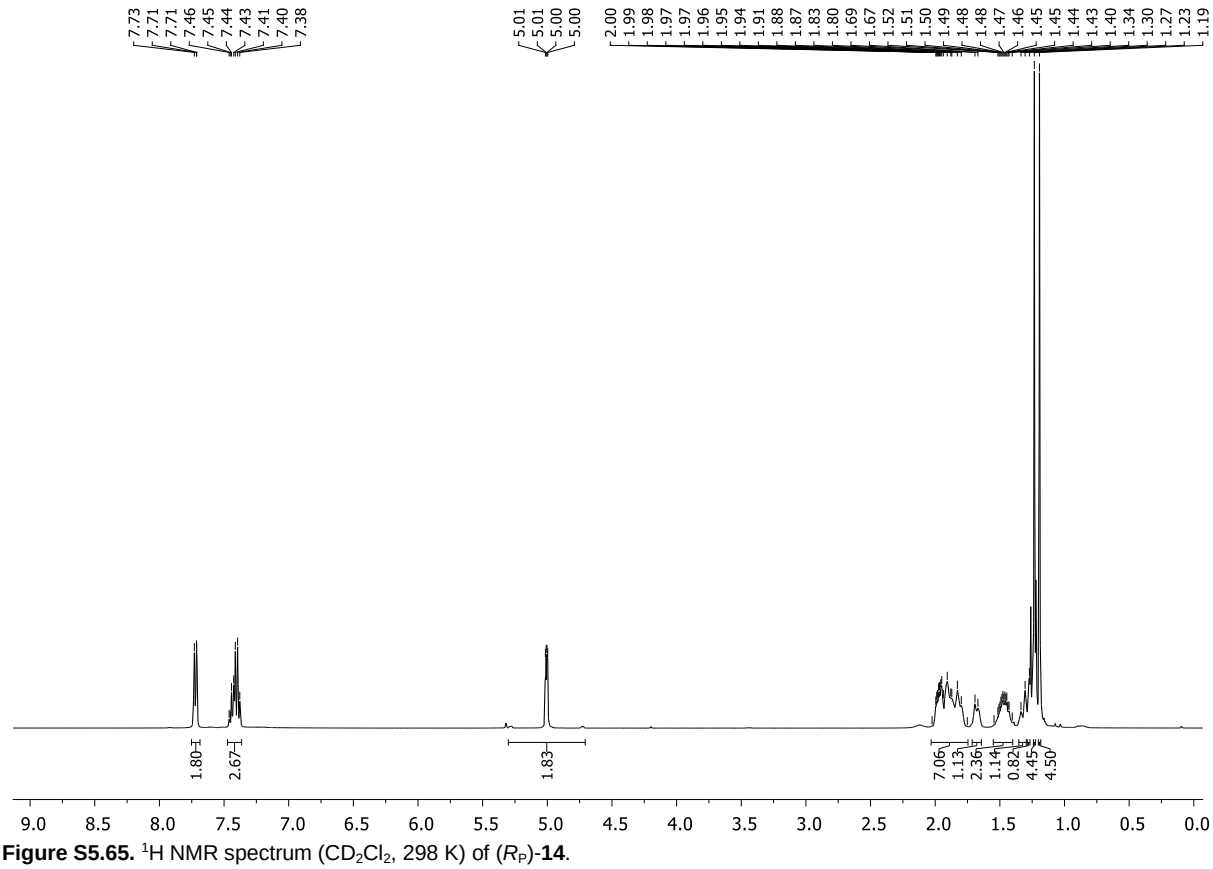

Figure S5.65. ^{1}H NMR spectrum (CD_2Cl_2, 298 K) of (R_P)-**14**.

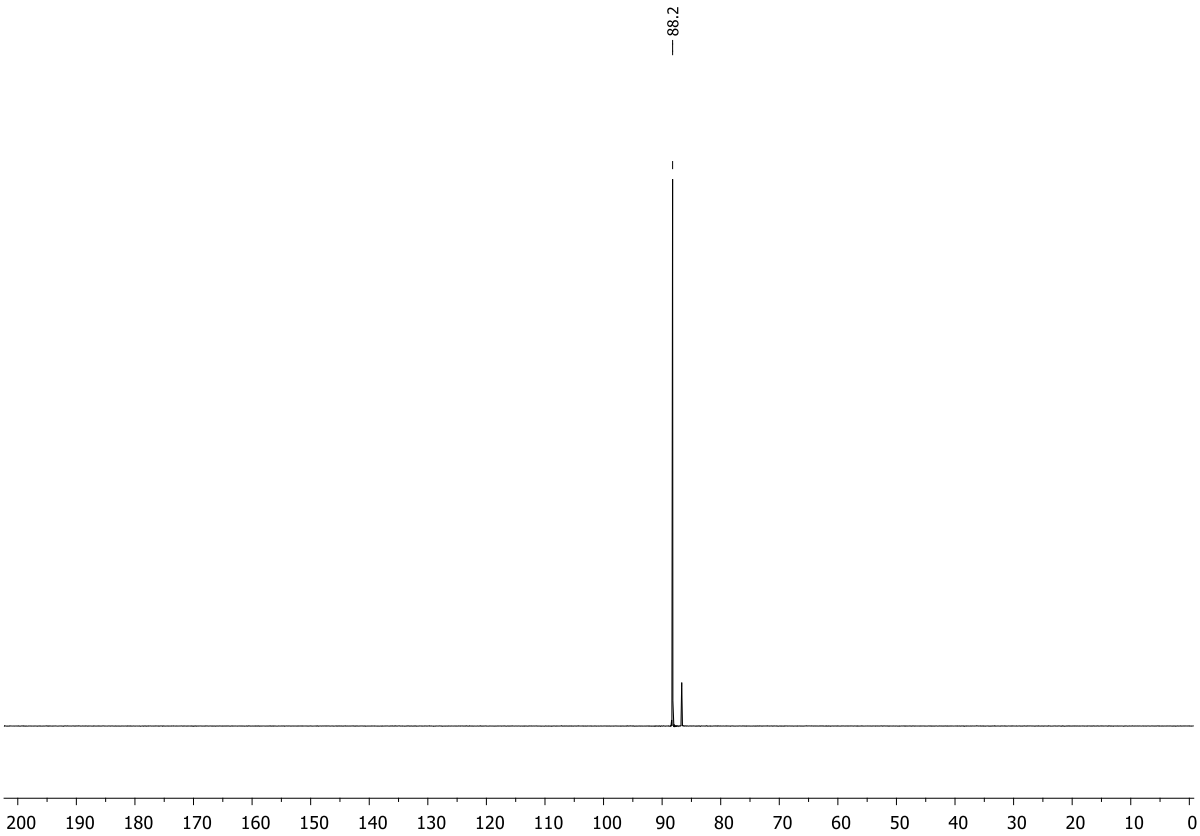

Figure S5.66. $^{31}P\{^{1}H\}$ NMR spectrum (CD_2Cl_2, 298 K) of (R_P)-**14**.

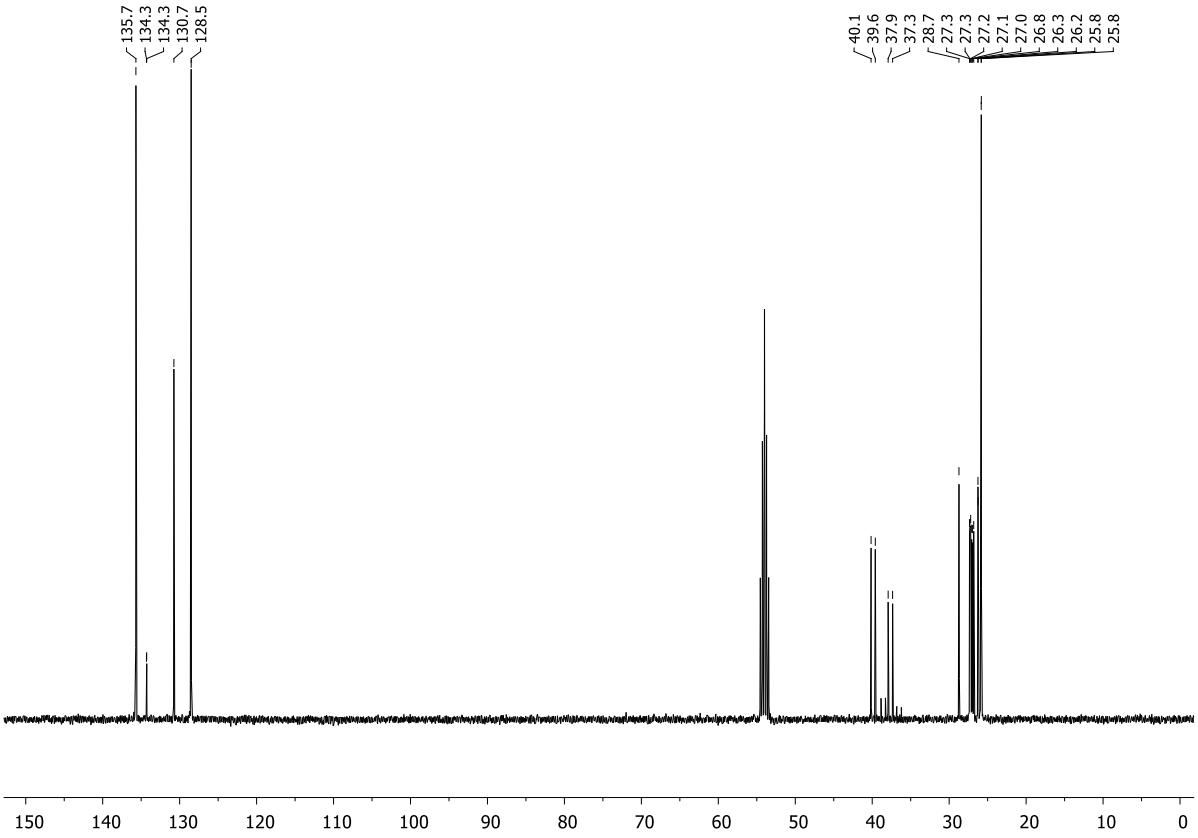

Figure S5.67. $^{13}C\{^{1}H\}$ NMR spectrum (CD_2Cl_2, 298 K) of (R_P)-**14**.

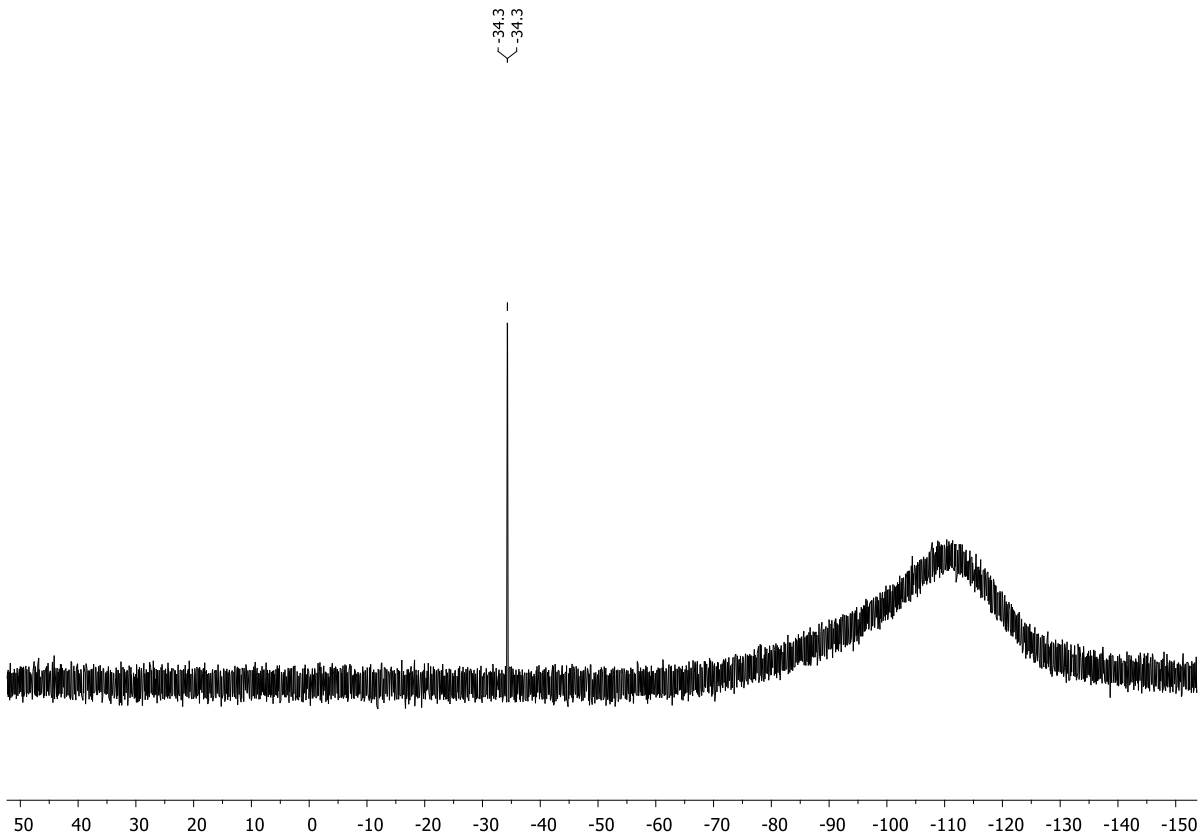

Figure S5.68. $^{29}Si\{^{1}H\}$ NMR spectrum (CD_2Cl_2, 298 K) of (R_P)-**14**.

5.6.2.13. Reaction of (R_P)-14 with BCF

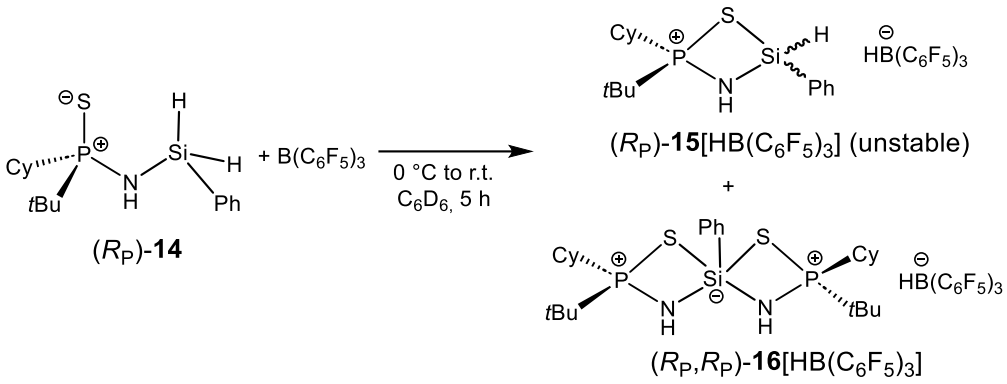

A solution of compound (R_P)-**14** (34.7 mg, 0.11 mmol, 1.0 equiv.) in C_6D_6 (1.0 mL) was added to a solution of tris(pentafluorophenyl)borane (54.6 mg, 0.11 mmol, 1.0 equiv.) in C_6D_6 (0.5 mL) at 0 °C in a Young NMR tube. The mixture was allowed to slowly warm to room temperature, affording a colorless solution. NMR spectroscopy of the crude reaction mixture was carried out without any purification, showing (R_P)-**15**[$HB(C_6F_5)_3$] and (R_P,R_P)-**16**[$HB(C_6F_5)_3$]. Then, all volatiles were removed in vacuo and the remaining solid was washed with pentane. After drying the resulting colorless solid in vacuo, NMR spectroscopy was carried out in CD_2Cl_2, showing only (R_P,R_P)-**16**[$HB(C_6F_5)_3$].

Crude reaction mixture containing (R_P)-**15**[$HB(C_6F_5)_3$] and (R_P,R_P)-**16**[$HB(C_6F_5)_3$]:
^{1}H NMR (400.13 MHz, C_6D_6, 298 K): δ = 0.70 (d, $^3J_{H–P}$ = 18.3 Hz, 5.1H, PC(CH_3)$_3$, (R_P)-**16**), 0.80 (d, $^3J_{H–P}$ = 19.8 Hz, 9H, PC(CH_3)$_3$, (R_P)-**15**), 0.86–1.08 (m, 10H, overlapping C*H* and CH_2 signals), 1.19–1.31 (m, 2H, overlapping CH_2 signals), 1.39–1.70 (m, 8H, overlapping CH_2 signals), 1.78–1.80 (m, 1H, overlapping CH_2 signals), 1.97–2.03 (m, 1H, overlapping CH_2 signals), 3.32 (d, $^2J_{H–P}$ = 3.9 Hz, 0.5H, N*H*, (R_P)-**16**), 3.99 (br, 1H, N*H*, (R_P)-**15**), 5.35 (br, 1H, Si*H*, (R_P)-**15**), 7.11–7.19 (m, 5H, overlapping H_{Ph} signals), 7.42–7.44 (m, 2H, overlapping H_{Ph} signals). **^{31}P{^{1}H} NMR** (162.04 MHz, C_6D_6, 298 K): δ = 108.2 (s, 0.62P, (R_P)-**15**), 95.6 (s, 0.38P, (R_P)-**16**). **^{13}C{^{1}H} NMR** (100.61 MHz, C_6D_6, 298 K): δ = 23.0 (d, $^2J_{C–P}$ = 1.9 Hz, PC(CH_3)$_3$), 23.9 (d, $^3J_{C–P}$ = 2.1 Hz, CH_2), 25.5 (d, $^2J_{C–P}$ = 13.3 Hz, CH_2), 25.9 (d, $^2J_{C–P}$ = 26.1 Hz, CH_2), 28.0 (d, $^3J_{C–P}$ = 2.5 Hz, CH_2), 28.5 (d, $^4J_{C–P}$ = 1.9 Hz, CH_2), 37.7 (d, $^1J_{C–P}$ = 34.9 Hz, PC(CH_3)$_3$), 38.6 (d, $^1J_{C–P}$ = 37.8 Hz, PCH), 129.1 (s, C_{Ph}), 133.1 (s, C_{Ph}), 134.1 (s, C_{Ph}), 134.3 (s, C_{Ph}), 137.5 (d, $^1J_{C–F}$ = 253.9 Hz, $C_{Ar\text{-}borate}$), 148.9 (d, $^1J_{C–F}$ = 229.5 Hz, $C_{Ar\text{-}borate}$), signals of (R_P)-**16** not visible. **^{11}B{^{1}H} NMR** (128.43 MHz, C_6D_6, 298 K): δ = −24.5 (s). **^{19}F{^{1}H} NMR** (376.66 MHz, C_6D_6, 298 K): δ = −166.7 (m, 6F, *meta*-$F_{Ar\text{-}borate}$), −162.5 (m, 3F, *para*-$F_{Ar\text{-}borate}$), −133.5 (m, 6F, *ortho*-$F_{Ar\text{-}borate}$).

(R_P,R_P)-**16**[$HB(C_6F_5)_3$]; after washing with pentane:
^{1}H NMR (400.13 MHz, CD_2Cl_2, 298 K): δ = 1.15 (d, $^3J_{H–P}$ = 18.4 Hz, 18H, PC(CH_3)$_3$), 1.63–2.03 (m, 20H, C*H*/CH_2), 2.24–2.33 (m, 2H, C*H*/CH_2), 3.73 (d, $^2J_{H–P}$ = 4.1 Hz, 2H, N*H*), 7.38–7.42 (m, 2H, H_{Ph}), 7.61–7.64 (m, 3H, H_{Ph}). **^{31}P{^{1}H} NMR** (162.04 MHz, CD_2Cl_2, 298 K): δ = 96.3 (s). **^{13}C{^{1}H} NMR**

(100.61 MHz, CD_2Cl_2, 298 K): δ = 24.6 (d, $^2J_{C–P}$ = 2.1 Hz, PC(CH_3)$_3$), 25.7 (d, $^3J_{C–P}$ = 1.9 Hz, CH_2), 26.5 (d, $^2J_{C–P}$ = 13.6 Hz, CH_2), 26.6 (d, $^2J_{C–P}$ = 14.8 Hz, CH_2), 28.4 (d, $^3J_{C–P}$ = 4.3 Hz, CH_2), 29.2 (d, $^4J_{C–P}$ = 2.5 Hz, CH_2), 36.9 (d, $^1J_{C–P}$ = 41.6 Hz, PC(CH_3)$_3$), 37.8 (d, $^1J_{C–P}$ = 44.6 Hz, PCH), 128.1 (s, C_{Ph}), 130.4 (s, C_{Ph}), 131.8 (s, C_{Ph}), 133.3 (s, C_{Ph}), 137.4 (d, $^1J_{C–F}$ = 250.2 Hz, $C_{Ar\text{-}borate}$), 148.7 (d, $^1J_{C–F}$ = 246.4 Hz, $C_{Ar\text{-}borate}$). **^{11}B{^{1}H} NMR** (128.43 MHz, CD_2Cl_2, 298 K): δ = –25.3 (s). **^{19}F{^{1}H} NMR** (376.66 MHz, CD_2Cl_2, 298 K): δ = –166.7 (m, 6F, *meta*-$F_{Ar\text{-}borate}$), –163.5 (m, 3F, *para*-$F_{Ar\text{-}borate}$), –134.6 (m, 6F, *ortho*-$F_{Ar\text{-}borate}$). **^{29}Si{^{1}H} NMR** (79.49 MHz, CD_2Cl_2, 298 K): δ = –81.7 (s).

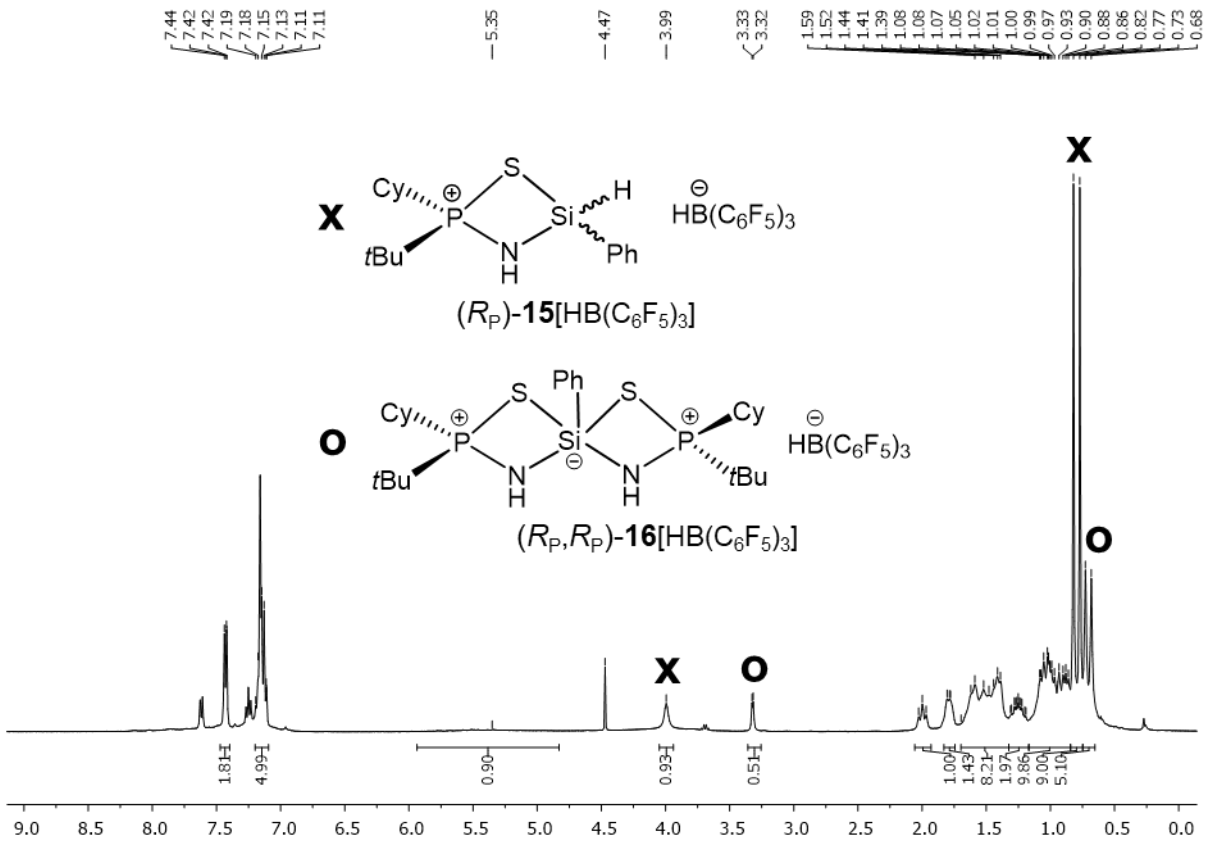

Figure S5.69. ^{1}H NMR spectrum (C_6D_6, 298 K) of the crude reaction mixture containing (R_P)-**15**[$HB(C_6F_5)_3$] and (R_P,R_P)-**16**[$HB(C_6F_5)_3$].

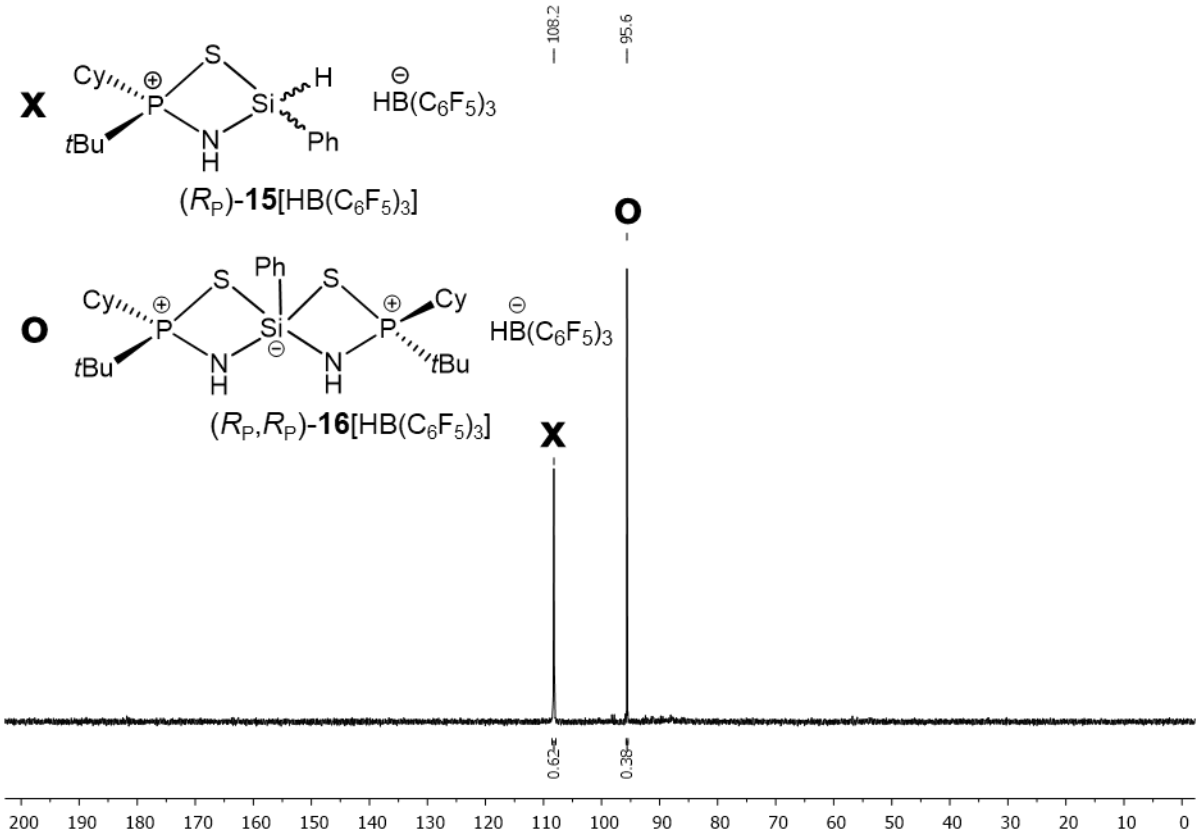

Figure S5.70. $^{31}P\{^{1}H\}$ NMR spectrum (C_6D_6, 298 K) of the crude reaction mixture containing (R_P)-**15**[$HB(C_6F_5)_3$] and (R_P,R_P)-**16**[$HB(C_6F_5)_3$].

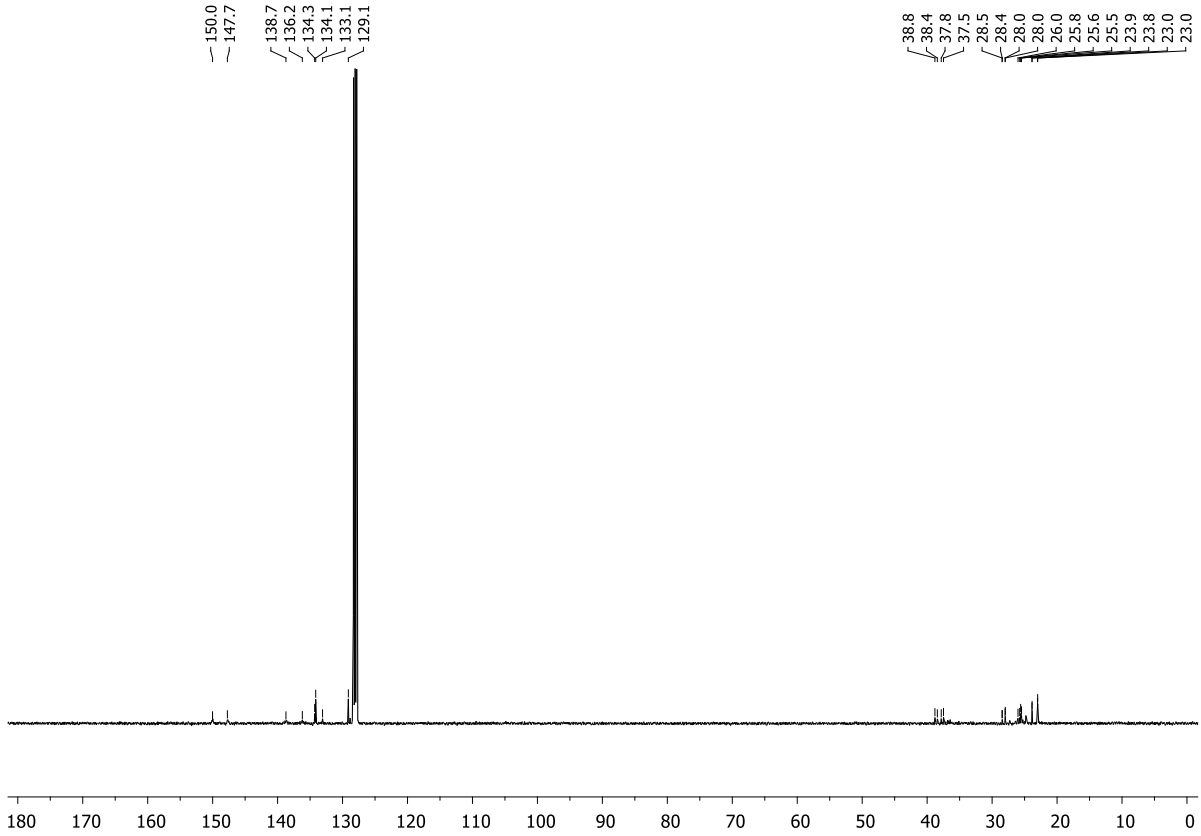

Figure S5.71. $^{13}C\{^{1}H\}$ NMR spectrum (C_6D_6, 298 K) of the crude reaction mixture containing (R_P)-**15**[$HB(C_6F_5)_3$] and (R_P,R_P)-**16**[$HB(C_6F_5)_3$].

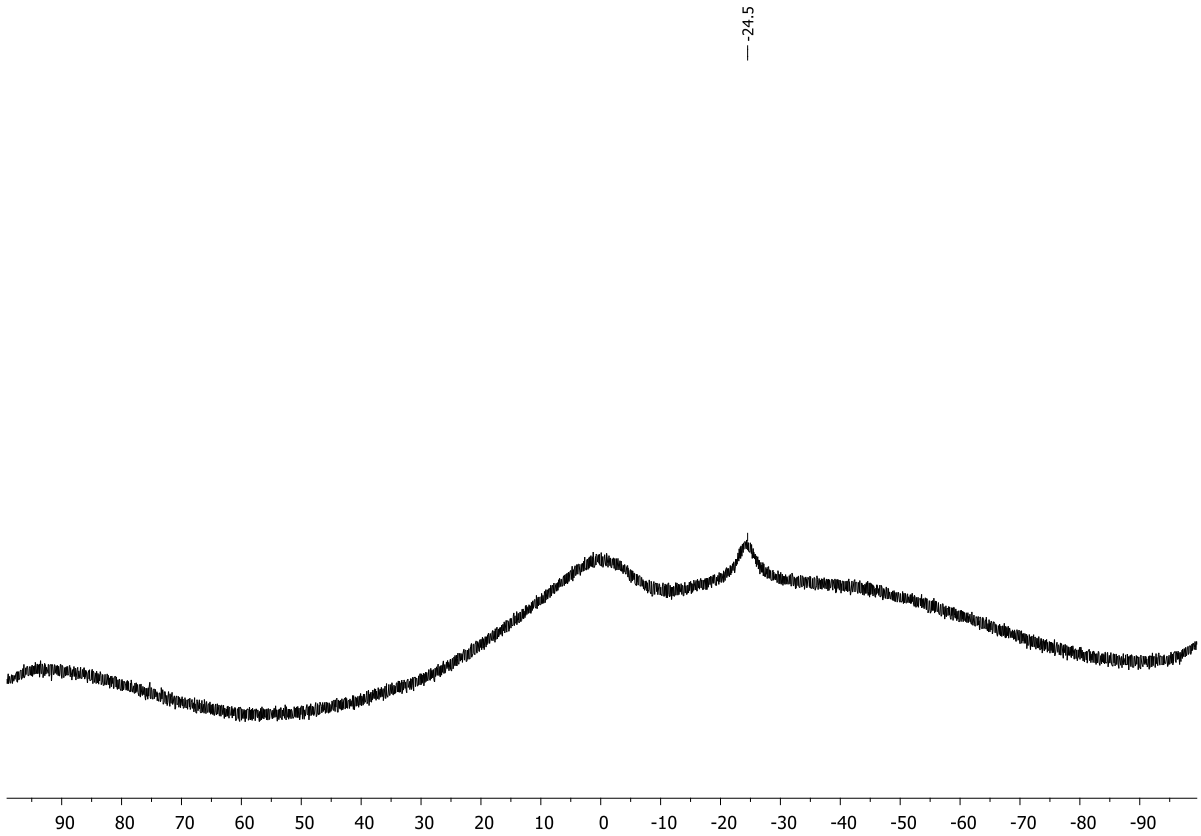

Figure S5.72. $^{13}B\{^{1}H\}$ NMR spectrum (C_6D_6, 298 K) of the crude reaction mixture containing (R_P)-**15**[$HB(C_6F_5)_3$] and (R_P,R_P)-**16**[$HB(C_6F_5)_3$].

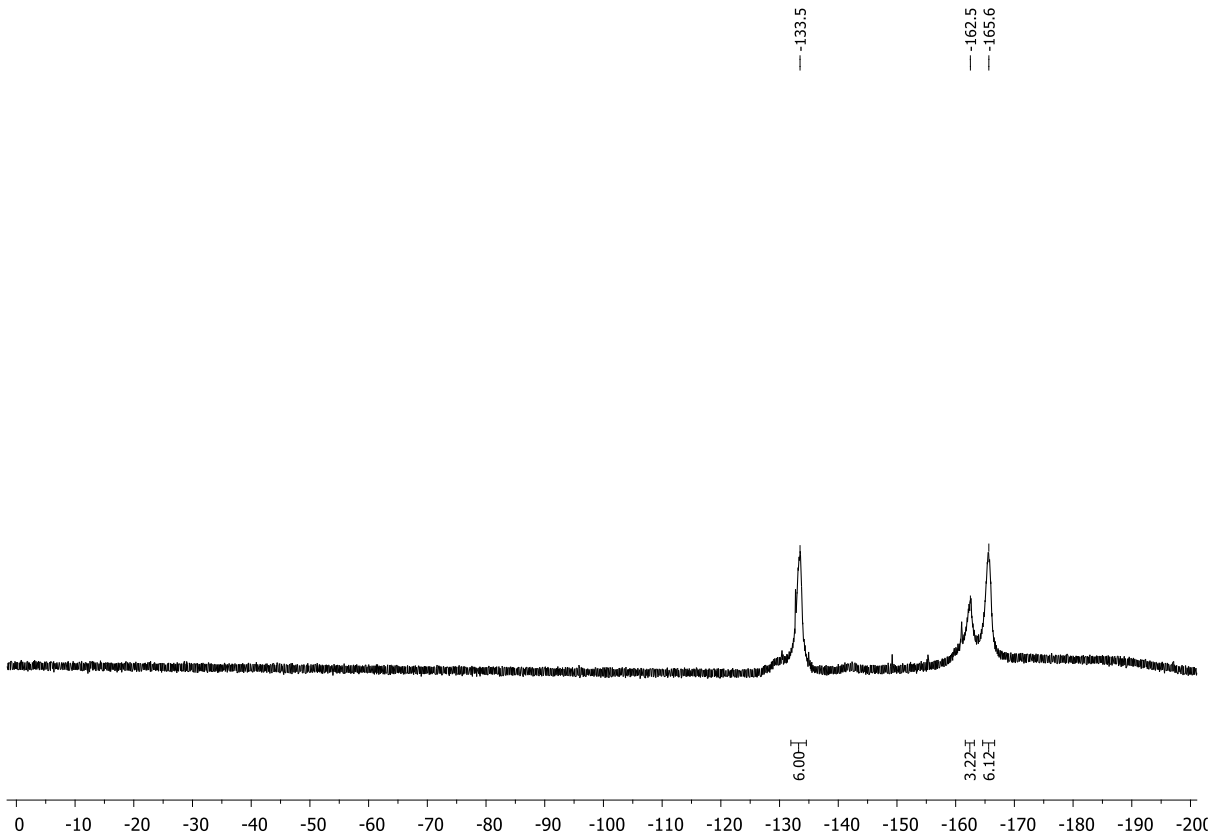

Figure S5.73. $^{19}F\{^{1}H\}$ NMR spectrum (C_6D_6, 298 K) of the crude reaction mixture containing (R_P)-**15**[$HB(C_6F_5)_3$] and (R_P,R_P)-**16**[$HB(C_6F_5)_3$].

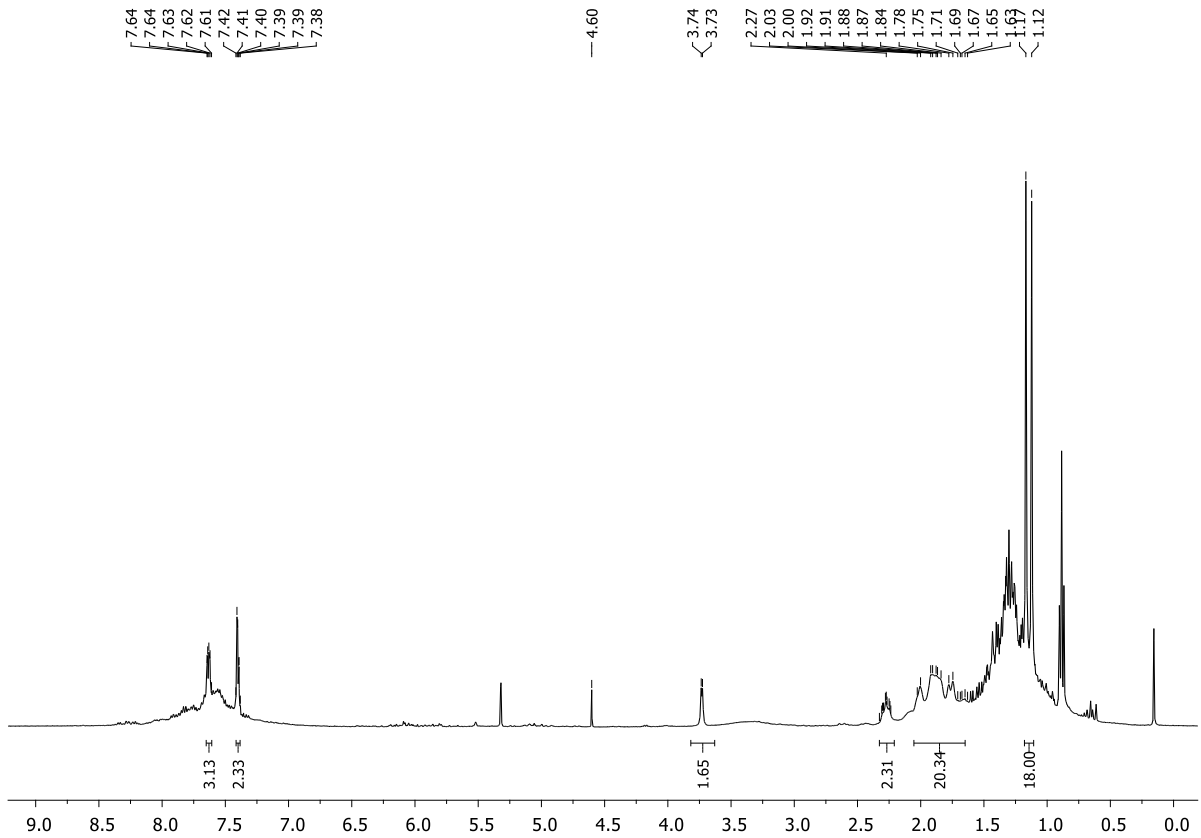

Figure S5.74. ^{1}H NMR spectrum (CD_2Cl_2, 298 K) of (R_P,R_P)-**16**[$HB(C_6F_5)_3$] with residues of pentane.

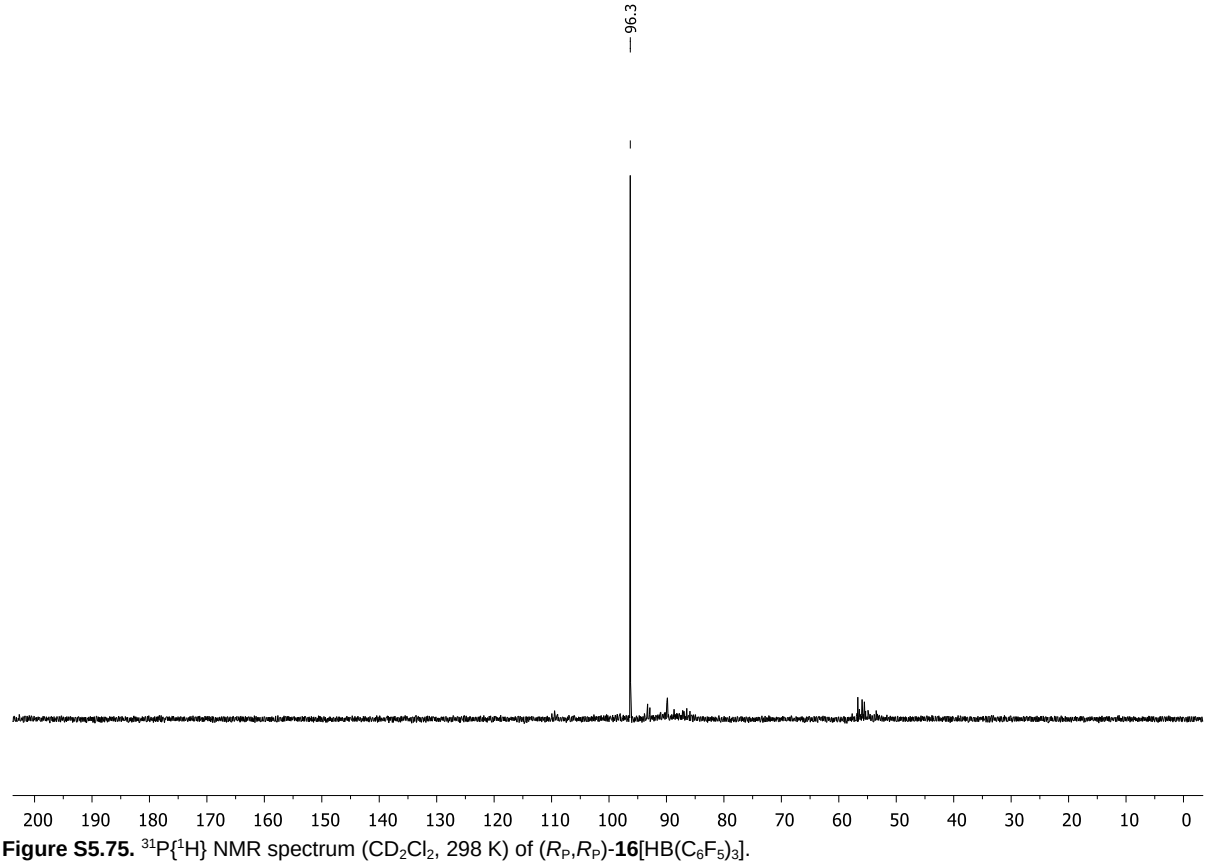

Figure S5.75. $^{31}P\{^{1}H\}$ NMR spectrum (CD_2Cl_2, 298 K) of (R_P,R_P)-**16**[$HB(C_6F_5)_3$].

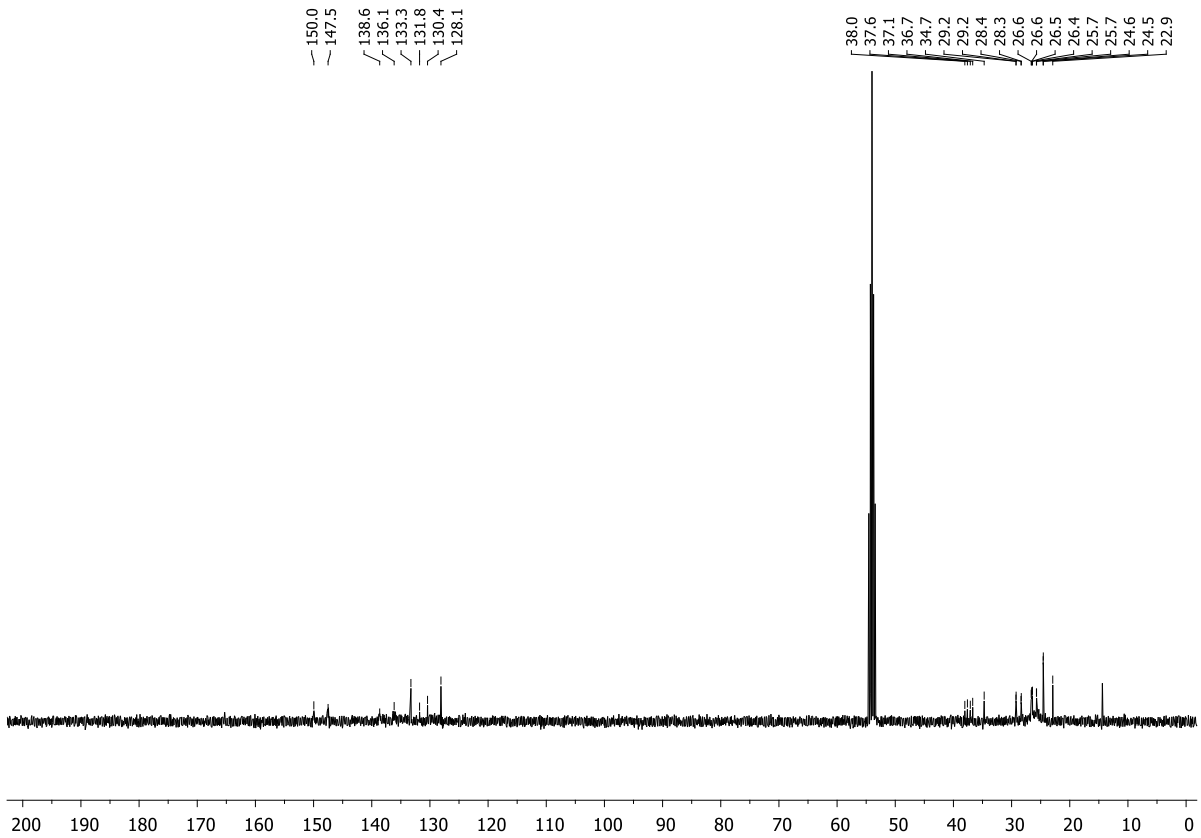

Figure S5.76. $^{13}C\{^{1}H\}$ NMR spectrum (CD_2Cl_2, 298 K) of (R_P,R_P)-**16**[$HB(C_6F_5)_3$].

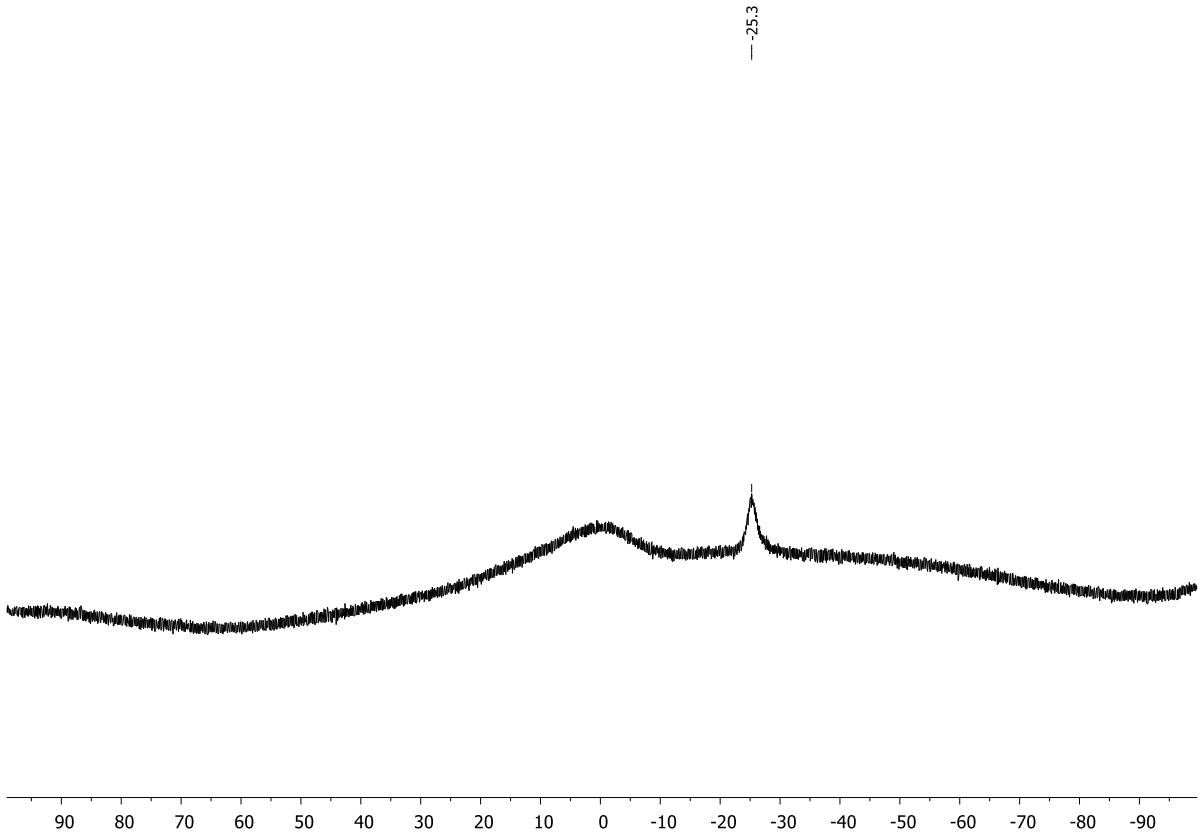

Figure S5.77. $^{11}B\{^{1}H\}$ NMR spectrum (CD_2Cl_2, 298 K) of (R_P,R_P)-**16**[$HB(C_6F_5)_3$].

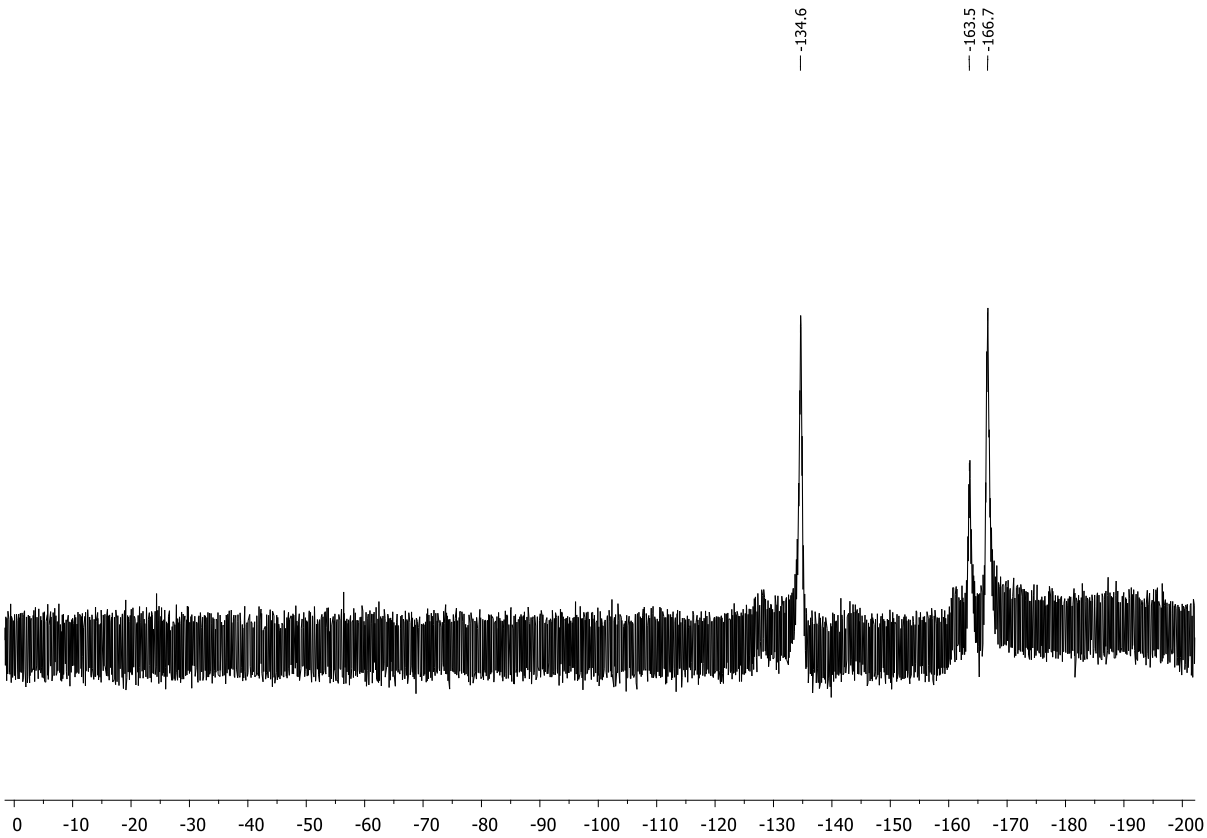

Figure S5.78. $^{19}F\{^{1}H\}$ NMR spectrum (CD_2Cl_2, 298 K) of (R_P,R_P)-**16**[$HB(C_6F_5)_3$].

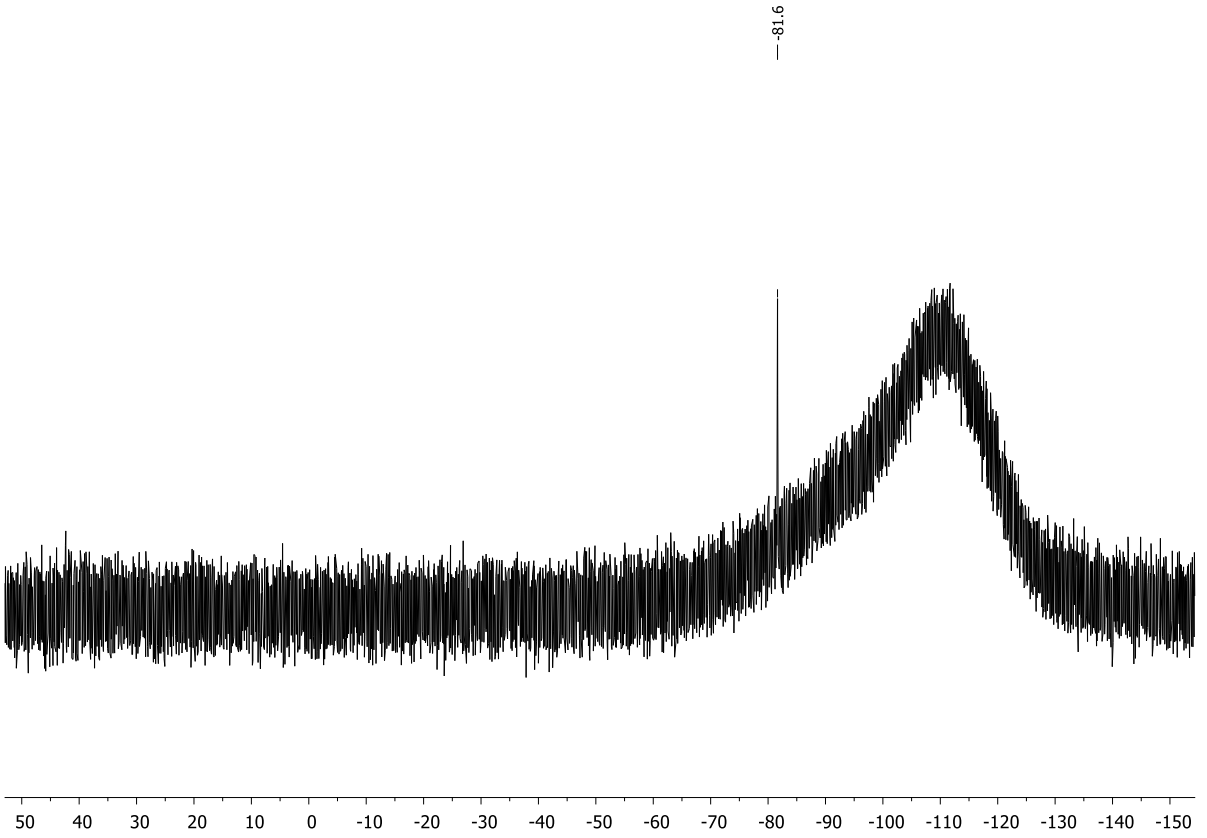

Figure S5.79. $^{29}Si\{^{1}H\}$ NMR spectrum (CD_2Cl_2, 298 K) of (R_P,R_P)-**16**[$HB(C_6F_5)_3$].

5.6.2.14. Synthesis of (R_P,S_{Si})-*t*BuCy(PS)NH(SiH*t*BuPh) [(R_P,S_{Si})-17)] and (R_P,R_{Si})-*t*BuCy(PS)NH(SiH*t*BuPh) [(R_P,R_{Si})-17)]

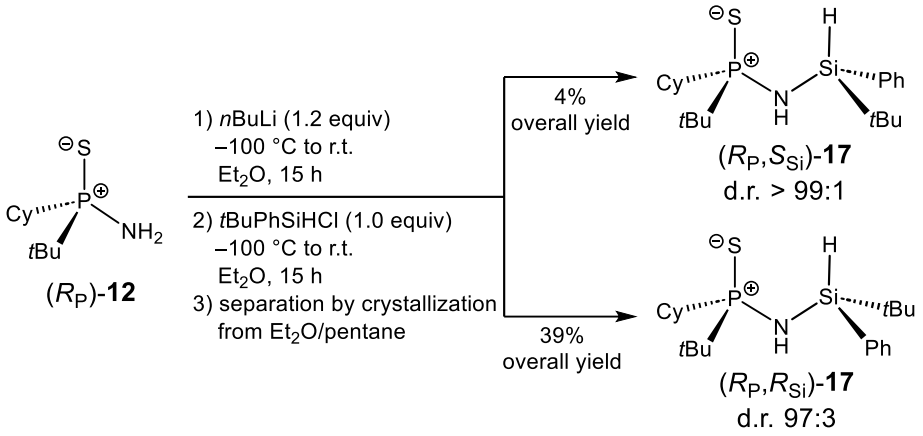

*n*Butyllithium (0.9 mL, 2.18 mmol, 1.2 equiv., 2.5 M in hexane) was added dropwise to a solution of (R_P)-*P*-(*tert*-butyl)-*P*-cyclohexylphosphinothioic amide [(R_P)-**12**] (400 mg, 1.82 mmol, 1.0 equiv.) in diethyl ether (10 mL) at −100 °C. The solution was allowed to slowly warm to room temperature and stirred for 15 h. Following, the colorless suspension was cooled to −100 °C again and *tert*-butylchlorophenylsilane (360 mg, 1.82 mmol, 1.0 equiv.) was added dropwise. The reaction mixture was allowed to slowly warm to room temperature and stirred for 15 h affording a colorless suspension. The precipitated lithium chloride was filtered off via cannula filtration and washed with diethyl ether. Then, all volatiles of the filtrate were removed under vacuum. Almost full conversion (86%) of the starting material and formation of the desired products (R_P,S_{Si})-**17** and (R_P,R_{Si})-**17** (d.r. 11:89) was confirmed by ^{1}H and ^{31}P{^{1}H} NMR spectroscopy. Twofold crystallization from a diethyl ether solution that was layered with pentane at room temperature afforded the diastereomerically enriched products, which could be each even higher enriched by a third recrystallization step. For every crystallization step, the minimum amount of diethyl ether, that was needed to completely solve the substrate, was used and carefully layered with 10 mL of pentane. In the first crystallization step, all leftover starting material was removed and only the diastereomeric products (R_P,S_{Si})-**17** and (R_P,R_{Si})-**17** (d.r. 25:75, 451 mg) were present in the formed crystals. In the second crystallization step, the two diastereomers could be almost fully separated. After filtration, washing with pentane and drying in vacuo, (R_P,S_{Si})-**17** was isolated as colorless crystals (d.r. 98:2), which were suitable for single-crystal X-ray analysis. A third recrystallization step lead to an even higher diastereomeric enrichment of (R_P,S_{Si})-**17**, which was again obtained as colorless crystals (26.0 mg, 0.07 mmol, 4%, d.r. >99:1). (R_P,R_{Si})-**17**, which remained in the mother liquor of the second crystallization step, was obtained as a colorless solid (d.r. 95:5) after removing all volatiles and drying in vacuo. It was recrystallized a third time to obtain an even higher diastereomeric enrichment in the mother liquor. After removing all volatiles and drying in vacuo, (R_P,R_{Si})-**17** was obtained as a colorless solid (272 mg, 0.71 mmol, 39%, d.r. 97:3). Attempts to receive measurable single crystals of this diastereomer has failed several times.

(R_P,S_{Si})-**17**:

^{1}H NMR (400.13 MHz, C_6D_6, 298 K): δ = 1.00 (s, 9H, SiC(CH_3)$_3$), 1.05 (d, $^3J_{H–P}$ = 15.7 Hz, 9H, PC(CH_3)$_3$), 1.52 (br, 1H, N*H*), 1.57–1.80 (m, 6H, CH_2), 1.91–1.94 (m, 1H, CH_2), 2.04–2.07 (m, 1H, CH_2), 5.26 (m, 1H, Si*H*), 7.18–7.22 (m, 3H, H_{Ph}), 7.56–7.60 (m, 2H, H_{Ph}). **^{31}P{^{1}H} NMR** (162.04 MHz, C_6D_6, 298 K): δ = 86.8 (s). **^{13}C{^{1}H} NMR** (100.61 MHz, C_6D_6, 298 K): δ = 18.1 (d, $^3J_{C–P}$ = 3.1 Hz, Si*C*(CH$_3$)$_3$), 26.0 (d, $^2J_{C–P}$ = 1.6 Hz, PC(*C*H$_3$)$_3$), 26.1 (d, $^3J_{C–P}$ = 1.5 Hz, *C*H$_2$), 26.8 (d, $^2J_{C–P}$ = 14.1 Hz, *C*H$_2$), 27.0 (d, $^2J_{C–P}$ = 12.6 Hz, *C*H$_2$), 27.1 (s, SiC(*C*H$_3$)$_3$), 27.7 (d, $^3J_{C–P}$ = 3.7 Hz, *C*H$_2$), 28.6 (d, $^4J_{C–P}$ = 0.8 Hz, *C*H$_2$), 37.5 (d, $^1J_{C–P}$ = 59.2 Hz, P*C*(CH$_3$)$_3$), 40.5 (d, $^1J_{C–P}$ = 56.5 Hz, P*C*H), 128.1 (s, C_{Ph}), 130.0 (s, C_{Ph}), 135.0 (s, C_{Ph}), 135.5 (d, $^3J_{C–P}$ = 0.8 Hz, C_{ipso}). **^{29}Si{^{1}H} NMR** (79.49 MHz, C_6D_6, 298 K): δ = –6.4 (d, $^2J_{P–Si}$ = 4.5 Hz).

^{1}H NMR (400.13 MHz, CD_2Cl_2, 298 K): δ = 0.97 (s, 9H, SiC(CH_3)$_3$), 1.14 (d, $^3J_{H–P}$ = 15.9 Hz, 9H, PC(CH_3)$_3$), 1.22–1.32 (m, 3H, CH_2), 1.42–1.53 (m, 2H, CH_2), 1.67–1.69 (m, 1H, C*H*), 1.78–1.89 (m, 3H, CH_2), 1.91–2.01 (m, 2H, CH_2), 2.05 (br, 1H, N*H*), 4.78 (m, 1H, Si*H*), 7.34–7.42 (m, 3H, H_{Ph}), 7.55–7.58 (m, 2H, H_{Ph}). **^{31}P{^{1}H} NMR** (162.04 MHz, CD_2Cl_2, 298 K): δ = 87.5 (s). **^{13}C{^{1}H} NMR** (100.61 MHz, CD_2Cl_2, 298 K): δ = 18.2 (d, $^3J_{C–P}$ = 3.7 Hz, Si*C*(CH$_3$)$_3$), 26.2 (d, $^2J_{C–P}$ = 1.6 Hz, PC(*C*H$_3$)$_3$), 26.4 (d, $^3J_{C–P}$ = 1.6 Hz, *C*H$_2$), 27.1 (d, $^2J_{C–P}$ = 13.8 Hz, *C*H$_2$), 27.1 (s, SiC(*C*H$_3$)$_3$), 27.2 (d, $^2J_{C–P}$ = 12.1 Hz, *C*H$_2$), 28.0 (d, $^3J_{C–P}$ = 3.9 Hz, *C*H$_2$), 29.0 (d, $^4J_{C–P}$ = 1.3 Hz, *C*H$_2$), 37.6 (d, $^1J_{C–P}$ = 58.9 Hz, P*C*(CH$_3$)$_3$), 40.8 (d, $^1J_{C–P}$ = 56.0 Hz, P*C*H), 128.2 (s, C_{Ph}), 130.1 (s, C_{Ph}), 135.1 (s, C_{Ph}), 135.8 (s, C_{ipso}).

Elemental analysis: $C_{20}H_{36}NPSSi$: calcd.: C 62.95, H 9.51, N 3.67; found: C 62.48, H 9.20, N 3.50.

HR(+ESI)-MS: calcd. *m/z* for $C_{20}H_{37}NPSSi$ [(M+H)$^+$]: 382.2148, found: 382.2159.

(R_P,R_{Si})-**17**:

^{1}H NMR (400.13 MHz, C_6D_6, 298 K): δ = 0.97 (s, 9H, SiC(CH_3)$_3$), 1.14 (d, $^3J_{H–P}$ = 15.6 Hz, 9H, PC(CH_3)$_3$), 1.40–1.53 (m, 3H, CH_2/N*H*), 1.57–1.78 (m, 4H, CH_2), 1.80–1.90 (m, 1H, CH_2), 1.92–2.02 (m, 1H, CH_2), 5.21 (m, 1H, Si*H*), 7.18–7.24 (m, 3H, H_{Ph}), 7.63–7.66 (m, 2H, H_{Ph}). **^{31}P{^{1}H} NMR** (162.04 MHz, C_6D_6, 298 K): δ = 86.1 (s). **^{13}C{^{1}H} NMR** (100.61 MHz, C_6D_6, 298 K): δ = 17.9 (d, $^3J_{C–P}$ = 4.2 Hz, Si*C*(CH$_3$)$_3$), 25.9 (d, $^2J_{C–P}$ = 1.5 Hz, PC(*C*H$_3$)$_3$), 26.0 (d, $^3J_{C–P}$ = 1.5 Hz, *C*H$_2$), 26.9 (d, $^2J_{C–P}$ = 14.6 Hz, *C*H$_2$), 27.0 (d, $^2J_{C–P}$ = 13.2 Hz, *C*H$_2$), 27.2 (s, SiC(*C*H$_3$)$_3$), 27.8 (d, $^3J_{C–P}$ = 3.7 Hz, *C*H$_2$), 28.8 (d, $^4J_{C–P}$ = 1.0 Hz, *C*H$_2$), 37.8 (d, $^1J_{C–P}$ = 58.8 Hz, P*C*(CH$_3$)$_3$), 39.6 (d, $^1J_{C–P}$ = 56.2 Hz, P*C*H), 128.0 (s, C_{Ph}), 130.0 (s, C_{Ph}), 135.0 (s, C_{Ph}), 135.9 (s, C_{ipso}). **^{29}Si NMR** (79.49 MHz, C_6D_6, 298 K): δ = –6.2 (d, $^1J_{P–Si}$ = 4.5 Hz).

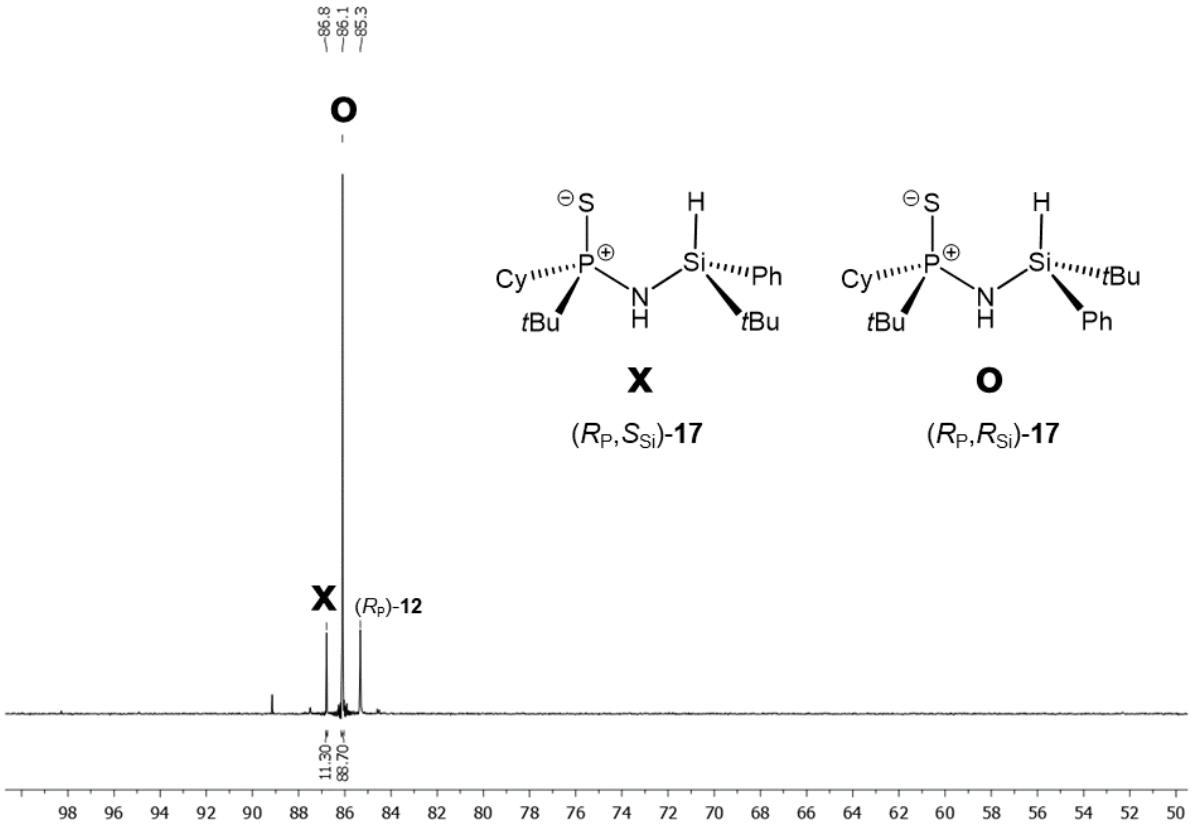

Figure S5.80. $^{31}P\{^{1}H\}$ NMR spectrum (C_6D_6, 298 K) of the crude reaction mixture for determining the diastereomeric ratio. Compounds (R_P,S_{Si})-**17** and(R_P,R_{Si})-**17** were formed in a 11:89 diastereomeric ratio. 14% of the starting material (R_P)-**12** remained unreacted.

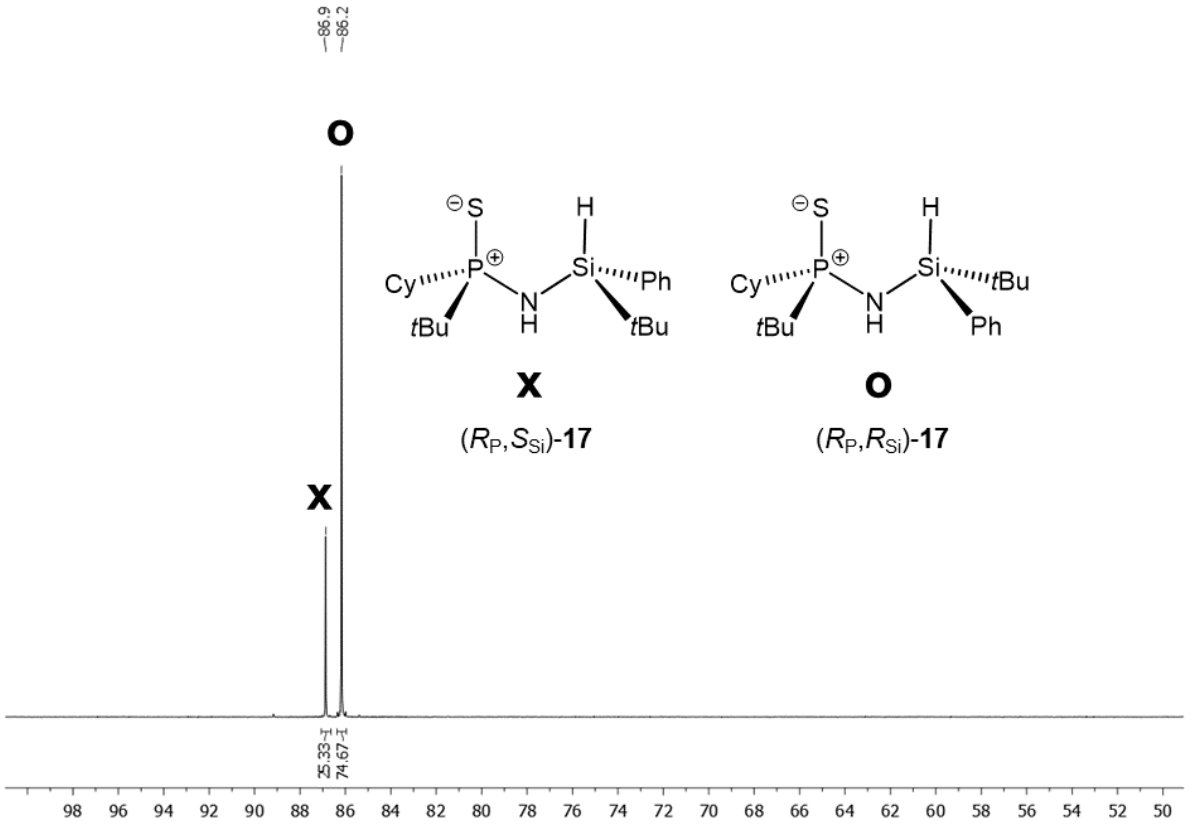

Figure S5.81. $^{31}P\{^{1}H\}$ NMR spectrum (C_6D_6, 298 K) of compounds (R_P,S_{Si})-**17** and(R_P,R_{Si})-**17** after the first crystallization step showing a 25:75 diastereomeric ratio.

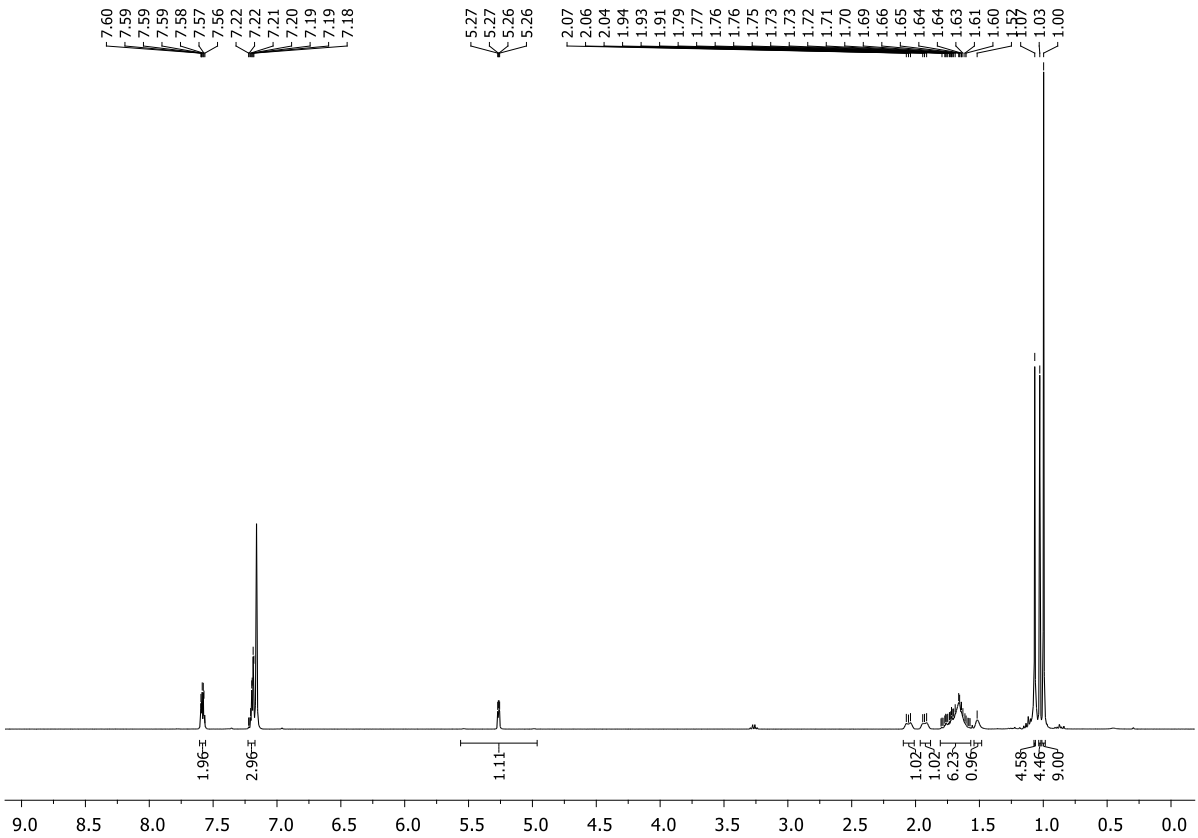

Figure S5.82. ^{1}H NMR spectrum (C_6D_6, 298 K) of (R_P,S_{Si})-**17**.

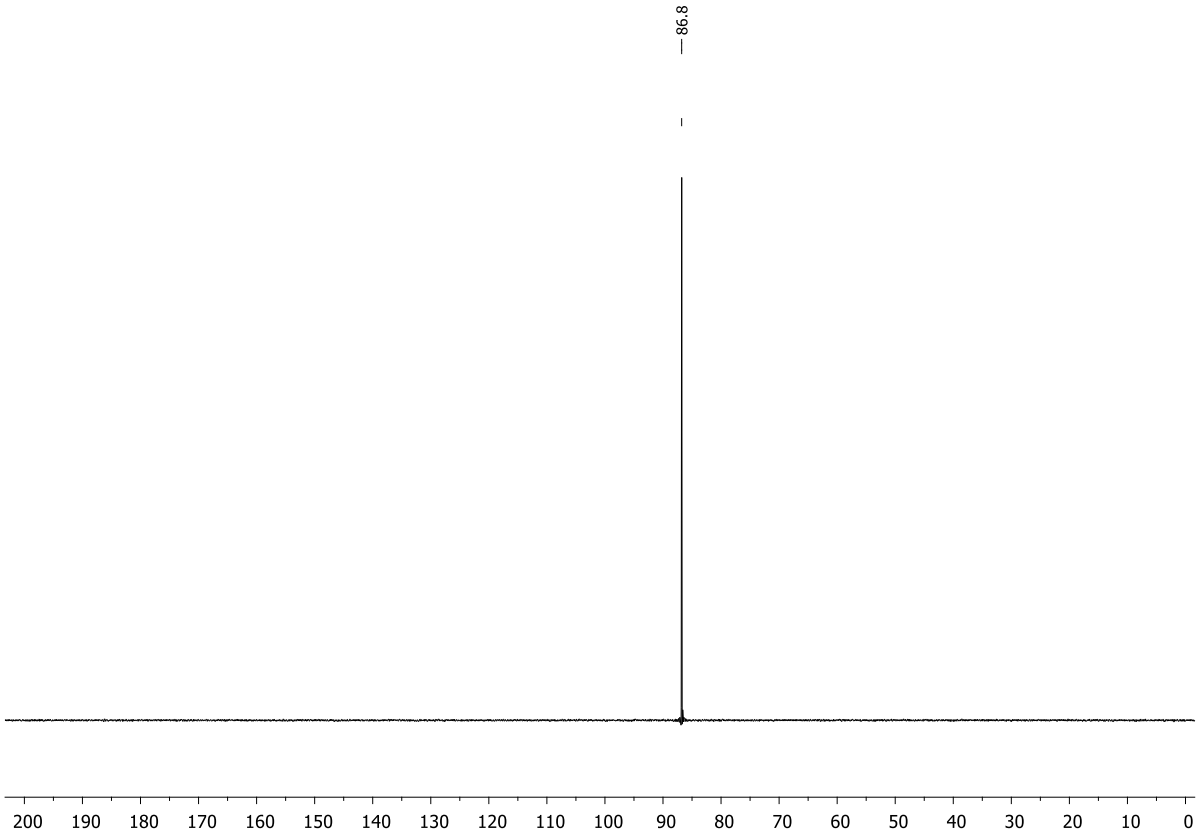

Figure S5.83. $^{31}P\{^{1}H\}$ NMR spectrum (C_6D_6, 298 K) of (R_P,S_{Si})-**17**.

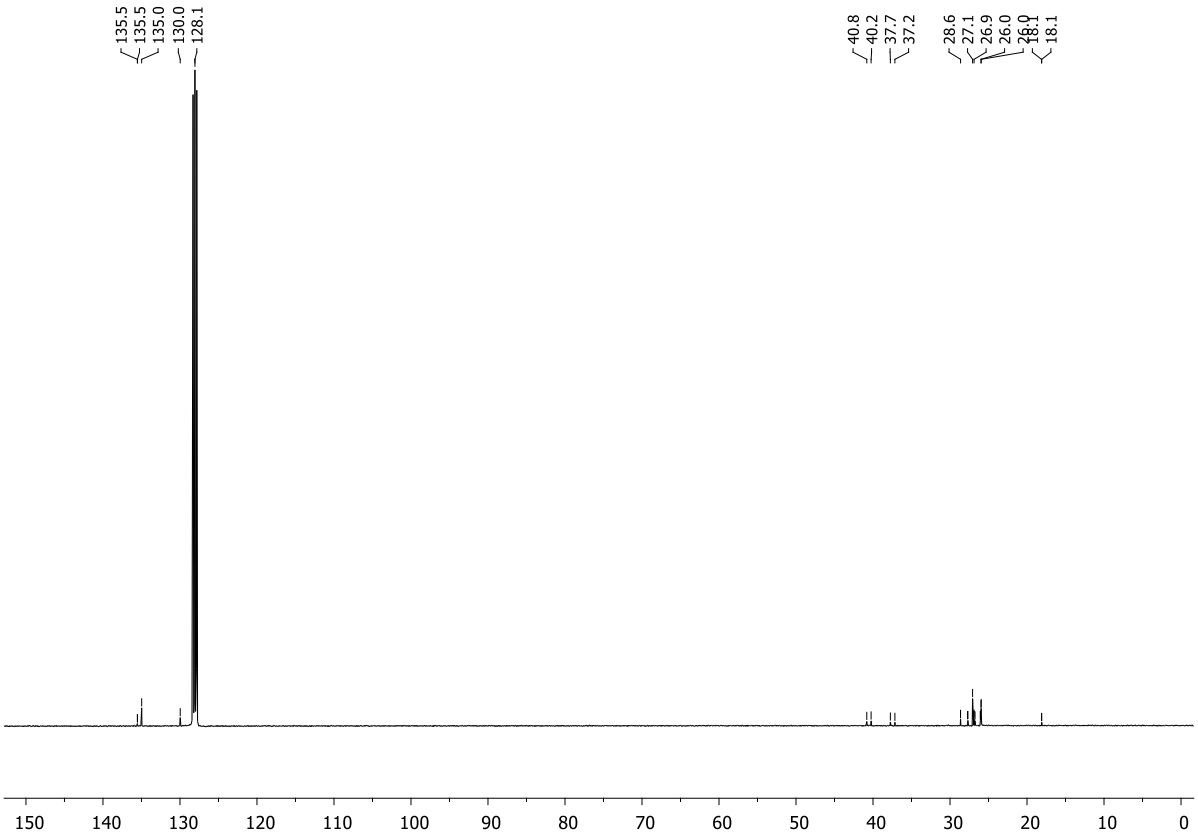

Figure S5.84. $^{13}C\{^{1}H\}$ NMR spectrum (C_6D_6, 298 K) of (R_P,S_{Si})-**17**.

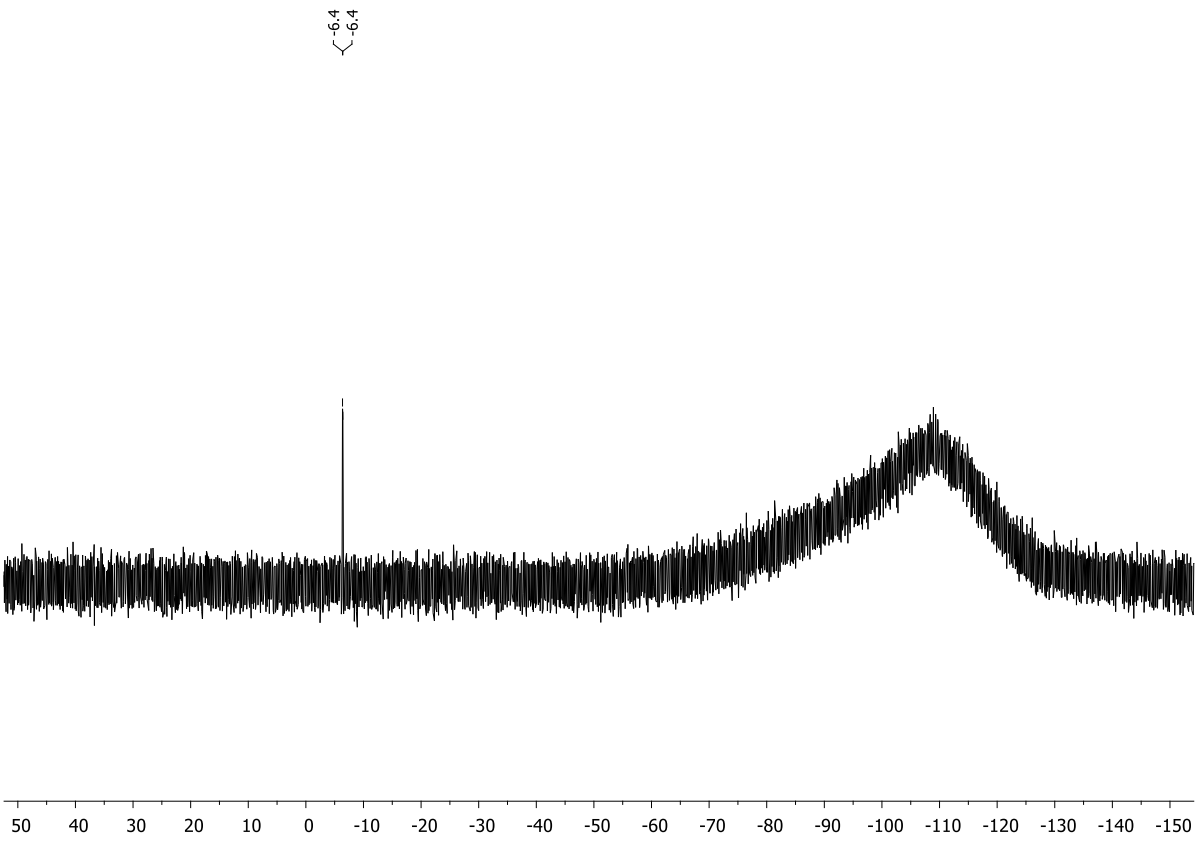

Figure S5.85. $^{29}Si\{^{1}H\}$ NMR spectrum (C_6D_6, 298 K) of (R_P,S_{Si})-**17**.

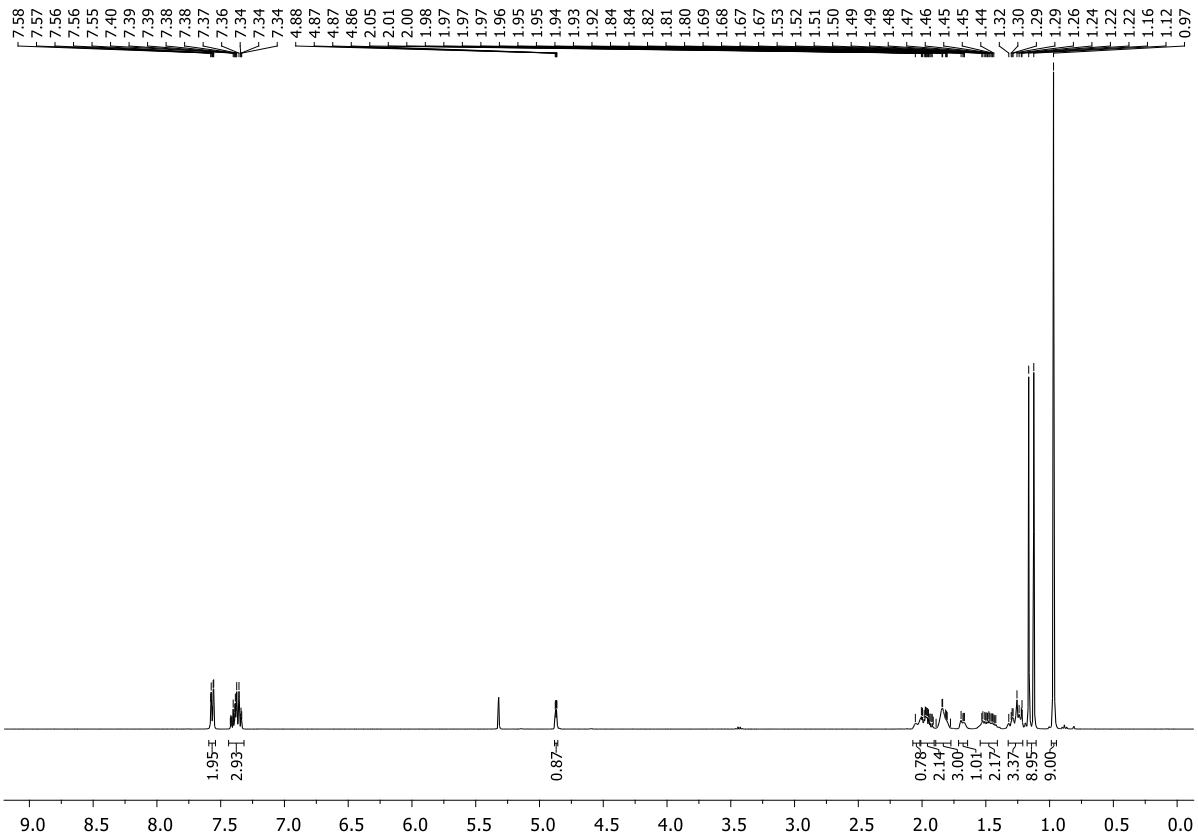

Figure S5.86. ^{1}H NMR spectrum (CD_2Cl_2, 298 K) of (R_P,S_{Si})-**17**.

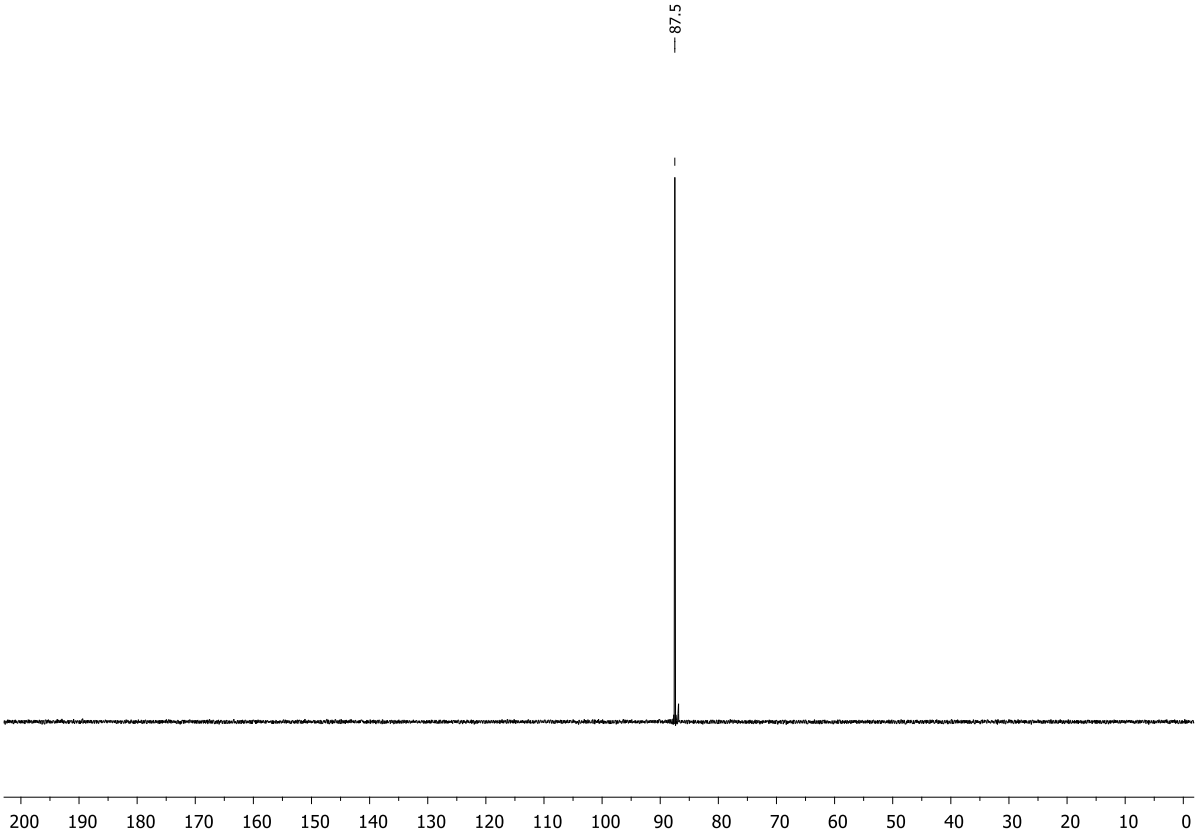

Figure S5.87. ^{31}P{^{1}H] NMR spectrum (CD_2Cl_2, 298 K) of (R_P,S_{Si})-**17**.

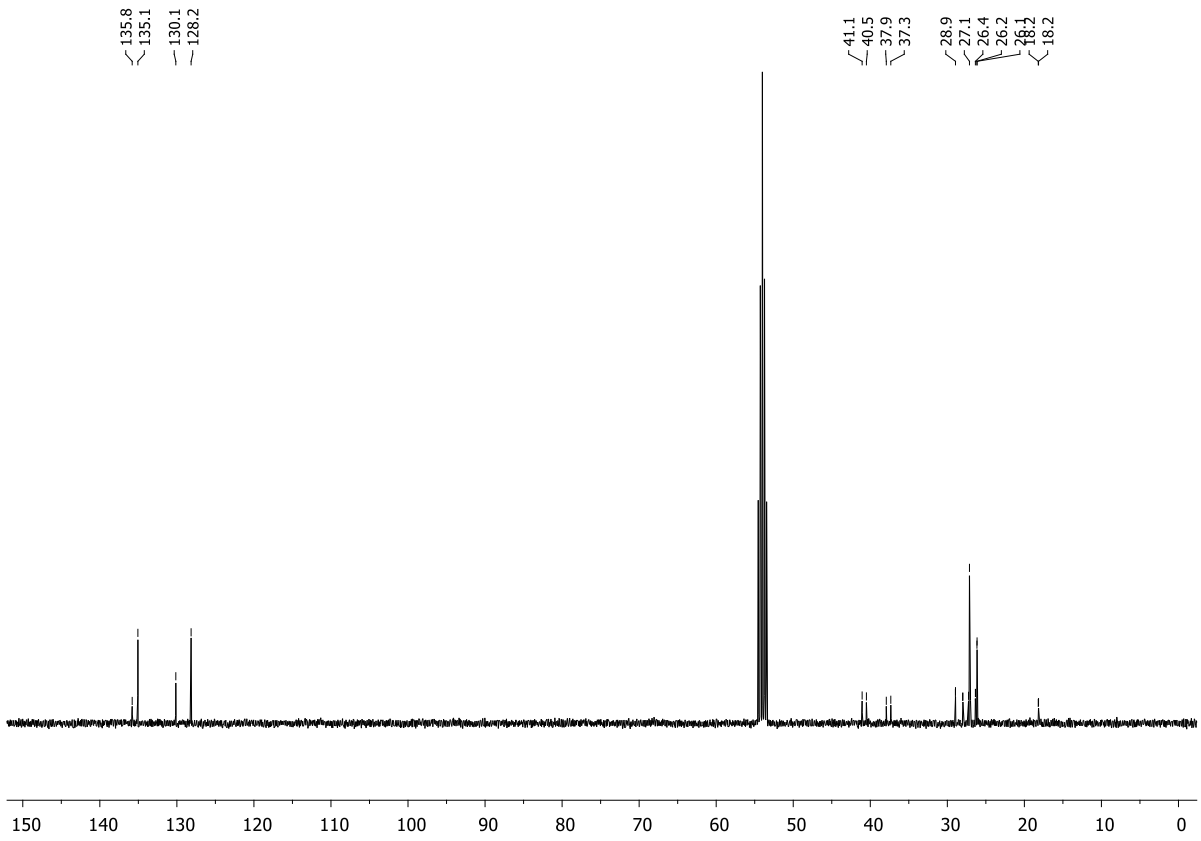

Figure S5.88. $^{13}C\{^{1}H\}$ NMR spectrum (CD_2Cl_2, 298 K) of (R_P,S_{Si})-**17**.

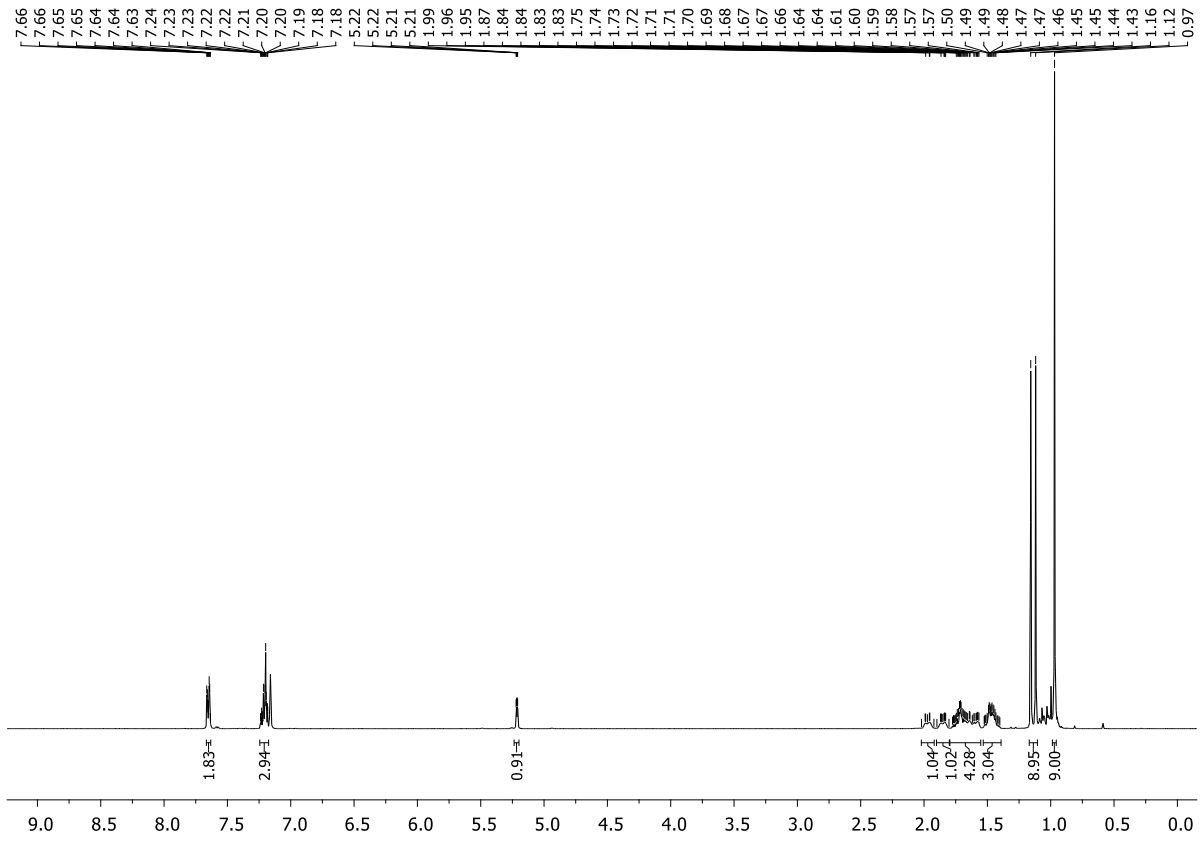

Figure S5.89. ^{1}H NMR spectrum (C_6D_6, 298 K) of (R_P,R_{Si})-**17**.

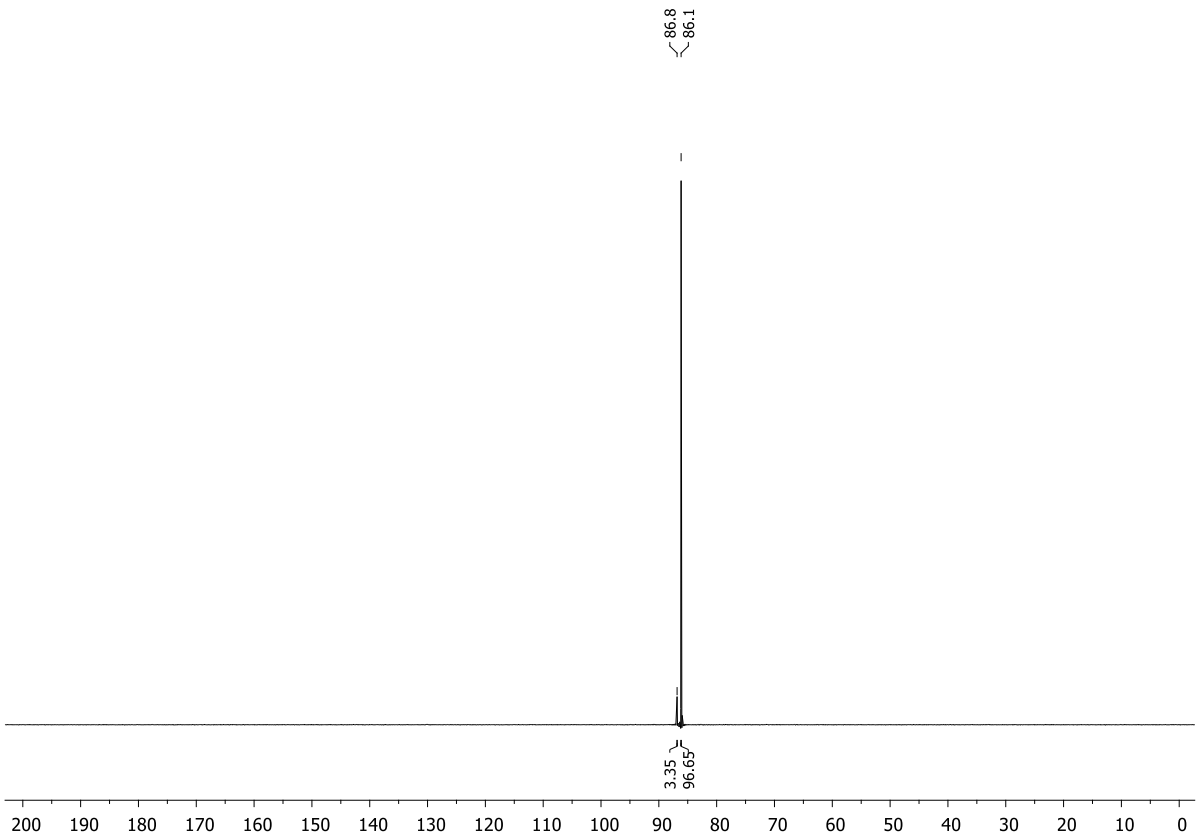

Figure S5.90. $^{31}P\{^{1}H\}$ NMR spectrum (C_6D_6, 298 K) of (R_P,R_{Si})-**17**.

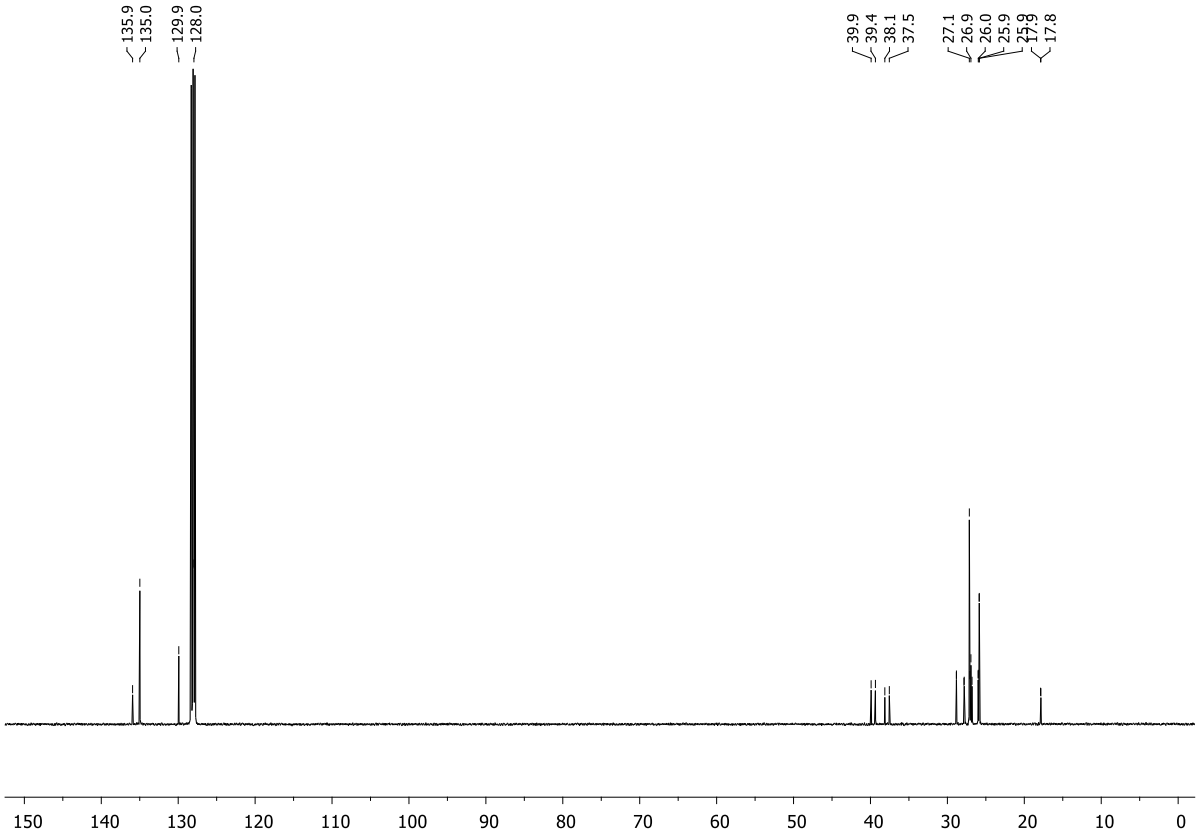

Figure S5.91. $^{13}C\{^{1}H\}$ NMR spectrum (C_6D_6, 298 K) of (R_P,R_{Si})-**17**.

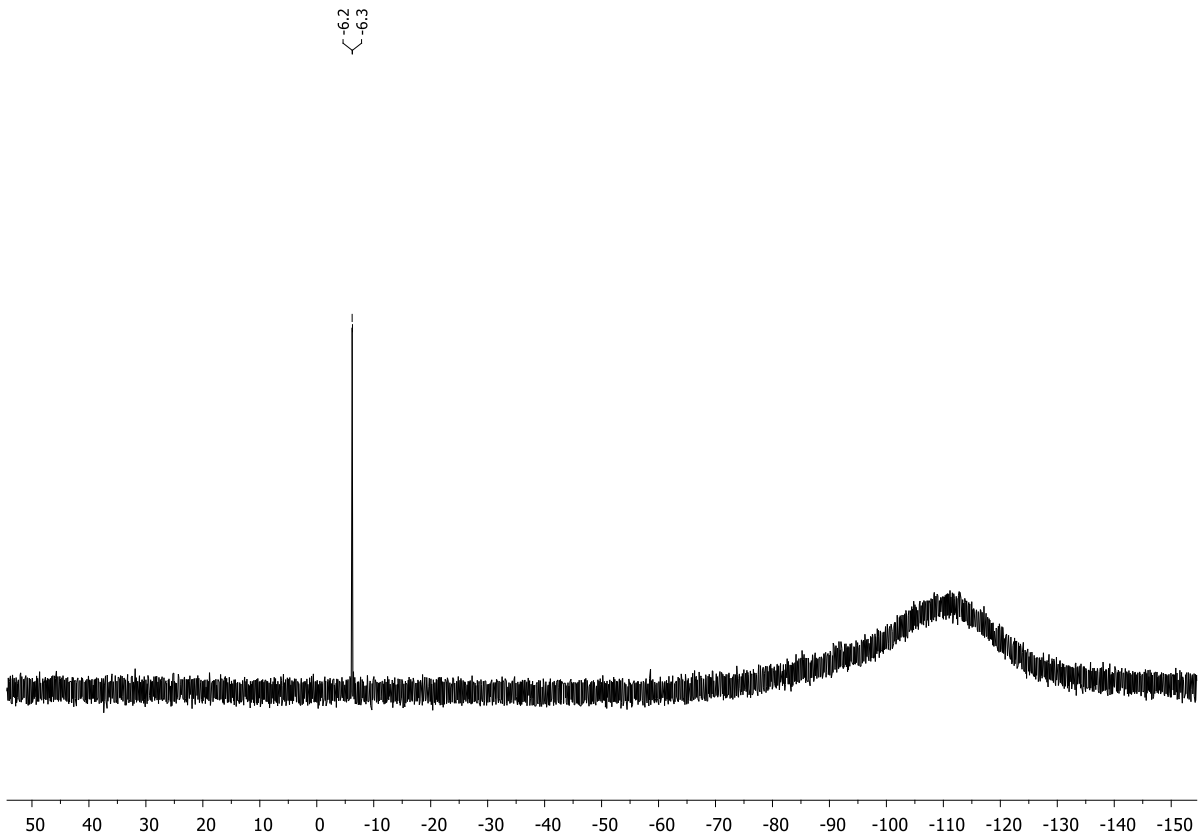

Figure S5.92. $^{29}Si\{^{1}H\}$ NMR spectrum (C_6D_6, 298 K) of (R_P,R_{Si})-**17**.

5.6.2.15. Synthesis of (R_P,R_{Si}/S_{Si})-*t*BuCy(PS)NH(Si*t*BuPh)$^+$ [HB(C_6F_5)$_3$]$^-$ {(R_P,R_{Si}/S_{Si})-**18**)[HB(C_6F_5)$_3$], d.r. 78:22 or 22:78}

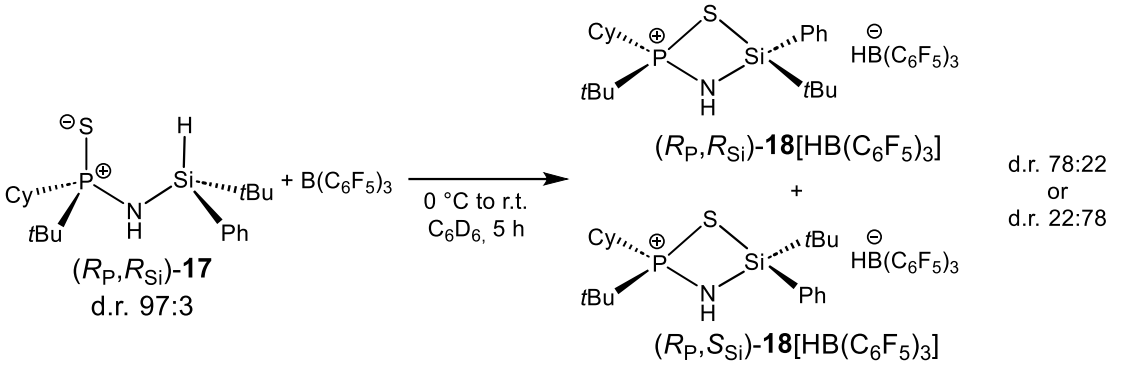

A solution of compound (R_P,R_{Si})-**17** (80.9 mg, 0.21 mmol, 1.0 equiv., d.r. 97:3) in C_6D_6 (1.0 mL) was added to a solution of tris(pentafluorophenyl)borane (109 mg, 0.21 mmol, 1.0 equiv.) in C_6D_6 (0.5 mL) at 0 °C in a Young NMR tube. The mixture was allowed to slowly warm to room temperature, affording a colorless solution. NMR spectroscopy was carried out without any purification 5 h after the starting materials were combined. Compound (R_P,R_{Si}/S_{Si})-**18**[HB(C_6F_5)$_3$] was obtained in a diastereomeric ratio of 78:22 or 22:78, respectively, according to ^{1}H and ^{31}P{^{1}H} NMR spectroscopy. Colorless crystals of diastereomer (R_P,S_{Si})-**18**[HB(C_6F_5)$_3$] were obtained after five days by layering the C_6D_6 solution with pentane at room temperature and subjected to a single-crystal X-Ray measurement. Before the crystals could be separated from the mother liquor, decomposition took place to form an oily precipitate.

^{1}H NMR (400.13 MHz, C_6D_6, 298 K): δ = 0.55 (d, $^3J_{H–P}$ = 19.8 Hz, 9H, PC(C*H*$_3$)$_3$, major product), 0.81 (d, $^3J_{H–P}$ = 20.0 Hz, 2.6H, PC(C*H*$_3$)$_3$, minor product), 0.82 (s, 2.6H, SiC(C*H*$_3$)$_3$, minor product), 0.84 (s, 9H, SiC(C*H*$_3$)$_3$, major product), 0.89–1.61 (m, 16H, overlapping C*H* and C*H*$_2$ signals), 1.87–2.04 (m, 2H, overlapping C*H*$_2$ signals), 4.38 (d, $^2J_{H–P}$ = 2.8 Hz, 0.3H, N*H*, minor product), 4.44 (d, $^2J_{H–P}$ = 3.4 Hz, 1H, N*H*, major product), 7.09–7.21 (m, 6H, overlapping *H*$_{Ph}$ signals), 7.43–7.48 (m, 2H, overlapping *H*$_{Ph}$ signals). **^{31}P{^{1}H} NMR** (162.04 MHz, C_6D_6, 298 K): δ = 105.8 (s, 0.78P, major product), 106.4 (s, 0.22P, minor product). **^{13}C{^{1}H} NMR** (100.61 MHz, C_6D_6, 298 K): δ = 22.8 (d, $^3J_{C–P}$ = 2.3 Hz, Si*C*(CH$_3$)$_3$), 23.2 (s, PC(*C*H$_3$)$_3$), 24.2 (s, SiC(*C*H$_3$)$_3$), 25.0 (d, $^3J_{C–P}$ = 1.7 Hz, *C*H$_2$), 25.9 (d, $^2J_{C–P}$ = 14.4 Hz, *C*H$_2$), 26.1 (d, $^2J_{C–P}$ = 15.2 Hz, *C*H$_2$), 27.3 (d, $^3J_{C–P}$ = 4.4 Hz, *C*H$_2$), 29.0 (d, $^4J_{C–P}$ = 3.1 Hz, *C*H$_2$), 38.1 (d, $^1J_{C–P}$ = 35.2 Hz, P*C*(CH$_3$)$_3$), 39.1 (d, $^1J_{C–P}$ = 38.1 Hz, P*C*H), 128.8 (s, *C*$_{Ph}$), 129.5 (s, *C*$_{Ph}$), 132.2 (s, *C*$_{Ph}$), 133.2 (s, *C*$_{Ph}$), 137.7 (d, $^1J_{C–F}$ = 259.2 Hz, *C*$_{Ar\text{-}borate}$), 148.6 (d, $^1J_{C–F}$ = 246.4 Hz, *C*$_{Ar\text{-}borate}$), signals of minor product not visible. **^{11}B{^{1}H} NMR** (128.43 MHz, C_6D_6, 298 K): δ = −24.1 (s). **^{19}F{^{1}H} NMR** (376.66 MHz, C_6D_6, 298 K): δ = −166.0 (m, 6F, *meta*-*F*$_{Ar\text{-}borate}$), −162.5 (m, 3F, *para*-*F*$_{Ar\text{-}borate}$), −132.8 (m, 6F, *ortho*-*F*$_{Ar\text{-}borate}$). **^{29}Si{^{1}H} NMR** (79.49 MHz, C_6D_6, 298 K): δ = 20.3 (d, $^2J_{P–Si}$ = 3.9 Hz), 21.6 (d, $^2J_{P–Si}$ = 3.4 Hz).

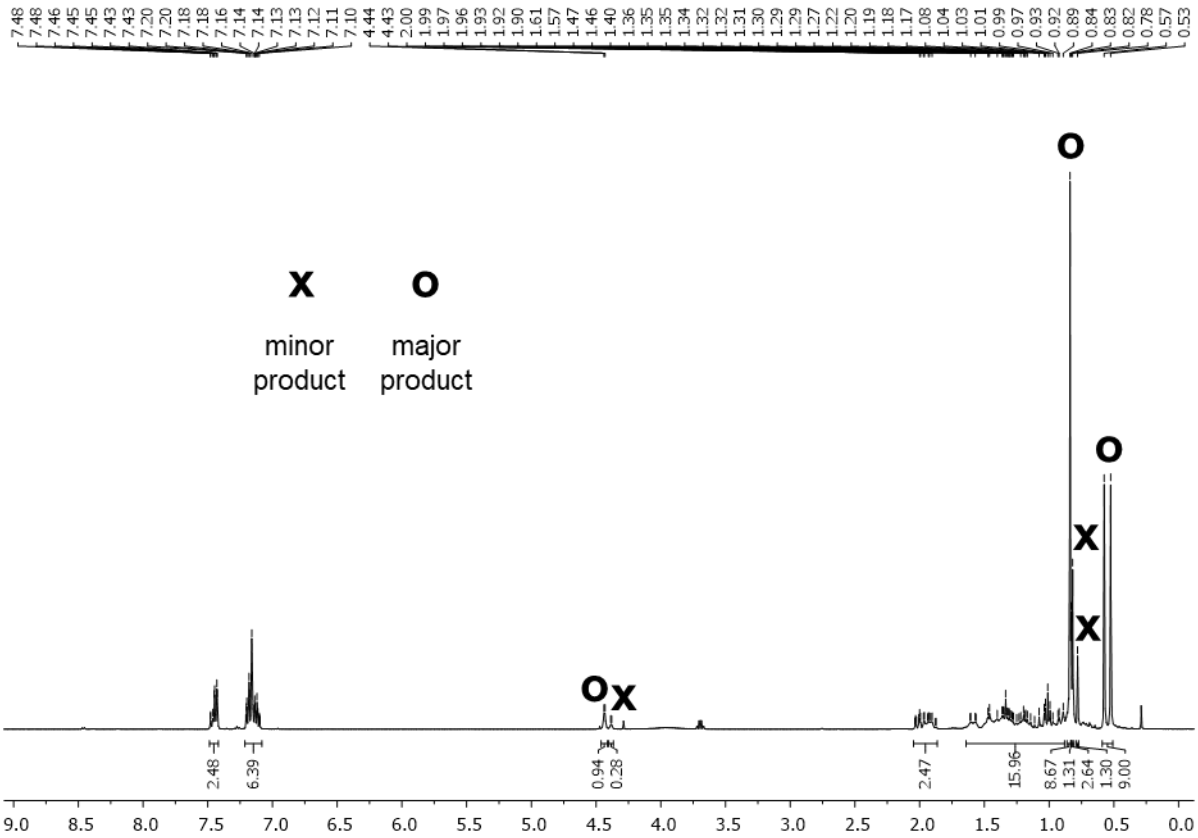

Figure S5.93. ^{1}H NMR spectrum (C_6D_6, 298 K) of (R_P,R_{Si}/S_{Si})-**18**[HB(C_6F_5)$_3$].

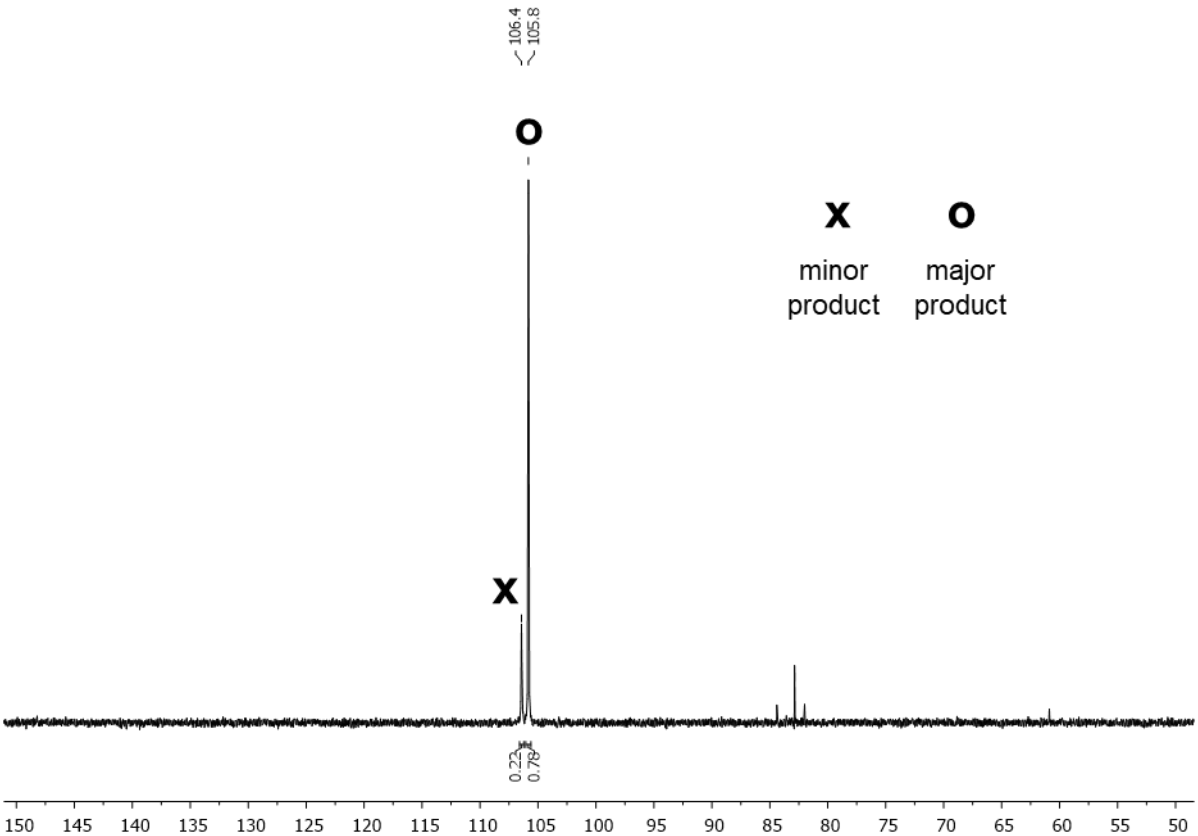

Figure S5.94. ^{31}P{^{1}H} NMR spectrum (C_6D_6, 298 K) of (R_P,R_{Si}/S_{Si})-**18**[HB(C_6F_5)$_3$].

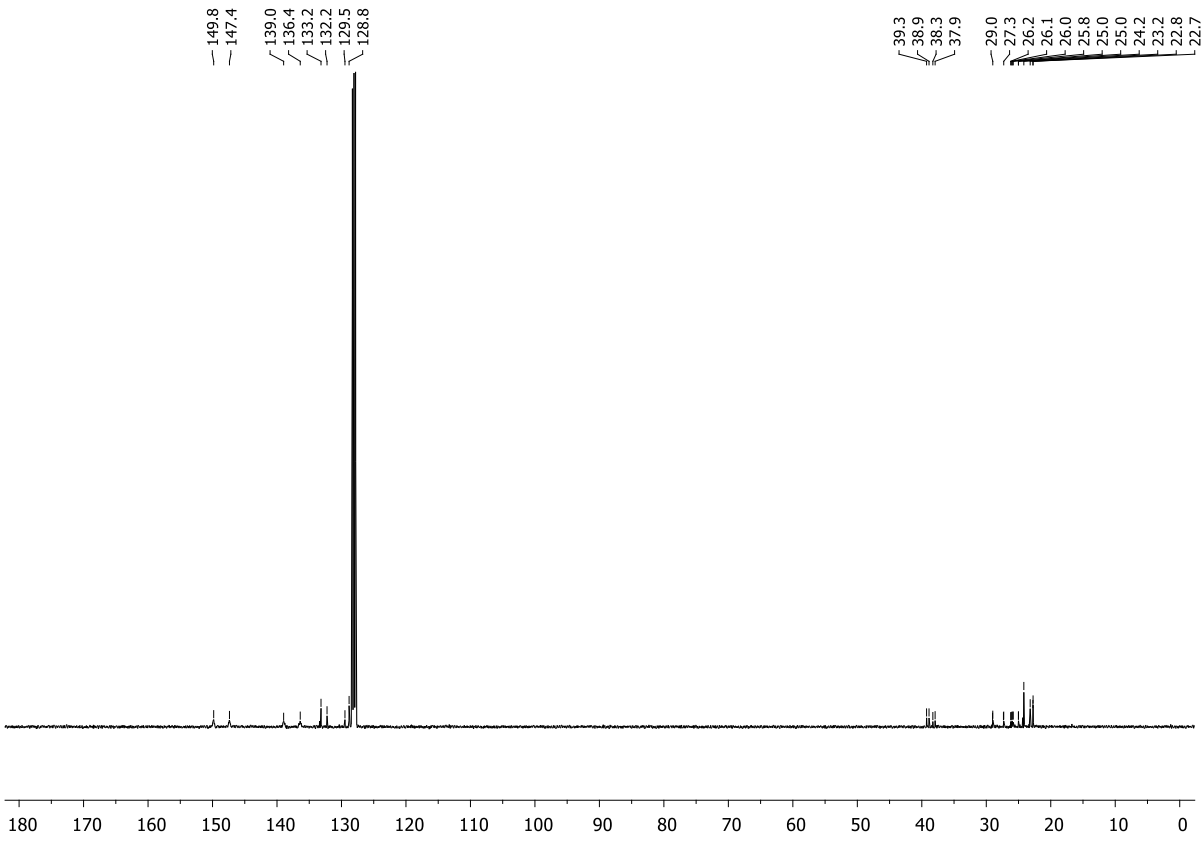

Figure S5.95. $^{13}C\{^{1}H\}$ NMR spectrum (C_6D_6, 298 K) of (R_P,R_{Si}/S_{Si})-**18**[$HB(C_6F_5)_3$].

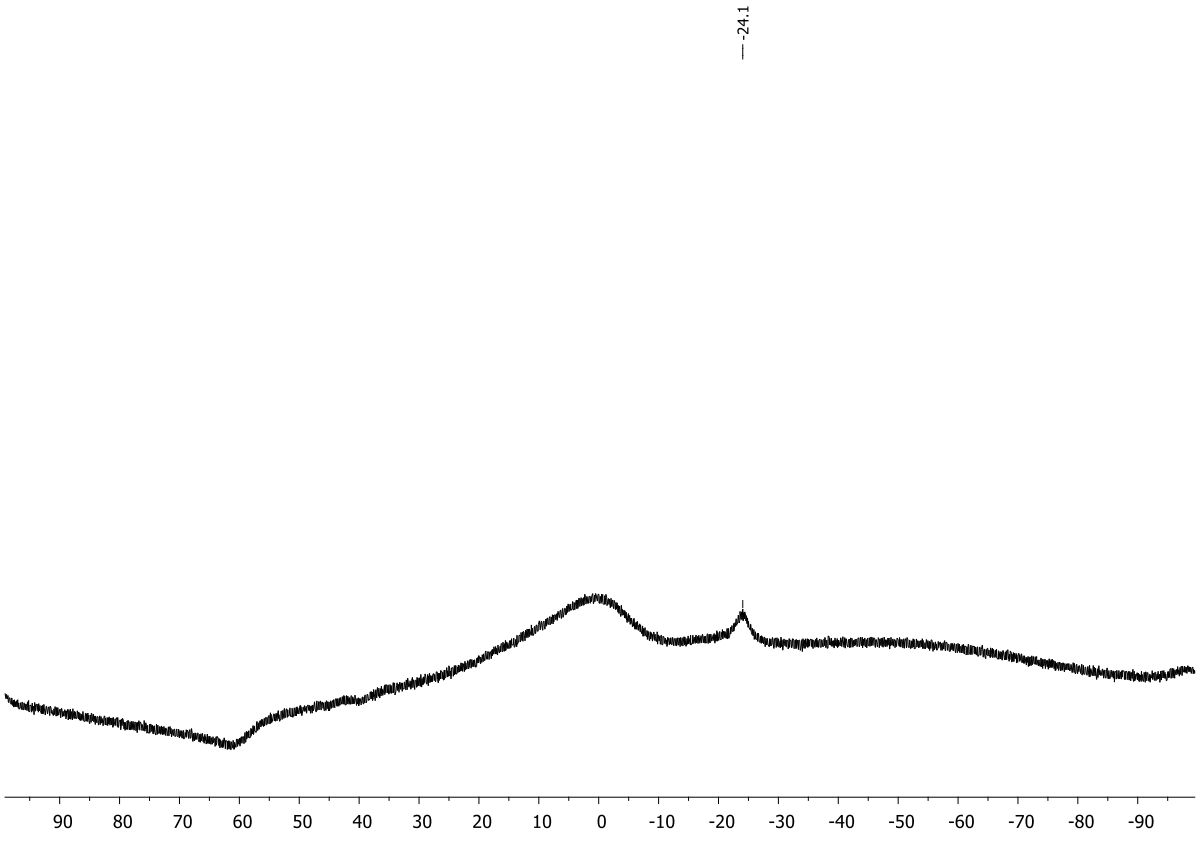

Figure S5.96. $^{11}B\{^{1}H\}$ NMR spectrum (C_6D_6, 298 K) of (R_P,R_{Si}/S_{Si})-**18**[$HB(C_6F_5)_3$].

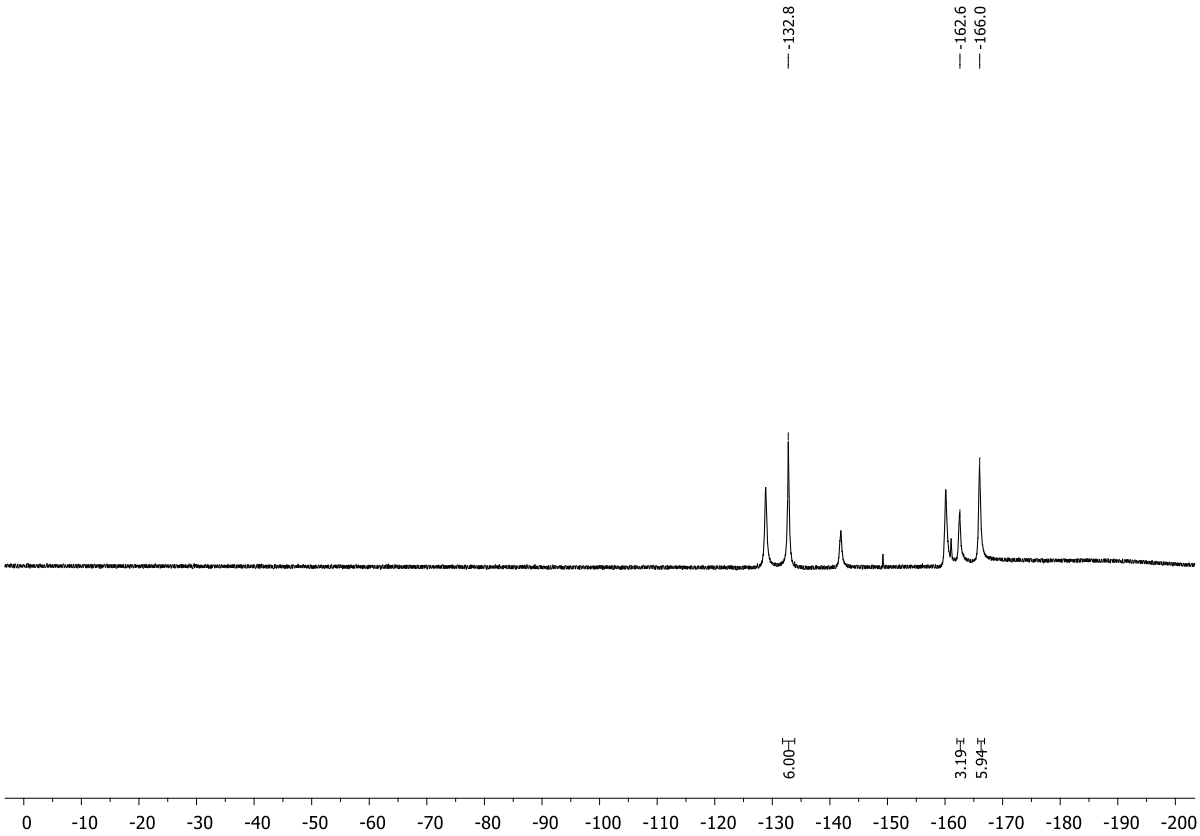

Figure S5.97. $^{19}F\{^{1}H\}$ NMR spectrum (CD_2Cl_2, 298 K) of (R_P,R_{Si}/S_{Si})-**18**[$HB(C_6F_5)_3$] with impurities of BCF.

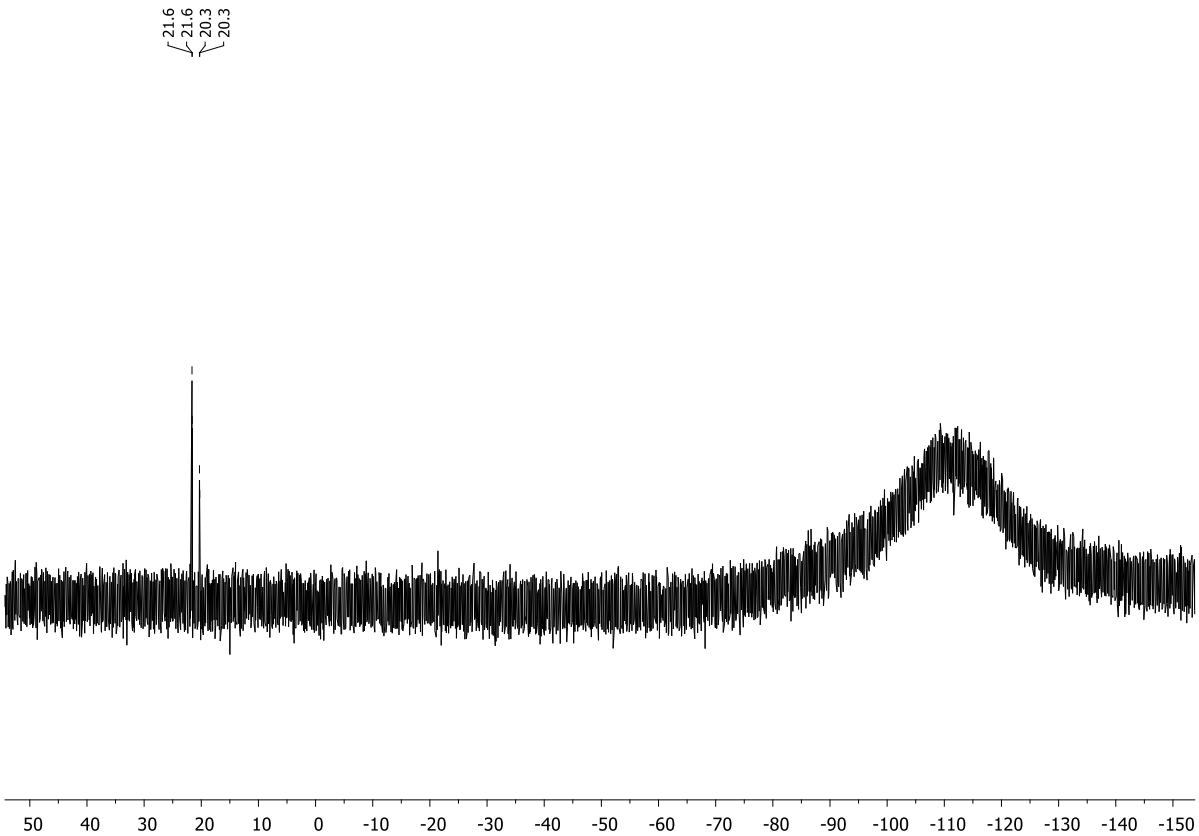

Figure S5.98. $^{29}Si\{^{1}H\}$ NMR spectrum (C_6D_6, 298 K) of (R_P,R_{Si}/S_{Si})-**18**[$HB(C_6F_5)_3$].

5.6.2.16. Attempt to Ring Opening of (R_P,R_{Si}/S_{Si})-18)[HB(C_6F_5)$_3$]

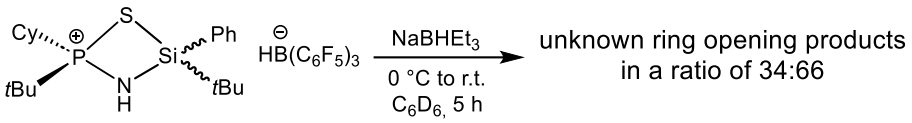

(R_P,S_{Si}/R_{Si})-**18**[HB(C_6F_5)$_3$]

The crude reaction mixture of compound (R_P,R_{Si}/S_{Si})-**18**[HB(C_6F_5)$_3$] (0.21 mmol, 1.0 equiv.) in C_6D_6 was treated with an excess of sodium triethylborohydride (0.25 mL, 0.25 mmol, 1.2 equiv., 1.0 M in toluene) at 0 °C. The mixture was allowed to slowly warm to room temperature, affording a colorless suspension. NMR spectroscopy was carried out without any purification.

^{1}H NMR (400.13 MHz, C_6D_6, 298 K): 1.07 (br, 0.66H, PC(CH_3)$_3$, major product), 1.31 (br, 0.34H, PC(CH_3)$_3$, minor product), other product signals not visible due to strong broadening. **^{31}P{^{1}H} NMR** (162.04 MHz, C_6D_6, 298 K): δ = 71.5 (s, 0.34P, minor product), 70.3 (s, 0.66P, major product).

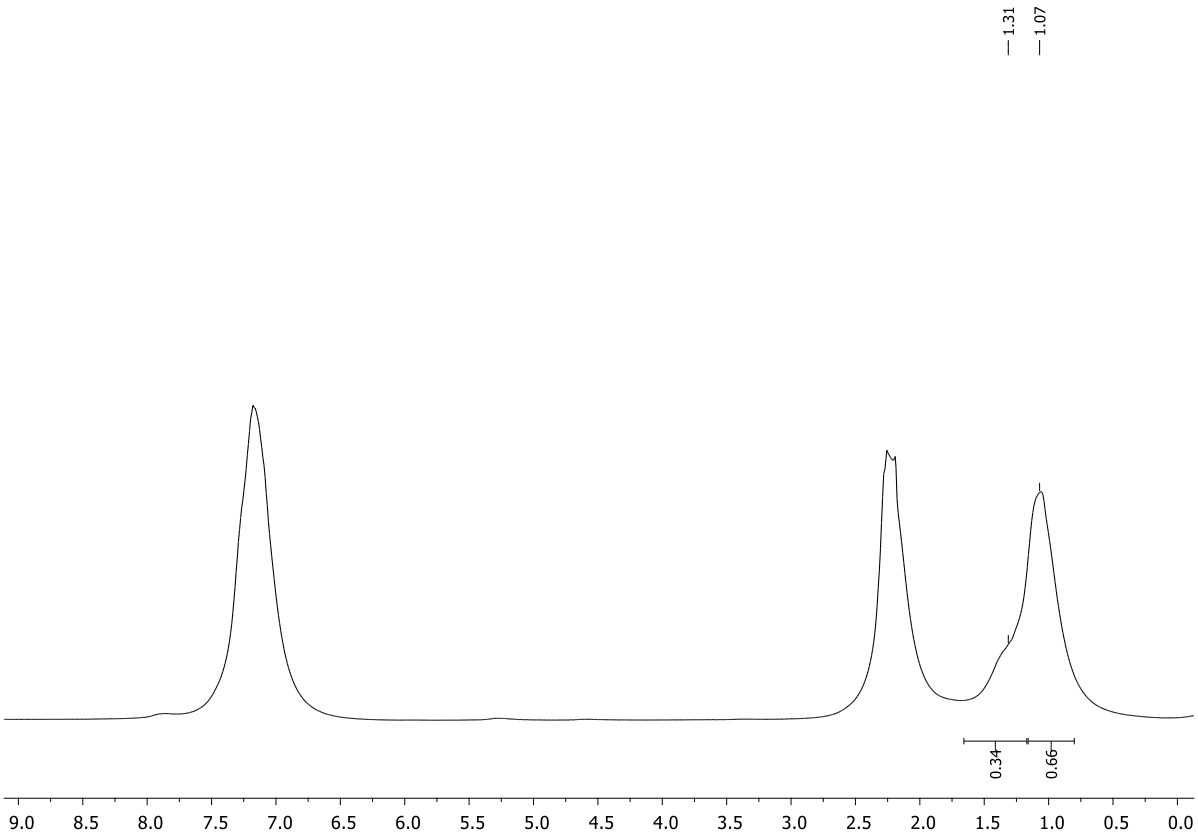

Figure S5.99. ^{1}H NMR spectrum (C_6D_6, 298 K) of the ring opening attempt of compound (R_P,R_{Si}/S_{Si})-**18**[HB(C_6F_5)$_3$].

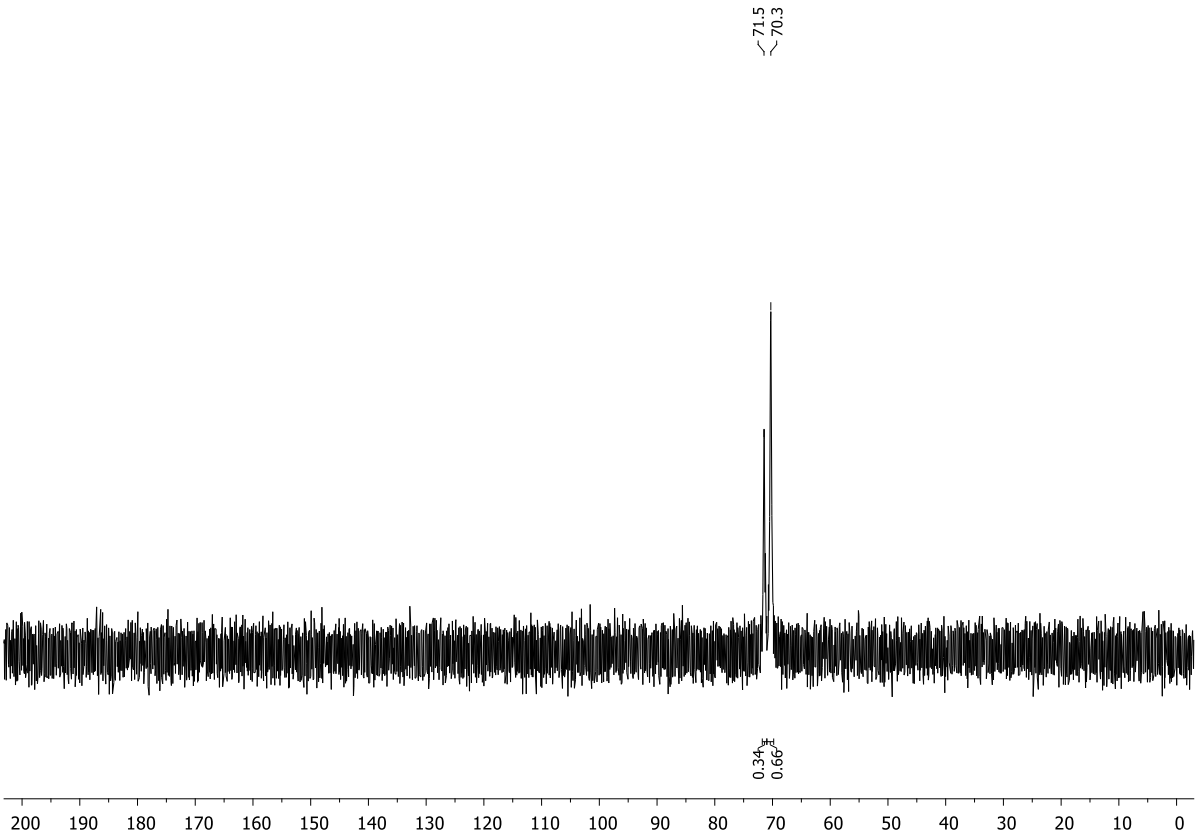

Figure S5.100. ^{31}P{^{1}H} NMR spectrum (C_6D_6, 298 K) of the ring opening attempt of compound (R_P,R_{Si}/S_{Si})-**18**[HB(C_6F_5)$_3$].

5.6.3. Six-Membered NPSSiOSi Ring System and Its Precursors

5.6.3.1. Synthesis of *t*Bu$_2$(PS)NH(SiPh$_2$OSi*t*BuHPh) (*rac*-19)

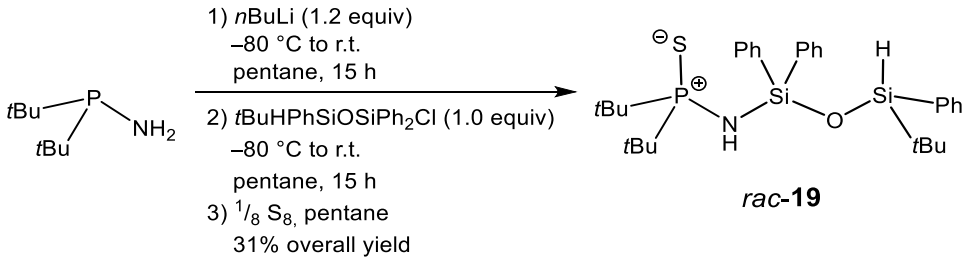

rac-**19**

*n*Butyllithium (2.33 mL, 3.72 mmol, 1.2 equiv., 1.6 M in hexane) was added dropwise to a solution of *P*,*P*-di-*tert*-butylaminophosphine (0.50 g, 3.10 mmol, 1.0 equiv.) in *n*-pentane (10 mL) at –80 °C. The solution was allowed to slowly warm to room temperature and stirred for 15 h. Following, the colorless solution was cooled to –80 °C again and 3-(*tert*-butyl)-1-chloro-1,1,3-triphenyldisiloxane (1.23 g, 3.10 mmol, 1.0 equiv.) was added dropwise. The reaction mixture was allowed to slowly warm to room temperature and stirred for 15 h affording a yellow suspension. The precipitated lithium chloride was filtered off via cannula filtration and washed with *n*-pentane. Then, all volatiles of the filtrate were removed under vacuum. The crude oily mixture was purified by Kugelrohr distillation (230 °C oven temperature, 1.0×10^{-2} mbar). The unoxidized intermediate *t*Bu$_2$PNHSiPh$_2$OSi*t*BuHPh was obtained as a yellowish viscous oil (0.58 g, 1.11 mmol, 36%).
For oxidation, sulfur (0.036 g, 1.11 mmol, 1.0 equiv.) was suspended in 1 mL pentane and cooled to 0 °C. *t*Bu$_2$PNHSiPh$_2$OSi*t*BuHPh (0.58 g, 1.11 mmol, 1.0 equiv.) in 5 mL pentane was added dropwise to the suspension. The mixture was allowed to slowly warm to room temperature and stirred for 15 h. Then, all volatiles were removed in vacuo and the product was extracted with pentane. After removing the solvent and drying in vacuo, compound *rac*-**19** was obtained as a colorless viscous oil (0.54 g, 0.97 mmol, 87%).

^{1}H NMR (400.13 MHz, CD_2Cl_2, 298 K): δ = 0.92 (s, 9H, SiC(C*H*$_3$)$_3$), 1.15 (d, $^3J_{H–P}$ = 15.5 Hz, 9H, PC(C*H*$_3$)$_3$), 1.16 (d, $^3J_{H–P}$ = 15.5 Hz, 9H, PC(C*H*$_3$)$_3$), 2.53 (br, 1H, N*H*), 5.02 (s, 1H, Si*H*), 7.29–7.44 (m, 10H, *H*$_{Ph}$), 7.57–7.59 (m, 2H, *H*$_{Ph}$), 7.76–7.79 (m, 3H, *H*$_{Ph}$). **^{31}P{^{1}H} NMR** (162.04 MHz, CD_2Cl_2, 298 K): δ = 91.0 (s). **^{13}C{^{1}H} NMR** (100.61 MHz, CD_2Cl_2, 298 K): δ = 18.9 (s, Si*C*(CH$_3$)$_3$), 26.0 (s, SiC(*C*H$_3$)$_3$), 27.8 (d, $^2J_{C–P}$ = 1.6 Hz, PC(*C*H$_3$)$_3$), 27.8 (d, $^2J_{C–P}$ = 1.7 Hz, PC(*C*H$_3$)$_3$), 40.0 (d, $^1J_{C–P}$ = 53.4 Hz, P*C*(CH$_3$)$_3$), 40.1 (d, $^1J_{C–P}$ = 53.3 Hz, P*C*(CH$_3$)$_3$), 127.9 (s, *C*$_{Ph}$), 128.0 (s, *C*$_{Ph}$), 128.2 (s, *C*$_{Ph}$), 130.4 (s, *C*$_{Ph}$), 130.5 (s, *C*$_{Ph}$), 130.5 (s, *C*$_{Ph}$), 135.1 (s, *C*$_{Ph}$), 135.4 (s, *C*$_{Ph}$), 135.8 (s, *C*$_{Ph}$), 136.0 (s, *C*$_{Ph}$). **^{29}Si NMR** (79.49 MHz, CD_2Cl_2, 298 K): δ = –32.8 (s, *Si*Ph$_2$), –5.6 (d, $^1J_{Si–H}$ = 209.7 Hz, *t*BuPhH*Si*).
Elemental analysis: $C_{33}H_{44}NOPSSi_2$: calcd.: C 65.05, H 8.01, N 2.53; found: C 65.20, H 7.14, N 2.30.
HR(+ESI)-MS: calcd. *m/z* for $C_{33}H_{44}NOPSSi_2$ [(M+H)$^+$]: 554.2493, found: 554.2497.

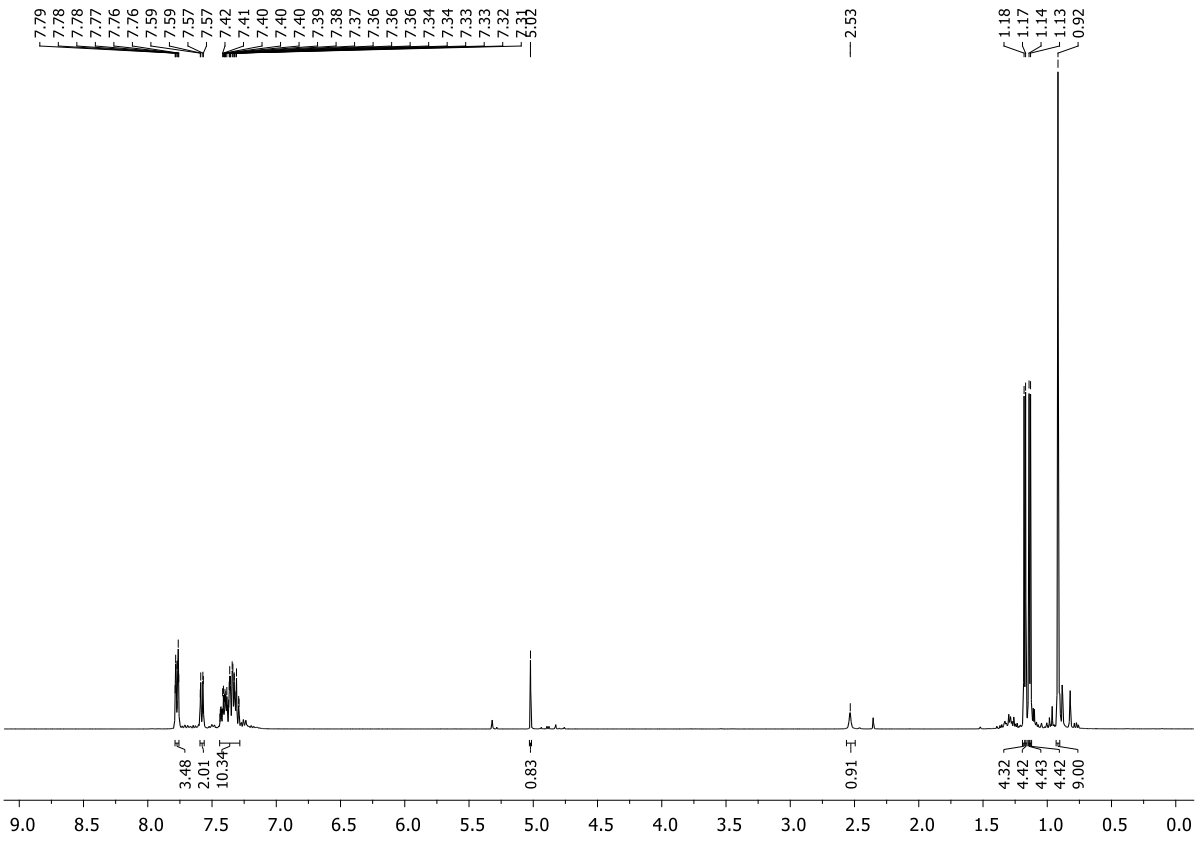

Figure S5.101. ^{1}H NMR spectrum (CD_2Cl_2, 298 K) of *rac*-**19**.

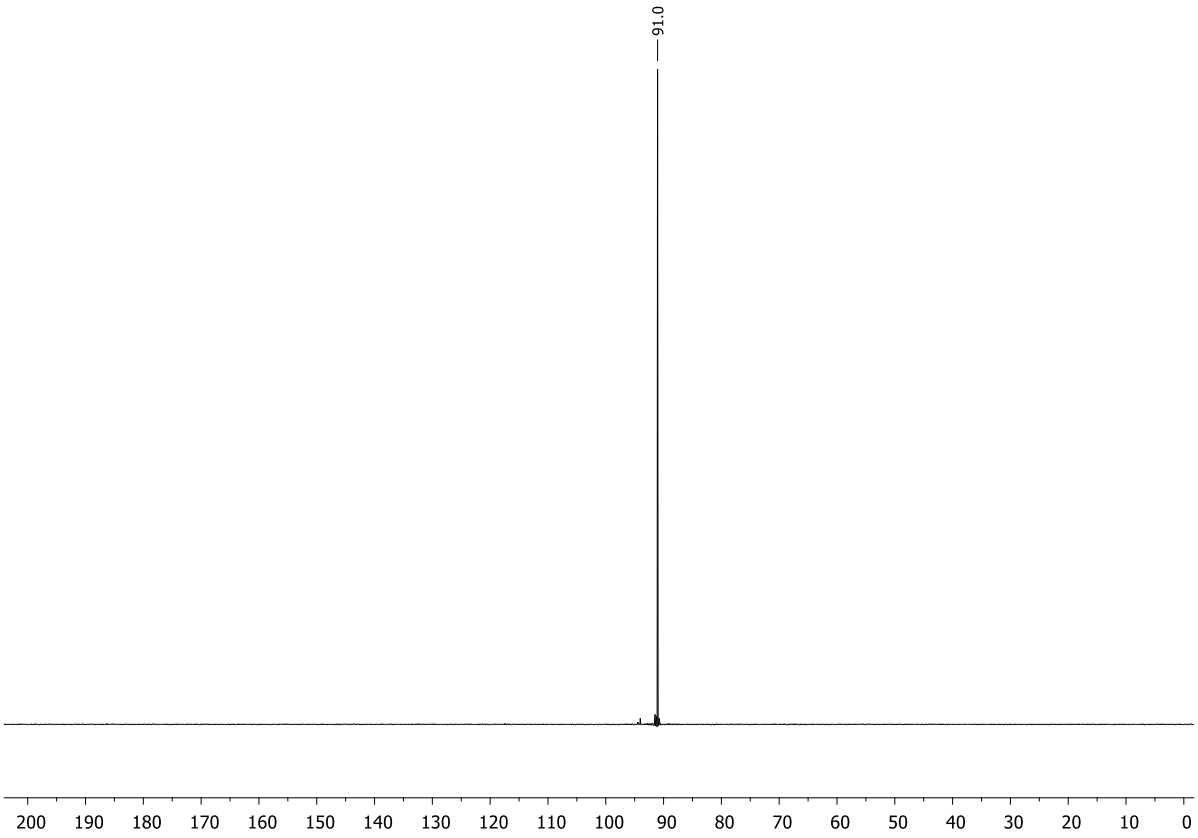

Figure S5.102. $^{31}P\{^{1}H\}$ NMR spectrum (CD_2Cl_2, 298 K) of *rac*-**19**.

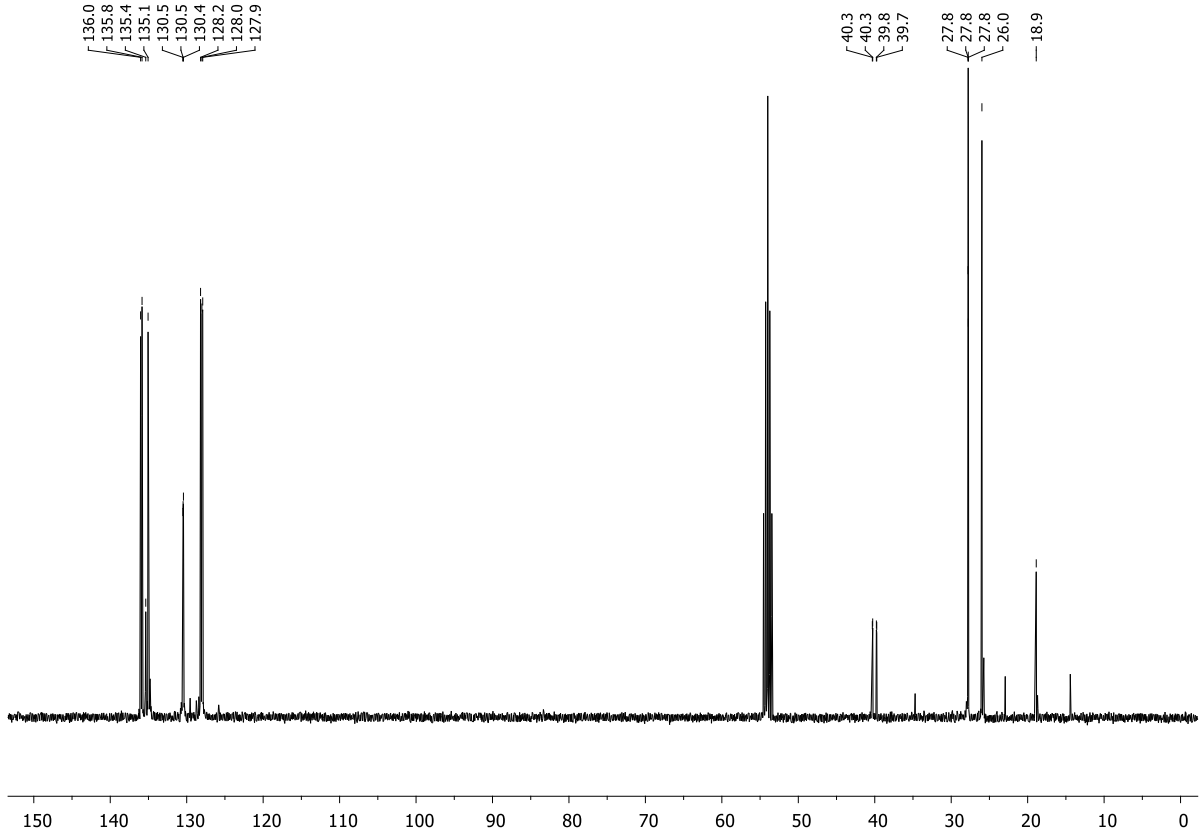

Figure S5.103. $^{13}C\{^{1}H\}$ NMR spectrum (CD_2Cl_2, 298 K) of *rac*-**19**.

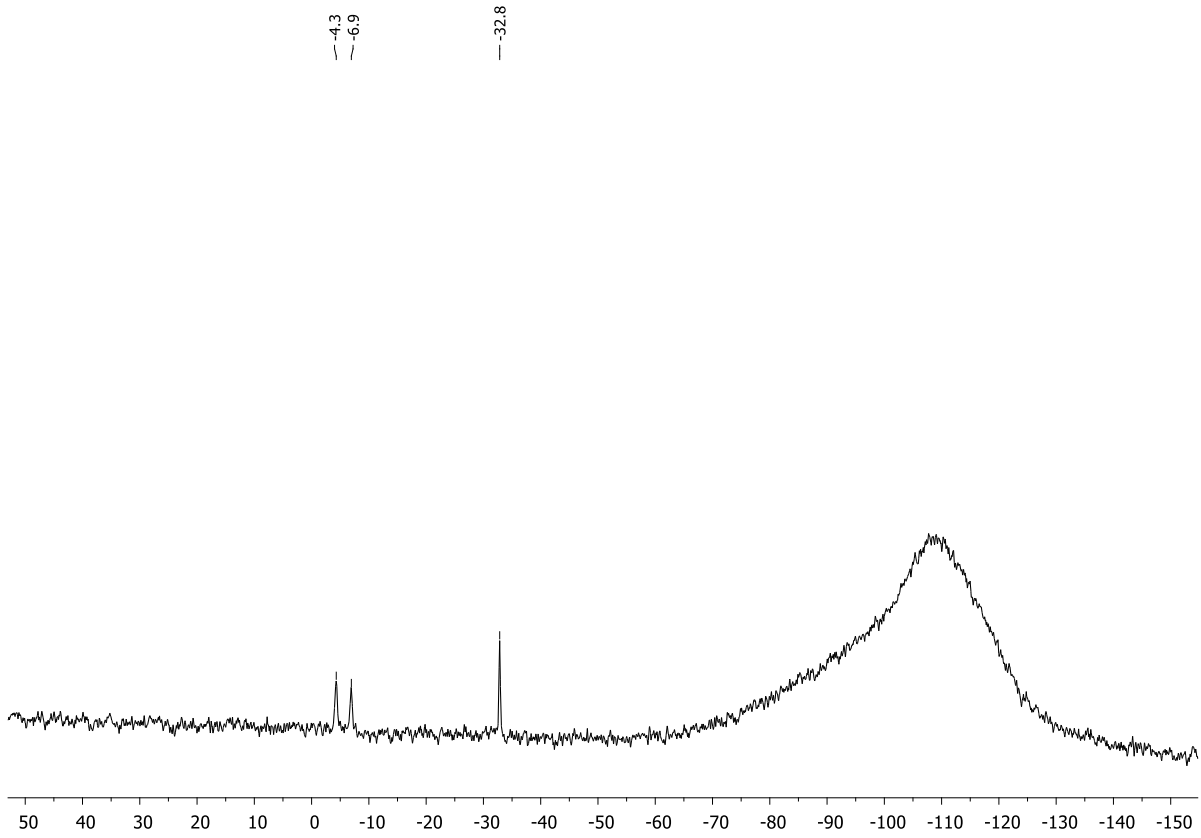

Figure S5.104. ^{29}Si NMR spectrum (CD_2Cl_2, 298 K) of *rac*-**19**.

5.6.3.2. Synthesis of [*t*Bu$_2$(PS)NH(SiPh$_2$OSi*t*BuPh)]$^+$ [HB(C$_6$F$_5$)$_3$]$^-$ {rac-20[HB(C$_6$F$_5$)$_3$]} and crystallization of [*t*Bu$_2$(PSH)NH$_2$]$^+$ [(μ-OH)(BCF)$_2$]$^-$ {21[(μ-OH)(BCF)$_2$]}

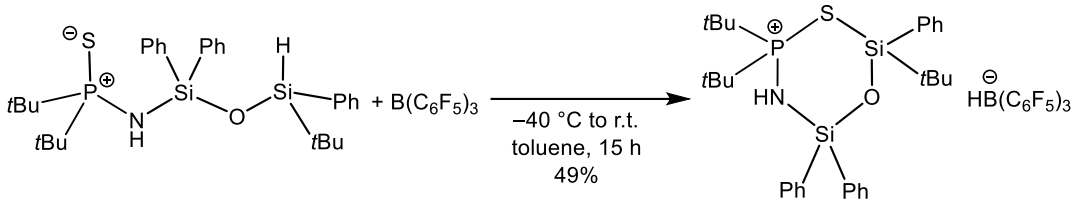

rac-**19** *rac*-**20**[HB(C$_6$F$_5$)$_3$]

A solution of compound *rac*-**19** (0.97 g, 1.75 mmol, 1.0 equiv.) in toluene (10 mL) was added to a solution of tris(pentafluorophenyl)borane (0.90 g, 1.75 mmol, 1.0 equiv.) in toluene (10 mL) at –40 °C. The solution was allowed to slowly warm to room temperature and stirred for 15 h. The oily crude product was precipitated by slowly transferring the resulting colorless solution into another Schlenk flask containing pentane (50 mL). The upper liquid phase was decanted, and the oily lower phase was washed with pentane. After drying in vacuo, compound *rac*-**20**[HB(C$_6$F$_5$)$_3$] was obtained as a foamy colorless solid (0.92 g, 0.86 mmol, 49%).

^{1}H NMR (400.13 MHz, CD_2Cl_2, 298 K): δ = 1.12 (s, 9H, SiC(C*H*$_3$)$_3$), 1.30 (d, $^3J_{H–P}$ = 18.6 Hz, 9H, PC(C*H*$_3$)$_3$), 1.38 (d, $^3J_{H–P}$ = 18.7 Hz, 9H, PC(C*H*$_3$)$_3$), 2.87 (br, 1H, N*H*), 7.38–7.39 (m, 4H, *H*$_{Ph}$), 7.42–7.46 (m, 2H, *H*$_{Ph}$), 7.54–7.68 (m, 7H, *H*$_{Ph}$), 7.74–7.77 (m, 2H, *H*$_{Ph}$). **^{31}P{^{1}H} NMR** (162.04 MHz, CD_2Cl_2, 298 K): δ = 100.1 (s). **^{13}C{^{1}H} NMR** (100.61 MHz, CD_2Cl_2, 298 K): δ = 23.4 (s, Si*C*(CH$_3$)$_3$), 25.1 (s, SiC(*C*H$_3$)$_3$), 26.8 (d, $^2J_{C–P}$ = 1.3 Hz, PC(*C*H$_3$)$_3$), 26.9 (d, $^2J_{C–P}$ = 1.6 Hz, PC(*C*H$_3$)$_3$), 42.7 (d, $^1J_{C–P}$ = 39.6 Hz, P*C*(CH$_3$)$_3$), 43.5 (d, $^1J_{C–P}$ = 41.3 Hz, P*C*(CH$_3$)$_3$), 129.1 (s, *C*$_{Ph}$), 129.2 (s, *C*$_{Ph}$), 129.5 (s, *C*$_{Ph}$), 132.9 (s, *C*$_{Ph}$), 133.0 (s, *C*$_{Ph}$), 133.2 (s, *C*$_{Ph}$), 135.1 (s, *C*$_{Ph}$), 135.2 (s, *C*$_{Ph}$), 135.5 (s, *C*$_{Ph}$). **^{11}B{^{1}H} NMR** (128.43 MHz, CD_2Cl_2, 298 K): δ = –25.6 (s). **^{19}F{^{1}H} NMR** (376.66 MHz, CD_2Cl_2, 298 K): δ = –165.6 (m, 6F, *meta*-*F*$_{Ar\text{-}borate}$), –159.5 (m, 3F, *para*-*F*$_{Ar\text{-}borate}$), –133.2 (m, 6F, *ortho*-*F*$_{Ar\text{-}borate}$). **^{29}Si{^{1}H} NMR** (79.49 MHz, CD_2Cl_2, 298 K): δ = –26.1 (d, $^2J_{Si–P}$ = 6.6 Hz, *Si*Ph$_2$), –3.3 (d, $^2J_{Si–P}$ = 4.3 Hz, *t*BuPh*Si*).

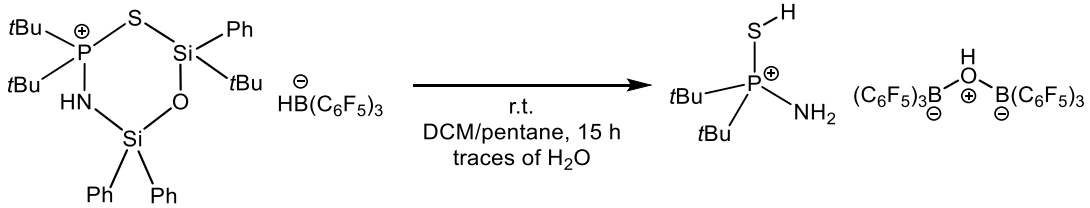

rac-**20**[HB(C$_6$F$_5$)$_3$] **21**[(μ-OH)(BCF)$_2$]

Crystallization of *rac*-**20**[HB(C$_6$F$_5$)$_3$] turned out to be challenging and mostly lead to oily precipitates. Only once, crystals suitable for single-crystal X-ray analysis could be obtained by layering a DCM solution with pentane. X-ray measurement revealed that the siloxane moiety has cleaved from the cation and that the anion has dimerized, very likely due to moisture. The crystal structure of **21**[(μ-OH)(BCF)$_2$] could be obtained.

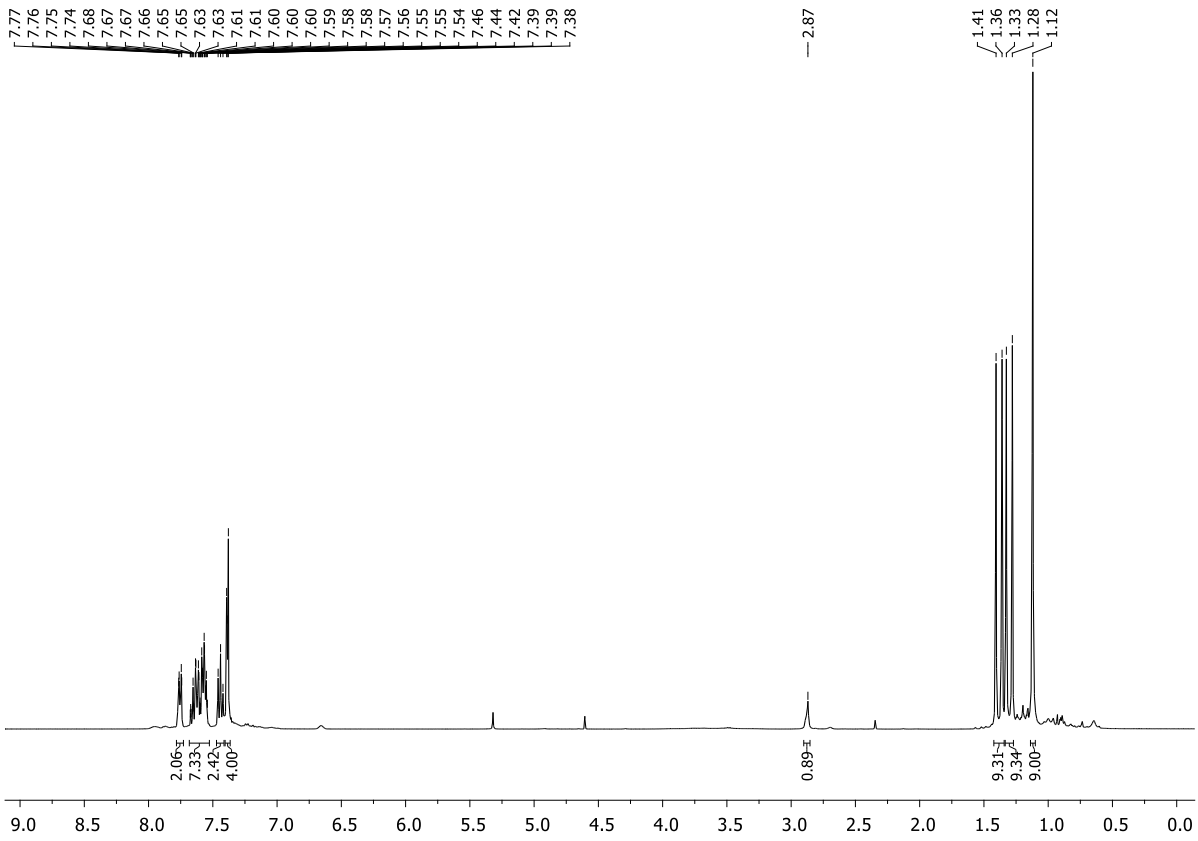

Figure S5.105. ^{1}H NMR spectrum (CD_2Cl_2, 298 K) of *rac*-**20**[$HB(C_6F_5)_3$].

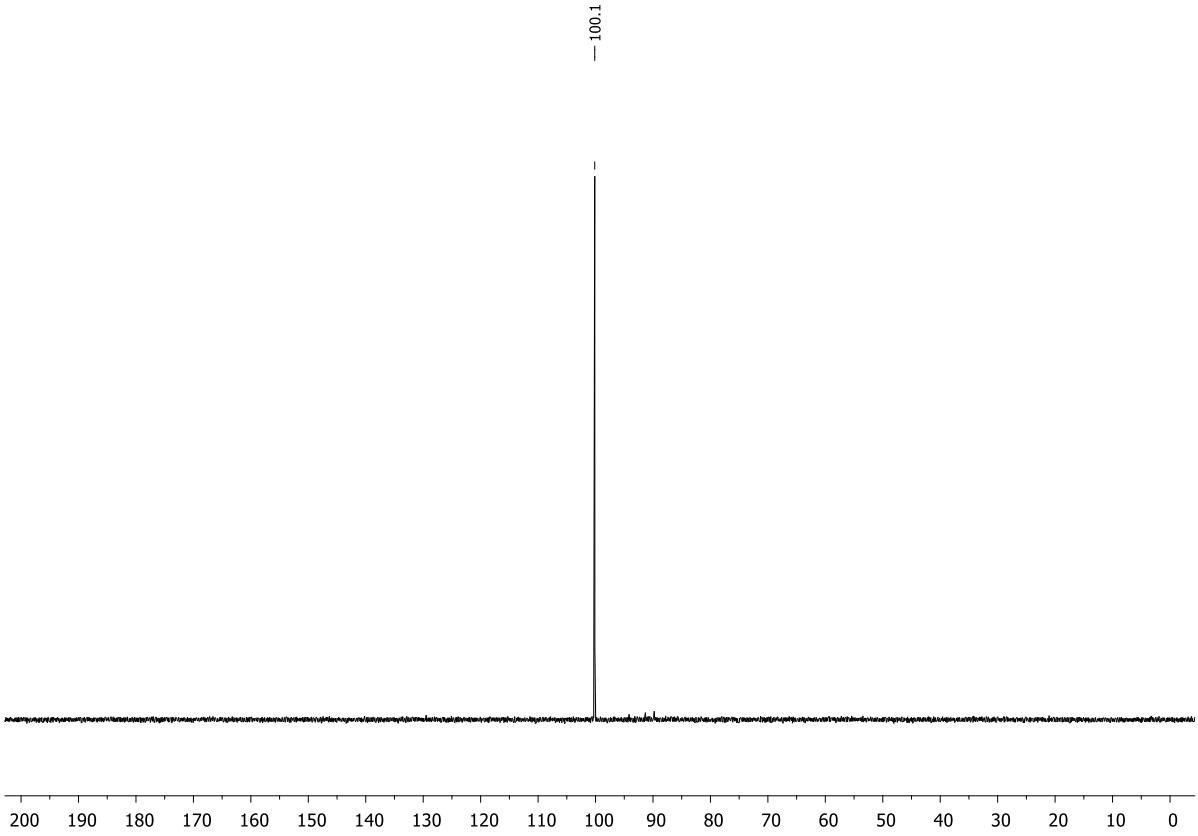

Figure S5.106. $^{31}P\{^{1}H\}$ NMR spectrum (CD_2Cl_2, 298 K) of *rac*-**20**[$HB(C_6F_5)_3$].

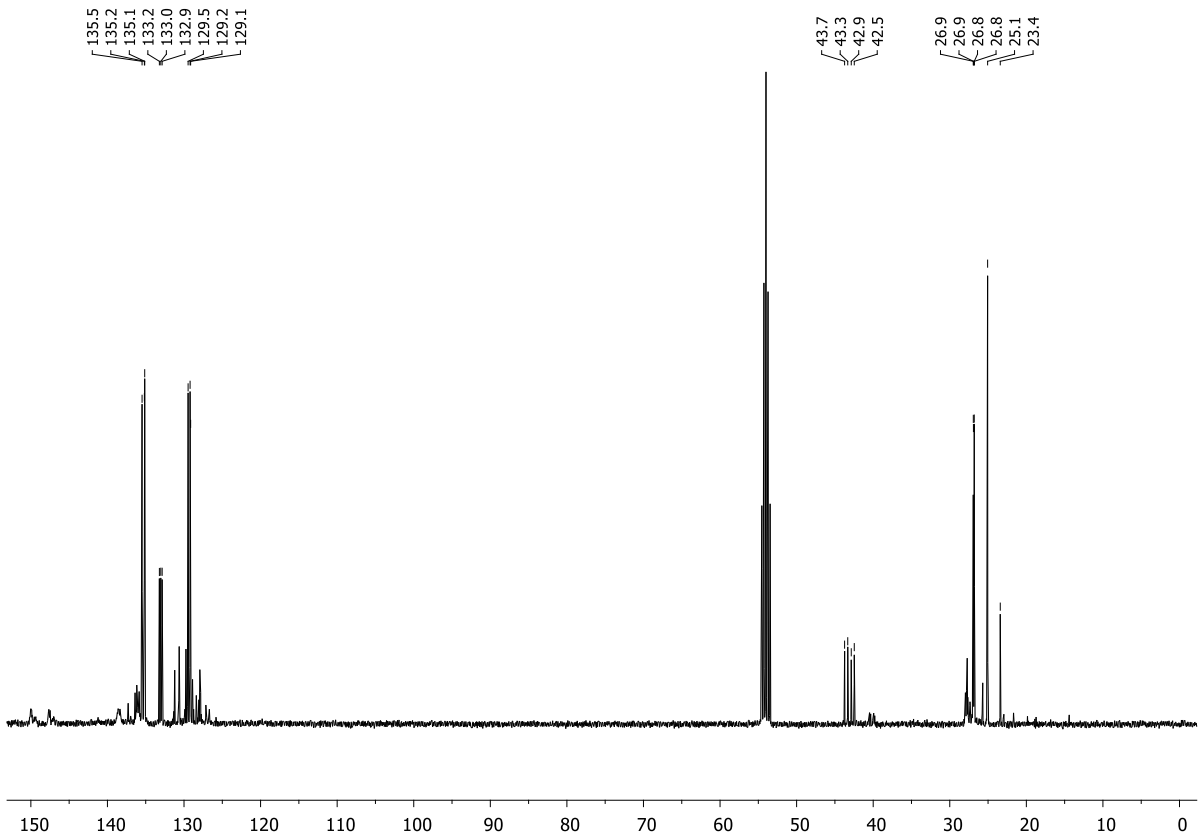

Figure S5.107. $^{13}C\{^{1}H\}$ NMR spectrum (CD_2Cl_2, 298 K) of *rac*-**20**[$HB(C_6F_5)_3$].

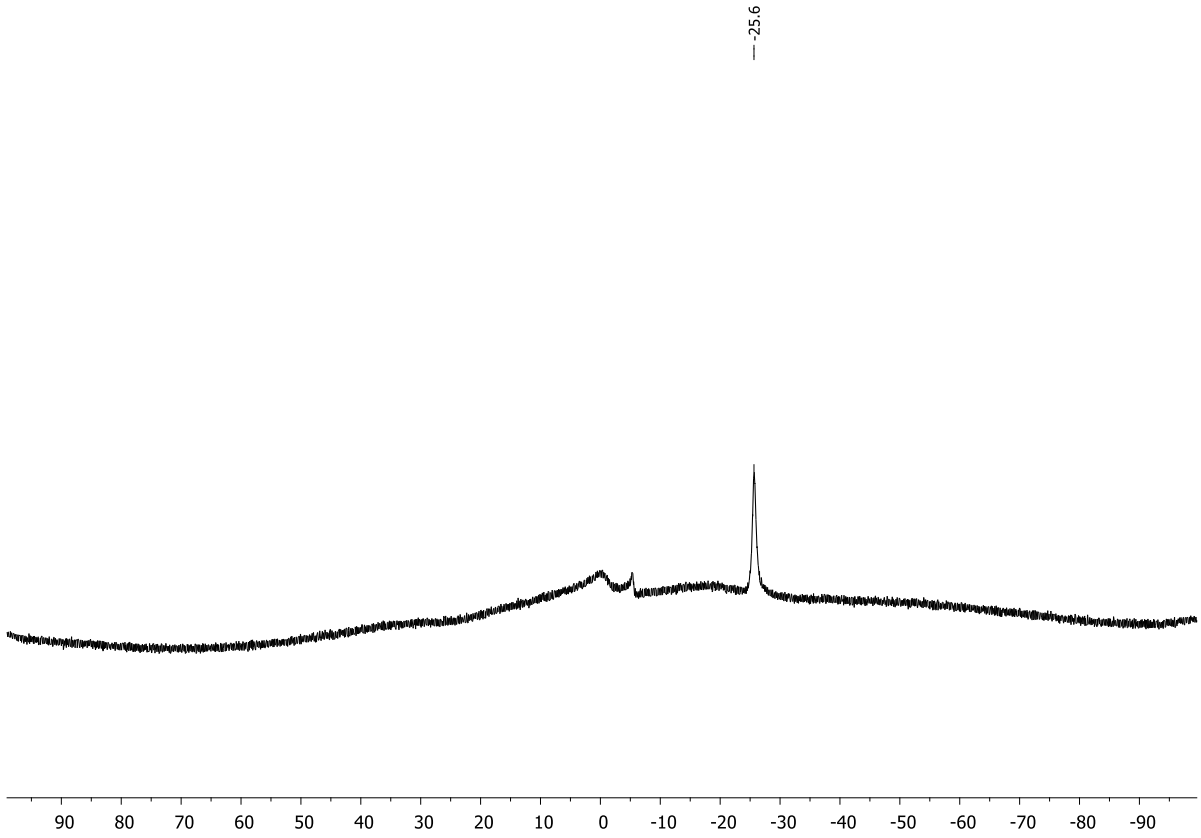

Figure S5.108. $^{11}B\{^{1}H\}$ NMR spectrum (CD_2Cl_2, 298 K) of *rac*-**20**[$HB(C_6F_5)_3$].

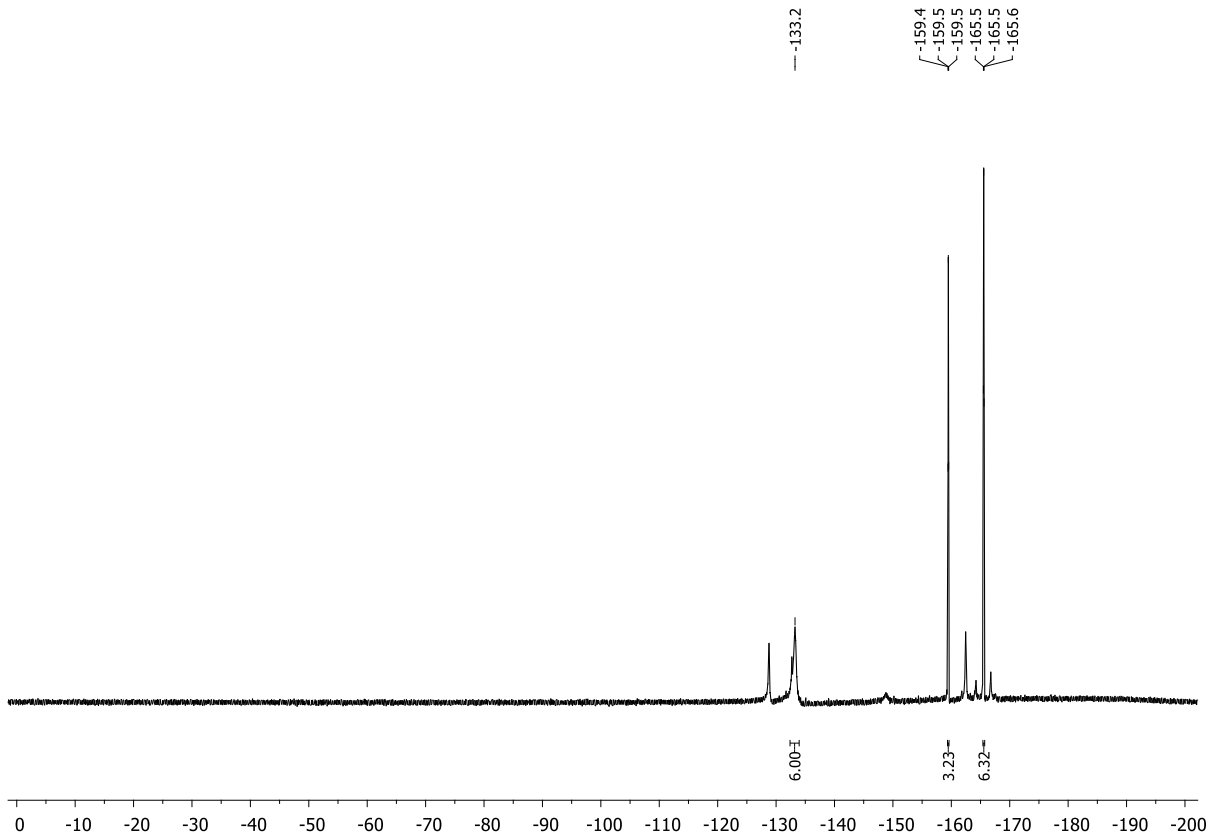

Figure S5.109. $^{19}F\{^{1}H\}$ NMR spectrum (CD_2Cl_2, 298 K) of *rac*-**20**[$HB(C_6F_5)_3$].

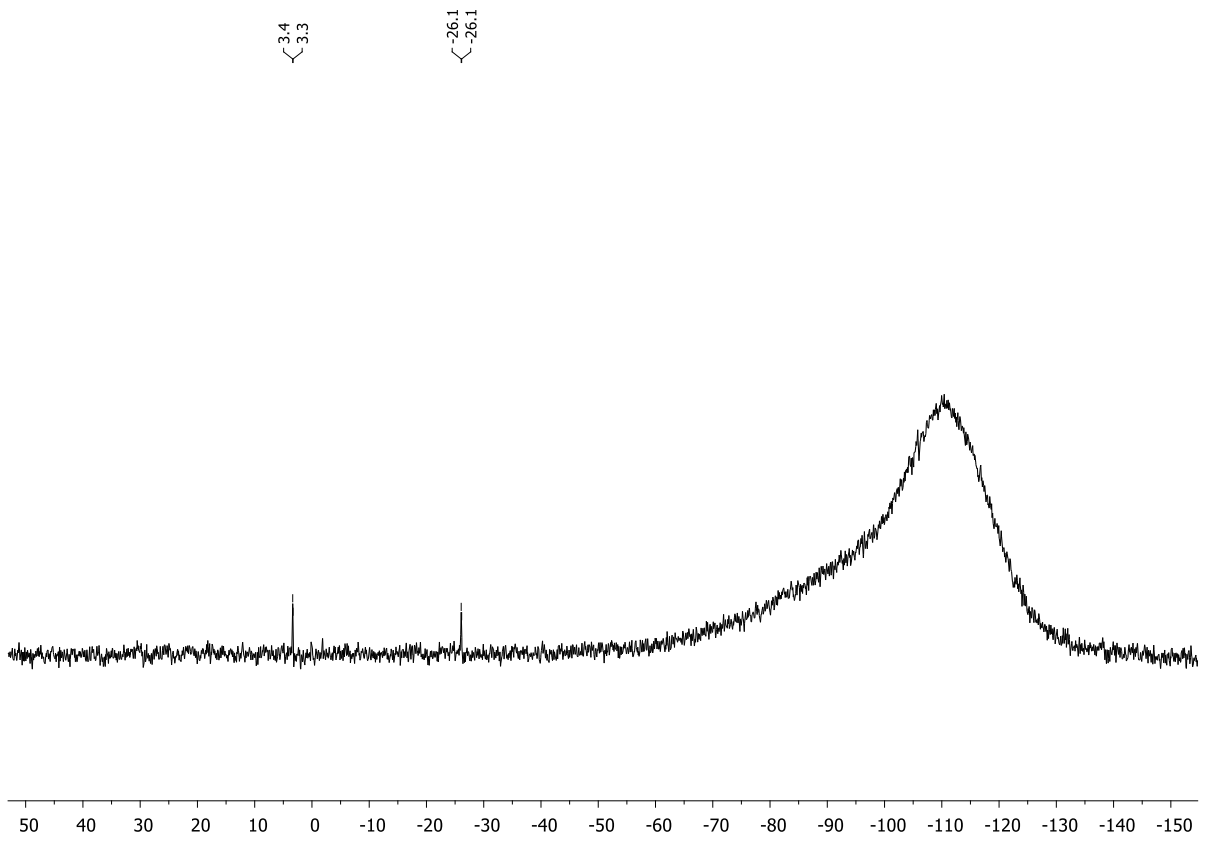

Figure S5.110. $^{29}Si\{^{1}H\}$ NMR spectrum (CD_2Cl_2, 298 K) of *rac*-**20**[$HB(C_6F_5)_3$].

5.7. X-Ray Crystallographic Details

The crystals were selected and measured on a XtaLAB Synergy R, DW system, HyPix-Arc 150 {**2**, **3**[HB(C_6F_5)$_3$], **4**, **5**[HB(C_6F_5)$_3$], **9**[HB(C_6F_5)$_3$], **10**, (R_P)-**13**, (R_P)-**14**, (R_P,S_{Si})-**17**, (R_P,S_{Si})-**18**[HB(C_6F_5)$_3$], *rac*-**21**[(μ-OH)(BCF)$_2$]}, on a Xcalibur, AtlasS2, Gemini ultra (*rac*-**6**), on a GV1000, TitanS2 {*rac*-**7**[HB(C_6F_5)$_3$]}, on a SuperNova, Dualflex, TitanS2 (*rac*-**8** · NH_4^+ HB(C_6F_5)$_3^-$). The crystals were kept at T = 123(1) K {**2**, **3**[HB(C_6F_5)$_3$], **4**, **5**[HB(C_6F_5)$_3$], *rac*-**8** · NH_4^+ HB(C_6F_5)$_3^-$, **10**, (R_P)-**13**, (R_P)-**14**, (R_P,S_{Si})-**17**, (R_P,S_{Si})-**18**[HB(C_6F_5)$_3$]}, 100(1) K {**9**[HB(C_6F_5)$_3$], *rac*-**21**[(μ-OH)(BCF)$_2$]}, 293(2) K (*rac*-**6**) or 166(60) K {*rac*-**7**[HB(C_6F_5)$_3$]} during data collection. Data collection and reduction were performed with **CrysAlisPro** Version 1.171.42.95a {**2**, **3**[HB(C_6F_5)$_3$], **4**, **5**[HB(C_6F_5)$_3$], **10**, (R_P)-**14**, (R_P,S_{Si})-**17**}, Version 1.171.39.46 (*rac*-**6**), Version 1.171.41.76a {*rac*-**7**[HB(C_6F_5)$_3$]}, Version 1.171.40.66a (*rac*-**8** · NH_4^+ HB(C_6F_5)$_3^-$), Version 1.171.41.83a {**9**[HB(C_6F_5)$_3$]}, Version 1.171.41.93a [(R_P)-**13**] or Version 1.171.42.58a {(R_P,S_{Si})-**18**[HB(C_6F_5)$_3$]}.[6] For all compounds a numerical absorption correction based on gaussian integration over a multifaceted crystal model and an empirical absorption correction using spherical harmonics as implemented in SCALE3 ABSPACK was applied. Using **Olex2**[7], the structures were solved with **ShelXT**[8] and a least-square refinement on F_2 was carried out with **ShelXL**[9] for all structures. All non-hydrogen atoms were refined anisotropically. Hydrogen atoms at the carbon atoms were located in idealized positions and refined isotropically according to the riding model. Hydrogen atoms at the nitrogen, silicon, sulfur and oxygen atoms were located from the difference Fourier map and refined without restraints, except for (R_P,S_{Si})-**18**[HB(C_6F_5)$_3$], whose hydrogen atoms at the nitrogen atoms were located in idealized positions and refined isotropically according to the riding model. Hydrogen atoms at the boron atoms in compounds **3**[HB(C_6F_5)$_3$], **5**[HB(C_6F_5)$_3$] and (R_P,S_{Si})-**18**[HB(C_6F_5)$_3$] were located in idealized positions and refined isotropically according to the riding model. Hydrogen atoms at the boron atoms in *rac*-**7**[HB(C_6F_5)$_3$], *rac*-**8** · NH_4^+ HB(C_6F_5)$_3^-$ and **9**[HB(C_6F_5)$_3$] were located from the difference Fourier map and refined without restraints. Figures were created with Olex2.[7]

Compound **2**: The asymmetric unit contains one molecule.
Compound **3**[HB(C_6F_5)$_3$]: The asymmetric unit contains one molecule of the cation and one molecule of the anion.
Compound **4**: The asymmetric unit contains one molecule.
Compound **5**[HB(C_6F_5)$_3$]: The asymmetric unit contains one molecule of the cation and one molecule of the anion.
Compound *rac*-**6**: The asymmetric unit contains one molecule.
Compound *rac*-**7**[HB(C_6F_5)$_3$]: The asymmetric unit contains one molecule of the cation and one molecule of the anion.
Compound *rac*-**8** · NH_4^+ HB(C_6F_5)$_3^-$: The asymmetric unit contains one molecule of the uncharged *N*-hydrosilyl-substituted aminophosphine sulfide, one disordered ammonium cation and one borate anion. The *tert*-butyl moieties at the phosphorus atom (C2, C3, C4 and C6, C7, C8) are disordered

over two positions and split into two parts with occupancies of 78:22 or 76:24, respectively. SADI and RIGU restraints were used to model these disorders. SIMU, SADI and RIGU restraints were used to model the disorder of the protons in the ammonium cation.

Compound **9**[$HB(C_6F_5)_3$]: The asymmetric unit contains one molecule.

Compound **10**: The asymmetric unit contains one molecule.

Compound (R_P)-**13**: The asymmetric unit contains one molecule.

Compound (R_P)-**14**: The asymmetric unit contains one molecule.

Compound (R_P,S_{Si})-**17**: The asymmetric unit contains one molecule. The *tert*-butyl moiety at the silicon atom (C12, C13, C14) is disordered over two positions and split into two parts with occupancies of 69:31. The phenyl moiety at the silicon atom (C15, C16, C17, C18, C19, C20) is disordered over two positions and split into two parts with occupancies of 56:44. SIMU and SADI restraints were used to model these disorders.

Compound (R_P,S_{Si})-**18**[$HB(C_6F_5)_3$]: The asymmetric unit contains four molecules of the cation and four molecules of the anion. Two of the cations (N3, P1A, S3, Si3 + the respective C atoms and N4, P2A, S4, Si4 + the respective C atoms) are disordered over two positions and split into two parts with occupancies of 41:59 or 33:67, respectively. One C_6F_5 moiety at B3 is disordered over two positions and split into two parts with occupancies of 77:23. SADI, SIMU, RIGU and ISOR restraints were used to model these disorders.

Compound *rac*-**21**[(μ-OH)$(BCF)_2$]: The asymmetric unit contains one molecule of the cation and one molecule of the anion. The asymmetric unit contains half a molecule dichloromethane (C45A, Cl1A, Cl2A), which is disordered over two positions and split into two parts with occupancies of 34:16. DANG, DFIX and SIMU restraints were used to model these disorders.

Table S5.1. Crystallographic data for compounds **2**, **3**[$HB(C_6F_5)_3$] and **4**.

Compound	**2**	**3**[$HB(C_6F_5)_3$]	**4**
Data Set (internal naming)	**BK11**	**BK17**	**BK15**
Formula	$C_{20}H_{30}NPSSi$	$C_{38}H_{30}BF_{15}NPSSi$	$C_{14}H_{34}NPSSi$
$\rho_{calc.}$ / g·cm^{-3}	1.182	1.555	1.080
μ/mm^{-1}	2.617	2.421	2.808
Formula Weight	375.57	887.56	307.54
Color	clear colorless	clear colorless	clear colorless
Shape	needle	block	needle
Size/mm^3	0.4 × 0.09 × 0.05	0.43 × 0.22 × 0.14	0.32 × 0.07 × 0.05
T/K	123.01(10)	123.00(10)	123.00(10)
Crystal System	orthorhombic	monoclinic	monoclinic
Flack Parameter	−0.01(4)	–	–
Hooft Parameter	–	–	–
Space Group	$Pna2_1$	$P2_1/n$	$P2_1/c$
a/Å	16.9481(2)	11.42660(10)	16.2223(2)
b/Å	20.0823(3)	18.95120(10)	6.22620(10)
c/Å	6.20240(10)	17.58030(10)	19.7590(2)
α/°	90	90	90
β/°	90	95.3400(10)	108.6420(10)
γ/°	90	90	90
V/Å^3	2111.03(5)	3790.45(4)	1891.02(4)
Z	4	4	4
Z'	1	1	1
Wavelength/Å	1.54184	1.54184	1.54184
Radiation Type	Cu K_α	Cu K_α	Cu K_α
$2\theta_{min}$/°	6.824	6.874	5.75
$2\theta_{max}$/°	150.572	150.39	150.574
Measured Refl.	16655	71997	27160
Independent Refl.	3714	7776	3881
R_{int}	0.0451	0.0377	0.0376
Parameters	231	533	181
Restraints	1	0	0
Largest Peak	0.54	0.29	0.48
Deepest Hole	−0.62	−0.44	−0.38
GooF	1.168	1.060	1.061
wR_2 (all data)	0.1695	0.1008	0.0891
wR_2	0.1679	0.0986	0.0876
R_1 (all data)	0.0591	0.0400	0.0335
R_1	0.0576	0.0364	0.0315

Table S5.2. Crystallographic data for compounds and **5**[$HB(C_6F_5)_3$], *rac*-**6** and *rac*-**7**[$HB(C_6F_5)_3$].

Compound	**5**[$HB(C_6F_5)_3$]	*rac*-**6**	*rac*-**7**[$HB(C_6F_5)_3$]
Data Set (internal naming)	**TH519**	**TH055**	**TH112**
Formula	$C_{32}H_{34}BF_{15}NPSSi$	$C_{18}H_{34}NPSSi$	$C_{36}H_{34}BF_{15}NPSSi$
$\rho_{calc.}$ / g·cm^{-3}	1.500	1.134	1.527
μ/mm^{-1}	2.470	2.619	2.412
Formula Weight	819.53	355.58	867.57
Color	clear colorless	clear colorless	clear colorless
Shape	plate	block	block
Size/mm^3	0.5 × 0.45 × 0.15	0.31 × 0.224 × 0.099	0.31 × 0.147 × 0.118
T/K	123.01(10)	293(2)	166(60)
Crystal System	monoclinic	monoclinic	orthorhombic
Flack Parameter	–	–	−0.02(3)
Hooft Parameter	–	–	–
Space Group	$P2_1/c$	$P2_1/c$	$Pna2_1$
a/Å	17.40980(10)	18.0296(3)	17.1324(6)
b/Å	11.83110(10)	6.41460(10)	21.2722(9)
c/Å	17.67910(10)	19.6993(3)	10.3571(3)
α/°	90	90	90
β/°	94.8860(10)	113.920(2)	90
γ/°	90	90	90
V/Å^3	3628.26(4)	2082.60(6)	3774.6(2)
Z	4	4	4
Z'	1	1	1
Wavelength/Å	1.54184	1.54184	1.54184
Radiation Type	Cu K_α	Cu K_α	Cu K_α
$2\theta_{min}$/°	5.094	9.084	6.624
$2\theta_{max}$/°	147.914	143.724	148.74
Measured Refl.	47329	13452	19563
Independent Refl.	7165	3987	7204
R_{int}	0.0270	0.0252	0.0416
Parameters	483	226	522
Restraints	0	0	1
Largest Peak	0.61	0.35	0.33
Deepest Hole	−0.45	−0.20	−0.39
GooF	1.030	1.035	1.044
wR_2 (all data)	0.0992	0.0755	0.1305
wR_2	0.0982	0.0728	0.1264
R_1 (all data)	0.0389	0.0323	0.0538
R_1	0.0374	0.0290	0.0492

Table S5.3. Crystallographic data for compounds *rac*-**8** · NH_4^+ $HB(C_6F_5)_3^-$, **9**[$HB(C_6F_5)_3$] and **10**.

Compound	*rac*-**8** · NH_4^+ $HB(C_6F_5)_3^-$	**9**[$HB(C_6F_5)_3$]	**10**
Data Set (internal naming)	**TH366**	**TH148**	**BK10**
Formula	$C_{36}H_{39}BF_{15}N_2OPSSi$	$C_{27}H_{18}BF_{15}N_2$	$C_{14}H_{26}NPSSi$
$\rho_{calc.}$ / g·cm^{-3}	1.432	1.689	1.167
μ/mm^{-1}	2.221	1.572	3.113
Formula Weight	902.65	666.24	299.48
Color	clear colorless	clear colorless	clear colorless
Shape	block	block	needle
Size/mm^3	0.238 × 0.2 × 0.153	0.52 × 0.29 × 0.28	0.33 × 0.06 × 0.06
T/K	123.15	100.15	123.00(10)
Crystal System	triclinic	monoclinic	orthorhombic
Flack Parameter	–	–	0.11(5)
Hooft Parameter	–	–	0.11(5)
Space Group	P-1	$P2_1/n$	$P2_12_12_1$
a/Å	10.7415(2)	8.71110(10)	6.14000(10)
b/Å	14.1355(3)	28.57560(10)	15.7849(2)
c/Å	15.1402(3)	11.13960(10)	17.5939(3)
α/°	102.729(2)	90	90
β/°	99.937(2)	109.1290(10)	90
γ/°	105.607(2)	90	90
V/Å^3	2092.86(8)	2619.81(4)	1705.19(5)
Z	2	4	4
Z'	1	1	1
Wavelength/Å	1.54184	1.54184	1.54184
Radiation Type	Cu K_α	Cu K_α	Cu K_α
$2\theta_{min}$/°	7.78	6.186	7.524
$2\theta_{max}$/°	134.08	150.496	150.788
Measured Refl.	30902	42427	17786
Independent Refl.	7417	5377	3498
R_{int}	0.0578	0.0225	0.0532
Parameters	622	414	179
Restraints	455	0	0
Largest Peak	0.40	0.32	0.55
Deepest Hole	−0.41	−0.23	−0.81
GooF	1.060	1.064	1.105
wR_2 (all data)	0.1237	0.0788	0.1733
wR_2	0.1184	0.0784	0.1602
R_1 (all data)	0.0477	0.0319	0.0599
R_1	0.0436	0.0314	0.0540

Table S5.4. Crystallographic data for compounds (R_P)-**13**, (R_P)-**14** and (R_P,S_{Si})-**17**.

Compound	(R_P)-**13**	(R_P)-**14**	(R_P,S_{Si})-**17**
Data Set (internal naming)	**TH501**	**BK13**	**TH510**
Formula	$C_{16}H_{36}NPSSi$	$C_{16}H_{28}NPSSi$	$C_{20}H_{36}NPSSi$
$\rho_{calc.}$ / g·cm^{-3}	1.095	1.179	1.109
μ/mm^{-1}	2.661	2.934	2.417
Formula Weight	333.58	325.51	381.62
Color	clear colorless	clear colorless	clear colorless
Shape	block	block	plate
Size/mm^3	0.26 × 0.12 × 0.06	0.33 × 0.09 × 0.07	0.23 × 0.1 × 0.07
T/K	123.01(10)	123.01(10)	123.00(10)
Crystal System	monoclinic	orthorhombic	orthorhombic
Flack Parameter	–0.02(3)	0.01(2)	–0.00(3)
Hooft Parameter	–0.02(3)	0.01(2)	–0.00(3)
Space Group	$P2_1$	$P2_12_12_1$	$P2_12_12_1$
a/Å	6.20850(10)	10.24910(10)	10.75220(10)
b/Å	19.7623(2)	11.71930(10)	12.11670(10)
c/Å	8.34720(10)	15.2652(2)	17.5507(2)
α/°	90	90	90
β/°	99.0760(10)	90	90
γ/°	90	90	90
V/Å^3	1011.33(2)	1833.54(3)	2286.53(4)
Z	2	4	4
Z'	1	1	1
Wavelength/Å	1.54184	1.54184	1.54184
Radiation Type	Cu K_α	Cu K_α	Cu K_α
$2\theta_{min}$/°	8.95	9.514	8.868
$2\theta_{max}$/°	145.92	150.348	146.484
Measured Refl.	13511	19541	20852
Independent Refl.	3879	3722	4500
R_{int}	0.0248	0.0275	0.0289
Parameters	196	194	317
Restraints	1	0	228
Largest Peak	0.27	0.18	0.40
Deepest Hole	–0.39	–0.30	–0.22
GooF	1.117	1.061	1.030
wR_2 (all data)	0.0819	0.0660	0.1053
wR_2	0.0816	0.0658	0.1047
R_1 (all data)	0.0327	0.0239	0.0378
R_1	0.0320	0.0236	0.0371

Table S5.5. Crystallographic data for compounds (R_P,S_{Si})-**18**[$HB(C_6F_5)_3$] and *rac*-**21**[(μ-OH)$(BCF)_2$].

Compound	(R_P,S_{Si})-**18**[$HB(C_6F_5)_3$]	*rac*-**21**[(μ-OH)$(BCF)_2$]
Data Set (internal naming)	**TH527**	**TH154**
Formula	$C_{38}H_{36}BF_{15}NPSSi$	$C_{44}H_{22}B_2F_{30}NOPS\cdot½CH_2Cl_2$
$\rho_{calc.}$ / g·cm^{-3}	1.489	1.787
μ/mm^{-1}	2.302	2.915
Formula Weight	893.61	1277.74
Color	clear colorless	clear colorless
Shape	block	needle
Size/mm^3	0.19 × 0.119 × 0.112	0.48 × 0.1 × 0.09
T/K	123.00(10)	100.00(10)
Crystal System	monoclinic	triclinic
Flack Parameter	0.056(10)	–
Hooft Parameter	0.06(3)	–
Space Group	$P2_1$	P-1
a/Å	10.22120(10)	11.3986(2)
b/Å	36.6956(5)	13.1673(3)
c/Å	21.2608(2)	16.6394(3)
α/°	90	74.882(2)
β/°	90.2030(10)	80.022(2)
γ/°	90	87.981(2)
V/Å^3	7974.30(15)	2374.36(8)
Z	8	2
Z'	4	1
Wavelength/Å	1.54184	1.54184
Radiation Type	Cu K_α	Cu K_α
$2\theta_{min}$/°	4.804	5.582
$2\theta_{max}$/°	134.16	148.202
Measured Refl.	94551	80412
Independent Refl.	26550	9249
R_{int}	0.0512	0.0557
Parameters	2500	797
Restraints	2130	67
Largest Peak	0.63	0.39
Deepest Hole	−0.39	−0.63
GooF	1.040	1.086
wR_2 (all data)	0.1889	0.1305
wR_2	0.1789	0.1265
R_1 (all data)	0.0788	0.0523
R_1	0.0670	0.0453

Compound 2:

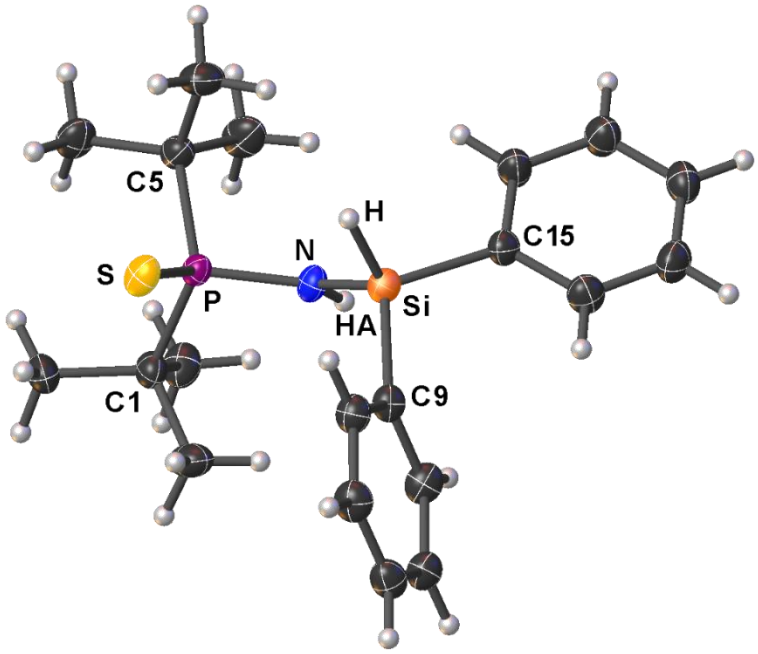

Selected Bond Lengths in Å		Selected Bond Angles in °	
P–S	1.9631(17)	N–P–S	111.11(16)
P–N	1.654(4)	N–P–C5	105.2(2)
P–C5	1.871(5)	N–P–C1	105.8(2)
P–C1	1.866(5)	N–Si–C9	113.41(19)
Si–N	1.751(4)	N–Si–C15	106.0(2)
Si–C9	1.873(4)	N–Si–H	107.3(18)
Si–C15	1.878(5)	P–N–Si	127.3(3)
Si–H	1.40(5)		
N–HA	0.83(8)		

Compound 3[$HB(C_6F_5)_3$]**:**

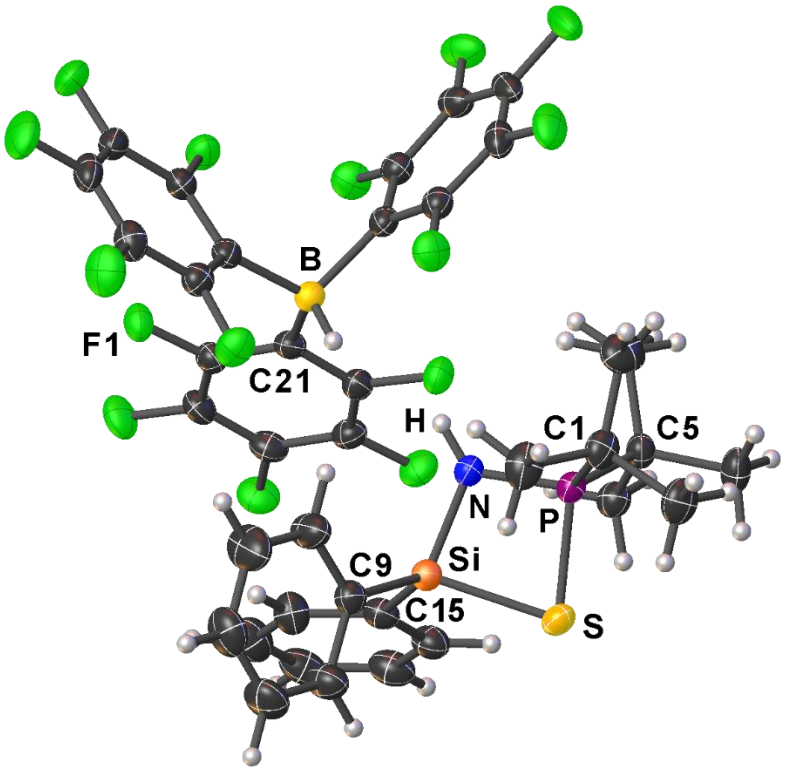

Selected Bond Lengths in Å		Selected Bond Angles in °	
S–P	2.0657(6)	P–S–Si	76.95(2)
S–Si	2.1967(6)	N–Si–S	86.49(5)
Si–N	1.7490(15)	P–N–Si	102.81(8)
P–N	1.6458(14)	N–P–S	93.69(5)
Si–C9	1.8504(17)	C15–Si–C9	109.80(8)
Si–C15	1.8468(18)	C1–P–C5	115.63(8)
P–C1	1.8499(18)		
P–C5	1.8421(17)		
N–H	0.86(3)		

Compound 4:

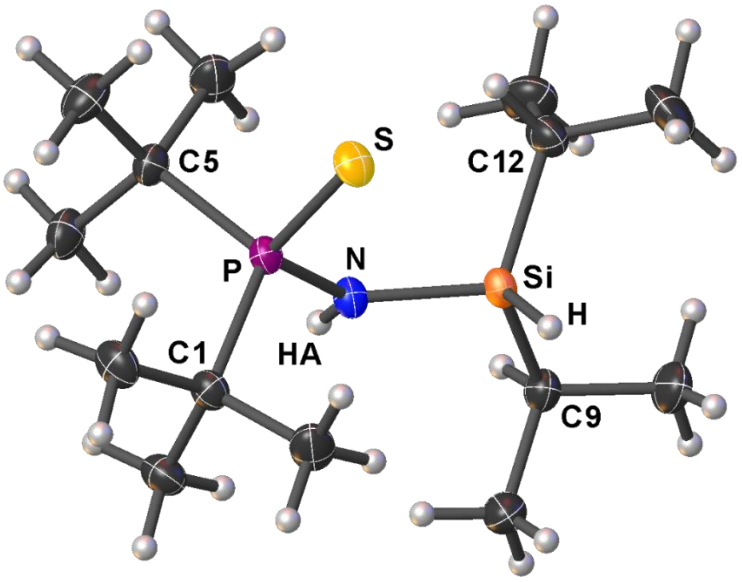

Selected Bond Lengths in Å		Selected Bond Angles in °	
P–S	1.9647(5)	N–P–S	110.16(4)
P–N	1.6551(11)	N–P–C5	106.89(6)
P–C5	1.8702(13)	N–P–C1	105.22(6)
P–C1	1.8696(14)	N–Si–C9	104.97(6)
Si–N	1.7550(12)	N–Si–C12	111.20(6)
Si–C9	1.8798(15)	N–Si–H	109.9(7)
Si–C12	1.8767(14)	P–N–Si	127.90(7)
Si–H	1.405(17)		
N–HA	0.76(2)		

Compound 5[$HB(C_6F_5)_3$]**:**

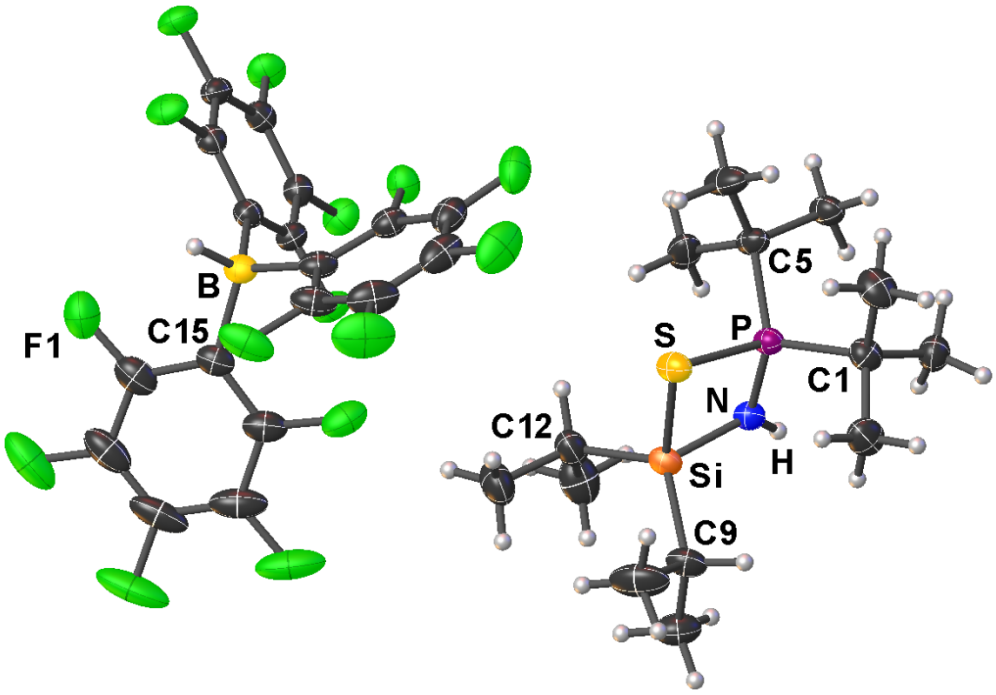

Selected Bond Lengths in Å		Selected Bond Angles in °	
S–P	2.0586(6)	P–S–Si	76.83(2)
S–Si	2.2074(6)	N–Si–S	86.24(5)
Si–N	1.7530(15)	P–N–Si	102.69(8)
P–N	1.6434(15)	N–P–S	94.24(6)
Si–C9	1.8652(19)	C12–Si–C9	117.74(9)
Si–C12	1.867(2)	C1–P–C5	115.32(9)
P–C1	1.8443(19)		
P–C5	1.8545(18)		
N–H	0.86(3)		

Compound *rac*-6:

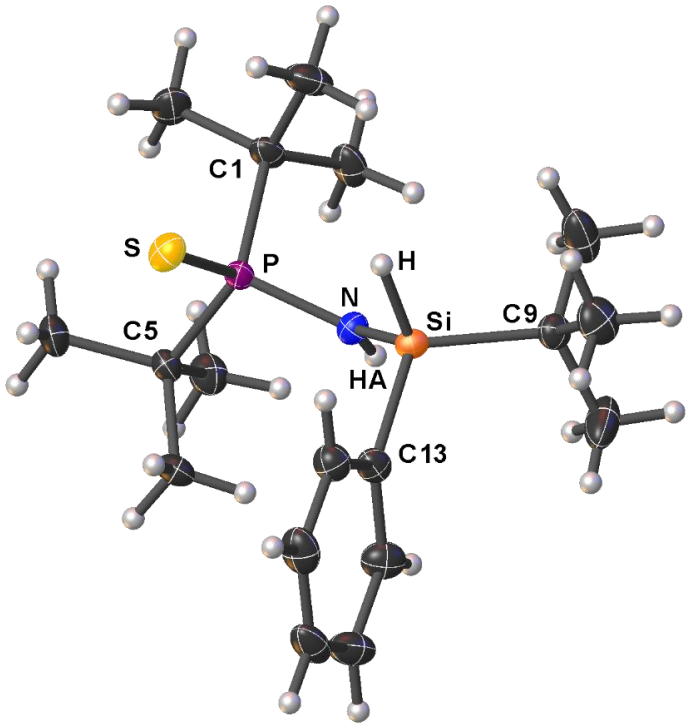

Selected Bond Lengths in Å		Selected Bond Angles in °	
P–S	1.9646(5)	N–P–S	111.36(4)
P–N	1.6683(11)	N–P–C5	106.14(6)
P–C5	1.8662(14)	N–P–C1	104.88(6)
P–C1	1.8699(13)	N–Si–C9	109.91(6)
Si–N	1.7500(11)	N–Si–C13	112.05(6)
Si–C9	1.8935(14)	N–Si–H	107.6(7)
Si–C13	1.8716(14)	P–N–Si	125.83(8)
Si–H	1.374(18)		
N–HA	0.76(2)		

Compound *rac*-7[HB(C_6F_5)$_3$]:

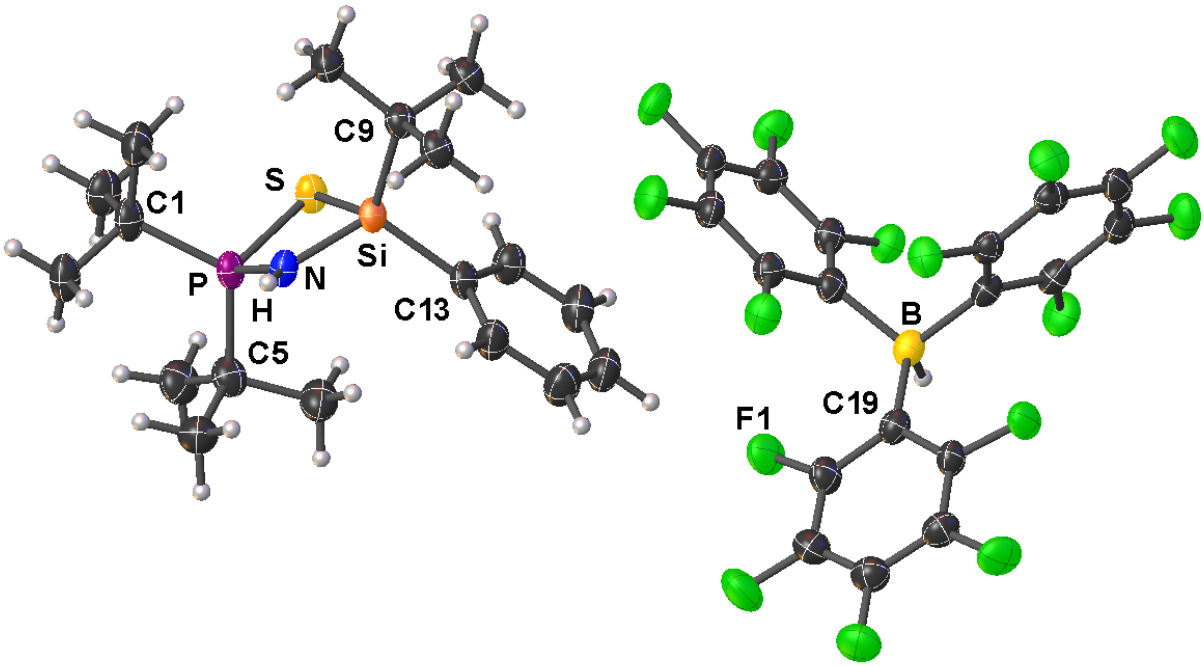

Selected Bond Lengths in Å		Selected Bond Angles in °	
S–P	2.0692(16)	P–S–Si	76.83(6)
S–Si	2.1937(16)	N–Si–S	86.51(15)
Si–N	1.752(4)	P–N–Si	102.5(2)
P–N	1.646(4)	N–P–S	93.57(16)
Si–C9	1.873(5)	C13–Si–C9	111.6(2)
Si–C13	1.860(5)	C1–P–C5	115.0(3)
P–C1	1.848(6)		
P–C5	1.870(6)		
N–H	0.81(7)		

Compound *rac*-8 · NH_4^+ $HB(C_6F_5)_3^-$:

Part 1 [78%(C2–C4)/76%(C6–C8)]

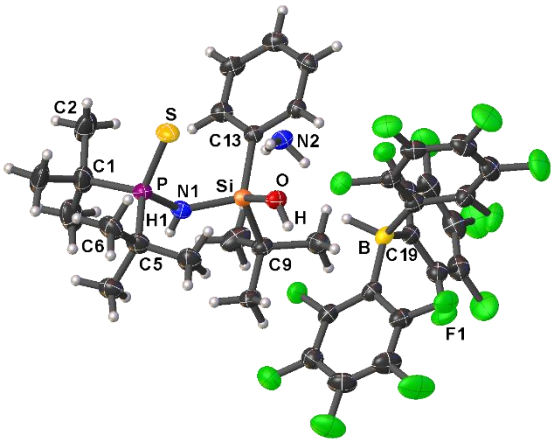

Part 2 [22%(C2a–C4a)/24%(C6a–C8a)]

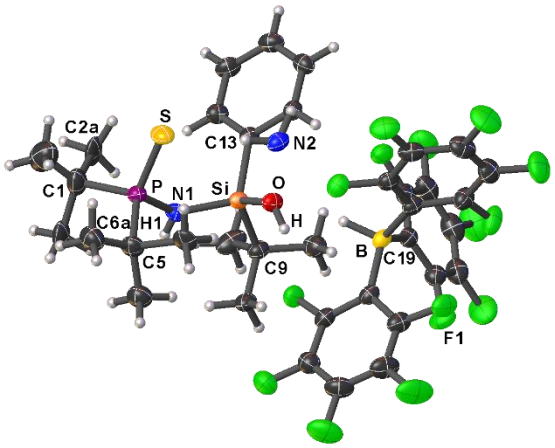

Selected Bond Lengths in Å		Selected Bond Angles in °	
P–S	1.9732(7)	N1–P–S	111.08(6)
P–N1	1.6663(16)	N1–P–C5	107.10(9)
P–C5	1.863(2)	N1–P–C1	105.26(10)
P–C1	1.858(2)	N1–Si–C9	104.68(8)
Si–N1	1.7362(17)	N1–Si–C13	112.84(8)
Si–C9	1.8855(19)	N1–Si–O	112.20(7)
Si–C13	1.8665(18)	P–N1–Si	132.95(11)
Si–O	1.6473(13)		
N–H1	0.76(3)		

Compound 9[$HB(C_6F_5)_3$]:

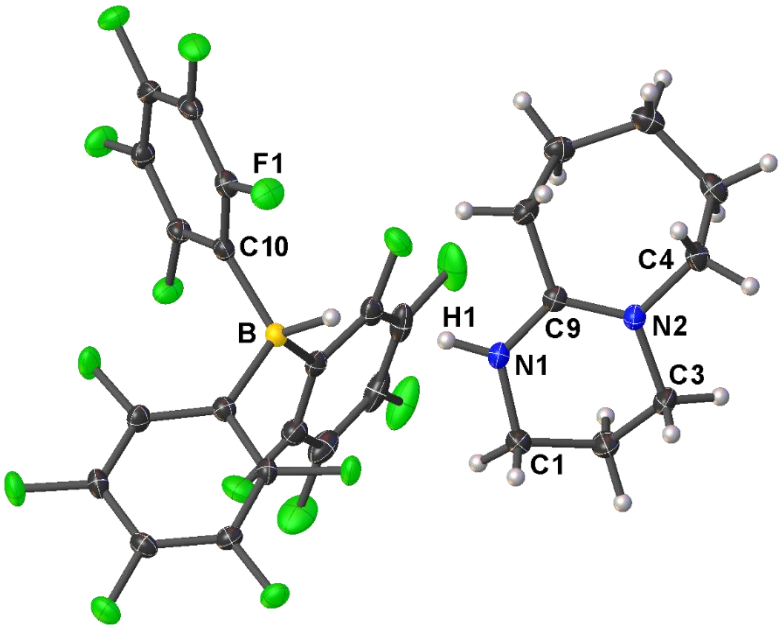

Selected Bond Lengths in Å		Selected Bond Angles in °	
N1–C1	1.4637(16)	C9–N1–C1	124.03(10)
N1–C9	1.3232(16)	C9–N2–C4	122.03(10)
N1–H1	0.882(18)	C9–N2–C3	121.40(10)
N2–C3	1.4739(16)	C3–N2–C4	116.52(10)
N2–C4	1.4787(15)		
N2–C9	1.3183(16)		

Compound 10:

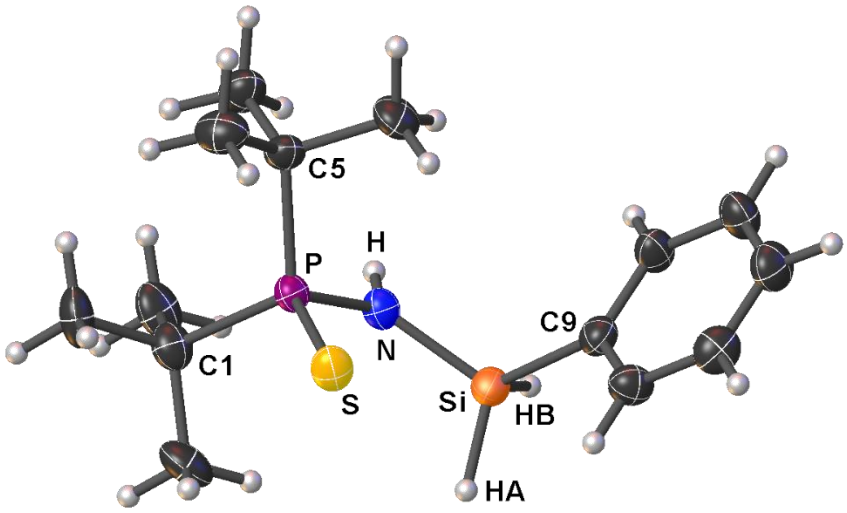

Selected Bond Lengths in Å		Selected Bond Angles in °	
P–S	1.9669(18)	N–P–S	109.20(17)
P–N	1.645(4)	N–P–C5	106.9(2)
P–C5	1.866(5)	N–P–C1	104.7(2)
P–C1	1.869(6)	N–Si–C9	116.1(2)
Si–N	1.744(5)	N–Si–Ha	112(3)
Si–C9	1.861(5)	N–Si–Hb	103(2)
Si–Ha	1.45(7)	P–N–Si	127.4(3)
Si–Hb	1.52(7)		
N–H	0.89(7)		

Compound (R_P)**-13:**

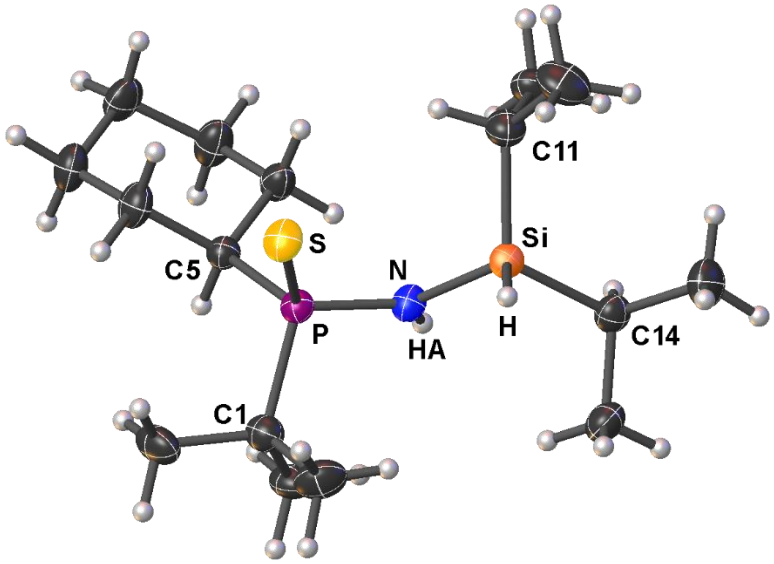

Selected Bond Lengths in Å		Selected Bond Angles in °	
P–S	1.9593(10)	N–P–S	109.60(10)
P–N	1.649(3)	N–P–C5	108.77(14)
P–C5	1.855(3)	N–P–C1	105.89(14)
P–C1	1.852(3)	N–Si–C11	109.41(15)
Si–N	1.756(3)	N–Si–C14	104.92(14)
Si–C11	1.876(3)	N–Si–H	111.1(14)
Si–C14	1.878(3)	P–N–Si	128.02(16)
Si–H	1.40(3)		
N–Ha	0.81(4)		

Compound (R_P)-14:

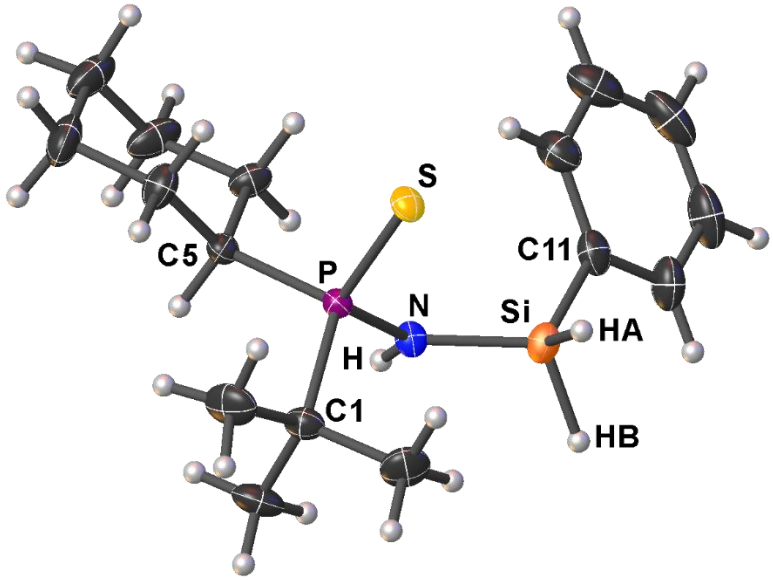

Selected Bond Lengths in Å		Selected Bond Angles in °	
P–S	1.9656(7)	N–P–S	111.51(7)
P–N	1.6653(18)	N–P–C5	105.40(9)
P–C5	1.834(2)	N–P–C1	104.79(10)
P–C1	1.853(2)	N–Si–C11	111.66(10)
Si–N	1.7385(18)	N–Si–Ha	107.7(11)
Si–C11	1.860(3)	N–Si–Hb	111.2(12)
Si–HA	1.43(3)	P–N–Si	128.39(11)
Si–HB	1.42(3)		
N–H	0.83(2)		

Compound (R_P,S_{Si})-17:

Part 1 [69%(C12–C14)/56%(C15–C20)]

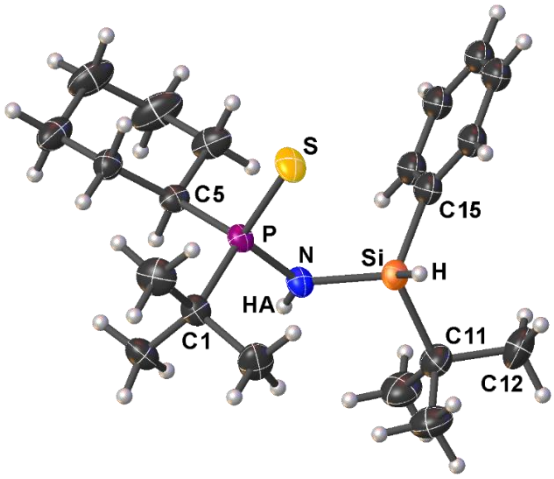

Part 2 [31%(C12A–C14A)/44%(C15A–C20A)]

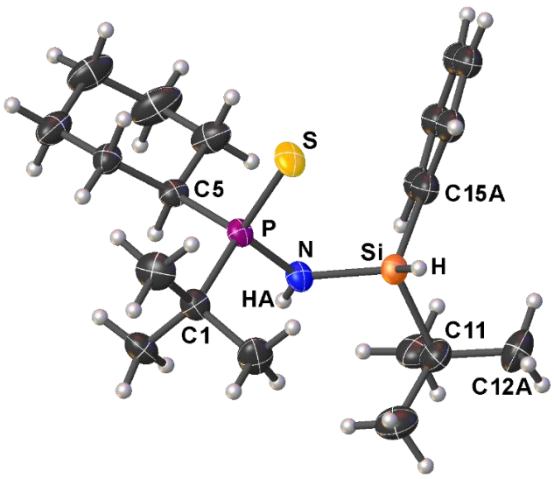

Selected Bond Lengths in Å		Selected Bond Angles in °	
P–S	1.9612(10)	N–P–S	110.97(10)
P–N	1.669(3)	N–P–C5	104.41(13)
P–C5	1.828(3)	N–P–C1	105.74(14)
P–C1	1.859(3)	N–Si–C11	108.81(15)
Si–N	1.744(3)	N–Si–C15	112.0(5)
Si–C11	1.888(4)	N–Si–C15A	110.1(6)
Si–C15	1.864(9)	N–Si–H	109.5(17)
Si–C15A	1.873(11)	P–N–Si	126.65(16)
Si–H	1.43(4)		
N–HA	0.81(4)		

Compound (R_P,S_{Si})-**18**[$HB(C_6F_5)_3$]**:**

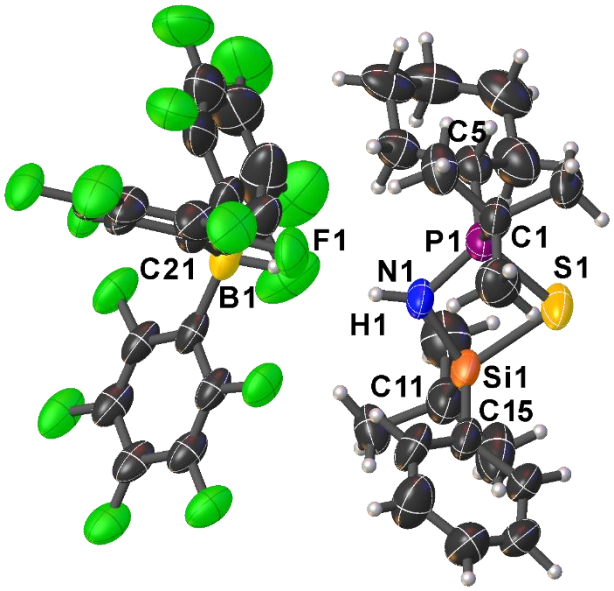

Part 1 (multicolored) [41%(N3,P1A,S3,Si3 + respective C atoms)/ 33%(N4,P2A,S4,Si4 + respective C atoms)/ 77%(C1G–C67,F17–F19)]

Part 2 (marked green shaded) [59%(N1A,P1B,S1A,Si1A + respective C atoms)/ 67%(N2A,P2B,S2A,Si2A + respective C atoms)/ 23%(C03M–C03N,F01D–F01E)]

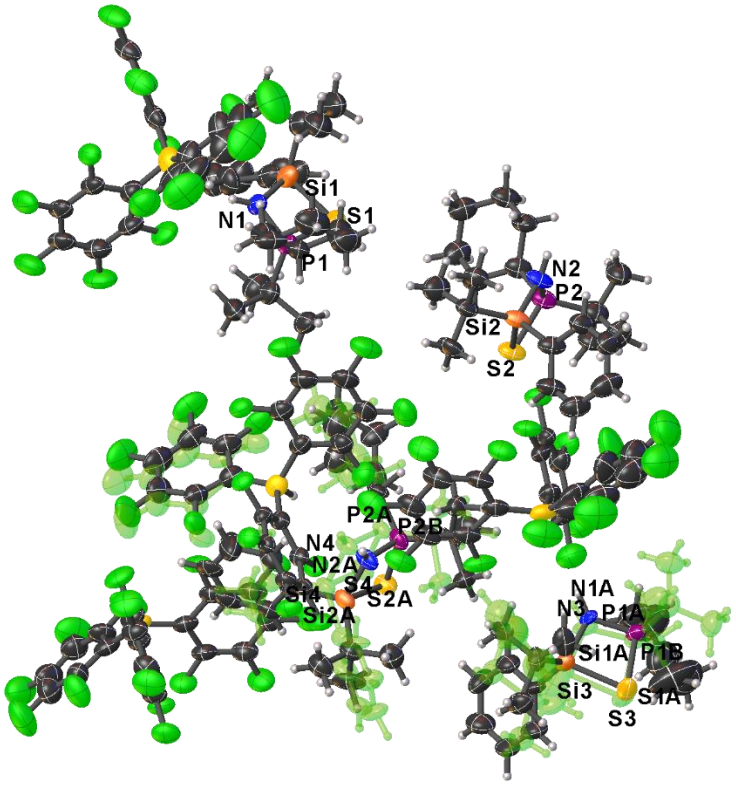

Selected Bond Lengths in Å		Selected Bond Angles in °	
P1–S1	2.076(4)	P1–S1–Si1	76.76(14)
S1–Si1	2.180(4)	N1–Si1–S1	87.9(3)
P1–N1	1.668(9)	P1–N1–Si1	102.1(5)
P1–C5	1.792(13)	N1–P1–S1	93.1(3)
P1–C1	1.826(12)	C15–Si1–C11	110.7(7)
Si1–N1	1.731(9)	C1–P1–C5	109.1(5)
Si1–C11	1.872(15)		
Si1–C15	1.825(16)		

Compound *rac*-**21**[(μ-OH)(BCF)$_2$]:

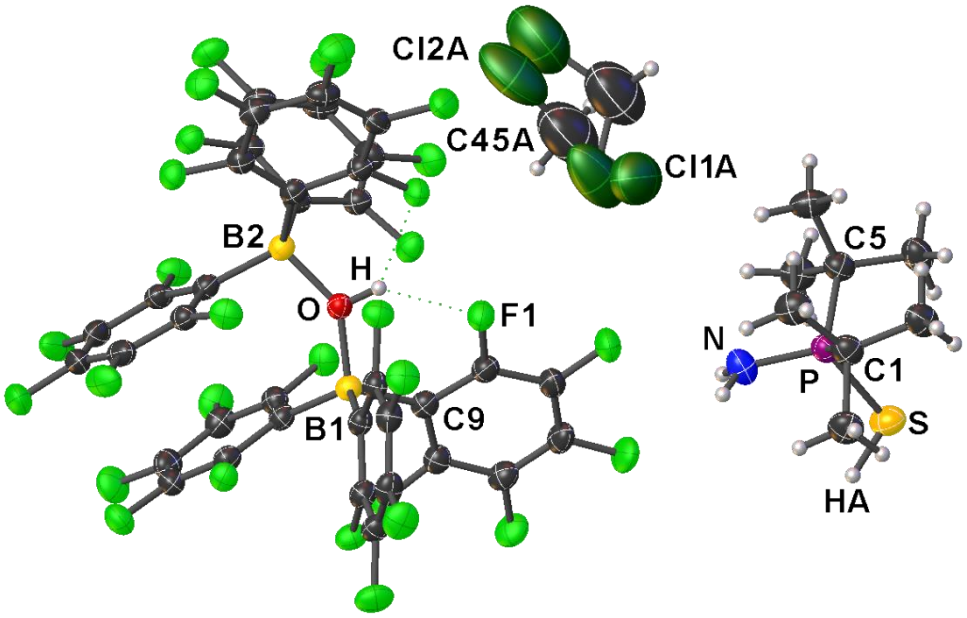

Selected Bond Lengths in Å		Selected Bond Angles in °	
P–S	2.0796(9)	N–P–S	112.94(10)
P–N	1.626(2)	N–P–C5	107.21(13)
P–C5	1.842(3)	N–P–C1	105.79(13)
P–C1	1.847(3)	C5–P–S	103.18(9)
S–HA	1.30(3)	C5–P–C1	118.53(12)
O–H	0.84(3)	C1–P–S	109.40(9)

5.8. Supplementary References

[1] a) M. J. P. Harger, M. A. Stephen, *J. Chem. Soc., Perkin Trans.* **1980**, 705–711; b) M. Köster, A. Kreher, C. von Hänisch, *Dalton Trans.* **2018**, *47*, 7875–7878; c) T. C. Jankins, Z.-Y. Qin, K. M. Engle, *Tetrahedron* **2019**, *75*, 3272–3281.

[2] N. Fontana, N. A. Espinosa-Jalapa, M. Seidl, J. O. Bauer, *Chem. Commun.* **2022**, *58*, 2144–2147.

[3] Y. Soltani, L. C. Wilkins, R. L. Melen, *Angew. Chem. Int. Ed.* **2017**, *56*, 11995–11999; *Angew. Chem.* **2017**, *129*, 12157–12161.

[4] W. Uhlig, A. Tzschach, *J. Organomet. Chem.* **1989**, *378*, C1–C5.

[5] T. Huber, N. A. Espinosa-Jalapa, J. O. Bauer, *Chem. Eur. J.* **2022**, *28*, e202202608.

[6] CrysAlisPro Software System, Rigaku Oxford Diffraction **2023**.

[7] O. V. Dolomanov, L. J. Bourhis, R. J. Gildea, J. A. K. Howard, H. Puschmann, *J. Appl. Crystallogr.* **2009**, *42*, 339–341.

[8] G. M. Sheldrick, *Acta Cryst.* **2015**, *A71*, 3–8.

[9] G. M. Sheldrick, *Acta Cryst.* **2015**, *C71*, 3–8.

6. Additional Findings

Preface

The following chapter and supporting information contain additional findings that were not discussed in the previous chapters. It includes fully characterized compounds, as well as compounds for which detailed characterization is missing. The collected procedures and data are available for further use by the group of PD Dr. J. O. Bauer.

Authors

Tanja Huber, Florian Meurer, Michael Seidl, Jonathan O. Bauer.

Author contribution

All syntheses and characterisations reported in this work were performed by T. Huber. Single crystal X-ray diffraction and structure refinements were performed by T. Huber, except for **2·HCl**, which was refined by Dr. M. Seidl, and except for **[(1–H)$^+$]$_2$H$_3$O$^+$}(OTf$^-$)$_3$**, which was refined by F. Meurer. The manuscript and the supporting information were drafted by T. Huber and revised by PD Dr. J. O. Bauer.

Acknowledgements

This work was supported by the Elite Network of Bavaria (ENB), the Bavarian State Ministry of Science and the Arts (StMWK), and the University of Regensburg (N-LW-NW-2016-366).

6.1. Results and Discussion

This chapter summarizes additional findings regarding the complexation and aggregation ability of aminophosphine sulfides.

6.1.1. Preparation and Crystal Structures of (1·Li)$_4$ and 2·HCl

During investigations on chapter five, the question arose as to what the solid-state structure of the lithiated starting material **1** would look like. In the past, the Bauer group has already dealt with the structure of lithium salts in the solid state and in solution.[1]

For the lithiation reaction, **1** was suspended in pentane and cooled to –30 °C before *n*-butyllithium was added. After stirring for 15 h, filtering and drying the colorless solid, crystallization was successful from a DCM solution, that was slowly layered with pentane and then stored at –10 °C. Single-crystal X-ray structure analysis revealed a tetrameric structure **(1·Li)$_4$**, which forms a very distorted cube (Scheme 6.1). Similar structures are known from literature for compounds with lithium[2] and other alkali metals.[2a,3] The corners of the highly distorted cubic core are alternately occupied by lithium and nitrogen, and the areas of the cube resemble rather a rhombus than a square.

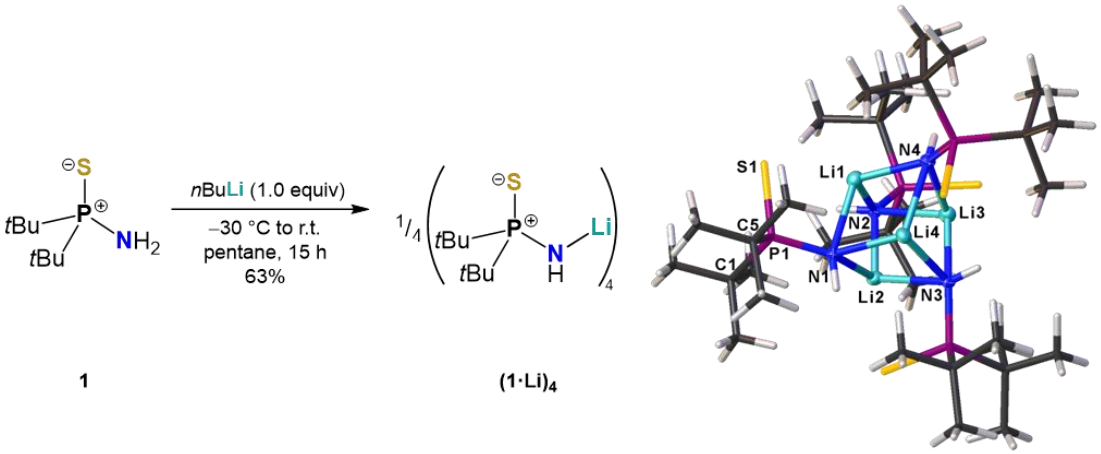

Scheme 6.1. Synthesis and crystal structure of **(1·Li)$_4$** (displacement ellipsoids set at the 50% probability level).

As described in chapter five for compound **1**, also non-oxidized *P*,*P*-di-*tert*-butylaminophosphine was attempted to be coupled with one or even two equivalents of chlorosilane. Besides deprotonation with *n*-butyllithium, experiments with triethylamine as the base were performed. Disubstituted and also monosubstituted coupling products (**2**) could never be obtained in pure form. The most likely reason for the latter fact is the tendency of **2** to partially form a zwitterionic species (**2a**) by transferring the NH hydrogen atom to the phosphorus lone electron pair (Scheme 6.2, top). Due to the difficulty in interpreting the crude NMR spectra, the actual presence of these molecules cannot be determined with certainty. Furthermore, in the course of a reaction of *P*,*P*-di-*tert*-butylaminophosphine with two equivalents of *tert*-butylchlorophenylsilane in the presence of two

equivalents of triethylamine, crystalline needles suitable for single-crystal X-ray analysis were obtained. Apparently, the base triethylamine could not fully scavenge the formed hydrogen chloride and, in turn, the adduct **2·HCl** was formed (Scheme 6.2, bottom). Between the NH hydrogen atom and the chloride anion, a hydrogen bond with an NH···Cl distance of 2.28 Å can be observed in the solid-state structure. Since the crystallization batch contained also some other unknown products (possibly **2** and **2a**), it was not possible to obtain more analytical data of **2·HCl**.

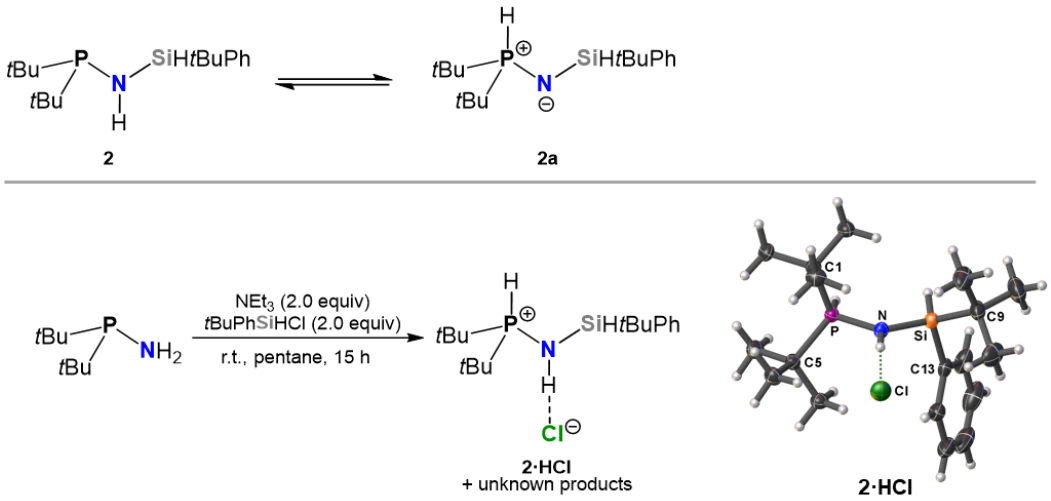

Scheme 6.2. Top: Presumed equilibrium of **2** with its zwitterionic form **2a**. Bottom: Experimental procedure and crystal structure of adduct **2·HCl** (displacement ellipsoids set at the 50% probability level).

6.1.2. Hydrogen-Bond-Based Structures of Aminophosphine Sulfides with Group-14-Elements and Transition Metals

To extend the scope of hydrogen-bond-based supramolecular synthons, the gradual expansion of the cubic clusters in chapter four was pursued. The aim was to use the free sulfide functions of compound **(1·HCl)$_4$** as ligands for the coordination of metal cations.

It was attempted to coordinate germanium(II) or tin(II), while maintaining the cubic structure of compound **(1·HCl)$_4$**. To ensure that the starting material is in its tetrameric form from the beginning, the reaction was performed in a 100 mM solution in DCM. Compound **(1·HCl)$_4$** and MCl_2 (M = Ge, Sn) were simultaneously dissolved in DCM and stirred for 15 h (Scheme 6.3). Insoluble solids were removed by filtration and the filtrate was layered with pentane to obtain colorless crystals that were suitable for single-crystal X-ray structure analysis for both reactions. The introduction of Ge(II) or Sn(II) into the products was indeed successful, however, the desired cubic shape could not be detected anymore. Nevertheless, both structures showed hydrogen-bonded patterns with crucial differences. The first dissimilarity that can be noticed is, that in the product with Ge(II), the amino moiety in **1** is still protonated and the chloride anion sticks to $GeCl_2$ to form trichlorogermanat(II). In contrast to that, the product with Sn(II) is free from the formerly present hydrogen chloride and $SnCl_2$ is coordinated by the sulfur unit of **1**. Accordingly, the products are named **(1–H)$^+$ GeCl$_3^-$** and **1·SnCl$_2$**. While the crystal structure of **(1–H)$^+$ GeCl$_3^-$** resembles a hydrogen-bonded, closed cage in the solid state, **1·SnCl$_2$** forms a ladder-like pattern made from ten-membered, hydrogen-bonded

rings (Scheme 6.3). The hydrogen bonds in **1·SnCl₂** with a NH···Cl distance of 2.56–2.71 Å are weaker than those in **(1–H)⁺ GeCl₃⁻**, that have a NH···Cl distance of 2.43–2.48 Å.

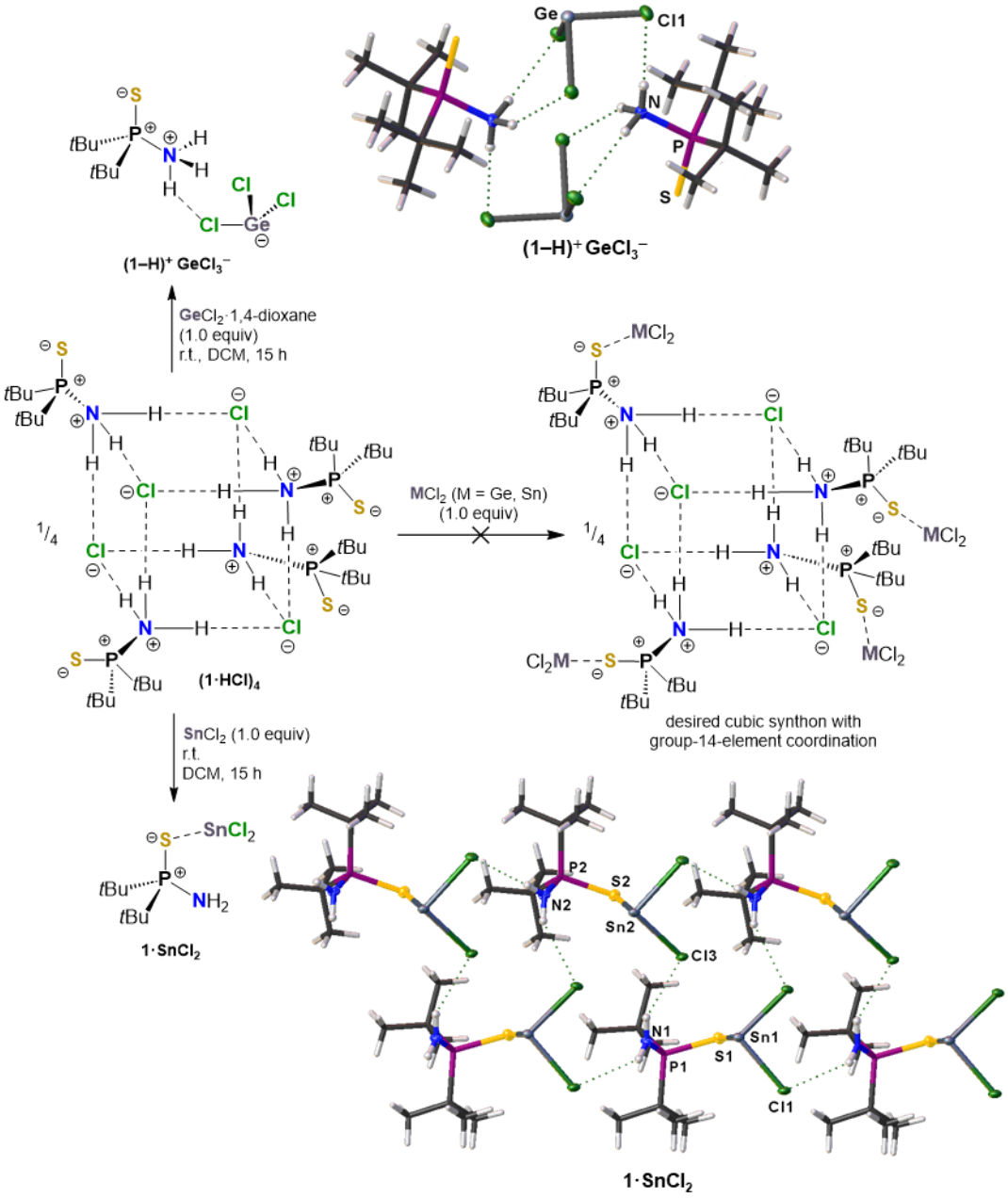

Scheme 6.3. Synthesis and grown crystal structures with hydrogen bonding of compounds **(1–H)⁺ GeCl₃⁻** and **1·SnCl₂** (displacement ellipsoids set at the 50% probability level).

Compound **(1·HCl)₄** was likewise reacted with AuCl. The cubic structure could again not be maintained and the analytical data were in accordance with those obtained by N. Fontana[4], when reacting compound **1** with AuCl (Scheme 6.4, top). The corresponding crystal structure of the product **[1₂·AuCl]₂** revealed an aurophilic interaction between two Au(I) cations,[5] that were each complexed by the sulfur moieties of two equivalents of compound **1**. The Au(I)–Au(I) distance of 3.02 Å[4] is in the typical range[5] for such a metallophilic interaction.

Surprisingly, a different structural result was obtained using enantiomerically pure compound (R_P)-**3** as the starting material. After reaction with AuCl in DCM for 15 h and subsequent filtration, colorless

crystals of **[(*R*P)-3]$_2$·AuCl** were obtained from the filtrate at −35 °C (Scheme 6.4, bottom). As with the achiral sample, although equimolar amounts of (*R*P)-**3** and AuCl were used, the product contained two equivalents of (*R*P)-**3** per metal ion center. The Au(I) cations were each coordinated by the sulfur units of two (*R*P)-**3** ligands, but no Au(I)–Au(I) interaction could be observed. Instead, a hydrogen-bonded zigzag chain of alternating amino groups and chloride anions was detected. The NH···Cl bond distances were between 2.34 Å and 2.37 Å.

Possibly, the formation of a dense, hydrogen-bonded network is not possible with the achiral sample[4] due to steric reasons, since two bulky tert-butyl groups are present in ligand **1**.

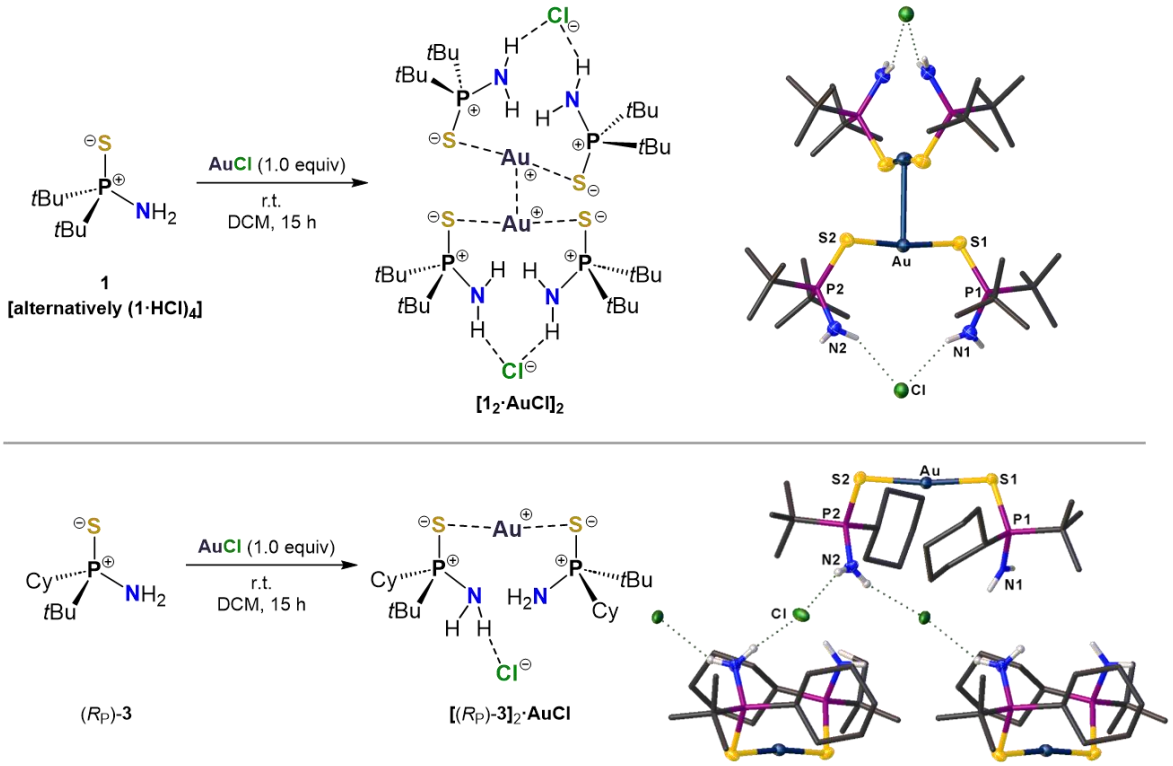

Scheme 6.4. Top: Synthesis and grown crystal structure with Au(I)–Au(I) interaction of compound **[1$_2$·AuCl]$_2$**.[4] Bottom: Synthesis and grown crystal structure with hydrogen bonded zigzag chain of compound **[(*R*P)-3]$_2$·AuCl** (displacement ellipsoids set at the 50% probability level; hydrogen atoms, except for NH, omitted for clarity).

6.1.3. Hydrogen-Bond-Based Structures of 1 with Tosylate and Triflate Anions

Besides chloride (see Chapter four), also other strongly coordinating anions are suitable for the formation of hydrogen-bonded, cube-like clusters.[6] With this in mind, *p*-toluenesulfonic acid and triflic acid were used for the protonation of compound **1**. Since the cubic structure of the chloride-based product **(1·HCl)$_4$** could not be maintained by reaction with group-14-element or transition metal salts, it was believed, that by changing the anion, more stable clusters would be formed.

Compound **1** was reacted with one equivalent of either *p*-toluenesulfonic acid or triflic acid in DCM for 15 h (Scheme 6.5). After removing all volatiles, the colorless solids were each converted into crystals suitable for single-crystal X-ray analysis by layering a DCM solution with pentane.

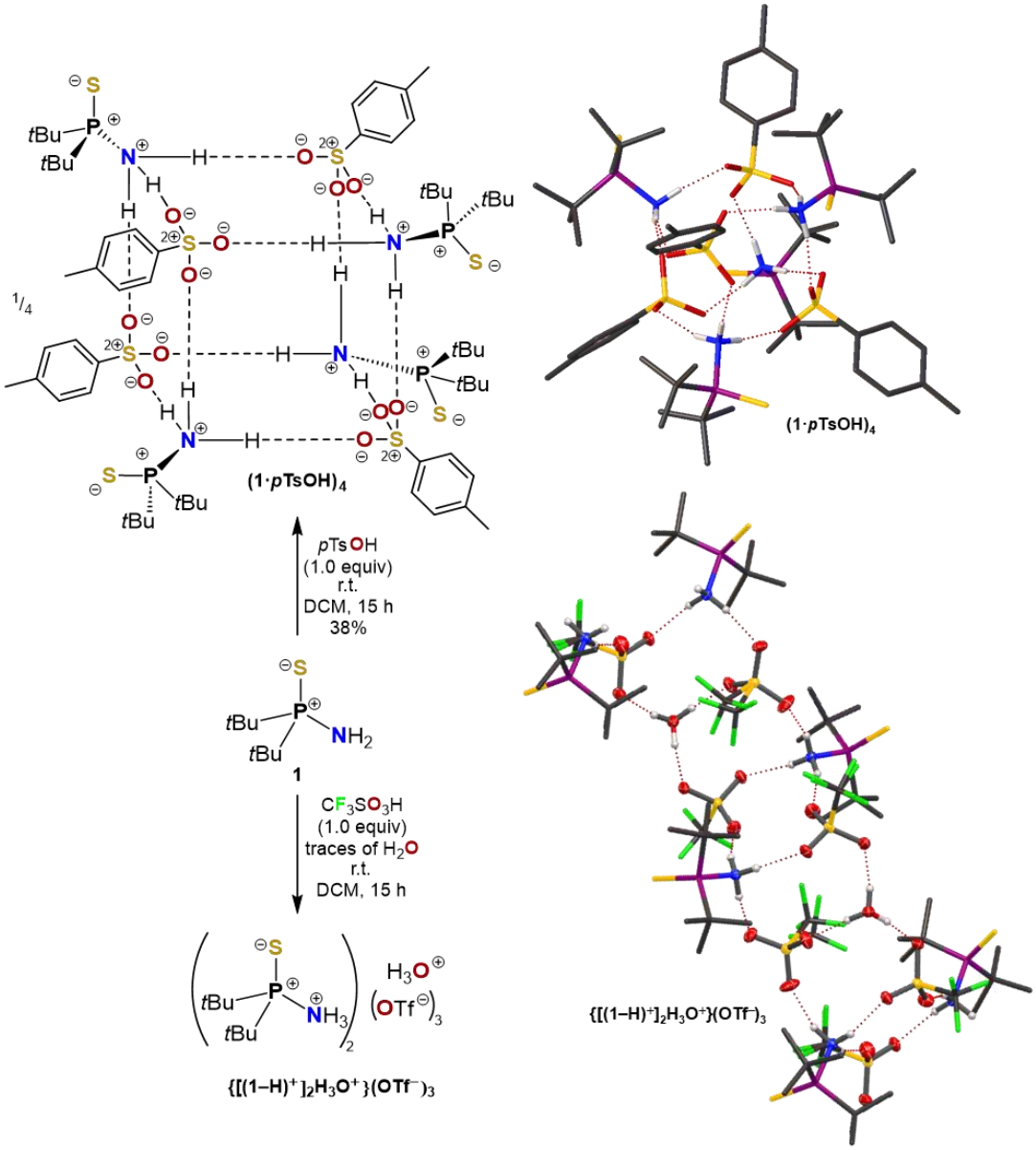

Scheme 6.5. Synthesis and grown crystal structure of compounds **(1·*p*TsOH)$_4$** and **{[(1–H)$^+$]$_2$H$_3$O$^+$}(OTf$^-$)$_3$** (displacement ellipsoids set at the 50% probability level; hydrogen atoms, except for NH and OH, omitted for clarity).

Using *p*-toluenesulfonic acid, the desired cubic product **(1·*p*TsOH)$_4$** was obtained (Scheme 6.5). Due to the SO_3^- moiety, the cube was much more distorted than the cubic core of compound **(1·HCl)$_4$** (see Chapter four) and the hydrogen bonds were much stronger. While the NH···Cl bond distances of **(1·HCl)$_4$** range from 2.24 Å to 2.33 Å, the NH···O bond distances of **(1·*p*TsOH)$_4$** are only 1.85–1.90 Å. Thus, it can be assumed that the inner cluster of compound **(1·*p*TsOH)$_4$** is indeed more stable and that the terminal sulfur units could be suitable for the complexation of metal cations, while the cubic core is preserved. Furthermore, variable concentration and variable temperature NMR studies of **(1·*p*TsOH)$_4$** in CD_2Cl_2 did not reveal such a pronounced dependence as observed for **(1·HCl)$_4$**. The ^{1}H and ^{31}P{^{1}H} NMR spectra showed indeed slightly shifted signals by changing the concentration or temperature, however, a downfield shifted NH_3 signal could be observed in every recorded ^{1}H NMR spectrum. This suggests that the cubic cluster of **(1·*p*TsOH)$_4$** is also

present in low concentration, which matches with the presence of very strong hydrogen bonds in the solid state.

Coordination experiments of several cations, such as Au(I), Al(III), Sn(II) and Ge(II) were performed with **(1·*p*TsOH)$_4$**. Since no crystals that were suitable for single-crystal X-ray structure analysis could be obtained from any of these experiments, no explicit evidence for the successful preservation of the cubic core could be found, but the aggregation properties of **(1·*p*TsOH)$_4$** are promising for this hypothesis.

Due to the similarity of *p*-toluenesulfonic acid and triflic acid regarding the SO_3H moiety, analogous products were expected for both reagents. However, a very different situation was found, when using triflic acid instead of *p*-toluenesulfonic acid for the protonation of compound **1**. The crystal structure of the product revealed that oxonium ions are incorporated and form a hydrogen-bonded, ladder-shaped network with the triflate ions and the protonated starting material **1** (Scheme 6.5). Structures containing ammonium ions, oxonium ions and triflate ions were recently described.[7] In the present case, for each oxonium ion there are two **(1–H)$^+$** cations and three triflate ions, giving in total a species named **{[(1–H)$^+$]$_2$H$_3$O$^+$}(OTf$^-$)$_3$**. Most likely, due to the hygroscopicity of triflic acid, traces of water were present, that were logically protonated to oxonium ions in the acidic medium. The hydrogen bonds are very strong with NH···O bond distances of 1.90–1.99 Å and OH···O bond distances of 1.68–1.74 Å.

6.2. References

[1] N. A. Espinosa-Jalapa, N. Berg, M. Seidl, I. G. Shenderovich, R. M. Gschwind, J. O. Bauer, *Chem. Commun.* **2020**, *56*, 13335–13338.

[2] a) T. Gröb, S. Chitsaz, K. Harms, K. Dehnicke, *Z. Anorg. Allg. Chem.* **2002**, *628*, 473–479; b) S. Courtenay, P. Wei, D. W. Stephan, *Can. J. Chem.* **2003**, *81*, 1471–1476.

[3] T. Gröb, K. Harms, K. Dehnicke, *Z. Anorg. Allg. Chem.* **2000**, *626*, 1065–1072.

[4] N. Fontana, *PhD thesis,* **2022**, Universität Regensburg.

[5] H. Schmidbaur, *Chem. Soc. Rev.* **1995**, *24*, 391–400.

[6] a) K. Sada, T. Watanabe, J. Miyamoto, T. Fukuda, N. Tohnai, M. Miyata, T. Kitayama, K. Maehara, K. Ute, *Chem. Lett.* **2004**, *33*, 160–161; b) B. Becker, K. Baranowska, J. Chojnacki, W. Wojnowski, *Chem. Commun.* **2004**, 620–621; c) T. Yuge, N. Tohnai, T. Fukuda, I. Hisaki, M. Miyata, *Chem. Eur. J.* **2007**, *13*, 4163–4168; d) N. Tohnai, Y. Mizobe, M. Doi, S. Sukata, T. Hinoue, T. Yuge, I. Hisaki, Y. Matsukawa, M. Miyata, *Angew. Chem. Int. Ed.* **2007**, *46*, 2220–2223, *Angew. Chem.* **2007**, *119*, 2270–2273; e) T. Yuge, N. Kai, I. Hisaki, M. Miyata, T. Norimitsu, *Chem. Lett.* **2007**, *36*, 1390–1391; f) T. Yuge, I. Hisaki, M. Miyata, N. Tohnai, *CrystEngComm* **2008**, *10*, 263–266.

[7] S. G. Dutremez, X. Dumail, S. Mallet-Ladeira, A. van der Lee, D. Granier, N. Masquelez, J.-S. Filhol, *Cryst. Growth Des.* **2021**, *21*, 2028–2045.

6.3. Syntheses and Characterizations

6.3.1. General Remarks

All experiments were performed in an inert atmosphere of purified nitrogen by using standard Schlenk techniques or an MBraun Unilab 1200/780 glovebox. Glassware was heated at 140 °C prior to use. Diethyl ether (Et_2O), dichloromethane (DCM), *n*-hexane, *n*-pentane, tetrahydrofuran (THF), and toluene were dried and degassed with an MBraun SP800 solvent purification system.
n-Butyllithium (2.5 M solution in hexane, Merck), triethylamine (≥99%, Merck), $GeCl_2$·1,4-dioxane (1:1 complex, Merck), tin(II) chloride (98%, Merck), gold(I) chloride (97%, abcr), *p*-toluenesulfonic acid (98%, Merck), triflic acid (98%, Merck) were used without further purification.
1 and *P*,*P*-di-*tert*-butylaminophosphine were synthesized following literature procedures.[1]
tert-Butylchlorophenylsilane was synthesized following a procedure published by our group.[2]
(1·HCl)$_4$ was synthesized following a procedure, which can be found in Chapter four of this work.
(R_P)-**3** was synthesized following a procedure published by our group.[3]
C_6D_6 (≥ 99.6%, Merck) was used for NMR spectroscopy as purchased. CD_2Cl_2 (> 99.8%, Fluorochem) was degassed and dried over molecular sieve (3 Å) prior to use. NMR spectra were either recorded using a Bruker Avance 400 (400.13 MHz) or a Bruker Avance III HD 400 (400.13 MHz) at 25 °C. Chemical shifts (δ) are reported in parts per million (ppm). ^{1}H and ^{13}C{^{1}H} NMR spectra are referenced to tetramethylsilane ($SiMe_4$, δ = 0.0 ppm) as external standard, with the deuterium signal of the solvent serving as internal lock and the residual solvent signal as an additional reference. ^{31}P{^{1}H} NMR spectra are referenced to H_3PO_4. For the assignment of the multiplicities, the following abbreviations are used: s = singlet, d = doublet, t = triplet, m = multiplet, br = broad signal. Elemental analyses were performed on a Vario MICRO cube apparatus.

6.3.2. Synthetic Procedures

6.3.2.1. Synthesis of (1·Li)$_4$

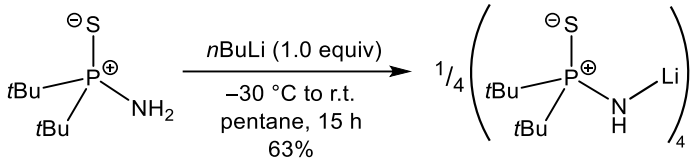

1 **(1·Li)$_4$**

*n*Butyllithium (2.1 mL, 5.17 mmol, 1.0 equiv., 2.5 M in hexane) was added dropwise to a suspension of *P*,*P*-di-*tert*-butylaminophosphine sulfide (**1**) (1.00 g, 5.17 mmol, 1.0 equiv.) in pentane (20 mL) at −30 °C. The suspension was allowed to slowly warm to room temperature and stirred for 15 h. The liquid phase was filtered off and the remaining solid was washed with pentane. After drying in vacuo, compound **(1·Li)$_4$** was obtained as a colorless solid (0.65 g, 3.27 mmol, 63%). Crystals suitable for single-crystal X-ray analysis were obtained from a DCM solution after slow layering with pentane and storing at −10 °C.

^{1}H NMR (400.13 MHz, CD_2Cl_2, 298 K): δ = 0.45 (d, $^2J_{H–P}$ = 12.1 Hz, 1H, N*H*), 1.32 (d, $^3J_{H–P}$ = 14.7 Hz, 18H, PC(C*H*$_3$)$_3$). **^{31}P{^{1}H} NMR** (162.04 MHz, CD_2Cl_2, 298 K): δ = 101.0 (s). **^{13}C{^{1}H} NMR** (100.61 MHz, CD_2Cl_2, 298 K): δ = 28.4 (s, PC(*C*H$_3$)$_3$), 39.9 (d, $^1J_{C–P}$ = 48.3 Hz, P*C*(CH$_3$)$_3$).
Elemental analysis: $C_8H_{19}LiNPS$: calcd.: C 48.23, H 9.61, N 7.03; found: C 48.68, H 9.53, N 7.01.

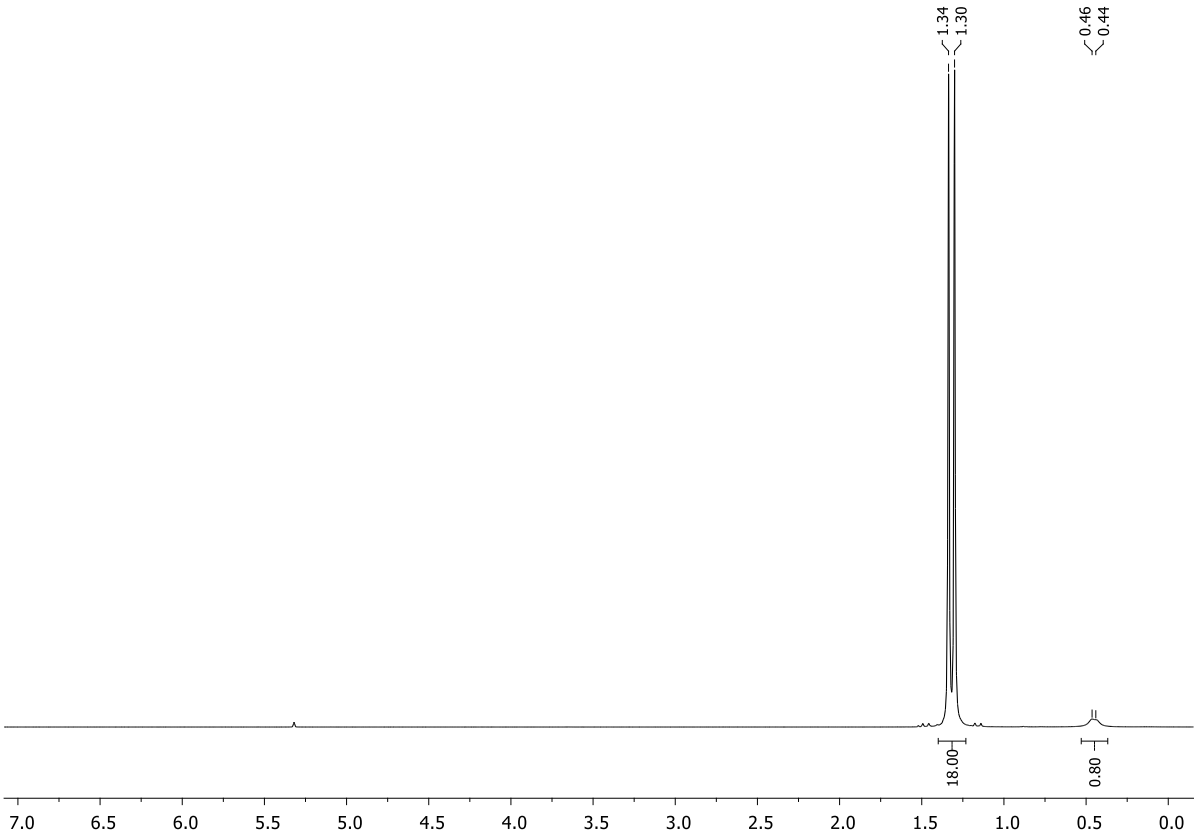

Figure S6.1. ^{1}H NMR spectrum (CD_2Cl_2, 298 K) of **(1·Li)$_4$**.

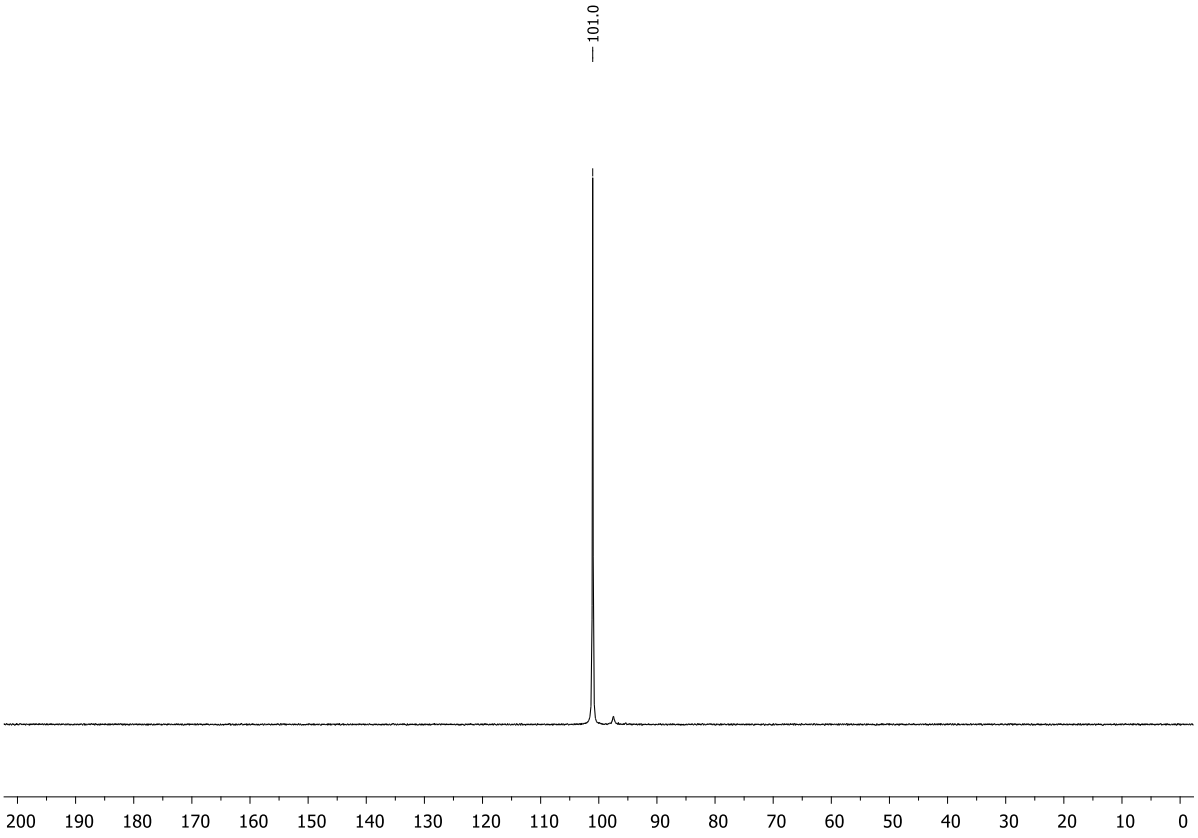

Figure S6.2. ^{31}P{^{1}H} NMR spectrum (CD_2Cl_2, 298 K) of **(1·Li)$_4$**.

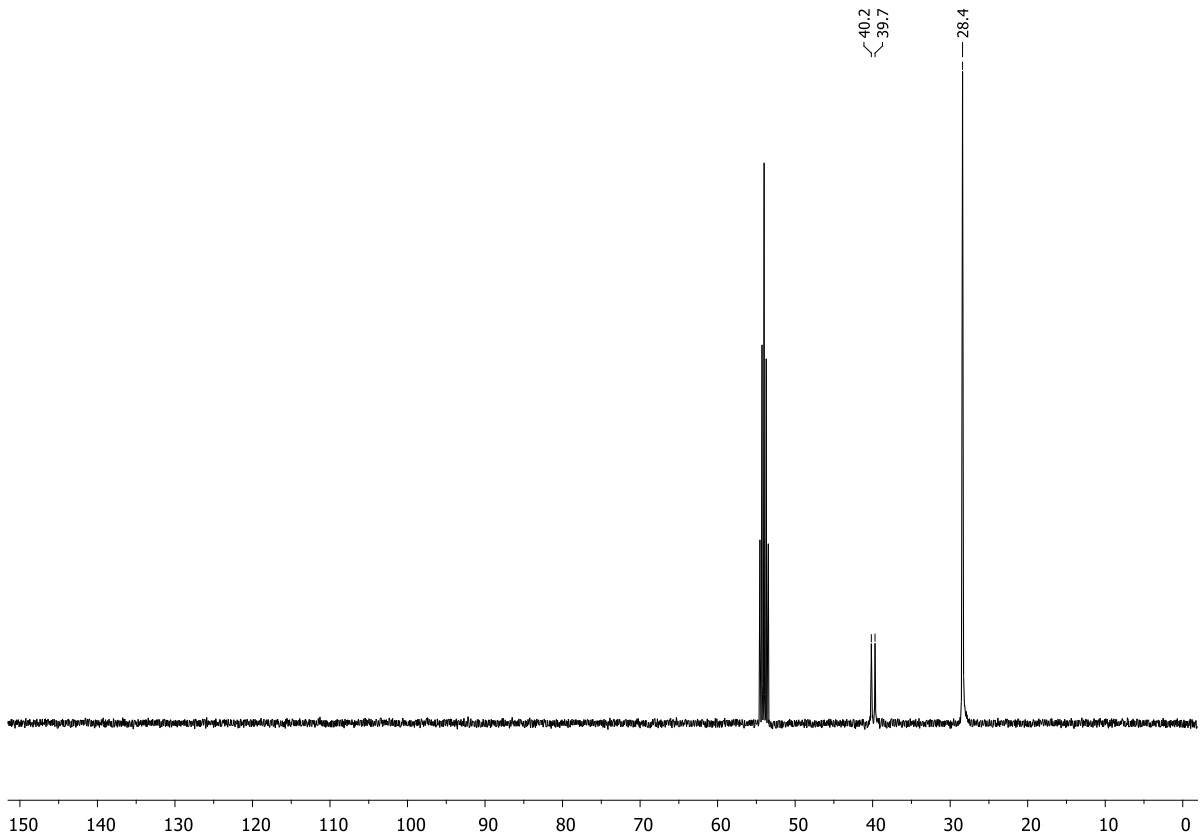

Figure S6.3. $^{13}C\{^{1}H\}$ NMR spectrum (CD_2Cl_2, 298 K) of **(1·Li)$_4$**.

6.3.2.2. Synthesis of 2·HCl

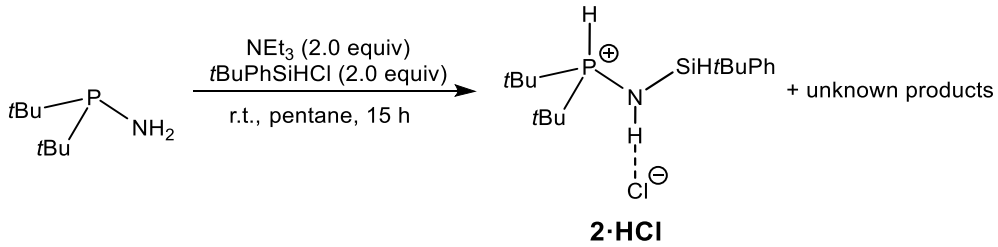

2·HCl

Triethylamine (1.5 mL, 10.58 mmol, 2.0 equiv.) was added to a solution of *P*,*P*-di-*tert*-butylaminophosphine (0.85 g, 5.29 mmol, 1.0 equiv.) in pentane (20 mL) at room temperature. Then, *tert*-butylchlorophenylsilane (2.10 g, 10.58 mmol, 2.0 equiv.) was added and the suspension was stirred for 15 h. The precipitate was removed by filtration and washed with pentane. All volatiles were removed from the filtrate and the remaining colorless solid was subjected to several recrystallizations from DCM/pentane until compound **2·HCl** eventually crystallized as thin colorless needles suitable for single-crystal X-ray analysis.

6.3.2.3. Synthesis of $(1–H)^+$ $GeCl_3^–$

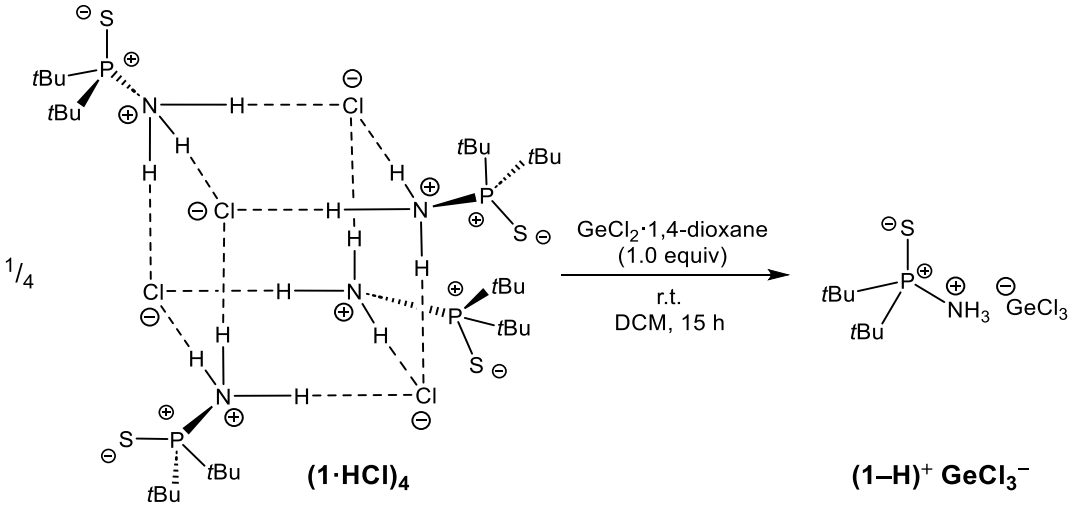

$(1·HCl)_4$ (60 mg, 0.25 mmol, 1.0 equiv) and $GeCl_2$·1,4-dioxane complex (60 mg, 0.25 mmol, 1.0 equiv) were suspended in DCM (2.5 mL) at room temperature and the mixture was stirred for 15 h. The resulting suspension was filtered and the filtrate was layered with pentane. Crystals suitable for single-crystal X-ray analysis of compound **$(1–H)^+$ $GeCl_3^–$** were obtained at room temperature.

^{1}H NMR (400.13 MHz, CD_2Cl_2, 298 K): δ = 1.41 (d, $^3J_{H–P}$ = 16.8 Hz, 18H, PC(CH_3)$_3$), 3.35 (d, 2H, N*H*). **^{31}P{^{1}H} NMR** (162.04 MHz, CD_2Cl_2, 298 K): δ = 94.7 (s). **^{13}C{^{1}H} NMR** (100.61 MHz, CD_2Cl_2, 298 K): δ = 27.1 (d, $^2J_{C–P}$ = 1.3 Hz, PC(CH_3)$_3$), 39.1 (d, $^1J_{C–P}$ = 50.7 Hz, PC(CH_3)$_3$).

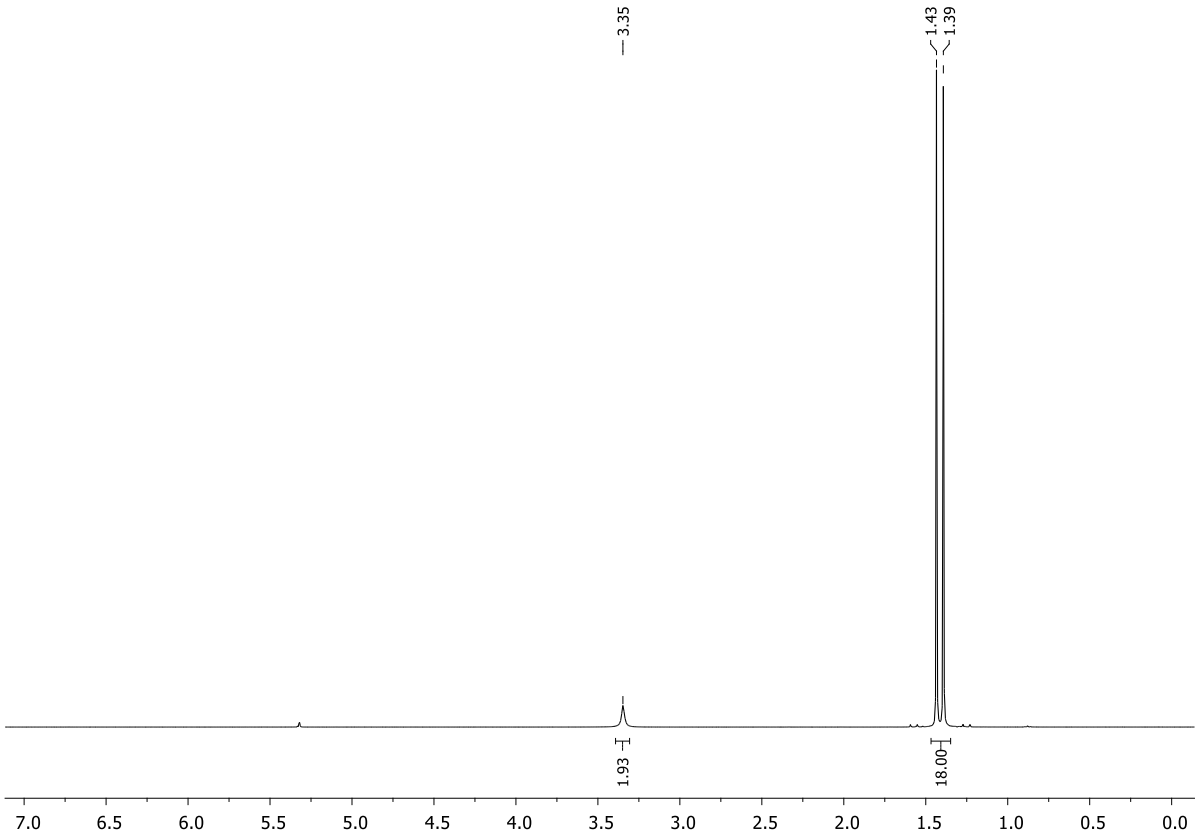

Figure S6.4. ^{1}H NMR spectrum (CD_2Cl_2, 298 K) of **$(1–H)^+$ $GeCl_3^–$**.

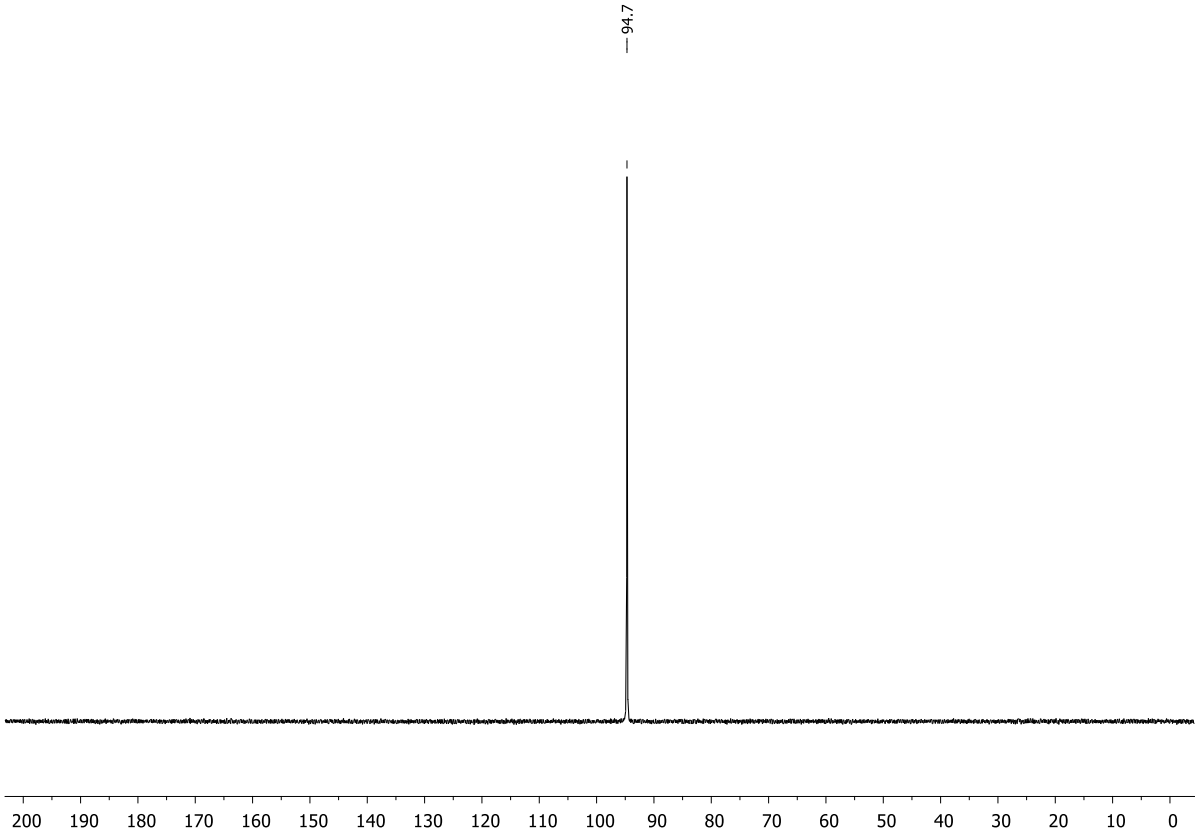

Figure S6.5. $^{31}P\{^{1}H\}$ NMR spectrum (CD_2Cl_2, 298 K) of **$(1–H)^+$ $GeCl_3^–$**.

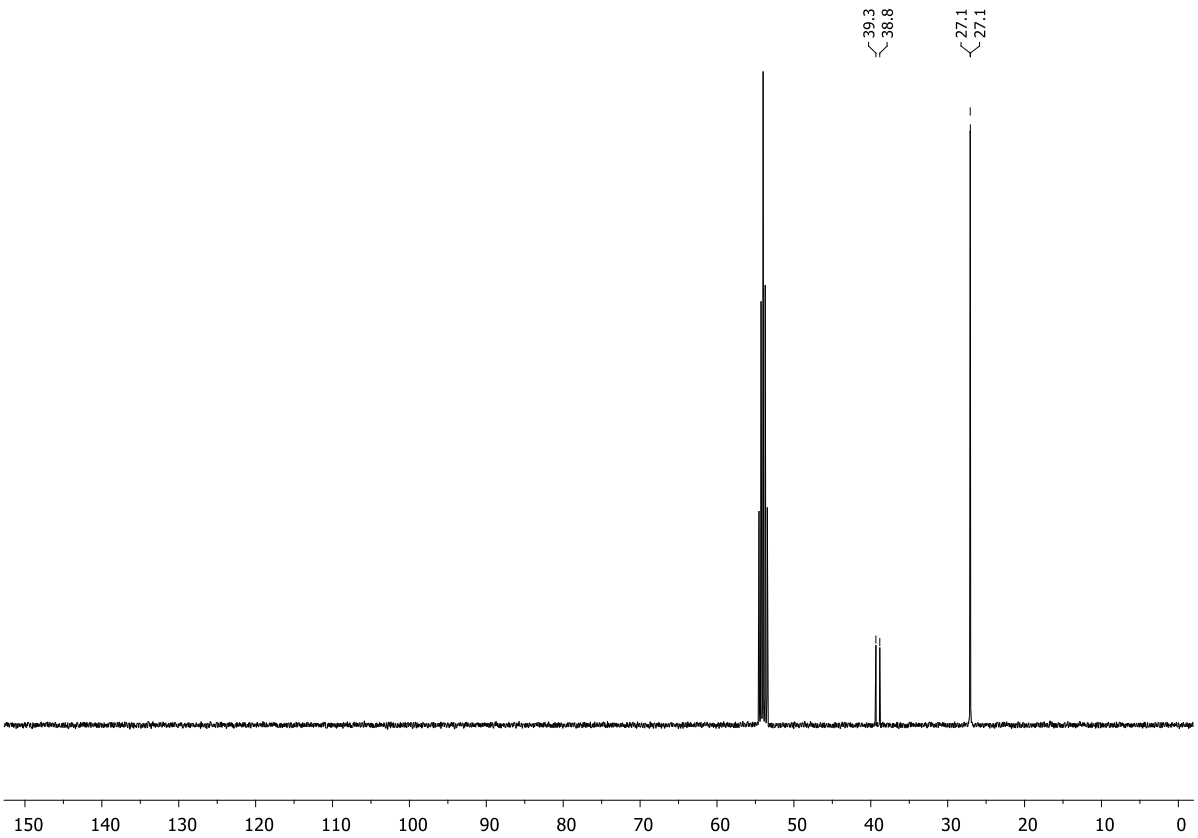

Figure S6.6. $^{13}C\{^{1}H\}$ NMR spectrum (CD_2Cl_2, 298 K) of **$(1–H)^+$ $GeCl_3^-$**.

6.3.2.4. Synthesis of 1·$SnCl_2$

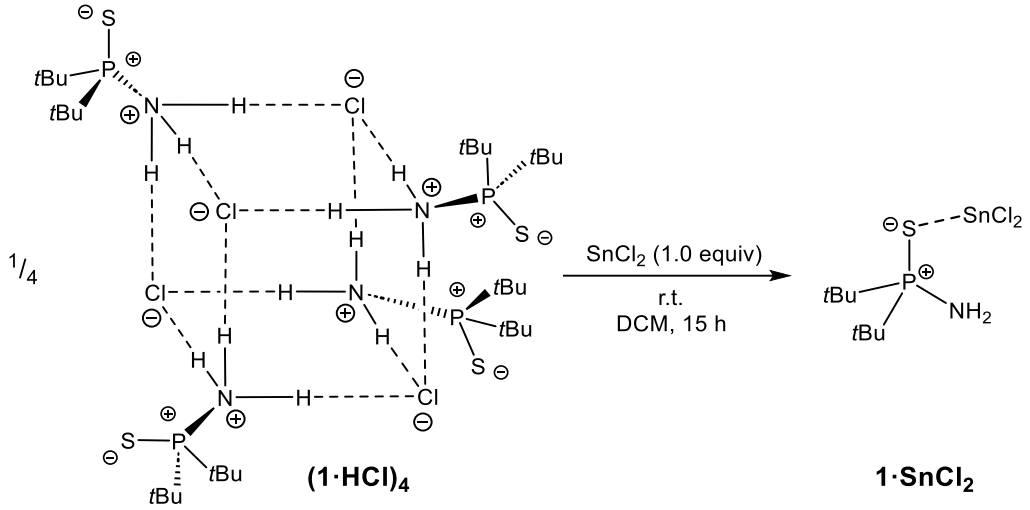

(1·HCl)$_4$ (60 mg, 0.25 mmol, 1.0 equiv) and $SnCl_2$ (50 mg, 0.25 mmol, 1.0 equiv) were suspended in DCM (2.5 mL) at room temperature and the mixture was stirred for 15 h. The resulting suspension was filtered and the filtrate was layered with pentane. Crystals suitable for single-crystal X-ray analysis of compound **1·$SnCl_2$** were obtained at room temperature.

^{1}H NMR (400.13 MHz, CD_2Cl_2, 298 K): δ = 1.42 (d, $^3J_{H–P}$ = 16.8 Hz, 18H, PC(C*H*$_3$)$_3$), 3.39 (d, 2H, N*H*). **^{31}P{^{1}H} NMR** (162.04 MHz, CD_2Cl_2, 298 K): δ = 94.6 (s). **^{13}C{^{1}H} NMR** (100.61 MHz, CD_2Cl_2, 298 K): δ = 27.2 (d, $^2J_{C–P}$ = 1.2 Hz, PC(*C*H$_3$)$_3$), 39.0 (d, $^1J_{C–P}$ = 51.2 Hz, P*C*(CH$_3$)$_3$).

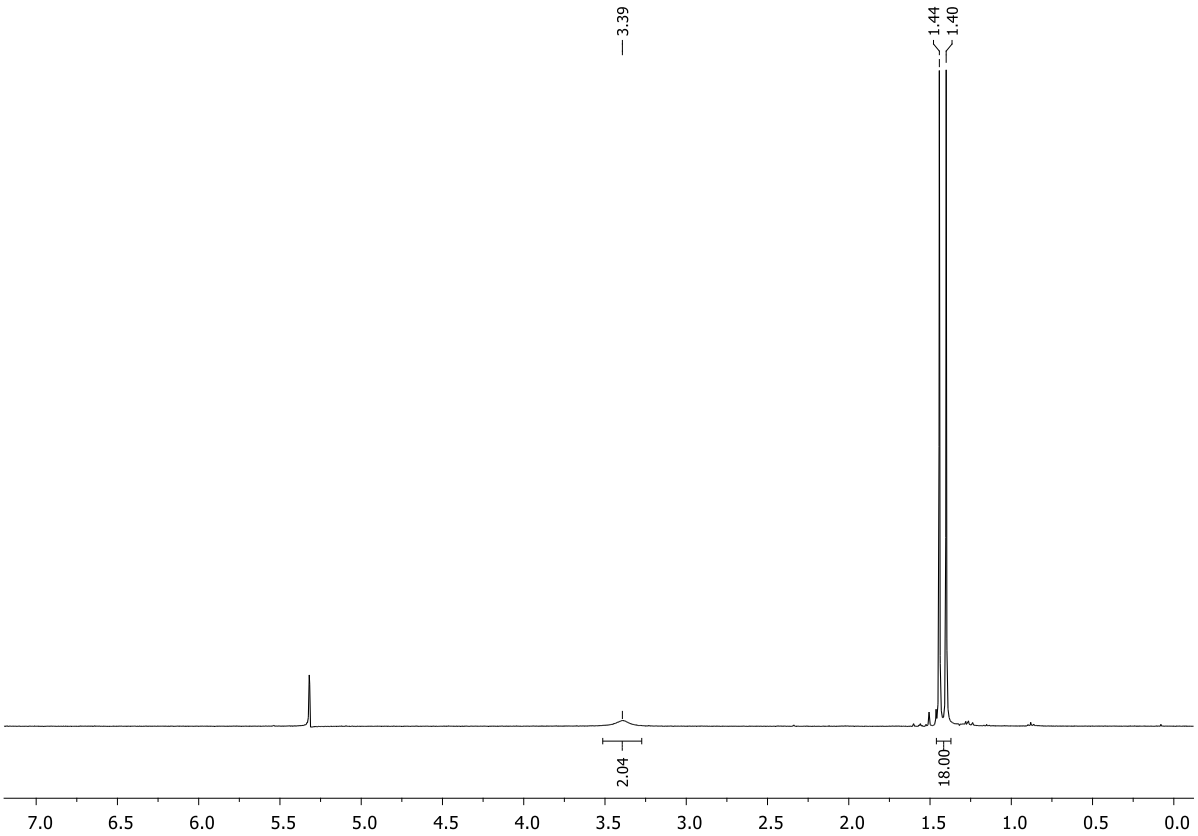

Figure S6.7. ^{1}H NMR spectrum (CD_2Cl_2, 298 K) of **1·SnCl$_2$**.

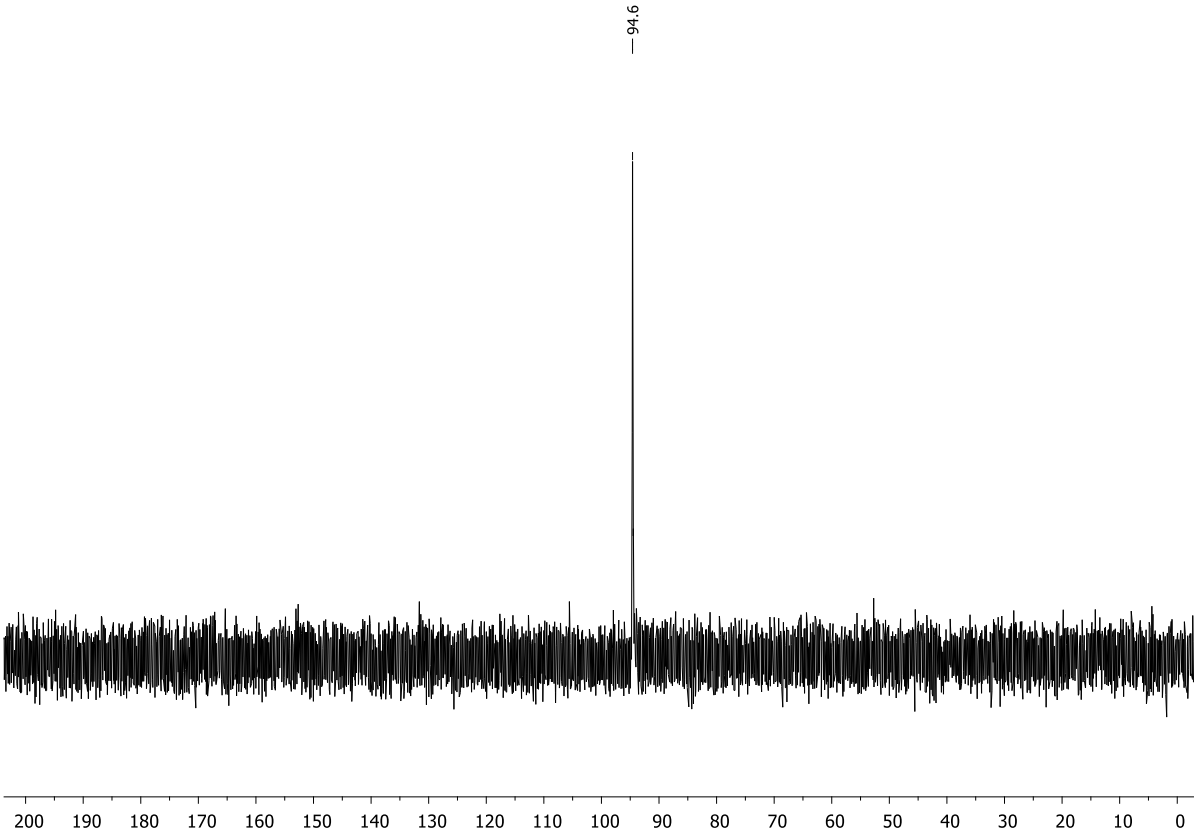

Figure S6.8. $^{31}P\{^{1}H\}$ NMR spectrum (CD_2Cl_2, 298 K) of **1·SnCl$_2$**.

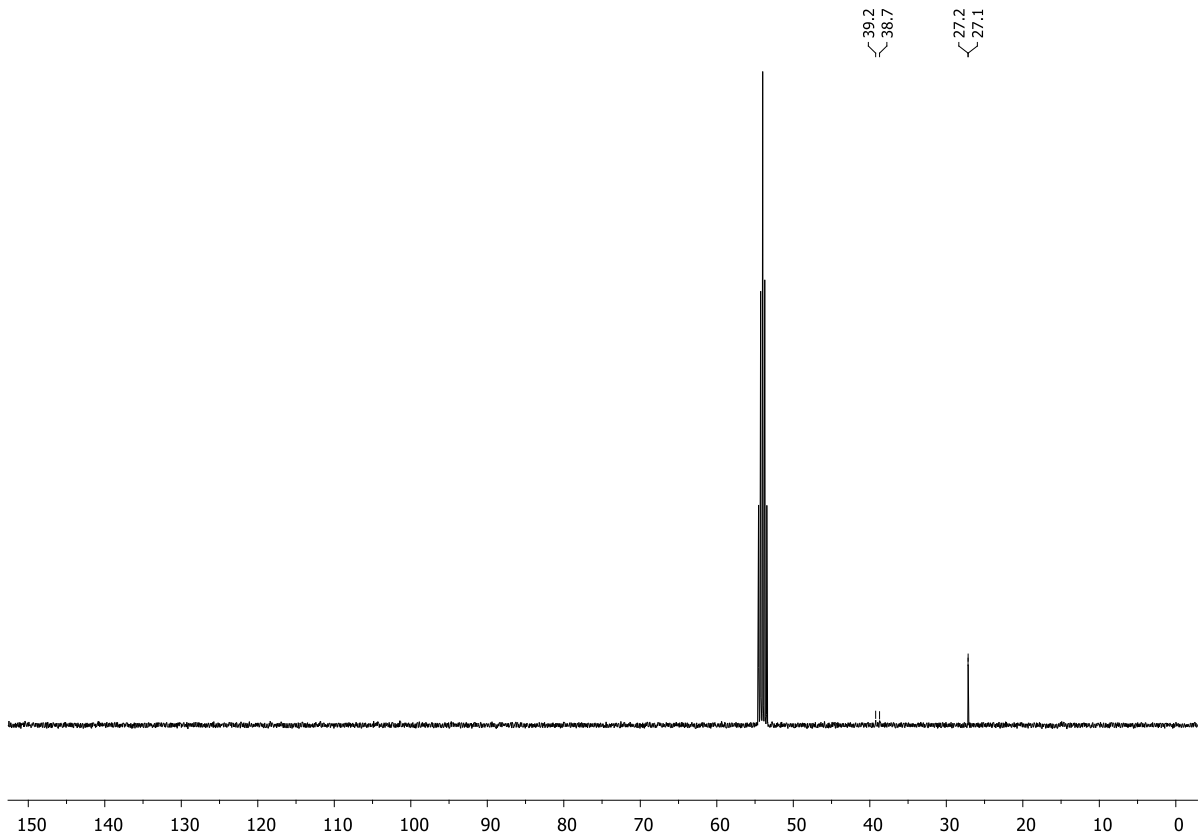

Figure S6.9. $^{13}C\{^{1}H\}$ NMR spectrum (CD_2Cl_2, 298 K) of **1·SnCl₂**.

6.3.2.5. Synthesis of [(R_P)-3]$_2$·AuCl

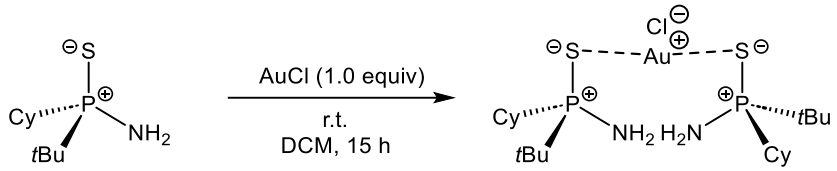

(R_P)-**3** **[(R_P)-3]$_2$·AuCl**

(R_P)-**3** (e.r. > 99:1) (30 mg, 0.14 mmol, 1.0 equiv) and AuCl (32 mg, 0.14 mmol, 1.0 equiv) were suspended in DCM (2.5 mL) at room temperature and the mixture was stirred for 15 h. The resulting suspension was filtered and the filtrate was layered with pentane. Crystals suitable for single-crystal X-ray analysis of compound **[(R_P)-3]$_2$·AuCl** were obtained at −35 °C.

^{1}H NMR (400.13 MHz, CD_2Cl_2, 298 K): δ = 1.20–1.40 (m, 6H, CH_2), 1.32 (d, $^3J_{H–P}$ = 16.5 Hz, 18H, PC(CH_3)$_3$), 1.55–1.74 (m, 6H, CH_2), 1.81–1.94 (m, 4H, CH_2), 1.96–2.06 (m, 4H, CH_2), 2.13–2.24 (m, 2H, CH), 2.98 (br, 4H, NH_2). **^{31}P{^{1}H} NMR** (162.04 MHz, CD_2Cl_2, 298 K): δ = 86.7 (s). **^{13}C{^{1}H} NMR** (100.61 MHz, CD_2Cl_2, 298 K): δ = 26.1 (s, PC(CH$_3$)$_3$), 26.8 (d, $^2J_{C–P}$ = 14.6 Hz, CH$_2$), 27.2 (d, $^2J_{C–P}$ = 13.1 Hz, CH$_2$), 27.3 (s, CH$_2$), 27.3 (s, CH$_2$), 28.7 (s, CH$_2$), 36.6 (d, $^1J_{C–P}$ = 57.9 Hz, PC(CH$_3$)$_3$), 38.4 (d, $^1J_{C–P}$ = 55.3 Hz, PCH).

Elemental analysis: $C_{20}H_{44}AuClN_2P_2S_2$ · 0.25 C_5H_{12} (pentane): calcd.: C 37.04, H 6.87, N 4.07; found: C 37.18, H 6.61, N 4.08.

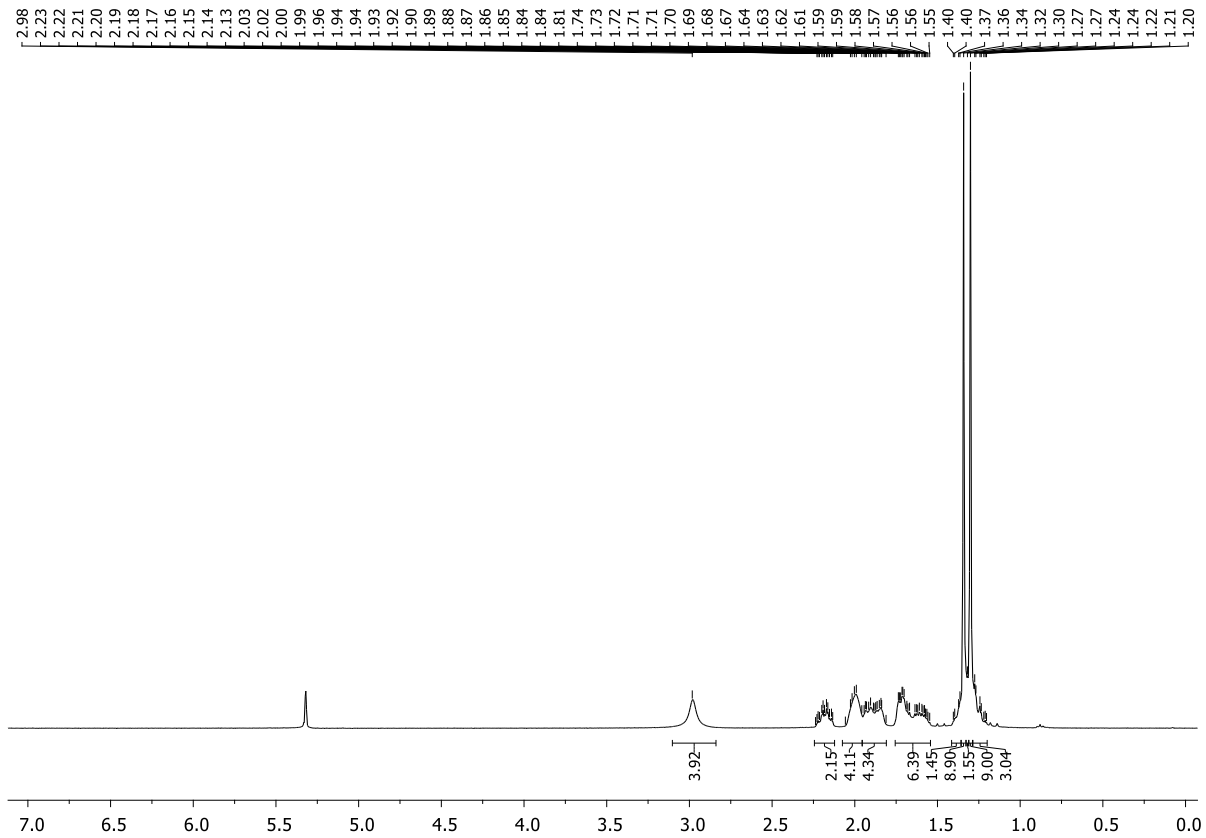

Figure S6.10. ^{1}H NMR spectrum (CD_2Cl_2, 298 K) of **[**(R_P)-**3]$_2$·AuCl**.

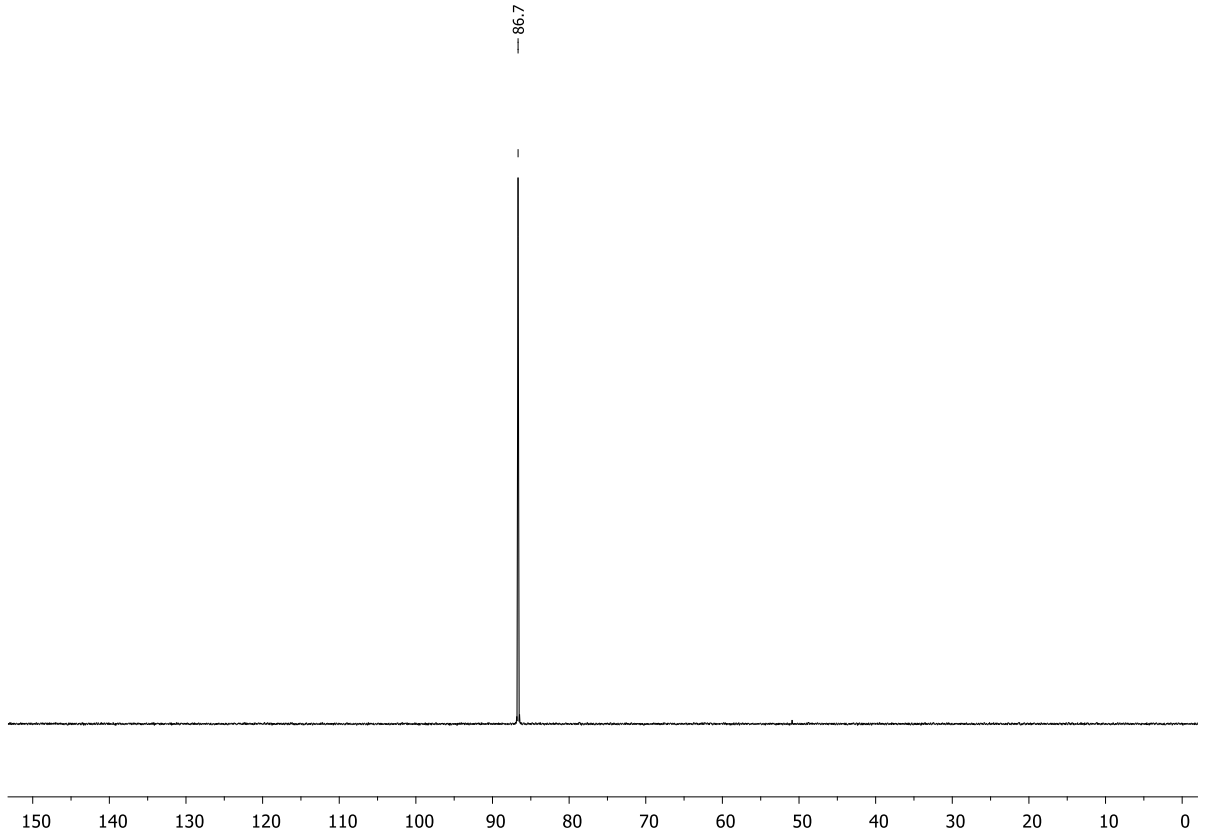

Figure S6.11. $^{31}P\{^{1}H\}$ NMR spectrum (CD_2Cl_2, 298 K) of **[**(R_P)-**3]$_2$·AuCl**.

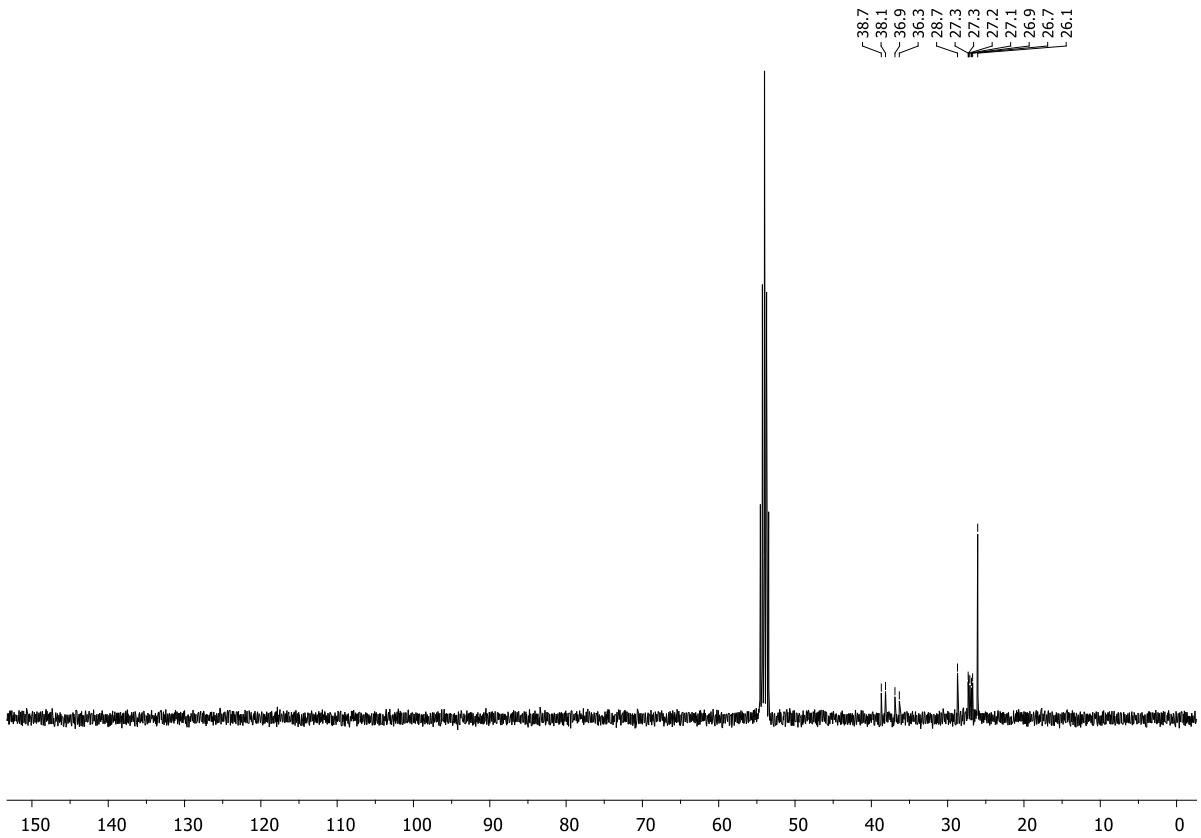

Figure S6.12. $^{13}C\{^{1}H\}$ NMR spectrum (CD_2Cl_2, 298 K) of **[**(R_P)-**3]$_2$·AuCl**.

6.3.2.6. Synthesis of (1·*p*TsOH)$_4$

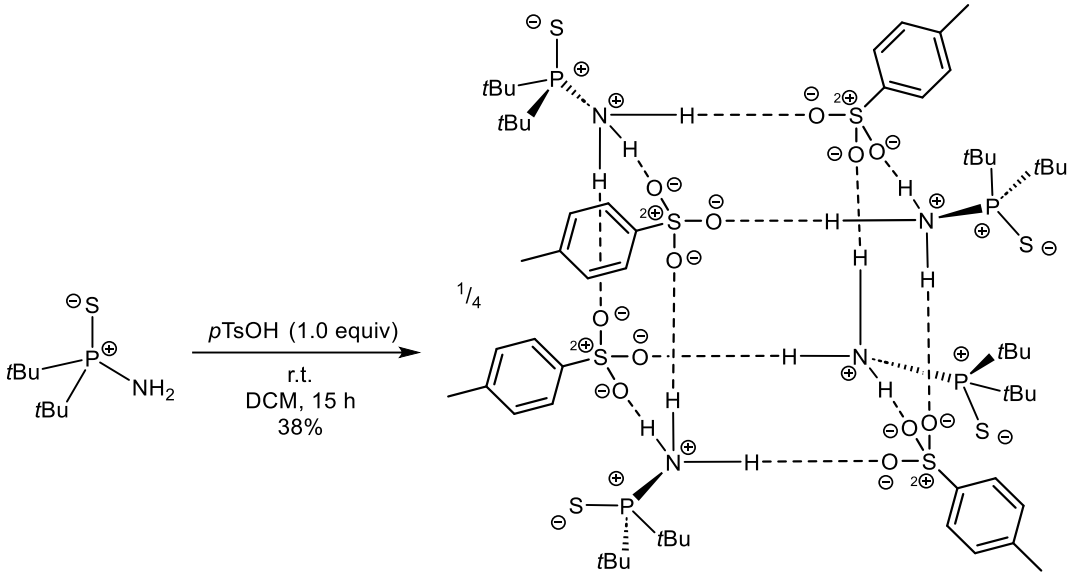

1 **(1·*p*TsOH)$_4$**

1 (0.97 g, 5.00 mmol, 1.0 equiv) and *p*TsOH (0.86 g, 5.00 mmol, 1.0 equiv) were solved in DCM (20 mL) at room temperature and the mixture was stirred for 15 h. All volatiles were removed from the resulting solution and the remaining colorless solid was dried in vacuo to obtain compound **(1·*p*TsOH)$_4$** (0.70 g, 1.92 mmol, 38%). Crystals suitable for single-crystal X-ray analysis were obtained from a DCM solution after layering with pentane.

^{1}H NMR (400.13 MHz, CD_2Cl_2, 298 K): δ = 1.39 (d, $^3J_{H–P}$ = 17.0 Hz, 18H, PC(C*H*$_3$)$_3$), 2.38 (s, C*H*$_3$), 7.20 (d, $^3J_{H–H}$ = 8.0 Hz, 2H, *H*$_{Ph}$), 7.73 (d, $^3J_{H–H}$ = 8.2 Hz, 2H, *H*$_{Ph}$), 7.93 (br, 3H, N*H*). **^{31}P{^{1}H} NMR** (162.04 MHz, CD_2Cl_2, 298 K): δ = 107.0 (s). **^{13}C{^{1}H} NMR** (100.61 MHz, CD_2Cl_2, 298 K): δ = 21.7 (s, *C*H$_3$), 27.2 (d, $^2J_{C–P}$ = 1.8 Hz, PC(*C*H$_3$)$_3$), 40.1 (d, $^1J_{C–P}$ = 46.4 Hz, P*C*(CH$_3$)$_3$), 126.7 (s, *C*$_{Ph}$), 129.5 (s, *C*$_{Ph}$), 140.6 (s, *C*$_{Ph}$), 142.0 (s, *C*$_{Ph}$).

Elemental analysis: $C_{15}H_{28}NO_3PS_2$ · 0.4 CH_2Cl_2: calcd.: C 46.30, H 7.27, N 3.51; found: C 46.07, H 7.35, N 3.49.

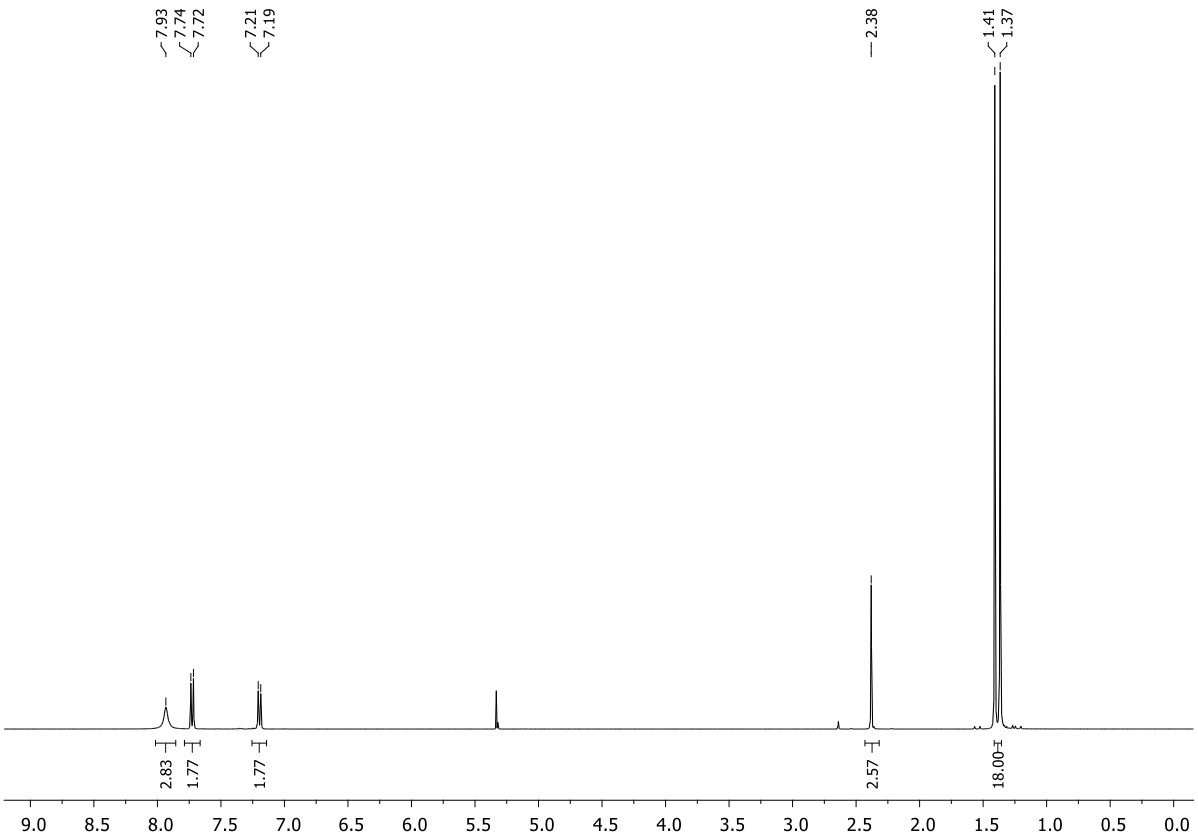

Figure S6.13. ^{1}H NMR spectrum (CD_2Cl_2, 298 K) of **(1·*p*TsOH)$_4$**.

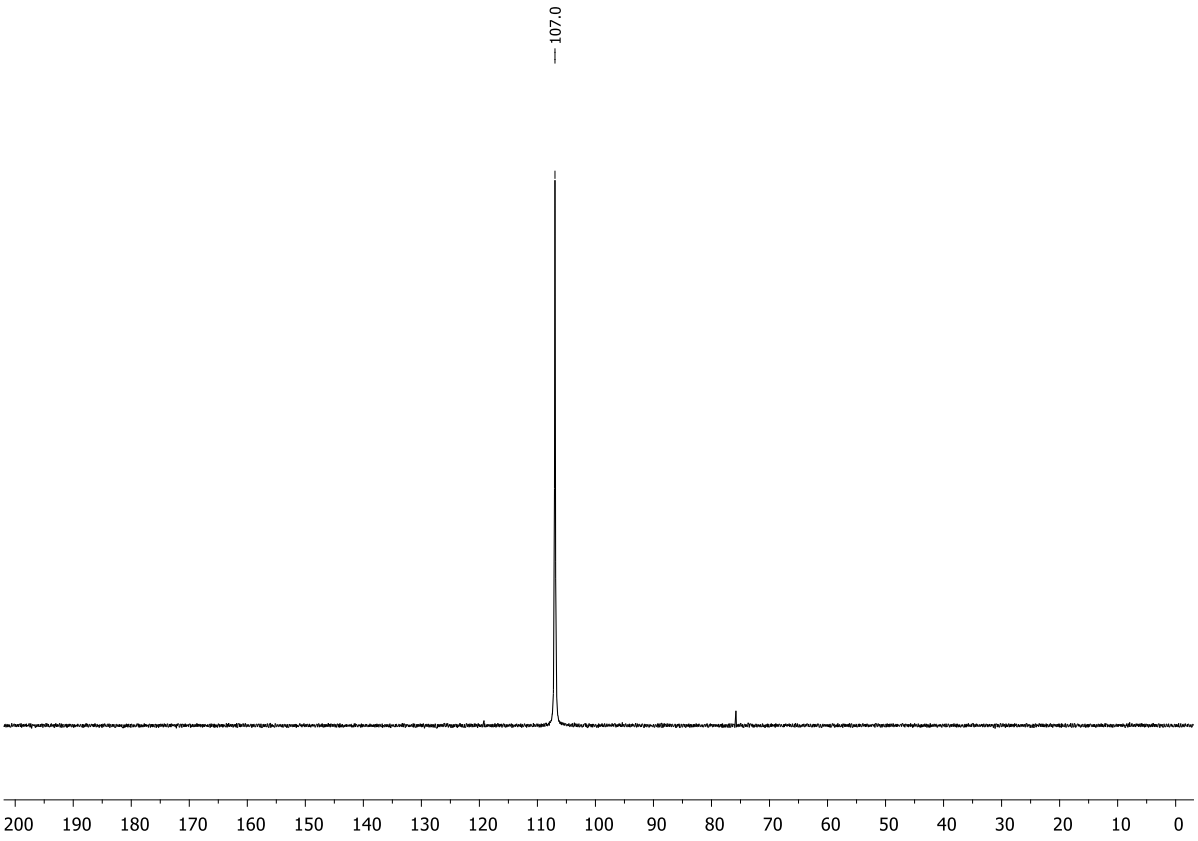

Figure S6.14. $^{31}P\{^{1}H\}$ NMR spectrum (CD_2Cl_2, 298 K) of **(1·*p*TsOH)$_4$**.

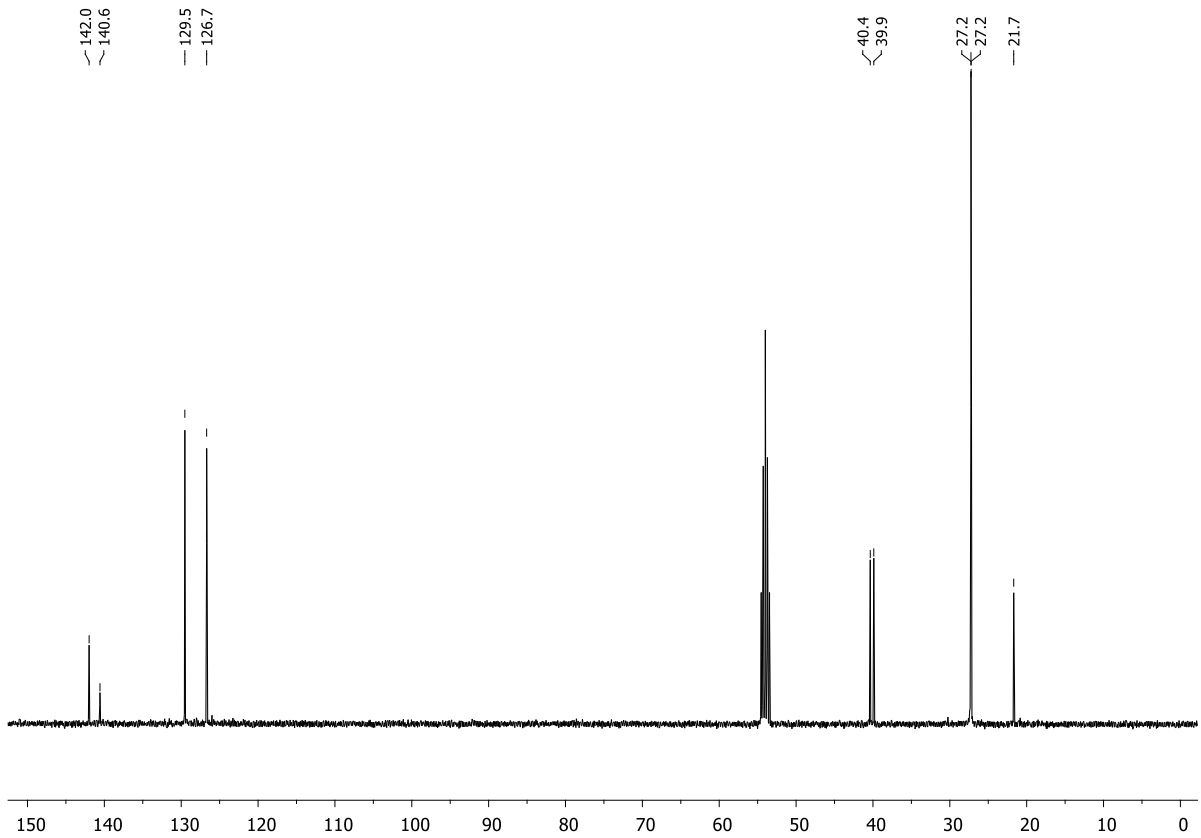

Figure S6.15. $^{13}C\{^{1}H\}$ NMR spectrum (CD_2Cl_2, 298 K) of **(1·*p*TsOH)$_4$**.

6.3.2.7. Synthesis of {[(1–H)$^+$]$_2$H$_3$O$^+$}(OTf)$_3^-$

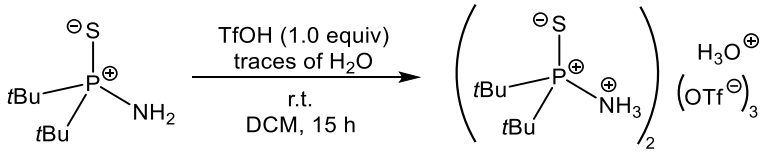

1 **{[(1–H)$^+$]$_2$H$_3$O$^+$}(OTf$^-$)$_3$**

1 (0.30 g, 1.55 mmol, 1.0 equiv) was solved in DCM (20 mL) and triflic acid (0.14 mL,1.55 mmol, 1.0 equiv) was added dropwise at room temperature. After stirring the mixture for 15 h, all volatiles were removed from the resulting solution and the remaining colorless solid was dried in vacuo to obtain compound **{[(1–H)$^+$]$_2$H$_3$O$^+$}(OTf$^-$)$_3$**. Crystals suitable for single-crystal X-ray analysis were obtained from a DCM solution after layering with pentane.

6.4. X-Ray Crystallographic Details

The crystals were selected and measured on a XtaLAB Synergy R, DW system, HyPix-Arc 150 {**(1·Li)$_4$**, **(1–H)$^+$ GeCl$_3^-$**, **1·SnCl$_2$**, **[(*R*$_P$)-3]$_2$·AuCl**, **(1·*p*TsOH)$_4$**}, on a GV1000, TitanS2 (**2·HCl**) or on a SuperNova, Dualflex, TitanS2 {**{[(1–H)$^+$]$_2$H$_3$O$^+$}(OTf$^-$)$_3$**}. The crystals were kept at T = 123(1) K {**(1·Li)$_4$**, **2·HCl**, **1·SnCl$_2$**, **[(*R*$_P$)-3]$_2$·AuCl**, **(1·*p*TsOH)$_4$**, **{[(1–H)$^+$]$_2$H$_3$O$^+$}(OTf$^-$)$_3$**} or 100(1) K [**(1–H)$^+$ GeCl$_3^-$**] during data collection. Data collection and reduction were performed with **CrysAlisPro** Version 1.171.41.93a [**(1·Li)$_4$**, **(1–H)$^+$ GeCl$_3^-$**, **1·SnCl$_2$**, **(1·*p*TsOH)$_4$**], Version 1.171.41.54a (**2·HCl**), Version 1.171.41.83a {**[(*R*$_P$)-3]$_2$·AuCl**}, Version 1.171.42.95a {**{[(1–H)$^+$]$_2$H$_3$O$^+$}(OTf$^-$)$_3$**}.[4] For all compounds a numerical absorption correction based on gaussian integration over a multifaceted crystal model and an empirical absorption correction using spherical harmonics as implemented in SCALE3 ABSPACK was applied. Using **Olex2**[5], the structures were solved with **ShelXT**[6] and a least-square refinement on F_2 was carried out with **ShelXL**[7] for all structures. All non-hydrogen atoms were refined anisotropically. Hydrogen atoms at the carbon atoms were located in idealized positions and refined isotropically according to the riding model. Hydrogen atoms at the nitrogen atoms in compounds **1·SnCl$_2$**, **[(*R*$_P$)-3]$_2$·AuCl**, **{[(1–H)$^+$]$_2$H$_3$O$^+$}(OTf$^-$)$_3$** were located in idealized positions and refined isotropically according to the riding model. Hydrogen atoms at the nitrogen atoms in compounds **(1·Li)$_4$**, **2·HCl**, **(1–H)$^+$ GeCl$_3^-$**, **(1·*p*TsOH)$_4$** were located from the difference Fourier map and refined without restraints. The hydrogen atom at the silicon atom in **2·HCl** was located in idealized position and refined isotropically according to the riding model. The hydrogen atom at the phosphorus atom in **2·HCl** was located from the difference Fourier map and refined without restraints. Two hydrogen atoms at the oxygen atom in **{[(1–H)$^+$]$_2$H$_3$O$^+$}(OTf$^-$)$_3$** were located in idealized positions and refined isotropically according to the riding model, while the third hydrogen atom was located from the difference Fourier map and refined without restraints. Figures were created with Olex2.[5]

Compound **(1·Li)$_4$**: The asymmetric unit contains eight lithium cations, eight anions (**1**$_{-H}$)$^-$ and two molecules of DCM.

Compound **2·HCl**: The asymmetric unit contains one cation **(2–H)$^+$** and one chloride anion.

Compound **(1–H)$^+$ GeCl$_3^-$**: The asymmetric unit contains one cation **(1–H)$^+$** and one anion **GeCl$_3^-$**.

Compound **1·SnCl$_2$**: The asymmetric unit contains two molecules. The bad values for R_{int}, max. peak and min. peak are due to the high residual electron density caused by the presence of tin.

Compound **[(*R*$_P$)-3]$_2$·AuCl**: The asymmetric unit contains one gold(I) complex with two (*R*$_P$)-**3**-ligands and one chloride anion.

Compound **(1·*p*TsOH)$_4$**: The asymmetric unit contains one cation **(1–H)$^+$**, one tosylate anion and half a molecule of DCM.

Compound **{[(1–H)$^+$]$_2$H$_3$O$^+$}(OTf$^-$)$_3$**: The asymmetric unit contains two cations **(1–H)$^+$**, one oxonium cation and three triflate anions. Two of the triflate anions (F00A, F00O, F00P and F00S, F00T, F00W, C01B) are disordered over two positions and split into two parts with occupancies of 43:57

and 72:28, respectively. SIMU, SADI, RIGU and ISOR restraints were used to model these disorders.

Table S6.1. Crystallographic data for compounds **(1·Li)$_4$**, **2·HCl** and **(1–H)$^+$ GeCl$_3^-$**.

Compound	**(1·Li)$_4$**	**2·HCl**	**(1–H)$^+$ GeCl$_3^-$**
Data Set (internal naming)	**TH356**	**TH004a**	**TH470**
Formula	$C_{64}H_{152}Li_8N_8P_8S_8 \cdot 2\ CH_2Cl_2$	$C_{18}H_{35}ClNPSi$	$C_8H_{21}Cl_3GeNPS$
$\rho_{calc.}$ / g·cm^{-3}	1.176	1.117	1.562
μ/mm^{-1}	0.453	2.785	9.240
Formula Weight	1763.54	359.98	373.23
Color	clear colorless	clear colorless	clear colorless
Shape	prism	needle	plate
Size/mm^3	0.57 × 0.26 × 0.21	0.406 × 0.037 × 0.026	0.32 × 0.22 × 0.08
T/K	123.00(10)	123.00(10)	100.01(10)
Crystal System	orthorhombic	monoclinic	monoclinic
Flack Parameter	0.00(2)	–	–
Hooft Parameter	0.00(2)	–	–
Space Group	$P2_12_12_1$	$P2_1/c$	$P2_1/c$
a/Å	20.56660(10)	15.5590(10)	8.97660(10)
b/Å	20.64060(10)	10.8837(6)	10.45140(10)
c/Å	23.4568(2)	13.0428(8)	17.2759(2)
α/°	90	90	90
β/°	90	104.273(6)	101.6720(10)
γ/°	90	90	90
V/Å^3	9957.58(11)	2140.5(2)	1587.28(3)
Z	4	4	4
Z'	1	1	1
Wavelength/Å	0.71073	1.54184	1.54184
Radiation Type	Mo K_α	Cu K_α	Cu K_α
$2\theta_{min}$/°	3.994	10.024	9.948
$2\theta_{max}$/°	104.332	147.408	147.39
Measured Refl.	165232	7330	19624
Independent Refl.	71901	4108	3098
R_{int}	0.0213	0.0466	0.0554
Parameters	999	216	154
Restraints	0	0	0
Largest Peak	1.18	0.40	0.47
Deepest Hole	−0.76	−0.44	−0.49
GooF	0.991	1.067	1.082
wR_2 (all data)	0.1004	0.1200	0.0841
wR_2	0.0909	0.1143	0.0835
R_1 (all data)	0.0722	0.0588	0.0314
R_1	0.0388	0.0458	0.0306

Table S6.2. Crystallographic data for compounds **1·SnCl$_2$**, **[(*R*$_P$)-3]$_2$·AuCl**, **(1·*p*TsOH)$_4$** and **{[(1–H)$^+$]$_2$H$_3$O$^+$}(OTf$^-$)$_3$**.

Compound	**1·SnCl$_2$**	**[(*R*$_P$)-3]$_2$·AuCl**	**(1·*p*TsOH)$_4$**	**{[(1–H)$^+$]$_2$H$_3$O$^+$}(OTf$^-$)$_3$**
Data Set (internal naming)	**TH467**	**TH246**	**TH421**	**TH526**
Formula	$C_{16}H_{40}Cl_4N_2P_2S_2Sn_2$	$C_{20}H_{44}AuClN_2P_2S_2$	$C_{15}H_{28}NO_3PS_2 \cdot ½CH_2Cl_2$	$C_{19}H_{45}F_9N_2O_{10}P_2S_5$
$\rho_{calc.}$ / g·cm^{-3}	1.698	1.634	1.238	1.475
μ/mm^{-1}	18.923	13.640	4.121	4.389
Formula Weight	765.74	671.05	407.94	854.84
Color	clear colorless	clear colorless	clear colorless	clear colorless
Shape	needle	needle	block	block
Size/mm^3	0.8 × 0.12 × 0.11	0.36 × 0.14 × 0.09	0.61 × 0.31 × 0.23	0.47 × 0.39 × 0.32
T/K	123.01(10)	123.01(10)	123.00(10)	123.15
Crystal System	monoclinic	orthorhombic	tetragonal	orthorhombic
Flack Parameter	–	–0.033(4)	–0.001(4)	0.354(7)
Hooft Parameter	–	–	–	–
Space Group	$P2_1/n$	$P2_12_12_1$	P-4n2	$P2_12_12_1$
a/Å	7.51040(10)	9.94820(10)	18.40640(10)	12.1546(1)
b/Å	26.3361(2)	14.83780(10)	18.40640(10)	17.6478(1)
c/Å	15.20040(10)	18.47890(10)	12.92390(10)	17.9402(1)
α/°	90	90	90	90
β/°	95.1100(10)	90	90	90
γ/°	90	90	90	90
V/Å^3	2994.61(5)	2727.66(4)	4378.56(6)	3848.21(4)
Z	4	4	8	4
Z'	1	1	1	1
Wavelength/Å	1.54184	1.54184	1.54184	1.54184
Radiation Type	Cu K$_\alpha$	Cu K$_\alpha$	Cu K$_\alpha$	Cu K$_\alpha$
$2\theta_{min}$/°	6.712	7.642	6.792	7.02
$2\theta_{max}$/°	151.336	146.238	150.236	133.4
Measured Refl.	44661	26344	51474	33349
Independent Refl.	5989	5250	4446	6794
R_{int}	0.1211	0.0350	0.0581	0.0569
Parameters	265	259	232	511
Restraints	0	0	0	182
Largest Peak	2.19	0.92	0.24	0.40
Deepest Hole	–2.06	–1.60	–0.27	–0.29
GooF	1.097	1.106	1.081	1.044
wR_2 (all data)	0.1606	0.0579	0.0708	0.0874
wR_2	0.1588	0.0577	0.0705	0.0862
R_1 (all data)	0.0558	0.0236	0.0271	0.0345
R_1	0.0544	0.0233	0.0265	0.0335

Compound $(1 \cdot Li)_4$:

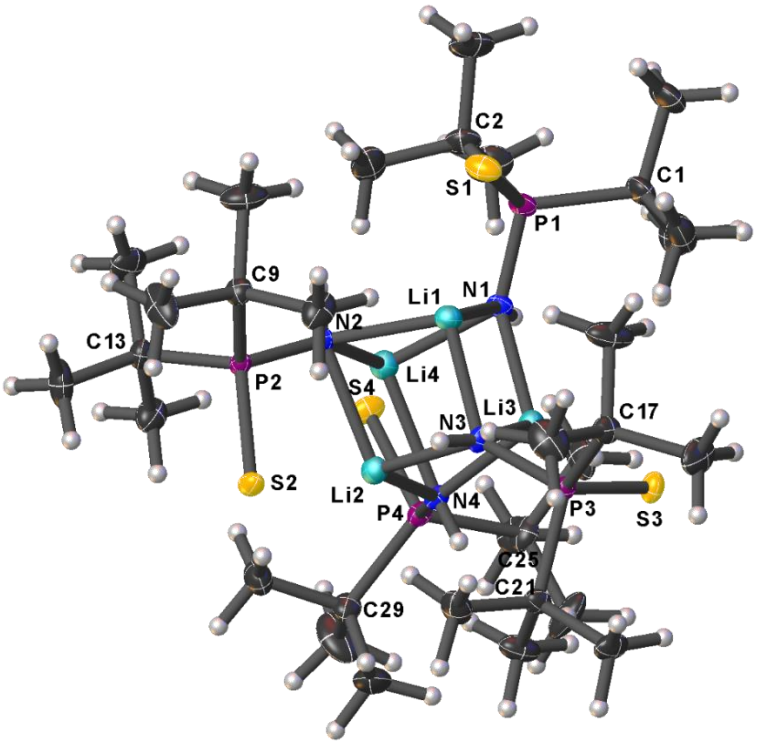

second cube with solvent molecules:

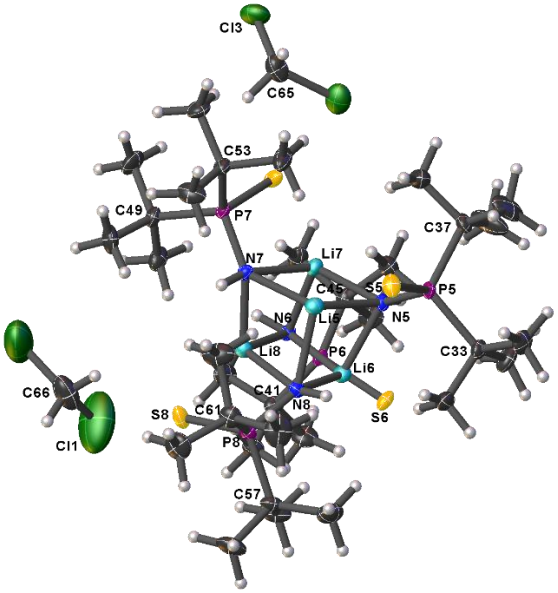

Selected Bond Lengths in Å		Selected Bond Angles in °	
P1–S1	1.9974(5)	N1–P1–S1	108.41(4)
P1–N1	1.6361(11)	N1–P1–C2	109.08(6)
P1–C2	1.8770(15)	N1–P1–C1	109.01(6)
P1–C1	1.8755(14)	C1–P1–C2	112.05(7)
N1–Li1	2.198(3)	P1–N1–Li1	93.54(8)

Compound 2·HCl:

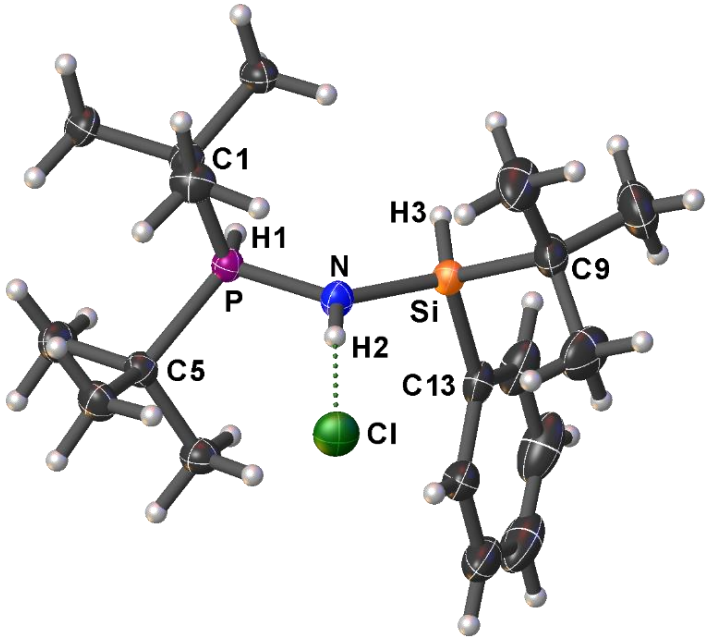

Selected Bond Lengths in Å		Selected Bond Angles in °	
P–N	1.6251(19)	N–P–C5	112.56(10)
P–C5	1.841(2)	N–P–C1	109.92(11)
P–C1	1.836(2)	N–P–H1	106.9(14)
P–H1	1.27(3)	N–Si–C13	110.45(10)
Si–N	1.7477(19)	N–Si–C9	110.31(11)
Si–C13	1.872(3)	P–N–Si	126.83(12)
Si–C9	1.888(3)		

Compound $(1–H)^+$ $GeCl_3^–$:

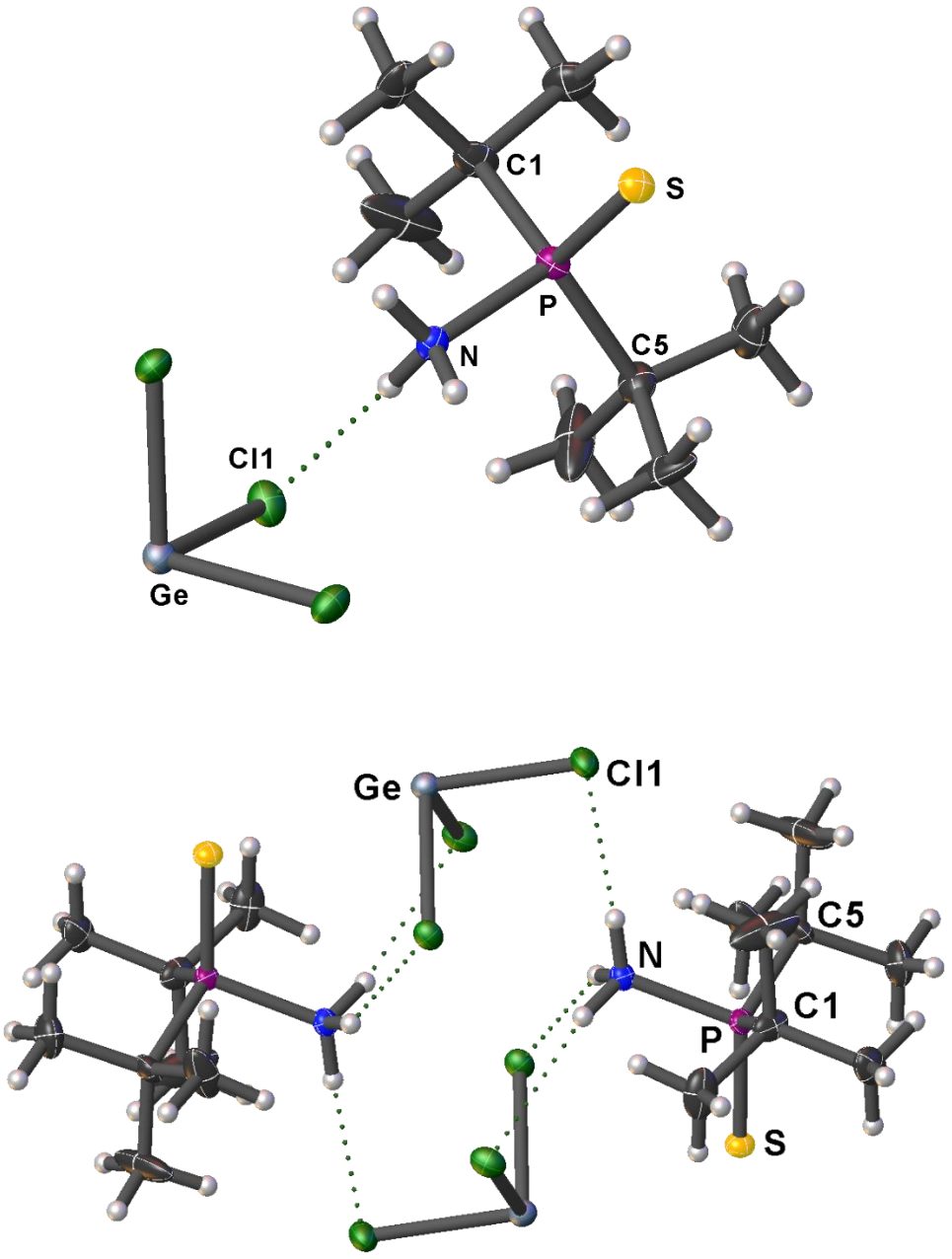

Selected Bond Lengths in Å		Selected Bond Angles in °	
P–S	1.9373(8)	N–P–S	109.06(7)
P–N	1.810(2)	N–P–C5	100.88(10)
P–C5	1.862(2)	N–P–C1	101.11(10)
P–C1	1.859(2)	C1–P–C5	117.33(12)
Ge–Cl1	2.3445(6)	Cl1–Ge–Cl2	91.07(2)

Compound 1·$SnCl_2$:

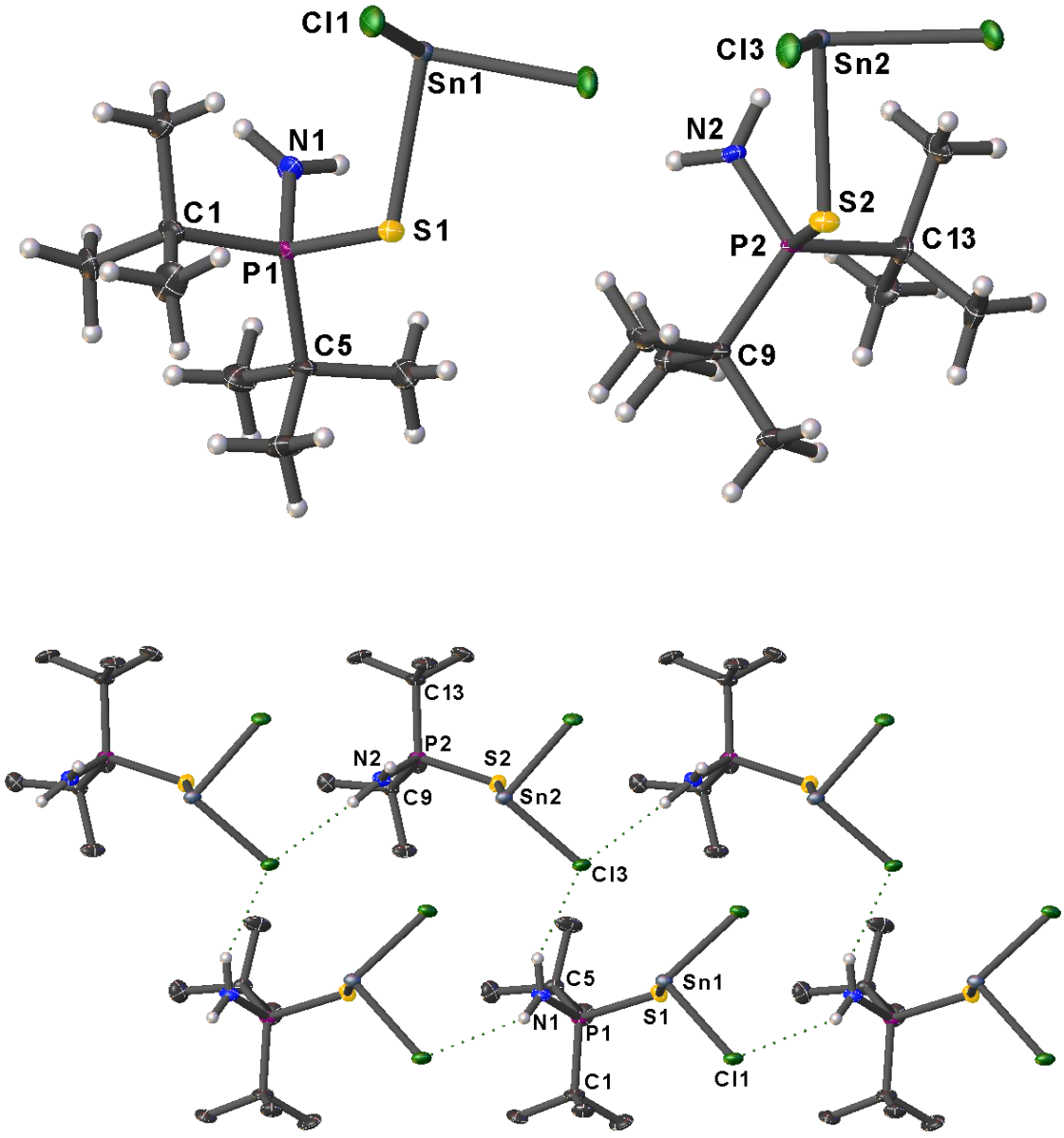

Selected Bond Lengths in Å		Selected Bond Angles in °	
S1–P1	2.0216(16)	N1–P1–S1	109.76(15)
P1–N1	1.648(4)	N1–P1–C1	104.8(2)
P1–C1	1.855(4)	N1–P1–C5	109.7(2)
P1–C5	1.861(5)	C1–P1–C5	115.7(2)
Sn1–S1	2.6083(10)	P1–S1–Sn1	101.28(5)
Sn1–Cl1	2.5093(11)	Cl1–Sn1–S1	91.44(4)

Compound [(R_P)-3]$_2$·AuCl:

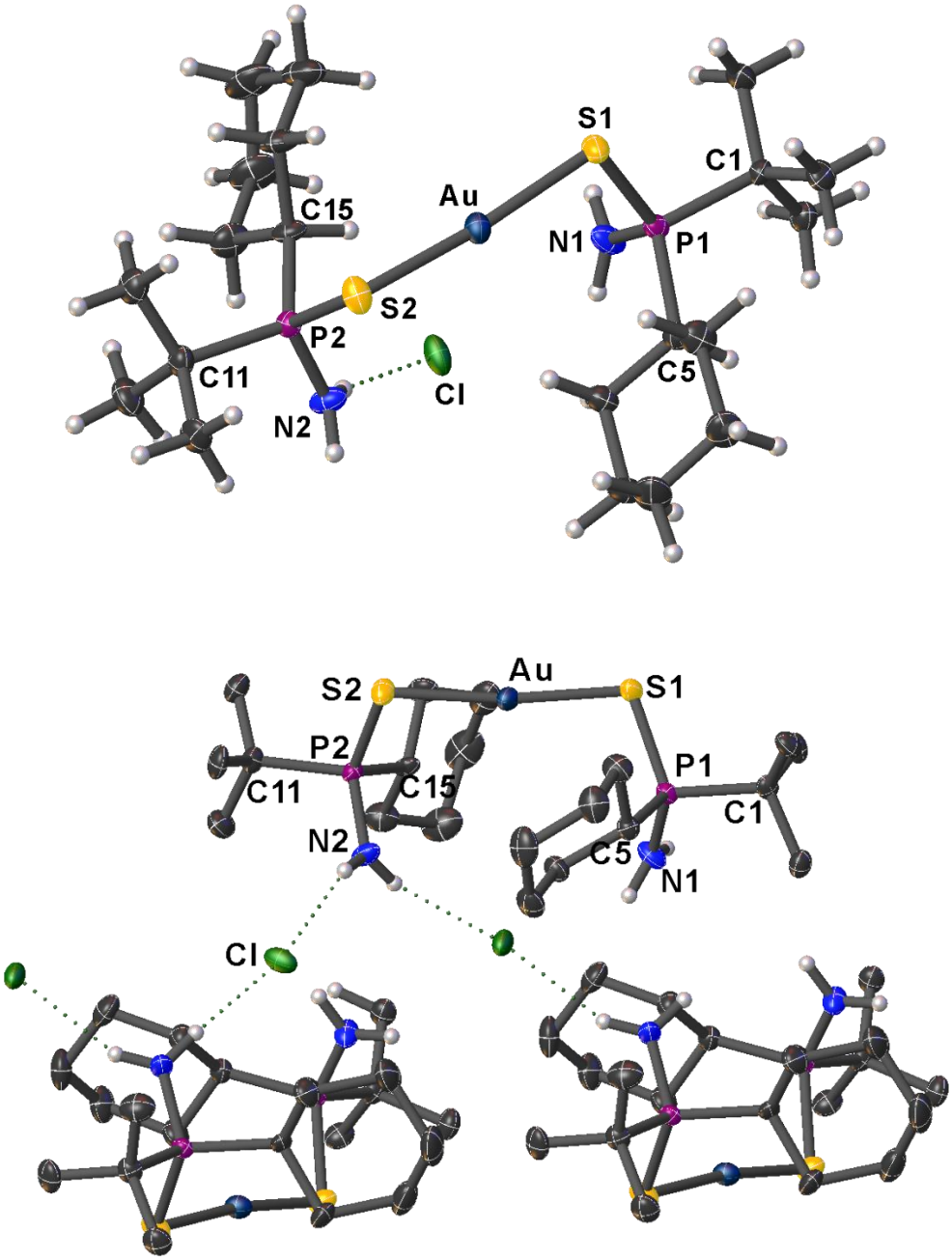

Selected Bond Lengths in Å		Selected Bond Angles in °	
P1–S1	2.0431(19)	N1–P1–S1	116.8(2)
P1–N1	1.624(5)	N1–P1–C1	104.9(3)
P1–C1	1.855(6)	N1–P1–C5	106.7(3)
P1–C5	1.847(6)	C5–P1–C1	110.2(2)
Au–S1	2.2820(16)	S1–Au–S2	172.91(5)
Au–S2	2.2968(15)		

Compound (1·*p*TsOH)$_4$:

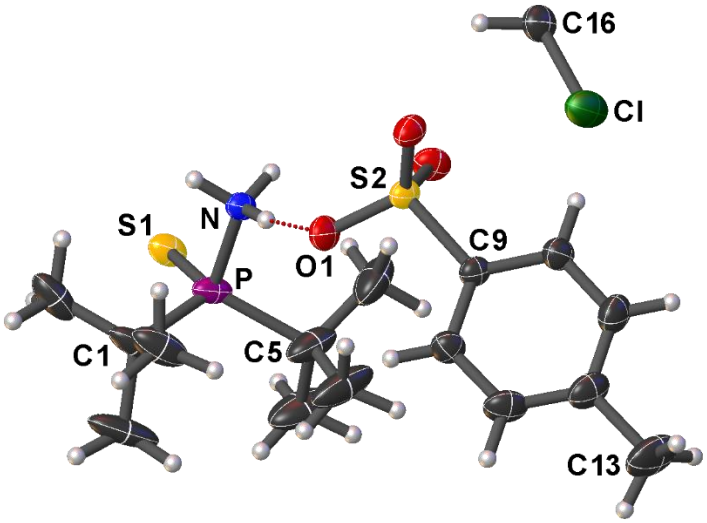

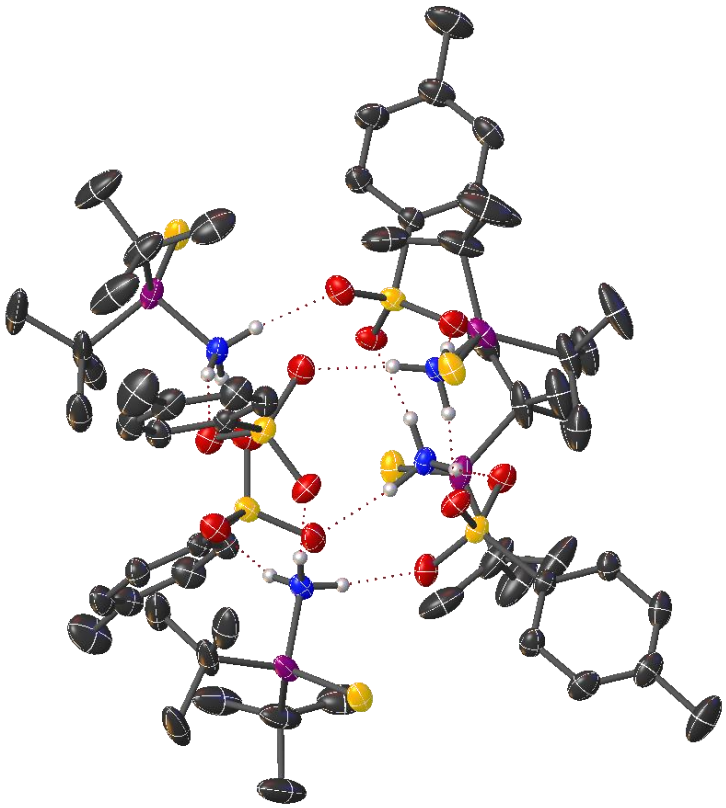

Selected Bond Lengths in Å		Selected Bond Angles in °	
S1–P	1.9378(8)	N-P-S1	109.73(7)
P–N	1.775(2)	N–P–C1	102.08(12)
P–C1	1.855(3)	N–P–C5	102.35(12)
P–C5	1.861(3)	C1–P–C5	115.93(16)

Compound $\{[(1–H)^+]_2H_3O^+\}(OTf^-)_3$:

Part 1 (multicolored)
[43%(F00A,F00O,F00P)/
72%(F00S,F00T,F00W,C01B)]

Part 2 (marked green shaded)
[57%(F3,F2,F00Q)/
28%(F1,F00U,F00X,C01C)]

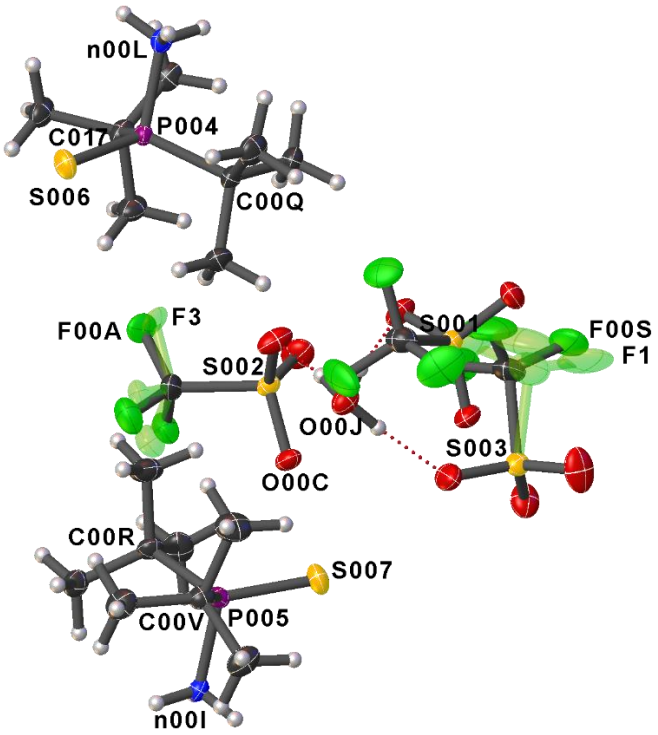

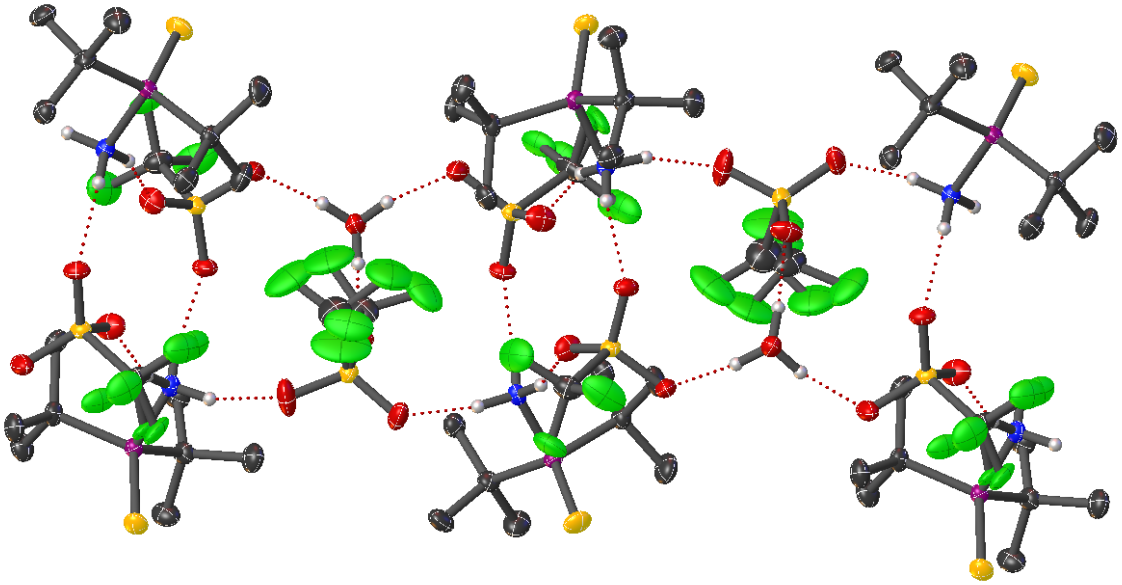

Selected Bond Lengths in Å		Selected Bond Angles in °	
P004–S006	1.9275(9)	n00L–P004–S006	108.33(8)
P004–n00L	1.792(2)	C017–P004–n00L	100.68(11)
P004–C00Q	1.860(3)	C00Q–P004–n00L	101.79(11)
P004–C017	1.864(3)	C017–P004–C00Q	115.12(12)

6.5. Supplementary References

[1] a) M. J. P. Harger, M. A. Stephen, *J. Chem. Soc., Perkin Trans.* **1980**, 705–711; b) M. Köster, A. Kreher, C. von Hänisch, *Dalton Trans.* **2018**, *47*, 7875–7878; c) T. C. Jankins, Z. Qin, K. M. Engle, *Tetrahedron* **2019**, *75*, 3272–3281.

[2] N. Fontana, N. A. Espinosa-Jalapa, M. Seidl, J. O. Bauer, *Chem. Commun.* **2022**, *58*, 2144–2147.

[3] T. Huber, N. A. Espinosa-Jalapa, J. O. Bauer, *Chem. Eur. J.* **2022**, *28*, e202202608.

[4] CrysAlisPro Software System, Rigaku Oxford Diffraction **2023**.

[5] O. V. Dolomanov, L. J. Bourhis, R. J. Gildea, J. A. K. Howard, H. Puschmann, *J. Appl. Crystallogr.* **2009**, *42*, 339–341.

[6] G. M. Sheldrick, *Acta Cryst.* **2015**, *A71*, 3–8.

[7] G. M. Sheldrick, *Acta Cryst.* **2015**, *C71*, 3–8.

7. Conclusions

This work presented the stereoselective preparation of aminophosphine sulfides, methods to influence their aggregation properties and novel applications as *N*-silyl-substituted building blocks. Unless otherwise stated, the products have generally been structurally characterized by classical analytical methods such as NMR spectroscopy, elemental analysis, mass spectrometry and single crystal X-ray diffraction. For chiral compounds, the absolute configurations were determined from the crystal structures obtained by single crystal X-ray diffraction analysis.

The first chapter gave a thorough overview of historical and modern research on *P*-stereogenic aminophosphines and shows the potential of chiral P–N compounds in terms of reactivity and applications. Preparative options for *P*-stereogenic aminophosphine chalcogenides and boranes ranging from the use of chiral auxiliaries to transition metal-based methods were reviewed before their applications in asymmetric catalysis were discussed. Non-oxidized aminophosphines serve as ligands in transition metal catalysis, whereas aminophosphine oxides are used in organocatalysis. Aminophosphine chalcogenides of the higher homologues are relatively unexplored in these areas but may inspire researchers to investigate their advantages in terms of catalytic applicability. In Chapter three, we first paved the way to *P*-stereogenic, enantiomerically pure primary aminophosphine sulfides. Using a chiral-auxiliary-based method, we eventually succeeded to obtain a representative with only alkyl substituents at the phosphorus atom (Scheme 7.1).

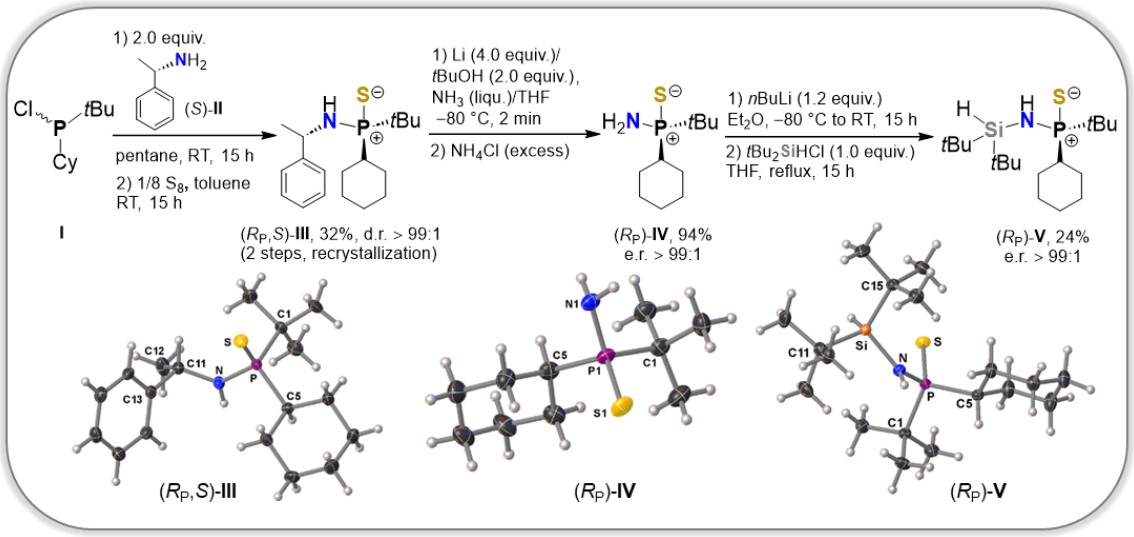

Scheme 7.1. Stereospecific, reductive C–N bond cleavage of (R_P,*S*)-**III** to enantiomerically pure *P*-chiral primary aminophosphine sulfide (R_P)-**IV** and subsequent silylation to (R_P)-**V**.

(*S*)-Methylbenzylamine [(*S*)-**II**] was used as the chiral anchor and coupled with *tert*-butylchlorocyclohexylphosphine (**I**). After oxidation with elemental sulfur, the diastereomerically pure product (R_P,*S*)-**III** was obtained by fractional crystallization. To cleave the chiral auxiliary and release the primary aminophosphine sulfide (R_P)-**IV**, a reductive C–N bond cleavage was carried out in a solution of lithium in liquid ammonia. Subsequent functionalization of the amino function with a hydrosilyl moiety to obtain (R_P)-**V** was successful and forms the basis of investigations

towards new heterocyclic aminophosphonium cations with *P*- and *Si*-centered chirality, which were taken up in Chapter five. The substrates, that were initially investigated, contained a phenyl moiety on the phosphorus atom, which was attacked by the highly reductive conditions resulting in a Birch type reaction. While this issue was known and rectified for P(III) compounds, no simple solution such as an exchange of the chiral anchor was helpful for P(V) compounds. Not only the Birch reduction of the phenyl ring, but also the concomitant P–Ph and P–S cleavages increase the level of difficulty for solving this circumstance. Time-dependent studies were carried out to gain more insight into the rapid reductive decomposition of the diastereomeric substrates. In the end, there was no other choice but to replace the phenyl with a cyclohexyl moiety, which made the diastereomeric separation more difficult but also allowed the C–N bond cleavage reaction to proceed in a very clean way and with excellent yield (Scheme 7.1). In addition, (*R*)-BINOL-PSSLi was successfully used as chiral shift reagent to prove the enantiomeric purity of primary aminophosphine sulfides. The associated NMR spectroscopy experiments and quantum chemical calculations indicated the formation of a complex between (*R*)-BINOL-PSSLi and the respective aminophosphine sulfide in CD_2Cl_2 solution. Both coordinative and hydrogen bonding interactions are involved in the proposed structure. Hydrogen-bond-based model systems also play the major role in Chapter four. Several aminophosphine chalcogenides have been subjected to a protonation with hydrogen chloride or Jutzi's acid (Scheme 7.2). Although this may sound simple from a synthetic point of view, the bifunctional pattern with NH_2 and $P^+–Ch^-$ (Ch = O, S, Se) moiety provides interesting insights into the possibilities of hydrogen bonding interactions in the solid state and in solution. Upon reaction with hydrogen chloride, achiral aminophosphine sulfide **VI** and selenide **VIII** were protonated at the amino group and formed a tetrameric cubic supermolecule with the chloride anions in the solid state [**(VI·HCl)$_4$** and **(VIII·HCl)$_4$**, respectively]. With $[B(C_6F_5)_4]^-$ as a weakly coordinating anion, such hydrogen bonds could not be formed and the protonation at the $P^+–S^-$ or $P^+–Se^-$ entity appeared to be energetically more favorable [**(VI–SH)$^+$ WCA$^-$** and **(VIII–SeH)$^+$ WCA$^-$**, respectively]. The same observations were also made for both *P*-stereogenic, enantiomerically pure [(R_P)-**VII**] and racemic (*rac*-**VII**) aminophosphine sulfides. An achiral oxygen analogue **IX** was always protonated at the $P^+–O^-$ entity, whether $[B(C_6F_5)_4]^-$ [**(IX–OH)$^+$ WCA$^-$**] or Cl^- (**IX·HCl**) was used as the counterion. However, only with the chloride anion, the formation of a ladder-shaped, hydrogen-bonded network was observed in the solid state, whereas no intermolecular interactions could be found in the presence of a weakly coordinating anion. The different protonation behavior of the oxygen-substituted congener when hydrogen chloride is used is easily explained by the fact that oxygen is by far more Lewis-basic than its higher homologues. All solid state structural information is derived from single crystal X-ray diffraction and in some cases also from NMR spectroscopy. For the aggregation properties in CD_2Cl_2 or CH_2Cl_2 solution, we used NMR and IR spectroscopy as well as computational calculations. Interestingly, the aggregation behavior of aminophosphine sulfides and selenides with chloride was found to be strongly dependent on concentration and temperature. The tetrameric structure tended to be preserved at high concentrations and at low temperatures. No such tendency was found for aminophosphine oxides.

Furthermore, for aminophosphine sulfides and selenides in the presence of $[B(C_6F_5)_4]^-$, a rapid exchange of NH_2 and ChH protons was suggested, which could be observed on the NMR timescale.

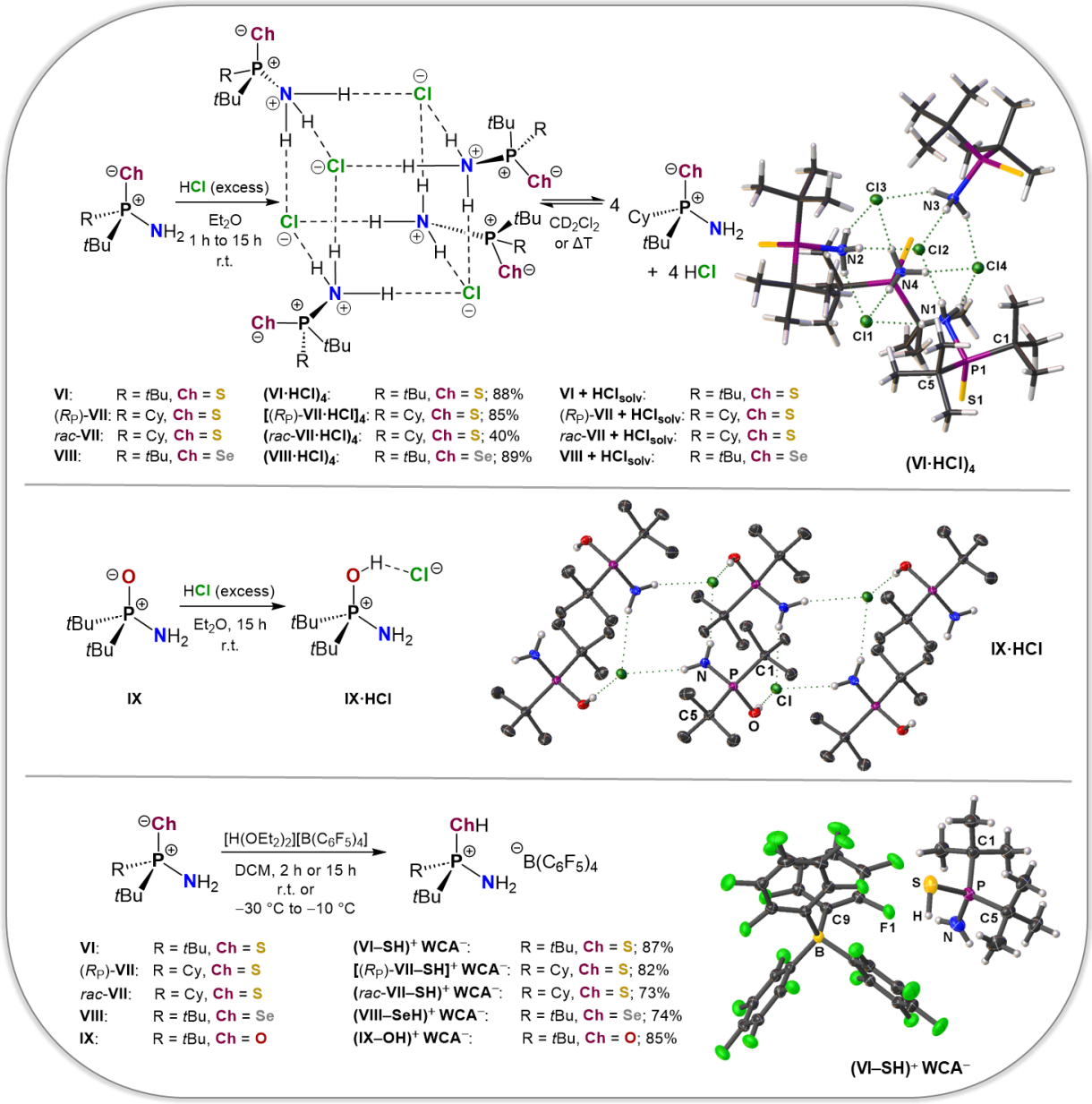

Scheme 7.2. Similarities and differences in the reaction products of **VI**, (R_P)-**VII**, *rac*-**VII**, **VIII** and **IX** with HCl or Jutzi's acid. The phosphorus atom in *rac*-**VII** must be seen without stereoinformation.

The fact that aminophosphine chalcogenides are potent and indispensable reaction intermediates in modern synthetic chemistry was discussed in Chapter one and was even experienced during the experimental work for Chapter three, when a *P*-stereogenic, enantiomerically pure aminophosphine sulfide was used as a building block for the functionalization with a hydrosilane moiety. The scope of hydrosilylation possibilities was extended in Chapter five. Achiral and *P*-chiral aminophosphine sulfides were left to react with achiral or *Si*-racemic hydrosilyl chlorides or triflates after deprotonation with *n*BuLi. Hydride abstraction reactions of the resulting *N*-hydrosilyl-substituted aminophosphine sulfides were carried out using the Lewis acid $B(C_6F_5)_3$ (BCF). The highly reactive

silylium centre was immediately stabilized by the Lewis-basic P^+–S^- unit to form an intramolecular S^-–Si bond. Although this ring-forming reaction generally gave more stable products for the achiral samples, the chiral precursors were significant for reactivity studies and stereochemical investigations. For example, a thermodynamic dependence on the stereoselective outcome of the ring closing reaction using a diastereomerically pure *P*- and *Si*-chiral precursor was found (Scheme 7.3).

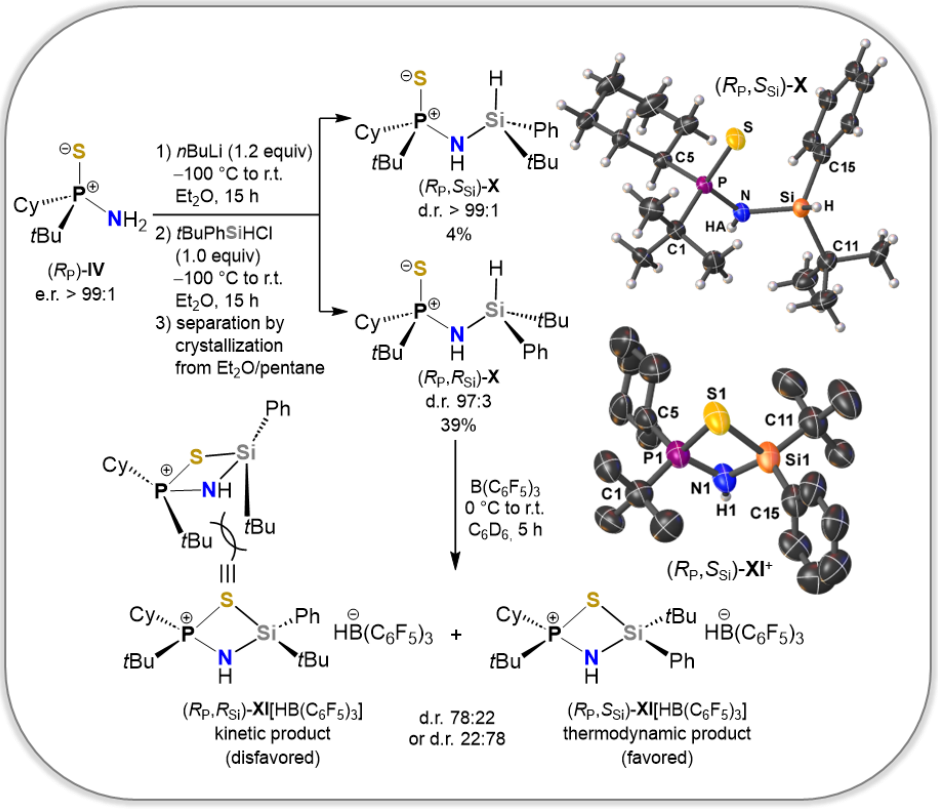

Scheme 7.3. Synthesis of the diastereomeric *P*- and *Si*-chiral cyclic aminophosphonium compounds (R_P,R_{Si})-**XI**[$HB(C_6F_5)_3$] and (R_P,S_{Si})-**XI**[$HB(C_6F_5)_3$] starting from (R_P)-**IV**.

In summary, it was shown that *P*-stereogenic primary aminophosphine sulfides are valuable compounds for promising applications as synthetic building blocks or as precursors for supramolecular synthons. They provide a molecular basis for the tailored design of new chiral ligand systems for transition metal catalysis but also for metal-free organocatalysis, such as hydrogen-bonding/ion-pairing catalysis. The possibilities for using *P*-stereogenic primary aminophosphine sulfides in synthetic inorganic and organic chemistry are far from being exhausted and will continue to be explored. This work is expected to be an inspiration to researchers with a background in the fields of asymmetric catalysis, supramolecular chemistry and *P*-chiral synthesis methodologies.

Acknowledgements

Auf der letzten Seite meiner Doktorarbeit möchte ich allen Leuten danken, die mich während meiner Promotion auf verschiedene Weise unterstützt haben.

PD Dr. Jonathan Bauer für die Aufnahme in seine Forschungsgruppe, was es mir ermöglicht hat diese Doktorarbeit zu verfassen und meine Promotionszeit im schönen Regensburg zu verbringen, für zahlreiche Gespräche und die Möglichkeit meine Forschungsergebnisse auf internationalen Konferenzen zu präsentieren.

Prof. Dr. Manfred Scheer für die Übernahme des Zweitgutachtens und die Unterstützung unserer Forschungsgruppe in den letzten Jahren.

Prof. Dr. Frank-Michael Matysik und Apl. Prof. Dr. Rainer Müller für die Bereitschaft als Drittprüfer bzw. als Vorsitzender meiner Verteidigung zur Verfügung zu stehen.

Meinem Arbeitskreis AK Bauer (Schlager/Malle-Lab: Dr. Tobi; Metal-Lab: Dr. Nicolò, Robin; New-Lab: Dr. Noel-Sí, Alex, Manuel) dafür, dass ihr eine Atmosphäre geschaffen habt, in der ich mich sehr wohl gefühlt habe; sowohl bei Labor- und Flurgesprächen als auch in den (Schafkopf-)Mittagspausen und bei diversen gemeinsamen Unternehmungen. Eure Kollegialität und unentwegte Hilfsbereitschaft waren großartig. Ich werde mich gerne an die Zeit mit euch zurückerinnern.

Den Arbeitskreisen des dritten Stocks (AK Scheer, AK Wolf, AK Korber), den technischen Angestellten (Martina, Petra, Schotti, Lukas, Tuan, Birgit, Sabine) und Gabor für das tägliche Miteinander, diverse technische und fachliche Hilfe.

Allen Menschen, die mich inner- und außerhalb der Uni in den vergangenen Jahren auf positivem Wege begleitet haben, allen langjährigen Freundinnen und Freunden, sowie denen, die es in der letzten Zeit geworden sind. Spieleabende, Konzerte, Festivals, Ausflüge, Urlaube, zusammen kochen, gemeinsam Sport machen und diverse andere Ablenkungen haben meinen Alltag bereichert. Besonderer Dank gilt dabei Franzi S.; dein Zuspruch und unsere gemeinsamen Unternehmungen haben mich immer aufgebaut.

Stefan dafür, dass du mich jeden Tag inspirierst und in den letzten Jahren dafür gesorgt hast, dass ich den Glauben an mich nicht verliere. Dafür, dass du mich verstehst, moralisch unterstützt und mir den Rückhalt gibst, den ich brauche. Ich bin dankbar dafür, dass wir die gleichen Werte teilen und unsere Träume gemeinsam leben. Ich kann unser nächstes Abenteuer kaum erwarten.

Meinen Eltern für das bedingungslose Vertrauen, das ihr mir entgegenbringt, und die Unterstützung aller meiner Lebenspläne. Das Wissen, mich darauf verlassen zu können, schenkt mir Kraft, Gelassenheit und Rückenwind.